Conf-790631 - - (vol. 2)
Volume 2
(of 2 Volumes)

5/2/80

PROCEEDINGS

of the

MASTER DR. 1125

Ocean Thermal Energy Conversion

6th OTEC CONFERENCE

Ocean Thermal Energy for the 80's

WASHINGTON, D. C. June 19 - 22, 1979

Sponsored by
Ocean Systems Branch
Division of Central Solar Technology
U.S. Department of Energy

DISTRIBUTION OF THIS DOCUMENT IS UNLIMITED

DISCLAIMER

This report was prepared as an account of work sponsored by an agency of the United States Government. Neither the United States Government nor any agency Thereof, nor any of their employees, makes any warranty, express or implied, or assumes any legal liability or responsibility for the accuracy, completeness, or usefulness of any information, apparatus, product, or process disclosed, or represents that its use would not infringe privately owned rights. Reference herein to any specific commercial product, process, or service by trade name, trademark, manufacturer, or otherwise does not necessarily constitute or imply its endorsement, recommendation, or favoring by the United States Government or any agency thereof. The views and opinions of authors expressed herein do not necessarily state or reflect those of the United States Government or any agency thereof.

DISCLAIMER

Portions of this document may be illegible in electronic image products. Images are produced from the best available original document.

NOTICE

This report was prepared as an account of work sponsored by the United States Government. Neither the United States nor the United States Department of Energy, nor any of their employees, nor any of their contractors, subcontractors, or their employees, makes any warranty, express or implied, or assumes any legal liability or responsibility for the accuracy, completeness or usefulness of any information, apparatus, product or process disclosed, or represents that its use would not infringe privately-owned rights. Mention of commercial products, their manufacturers, or their suppliers in this publication does not imply or connote approval or disapproval of the product by the U. S. Department of Energy.

Conf-790631
Volume 2
(of 2 Volumes)

PROCEEDINGS

of the

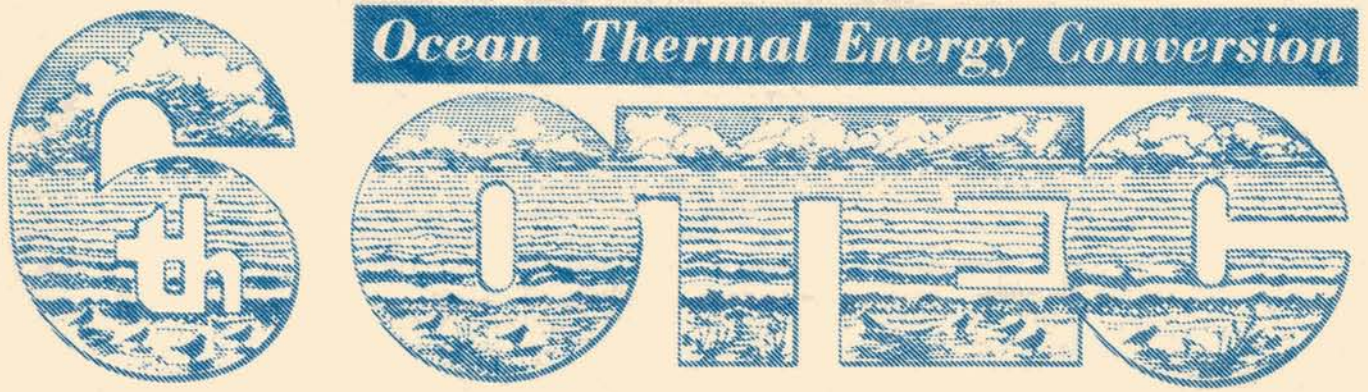

CONFERENCE

Ocean Thermal Energy for the 80's

WASHINGTON, D. C. June 19 - 22, 1979

Sponsored by
Ocean Systems Branch
Division of Central Solar Technology
U.S. Department of Energy

NOTICE

This report was prepared as an account of work sponsored by the United States Government. Neither the United States nor the United States Department of Energy, nor any of their employees, nor any of their contractors, subcontractors, or their employees, makes any warranty, express or implied, or assumes any legal liability or responsibility for the accuracy, completeness or usefulness of any information, apparatus, product or process disclosed, or represents that its use would not infringe privately-owned rights. Mention of commercial products, their manufacturers, or their suppliers in this publication does not imply or connote approval or disapproval of the product by the U. S. Department of Energy.

PROCEEDINGS

Conf-790631
Volume 2
(of 2 Volumes)

of the

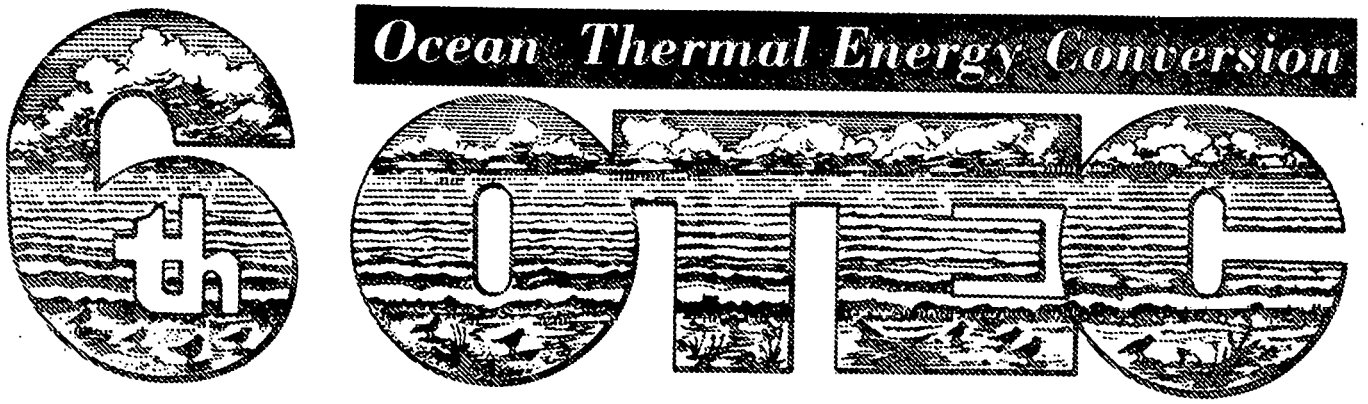

CONFERENCE

Ocean Thermal Energy for the 80's

WASHINGTON, D. C. June 19 - 22, 1979

Gordon L. Dugger, Editor

Sponsored by
Ocean Systems Branch
Division of Central Solar Technology
U.S. Department of Energy

Organized by
The Johns Hopkins University
Applied Physics Laboratory
Laurel, Md. 20810

FOREWORD

The purpose of the 6th Ocean Thermal Energy Conversion (OTEC) Conference, like that of its predecessors, was to provide opportunities for information exchange and for discussion of the national OTEC program. The latest research and development work, test results, component design information, system integration efforts, and application investigations were presented. Not only the technical aspects but also the commercial, institutional, legal, environmental, and international aspects of OTEC implementation were discussed.

The reports of six working groups are featured at the beginning of Volume I of these Proceedings. Each working group held intensive discussions of a major subject area of the OTEC program. Every attendee was invited to participate in the working group of his or her choice. The reports, prepared by the executive committees of the working groups, address the technical and/or institutional status of the program; the critical-path activities needed to prepare for and achieve pilot plant design, construction and operation at early dates with acceptable risk levels; the pilot plant missions; and further work and actions needed to bring about cost-competitive, commercial OTEC plants in a timely manner. On the whole, the reports are quite positive in tone relative to readiness for the pilot plant phase.

The interesting presentations and remarks by the speakers at the plenary session, the luncheon, and the banquet follow the working group reports in Volume I.

Preprints of the majority of the technical papers were available in two volumes at the Conference. Some of the papers were represented by abstracts; none had been reviewed. Many of the authors included more current material in their oral presentations. The preprinted papers were then reviewed (but less formally than for a journal) for acceptability and clarity for use in these Proceedings. Although a few papers were declined, and two authors defaulted, these Proceedings contain, in final form, 95% of the papers that were presented. At the Conference we attempted to tape the discussions of the papers, and, where possible, the discussion follows each paper. The papers are arranged by subject matter into two volumes as shown in the Table of Contents.

The list of the 585 attendees with their addresses and, in most cases, their telephone numbers, is at the end of Volume II. The total turnout for the banquet was 600.

Two important aspects of this Conference were that 27 participating organizations aided us in organizing and publicizing the Conference, and there were 21 exhibitors, listed on page iv. The exhibits added greatly to the value of the meeting for the attendees, the press, and the general public. On the evening of the banquet, a reception was hosted by Rums of Puerto Rico, enjoyed by all.

Bob Cohen was the Department of Energy contact as sponsor for the Conference. He and Bill Richards, Chief of the Ocean Systems Branch, and the other program managers in the Branch--Sig Gronich, Bill Sherwood, Lloyd Lewis, Ken Read, and Gene Kinelski--aided in the session planning. The conference committees and session chairmen are listed on page v. The Steering Committee made the planning decisions about the content and makeup of the Conference. The Papers Committee reviewed the 170 abstracts that were submitted and accepted 125 papers for presentation at the Conference. The Session Chairmen and Co-Chairmen did fine jobs in running the sessions, and they and many of the authors joined the listed Papers Committee in reviewing the preprints for use in these Proceedings. The Exhibits and Arrangements Committee from APL/JHU headed by Bud Francis did an excellent job and were supported by many others at APL. Bob Kroll of APL handled the editorial services for both the preprints and these Proceedings, with support from many others. To all of these stalwarts I say thank you for jobs well done!

My sincere thanks for all-around help with the Conference also go to Ed MacCutcheon, Consultant. He appeared, and worked behind the scenes, in many roles and is now helping Bob Scott of Gibbs & Cox, Inc., to organize the 7th Ocean Energy Conference, which will be held at the Shoreham Hotel in Washington, D.C., June 2-5, 1980. We wish them every success.

Gordon L. Dugger
Chairman
6th OTEC Conference

6th OTEC CONFERENCE
PARTICIPATING ORGANIZATIONS

The Aluminum Association

American Chemical Society
Division of Industrial and Engineering Chemistry

American Institute of Aeronautics and Astronautics

American Institute of Chemical Engineers

American Society of Mechanical Engineers

American Oceanic Organization

American Society of Naval Engineers

American Society for Testing and Materials

Center for Oceans Law and Policy, University of Virginia

Electric Power Research Institute

Institute of Electrical and Electronics Engineers, Inc./Oceanic Engineering Council

International Association for Hydrogen Energy

International Solar Energy Society

ANZ Section
American Section
Italian Section
Japanese Section
Dutch Section
Belgian Section
Irish Section
Scandinavian Section
U.K. Section
South African Section
Arab Section
German Section
Indian Section

Marine Technology Society

National Association of Corrosion Engineers

National Energy Resources Organization

National Ocean Industries Association

National Science Foundation, Division of Engineering

Shipbuilders Council of America

The Society of Naval Architects and Marine Engineers

Solar Energy Industries Association

Solar Energy Research Institute

United Nations Educational, Scientific and Cultural Organization

U.S. Coast Guard
Office of Merchant Marine Safety

U.S. Department of Commerce
Maritime Administration
National Oceanic and Atmospheric Administration

U.S. Navy Department
Oceanographer of the Navy

6th OTEC CONFERENCE
EXHIBITORS

Alfa-Laval Thermal

Advanced Marine Enterprises

Department of Energy

Gibbs & Cox, Inc.

General Electric Co.

Global Marine Development, Inc.

State of Hawaii

Hydronautics, Inc.

Lockheed Ocean Systems

M. Rosenblatt & Son, Inc.

National Oceanic and Atmospheric Administration

ORI, Inc.

Offshore Technology Corporation

Puerto Rico

Rotoflow Corporation

Solar Energy Research Institute

Solar Ocean Energy Liaison

The Johns Hopkins University, Applied Physics Laboratory

TRW, Inc.

Westinghouse Electric Corporation

Worthington Pump Company

6th OTEC CONFERENCE
COMMITTEES AND SESSION CHAIRMEN

STEERING COMMITTEE

Gordon Dugger, Chairman
Robert Cohen
Phillip Eisenberg
Evans J. Francis
Robert Hindle
Raleigh E. Guynes
Robert B. Leamer
E. M. MacCutcheon
Richards T. Miller
Merle Olmsted
Paul D. Ritland
David Shapiro
J. Paul Walsh
Byron Washom

PAPERS COMMITTEE

Paal Bakstad
Roderick Barr
Kenneth Bell
Peter Benson
Ralph Blevins
Robert Cohen
Paul Curto
J. B. Darby, Jr.
John D. Ditmars
Robert Douglass
Gordon Dugger
Evans J. Francis
James F. George
Donald Guild
Freeman Hill
Robert Hindle
Eugene H. Kinelski
T. S. Lee
Lloyd Lewis
Brenda Little
Dan Lott
Robert F. Mast
Terence McGuinness
Maxwell S. McKnight
John Michel
Richards T. Miller
Ralph Mitchell
Robert L. Molinari
Frederick Naef
J. R. Paulling
R. J. Pont
Glenn F. Popper
Kenneth Read
Robert Scott
Wilbur Sherwood
Robert E. Stein
Anthony Thomas
Rodney D. Titcomb
J. Paul Walsh
Laskar Wechsler
Byron Washom
Pat Wilde

ARRANGEMENTS AND EXHIBITS COMMITTEE

Evans J. "Bud" Francis, Chairman
William Buchanan
Joan Handiboe
Jacqueline Hentgen
William Kehoe
Phillip Lewellen

SESSION CHAIRMEN AND CO-CHAIRMEN

William H. Avery
Paal Bakstad
Roderick Barr
Eugene Barsness
Kenneth J. Bell
Charles Cochran
Robert Cohen
Joseph Darby
John Ditmars
Robert Douglass
Joseph Draley
Douglas Evans
Evans J. Francis
James F. George
Julio Giannotti
Eugene Kinelski
Frank LaQue
Lloyd Lewis
Terence McGuinness
John Michel
Ralph Mitchell
Robert Molinari
Frederick Naef
J. D. Nyhart
William Owens
Robert A. Paddock
Glenn Popper
T. J. Rabas
Kenneth F. Read
Dennis Richards
S. L. Ridgway
Norman Sather
Richard Scotti
Ben Shelpuk
Wilbur Sherwood
Feat Szeto
Joseph Vadus
Keith Waite
J. Paul Walsh
Byron Washom
Laskar Wechsler
Pat Wilde

THIS PAGE

WAS INTENTIONALLY

LEFT BLANK

CONTENTS

VOLUME I

1. WORKING GROUP REPORTS 1

2. PLENARY SESSION AND TALKS

Welcoming Remarks, Bennett Miller 2.1

The Need for OTEC, Gerry E. Studds 2.2

Energy From the Oceans — Lessons from the North Sea, John Derrington 2.3

The U.S. Ocean Energy Systems Program, W. E. Richards . . 2.4

Remarks at the 6th OTEC Conference Luncheon, Edwin M. Hood . 2.5

Remarks at the 6th OTEC Conference Luncheon, Charles Matthews 2.6

Keynote Address at the 6th OTEC Conference Luncheon, Charles H. S. Eaton 2.7

Introductory Remarks at the 6th OTEC Conference Banquet, Robert Cohen 2.8

Remarks at the 6th OTEC Conference Banquet, John M. Deutch . 2.9

Keynote Address at the 6th OTEC Conference Banquet, Carlos Romero-Barceló 2.10

3. OTEC PROGRAMS OF EUROCEAN, FRANCE, AND JAPAN

EUROCEAN OTEC Project, Bengt A.P.L. Lachmann . . . 3.1

The French OTEC Program, Philippe Marchand 3.2

An Overview of the Japanese OTEC Development, Takuya Homma and Hiroshi Kamogawa 3.3

4. OTHER OCEAN ENERGY SYSTEMS

Waves, Salinity Gradients, and Ocean Currents — Alternative Energy Sources, Michael E. McCormick 4.1

5. CLOSED-CYCLE OTEC PLATFORMS

OTEC Ocean Engineering Progress Report, Wilbur G. Sherwood and J. Paul Walsh 5.1

OTEC Goes to Sea (A Review of Mini-OTEC), Lloyd C. Trimble and Roger L. Potash 5.2

An Overview of the OTEC-1 Design, N. A. Svensen . . . 5.3

Development of a Test Program for OTEC-1, Phil Archbold. . 5.4

System Design Considerations for a Floating OTEC Modular Experiment Platform, James F. George 5.5

Conceptual Designs and Costs of OTEC 10/40 MW Spar Platforms, R. J. Scott 5.6

Design Considerations on 100 MW_e Commercial Scale OTEC Power Plant and a 1-MW_e Class Engineering Test Plant, T. Homma, H. Kamogawa, S. Nagasaki, H. Uehara, T. Teramoto, and T. Kajikawa 5.7

Station Keeping Subsystem Designs for Modular Experiment OTEC Plants, Nedret S. Basar, John C. Daidola, and Richard C. Sheffield 5.8

A Feasibility Study of an OTEC Guyed Tower Concept, Eugene H. Pharr 5.9

Land-Based OTEC Plants — Cold Water Pipe Concepts, John H. Brewer 5.10

6. COLD-WATER PIPES

Preliminary Designs of Cold-Water Pipes for Barge and Spar-Type OTEC Plants, Terence McGuinness, Arthur Griffin, and Duane Hove 6.1

Cold Water Pipe Verification Test, H. L. Donnelly, J. T. Stadter, and R. O. Weiss 6.2

Analytical and Experimental Methods for Determining OTEC Plant Dynamics and CWP Loads, Roderick A. Barr and Virgil E. Johnson, Jr. 6.3

A Limiting Mechanism for the Heave-Induced Mathieu Type Instability of a Cold Water Pipe, Arnold E. Galef . . 6.4

Practical Schemes for Reducing Cold Water Pipe Loads, William P. Deuchler, Julio G. Giannotti, and William W. Rogalski 6.5

Development of a Lightweight Concrete for OTEC Cold Water Pipes, A. Litvin and A. E. Fiorato 6.6

Oscillations of and Drift Force Acting on an OTEC-CWP Structure, S. Nagasaki, M. Nagatsuka, and H. Kobayashi . 6.7

Dynamic Analysis of Cold-Water-Pipe Systems for Ocean Thermal Power Generation Plants, Takeshi Yokoyama, Yasumasa Arai, and Tashio Katoh 6.8

Vortex Excited Oscillations of Marine Structures with Application to the OTEC Cold Water Pipe, Owen M. Griffin . 6.9

Current-Wave Coupling and Hydrodynamics, Giulio Venezian . 6.10

The Effects of Shear on Vortex Shedding Patterns in High Reynolds Number Flow: An Experimental Study, David Rooney, Rodney Pelzer, Jon Buck, and John Baxter . . 6.11

Development of Ocean Current Information Needed to Address the Problem of Vortex Shedding on the OTEC Cold-Water Pipe, J. A. Pompa and J. R. Buck 6.12

7. OTEC POWER TRANSMISSION CABLES

A Theoretical Study of Technical and Economical Feasibility of Bottom Submarine Cables for OTEC Plants, T. F. Garrity and A. Morello 7.1

The Development of Riser Cable Systems for OTEC Plants, C. A. Pieroni, R. T. Traut, D. O. Libby, and T. F. Garrity . 7.2

Load Criteria for OTEC Riser Cable Design, James C. Oliver and William K. Jawish 7.3

8. CLOSED-CYCLE OTEC POWER SYSTEMS

Preliminary Designs of 10 MW_e and 50 MW_e Power Modules, R. T. Miller, J. J. Gertz and S. Cunninghis . . . 8.1

Design of a 10 MW_e (Net) OTEC Power Module Using Vertical Falling-Film Heat Exchangers, Paal J. Bakstad and Russell O. Pearson 8.2

Design of a 0.2-MW_e (Net), Plate-Type, OTEC Heat Exchanger Test Article and a 10-MW_e (Net) Power Module, J. W. Denton, P. Bakstad, and K. McIlroy 8.3

Design of a 10 MW(e) Power System and Heat Exchanger Test Articles Using Plate Heat Exchangers, Murray I. Leitner and James W. Connell 8.4

Optimizing Plant Design for Minimum Cost Per Kilowatt and Refrigerant-22 Working Fluid, M. G. Olmsted, M. J. Mann, and C. S. Yang 8.5

Ocean Thermal Energy Conversion Plant with Freon 22, Haruo Uehara, Hisao Kusuda, Masanori Monde, Tsutomu Nakaoka, and Shiro Mikazaki 8.6

Performance Optimization of an OTEC Turbine, Semon P. Vincent and Charles H. Kostors 8.7

OTEC System Response and Control Analysis, W. L. Owens . . 8.8

Dynamic and Off-Design Analysis of OTEC Closed Cycle Power Systems, Arthur W. Westerberg, Shichune Yao, Stephen J. Jennings, and William H. Coleman 8.9

Steady-State and Dynamic Performance of an OTEC Plant, Myron Kayton 8.10

Off-Design Performance and Control Considerations for an OTEC Plantship, D. Richards, P. J. McEvaddy, and L. L. Perini 8.11

9. OPEN-CYCLE OTEC POWER SYSTEMS AND OTEC CYCLE INNOVATIONS

OTEC 100-MW_e Alternate Power Systems Study, Thomas J. Rabas, J. Michael Wittig, and Klemens Finsterwalder . . 9.1

Recent Developments in the Foam OTEC System, Clarence Zener, Alberto Molini, Tomlinson Fort, Jr., John Fetkovich, and Martin Greenstein 9.2

Description and Status Report of a Program to Define Seawater-Surfacant Interactions in Relation to the Foam System, M. I. Kay 9.3

Design of Land-Based, Foam OTEC Plants for Bottoming Cycles, A. E. Molini, M. Santiago, A. Herrera, J. A. Lopez, R. Martinez, C. Zener, and T. Fort, Jr. 9.4

Multiple Staging of the Cold Water in the Open Cycle OTEC Systems, Alberto E. Molini, Clarence Zener, and Tomlinson Fort, Jr. 9.5

The Mist-Transport Cycle: Progress in Economic and Experimental Studies, A. F. Charwat, R. P. Hammond, and S. L. Ridgway 9.6

Land-Based Application of an OTEC Open-Cycle Power System, F. C. Chen 9.7

Waste Heat from OTEC Condenser Water to Melt Icebergs for Irrigation Water, John M. Randall, Wayne M. Camirand, and Earl Hautala 9.8

Examination of a Gravity-Opposed Heat Pipe for Otec Application, George Peter Wachtell 9.9

Thermoelectric OTEC, T. S. Jayadev, D. K. Benson, and M. S. Bohn 9.10

Hybrid OTEC Air Cycle Avoids Indirect Heat Exchangers, C. E. Jahnig 9.11

10. OTEC APPLICATIONS, ECONOMICS, AND INTEGRATION

Potential for Ocean Thermal Energy Conversion, Electric Power Generation in the Southeast Region, Paul R. Sutherland, F. George Arey, Jr., and Donald H. Guild 10.1

A Case Study of OTEC Plant Financing for the Middle South Utilities, B. Jennine Anderson 10.2

Electric Utility System Planning Studies for OTEC Power Integration, Fernando Pérez Bracetti 10.3

Financing Under a Tax-Exempt Situation — Key to OTEC Commercialization? N. Famadas and J. R. Capo 10.4

Analysis of Prospects for OTEC Commercialization for Baseload Power, Willis E. Jacobsen and Richard N. Manley . . 10.5

Commercial Ocean Thermal Energy Conversion (OTEC) Plants by the Mid-1980's, Evans J. Francis, John F. Babbitt, and Myron H. Nordquist 10.6

Status of Solid Polymer Electrolyte Electrochemical Cell Technology for Electrolytic Hydrogen Generation and Fuel Cell Power Generation, L. J. Nuttall 10.7

Large Alkaline Electrolysis Systems for OTEC, William C. Kincaide 10.8

Integration Issues of OTEC Technology to the American Aluminum Industry, M. S. Jones, Jr., K. Sathyanarayana, A. L. Markel, and J. E. Snyder, III 10.9

OTEC Power for Ocean Minerals, E. H. Harlow 10.10

VOLUME II

11. CLOSED-CYCLE OTEC HEAT EXCHANGERS

Performance Tests of 1 MWt Shell-and-Tube and Compact Heat Exchangers for OTEC, Anthony Thomas, James J. Lorenz, David L. Hillis, David T. Yung, and Norman F. Sather . 11.1

Core Unit Testing of the APL/JHU Shell-Less Folded Tube Heat Exchangers, James L. Keirsey, John A. Funk, Peter P. Pandolfini, and Richard T. Cusick 11.2

1 MW_e Heat Exchangers for OTEC — Status Report, June 1979, J. E. Snyder, III, M. H. Seidman, A. M. Sprouse, and A. L. Yarden 11.3

Compact Heat Exchanger Design Progress, J. H. Anderson, Jr. and P. B. Pribis 11.4

Studies on OTEC Power System Characteristics and Enhanced Heat Transfer Performance, T. Kajikawa, T. Agawa, H. Takazawa, M. Amano, K. Nishiyama, and T. Homma . . 11.5

Flow-Induced Vibration in Shell-and-Tube Heat Exchangers for Ocean Thermal Energy Conversion (OTEC), J. J. Lorenz and D. Yung 11.6

A Summary of Recent Experimental and Analytical OTEC Studies at ORNL, J. W. Michel 11.7

Heat Transfer Enhancement by Surface Extension in Horizontal Ammonia-Film Evaporators, Raul J. Conti 11.8

Ammonia Vaporization and Condensation Investigations Related to OTEC Heat Exchangers, C. M. Sabin and H. F. Poppendiek 11.9

The Modeling of Thin Film Heat Exchangers, Shi-chune Yao, Arthur W. Westerberg, and Nien H. Chao 11.10

Variflux and Finned-Plate OTEC Heat Exchanger Technology Status, D. Wright, W. Wagner, and J. Shoji 11.11

12. MATERIALS, BIOFOULING, AND COUNTERMEASURES

Biofouling, Corrosion, and Materials Overview, Eugene H. Kinelski 12.1

Qualifying Aluminum and Stainless Alloys for OTEC Heat Exchangers, F. L. LaQue 12.2

Use of the New Stainless Alloys for OTEC Heat Exchangers, Jack R.\Maurer 12.3

Oxygen, Temperature, and pH Effects on Corrosion of Aluminum in Seawater, Stephen C. Dexter 12.4

Interleakage of Ammonia and Seawater in OTEC Heat Exchangers, Effects on Corrosion and Scale Formation, C. F. Schrieber, W. B. Grimes, and W. F McIlhenny 12.5

Review of Corrosion of Steel in Concrete, Aziz Siman, Changiz Dehghanian, and Carl E. Locke 12.6

The Effects of Biofouling and Corrosion on Heat Transfer Measurements, B. E. Liebert, L. R. Berger, H. J. White, J. Moore, Wm. McCoy, J. A. Berger, and J. Larsen-Basse . 12.7

Experiments on Ultrasonic Cleaning of a Shell-Less Folded-Aluminum-Tube, OTEC Heat Exchanger, Peter P. Pandolfini, William H. Avery, and Freeman K. Hill 12.8

The LMSC Biofouling Measurement Device, W. L. Owens . . 12.9

Possible Cu-Ni-Clad Steel Material and Abrasive Slurry Cleaning System for Plate-Fin-Type OTEC Heat Exchangers, Michael J. Mann 12.10

Possible Use of the Cathelco System to Control Fouling in OTEC Systems, Clifford W. Smith, Barry J. Kirk, and William J. Blume 12.11

Fouling Countermeasures — Status of Two Mechanical Cleaning Systems and Chlorination, Daniel F. Lott and Susan M. Tuovila 12.12

A Biofouling and Corrosion Study of Ocean Thermal Energy Conversion (OTEC) Heat Exchanger Candidate Metals, Brenda Little, John Morse, George Loeb, and Frank Spiehler 12.13

Field Demonstration of Rapid Microfouling in Model Heat Exchangers: Gulf of Mexico, November 1978, V. A. DePalma, D. W. Goupil, and C. K. Akers 12.14

Microbial Film Development and Associated Energy Losses, J. D. Bryers, W. G. Characklis, N. Zelver, and M. G. Nimmons . 12.15

Ultrasonic Detection of Microbial Slime Films, George Loeb and Jacek Jarzynski 12.16

Design for an OTEC Seacoast Test Facility at Ke-Ahole Point, Kona, Hawaii, W. Grantz, J. Belvedere, L. Hallanger, E. Noda, and H. White 12.17

Design and Construction Phase of a Biofouling, Corrosion, and Materials Study from a Moored Platform at Punta Tuna, Puerto Rico, Donald S. Sasscer, Thomas R. Tosteson, Kund B. Pedersen, Ferdinan Rosa, and Fernando L. Benitez . 12.18

13. THE OTEC RESOURCE: ENVIRONMENT AND SITING

OTEC Environmental and Resource Assessment Program, Lloyd F. Lewis 13.1

Ocean Thermal and Current Velocity Data Requirements for Design of an OTEC Plant — An Update, Robert L. Molinari. 13.2

Thermal and Current Data from the Gulf of Mexico and South Atlantic Relative to Placement of OTEC Plants, Robert L. Molinari 13.3

OTEC Data Base and Data Products, James Churgin and Harry Iredale 13.4

OTEC World Thermal Resource, William A. Wolff, William E. Hubert, and Paul M. Wolff 13.5

Regional-Scale Sea Surface Temperature Determination from the Geostationary Environmental Operational Satellite, George A. Maul 13.6

Large Cold Tongues in the Eastern Gulf of Mexico and Their Potential Effect on OTEC, Fred M. Vukovich . . . 13.7

Use of Satellite-Derived Sea Surface Temperatures by Cruising OTEC Plants, F. K. Hill and G. L. Dugger . 13.8

Preliminary Results of a Program to Study OTEC Oceanic Environmental Parameters at Punta Tuna, Puerto Rico, Gary C. Goldman and Daniel Pesante 13.9

Observations of Water Mass Structure and Variability North of St. Croix, U. S. Virgin Islands for OTEC Assessment, Robert S. C. Munier, Thomas N. Lee, and Sherman Chiu . 13.10

OTEC Physical and Climatic Environmental Impacts, John D. Ditmars and Robert A. Paddock 13.11

Results of a Near Field Physical Model Study, E. Eric Adams, David J. Fry, and David H. Coxe 13.12

Environmental Impact Assessment for OTEC-1, Linda Sinay-Friedman and John Reitzel 13.13

Modeling the Intermediate Field of Ocean Thermal Energy Conversion Plant Discharges, Gerhard H. Jirka, Janet M. Jones, and Frank E. Sargent 13.14

A Whole Basin Model of the Gulf of Mexico, Alan F. Blumberg and George L. Mellor 13.15

Programmatic Environmental Assessment for Operational OTEC Platforms — A Progress Report, M. Dale Sands . . . 13.16

Environmental Monitoring and Assessment Program at Potential OTEC Sites, P. Wilde 13.17

A Review of the Biological Information Relating to OTEC Operation, S. Mack Sullivan 13.18

Comparison of Nutrient Data from Four Potential OTEC Sites, Mary S. Quinby-Hunt 13.19

Zooplankton from OTEC Sites in the Gulf of Mexico and the Caribbean, M. L. Commins and A. J. Horen . . . 13.20

Phytoplankton and Biomass Distribution at Potential OTEC Sites, P. W. Johnson and A. J. Horne 13.21

The Marine Mammal Fauna of Potential OTEC Sites in the Gulf of Mexico and Hawaii, Susan F. Payne 13.22

14. LEGAL AND INSTITUTIONAL

Legal Aspects of Siting OTEC Plants Offshore the United States, on the High Seas, and Offshore Other Countries, J. D. Nyhart 14.1

Legal and Institutional Aspects, Ved P. Nanda . . . 14.2

Research in OTEC Institutional and Legal Matters, R. Clark Tefft, Ratus L. Kelly, C. Mathews Dick, Jr., and Kathleen M. Stevenson 14.3

Lead Agency Designation and Proposed Licensing Procedures for Ocean Thermal Energy Conversion Facilities, Edward J. Linky 14.4

15. LIST OF ATTENDEES 15.1

11. CLOSED-CYCLE OTEC HEAT EXCHANGERS

PERFORMANCE TESTS OF 1 MWt SHELL-AND-TUBE AND COMPACT HEAT EXCHANGERS FOR OTEC*

Anthony Thomas, James J. Lorenz, David L. Hillis, David T. Yung, and Norman F. Sather

Argonne National Laboratory
9700 South Cass Avenue
Argonne, Illinois 60439

Abstract

Final test results are reported for the five 1 MWt shell-and-tube heat exchangers tested at Argonne National Laboratory. In addition, preliminary results are reported for two 1 MWt shell-less, or compact, heat exchangers. The five shell-and-tube heat exchangers are the Union Carbide flooded-bundle evaporator, the Union Carbide sprayed-bundle evaporator, the Union Carbide enhanced-tube condenser, the Carnegie-Mellon vertical fluted-tube evaporator, and the Carnegie-Mellon vertical fluted-tube condenser. The two compact heat exchangers are the APL/JHU folded-tube evaporator and the Trane plate-fin evaporator. Performance parameters measured include the overall heat transfer coefficient (U_o), the water-side pressure drop, and the vapor quality. Also measured were operational characteristics of the heat exchangers such as repeatability of results and the dependence of U_o on heat duty, ammonia flow rate, and subcooling. Individual water-side and ammonia-side coefficients were deduced using the Wilson-plot method.

Introduction

The Ocean Thermal Energy Conversion (OTEC) test program at Argonne began in 1977 with the specific purpose of obtaining performance data on small (1 MWt) heat exchangers. This information is necessary for the development of design methods for full-scale OTEC heat exchangers. Although single-tube experimental data are available for some configurations,[1,2,3,4] such results are not by themselves sufficient for scale-up.

Preliminary results for two of the five shell-and-tube heat exchangers tested were reported at the Fifth OTEC Conference in Miami Beach, Florida. In this paper, the final experimental results for all five 1 MWt shell-and-tube heat exchangers are reported, along with preliminary results for two shell-less, or compact, heat exchangers. The five shell-and-tube heat exchangers are the Union Carbide flooded-bundle evaporator, the Union Carbide sprayed-bundle evaporator, the Union Carbide enhanced-tube condenser, the Carnegie-Mellon vertical fluted-tube evaporator, and the Carnegie-Mellon vertical fluted-tube condenser. The two compact heat exchangers are the APL/JHU folded-tube evaporator and the Trane plate-fin evaporator. Performance parameters measured include the overall heat transfer coefficient (U_o), the water-side pressure drop, and the vapor quality. Also measured were operational characteristics of these heat exchangers such as repeatability of results and the dependence of U_o on heat duty, ammonia flow rate, and subcooling. Individual water-side and ammonia-side heat transfer coefficients were deduced using the Wilson-plot method.

The material in this paper is presented in four parts. First, brief descriptions of the heat exchangers tested are given. Second, the experimental facility and instrumentation are described. Third, the formulation and methods used to deduce the overall and individual heat transfer coefficients and their possible errors are discussed. Finally, the experimental results for the five shell-and-tube and two compact heat exchangers are presented.

Test Heat Exchangers

The five 1 MWt shell-and-tube heat exchangers that have been tested are:

1. A flooded-bundle evaporator supplied by the Linde Division of Union Carbide Corporation. This unit is a horizontal three-pass shell-and-tube heat exchanger containing 279 tubes each 1.5 in. OD by 75 in. long. The tubes are made of titanium and are coated with a porous aluminum High Flux surface on the ammonia side. Water flows through the tubes, which are circular and unenhanced on the inside.

2. A horizontal sprayed-bundle evaporator supplied by Union Carbide/Linde and containing titanium tubes coated with the porous aluminum High Flux surface. Liquid ammonia is sprayed onto the outside surface of the tubes by means of perforated feed tubes in the top row of the tube bundle. Water flows through the tubes, which are unenhanced on the water side, in a four-pass arrangement. This unit has 388 tubes each 1.5 in. OD by 55 in. long.

3. A horizontal enhanced-tube condenser provided by Union Carbide/Linde containing aluminum tubes with internal axial fins on the water side and a thin-film promoter on the outside to enhance the condensation of ammonia (Fig. 1). This unit has 147 tubes each 1.5 in. OD by 155 in. long.

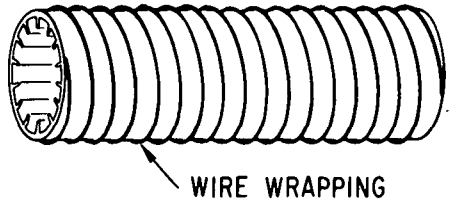

Fig. 1 Linde condenser tube with internal axial fins and external wrapped wire enhancement.

* This work was sponsored by DOE's Ocean Systems Branch, Division of Central Solar Technology, and was performed under Contract No. 09ENG38 with the University of Chicago, operator of Argonne National Laboratory.

4. A vertical fluted-tube evaporator designed by Carnegie-Mellon University (C-MU). This heat exchanger contains 240 fluted aluminum tubes, 1 in. in diameter (nominal) by 172 in. long. The tubes are fluted on both the inside and outside. Ammonia is fed in a thin film onto the outside of the tops of the tubes, and water flows downward on the inside.

5. A vertical fluted-tube condenser, also designed by Carnegie-Mellon. This unit is identical in all respects to the fluted-tube evaporator described above, except that the external (ammonia-side) surface of each tube contains 33 flutes, rather than 42 (Fig. 2).

The two 1 MWt shell-less heat exchangers are:

1. A folded-tube evaporator designed by the Applied Physics Laboratory of Johns Hopkins University (APL/JHU). This unit is composed of three 3 in. OD aluminum tubes, each of which is folded into 43 horizontal passes in a vertical plane. Ammonia is evaporated as it flows upward in the tubes, while water from a head pond at the top flows downward over the tubes by the action of gravity.

2. A brazed-aluminum plate-fin evaporator furnished by the Trane Company. Warm water flows upward through straight, unenhanced passages, and ammonia is evaporated while flowing upward through finned passages.

Test Facility

During 1977 a test facility was designed and constructed at Argonne in order to measure the performance of test heat exchangers operating under simulated OTEC conditions. The test facility, shown in Fig. 3, is designed to measure heat transfer rates and water pumping requirements of evaporators and condensers sized to handle a nominal heat duty of 3.2 million Btu/hr. The facility is

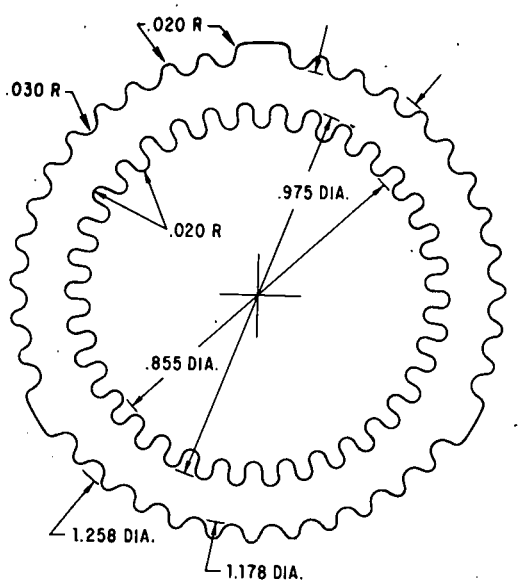

Fig. 2 Cross section of C-MU fluted condenser tube (all dimensions in inches).

designed for steady-state operation over a range of temperatures and flow rates of warm and cold water shown in Table 1. A detailed description of this facility is reported elsewhere.[5,6] Provision is made for control of temperatures and flow rates at preselected values and for measurement of all quantities necessary for calculation of the overall heat transfer coefficient and water-side pressure drops of the test units. The operating conditions of the heat exchangers during the test are typical in all respects of those expected of actual OTEC plants except that deionized water, chemically treated to inhibit the effects of biofouling and corrosion, is used instead of ocean water. The data obtained

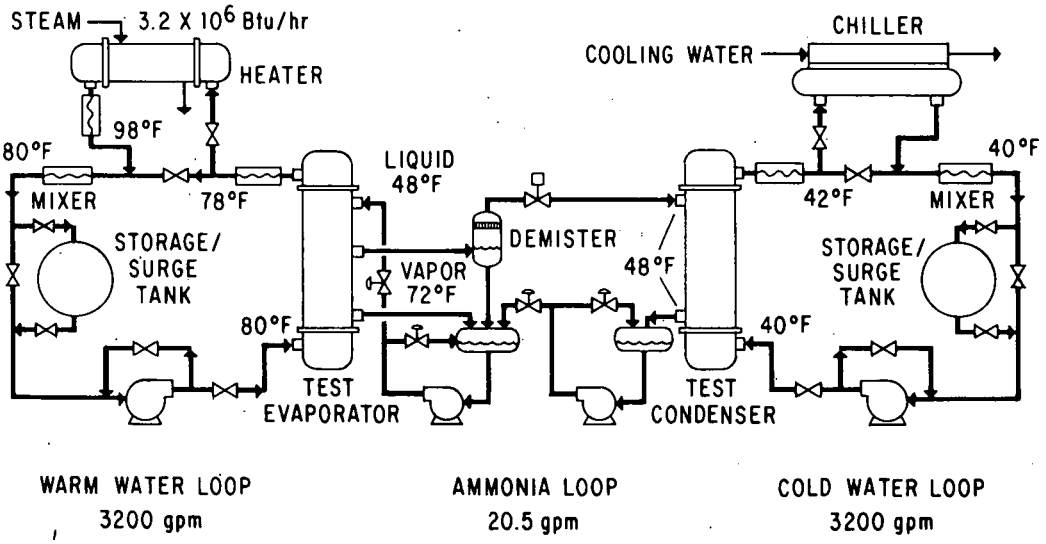

Fig. 3 OTEC heat exchanger test loop.

Table 1 Test Facility Operating Conditions

Parameter	Nominal Value	Range
Heat Duty of Test Units, Btu/hr	3.2 million	2.4 million-4.0 million
Warm Water Supply Temperature, °F	80°	75-85°
Cold Water Supply Temperature, °F	40°	38-45°
Water Temperature Change, °F	2°	2-4°
Log-Mean Temperature Difference, °F	7°	4-10°
Water Flow Rate, gpm	3200	1500-5000

on clean-tube performance, combined with information on the effects of biofouling, provide a means for predicting the performance of similar evaporators and condensers in an ocean environment.

The accuracy goals for the measurements characterizing the overall performance of the test units are ±3% for the overall heat transfer coefficients and ±5% for the water-side pressure drops across the heat exchangers. The equipment used for making these measurements is described in the Data Reduction section. In general, the actual measurement accuracy far exceeds the accuracy goals of the test program.

The test facility has a computer-based data system that can, on command, read the sources of data, apply calibration and correction factors to these data, compute heat balances and overall heat transfer coefficients, and produce hard-copy records of all measured and calculated quantities.

Data Reduction

There are three independent ways of determining the heat duty (q) of the heat exchangers: a) from the temperature change of the water passing through the heat exchangers; b) from an energy balance on the ammonia side; and c) from an overall energy balance on the warm water and cold water loops. Of these three possible methods, the first was determined to be the most accurate and is used exclusively in all subsequent calculations.

Overall Heat Transfer Coefficient

Once a value of the heat exchanger heat duty, q, is obtained, the overall heat transfer coefficient, U_o, is calculated from the conventional definition:

$$U_o = \frac{q}{A_o \Delta T_{lm}} \qquad (1)$$

where:

A_o = the outside surface area of the tubes (mean outside surface area for fluted tubes; also see footnote 2 in Table 3 for exceptions), and

ΔT_{lm} = the log-mean temperature difference between the water and ammonia streams.

ΔT_{lm} can be expressed in equation form as follows:

$$\Delta T_{lm} = \frac{T_i - T_o}{\ln\left[\frac{T_i - T'_o}{T_o - T'_o}\right]} \qquad (2)$$

where:

T'_o = the ammonia temperature,

T_i = the inlet water temperature, and

T_o = the outlet water temperature.

The instruments used to measure the water-side pressure drop and the quantities required for calculating the overall heat transfer coefficient are shown in Table 2, along with their respective accuracies. With the present instrumentation, the probable errors in both the overall heat transfer coefficient and the water-side pressure drop are within ±1%, well within the accuracy goals of the test program (see Test Facility section).

Individual Heat Transfer Coefficients

Individual ammonia-side and water-side heat transfer coefficients can be determined by the standard Wilson procedure. This procedure makes use of the relationship between U_o and the individual coefficients that expresses the total heat transfer resistance as the sum of its separate components. This can be expressed as:

$$\frac{1}{U_o} = \frac{A_o}{h_i A_i} + \frac{1}{h_o} + \frac{\Delta r A_o}{k A_{lm}} + \frac{1}{h_{fo}} + \frac{A_o}{h_{fi} A_i} \qquad (3)$$

where A_o and A_i are selected as the outside and inside areas, respectively. (For the fluted tubes, the mean inside and outside areas are employed.) The third term on the right-hand side of Eq. 3 is the wall resistance. In general, the water-side heat transfer coefficient, h_i, is proportional to some power, n, of the water flow rate, w. For the Union Carbide enhanced-tube condenser, n = 0.66 in accordance with the empirical correlation of Noranda,[7] and for the APL/JHU evaporator, n = 0.6 in accordance with the Zhukauskas correlation. For all other heat exchangers tested the standard value of n = 0.8 is employed. If a series of runs are made over a range of water flow rates under

Table 2 Instruments and Measurement Accuracy

Quantity Measured	Instrument	Accuracy of Measurement
Temperature of:		
Water into and out of heat exchanger Ammonia vapor in evaporator and after expansion valve	Quartz crystal thermometer	±0.010°F
Water into and out of heater and chiller	Copper-constantan thermocouple	±0.1°F
Pressure of:		
Ammonia vapor in heat exchanger and after expansion valve	Quartz crystal transducer	±0.005 psia
Pressure difference of:		
Water into and out of heat exchanger Water into and out of pump Static head of liquid ammonia in evaporator (liquid level)	Strain gauge transducer	±0.5% of reading
Flow rate of:		
Water through heat exchanger Water through heater and chiller	Turbine meter	±0.15% of reading
Liquid ammonia feed to evaporator	Turbine meter	±0.5% of reading

conditions where h_o is constant, a plot of the values of U_o^{-1} versus w^{-n} should fall on a straight line. Extrapolation of the line to the intercept at $w^{-n} = 0$ will yield a value of U_o^{-1} that is equal to the sum of the last four terms on the right side of Eq. 3. The value of the ammonia-side coefficient, h_o, can then be determined by subtracting the values of the tube wall and fouling resistances, if they are known. Finally, the values of the water-side coefficient, h_i, can be obtained for each value of w. It should be pointed out that the ammonia-side heat transfer coefficient is generally a function of location within the heat exchanger; consequently, the h_o value in Eq. 3 represents an average value.

Clearly, the use of this procedure for determining h_o and h_i (w) requires that the data on U_o (w) be obtained under conditions where the average value of h_o is constant and the fouling coefficients, h_{fo} and h_{fi}, are known. In order to ensure that h_o remained the same during the runs at different water velocities, the heat duty, q, was held constant at the nominal design value of 3.2 million Btu/hr, and the ammonia feed rate (for test evaporators) was held constant. Although the inlet water temperature remained unchanged, the ammonia-side temperature had to vary slightly from run to run in order to accommodate the different values of U_o. Consequently, the profiles of the local difference between the water and ammonia temperature along the length of the tubes were not identical for the different flow rates. Nevertheless, the average ammonia-side coefficient, h_o, remained approximately the same because the heat duty was held constant.

The requirement that the fouling resistances be known is a somewhat less certain matter, particularly in the case of the water-side fouling coefficient, h_{fi}. Because of precautions taken to maintain the cleanliness of the ammonia system, it is unlikely that foreign materials from this system could foul the ammonia-side surfaces. The water system has been maintained under a nitrogen blanket since the initial filling. The water is continuously filtered during operation by high-capacity filters located in bypass lines around the water pumps. The cleanliness of the system and the effectiveness of the corrosion inhibitor in scavenging oxygen and preventing the deposit of hard calcium lead us to expect that the magnitude of the water-side fouling resistance approaches zero. Thus it is assumed that the last two terms in Eq. 3 are small enough to be neglected in determining h_o and h_i by the Wilson procedure.

Test Results

Union Carbide Flooded-Bundle Evaporator

A summary of test results for the Union Carbide flooded-bundle evaporator, as well as for the other heat exchangers, is given in Table 3. Under nominal operating conditions (3200 gpm water flow* and 3.2 million Btu/hr heat duty), the overall heat transfer coefficient (U_o) is 785 Btu/hr·ft^2·°F and the ammonia-side and water-side coefficients are 4800 Btu/hr·ft^2·°F and 1400 Btu/hr·ft^2·°F, respectively. The water-side pressure drop is 2.7 psi.

The tests on the Linde flooded-bundle evaporator show that the heat transfer performance depends in part on the exchanger's immediate past history of operation. In particular, contact between the liquid ammonia and the High Flux tube surface under nonboiling conditions appears to deactivate nucleate

*This corresponds to a tube-side velocity of ≈ 6.5 ft/sec, except in the case of the Linde condenser for which the velocity is 5.0 ft/sec.

Table 3 Summary of Test Results for 1 MWt OTEC Heat Exchangers

Heat Exchanger Type	Type of Enhancement	Tube Material Diameter (in.) Length (in.)	U_o [1,2]	h_{NH_3} [1,3]	h_{H_2O} [1,3]	H_2O-side Δp (psi)	Comments
Linde Flooded Evaporator (horizontal 3-pass)	High Flux on NH_3 side; no enhancement on H_2O side	Ti OD = 1.5 ID = 1.43 L = 75	785	4800	1400 (8% higher than predicted by Sieder-Tate	2.7	Approx. 100 hr of continuous running required to reach steady state after full deactivation
Linde Spray Evaporator (horizontal 4-pass)	High Flux on NH_3 side; no enhancement on H_2O side	Ti OD = 1.5 ID = 1.43 L = 55	760	4590	1295 (5% higher than predicted by Sieder-Tate)	4.0	Performance was insensitive to recirculation ratio if greater than 1.27[4]
Linde Condenser (horizontal single-pass)	Proprietary enhancement on NH_3 side; fins on H_2O side	Al 3003 OD = 1.5 ID = 1.37 L = 155	820	5180	1125 (enhancement ratio = 1.6; area ratio = 1.8)[6]	1.8[5]	Within ranges tested U_o was independent of heat duty, and hence liquid loading
C-MU Evaporator (vertical single-pass)	Fluted on both sides (40/40 flutes)	Al 6061 OD = 1.21 ID = 0.91 L = 172	825[4,7]	1800	2610 (enhancement ratio = 1.95; area ratio = 2.07)[6]	3.2	U_o repeatable during any continuous run, but not from one run to the next
C-MU Condenser (vertical single-pass)	Fluted on both sides (40/60 flutes)	Al 6061 OD = 1.21 ID = 0.91 L = 172	1045	3590	2470 (enhancement ratio = 2.5; area ratio = 2.07)[6]	3.3	Performance insensitive to inlet vapor states ranging from 90% quality to superheated
APL/JHU Shell-less Folded-Tube Evaporator	No enhancement	Al 3003 OD = 3.0 ID = 2.69 L = 171 (per pass)	410[8]	1160	690	1.0[10]	Performance the same with or without inlet swirler
Trane Compact Plate-Fin Evaporator	Fins on NH_3 side; no enhancement on H_2O side	Al 3003 Proprietary geometry; reference area=775 ft^2	1230[8]	4540[9]	1720	3.1	Fins appear to be very effective in augmenting heat transfer

[1]All results at nominal heat duty (3.2 million Btu/hr) and water flow rate (3200 gpm); U_o and h are in Btu/hr·ft^2·°F.

[2]U_o is referred to tube outer area; for C-MU units U_o is based on mean outer area; for APL/JHU unit U_o is based on tube inside area; and for Trane unit U_o is based on flat plate surface area.

[3]Calculated via Wilson plot with $V^{-0.8}$, except for Linde condenser where $V^{-0.66}$ was used in accordance with Noranda correlation, and for APL/JHU unit where $V^{-0.6}$ was used in accordance with Zhukauskas correlation.

[4]Recirculation ratio = mass rate of liquid feed/mass rate of evaporation.

[5]Δp is relatively small because the velocity is only 5 ft/sec compared to ≈6.5 ft/sec for the other units.

[6]Value given for h_{H_2O} is based on mean inside area for C-MU units and smooth inside area (based on tube ID) for Linde condenser. Enhancement ratio is the ratio of the actual h_{H_2O} to the predicted h_{H_2O} (using Sieder-Tate) for a smooth tube; area ratio is the ratio of actual inside area to smooth tube inside area.

[7]Recirculation ratio = 5.

[8]Based on nominal NH_3 flow rate of 12 gpm (per tube) for APL and 27 gpm for Trane.

[9]Wall resistance included.

[10]Δp is small because the nominal velocity is only 2.4 ft/sec.

boiling sites, thus reducing the heat transfer coefficient. The observed rate of deactivation is fairly rapid at first: a boiling stoppage of only one hour caused a drop in U_o from 750 to 690 Btu/hr $\cdot ft^2 \cdot °F$. The rate slows to zero over a shutdown period of several hours at the end of which the value of U_o has reached its ultimate minimum of some 600 Btu/hr$\cdot ft^2 \cdot °F$. Operation of the evaporator under boiling conditions reverses this effect, but at a much slower rate. About 100 hours of continuous boiling at nominal design operating conditions are required to fully reactivate the High Flux surface to a U_o value of 785 Btu/hr$\cdot ft^2 \cdot °F$ from an initial value of 600 Btu/hr$\cdot ft^2 \cdot °F$. This behavior is illustrated in Fig. 4. Preliminary tests indicated that reactivation could be accelerated by circulating warm water with no liquid ammonia in the evaporator. This causes a rapid vaporization of liquid ammonia occluding the pores of the High Flux surface and, hence, a more rapid reactivation than that which occurs during normal ammonia boiling.

The value of 4800 Btu/hr$\cdot ft^2 \cdot °F$ obtained for the ammonia-side coefficient can be compared to a value of 5500 Btu/hr$\cdot ft^2 \cdot °F$ measured for clean High Flux tubes in a bench-scale test at Union Carbide Corporation. The small difference between these two values may be due to the presence of fouling on the tube surfaces in the exchanger tested at Argonne; a fouling film with a resistance of only 0.000027 hr$\cdot ft^2 \cdot °F$/Btu, which would account for the difference between the two values of h_o, could have formed on the tube walls from residues left during cleaning and hydrotesting.

With respect to other matters pertaining to the performance of the flooded-bundle evaporator, it was found that the amount of liquid droplet entrainment is so small as to be undetectable; this indicates that the vapor quality is >99.9%. It was also found that varying the heat duty from 3.2 million to 4.6 million Btu/hr produced no measurable changes in U_o.

Finally, reducing the subcooling of the liquid ammonia feed to the evaporator had only a slight effect on thermal performance. In particular, raising the liquid ammonia feed temperature from 48°F to 64°F resulted in an increase in U_o of only 10 Btu/hr$\cdot ft^2 \cdot °F$. Consequently, it is doubtful that the use of an ammonia preheater can be justified on a cost basis.

Union Carbide Sprayed-Bundle Evaporator

Under nominal operating conditions (3200 gpm water flow, 3.2 million Btu/hr heat duty, and 40 gpm ammonia feed rate), the overall heat transfer coefficient is 760 Btu/hr$\cdot ft^2 \cdot °F$ and the ammonia-side and water-side coefficients are 4590 Btu/hr $\cdot ft^2 \cdot °F$ and 1295 Btu/hr$\cdot ft^2 \cdot °F$, respectively. The water-side pressure drop is 4.0 psi.

As with the flooded-bundle evaporator, the past history of the High Flux surface can have a marked effect on the heat transfer performance of this exchanger. Contact between the liquid ammonia and the High Flux surface under nonboiling conditions appears to deactivate the nucleation sites, reducing the heat transfer coefficient to <700 Btu/hr $\cdot ft^2 \cdot °F$. It was found that a deactivated High Flux surface could generally be reactivated by "drying out" the surface while maintaining constant warm water flow. However, if the "dryout" was conducted when the surface was already activated, the heat transfer coefficient actually decreased; this was attributed to incomplete rewetting of tubes following the dryout. Whereas the tubes within the flooded bundle are totally immersed in ammonia, the tubes within the spray evaporator are wetted by a thin falling film of

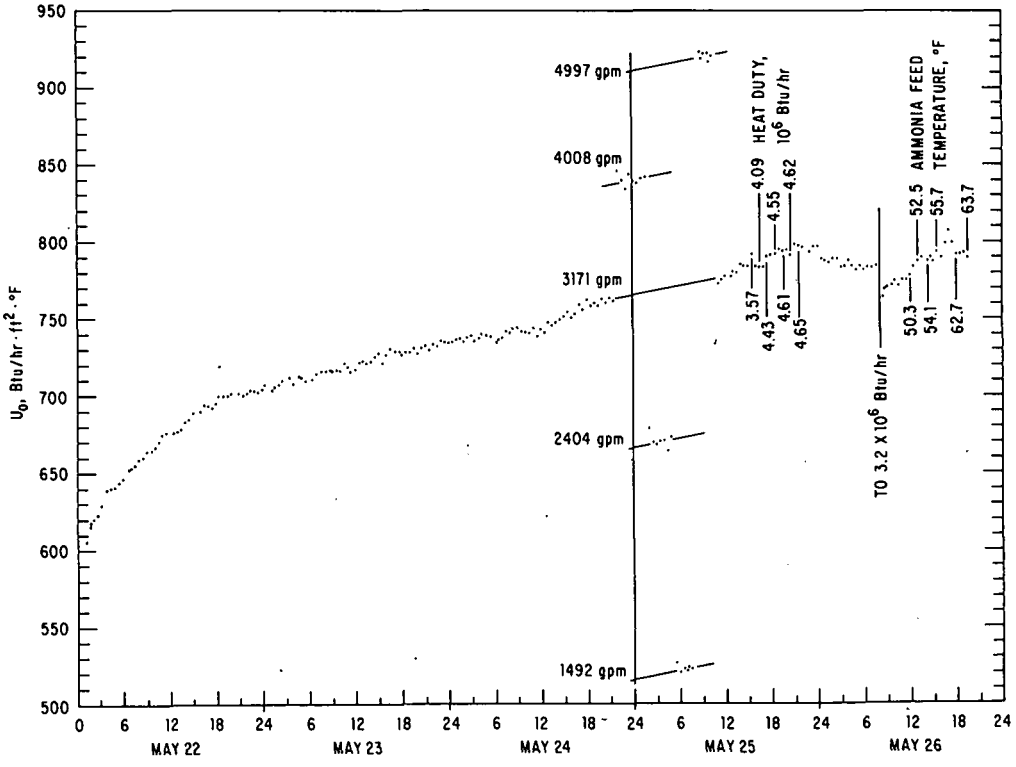

Fig. 4 Extended run results for the Linde flooded-bundle evaporator.

ammonia. Rewetting a dry heated surface by a thin liquid film is known to be very difficult. The surface becomes covered with dry patches that can be eliminated only by "flooding" the surface or by reducing the surface temperature. (Once the dry spots are eliminated, the liquid flow rate can be reduced to a much lower value before dry areas reappear.) These dry patches represent regions of poor heat transfer, and hence result in a lower overall heat transfer coefficient.

The overall heat transfer coefficient was found to be insensitive to ammonia feed rates above the nominal (i.e., up to 100 gpm). However, as shown in Table 4, at a given heat duty there exists a minimum ammonia feed rate below which U_o drops off sharply. During the runs at 3.2 million Btu/hr, the "break" occurred between 26 and 24 gpm, implying a minimum recirculation ratio of about 1.27 to maintain full heat transfer effectiveness. In the tests at 4.0 million Btu/hr, the break was between 30 and 28 gpm, as shown in Fig. 5. The corresponding recirculation ratio was 1.17. Also in Fig. 5, note that the heat transfer coefficient recovered when the ammonia feed rate was increased to 52 gpm. At 2.4 million Btu/hr, the break occurred between 20 and 18 gpm and the recirculation ratio was 1.29.

The sharp drop in U_o at the breakpoint in Fig. 5 most likely reflects the initiation of dry patches on the lower tubes. At the breakpoint for each heat duty, Table 4 gives the corresponding critical loading on the bottom row of tubes. These "local" values were readily estimated from appropriate heat balances on the tube bundle. It can be seen that the critical loadings are all in the neighborhood of 20 lb/hr·ft, with no apparent dependence on heat duty.* Since this critical loading is a local limiting value, it should apply to essentially any size spray evaporator having Union Carbide High Flux tubes. To ensure good heat transfer perfor-

*These results agree favorably with the single-tube results of Czikk et al.,[1] who measured the minimum loading on High Flux tubes as a function of vapor crossflow velocity and heat flux. No discernable heat flux dependence was found, and at low vapor velocities the minimum loadings were scattered within a band ranging from 15 lb/hr·ft to 30 lb/hr·ft.

Table 4 Minimum Feed Rates and Critical Loadings for the Sprayed-Bundle Evaporator at Various Heat Duties

Nominal Heat Duty (million Btu/hr)	Ammonia Evaporation Rate (gpm liquid)	Minimum Ammonia Feed Rate (gpm)	Minimum Recirculation Ratio[a]	Critical Loading on Bottom Row of Tubes (lb/hr·ft)
2.4	14.7	19	1.29	18
3.2	19.7	25	1.27	22
4.0	24.7	29	1.17	20

[a]Recirculation ratio = mass rate of liquid feed/mass rate of evaporation.

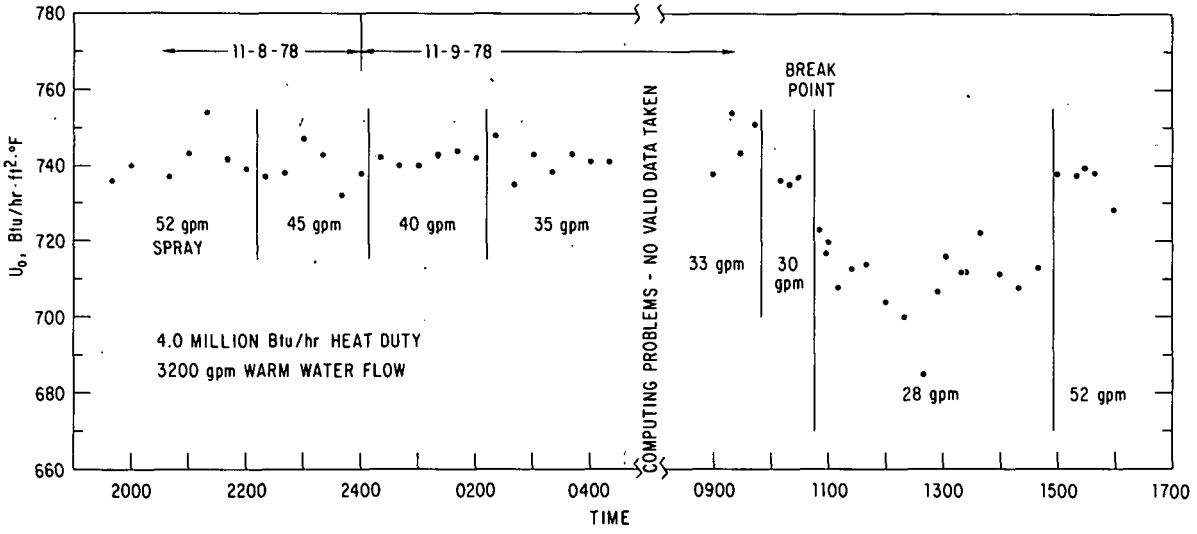

Fig. 5 Determination of minimum ammonia feed rate for the Linde sprayed-bundle evaporator.

mance, it is necessary to design the feed system such that all tubes receive at least the critical loading of 20 lb/hr·ft.

It should be emphasized that this minimum loading is the limiting value approached from a completely wetted, well-activated state. No tests were conducted to determine the minimum loading when approached from an incompletely wetted condition, but the loading would probably be greater.

In addition to the foregoing, vapor quality, heat duty, and ammonia inlet subcooling were also studied. In all cases the measured vapor quality was of the order of 99%. The 1% liquid entrainment created sufficient fog to obscure one's view of the tube bundle. The overall heat transfer coefficient was not significantly affected by variations in heat duty from 2.4 million Btu/hr to 4.0 million Btu/hr nor by changes in ammonia inlet temperature in the range of 52°F to 70°F.

Union Carbide Enhanced-Tube Condenser

Under nominal operating conditions, the overall heat transfer coefficient is 820 Btu/hr·ft^2·°F and the ammonia-side and water-side heat transfer coefficients are 5180 and 1125 Btu/hr·ft^2·°F, respectively. The water-side velocity is 5.0 ft/sec and the pressure drop is 1.8 psi.

The values for the ammonia-side and water-side heat transfer coefficients were obtained using the Wilson-plot method, but with a velocity power of $v^{-0.66}$ conforming to the Noranda correlation for finned tubes (see Fig. 6). The ammonia-side heat transfer coefficient, 5180 Btu/hr·ft^2·°F, is about two times the value predicted by the Nusselt expression for condensation on a smooth tube.

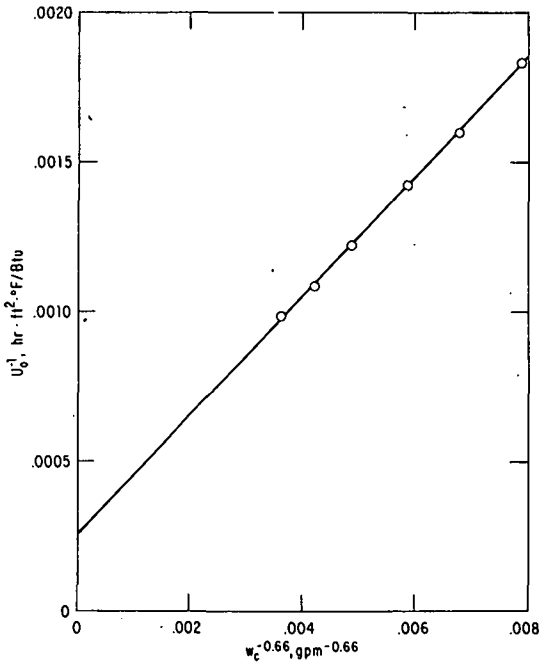

Fig. 6 Wilson plot for the Linde enhanced-tube condenser.*

In Fig. 7 it can be seen that the values of the water-side coefficient are correlated well by the velocity power based on the Noranda correlation and that they are very close to those predicted by the Noranda correlation (about 3% higher). For comparison, the Sieder-Tate correlation for smooth unenhanced tubes is also plotted in Fig. 7. In the present range of water flow rates, the h_i values are about 1.50 to 1.75 times larger than those predicted by the Sieder-Tate equation. These enhancement ratios, incidentally, are consistent with the 1.8 ratio of the actual wetted inside surface area to the nominal inside surface area.

It was found that the individual coefficients as determined by the Wilson method are very sensitive to the choice of the velocity exponent. For example, using the conventional -0.8 power, rather than the -0.66 power as in the Noranda correlation, yields an ammonia-side coefficient of 2620 Btu/hr·ft^2·°F and a water-side coefficient of 1410 Btu/hr·ft^2·°F. Consequently, the accuracy of the calculated individual coefficients is strongly dependent on the accuracy of the exponent in the Noranda correlation.

Additional tests were conducted to study the effects of heat duty and noncondensables. The overall heat transfer coefficient was not affected when the heat duty was varied from 2.4 million to 4.0 million Btu/hr. Since the condensate flow rate is proportional to the heat duty, this implies that the ammonia-side heat transfer coefficient is essentially independent of liquid loading within that range. Apparently, small amounts of noncondensable gases were present throughout the testing, as evidenced by a 3% increase in the U_o value following a purge at the conclusion of the test period.

C-MU Vertical Fluted-Tube Evaporator

Under nominal operating conditions (3200 gpm water flow, 3.2 million Btu/hr heat duty, and 100

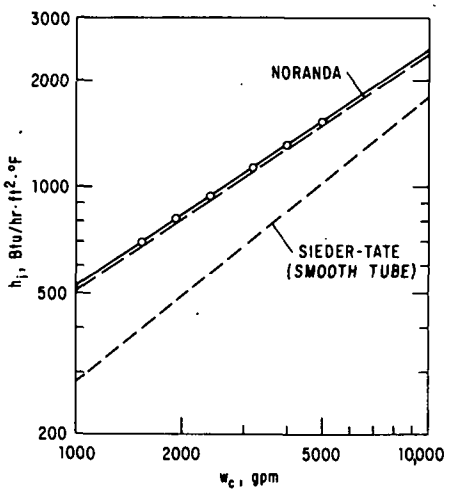

Fig. 7 Variation of water-side coefficient with water flow rate for the Linde condenser.*

*The mean flow velocity v (ft/sec) and the flow rate w_c (gpm) are related by $v = 0.00157\ w_c$.

gpm ammonia feed rate), the overall heat transfer coefficient is 825 Btu/hr·ft^2·°F and the ammonia-side and water-side heat transfer coefficients are 1800 Btu/hr·ft^2·°F and 2610 Btu/hr·ft^2·°F, respectively. The water-side heat transfer coefficient of 2610 Btu/hr·ft^2·°F represents an enhancement ratio of 1.95, which is nearly equal to the area ratio of 2.07. The heat transfer enhancement on the ammonia side is about 2.5, which is higher than the area ratio of 1.6. At nominal operating conditions, the water-side pressure drop is 3.2 psi, the recirculation ratio is 5, the ammonia quality exceeds 99%, and the ammonia temperature entering the evaporator is 67°F.

The measured U_o values were found to be stable and repeatable during any continuous run; however, they were not always repeatable from run to run or even following a brief ammonia flow shutdown. This behavior is illustrated in Figs. 8 and 9 at heat duties of 3.2 million Btu/hr and 4.0 million Btu/hr. The expected parametric trend in the U_o versus ammonia feed rate curve is observed (i.e., U_o increases with feed flow), but the U_o values for the runs on December 13 and 14 are 20-60% higher than those of the previous week. (All subsequent U_o values fell within these limits.) Runs at a heat duty of 2.4 million Btu/hr exhibited a similar degree of nonrepeatability from one week to the next. These repeatability problems are attributed to variations in tube wetting and to the poor design of the feed channels by which the liquid ammonia film is applied to the tops of the tubes; for good evaporator performance well-wetted tube surfaces are essential. It is reasonable to expect that the extent of tube wetting is influenced by the initial rate at which ammonia is fed to the tubes, which are completely dry before starting up. This may explain the difference in performance from one week to the next that was observed in Figs. 8 and 9. In the runs on December 5 and 8 the system was started with a feed rate of 60 gpm, while on December 13 and 14 the initial feed rates were 100 and 110 gpm, respectively. It is likely that in the latter case "flooding" of the surfaces resulted in well-wetted tubes and high U_o values. On the other hand, in the former case the lower feed rate resulted in the formation of dry patches and lower U_o values. The foregoing suggests that to ensure sufficient wetting and good thermal performance, the system should be started with a high ammonia feed rate and then cut back to the desired operating value.

Heat transfer performance is strongly dependent on proper distribution of liquid ammonia. One measure of applicator performance is the uniformity of the liquid feed around the periphery of each tube. It should be evident that a nonuniform feed can contribute to the problem of tube wetting. Another measure of applicator performance is the degree to which liquid ammonia remains on the tubes. With the present applicator design there was a tendency for the liquid ammonia to run along the underside of the metering plate and down the inside surface of the evaporator shell. Furthermore, there was a tendency for the liquid to spray from the tube surface in the region of application and then fall as "rain" within the heat exchanger. For identical operating conditions, the amount of rain observed varied significantly. During the runs on December 5 and 8 there was considerable rain (and U_o was relatively low); in contrast, during the following week there was only a little rain (and U_o was relatively high). This inconsistent behavior reflects a poorly operating applicator. In other tests, C-MU has found that an applicator section with a sleeve extending down over the top of the fluted section performs much more effectively than the uncovered

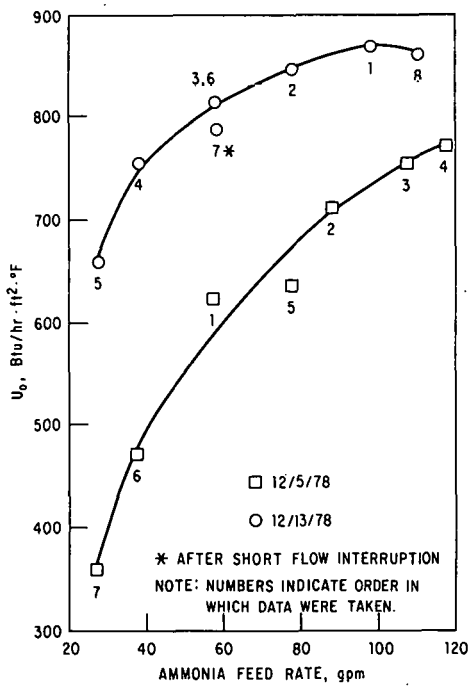

Fig. 8 U_o versus ammonia feed rate at 3.2 million Btu/hr for the C-MU evaporator.

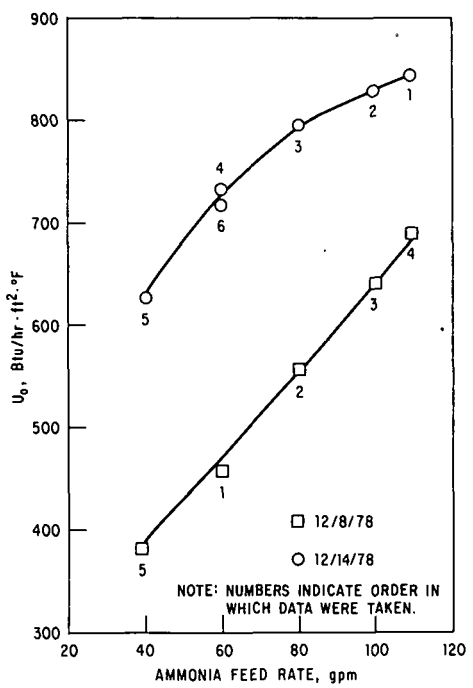

Fig. 9 U_o versus ammonia feed rate at 4.0 million Btu/hr for the C-MU evaporator.

applicator used in the evaporator tested at Argonne.

As mentioned above, for heat duties of 3.2 million and 4.0 million Btu/hr Figs. 8 and 9 exhibit the expected increase in U_o with higher ammonia feed rates. No maximum is observed, which according to Rothfus[8] is characteristic of performance with an applicator having uncovered truncated flutes. Rothfus has found that with the sleeve configuration the curves exhibit a maximum in the vicinity of the laminar-turbulent transition. This occurs at a film Reynolds number of 1500-2000, which corresponds to an ammonia loading of 32-42 gpm.

Comparing Figs. 8 and 9, it is evident that the U_o values increase with decreasing heat duty. This result was anticipated because at lower heat duties less ammonia is evaporated, so the amount of ammonia liquid on the tubes is greater.

C-MU Vertical Fluted-Tube Condenser

Under nominal operating conditions, the overall heat transfer coefficient is 1045 Btu/hr·ft^2·°F and the ammonia-side and water-side heat transfer coefficients are 3590 Btu/hr·ft^2·°F and 2470 Btu/hr·ft^2·°F, respectively. The water-side heat transfer coefficient of 2470 Btu/hr·ft^2·°F represents an enhancement ratio of 2.5, which is about 20% higher than the area ratio of 2.07. The heat transfer enhancement on the ammonia side is about 3.0, which is higher than the area ratio of 1.6. At nominal operating conditions, the water-side pressure drop is 3.3 psi. The overall heat transfer coefficient increased slightly when the heat duty was varied from 2.4 million Btu/hr to 4.0 million Btu/hr.

The pressure of the vapor available to the Carnegie-Mellon condenser can be adjusted to correspond to the exhaust pressure expected from a turbine. The thermodynamic state of the superheated vapor discharged from the expansion valve in the test loop is different from that of a typical turbine exhaust, since the turbine exhaust is expected to be wet and to have micron-sized liquid droplets entrained in the saturated vapor. The mass flow rate of the droplets may be several percent of the total mass flow rate from the turbine.

The Argonne test facility is equipped with a spray type of desuperheater that provides a vapor stream containing liquid ammonia droplets. This desuperheater contains 48 spray nozzles that use high-velocity ammonia vapor jets to atomize small liquid ammonia jets. The liquid ammonia is obtained from the receiver at the bottom of the condenser, and the high-velocity vapor jets are supplied with ammonia vapor at the evaporator pressure. These spray heads are rated to produce 90% of the flow of droplets under 10 microns in diameter.

The effect of vapor quality on the Carnegie-Mellon condenser was measured during a series of runs at the design heat duty of 3.2 million Btu/hr. U_o was first measured while using the superheated ammonia vapor available from the evaporator. Feed valves were then opened to permit a flow of 2.04 gpm of liquid ammonia to the desuperheater spray nozzles; this produced a "wet" ammonia feed (90% quality) to the condenser. Values of U_o for this "wet" condition were determined. Finally, the spray desuperheater was shut off to repeat the superheated condition.

The observed value of U_o with 90% vapor quality was slightly less (about 1%) than with superheated vapor. This decrease was of the same order of magnitude as the scatter in the measured values of U_o at constant operating conditions. We may, therefore, conclude that wet vapor (90% quality) has no significant effect on the condenser performance.

APL/JHU Folded-Tube Evaporator

Under nominal operating conditions, the overall heat transfer coefficient is 410 Btu/hr·ft^2·°F and the ammonia-side and water-side coefficients are 1160 Btu/hr·ft^2·°F and 690 Btu/hr·ft^2·°F, respectively. The individual coefficients were determined from the Wilson-plot technique using an exponent of -0.6 in accordance with the Zhukauskas correlation for tube bundles in crossflow.

Figure 10 shows the dependence of U_o on heat duty and ammonia flow rate. The solid curves represent the best fit to the data at three different heat duties. Actual data points fell within ±3% of the solid curves. The dashed lines of constant exit quality were constructed by fitting smooth curves through points of constant quality on the solid curves. (Qualities at points on the solid curves were calculated from the respective heat duties and ammonia flow rates.) It can be seen that for a given quality the overall U_o values increase with ammonia flow rate. This is characteristic of high-quality forced-convective heat transfer and is analogous to the Reynolds number dependence of the single-phase heat transfer coefficient. Figure 10 also shows that U_o increases with exit quality. This increase is due to the fact that the annular film becomes thinner and has less resistance to heat transfer. At the nominal

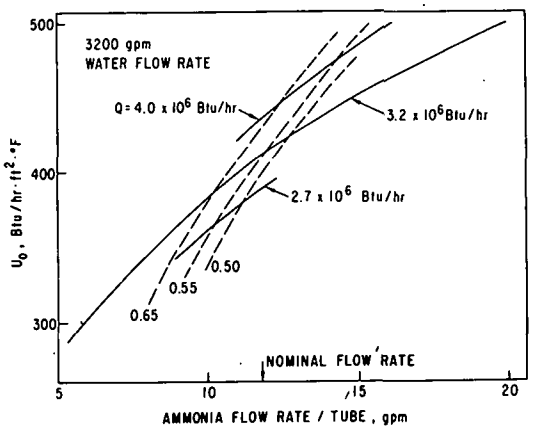

Fig. 10 U_o versus ammonia feed rate for the APL/JHU evaporator. (Solid curves represent best fit to data at a given heat duty; dashed curves represent lines of constant exit quality.)

ammonia flow rate of 12 gpm (per tube) the exit quality is about 55%.

Other test results for the APL evaporator are summarized as follows:

- The value of U_o was not significantly affected when the subcooling of the ammonia feed was varied from 4°F to 16°F.
- Test results with and without the inlet swirler were nearly identical. (Initially the swirlers were thought to be necessary for the promotion of nucleation within the first pass.)
- Two-phase flow instabilities were not encountered under any operating conditions. Initial tests were conducted with a turbine flowmeter at the inlet of each tube, and this was thought to have had a stabilizing influence. However, performance was found to remain stable in subsequent tests with the flowmeters removed.

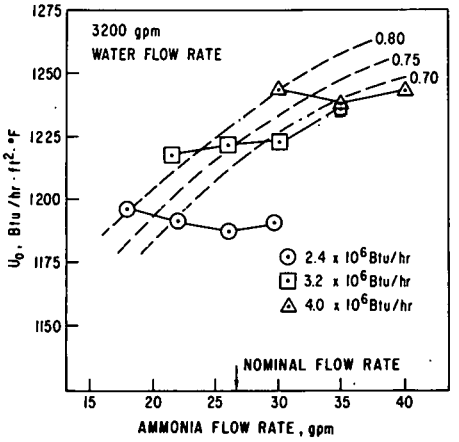

Fig. 11 U_o versus ammonia feed rate for the Trane evaporator. (Solid lines connect data points at a given heat duty; dashed curves represent lines of constant exit quality.)

Trane Plate-Fin Evaporator

Under nominal operating conditions, the overall heat transfer coefficient is 1230 Btu/hr·ft^2·°F and the ammonia-side and water-side heat transfer coefficients are 4540 Btu/hr·ft^2·°F and 1720 Btu/hr·ft^2·°F, respectively. The individual coefficients were determined from a Wilson plot using an exponent of -0.8 for flow between parallel plates. At the nominal water-side flow rate of 3200 gpm, the pressure drop is 3.1 psi.

The ammonia-side coefficient of 4540 Btu/hr·ft^2·°F is not the actual coefficient based on the finned area, but an effective coefficient based on the flat plate surface area. The ratio of the total area with fins in contact with ammonia to the flat area without fins is approximately 3.5; however, the exact geometry of the fins is proprietary. Based on limited information, we estimated the fin efficiency to be about 65% and the actual ammonia-side heat transfer coefficient to be about 1750 Btu/hr·ft^2·°F.

Figure 11 is a plot of typical experimental results for the Trane evaporator. The data shown were taken at an ammonia subcooling of 3°F. (The effect of subcooling on U_o was tested over a limited range, i.e., 3°F to 10°F, and found to be negligibly small.) Compared to the APL results shown in Fig. 10, the lines of constant exit quality for the Trane evaporator exhibit a relatively weak dependence on ammonia flow rate. This result was expected since the water-side resistance is controlling and changes on the ammonia side do not significantly affect the overall heat transfer coefficient. At the nominal ammonia flow rate of 27 gpm, the exit quality is about 75%.

In Fig. 11, the following data point was deleted since it would confuse the presentation and interpretation of the other data: U_o = 1210 Btu/hr·ft^2·°F; ammonia flow rate = 26 gpm; and heat duty = 4.0 million Btu/hr. Based on the trend of the other data, a higher U_o value might be expected for this data point. However, the exit quality for this point was calculated to be about 94%, and it is known that the two-phase forced-convective heat transfer coefficient begins to decrease rapidly at qualities greater than 80-90%. Common design practice is to limit the exit quality to less than 80%. The low value of the data point in question most likely reflects high-quality degradation of the ammonia-side heat transfer coefficient.

Concluding Remarks

The experimental data obtained at the Argonne OTEC test facility can be used to predict the performance of larger units. Of course, the extension of the results to exchangers of a different size and/or geometry must take into account the range and limitations of the tests, in addition to other considerations. For example, with the Union Carbide flooded-bundle evaporator, the static head penalty must be considered. With the Union Carbide sprayed-bundle evaporator, the ammonia distribution system must be designed to provide the minimum of 20 lb/hr·ft to each tube. In the case of large sprayed bundles having high vapor velocity, the problem of vapor/liquid interaction and entrainment must also be considered.[9] For the Union Carbide and C-MU condensers, the influence of heat duty (and hence liquid loading) was examined over a limited range, and any extrapolation beyond that range must be made via a sound analytical model. Of all the units tested, the C-MU evaporator results are the most difficult to scale up because: 1) the dependence of U_o on ammonia feed rate was not measured beyond 110 gpm; 2) uncertainty exists regarding the ammonia applicator performance; and 3) an analytical model describing the fundamental mechanism of evaporation on fluted tubes is lacking.

ANL is carrying on an active analytical modeling program aimed at establishing the required models and algorithms for scaling the test results. The procedures for scaling will be very useful as the program progresses into additional tests of the plate-and-fin heat exchangers as well as the PSD-I and PSD-II test articles.

Acknowledgments

The authors wish to express their appreciation to O. Despe for his contribution to instrumentation, to R. Mandernack for supervision of facility operations, to C. Lemberg for her editorial effort, and to R. Walker for secretarial assistance.

References

1. Czikk, A.M., et al., Fluid Dynamic and Heat Transfer Studies of OTEC Heat Exchangers, Proc. Fifth Ocean Thermal Energy Conversion Conf., Miami Beach, Fla., Vol. 3, Feb. 1978.

2. Pandolfini, P.P., et al., Tests of the JHU/APL Heat Exchanger Concept, Proc. Fifth Ocean Thermal Energy Conversion Conf., Miami Beach, Fla., Vol. 3, Feb. 1978.

3. Michel, J.W., Analytical and Experimental Studies of OTEC Heat Transfer Problems at Oak Ridge National Laboratory, Proc. Fourth Annual Conf. on Ocean Thermal Energy Conversion, New Orleans, La., March 1977.

4. Rothfus, R.R., and C.P. Neuman, The OTEC Program at Carnegie-Mellon University--Heat Transfer Research and Power Cycle Transient Modeling, Proc. Fourth Annual Conf. on Ocean Thermal Energy Conversion, New Orleans, La., March 1977.

5. Sather, N.F., et al., Performance Tests of 1 MWt OTEC Heat Exchangers, Proc. Fifth Ocean Thermal Energy Conversion Conf., Miami Beach, Fla., Vol. 3, Feb. 1978.

6. Lewis, L.G., and N.F. Sather, OTEC Performance Tests of the Union Carbide Flooded-Bundle Evaporator, Argonne National Laboratory Report ANL/OTEC-PS-1, Dec. 1978.

7. Jacobs, M., Union Carbide Corporation, personal communication, Dec. 1978.

8. Rothfus, R.R., Carnegie-Mellon University, personal communication, Dec. 1978.

9. Yung, D., et al., Vapor/Liquid Interaction and Entrainment in Shell-and-Tube Evaporators, ASME Paper No. 78-WA/HT-35, 1978.

DISCUSSION

J. Michel, ORNL: Upon what area is the overall coefficient based for the Trane model? Is it finned on the ammonia side, and what is the area ratio?

A. Thomas: The coefficient is based on the flat area that is in contact with the water. The ammonia side is finned, and the area ratio is 3.5.

P. Pribis, GE: In presenting your data, why didn't you use the NTU method to compare the different heat exchangers from a performance standpoint? How confident are you about the validity of using the log-mean temperature difference (LMTD) as the true mean temperature difference in the calculation of the U value?

A. Thomas: There are other factors, in addition to heat transfer, that enter into the determination of heat exchanger cost-effectiveness in an OTEC system, and hence a comparison based on NTU is incomplete. As for the second part of your question, we recognize that the LMTD is not necessarily the ideal entity to use, especially in the case of two-phase heat exchangers such as the APL and Trane concepts. The APL people have internal instrumentation in their unit to measure local temperatures and pressures. The difference in the U value computed by this method and by our LMTD method was only 3 to 5%. Thus, we use the LMTD method because we believe that it is useful for system comparisons.

Question: What sort of fluctuations do you see, and how do you know that your system is equilibrated?

A. Thomas: We see fluctuations in the readings of about 1 to 1.5% of the mean, which we believe are caused by system transients; in fact, in the later runs the readings are averaged over periods of time that would eliminate the fine structure. Experience has shown that in one to two hours the temperature readings reach steady state.

Question: What fraction of the tube bundle is submerged in the pool boiler? Is it subject to forced-convection heat transfer?

A. Thomas: All the heat exchanger tubes are below the liquid ammonia level, and nucleate boiling dominates the heat transfer.

Question: In the pool boiler, is there any indication of less boiling (i.e., less heat transfer) at the bottom of the heat exchanger than at the top?

A. Thomas: No direct measurements were made; however, with the Hi-Flux surface we expect subcooled nucleate boiling on the lower tubes.

Question: Do you know what the ammonia-side construction of the Trane heat exchanger looks like?

A. Thomas: The ammonia side is finned, but the details are proprietary information of the Trane Company.

Bakstaad, TRW: In the Trane unit, what are the Δp's on the water and ammonia side?

A. Thomas: At nominal flow conditions the water-side Δp was about 3 psi, which is not that far out of line from any of the others. For the ammonia side it was 1.8 psi. Both of these numbers were predicted by Trane.

CORE UNIT TESTING OF THE JHU/APL SHELL-LESS FOLDED TUBE HEAT EXCHANGER*

James L. Keirsey**, John A. Funk***
Peter P. Pandolfini+ and Richard T. Cusick+

The Johns Hopkins University
Applied Physics Laboratory
Johns Hopkins Road
Laurel, Maryland 20810

Abstract

A heat exchanger that meets the minimum overall objective for Ocean Thermal Energy Conversion (OTEC) plant-ships may not necessarily have the highest heat transfer performance but should have low fabrication cost, cleanability, modularity and maintainability. The shell-less, folded-tube heat exchanger being investigated by APL/JHU appears to offer advantages in these areas compared with some alternative designs. A full-scale core unit is being tested at the Argonne National Laboratory. The objectives of this core test are as follows: (a) to obtain experimental data on this novel design and (b) to validate or to provide a basis for modification of the APL computer code that will be used to estimate performance of a full-scale operational unit. The core test unit is described and is compared with a full-scale, 2.5-MW_e, operational heat exchanger module. Results of evaporator core tests which began in April 1979 are compared with performance predictions and with results of separate internal and external heat transfer tests carried out in 1976-77.

Introduction

The main objective of the OTEC program is to produce useable energy at a minimum overall cost. A heat exchanger design that meets this objective may not necessarily have the highest overall heat transfer coefficient or the lowest overall working fluid pressure drops. Although these factors are important, low fabrication cost, modularity, cleanability and maintainability are equally important. The design conceived by APL/JHU appears to offer advantages in these areas. This shell-less, folded-tube heat exchanger concept is illustrated in Fig. 1 as an evaporator. Ammonia is used as the working fluid inside 3-in. O.D., Alclad 3004 aluminum tubes with warm sea water flowing downward over the tube(s) by gravity from a head pond at the top. The subcooled liquid ammonia is fed to the bottom of each tube via a manifold and short riser. Liquid heat-up removing most of the subcooling occurs in the first pass and evaporation begins near the end of the first or in the second pass. Two-phase ammonia flows upward through the folded tube with each pass contributing to additional vaporization until the vapor quality leaving the last pass is near 70%. The liquid and vapor are partly separated in the exit manifold, and the rest of the liquid is taken out by a demister. This liquid is mixed with that coming from the condenser and is returned to the evaporator inlet.

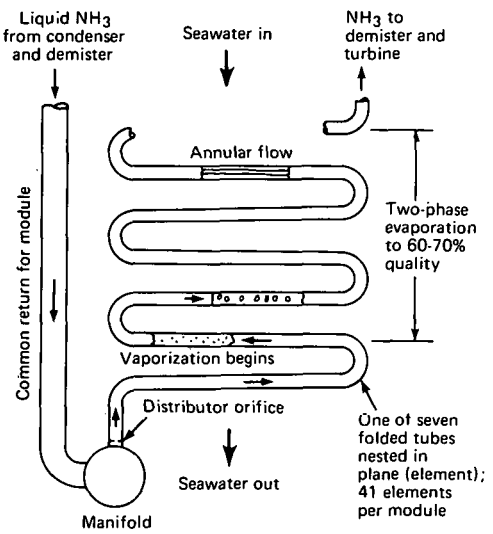

Fig. 1 The APL concept for multipass, two-phase-flow heat exchangers with the ammonia inside the tubes.

The condenser is conceptually similar to the evaporator except that ammonia vapor enters the top of each tube, condenses as it flows down the tube, and enters a sump at the bottom.

In a pilot or commercial plantship, each heat exchanger will consist of an array of these 3-in.-O.D., horizontal, folded tubes. Each module will be housed in an open rectangular compartment within the concrete hull structure so that no separate heat exchanger shell is required. The water will be pumped to a head pond above the heat exchanger, and will flow out the bottom of the vessel (see Ref. 1 for a more complete description of the plantship and heat exchanger arrangement). This heat exchanger design approach has the following advantages:

(a) Use of relatively large tube diameter reduces the number of tube joints, thus reducing fabrication and assembly costs.

(b) No heat exchanger shells *per se* are required.

(c) There is strong potential for econimical, *in situ* cleaning of the heat exchangers without interruption of operations.

* Sponsored by the Department of Energy, Division of Solar Technology
** Asst. Group Supervisor, Propulsion, Aeronautics Division
*** Engineer, Propulsion Group, Aeronautics Division
+ Engineer, Propulsion Group, Aeronautics Division
∓ Instrumentation Section Supervisor, Propulsion Group, Aeronautics Division

(d) The high degree of modularity will permit regularly scheduled inspection and maintenance, one module at a time, without a significant reduction in total power output.

These advantages of a simple design could outweigh the advantages of an initial higher efficiency and the somewhat smaller size of a more complex heat exchanger.

Although all prior performance analyses [2] and tests of internal[3,4] and external[5] heat transfer coefficients on sections of the heat exchanger have been encouraging, tests of a full-scale core unit were clearly needed to demonstrate overall performance and evaluate possible internal flow instability problems and ways to avoid them.

The design concept for a 2.5 MW_e (net) heat exchanger module is depicted in Fig. 2 in the condenser configuration. Ammonia vapor is fed into the

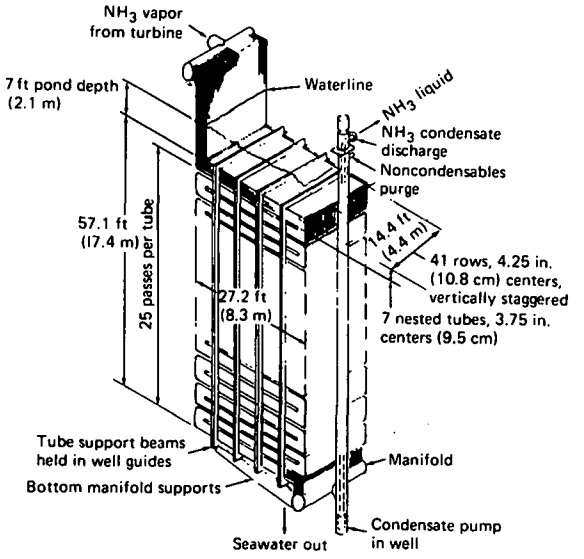

Fig. 2 Three-quarter view of 2.5 MW_e (net) condenser module having 1.5 x 10^5 ft^2 (1.4 x 10^4 m^2) (nominal) surface area.

top manifold which feeds each tube. The unit has seven tubes "nested" in a single vertical plane, with each tube having 25 horizontal passes. The tubes have a 3-in. O.D., and .060-.075-in. wall, and are made of Alclad 3004 aluminum. The nesting feature provides the appropriate tube surface area for all the flow conditions in the desired vertical height for efficient packaging into a plant-ship. In addition, the nesting provides a 1.25-inch clearance between vertical rows for passing a cleaning head to remove biofouling as required. (Related efforts on biofouling and cleaning are presented in Refs. 6 and 7 as well as the companion paper, Ref. 8.) The module has 41 rows, vertically staggered, giving a total surface area of approximately 1.5 x 10^5 sq. ft.. The overall dimensions of the heat exchanger module are 27.2 ft x 14.4 ft x 57.1 ft, with a 7-ft-deep water head pond. Operated as an evaporator, the module would have the same overall dimensions, but liquid ammonia would be delivered to the bottom header by a single downcomer.

Results of Prior Tests

The measured performance of the model core unit is to be compared with predictions made with the performance simulation[9] with prior results of single-pass experiments measuring the ammonia performance, and with the results of external (water-side) tests made on tube bank sections. Those prior results are synopsized below.

Two-Phase Heat Transfer Tests[3]

In 1976, tests were conducted at APL/JHU using a single 20-ft pass of 3-in. O.D. x 0.156-in.-wall, aluminum smooth bore tube, through which ammonia at mass qualities up to 20% flowed. The tube was instrumented for measuring heat transfer coefficients and had a U-bend at each end to simulate internal end-flow conditions. A steam preheater was used upstream of the test section to adjust the entrance vapor quality. Heat flux densities in the range of plant operations (1000-4000 Btu/hr-ft^2) were applied to the tube with an electrical heating tape wound around the tube over its entire length and insulated to prevent losses from the test section. Although this arrangement does not simulate the circumferential variation in heat input that will be experienced with warm water through a heat exchanger, it does permit reasonably good determination of the internal two-phase heat transfer coefficients. The results of the experiments confirmed the applicability of the existing Chaddock-Brunemann correlations[10] predicting two-phase ammonia heat transfer coefficients at the conditions tested.

Onset-of-Vapor-Generation Tests[4]

In 1977 tests were conducted at APL/JHU using the same ammonia flow loop described above, but with the addition of a chiller. Tests were run with liquid ammonia at various levels of subcooling, mass flow rates, and heat flux levels to determine the conditions for onset of significant vapor generation in the 3-in. smooth bore aluminum tube. Results of the tests confirmed the applicability of existing correlations[11] for predicting the occurrence of onset of significant vapor generation (boiling), although the occurrence of initial vapor generation may differ from the classical "onset of nucleate boiling" because of circumferential convection currents which carry warm liquid to the top of the tube, plus the increased turbulence introduced by the U-bends.

External (Water-side) Heat Transfer and Pressure Drop Tests[5]

In 1977 tests were also conducted using tube bank sections consisting of five vertical rows of 4-in.-diameter tubes, with ten tubes in each vertical row, mounted in a water box. Water was pumped into a head tank and flowed vertically downward by gravity. Four instrumented tubes were located in the center row at different positions vertically within the bank. Each instrumented tube contained a heating element that was used to determine water-side heat transfer coefficient, h_w, in each of four quadrants oriented circumferentially around the tube. This same apparatus was later used at Ke-Ahole Point, Hawaii for fouling measurement and cleaning tests[6]. Results of tests both at APL and Hawaii indicate that the circumferential distribution of the water-side heat transfer coefficient h_w was essentially

uniform for tubes interior to the bank, and averaged values were higher (20-100%) than predicted from existing correlations[10]. In addition, pressure drops measured across the tube banks were consistent with existing correlations developed for larger longitudinal pitches. It is therefore believed that the APL computer code using a correlation by Zukauskas for h_w is conservative; measured values of h_w may be as much as 100% higher, which would increase the overall performance of the core unit by approximately 33%.

The external flow model was also used to measure effects of biofouling on the heat transfer coefficients and to evaluate cleaning requirements and techniques needed to control the fouling as described in Refs. 6 and 7.

Core Test Unit Description

A simplified drawing of the core test unit is presented in Fig. 3. The unit is full scale

The three active tubes (with ammonia flowing inside) are contained within an inner water box, through which water flows vertically downward. A row of dummy (inactive) half-tubes is mounted on the inner wall of this inner water box to provide the proper water-flow geometry. The outer water box supports the hydrostatic head. This arrangement allows the maintenance of suitable fabrication tolerances for the walls of the inner box. Each tube has 43 passes of 14.3-ft length.

For testing the unit as an evaporator, subcooled liquid ammonia is fed into the three tubes at the bottom, and a two-phase mixture issues from the top. Warm water (80-82°F) is pumped into the head pond which has a free surface and is exhausted through a 12-in. pipe at the bottom.

The difference in number of passes and tube length per pass between the 2.5-MW_e operational module and the core test unit is due to several factors:

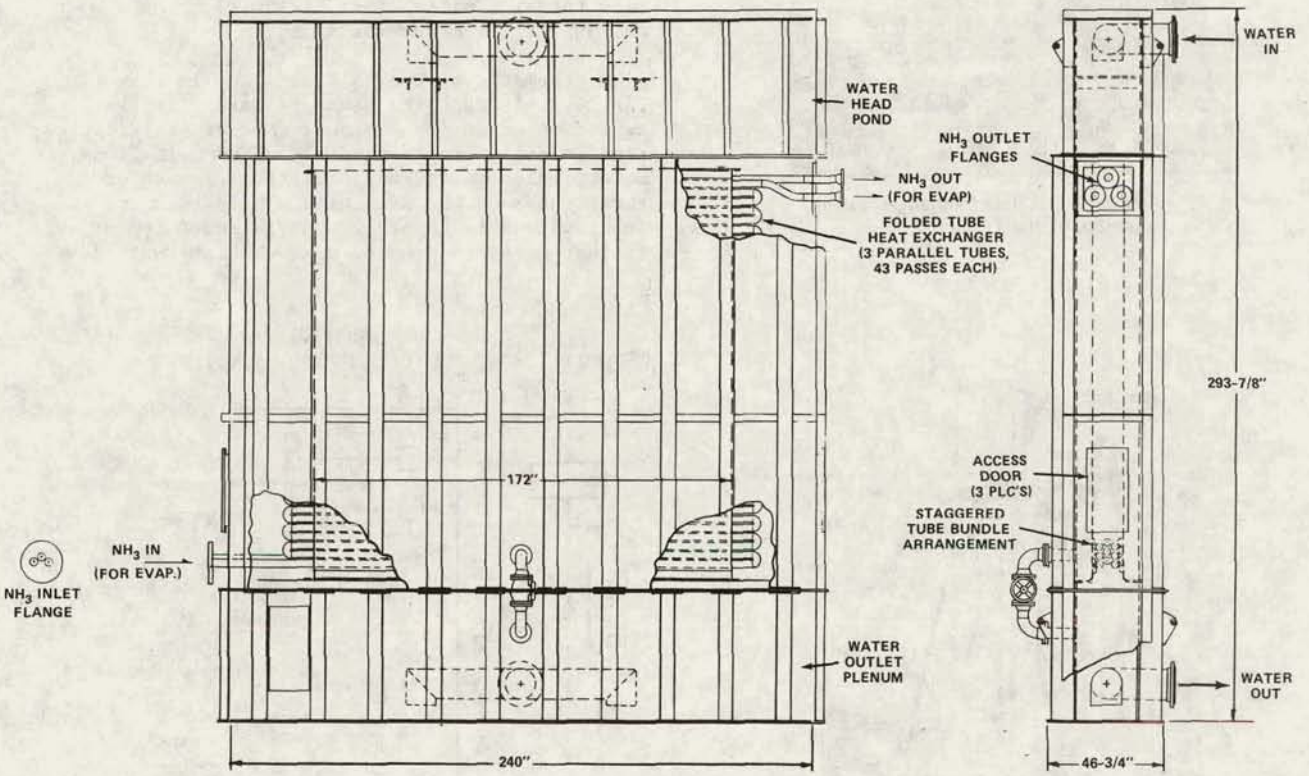

Fig. 3 OTEC core test heat exchanger APL/JHU.

with respect to the diameter and length of each folded tube and simulates a complete full-scale heat exchanger module as nearly as possible within the sizing and testing constraints imposed by the Argonne National Laboratory (ANL) test facility. The ammonia and water flow rates, velocities and temperatures are properly simulated. The core unit has about 1/96th of the surface area of the 2.5-MW_e (net) module, as it has 3 tubes flowing in parallel compared with 287 parallel flowing tubes for the operational module.

(a) the nominal water flow rate (3200 gpm) available at ANL required a smaller clear space between tubes in order to simulate the full scale water velocity of 2.5 fps,

(b) the related requirement to space the tubes closer together in the core test unit than for the operational module due to the absence of "nesting" in a vertical plane in the core test unit (the minimum gap turned out to be 0.59 in. due to assembly of the U-bends), and

(c) the desire to have approximately the same total surface area per tube in the core test unit and the operational modular unit.

The assembled core test unit is shown in Fig. 4.

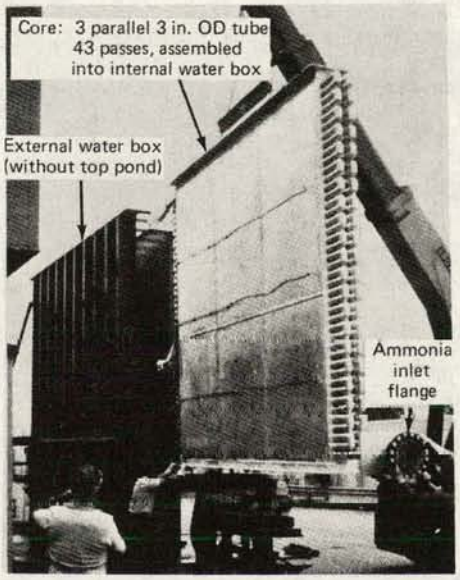

Fig. 4a APL core test heat exchanger during assembly at the Trane Co.

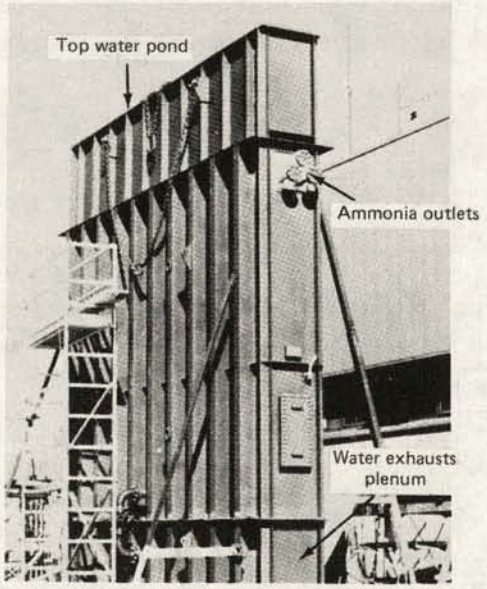

Fig. 4b APL core test unit assembled.

The core test unit is being tested with and without a swirl element (Fig. 5) in the first pass of each tube. The purpose of the swirl elements is to enhance liquid flow heat transfer coefficients in order to remove most of the liquid sub-

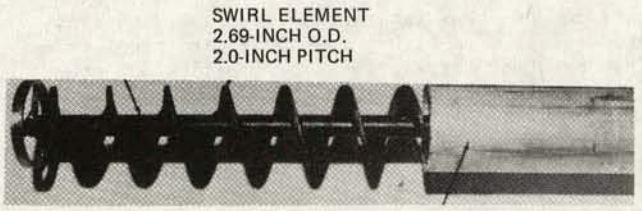

PURPOSE: TO ENSURE EARLY ONSET OF BOILING BY HEAT TRANSFER ENHANCEMENT

Fig. 5 First pass swirl element.

cooling so that vapor generation could occur within the first pass or near the beginning of the second pass. The increased velocity and turbulence imparted to the liquid by the swirl element is expected to provide a liquid temperature rise between 8° and 11°F in a 14-ft tube compared to 4-4.5°F rise without the swirler at nominal flow rates. Initial test runs will be made with the swirler elements installed.

A schematic of the ANL test loop is shown in Fig. 6. Although the setup is basically the same as for other core tests performed at ANL[13], attention is called to the individual ammonia flowmeter, inlet valve, and demister for each of the three tubes of the APL unit. The purpose of the inlet valves is to permit the introduction of sufficient pressure drop to make the internal flow

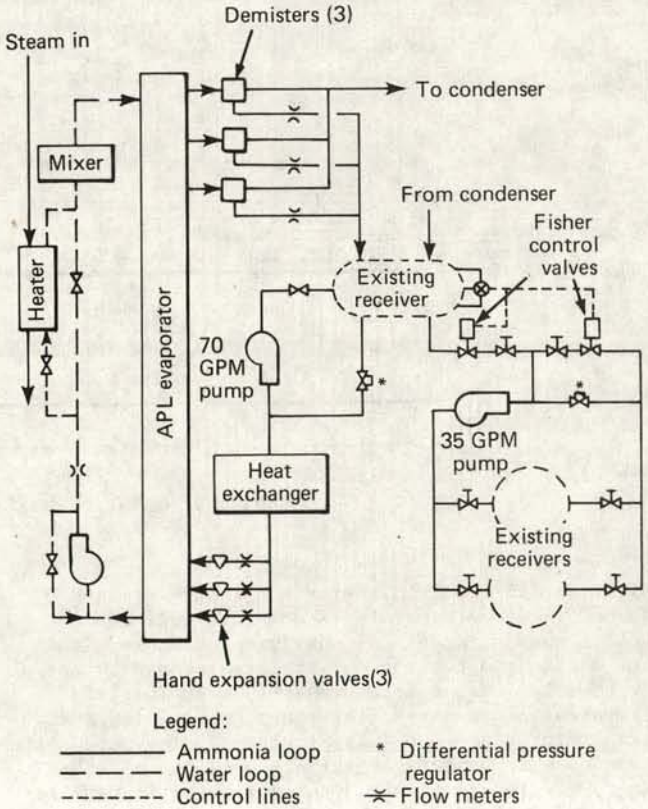

Fig. 6 Test loop schematic.

divide evenly between the tubes, and to isolate and dampen any fluctuations and variations in flow conditions (due perhaps to possible density wave instabilities), if present in any tube. The small heat exchanger shown just upstream of the flowmeters is used to vary the degree of subcooling of the ammonia to the core unit. The evaporator is also to be tested with the three tubes manifolded into a common demister.

Core Test Results

Fifty-six test runs were made on the APL core test unit during May and June 1979. The primary test variables are shown in Table I. The first pass swirlers were included in runs 1-38, then removed for runs 39-56.

Table I

Core test conditions (evaporator)

	NOMINAL	VARIATION
HEAT DUTY	3.2×10^6 Btu/HR.	$(2.8 \text{ TO } 4.6) \times 10^6$
WATER FLOW RATE	3200 GAL/MIN.	1500 TO 4700
WATER INLET TEMP.	80° F	78° TO 82°
AMMONIA FLOW RATE	1.0 LBM/SEC PER TUBE	0.7 TO 2.0
AMMONIA INLET TEMP.	72°F	55 TO 72°
AMMONIA INLET VALVE PRESSURE DROP	2 PSID	0 TO 4
DEMISTER(S)	INDIVIDUAL FOR EACH TUBE	SINGLE COMMON
SWIRL ELEMENT(S)	INSTALLED IN FIRST PASS OF EACH TUBE	REMOVED

Stability of the Unit After Start-up

The system, which included not only the evaporator core unit but also a condenser, pumps, steam heater and connecting pipes, would typically reach a stable operating condition in about 2 hours after start-up. The unit operated very stably at all conditions tested. Typical of the operation was a condition where data were recorded at approximately 30-minute intervals over a 6-hour running period at a constant heat duty of 3.56×10^6 Btu/hr; during this period the core unit exhibited stable operating characteristics with the water inlet and outlet temperatures varying by $\pm$ 0.2°F while the water flow rate varied only $\pm$ 0.2%. Inlet ammonia flowmeters indicated that the flow divided equally among the three tubes to $\pm$ 2% and the flow rate had a maximum variation of $\pm$ 5%. It was unnecessary to introduce any Δp with the inlet valves to stabilize the unit.

In making the 56 test runs, changes were routinely made in flow rate settings of the ammonia and/or the water and loop stabilization times ranged from 1 to 2 hours depending upon the changes made. No difficulties whatever were encountered in stabilizing the flow. The loop was judged to be stable when water inlet temperature changes were about $\pm$ 0.1°F or less. Overall, the unit ran quietly and was free of significant vibration.

Performance at Nominal Conditions

The nominal condition for the core unit was specified prior to the test as being a condition that simulated the water inlet temperature and velocity, the ammonia inlet temperature and velocity, and the heat fluxes of an "optimized" operational unit. The term "optimized" refers to a condition of maximum net power output of the power system cycle when the estimated performance of all system components (evaporator, pumps, turbines and ship propulsion) is accounted for including deductions for their associated parasitic powers. The optimized system condition was estimated by an analysis[14] made several years ago based on available heat transfer correlations and pressure losses, some of which have since been proved somewhat conservative by experiments discussed earlier (Refs. 3-5). The core unit testing itself, in some respects, has indicated the conservatism of the original analysis. This analysis yielded an optimized system condition with a heat exchanger having an ammonia flow rate of 1.0 lbm/sec/tube and a water velocity of 2.5 ft/sec in the minimum gaps between tubes with the 7-nested arrangement. For the core test unit, therefore, the nominal test condition was defined as corresponding to values of 3200 gpm water flow rate, 1 lbm/sec/tube ammonia flow rate, and a heat duty of 3.2×10^6 Btu/hr.

Since the overall coefficient of heat transfer, U, is used as one parameter in describing heat exchanger performance, and U may be computed in several ways, the technique used herein for calculating U is defined as follows:

$$U = \frac{Q_{net}}{A'_{inner}\ \Delta T_m}, \quad \text{Btu/hr-ft}^2\text{-}^\circ\text{F}$$

where Q_{net} is the total heat duty (Q_w) minus the heat duty needed to raise the ammonia from input temperature to the saturation temperature corresponding to the measured pressure at exit of the first pass:

$$Q_{net} = Q_w - C_{pL} \sum_1^3 \dot{w}_m \, (t_{sat\ in} - t_{in})$$

where Q_w is the total heat duty (Btu/hr)

C_{pL} is the specific heat of the liquid ammonia. A function of the average ammonia temperature in the first pass.

$\sum_1^3 \dot{w}_m$ is the sum of the ammonia liquid flow entering the first pass of each of the three tubes.

A'_{inner} is A_{inner} (described above) minus the area of the first pass of each tube. Equal to 1263.6 ft^2.

ΔT_m is a log mean temperature difference (°F) defined as follows

$$\Delta T_m = \frac{(T_{in} - t_{out}) - (T_{out} - t_{sat\ in})}{\ell n \left[\dfrac{(T_{in} - t_{out})}{(T_{out} - t_{sat_{in}})} \right]}$$

where T_{in} is the entrance water temperature. Used ANL entrance thermometer reading.

T_{out} is the exit water temperature. Used ANL exit thermometer reading.

$t_{sat\ in}$ is the saturation temperature (°F) corresponding to the measured pressure at exit of the first pass.

t_{out} is the exit ammonia temperature (°F).

Table II indicates the measured performance of the unit at the nominal condition defined above and compares it with the performance predicted by the APL analytical simulation. It is noted that the

Table II

Summary of evaporator performance at nominal conditions

WATER FLOW RATE – 3200 gpm
AMMONIA FLOW RATE – 1.0 lbm/sec/tube
HEAT DUTY – 3.2×10^6 Btu/hr
QUALITY – 58%

	PREDICTED	MEASURED, WITH SWIRLERS (avg 5 runs)	MEASURED WITHOUT SWIRLERS (avg 3 runs)
OVERALL U, (Btu/hr-ft^2-°F)	360	395	400
AMMONIA-SIDE Δp, (psi)	5.6	5.0	4.9
WATER-SIDE Δp, (psi)	0.90	0.95	0.95

NOTE: AVERAGE AMMONIA INLET SUBCOOLING FOR 5 RUNS WITH SWIRLERS = 9.2°F, AND FOR 3 RUNS WITHOUT SWIRLERS = 6.7°F

measured performance is insensitive to the presence or absence of the swirlers in the first passes and the pressure drops with the swirlers in the first passes were very small, in accordance with predictions. The overall U measured is 11% higher than predicted, the ammonia pressure drop from the entrance to exit (1st pass entrance to 43rd exit) is 10% lower than predicted, and the water pressure drop across the tube bend is 5% higher than predicted. Modifications to the analytical simulation which reflect these measurements of U and the pressure drops yield an improved performance of 13% in the net power output of the system when the system is constrained to the same geometry, entrance ammonia temperature flow rates, water temperatures and pond heights. It should be noted here then in light of the improved performance of the evaporator (and possibly correspondingly improved performance of a condenser with similar geometry), true optimum operating conditions may be different from the nominal conditions specified above.

Core Test Performance Over a Range of Operating Conditions

During the course of evaporator testing, a range of operating conditions for the water flow, ammonia flow, entrance subcooling, and heat duties were covered as outlined in Table I.

Overall U. The effect of water flow rate on the overall U measured is shown in Fig. 7 at two combination conditions of ammonia flow rate and heat duty and both with and without the swirler in the first passes. The swirlers are seen to have only a small effect on the total unit performance. The strong effect of water velocity is apparent from these data. At 3200 gpm the water velocity in the minimum gap between the tubes is 2.5 ft/sec and at 5000 gpm this velocity is 3.9 ft/sec. Entrance subcooling, which was varied between 5°F and 16°F, had no observable effect on overall U.

Figure 8 illustrates the effect of ammonia flow rate on U for two different water flow rates. In the lower group of data, the heat duty has only a small (secondary) effect on U within the range of testing, but the overall U is a strong function of the ammonia flow.

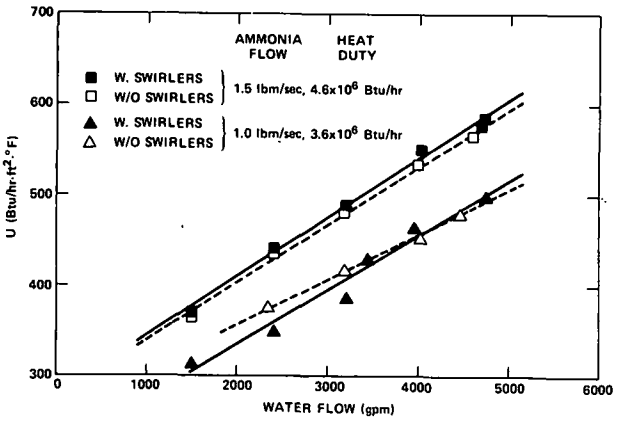

Fig. 7 Effect of water flow on U.

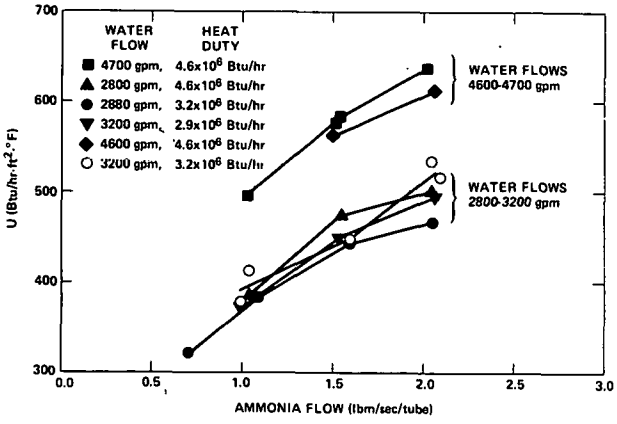

Fig. 8 Effect of ammonia flow rate on U.

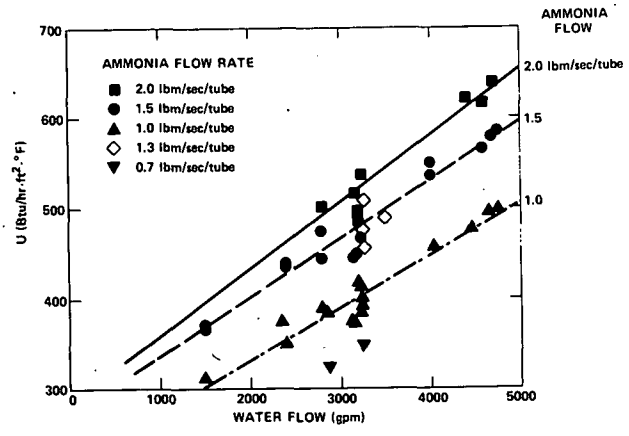

Fig. 9 Summary of all U measurements with data for all heat duties and swirler configurations, parametric with respect to ammonia flow.

A summary for all data taken at ANL showing U vs. water flow rate is shown in Figure 9 with

linear regression fits of the data at different ammonia flow rates. The highest U observed was 637 Btu/hr-ft^2-°F measured at the largest water flow rate, the largest ammonia flow rate, and the highest heat duty that could be achieved at the testing facility. From the trend of the data it appears that the U would be higher for still larger flow rate.

Ammonia-side Pressure Drop. Figure 10 is a plot of ammonia-side pressure drop across the core

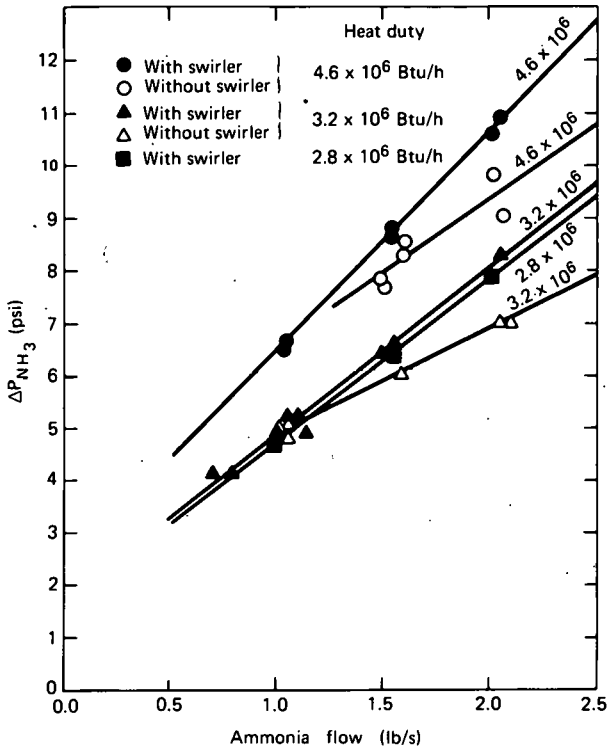

Fig. 10 Effect of ammonia flow rate on pressure drops.

unit as a function of ammonia flow rate, at various heat duty values, both with and without the swirlers. The analytical simulation adjustment is made to be consistent with these values by altering the U-bend losses and friction losses. It now appears that the estimates of these losses can be resolved with the experiments by setting the friction and bend loss coefficients in the two-phase multiplier term about 30% lower than the values used in the original simulation.[14] Further discussion of this adjustment in the analytical simulation is included later in the paper.

Water Side Pressure Drop. The pressure drop across a tube bank is a function of the transverse and lateral pitch ratios of the bank, the fluid, and the maximum velocity in the minimum area passages of the bank. It is characterized by an Euler number as defined on Fig. 11. For a staggered tube bank, the transverse pitch is defined as the distance (normal to flow) between similar rows (6.0" for the core unit) and the lateral pitch is defined as one-half the distance between tubes in the same tube row along the direction of the flow (1.875 for the core unit). The pitch ratios with respect to tube diameter for the core unit are 2.0 x 0.625.

Data from Ref. 12 suggest that the Euler number is determined mainly by the transverse pitch ratio and the flow Reynolds number; the Euler number decreases with an increase in this pitch ratio and the Reynolds number in the range of interest (33,000-100,000). This reference shows the Euler number went from 0.15 to 0.11 for Reynolds numbers 30,000-70,000 for a bank with a transverse pitch ratio of 2.2. Data from the present tests (Fig. 11) show that the Euler number varied from about 0.15 to 0.13 over the range of test conditions which agrees with the trends of Ref. 12 with respect to Reynolds number and transverse pitch ratio. It should be noted that the full scale pilot plant design uses a 2.83 x 0.63 staggered tube configuration which should have a lower Euler number (see Refs. 5 and 12) than that measured in these experiments.

$$Eu = \frac{\Delta P_W \, g_c \times 144}{\rho V_W^{\,2} \, (2 N_T - 1)}$$

g_c = 32.174 lbm-ft/lbf-sec^2
ρ = 62.4 lbm/ft^3
N_T = no. of tubes (43)
V_W = water velocity in minimum area, ft/sec

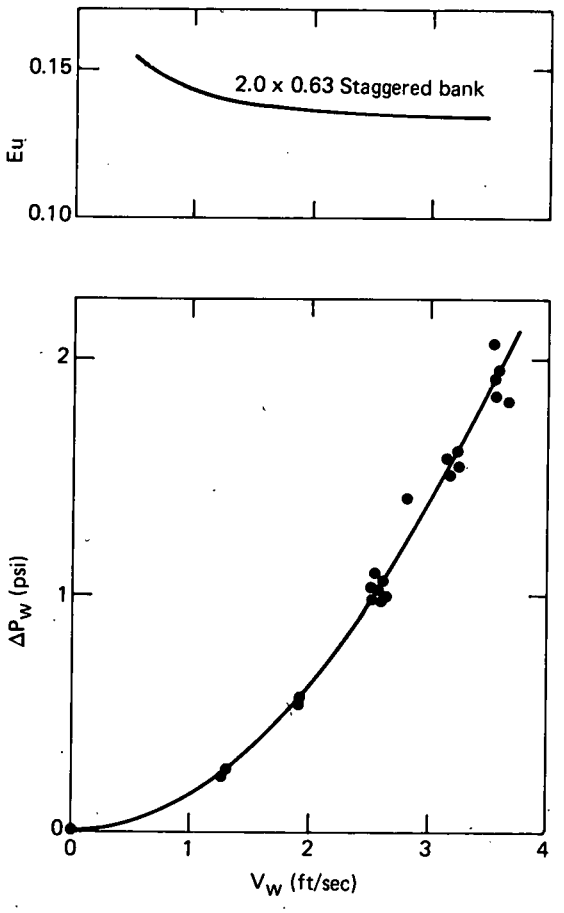

Fig. 11 Water pressure drop (ΔP_W) vs. water velocity in minimum area (V_W) and Euler number vs. V_W for Core Test Unit (2.0 x 0.63 staggered tube bank configuration).

Comparisons of Predictions of the Unmodified Analytical Simulation with Experimental Observations

Comparison of U. From the correlation of the data it was found that the equation

$$U^*_{meas} = 0.0243\left(\sqrt{Re_w\ Re_{NH_3}}\right)^{0.885}$$

represented all the data within ± 10%, where U^* is defined on Figure 12. Figure 12 is a curve showing the data correlation compared with the predictions of the analytical simulations:

$$U^*_{pred} = 2.17\left(\sqrt{Re_w\ Re_{NH_3}}\right)^{0.469}$$

$$U = \left[1/h_{NH_3} + \frac{d_i \ln d_o/d_i}{2k} + d_i/d_o\, h_w\right]^{-1}$$

$$U^* = \left[1/U - \frac{d_i \ln d_o/d_i}{2k}\right]^{-1} \qquad d_i = 0.224'$$

$$d_o = 0.250'$$

$$\frac{d_i \ln d_o/d_i}{2k} = 0.0001272 \qquad k = 96.67\ \text{Btu/hr} \cdot \text{ft} \cdot °\text{F}$$

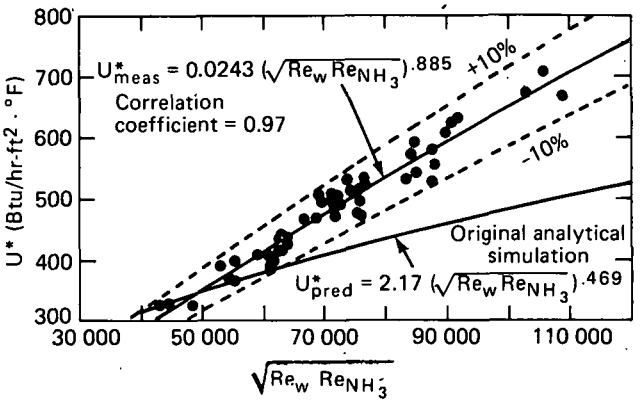

Fig. 12 Correlation of data.

By examining these two curves it is clear that the simulation underpredicts the overall U by an increasing amount as the parameter $Re_w\ Re_{NH_3}$ increases. The basis for both correlations was to fit U^* as a function of $Re_w\ Re_{NH_3}$ as follows:

$$\frac{1}{U^*} = \left[\frac{1}{U} - \frac{d_1\ \ell n\ d_o/d_i}{2K}\right] = \frac{1}{h_{NH_3}} + \frac{d_i}{d_o h_w}$$

$$U^* = \frac{h_{NH_3}\ h_w}{h_w + (d_o/d_i)\ h_{NH_3}} = f\left[\sqrt{Re_w\ Re_{NH_3}}\right]$$

where h_w and h_{NH_3} are functions of Re_w and Re_{NH_3}, respectively. If a modification to both the water and ammonia side film coefficients is made through multiplication by factors C_W and C_{NH_3},

$$\frac{1}{U^*} = \frac{1}{C_{NH_3} h_{NH_3}} + \frac{d_i}{C_W d_o h_w}$$

a modified correlation will become

$$U^*_{meas} = f\left(\sqrt{C_W\ C_{NH_3}}\ \sqrt{Re_w\ Re_{NH_3}}\right)$$

From this

$$\frac{U^*_{meas}}{U^*_{pred}} \sim \sqrt{C_W\ C_{NH_3}} = 0.01122\ \sqrt{Re_w Re_{NH_3}}^{0.417}$$

This factor, $C_W\ C_{NH_3}$, can be used to modify the analytic simulation to produce the experimental results.

Comparison of Δp_{NH_3}. The frictional and bend components of the two-phase pressure drop are computed by the simulation using the Chisolm method (see Ref. 15) where

$$\Delta p_{NH_3} \sim \phi_f^2\ (1 - x)^{1.75}$$

and

$$\phi_f^2 = 1 + \frac{C}{X_{tt}} + \frac{1}{X^2_{tt}} .$$

In the simulation results, the value of C for both the straight runs and bends was set equal to 10.0. In all instances, this value for C resulted in an overprediction of the two-phase pressure drop. Examining the results with and without swirlers suggests that C = 7.1 ± 0.9 for the former and C = 5.4 ± 1.0 for the latter. A general value of C = 7.0 seems to be a good choice that will conservatively predict the test results but still be an improvement over the original value.

Effect of Test Results on Pilot Plant Design

The performance of the core test unit as an evaporator and the subsequent modification of the analytical simulation leads to a re-examination of the expected performance of the proposed pilot plant. This plant was designed to produce 10 MW net with 4 heat exchanger modules (4 each of evaporators and condensers). Each heat exchanger consists of 41 rows of seven-nested 3-in. O.D. types with a pass length of 23.3 ft and a total height of 65 ft. The geometry of the ship is considered a fixed constraint for this comparison. For the baseline case the modified simulation estimates an increase of about 13% in the net power output; as the ammonia flow is increased to 1.5 and 2 lbm/sec/tube this gain in net power increases to about 18 and 22%, respectively.

Conclusions and Recommendations

The results of the core tests of the folded tube heat exchanger concept have been very encouraging. From these tests it is concluded:

(a) The unit, which had 3 parallel tubes with ammonia flow internally, operated with remarkable stability. The flow divided between the 3 tubes to within a few percent and variations in fluid conditions over a several-hour running period were shown to be negligible.

(b) The unit could be started under conditions similar to an ocean environment where the maximum water temperature available does not exceed about 83°F.

(c) The measured overall U exceeded the values predicted by the APL analytical simulation by about 11% at nominal conditions, and an increasing amount at higher flow rates.

(d) The combined friction, bend, acceleration, and gravity two-phase pressure drop was less than those predicted by the simulation.

(e) The water-side pressure drop was in line with predictions and previous measurements at nominal flow rates.

(f) For the baseline case, the modified simulation estimates an increase of about 13% in the net power output; as the ammonia flow is increased to 1.5 and 2 lbm/sec/tube this gain in net power increases to about 18 and 22%, respectively

(g) The effect of the swirlers in the first passes did not significantly affect the overall operation of the unit.

Since it has been demonstrated that the folded-tube shell-less heat exchanger designed for use as part of a pilot-plant works well as an evaporator and presents a viable option for OTEC, it is recommended that:

(a) The core unit be tested as a condenser by ANL as soon as practicable so that similar performance data may be obtained for modification of APL simulation.

(b) Plans be formulated for testing a sea-borne, folded-tube heat exchanger unit.

(c) Cleaning system development and other associated systems compatible with this concept be continued.

(d) Further system optimization studies be conducted using the modified heat exchanger analysis to either confirm or re-establish an optimized working condition for the heat exchangers.

Acknowledgments

The conceptual design and performance evaluation of the operational heat exchanger module and core unit was done by APL/JHU, and the detailed design and fabrication of the unit by the Trane Co., LaCrosse, Wisc. The core tests are performed by the Argonne National Laboratory, Argonne, Ill. Acknowledgments for work on biofouling and cleaning are contained in Reference 6.

References

1. J.F. George, "System Design Considerations for a Floating OTEC Modular Experiment Platform," APL/JHU, presented at the 6th OTEC Conference, Wash., D.C., June 1979.

2. G.L. Dugger, H.L. Olsen, P.P. Pandolfini and W.H. Avery, "Experiments on and Design of Low-Cost Aluminum Heat Exchangers for OTEC Plant Ships," APL/JHU AEO-77-072, March 1977.

3. H.L. Olsen, P.P. Pandolfini and J.L. Rice, "Internal Heat Transfer Experiments in a Simulated OTEC Evaporator Tube," APL/JHU AEO-76-066, November 1976.

4. P.P. Pandolfini, J.L. Keirsey and J.L. Rice, "An Experimental Investigation of the Onset of Nucleate Boiling in Ammonia Flowing Inside a Large-Diameter Smooth Aluminum Tube," APL/JHU BBP 78-28, March 15, 1978.

5. P.P. Pandolfini and R.A. Makofski, "Circumferential Heat Transfer and Pressure Drop in Tube Arrays with a Low-Lateral-Pitch Ratio in Crossflow," APL/JHU CP-066, June 1978.

6. P.P. Pandolfini and W.H. Avery, "Measurement of the Effect of Biofouling and Cleaning on the Heat Transfer Characteristics of Large Diameter Tubes," APL/JHU BBP 79-46, final report submitted to the Office of Sea Grant, U.S. Dept. of Commerce, March 1979.

7. P.P. Pandolfini, W.H. Avery and L.R. Berger, "Effect of Biofouling and Cleaning on Heat Transfer of the Exterior of Large Diameter Tubes," 5th OTEC Conference, Miami, Fla., Feb. 20-23, 1978.

8. P.P. Pandolfini, W.H. Avery and F.K. Hill, "Experiments in Cleaning of APL/OTEC Heat Exchanger Biofouling with an Ultrasonic Device," 6th OTEC Conference, Wash., D.C., June 19-22, 1979.

9. J.A. Funk and P.P. Pandolfini, "Pre-Test Data Package for the APL Core Heat Exchanger as an Evaporator," APL/JHU BBP 79-25, February 13, 1979.

10. Pujol, L. and Stenning, A.H., "Effect of Flow Direction on the Boiling Heat Transfer Coefficient in Vertical Tubes," from Cocurrent Gas-Liquid Flow, Rhodes and Scott, Plenum Press, New York, 1969.

11. Frost, W. and Dzakowic, G.S., "An Extension of the Method for Predicting Incipient Boiling on Commercially Finished Surfaces," Paper No. 67-HT-61, presented at ASME-AIChE Heat Transfer Conference, Seattle, August 1967.

12. Afgan, N.H. and Schlünder, E.U., Heat Exchangers: Design and Theory Source Book, Chapter 4, Scripta Book Co., Washington, D.C., 1974.

13. L.G. Lewis and N.F. Sather, "OTEC Performance Tests of the Union Carbide Flooded-Bundle Evaporator," ANL/OTEC-PS-1, Argonne National Laboratory, December 1978.

14. H.L. Olsen and P.P. Pandolfini, "Analytical Study of Two-Phase-Flow Heat Exchangers for OTEC Systems," APL/JHU AEO-75-37, November 1975.

15. J.G. Collier, Convective Boiling and Condensation, McGraw-Hill Co., 1972, p. 50.

DISCUSSION

Question: How was the overall U calculated when based on the mean boiling temperature of ammonia, and what area was used in the calculation?

J. Keirsey: Dr. Pandolfini, take that question, please.

P. Pandolfini, JHU/APL: The area used to calculate the overall U's was based on the inside diameter of the tubing and the length from the end of the first (bottom) pass to the end of the last (43rd) pass. It was assumed that the sensible heat input needed to raise the temperature of the incoming subcooled ammonia to the saturation value was supplied in the first pass. Thus, this sensible heat was subtracted from the measured heat duty, and the area of the first pass was subtracted from the total area. The U's, which represent the two-phase flow, were then computed using the log mean temperature difference based the ammonia saturation temperature corresponding to the pressure measured at the end of the first pass, the ammonia temperature measured at the end of the last pass, and the water inlet and exit temperatures. The U's computed are not very sensitive to this assumption, which was further borne out that they were insensitive to both the degree of subcooling (in the range tested) and to the presence or absence of the swirlers in the first pass.

Question: Is there any indication of instability in this system?

J. Keirsey: No, no indication of any instability at all. The ammonia divided evenly among the three tubes, as shown by the numbers in the paper. There was no indication of significant density wave instabilities in the tubes. Maybe it is the U-bend losses and internal friction that stabilizes the unit.

Question: What kind of tests are you preparing for cleaning?

J. Keirsey: There is a paper by Dr. Pandolfini on that subject in this Conference. The most promising system at this time is the ultrasonic system. In the design of a commercial unit, there is space enough between the tube rows, 1½ inches, for a cleaning head to be lowered and raised.

D. Aronson, Consultant: You spoke about arriving at an optimum. Will that not be a variable depending on the relative cost of the heat exchangers with respect to the whole system?

J. Keirsey: It certainly will. Our objective is to find the minimum overall system cost. Reliable cost data for all of the OTEC system components are being sought as time and funding permit.

1 MW_e HEAT EXCHANGERS FOR OTEC - STATUS REPORT, JUNE 1979

J. E. Snyder III, M. H. Seidman and A. M. Sprouse

TRW, Inc.
Redondo Beach, California 90278

A. L. Yarden

Southwestern Engineering Company
Los Angeles, California 90054

Abstract

The 1 MWe heat exchanger for OTEC project has the objective of delivering two test article heat exchangers for evaluation on an ocean-going platform, the OTEC-1. These heat exchangers, one evaporator and one condenser, are shell-and-tube design with seawater inside titanium tubes and ammonia working fluid on the outside.

The evaporator is designed to permit evaluation of both smooth tubes and high-flux enhanced surface tubes. Flexible operation permits evaluation as a sprayed bundle or pool-boiling unit. In the sprayed bundle mode, use of removable shrouds can alter vapor velocity distribution to simulate a 4 MWe unit.

Both units contain extensive instrumentation for the purpose of evaluating biofouling and cleaning systems under operational conditions expected in large-scale OTEC plants.

Introduction

In July 1977, the U. S. Department of Energy (DOE) awarded a contract to TRW for the design, fabrication, instrumentation, and test support of two heat exchangers for Ocean Thermal Energy Conversion (OTEC). These heat exchangers consist of an evaporator (to vaporize liquid ammonia) and a condenser (to condense ammonia vapor) and have a nominal thermal duty of 40 MW (or 1 MW electrical if an overall OTEC plant efficiency of 2.5 percent is assumed).

The purpose of these 1 MWe heat exchangers is to evaluate heat transfer performance of large size units at sea under realistic OTEC operation conditions including sea state induced motions and marine biofouling and corrosion.

The heat exchangers are designed to obtain a maximum amount of heat transfer data which will be of use in the design of future and potentially larger size units. To ensure that the heat transfer and biofouling control evaluation objectives are achieved with minimum risk, conventional fabrication techniques (shell and tube construction) and proven materials (e.g., titanium tubes and carbon steel shell) are being used wherever possible.

Project Status

The heat exchangers are currently being fabricated at Southwestern Engineering Company with delivery scheduled for October, 1979. Figure 1 shows the units in late May 1979 with the evaporator on the right and the condenser shell on the left. The final designs of the evaporator and condenser have been completed and were the subject of a previous paper[1].

The 1 MWe heat exchangers are part of an overall program sponsored by the U. S. Department of Energy to deploy heat exchanger test articles on an ocean-going test platform designated as OTEC-1 in early 1980. The 1 MWe test article heat exchangers are being provided by TRW as the test article contractor (TAC), the test platform is being developed under a systems integration contract (SIC) by Global Marine Development, Inc., and the test director contractor (TDC) is the Energy Technology Engineering Center (ETEC) division of Rockwell International.

Figure 1. 1 MWe evaporator and condenser shells during fabrication, May 1979.

This paper will concentrate on the various configurations in which the heat exchangers are capable of being operated, instrumentation to be employed, a description of the test loop, test plans and expected performance.

General Description of Heat Exchangers

Both heat exchangers are of conventional shell and tube design as shown in Figures 2 and 3. Seawater flows on the inside of horizontal titanium tubes in a single pass and ammonia flows across the outside of the tubes. Titanium was selected as the tube material because of its durability in seawater service and compatibility with ammonia. The pressure vessels or shells are fabricated from SA 516 Grade 70 steel which is not subject to stress corrosion attack in anhydrous ammonia. The tubesheets for both units are steel, explosively clad with a 3/8" nominal thickness of titanium on the seawater side. The tubes are rolled into grooves in the steel portion of the tubesheet and welded to the titanium cladding as an added protection against leakage.

Evaporator

In the evaporator liquid ammonia is forced to boil or evaporate by contact with the outside walls of the heat transfer tubes heated by warm seawater. The basic evaporator is shown in Figure 2. It has been designed to operate primarily as a sprayed bundle unit but can also be operated in a flooded bundle (pool boiling) mode as discussed in a following section.

The tube bundle is arranged so that the cross section is square in order to provide data which is representative of a section of a larger bundle and permit better control over experimental variables.

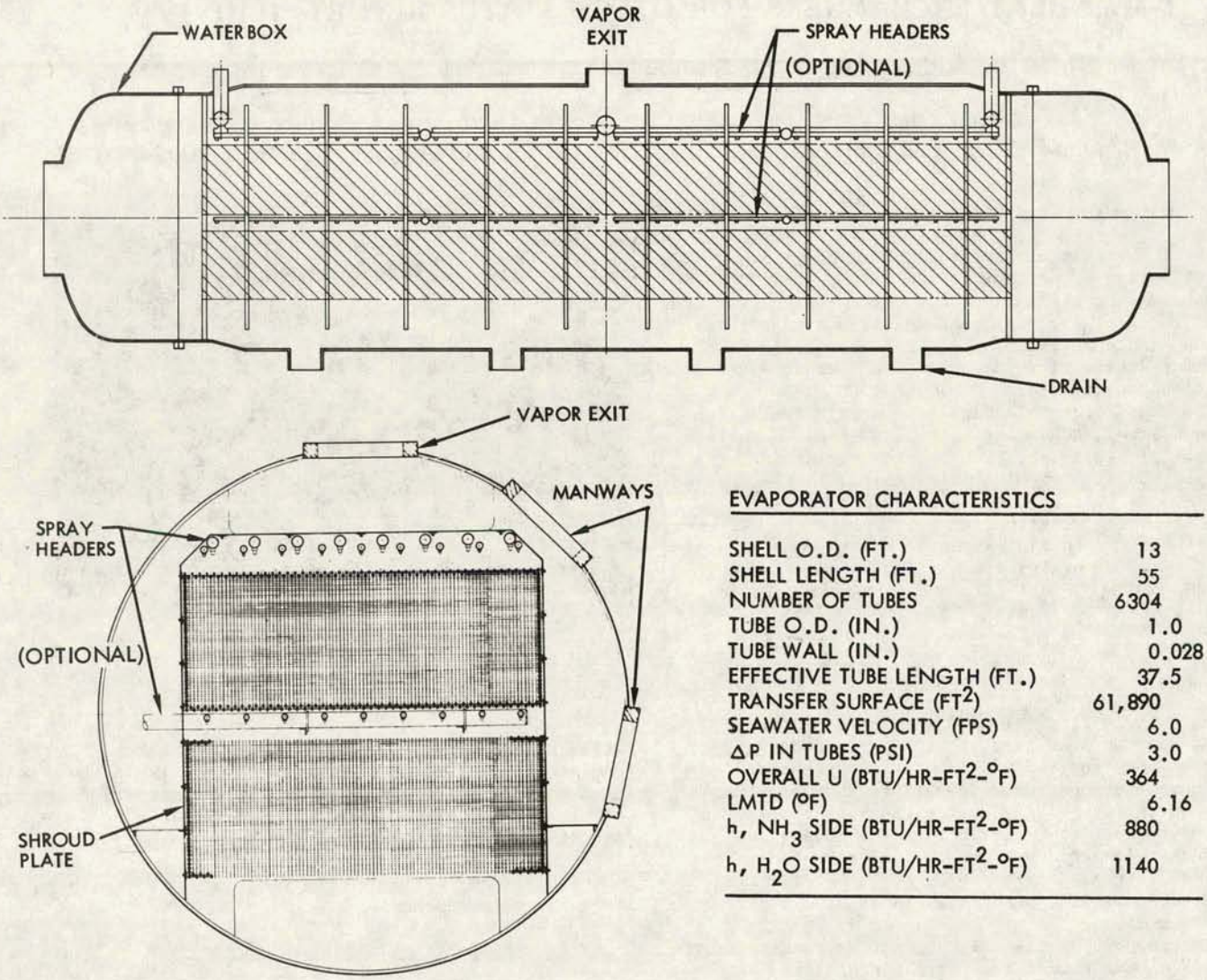

EVAPORATOR CHARACTERISTICS

SHELL O.D. (FT.)	13
SHELL LENGTH (FT.)	55
NUMBER OF TUBES	6304
TUBE O.D. (IN.)	1.0
TUBE WALL (IN.)	0.028
EFFECTIVE TUBE LENGTH (FT.)	37.5
TRANSFER SURFACE (FT^2)	61,890
SEAWATER VELOCITY (FPS)	6.0
ΔP IN TUBES (PSI)	3.0
OVERALL U ($BTU/HR-FT^2-^oF$)	364
LMTD (^oF)	6.16
h, NH_3 SIDE ($BTU/HR-FT^2-^oF$)	880
h, H_2O SIDE ($BTU/HR-FT^2-^oF$)	1140

Figure 2. 1 MWe evaporator design and characteristics.

Liquid ammonia is fed to the tubes from two separate feed planes as can be seen in Figure 4. The liquid ammonia is distributed through spray nozzles projecting from a network of headers. Uniformity of spray pattern among nozzles is assured by providing the controlling pressure drop through each nozzle rather than inside the header pipes.

The evaporator bundle is physically divided into two equal tube banks by the internal spray feed plane. All the tubes in the lower half are enhanced with the Union Carbide/Linde "High Flux" surface coating on the outside only. This coating acts to promote nucleation during evaporation thereby reducing the temperature difference between tube surface and saturated liquid that is required for boiling. Improved performance has been demonstrated for both the thin film, or sprayed bundle, and pool boiling modes in units built by Union Carbide/Linde for testing at the Argonne National Laboratory.

The nominal waterside operating conditions call for an in-tube water velocity of 6 ft/sec and fouling resistance of 0.0005 $hr-ft^2-^oF/Btu$. In the smooth tube portion of the 1 MWe evaporator, the resulting heat transfer performance will be ammonia side limited: the thermal resistance in the film of evaporating ammonia dominates the other terms making up the overall heat transfer coefficient, U. The evaporator design permits individual performance evaluation of both smooth and enhanced tube bundles under a variety of operating conditions.

The evaporator is connected to a drain or surge tank located below the unit. This tank acts as a reservoir to reduce surges in flow from either the ammonia recirculation pumps or ammonia feed pumps.

The sections which follow describe the various configurations in which the heat exchangers can be operated to obtain performance data.

Phase Separator

A design goal for the 1 MWe evaporator is an exit vapor of 99% quality or better. The actual amount of liquid ammonia carryover anticipated from the sprayed bundle can only be estimated, but the quality may be as low as 95%. A phase separator is required to assure the higher exit vapor quality. A separate external vessel was chosen, primarily because of size limitations within the evaporator. The evaporator is already very nearly the largest

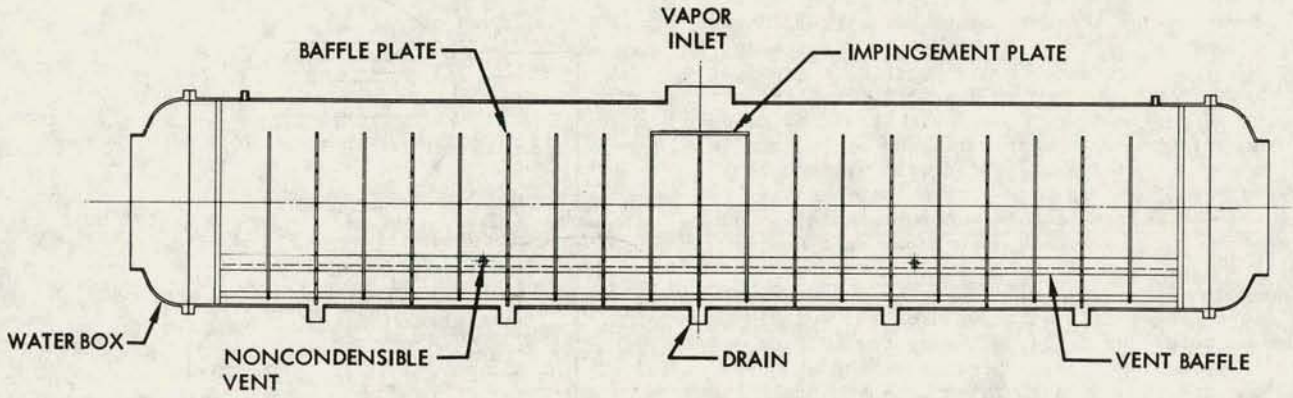

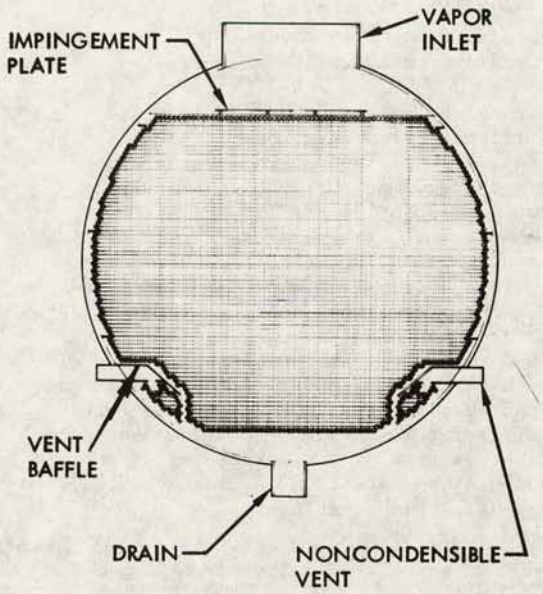

CONDENSER CHARACTERISTICS

SHELL O.D. (FT.)	9.2
SHELL LENGTH (FT.)	50.5
NUMBER OF TUBES	5526
TUBE O.D. (IN.)	1.0
TUBE WALL (IN.)	0.028
EFFECTIVE TUBE LENGTH (FT.)	42
TRANSFER SURFACE (FT^2)	59,800
SEAWATER VELOCITY (FPS)	5.6
ΔP IN TUBES (PSI)	3.3
OVERALL U (BTU/HR-FT^2-^oF)	403
LMTD (^oF)	5.7
h, NH_3 SIDE (BTU/HR-FT^2-^oF)	1428
h, H_2O SIDE (BTU/HR-FT^2-^oF)	963

Figure 3. 1 MWe condenser design and characteristics

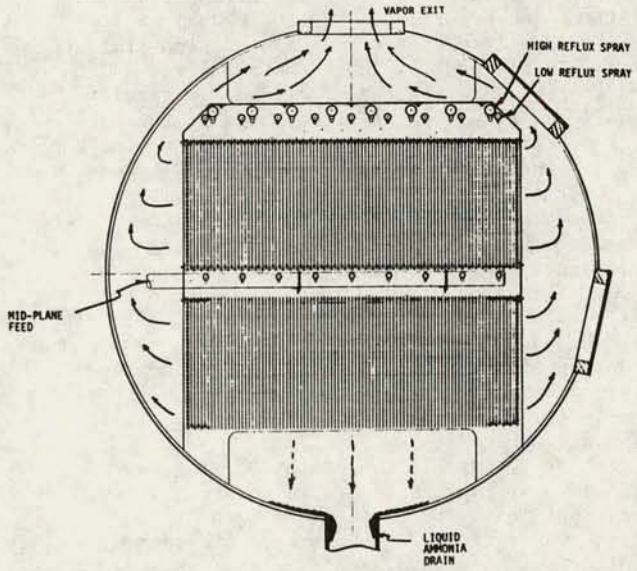

Figure 4. Evaporator cross-section showing ammonia spray feed planes and vapor path.

vessel that could be constructed and shipped by the fabricator, and space available inside the shell above the bundle is filled with the system of spray headers that feeds the bundle. Use of an external phase separator also permits measurement of the entrainment rate. Data on the variation of liquid carryover with evaporative rate and vapor exit velocity are important for design of larger evaporators.

Separation is accomplished by a combination of hook-and-vane and wire mesh, both of which stop entrained liquid by impingement and allow drainage by gravity to a collection point. The pad area is sized based on industrial experience for water and is a function of vapor quality and velocity head. The vanes and mesh are arranged to present a large frontal area to the incoming vapor flow. The liquid ammonia drains down the face of the pad to the bottom of the vessel where it is collected and piped into the drain tank below the evaporator.

Condenser

The condenser is designed along conventional lines with vapor entering the top of the unit in a downflow configuration. The tube bundle is nearly circular in cross-section in order to fill all available shell space. Tube pattern is not as

crucial to performance as for the evaporator since the incoming vapor tends to distribute itself naturally. Wherever the vapor is condensing at a high rate, the local pressure drops, creating a gradient that causes more vapor to be drawn to the site. Thus, the vapor tends to distribute itself as needed. For example, the cold water inlet end of the bundle will be more effective and vapor will migrate to this end. The tube support plates (baffles) are segmented to facilitate this vapor migration. Vapor is fed from the top and straight down across the bundle.

Noncondensible gases will be present from start-up since nitrogen is used to blanket the vessels during shipping and to purge the system between tests. Performance can be greatly reduced by even small amounts of noncondensibles because local pressure gradients draw these gases to the tube surfaces where they accumulate and act as an insulating gas layer through which the ammonia must diffuse to reach the condensing surface thus "blanketing" the condenser. The 1 MWe condenser has 2 noncondensible vents on each side located along the lower curve of the shell where the natural vapor draft tends to drive them. This vapor draft is aided by having a small sub-bundle adjacent to the vents which is shielded from falling condensate and thus produces a greater condensation rate than the surrounding condensate-covered tubes.

As in the evaporator, the condensate drains are sufficiently large to permit full gravity flow with no standing condensate in the shell. Five separate metered drains have been provided at equal spacings along the length of the unit to evaluate zone-by-zone performance.

Evaporator Operation

The evaporator is the more critical of the two heat exchangers. Problems associated with uniform liquid distribution and avoiding liquid entrainment in the exit vapor have guided the design of the 1 MWe evaporator to include a high degree of operational flexibility.

Mid-plane Feed

The evaporator mid-plane feed system is intended to supply liquid ammonia at the center of the bundle in sufficient quantity to make up the liquid evaporated during passage through the upper half of the tube bundle. This allows more flexibility in providing the desired liquid loading on individual tubes. Liquid loading is an important parameter in determining the heat transfer performance of a heat exchanger tube. At very low values of liquid loading, the film on the tube is insufficient and dry-out occurs reducing overall heat transfer. At high rates of liquid loading, the increased film thickness becomes a barrier to heat transfer and again performance is reduced. Ideally, each tube should be uniformly covered with the minimum film thickness necessary to avoid dry-out.

The mid-plane feed system reduces the liquid loading which must be supplied to the top tube rows to avoid dry-out at the bottom rows. The result is a lower average tube liquid loading film thickness and hence higher average heat transfer performance. Additional feed planes would further reduce average liquid film thickness but result in greater complexity and cost for the feed system.

The evaporator liquid ammonia feed system is shown schematically in Figure 5. The primary purpose of the mid-plane feed is to provide make-up

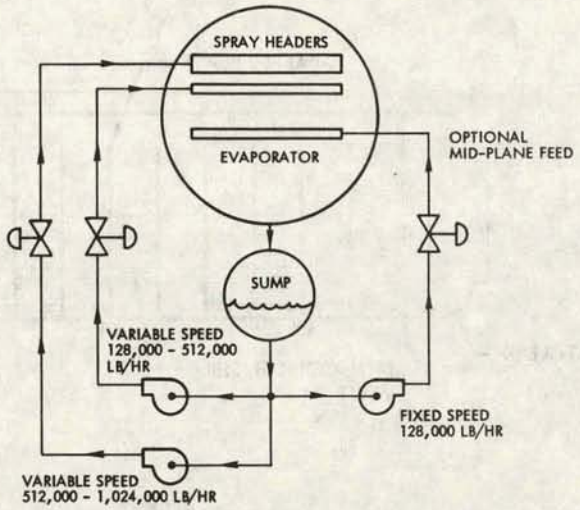

Figure 5. Schematic of evaporator liquid ammonia feed and reflux system.

liquid at a constant rate and thus a fixed speed pump with a trimmer valve was chosen to provide the required flows. The piping feeding the spray nozzles has been designed so that the controlling pressure drop is across the nozzles and the headers merely act as plenums. The nozzles are standard full-cone spray nozzles, selected for their wide angle and uniform coverage. Later incorporation of the enhanced surface tubes into the lower half of the evaporator has added another use for the mid-plane feed system. It allows separate feed of the enhanced tubes so that their performance in the spray mode can be evaluated independently of the smooth tubes. For this purpose, it is necessary to provide a tie-in to one of the larger reflux pumps since the evaporation rate from the enhanced tubes is expected to be somewhat greater.

Vapor Shrouds

In the evaporator, vapor generated within the tube bundle exits by side draft. Permanent shrouding in place at the top of the bundle forces the vapor to take a path that is nearly horizontal. Because the bundle was designed with a square cross-section, flow is essentially one-dimensional and modelling and description of flow phenomena are greatly simplified. For the case of side draft the vapor velocity profile is as shown in Figure 6: zero at the center of the bundle and increasing linearly to a maximum at either side of the bundle.

By blocking vapor flow from one side of the bundle, all the vapor can be forced to exit through the other side. In this case, the velocity profile is zero at the blocked edge and builds linearly to a maximum that is twice the maximum velocity that would occur in the bundle with draft from both sides. This flow profile is equivalent to that which would occur in a bundle twice as wide, so that the bundle with side shrouding can be used as an analog of a 4 MWe scale unit, four times as large, as shown in Figure 7. Distribution problems associated with high vapor velocities can be investigated in this fashion.

A major concern in the design of large sprayed bundle evaporators is the entrainment that occurs when fine liquid droplets are carried away by the exiting vapor flow. At high rates of vapor flow, maldistribution of the liquid on the tubes may also occur because the path of falling liquid droplets

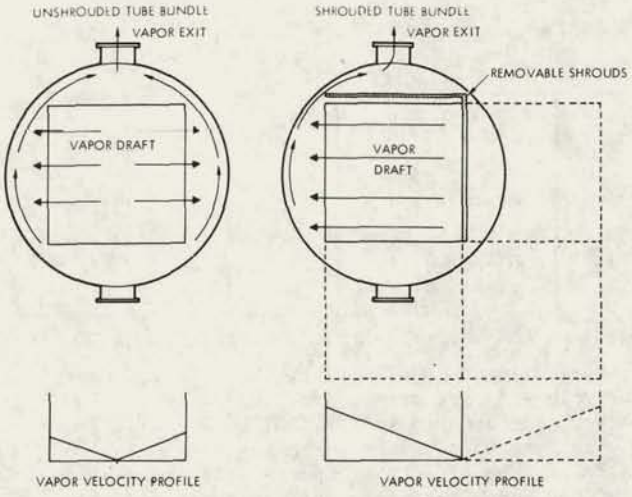

Figure 6. Figure 7.

Figure 6. Vapor velocity profile in baseline evaporator.

Figure 7. Vapor velocity profile in shrouded evaporator showing simulation of 4 MWe scale bundle.

may be altered in the direction of flow. Both of these problems lead to a loss in efficiency of heat transfer. Data for the case of a 4 MWe scale evaporator can be obtained by bolting shroud plates along one side of the bundle as previously described. When used in conjunction with an external phase separator with a metered drain, rate of entrainment can be determined.

The shrouds to be used for this test are steel plates sized so that they will fit through manways provided at intervals along the shell. The vessel must be purged of any ammonia remaining from previous operation. The shrouds are then bolted into place to a framework alongside the tube bundle. Each shroud is neoprene-gasketed to provide a seal with small leakage rates. Identical shrouds are used for other alterations to the evaporator configurations, but they are deployed differently, as in the case of pool boiling.

Pool Boiling

The evaporator has been designed so that it may be flooded and operated as a pool boiler. It is thus possible to obtain data on performance in more than one mode of heat transfer.

The evaporator is converted to a pool boiler by use of spectacle blinds on the drain downcomers and by connection of spillover drain lines between the shell and the drain tank. A drawing of the evaporator when operated as a pool boiler is shown in Figure 8. The spillover nozzles are located two to a side on both sides of the vessel and at two levels, suitable for maintaining a level at the top of either the mid-plane or the full bundle. An additional nozzle is provided near the bottom of the vessel for feeding the pool boiler; it is connected into the regular feed system which uses a variable speed pump to provide the range of flow rates. Neoprene-gasketed shrouds are installed internally along the sides of the bundle to avoid the establishment of convection currents in the void areas between the shell and the square tube bundle. This permits a closer approach to the behavior of a segment of a larger pool boiler. The shrouds also

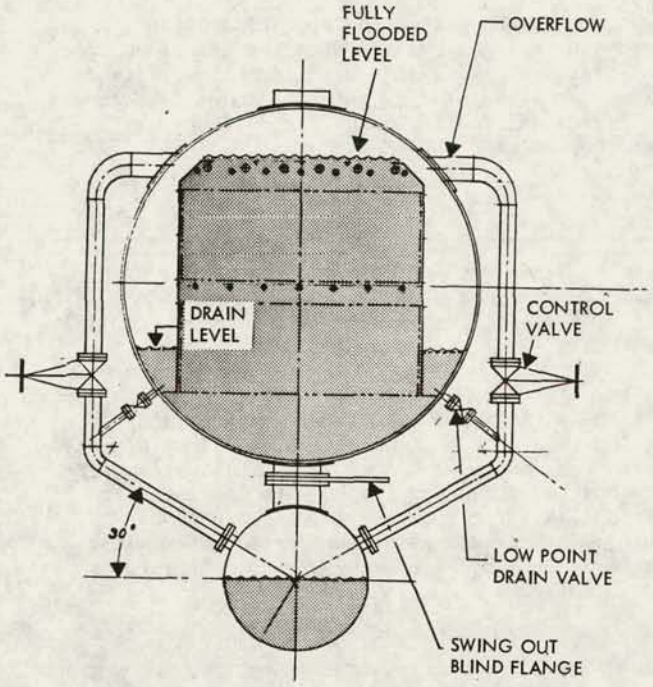

Figure 8. Outline drawing of the evaporator.

have the advantage of reducing the ammonia inventory required. and of acting as baffles to prevent the formation of waves on the free liquid surface. Additional drains are provided at the low points so that the untubed areas may be kept completely drained of ammonia if desired.

By installing the shrouds only half-way up the bundle, the enhanced tube portion may be tested separately.

Predicted Performance

Evaporator heat transfer performance predictions are based on measurements of boiling temperature difference as a function of heat flux. Both the thin film and pool boiling modes of evaporation were tested in ammonia using single tubes with High Flux and smooth surfaces[2], [3]. This data is plotted in Figure 9. The ammonia side heat transfer coefficient, h_a, can be calculated from the data using the equation

$$Q/A = h_a \Delta T \qquad (1)$$

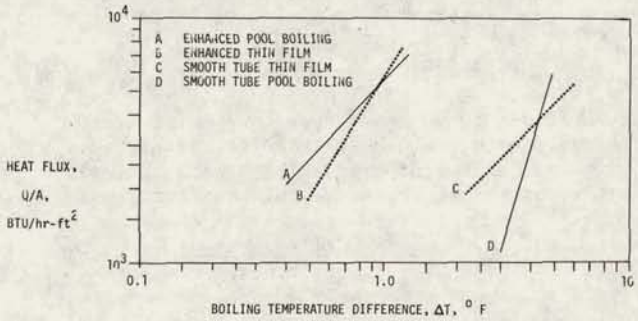

Figure 9. Smooth and enhanced single tube heat transfer performance in ammonia for thin film and pool boiling evaporation modes.

To obtain the evaporator operating points, a system curve is calculated from the equations for heat transfer performance using previously fixed values for seawater flow rate and inlet temperature, exchange area, fouling factor, and ammonia saturation temperature.

$$Q/A = \frac{\dot{m}_w \, C_{p_w} \, (T_{wi} - T_{wo})}{A} \qquad (2)$$

$$U = \Sigma \, a_i \frac{1}{h_i} = \frac{\dot{m}_w \, C_{p_w}}{A} \ln \frac{T_{wi} - T_{ae}}{T_{wo} - T_{ae}} \qquad (3)$$

The outlet seawater temperature, T_{wo}, is the only unknown on the right sides of these equations. Picking values of T_{wo} enables calculations of corresponding values of Q/A and h_a. This system performance curve can be plotted with the tube performance data for h_a, both in the form of h_a = f(Q/A). Intersections of tube performance with system performance represent operating points as shown in Figure 10.

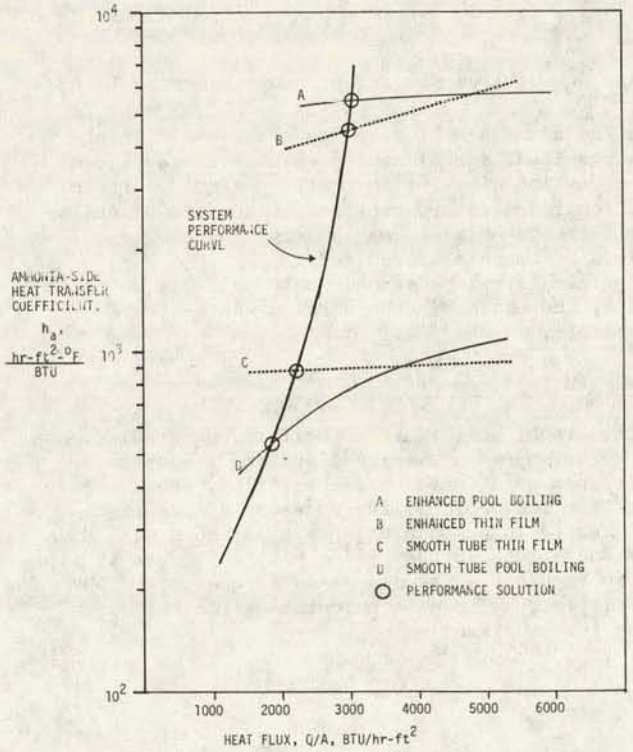

Figure 10. 1 MWe evaporator system performance in sprayed bundle and pool boiler operation.

When Q/A and h_a for each operating point are determined, the overall heat transfer coefficient, U, can be calculated from equation 3, and the evaporative vapor volume can be calculated from

$$m_a = \frac{A \, (Q/A)}{C_{p_a} \, (T_{ae} - T_{ac}) + \Delta H_{fg}|_{T_{ac}}} \qquad (4)$$

These calculations are summarized in Table 1.

Comparison of these numbers show that in the sprayed bundle, the enhanced surface tube bank will produce nearly a third more vapor than the smooth tube bank. In the pool-boiler, the enhanced tubes' vapor volume is greater by about 63 percent.

Table 1. Predicted Evaporator Operating Points

Tube	Mode	Q/A, Btu/hr-ft^2	h_a hr-^{o}F-ft^2	U, hr-^{o}F-ft	m_a, lb/hr
High Flux	Pool Boiling	3020	5500	557	175,000
High Flux	Thin Film	2920	4400	543	169,200
Smooth	Pool Boiling	1850	540	289	107,300
Smooth	Thin Film	2200	880	364	127,600

Actual performance in the pool boiler will probably be less than indicated by the single tube data due to the effects of hydrostatic suppression. The higher hydrostatic pressure at greater depths in the liquid ammonia will suppress boiling; at the bottom row of tubes this could be as much as 0.8^{o}F. It is expected that the nucleation-promoting features of the High Flux surface will help alleviate this boiling suppression and that the additional vapor generated in the lower tube bank may improve smooth tube pool boiling performance by increasing liquid circulation and reducing the hydrostatic pressure in the upper bundle because of the large amounts of vapor present in the two phase mixture.

Actual spray bundle performance may also be less than predicted in Table 1 due to non-uniformities in liquid loading. Maintaining a uniform thin film in practice is extremely difficult, especially at low liquid loading rates.

Relative to spray bundle operation, the pool boiler may give better overall heat transfer performance because its liquid feed supply is more continuous and uniform except at very high rates of vapor generation when slugging may occur. The High Flux surface is not expected to display as marked a difference in performance due to liquid loading rate. The porous surface acts to hold and distribute liquid along each tube so that the thin film of liquid is self-maintained.

Condenser Operation

The condenser is divided along its length into five zones by support plates that are fixed at the bottom of the shell. Each zone is separately drained by free gravity drainage into a collection vessel called a drain pot. The purpose of dividing the condenser in this fashion is to measure the variation in condensation rate along the length of the tubes. The double-segmental baffles in the condenser allow the vapor to migrate to areas of greater condensation rate. At localities such as near the seawater inlet, where ammonia vapor is condensing at a high rate, the local pressure drops to create a gradient that draws more vapor to the site. Thus, the amount of vapor condensed by the first fifth of the tube length will be considerably greater than that condensed by the last fifth.

The liquid level in each drain pot is controlled to a fixed reference by means of a sensing element and flow control valve. By keeping the level in the drain pot constant, the flow rate measured at the exit connection to the pot is the instantaneous measurement of condensate flow for the zone above the drain pot: no accumulation of liquid is permitted in either the condenser shell or drain pot which would effect the condensate flow measurement. The drain pots also provide a reservoir for collecting liquid outside the shell where it will not slosh

into the lower tube bundle and interface with condensation. Perforated plate sections have been incorporated into the design of the drain pots to prevent sea-state induced motions such as sloshing and U-tubing. These motions must be minimized if a reasonably constant level is to be maintained.

Instrumentation

The heat exchangers are to be cleaned by a circulating sponge ball cleaning system developed by Amertap[4]. Performance measurements will include an evaluation of biofouling control including the Amertap system.

The heat exchangers have been instrumented to measure the following performance characteristics:

1. Seawater pumping power requirements (ΔP between waterboxes).

2. Overall heat transfer coefficient (seawater ΔT, bulk seawater mass flow rate, ammonia saturation temperature).

3. Local heat transfer coefficients (seawater ΔT and flow rate will be measured for 20 individual tubes located throughout the tube field).

4. Effect on performance due to biofouling (compare heat transfer in three types of tubes: Amertap-cleaned tubes, uncleaned tubes, and closed loop tubes circulating deionized water).

Temperature

The sensors used for temperature measurement are three-wire platinum element resistance temperature detectors (RTD's) with an accuracy to about 0.13°F.

The primary temperature measurements to be used for performance evaluation are nearly the same for both evaporator and condenser and are made in the inlet waterbox (4 sensors), the outlet waterbox (14 sensors), and the shell (10 evaporator sensors, 5 condenser sensors). Individual measurements will be averaged to get values of inlet and outlet water temperature and ammonia saturation temperature for use in computing overall heat transfer performance according to the equation:

$$UA\Delta T_{lm} = (\dot{m}Cp\ \Delta T)_{seawater} \qquad (5)$$

Since these RTD readings will be averaged, it is essential to locate the sensors to get as fair a distribution as possible. It was assumed that the heat exchange performance would be symmetrical left and right of the center vertical plane. To get the maximum information from a limited number of RTD's, they were concentrated on one side of the vessel with a few placed to check the degree of symmetry. Locations were chosen at least 6" from the wall to avoid probable anomalies in this region. It was not practical to thread wiring in and out of the tube bundle, so no temperature measurements are made on ammonia vapor near the tube surfaces or on the tube walls. There are, however, additional RTD's on the ammonia side to measure inlet and outlet temperatures of both liquid and vapor. These are intended to serve as a back-up to in-vessel measurements.

Pressure

Pressure is measured through a tap in the vessel wall and transmitted by a diffused silicone type transducer with an accuracy of about 0.25% of span. Valving between the tap and the transmitter allows zeroing and calibration. The important pressure measurements are made through four taps in each waterbox at 12, 3, 6 and 9 o'clock and one in the top center of each shell. The waterbox taps give the difference in pressure due to friction losses in the exchanger tubes.

Instrumented Loops

The instrumented loops are designed to indicate the variations in local heat transfer and the effects of biofouling. Thirty of these loops will be installed in each unit: six containing deionized water, twenty cleaned by Amertap, and four containing seawater, but not cleaned. The instrumentation for each loop consists of an RTD to sense the temperature of the seawater as it leaves the exchanger and a flow meter. By collecting the exit seawater from these individual tubes and measuring its temperature and flow rate, the local heat transfer can be calculated. Seawater enters Amertap-cleaned and uncleaned tubes normally from the inlet waterbox, but the deionized water loops are closed and their water is recirculated after being heated or chilled to inlet waterbox temperature. Comparing the heat transferred in these three types of tubes over a period of time, the progress of biofouling and the effectiveness of the Amertap system can be observed.

Sites for the instrumented tubes have been selected throughout the bundle to test several hypotheses as well as measure performance by region. It is expected that edge tubes will be anomalous and that performance in the left and right sides of the bundle will be symmetrical. A variation in performance with bundle depth is also expected. Clean water, uncleaned, and Amertap-cleaned tubes are grouped so that their performance characteristics can be compared. Several instrumented tubes have been placed in the region of the non-condensible vents and build-up of non-condensibles will be indicated by an observable decline in the measured heat transfer coefficient for these tubes.

Test Plans

The final test plan will be developed by the Test Director Contractor and will consider the potential experiments which would contribute to evaluation of the heat transfer and biofouling control performance of the 1 MWe heat exchangers and which exploit the capabilities of the hardware and instrumentation. Final test plans must necessarily reflect DOE's budget and schedule constraints.

Summary

The 1 MWe heat exchangers represent the first large scale test of an OTEC evaporator and condenser in a representative ocean environment. The units were designed to provide maximum operational flexibility based on the 1 MWe test objectives specified by DOE. Measurements were developed to achieve these test objectives and sensors have been placed to make the desired measurements. Operation of the units on-board OTEC-1 in early 1980 off the island of Hawaii will provide valuable design data for future and larger scale OTEC heat exchangers.

Nomenclature

a = area ratio conversion to outer tube surface area

A = heat transfer surface area

C_{p_w}, C_{p_a} = specific heat at constant pressure of water and of ammonia

ΔT = temperature difference between inlet and outlet or across film

ΔT_{lm} = log mean temperature difference

$$= \frac{\Delta Ta - \Delta Tb}{\log (\Delta Ta/\Delta Tb)}$$

where $\Delta Ta = (Tw_{in} - Ta)$

$\Delta Tb = (Tw_{out} - Ta)$

and Tw_{in}, Tw_{out} = inlet and outlet water temperature

Ta = bulk ammonia temperature

h = heat transfer coefficient

h_a = heat transfer coefficient due to ammonia

H_{fg} = specific enthalpy of vaporization

$\dot{m}_w$, $\dot{m}_a$ = mass flow rate of water and of ammonia

Q = heat transfer rate

T_{wi}, T_{wo} = inlet and outlet water temperature

T_{ac}, T_{ae} = bulk ammonia temperature at condensing and evaporating conditions

U = overall heat transfer coefficient

References

1. Snyder, J. E., "1 MWe Heat Exchangers for OTEC Status Report February 1978," presented at the Fifth Annual Conference on OTEC, Miami Beach, Florida, 20-23 February 1978.

2. Sather, N. F., L. G. Lewis, J. J. Lorenz and D. Yung, "Performance Tests of 1 MWt OTEC Heat Exchangers," Argonne National Laboratory, presented at the Fifth Annual OTEC Conference, Miami Beach, Florida, 20-23 February 1978.

3. Lewis, L. G. Lewis and N. F. Sather, "OTEC Performance Tests of the Union Carbide Flooded-Bundle Evaporator," Argonne National Laboratory Report ANL/OTEC-PS-1, December 1978.

4. Kern, W. I., "Increasing Heat Exchanger Efficiency Through Continuous Mechanical Tube Maintenance," Fourth Annual OTEC Conference, New Orleans, Louisiana, 22-24 March, 1977.

COMPACT HEAT EXCHANGER DESIGN PROGRESS

J. H. Anderson, Jr.

Sea Solar Power, Inc.
2422 South Queen Street
York, Pennsylvania 17402

and

P. B. Pribis

General Electric Company
1 River Road
Schenectady, New York 12345

Abstract

Plate type heat exchangers with horizontal, single pass water flow passages, vertical downflow condenser passages, and vertical upflow boiler passages are being investigated for use in Ocean Thermal Energy Conversion (OTEC) power plants.

The design is attractive because of simplicity of flow paths, controls and manufacture and its adaptability for variations in water side and boiling and condensing surface designs. High heat transfer coefficients are possible, along with low pressure drops on both the water and working fluid sides.

Aluminum, cupro-nickel, titanium, steel or combinations of different materials can be used in the form of clads.

Heat exchanger tests using different surfaces, and Refrigerants 12 and 22 are in progress.

Results to date are:

(1) The plate heat exchanger is a cost effective solution to OTEC heat exchanger design requirements;

(2) Small scale units have been mechanically assembled and successfully operated;

(3) Special test devices have been employed to develop surfaces with film coefficients for condensing as high as 4500 Btu/hr ft^2°F, and for boiling as high as 2500 Btu/hr ft^2°F at 4000 Btu/hr ft^2; and

(4) Overall heat transfer coefficients of 1200-1400 Btu/hr ft^2°F for boiling and condensing can be obtained.

Introduction

It has been recognized that the key element affecting the economic feasibility of ocean thermal power is the cost of the heat exchangers. Consequently, many years ago, the first author and his father, J. Hilbert Anderson, Sr. concluded that conventional heat exchanger equipment could be improved upon for application in Sea Solar Power Plants. By building a heat exchanger for very low pressure differences, an inexpensive heat exchanger could be built. By submerging the heat exchangers to a depth in the water where the working fluid pressure was balanced by the hydrostatic pressure, a heat exchanger could be made of thin material, and relatively low cost, compared to conventional, high pressure, heat exchangers. Furthermore, a flat plate heat exchanger was envisioned that could be assembled simply and rapidly. It could be brazed or mechanically assembled into single or modular units.

Over the years, we developed the concept for a mechanically assembled, plate type, crossflow, heat exchanger which could be utilized as an evaporator or condenser for OTEC. It would be a design utilizing a completely mechanical construction, with no welding or brazing which might be subjected to corrosive action in seawater.

The water channels would be horizontal and the working fluid channels would be vertical. The objective is to have very low head loss on the water side and very low pressure losses on the working fluid side. These factors are extremely important in the design of OTEC Plants because water side head losses cost a lot of money in pumping power, and pressure losses on the working fluid side decrease the operating efficiency of the power plant.

A promising design evolved for this mechanically assembled cross flow flat plate heat exchanger. However, there was virtually no heat transfer data available for this type of heat exchanger configuration and, furthermore, there was little information concerning the possibility for assembling and sealing such a heat exchanger. In order to evaluate these two major questions about such a heat exchanger design, it was decided to actually build some heat exchangers and test them.

We designed and built two heat exchangers. These heat exchangers were a scaled down boiler and condenser of an operating model. They were sized for a heat duty of about 100,000 Btu/hr. The primary objective for building these units was to demonstrate that they could be built and sealed to our satisfaction.

A test loop was designed and built which could adequately test the boiler and the condenser performance and which could be flexible enough to allow for rapid removal and replacement of each heat exchanger. The test loop worked extremely well and allowed a wide range of heat duties and water velocities as follows:

Heat duties: 1800 Btu./hr.ft.^{2} to 7000 Btu./hr ft^2

Water velocities: 2 ft/sec. to 13 ft/sec.

It was then decided to examine in detail the heat transfer coefficients on the working fluid side. A small test apparatus that could be run in conjunction with the test loop was designed. This apparatus was made such that a visual observation of boiling and condensing could be made and accurate test data of film side heat transfer coefficients could be obtained. In this way, one could quickly evaluate refrigerant side surface configurations before they were applied to the plates in the larger test heat exchangers. Two test loops were built and have been running. The first loop was built for

R-12 and the second loop for R-22.

Since the fouling was being well studied and documented by the University of Hawaii in their test at Keahole Point as well as others in the OTEC program, it was felt that the last remaining area where improvement could be hoped for was the water side heat transfer coefficient. The decision was made to build and test a third addition to the test loop to measure heat transfer and pressure drop on the water side. This loop was designed to be run in parallel with the main test loop. It is made to evaluate performance achievable with various enhancement techniques. It is being assembled and testing will commence shortly.

The advantages of having three test loops is that one can now quickly change surface enhancements on the refrigerant sides and on the water sides and evaluate their individual performances. Then we can apply the selected surfaces to the plates for the larger heat exchangers and test an overall performance for the heat exchanger. Testing time is minimized and a great variety of surface enhancements can be tried in both the refrigerant side and water side units. For instance, a test plate can be inserted and tested in the small fluid side test chamber in a period of one or two days. Furthermore, we have come to recognize that full size heat exchangers of this type can be built at a relatively low cost. This type of heat exchanger can be built not only as a pressure balanced heat exchanger, but also as a pressurized heat exchanger. Naturally, it will be heavier than the pressure balanced heat exchanger, but nevertheless, it will be more than competitive with shell and tube or conventional heat exchangers.

Mechanically Assembled Plate Heat Exchanger Design

General

Since the initial work, it has been our objective to use a flat plate design heat exchanger for sea thermal power plants. Since these heat exchangers can be built for pressure balanced design, they can be built with very thin plates that would not have to withstand much pressure. However, as we continued in our studies, it was found that this same design could be built to withstand pressure. The design selected for the evaporator is called a flooded evaporator, the entire surface area of the working fluid side is submerged in a pool of refrigerant. Boiling bubbles form along the surface submerged in the pool of liquid and rise to the top. Flooded evaporators have commonly been used in the refrigeration industry. As an adjunct to the flooded evaporator design, we are adding recirculation which is also commonly used in the refrigeration industry and improves heat transfer conditions in the working fluid channels by permitting some of the working fluid to flow across the heated channels and be recirculated around the second time. Excess liquid is circulated through the evaporator so as to produce somewhat higher liquid velocity and boiling coefficients at the bottom of the evaporator where the liquid enters. This also tends to produce better distribution of liquid over the surface and avoid the problem of having gas flow through part of the surfaces with poor distribution flow and incomplete wetting of the surfaces (blanket boiling). The ideal design approaches DNB (departure from nucleate boiling) as closely as is practical for maximum heat transfer conditions. It is very important for OTEC power plants to keep the vertical height of the flow path low enough so that the static head penalty does not become too large. In the selected design a flow passage height of 2 ft. would produce a static head penalty of roughly 1/2° using R-22 as the working fluid.

In addition to the boiling channels there are some preheating channels that run counterflow to the water. These channels heat the working fluid from the temperature of the condenser to the saturation point entering the boiler.

The water flow channels are horizontal. They are straight through so as to minimize head loss in the channel. They can be cleaned either mechanically by brushes, chemically, or by a slurry solution. Numerous enhancement possibilities can be used on the water channels. This will depend upon the ultimate technique of manufacturing, the cost of enhancement, and the improved heat transfer of the enhancement compared to the increased pressure drop.

At the top of the boiler channels a demister is inserted. The velocity of the gas leaving the evaporator channels is low so that liquid droplets run off the screen type demister and flow back into the flooded area. Gas proceeds on through the piping manifold. In this way, there is no acceleration and deceleration of gas out of the boiler and back into a separate chamber demister. Furthermore, a separate chamber demister along with the piping is not necessary in the circuit.

The condenser is very similar to the boiler, except that vapor enters at the top and is condensed on the cold plates as it proceeds down through the 2 ft. high working fluid channels. The mechanical assembly of the condenser is identical to the boiler with the exception that there is no demister at the top of the condenser. Plates that are identical or similar in construction can be used in the boiler and the condenser. The condenser working fluid channels are wide and the velocities low enough to prevent a large pressure drop on the vapor side in the condenser.

Plate Fabrication

The objective in fabricating a plate type heat exchanger is to take full advantage of the ability to assemble the unit mechanically, or possibly by brazing and thereby eliminate costly labor intensive activities, such as welding, tube rolling, etc. Figure 1 is an exploded view of such a heat exchanger.

A method being investigated which potentially may reduce fabrication costs is to make all the sheets by cutting and folding one larger sheet. This has the advantage of eliminating one-fourth of the sealing surface. The design is also directly affected by the heat transfer coefficients obtainable. The produce of the coefficient and area should be as close as possible for each (water and working fluid) side. To achieve this, it may be necessary to use the ribs on the working fluid side instead of the water side as shown in Figure 1. If this is done, they must support a tension load instead of compression, and must be attached accordingly. If the ribs (surface expansion) are used on the water side, their loading is in compression. One easy solution to this dilemma is to separate the plates by ridges die pressed into the plates. Such a plate is shown in Figure 2.

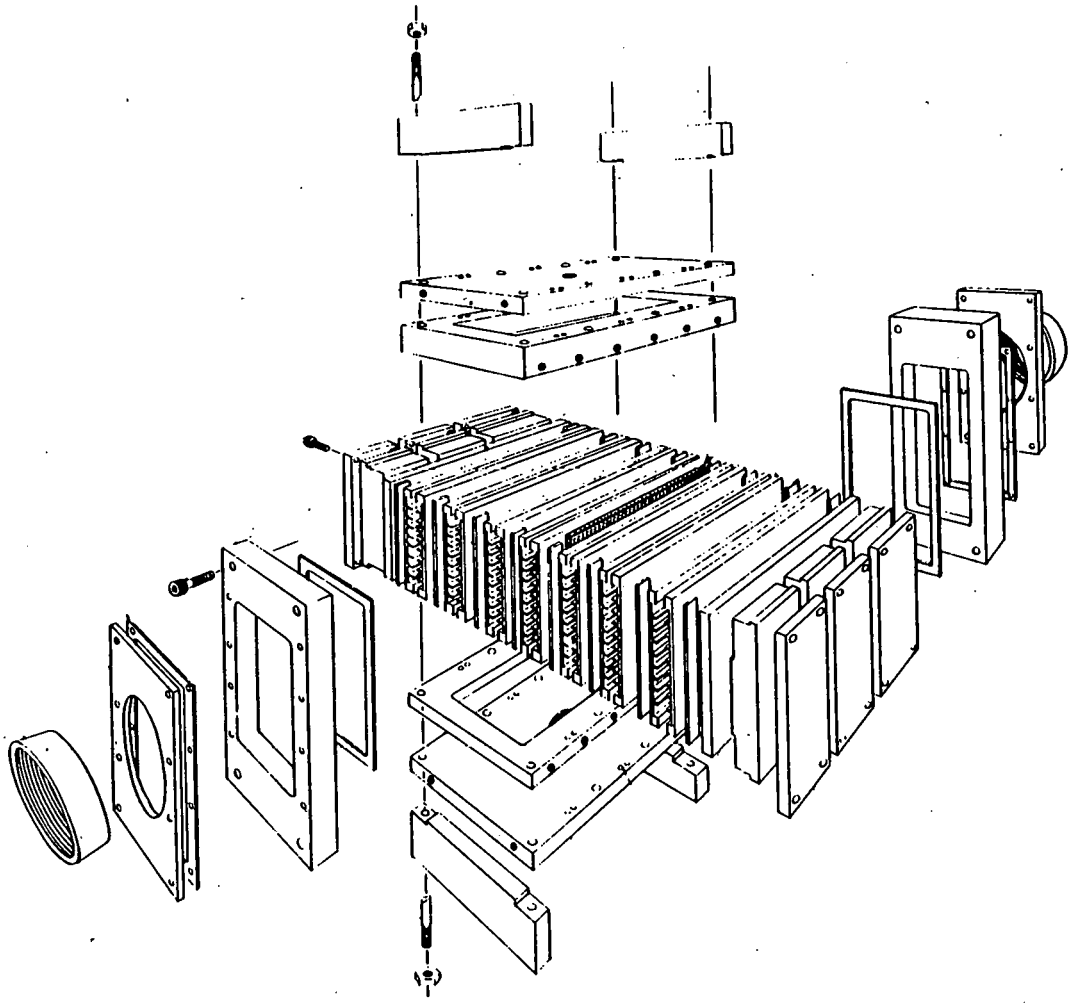

Fig. 1 Plate Type Heat Exchanger (Exploded View)

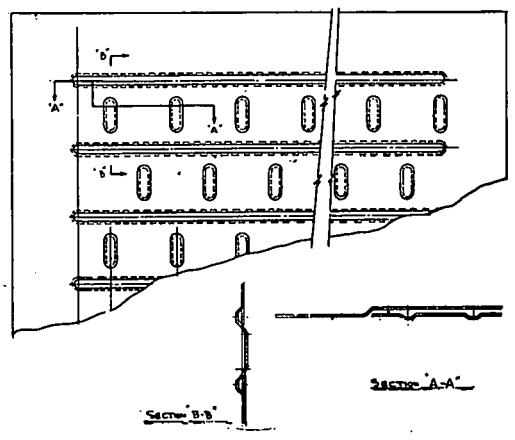

Fig. 2 Possible Plate Configuration

Materials

Cladded plates are available which permit the use of different materials on the water side and working fluid side. These cladded plates have proven to be sturdy (Have you ever seen a delaminated quarter?) and the interface produces insignificant thermal resistance. A material such as 90%-10% copper-nickel can now be used on the water side in a thin application. The antifouling benefits are realized at a fraction of the previous costs. Working fluid side material may be dependent on the fluid used, but typically would be copper for halocarbon working fluids.

An additional technique to further reduce costs, feasible with cladded plates, is to use only thin surfaces and a cheap filler material between them. A carbon steel filler has the advantages of low cost and adds enough strength to allow the thin clad surfaces to be used.

In attempting to match the products of the heat transfer coefficients and the areas for the working fluid side and the water side, it may be necessary

to enhance the water side. A sprayed metal surface, of 90%-10% copper-nickel can be used, resulting in potentially excellent antifouling characteristics and cathodic protection of the substrate. However, testing is required to verify this.

Heat Exchanger Test Loop

After designing the heat exchangers and constructing a wooden model, it was necessary to build an actual set of the heat exchangers. The test loop for these was patterned after a refrigeration test loop. A compressor was employed to put hot gas into the condenser. From the condenser liquid flows into an evaporator on its way back to the suction of the compressor. The loop is pictured in Figure 3.

To simulate OTEC conditions the test loop was set up such that the compressor discharged into a desuperheater. This is nothing more than a tube-in-tube string of copper tube using city water to cool the superheated gas to approximately saturation conditions entering the condenser as it would be in an OTEC plant. The saturated gas is condensed, and collects in a small receiver beneath the condenser. From here the liquid flows through a tube-in-tube subcooler where it is cooled slightly below saturation conditions, again to simulate the conditions of an OTEC plant where liquid from the condenser is subcooled below saturation conditions for the boiler. The condensate is metered and flows into the bottom of the boiler.

The only difference between this test loop and the actual OTEC cycle is that the condenser is operating at slightly higher temperatures and pressures than the evaporator. This condition does not have a large effect on the heat transfer coefficients.

The water flow channels are in series so that the water first flows through one channel of the condenser and into the boiler, then back through the second channel of the boiler into the second channel of the condenser, then back through the third channel of the condenser, through the third channel of the boiler and so forth. The total temperature rise from beginning to end is practically nil. The heat added to the water in the condenser is taken out in the evaporator and so forth. Because each of the heat exchangers is only 2 ft. long and the rise and drop of the water temperature through each unit is less than .2°F, we have made our calculations on the basis of a constant water temperature through the condenser and the boiler. The flow velocities in the water channels are measured by a calibrated orifice on the discharge line of the pump. The orifice is placed in an 8 ft. long straight section of pipe to minimize disturbance entering the orifice. From the quantity of water flowing and the cross-sectional area of the water flow channels, one can calculate the mean velocity of the water in the heat exchanger passages.

The operating conditions of the heat exchangers are measured by reading the pressure in the boiler and condenser using a dead weight gauge tester. The flow through the boiler and condenser is measured with a liquid flow meter. A barometer is used to read atmospheric pressure. The barometer was calibrated against a standard to read the actual Pressure inside the chambers relative to conditions as set in the ASHRAE tables. The ASHRAE tables are then used to give the corresponding temperatures at the saturation pressures in the boiler and condenser.

A computer program was written to take raw data and calculate the performance of each boiler and condenser at various loading points. The water velocity may be varied from a low of about 2 ft./sec., to 13 ft./sec.

This small test unit is a valuable tool because a complete boiler or condenser can be assembled and inserted in place in about 6 hours. A complete set of test data can be taken in a few days.

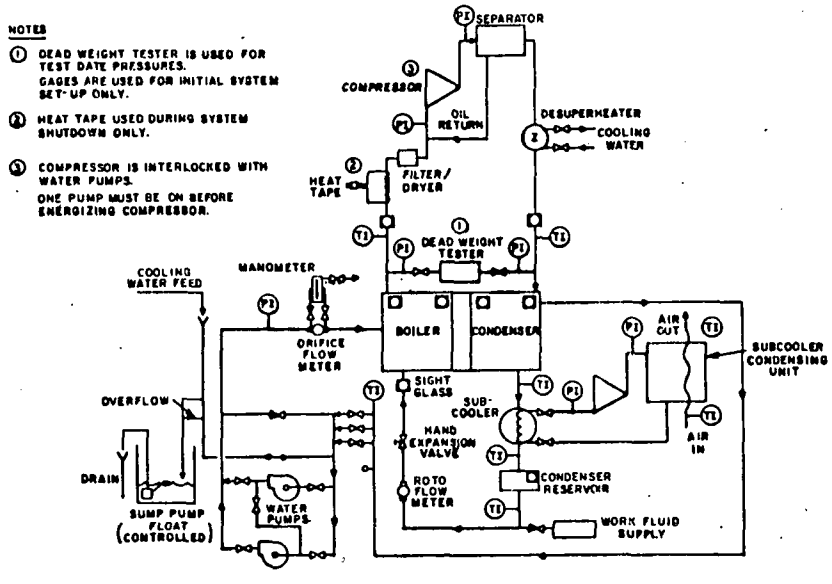

Fig. 3 Heat Exchanger Test Loop

Film Coefficient Test Chambers

Figure 4 shows the device which consists of two chambers separated by a plate. Working-fluid conditions are established such that condensing occurs in one chamber while boiling occurs in the other. Figure 5 is a schematic of the support system which establishes the correct working fluid conditions in each chamber. By measuring plate midplane temperatures, film coefficients for both sides of the plate can be determined, providing fluid conditions and flow rates are known. A secondary function of the test chamber is to allow the visual observation of various enhanced surfaces in the boiling and condensing modes.

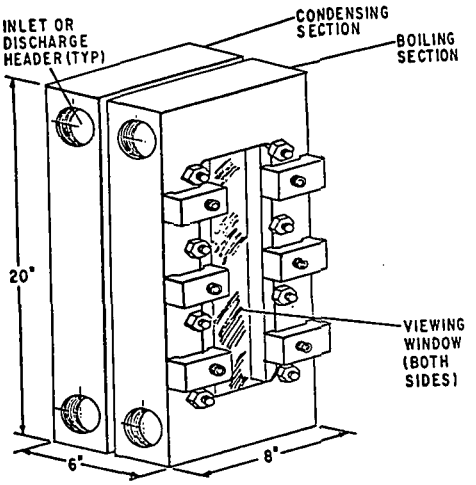

Fig. 4 Film Coefficient Test Chamber

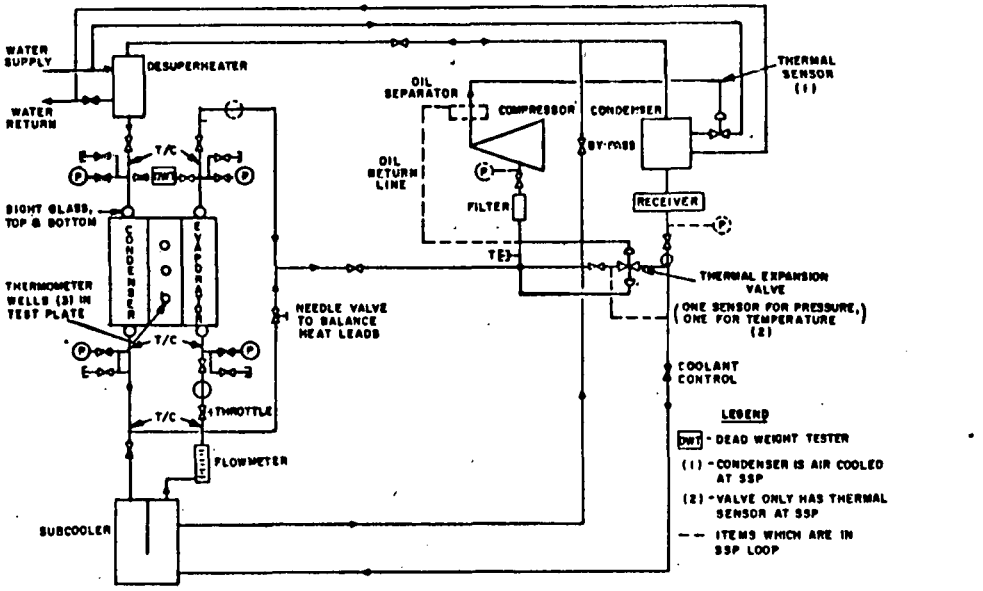

Fig. 5 Film Coefficient Test Loop

The device can simulate OTEC conditions in regards to (a) heat load (b) surface velocities and Reynolds numbers, (c) and degree of subcooling. It uses a desuperheater to insure that vapor entering the condenser is very close to saturated conditions, as would be the case in an operating OTEC system.

The bulk temperatures for the working fluid in each side of the chamber is taken to be the saturated temperature for the pressure, as this is the temperature at which most of the heat transfer occurs. Fluid properties are taken at their bulk temperatures. The heat transferred through the plate is calculated for each side by multiplying the change in enthalpy by the mass flow rate. The average heat transfer rate is used to calculate the temperature drop across the 1/2" thick plate, and this temperature drop is used to calculate plate surface temperatures. High conductivity plates are used so that plate surface temperatures are not subject to large errors. Film coefficients are then calculated from

$$h = Q/AdT$$

where dT is the temperature difference between the bulk fluid temperature and plate surface temperature. Enhancement ratios are determined by comparing the resultant film coefficients to those calculated from theoretical correlations (Ref. 1-5) and those measured in the test chamber for a flat plate with no enhancement.

Water Film Coefficient Test Loop

Working fluid side enhancements result in film coefficients large enough that the water side film coefficient becomes limiting in the development of a highly efficient water-to-working fluid exchanger.

A test unit long enough to have a reasonably high L/D and with an entrance section thermally isolated from the test section was designed to evaluate en-

hanced water side surfaces. This test section has six (6) individual channels .446" x .438" in cross-section. Four channels are active and two channels are stagnant to serve as buffers to minimize edge effects.

The water is heated as it passes through the active channels by condensing refrigerant on the back sides of the active channels.

Figure 6 shows a cross section of the test unit showing the active channels, buffer channels, gas condensing space, pressure taps and thermometer wells. Not shown are the heat barriers which are a combination of slots and plastic to minimize heat transfer from the condensing space to the 12" long straightening section of the water channels. This will minimize entrance effect on film coefficient. Heat losses to the atmosphere will be minimized by insulation and running system temperatures as close to atmospheric temperature as possible.

Figure 7 is a schematic of the refrigerant and water piping for the test loop. Water and refrigerant conditions are established by the main loop, then the required quantities are bled to the water film coefficient test loop.

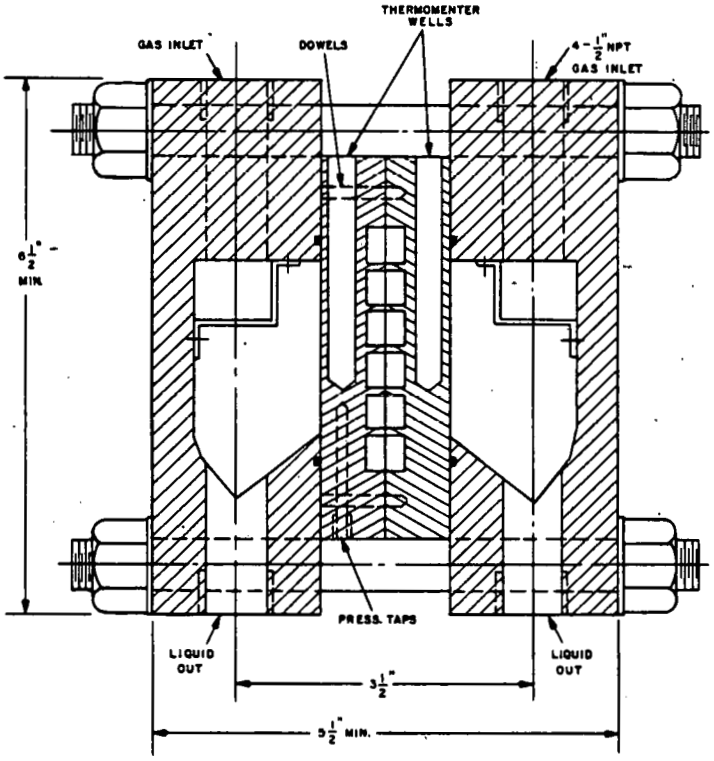

Fig. 6 Water Film Coefficient Test Chamber (Cross Section)

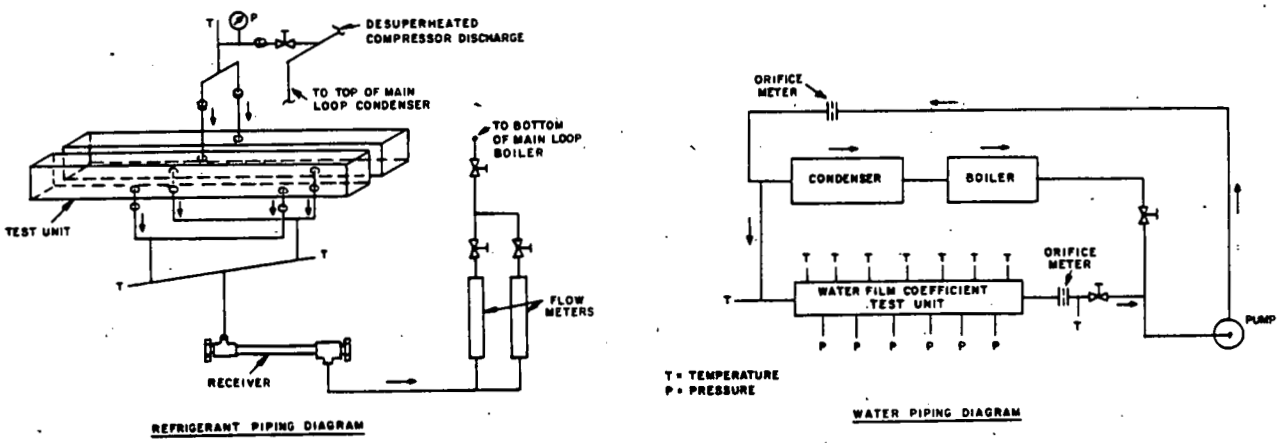

Fig. 7 Water Film Coefficient Test Loop

Since the heat transfer area is known, by measuring the entering and leaving enthalpy of the refrigerant the heat flux is obtained. Since the conductivity of the metal is known, by measuring the temperature of the metal at a known distance from the water surface, metal surface temperature can be determined. The log mean temperature difference (LMTD) and film coefficients can be determined, and a heat balance can be performed, by measuring the entering and leaving water temperature.

Test Results

Our first test on the condenser and boiler in the larger test loop involved straight rectangular water channels, a surface covered with fine screen on the boiling side, and a surface with louvered plates on the condensing side. The second set of tests were the same except using flat plate aluminum surfaces on both the boiler and the condenser. As shown by Figure 8 the overall coefficients for both boiling and condensing were improved somewhat for the screen surface and louvered surface over the flat plate data. However, they were not as good as we had hoped they would be, and it appeared that the screens did not fully act as nucleating surfaces but tended to blanket the surface between the pressure points holding the screen to the surface.

Testing of various surfaces in the film coefficient test chambers is still in progress, and, therefore, no end result statement can be made at this time. Testing to date has shown the following:

1. Testing flat plates has shown that this system gives data which correlates well with predictions made by theoretical correlations. (Ref. 1-5) Results also correlate well with those of a larger test system in the refrigeration industry.

2. The ability to observe the boiling and condensing phenomena has proven valuable in designing new types of surfaces which result in higher film coefficients. Observations made thru magnifying lenses, and slow motion photography have proved extremely useful.

The latter type of investigations have suggested the testing of sprayed metal surfaces -- inexpensive surfaces which provide a large number of nucleation sites for pool boiling. Observation of this surface operating in the boiling mode shows a large number of small bubbles leaving the surface at low heat fluxes (typical of OTEC condition). Higher heat fluxes drive the surface past the point of departure from nucleate boiling (DMB) and blanket boiling is observed. Film coefficients range from 1400 Btu/hr.^{2}°F-ft.^{2} at low heat fluxes, to 4000 Btu/hr. °F-ft.^{2} at high heat fluxes. The particular surface tested was one of random application techniques. To optimize the surface, the following variables of application need to be studied: (1) surface finish and density, (2) surface material, (3) and surface thickness. A fourth variable, (4) surface configuration, is added when the condensing mode is considered.

The total resistance to heat transfer in the small test chamber is the sum of the resistance due to the base metal, the substrate spray metal interface, the spray metal, and the film coefficient. The base metal resistance is relatively small, is fixed for a given design, and need not vary in these experiments. The resistance of the sprayed metal layer varies with its density and composition. As an example, copper can be used instead of aluminum. The effect of the film coefficient, which is usually the largest resistance, can be varied by changing the surface finish (effect on Reynold's number) and by changing the surface density and thickness (effect on number and size of nucleation sites). The substrate-sprayed layer interface resistance is changed by the materials used, and atmosphere in which applications are done in.

Testing to date has not covered all of the above mentioned variables, as this was not necessary to determine a surface which showed promising results, for testing in the larger unit and verifying heat transfer coefficients used in plant design calculations.

Surface configuration variations being tested for the condensing mode include the application of the spray metal surfaces in vertical strips. Initial testing showed that the random surface, applied in 1/16" vertical strips, gave results not much better than a flat plate. It was evident that capillary action retained the fluid on the plate, and retarded its drainage. This indicates a change in surface finish, and/or a change in density is required. This is easily accomplished by varying application system parameters (i.e., - hold gun closer to surface, use higher air pressure if electric arc spraying, or use oxygen -- acetylene method of application, spray in reduced atmosphere, etc.)

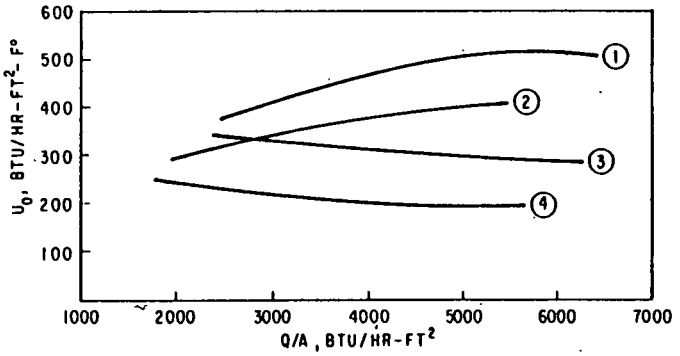

1. BOILING COEFFICIENT, USING SCREENS
2. BOILING COEFFICIENT, SMOOTH PLATE
3. CONDENSING COEFFICIENT, LOUVERED SURFACE
4. CONDENSING COEFFICIENT SMOOTH SURFACE

Fig. 8 Heat Exchanger Test Results

A change in finish is accomplished by wire brushing after application.

Other working fluid side heat transfer enhancements for boiling and condensing are being investigated. These focus on Gregoric type surface enhancements which both increase surface area and create vertical channels.

While not many tests have been made to date, these tests are rapidly progressing, and we can draw a few overall conclusions as to performance of condensers and evaporators from the tests we have run.

The latest fouling factor, including data from tests at Keahole Point, show that a fouling factor of .0001 hr.-ft.^{2}-°F/Btu is maintainable with cleaning at moderate time intervals. (Ref.6-7) If we use this fouling factor in conjunction with the condensing coefficients achievable with the grooved surface, and the water side coefficients that we have attained on the complete condenser and boiler at a water velocity of 6 ft./sec., it appears that we will attain an overall heat transfer coefficient (U_o) referred to the projected area of the refrigerant surface of about 1400 Btu/hr-ft^2°F.

If we similarly calculate overall boiling coefficients (U_o's) using the sprayed surface for the boiler and the water side coefficients that we have attained on the boiler and condenser tests, then it also appears that we can attain approximately 1200-1400 Btu/hr.ft.^{2}°F referred to the projected area of the refrigerant surface at average boiler operating conditions.

It is too early to predict these coefficients more accurately, but they appear to be quite clearly attainable in actual practice.

Our test and development program is showing continual improvement in working fluid and water side surface enhancement techniques. This will have a very major and important effect on the basic economy of the heat exchangers and in the overall sea thermal power plant performance.

Conclusion

The three test loops that have been described here make it possible for us to measure an overall heat transfer coefficient for simulated OTEC evaporator and condenser conditions, the film coefficient for boiling and condensing, and the water side heat transfer coefficient. Furthermore, building the heat exchangers has shown us that a mechanically assembled heat exchanger can be built and assembled simply and reliably. The test loops are all easily accessible, and can be operated in a simple, reliable manner. Data can be taken quickly and accurately. Test plates and test units can be changed quickly.

From the data that we have already obtained, we can expect overall heat transfer coefficients for OTEC power plants near 1200 Btu/hr-ft^2-°F and larger using R-22 as a working fluid. The heat exchanger configuration described herein appears to offer a very practical, low cost solution for Ocean Thermal Energy Conversion plants.

REFERENCES

1. "Heat Transfer", Chapter 2, ASHRAE Handbook of Fundamentals, Page 268, ASHRAE, New York, 1972.
2. F. Krieth, Principles of Heat Transfer, 2nd Edition, Page 464, 1965.
3. "Condensation", Section 506, GE Heat Transfer Data Book, Page 3, GE R&D Center, Schenectady, N.Y., 1977.
4. "Condensation", Section 506, GE Heat Transfer Data Book, Page 5, GE R&D Center, Schenectady, N.Y., 1977.
5. W. M. Rohsenhow, "A Method of Correlating Heat Transfer Data for Surface Boiling of Liquids", Trans. Am. Soc. Mech. Engrs., Page 969 [August 1952].
6. Aftring, R.P., Capone, D.C., Dugnay, L., Fell, J., Master, I.M., and Taylor, B.F. "Biofouling and Site Characterization Studies in an Ocean Thermal Energy Conversion (OTEC)." Experiment at St. Croix, U.S. Virgin Islands.
7. All Proceedings. (1978). Ocean Thermal Energy Conversion Conference, 5th. University of Miami, Feb., Vol. 4.

STUDIES ON OTEC POWER SYSTEM CHARACTERISTICS AND ENHANCED HEAT TRANSFER PERFORMANCE

T. Kajikawa*, T. Agawa, H. Takazawa, M. Amano, K. Nishiyama, & T. Homma**

Energy Division, Electrotechnical Laboratory
Ministry International Trade and Industry
Tanashi, Tokyo, Japan 188

Abstract

Preliminary experiment on dynamic response of OTEC power system, evaluation of the noncondensible gas effect and the performance tests of the several kinds of the enhanced heat transfer surfaces have been carried out with ETL-OTEC-II (small scale OTEC power generation test facility) as a part of the OTEC System characteristics study.

The power system responses due to the surface water temperature changes and the step changes of the warm and cold water flow rates were experimentally obtained.

In the experiment on the noncondensible gas effect, the measurement showed that the air concentration ratio of only 0.1 wt% highly affects the performance of the OTEC power system, so that it is suggested that the noncondensible gas concentration ratio should be kept to be less than 0.05 wt% for the condenser.

The test results on the new porous surfaces made of metal fiber at the evaporator and the double fluted tube with drain collars at the condenser with ETL-OTEC-II test facility using Freon 114 as a working fluid indicated that substantial gain could be obtained by them as compared with powder coating surface and conventional double fluted surface, respectively.

The small heat exchanger test facility is introduced, which has been constructed at ETL in order to confirm the heat transfer performance with ammonia and Freon 22. Several kinds of heat transfer surfaces to be tested are discussed.

Introduction

It is necessary to clarify the OTEC power system characteristics from the various aspects in order to establish the precise design method and the most efficient control method of an OTEC power system. In ETL the system characteristics have been clarified with ETL-OTEC-II experimental facility, which featured all major components of OTEC power system.[1]

The effects of the temperature difference, the temperature range and the warm and the cold water flow rates on the system performance were experimentally studied at the steady state. The characteristics of the heat exchangers and also the interaction between the performance of the evaporator and that of the condenser were detected in the OTEC power generation. The OTEC power cycle was simulated with a closed loop model, and the mutual relation among major system variables was obtained theoretically.

As the various factors; for example, noncondensible gas concentration, lubricating oil concentration, water concentration and so on, affect OTEC power system performance, their sensitivity should be investigated to grasp more precise system characteristics. In order to get the information on the most efficient control, the dynamic response of the OTEC system should be clarified.

The present work adresses some preliminary experimental results on dynamic response, noncondensible gas effect, and the performance tests of enhanced heat transfer surfaces.

Preliminary experiments on dynamic responses with ETL-OTEC-II

As the input conditions unexpectedly and uncontrollably change and also the palasitic loss should be supressed as possible, the peculiar control system is required for an OTEC power system. Offshore of Osumi islands and Toyama bay are selected as the representative OTEC sites in Japan.[3] The maximum changes in the surface water temperature through a year are 8.45°C at Osumi and 11.84°C at Toyama, even through the minimum available temperature difference is adopted 15.0°C in the case of Toyama.

According to the measurement, the dialy variations of the surface layer water temperature are about 1.5 - 2.5°C in August near Kyushu as shown in Fig. 1. It means that the temperature difference varies about 7 - 12 % on the base of the designed overall temperature difference $\Delta T = 21°C$. As the power output is strongly sensitive to the overall temperature difference, the power output is estimated to change by 1.14 - 1.25 times. The changes in the temperature suddenly happen sometimes.

The preliminary experiment was carried out with ETL-OTEC-II to get dynamic characteristics of the system prior to the theoretical works. The dynamic behaviors of the system due to the step changes of warm water temperature and of warm and cold water flow rates were detected. The responses of the gas temperature at the evaporator and the condenser, power output and other system variables were detected under the constant rotation speed of the turbine. The rotation speed of the turbine was kept 3600 rpm constant by the control of electric loads through the experiment. In order to obtain the instantaneous measurement, pressure and temperature were measured by semiconductor pressure detector and

* Chief, Ocean Energy Section
** Chief, Energy Conversion Section

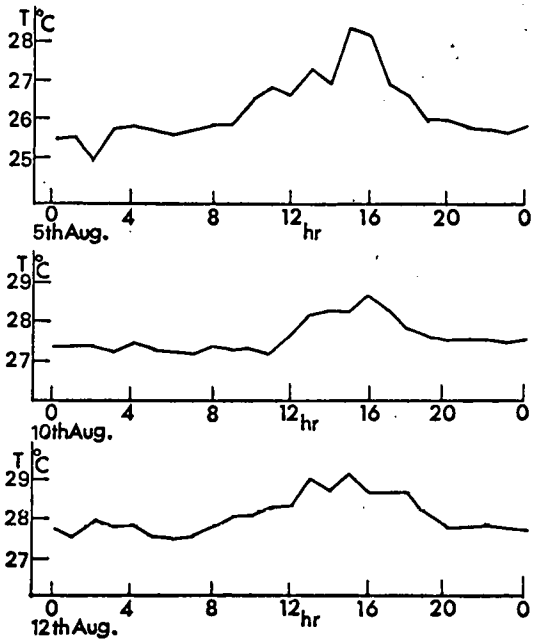

Fig. 1 The surface water temperature change near Kyushu, southern part of Japan

platinum resistance therometer, respectively.

Experimental results

In the experiment each step change was independently applied to the system to clarify each dynamic characteristic. For real control system all variables are systematically changed to respond the variation in the inlet temperature and external electric loads in order to get the most efficient operation of the overall power system.

The system responses to the change of the inlet warm water temperature were examined. The sharp

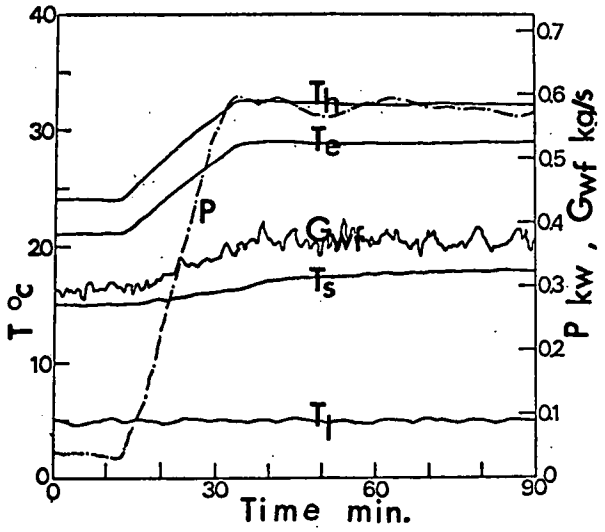

Fig. 2 System response to the increasing change of warm water temperature, where Th and Tl are warm water and cold water temperature, respectively.

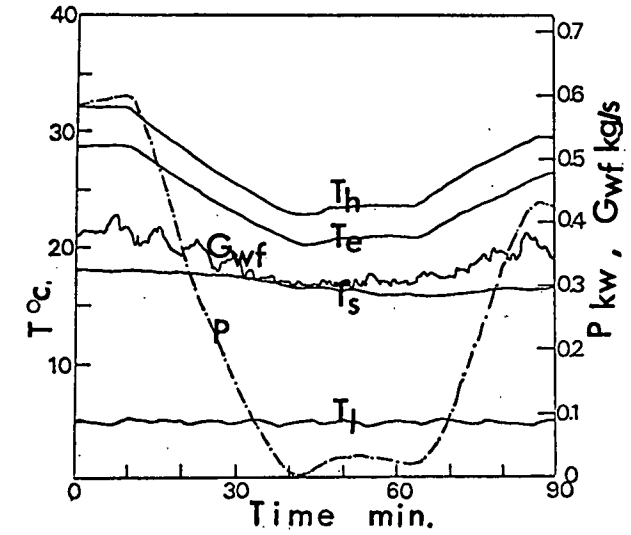

Fig. 3 System response to the decreasing change of warm water temperature

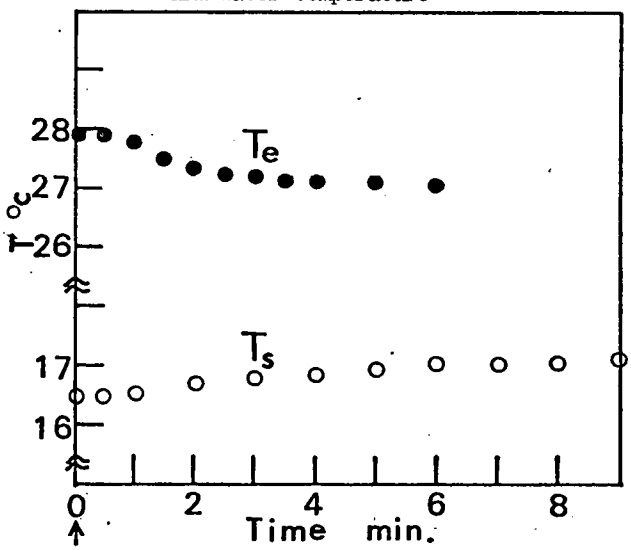

Fig. 4 System response to the decreasing step change of water flow rate for both warm and cold water

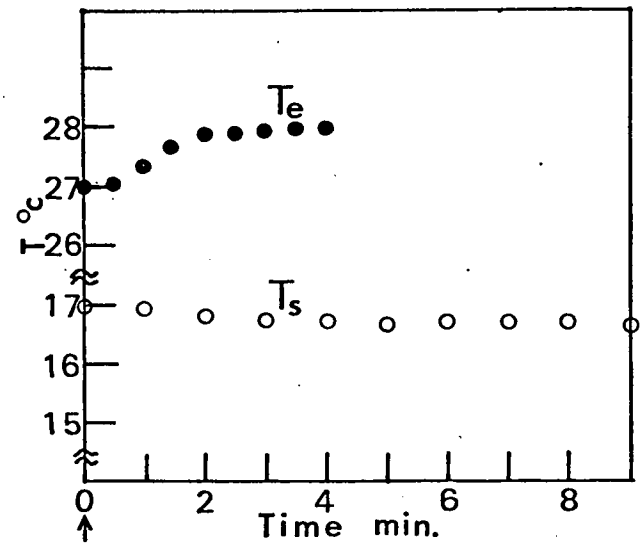

Fig. 5 System response to the increasing step change of water flow rate for both warm and cold water

step change could not apply in the cause of unsatisfactory heat supply system. After the system reached to the steady state at the warm water temperature 24°C, the inlet warm water temperature was varied to 32°C at the rate of 0.4°C/min. The power output P, the outlet temperature T_E at the evaporator, the inlet temperature T_S at the condenser and working fluid flow rate Gwf were measured as shown in Fig. 2. The power output sensitively followed with the variation of the inlet temperature. The response of the working fluid flow rate was slightly delayed. The gas temperature at the outlet of the evaporator and at the inlet of the condenser required longer time to reach to the steady state. The delay times were about 60 sec. and 120 sec. at the evaporator and the condenser, respectively. After the system reached to another steady state at the warm water temperature 32°C, the inlet warm water temperature was decreased to 24°C at the rate of 0.27°C/min. The same system variables were measured as shown in Fig. 3. These results showed that even though the apparent power output followed with the variation, the response of the gas temperature indicated that the system was actually transient. The power level seemed to be unstable for a while after the warm water temperature reached to the steady state.

The system responses to the step change of the both warm and cold water flow rates were examined. The water flow velocity was changed from 2.56 m/s to 1.42 m/s at the evaporator and from 2.69 m/s to 1.42 m/s at the condenser. The set-up and set-down time were about 10 sec. The dynamic responses of the gas temperature at the outlet of the evaporator and at the inlet of the condenser are shown in Fig. 4 and 5. Resultant change width in the gas temperature depends on the heat exchanger performance. The effect of the water flow rate on the heat exchanger performance in the evaporator is more sensitive than in the condenser. The time constant of the gas temperature at the evaporator was about 100 sec., while the response of the gas temperature at the condenser was rather insensitive. The pressure measurement at the condenser indicated that the condensation pressure reached to the steady state after 20 sec.

Noncondensible gas effect on power system performance

It is well known that the noncondensible gas degrades the performance of the condenser. Paticularly, in OTEC power plant the degradation might affect the whole power system performance, because the temperature difference for heat transfer is comparable to the temperature drop for efficient work. Therefore, the noncondensible gas effect on the power system performance was experimentally examined with ETL-OTEC-II experimental facility. In the experiment a certain amount of air was artificially injected into the condenser in sequence. After each 30 min.-operation to reach to the steady state, the power system performance was measured. The air concentration ratio was measured by gas chromatography. The sample gas was extracted from both the top and bottom positions of the condenser.

Experimental results

According to the measurements of air concentration ratio at two positions, it was clarified that the air concentration ratio at the bottom was larger than that at the top by 2-3 times. The condensation temperature, power output, heat duty in the condenser and the evaporator, and overall heat transfer coefficient at the condenser varied with the air concentration ratio as shown in Fig. 6 and 7. For example, if the air concentration ratio is 0.1 wt%, the power output decreases by 13.8 % and the overall heat transfer coefficient degrades to 75 %. For the OTEC power plant the permissible noncondensible gas concentration ratio is consequently suggested to be less than 0.05 wt%.

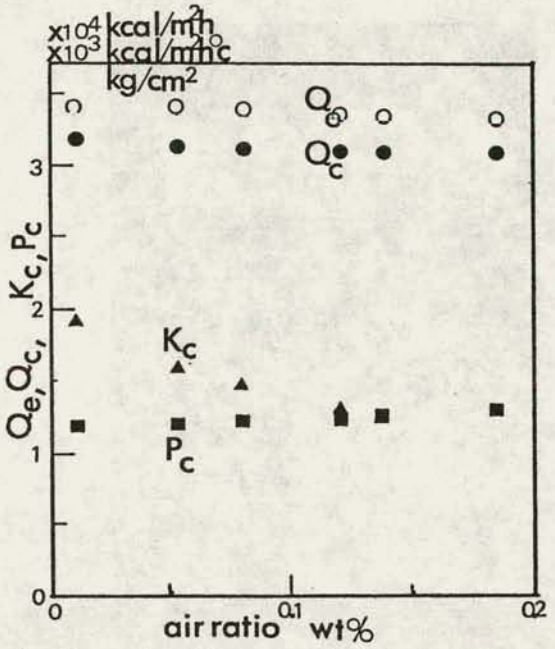

Fig. 6 Noncondensible gas effect on heat duty, heat transfer coefficient and condensation pressure.

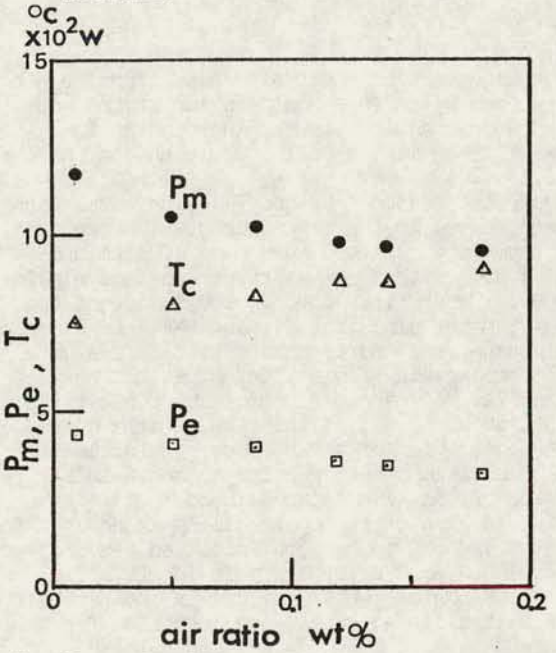

Fig. 7 Noncondensible gas effect on power output and condensation temperature, where Pm, Pe and Tc are mechanical power output, electrical power output and condensation temperature, respectively.

Fig. 8 Micrographic crosssectional view of metal fiber coated tube

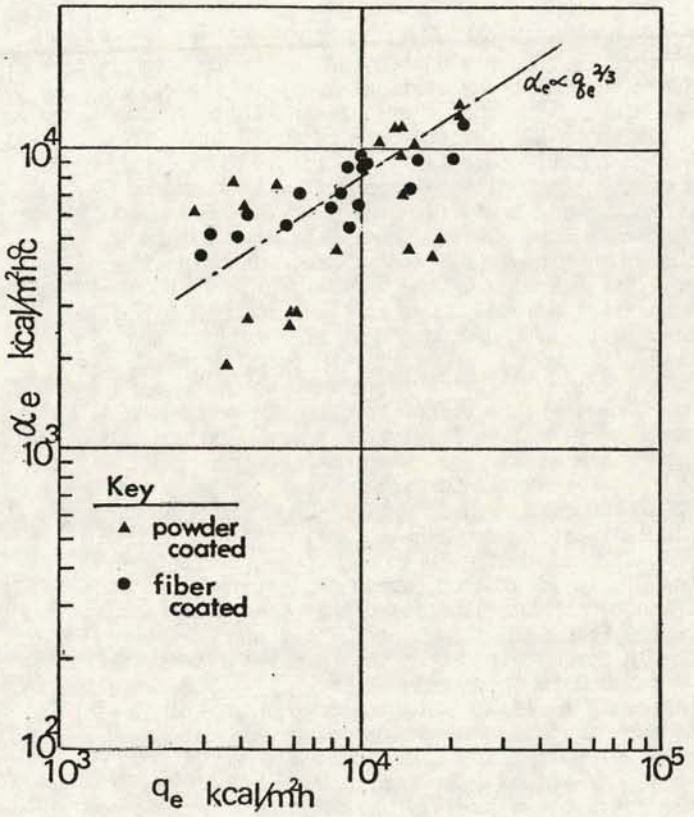

Fig 9 Heat transfer performance for two kinds of porous evaporating surface

Enhancement of heat exchanger performance

Evaporator

The enhancement of shell side heat transfer has been achieved by surface modification of the tube. One of the approach for the enhancement of an evaporator is to make a nucleation enhancing porous surface.

The surface coated tube and FMF(Fine Metal Fiber) tube were tested in the experiments. The surface coated tube is the fluted tube made of aluminum (A6063) coated with a porous copper surface similar to HYFLUX. Water flows through the inside of the tubes, which are also fluted. The FMF tube is made of stainless steel and is coated with a fine metal fiber on the working fluid side. The thickness of the fiber layer is about 0.3 mm. The porocity is estimated about 50 %. As the results of a micrographic observation of the surface, the nucleation enhancing positions were regular as shown in Fig. 8. The inside of the tube is unenhanced.

In a half part of the pool boiling evaporator for ETL-OTEC-II 24 FMF tubes were installed, each of which was 20.0 mm O.D. by 1.8 m in length. Two kinds of FMF surface were tested. In another half part 24 coated fluted tubes were installed for the reference.

Experimental results in the evaporator

The water flow rate and inlet and exit temperature for each tube were individually measured. The overall heat transfer coefficient K_E was obtained from the heat duty calculated by the water flow rate and the difference (Ti-To) between inlet and exit water temperature of the tube and the log mean temperature difference θm. Each temperature was measured by thermister and data were recorded by the data acquisition system.

$$K_E = Gh\ (Ti-To)/A/\theta m \qquad (1)$$

where Cp, Gh, A are heat capacity, water flow rate and heat transfer area respectively. The evaporating temperature was determined by averaging the gas and saturated liquid temperature at four points in the evaporator. The water side heat transfer

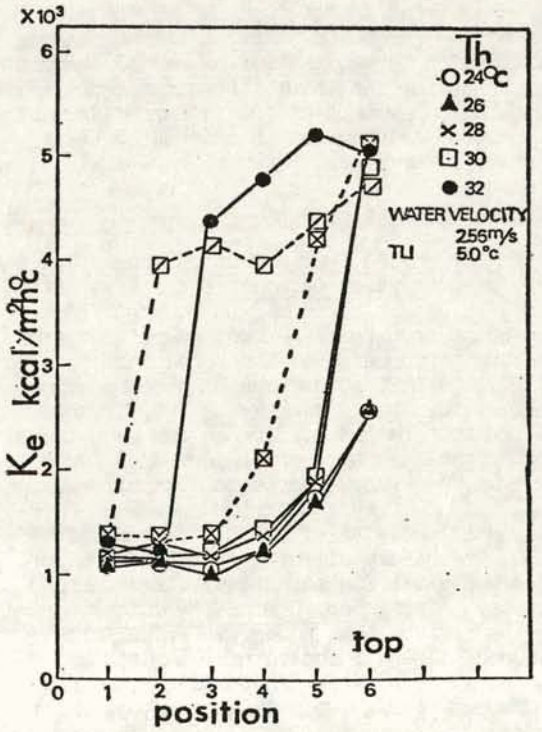

Fig. 10 Distribution of evaporating heat transfer coefficient in the shell for powder coated tube, where Th is a warm water temperature and T_{LI} is a cold water inlet temperature.

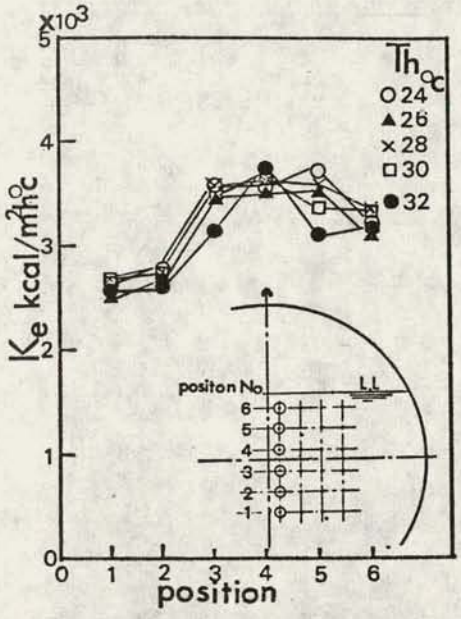

Fig. 11 Distribution of evaporating heat transfer coefficient in the shell for FMF tube, where Th is a warm water temperature and T_{LL} is kept 5°C constant.

coefficient was determined by Colburn's equation.

$$Nu = 0.023\ Ref^{0.2}\ Rem\ Prf^{1/3}\ Prm \qquad (2)$$

where subscript f and m represent that fluid properties are evaluated at a film temperature and at the averaged fluid temperature, respectively. In the case of FMF tube, thermal conductance at the wall was added in the calculation because of low thermal conductivity of stainless steel, while in the case of coating tube the effect of wall thickness was neglected.

The results of the experiment are shown in Fig. 9. The relation between heat flux ge and evaporating heat transfer coefficient e is represented in the figure. It can be seen that FMF surface has almost the same performance as a powder coating surface.

On the other hand, the results of the distribution of the performance in the evaporator were peculiar as shown in Fig. 10 and 11. It seem that the vertical profiles of the performance at coating tube vary with the temperature difference and the heat duty, in paticular, the bubble density near the surface of the tube. Fig. 11 shows that the distribution of heat transfer performance is rather uniform at FMF tube. This tendency was obtained in every row of the tubes.

Condenser

It is considered that the fluted surface is one of the most promising surface as the enhancement of the condensation heat transfer for an OTEC power system. The number of related research has been increasing in OTEC Conference[4,5]. In the research on a fluted surface the optimization of the covex surface and the design of the drainage groove are essential. It should be noted as often pointed out that operation at a longer fluted tube causes flooding of the drainage channel with decreasing the overall heat transfer performance.

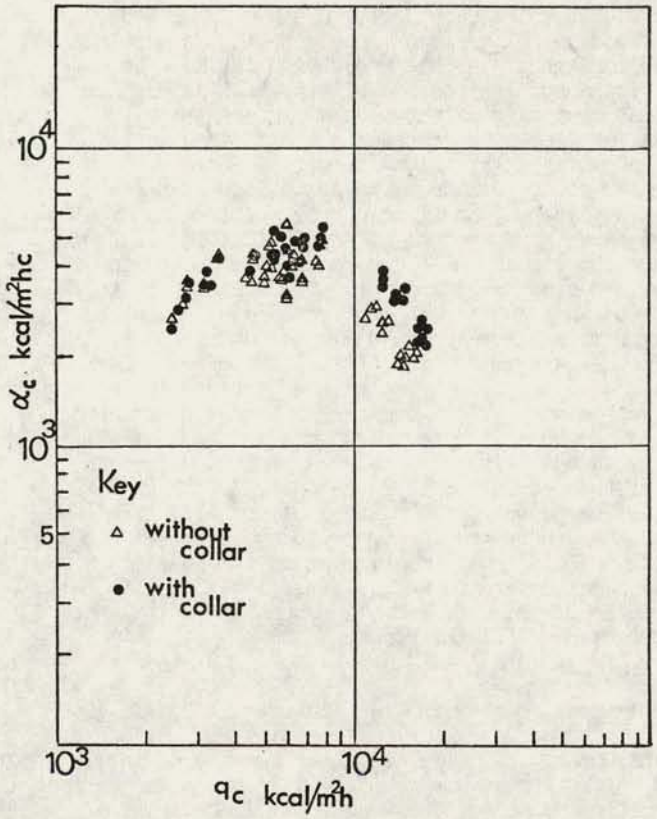

Fig. 12 Heat transfer performance for fluted surface

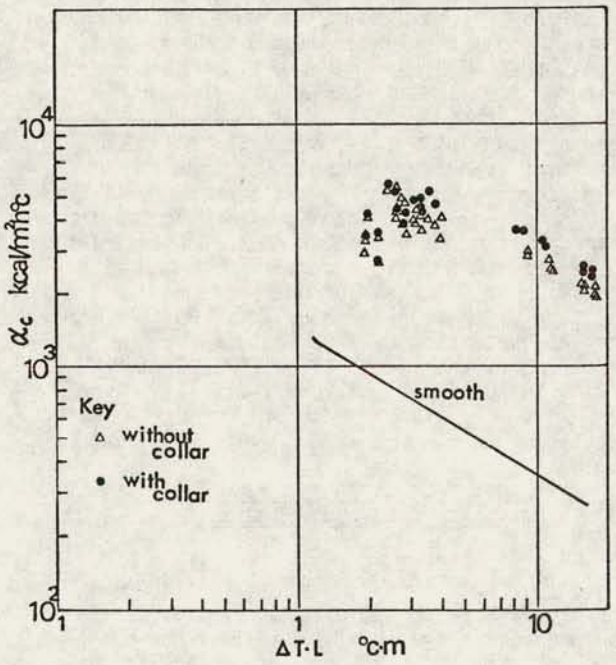

Fig. 13 Heat transfer coefficient vs $\Delta T \cdot L$ for fluted tube with and without drainage collars: $\Delta T (= Tc - Tw)$ is the temperature difference between condensate temperature and wall temperature, and L is a tube length.

In order to overwhelm this defect the fluted tube with the drainage collar has been proposed[1]. The drainage collar accumulates the liquid working fluid condensated at the upper part of the tube and discharged it from the exit of drainage collar, so that most part of the fluted surface below the collar is kept to be renewal. The drainage collar was made of thin stainless steel. The outer diameter of the collar is the same size as the outer diameter of the fluted tube. This means that there is nothing speical at the fablication of the heat exchanger and also does not cause increasing the vapor side pressure drop. The fluted tube reported in the 5th OTEC Conference has 72 flutes, 20 mm nominal diameter, and 2.4 m length.

In the experiment each of the fluted tubes with drainage collar has three drainage collars in the two path condenser. A drainage collar was attached at the center of the on-going tube and two collars were attached at the 1/3 and 2/3 positions from the top of the return tube. Each 6 pairs of fluted tube with and without drainage collars was installed in the condenser. In order to avoid the effect of the position on the performance, the positions of each pair of tubes were diversified. The procedure of the data reduction was similar to that in the evaporating performance.

Experimental results in the condenser

The experiments were made over a range of inlet cold water temperature of 4°C - 11°C and a range of water flow velocity of 2.7 m/s - 0.71 m/s. The temperature difference and water flow rate were measured for each tube. The area derived from the nominal outer diameter of the tube in the calculation of the heat transfer coefficient on the working fluid side. The data were averaged to minimize the error due to the position of the tube and time. The experimental results presented in Fig. 12 indicate that the performance at the fluted tube with drainage collars is slightly better than at the fluted tube without collar. The drainage collar effect is shown in Fig. 13, where the relation between heat transfer coefficient and the temperature difference by tube length is presented. The attachment of collar without special effort being made to optimize the position and the number of the collar was found to have a better performance by about 1.2 times than that of the perfomrance at the fluted tube without drainage collar. Further experiments and evaluation will be made as for the optimization of the overall longer fluted tube including the drainage collar effect.

Single tube heat exchanger test facility for ammonia and Freon 22

Experimental facility

The experiments on the system characteristics and the heat exchanger performance have been carried out with Freon 114 as the working fluid in ETL-OTEC-II , because handling Freon 114 is easy. The system characteristics on a closed cycle type low temperature difference power plant such as an OTEC power plant have been clarified by not only experiments but also theoretical model simulation[1]. The importance of the enhancement of heat exchangers has been recognized in the system. The major candidate of the working fluid for a commercial scale

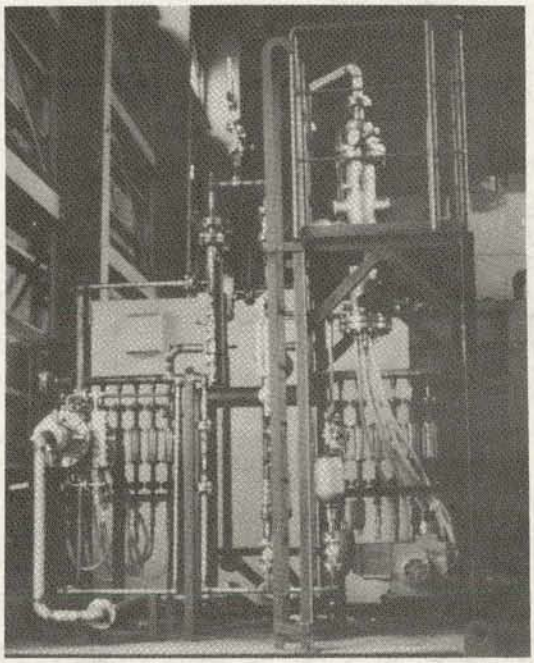

Fig. 14 Single tube heat transfer test facility

OTEC power plant is considered to be ammonia according to the results by OTEC Committee in Japan reported in the fifth OTEC Conference[6]. Therefore, at least the experiment on the heat transfer characteristics with ammonia should be achieved to obtain the more precise data for ammonia cycle OTEC power plant. The small scale heat exchanger test facility with ammonia or Freon 22 (R22) has been constructed at Electrotechnical Laboratory. The objectives of this facility are as follows:

(1) To confirm the relation between the single tube heat transfer performacne and the heat exchanger performance in the OTEC system.
(2) To determine the heat transfer coefficient of The single evaporating and condensation tube or plate with ammonia and Freon 22.
(3) To achieve the enhancement of heat transfer on the ammonia side.

This facility, as shown in Fig. 14, encompasses a closed warm water loop, a closed ammonia cycle (or Freon 22 cycle) and a closed cold water loop. The ammonia cycle features a demister, a relief valve, an expansion valve, a buffer tank(which can be modified to a spray desuperheater), a liquid return pump, a storage tank and the test evaporator and condenser, which are shell and tube-type heat exchangers in a present stage and also are intended to be tested plate-type in the future.

The heat duty ranges from about 3 kw to about 10 kw. The water is heated by electric heater and the temperature adjustment is achieved by SCR control. The supply sytem can supply over a range of warm water temperature of 20-35°C. The system is capable of maintaining the temperature stable within better than $\pm$ 0.1°C. The water flow velocity in the tube is over a range of 0.5-3.0 m/s. The total maximum water flow rate is 17.5 m^3/h. The supply system of a cold water has a similar capacity. The chiller combined with electric heater system is adopted in order to achieve the accuracy of the cold water temperature within $\pm$ 0.1°C. In the ammonia loop the maximum working fluid flow rate is 20.0 kg/h in an ammonia cycle and 120.0 kg/h in a Freon 22 cycle.

Instrumentation

Temperature, flow rates, and pressures are measured in each of heat exchanger tubes and each of the three loops. In order to achieve the accurate measurements characterizing the performance of the heat exchangers within ± 3 %, fine differential temperature-volt converter is instrumented. Pressure is detected by the semiconductor pressure detector and pressure gauges. The test facility has a computer based data acquisition system. The ammonia droplets are caught at the demister and returned to the evaporator as a liquid stream from the bottom of the demister vessel via the volume measurement section at a certain interval in order to detect the quality of the vapor.

Test heat exchangers

At a present stage the test heat exchangers are considered to be shell and tube-type. Each of them consists of seven tubes, whose diameter is 20.0 mm O.D.. The 60° pitch for both heat exchangers is adopted. The ratio of pitch to tube diameter is 1.5. For the evaporator the length of the tube is 0.8 m and the total heat transfer area based on the outer diameter is 0.352 m^2. For the condenser the length of the tube is 1.0 m and the total heat transfer area is 0.440 m^2 based on the nominal diameter.

There are provided five heat transfer surfaces including three kinds of evaporating and two types of a fluted. These include the following:

1. The coating tube is the fluted tube made of aluminum coated with a porous nickel and with a porous stainless steel. The micrographic crosssectional view of the surface is shown Fig. 15 as an example.
2. Another coated tube is the smooth tube made of stainless steel coated with a fine metal fiber in order to get the uniform porous surface. The thickness of the fiber is about 0.3 mm. In the future the thickness of the layer and the size of the fiber are intended to be varied in order to obtain the optimum performance, because the porosity of the surface can be controlled in that surface.
3. The porous surface made by the chemical process is presented. Preliminary single tube experiment and the micrographic crosssectional view as shown in Fig. 16 indicated the possibility of the high performance. According to this approach it is possible to control the surface roughness.
4. The double fluted tube made of aluminum (A6063) is presented. The fluted tube is the same shape and pitch as the one which has been experimented with ETL-OTEC-II experimental facility.
5. Another double fluted tube is made based on the optimization process[5]. The micrographic crosssectional view is shown in Fig. 17. As the designed shape must be constructed accurately, the tube material is adopted A1050S.

The measured performance will be used to evaluate analytical methods for designing heat exchangers in connection with the data obtained in the system experiments at ETL-OTEC-II facility.

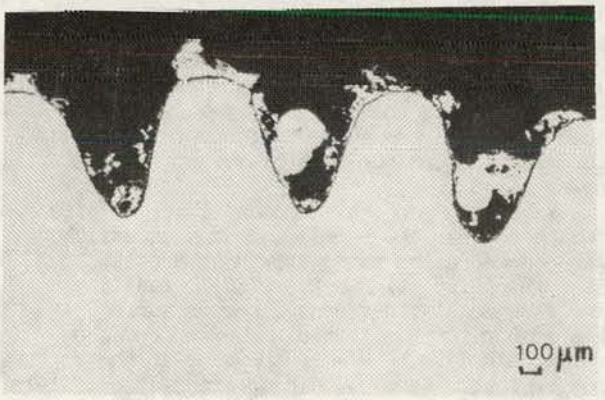

Fig. 15 Micrographic crosssectional view of coated fluted surface

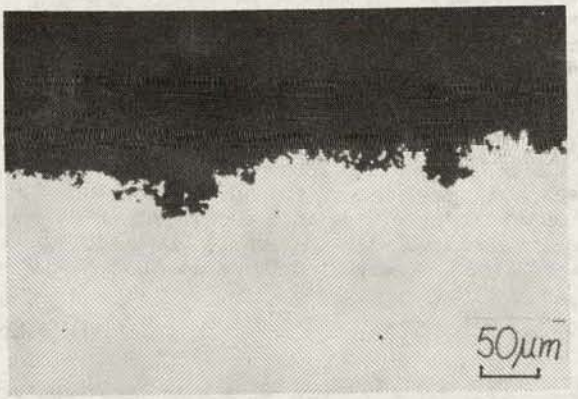

Fig. 16 Micrographic crosssectional view of chemically treated tube

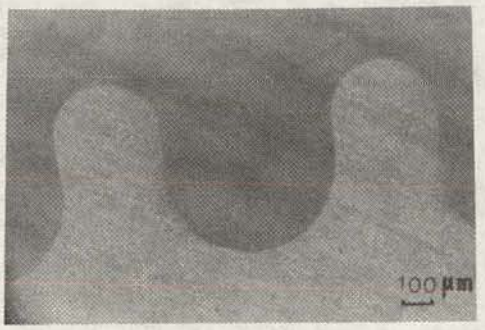

Fig. 17 Micrographic crosssectional view of fluted tube

Conclusions

The conclusions are offered as follows:

(1) In order to clarify the OTEC power system characteristics, preliminary experiments on the dynamic behavior in ETL-OTEC-II were carried out.
The responses of system variables to the step change of input conditions were investigated to get each dynamic characteristic.
The results presented in this paper are primitive and should be regarded as approximate.
The response to the change of bypass working

fluid flow rate, the responses to the sharp change of the inlet temperature simulating real condition, the dependency of change width and the response to the change of the external load should be the subjects for a future study to offer the optimum control system for OTEC power plant.

(2) The experiment on the noncondensible gas effect indicated that the permissible noncondensible gas concentration ratio should be kept to be less than 0.05 wt% for ETL-OTEC-II facility.

(3) The fine metal fiber coated porous surface at the evaporator was tested. The performance was obtained to be almost the same at the powder coated tube. The heat transfer coefficient was about 10000 kcal/m^2h°C. The results are sufficient encouraging to pursue the optimization of the surface and the manufacture for OTEC application.

(4) The effect of drainage collar was confirmed in the experiment. The enhancement of the heat transfer performance was about 1.2 times in comparison with the fluted tube without drainage collar. The experiment by using longer fluted tube should be necessarily tested as a next step.

(5) The single tube heat exchanger test facility for ammonia and Freon 22 constructed at Electrotechnical Laboratory and the line-up enhanced surfaces were introduced. These results combined with the results in the OTEC power system are expected to be useful to achieve the precise system design for a large scale OTEC power plant.

Acknowledgement

The authors express the appreciation to Dr. T. Todoroki, Chief of Energy Division in ETL, who gave much encouragement in this study. Moreover, they also express the gratitude to Dr. H. Kamogawa in Toshiba Elec. Co., on this study. The research is financially supported by the Sunshine Project in AIST, MITI.

References

1. T. Kajikawa etal ; Proceedings 5th OTEC Conference, v164 - v198, Miami, Florida, Feb. (1978)
2. S. A. Hetyei and C. P. Newman ; Report:NSF/RANN /SE/GI-39114/PR/75/7 (1975)
3. T. Homma etal ; Presented at 6th OTEC Conference, Washington D.C. June (1979)
4. R. R. Rothfus and G. H. Lavi ; Proceedings 5th OTEC Conference, v190 -v1110, Miami, Florida, Feb. (1978)
5. R. L. Webb ; Proceedings 5th OTEC Conference, v1123 - v1145, Miami, Florida, Feb. (1978)
6. T. Homma and H. kamogawa ; Proceedings 5th OTEC Conference, v91 - v116, Miami, Florida, Feb. (1978)

DISCUSSION

R. Webb, Penn State University: Could you comment on how the fine metal fiber was attached to the tube, and the possible cost difference between that and the porous coated tube?

T. Kajikawa: This surface is made by attaching the fibers on the metal under high temperatures. We can not estimate cost because the surface is not in production at the present stage; it's comparable with the porous coated tubes.

Question: Have you considered the use of the Hitachi surface in either the boiler or the condenser?

T. Kajikawa: I am very interested in that surface, but we haven't carried out any experiments.

N. Sather: Could you say a little more about the chemical process used to produce the porous surface in the picture that you presented? Is that a commercial surface?

T. Kajikawa: No. It is produced by the modified etching process.

FLOW-INDUCED VIBRATION IN SHELL-AND-TUBE HEAT EXCHANGERS FOR OCEAN THERMAL ENERGY CONVERSION (OTEC)

J. J. Lorenz and D. Yung

Argonne National Laboratory
Argonne, Illinois 60439

Abstract

The problem of crossflow-induced vibration in shell-and-tube heat exchangers for OTEC is considered. Models of the dominant excitation mechanisms are discussed: vortex shedding, turbulent buffeting, fluidelastic instability, and acoustic excitation. Criteria are presented for assessing vibration and equations are derived for predicting the maximum allowable span length as a function of crossflow velocity and other system variables. Also regions of acoustic resonance and noise are defined. Among the system variables studied are tube diameter, tube material, tube-field layout, and pitch-to-diameter ratio. All models are presented in a simple form that can readily be applied to the mechanical design of OTEC heat exchangers.

Nomenclature

c	speed of sound, m/s
D	tube outer diameter, m
D_i	tube inner diameter, m
E	modulus of elasticity, N/m^2
f_a	acoustic frequency, 1/s
f_n	natural frequency (fundamental mode), 1/s
f_t	dominant buffeting frequency, 1/s
f_v	vortex shedding frequency, 1/s
g	gravitational acceleration, m/s^2
g_c	gravitational coefficient, 1 $kg \cdot m/N \cdot s^2$
I	cross-sectional moment of inertia, m^4
ℓ	longitudinal tube pitch, m
L	tube span length, m
L_{max}	maximum allowable tube span length, m
m	mode number
P_s	system pressure, N/m^2
P/D	pitch-to-diameter ratio
Re	Reynolds number
S_v	Strouhal number, Eq. (4)
t	transverse tube pitch, m
V	crossflow velocity in transverse gap, m/s
V_c	critical velocity for fluidelastic instability, m/s
W_e	effective mass per unit length, kg/m
W_m	mass of tube per unit length, kg/m
W_s	added mass due to shell-side fluid per unit length, kg/m
W_t	mass of fluid inside tube per unit length, kg/m
Y	characteristic length, m
β	instability threshold constant
δ_o	log-decrement of the tube in still fluid
ζ	constant, Eqs. (5) and (8)
ρ_s	density of shell side fluid, kg/m^3

Introduction

Flow-induced vibration in heat exchangers is a potential cause of acoustic noise and mechanical failure of tubes. Failure can result from fatigue, wear, collision of tubes, cutting at baffles, and leaks at tube joints. It has been found that tube vibration can also lead to an increased shell-side pressure drop. Over the years, numerous methods have been developed for predicting flow-induced vibration in shell-and-tube heat exchangers [1-11], and a number of excellent reviews have been published [12-14]. However, at the present time a complete solution to the problem is unavailable.

The present work considers crossflow-induced vibrations in shell-and-tube heat exchangers for Ocean Thermal Energy Conversion (OTEC). Here the shell-side fluid is a vapor, such as ammonia, and the tube-side fluid is seawater. (Flooded-bundle evaporators are not considered.) The purpose of this paper is to assess the problem of flow-induced vibration in light of existing predictive methods. Models of the dominant excitation mechanisms are discussed: vortex shedding, turbulent buffeting, fluidelastic instability, and acoustic excitation. Criteria are presented for assessing vibration and equations are derived for predicting the maximum allowable span length as a function of crossflow velocity and other system variables. Also, regions of acoustic resonance and noise are defined. Among the system variables studied are tube diameter, tube material, tube-field layout, and pitch-to-diameter ratio. All models are presented in a simple form that can readily be applied to the mechanical design of OTEC heat exchangers.

Methods for Predicting Flow-Induced Vibration

Natural Frequency of Tube Vibration

Before discussing the various excitation mechanisms, the vibration characteristics of a tube will be considered. For conservatism (and simplicity) in vibration calculations, it is common practice to consider only the fundamental mode of tube vibration. The natural frequency (fundamental mode) of a uniform tube with equal span lengths and simple supports is [15]:

$$f_n = \frac{\pi}{2L^2}\sqrt{\frac{EIg_c}{W_e}} \quad (1)$$

where f_n is the natural frequency; E is the modulus of elasticity; I is the cross-sectional moment of inertia; L is the tube span length; W_e is the effective mass per unit length; and g_c is the gravitational coefficient.

The cross-sectional moment of inertia I is calculated from:

$$I = \pi (D^4 - D_i^4)/64 \quad (2)$$

where D and D_i are the tube outside and inside diameters, respectively. The effective mass per unit length W_e is defined as:

$$W_e = W_m + W_t + W_s \quad (3)$$

where W_m is the mass of tube per unit length; W_t is the mass of fluid inside tube per unit length; and W_s is the added mass per unit length for shell-side fluid. For a single cylinder in an infinite fluid, $W_s = \rho_s \pi D^2/4$, where ρ_s is the density of the shell-side fluid. In a tube bundle, the effect of adjacent tubes tends to increase the added mass. For OTEC heat exchangers, however, the added mass term is insignificant when compared with the other terms because the shell-side fluid is a vapor. (The mass of the thin liquid film and droplets on the shell-side is negligibly small.)

In general the natural frequency depends on the end conditions, number of spans, and type of intermediate supports. Equation (1) is strictly valid only for simply supported ends, but is a very good approximation even for clamped ends when the number of spans is greater than about 7, see Ref. [14]. The natural frequency is weakly dependent on tube-to-baffle hole clearance [16]. Clearance is important in that it has a strong influence on system damping.

Vortex Shedding

Excitation by vortex shedding has been studied extensively by Chen [1]. The vortex shedding frequency is given by the following expression:

$$f_v = \frac{S_v V}{D} \quad (4)$$

where S_v is the Strouhal number; V is the velocity (free stream for single tube and transverse gap for tube banks); and D is the tube outer diameter. When the vortex shedding frequency is near the natural frequency of the tube, resonance occurs and large amplitude vibrations are possible. The frequency of vortex shedding from a single cylinder has been investigated by a great number of authors, see review by Chen [1]. The Strouhal number remains nearly constant with a value of 0.20 in the Reynolds number range of 300 to 2×10^5. Vortex shedding in a heat exchanger tube bank is considerably more complicated than vortex shedding behind isolated cylinders. For a tube bank, the Strouhal number depends on the tube arrangement. Tube fields are generally laid out with equilateral pitches in either square or triangular arrays. The most common arrangements are 30°-triangular, 60°-triangular, 45°-square, and 90°-square. Figure 1 shows a plot of Strouhal number versus pitch-to-diameter ratio constructed by Chenoweth [14] from the data of Chen [1]. Unfortunately, Chen obtained little data at the smaller pitch-to-diameter ratios of interest to OTEC. At small P/D values the curves in Fig. 1 were obtained essentially by extrapolation and, therefore, should be regarded as approximate. Recent studies by Chen [2,3] have indicated that for small P/D values the excitation mechanism changes from vortex shedding to other mechanisms such as wake swing, jet swing, and jet instability. Moreover the dynamic forces associated with these latter mechanisms are smaller than those associated with vortex shedding. In the present study where the P/D values are relatively small, we will nevertheless refer to the excitation process as vortex shedding even though we recognize that other mechanisms may come into play.

For a tube bank, the velocity term in Eq. (4) is the transverse gap velocity and not the diagonal gap velocity. This is in contrast to the practice employed for heat transfer and pressure drop calculations. Although the transverse gap velocity is commonly used for flow-induced vibration calculations, investigators have considered other possible definitions [12,14]. When the vapor crossflow is not truly perpendicular to the transverse gap, which typically occurs in heat exchangers experiencing radial inflow or outflow, there is no universally accepted definition of velocity for flow-induced vibration calculations. For this situation it is suggested that the designer conservatively assume that the entire crossflow is directed perpendicular to the gap.

Vibration can occur if f_v/f_n is greater than some constant ζ. The condition for the onset of vibration is then:

$$\frac{f_v}{f_n} = \zeta \quad (5)$$

Chenoweth [14] compared experimental data with predictions using $\zeta = 0.5$ and $\zeta = 1.0$. For heat exchangers with vapor on the shell-side, their study indicated that $\zeta = 1$ yields the best agreement with experimental data from TEMA and HTRI data

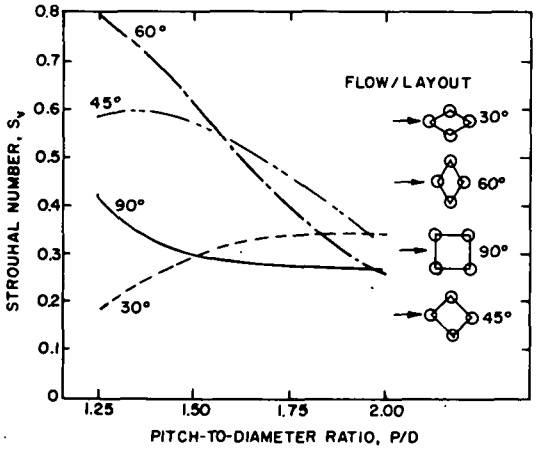

Fig. 1 Strouhal number for different tube field layouts (from Ref. [14]).

banks. Further comments on the selection of ζ will be given later. Upon substituting Eqs. (1) and (4) for f_v and f_n into Eq. (5) and letting $\zeta = 1$, the following expression for the maximum allowable span length, L_{max}, is obtained after some rearrangement:

$$L_{max} = \left(\frac{\pi}{2}\right)^{1/2} \left(\frac{D}{S_v}\right)^{1/2} \left(\frac{EIg_c}{W_e V^2}\right)^{1/4} \tag{6}$$

where S_v is determined from Fig. 1 for a given tube arrangement and P/D ratio. Reliable heat exchanger design requires that the span length be less than L_{max} to avoid tube vibration.

Turbulent Buffeting

For closely packed tube banks Owen [4] abandoned the idea of a coherent vortex shedding process. Instead, he considers a spectrum of turbulence with a dominant frequency which is proportional to the average flow velocity within the bank. Owen [4] gives the following equation for the dominant turbulent buffeting frequency, f_t:

$$f_t = \frac{VD}{\ell t}\left[3.05\left(1 - \frac{D}{t}\right)^2 + .28\right] \tag{7}$$

where V is the transverse gap velocity; ℓ is the longitudinal tube pitch; and t is the transverse pitch, see Fig. 2.

Following the logic of the preceding section, the criteria for the onset of vibration is given by:

$$\frac{f_t}{f_n} = \zeta \tag{8}$$

Again the constant ζ is set equal to unity. Upon substituting Eqs. (1) and (7) for f_t and f_n into Eq. (8), the following expression for maximum allowable span length L_{max} is obtained after rearrangement:

$$L_{max} = \left(\frac{\pi}{2}\right)^{1/2} \left(\frac{\ell t}{D\theta}\right)^{1/2} \left(\frac{EIg_c}{W_e V^2}\right)^{1/4} \tag{9}$$

where $\theta = 3.05\left(1 - \frac{D}{t}\right)^2 + 0.28$ (9a)

Fluidelastic Instability

Connors [5] identified a fluidelastic instability which occurs when the work done on the tube system by the fluid exceeds the energy dissipated by system damping. When a critical velocity is exceeded the tubes vibrate in an orbital or whirling manner. Connors [5] gives the following equation for the critical velocity, V_c, beyond which fluidelastic whirling occurs:

$$V_c = \beta f_n D \sqrt{\frac{W_e \delta_o}{\rho_s D^2}} \tag{10}$$

where W_e is the effective mass per unit length [Eq. (3)]; f_n is the tube natural frequency; β is the instability threshold constant; and δ_o the log-decrement of the tube in still fluid. Based on the

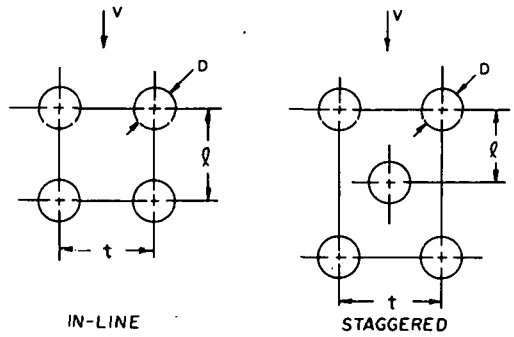

Fig. 2 Definition of pitch for turbulent buffeting model, Eq. (7).

work of Chenoweth [14], the following values were selected for heat exchangers where the shell-side fluid is a gas; $\beta = 9.9$ and $\delta_o = 0.0033$. In general the instability constant β is a function of tube-field layout, and the log decrement δ_o is a function of fluid viscosity, tube material, and bundle geometry. Unfortunately no general methods are yet available for predicting the dependence of β and δ_o on system parameters. In a recent paper, Connors [18] gives a correlation for β as a function of P/D for a 90° tube-field layout. However the correlation is valid only for pitch-to-diameter ratios in the range $1.41 < P/D < 2.12$, and is not applicable to other tube-field layouts. Until more is known about the behavior of β and δ_o, the single values from the work of Chenoweth will be employed.

The critical condition for the onset of fluidelastic whirling is when the transverse gap velocity, V, equals the critical velocity for fluidelastic instability, V_c:

$$\frac{V}{V_c} = 1 \tag{11}$$

Upon substituting Eq. (1) for f_n into Eq. (11), the following expression for the maximum allowable span length is obtained.

$$L_{max} = \left(\frac{\pi}{2}\right)^{1/2} \beta^{1/2} \left(\frac{EI\delta_o g_c}{\rho_s V^2}\right)^{1/4} \tag{12}$$

Acoustic Excitation

When the shell-side fluid is a vapor, acoustic waves can be excited by either vortex shedding or turbulent buffeting. The acoustic frequency, f_a, of a heat exchanger is given by Chenoweth [14] as:

$$f_a = \frac{mc}{2Y} \tag{13}$$

where m is the mode number; Y is a characteristic length, taken as the shell-diameter of the heat exchanger; and c is the speed of sound in the shell-side fluid, which can be approximated by:

$$c = \alpha \sqrt{\frac{P_s g_c}{\rho_s}}$$

where the constant $\alpha = 1.19$; P_s is the system pressure; and ρ_s is the density of the shell-side

gas.

If either the vortex shedding frequency or turbulent buffeting frequency is within 20% of the acoustic frequency, a loud noise can be generated within the heat exchanger shell [14]. Although mechanical damage from acoustic noise is unlikely, the sound may be intolerable and exceed OSHA safety limits. In accordance with the condition that the vortex shedding frequency or turbulent buffeting frequency should not lie within 20% of the acoustic frequency, the following equations are easily derived for the upper and lower limits on the heat exchanger shell diameter:

Vortex shedding:

$$Y = K \frac{m}{2}\left(\frac{D}{S_v}\right) \frac{c}{V} \tag{14}$$

Turbulent buffeting:

$$Y = K \frac{m}{2} \left(\frac{\ell t}{D\theta}\right) \frac{c}{V} \tag{15}$$

where K = 1.2 for the upper limits and K = 0.8 for the lower limits. Acoustic noise is probable when the heat exchanger shell diameter Y lies either within the region bounded by Eq. (14) with K = 1.2 and 0.8 or by Eq. (15) with K = 1.2 and K = 0.8. In acoustic vibration calculations it is usually sufficient to consider only the fundamental mode, i.e., m = 1.

A potentially detrimental situation can occur when the acoustic vibration is in resonance with heat exchanger tube vibration. Resonance is probable when the natural frequency of tube vibration is within, say, 20% of the acoustic frequency. This leads to the following equation for the upper and lower limits on the heat exchanger shell diameter:

$$Y = \frac{Kmc}{\pi} \left(\frac{W_e}{F.I g_c}\right)^{\frac{1}{2}} L^2 \tag{16}$$

where K = 1.2 for the upper limit and K = 0.8 for the lower limit. The mode number is again taken to be m = 1. If the shell diameter lies within the region bounded by Eq. (16) with K = 1.2 and 0.8, it is probable that resonance will occur.

When either acoustic noise or resonance is predicted, appropriate corrective measures should be taken. Generally this problem is remedied by inserting detuning plates parallel to the direction of crossflow. This changes the acoustic frequency by changing the characteristic length, but does not affect the heat transfer performance and pressure drop [14].

Other Methods for Predicting Flow-Induced Vibration

The foregoing are among the more popular methods for predicting flow-induced vibration, and will be the only ones employed in the present work. Nevertheless some of the other methods which have been developed over the years are noteworthy: Thorngren [6]; Gregorig [7]; Fitz-Hugh [8]; Walker and Reising [9]; and Brothman [10].

Results and Discussion

Chenoweth [14] examined the accuracy of the various predictive methods by comparing predictions with experimental data from TEMA and HTRI data banks. Correct predictions were defined as either when vibration was predicted where it was reported or when vibration was not predicted where it was not reported. For cases where the shell-side fluid is a gas, the following constants appear to yield the best agreement with the data: $\zeta = 1$ (vortex shedding and turbulent buffeting); and $\beta = 9.9$, $\delta_o = 0.0033$ (fluidelastic instability). Utilizing these constants, the various methods generally predict vibration where it was reported. However, the methods tend to be conservative in that they often predict vibration where it did not occur. For example, on the basis of vortex shedding and turbulent buffeting, tube vibration was predicted to occur in nearly all cases although no vibration was reported in 11 out of 20 cases in the two data banks combined. Chenoweth [14] points out that possibly a different definition of velocity is needed to improve the predictions. It is hoped that future research in flow-induced vibration will bring forth improvements in all the predictive methods.

In the previous section, equations were derived for predicting the maximum allowable tube span length based on considerations of vortex shedding, turbulent buffeting, and fluidelastic instability. Also, equations were presented for determining regions of acoustic resonance and noise. To illustrate the use of these equations consider a shell-and-tube heat exchanger having titanium or aluminum tubes in a 30°-triangular configuration with D = 2.54 cm and P/D = 1.25. Tube wall thickness for various tube diameters are specified in Table I. The two materials listed in Table I, titanium and aluminum, are leading candidates for OTEC because of their corrosion resistance and compatability with the working fluid.

For the various excitation mechanism, Fig. 3 shows the maximum span length as a function of crossflow velocity. Vibration is expected in the region above the fluidelastic curve, while no vibration is expected in the region below the turbulent buffeting curve. The area in between is a region of uncertainty, reflecting the variance in predictions using different models. On the basis of fluidelastic instability, this region appears to be safe; but on the basis of turbulent buffeting, vibration would be expected. For design purposes the span length should be chosen to lie below the region of uncertainty. If the expected crossflow velocity is, say, 1 m/s, then the maximum allowable tube span length is 1.8 m. For reference, the TEMA maximum span length is also plotted. As stated in Ref. [14], the 1940 TEMA Standards somewhat arbitrarily specified maximum span lengths for different tube sizes and materials. Common practice is to limit the maximum span length to 80% of the TEMA values. For the particular case considered in Fig. 3, it can be seen that for crossflow velocities less than 1.4 m/s the TEMA maximum span would imply a conservative design. For velocities larger than 1.4 m/s the design would be somewhat uncertain.

Figure 4 shows the region of potential acoustic noise. The upper boundary is set by Eq. (14) with K = 1.2 and the lower boundary by Eq. (15) with K = 0.8. (It should be pointed out that the regions bounded by Eq. (14) with K = 1.2 and K =

Table I Wall Thicknesses for Aluminum and Titanium Tubes

Outer diameter	Wall thickness, cm	
cm	Aluminum	Titanium
2.54	0.165	0.071
3.81	0.218	0.091
5.08	0.262	0.122

0.8 and by Eq. (15) with K = 1.2 and K = 0.8 overlap; consequently it is only necessary to plot the two limiting curves.) For a crossflow velocity of 1 m/s acoustic noise may occur if the heat exchanger shell diameter is between 15 m and 32 m. The more severe problem of acoustic resonance is considered in Fig. 5. Assume that the crossflow velocity is 1 m/s and that a 1.8 m span length is chosen in accordance with Fig. 3 to avoid tube vibration. Then Fig. 5 indicates that resonance can occur if the shell diameter is between 15 m and 23 m. When either acoustic noise or resonance is predicted, appropriate corrective measures should be taken. Generally this problem is remedied by inserting detuning plates parallel to the direction of crossflow. This changes the acoustic frequency by changing the characteristic length, but does not affect the heat transfer performance and pressure drop [14].

The effect of increasing tube diameter from 2.54 cm to 5.08 cm is illustrated in Fig. 6. In these calculations the wall thickness for a given outer diameter is taken from Table I. When the tube diameter is increased from 2.54 cm to 5.08 cm, the predicted maximum allowable span length increases from 1.8 m to 3.5 m, assuming a crossflow velocity of 1 m/s. The increase in allowable span length is essentially due to an increase in tube stiffness.

In addition to tube diameter, a number of other system variables were studied: tube pitch-to-diameter, tube material, and tube-field layout. Changing the tube pitch-to-diameter ratio from P/D = 1.25 to 1.5 and the tube material from titanium to aluminum had little effect on the overall results. Using an approach similar to that of Ref. [17], a crude comparison was made of the severity of tube vibration for various tube-field layouts (30°-triangular, 60°-triangular, 45°-square, and

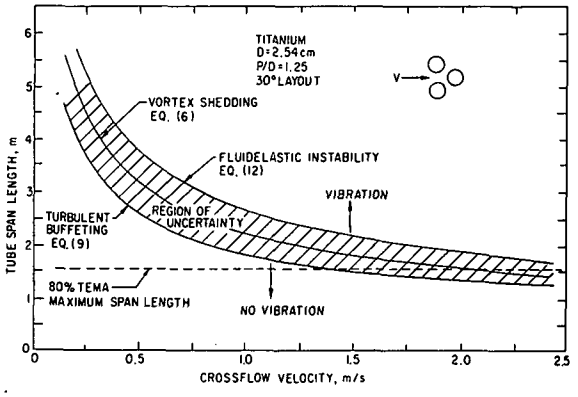

Fig. 3 Maximum allowable tube span length.

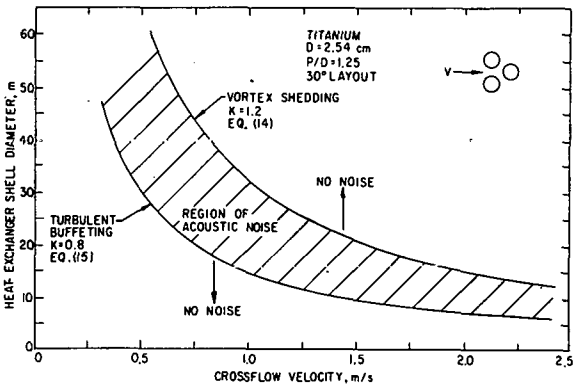

Fig. 4 Region of acoustic noise.

90°-square). It was found that all of the arrangements are affected about the same. Although differences were not very significant and should not be over emphasized, it was interesting to note that the 45° arrangement was the best (i.e., least vulnerable to vibration) followed closely by the 30°, 60°, and 90° configurations in that order.

Concluding Remarks

In this paper, some of the more popular methods for predicting flow-induced vibration were presented. These methods, although simple and based on a limited amount of experimental data, are extremely valuable tools for vibration analysis of shell-and-tube heat exchangers. As more and more field data becomes available, the accuracy of the predictive methods can be improved, and, consequently, design uncertainties can be further reduced.

References

1. Chen, Y. N., "Flow-Induced Vibration and Noise in Tube-Bank Heat Exchangers Due to Von Karman Streets," Trans. ASME, Series B, J. of Eng. for Industry, Vol. 90, Feb. 1968.

2. Chen, Y. N., "Excitation Sources of The Flow-Induced Vibrations and Noise in Tube-Bank

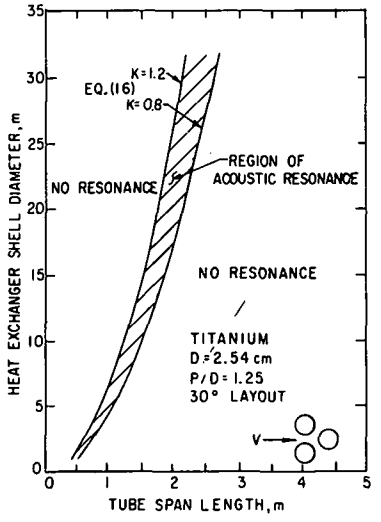

Fig. 5 Region of acoustic resonance.

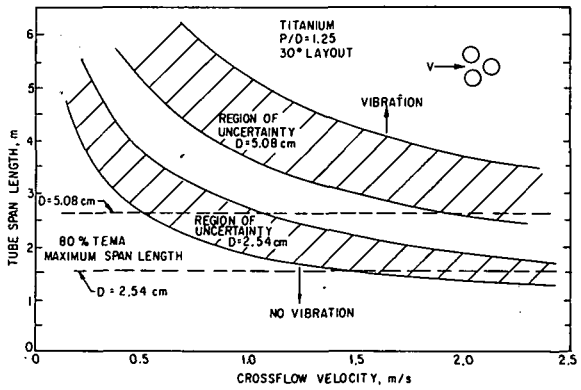

Fig. 6 Influence of tube diameter on the maximum allowable tube span length.

Heat Exchangers," ASME Winter Annual Meeting, Atlanta, GA, Nov. 1977.

3. Chen, Y. N., "The Sensitive Tube Spacing Region of Tube Bank Heat Exchangers for Fluid-Elastic Coupling in Cross Flow," Published in Fluid Structure Interaction Phenomena in Pressure Vessel and Piping Systems, PVP-PB-026, ASME Winter Annual Meeting, Atlanta, GA, Nov. 1977.

4. Owen, P. R., "Buffeting Excitation of Boiler Tube Vibration," J. Mech. Eng. Sci., Vol. 7, No. 4, 1965.

5. Connors, H. J. Jr., "Fluidelastic Vibration of Tube Arrays Excited by Cross Flow," Symp. on Flow-Induced Vibration in Heat Exchangers, ASME Winter Annual Meeting, New York, Dec. 1970.

6. Thorngren, J. T., "Predict Exchanger Tube Damage," Hydrocarbon Processing, Vol. X, April 1970.

7. Gregorig, R., et al., "Vibration Criteria of a Tube in Crossflow, Part 3: Vibration of Tube Bundles," Chemie-Ing.-Techn., Vol. 40, 1968.

8. Fitz-Hugh, J. S., "Flow-Induced Vibration in Heat Exchangers," Paper No. 427, Proc. Int. Symp. on Vibration Problems in Industry," Keswick, V. K., April 1973.

9. Walker, W. M., and Reising, G. F. S., "Flow-Induced Vibrations in Cross Flow Heat Exchangers," Chem. and Process Eng., Vol. 49, No. 11, 1968.

10. Brothman, A., et al., "A Tube Vibration Analysis Method," AIChE Symposium Series 138, Vol. 70, 1974.

11. Chen, S. S., "Crossflow-Induced Vibration of Heat Exchanger Tube Banks," Nuclear Eng. and Design, Vol. 47, 1978.

12. Shin, Y. S. and Wambsganss, M. W., "Flow-Induced Vibration in LMFBR Steam Generators: A State-of-the-Art Review," Nucl. Eng. and Design, Vol. 40, No. 2, 1977.

13. Moretti, P. M., "A Critical Review of the Literature and Research on Flow-Induced Vibrations in Heat Exchangers," AIChE Symposium Series 138, Vol. 70, 1974.

14. Chenoweth, J. M., "Flow-Induced Vibration in Shell-and-Tube Heat Exchangers," SAN/1273-1, Feb. 1977.

15. Timoshenko, S. P., Vibration Problems in Engineering, Van Nostrand, New York, 1955.

16. Shin, Y. S., et al., "Effect of Tube/Support Interaction on the Vibration of a Tube on Multiple Supports," Argonne National Laboratory Report No. ANL-CT-77-5, Jan. 1977.

17. Yung, D., Lorenz, J. J., and Ganic, E. N., "Vapor/Liquid Interaction and Entrainment in Shell-and-Tube Evaporators," ASME Paper No. 78-WA/HT-35, 1978.

18. Connors, H. J., "Fluidelastic Vibration of Heat Exchanger Tube Arrays," ASME Paper No. 77-DET-90, 1977.

A SUMMARY OF RECENT EXPERIMENTAL AND ANALYTICAL OTEC STUDIES AT ORNL*

J. W. Michel

Energy Division
Oak Ridge National Laboratory
Oak Ridge, Tennessee 37830

Abstract

The results of ammonia heat transfer experiments and various analytical studies of Ocean Thermal Energy Conversion (OTEC) heat exchangers are summarized. Work done in 1978 and early 1979 includes additional ammonia condensation tests on several vertical fluted tubes and on tubes inclined at 30° from the vertical. The high condensation coefficients previously reported for fluted tubes have been verified, and they seem to be insensitive to tube length over the range tested. Also, tilting the tubes significantly improves the performance of smooth tubes and causes a slight decrease in the performance of fluted tubes. Testing of vertical tubes for ammonia evaporation is in progress with evaluation of both in-tube and outside tube evaporation experiments planned.

Analytical studies include evaluation of the cost effectiveness of various types of heat transfer enhancement and a survey of heat exchanger joinability. Also, several studies are in progress relative to OTEC alternate cycles and components for these cycles.

Introduction

Development work at ORNL on OTEC projects includes basic ammonia heat transfer experiments and studies related to the closed-cycle concepts, and experimental and contract management relative to open or alternate cycles. Closed-cycle work began in early 1976 while alternate-cycle activities began in mid-1978. This paper summarizes the results of these activities that have been obtained this past year. Summaries of prior work have been presented in Refs. 1 and 2.

Heat Transfer Experiments

The design and operation of an ammonia condensation heat transfer test loop has been previously described[3] and the data obtained on a vertical smooth tube and several fluted tubes, all 4 ft in length, were presented. Subsequent condensation tests[4] with vertical tubes have consisted of tests of a fluted tube (tube F) of 6-in. equivalent length, a double fluted tube (tube H) similar to that used in the CMU condenser[2] and a smooth tube tilted at an angle of 30° from the vertical (tube A–T). Photographs of sample sections of these 1-in.-OD tubes are shown in Fig. 1, and the characteristics physical parameters summarized in Table 1.

The heat transfer results are summarized in Figs. 2 through 4. Figure 2 compares the performance of tube F with an equivalent length of 6 in. (seven equally spaced drain-off skirts attached) to data previously obtained with tube F and with tube A. As indicated, the effect of tube length over the range of 1/2 to 4 ft on the condensation heat transfer coefficient is insignificant except perhaps at the high heat fluxes, which are much higher than for typical OTEC operation. The implication is that a fluted tube several times longer than 4 ft would still perform well at low heat fluxes and not suffer potential performance loss due to condensate flooding of the rills. The condensation heat transfer results for tube H are shown in Fig. 3, as a plot of heat load versus overall mean temperature difference for several values of inside

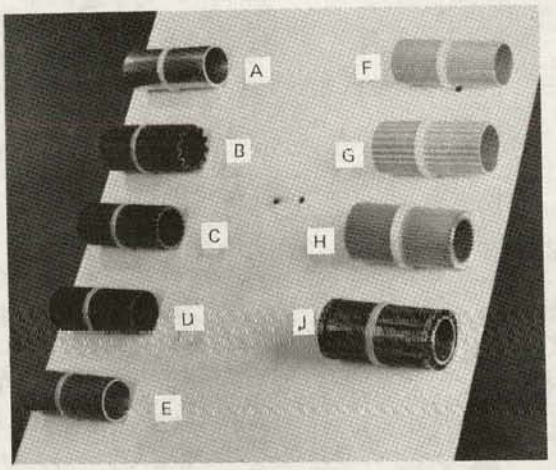

Fig. 1 Examples of experimental fluted tubes.

Table 1 Characteristics of Tubes Tested

Cross section	Tube	Inside diameter, cm	Outside perimeter, cm	Outside area, m^2	Outside area, ft^2	No. of flutes
	A/A-T	2.21	7.98	0.0974	1.05	–
	E	2.21	12.70	0.1490	1.60	60
	F	2.29	8.26	0.0964	1.04	48
	G	2.54	9.75	0.1143	1.23	24
	H	–	14.00	0.163	1.76	42[a]

[a]Also contains 34 inside flutes.

*Research sponsored by the Division of Central Solar Technology, U.S. Department of Energy, under contract W-7405-eng-26 with Union Carbide Corporation.

By acceptance of this article, the publisher or recipient acknowledges the U.S. Government's right to retain a nonexclusive, royalty-free license in and to any copyright covering the article.

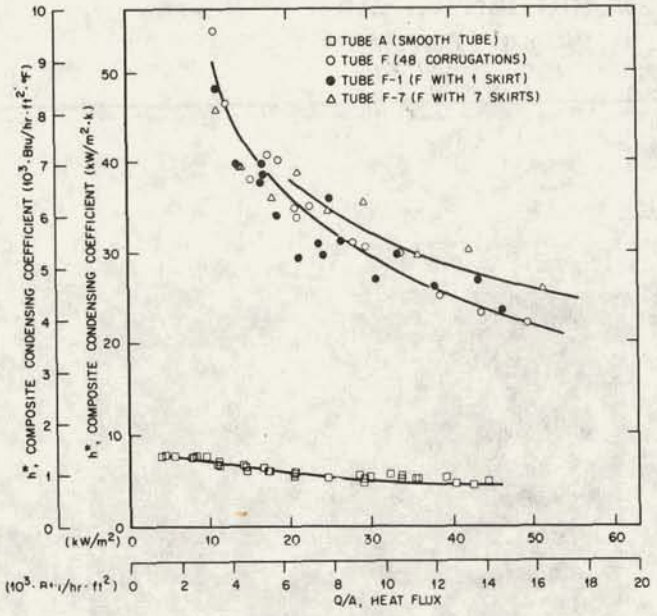

Fig. 2 Comparison of heat transfer performance between tube F (48 corrugations) and duplicate tubes containing equally spaced drainage skirts — h* vs Q/A.

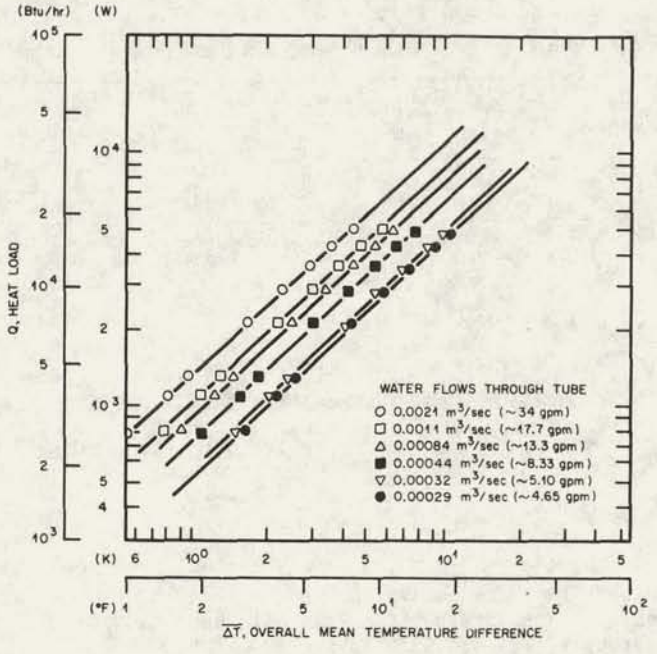

Fig. 3 Heat transfer performance of tube H. Ammonia is condensing on the outside surface and water is flowing through the inside of the tube (no rod inside); 0.00084 m^3/sec (~13.3 gpm) corresponds to a water velocity of 2 m/sec (6.5 fps) — a typical design value for OTEC plants.

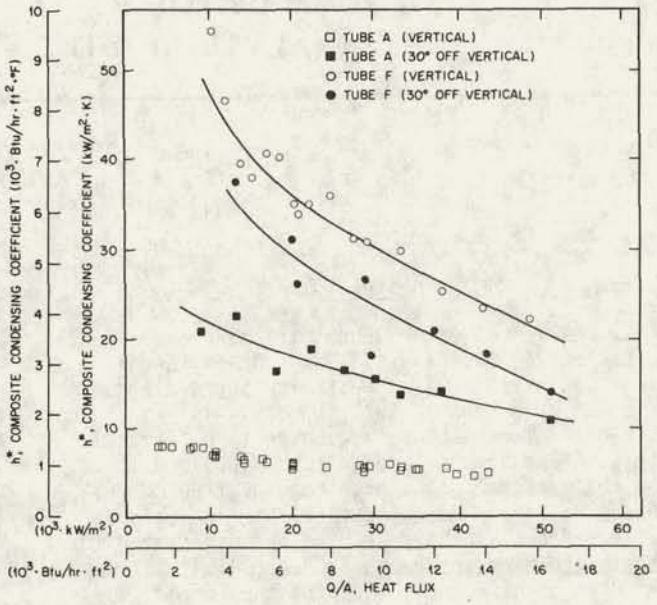

Fig. 4 Comparison of heat transfer performance of a smooth and a fluted tube for vertical and 30° off vertical orientations — h* vs Q/A.

cooling water flow rate. This method of displaying the results was chosen since the Wilson plots ($1/U_o$ versus $1/V^{0.8}$) did not give straight lines, thus making the extrapolation for obtaining the condensation coefficient uncertain. It appeared that a lower exponent (0.6 or 0.7) for water velocity would be required to give a straight line for the Wilson plot. For a typical OTEC water-side velocity of 7 ft/s, the overall coefficient* for this tube would be from 850 to 950 Btu/hr·ft²·°F over a Δt range of 10 to 2°F, respectively.

The results of the tilted tube testing, shown in Fig. 4, indicate that the 30° tilt from the vertical decreases the coefficient for the fluted tube from ~14 to 40% (low to high heat flux). For the smooth tube, tilting increases the coefficient by over a factor of 3 at low heat flux to about a factor of 2 at high heat flux. Based on the McAdams[5] model and assuming ideal condensate flow vectors, a factor of 2.7 would be expected for a single tube. Translating these results to the performance of a tube bundle would, however, be risky since it is not known how the condensate would flow down to the bottom of the unit — more tests are planned to clarify this.

Although not part of the ORNL OTEC project, condensation data have been obtained[6] with R-22 on both smooth and enhanced tubes; also 1-in.-OD by 4 ft long. The results of these tests (Fig. 5) show, as expected, considerably lower heat transfer coefficients than obtained with NH_3 on the same tubes (tubes E and A). In fact, tube E with R-22 is approximately equivalent in performance to tube A (smooth) with NH_3.

*Based on the actual outside tube area, 1.76 ft² (4 ft long).

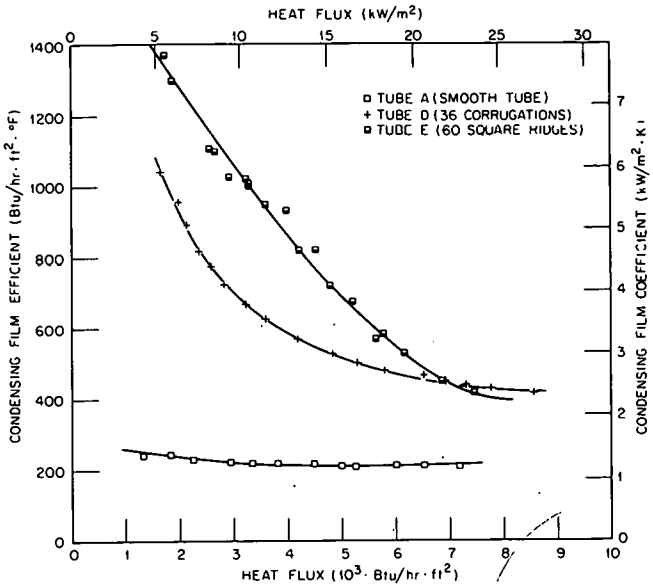

Fig. 5 Condensing film coefficient vs heat flux for R-22.

Cost Effectiveness of Fluted Tubes

Using fluted tubes to enhance the heat transfer rate in a heat exchanger will increase the tube material and, thus, the cost to manufacture this surface configuration. The additional material requirement will depend on the shape of the flute, the number of flutes, and the trough-to-crest depth. Measurements and calculations of the material increment on four ORNL test tubes, designated E, F, G, and H, were performed. The relevant dimensions, wall cross-sectional areas, and percentage increments of the tubes are shown in Table 2 and compared with data on a smooth tube.

The material increment calculations were also done for repeated-rib-type, inside enhancement tubes, as recommended by Bergles.[7] It was found that the material increment for this type of enhancement was small. For instance, for the Webb[8] 01/10 tube [outside diameter = 5.1 cm (2.0 in.); wall thickness (T_W) = 0.165 cm (0.056 in.); rib thickness = 0.051 cm (0.020 in.); rib depth = 0.0475 cm (0.0187 in.); and pitch = 0.475 cm (0.187 in.)]; the tube material is only increased by 2.9%, as compared to the corresponding smooth tube.

Table 3 shows a comparison of the measured condensation heat transfer performance for the five tubes tested with the amount of extra metal used in forming the flutes. It is assumed that the performance improvement will directly result in a decrease in the required heat transfer area and thus the total amount of tubing or tube metal required, and therefore a corresponding reduction in the cost of the heat exchanger. It should be recognized that for a system optimized heat exchanger this may not be exactly true. Also, the tubing cost is only part, albeit a large fraction, of the cost of the heat exchanger. A computed cost-effectiveness factor, the ratio of the increase in the heat load capability corrected for constant water-side and fouling conditions (defined in Table 3) to the increase in the amount of tube metal used, all compared to an unenhanced (smooth wall) tube, is the basis for making the comparisons.

Without water-side enhancement, tube F appears to be the most cost effective design for the fluted tubes. As noted above, the tilted smooth enhancement effect may not be completely realized in a large tube bundle. Incorporating (theoretically) the "Webb" type water-side enhancement still shows that tube F would be the most cost-effective design. On this basis, it is apparent that the extra metal required to produce the enhancement effect for tube H may not be cost effective. Figure 6 shows the comparative effectiveness of the enhancement achieved by the various tubes tested so far.

Table 2 Comparison of the Material Requirements for Several Enhanced Tubes

Tube Designation	A	E	E (heavy wall)	F	F (heavy wall)	G	G (heavy wall)	H (double fluted)
Diameter								
Outside, in.	1.00	1.00	1.00	1.00	1.00	1.15	1.15	1.185
Inside, in.	0.87	0.83	0.82	0.90	0.84	1.01	0.958	0.855
Wall Thickness								
To trough, in.	0.065	0.040	0.965	0.037	0.065	0.042	0.065	0.065
To crest, in.	0.065	0.065	0.090	0.050	0.078	0.074	0.096	0.065
Number of flutes	nil	60	60	48	48	24	24	42/34
Wall Cross-sectional Area								
Smooth tube,[a] in.²	0.19	0.11	0.18	0.109	0.186	0.139	0.210	0.212
Fluted tube, in.²	0.19	0.15	0.22	0.207	0.193	0.193	0.264	0.377
Wall Material Increment from smooth tube %	nil	32.9	19.8	18.4	11.4	38.5	25.6	43.7
Fluted Outside Height, in.	–	0.025		0.013		0.031		0.040[b]

[a]The corresponding smooth tube is defined as having smaller constant wall thickness (i.e., to trough).

[b]Inside tube flute (34) height is 0.060 in.

Table 3 Comparison of Performance Improvement with Tube Metal Requirements
(Adjusted to Constant Tube wall thickness of 0.065 in.)

Tube Type →	A	A-T	E	F	G	H
Ammonia Enhancement						
Ratio of h_{NH_3} (Q/A = 3000)	1.0 (1300)	3.0	5.3	7.2	4.8	?
Ratio[a] of Q's	1.0 (3160)	1.36	1.55	1.46	1.45	2.20
Ratio of tube metal requirements/ft	1.0	1.0	1.20	1.11	1.26	1.44
$\frac{\text{Total tube A metal}}{\text{Total enhanced tube metal}}$	1.0	1.0	1.29	1.31	1.15	1.53
Ammonia Plus Water Enhancement[b]						
Ratio[a] of Q's	1.0	1.82	2.28	2.12	2.03	2.20
$\frac{\text{Total tube A metal}}{\text{Total enhanced tube metal}}$	1.0	1.77	1.85	1.86	1.57	1.53

[a]Values of Q (Btu/hr) are for a ΔT_m = 6°F, velocity of water = 6 ft/s, and fouling factor = 0.0003 ft²·°F·hr/Btu.

[b]Assumes use of "Webb" type enhancement; h_{H_2O} X 2 for tubes A-T, E, F, and G.

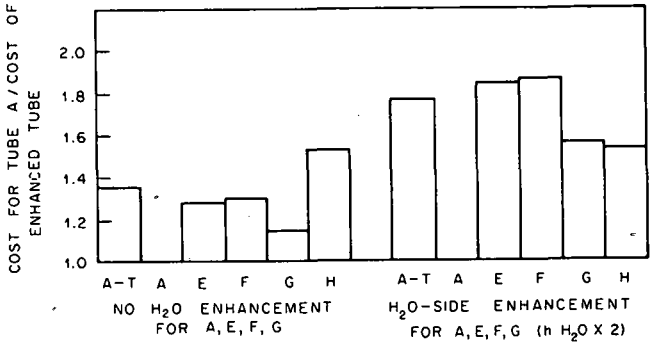

Fig. 6 Potential cost savings for use of enhanced tubes.

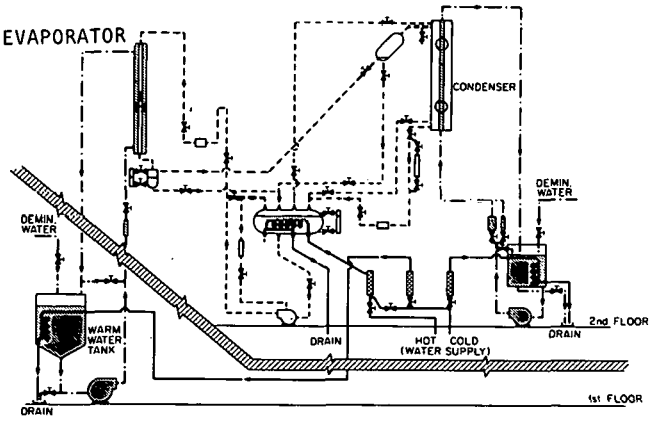

Fig. 7 OTEC vertical tube evaporator/ condenser test loop.

Ammonia Evaporation Studies

The condensation heat transfer test loop was modified to perform ammonia evaporation experiments for both inside tube and outside tube evaporation on vertical smooth and fluted tubes. As with the condensation experiments, this test program is also based on the use of the Wilson-plot method for computing the ammonia evaporation heat transfer coefficients. A schematic diagram of the test loop is shown in Fig. 7. Under directions from DOE, experiments were first run on inside tube evaporation; but due to lack of commercial interest, these tests were terminated after completing some preliminary tests on a smooth tube and tube H. These results are shown in Fig. 8, although some reservations are made relative to their accuracy due to lack of more extensive verification experiments.

The results of tests to date on a smooth tube at two ammonia feed rates are also shown in Fig. 8. Tests on a variety of fluted tubes are planned to determine the most cost-effective enhanced tube design.

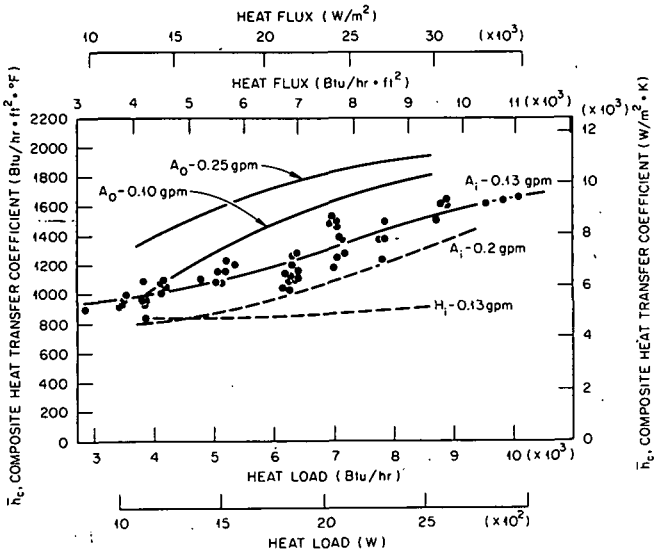

Fig. 8 Composite heat transfer coefficients for ammonia evaporation (subscripts O & i refer to evaporation on the outside and inside tube wall respectively, gpm is the ammonia top feed rate).

Other Studies on Closed and Alternate OTEC Cycles

A literature review and state-of-the-art discussion paper on joinability as related to OTEC heat exchangers was completed by the Metals and Ceramics Division.[9] The paper includes discussions on welding, brazing, soldering, and adhesive processes as applied to the candidate OTEC materials for both shell and tube and compact plate/fin designs.

In April 1978, the OTEC Alternate Cycles Program was initiated. The objective of this program is to provide the DOE Ocean Systems Branch with technical and managerial assistance and to perform subcontract monitoring, in-house research, and ad hoc studies for the development of OTEC alternate power cycles technology.

To accomplish the objectives, work is being carried out to provide the Ocean Systems Branch with program planning and analysis assistance; site visits were carried out to monitor subcontractor performance; and research work and ad hoc tasks were performed as needed in critical technology development areas.

The OTEC Alternate Cycles Program, as opposed to the closed-cycle program, has more thermodynamic cycle alternates available for base-load power generation, including open, hybrid, and lift cycles. The alternate cycles are generally considered second-generation OTEC technology and, in some arrangements, can operate as a dual-purpose plant. The open cycle, with surface condenser, and the hybrid cycle not only generate electricity but also produce fresh water. The recently invented lift-cycle concepts, though yet to be proven, may offer more efficient energy extraction from the renewable ocean thermal resources.

The open cycle uses essentially seawater as the working fluid; steam is flashed from the warm surface seawater, passed through a turbine, and condensed with cold seawater, either in a surface condenser or a direct-contact unit. The hybrid cycle combines the open and closed cycles; steam from a seawater flash evaporator is condensed in an ammonia boiler that is part of a closed-cycle system. These two cycles have a further option of producing distilled or desalted water as a by-product.

There are two types of lift cycles currently under development and supported by DOE: foam lift and mist lift. In the foam-lift concept, warm seawater containing a small amount of an added surfactant is partially flashed in a foam generator, producing a stable column of foam. The foam flows upward by the pressure driving force created by the difference in vapor pressure between warm and cold seawater. The foam is broken at the top of the column, and the associated steam is condensed by a cold seawater spray. The seawater entrained in the foam is collected and passed down through a hydraulic turbine to create work. The mist concept is similar to the foam, except that seawater is lifted as a fine mist by high-velocity steam flashed from the warm seawater.

The DOE program involves six projects in alternate power cycles. These subcontract projects are summarized in Table 4. In performing the technical support function, we have studied and reviewed the technical reports of each of the projects and have become acquainted with the technical implication and progress to date. Subcontractor site visits have been conducted to learn about their facilities, experiments, and personnel. The information acquired has become the basis for performing cost effectiveness studies and future planning work. In addition, an OTEC Alternate Cycles Contractors'

Table 4 OTEC Alternate Cycles Research and Development Projects

Institution	Location	Power Cycle Application	Project Goal
Westinghouse Electric	Lester, Pa.	Open cycle; hybrid cycle	To provide conceptual designs of 100-MWe power systems for the open and hybrid OTEC cycles and to define the systems' costs and to evaluate these costs against other OTEC systems.
Colorado School of Mines	Golden, Colo.	Open cycle	To design, fabricate, and test an apparatus suitable for measuring the steam production rate for seawater for various flash evaporator configurations.
Carnegie-Mellon University	Pittsburgh, Pa.	Foam lift cycle	To establish the scientific feasibility of foam OTEC power plant, to investigate the technical feasibility of generating 1 g/cm^2/sec and to break this foam at desired height.
University of Puerto Rico	Mayaguez, Puerto Rico	Foam lift cycle	To investigate the seawater-surfactant system and to establish the minimum surfactant concentration for effective foam generation.
R&D Associates	Marina del Rey, Calif.	Mist lift cycle	To determine the feasibility of the mist flow ocean thermal energy process and to investigate the lift tube performance so that reasonable projections of the operating characteristics and the possible range of cost estimates can be made.
University of California at Los Angeles	Los Angeles, Calif.	Mist lift cycle	To design and operate an experimental facility that can test the key components and demonstrate the scientific feasibility of the mist lift power cycle.

information exchange meeting and workshop[10] was organized and held in Washington, D.C.; it was designated to disseminate the research and development information to the technical community and to the general public and to effectively support the headquarters branch in program planning.

OTEC alternate-cycle power systems will operate at subatmospheric conditions; that is, the inner volume of the power-system components is below atmospheric pressure. Seawater is the working fluid in alternate cycles. Dissolved gases in seawater will be released in the flash evaporator and in the condenser, if direct-contact condensation is being used. If not removed, the noncondensable gases will impair the performance of the power cycles.

A review of the literature on the gas desorption phenomena of seawater and on the degasification process revealed the need for additional design information on degasifiers for OTEC applications. In order to obtain design data to establish suitable gas removal processes for alternate power cycles, a test loop is being built. This loop will be capable of performing tests of various gas desorption designs, including packed-column, tray-column, shallow-pool, thin-film, and vacuum-spray types.

Acknowledgements

The work reported herein has been supported by the Ocean Systems Branch of the Central Solar Technology Division of the U.S. Department of Energy. The experimental heat transfer work was performed under direction of R. W. Murphy by S. K. Combs and G. S. Mailen. The work on heat exchanger joinability was performed by R. J. Beaver and the Program Manager for Alternate Cycles Development is F. C. Chen.

References

1. G. E. Ioup, ed., Proceedings Fourth Annual Conference on Ocean Thermal Energy Conversion (OTEC), University of New Orleans, New Orleans, Louisiana, March 22-24, 1977, University of New Orleans, New Orleans, Louisiana, July 1977.
2. T. N. Veziroglu, ed., Proceedings of the Fifth Ocean Thermal Energy Conversion Conference, February 20-22, 1978, Miami Beach, Florida, University of Miami, Coral Gables, Florida, September 1978.
3. S. K. Combs, "An Experimental Study of Heat Transfer Enhancement for Ammonia Condensing on Vertical Fluted Tubes," ORNL-5356, January 1978.
4. S. K. Combs, "Experimental Data for Ammonia Condensation on Vertical and Inclined Fluted Tubes," ORNL-5488, January 1979.
5. W. H. McAdams, Heat Transmission, 3d ed., McGraw-Hill, New York, 1954, p. 329.
6. S. K. Combs, G. S. Mailen, R. W. Murphy, "Condensation of Regrigerants on Vertical Tubes," ORNL/TM-5848, August 1978.
7. A. E. Bergles and M. K. Jensen, "Enhanced Single-Phase Heat Transfer for Ocean Thermal Energy Conversion Systems," ORNL/Sub-77/14216/1, April 1977.
8. R. L. Webb et al., "Heat Transfer and Friction in Tubes with Repeated-Rib Roughness," *Int. J. Heat Mass Transfer*, 14: 601–17 (1971).
9. R. J. Beaver, "State-of-the-Art Survey of Joinability of Materials for OTEC Heat Exchangers," ORNL/TM-6284, December 1978.
10. F. C. Chen and J. W. Michel, eds., "Report of the Proceedings of the OTEC Alternate Cycles Contractors' Information Exchange Meeting," Conf-780934, Ocean Systems Branch, Division of Central Solar Technology, U.S. Department of Energy, December 1978.

DISCUSSION

Question: What is the physical mechanism for the enhancement resulting from inclining the tube?

J. Michel: I think it results from the reduction in condensate flow length and hence in film thickness. On a vertical tube, condensate flows down the whole length and the film thickness builds up continually as you go down. On an inclined tube, the buildup of the film thickness cannot be very big except on a line along the bottom where the condensate is running down the bottom of the tube.

G. Loeb, NRL: Isn't there a serious question about cleanability of an enhanced surface where you have transverse ribs or flutes?

J. Michel: Yes, that is certainly a consideration that has to be factored into the whole problem. Are these separable problems? Should we be developing the best waterside enhancement from a heat-transfer point and hope that the biofouling countermeasures people will have clorination, brushes, or sponge balls, or something that will handle it? At the moment we have not put that together in the development program. It is something, I think, that needs to be done. By the way, a variation of this design was used in the PSD-I [Power System Design-I] where it was assumed that a mechanically driven brush in the tube would fit the contours of the axial flutes to keep them clean. There is some argument that these transverse repeating ribs might be sort of self-cleaning because of the turbulence and added shear that they provide — that's kind of an arm-waving argument — but we need to consider it more.

D. Aronson: In regard to enhancement, I believe that some reports exist because they've been used in European reactors. But I don't know whether they were helical or a series of ridges. If they were made helical, I imagine there is some kind of cleaner that moves in a helical motion. Do you have any information on that?

J. Michel: Bergles discusses several types in his report — spring wires, twisted tapes, repeated ribs, protrusions, and dents. They all show some degree of enhancement, but the thing that has to be kept in mind is the balance between heat-transfer enhancement and the relative pressure drop incurred. The one we selected had, I think, the most promise among the things that Bergles reported. There is another new tube that Jack Yampolsky is working on that has a rotating flow that has some interesting effects on water-side enhancement.

HEAT TRANSFER ENHANCEMENT BY SURFACE EXTENSION IN HORIZONTAL AMMONIA-FILM EVAPORATORS

Raul J. Conti*

Lockheed Palo Alto Research Laboratory
Lockheed Missiles & Space Company, Inc.
3251 Hanover Street Palo Alto, California 94304

Abstract

A pressure vessel containing saturated ammonia vapor is used to explore experimentally the potential for heat-transfer enhancement by surface extension. Attention is focused on practical and cost-effective techniques for enhancement of shell-side heat transfer in thin-film evaporators for OTEC application. In particular, the shell-side thermal conductance is measured using horizontal evaporator tube specimens with integral helical fins subjected to overhead feed of liquid ammonia. Measurements show that the fins increase the thermal conductance significantly, up to 3.6 times the values measured on smooth tubes with the same reference area (the largest cylindrical surface through solid material). This increment surpasses the geometrical extension of surface area, indicating an enhancement of the heat transfer process due to the fins. The results indicate that at low and moderate feed rates, up to approximately 200 lb/hr per foot of tube length, the effective amount of surface extension achievable is limited by the requirement of tube wettability. This is a three-dimensional phenomenon related to the flow regime of the liquid feed, which may fall on the evaporator tube in the form of a continuous sheet, discrete columns, or intermittent drops, depending on the feed rate. Results are presented for the transition points between flow regimes, and for heat transfer on three commercially available finned tubes with 20 and 34 fins per inch, as well as on a tube with fins reduced in height to make better use of surface extension.

Introduction

It is well-known that OTEC plants, in exploiting a low-grade thermal resource, would place a heavy burden on evaporators and condensers, particularly if closed thermodynamic cycles are used. As a consequence, these heat exchangers would be of unprecedented size, and would become some of the costliest components in the system. This makes it attractive to seek enhancement of heat transfer in order to improve the performance and reduce the size of the heat exchangers. In fact, many of the heat-exchanger designs now under consideration or under implementation for OTEC incorporate some form of heat-transfer enhancement, such as induced nucleate boiling or surface extension by means of fins, flutes, etc. The investigation reported in this paper concentrated on surface extension by means of integral, closely spaced, helical fins. This method has the advantages of relatively low cost and high reliability, since it does not rely on active phenomena such as boiling or dropwise condensation, which may be affected by external agents or time. In addition, because of the confining effect of the fins, surface tension is more predominant here than in plain tubes, and less aerosol formation may be expected; certainly much less than the mist generated by boiling.

Circumferential fins and grooves to enhance condensation on horizontal tubes have been used extensively, and design criteria are available (see, for instance, the classical paper by Gregorig[1] and the recent paper by Webb[2]). However, less information is available for evaporation from such surfaces. For instance, the analytical and numerical models of Edwards et al.[3,4], while providing some insight, are restricted to tapered fins with liquid meniscus attached to the tip, and do not address the three-dimensional aspect of the liquid feed, which turns out to be a limiting factor, as will be seen. Therefore, the purpose of this work was to explore experimentally the potential for enhancing ammonia evaporation on horizontal tubes by means of circumferential fins. Preliminary work with custom-made grooved surfaces, reported by the author at the Fifth OTEC Conference[5] indicated that substantial gains could be obtained by this method. It remained to answer questions such as the effects of feed rate, fin pitch, height, etc., that might affect the practical limits of surface extension. The present work addresses some of these issues, concentrating on commercially available finned tubes.

Experimental Technique

Facility

The facility used for the present investigation, shown schematically in Fig. 1, has been reported on previously[5] and will be described here only briefly. It consists essentially of a pressure vessel about 1 ft in diameter and 6 ft long, a liquid ammonia feed loop, instrumentation, and a data acquisition system. The pressure chamber is partially filled with liquid ammonia, and the internal environment is maintained at the working pressure by means of a submerged heater and a pressure regulator. All tests were performed in a saturated vapor environment at nominal conditions of 72° F and 133 psia. The system is capable of maintaining the temperature stable within better than 0.01° F.

The feed system consists of a closed loop that draws liquid ammonia from the sump in the pressure chamber, pumps it through flow meters and a metering valve, and delivers it to the feed unit above the test specimen. Various types of feed unit were used, such as a perforated tube with pressure feed, a slotted tube with overflow at the top generator, and a tray with a porous surface on the bottom. The flow pattern from the various feed units was generally similar to the drip pattern from the test specimen itself; in order to ensure further similarity, a dummy tube was placed between the feed unit and the test specimen. This tube was geometrically identical to the test specimen, but was not heated. The temperature measured within the feed unit was very close to the chamber temperature, and since the dummy tube was also at chamber temperature, the feed to the test specimen can be considered to be at saturated vapor temperature.

Instrumentation. The low temperature differentials involved in simulating OTEC conditions pose a special instrumentation problem, and care was devoted to meeting instrumentation requirements. The vapor pressure in

*Senior Staff Scientist, Applied Mechanics Laboratory.
The present investigation was sponsored by the Lockheed Independent Research and Development Program.

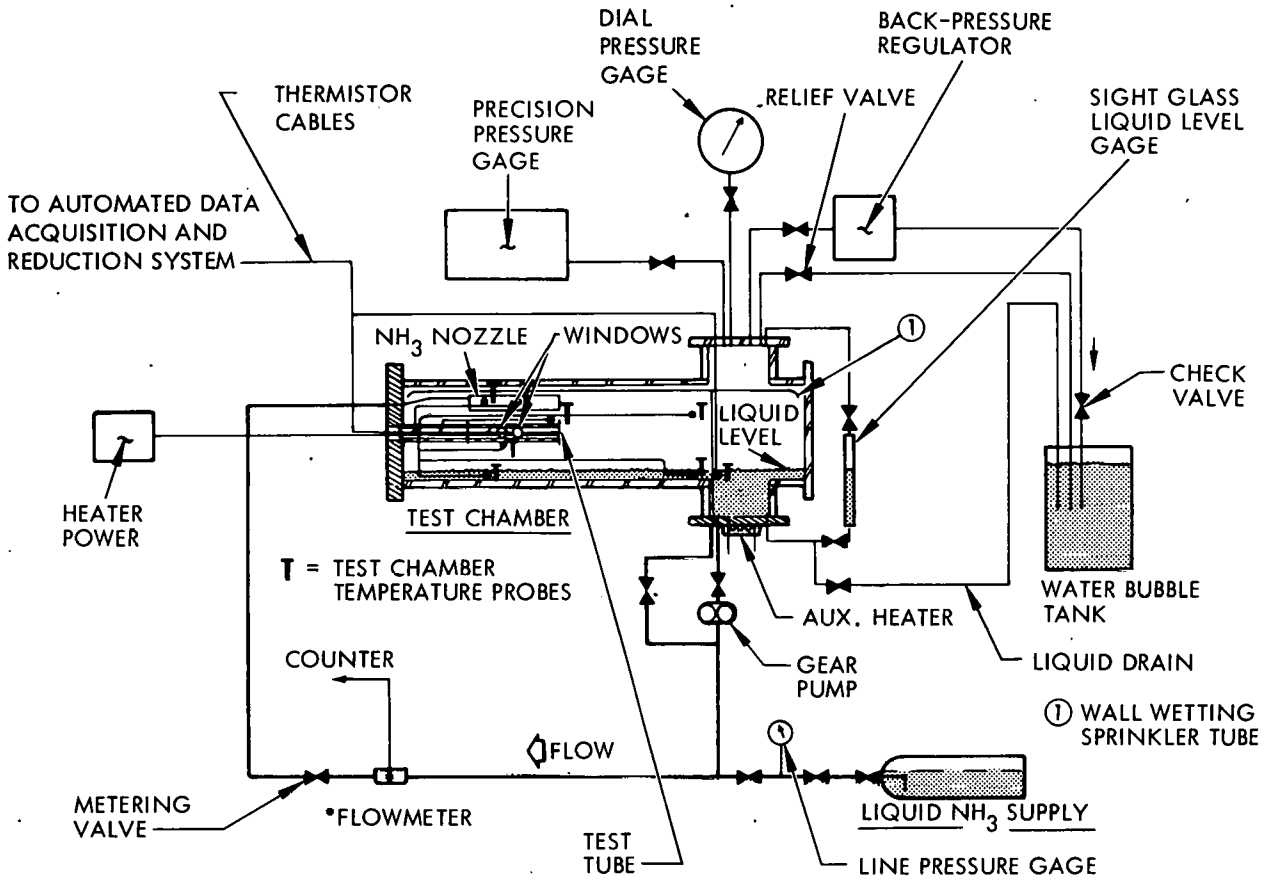

Fig. 1 Schematic of shell-side heat-transfer facility.

the chamber was measured with a fused-quartz gage calibrated to within 0.04 psi. This measurement was used to check the liquid and vapor temperatures measured at various stations within the chamber against tabular values for saturated ammonia. The accuracy of these measurements is estimated to be no worse than 0.02° F, and often better than this value. The flow rate for the feed system was measured with an accuracy of about 2 percent, as established from special calibration. The electrical power to heat the test specimen was measured with an accuracy of better than 1 percent.

The crucial measurement is that of wall temperature in the test specimen. Because of the small differential with the ambient temperature in the saturated vapor (ranging from 1° to 3.5° F) and the confined space available, special sensor installation techniques were used, similar to those reported earlier.[5] An additional problem was posed by the finned tubes, since the temperature distribution within the fin is nonuniform. Moreover, since the fins have a channeling effect on the liquid flow, the axial distribution of evaporation and heating may be nonuniform as well. In view of these problems, point measurements of the temperature field were abandoned in favor of average measurements over axial distances of about one tube diameter. This was achieved by mounting the temperature sensors on strips of high-conductivity material, which were, in turn, mounted axially on the internal surface of the tube specimens. Because of the uncertainties mentioned, and in spite of the fact that the measurement system is capable of a precision no worse than a few hundredths of a degree Fahrenheit, it is difficult to place a uniform lower bound on the accuracy of the measurements.

Data acquisition system. The analog signals generated by the temperature transducers are routed to a computer-controlled data acquisition system, which is programmed to scan the channels, average the digitized signal from each data channel over a preselected time interval to minimize random errors, convert to engineering units, perform other data reduction calculations, and output the final data on a printer and x-y plotter. The conversion to engineering units is based on calibrations of the system performed with a temperature standard.

Test Articles

The test articles consisted of samples of commercial finned tubes ("low fin") of the type often used for condenser duty. The fins are an integral part of the tube and run on a helical pattern. The fin profile is slightly tapered, with flat top and rounded valley. The three tubes tested had an overall diameter of 1 in.; the first one had a pitch of 20 fins/in. and fin height of 0.060 in., the second one had the same pitch but a fin height of 0.037 in., and the third one had a pitch of 34 fins/in. and fin height of 0.050 in. They were all made of aluminum alloy 5052. Eight-inch samples of the tubes were instrumented in at least two cross sections, fitted with an electrical heater located on the tube axis, and mounted in the test chamber with both ends insulated. The modified test article consisted of a standard tube with 20 fins/in., which were turned down to an average height of 0.020 in.

Test Procedure

Before each series of tests the entire data system was calibrated by immersing the test article in a constant-temperature bath together with a standard sensor of known calibration. The calibration points thus generated were fitted with nonlinear curves using the least-squares method, and the coefficients were stored on magnetic tape. The test article was then placed in the chamber and subjected to a vacuum for several hours to minimize contamination. After ammonia was loaded in the chamber, test runs were made at three levels of heat flux and throughout a range of feed rates to simulate the feed conditions for tubes in a stack that is irrigated at the top. The constant heat-flux condition does not correspond exactly to the envisioned application, where the heat flux would be limited by the temperature available in the sea water; however, the parametric data at various levels of the heat flux can be used by the designer to calculate the performance that can be expected under temperature-limited conditions. Nevertheless, a complication arises when dry areas are present in the test article, since the thermal behavior of the wall in the vicinity of these areas can be expected to be different for the heat-flux and temperature-limited cases. It will be seen that such areas were observed in some of the tests, particularly at low feed rates; therefore, care must be used in interpreting those results. Some redeeming arguments can be invoked: the dry areas, although of significant magnitude, were not extensive, but rather distributed in a periodic pattern, thus avoiding gross distortion of the temperature field; also the wall material has high conductivity, which tends to average out the temperature distortions. In any case, the situation of reduced performance due to dry areas is one to be avoided, and the corresponding data have more qualitative than quantitative value.

Data Reduction. Measurement of the electrical power dissipated in the test article and the corresponding wall temperatures attained allows computation of the shell-side thermal conductance according to the formula

$$h = \frac{\dot{Q}}{A_r (T_r - T_s)}$$

where h is the thermal conductance; $\dot{Q}$ is the overall rate of heat flow; A_r is the reference area, equal to the area of a cylindrical surface through the fin root; T_r is the reference temperature obtained by extrapolating the temperature measured in the wall to the reference surface, using the average heat flux; and T_s is the saturated vapor temperature, measured near the liquid-vapor interphase at the bottom of the test chamber. The conductance thus calculated is area-averaged around the instrumented cross section, and further averaged with the other cross section(s) to obtain the values reported in this paper.

Results

Three standard finned tubes were tested, having 20 fins per inch, 0.037 and 0.060 in. high, and 34 fins per inch, 0.050 in. high. All tubes were 1 in. in diameter and were made of aluminum alloy. In addition, one sample of the tube with 20 fins per inch was modified by turning down the fins to approximately 0.020 in., and was then tested under the same conditions. The feed rate ranged from about 10 lb/hr ft to about 750 lb/hr ft, which covers the flow rates that would exist in a stack of approximately 300 tubes. Three levels of heat flux were used – approximately 2,800, 5,000, and 6,500 Btu/ft^2 hr – which covers the range envisioned for OTEC applications.

Liquid Flow Regimes

The liquid flow over finned tubes shows marked differences with that over smooth tubes, because axial communication is restricted by the fins. At high feed rates this results in a more regular pattern, since disrupting axial waves are greatly reduced. On the other hand, at moderate and low feed rates the channeling effect of the fins creates a three-dimensional pattern of wetted and starved sections, which becomes more severe as the fin height is increased. This has a bearing on heat-transfer efficiency, and merits further attention.

Three basic flow regimes were observed in the tests, and identified as the sheet, column, and drop regimes. The sheet regime is characterized by uniform conditions in the axial direction and fully wetted tube, as shown in Fig. 2. The glassy appearance shown may change to a rougher pattern as the feed rate is increased, without significant effect on tube wettability. This regime was observed at feed rates greater than about 300 lb/hr ft, and it is more stable than similar flow over smooth tubes.

The column regime, observed between roughly 80 and 300 lb/hr ft, is characterized by discrete columns falling at fairly regular intervals. At the low end of this regime, up to about 150 lb/hr ft, the columns may break intermittently into drop strings, as shown in Fig. 3. The fins do not appear to play a significant role in the formation of columns, which are also observed in smooth tubes, but they are important in channeling the flow into narrow vertical bands, creating a pattern of alternating wet and dry areas, which correlates with decreased average conductance. The spacing between columns can be calculated by analyzing the Taylor instability on the bottom generator of the tube, and is given by Whitney[6] (for a thin liquid film) as

$$\lambda = 2\pi\sqrt{\frac{2\sigma}{\rho g}}$$

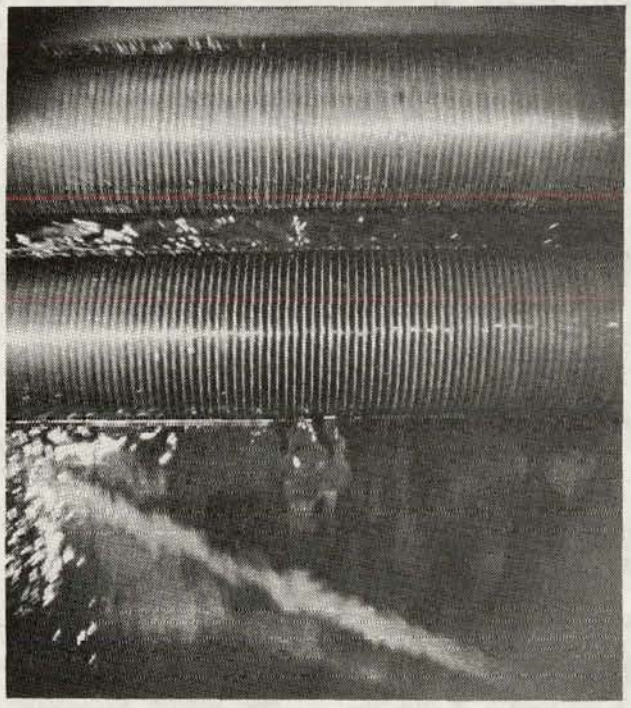

Fig. 2. Ammonia film on standard 1-in. finned tube with 20 fins/in. at a feed rate of 325 lb/hr ft – liquid sheet regime.

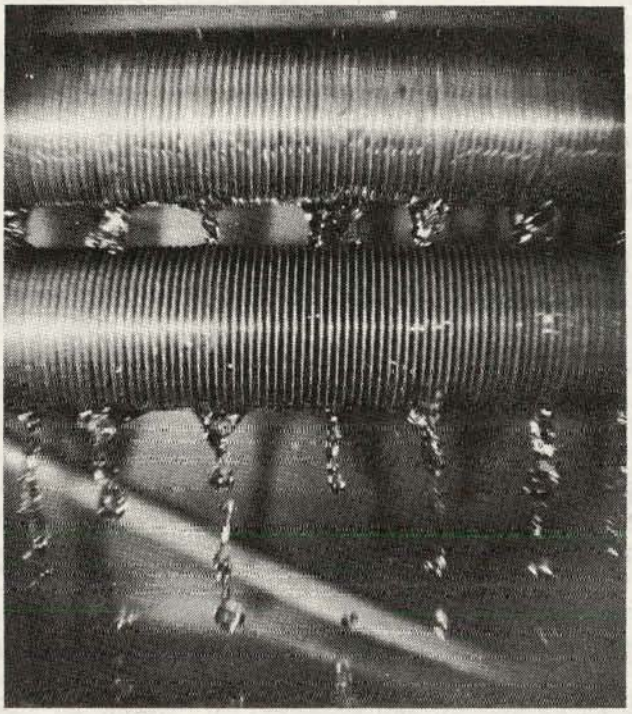

Fig. 3. Ammonia film on standard 1-in. finned tube with 20 fins/in. at a feed rate of 145 lb/hr ft – liquid column regime.

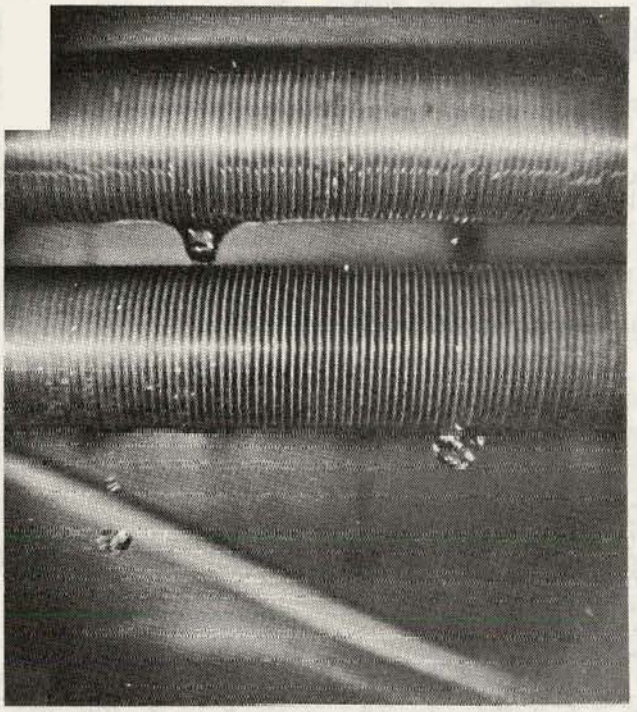

Fig. 4. Ammonia film on standard 1-in. finned tube with 20 fins/in. at a feed rate of 24 lb/hr ft – liquid drop regime.

where σ and ρ are the surface tension and density of the liquid, and g the gravitational acceleration. A similar formula, with a factor of 3 instead of 2 within the square root, was quoted previously by Yung et al.[7], and it applies to a thick liquid layer. Table 1 shows a comparison between measured values of column spacing and those calculated with the formula given above. The measured values fall between the thin layer and thick layer estimates, favoring Whitney's thin-layer estimate.

The drop regime, illustrated in Fig. 4, was observed at feed rates below 80 lb/hr ft. This regime has the same general characteristics as the column regime, and the same comments apply.

Small inclination of the tube from the horizontal position or motion about the horizontal position did not alter the character of the liquid flow regimes, but were observed to have a beneficial effect on tube wettability, with a corresponding improvement in heat transfer.

Table 1

CALCULATED AND MEASURED LIQUID COLUMN SPACING

Fluid	σ (dynes/cm)	ρ (g/cm^3)	Calculated Spacing, λ (cm)	Measured Average Spacing (cm)
Water	72.7	1.000	2.42	2.1
Ethyl Alcohol	22.3	0.792	1.51	1.3
Ammonia	20.7	0.607	1.66	1.7

Heat Transfer

The average shell-side heat conductance measured on the tube with 20 fins/in., 0.060 in. high, is shown in Fig. 5. Within the liquid-sheet regime, at feed rates above 300 lb/hr ft, the conductance is insensitive to feed rate and heat flux. The increment in conductance over that of a smooth tube with the same reference area surpasses the increment in surface area (3.17), which indicates that the fins improve the efficiency of the heat-transfer process. In the range of feed rates between 200 and 300 lb/hr ft, corresponding to the transition zone between the sheet and column regimes, unsteadiness of the liquid flow pattern results in some scatter of the data, with occasional peaks in conductance. Within the column and drop regimes, below 200 lb/hr ft, there is a monotonic deterioration of heat conductance as the feed rate is decreased, becoming severe at the low end of the drop regime. This is attributed to the presence of dry areas, as discussed before. Under partial dryout conditions the accuracy of the data is questionable; however, there is little doubt that the qualitative trend is correct. It should be noted that the feed rates in question are of practical importance, since at a heat flux of 5000 Btu/ft^2 hr a feed rate of 200 lb/hr ft corresponds approximately to a stack of 88 tubes, which would suffer from partial dryout. This indicates that a fin height of 0.060 in. is excessive.

A tube with lower fins (0.037 in. high) and the same pitch was tested in search of a better configuration. The results of these tests are shown on Fig. 6. The situation is not improved, since there is a general decrease in heat conductance, and partial dryout is still present at the same feed rates observed on the tube with higher fins.

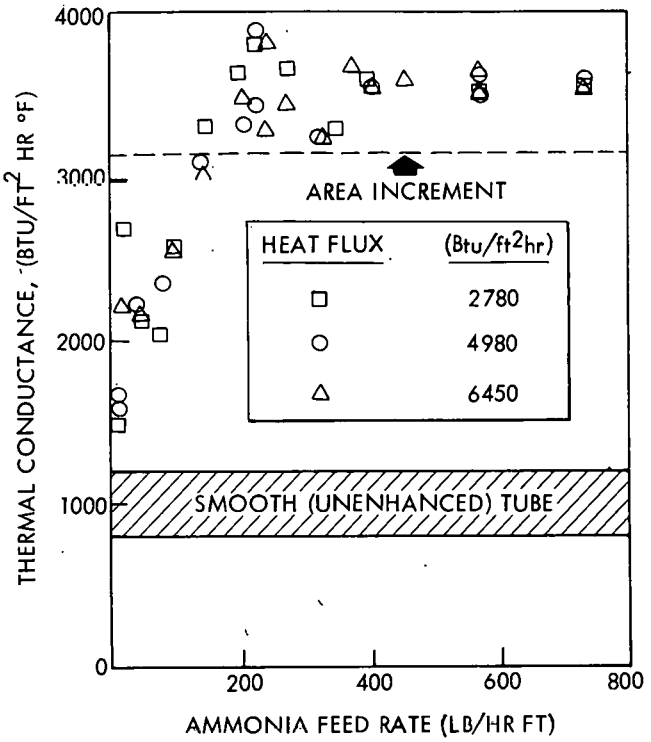

Fig. 5. Shell-side heat transfer for ammonia evaporation on standard 1-in. aluminum tube with 20 fins/in., 0.060 in. high.

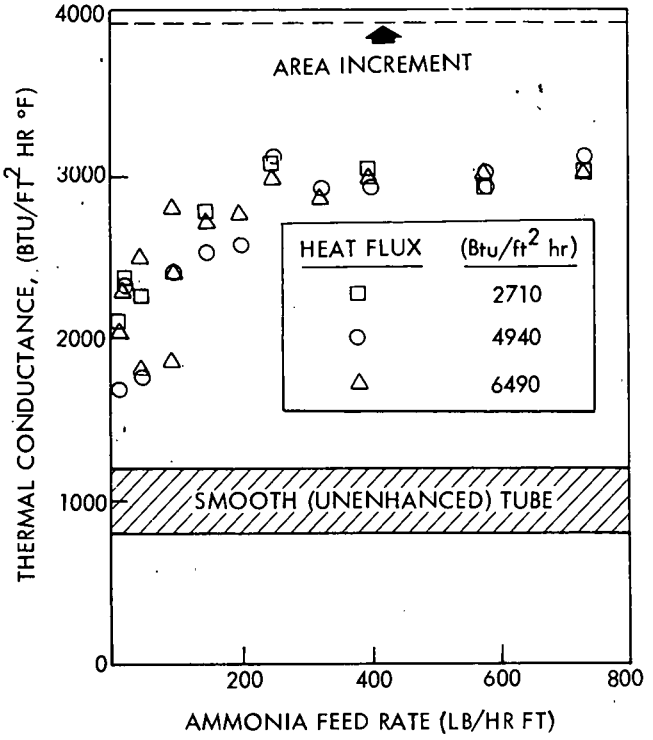

Fig. 7. Shell-side heat transfer for ammonia evaporation on standard 1-in. aluminum tube with 34 fins/in., 0.050 in. high.

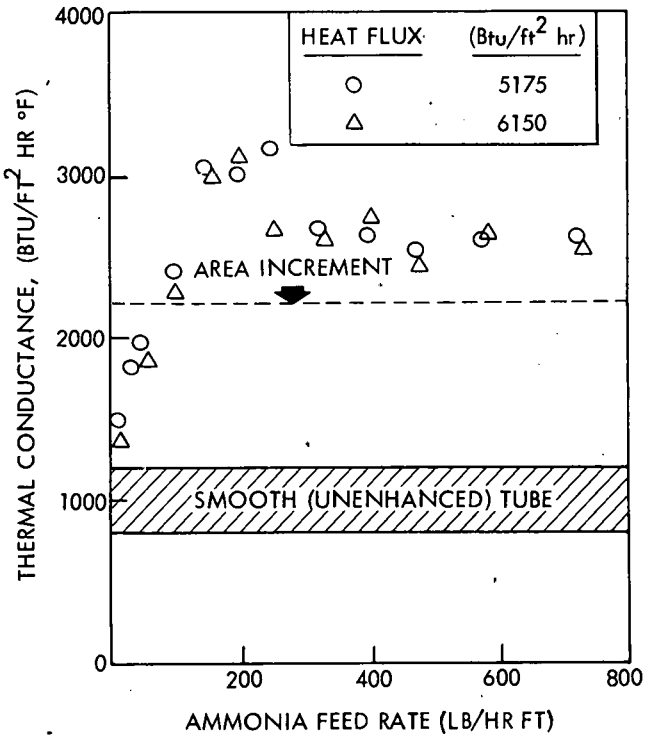

Fig. 6. Shell-side heat transfer for ammonia evaporation on standard 1-in. aluminum tube with 20 fins/in., 0.037 in. high.

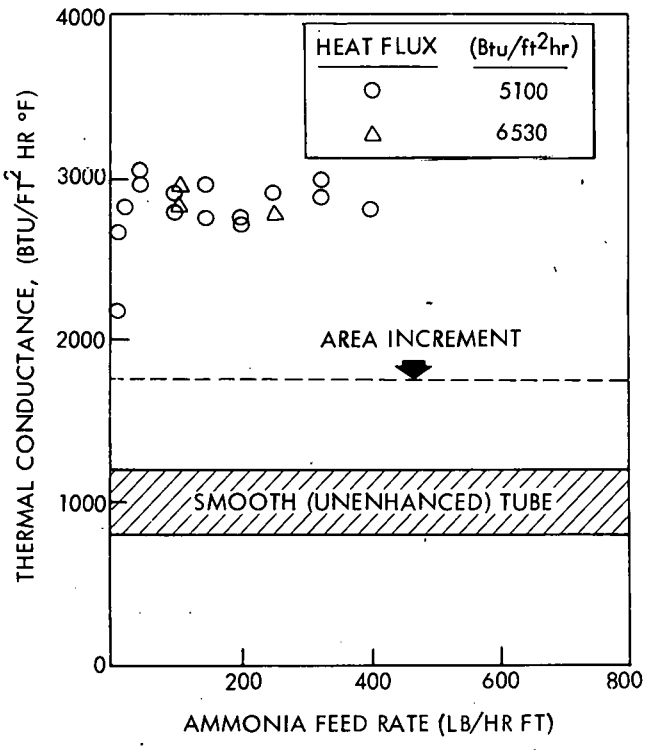

Fig. 8. Shell-side heat transfer for ammonia evaporation on modified 1-in. aluminum tube with 20 fins/in., 0.020 in. high.

To maintain the amount of surface extension with lower fins one may decrease the fin pitch, and to pursue this alternative a third standard tube was tested – this time with 34 fins/in. and a fin height of 0.050 in. – yielding a surface area ratio of 3.9. The results of the tests are shown on Fig. 7. This configuration is considerably less efficient than the one with 20 fins/in., 0.060 in. high, since it yields lower conductance with greater surface extension.

In an effort to improve tube wettability with a moderate loss in surface extension, the fins of the tube with 20 fins/in. were turned down to 0.020 in. and tested under the same conditions as the others, with the results shown on Fig. 8. Tube wettability was improved significantly, and the heat conductance was constant at feed rates down to approximately 30 lb/hr ft, having suffered a reduction of about 28 percent with respect to that measured on the same test specimen with the original 0.060-in. fins. It should be noted that the performance achieved is not claimed to be optimal, and it is likely that further improvements are possible.

Conclusions

- This investigation shows that low circumferential fins can increase significantly the heat conductance of aluminum tubes for duty in horizontal ammonia-film evaporators under OTEC working conditions.
- A tube with 20 fins/in., 0.020 in. high, has about three times more shell-side conductance than a smooth tube with the same cylindrical reference area. Without tube-side enhancement, this would result in an increase of approximately 50 percent overall heat conductance. The configuration described is not necessarily optimal, and further improvements are likely.
- Commercial tubes of the "low fin" type, often used in condensers, have fins that are too high for duty in horizontal ammonia-film evaporators as envisioned for OTEC application.
- There is a limit to effective surface extension with increasing fin height, imposed by tube dryout at intermediate and low feed rates. This is a three-dimensional flow phenomenon related to the flow regimes of the falling liquid film, and it is not taken into account in current mathematical models of heat transfer in finned tubes.
- It appears that flow unsteadiness and tube inclination have a significant effect on tube wettability and heat transfer. A systematic investigation of these phenomena seems warranted.

References

1. R. Gregorig, "Hautkondensation an feingewellten Oberflachen bei Beruksichtigung der Oberflachenspannungen," Zeitchrift fur angewandte Mathematik und Physik, Vol. V, 1954, pp. 36–49
2. R. L. Webb, "A Generalized Procedure for the Design and Optimization of Fluted Gregorig Condensing Surfaces," Proceedings of the Fifth Ocean Thermal Energy Conversion Conference, Vol. 3, Miami Beach, Florida, 20–22 Feb, 1978
3. D. K. Edwards, K. D. Gier, P. S. Ayyaswamy, and I. Catton, "Evaporation and Condensation in Circumferential Grooves on Horizontal Tubes," ASME Paper 73-HT-25
4. D. K. Edwards, A. Balakrishnan, and I. Catton, "Power-Law Solutions for Evaporation from a Finned Surface," J. Heat Transfer, Aug 1974, pp. 423–425
5. R. J. Conti, "Experimental Investigation of Horizontal-Tube Ammonia Film Evaporators With Small Temperature Differentials," Proceedings of the Fifth Ocean Thermal Energy Conversion Conference, Vol. 3, Miami Beach, Florida, 1978
6. A. K. Whitney, private communication
7. D. Yung, J. J. Lorenz, and E. N. Ganic, "Vapor/Liquid Interaction and Entrainment in Shell-and-Tube Evaporators," Argonne National Laboratory Tech. Memorandum ANL-OTEC-78-2, Jun 1978

DISCUSSION

J. Michel, Oak Ridge: Did you detect any boiling in this test or was it still surface evaporation?

R. Conti: No, we did not have any boiling; again, the superheat was not very high. The greatest superheat we had at the reference surface was about 3°F, and we didn't push the heat flux beyond that. We were already getting approximately 6500 Btu per square foot per hour and have had no indication of boiling at all.

R. Webb, Penn State: When you spoke about the effect of wettability as a function of fin height, were you referring to the fact that the high fins can prevent distribution of the liquid that drops from the upper tube so that it can not wet other zones on the tube?

R. Conti: Yes, there are two problems with the higher fins. You mentioned one – that they impede axial distribution – so any break in the feed will give you a dry area. The other problem is that the common commerical fins that we were testing drain fast enough so that the tall fins are partially in the vapor and so wetted area as well as axial communication are lost.

R. Webb: One follow-up question. You state that inclination helps on heat transfer, but I don't think your paper contains any data on that. Could you comment on that point?

R. Conti: No, I cannot say much about that, because it hasn't been explored extensively. We just observed that inclination, as shown in the movie, gave heat transfer that was comparable to the fully wetted tube. Generally, I think, unsteadiness and inclination tend to improve things. We will look into this in the future.

B. Keramati, General Electric: Are you planning to run any tests with nucleation enhancer surfaces, such as the Linde surface, so that you induce boiling even at these low ΔT's?

R. Conti: Our plans are uncertain. I understand that you're not talking about double enhancement, that you want fins or Linde surface.

B. Keramati: I envision a Linde-type surface on the fins.

R. Conti: Oh, that's a good one. We'll think about it. Maybe Linde would be interested in hearing that one.

AMMONIA VAPORIZATION AND CONDENSATION INVESTIGATIONS RELATED TO OTEC HEAT EXCHANGERS

C. M. Sabin* and H. F. Poppendiek**

Geoscience Ltd
Solana Beach, California 92075

Abstract

The Geoscience program consists of three separate tasks, all appropriate to OTEC closed cycle power plant heat exchangers.

The first of these tasks is the measurement of heat transfer conductances of liquid ammonia films evaporating over horizontal round tubes. Investigated in this task were the effect of the materials, the effect of flow rate, and the effects of several tube surface modifications. The tube material influenced neither the wettability by liquid ammonia, nor the measured heat transfer conductances. The heat transfer conductances measured were within limits presently used by designers over the entire flow rate range. An unexpected result was the behavior of Linde Hi-Flux, which exhibited a transition from non-nucleating to high conductance, nucleating behavior as heat flux was increased. The observed transition occurred in the heat flux range for which the 1 MWe heat exchangers have been designed.

The second task is the measurement of heat transfer conductances for ammonia condensing over horizontal tubes with modified surfaces similar to the Gregorig surfaces found advantageous for condensation over vertical tubes. Surface modifications improved heat transfer performance.

The third task is the measurement of shear entrainment of liquid from horizontal tube bundles subjected to vapor cross flow. Qualitative and quantitative data are described.

Introduction

OTEC heat exchanger designers require test data at realistic heat flux levels, temperature levels, and liquid flow rates to support theoretical predictions and correlations. The Geoscience program addresses three subject areas intended to provide basic design data relating to heat exchangers in the closed cycle power plant. The three subject areas are: heat transfer to ammonia films evaporating over horizontal tubes, condensation over horizontal tubes with modified surfaces, and shear entrainment of liquid within horizontal tube banks by transverse vapor flow. This work is part of a continuing program in heat transfer and fluid flow, particularly in conductance enhancement, supported by DOE OTEC project.***

* Vice President.

** President.

*** Contract EY-76-C-03-1094.

Film Evaporation

The present film evaporation tests, which extend work by Geoscience reported earlier,[1,2] cover three aspects of system design which affect heat transfer to liquid films. These are: the effect of tube surface material, the effect of liquid flow rates, and the effects of various surface modifications.

Effects of Tube Material

Geoscience tests of the film evaporation process in 1977 demonstrated some aberrations in wettability of surfaces by ammonia liquid. This phenomenon was attributed to the specific cleaning procedure which was used at that time. That conclusion has since been verified by tests at TRW.[3] However, there was still some concern that the heat transfer rates might be affected by variations in wetting behavior of the material itself. Therefore, tests were made of the film evaporation heat transfer properties of as-drawn tubing from several different materials, all of which are presently being proposed for use in the OTEC plant. These are commercially-pure titanium, the aluminum alloy 5052, the copper-nickel alloy 90-10, and the Allegheny-Ludnum stainless steel 6X. According to the manufacturer, the corrosion resistance of this latter material is strongly dependent on the heat treatment and since the heat treatment affects the grain structure, there was some possibility that this might effect the wettability and, through that, the heat transfer. The material was, therefore, obtained heat treated for corrosion resistance, and with a ground finish rather than as-drawn. All of these materials appeared to wet immediately, and no effect of the material on the heat transfer has been observed. The results for the various materials are identical within the experimental accuracy. A comparison of heat transfer rates for the various materials is shown in Figure 1.

Effect of Flow Rate

The liquid flow rate range investigated in the first program extended up to about 25 pounds per hour of liquid per foot of tube length. Since some designs utilize considerably higher flows than this in portions of the bundle, the flow rate range was extended to 150 lb/hr ft.

Figure 2 shows the variation in heat transfer conductance which can be expected as a result of the liquid flow rates. The liquid layers are laminar, based on a Reynolds modulus utilizing the liquid film thickness and transition criteria appropriate to a smooth inclined plate,

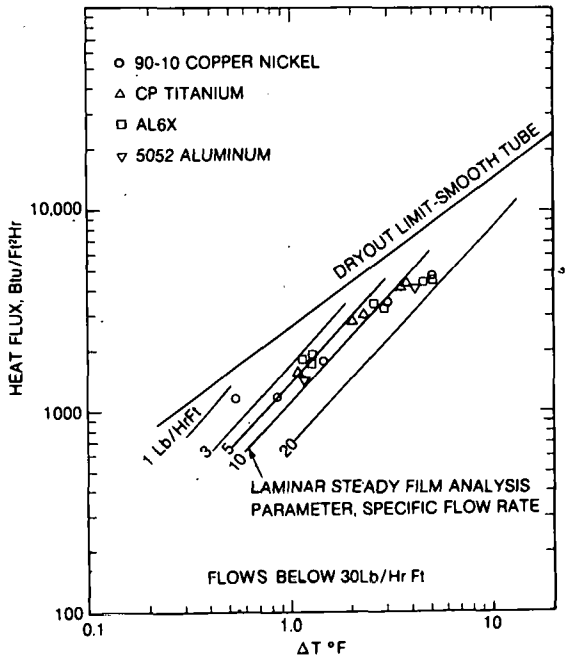

Figure 1. Heat flux versus temperature difference, smooth tubes with low flows.

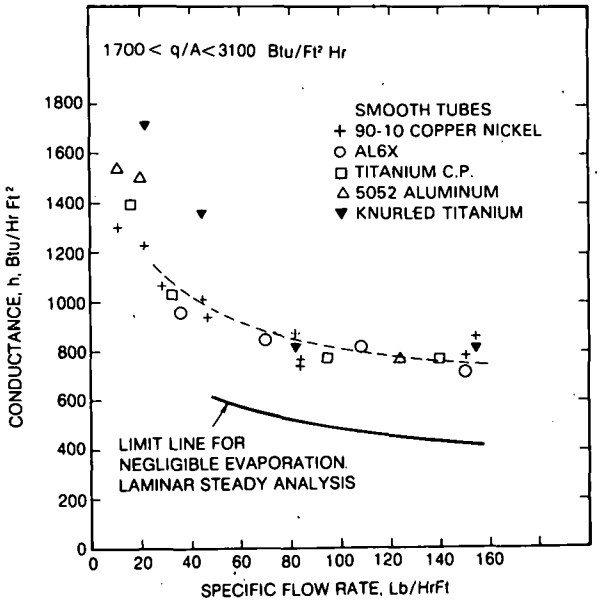

Figure 2. Heat transfer conductance as a function of flow rate.

throughout this range. However, visually they appear irregular and unsteady because of the liquid application process. At a liquid loading of 150 lb/hr ft, the flow between tubes consists of intermittent columns and droplets, and the dropping points move in an apparently random manner and there is some splashing. This randomness persists down to the lowest flows tested although the between tube flow is purely dropwise.

The weak relationship between average flow rate and measured conductance is believed to be caused by the nature of the intermittent liquid application. The unsteadiness of these flows is in sharp contrast to the uniform steady films of condensation, where the laminar analysis predicts heat transfer conductances accurately. Because of the highly nonlinear relationship between film thickness and flow rate, most of the volume of a droplet runs off the tube quickly, leaving a more slowly moving thin film. The average film thickness is, therefore, changed only a small amount by fairly large changes in applied flow. All of the data for flows over smooth tubes up to at least 30 lb/hr ft cluster around the predictions for a laminar film with a steady flow of five to 20 lb/hr ft.

Effects of Surface Modification

Modified surfaces tested included sandblasted, diamond-knurled, double-screen covered, and Linde Hi-Flux. This latter treatment was composed of aluminum over titanium.

Both the diamond-knurled and sandblasted finishes are effective in enhancing the heat transfer at low flow rates where the films are thin. At low flow the diamond-knurl spreads the liquid along the tube and thins the liquid layer enough to enhance the heat transfer significantly. The sandblasted finish has a small enhancement effect probably due to improved liquid distribution over the surface. However, with the thick liquid layers encountered with high flow rates, the surface modifications no longer influence conductances significantly. These effects may be seen in Figure 3.

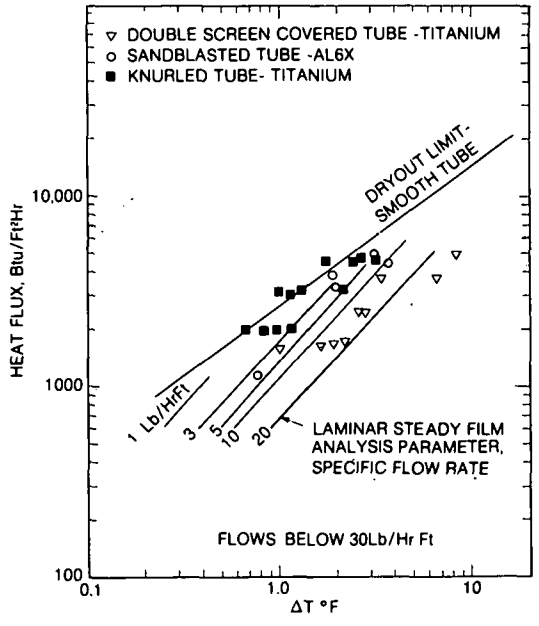

Figure 3. Conductances measured for non-nucleating modified surfaces at low specific flow rate.

The double-screen arrangement, which was developed by Geoscience specifically to enhance nucleation in submerged tube boiling, was tested for film evaporation at the request of the OTEC office. It was hoped that the double-screen would cause the film to nucleate, thereby enhancing the film heat transfer. No nucleation

was observed with this surface throughout the range of flows and heat fluxes appropriate to the OTEC heat exchangers. In the absence of nucleation, the effect of the double-screen is to greatly impede the flow of liquid over the surface thereby thickening the film, and trapping slow moving liquid adjacent to the surface. The heat transfer conductances are low. Film boiling was encountered with this surface above 4000 Btu/ft^2 hr. This may be seen in Figure 3. One would expect the double-screen arrangement to be a rather poor choice for horizontal tube film evaporators.

The Linde Hi-Flux surface exhibited a curious performance with regard to film evaporation heat transfer. It had been observed that the iron Hi-Flux coating over a steel tube, which was tested in the preceding program, did not nucleate,[2] and this was apparently in contrast to the experience with Hi-Flux at other laboratories, although Conti, at Lockheed, observed that steady state nucleation was only reached after several hours.[4] Both non-nucleating and nucleating behavior were observed with the aluminum Hi-Flux in the present tests and the heat transfer conductances measured in the two regimes are vastly different. This may be seen in Figure 4. A

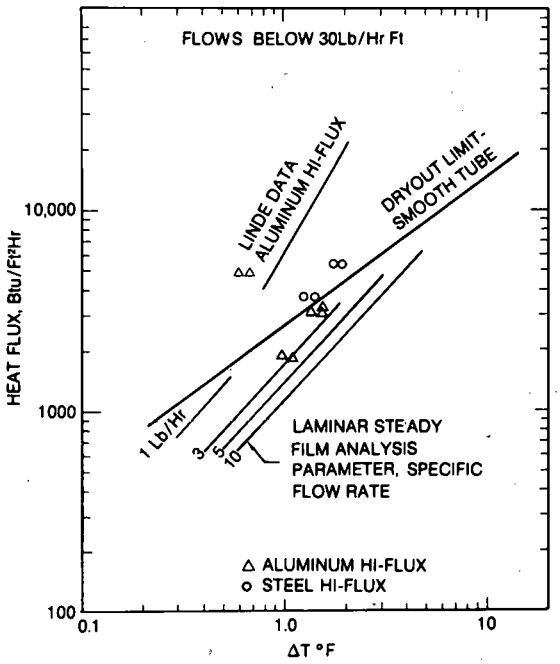

Figure 4. Conductances measured for Hi-Flux coated tube.

history of the performance of this surface during a particular day's run is shown in Figure 5. At start-up, the applied heat flux was small and the flow rate large. With constant heat flux, the flow rate was decreased in steps. This sequence corresponds to Curve 1 in the figure. During this sequence there was no visible nucleation and the film evaporation conductances were similar to those observed previously with the iron sample. The heat flux was then increased at low flow, and the flow rate increased in steps until the maximum was reached. This sequence is labeled Curve 2. The heat flux was then

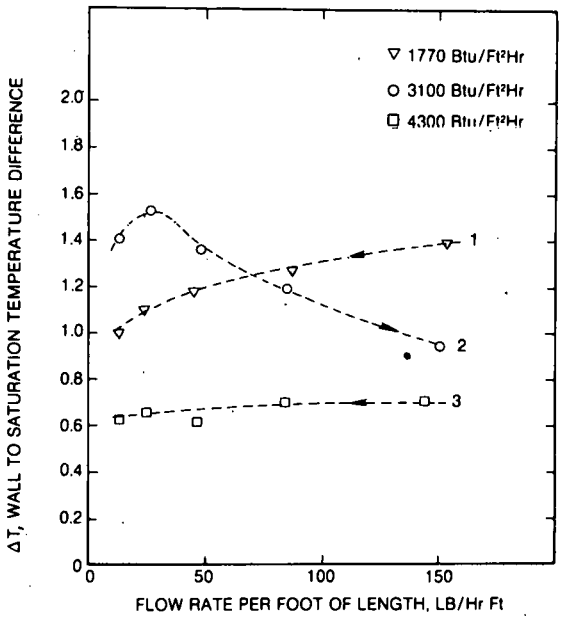

Figure 5. Temperature differences measured as a function of time for Hi-Flux.

increased again and the flow rate decreased in steps to generate Curve 3. During this procedure, the surface began to nucleate, and a massive change in heat transfer conductance was observed. It may be seen in the figure that despite the fact that the heat flux was increased by over a factor of two, the temperature difference from Sequence 1 to 3 decreased significantly. Once nucleation had been established on this surface it was possible to decrease both the heat flux and the flow rate and maintain nucleation down to a fairly low level.

The nucleating behavior is probably influenced by the fill procedure used in the tests. In order to remove the air from the Geoscience apparatus, it is evacuated. Usually the pressure in the container is reduced to 10^{-1} torr before introducing the ammonia into the tank. Nucleating surfaces, such as Hi-Flux, depend upon vapor or inert gas trapped in microscopic reentrant surface cavities to provide nucleation sites. Evacuation of the apparatus effectively removes inert gas, so ammonia vapor must be generated in these cavities subsequent to the fill procedure to initiate nucleation. Since the TRW 1 MWe evaporator has the lower half of its tube array covered with this material, and since the design heat flux is between the values for Curves 1 and 2, it may be necessary to start the evaporator at a higher temperature difference to initiate nucleation or, alternatively, to avoid evacuation before filling.

Condensation

Investigations of enhanced conductance condensing surfaces used by other investigators in the OTEC program have been directed toward fluted vertical tubes, while the heat exchangers being designed for near term construction utilize horizontal tubes. The tests described here are of tubes which approximate the vertical tube

Gregorig surfaces, but with the ridges formed in a helix of small pitch at almost right angles to the horizontal tube axis. The condensation tests have been done in the same apparatus used to perform Geoscience's film evaporation work. The test samples are thick-walled tubes, cooled on the inside by a high velocity flow of refrigerated water and provided with radially-spaced thermocouples placed so that the temperature drop through the wall can be measured to establish the heat flux.

Condensation tests have been performed on one plain tube and three modified tube surfaces. The modified surfaces consist of two different types. In one, grooves have been cut into the surface. The liquid condensate is drawn by surface tension into the grooves so that the layers on the ridges are thin. The ridges then act as the principal heat transfer surfaces. The other type consists of a smooth tube sample with a wire wrapped around in a helix. Surface tension draws the liquid through the wires so that the unmodified tube surface between acts as the heat transfer surface. Because of scheduling it was not possible to present the data here; however, all of these modifications enhance the condensation heat transfer conductances compared to the plain tube.

Shear Entrainment

The shear entrainment matrix under test is shown in Figure 6. This assembly is installed in a pressure

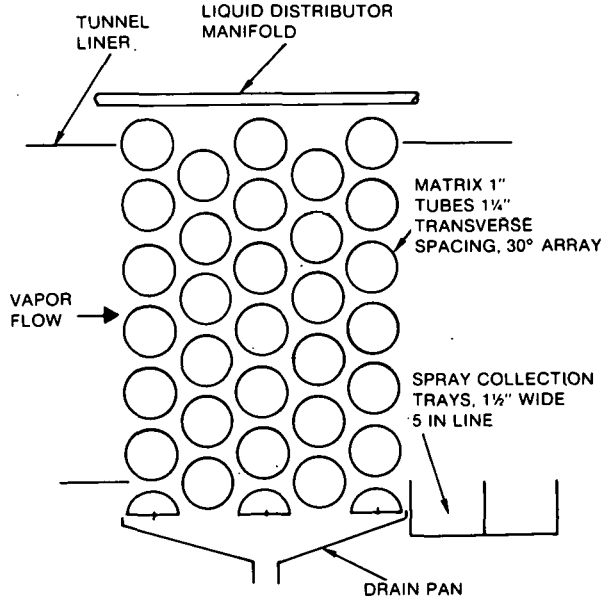

Figure 6. Shear entrainment test matrix.

vessel wind tunnel. The matrix array duplicates that installed in the 1 MWe evaporator. The liquid is introduced over the top of this array by a manifold assembly at points approximating the spacing of droplets that would naturally fall from a tube row directly above those in the matrix.

Variations in the liquid flow between a fraction of a pound an hour per foot of tube length and 150 pounds per hour per foot of length are within the capability of the equipment. Testing with ammonia liquid and vapor is not complete; the tests described here have been done with air saturated with Freon 113 vapor and Freon 113 liquid. The density of the saturated air is high, within a factor of two of ammonia vapor.

Drying of the front sides of the tubes begins to occur at quite low velocities, and ejection of liquid from the back of the bundle occurs at a somewhat higher velocity as given in Table I. Figure 7 shows the shape of the

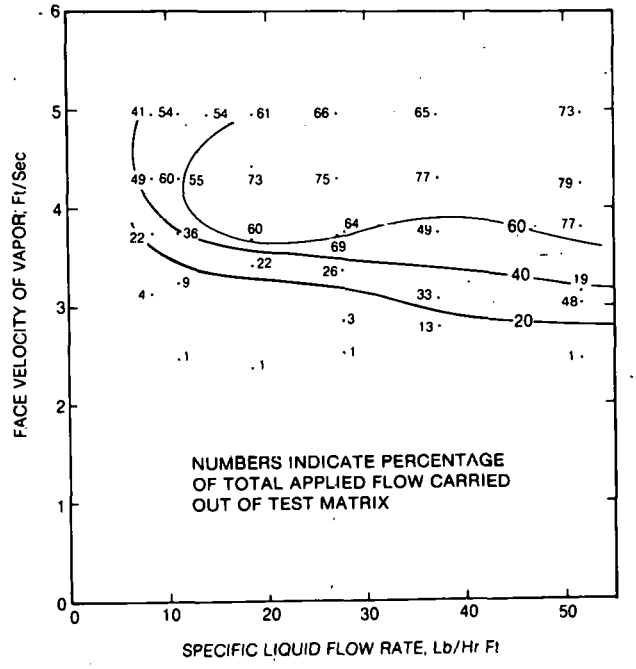

Figure 7. Shear entrainment contours for Freon 113 and air.

percentage entrainment contours as functions of the liquid and vapor flow rates. These entrainment contours are illustrative only, and are specific to the matrix tested. Clearly, a single row heat exchanger of great height would show 100 percent entrainment at adequate velocity, while one of great thickness would show some lower value.

Inspection of the array in Figure 6 shows that a large portion of the liquid shorn from a tube in one row would impinge on the next lower tube in the row downstream regardless of the vapor velocity, as long as it was above some threshold. Liquid would, therefore, migrate down through the bundle even at very high vapor velocity. The maximum entrainment observed in the matrix used in these tests is about 80 percent.

The analysis used to generalize these data and the forthcoming ammonia data is beyond the scope of this paper. However, Reference 5 provides criteria for some limiting cases, which are general. According to Equation (8) of that reference, the critical velocity for droplets falling from a tube to miss the tube directly below in the array is, for conditions of the present tests, 20 ft/sec, almost a factor of two higher than the experimentally observed upper value of 10.5 ft/sec. The failure of the model to accurately predict onset of entrainment does not appear to be caused by an inadequate

Table I. Vapor-Liquid Interaction Thresholds
Freon 113 Vapor-Air Mixture and Freon 113 Liquid

Condition	Vapor Velocity,* ft/sec
Fifth tube in first row completely dry	1.7
Front faces of first row tubes dry	1.0
Droplets ejected from back of matrix:	
To first tray	0.7
To second tray	2.1

ρ_L = 94 lb/ft^3; ρ_v = 0.23 lb/ft^3
Liquid loading 30 lb/hr ft.

physical representation of the droplet motion in the vapor stream, but instead from inaccurate initial conditions. The model presumes the droplets fall from the lowest point on the tube, whereas even very small transverse vapor flows move the release point around toward the approximate location of vapor flow separation in back of the tube. The model also presumes the droplet size is determined by surface tension forces. Observations of the Freon-air tests indicate that most entrained droplets are smaller than the measured quiescent drop size of 0.11 inches for Freon 113.

References

1. Sabin, C. M.; H. F. Poppendiek; D. J. Connelly; J. G. Dunbar, "Annual Report, Heat Transfer Enhancement for the OTEC Evaporator," Geoscience Ltd Report GLR-197, for U. S. Department of Energy, Contract AT(04-3)-1094, Dec 1977.

2. Sabin, C. M.; H. F. Poppendiek, "Film Evaporation of Ammonia Over Horizontal Round Tubes," Fifth OTEC Conference, Vol 3, Feb 20-22, 1978.

3. 1 MWe Heat Exchanger Preliminary Design Briefing Document, TRW, Inc., Mar 28, 1978.

4. Conti, R. J., "Experimental Investigation of Horizontal-Tube Ammonia Film Evaporators with Small Temperature Differentials," Fifth OTEC Conference, Vol 3, Feb 20-22, 1978.

5. Yung, D; J. J. Lorenz; E. N. Ganic, "Vapor/Liquid Interaction and Entrainment in Shell-and-Tube Evaporators," ANL-OTEC-78-2, June 1978.

* Face velocity. Velocity in minimum free flow area is five times larger.

DISCUSSION

D. Aronson: You've been talking about boiling evaporation; does that mean you are getting evaporation without bubble formation?

C. Sabin: That's correct.

D. Aronson: There was concern at one time about the fact that, as the stuff dropped down, you get droplets that would pose a problem in entrainment and carryover. Has that been confirmed or is that not really it?

C. Sabin: My own experience on that is that with nucleation enhancement, you get very active boiling accompanied by a mist. There is a dramatic difference between the boiling on the thin film like this and the nonboiling situation. We have done a limited number of tests with a Linde surface, and we have observed a fairly heavy mist coming from the boiling. I think the Argonne Lab had a similar experience.

THE MODELING OF THIN FILM HEAT EXCHANGERS

Shi-chune Yao*, Arthur W. Westerberg†, and Nien H. Chao**

Carnegie-Mellon University
Pittsburgh, Pennsylvania 15213

Abstract

The steady and dynamic behavior of thin film evaporators and condensers are simulated with a general thin film heat exchanger model. The dynamics of the gravity-controlled falling laminar film on horizontal or vertical tubes are studied in detail. For a first approach or for a slow transient a single-lumped model can be used. For a refined simulation or for a severe transient a grouped model is proposed. The grouped model preserves the unique feature of delay-time and wave-distortion of a transient, which was observed in a separate precise analysis.

The thin film heat exchanger models are used in the dynamic simulation computer programs ODSP3 and OSCAR which were established at CMU for OTEC systems. Typical results are presented to demonstrate the capability of the model.

Introduction

The design of shell and tube condensers has achieved substantial attention in the past as indicated in the review paper [1]. Thin film evaporators also have been studied extensively in the area of desalination and OTEC applications [2,3]. However, appropriate literature is not available for dynamic modeling of these components.

The evaporator in an OTEC system generates vapor from a flowing liquid film on horizontal or vertical tubes. The vapor passes the turbine and then condenses in the condenser as a liquid film, again on horizontal or vertical tubes. The common feature of evaporators and condensers is that the major transport process happens at the liquid films. Therefore, it becomes possible to simulate the dynamic behavior of these components by a unified approach which models "Thin Film Heat Exchangers" in general.

In a thin film heat exchanger the motion of a liquid film can be influenced by the motion of the flowing vapor. However, near the central region of the bundle where vapor flow is insignificant, the film falls mainly due to gravity. A schematic of the flow regimes in a thin film evaporator is shown in Figure 1.

At close to the edge of the bundle the vapor cross flow can be strong enough to break the liquid film by shear stresses. The transition of film flow between the shear-controlled and gravity-controlled regimes on horizontal tube bundles can be well described by a dimensionless gas velocity Jg*[4]. In addition, the liquid entrainment and the breakdown of films have been analyzed in [5,6], respectively. In spite of this, the general behavior of this shear dominant film flow is still not well known.

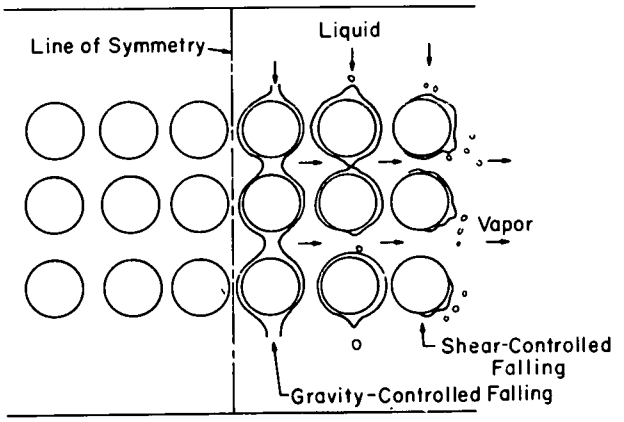

Figure 1. Flow Regimes in a Thin Film Heat Exchanger.

On the other hand, gravity-controlled steady state film flow and heat transfer behavior have been studied extensively in the past [7,8] and the dynamic simulation based upon this flow regime is more feasible at the present time. In the present unified approach, a column of horizontal tubes or a single section of vertical tube in an evaporator or a condenser is considered. The liquid film falls vertically due to gravity. The film thickness either increases or decreases depending upon whether the unit is a condenser or an evaporator.

Practically, in the thin film OTEC evaporator the feed rate of the working fluid onto the bundle is considered as one of the most effective parameters for the control of the system. Generally, slow transients of the liquid film flow occur for conventional operation of an evaporator; however, severe film transients occur at emergency operations. For example, a sudden drop of the load to the generator causes the torque on the turbine to disappear. The turbine may overspeed if the vapor flow through the turbine is not rapidly reduced. Opening the bypass valve and shutting the feed to the evaporator reduce the pressure drop over the turbine and reduce the vapor flow through it; however they must react within about one second. With these process upsets, the liquid film on the evaporator tubes experiences severe transients.

The classification of flow transients in a thin film heat exchanger can be made by the following argument. At steady operation the liquid is fed to the top of the bundle with sufficient over-flow. The time required for the liquid traveling to the bottom of the bundle is, typically, in the order of 5 seconds. For a variation of feeding with a characteristic time longer than 5 second, the quasi-steady approach for the film dynamics can be used with reasonable accuracy. For the variation of feeding with a characteristic time less than 5 seconds, the quasi-steady approach does not give a reasonable result. More precise modeling will be necessary.

In the quasi-steady approach, the flow transient should be slow. At any intant throughout flow conditions the bundle are very similar. Therefore, all the tubes in a bundle may be considered as a single representative tube. In other words, the whole bundle

*Assistant Professor, Mechanical Engineering Dept.
†Professor, Chemical Engineering Department
**Graduate Student, Mechanical Engineering Dept.

in a thin film heat exchanger may be simulated by a single-lumped tube, with steady state solution applied at each moment.

At severe transients the model should consider the whole horizontal tube column as a series of grouped-control-volumes, with each group containing several tubes. The most accurate analysis considers each horizontal tube as a group. If only one group is used for the whole column, this model becomes a single-lumped approximation. The practical selection of the number of groups should be based upon the expected typical transient of the feed. With these lumped subsystems arranged in a vertical series, the time response of a film is simulated while keeping calculational effort to a minimum.

In each lumped subsystem the film thickness and the heat transfer coefficients are taken from the results of theoretical studies or empirical correlations. The dynamic behavior of the film is studied with quasi-steady analysis, and some typical results of the model will be compared with a much more detailed calculation of transients.

In the following sections the quasi-steady approach and the grouped approach film transients will be presented in detail. Additionally, the results of a separate detailed analysis on film transients are compared to the proposed model. The incorporation of this model into a heat exchanger model is described in the section "The Modeling of Heat Exchangers" as the heat exchanger model is to be used in dynamic simulation computer programs written at CMU. Finally, a typical result is shown of the dynamic behavior of a thin film exchanger using the proposed grouped model.

The Quasi-Steady Approach to Film Dynamics

A. Horizontal Tubes

We start by considering a single tube operating at steady-state. The initial condition at x=0 is that the inlet volume flow rate per unit length equals $2\Gamma_o$. For laminar flow with constant wall heat flux the film thickness δ is [12]

$$\delta = \{[(\frac{3\nu\Gamma_o}{g}) - (\frac{q_w}{\rho_\ell h_{fg}})(\frac{3\nu R}{g})(\frac{x}{R})]/\sin(\frac{x}{R})\}^{1/3} \quad (1)$$

where ν is the kinematic viscosity, q_w is the wall heat flux leaving the surface, ρ_ℓ and h_{fg} are the liquid density and latent heat of vaporization, R is the radius of the horizontal tube, and x is the distance measured from the top of the tube along the surface. We may set $\sin(\frac{x}{R}) = 1$ in the equation (1) for vertical tubes. In most cases, the rate of evaporation of the liquid on an horizontal tube is very much less than the liquid flow rate.

In some cases the tubes are coated with heat transfer augmentation material such that boiling occurs in the evaporator. The heat transfer coefficient of the boiling thin film can be put in a general form [9]

$$h = C(T_w - T_v)^n \quad (2)$$

In a condenser or when pure evaporation occurs in the laminar film the heat transfer coefficient is related to the film thickness as [10]

$$h = k/\delta \quad (3)$$

B. Vertical Tubes

Liquid falling on a vertical tube is very likely to be in wavy laminar flow or in turbulent flow. Correlations are presented here for smooth tubes. The film thickness is described as [11]

$$\delta/(\frac{\nu^2}{g})^{1/3} = 0.36(\frac{\nu\delta}{\nu})^{0.55} \quad (4)$$

The heat transfer coefficient for wavy laminar flow is

$$h = 0.606\,(k^3 g/\nu^2)^{1/3}\,[\Gamma/\mu]^{-0.22} \quad (5)$$

and for turbulent flow

$$h = 3.8\times10^{-3}(k^3 g/\nu^2)\,(4\Gamma/\mu)^{0.4}\,(\frac{\nu}{\alpha})^{0.65} \quad (6)$$

with laminar to turbulent transition [7] at

$$\frac{4\Gamma}{\mu} = 5800\,(\frac{\nu}{\alpha})^{-1.06} \quad (7)$$

Grouped Approach to Film Dynamics

In this approach lumped subsystems are assigned to several consecutive horizontal tubes or a section of vertical tubes. Figure 2 shows the schematic of the model. Within each subsystem, a proper delay time is chosen to take into account the free falling of liquid between horizontal tubes as well as the finite liquid flow velocity along the tube. When the number of horizontal tubes in a subsystem equals the total number of tubes in a column or the length of the vertical section equals the total length of the vertical tube, the present model corresponds to the single-lumped model. When there is only one horizontal tube in a subsystem or when the length of vertical section in a subsystem is very short, the present model approaches the exact case.

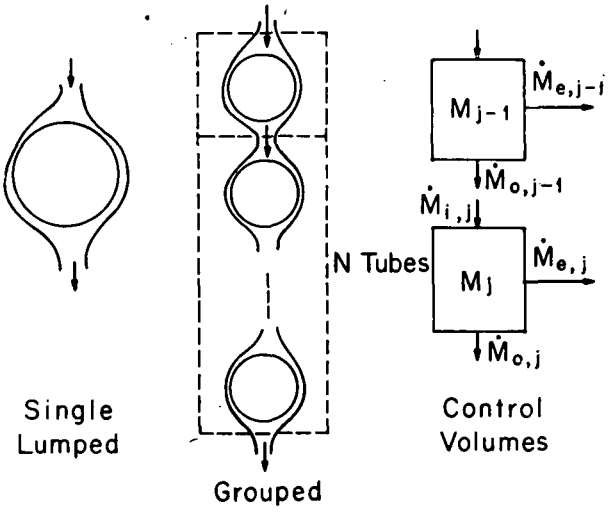

Figure 2. Single-Lumped and Grouped Models.

The mass balance of each lumped subsystem j can be written as

$$\frac{dM_j}{dt} = \dot{m}_{i.j} - \dot{m}_{o.j} - \dot{m}_{e.j} \quad (8)$$

where $\dot{m}_{i.j}$ is the inflow to control volume j, $\dot{m}_{o.j}$ is the outflow from control volume j, $\dot{m}_{e.j}$ is positive for evaporation and negative for condensation. In order to solve this equation, all the $\dot{m}$'s must be present in terms of M's.

In the evaporator, dryout of the liquid film may occur during a transient. This corresponds to $M_j=0$ in a subsystem.

A. Horizontal Tubes

At initial steady state, the total mass in the subsystem is

$$M_j = N_j \rho_\ell \int_0^{\pi R} \delta(x)dx \qquad (9)$$

where N_j is the number of horizontal tubes in the control volume j. Using equation (1) for $\delta(x)$, with $q_w \cong 0$, we get

$$M_j=2N_j\rho_\ell R\left[\frac{3\nu\dot{m}_{i.j}}{2\rho_\ell g}\right]^{-1/3} \int_\Delta^{\pi-\Delta} \sin y^{-1/3}\, dy \qquad (10)$$

The values of the Δ is assigned to be the half thickness of the falling film between horizontal tubes.

The flow rate at the inlet of subsystem j comes from subsystem j-1.

$$\dot{m}_{i.j}(t) = \dot{m}_{o.j-1}(t) \qquad (11)$$

In this subsystem, $\dot{m}_{o.j}$ is related to $\dot{m}_{i.j}$ by a delay time $\bar{t}_j$. That is

$$\dot{m}_{o.j}(t) = \dot{m}_{i.j}(t-\bar{t}_j)\frac{1}{\bar{t}_j}\int_{t-\bar{t}_j}^{t} \dot{m}_{e.j}(t)dt \qquad (12)$$

such that equation (8) becomes

$$\frac{dM_j}{dt} = \dot{m}_{o.j-1}(t) - \dot{m}_{i.j}(t-\bar{t}_j)\dot{m}_{e.j}(t) + \frac{1}{\bar{t}_j}\int_{t-\bar{t}_j}^{t} \dot{m}_{e.j}(t)\,dt \qquad (13)$$

The evaluation of the delay time $\bar{t}_j$ will depend upon the transient film behavior and the falling of the film between the tubes.

For a quasi-steady system the delay time is the time for the fluid to travel through a subsystem

$$\bar{t}_j = f(M_j)= \frac{N_j\,\pi R}{0.806}\left(\frac{3\nu}{g}\right)\left[\frac{2N_j\rho_\ell R}{M_j}\int_\Delta^{\pi-\Delta} \sin y^{-1/3\ 2}\, dy\right] \qquad (14)$$

For a fast transient, the total mass M_j can vary as a function of the time, and the film thickness. in the subsystem can also vary as a function of location. The selection of the proper M_j for the evaluation of $\bar{t}_j$ is not straightforward. The exact solution of transient film motion was obtained by the authors.[12] Figure 3 shows the flow decay at various locations on a tube column. Also it appears that the thicker the film the faster it moves. For a film with non-uniform thickness the thicker film will catch up with the film in front of it. In other words, the thick part of the film travels with higher speed and dominates the transient behavior.

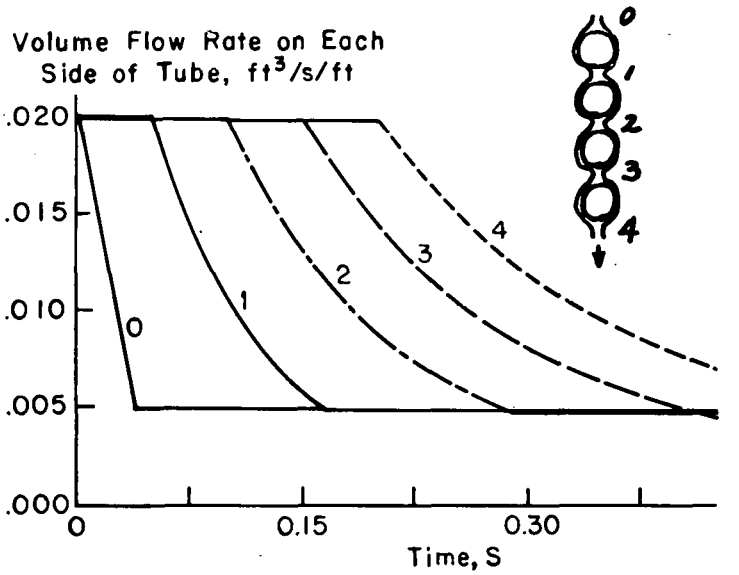

Figure 3. Evaporating Ammonia Film on One-Inch Tubes - Transient Analysis.

Since the flow has a delay time $\bar{t}_j$ the value of the total fluid mass for equation (14) can be selected at the time t, or the time $t-\bar{t}_j$, or the time between these two limits. For example, a transient with increasing flow will have the total fluid mass at time t more than the total fluid mass at time $t-\bar{t}_j$. Then $M_j(t)$ should be used in equation (14). A transient with decreasing flow will have the total fluid mass at time t less than the total fluid mass at time $t-\bar{t}_j$. Therefore, $M_j(t-\bar{t}_j)$ should be used for equation (14). In a general form we can use a weighted combination for the time delay. For example,

$$\bar{t}_j = N_j\sqrt{\frac{2H}{g}} + \varepsilon f(M_j(t-\bar{t}_j)) + (1-\varepsilon)\, f\,(M_j(t)) \qquad (15)$$

where the first term on the right side is due to the falling of the film between tubes. $\bar{t}_j$ is solved by iteration in equation (15). The selection of ε is quite flexible. A smooth function is constructed for this purpose.

Finally, the evaporation rate can be calculated using

$$\dot{m}_{e.j} = \bar{h}\ 2N_j\pi R(T_w - T_v)/h_{fg} \qquad (17)$$

where

$$h = \frac{1}{\pi R}\int_0^{\pi R} h(x)dx \qquad (18)$$

with h(x) given from equations (2) or (3) and presented in terms of M_j.

A typical result of the variation of flow rate on a system containing 20 consecutive horizontal tubes is shown in Figure 4. Each tube is treated as a single subgroup. The effect of delay time is clearly presented.

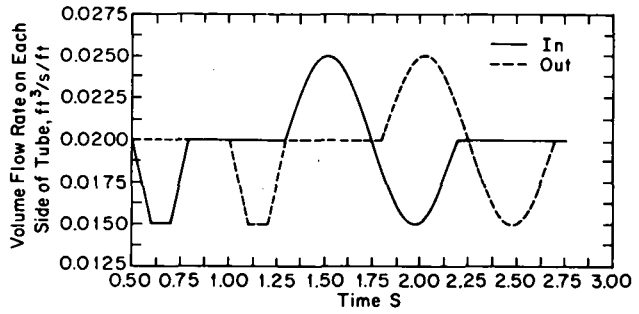

Figure 4. Evaporating Ammonia Film on 20 Consecutive One Inch Tubes Result of Grouped Model.

B. Vertical Tubes

Equation (8) can also be used for vertical tubes. The total mass in the subsystem is

$$M_j = L_j \pi D \delta \rho_\ell \tag{19}$$

Using equation (4) for δ, we get

$$M_j = 0.36\, L_j (\pi D \rho_\ell)^{0.45} \left(\frac{\nu^2}{g}\right)^{1/3} \left(\frac{m_{o.j}}{\nu}\right)^{0.55} \tag{20}$$

The evaporation rate is then

$$\dot{m}_{evap.j} = \bar{h}\, \pi D L_j\, (T_w - T_v)/h_{fg} \tag{21}$$

and $\bar{h}$ is the averaged heat transfer coefficient using h(x) as given by equation (5) and (6).

The Modeling of Heat Exchangers

The models for the condensers and evaporators are complicated. Transient heat balances are formulated for the water, the tube, the ammonia liquid on the tube and the vapor in the vessel, and finally for the liquid in hotwell.

The transient heat balance of the water considers the heat transfer to the tube and the incoming and outgoing enthalpies of water. To approximate the dynamic behavior, the transit times for the water are introduced as a time delay. The transient enthalpy balance for the ammonia liquid on the tubes and ammonia vapor in the vessel considers the heat transfer from tubes to vapor, liquid feed onto the the hotwell during depressurization, and the vapor leaving the vessel.

Mass balances are also formulated separately to describe the holdup for the vapor, the liquid ammonia on the tube, and the liquid in hotwell. Additionally, the state equation for the vapor temperature is written with the assumption that the vapor in the condenser is in the saturated state and also that it follows the ideal gas law.

In general, this model can be applied to both the condenser and the evaporator. Specific consideration is given to the differences between the evaporator and the condenser. The condenser does not have liquid feed onto the tube and no vapor leaves the vessel. On the other hand, no vapor comes into the evaporator. Under normal operating conditions the evaporator will have ammonia transport from the liquid film to vapor in vessel; this transport will be a negative quantity for the condenser.

The liquid in the hotwell will flash when the vessel pressure is reduced to a value lower than the saturation pressure of the hotwell liquid. Also at some conditions, the evaporator may operate at a low recirculation rate and the tube may experience partial or complete dry-out during transients. Since the exact relationship between the heat transfer and film flow during partial dryout is not available in the open literature, only complete dryout is modeled for each subsystem in the grouped model.

The details of the heat exchanger modeling are presented in the Reference [13].

Results

Two computer programs were written at the Carnegie-Mellon University for the dynamic simulation of OTEC power plants. The program ODSP3 [14] used the single-lumped approach for modeling heat exchanger transients. The program OSCAR [13] uses the grouped model in simulation.

A typical OTEC closed cycle loop contains an evaporator and a condenser with the turbine in between. There is also a bypass valve installed between the evaporator and condenser. During a hypothetical accident the load of the generator is dropped and the turbine rotation speeds up drastically. At this moment, the by-pass valve opens and the feeding of ammonia to the evaporator is stopped. The vapor pressure in the evaporator tends to decrease due to the reduced vapor generation and the increased vapor outflow from the evaporator. The vapor pressure in the condenser increases initially due to the opening of the by-pass valve. But, eventually, the pressure in condenser decays because the vapor pressure in evaporator also decays.

Figure 5 shows the results of this calculation. The action of the by-pass valve and the ammonia feed valve to the evaporator was initiated at time 0.5s after the drop of the load. The dynamic response of the evaporator and the condenser is as we expected.

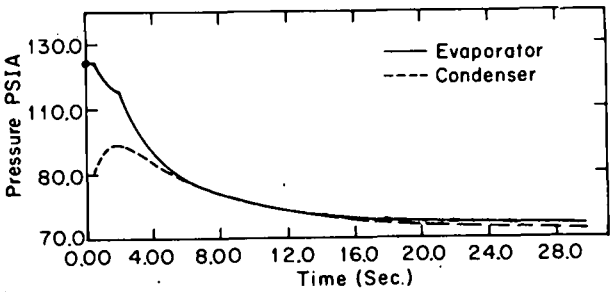

Figure 5. The Pressures in Evaporator and Condenser at a System Transient.

Acknowledgement

This material is based upon the work sponsored by the U.S. Energy Research & Development Administration/Department of Energy under contract No.EY-76-S-02-2641-A004. The constructive communication with the Westinghouse Electric Company is greatly appreciated.

References

1. Butterworth, D.,"Development in the Design of Shell and Tube Condensers," ASME Paper No. 77-WA/HT-24.

2. Fletcher, L.S., Sevnas, V., and Parker, W., "Evaporation Heat Transfer Coefficients for Thin Sea Water Films on Horizontal Tubes," Ind. Eng. Chem., Process Des. Dev., Vol.14, NO.4 (1975), pp.411-416.

3. Ganic, E.N. and Czikk, A.M., "An Analytical Model of the Sprayed Bundle Evaporators," Union Carbide Linde Division.OTEC Contract E(49-18)-2448.

4. Ishihara, K., Paten, J., and Taborek, J., "Critical Review of Correlations for Predicting Two-Phase Flow Pressure Drop Across Tube Banks," ASME Paper No.77-WA/HT-23.

5. Yung, D., Lorenz, J., and Gamic, E., "Vapor-Liquid Interaction and Entrainment in Shell-and-Tube Evaporators," ANL-OTEC-78-2.

6. Ihiratowicz, E., Gumkowski, S., and Mikidlewicz, "Experimental Study of Evaporation and Breakdown of Thin Liquid Films Driven by Shear Stresses," ASME Paper No.77-WA/HT-7.

7. Chun, K. and Seban, R., "Performance Prediction of Falling Film Evaporators," Trans. ASME J. of Heat Transfer, Nov.1972, pp.432-436.

8. Lorenz, J. and Yung, D., "An Analysis of Heat Transfer in Horizontal Tube Falling Film Evaporators," ANL-OTEC-78-1.

9. Collier, J., "Convective Boiling and Condensation," McGraw Hill Company, 1972.

10. Nusselt, W., "Die Oberflachenkondensation des Wasserdampfes," Zeitschr. Ver.deutsh. Ing.,60, 541 and 569 (1916).

11. Seban, R., "Transport to Falling Film," Paper K-30, 6th Int. Heat Transfer Conference (1978).

12. Yao, S.C., Chao, N.H. and Westerberg, A.W., "Transient Behavior of Condensing or Evaporating Films on Horizontal Tubes," 2nd Multi-Phase Flow and Heat Transfer Symposium, Miami Beach, April 1979.

13. Westerberg, A., Suuberg, E. and Yao, S., etal, "A Dynamic Simulation Program for OTEC," CMU-Rept. OTEC Contract No. EG-7-03-C1569.

14. Westerberg, A.W., Yao, S.C., et al., "Six Month Report for OTEC Dynamic and Control System Modeling," CMU-Rept. OTEC Contract No. DOE EY-76-S-02-2641-A004, September 1978.

DISCUSSION

D. Johnson, APL/JHU: First of all, a disclaimer. I know nothing about thin-film heat transfer, but it seemed to me that the talk from Mr. Conti indicated that wave propagation in the thin film was a very important factor, and that your model doesn't include that at all — it couldn't include it. Do you verify your model by comparing it with so-called exact solutions?

A. Westerberg: We can at least include the wave propagation by the choice of the film coefficient for heat transfer. We haven't taken into account the other aspects. I would like to point out that our heat transfer expert is Yao; I am the systems modeler, and I can not pretend to answer beyond that point.

J. Lorenz, Argonne National Lab: Assume you just have one horizontal tube, and I cut the flow from it. You're going to have drops hanging at the bottom due to surface tension. Have you done anything in your modeling to account for that residual liquid that hangs there due to surface tension on each tube? It could hang there for a significant amount of time before it evaporates. How might this effect your model?

A. Westerberg: We do not have that in the model. Although my guess is that that would not be a significant amount of liquid relative to the thin film, I do not know. Again, Yao could answer that.

K. Bell, Oklahoma State U: I think I can say that those of us who have worked, or have worried at least, about thin-film flow on banks of horizontal tubes, condensers or evaporators, look forward to the day when you have to come face to face with what is the local heat-transfer coefficient on each of those tubes. After about the second one...

D. Aronson: I wonder whether or not in your program you limited yourself in methods of control. For example, I can see that the turbine might be a radial inflow turbine with adjustable guide vanes, so that you would not have a bypass. The other aspect of it, of course, would be that you do not attempt to make rapid changes but either put a parasitic loss in your pump or other device which is loading the system, so if you lose our cable you have something you can hold onto until you can bring the system into equilibrium. These are real considerations, I think, that are options. Did your program allow for these alternatives?

A. Westerberg: There are two ways to answer that. Number one is that we have developed an executive capability — which is where I come in — which would allow any model you wish to put into the sytem to be put into it and handled in a very nice way. In other words, it can be used for both design and rating calculations and both dynamic and steady state. But the other side of the coin, the particular models that we have developed at the moment do not include that; however, we could add them to the system fairly readily. It's a modular flow-sheeting system that allows both arbitrary configuration and the adding of models by anybody who wishes to in a fairly straightforward fashion.

Question: It sounds like the model could lend itself, aside from OTEC, to other systems such as flashing conditions in a power system, in a turbine. Is this program in the public domain?

A. Westerberg: This program will be in the public domain since it has been basically developed with DOE money.

VARIFLUX AND FINNED-PLATE OTEC HEAT EXCHANGER TECHNOLOGY STATUS

D. Wright, W. Wagner, and J. Shoji

Rockwell International/Rocketdyne Division
Canoga Park, California 91304

Abstract

The competitiveness of the Ocean Thermal Energy Conversion (OTEC) Power System with other existing and proposed "nonfueled" energy systems is predicated upon the development of low capital cost, high-performance, low-maintenance heat exchangers (evaporator and condenser). Advances in the heat exchanger areas of increased performance and lowered cost can bring the OTEC concept closer toward a manufacturing and commercialization reality. The design approach discussed ~~in this paper~~ is directed toward minimization of the heat exchanger surface area to reduce manufacturing costs and improve efficiency through enhancement of both the working fluid and sea-water surfaces and the utilization of high-thermal conductivity, low-cost, corrosion resistant aluminum alloys. The heat exchanger concepts include: (1) a unique shell-less and scalable element consisting of a dual concentric tube element ("Variflux tube") and (2) a finned plate modular approach. Overall heat-transfer coefficients exceeding 1200 Btu/ft^2-hr-R (2 to 3 times conventional values) have been achieved. In addition, improved Variflux and finned-plate configurations predicted to yield overall heat-transfer coefficients exceeding 2000 Btu/ft^2-hr-R have been configured and experimental evaluation planned. These experimental data, the resulting conclusions, and the status of the two concepts are presented ~~in this paper.~~

Introduction

The requirements of the OTEC Energy Program to develop reliable, efficient, low-cost, and compact heat exchangers have been outlined during previous studies.[1,2] The analytical and experimental evaluation of the Variflux and plate-fin heat exchanger configurations are being performed to determine the potential of these concepts in an OTEC system. The Variflux concept as applied to the OTEC heat exchangers was initially presented in Ref. 3 along with initial test results.

Concepts discussed in this paper are the result of aerospace technology in high-performance, heat-exchanger design and production fabrication technology to achieve low fabrication costs. The incorportation of fins in a high-thermal conductivity, low-cost material such as an aluminum alloy can potentially offer a low-cost, high-performance, compact heat exchanger which can be modularized.

Programs to further experimentally evaluate the potential to the Variflux and the plate-fin heat-exchanger concepts are currently being negotiated.

Description of Concepts

High-performance heat exchangers have been designed, engineered, fabricated, and tested at Rocketdyne initially to remove heat from rocket engine components and more recently for power conversion devices. One result of its search for high-heat-flux heat exchangers has been the patented Variflux design (Fig. 1). As employed in the OTEC program, a Variflux tube configuration consists of a dual, concentric-tube element with water flowing in the inner tube and ammonia in the annulus between the tubes. The annulus may also contain lengthwise, constant or variable heat-transfer enhancement devices, such as fins, wire wraps, coatings, roughened or treated surfaces, etc. The inner tube may also incorporate a finned or another enhanced surface. The basic Variflux design is capable of producing increased heat flux levels, as compared to conventional designs, thereby resulting in reduced surface area and tube material weight. The design results in uniform circumferential tube wall temperatures and controllable axial temperature gradients.

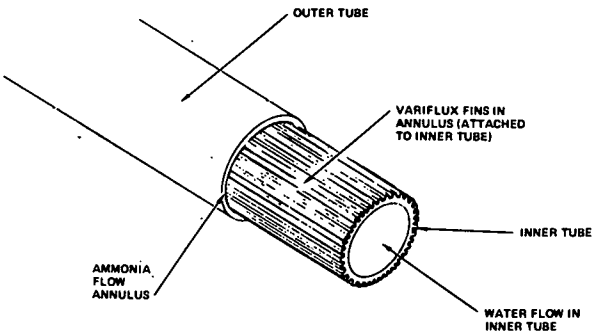

Fig. 1. Variflux Dual-Concentric Tube Assembly

A plate fin evaporator, conceptually shown in Fig. 2, has a surface area advantage compared to the Variflux tube concept since both sides of the plate design elements are wetted by the driving fluid (sea-water). In the Variflux tube design, the outer tube surface element does not play a thermal role except to provide a flow guide and structural containment of the ammonia flow. Therefore, on a surface area and weight basis for equal sea-water finning enhancement, the basic weight advantage for plate design would be from 10 to 40 percent depending on the outside wall thickness, fin, weight, and the inside wall thickness.

Disadvantages of the plate design are the lack of spanwise rigidity of the thin-plate cross section in large sections (6 by 25 feet) and the end manifold capping and joining on the ammonia flow passage. This is an analogous to the problem of joining tubes to the two tube sheets for the Variflux tube design. Another disadvantage of the plate design is

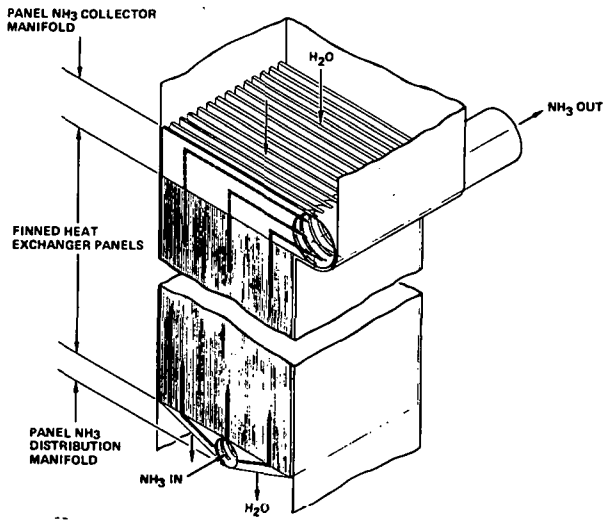

Fig. 2. Typical Plate-Fin Heat Exchanger Concept

the increased difficulty in cleaning the sea-water side over that of a tube. An added advantage of the plate-fin design is that one large panel (6 by 25 feet) would equal 19 tube assemblies (2.4-inch diameter tubes). A larger panel width would further decrease the number of plate assemblies; however, the exit manifold area requirements may present a difficult problem at the panel ammonia exit.

In the Variflux and plate-fin heat exchanger designs, the performance and operation of each tube or panel is identical, which is not the case for many types of tube and shell heat exchanger configurations where spatial flow nonuniformities exist. The advantages of tube performance uniformity are twofold: (1) each tube or panel in the heat exchanger provides its maximum performance (i.e., performance is not degraded by the location of the tube or panel in the heat exchanger) and (2) scaling difficulties or uncertainties are avoided. Because all Variflux tube or plate-fin panel elements perform and operate in an identical manner, accurate test data can be obtained in single-tube element of multi-panel testing, and the scaling in terms of module size is simply a matter of changing the number of tube or panel elements. This latter point permits the desirable feature of heat exchanger modularization. Tube or panel sizes and lengths are the same for various power level modules; only the number of tube or panel elements change. For example, 5 MWe plant system heat exchangers (for the same cycle parameters) will require one-fifth the tube elements of a 25-MWe powerplant unit; a 1-MWe test unit heat exchanger will require one-fifth the tube elements of the 5 MWe system.

Thermal Performance Characteristics

Extensive computer parametric thermal performance results for the Variflux OTEC evaporator tube elements have been run. In the design analysis, the inner tube's outer surface (ammonia side) was finned to enhance the heat transfer. Parameters varied in the analysis were the tube and fin dimensions, and the tube material. Figure 3 presents the calculated overall heat-transfer coefficient (U) versus fin pitch (P) for a fixed tube thickness (t), fin thickness (b), fin height (H), for the following

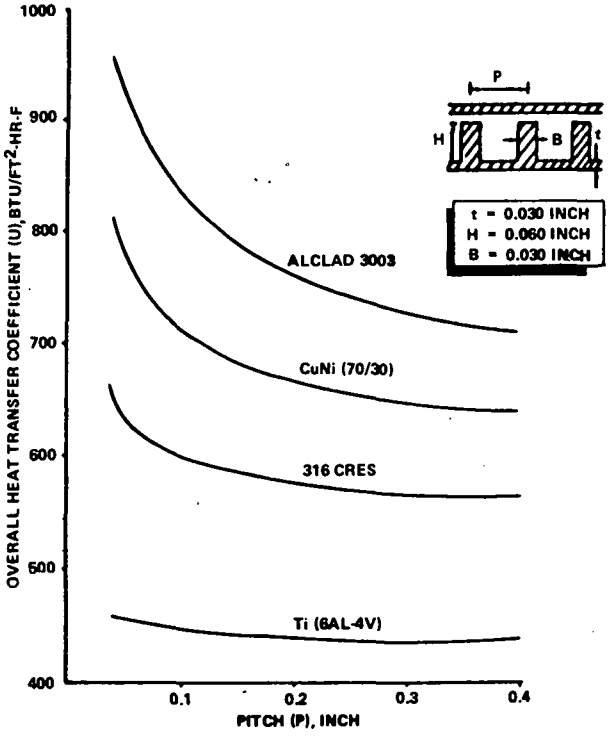

Fig. 3. Finned-Tube Design Overall Heat-Transfer Coefficient

materials: Al 3003, 5086, and 5052, Cu-Ni 70/30, CRES 316, and titanium (6Al-4V). The Al 3003 material provided the highest U values as a result of highest conductivity. Analyses of various finned aluminum configurations have resulted in predictions of average U values as high as 2200 to 3000 Btu/ft^2-hr-R.

Aluminum alloys are attractive materials because of their high-thermal conductivity, low-cost, ease of fabrication, and ready availability. The fact that complex shapes in aluminum can be extruded with relative ease, and at low cost, is important if finned heat-exchanger plate designs are employed. However, there are significant uncertainties as to the corrosion resistance of aluminum alloys to sea-water and to various mixtures of sea-water and ammonia. And, although not limited to aluminum alloys, degradation in heat transfer due to biological fouling is also an important consideration. Because of its immunity to sea-water corrosion, titanium has been the primary material considered for OTEC heat exchanger. However, titanium has several disadvantages: high cost, difficulty of fabrication, and low-thermal conductivity. Like aluminum, it has no currently known inherent resistance to biofouling.

One approach is to evaluate a suitable aluminum alloy which represents a near term, low cost approach for the OTEC plate-fin heat exchangers. Recent DOE-sponsored material test results have indicated corrosion problems associated with 6000 series aluminum. The same test program indicated that aluminum alloys to be considered in the proposed program should be 5052 and Alclad 3003. The fact that complex shapes from 5052 can be extruded and at low cost is especially advantageous for the heat exchanger design concepts being considered.

Experimental Program

Currently, the experimental test program regarding advanced OTEC heat exchangers at Rocketdyne has involved four areas:

- Working fluid film coefficient definition
- Subscale single Variflux tube assembly tests
- Full-scale single Variflux tube assembly fabrication and tests
- Plate-fin element fabrication and tests

Electrically Heated Tube Test Results

Low-temperature differential boiling and hydraulic characteristics have been obtained to provide basic thermal properties for four candidate working fluids. The test setup at the Rocketdyne Chem-Lab (Fig. 4) consisted of a single, electrically heated, stainless-steel tube 40 feet long (coiled into 12 coils) with a 0.125-inch outside diameter and a 0.016-inch wall thickness. This tube simulated one passage of a finned Variflux tube. The heat flux to the working fluid was provided by applying a-c power to the tube. Calibrated thermocouples were placed every 2 feet along the outside tube surface. Flowrate was controlled using a series of hand valves and measured with a sonic orifice.

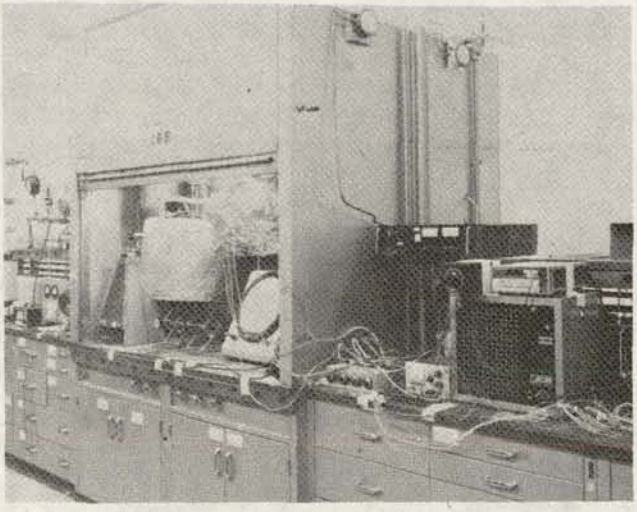

Fig. 4. Test Setup in Chem-Lab

The overall test conditions and specific test data for the four fluids are presented in Table 1 and Fig. 5. As shown, the ammonia heat transfer coefficients were significantly higher (a factor of 1.9 to 4.8) than those for the other three fluids even at one-half the mass velocity. The ammonia film coefficient substantially exceeded the anticipated baseline value of 1500 Btu/hr-ft^2-R in the 12 to 84 percent quality range and shows the advantage

Table 1. Electrically Heated Tube Test Summary

Parameter	Working Fluid			
	Ammonia	Freon-22	Freon-12	Propane
Number of Tests	19	23	20	19
Mass Velocity Range, lb/in.^{2}-sec	0.046 to 0.178	0.149 to 0.530	0.200 to 0.711	0.095 to 0.290
Inlet Pressure, psia	119.2 to 149.8	85.4 to 173.6	80.5 to 105.0	105.7 to 145.2
Outlet Quality Range	0.64 to > 1.0	0.37 to > 1.0	0.15 to > 1.0	0.35 to > 1.0
Heat Flux Range, Btu/ft^2-hr-R	793 to 5137	202 to 4712	1089 to 5101	985 to 5495

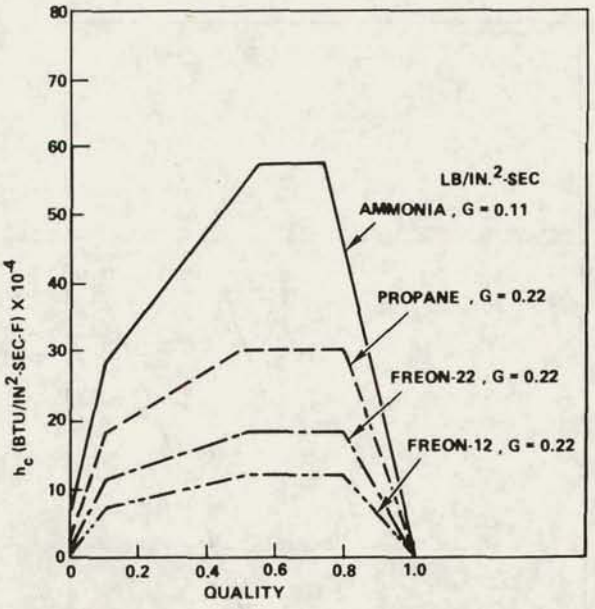

Fig. 5. Working Fluid Film Coefficient Test Results

of recirculating 10 to 25 percent of the flow. All of these fluids exhibited the trend of low liquid and vapor film coefficients (as analytically predicted) and high two-phase film coefficients. The magnitude of the two-phase film coefficient appears to be primarily a function of the fluid latent heat of vaporization. The influence of mass velocity (flowrate) is illustrated for "Freon-12" in Fig. 6.

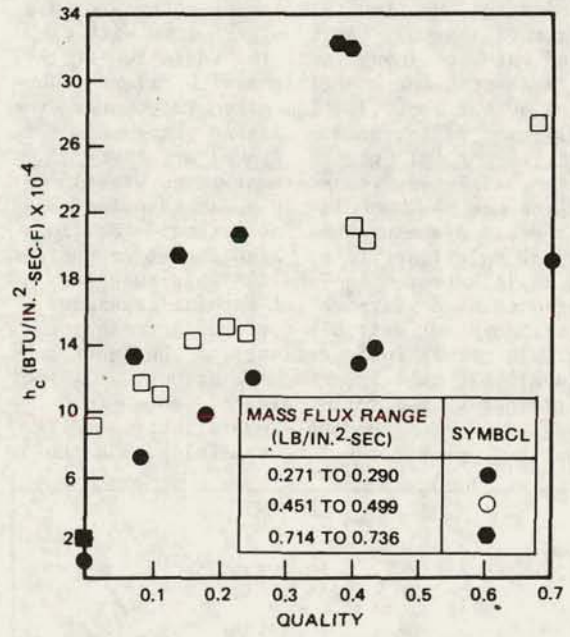

Fig. 6. Freon-12 Film Coefficient Data

The trend of increasing convection coefficient with increasing mass flowrate is applicable to all fluids tested. Typical measured pressure drop data for ammonia tests are also presented in Fig. 7.

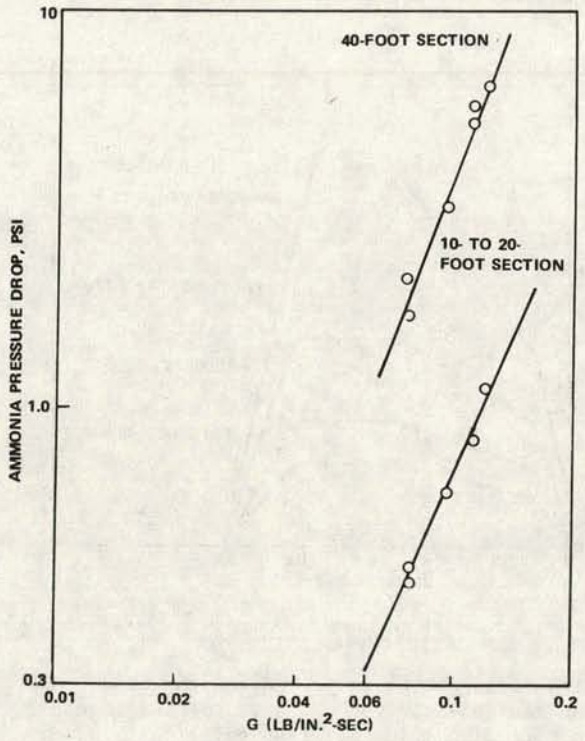

Fig. 7. Ammonia Pressure Drop Data

Single Variflux Tube Assembly Experimental Verification

A successful experimental evaluation of a single Variflux tube assembly has been performed with ammonia and water to investigate the variation of the overall heat transfer coefficient with orientation (vertical or horizontal), flow circuit (counter or parallel), and different ammonia and water mass velocities. For this company-funded experimental evaluation, a 12-foot finned inner tube, with 45 fins to enhance the ammonia-side heat transfer on a 1.5-inch basic diameter, was fabricated. The fin geometry of this inner tube, which is not an optimum design, is illustrated in Fig. 8. This tube was fabricated using a gear-hobbing machine technique which, although not suitable for manufacturing production, did permit rapid delivery of the inner tube. Due to available tube length restrictions, a 12-foot length (rather than a full-scale, 30- to 40-foot tube length) of aluminum 6061-T6 was fabricated. The inner and outer tubes, the manifolds, and the inner tube centering tool are shown in Fig. 9 prior to assembly. The assembled tube is shown along with ammonia pressure taps and manifolds, and water line interface (Fig. 10).

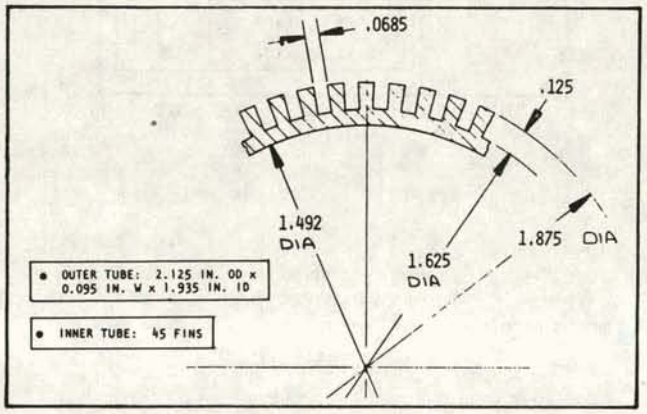

Fig. 8. Variflux Inner Tube Configuration

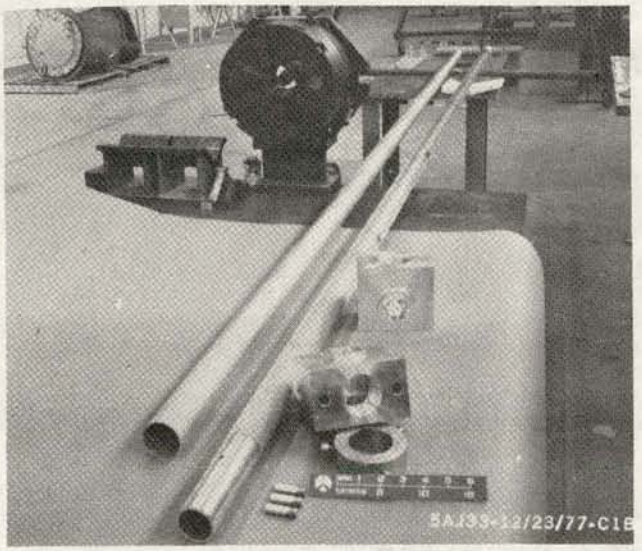

Fig. 9. Variflux Tube Components

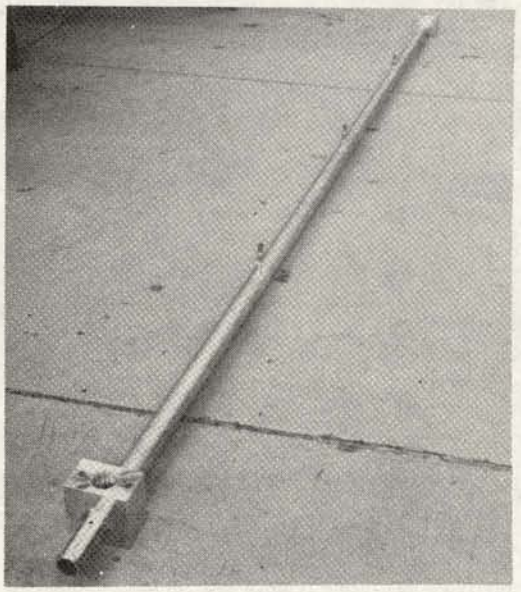

Fig. 10. Variflux Tube Assembly

A highly versatile test facility was constructed at the Rockwell International Thermal Lab for this single tube testing, and is capable of heating or cooling the water and ammonia over a wide range of flowrates to obtain desired test conditions (Fig. 11). With this system, a given configuration could be tested both as an evaporator and condenser without any plumbing modifications. In-place calibrated thermocouples were used to measure the ammonia and water temperatures, while static and differential gages were used for the associated pressure measurements. Also, numerous facility parameters were monitored to ensure accurate tube conditions and safe operation. To simulate the various sections of a full-scale tube (30 to 40 feet), the ammonia was preheated prior to entering the Variflux tube. By

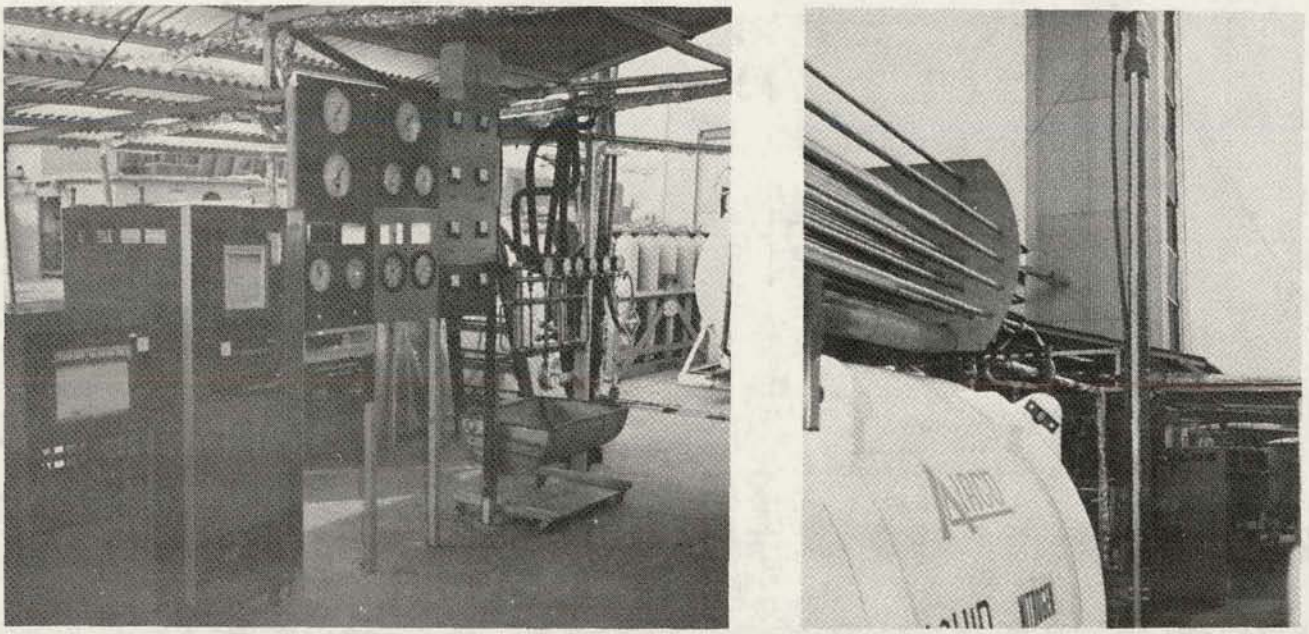

Fig. 11. Single Tube Variflux Overall Test Setup (Vertical Orientation)

regulating the ammonia and water inlet conditions, various lengths of the full-scale tube were simulated. The nominal flow conditions for the tube are 0.054 lbm/sec of ammonia and 6 lbm/sec of water.

Evaporator Test Results. Three evaporator configurations were evaluated: vertical, counterflow (ammonia flowing up); vertical, parallel flow (ammonia down); and horizontal, counterflow. As shown in the test summary in Table 2, a total of 57, 39, and 34 tests, respectively, were conducted using these three configurations. A comparison of the measured overall heat transfer coefficients, based on the water-side surface area for the tested configurations, is shown in Fig. 12 and 13. The overall heat transfer coefficient (U) was highest for the vertical, counterflow (ammonia up) configuration at 1160 Btu/ft^2-hr-R and was the lowest for the vertical, parallel flow (ammonia down) configuration at 607 Btu/ft^2-hr-R for nominal flow conditions.

The buoyancy of vapor ammonia in liquid ammonia is believed to be the key in explaining the measured overall U trends. In the vertical counterflow (ammonia up) configuration, the ammonia vapor formed tends to rise relative to the liquid allowing the liquid to be adjacent to the heater surface. This is basically the "liquid holdup" phenomenon typically discussed in vertical steam/water heat exchangers. For the vertical, parallel flow (ammonia down) configuration, the buoyant ammonia vapor would attempt to rise, which is in the opposite direction to flow. This apparently retards the evaporation process resulting in a lower overall U. As the ammonia flowrate is increased, this buoyant force would and does become less significant and the overall U increases and approaches the value of the vertical, counterflow (ammonia up) configuration.

The influence of ammonia quality at approximately the nominal flowrate is presented in Fig. 13. The vertical, counterflow (ammonia up) configuration achieved the highest overall U at approximately 50 to 60 percent quality. For ammonia quality higher than 50 to 60 percent, both vertical configurations

Table 2. Variflux Evaporator Test Summary

	Vertical Counterflow (Ammonia Up)	Vertical Parallel Flow (Ammonia Down)	Horizontal Counterflow
Number of Tests	57	39	34
NH_3 Flowrate, lb/sec	0.023 to 0.096	0.022 to 0.0180	0.035 to 0.177
NH_3 Mass Velocity, lb/in.^{2}-sec	0.038 to 0.156	0.036 to 0.293	0.035 to 0.177
NH_3 Outlet Pressure, psia	115 to 135	131 to 136	134 to 135
Inlet Quality (X_{NH_3})	0 to 0.65	0 to 0.94	0 to 0.70
Outlet Quality (X_{NH_3})	0.16 to 1.0	0.09 to 0.98	0.07 to 0.75
H_2O Flowrate, lb/sec	5.9 to 8.2	5.8 to 8.2	5.9 to 8.1
H_2O Velocity, ft/sec	7.8 to 10.8	7.7 to 10.8	7.8 to 10.7
H_2O Inlet Temperature, F	75.2 to 80.2	75.4 to 80.7	75.9 to 80.5

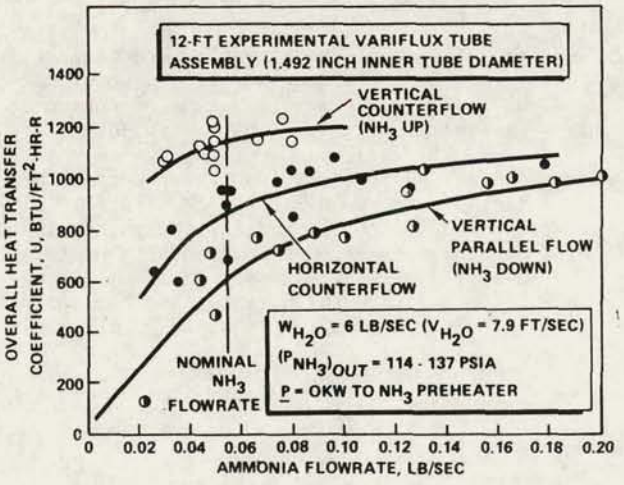

Fig. 12. Variflux Evaporator Heat Transfer Characteristics

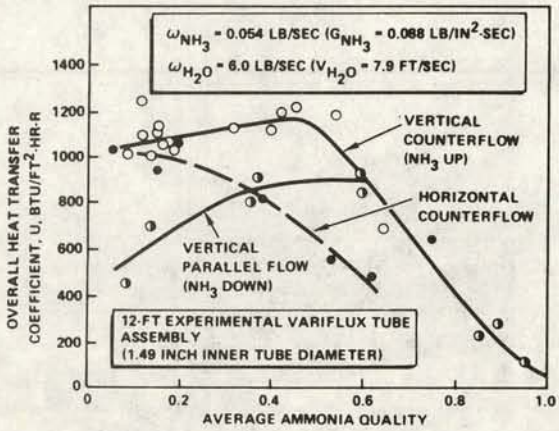

Fig. 13. Ammonia Quality Influence

achieved approximately the same overall U, while the horizontal configuration was lowest. Typical ammonia pressure drop data are presented in Fig. 14 as a function of flowrate and ammonia quality. As expected, the higher qualities resulted in higher pressure drops. No flow instabilities were encountered in the tests performed.

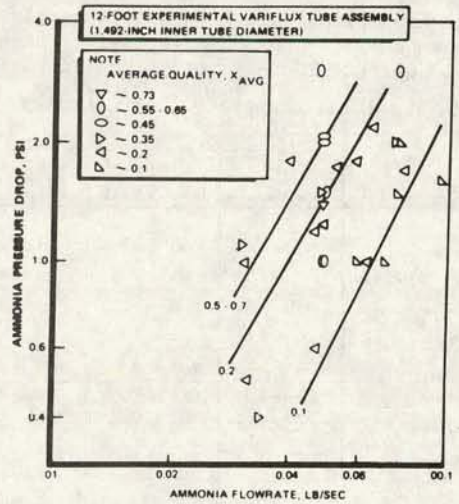

Fig. 14. Variflux Evaporator Ammonia Pressure Drop Data

With a maximum overall heat transfer coefficient of up to 1150 Btu/ft^2-hr-R, the Variflux concept has clearly demonstrated 2.9 times the value of conventional nonenhanced evaporators (400 Btu/ft^2-hr-R).

Condenser Test Results. Two condenser configurations have been evaluated using a 12-foot experimental Variflux tube assembly and include vertical, parallel flow (ammonia up); and horizontal, counterflow. As shown in Table 3, a total of 32 and 18 tests were performed with the vertical and horizontal

Table 3. Variflux Condenser Configuration Test Summary

	Vertical Parallel Flow (Ammonia Up)	Horizontal Counterflow
Number of Tests	32	18
NH_3 Flowrate, lb/sec	0.035 to 0.065	0.02 to 0.064
NH_3 Mass Velocity, lb/in.^{2}-sec	0.057 to 0.106	0.033 to 0.104
NH_3 Inlet Pressure, psia	88 to 126	89.4 to 114
Inlet Quality (X_{NH_3})	0.19 to 1.0	0.04 to 0.70
Outlet Quality (X_{NH_3})	0 to 1.0	0 to 0.63
H_2O Flowrate, lb/sec	1.5 to 8.2	2.3 to 6.5
H_2O Velocity, ft/sec	1.98 to 10.8	3.0 to 8.6
H_2O Inlet Temperature, F	36.1 to 52.9	42.0 to 47.2

configurations, respectively. Test data for the condenser resulted in overall heat transfer coefficients as high as 800 Btu/ft^2-hr-R. Although these values are not as high as those obtained for the evaporator, improvements to the condenser configurations are currently being evaluated. Again as in the evaporator tests, the flows were stable.

Full-Scale Single Variflux Tube Assembly Fabrication and Tests

A program to fabricate a full-scale Variflux tube assembly has been proposed to Argonne National Laboratory and contract negotiations are proceeding. This facility would perform the experimental evaluation of the unit. The design of a typical Variflux tube assembly is shown in Fig. 15.

Sea-water side cleaning of an externally and internally finned inner tube will be more difficult as compared to the externally finned tube, but the Mann brush system has been used to clean internally finned tubes. The externally and internally finned tube configuration shown in Fig. 16 enabled a factor

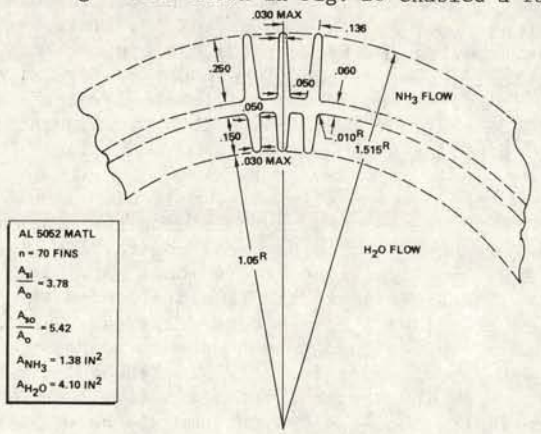

Fig. 16. OTEC Variflux Inner Tube Design Geometry for Argonne Evaporator

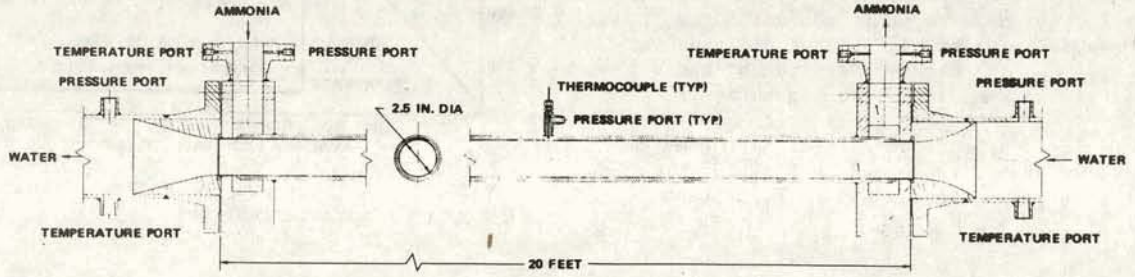

Fig. 15. Typical Concentric Tube Heat Exchanger

of two reduction in tube length and, therefore, provides a definite advantage. Currently, this design is to be extruded from 5052 aluminum alloy.

An overall heat transfer coefficient of 2200 to 3000 Btu/ft^2-hr-R is projected for this configuration based on analytical predictions and subscale tests.

Plate-Fin Element Fabrication and Tests

A program to design, fabricate, and test a plate-fin element has been proposed to the Department of Energy and contract negotiations are proceeding. Three plate-fin configurations (Fig. 17 and 18) are to be evaluated and will include:

1. Smooth water side with a roughened ammonia side
2. Smooth water side with finned ammonia side
3. Finned water side and a finned ammonia side

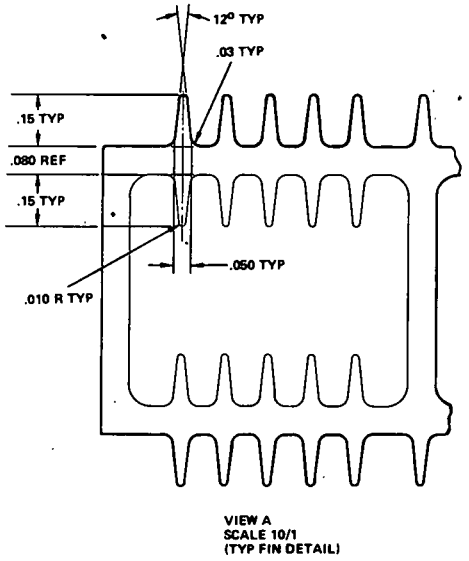

Fig. 17. Plate-Fin Heat Exchanger Panel Configuration

The panel and fin configurations shown in Fig. 17 and 18 represent configurations satisfactory from a thermal design and extrusion standpoint. Tapered fins were selected to save weight. Detailed dimensions of the final panel configuration will be determined during the proposed program. Overall U' up to 3000 Btu/ft^2-hr-R have been projected for the externally and internally finned-plate configuration.

Current panel fabrication techniques to be evaluated are: (1) complete extrusion and (2) open-face extrusion. The complete extrusion will provide low fabrication cost, but adds to the extrusion difficulty. The open-face extrusion (actually one-half the complete extrusion) simplifies the extrusion but the joining of the two halves will increase fabrication costs. Joint design approaches and the adhesive or bonding method are being evaluated (Fig. 19).

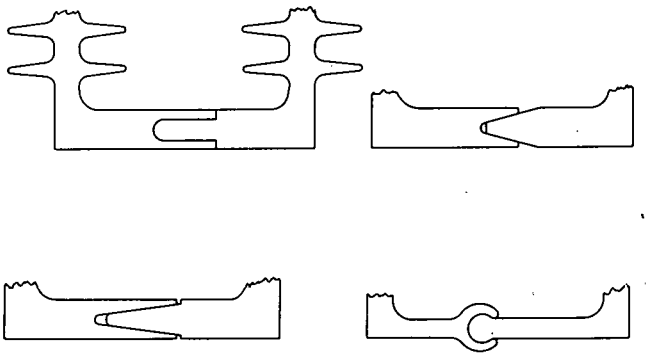

Fig. 19. Open-Face Extrusion Candidate Joint Designs

Variations of this latter approach are currently being investigated under a company-funded task. Currently, the complete extrusion approach is preferred.

The basic design approach is to fabricate one housing and have the flexibility of interchanging the panels. This approach will enable the three plate-fin configurations to be experimentally evaluated with one external housing at low cost and with minimal disturbance to plate-fin instrumentation. Several housing approaches will be evaluated. Currently, the bolted split channel approach (Fig. 20) is preferred due to its capability of allowing direct access to the individual panels, if necessary, during assembly.

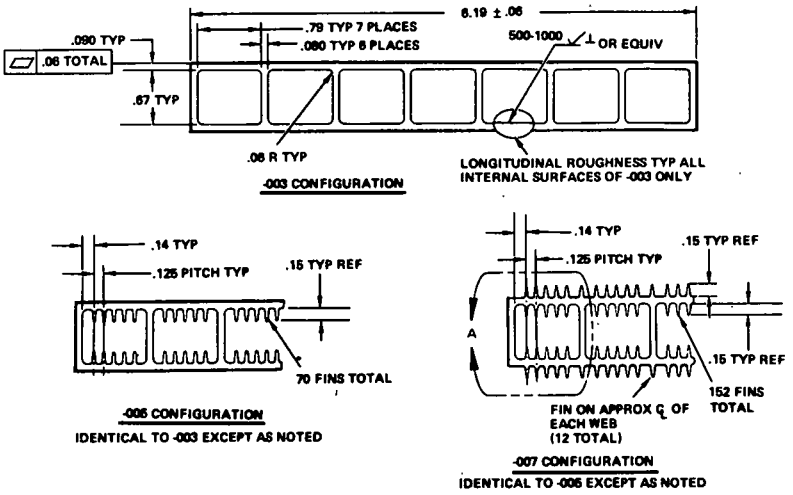

Fig. 18. Plate-Fin Heat Exchanger Panel Configurations

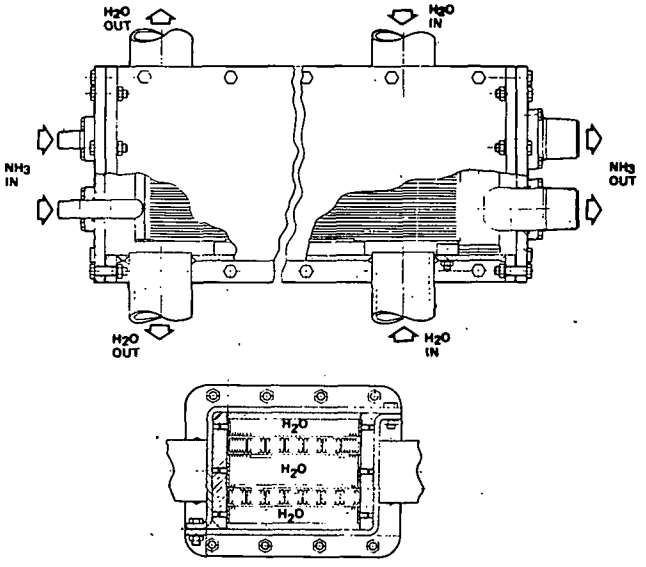

Fig. 20. Plate-Fin Heat Exchanger Element Assembly

Conclusions

The heat transfer characteristics for low temperature differential boiling of ammonia, Freon-22, Freon-12, and propane have been experimentally determined along with hydraulic characteristics. Ammonia demonstrated significantly higher two-phase coefficients than the other fluids due to its higher latent heat of vaporization.

The potential of the ammonia-side finned Variflux concept has been demonstrated as an evaporator and condenser section. Although this tube assembly did not represent the optimum design, overall heat transfer coefficients as high as 1150 Btu/ft^2-hr-R were consistently achieved for the evaporator section. Of the three evaporator sections evaluated, the vertical counterflow configuration with the ammonia flowing up provided the highest overall U. For the condenser section, the two configurations evaluated resulted in essentially the same overall U values at the nominal conditions; however, the horizontal configuration was less sensitive to water flowrate variations. Design improvements of ammonia-side surface enhancement technique, inner tube internal fins (sea-water side) will further improve the evaporator and condenser overall U and further reduce the heat exchanger size.

The design improvement of external and internal fins was incorporated in the full-scale Variflux tube assembly to be fabricated for Argonne National Laboratory. An overall U of 2200 to 3000 Btu/ft^2-hr-R is projected for this configuration.

The plate-fin configuration offers definite heat transfer advantages but problems may be encountered in manifold design and sea-water side cleaning approaches. Overall U's up to 3000 Btu/ft^2-hr-R are predicted for this concept.

The potential heat transfer and manufacturing cost advantages of these concepts are dependent on the corrosion resistance of aluminum alloys. Also, there remain further evaluation of manufacturing and cost reduction problems associated with high-speed production of extruded tube and finned-plate assemblies.

Acknowledgement

Support of the Rocketdyne Chem-Lab and the L.A. Division Thermal Lab personnel has been instrumental in the completed test effort to date. In particular, the important, contributing and detailed analysis, design and test support of J. Page, L. Yoshimoto, J. Fasheh, R. McCarter, D. Moses, W. Moen, R. Wagner, in this effort, is hereby acknowledged.

References

1. Ocean Thermal Energy Conversion V-3 Baseline System Concept, TRW Final Report, Contract NSF-C958, June 1975.
2. OTEC Heat Exchanger Design and Producibility Study Final Report, (LMSC-D507632) Contract E (04-3)-1291, Lockheed Missiles and Space Company, Inc., October 1976.
3. Wright, D., W. Wagner, J. Shoji, and J. Campbell, "Summary of Analysis and Testing on Advanced Variflux OTEC Scaled Evaporator and Condenser Components," presented at the Fifth Ocean Energy Conversion (OTEC) Conference, 20-22 February 1978.

DISCUSSION

Question: Can you say something about the relative performance of a condenser as compared to the evaporation between ammonia and some of the freons?

D. Wright: So far, as a condenser, there is nothing that has been as good as we had hoped or anticipated, but these results are being investigated at the present time. We are still in the process of reducing the data.

12. MATERIALS, BIOFOULING, AND COUNTERMEASURES

BIOFOULING, CORROSION, AND MATERIALS OVERVIEW

Eugene H. Kinelski

Department of Energy
Division of Central Solar Technology
600 E Street, N.W.-Room 413
Washington, D.C. 20585

Abstract

The OTEC Biofouling, Corrosion and Materials (BCM) Program has been structured to provide the data on materials and biofouling countermeasures needed to assure low-risk operation on the OTEC-10 Pilot Plant. Enumerated ~~in this paper~~ are the low-risk options available if the Pilot Plant were to be designed today. Also presented are the tests under way that will qualify additional options for the Pilot Plant preliminary design which is planned for Fiscal Year 1981. ~~This paper is~~ a brief overview of the BCM program and the ways it has met and will meet the needs of the OTEC program are described.

Introduction

The OTEC Biofouling, Corrosion and Materials (BCM) program has been in effect for three years. All of our major projects reflect concerns over the success of OTEC, which is highly dependent upon the materials used and the control of biofouling.

As shown in Fig. 1, two major developments are planned: an OTEC-1 Test Facility, which will be used mainly to evaluate performance of heat exchangers and BCM concerns, and an OTEC-10 Pilot Plant. The OTEC-1 Early Test Article 1-MW(e) heat exchanger will be equipped with heat transfer monitors to measure the effectiveness of the Amertap anc chlorination systems used. In addition to the monitors, selected tubes in the heat exchangers are to be isolated on the seawater side to evaluate the effects of Amertap and chlorination. The PSD-I and II heat exchanger tests will also be provided with heat transfer monitors to assess the biofouling countermeasures used. These devices, developed by Carnegie-Mellon University, measure the resistance to heat transfer as influenced by fouling, R_f, versus time. In addition, test monitors specifically applicable to each design will be employed.

It is planned to initiate an OTEC-10 Pilot Plant preliminary design in FY 1981. In this design, the entire OTEC plant will be brought together:

- 10 MW(e) power system
- Cold water pipe large enough for 40 MW(e)--30' in diameter
- Platform large enough for up to 40 MW(e) power generation
- 40 MW(e) electric cable to shore

All of the developmental work in the BCM Program is directed to a successful design of OTEC-10. The materials must be cost-effective and give promise of a 30-year life (or economically viable replacement during a 30-year life), the biofouling countermeasures should be effective in maintaining an R_f of less than 0.001 ft^2-hr-°F/Btu as a target with low parasitic power losses, and the plant must withstand a hostile ocean environment.

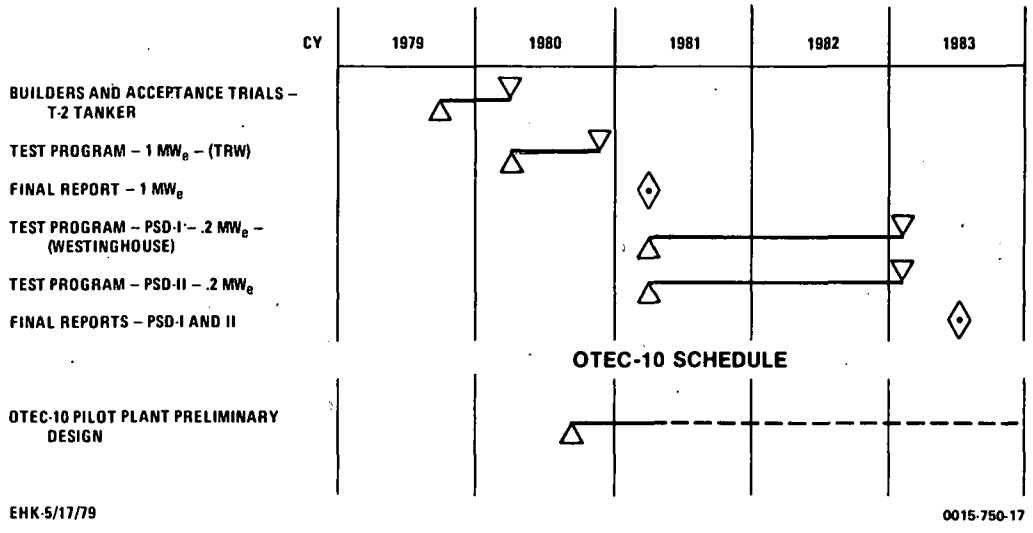

Fig. 1 OTEC-1 schedule.

Justification of a Preliminary Design for an OTEC-10 Pilot Plant for Fiscal Year 1981

In view of the cost of the proposed OTEC-10 Pilot Plant and the possible adverse effect of a failure on subsequent OTEC development, it is believed that a preliminary design should be committed only if the risk of failure is believed to be small. This assumes that there is a good probability of successful solution of all design problems. From the viewpoint of the BCM Program, we have examined material and design options. The following low-risk choices have been identified at this time. It should be emphasized that as more data become available, certain high risks may become low risk.

Heat Exchangers

In heat exchanger designs, both cost and other factors such as corrosion and biofouling must be taken into account to determine the level of durability and maintenance of operational capability that will be required throughout the whole system. Only shell-and-tube evaporators and condensers can now be considered low risk using ammonia as a working fluid. The water-side surfaces should be smooth to provide the best possibility for success of the biofouling countermeasures.

With regard to heat exchanger joints, low risk is attributed to the following types:

Welded tube-to-tubesheet
Welded tubesheet-to-shell
Mechanical waterbox to tubesheet

The heat exchanger cores are low risk items if titanium or selected high chrome-moly stainless steel (e.g., AL-6X or 29 Cr-2 Ni-4 Mo-Bal-Fe) alloys are chosen.

The shells are a low risk with Type 403 stainless steel. Fear of the use of stressed steel shells in ammonia with insufficient water to inhibit possible stress corrosion cracking places steel in the higher risk category. Although stress-relieved steel could be considered, the problems of stress-relieving such large components, especially at welds, pose a higher risk option.

The tubesheets should be steel clad with titanium for the titanium core, or an alloy compatible with stainless steel for the stainless steel core. The problem of keeping the tubesheet free of macrofouling on the seawater side is not solved and further studies are needed. The water boxes should be steel clad with an antifouling copper alloy or solid copper-nickel Alloy 706.

Fouling Countermeasures

Although a large effort is being devoted to qualifying countermeasures for microfouling, no mechanical cleaning system with or without chlorination can be characterized as low risk at this time. Further studies are needed to qualify a method that yields an acceptable level of risk. Although biofilm kinetics research could aid in these developments, this has not been possible with the emphasis being placed on development efforts. The effect of downtime and failures resulting in stagnant seawater is another concern because of the heavy macrofouling that could occur.

Distribution Piping, Pumps and Valves

Distribution piping for the OTEC platform for ammonia is a low risk with stress-relieved steel or Type 403 stainless steel. The seawater piping can be steel clad with an antifouling copper alloy or solid copper-nickel Alloy 706. Chromium-nickel-molybdenum stainless steels of appropriate compositions are qualified for use in sea water pumps and valves.

Turbines

Because of the planned use of ammonia as the working fluid there is a potential stress-corrosion-cracking problem in the OTEC turbine, and hence a small risk, if steels, stainless steels, or aluminum alloys are used.

Screens

Unfortunately, screens are usually the last items to be considered - both from a design as well as a materials choice viewpoint. In an OTEC plant, trash racks can be employed at the end of the cold water pipe and warm water intake. The low-risk material choices are steel clad with antifouling copper alloy and solid copper-nickel Alloy 706. The screens, which could be located in the sump on the platform, could use copper-nickel Alloy 706 as a low risk, antifouling alloy. Although either a static or traveling screen could be used, the ability to keep a traveling screen free of debris automatically is an advantage over a static screen.

Cold Water Pipe and Hull

Any design of a cold water pipe will require materials selection with particular attention to fatigue properties. Available materials for which risk may be acceptable are steel and reinforced concrete. The latter materials are judged to represent low risk for the hull, but possible interactions of steel with, e.g., aluminum heat exchangers, must be taken into account.

Cable

The electric cable to transmit power ashore presents no serious material problems with the bottom cable. The riser cable has problems with fatigue and the use of armoring materials. These problems will influence design and choice of materials.

Moorings

Synthetic fiber cables are low-risk choices for mooring lines. Possible fatigue of connections will require attention. Also, fish bite may be a potential problem. Steel cables will have a limited life and require replacement.

What Does the Future Hold for OTEC Technology?

Let me mention now some of the technology developments that may produce additional low-risk options by 1981. Figure 2 is the schedule for the BCM program. Since biofouling countermeasures are our main unknown at present, a major effort is devoted to tests at Panama City, Florida, and a new, to-be-selected laboratory during the next two years. As soon as the Seacoast Test Facility is ready for operation--about September 1980--all tests will be transferred to that facility. In the meantime, tests using cold water on the second phase of Mini-OTEC could be conducted, and tests will be starting on OTEC-1. These OTEC-1 tests will involve 8 BCM heat transfer monitors for the 1-MW(e) heat exchanger tests. Monitors will be used to test the following operating conditions on the evaporator as

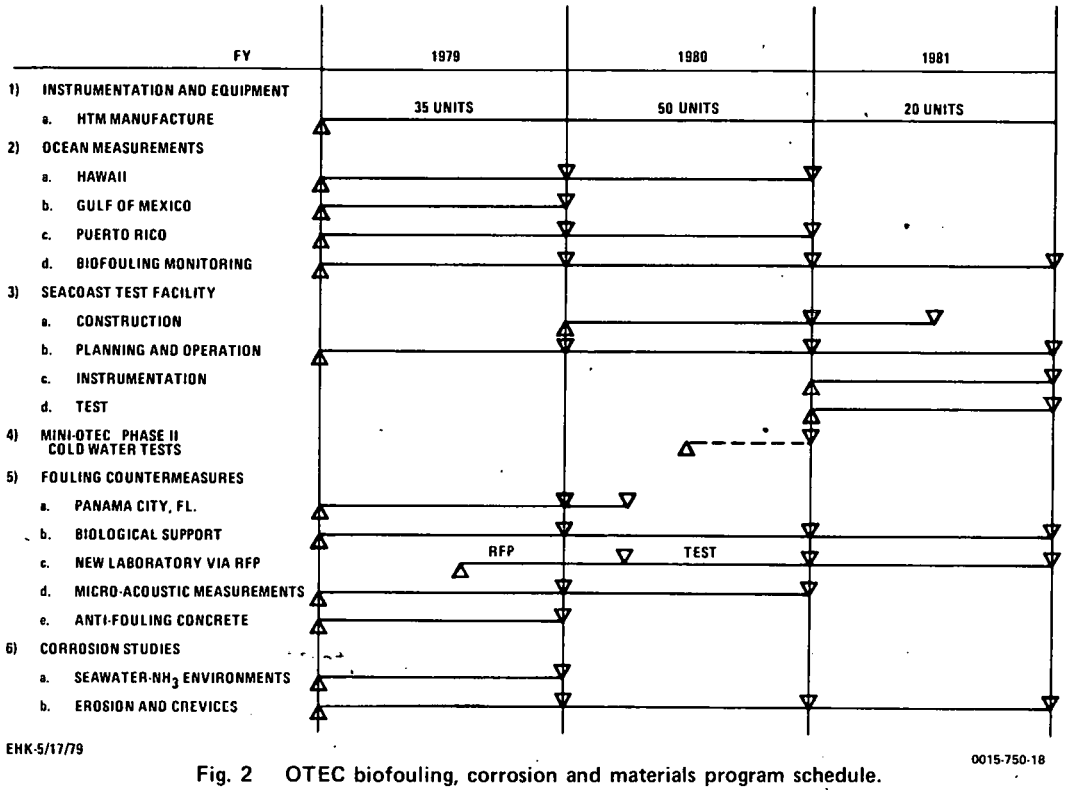

Fig. 2 OTEC biofouling, corrosion and materials program schedule.

well as the condenser:

a) No countermeasure--base line
b) Chlorination only
c) Amertap and chlorination upstream of the heat exchangers
d) Amertap and chlorination downstream of the heat exchangers

Case (a) above will be supplied with water on a continuous basis, even though the 1-MW(e) heat exchanger may not be in operation. Cases (b), (c), and (d) will be supplied with water only when the 1-MW(e) heat exchanger is operating. Titanium tubes will be used in the monitors to duplicate the tubes in the 1-MW(e) heat exchangers.

Corrosion investigations are needed to qualify a number of alternatives to titanium as heat exchanger metals. Since the quantities of metals are anticipated to be quite large with commercial OTEC plant production, the use of the high chromium-molybdenum-nickel-iron alloys present satisfactory alternatives. Copper-nickel alloys 706 and 772 present excellent properties - especially their antifouling characteristics - for use in OTEC heat exchangers on the seawater side. Extensive testing in ammonia and mixtures of ammonia and seawater is needed to qualify these alloys. One possibility of their use would be as copper-nickel clad steel, with steel on the ammonia side.

Additional studies on Alclad aluminum alloys 3003 and 3004 and bare 5052 and 3003 are needed to establish their service lives as functions of base metal and/or cladding thickness.

Corrosion resistance is evaluated at each of the ocean test sites when the heat transfer monitors are disassembled for inspection. Dow Chemical Laboratory, Freeport, Texas, is conducting corrosion tests of the Ti, Al, Cu-Ni, and stainless alloys in ammonia and in mixtures of ammonia and seawater. Erosion and crevice corrosion tests are under way at the LaQue Center for Corrosion Technology in Wrightsville Beach, North Carolina. Corrosion fatigue tests on cable and cold water pipe components are planned for the near future. Before such tests can be initiated, the designs and stress levels need to be selected to guide the test efforts.

QUALIFYING ALUMINUM AND STAINLESS ALLOYS FOR OTEC HEAT EXCHANGERS†

F. L. LaQue

Claridge House I
Verona, New Jersey 07044

Abstract

This paper reviews the basis for qualification of aluminum and stainless steel as materials for use in Ocean Thermal Energy Conversion (OTEC) heat exchangers. Existing data are not adequate either to qualify or disqualify aluminum, but they do identify Alclad 3003 or 3004 and the 5052 alloys as the most worthy candidates. Representatives of the aluminum industry support roll-welded Alclad materials as the most likely candidates for economical OTEC heat exchangers** with a service life of ten years or more. The principal deficiency of test data from long time tests in sea water is that in nearly all cases the specimens were allowed to be fouled by marine organisms under static conditions; possible effects of periodic mechanical treatments to remove fouling or chlorination to prevent it were not taken into account. A current testing program sponsored by DOE through Argonne National Laboratories is designed to provide the needed data. Susceptibility to crevice corrosion will require careful design at tube supports in shell-less heat exchangers with water outside the tubes. Vibration must be minimized to avoid fretting corrosion of the tube at tube supports and corrosion fatigue in shell-and-tube heat exchangers. Experience showing severe crevice corrosion of aluminum in plate-type heat exchangers in desalination plants would appear to disqualify aluminum for plate-type exchangers. Galvanic couples with other metals, particularly copper alloys, must be avoided. Ammonia leakage into supersaturated sea water could trigger deposition of calcium scales. With respect to stainless steel, existing data qualify the AL-6X alloy (24% Ni, 20% Cr, 6% Mo) for OTEC heat exchangers.

Introduction

The principal issues in selecting materials and appropriately related designs for the heat exchangers in Ocean Thermal Energy Conversion (OTEC) plants are cost and service life. Titanium would be clearly preferred--it does not corrode in seawater, it has high strength/weight ratios, and it offers unquestioned 30-yr life--were it not for its cost. Even so, either titanium or an appropriate stainless steel alloy may be the preferred material for compact plate-type heat exchangers[1] and/or for the tubing of vertical shell-and-tube heat exchangers (the latter type being attractive, e.g., for spar-type OTEC platforms[2]). However, aluminum alloys offer lowest initial cost, especially for the low-cost, shell-less, folded-tube heat exchangers designed for integration with low-cost, barge-type, cruising OTEC platforms.[3] The question then becomes one of the life of aluminum heat exchangers in any appropriate OTEC application as it impacts the overall system cost. If a cruising OTEC plant producing an energy-intensive product on board is financed, e.g., by private chemical or metal industry firms or other venture capital groups who look for rapid capital recovery (as opposed to electric utility practice of 30-yr-life financing), a life of 15 to 20 years may prove to be adequate, and initial cost may far outweigh the ultimate heat-exchanger life considerations.[4] Even for utility customers, a one-time replacement (after 15 yr of a 30-yr life) could be acceptable if aluminum shows better present-value economics than alternative materials[5] (see also the footnote at left).** Thus, qualification of aluminum alloys is an extremely important issue with respect to the probable rate of commercialization of OTEC energy for the nation.

Further discussion of OTEC economics may be found in other papers in these 6th OTEC Conference Proceedings and elsewhere. This paper addresses the qualification/life questions for aluminum and stainless-steel

† The views expressed and conclusions reached are those of the author. They do not necessarily represent those of the Argonne National Laboratory nor the Department of Energy.

* Consultant to Argonne National Laboratory.

** Representatives of the aluminum industry have suggested that the estimate of 10 years as the life of Alclad tubes is too conservative because it does not give sufficient credit to the survival of the core alloy after the cladding is gone. In view of uncertainties relative to the effects of cleaning on the life of the cladding and possibly high rates of subsequent pitting on the core alloy, the author is inclined to stick to his estimate of a 10 year life, pending development of data from new tests that could support an expectation of a longer life.

alloys by summarizing Refs. 6 and 7, which were prepared for the Department of Energy through Argonne National Laboratory.

Aluminum

Corrosion Rates and Cleaning Effects

While there are extensive historical data from corrosion tests in sea water, the tests were not made under environmental conditions pertinent to OTEC heat exchangers. The catalogued data on aluminum corrosion rates led to the following principal conclusions:[8]

> "Pitting and crevice corrosion proved to be the types of attack that predominated. The catalogued data are the results of many static tests conducted under natural conditions of marine fouling, hence they must be used carefully in qualifying aluminum for OTEC purposes. These data can serve the OTEC program best as a basis for selecting aluminum alloys that appear promising as candidates for further evaluation. The aluminum alloy 5052 and Alcald (7072) 3003 fall into this category."

To elaborate on the second sentence of this quotation, the possibly protective effect of the extensive accumulations of fouling organisms such as occurred in static tests makes the results of such tests questionable for prediction of corrosion behavior in OTEC service where it will be necessary to prevent similar accumulation of fouling or remove it by periodic cleaning.

In several tests for aluminum the maximum pit depth varied with $t^{1/3}$ (where t is time). Such a relationship could be accounted for by assuming that a mature pit is in the shape of a hemisphere whose radius increases with $t^{1/3}$, so that the volume of the pit increases linearly with time.[9] This observation was based on specimens which were exposed for long periods without disturbance of the metal surface. Again, periodic cleaning might expose fresh surfaces so as to re-initiate corrosion at frequent intervals. On the other hand, cleaning would reduce the initiation of pitting by providing a more uniform surface free from deposits which might otherwise promote pitting by crevice effects. Uniform corrosion data more directly applicable to periodically cleaned OTEC heat exchangers have been provided from two recent tests of the 5052 alloy: Liebert[10] tested it in sea water flowing at 3 to 6 ft/sec at Keahole Pt., Hawaii for periods from 3 hours to 8 months. Schrieber[11] tested it in seawater flowing at 5 ft/sec at Freeport, Texas for periods from 15 to 59 days.

For the purpose of this paper, Liebert plotted the results of both tests in Fig. 1. The exposure conditions at Freeport were evidently more aggressive than at Keahole Pt. Both sets of results showed that the progress of corrosion was proportional to $t^{1/2}$. Such behavior was consistent with historical data from tests of much longer duration at several locations as described by Godard et al.[2] (table 123, p. 130).

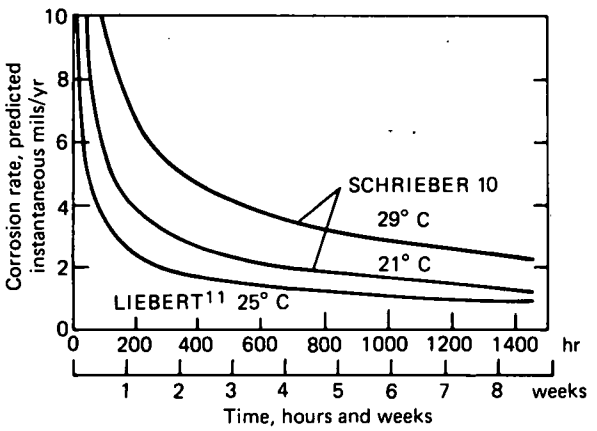

Fig. 1 Effect of time of exposure on corrosion of 5052 aluminum in seawater flowing at 3 to 6 ft/sec.

The curves in Fig. 1 based on data from Schrieber cover tests at ambient temperatures of 21° to 29°C. This difference in temperature would account for the higher rates in the latter test. It can be expected that aluminum will be corroded at lower rates in condensers than in evaporators.

It is possible from Fig. 1 to estimate the rates of corrosion of the 5052 aluminum alloy and possibly other aluminum alloys such as Alclad 3003 that might be encountered in OTEC heat exchangers subjected to periodic cleaning to maintain the desired heat-transfer coefficients. Such rates would be affected by the severity of the effect of cleaning on preservation of protective films prior to, or during, the intervals between cleanings. If an adequate cleaning treatment and cleaning cycle does not remove the protective film formed prior to cleaning, the critical corrosion rate will be that established by the time of the first cleaning and may diminish during periods between successive cleanings. Some biofouling/cleaning tests have indicated that cleaning at intervals of 2-4 weeks will suffice.[10,12,13]

On the basis of the data in Fig. 1, if the cleaning treatment did not remove the protecting film that had formed in 30 days, the rates of corrosion that would occur during successive 30-day periods would be from 2 to 3 mils/yr based on Schrieber's results and about 1 mil/yr based on Liebert's data.

Experience with effects of rather drastic mechanical cleaning of aluminum tubing has indicated that effects of cleaning

methods under consideration for OTEC, such as M.A.N. brushes and Amertap balls, can be tolerated. This expectation needs to be confirmed by an appropriate testing program. In the meantine, it may be noted that in Liebert's tests a cleaning treatment using 20 passes of a M.A.N. brush at the end of 13, 22 and 29 weeks had a negligible effect on the progress of corrosion.

In Schrieber's tests specimens were cleaned with 6 passes of brushes to simulate cleaning by M.A.N. brushes after periods of exposure of 1, 2, 3 and 7 months and then re-exposed for a total of 10 months. The specimens subjected to this periodic cleaning were corroded uniformly at a rate of 1.5 mils/yr. This rate was only slightly higher than that of uncleaned controls.

Schrieber's tests included effects of various methods of chemical cleaning. The most effective of these was cleaning with 10% by volume sulfuric acid plus 2% by weight chromic acid for 4 hours at ambient temperature. However, this acid treatment increased corrosion to about 2 1/2 times that of uncleaned specimens. It might be expected that acid cleaning could result in restarting corrosion at an initial rate after each cleaning treatment.

Occasional cleaning could reduce the initiation of pitting by providing a more uniform surface free from deposits which might otherwise promote pitting by crevice effects. This would be more important with respect to 5052 than Alclad. Unfortunately, Alclad 3003 was not included in either Liebert's or Schrieber's tests. However, in the absence of more specific data, it seems reasonable to assume that the rate of uniform corrosion of the cladding alloy will not be greatly different from that of the 5052 alloy.

At present the available data on uniform corrosion support the possibility that Alclad aluminum tubes with 10 mils of cladding could survive for about 10 years in an OTEC heat exchanger with cleaning at appropriate intervals to remove fouling, based on two assumptions: a) so long as a substantial area of cladding remains there would be no penetration of the 3003 alloy core, and b) the cleaning treatment will not eliminate protection provided by films formed prior to each cleaning. The 5052 alloy might have a similar life with respect to uniform corrosion but would be more vulnerable to penetration by pitting.

Pitting

For 5052 and Alclad 3003, there was a very wide scatter of data in the Alcoa Catalogue on depths of pitting in both surface and deep waters.[8] The confusion generated by the need to choose among data sources is illustrated by Table 1 in which choices by three designers and those of the author (abstracted from the Alcoa Catalogue) are presented. (This presentation in Table 1 is not intended to be used as a basis for estimating the probable life of aluminum in OTEC heat exchangers.)

Table 1 Reported rates of penetration of aluminum alloys in sea water in mils/yr

	Maximum		Minimum	
Source[a]	Surface water	Deep water	Surface water	Deep water
a) 5052 aluminum alloy				
A	29	65	0	0
B	52	62	0	0
C	29	39	0	0
D	5	35	0	0
b) Alclad 3003				
A	13	14	-	-
B	4	-	-	30
C	22	-	4	-
D	13	b	0.3	0

[a] A = Lockheed, B = Westinghouse, and C = TRW in their respective 1978 Conceptual Design Reports; D = Data chosen from Ref. 8.

[b] Depth of pitting was 20 mils in 123 days at which time a large area of cladding was gone.

Some unpublished data provided by T. E. Wright[14] covering results of Alcan IS-1200 for 3 years at Harbor Island, N.C. are summarized in Table 2. After test the pipes with D $\geq$ 2 in. were covered with "mossy" marine organisms and small barnacles, which would have reduced the velocity to practically zero at the metal surface. For pipes with D $\leq$ 1.5 in., there had been relatively little persistent fouling by marine organisms.

Table 2 Maximum depths of pitting of aluminum 1200 in seawater flowing through pipes at ambient temperature for 3 years at Harbor Island, N.C.[14]

Nominal pipe size diam, D, in.	Range of v_w, ft/sec	Pit depths, mils	Macro-fouling
3	0.17-1.6	58	yes
2.5	0.26-2.4	54	yes
2	0.36-3.4	35	yes
1.5	0.6-5.6	34	no
1	1.6-15	34	no
0.75	2.3-21	46	no
0.5	4.0-38	109*	no

* Perforated.

These results suggest that a sustained $v_w \geq 2.5$ ft/sec can be expected to minimize persistent macrofouling. This v_w is consistent in order of magnitude with results of other observations indicating a critical velocity near 4 ft/sec to avoid macrofouling. (This critical velocity does not apply to fouling by micro-organisms such as bacterial slimes. Recent studies of effects of such slimes on heat transfer have shown that bacterial slimes can adhere at velocities up to at least 6 ft/sec.)

Corrosion within the complete range of v_w was predominantly in the form of multitudes of rather deep pits. The maximum depth occurred at the lowest and highest velocities as shown in Table 2. Thus, it would appear that there was no controlling effect of the marine growths on the extent of pitting and that a v_w near 5 ft/sec was less aggressive than higher or lower velocities. However, these results may have limited applicability for aluminum OTEC heat exchangers because of uncertainties related to the wide ranges of v_w and the interrelated effects of fouling organisms that would not exist in OTEC service.

Additional data have been provided by another test of aluminum in the form of pipes at Harbor Island, N.C. This was undertaken in an effort to qualify 1-in.-O.D. x 0.133-in.-wall aluminum for use in seawater piping systems by the U.S. Navy.[15] The alloys tested were 3003, Alclad 3003 and 5052. Two 32-in. lengths of each alloy were assembled in lines containing a 90° short-radius Saran elbow to induce a turbulence effect. The assemblies were downstream of, but insulated from, a system containing copper-nickel alloys. The tests were run at v_w = 10 ft/sec for 30 to 42 months for the 3003 pipes and 12 to 24 months for the Alclad 3003 and 5052 alloys. Apparently there was no fouling of the pipes in this test. Corrosion was in the form of pitting (Table 3) not initiated by intergranular attack. There was erosion of the inlet edges. This did not occur downstream of the elbows. The investigators concluded that 3003 or Alclad 3003 piping might have a life expectancy of 10 years.

Table 3 Pitting of aluminum pipes in seawater flowing at 10 ft/sec at ambient temperature at Harbor Island, N.C.

Alloy	Maximum depth of pitting (mils)	Duration of exposure (months)
3003	40	42
Alclad 3003	19*	24
5052	41	24

*Pitting was confined to the cladding and did not penetrate into the 3003 core.

Current Corrosion Research

The current research program includes an effort to account for the severe pitting of some aluminum alloys at depths from which condenser cooling water may be taken.[16] Dexter[17] has given special attention to individual and possibly synergistic effects of critical levels of pH and oxygen concentration. The results of this research will aid characterization of the proposed OTEC plant locations with respect to the possibility of encountering water that might have exceptional capacity to promote pitting of aluminum.

Programs carried out at Keahole Pt. in Hawaii[10] and St. Croix in the Virgin Is. were designed to study effects of fouling on heat transfer at v_w's that might be encountered in OTEC exchangers. Unfortunately, the 6061 alloy used in these tests was chosen by those concerned primarily with heat transfer because of its ease in machining for use in the heat transfer device. The corrosion resistance of 6061 is well below that of 5052 or Alclad 3003, the preferred candidates for OTEC service.

Crevice Corrosion

Crevice corrosion in aluminum OTEC heat exchangers is more likely to be encountered in shell-less heat exchangers with water outside the tubes where crevices may be formed by tube supports, and in plate-type heat exchangers at points of contact between overlapping plates and under gaskets.

The danger of serious corrosion in plate-type heat exchangers is illustrated by experience with such an exchanger operated in a freezing-process desalination unit using freon at the Office of Water Technology demonstration plant at Wrightsville Beach, N.C. This heat exchanger was used to precool incoming seawater with product water or brine. Typical plates made of the 3003 alloy 0.025 inch thick were removed for examination after service for about 3 years and actual contact with seawater for about half that period. Crevice corrosion to a depth of about 12 mils had occurred at several points of contact between overlapping plates. In addition, there was one perforation of a 0.025-in.-thick plate at a contact point.

Similar crevice corrosion was said to be responsible for failure of aluminum (alloy not identified) in plate-type heat rejection condensers in a desalination plant in Israel:[18]

> "The plates were attacked mainly by crevice corrosion; as aluminum plates could not stand up to the severe conditions, titanium plates are now installed."

Crevice corrosion of Alclad 3003 was observed in the deep submergence tests reported by F. M. Reinhart.[16] The most severe crevice attack, to a depth of 15 mils with most of the cladding gone, occurred in exposure for 123 days at a depth of 5460 ft. This was accompanied by pitting to a maximum depth of 18 mils. Crevice corrosion of Alclad did not occur in surface water over a period of 588 days, but there was pitting to a depth of 17 mils.

The 5052 alloy experienced crevice corrosion to a depth of 65 mils in 123 days at a depth of 5640 ft. There was no pitting outside the crevice. In surface water the maximum depth of crevice corrosion was 5 mils in 366 days with pitting to the same depth outside the crevice. As for Alclad 3003, these results for 5052 suggest that crevice corrosion may be more severe in condensers using deep water than in evaporators using surface water. The reverse may be true with respect to pitting. In any event, Alclad would be expected to have a better chance than unclad alloys in resisting corrosion in crevices.

Crevice corrosion tests of the 6061 alloy at Key West, Florida, showed that a modest increase in v_w greatly increased the severity of crevice corrosion.[19] Specimens suffered crevice corrosion to a depth of 8 mils in 2 years in quiet surface water. Similar specimens exposed to water flowing in a flume at a velocity of 0.75 ft/sec were perforated (0.0625 in.) during the two year test period.

Comments on crevice corrosion in the Alcoa Catalogue[8] included the following:

"The existing data do not show to what extent crevice corrosion would be encountered on aluminum in OTEC power plant heat exchangers. OTEC heat exchangers should be designed to avoid crevices." It was suggested that crevices might be avoided "thru the use of appropriate gaskets and sealants and increasing the tightness of joints." In this context it will be necessary to insure that the gasket or sealant be firmly and continuously bonded to the metal so as not to create another crevice.

Effects of Seawater Velocity v_w

The oxide films on which aluminum depends for resistance to corrosion could be eroded by shear forces resulting from flow over the surface above some critical v_w. A limited amount of data[20] including those from the Navy Engineering Experiment Station[15] indicate that such a critical velocity is likely to be over 10 ft/sec and, therefore, above the 6 ft/sec proposed for OTEC shell and tube heat exchangers and the lower velocity in the shell-less heat exchangers proposed by The Johns Hopkins Applied Physics Laboratory.

The manner by which v_w is achieved in a test can have a considerable influence on its damaging effect. A uniform high velocity over the whole of a test surface[20] is likely to be less damaging than a localized high velocity such as achieved by a submerged jet. The local removal of a protective film adjacent to filmed surfaces can set up local corrosion cells causing accelerated attack where the film has been removed. Such localized velocity effects could restrain the use of submerged jets for cleaning shell-less aluminum heat exchangers. This issue should be established by an appropriate test program.

A similar limitation may be imposed on the use of an ultrasonic (high frequency vibration) cleaning device designed to induce cavitation in the water. Tests using high frequency vibration to evaluate resistance to cavitation erosion have shown that aluminum has a relatively low resistance to cavitation erosion.[21,22]

In the absence of abrasive material in suspension, it is conceivable that a modestly high velocity, e.g., the 6 ft/sec proposed for OTEC heat exchangers, could be favorable to a good performance of aluminum as well as other metals. The beneficial effect would be the prevention or removal of various deposits which might otherwise promote localized attack in crevices under such deposits. The additional corrosion tests being carried out at several locations will permit observations of effects of v_w that were not involved in the tests that have provided most of the historical data on corrosion of aluminum as discussed elsewhere in this report. An increase to $v_w >$ 6 ft/sec would be expected to aggravate crevice corrosion as observed by Peterson and Lennox.[19]

Galvanic Effects

The vulnerability of aluminum to acceleration of corrosion by galvanic action in contact with most other metals needed for OTEC system components and by effects of heavy metals (copper) from corrosion upstream of aluminum components will limit choices of materials for such components. This could increase costs of such components and limit means of avoiding fouling in piping, screens and water boxes by use of anti-fouling coatings containing copper or of copper alloys naturally resistant to fouling by barnacles, etc. If antifouling coatings are to be used, they should be based on tributyl tin rather than copper.

Steel piping and water boxes could be coated to avoid effects of galvanic corrosion and iron corrosion products including detached scale on associated aluminum. Epoxy formulations have been proposed as being appropriate coatings. These should be supplemented by cathodic protection to take care of possible bare spots. There

have been reports of adverse effects of detached portions of elastomer linings. Cathodic protection at much higher current densities could conceivably be effective with bare steel pipes and water boxes.

Coating of steel with aluminum has been proposed as a cost-effective alternative. Consideration could be given also, to the use of solid aluminum for water boxes and tube plates.

Effect of Chlorination

Chlorination may be used as a supplement to mechanical cleaning to maintain the desired level of heat transfer. Chlorination may also be necessary to control macrofouling, especially in conjunction with the use of aluminum in heat exchangers which would restrict the use of copper alloys for components upstream of the aluminum. The concentration of chlorine proposed to be used, e.g., less than 0.2 ppm, is not expected to aggravate corrosion of aluminum. For environmental reasons it is desirable to avoid use of chlorination if possible.

Effects of Ammonia

The possibility of serious corrosion of aluminum as a result of leakage of ammonia into sea water was suggested by results of tests with very dilute concentrations of ammonia in pure water.[8] In these tests, mixtures with sea water were found to be less aggressive.

Such possible effects have been investigated at Freeport, Texas in tests covering ammonia additions from 8 to 800 ppm at 5°C and 30°C, and v_w's of 2.5 and 5.6 ft/sec.[11] The 8-ppm concentration was most aggressive in increasing the extent of pitting at both 5°C and 30°C as compared with seawater containing no ammonia. In the case of the 3003 alloy, pitting at 30°C increased from practically zero to 14 mils in 64 days at v_w = 2.5 ft/sec. With the 5052 alloy pitting increased to 21 mils in 64 days under the same conditions.

The effect of 8 ppm of ammonia was less at 5.6 ft/sec. Ammonia concentrations greater than 8 ppm were less damaging under all the testing conditions. The presence of ammonia did not increase rates of uniform corrosion.

The observed effects of ammonia on corrosion are less serious than the important effect of ammonia in precipitating calcium carbonate scale from water that is likely to be supersaturated in calcium carbonate. Such scaling was observed in this test program. Since the scale resulting from such precipitation would be intolerable in OTEC heat exchangers, there will be a need to avoid even slight leakage of ammonia, irrespective of possible effects on corrosion of aluminum.

This need to take extraordinary steps to avoid, detect and correct leakage of ammonia extends as well to heat exchangers using any other metal for tubing. The effect of ammonia leakage in forming scales would be most critical in plate-type heat exchangers in which nuclei originating from a leak in one plate could result in precipitation of scale on all downstream plates.

It is possible, also, that scale precipitation nuclei could be transported by M.A.N. brushes or Amertap balls from a local source in a tube to the main body of water in a water box.

The tests by Schrieber et al.[11] extended to possible effects of leakage of seawater into ammonia to the extent of 0.14%. Their results indicated that such leakage would not present a problem of accelerated corrosion of aluminum nor deposition of scale.

Economic considerations will also require avoidance of even slight ammonia leakage; for example, leakage sufficient to add 1 ppm to the seawater in a 250 MW_e (net) OTEC plant would result in an intolerable loss of 20 tons of ammonia per day.

Currently there is a possible obstacle to the use of aluminum in a system involving ammonia. U.S. Coast Guard Regulation CG-257 prohibits the use of aluminum for components that come into contact with ammonia. The basis for this exclusion is obscure. It is possible that the Coast Guard could be persuaded to waive this prohibition on the basis of existing data and experience plus the results of Ref. 11.

A pending IMCO (Inter-Governmental Maritime Consultative Organization) standard (Section 154, 1700, Table 4) does not prohibit the use of aluminum in contact with ammonia. This conflict with the Coast Guard Regulation would presumably be taken into account by the Coast Guard in reaching a final decision on waiving their prohibition of aluminum in OTEC ammonia systems.

Effects of Vibration

Corrosion fatigue. The relatively low corrosion fatigue strength of aluminum alloys, e.g., from 3000 to 8000 psi as shown by conventional rotating beam tests in seawater,[23] has led to attention to calculation of the extent of danger from this source. These studies have indicated that corrosion fatigue of tubes in heat exchangers need not present a problem with proper spacing of tube supports.

Fretting. There have been instances of severe deterioration of aluminum tubes as a result of vibration in tube support plates. The Alcoa Catalogue[8] drew attention to this with a photograph of a particularly severe example along with erosion by high velocity steam in the same installation. They con-

cluded that the need to minimize vibration was related more to avoiding damage by fretting than by corrosion fatigue.

Service Records

The situation on records of service related to OTEC heat exchangers has been summarized as follows:[8] "Available service histories also proved inadequate for qualifying alloys for the OTEC applications, but they do support the selection of Alclad (7072) 3003 as a tubing alloy worthy of further consideration. Performance data covering areas of investigation peculiar to OTEC power plants is needed to permit a firm decision for or against aluminum alloy tubes." Exclusion of the 5052 alloy in this quotation may have been inadvertent, since elsewhere in the report the 5052 was identified as a "promising candidate for further evaluation."

More recently, representatives of the aluminum industry have identified Alclad 3003 or 3004 as being the most likely to qualify as economical materials for OTEC heat exchangers.

Roll-formed-and-welded Alclad tubing is considerably lower in cost than extruded material and is available in some enhanced-surface configurations.

Experience with aluminum in desalination plant heat exchangers has limited applicability to OTEC service. Pertinent data are restricted to heat-rejection condensers handling raw seawater.[18] In other desalinization heat exchangers the water has been deaerated and treated to prevent scaling. However, it was subjected to considerably higher (more adverse) temperatures than will be encountered in OTEC systems.

The most pertinent service records are the following:

Alclad 3003 tubes 3/4-in.-O.D. with a 0.064-in. wall were used in an oil cooler on the S.S. Alcoa Clipper.[8] After 10 years, 24% of the 0.01 inch cladding remained with no penetration into the 3003 core.

A generally similar life was shown by Alclad used for salt water piping in the Royal Canadian Navy as described by W. R. Chinn and T. H. Rogers.[24] Services involved circulatory lines to the main engines, sanitary lines and auxiliary equipment with flow velocities from 5 to 10 ft/sec. Experience with Alclad 3003 showed gradual loss of large areas of cladding 0.013-in. thick after service for 8 years, but there was no penetration into the 3003 alloy core. The authors estimated that a 10-yr life would be expected from 4-inch pipe with 0.013-in. cladding in this service.

The installations in the Royal Canadian Navy also included piping of the 5052 alloy in the same service as the Alclad 3003. The performance of the 5052 alloy was quite unsatisfactory. Failures by perforation were experienced in less than 2 years.

Experience in other heat exchangers. It is difficult to relate experience with aluminum in heat exchangers to other services such as power plants to qualification of aluminum for OTEC applications.

Water-side damage that occurred could have been from effects of suspended sediments and corrosive constituents that would not be present in clean seawater. The situation is illustrated by attempts several years ago to use aluminum tubes in condensers in nine power plants.[25] The performance of the aluminum was generally unsatisfactory because of steam erosion, water erosion and pitting. Attention to problems disclosed by early experience resulted in improved performance in later power plant installations mostly using fresh water for cooling.[26]

Summary of service records. The experience with the oil cooler on the Alcoa Clipper and with the piping in the Royal Canadian Navy supports the conclusion that Alclad 3003 tubes could survive for at least 10 years in OTEC heat exchangers. This estimate is supported by test data in the present paper on the progress of uniform corrosion with time.

The data with respect to the 5052 alloy are less encouraging as illustrated, for example, by its performance in comparison with Alclad 3003 in the piping installations in the Royal Canadian Navy. The ability of cladding to arrest pitting penetration of the core should be particularly attractive for thin-wall heater exchanger tubing where resistance to local penetration is especially important. Nevertheless, the 5052 alloy should remain a candidate for further evaluation in test programs for use in tube supports or tube sheets.

There is a possibility that the life of cladding could be extended by the development of a less active cladding alloy, e.g., one with a lower zinc content. There appears to be less scope for finding an effective cladding alloy for use over the 5052 composition which has a more negative corrosion potential than the 3003 alloy.

Stainless Alloys

The stainless alloys to be qualified for use in OTEC heat exchangers are represented by AL6X, a proprietary product of the Allegheny Ludlow Steel Company. It has a nominal composition of 24% Ni, 20% Cr, 6% Mo, and the balance iron. Other alloys characterized by a critical total chromium plus molybdenum content, as shown in Fig. 2, may be found to be equivalent to AL6X. The latter has been qualified already on the basis of more extensive evaluation tests and service experience than other candidates being subjected to similar evaluation.

This paper reviews the qualification of the AL-6X alloy.

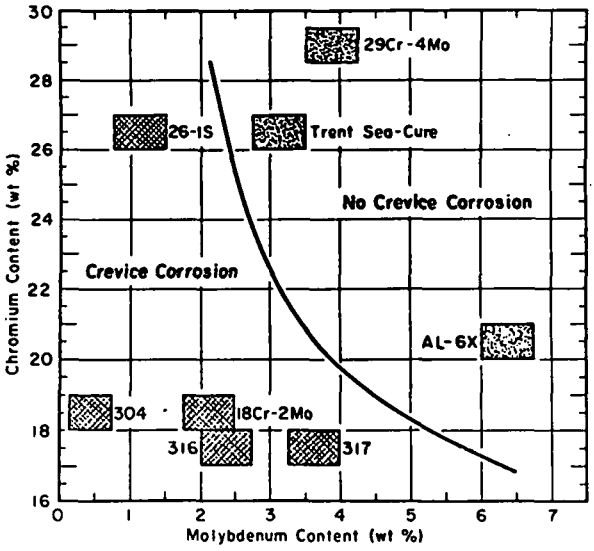

Fig. 2 Susceptibility of alloys to crevice corrosion as a function of chromium and molybdenum content.

The AL6X alloy is related to alloy IN-748, which is 27% Ni, 20% Cr, and 8.5% Mo. The latter alloy, covered by U.S. Patent No. 3,547,625, was developed by the International Nickel Company, Inc. for use in high-strength wire rope that could be used in marine environments without the failures from crevice corrosion encountered in wire rope made from 300-series grades of stainless steel. It came to the attention of fabricators of stainless steels, including Allegheny Ludlum, who were interested in developing an alloy that would not be subject to corrosion in crevices under deposits on salt-water-cooled condenser tubes made of Types 304 and 316 stainless steel.

Allegheny Ludlum modified the alloy to suit their production practices while maintaining the required resistance to crevice corrosion and pitting. Comparative tests of the two alloys have shown that AL-6X retains the resistance to pitting and crevice corrosion in seawater that was the target for the development of the IN-748 alloy.

Test Program

In the course of the alloy development program, it was found necessary to avoid the presence of intermetallic sigma phase rich in chromium and molybdenum. This impaired resistance to corrosion in the alloy-depleted zones adjacent to the sigma.[27] Poor performance attributed to sigma varied with the amount of sigma present, and, particularly, on its most damaging location at grain boundaries, as well as with the method of test. Sigma phase was responsible for poor performance in accelerated laboratory tests using ferric chloride. However, it was not found to be harmful in some early trial installations in which improperly heat-treated material performed satisfactorily despite the presence of a sigma phase.

An example of what has been described was provided by tests of the AL-6X alloy by the U.S. Naval Research Laboratory at Key West, Florida.[28] Specimens exposed for 218 days under conditions of quiet immersion suffered crevice corrosion to a depth of about 0.01 inch.

Corrosion specimens were also exposed to seawater flowing at a rate of 180 ml/min in a test cell at Key West Laboratory. Under these conditions, an AL-6X specimen exposed for 218 days was perforated 0.065 in. while companion specimens exposed 552 days suffered practically no crevice corrosion.

It seems likely that the absence of crevice corrosion of the AL-6X alloy in the much longer test period was no more than an example of the statistical probability feature of the incidence of crevice corrosion of stainless steels. Such attack may not occur within all crevices of test specimens containing several crevices.

Incidentally, specimens of a 26% Cr 1% Mo alloy with a thickness of 0.06 in. suffered crevice corrosion to a depth of 0.05 in. in the quiet immersion test at Key West and perforated in the 552-day test in the flowing water cell.

The effects of sigma phase and its elimination by proper heat treatment of the AL-6X alloy were demonstrated by crevice corrosion tests in hot sea water at Harbor Island, North Carolina. The test used was the multiple crevice technique developed by D. B. Anderson.[29] Twenty crevices are created on each side of a 4 x 6 in., flat specimen by pressing a serrated Delrin washer against the surface of the metal. The ratio of shielded-to-freely-exposed area is 1 to 85. After exposure, the depths of attack at any of the 40 crevices are measured and subjected to statistical analysis of the frequency and depths of attack.

This approach is responsive to observations that crevice corrosion of stainless steels in seawater is a matter of probability as well as intensity. The probability factor was illustrated dramatically in Ref. 30 as described previously. Effects of annealing temperature are indicated in Table 4.

Several types of acclerated screening tests have been used in the development of stainless steels that will resist pitting and crevice corrosion. Most important of these are tests using ferric chloride. In Ref. 30 the specimens did not include any crevices. Subsequent modifications using specimens with crevices have been found to be more discriminating in predicting resistance to pitting and crevice corrosion under conditions of long-time exposure to

Table 4 Effect of heat treatment on resistance of AL-6X to crevice corrosion in seawater at Harbor Island, N.C., for 30 Days at 50°C.[a]

Annealing temperature	Attack initiated,%	Attack propagating to 0.25 mm, %	Maximum depth of attack, mm
2200°F (1204°C)	0	0	0
1600°F (871°C)[b]	17.5	0	0

[a] Private communication, International Nickel Co., Inc.

[b] To promote presence of sigma phase.

natural seawater. Table 5 shows results of such tests conducted in the course of the development of the IN-748 and AL-6X alloys.

Table 5 Results of exposure to 10% $FeCl_3$ for 72 hr at room temperature

Alloy	Weight loss, %	Crevice attack	Pitting
304	2.5-5.1	Severe	Severe
316	2.5-5.1	Severe	Severe
317	0.8-1.1	-	-
29% Cr 4% Mo	0	0	0
25% Cr 1% Mo	0	0	0
AL-6X	0	0	0
Titanium	0	0	0

Another ferric chloride test to measure resistance to crevice corrosion was developed by Brigham.[31,32] The test is run to determine at a series of increasing temperatures the highest temperature at which a significant increase in crevice corrosion occurs. Results reported by Bond et al.,[33] presented in Table 6, showed the improved resistance of AL-6X and the other highly alloyed compositions compared to the 316 alloy.

Another approach to screening is an electrochemical test[34] in which current is applied to a specimen in a series of increasing potentials. Observations of the amount of current that is passed can define the "breakthrough" or "rupture" potential coincident with a substantial increase in current. The higher this potential, the greater the expected resistance to pitting and crevice corrosion. Representative results are shown in Table 7.[35]

Table 6 Critical crevice corrosion temperatures in 10% $FeCl_3$, pH 1

Alloy	Temp. of no crevice corrosion, °C	Temp. of slight crevice corrosion, °C
304	-	-2.5
316L (17% Cr 12% Ni 2.5% Mo)	-	0
27% Cr 1.5% Mo 4% Ni	5	7.5
25% Cr 3.5% Mo	47.5	50
26% Cr 1% Mo	20-22.5	22.5-25
AL-6X	17.5-20	20-22.5

Table 7 Breakthrough potential tests of stainless steels in chloride solutions

Alloy	Minimum breakthrough potential, mV 0.1% chloride	1% chloride
304	220	180
316	330	250
AL-6X	1000+[a]	940

[a] Beyond range of test.

Crevice Corrosion Tests in Seawater

Although results of ferric chloride and other screening tests indicated that AL-6X alloy would have high resistance to crevice corrosion and pitting in natural seawater, it was necessary to confirm this expectation by long-time tests using the Anderson multiple-crevice technique. Specimens were exposed at Harbor Island, N.C. for 5 years (Table 8). The specimens were free of pitting and free of corrosion in the crevices. No localized corrosion was found under the several varieties of fouling organisms that became attached to the alloy during the test period.

Table 8 Results of multiple crevice corrosion test in flowing seawater in ambient temperatures at Harbor Island, N.C. for 5 years

Alloy	Avg. Wt. loss, g	Probability, % Initiation	10 mils	50 mils	Max. depth, mils
316[a]	0.14	6	6	0	38
AL-6X	0.01	0	0	0	0

[a] Tested for 126 days.

Trial Installations

Trial lots of welded AL-6X tubes and 304, 316 and 216 stainless steels were placed in service in operating power plant condensers at New Haven, Conn. and Oldsmar, Fla. The Connecticut location had been the site of failures of type 316 stainless tubes by crevice corrosion under deposits.

In the Connecticut tests, some of the 216 and AL-6X tubes were installed with inlet and restrictions to reduce v_w from the normal 8 ft/sec to 0.1 ft/sec to promote deposition of solids, which had been found to have been the principal factor in the failure of type 316 tubes. Withdrawals of tubes after 1 and 3 years disclosed serious pitting in the types 304 and 316 but none in the 216 and AL-6X tubes at either site.

After 6 years, the single remaining 304 tube in the Florida installation contained many small pits. The 316 tubes showed many smaller pits. Both the 216 and AL-6X tubes tested with unrestricted flow remained free of pits after 6 years at both locations.

The partially restricted 216 tubes in the New Haven test showed larger pits than the unrestricted type 316. The partially restricted AL-6X tubes showed some light but insignificant attack. There was no attack in the crevice under the plug used to restrict flow.

The AL-6X tubes used in these trial installations had been made at a time when the annealing cycle did not avoid the presence of the sigma phase shown to be harmful in accelerated laboratory tests. Samples from the tubes used in the trial installations were re-heat-treated in accordance with the improved current production practice and subjected to the laboratory crevice corrosion screening test for comparison with samples of the test tubes in their original improperly heat treated condition. The properly heat-treated material performed satisfactorily in the crevice corrosion test.

It would appear that the crevice corrosion screening test is much more drastic toward the AL-6X alloy than the restricted flow conditions established in the Connecticut trial installation designed to promote pitting under deposited solids.

Full-Scale Installations

By the end of 1978, several million feet of AL-6X tubes had been installed in salt-water-cooled condensers in coastal power plants in the United States (Table 9). In addition, thousands of AL-6X inserts are being used by power companies to extend the life of brass tubes that have suffered inlet-end erosion. Except for one instance, no trouble has been encountered.

The one exception was the result of abnormal circumstances encountered early in 1977 at the United Illuminating Company station at Bridgeport, Conn. As a result of failure of a steam-impingement baffle in front of six AL-6X tubes, 7/8-in.-diam, 0.028-in. wall, in an upper row of the condenser, high velocity steam bled from a heater drain vent or a gland was dumped into the condenser through a line at 600 to 1000°F. The steam ruptured the baffle and impinged directly on the tubes to cause the failure.

Table 9 AL-6X installations

Company	Plant	Date
United Illuminating	Bridgeport Harbor No. 1	1973
	Bridgeport Harbor No. 2	1976
Tampa Electric	Big Bend No. 1	1976
	Hooker's Point No. 5	1976
	Gannon No. 6	1977
Public Service Elec. & Gas, New Jersey	Linden	1977
	Sewaren	1978
New Orleans Public Service	Michoud No. 3	1977
	Michoud No. 2	1978
Long Island Lighting	Northport No. 1	1978
	Northport No. 2	1979
New England Electric	Brayton Point No. 1	1978
	Brayton Point No. 2	1978
Maine Yankee		1978

Any of the other materials being considered for OTEC heat exchangers would have been similarly damaged by the abnormal conditions that caused the failure of the AL-6X tubes.

The normal operating conditions in the condenser at the Bridgeport station are particularly severe, since they involve peaking service with daily shutdown and start ups. The steam velocities are high but have not led to any failures from vibration. The steam contains some ammonia from the feed-water treatment.

Supplementary Information

Galvanic behavior. The AL-6X alloy occupies a position in a galvanic series in seawater shown by Table 10. It can be expected that the AL-6X alloy will not be subject to accelerated corrosion by galvanic contact with any of the materials with which it may become associated in OTEC systems.

Table 10 Galvanic series in seawater for alloys of interest in OTEC systems

Material	Range in potential vs sat. calomel half-cell, mV
Aluminum 5052[a]	-880 to -1080
Steel	-600 to -700
Copper	-300 to -350
90:10 Cu-Ni (706)	-210 to -280
70:30 Cu-Ni (715)	-170 to -230
Stainless Steel (Type 316)	-350 to -450 (Active) -100 to 0 (Passive)
26% Cr 1% Mo[28]	-100 to +100
Titanium	-50 to +50
AL-6X[b]	-50 to +280

[a] From Marine Corrosion, John Wiley and Sons, Inc., 1975, Fig. 6-1.

[b] From T. J. Lennox, Jr., Naval Research Laboratory Report 3622, 1977.

The AL-6X alloy could accelerate corrosion of aluminum, steel or other less noble metals if coupled to them. The extent of this galvanic effect would be about the same as that expected from similar combinations involving titanium and copper-nickel alloys.

In new condensers, it would be desirable to use steel tube plates clad with a stainless steel of high molybdenum content such as Jessop* 700 containing 21% Cr, 25% Ni, and 4.5% Mo if steel clad with AL-6X should not be available. Second choices would be cladding with Incoloy** 825 or Carpenter 20 Cb.+ The use of such alloy-clad steel tube plates would facilitate seal welding of tubes, which could be desirable to prevent leakage of ammonia.

AL-6X tubes would be able to tolerate copper in corrosion products from copper alloys, such as the 90:10 Cu-Ni alloy 706 that might be used upstream to take advantage of its antifouling properties, in screens or piping.

Resistance to ammonia. Since AL-6X is a ferrous alloy, it is resistant to corrosion by ammonia.[36] Leakage of ammonia into seawater, or vice versa, would not be expected to impair resistance to attack by either. Less highly alloyed stainless steels have been used successfully as tubes in heat exchangers involving exposure to ammonia.

Resistance to chlorine. There have been no reported problems attributable to the use of chlorination in heat exchangers in which stainless steels less highly alloyed than AL-6X have been used. Because of its higher Mo content, AL-6X has superior resistance to chlorinated seawater as confirmed by a laboratory screening test in which it was not affected by exposure to a 5% solution of sodium hydrochlorite at 50°C.[37]

Biofouling and Cleaning

Mechanical cleaning of stainless steel heat-exchanger tubes by the Amertap system has been employed without damage to the tubes.[38] There is no record of the use of the Amertap system with AL-6X tubes but no damage to such tubes need be anticipated. The absence of corrosion products and maintenance of a smooth surface on AL-6X tubes should facilitate mechanical cleaning. Chlorination will not bother it.

Since AL-6X will not corrode, there will be no electrical currents from local corrosion action that might trigger deposition of calcium supersatured water, this gives AL-6X an additional advantage over aluminum, which is less resistant to corrosion.

Effects of Seawater Velocity v_w

AL-6X tubes are being used successfully in power plant condensers with a design v_w of 8 ft/sec, which is higher than the velocities to be used in OTEC heat exchangers. The closely related IN-748 alloy and stainless steels showed low erosion rates at v_w's up to 140 ft/sec (Table 11).

Such resistance to deterioration from impingement of high-velocity seawater would be an advantage for the AL-6X alloy, if seawater jets were to be used for cleaning OTEC heat-transfer surfaces. As noted previously, it will tolerate the even more dangerous conditions of exposure to slowly moving seawater in partially obstructed tubes and under attached marine organisms.

Stress Corrosion Cracking

The temperatures to be encountered in OTEC heat exchangers are well below those at which chloride stress-corrosion cracking of austenitic stainless steel has been observed (above 140°F).

The AL-6X alloy is susceptible to stress-corrosion cracking in boiling, concentrated magnesium chloride, which is considered to be the most aggressive medium for promoting stress-corrosion cracking of austenitic stainless steels. Other chlorides, including seawater, are much less aggressive. The relatively high nickel content of AL-6X improves its resistance[39] as was demonstrated by freedom from cracking in boiling 20% sodium chloride.[36]

*Trade Mark, Jessop Steel Co., Washington, PA

**Trade Mark, International Nickel Co., Inc., NY

+Trade Mark, Carpenter Technology Corp., Reading, PA

Table 11 Results of tests in high-velocity seawater[a]

Alloy	Weight loss, g	appearance
TEST 1. Specimens on rotation disc[b] at tip velocity of 27 ft/sec for 60 days at 16°C. Exposed area 7.2 in.^{2} (46 cm^2).		
IN-748	0.004	No visible corrosion
316 Stainless Steel	0.004	No visible corrosion
TEST 2. Extreme-velocity test,[c] 129 ft/sec[d] for 30 days at 9°C. Exposed area 3.5 in.^{2} (22 cm^2).		
IN-748	0.04	Trace
316 Stainless Steel	0.03	None

TEST 3X. Extreme-velocity test,[c] 130-140 ft/sec for 30 days at 15°C.

Alloy	Corrosion Rate mils/yr	mm/yr
304 Stainless Steel	1	0.025
316 Stainless Steel	1	0.025
90:10 Cu-Ni (CA-706)	25	0.63
6061 Aluminum	65	1.6
Carbon Steel	150	3.8

[a] International Nickel Co., Inc., private communication, 1977.

[b] F. L. LaQue, Marine Corrosion, John Wiley and Sons, Inc., New York, 1957, Fig. 3.14, p. 59.

[c] Ibid., Figs. 3.22-3.25, p. 64.

[d] Hole in specimen to induce cavitation.

Intergranular Corrosion

The AL-6X alloy is made with a sufficiently low carbon content (< 0.03%) to avoid sensitization to intergranular corrosion that results from precipitation of chromium carbides in austenitic stainless steels. Another form of sensitization caused by formation of a sigma phase, discussed previously, is avoided by appropriate heat treatment.

Corrosion Fatigue

No data are available on the corrosion fatigue properties of the AL-6X alloy. However, its high resistance to pitting, which otherwise could serve to create local stress-raising notches, can be expected to give the alloy an advantage over metals less resistant to local attack.

Vibration

There have been no instances of failure of AL-6X tubes that replace copper alloys. In these cases, the spacing of the tube supports had been designed for thicker-walled tubes of copper alloys. In new installations of AL-6X tubes, the spacing of the tube supports will, presumably, be related properly to the properties of the alloy and the dimensions of the tubes.

Choice of AL-6X in preference to titanium to replace copper alloys in condensers with tube supports designed for the copper alloys has been reported to have been based on vibration-related failures of thin-wall titanium tubes in such installations.[38] The higher modulus of elasticity of AL-6X (29 x 10^6) as compared with titanium (15 x 10^6) should be advantageous with respect to vibration.

Conclusions

Aluminum

1. Aluminum can neither be qualified nor disqualified for use for tubes in OTEC heat exchangers on the basis of available data on resistance to corrosion especially by pitting or crevice corrosion. Alloys worthy of further tests under conditions properly related to OTEC service are Alclad (7072) 3003 or 3004 and Al 5052. For thin-walled heat exchanger tubes the prime requirement is resistance to penetration by pitting. This suggests that Alclad would have a considerable advantage based on the ability of the cladding to arrest penetra-

tion of the core alloy so long as a substantial area of cladding remains. A principal target of further testing should be to establish whether periodic cleaning will increase the loss of cladding above the approximately 1 mil per year rate indicated by behavior in the absence of any effects of cleaning. Available data suggest a possible life of about 10 years for Alclad tubes with 10 mils of cladding. (Representatives of the aluminum industry have suggested that the latter estimate is too conservative because it does not give sufficient credit to the survival of the core alloy after the cladding is gone. In view of uncertainties relative to the effects of cleaning, the author is inclined to stick to his estimate of a 10 year life, pending development of additional data.)

2. The danger of crevice corrosion will have to be taken into account in connection with the use of aluminum in designs where crevices cannot be avoided, such as plate-type heat exchangers, or may be difficult to seal as at tube supports in heat exchangers with water outside the tubes. Crevice corrosion seems likely to be more severe in condensers handling water from great depths.

3. Water velocities below 8 ft/sec are not expected to result in intolerable erosion of aluminum.

4. The vulnerability of aluminum to acceleration of corrosion by galvanic action in contact with most other metals needed for OTEC system components, and by effects of heavy metals (copper) from corrosion upstream of aluminum, will limit choices of materials for such components.

5. The effects of leakage of ammonia in accelerating corrosion of aluminum will be less significant than the effect of ammonia leakage in triggering deposition of carbonate scale from water likely to be supersaturated with calcium carbonate. The latter effect, plus the economic penalty of loss of ammonia by leakage, will require steps to prevent, detect and correct even slight leakage of ammonia in OTEC heat exchangers irrespective of the metal to be used.

6. Aluminum heat exchangers must be designed to minimize vibration that could cause corrosion fatigue or fretting corrosion at tube supports.

7. There should be no problem of stress corrosion cracking of aluminum in either sea water or ammonia, or mixtures of the two.

8. There is no problem of supply of aluminum ore and of aluminum metal that would restrain the use of aluminum in any probable scale of OTEC operations.

9. Although the use of aluminum in contact with ammonia is currently prohibited by U.S. Coast Guard Regulation CG-257, it is permitted by a pending IMCO (Inter-Governmental Maritime Consultive Organization) standard. In view of this pending standard and any new data showing resistance of aluminum to attack by ammonia, the Coast Guard may waive its prohibition of aluminum as applied to OTEC systems.

Stainless Steels

1. The evidence compiled in this review supports continuing consideration of the AL-6X alloy as a desirable material for tubing in OTEC heat exchangers.

2. The high-purity, high Cr alloys containing from 1 to 4% Mo have performed well enough in evaluation tests to warrant furthere attention. To date, the number of trial or full-scale installations has not been adequate to provide a record of condenser service experience for the chromium alloys that is comparable to that of the AL-6X alloy.

3. Other alloy producers may, in the future, offer either the original IN-748 composition or a modification (containing at least 6% Mo) that could be expected to perform well in OTEC heat exchangers.

4. In a broader sense, alloys likely to demonstrate adequate resistance to pitting and crevice corrosion have chromium and molybdenum contents to the right of the line in Fig. 2.[40] The alloy in this figure, identified as Sea-Cure* has a nominal composition of 26% Cr, 3% Mo, and 2.5% Ni.

5. None of the commercial stainless steels in the 300 or 400 series has the level of resistance to pitting and crevice corrosion required for use in OTEC heat exchangers.

*Trade Mark, Colt Industries, Inc., Crucible Materials Research Center, Pittsburgh, PA.

References

1. Trimble, L. C. and Potash, R. L., "OTEC Goes to Sea (a Review of Mini-OTEC)," in Proceedings of the 6th OTEC Conference, Washington, D.C., June 19-22, 1979, G. L. Dugger, editor, Vol. I.

2. Bakstad, P. J. and Pearson, R. O., "Design of a 10-MW_e (Net) OTEC Power Module Using Vertical Falling-Film Heat Exchangers," loc. cit., Vol. I.

3. Keirsey, J. L., Funk, J. A., Pandolfini, P. P. and Cusick, R. T., "Core Unit Testing of the APL/JHU Shell-Less Folded Tube Heat Exchanger," loc. cit., Vol. II.

4. Francis, E. J., Avery, W. H., Babbitt, J. F. and Nordquist, M. H., "Commercial Ocean Thermal Energy Conversion (OTEC) Plants by the Mid-1980's," loc. cit. Vol. I.

5. Denton, J. W., Bakstad, P. and McIlroy, K., "Design of a 0.2-MW_e, Plate-Type, OTEC Heat Exchanger Test Article and a 10-MW_e (Net) Power Module," loc. cit., Vol. II.

6. LaQue, F. L., "Qualification of Aluminum for OTEC Heat Exchangers," ANL/OTEC-BCM-003, May 1979.*

7. LaQue, F. L., "Qualification of Stainless Steel for OTEC Heat Exchanger Tubing," ANL/OTEC-001, January 1979.*

8. Wagner, R. H. and Bonewitz, R. A., "Catalogue of Information on the Performance of Aluminum in Sea Water," Alcoa Rept. NXS-3, prepared for Battelle Pacific Northwest Laboratory, April 5, 1978.

9. Godard, Jepson, Bothwell and Kane, The Corrosion of Light Metals, Wiley, New York, 1967.

10. Liebert, B. E., "Corrosion of Aluminum and Titanium at Keahole Point Over an Eight Month Period," Proc. of the Ocean Thermal Energy Conversion Biofouling and Materials Workshop, Rosslyn, Va., Jan. 8-10, 1979, ANL/OTEC-BCM-00, pp. 189-196.*

11. Schrieber, C. F., Grimes, W. D. and McIllhenny, W. F., (Dow Chemical) "A Study of the Corrosive Effect on Aluminum and CP Titanium of Mixtures of Ammonia and Seawater that May Be Encountered in OTEC Heat Exchangers," ANL/OTEC-BCM-004, March 1979.*

12. Pandolfini, P. P., Avery, W. H. and Hill, F. K., "Experiments on Ultrasonic Cleaning of a Shell-Less Folded-Aluminum-Tube, OTEC Heat Exchanger," in Proceedings of the 6th OTEC Conference, Washington, D.C., June 19-22, 1979, G. L. Dugger, editor, Vol. II.

13. Little, Brenda, Morse, J., Loeb, G. and Spiehler, F., "A Biofouling & Corrosion Study of Ocean Thermal Energy Conversion (OTEC) Heat Exchanger Candidate Metals," loc. cit., Vol. II.

14. Private communication from T. E. Wright, Alcan Research Laboratory, Kingston, Ontario, Canada.

15. U.S. Navy Engineering Experiment Station Report 0 40037A(5), February 28, 1955.

16. Reinhart, F. M., "Corrosion of Metals and Alloys in the Deep Ocean," CEL Rept. T-R 834, Naval Construction Battl. Center, Port Hueneme, CA, February 1976, 265 pages.

17. Dexter, S. C., "Oxygen, Temperature and pH Effects on Corrosion of Aluminum in Seawater," in Proceedings of the 6th OTEC Conference, Washington, D.C., June 19-22, 1979, G. L. Dugger, editor, Vol. II.

18. Friedman, M., "Operational Experience of Vapour Compressing Plants," Proceedings of the Eleventh National Symposium on Desalination, Oslo, March 1975.

19. Peterson, M. H. and Lennox, T. J., Jr., "The Effects of Exposure Conditions on the Corrosion of A16061 T6 Aluminum in Sea Water," Materials Performance, April 1977, pp. 16-19.

20. Symonds, J., "Effects of Velocity on the Sea Water Corrosion Resistance of Two Aluminum Alloys," presented at OTEC Biofouling and Corrosion Conference, Miami, February 1978.

21. Kerr, S. L., Trans. ASME, 59, 373 (1937).

22. Plesset, M. S., Corrosion, 18, 5, 1962.

23. Czyryea, E. J., "Corrosion Fatigue Tests of Aluminum Alloys for Surface Effect Ship Hulls," Rept. No. 28-363, NSRDL, Carderock, Md., October 1972.

24. Chinn, W. R. and Rogers, T. H., "Aluminum in Ships of the Royal Canadian Navy," Corrosion, 15, August 1959, p. 403t.

25. "Aluminum Condenser Tubes, A Status Report," Power, March 1963.

26. Horst, R. L. and Marchese, R. T., Paper No. 62 WA-330, A.S.M.E., November 1962.

27. Brigham, R. J. and Tozer, E. W., Canadian Metallurgical Quarterly, 12, 2, 171-176, 1973.

28. Lennox, T. J., Jr. and Peterson, M. H., NACE Corrosion/76, Houston, TX, March 1976, Paper 78.

29. Anderson, D. B., American Society for Testing and Materials ASTM STP 576, 1976, pp. 231-242.

30. Smith, H., Metal Progress, 33, 596-600, 1938.

31. Brigham, R. J. and Tozer, E. W., Corrosion, 29, 1, 33-36, 1973.

32. Brigham, R. J., Corrosion, 30, 11, 396-398, 1974.

33. Bond, A. P., Dundas, H. J., Ekerot, S. and Semcrysen, M., Stainless Steel, 77, London, England.

34. Fujii, M. and Kumada, M., Japan Institute of Metals, 34, 6, 1970.

35. Deverell, H. E. and Maurer, J. R., NACE Corrosion 77, San Francisco, CA.

36. Maurer, J. R., Allegheny Ludlum Steel Co., private communication, 1977.

37. International Nickel Co., Inc., private communication, 1977.

38. Haskinson, D. W. and Kuester, D. W., ASME Series A, J. Eng. Power, 87, 401-404, 1965.

39. Copson, H. R., in Physical Metallurgy of Stress Corrosion Fracture, edited by T. Rhodes, Wiley Interscience, New York, 1959, p. 247.

40. Kovach, C. W., Inco Power Conference, Wrightsville Beach, N.C., August 1978.

*Argonne National Laboratory (ANL) OTEC reports are available from the National Technical Information Service, Springfield, VA 22161.

DISCUSSION

D. Sasscer, CEER: Do the curves from Schreiber and Leibert show a dependency of corrosion rate on temperature for aluminum? Do they mean that aluminum is better for condensers than it is for evaporators?

F. LaQue: The difference in the two tests of Schreiber's was attributed to temperature. However, I am more prepared to defend the shape of the curve than the numbers. What I was dealing with was not so much what the curves tell us about how fast aluminum is going to corrode but how much attention we have to pay to cleaning procedures that don't shove us back to instantaneous rates of corrosion. I think it is reasonable and I have suggested that we might visualize hybrid OTEC plants in which aluminum might be qualified for the condensers even though it might not be qualified for the evaporators.

C. Kovach, Crucible Steel: I would like to fill in a field service experience gap which exists for one of the new high alloy stainless steels described by Mr. LaQue, specifically, Trent Sea-Cure condenser tubing. This alloy is now on test as condenser tubing in approximately twenty electric utility condensers operating on brackish and sea cooling water in the USA and in Europe. Test results are now available from three sites with service times of approximately one year. No evidence has been observed of pitting or crevice corrosion initiation in any of these cases. In one of these instances the tube was severely fouled with barnacles and other marine growth because of a one-month stagnant condition. The alloy has also undergone about one year of coupon test exposure in low velocity natural seawater at Wrightsville Beach with no pitting or crevice corrosion at artificial crevices. We feel that the absence of localized corrosion in tests of one year duration strongly indicate that Sea-Cure will withstand natural seawater for much longer periods of time without initiating pitting or crevice corrosion. In considering the economics of material selection for the OTEC application it is pointed out that the general corrosion rate of stainless steels in chloride waters is essentially nil, and a thickness allowance for general corrosion is therefore not required. Also, considerable cost differences exist between these new high alloy stainless steels depending on such factors as alloy content, melting method, production characteristics and product form. Anyone analyzing costs should be sure to treat each alloy separately on its own merits.

E. Barkman, Reynolds Metals Co.: I am among the aluminum industry representatives who believe [as now noted by a footnote on Mr. LaQue's first page] that the estimated life for Alclad aluminum tubing should include an allowance for life of the base alloy after the cladding is gone. I would also note that data such as shown in Fig. 1 in the paper suggest that the corrosion rate may be less than 1 mil/yr after the first year.

USE OF THE NEW STAINLESS ALLOYS FOR OTEC HEAT EXCHANGERS

Jack R. Maurer*

Research Center
Allegheny Ludlum Steel Corporation
Brackenridge, Pennsylvania 15014

Abstract

Recent developments in melting and processing technology have made available a number of new alloys, resistant to sea water and other highly aggressive environments. These corrosion resistant properties have made the stainless steels into viable alternates for consideration in the OTEC heat exchangers. The paper discusses these new alloys with particular emphasis on AL-6X (20 Cr-24 Ni-6 Mo). Examples of 9 years of test experience and 5 years operating experience in power plant condensers are covered, including corrosion resistance, fouling, heat transfer and other areas of interest to OTEC applications. The new ferritic stainless steels are also reviewed as potential candidates for heat exchanger applications where performance and thin wall integrity are important. Details of condenser operating experiences in both brackish and fresh water environments are included. The paper covers both fossil and nuclear applications. Information regarding installation and fabrication is covered. Specific attention is given to both rolled and welded tube/tube sheet joints. This will include rolling procedures and examples of typical joint strength available using various combinations of materials. A review of tube sheet materials, compatible with various alloys is also made.

Introduction

The stainless steels have been used in power plant heat exchanger systems for over two decades with a high degree of success. At the present time, in excess of 600 million feet of stainless steel has been used for condenser applications. The reasons for the selection of stainless steel are numerous: overall corrosion resistance, resistance to ammonia stress corrosion cracking, resistance to steam impingement, inlet end and blockage erosion, virtually no corrosion product release, ease of installation and cleaning maintenance, etc. In addition, these materials have been cost effective as original purchases, as long term reliable products, and as efficient materials in the heat transfer cycle.

Until recently, most of these applications have been in fresh water areas where Type 304 stainless steel has proven to be an efficient, economical and reliable choice. Type 316 was used for sea water installation and met with mixed success. Some early researchers[1] projected that this alloy would have sufficient pitting resistance to perform in sea water environments. This did not include the presence of crevices, whether fabricated, natural or artificial. In power utility service (and others as well), clean crevice-free T-316 performs quite well in both fresh and polluted sea water. When crevices are present or allowed to form, this material can be quickly attacked.

Considerable research was initiated in the latter part of the 1960's and continues today to find materials which are compatible with long term sea water exposure. Our own program at Allegheny Ludlum was initiated in 1965 to develop a stainless alloy specifically for sea water condenser service. Specific design criteria were established for a successful alloy which must:

- Resist pitting and crevice corrosion in fresh and brackish sea water
- Be capable of operating with a fouled surface for extended periods with no evidence of deterioration or corrosion initiation
- Resist corrosion attack during lengthy outages under stagnant conditions
- Have the other attributes of stainless steels
- Be economically competitive with other alloys

Alloys certainly existed which met most of these criteria. Perhaps the most difficult was the item concerning cost effectiveness. In order for a material to receive serious consideration, its evaluated cost based on input of all advantages and disadvantages, must be economically justified. It is obvious that alloys designed to meet the above criteria must contain substantial amounts of expensive alloying additions to provide a high level corrosion resistance. These alloys are also generally more difficult to melt and/or process.

Part of the success in developing new alloys to meet our needs has been the introduction of new equipment and processes. Perhaps the most significant advance in

*Market Development Manager

melting technology has been the argon oxygen decarburization (AOD) process. Its introduction helped to resolve the major stumbling block to the successful commercial development of AL-6X as a sea water resistant condenser tube material which meets all of the specified design criteria outlined above. Other technological advancements such as the development of the electron beam furnace to produce low interstitial ferritics were major advances. Adaptation of that technology to enhanced vacuum induction melting techniques has helped to commercialize alloys such as 29 Cr-4 Mo and 29 Cr-4 Mo-2 Ni for sea water applications.

Materials and Properties

During the past decade, several researchers have investigated various material systems and proposed new alloys or at least categorized them. The most promising alloys for sea water corrosion resistance rely on the combined alloying effects of chromium and molybdenum. Studies regarding alloy compositions based on these two elements such as Brigham[2], Pessal and Nurmurin[3] and Bond and his coworkers[4] have documented their effects on pitting and crevice corrosion.

One alloy which has demonstrated its performance characteristics and cost effectiveness for sea water cooled power plant condensers is AL-6X. It is a promising candidate for OTEC heat exchangers. Another alloy which appears to be a worthwhile candidate for both these applications is 29-4 (and its companion product 29-4-2).

The typical compositions of these alloys are listed in Table 1 and the typical annealed mechanical properties in Table 2. Laboratory evaluation of these materials using ASTM G-48 (10% ferric chloride, rubber band test) and potentiostatic techniques provide a comparison of the properties of these materials against other more familiar alloys. The data are shown in Tables 3 and 4.

Table 1
Typical Analyses

	AL-6X	29-4	29-4-2
Chromium	20	29	29
Nickel	24	--	2
Molybdenum	6	4	4

Table 2
Typical Annealed Properties

	AL-6X	29-4	29-4-2
.2% YS·ksi	45	75	88
UTS ksi	94	91	98
% E (2")	45	25	23

Table 3

10% Ferric Chloride Rubber Band Test
72 Hours -- Room Temperature
ASTM G-48

Alloy	% Wt. Loss
AL-6X	0
29 Cr-4 Mo	0
29 Cr-4 Mo-2 Ni	0
Hastelloy C	0
Titanium	0
E-BRITE 26-1	0 - 0.01
AL-4X	0.04 - 0.06
216	0.2 - 0.45
26-1S	0.3 - 0.6
317	0.8 - 1.1
316	2.5 - 5.1
20Cb3	4.0 - 5.0
304	2.5 - 5.1

Table 4

Potentiostatic Measurements

Alloy	Min. Breakthrough Potential (Volt vs. SCE)
AL-6X	1.0+ (beyond range tested)
29-4	1.0+ (beyond range tested)
29-4-2	1.0+ (beyond range tested)
Hastelloy C	1.0+ (beyond range tested)
Titanium	1.0+ (beyond range tested)
26-1S	.98
216	.95
20Cb3	.55
18-2	.40
316	.33
439	.30
304	.22
430	.05

While neither of these laboratory tests provide a totally accurate prediction of a materials behavior in sea water, they have been generally accepted as screening devices to permit the selection of alloys for further study. In both cases, AL-6X and 29-4 demonstrate a resistance to pitting and crevice corrosion that is substantially better than the more commonly available stainless steels. Additional corrosion tests on these and other alloys have been performed and are discussed by the author in another publication[5]. These additional corrosion tests describe the alloys for broader applications, but have little bearing on power plant condensers or OTEC environments.

Applications

AL-6X has been tested in many locations. Table 5 lists some of the utilities and other companies in the USA and abroad who have used this material in test programs and heat exchanger tubes. The performance has been good in all areas to-date. The earliest tests were started in 1970 and some are still in progress, providing over 9 years of service experience. This experience has been excellent and the few

failures which have occurred have been traced to upset conditions or improper heat treatment during the early development years. This latter situation has been corrected and is now monitored through tight quality control procedures.

Table 5

AL-6X Test Installations

United Illuminating	Pacific G & E
Florida Power	Public Service E & G
Gulf States Utilities	Consolidated Edison
Northeast Utilities	Houston L & P
New England Electric	Maine Yankee
Potomac Electric	Connecticut Yankee
Virginia Electric	TVA
Baltimore G & E	Long Island Lighting
ENEL - Italy	PZEM - Netherlands
CEGB - England	Brown Boveri
Union Carbide	Upjohn
U.S. Navy	Lockheed Missile
Jos. E. Seagram	Amoco Research
Simpson Paper	Exxon

Complete installations have been made in 18 power plant condensers (Table 6). This represents approximately 17 million feet of tubing. In every case, AL-6X was used as retrofit tubing because some other material had failed to provide the service performance expected in the original design. This, of course, is typical of the development and usage of most new materials. The success of AL-6X has led one utility to announce that it would design its next new unit with this material.

A list of additional complete applications in areas other than power plants is included in Table 7. These applications utilize salt or brackish water for cooling purposes which is the primary reason for using AL-6X and, in most cases, the tubes are replacement bundles rather than original equipment.

The testing and use of 29-4 and 29-4-2 is much more limited since these are newer alloys. While their apparent corrosion resistance properties in laboratory studies are at least equivalent to or better than AL-6X, they have yet to be proven over long time exposures in operating environments. Table 8 lists a number of companies presently testing either or both of these alloys in highly aggressive environments. Samples exposed up to three years in salt water have shown no signs of general or localized corrosion attack.

While corrosion resistance and the integrity of the alloys used is of considerable importance, the heat transfer capabilities of these materials must also be considered. In the 1950's, utilities were highly reluctant to use stainless steels for condenser tubes because of their low coefficients of thermal conductivity. The first full installation of stainless steel at Monongahela Power in 1957 helped to resolve this problem. An analysis of that installation and the heat transfer characteristics of stainless was presented by author[6] at the 1961 Inco Power Conference.

Table 6

AL-6X Installations

United Illuminating	
Bridgeport Harbor #1	(1973)
Bridgeport Harbor #2	(1976)
Tampa Electric	
Big Bend #1	(1976)
Hooker's Point #5	(1976)
Gannon #6	(1977)
Public Service E & G	
Linden	(1977)
Sewaren	(1978)
Salem #1	(1979)
New Orleans Public Srvc.	
Michoud #3	(1977)
Michoud #2	(1978)
Long Island Lighting	
Northport #1	(1978)
Northport #2	(1979)
New England Electric	
Brayton Point #1	(1978)
Brayton Point #2	(1978)
Maine Yankee	(1978) (1979)
Southern Cal. Edison	
Mohave #1	(1979)
Mohave #2	(1980)
San Diego G & E	
South Bay #1	(1979)

Table 7

Additional AL-6X Applications

Alton Box Board	
Pulp & Paper	Evap. Condenser
Pittsburgh Plate Glass	
CPI	Glycol Cooler
Gillette	
Industrial Power	Steam Condenser
U.S. Borax	
CPI	Heating Coil
Evaporator Technology	
CPI	Caustic Cooler
Union Oil	
Geothermal	Condenser
Fluor	
CPI	Heat Exchanger

Table 8

29-4 and 29-4-2
Test Installations

United Illuminating
Consolidated Edison
Florida Power
New England Electric Service
Maine Yankee
Public Service Electric & Gas
Union Carbide
David Taylor Naval Ship R & D
Spiral Tube Corporation
Goslin
HCPC Construction
Spinal Tube Corporation
E. I. DuPont
Pennwalt Corp.
Getty Refining
Hooker Industrial Systems

Studies and a report by Lustender and Staub[7] helped to put the problem of heat transfer into proper perspective. Their results, shown in Figure 1, aptly illustrate the slight effect of the metal wall in comparison with internal and external surface films. Additional results presented by the author[8] and shown in Figure 2 provide a further insight into heat transfer performance. In this example, T-304 and Admiralty Brass tubes performed at the beginning of the study, just as one might expect. With exposure to the heat transfer fluids, fouling deposits and corrosion, the performance deteriorated, again as expected. Over a period of time, the overall heat transfer of the copper base alloy was considerably depressed by the formation of a corrosion product, while the stainless did not develop the additional barrier to heat transfer. These results have been confirmed by several utilities where replacement tubes of stainless steel did as well as or outperformed the original tube metal.

AL-6X has performed in a similar manner. The first tube installation at United Illuminating's Bridgeport Harbor has shown AL-6X to compete favorably with the previous tubes which were aluminum brass. Figure 3 shows the performance range for aluminum brass over the years comparing condenser back pressure against circulating water inlet temperature and includes data points for AL-6X tubes.

The fouling of tubes is one of the major concerns of heat transfer. Stainless alloys present a sterile surface to cooling water organisms and may be more susceptible to their growth than those materials which leach poisonous materials. Experience to-date confirms that stainless steel condenser tubes will foul although the degree is highly variable dependent on the cooling water source, amount of pollution, circulating water velocity and surface texture.

FIGURE 1

HEAT FLOW RESISTANCES

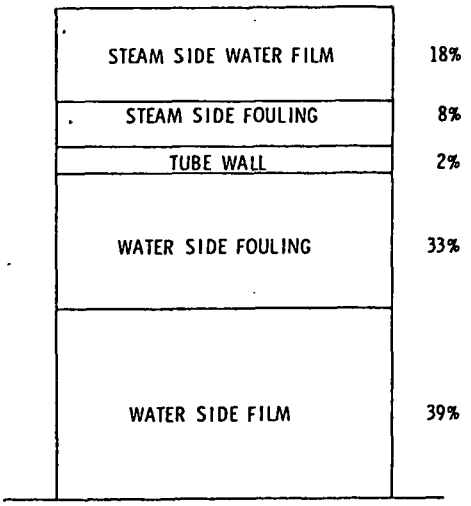

FIGURE 2

EFFECT OF EXPOSURE ON HEAT TRANSFER

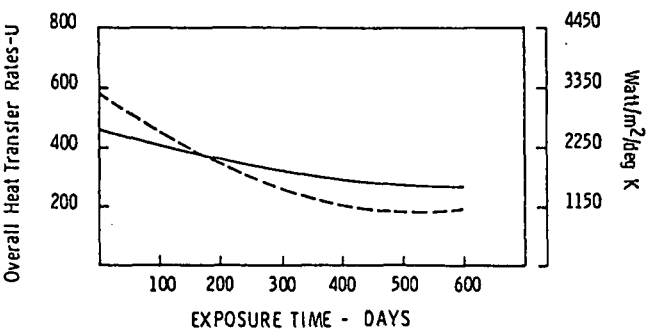

Figure 3
Condenser Performance Curves

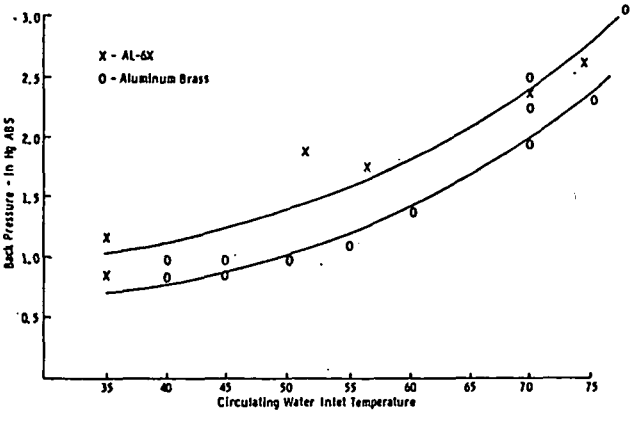

Tubes of AL-6X and T-316 removed from a Florida utility's condenser on relatively clean salt water illustrated a substantial difference in the degree of fouling and/or deposits which formed on the ID surfaces. The T-316 tubes had a heavier deposit, although both could be classified as "clean" in comparison to some applications investigated over the years. The difference in performance between these two alloys may have been the result of processing variables rather than the nature of the alloys or the cooling water. The T-316 tube was welded, cold drawn, annealed and pickled. The AL-6X tube was formed and welded from bright annealed strip and was not annealed or pickled following welding. Figure 4 shows secondary electron images of tube surfaces produced by various methods. There is a considerable variation in surface "roughness" and the number and degree of sites where biological growths can attach and grow. Additional research on commercially available surface finishes is necessary for a better understanding of the fouling tendencies of various materials.

Other Considerations

Two items which should be reviewed when considering tubes for a heat exchanger application are the tube sheet material and the method of joining tubes. These are important considerations if one wishes to optimize performance and reliability.

A. Tube Sheets

All AL-6X applications to-date have been retrofits and as a result, the original tube sheets are used. These include Muntz

Figure 4

Tube Surface Topographies - 1700X

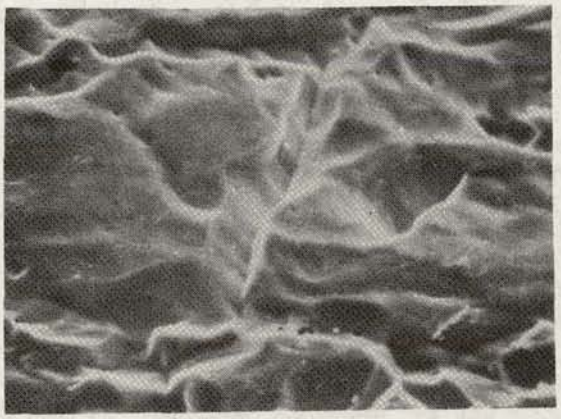

T-304 Cold Drawn, Annealed & Pickled

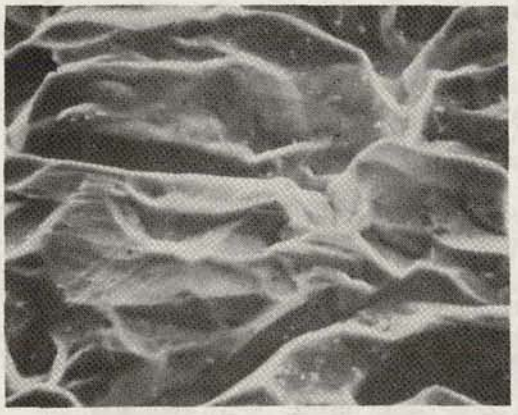

T-304 Welded, Annealed & Pickled

AL-6X As-Welded (bright annealed skelp)

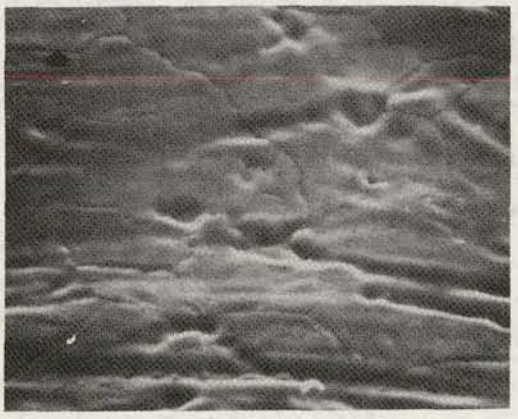

T-304 Welded, Bright Annealed

metal, aluminum bronze and T-316. There have been no severe galvanic problems, but there have been some signs of galvanic activity. Some of these installations have anodes or used impressed current for the protection of the tube sheet.

Allegheny Ludlum is presently investigating the galvanic compatibility of various tube materials with tube sheet materials. The initial results indicate that AL-6X (and 29-4) may react with certain tube sheet materials in such a way as to cause the degradation of the tube sheet. This has occurred with titanium tubes installed in various tube sheet alloys and was recently discussed by Peabody[9] at the American Power Conference.

A detailed presentation of our Research will be presented at an early date. Work to-date indicates that as more corrosion resistant materials are used for tubes, the cathode area expands. In other words, materials which corrode in an environment such as Admiralty Brass in sea water, provide a small cathode area encompassing a few diameters into the tube. More resistant materials such as 90-10 cupro nickel may extend the cathode to a few feet. Materials such as titanium, AL-6X, 29-4 and others with excellent resistance to sea water may develop cathodic areas as much as 20-40 feet. This increases a normally unfavorable cathode/anode ratio for tubes/tube sheet from 8/1 to 1000/1 and even more.

Tube sheets are less susceptible to damage than tubes for the simple reason they can be inspected and corrective measures applied. The success of these corrective measures varies and can be expensive (perhaps as much as $100,000). The proper choice of tube sheet material to prevent a problem from occurring is therefore of considerable concern.

The second phase of our program is to determine optimum material combinations for our alloys and perhaps others as well. The program will analyze the effect of tubes and tube sheet materials with proper anode/cathode relationships to guide materials selection. At the present time, based on our knowledge of material, their galvanic relationships and corrosion resistance in sea water, we would suggest the following for consideration in decreasing order of acceptance:

AL-4X*
T-216
T-317
T-316

*An alloy of 20 Cr-24 Ni-4.5 Mo-1.5 Cu - also produced by several other manufacturers under their own trade marked designations.

These alloys, clad to carbon steel, should also be acceptable.

B. Installation

Tight, strong, leak-free joints are of major concern. This is particularly true of nuclear power plants, but also of any heat exchanger system and certainly so of the OTEC project. The methods and techniques of accomplishing this would require too much space in this article. A few items should be noted:

1. It is possible to weld AL-6X and 29-4 to compatible tube sheets with or without filler metal.

2. Tight leak-free joints can be achieved by tube rolling or expansion if the proper parameters are chosen and competent supervision maintained.

3. A combination of tube expansion and the use of adhesive compounds can sometimes improve the quality of the joints.

To-date, none of the AL-6X installations have been welded. The technology exists to do this, but there has been little need, based on our ability to satisfactorily expand tubes. In a few cases, where tube sheet damage or distortion has been excessive, the addition of an adhesive compound in the joint has been very successful in preventing in-leakage.

The results of several roller expansion experiments are included in Table 9 and Figure 5. The table compares various tube materials and two tube sheet materials. Our results indicate that higher pull out strength can be achieved with heavier gage tubes and the use of adhesive compounds. It also demonstrates that greater expansion is possible with heavier gage tubes without tube sheet distortion. Figure 5 demonstrates pull out strengths achieved in our tests of AL-6X at various expansion amounts. It appears that distortion of a carbon steel tube sheet can occur between a .003" and .004" expansion. Other data indicate distortion of Muntz tube sheets between .0025" and .0035" expansion. Satisfactory joint strength can be achieved if these restrictions are used.

Several comments regarding stainless alloy tube installations are indicated:

1. Only expanders with 5 rollers should be used with thin wall tubes

2. Torque measurement is helpful but should never be "the" criteria for a successful tube expansion.

Table 9

Tube Expansion Test Results

Tubes	Block	Tube Wall (")	Expansion	Pull Out (Pounds)	Distortion	Adhesive
70/30	Muntz	.050	.004	1000	No	No
AL-6X	Muntz	.027	.002	750	No	No
Titanium	Muntz	.0265	.002	600	No	No
70/30	Steel	.050	.003	4500	No	No
AL-6X	Steel	.027	.003	2800	No	No
Titanium	Steel	.0265	.003	1500	No	No
304	Steel	.048	.003	2450	No	No
304	Steel	.048	.005	5500	No	No
304	Steel	.027	.003	3400	No	No
304	Steel	.027	.005	4350	Yes	No
AL-6X	Muntz	.027	.003	1500	No	No
AL-6X	Steel	.027	.003	3600	No	No
AL-6X	Muntz	.027	.003	4800	No	Yes
AL-6X	Steel	.027	.003	6300	No	Yes

Figure 5
AL-6X Tubes
Carbon Steel Test Block

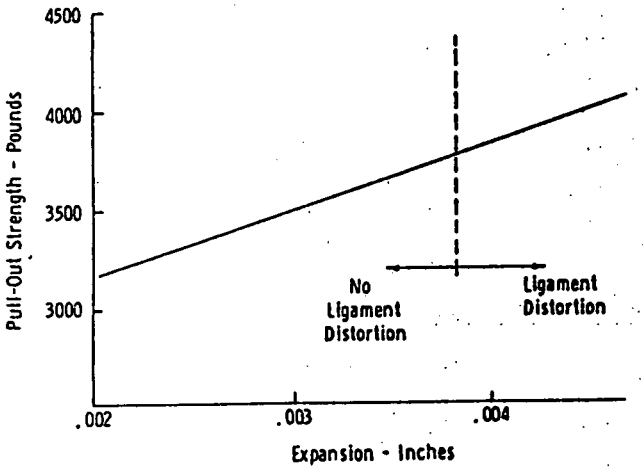

3. The key is selective ID measurement, "after" rolling and as a result of careful measurement of parameters "before" rolling.

4. Higher pull out joint strength can be achieved with steel tube and tube sheets than nonferrous alloy tube and tube sheets.

5. Grooves may be effective with these materials but only if steel tube sheets (carbon, stainless, clad, etc.) are used. While leak tightness might be improved, pull out strength will be diminished.

The above are made on the basis of our experience with tube installation and require additional study before they are used for a particular installation. This brief review obviously does not permit that.

Conclusions

During the past decade, we have been able to develop, install, observe and evaluate a new stainless alloy for sea water service that now has a sufficient pedigree for consideration as an OTEC heat exchanger tube material. In addition, we have been actively developing other materials which may ultimately prove to be even more suitable for this application.

The development and application of these new materials have established their overall suitability for sea water service,

provided heat transfer data and some information on fouling characteristics. Additional information has been developed on tube sheet materials as well as those techniques necessary to obtain strong, leak-free joints. Additional research is indicated in the areas of galvanic compatibility and biofouling.

References

1. Smith, H. A., Pit Corrosion of Stainless Steel, Metal Progress, 1938, 33 (6), pp. 596-600.

2. Brigham, R. J., Temperature as a Crevice Corrosion Criterion, Corrosion, 1974, 30 (11), pp. 396-398.

3. Pessall, N. and Nurminen, J. I., Developments of Ferritic Stainless Steels for Use in Desalination Plants, Corrosion/73, Paper 65.

4. Bond, A. P., Dundas, H. J., Elerot, S. and Senychyshen, M., Stainless Steels for Sea Water Service, Stainless Steel 77, pp. 197-203.

5. Maurer, J. R., Controlling Corrosion Problems with the New High Technology Stainless Steels, Proceedings 38th International Water Conferences, pp. 55-66.

6. Maurer, J. R., Basic Considerations in the Use of Stainless Steels in Modern Condenser Design, 1961 Inco Power Conference, Estes Park, Colorado.

7. Lustender, E. L. and Staub, F. W., Development Contribution to Compact Condenser Design, 1964 Inco Power Conference, Wrightsville Beach, N.C.

8. Maurer, J. R., The Use of Stainless Steel Tubing in Condenser and Related Power Plant Equipment, A Progress Report Southeastern Electric Exchange, 1966, Atlanta, Ga.

9. Peabody, A. W. - Corrosion Associated with Use of Titanium Tubes in Surface Condensers, 41st American Power Conference, 1979, Chicago, III.

DISCUSSION

P. Manning, Cabot Corp.: Alloys very similar to AL-6X (e.g. 20 Mod) show extremely high pitting resistance to the assimulated solution that would be found underneath scales or in severe crevices. That's adjusted to pH 2 with hydrocloric acid and 4% sodium chloride. I was wondering if, in your research at Alegheny Ludlum, you had examined other laboratory solutions or laboratory test methods to study better resistance success?

J. Maurer: As I pointed out, we have tested both products for many years now in actual service conditions. We have examined an alloy called 4X, which is something similar to your 20 Mod, and it appeared to be quite resistant to pitting corrosion in sea water. We have not tested any 4X yet; it is only in plate form at this time.

R. Zawierucha, UCC/Linde: From the standpoint of corrosion resistance, would you include 29-4 and AL-6X as titanium equivalents in general corrosion rate, which, for all practical purposes is nil?

J. Maurer: Yes. Based on the results I presented, it would take 400 years to corrode one mil. The stainless steels just do not generally corrode in sea water. If any corrosion does occur, it is pitting or crevice corrosion.

Shiro Sato, Japan: What is the allowable temperature for AL-6X in seawater service?

J. Maurer: I don't know at this point. Chuck Schreiber has tested it as high as 242° F in the AISID Solid Program at Freepoint, Texas, and it looked very good. That is as high as we have gone except, for a malfunction at Bridgeport Brass after which some condenser tubes were shut down. They did not need the total capacity of the condenser, so there was no water running through the tubes. They observed temperatures in the range of 700°F with saltwater still in the tubes; it boiled out and caused pitting and crevice corrosion at 700°F.

J. Halchak, Rockwell International: Are you actively pursuing a longitudinally-finned tube development?

J. Maurer: Not yet. I talked to the man who thought he could produce a tube, not longitudinally finned, but with very long spirals.

Roland: Are you familiar with the alloy Vesta SMO, and, if so, how would you rate it relative to AL-6X?

J. Maurer: We had a sample that was 20 parts chrome, 16 parts nickel, and 6 parts molybdenum containing a nitrogen stabilizer material. We have examined it and put it through the third claw test and it shows no signs of attack.

There is a partial supplementary answer to that question in a paper I am presenting later. There is a curve in the draft that divides the alloys into those that are likely to be useful from those that are not. If you paid attention to the reliability of that line, most any alloy that you might obtain that is on the right side of the line could be expected to perform well. You could apply that to the alloy that you are referring to, and it would be on the safe side.

Question: In view of the observed effects of certain heat treatments on development of the undesirable sigma phase, what are the chances of getting into any corrosion trouble from welding an AL-6X tube into a heavy tubesheet?

J. Maurer: AL-6X is produced in thin gauges at present because it does suffer from the formation of sigma phase, as Frank LaQue mentioned. The heavier the gauge, the slower the cooling treatment, and the greater is the tendency to form sigma, which robs the structure of chrome and moly. You end up with sigmatized sensitized material. Therefore, we do not make it in plate form and would use, where plates are concerned, something like 20 Mod or 4X 904L. We have taken thin tubes, however, and welded them into tubesheet configurations and tested them. We found that tubesheet acts as a heat sink to cool the joint very rapidly, and you do not have problems at the joint.

OXYGEN, TEMPERATURE, AND pH EFFECTS ON CORROSION OF ALUMINUM IN SEAWATER

Stephen C. Dexter

University of Delaware
College of Marine Studies
Lewes, Delaware 19958

Abstract

The effects of dissolved oxygen, pH and temperature on the rate of initiation and growth of pitting and crevice corrosion of aluminum alloy 5052 and pure aluminum have been determined. Variations in pH and temperature rather than dissolved oxygen are shown to account for increased corrosion rates of 5000 series aluminum alloys that have been reported for deep ocean exposures. A combination of on site hydrographic measurements and electrochemical laboratory testing will make it possible to identify the most corrosive depths at any candidate OTEC site. The impact of these results on the use of aluminum for OTEC heat exchanger tubing and on possible approaches to corrosion control are discussed, particularly in relation to location of cold and warm water intakes and conditions that may develop during shutdown periods.

Introduction

The long-term effectiveness of any Ocean Thermal Energy Conversion (OTEC) type power generating plant depends critically on the performance of the material selected as heat exchanger tubing for the evaporator and condenser[1]. Several aluminum alloys are prime candidates for this application due to the high strength-to-weight ratio, resistance to general corrosion and high thermal conductivity[2]. Alloy 5052, a weldable, nonheat-treatable aluminum-magnesium alloy which is readily available in seamless tubing has particularly been recommended for this service[3].

The corrosion behavior of aluminum alloy 5052 in surface seawater[2-14] and in desalination environments[15,16] has been studied and is reasonably well characterized. Less is known about its behavior in deep ocean waters[17-19] typical of those to which an OTEC installation will be subjected.

The corrosion data that are available for 5000 series aluminum alloys at various depths in the Pacific Ocean show that these alloys may suffer accelerated rates of corrosion in the deep ocean as compared to that at the surface[8,19]. The rates that were reported reached a maximum of three times that of the surface at a depth of 500 to 900 meters, then decreased again to twice the surface rate at 2000 meters. This is of concern to the OTEC Program because the cold water inlet pipe of proposed OTEC plants may be taking in deep ocean water similar to that in which the above maximum corrosion rates were reported. Figure 1 shows the variation with depth of dissolved oxygen, pH, temperature and salinity at the sites from which the deep Pacific Ocean corrosion data were obtained[19]. Note that the dissolved oxygen concentration reaches a minimum at the same 500 to 900 meter depth at which the maximum corrosion rate was reported. For this reason, it has usually been assumed that the low dissolved oxygen concentration was in some way responsible for the increased corrosion rate[8,19,20]. The objective of the research program whose results are given in this report was to assess what threat, if any, an increase in corrosion rate of 5000 series aluminum alloys in the deep ocean may pose to the use of aluminum alloy heat exchanger tubing in OTEC installations, and to determine whether or not decreased oxygen is the causal agent for the increased rate.

Other factors could also be important in determining the rate. For instance, the pH curve of Figure 1 has the same shape as that of the dissolved oxygen curve, and other data from the Pacific Ocean have shown[21] that the inorganic substances NO_3^-, SiO_3^{--} and PO_4^{3-} often reach maximum concentrations at the same 500 to 900 meter depth. It is known[9,22] that aluminum and its alloys suffer accelerated rates of attack at pH values above 10 and below 4 but there have been no detailed data reported on the effects of pH within the normal range (7.4 to 8.2) of open ocean seawater. It has been reported[16] that several aluminum alloys, including 5052, show little effect of dissolved oxygen in the range from 30 to 1000 ppb while the same alloys are sensitive to pH changes between 3.8 and 7.4.

Each of the variables discussed above can influence the overall corrosion rate by affecting 1) the induction time for pitting and crevice corrosion to initiate or 2) the rate of pit or crevice growth after initiation. Pit initiation, as distinguished from pit growth and from crevice corrosion, occurs at and above a well-defined critical potential[26]. When alloy 5052 is exposed to aerated clean seawater, the corrosion potential is normally active to the critical potential[13,14], and as long as this remains so, pitting corrosion does not initiate. Whenever the corrosion potential exceeds the critical value, the passive film is broken down locally, and the breakdown sites then become subject to accelerated corrosion[26].

Crevice corrosion on the other hand, is not initiated at a specific potential[27]. It occurs at sites where breakdown of passivity is induced by reduction of oxygen concentration or by the accumulation of acid anodic corrosion products such as aluminum chloride. These changes may be brought about through the operation of differential oxygen concentration cells acting at crevices. In an OTEC heat exchanger, crevices may be present at the interfaces between tubes and the tube sheet, or they may be created by deposits of fouling organisms. Although the initiation of pitting and crevice corrosion takes place by different mechanisms as described above, the rate of corrosion subsequent to initiation is controlled in each case by the rate of oxygen reduction or hydrogen evolution at cathodic sites on the metal surface[26].

The first part of the experimental program described in the following sections was to establish the effects on the corrosion potential of dissolved oxygen, pH, and temperature when varied both independently and in combination. Next, effects on the critical pitting potential were determined. The

critical potential is already known to be unaffected by dissolved oxygen and heavy metals[25]. Following this, effects on the initiation of pitting and crevice corrosion were determined by simple immersion tests under controlled conditions. Finally, the rate of corrosion after initiation was determined by measuring the current density upon cathodic polarization of an aluminum electrode either in a galvanic corrosion cell formed with a suitable anode or by potentiostatic methods. In this final set of experiments, an increase in cathodic current density upon changing the dissolved oxygen, pH, etc., from values characteristic of surface water to those of deep water was taken as a measure of increased pit and crevice growth rates under corresponding conditions in the deep ocean. Conversely, a decrease in current density was taken as an indication of decreased pit and crevice growth rates.

Experimental Techniques

The results reported in this paper were generated on cylindrical laboratory electrodes 2 to 5 cm long and 0.6 to 0.95 cm in diameter mounted with a teflon compression gasket to avoid crevice effects. The 5052 alloy electrodes were machined from 1.3 cm diameter extruded rod containing by weight: 2.44% Mg, 0.2% Cr, 0.19% Fe, 0.08% Si, 0.02% Mn and Ni, and 0.01% or less of Cu, Zn, Pb, Sn, and Ti supplied by Reynolds Metals Company.

In order to obtain reproducible corrosion potentials, it was necessary to strictly control the specimen preparation procedure, and the following sequence was finally adopted. A uniform surface was provided for all electrodes by abrading through 600 grit emery paper followed by pickling for 20 minutes in 20% nitric acid at 50 to 60°C, dipping in 1N sodium hydroxide for 5 seconds at 50 to 60°C, and rinsing in distilled water. After pickling, all electrodes were aged for one hour in distilled water before insertion into the test cell. After pickling, and again after aging, all electrodes were examined at 25X in a stereo microscope. Any electrode on which pits were found was recycled through the abrasion and pickling steps before using.

The seawater used was full strength (34 to 35°/oo salinity), clean surface water brought to the laboratory in 55 liter polyethylene jugs from 40 to 100 miles east of the mouth of Delaware Bay at two to three week intervals by the research vessel, Cape Henlopen. The seawater was kept in an air-conditioned compartment on the ship, and arrived in the laboratory within 24 hours after removal from the ocean. Once in the laboratory, the water was passed through glass fiber and 0.2 μm membrane (Milipore) filters in series to remove detritus and most marine microorganisms, and was kept aerated. The aluminum electrodes behaved consistently in this water for about 21 days, but the behavior often began to change during the fourth week.

Corrosion potentials of the test electrodes were measured against a saturated calomel reference electrode (SCE) using a high impedance Keithly Model 602 electrometer. The dissolved oxygen concentration was controlled between 0.6 ppm and air saturation by bubbling the proper air-nitrogen mixture from a premixed compressed gas cylinder through the electrolyte. Oxygen concentrations were measured using a YSi Model 57 oxygen meter.

The pH of the electrolyte was controlled either by small additions of 0.1 N HCl or NaOH, or by varying the partial pressure of CO_2 in the air-nitrogen mixture described above using flow meters. Control was achievable by the acid-base method to better than ±0.05 pH units, and by the CO_2 method to ±0.02 pH units. The temperature of the test cell was controlled by pumping precooled alcohol through a glass cooling coil inserted into the electrolyte. Precooling was done with an FTS Systems Model MC260SV Cooling Unit. Control was achieved to better than 0.5°C over the temperature range from 4 to 25°C. In all cases where no specific temperature is given, the test was run at room temperature (22 to 25°C).

Pit and crevice initiation tests were run in wide mouth 500 mℓ Erlenmeyer flasks. For tests at air saturation these were left open to the atmosphere. Tests at lower values of dissolved oxygen were run by bubbling the proper air-nitrogen mixture through a flask fitted with a rubber stopper through which were inserted the electrode holder, a gas bubbler for the appropriate nitrogen-oxygen mixture, a salt bridge and a gas outlet tube. For long-term low oxygen tests, the cell was sealed off by closing a stopcock on the gas inlet tube and plugging the outlet with a closed end glass tube. The freshly pickled and aged electrode was immersed in the seawater after the dissolved oxygen reached equilibrium (usually about one hour). Smooth electrodes were used for pit initiation tests. The same type electrodes were used for the crevice tests, with the crevice being formed by slipping a single rubber "o-ring" around each electrode.

Corrosion potentials of the test electrodes were measured at least daily on the SCE scale as described above. Each test was terminated as soon as the white aluminum hydroxide corrosion product was visible at a pit initiation site on the cylindrical surface of the electrode or adjacent to the rubber "o-ring" creating the test crevice. After the corrosion product was cleaned off by gently brushing under distilled water, corrosion was confirmed by examination in a stereo microscope.

Critical pitting potentials and cathodic polarization curves were measured with standard potentiostatic techniques[28,29] in a 1000 mℓ six neck polarization flask using either a Princeton Applied Research Model 173 or a Wenking Model 70TS1 potentiostat. The final value for the critical pitting potential was taken as the most noble potential that could be maintained for at least 12 hours with neither an increase in current density nor the development of pits on the electrode surface large enough to be observed at 25X in a stero microscope.

In the cathodic polarization experiments, the freshly pickled and aged electrode was allowed to come to steady state (usually about one hour after immersion) in seawater in which the pH and dissolved oxygen were being controlled as described above. No stirring was used during the test other than the mild agitation provided by the gas bubbler. The pH was continuously monitored during each run using a Fisher Accumet Digital pH metter with a combination pH electrode mounted through one of four outside necks of the flask. Polarization began from the steady state corrosion potential in discrete steps of 25 mv every five minutes in the active direction until the cathodic current density reached about 10 μa per square centimeter. Sets of cathodic polarization curves at successively more acidic pH values were run in three different ways: a) all on the same electrode without repickling between runs of a series, b) using a freshly pickled and aged electrode for each new pH value, or c) using a freshly pickled and aged electrode for each potential level within each curve.

Cathodic polarization was also achieved by the alternative method of connecting the test electrode

to a more active metal in a galvanic cell. In these experiments, alloy 5052 was coupled to a zinc electrode through an external circuit. Dissolved oxygen and pH within the cell were controlled as described previously, and the steady state cell current was measured using a zero resistance ammeter. The pH and/or dissolved oxygen of the test solution was then changed and a new steady state current measured. A steady pH value was maintained by connecting the test flask to a gravity feed flow through system having two large reservoirs, one adjusted to the initial and the other to the final pH desired. After measurements were made at the initial pH, a stopcock was turned to draw water from the other reservoir at the final pH.

Results

The critical pitting potential of alloy 5052 in seawater of salinity 32°/oo, pH 8.2 and 25°C, was measured by standard techniques and found to be -0.69 ± 0.01 V on the saturated calomel (SCE) scale. In seawater of salinity 35°/oo the measured value was slightly more active at -0.72 ± .015 V SCE. Measurements were also made at controlled pH values of 7.8 and 7.5 and at temperatures of 4 and 10°C, but any differences fell within the experimental error mentioned above. Therefore, since the critical pitting potential is not a function of dissolved oxygen[25], pH or temperature, it will not vary with depth and it can be eliminated from consideration as a factor responsible for increased corrosion rates of aluminum in the deep ocean.

Data illustrating how the corrosion potential of alloy 5052 varied with dissolved oxygen at pH 8.2 and with pH at air saturation over the range in which these variables are found in the open ocean are shown in Figure 2. Decreasing dissolved oxygen made the corrosion potential more active while decreasing pH made it more noble. The slope of the dissolved oxygen curve was always positive, the corrosion potential becoming more noble at the rate of 50 ± 5 mv for each ppm increase in dissolved oxygen. For pH, the slope was always negative with the corrosion potential becoming more active with rising pH at the rate of -37 ± 5 mv for each 0.1 pH unit down to pH 7.5. Below pH 7.5 the rate of change decreased because the corrosion potential began to approach the critical pitting potential. The vertical error bars shown in Figure 2, and throughout this report except where stated otherwise, represent the envelope of all data observed rather than the standard deviation.

Corrosion potential measurements were also made at the four combinations of pH and dissolved oxygen shown in Table I. Although the pH and DO effects are in opposite directions, the results in Figure 3 show that the pH effect predominates when both are varied together. The data in Figure 3 are a composite of four individual runs whose slopes varied from -12 to -35 mv per 0.1 pH unit with an average corresponding to the curve drawn through the data of -20 mv per 0.1 pH unit. In these tests, the lower oxygen made the pH effect less intense, and the corrosion potential was always active to the critical pitting potential. This is in contrast to the case of decreasing the pH alone (Figure 2) where the critical pitting potential was sometimes approached during the experiment.

Table 1 Approximate Ocean Depth Ranges Corresponding to Experimental Combinations of pH and Dissolved Oxygen (Figure 1)

pH	Temperature (°C)	DO (ppm)	Depth (m)
8.20	15.0	7.2 to 7.5	Surface
7.85	8.5	3.1	150 to 200
7.65	7.0	1.3	350 to 380
	or		or
	3.0		1060 to 1300
7.50	4.0 to 5.0	0.6	500 to 900

The effect of decreasing temperature on the corrosion potential of alloy 5052 in air saturated seawater at pH values of 7.7 and 8.2 is shown in Figure 4. As was the case for pH alone, a decrease in temperature, with all other factors held constant, causes the corrosion potential to shift in the noble direction. At air saturation, a decrease in temperature to 4°C is alone sufficient to raise the corrosion potential to within 20 mv of the critical pitting potential at pH 7.7, or to within 150 mv at pH 8.2. Decreasing the dissolved oxygen at the same time as temperature, however, reduces the amount of noble shift.

Pit and Crevice Initiation

The length of exposure to natural seawater necessary to initiate pitting and crevice corrosion was measured as a function of pH and dissolved oxygen concentration of the seawater. For alloy 5052, both pitting and crevice corrosion initiated on some of the samples in less than 15 days at pH 8.2, and the initiation times became shorter and more consistent as the pH decreased from 8.2 to 7.4. This is illustrated in Figure 5a) and b) where the solid points represent the average of all pit or crevice initiation times for those electrodes on which corrosion began in less than 30 days at a given pH, and the error bars represent the standard deviation. As soon as pitting had initiated, white specks of corrosion product were visible to the naked eye on the electrode surface and small spherical pits were observable under a low power stereo microscope. Each time pitting was visible on the surface, the potential of the electrode had shifted to -0.7 ± 0.02 V on the saturated calomel scale. This agrees closely with our measurements of the potentiostatic critical pitting potential of alloy 5052 under the same experimental conditions. All tests represented by Figure 5 were stopped after corrosion started or after 30 days, whichever was shorter. At pH 8.2, 70% of both the pit and crevice tests had not begun to corrode within 30 days. At pH 7.6, 12% of the pit initiation tests and one of the crevice initiation tests did not corrode within 30 days, but all tests, both pit and crevice, at pH 7.8 and 7.4 initiated within that time period. Several of the pit and crevice tests at pH 8.2 that survived the first 30 days without initiation were continued for longer times, and had still not begun to corrode after 12 months of continuous immersion.

Pit and crevice initiation times on alloy 5052 were prolonged at pH 8.2 and dissolved oxygen concentrations below air saturation. Corrosion did not initiate within the thirty day test period on any of the electrodes at dissolved oxygen concentrations of 3.1, 1.3, or 0.6 ppm. From these results, it is evident that decreased oxygen concentration in the deep ocean cannot be responsible for a decrease in pit or crevice initiation times, while a decrease in pH could produce that effect.

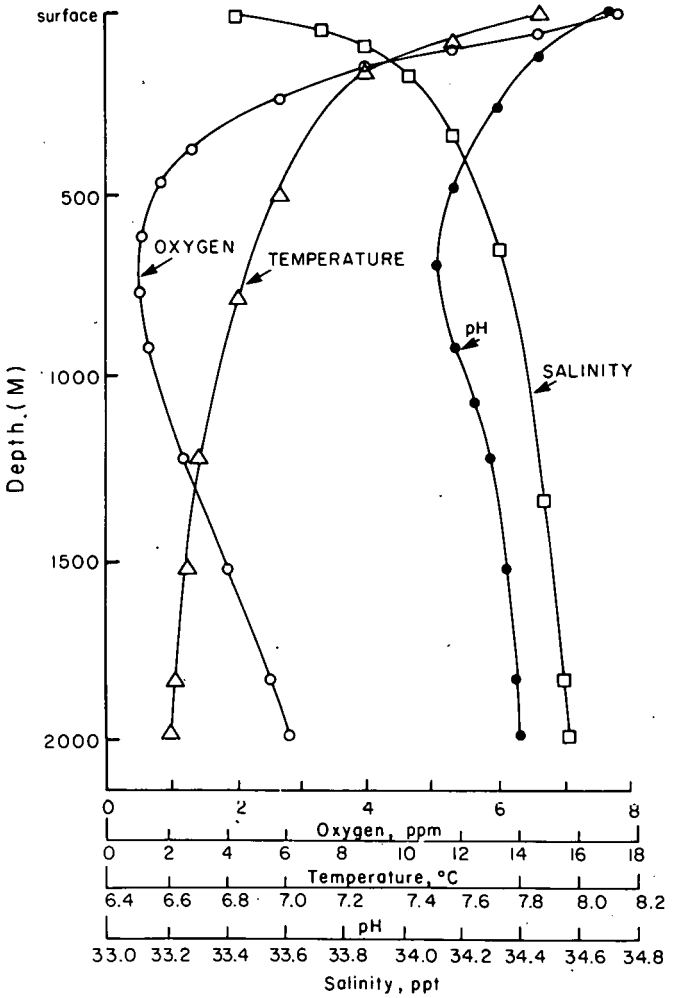

Figure 1. Hydrographic data as a function of depth at the site from which the deep Pacific Ocean corrosion data were taken[19].

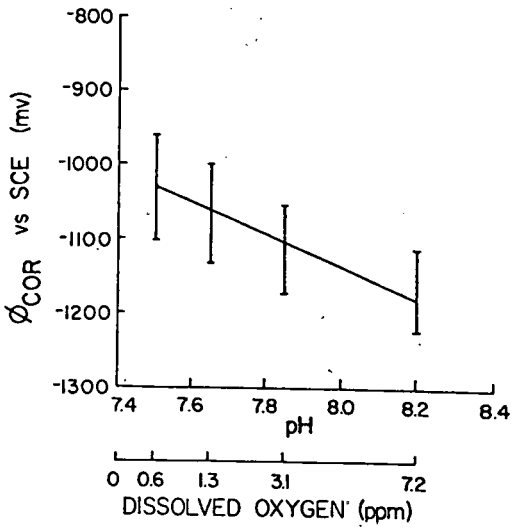

Figure 3. Effect of combinations of pH and DO found in the deep Pacific Ocean (See Figure 1 and Table 1) on the corrosion potential of alloy 5052 in seawater.

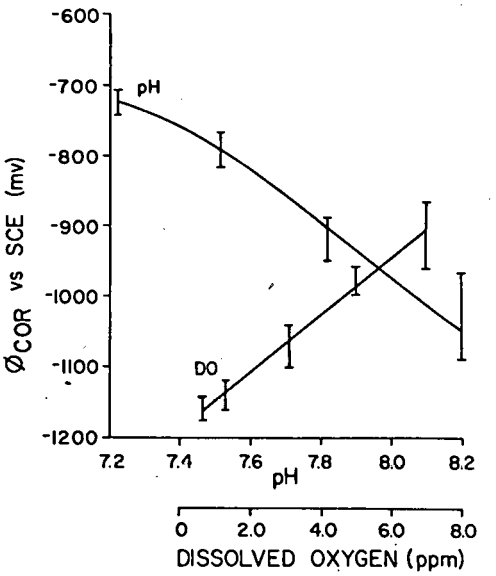

Figure 2. Effect of DO at pH 8.2 and of pH at air-saturation on the corrosion potential of alloy 5052 in seawater.

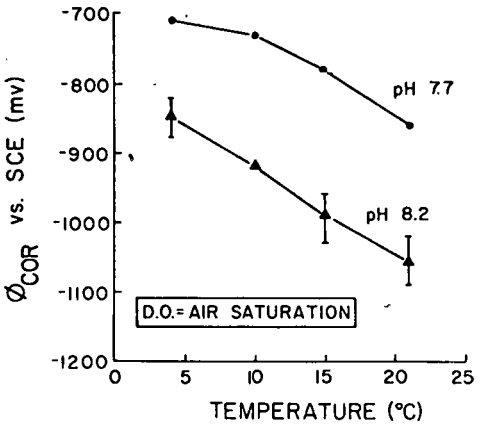

Figure 4. Effect of temperature at two pH values on the corrosion potential of alloy 5052 in air-saturated seawater.

Pit and Crevice Growth

The cathodic polarization of alloy 5052 was measured at pH 8.2 as a function of dissolved oxygen concentration by both the galvanic couple (Figure 6) and cathodic polarization (Figure 7) techniques. In both Figures 6 and 7, it is evident that decreasing the dissolved oxygen while maintaining everything else constant leads to a decrease in the cathodic current density. Thus a decrease in dissolved oxygen in the deep ocean cannot be responsible for an acceleration of either pit or crevice propagation rates.

In contrast to this behavior, is the effect of small changes in pH. In the galvanic couple tests, the steady state current density of alloy 5052 coupled to zinc in seawater was first determined at pH 8.2. The pH was then changed to a more acidic value, and a new steady state current density was measured. Figure 8 shows the ratio of the current density at the test pH to that at pH 8.2 as a function of the test pH. Each point plotted is the average of several runs. Individual ratios varied from 1.12 to 5.29 but were always greater than one, and were steady over the one to two hour time period over which each test was run. This result was independent of the direction of the pH change. If the test pH was established first, then a reduction in current density was observed upon changing the pH to 8.2.

In order to eliminate the possibility that the observed changes were taking place on the zinc electrode rather than on the aluminum, these experiments were run with an alumina thimble around the zinc electrode to isolate it from the pH change. The increase in current observed upon decreasing the pH from 8.2 to 7.6 is shown in Figure 9. The experiment was then repeated with the thimble around the aluminum electrode, and apart from a brief transient there was no lasting change in current upon decreasing the pH.

The pH effect was also observed by the potentiostatic method. Figure 10 shows a series of cathodic polarization curves of alloy 5052 in natural seawater all run on the same electrode at successive pH values of 8.2, 7.8, 7.5, and 7.2 using HCl control. Note that as the pH is decreased, the corrosion potential shifts in the noble direction (in agreement with Figure 3), and that each curve is progressively shifted toward higher current densities for any given value of the potential. Figure 11 shows the experimental variability encountered when a freshly pickled electrode is used for each curve at pH values of 8.2 and 7.2. The error bars represent the scatter in potential that was observed over at least 5 curves run under the same conditions. Also shown on Figure 11 are data (open points) taken by using a freshly pickled and aged electrode for each potential level within each curve. These data fall within the experimental scatter for curves run on a single electrode. In comparing Figures 10 and 11 note that the curves for pH 7.2 and 8.2 converge slower when succeeding curves are all run on the same electrode. This effect is probably an experimental artifact produced as each pH condition effects the next curve in the sequence. For the most accurate and reproducible data, separate electrodes should be used for each curve as was done in Figure 11. The pH 7.2 curve was repeated using both HCl additions and CO_2 partial pressure to control the pH. At current densities less than about 4 $\mu A\ cm^{-2}$, the differences fell within experimental error and either method of pH control can be used.

The strong systematic effect of pH on the cathodic polarization behavior of alloy 5052 at air saturation was modified at lower dissolved oxygen concentrations. The effect of reducing the dissolved oxygen to 3.0 is shown in Figure 12, in which the shaded areas represent the envelope of the data from Figure 11 for comparison. The data at pH 7.2 are not altered by the dissolved oxygen decrease, but the corrosion potentials at pH 7.7 and 8.2 are made more active. As the dissolved oxygen decreased still further to 0.6 ppm, the corrosion potentials became even more active. In addition, the slopes of the cathodic polarization curves at low current densities and low pH values became steeper.

When temperature was included as a variable in the cathodic polarization experiments, the results shown in Figures 13 through 15 were obtained. At 7.2 ppm dissolved oxygen and 4°C, the corrosion potentials at all pH values became noble (Figure 13), as would be expected from Figure 4. This proved to be a highly corrosive set of conditions, especially at low pH. The envelope of the data from Figure 11 is shown for comparison. While the curve at pH 7.2 is not changed by the low temperature, at pH 7.7 the combination of reduced pH and low temperature caused the corrosion potential to exceed the critical pitting potential. On every trial attempted at DO 7.2 ppm, pH 7.7 and 4°C, the corrosion potential rose to the critical value within ½ hour after immersion in the test cell, and pitting began on the cylindrical surface of the electrode before it had equilibrated sufficiently to begin polarization. It is not known why conditions were more corrosive at pH 7.7 than at pH 7.2.

Figure 14 shows the cathodic polarization data at intermediate values of temperature (15°C) and dissolved oxygen (5.0 ppm). This set of conditions was nearly as corrosive as that at pH 7.7 in Figure 13. The lower temperature compensated for the reduced dissolved oxygen, and again the corrosion potentials were near the critical pitting potential. The curve at pH 7.2 in Figure 14 appears to be anomalous. The corrosion potential is very noble, and one would expect the curve to show higher current densities at all potentials (that is, have a shallower slope) than that at pH 7.7. It is suggested that pitting began just as this run was started, and the current supplied by the active pit tended to polarize the electrode in the same direction as the potentiostat, thereby making the applied potentiostatic current artificially low. The data at both low temperature (4°C) and low oxygen (0.6 ppm) are shown in Figure 15. Such conditions appear to be less corrosive than those of Figures 13 and 14. The corrosion potentials are less noble due to the very low oxygen, and the curves at all pH values show rapid polarization.

Figure 16 summarizes cathodic polarization data approximating three of the open ocean conditions shown in Table 1 as well as the 15°C, 5.0 ppm DO, pH 7.7 curve from Figure 14. Note that at any given potential noble to -1100 mv SCE, the current density is highest for the two curves at the intermediate values of temperature, pH and oxygen.

In Table 2, is presented a summary of all the cathodic polarization data from Figures 11 through 16 plus several other DO, pH and temperature combinations not shown graphically. Each curve is characterized by its corrosion potential and by the current density at a potential of -1080 mv SCE. The rationale for choosing -1080 mv is discussed later in this report. The trend within any set combination of DO and temperature is for the corrosion potential to become more noble and the current density at -1080 mv to become larger with decreasing

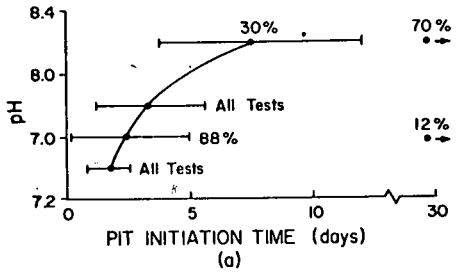

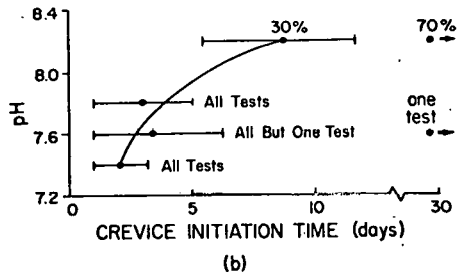

Figure 5. Effect of pH on initiation of pitting and crevice corrosion of alloy 5052 in air-saturated seawater. Horizontal error bars represent the standard deviation.

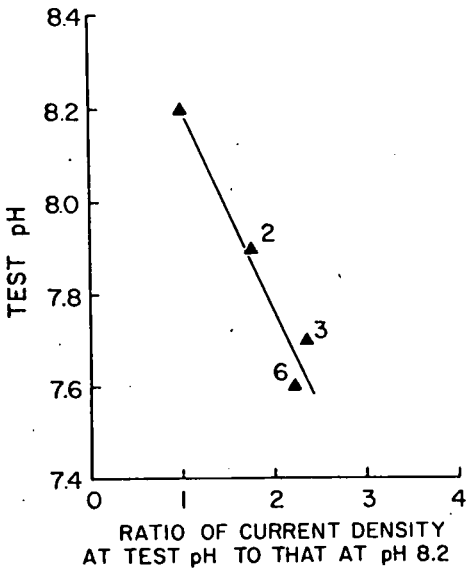

Figure 8. Increase in current density with decreasing pH on 5052 aluminum coupled to zinc in air-saturated seawater. Numerals beside each point represent the number of runs for which that point is the average.

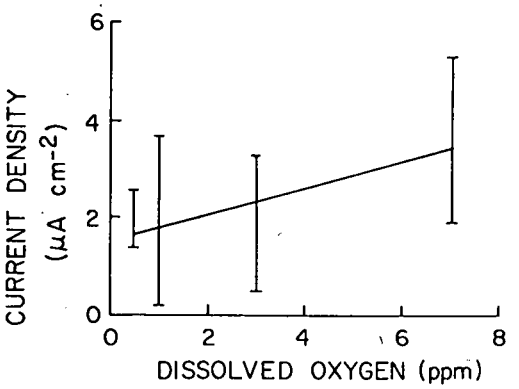

Figure 6. Effect of DO on the cathodic current density on alloy 5052 coupled to zinc in seawater at pH 8.2.

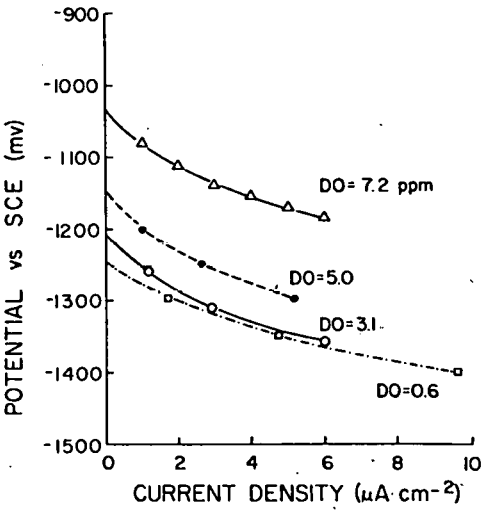

Figure 7. Effect of DO on the cathodic polarization of alloy 5052 in seawater at pH 8.2.

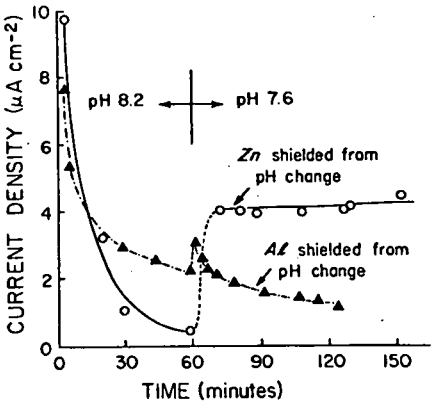

Figure 9. Influence of sudden pH change on the current density for an alloy 5052 -- zinc galvanic couple in seawater with the Zn and Al electrodes alternately shielded from the pH change.

pH. At 4°C and DO ≤ 5 ppm the current densities become very small and the trend with decreasing pH is reversed.

Table 2 Summary of Polarization Data for Alloy 5052

Temperature (°C)	DO (ppm)	pH	Corrosion Potential (mv SCE)	i(μA cm^{-2}) at -1080 mv
22	7.2	8.2	-1040	1.0
		7.7	- 850	2.3
		7.2	- 725	4.0
	5.0	8.2	-1140	0
		7.7	- 845	2.4
		7.2	- 735	2.4
	3.0	8.2	-1170	0
		7.7	- 820	1.3
		7.2	- 715	4.1
15	5.0	8.2	- 805	3.3
		7.7	- 750	4.4
		7.2	- 700	-
	3.0	8.2	- 840	0.8
		7.7	- 805	1.4
		7.2	- 750	2.7
8.5	3.0	7.8	- 770	1.4
4.0	7.2	8.2	- 880	1.2
		7.7	- 700	-
		7.2	- 725	3.9
	5.0	8.2	- 825	2.1
		7.7	- 775	1.4
		7.2	- 750	1.2
	3.0	8.2	- 860	1.3
		7.7	- 750	0.4
		7.2	- 740	0.6
	0.6	8.2	- 840	0.5
		7.7	- 770	0.8
		7.2	- 750	0.3

Discussion

The objective of this research was to determine what factors may have been responsible for the accelerated deep ocean corrosion rates of 5000 series aluminum alloys that have sometimes been observed, and to assess what an increased corrosion rate might mean to an OTEC installation using alloy 5052 heat exchanger and condenser tubing. It would be well, at this time, to keep in mind that it is only the average pit depth for all 5000 series alloys for which an apparent systematic variation with dissolved oxygen has been shown[19]. Data for individual 5000 series alloys in the deep ocean are widely scattered and may or may not follow the trend shown by the average.

The laboratory data presented in Figures 2 through 16 are consistent with both the average trend and the individual scatter. The data strongly support the possibility of increased deep ocean corrosion rates for alloy 5052, while at the same time, allowing us to better understand why a great deal of individual scatter has also been observed.

Although the data are consistant with increased corrosion rates in the deep ocean, they are not consistant with the idea[8,19] that low dissolved oxygen concentrations in the deep ocean are responsible. A decrease in dissolved oxygen, all other factors held constant, reduces rather than increases the rate of pit and crevice growth as measured by cathodic polarization (see Figures 6 and 7). In addition, the data on pit and crevice initiation indicate that a decrease in dissolved oxygen prolongs rather than decreases the induction time. This means that a decrease in dissolved oxygen with depth in the Pacific Ocean cannot be responsible for an increased corrosion rate. On the other hand, a decrease in pH (again all other factors held constant) from the 8.2 characteristic of surface seawater, to 7.5, typical of deep Pacific Ocean waters, both reduces the induction time for corrosion to start (Figure 5) and increases current density for a given potential at cathodic sites (i.e., decreases polarization, Figures 10 and 11). The cathodic current density controls and is proportional to the observed corrosion rate at anodic sites[26], and this means higher pit and crevice growth rates at low pH. The effect of a decrease in temperature when varied independently, was to increase the probability of pit and crevice initiation by making the corrosion potential more noble (Figure 4), but to decrease the growth rate by making cathodic polarization more rapid.

More important to OTEC than these individual variations is what happens when pH, oxygen and temperature are varied together as they do in the real ocean. The necessary information is contained in the cathodic polarization curves of Figure 12 through 16, but in order to relate this data to an OTEC plant, we must first have a calibration point. That is, we must determine at what value of potential the curves should be compared. Once this is known, current densities can be read directly from the appropriate curves, and converted to predicted average corrosion rates using Faraday's law which relates weight of metal corroded per unit time to current density.

The needed calibration point is most easily deduced from weight loss data. Using Faraday's law, one can calculate the average current density necessary to account for a given weight loss over a given period of time. From Godard's weight loss data[9] for alloy 5052 in Halifax surface water and Reinhart's data[19] in deep Pacific waters, it was calculated that the appropriate average current densities are approximately 0.3 to 1.0 μA cm^{-2} in surface water and 1.0 to 2.0 μA cm^{-2} in deep Pacific water. The higher numbers in each of these ranges are from short-term (one year or less) data and the lower numbers from longer term data, probably reflecting a decrease in corrosion rate with time as corrosion product films build up[9].

Returning now to Figure 16, where pH, dissolved oxygen and temperature are varied together, the potential corresponding to a current density of 1 μA cm^{-2} on the curve for surface water conditions (pH 8.2, DO 7.2 ppm) is about -1080 mv SCE. Presumably, the active pits have polarized the metal to this potential. Assume now that regardless of the initial environmental conditions, an active pit or crevice will always polarize the electrode to about this same -1080 mv. The intersections of each curve with a horizontal line at this potential can then be used to predict the cathodic current density under conditions corresponding to the curve of interest. The approximate Pacific Ocean depths corresponding to the curves in Figure 16 were shown in Table 1. The intersection of the horizontal line at -1080 mv with the curve corresponding to the DO-pH minimum is at 0.3 μA cm^{-2}. This predicts that pit and crevice growth rates will be slower here than at the surface. This does not necessarily mean lower overall corrosion rates than at the surface, however, because the corrosion potential at conditions corresponding to the DO-pH minimum is only about 50 mv active to the critical pitting

potential. Such a noble corrosion potential may encourage more rapid pit initiation than in surface water where the corrosion potential is 300 mv more active. It is difficult to say in any given situation whether initiation or growth will be more important, and this uncertainty could account for some of the scatter that has been observed in the data.

The two curves in Figure 16 which correspond to intermediate values of pH, DO and temperature both show current densities at -1080 mv higher than that for surface water conditions. In addition, these two curves also start from noble corrosion potentials. Both initiation and growth will be accelerated under these conditions, therefore, and overall corrosion rates are expected to be larger than at the surface. On this basis it is concluded that our data are consistent with increased corrosion rates in the deep ocean, but that the maximum rate will probably occur at a lesser depth than that of the dissolved oxygen minimum. Presumably, the existing data bank would show this effect if data were available at a greater variety of depths.

In general, the most corrosive conditions encountered in these experiments were ones combining low temperature and low pH with high dissolved oxygen. These conditions encourage both noble corrosion potentials, which can lead to rapid initiation, and increased cathodic current densities, which lead to higher growth rates. It is fortunate for OTEC that this most corrosive set of conditions is almost never found together in the real environment. Low dissolved oxygen and low pH are closely coupled in the ocean. The dissolved oxygen minimum is caused by biological decay of descending organic matter. This process not only consumes oxygen, but also produces CO_2, which simultaneously keeps the pH low[30]. Since the most corrosive combination of low pH and high DO do not occur together naturally, Figure 16 predicts that the most corrosive natural conditions will be those in the mid-range of all three variables. Here, the temperature and pH are both low enough to make the corrosion potential noble, but the DO is still high enough to permit reasonably high growth rates. In the Pacific Ocean (see Figure 1) these conditions are most usually found at depths of 150 to 400 meters, while in the Atlantic they may be found at greater depths due to the higher overall levels of oxygen[30]. The data strongly suggest that OTEC should avoid locating either warm or cold water intakes at such depths. Thus, it is recommended that: 1) profiles of DO, pH and temperature be obtained at all potential OTEC sites, and 2) cathodic polarization curves at all appropriate sets of conditions be run before the design depths of warm and cold water intakes are fixed for any future OTEC plant using aluminum tubing.

Recent results reported by Munier and Craig[31] are encouraging in that they encountered no pitting or crevice attack on heat exchanger tubing of either alloy 5052-0 or the less resistant 6061-T6, in the St. Croix OTEC corrosion experiments over a 72-day test period. Munier and Craig are quick to point out, however, that their results were obtained under ideal OTEC conditions of continuous flow, 27 to 29°C, 4 to 5 µg atm/ℓ of dissolved oxygen and pH 8.0 to 8.2. Our results confirm that these are, indeed, the least corrosive of naturally occurring seawater conditions. The benefit to OTEC of maintaining a continuous flow is also demonstrated by their data in that a number of their initial corrosion potentials were more noble than the critical pitting potential at their salinity (about -.725 volts Ag-AgCl), and yet they experienced no pitting. This should be attributed to the inhibitive effect on pit initiation of a continuous flow. Our results indicate that pitting would have occurred had their noble potentials been encountered under quiescent conditions. This shows the importance to OTEC of maintaining constant velocity conditions in the heat exchanger tubing. Times when the unit is shut down for maintenance will be particularly critical - especially during the initial installation period before protective corrosion products films have built up. If aluminum tubing is eventually chosen for OTEC, the data indicate that operational procedures should be developed that will prevent zero velocity conditions in the tubing from persisting for more than about 10 minutes during initial startup or 10 hours during subsequent shutdown periods. Some provision for complete drainage of the aluminum tubing should be provided in the design to accomodate longer shutdown periods.

Acknowledgements

Support of this work under ERDA/DOE Contract No. EY-76-S-02-2957 (formerly E(11-1)-2957) is gratefully acknowledged. In addition, thanks are due to D. Ferrick, R. Rotter and K. Lucas for help with the experimental work, and Prof. H. H. Uhlig for many helpful discussions.

References

1. S. C. Dexter. On the Localized Corrosion of Aluminum Alloys for OTEC Heat Exchangers. In Proc. OTEC Biofouling and Corrosion Symposium. R. H. Gray, editor. Seattle, p. 223, October (1977).
2. S. C. Dexter. Handbook of Oceanographic Engineering Materials, Wiley-Interscience, New York. In Press.
3. R. A. Bonewitz. Concurrent Studies of Enhanced Heat Transfer and Materials for Ocean Thermal Exchangers. Final Report ERDA Contract No. E(11-11)-2641, 69 pp. (1976).
4. W. H. Ailor, Jr. Five-year Corrosion of Alumi- Alloys at Several Marine Sites. British Corrosion Journal, 1, p. 327-343 (1966).
5. W. H. Ailor, Jr. Ten Year Seawater Tests on Aluminum. In: Corrosion in Natural Environments. ASTM STP 558, American Society for Testing and Materials, p. 117-134 (1974).
6. W. H. Ailor, Jr. and R. I. Lindberg. Corrosion Resistance of Aluminum Alloy 5083 in Marine Environments. J. American Soc. of Naval Eng., 73, No.3 (1961).
7. W. H. Ailor, Jr. and F. M. Reinhart. Three-year Tidewater Corrosion of Aluminum Alloys. Naval Engineers Journal, June (1964).
8. F. W. Fink and W. K. Boyd. The Corrosion of Metals in Marine Environments. Bayer and Co., Inc., Columbus, Ohio (also DMIC Report 245), p. 57-70 (1970).
9. H. P. Godard, W. B. Jepson, M. R. Bothwell and R. L. Kane. The Corrosion of Light Metals. John Wiley and Sons, Inc. (1967).
10. H. P. Godard and F. F. Booth. Corrosion Behavior of Aluminum Alloys in Seawater, In: Congress International de la Corrosion Marine et des Salissures, Cannes, France, p. 37-52 (1964).
11. C. R. Southwell, et al. Corrosion of Metals in Tropical Environments. Materials Protection, 15 (1976).

12. F. M. Reinhart. Corrosion of Materials in Surface Seawater after 6 Months Exposure. Naval Civil Engineering Laboratory, Port Hueneme, California, Technical Note N-1023 (1969).
13. R. E. Groover, T. J. Lennox, Jr. and M. H. Peterson. Cathodic Protection of Nineteen Aluminum Alloys Exposed to Seawater Corrosion. Materials Protection and Performance, 8, No.11 (1969).
14. R. E. Groover, T. J. Lennox, Jr. and M. H. Peterson. Characterization of the Corrosion Behavior and Response to Cathodic Protection of Nineteen Aluminum Alloys in Seawater. Naval Research Laboratory, Washington, D.C., NRL Memorandum Report No. 1961, AD685588, 23 pp. (1969).
15. J. S. Snodgrass. Progress in the Utilization of Aluminum in Desalting. Paper No. 90 presented at the N.A.C.E. sponsored Meeting CORROSION/72, 17 pp. (1972).
16. P. F. George, J. A. Manning, Jr., and C. F. Schrieber. Desalination Materials Manual. Dow Chemical Co., for the Office of Water Research and Technology, National Technical Information Service, PB-252 043 (1975).
17. W. H. Ailor, Jr. Evaluation of Aluminum Panels Exposed in the Pacific Ocean at 2340 feet for Six Months. Metallurqica, March (1967).
18. W. H. Ailor, Jr. Evaluation of Aluminum after One Year Deep Sea Exposure. Journal of Hydronautics, 2, No. 1, p. 26-33 (1968).
19. F. M. Reinhart. Corrosion of Materials in Hydrospace, Part V. Aluminum Alloys. U.S. Naval Civil Engineering Laboratory, Port Hueneme, California, Technical Note N-1008 (1969).
20. F. L. La Que. Marine Corrosion. John Wiley and Sons, Inc., 209 pp. (1975).
21. Broecker, W. S. Chemical Oceanography. Harcourt, Brace, Jovanovich, Inc., 6 pp. (1974).
22. H. L. Craig, Jr. Kinetic Studies of Aluminum Pitting Reactions, In: Localized Corrosion, R. W. Staehle, editor, N.A.C.E., Houston, Texas, p. 600-607 (1974).
23. F. C. Porter and S. E. Hadden. Corrosion of Aluminum in Supply Waters. J. Appl. Chem., 3: 385 (1953).
24. W. A. Bell and H. S. Campbell. Aluminum in Fresh Waters. British Corrosion Journal, 1: 72 (1965).
25. H. Bohni and H. H. Uhlig. Environmental Factors Affecting the Critical Pitting Potential of Aluminum. J. Electrochem. Soc., 116: 906 (1969).
26. Uhlig, H. H. Corrosion and Corrosion Control, Second Edition. John Wiley and Sons, Inc., 419 pp. (1971).

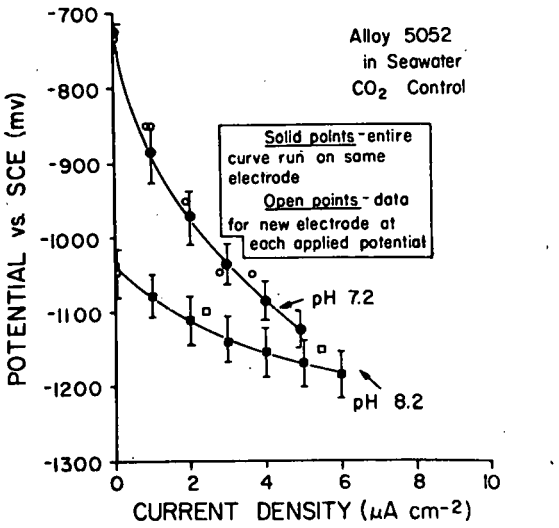

Figure 11. Experimental variability of the influence of pH on cathodic polarization when using 1) a separate electrode at each pH value or 2) a separate electrode at each potential level within each curve (open points).

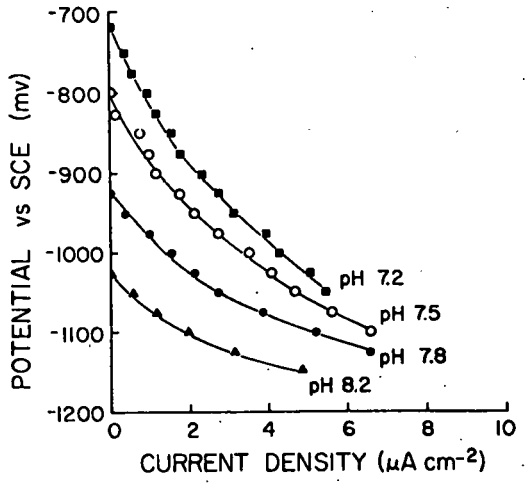

Figure 10. Influence of pH on cathodic polarization of alloy 5052 in air-saturated seawater. All curves were run in succession on the same electrode.

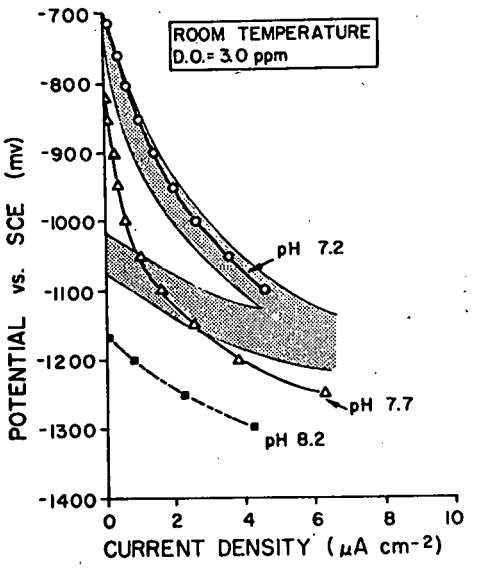

Figure 12. Effect of pH on cathodic polarization of alloy 5052 in seawater with 3 ppm DO at 23 ± 2°C. Shaded area represents the envelope of data from Figure 11.

27. B. E. Wilde. On the Pitting and Protection Potentials: Their Use and Misuses for Predicting Localized Corrosion Resistance of Stainless Alloys in Halide Media. In: Localized Corrosion. R. W. Staehle, editor, N.A.C.E., Houston, Texas, p. 342-352 (1974).
28. H. Leckie and H. Uhlig. J. Electrochem. Soc., 113, 1262 pp. (1966).
29. Handbook on Corrosion Testing and Evaluation. W. H. Ailor, Jr., editor. John Wiley and Sons, Inc., 171 pp. (1971).
30. S. C. Dexter and C. H. Culberson. Global Variability of Natural Seawater. Presented at CORROSION/79, NACE, Atlanta, March (1979).
31. R.S.C. Munier and H. L. Craig. OTEC Biofouling and Corrosion Experiment St. Croix, U. S. Virgin Islands, Part II Corrosion Studies, OTEC Report PNL-2739, February (1978).

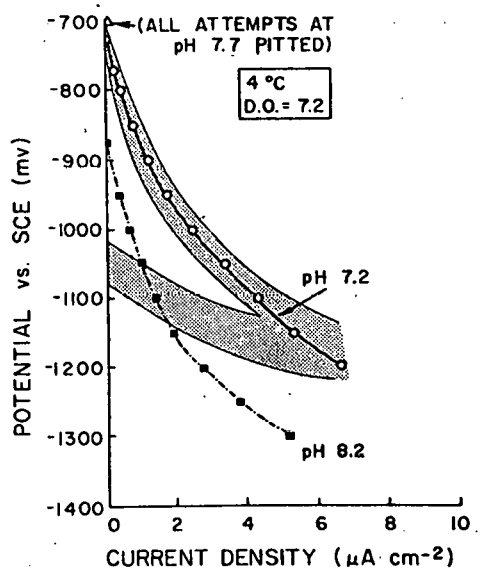

Figure 13. Effect of pH on cathodic polarization of alloy 5052 in seawater with 7.2 ppm DO at 4.0°C. Shaded area represents the envelope of data from Figure 11.

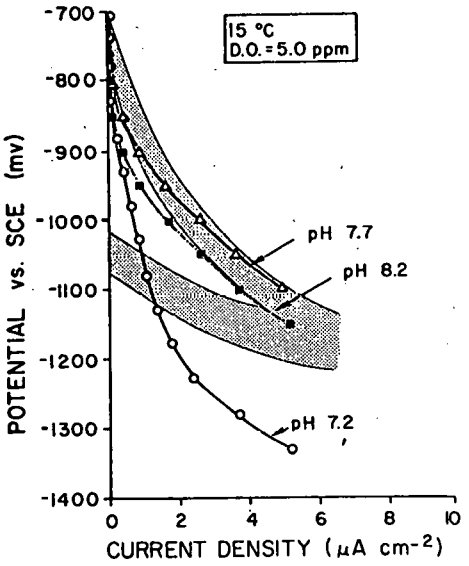

Figure 14. Effect of pH on cathodic polarization of alloy 5052 in seawater with 5.0 ppm DO at 15°C. Shaded area represents the envelope of data in Figure 11.

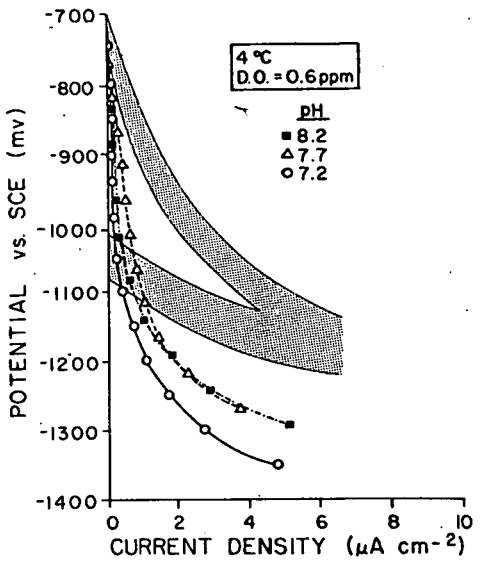

Figure 15. Effect of pH on cathodic polarization of alloy 5052 in seawater with 0.6 ppm DO at 4.0°C. Shaded area represents the envelope of data in Figure 11.

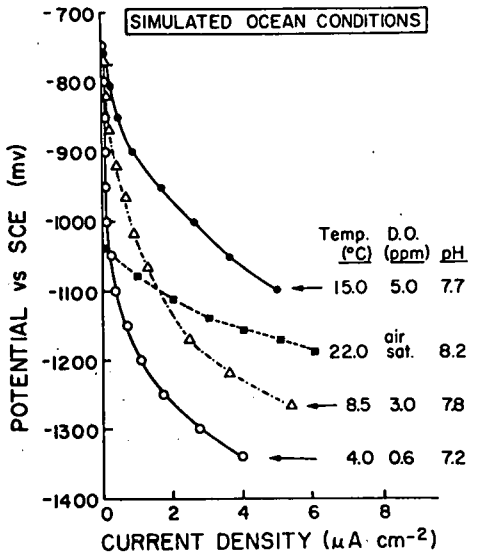

Figure 16. Cathodic polarization of alloy 5052 in seawater at combinations of pH, DO and temperature in the deep ocean (See Figure 1 and Table 1).

DISCUSSION

G. Kinelski: What will happen on OTEC-1 when the cold water is pumped into a sump, then pumped from the sump into the heat exchangers, and dumped overboard? I don't know the residence time in the sump but presumably it will be on the order of a one-half to a full minute. Presumably there will be some aeration taking place in that particular sump. Can you comment on that please?

S. C. Dexter: It would be a good idea to sample the water in the sump to measure temperature, oxygen, and pH. If we can do that, and correlate what happens, it will be very useful. If we get aeration and the aeration allows the pH to remain low, it could result in a very dangerous condition. Usually, when you aerate you drive off CO_2 and the pH rises. If the pH rises with the oxygen, you avoid the most corrosive set of conditions.

B. Liebert, Univ. of Hawaii: Do you look at the surface morphology of the samples after you finished testing them? Did you look at them topically or under the scanner?

S. C. Dexter: We did not use scanning electron microscope. We did it quite a number of times bebefore, but we did look at them in a stereo-microscope; in fact, we always verify the formation of the pits by looking in the stereo-microscope.

INTERLEAKAGE OF AMMONIA AND SEAWATER IN OTEC HEAT EXCHANGERS EFFECTS ON CORROSION AND SCALE FORMATION

C. F. Schrieber, W. D. Grimes, and W. F. McIlhenny

Resources Research Department
The Dow Chemical Company
Freeport, Texas 77541

Abstract

Coupon scale tests were conducted in mini-plant size equipment to assess scaling and corrosion behavior of CP titanium and aluminum alloys in environments which may possibly be encountered in OTEC heat exchangers. Exposures were completed for nominal 8, 30, 80, and 800 ppm additions of ammonia to seawater at 5°C and 30°C. The change in pH resulting from the ammonia addition has resulted in scaling at all ammonia concentrations, with calcite formation followed by aragonite and then brucite as concentrations increased. It is anticipated that a continuous cleaning process could control scale at 8 ppm, 30°C and 5°C, and at 30 ppm, 5°C, but that scaling at 80 ppm and 800 ppm additions is not economically controllable. Corrosion has been minimal except for measureable pitting on Al 3003, Al 5052, Al 5086 at 8 ppm, 30°C, and on Al 5052 at 8 ppm, 5°C. Ambient temperature seawater controls show general corrosion attack but insignificant pit attack. Exposures were also completed for 0, 0.1, 1.0, and 2.5% nominal seawater additions to commercially pure ammonia at 5°C. Both corrosion and scaling have been minimal for these exposures. The exposures reported herein indicate that CP titanium will give superior performance in an OTEC heat exchanger followed by pretreated aluminum alloy 5052.

Introduction

The possibility of either an ammonia or seawater leak in either the OTEC evaporator or condenser, constituted the stimulus for this research. The concern was that low concentrations of ammonia in seawater, and conversely, low concentrations of seawater in ammonia, may act to seriously impair material performance.

Testing was to remain on a coupon test scale, and relevant information sought included degree and definition of chemical scaling, average uniform penetration, final test interval corrosion rate, pitting, and crevice corrosion. Heat exchanger materials, as proposed by the Department of Energy included commercially pure (CP) titanium, and aluminum alloys 3003, 5052, and 5086. Additionally, at the recommendation of Dow personnel, specimens of aluminum alloy 5052, as pretreated in boiling deionized water were included in all exposures. Program methodology for this work is shown in Table 1.

Experimental Procedures

Test units

Seawater containing ammonia. Two test units designed to test the subject alloys in seawater plus small concentrations of ammonia at 30°C and 5°C were constructed as depicted in the generalized schematic in Figure 1. One unit operates at 30°C and is temperature controlled by either cooling water or steam. The low temperature, 5°C unit employs an external chiller circuit which removes heat from the loop by a cold glycol-water solution. Units are constructed of plastic-lined steel (polypropylene, Saran®, Teflon®, and Kynar®) and Alloy 20 stainless steel.

Table 1: Program Methodology

I. SEAWATER MIXED WITH AMMONIA

Test	Ammonia (ppm)	Exposures (days)	Velocity (fps)
Unit I: Evaporator Simulation	7.4 (a)	8,29,64	
	33 (a)	14,30,59	
	83	10,30,50 (b)	
	880	10 (b)	2.5 & 5.6
Unit II: Condenser Simulation 5°C	8.5 (a)	8,29,64	
	24 (a)	14,30,59	
	78	12,32,51 (b)	
	916 (a)	9.5 (b)	

II. AMMONIA MIXED WITH SEAWATER

Test	Seawater,%	Exposures (days)	Velocity (fps)
Unit III:	(151 ppm)	10,40	
Condenser	0.14	10,24	
Simulation	1.1	10,28,59	2.5
5°C	3.3	10,30,53	5.6

(a) Run in parallel with ambient seawater controls.
(b) Terminated early due to extensive calcareous scaling.

The test units contain approximately 22.7 liters (6 gal.) recirculating seawater. The seawater is refreshed at a rate of 7.6 to 1.9 l/min. (2.0 to 0.5 gpm).

Ammonia leakage into seawater was simulated by injection of ammonia solution into the refreshment seawater. Adequate mixing was assured by injection downstream of the recirculating pump and the use of aqueous ammonia as an injection fluid. Concentrations of ammonia in seawater are routinely obtained by analysis of the system blowdown. Both units contain all instruments necessary for automatic control and failsafe shutdown to prevent specimens from experiencing excessive ammonia concentrations.

Ammonia containing seawater. A test unit to employ mixtures of anhydrous ammonia plus low concentrations of seawater while operating at 5°C was constructed according to the generalized schematic in Figure 2. Construction materials are welded stainless steel 304 alloy, Teflon-lined steel, and Alloy 20 stainless

steel. The loop contains a suitable pump, temperature detectors, flow control and monitoring devices, as well as all automatic controls necessary for failsafe system operation. A chiller is incorporated in the circuit to maintain a 5°C environment within the test loop.

The test loop is designed for total recycle of 100 lbs. of anhydrous ammonia. Analysis performed on the ammonia-seawater mixtures included water content, chloride ion concentration, and sodium ion concentration.

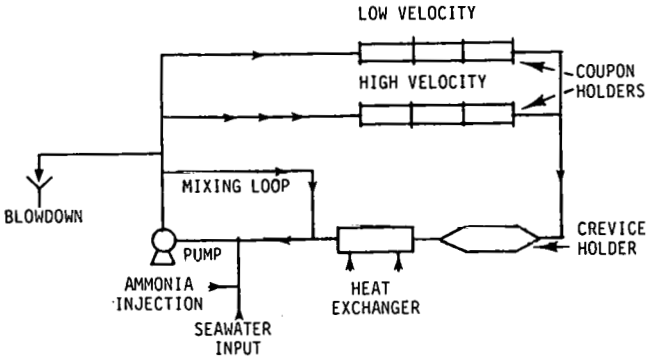

Figure 1: Simplified flowsheet of corrosion test unit to determine effect of low conc. of NH_3 in seawater (unites 1 & 2).

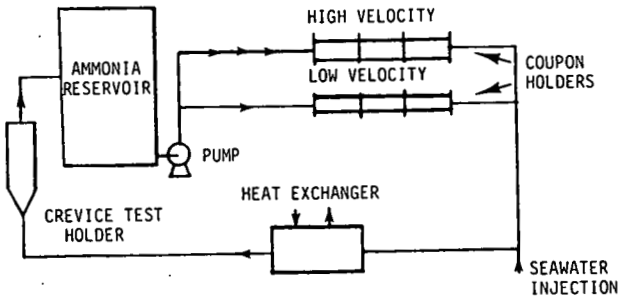

Figure 2: Simplified flowsheet of corrosion test unit to determine effect of low conc. of seawater in ammonia.

Seawater control test unit. This unit is of once-through flow design with automatic flow control downstream of the specimens. A filter is located upstream of the specimen holders. Incoming seawater temperature is not controlled.

Seawater. Seawater utilized in these tests is from the Gulf of Mexico intake basin located at The Dow Chemical Company's Texas Division industrial site "A" at Freeport, Texas. After large incoming debris is screened out at the Dow intake basin, the seawater is transferred through flumes (canals) to a second smaller sedimentation basin near the OTEC test facility. The seawater is then transferred through a system of copper-free piping to the test units where it is filtered to contain a maximum particle size of 25 microns.

Alloys and Specimen Preparation

The alloys specified for use in these tests include aluminum alloys 3003, 5052, and 5086, and CP titanium.

An addition made by Dow to the test alloy scheme consisted of a sample series of aluminum alloy 5052 pretreated in boiling deionized water for eight hours. One of the findings of the Office of Saline Water desalination materials programs indicated that the higher general and pitting corrosion attack of aluminum which occurs during the initial few weeks can be effectively reduced or eliminated by this pretreatment.

General and pitting corrosion rate determinations utilized (6" x 3/4" x (0.06-0.08)") nominal size coupons. These specimens were held in pipe spools line with polytetrafluorethylene (TFE, Teflon®) plastic. Fluid velocity past the specimens was accurately fixed by knowledge of the flow rate and available cross sectional area in the holder.

Crevice corrosion determinations utilized (3" x 3" x (0.06-0.08)") nominal size specimens with a centered (1/2") diameter hole. These specimens were mounted on a rod holder and individually separated by special crevice contactors. These contacts were specifically designed to form eight crevice areas on each side of the specimen faces with fluid stagnation points between the crevice areas. Contact pressure between separators and specimens was applied from each end of the crevice assembly.

Data Resolution

Weight loss and microscopic data was resolved into average penetration, final interval corrosion rate, maximum pit depth, and approximate pit density.

In order to facilitate data usage by the OTEC community, corrosion was expressed as corrosion penetration for the given period of exposure.

Data are commonly expressed in mils (mm) penetration. However, passivating alloys often experience a high initial penetration which is not indicative of long-term alloy performance. Thus, corrosion rate assessment of long-term performance of passivating alloys was more accurately represented by the "final interval" corrosion rate, or the time and penetration difference generated using the final two specimen pulls.

Ammonia in Seawater

Ammonia in recirculating seawater tests were performed at both 5°C and 30°C. Leakage severity was tested by forming nominal ammonia concentration levels in the seawater of 8, 30, 80, and 800 ppm at the two temperatures. In addition, ambient temperature seawater controls were run in parallel with the 8, 30, and 800 ppm ammonia in seawater tests to assess the corresponding influences of seawater corrosion and fouling behavior.

Scale Formation

Mixing of ammonia and water will result in hydrolysis of the ammonia to form ammonium and hydroxyl ions. The resulting solution is thus more alkaline, and in seawater an increase in alkalinity enhances calcium carbonate and magnesium hydroxide precipitate formation. Precipitates so formed may then nucleate and form scales on heat exchanger surfaces in a manner which will seriously

impair heat transfer.

This set of problems is due to the nature of the hydrolysis of ammonia and to the formation of hydroxyl ion:

$$NH_3^0 + NOH \rightarrow NH_4^+ + OH^-$$

As a result of the hydroxyl ion formation, solutions of ammonia in water are very basic. Then the hydroxyl ion in seawater reacts with bicarbonate (the predominant ionic form of carbon dioxide) to produce carbonate ion:

$$HCO_3^- + OH^- \rightarrow CO_3^= + HOH$$

which in turn will react with calcium present to precipitate calcium carbonate:

$$Ca^{++} + CO_3^= \rightarrow CaCO_3\downarrow$$

Or, alternately, the hydroxyl ion produced by the hydrolysis of ammonia can react directly with the magnesium present in seawater to precipitate magnewium hydroxide:

$$Mg^{++} + 2OH^- \rightarrow Mg(OH)_2\downarrow$$

In general, if sufficient ammonia is present, the sequence of chemical events would be:

1. conversion of HCO_3^- to $CO_3^=$
2. precipitation of $CaCO_3$
3. precipitation of $Mg(OH)_2$
4. elevation of solution pH

In these tests, ammonia was added to the recirculating seawater loop (with continuous refreshment) as ammonium hydroxide, ammonia already hydrolized to its product ions. The results, summarized in Figure 3 indicate greater rates of scale/fouling growth at higher temperatures and concentrations of ammonia. CP titanium and pretreated aluminum alloy 5052-H14 were observed to very slightly retard initial scale growth.

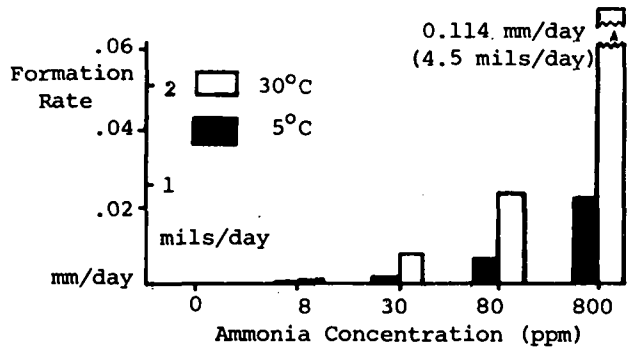

Figure 3: Scale-fouling growth.

Crystalline components of the scale were determined using X-ray diffraction, energy dispersive X-ray, and infrared spectral analysis. Scale composition development followed the pattern shown in Figure 4 with calcite forming initially followed by aragonite and brucite at higher ammonia concentrations and temperatures. At zero and 8 ppm ammonia in seawater, primary constituents of the surface deposit are amorphous muds and organics.

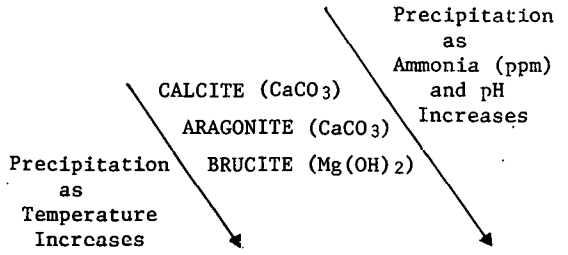

Figure 4: Scale composition and formation.

Corrosion

Information sought in these tests is final interval corrosion rate, maximum pit penetration and crevice attack.

Seawater controls. Corrosion on the seawater controls was marked by general, uniform surface attack and the absence of significant pitting. Average final interval corrosion rates for aluminum alloys 3003, 5052, and 5086 was 2.2 to 2.6 mpy, with aluminum alloy 5086 giving the most consistent performance of the three untreated alloys. Treated aluminum alloy 5052 was superior to all aluminum tested with a rate of 0.60 mpy. CP titanium showed negligible attack and was superior to all metals on test.

Addition of 8 ppm ammonia to seawater. For the test exposure at 30°C, aggressive pit attack was noted on aluminum alloys 3003, 5052, and 5086. Also, at 5°C, agressive pit attack was noted on aluminum alloy 5052. Parallel ambient temperature seawater controls showed greater average corrosion penetration but insignificant pit attack on these same alloys. Performance of the crevice test specimens was generally superior to that of the weight loss coupons. CP titanium showed negligible pit attack and constituted the superior metal at these exposures followed by pretreated aluminum alloy 5052.

Addition of 30 ppm ammonia to seawater. At 30°C, one or two pits 1-2 mils deep were noted on aluminum alloys 3003, 5052, and 5086. At 5°C, no significant pit attack occurred, Crevice corrosion was not observed at the 30°C temperature exposure. At 5°C, 1-2 mils crevice attack penetration was noted on aluminum alloys 3003, 5052, and 5086. CP titanium gave the best corrosion performance of any metal tested at this exposure followed by pretreated aluminum alloy 5052.

Addition of 80 ppm ammonia to seawater. Scaling was very noticeable at 10 days and excessive at 51 days. Exposures were terminated at this point. Final rates for the aluminum alloys at 30°C were 50-100% of the final corrosion rate of the ambient temperature seawater controls. Corrosion rates at 5°C were minimal. Maximum observed pit depth on any speciment was estimated at less than 1 mil penetration. No significant crevice attack was noted on either test after 50 days although some slight impressions were present at the lower temperature. Again, CP titanium and pretreated aluminum alloy 5052 showed overall superior performance.

Addition of 800 ppm ammonia to seawater. The

5°C and 30°C exposures at 800 ppm ammonia in seawater were terminated at 10 days because of excessive scaling. Both final interval corrosion rates and pitting were negligible, a factor probably related to the rapid scaling.

Comparative date for the subject alloys is given in Figures 5 (a) and 5 (b).

Seawater in Ammonia

Seawater in ammonia tests were performed at 5°C, the OTEC condenser temperature, and at addition severities of a nominal 0*, 0.1, 1.0, and 2.5% seawater concentration. Solution analyses performed for each exposure included percent water by volumetric evaporation or barium oxide adsorption, sodium ion concen-

* Measured water content ∿150 ppm

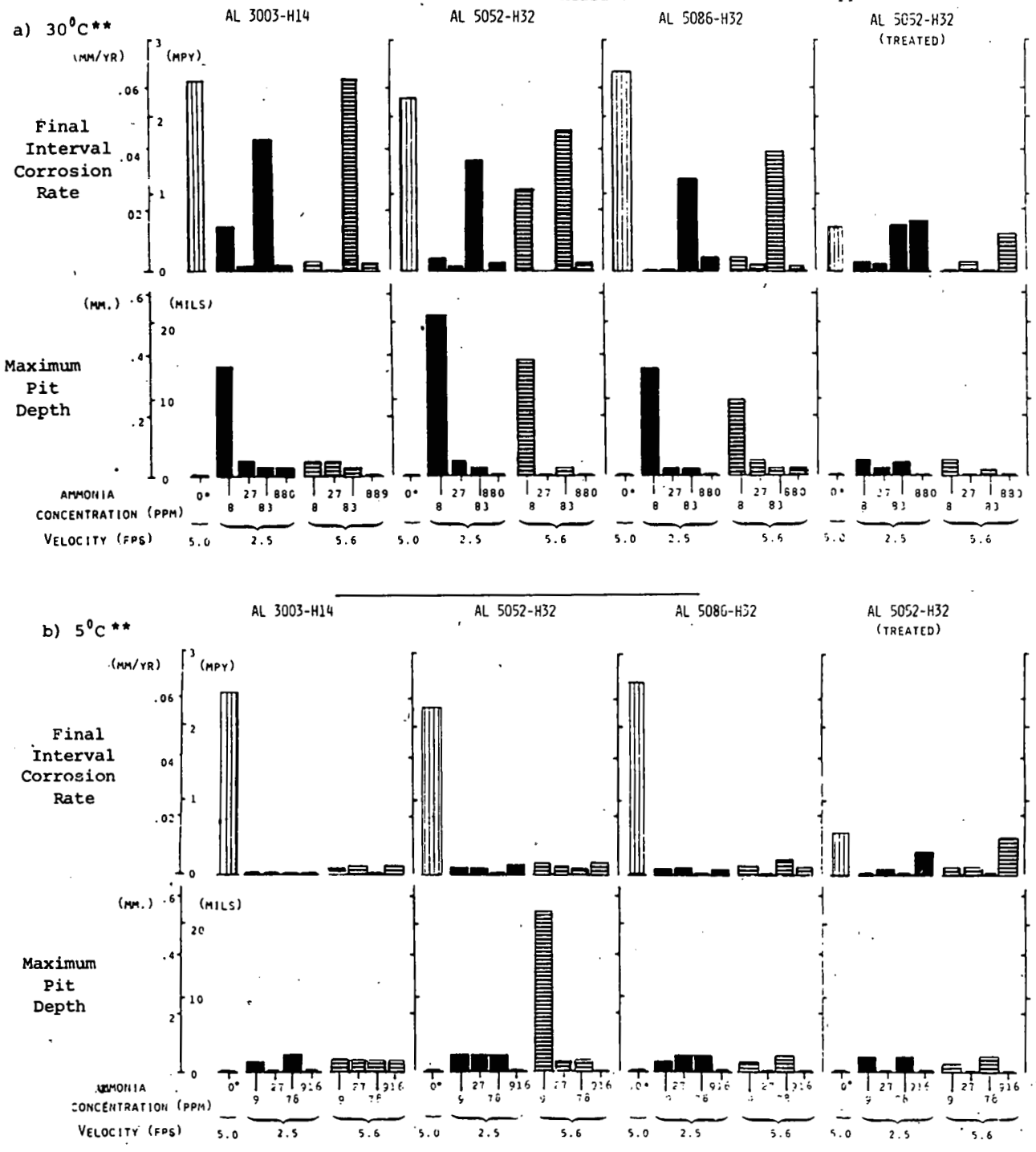

* Ambient temperature controls (mean value)
** Corrosion on CP titanium was negligible and not graphed

Figure 5: Corrosion summary: final interval corrosion rate and maximum pit depth; seawater mixed with ammonia.

tration by atomic adsorption analysis, and chloride ion concentration by Volhard analysis.

Scale Formation

Scale was not observed to form over the range of seawater concentrations investigated.

Corrosion

Again, relevant corrosion information sought consisted of final interval corrosion rates, maximum pit depth, and crevice attack.

Anhydrous ammonia. Pit, crevice, and uniform corrosion attack were minimal on all alloys tested. Initial high penetrations observed on pretreated aluminum alloy 5052 did not increase significantly for the subsequent exposure periods, so that at the conclusion of the test, all aluminum alloy penetrations were comparable. CP titanium demonstrated corrosion resistance superior to that of any metal tested, followed in order by pretreated aluminum alloy 5052 and aluminum alloys 5052, 3003, and 5086.

Anhydrous ammonia plus 0.1% seawater. Pitting and crevice attack were negligible for all alloys tested. final interval corrosion rates for aluminum alloys 3003, 5052, and 5086 were less than 0.12 mpy at 2.5 fps and 0.43 to 0.69 mpy at 5.6 fps, thus indicating a significant velocity effect. Initial high average corrosion penetrations for pretreated aluminum alloy 5052 gave a final interval corrosion rate at 24 days which was negligible. The superior metals at this exposure were CP titanium and pretreated aluminum alloy 5052.

Anhydrous ammonia plus 1.0% seawater. Pitting and crevice attack were negligible except for one pit observed on aluminum alloy 5052 at 5.6 fps. Initial high corrosion penetrations on pretreated aluminum alloy 5052 did not continue to increase significantly through the 53-day exposure. CP titanium again constituted the superior metal for this exposure followed by pretreated aluminum alloy 5052.

Anhydrous ammonia plus 2.5% seawater. Pit and crevice attack were negligible at this exposure although final interval corrosion rates for aluminum alloys 3003, 5052, and 5086 were greater than for ammonia exposures with lower seawater percentages. Initial high penetrations on pretreated aluminum alloy 5052 did not continue to increase significantly through the 53-day exposure. CP titanium again constituted the superior metal for this exposure followed by pretreated aluminum alloy 5052. Corrosion data are summarized in Figure 6.

Summary and Conclusions

Results of this effort are summarized by the following:

1. In all cases CP titanium performed in a manner superior to that of the aluminum alloys tested. Final interval corrosion rates for this material were less than 0.0028 mm/yr (0.11 mpy) in all environments tested. This compares to rates of 0.065 mm/yr (2.6 mpy) for all aluminum alloys in seawater and 0.0074 mm/yr. (0.28 mpy) in ammonia. Pit and crevice attack was minimal, and no significant penetration (>1 mil) was observed at any exposure. In contrast, pit attack of varying degrees was observed on all aluminum alloys tested.

   Additionally, chemical scales forming on titanium surfaces were less tenacious and therefore more readily removed than scales which formed on the aluminum surfaces.

2. Aluminum alloy 5052, which had been pretreated by immersion in boiling deionized water for 8 hours, was the best performer of the aluminum alloys tested. The boiling water pretreatment forms an impervious bohemite film on aluminum which prohibits the plating of pit-inducing heavy metal ions. The effect of this pretreatment is to significantly reduce the initially high corrosion rate associated with aluminum.

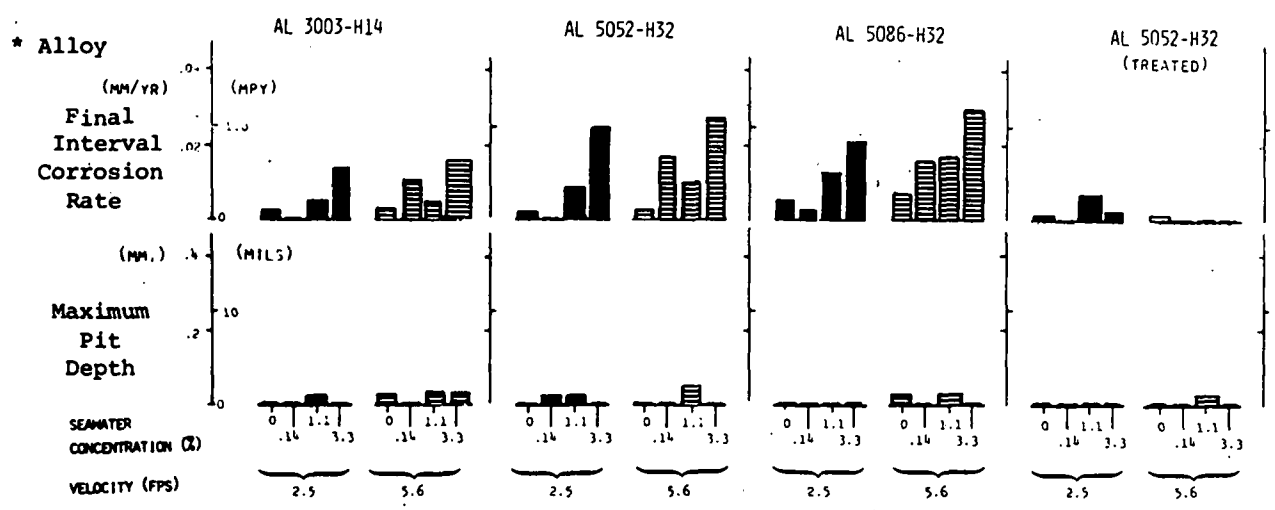

* Corrosion on CP titanium was negligible and not graphed

Figure 6: Corrosion summary: final interval corrosion rate and maximum pit depth; ammonia mixed with seawater: 5°C.

In ambient temperature seawater, pretreated aluminum alloy 5052 has a final interval corrosion rate of 0.015 mm/yr (0.59 mpy) as opposed to a final rate of 0.056 to 0.065 mm/yr (2.20 to 2.57 mpy) for untreated aluminum alloys 3003, 5052, and 5086. In mixtures of 30°C seawater plus lower concentrations of ammonia, the performance of pretreated aluminum alloy 5052 was also superior to other aluminum alloys, particularly to pit resistance which was minimal in all seawater-ammonia mixtures.

In anhydrous ammonia and ammonia-seawater mixtures, pretreated aluminum alloy 5052 showed an initial weight loss greater than that of the untreated aluminum alloys. However, the final rates for the pretreated alloy in this environment were consistently superior to the other aluminum alloys. In addition, the etched surface attack often observed on aluminum alloys was not apparent on pretreated aluminum alloy 5052. The surface appearance of this alloy was virtually unchanged by the exposure to the subject environments.

Scale and fouling removal was observed to occur as readily on pretreated aluminum alloy 5052 as on CP titanium.

3. The addition of ammonia to seawater will result in alkaline scale formation which may impair heat transfer. The increase in pH resulting from ammonia addition has resulted in scaling at all trial concentrations of ammonia in seawater (8, 30, 80, and 800 ppm), with calcite scale forming initially followed by aragonite and brucite as concentrations increase. It is anticipated that a continuous cleaning process could control scale at 8 ppm 30°C and 5°C, and at 30 ppm, 5°C, but that scale control at ammonia concentrations above 80 ppm (scale growth above 0.013 mm/day) is not economically controllable.

4. The addition of seawater to anhydrous ammonia within the scope of these tests has not resulted in any relevant scale formation.

5. The final interval corrosion rates for the aluminum alloys was generally greater in the control ambient temperature seawater than in seawater plus ammonia mixtures. Aluminum alloys 3003, 5052, and 5086 showed final corrosion rates of 0.056 to 0.065 mm/yr (2.20 to 2.57 mpy) in ambient temperature seawater. Treated aluminum alloy 5052 in this environment exhibited a rate one-fourth the above or 0.015 mm/yr (0.59 mpy). Pitting was minimal in ambient temperature seawater although measureable pitting was observed on the untreated aluminum alloys in seawater containing 8 ppm at 30°C.

6. Addition to anhydrous ammonia of greater quantities of seawater from 151 ppm to 2.5% was generally observed to increase the final interval corrosion rate of untreated aluminum alloys 3003, 5052, and 5086. No conclusive observation may be made concerning treated aluminum alloy 5052 and CP titanium.

7. The results of this test were inconclusive in determining a preferred velocity for the OTEC system.

DISCUSSION

M. Kaminsky, Argonne National Laboratory: You indicated that you pretreated aluminum alloy (5052-H32) for some short significant improvement of the performance. Tell me more about the treatment parameters. You mentioned that you boiled them (coupons) in deionized water. Could you tell me for how long and what else has been done?

C. Schrieber, The Dow Chemical Co.: The test coupons were boiled for 8 hours in deionized water. This procedure forms a boehmite film on them and the tube essentially acts like it's been under these conditions for 6 or 4 months. I'm not saying that, at the end of 3 or 2 years it would be any different between (boiled or untreated surfaces), but in the short tests we ran there was a difference.

M. Kaminski: Did you look at the surfaces after they had been pretreated?

C. Schrieber: Yes.

M. Kaminski: What analysis have you done and what did you find?

C. Schrieber: Well, [the surface] has a transparent, very, very thin boehmite type film on it. [The film] does discolor the panel in a lighter shade.

B. J. Freedman, Electric Boat Div., General Dynamics: What is the nature of the scale? Have you noted any salt buildup? What is the effect of the environment on surfaces newly cleaned by Amertap? Have you analyzed for chloramines?

C. Schrieber: The compositions are in the paper (Fig. 4), and were aragonite and calcite which are calcium carbonate, and brucite — which is magnesium hydroxide. The calcium-to-magnesium ratio changes depending on the ammonia inventory that's available. If the ammonia inventory is very high at a location, the amount of magnesium will rise. Brucite will be in preponderance. John Morse (Univ. of Miami) noted the same thing in his studies. There was no "salt" build-up in these studies, and we haven't had any reason to look for chloramines.

R. Zawierucha, UCC/Linde Div.: Do you have any plans for testing Alclad 3003 or 3004?

C. Schrieber: Yes, in July 1979.

REVIEW OF CORROSION OF STEEL IN CONCRETE

Aziz Siman, Changiz Dehghanian, and Carl E. Locke

School of Chemical Engineering
and Materials Science
University of Oklahoma
Norman, Oklahoma 73019

Abstract

The steel reinforcement in portland cement concrete is usually passivated due to the alkaline character of concrete which produces a pH of about 12.5. Preservation of this state is an essential condition to protect steel from corrosion. It is well known that a small amount of chloride ions will destroy the passive oxide film on steel. Many other variables such as concrete properties (water/cement ratio, type of cement and aggregate size and shape), steel surface and the presence of oxygen, carbon dioxide and moisture are of great importance in this corrosion process.

Premature failure of bridge decks due to deicing salt application is an example of reinforced concrete structure corrosion which has resulted in huge repair expenses. The structures exposed to marine environments such as piers, offshore platforms and underwater concrete coated pipelines also suffer the same problem. Since concrete is to be used as a material of construction in OTEC plants, consideration of these problems is necessary. In recent years, extensive efforts have been made to fully investigate the electrochemistry of steel in concrete and the methods of protection. ~~This paper reviews~~ general aspects of reinforcing steel corrosion in concrete are reviewed. Some electrochemical studies such as evaluation of embeddable solid reference electrodes for cathodic protection applications in concrete and corrosion rate measurements of salt contaminated concrete have also been discussed.

Introduction

The widespread use of reinforced concrete structures has attracted investigators to study the problems associated with corrosion of reinforcing steel in concrete. It is generally belived that a protective layer of γ-Fe_2O_3 formed on the surface of steel at the high alkaline environment of concrete will establish enough protection to resist corrosion. However, the introduction of chloride ions to the surface of embedded steel will destroy the passivity. The corrosion products formed are voluminous and concrete cracks will form eventually due to low tensile strength of concrete. These cracks will expose more steel surface to the corrosive environment and intensify the problem.

Premature deterioration of bridge decks due to deicing salt application is one of the most common types of this process.[1] Other reinforced concrete construction exposed to high chloride ion environments such as parking garages, piers and offshore platforms also suffer the same problem. The huge amounts of reinforced concrete planned to be used in cold water pipe and concrete gravity platforms of OTEC plants[2] necessitates more attention on the corrosion of the embedded steel in concrete. Deliberate addition of sea water in concrete mixture and $CaCl_2$ as accelarator are two other forms of chlorine contamination. Consequently, in any concrete structure which is in contact with chlorides, the possible corrosion problems should be carefully studied.

In recent years, extensive efforts have been made to investigate the electrochemical behavior of steel in concrete. The corrosion process of steel in concrete is a function of many variables such as the concrete properties, steel surface and the corrosive environments they are exposed to. Numerous techniques have been proposed to prevent or hinder the corrosion problem and some have already been applied.

This paper reviews general aspects of reinforcing steel corrosion in concrete. Evaluation of embeddable solid reference electrodes for cathodic protection applications in concrete will be described. Electrochemical studies such as polarization tests regarding the mechanism of corrosion process and determination of corrosion rates will also be discussed.

Theory and Background

Corrosion can be defined as the tendency of metals to go to their natural form. Any corrosion process includes an anode (oxidizing pole), a cathode (reducing pole), an electrolyte which is the conductive environment for ions and finally, a pathway for electrons from anode to cathode. The corrosion process of steel in concrete can be simplified as the oxidation of iron (anodic reaction)

$$Fe \longrightarrow Fe^{++} + 2e^{-} \qquad (1)$$

and cathodic reduction of oxygen (cathodic reaction)

$$\tfrac{1}{2}\, O_2 + H_2O + 2e^{-} \longrightarrow 2(OH)^{-} \qquad (2)$$

the combination of these two reactions will form different types of iron oxides which is commonly called rust.[3]

The corrosion process of reinforcing steel in concrete is a complex problem. This complication is due to the number of variables which are involved in making the concrete and steel, and the environment as well.

Three major groups of variables can be detected in this corrosion process. These include: a) variables which are associated with concrete design, b) variables which are associated with reinforcing steel and c) variables which are associated with the environment. The above mentioned factors have to be carefully taken into consideration in any research regarding this phenomena.

Concrete

The properties of concrete which serves as the electrolyte, plays the most significant role in this corrosion process. The concrete mix design which determines the amount of each constituent in the mixture should be selected carefully. Water/cement ratio is specifically important since it controls the moisture content of concrete. The moisture content will then effect other properties such as strength, conductivity and permeability. The change of conductivity influences the transfer of the ions and thus effects the corrosion reactions. The resistivity of concrete is in the range of 10000-200000Ω.Cm, however, in very dry conditions it increases to 10^6-10^7Ω.Cm.[4-5]

As can be seen from equation (2), oxygen and water are the major factors of this corrosion reaction. As long as water and oxygen are present, the cathodic reaction would proceed further. The elimination of one will stop further progress of corrosion. Moisture content not only increases the conductivity of concrete, but it also serves as a means for transfer of oxygen, chloride ions and carbon dioxide which lowers concrete alkalinity. The water/cement ratio effects the chloride ions migration, a lower w/c ratio provides a less permeable concrete which better protects the reinforcement. It has been shown[6] that under certain salt applications two inches of clear cover is needed for corrosion protection of concrete with w/c ratio of 0.4. This value, however, should be increased to three inches when w/c ratio is increased to 0.5. Permeability of concrete will also be reduced significantly when w/c ratio is lowered to 0.4.[7] Finally, w/c ratio controls the strength of concrete, the lower the w/c ratio, the higher the strength of concrete.

The selection of proper cement type is of great importance. There are five different types of portland cement produced in the U.S. which are used for different applications. Chemically, cement is a mixture of calcium silicates (3 $CaO.SiO_2$ and 2 $CaO.SiO_2$), aluminates (3 $CaO.Al_2O_3$) and ferrites (4 $CaO.Al_2O_3.Fe_2O_3$). Other compounds such as CaO, MgO, K_2SO_4, $CaSO_4$ and Na_2SO_4 are also present. Complete hydration of anhydrous compounds produces $Ca(OH)_2$ which is the major source of alkalinity. The amount of solid $Ca(OH)_2$ varies from a minimum of 20% in the type IV portland cement to a maximum of 30% for the type III portland cement.[8] Table 1 shows the composition of some compounds in portland cements with some of their application.

Table 1*

SOME APPLICATIONS AND COMPOSITIONS OF DIFFERENT TYPES OF CEMENT

Cement Type	Max C_3A%	Max CaO%	Application
I	14	1.5	ordinary
II	8	1.8	sulfate resistant
III	17	4.2	rapid hardening
IV	7	0.9	low heat generation
V	5	0.6	sulfate resistant

*Reference 7 and 9.

It has been reported that the presence of tricalcium aluminates (C_3A) is of great importance in corrosion process. C_3A can react with chlorides and form insoluble compounds (3 $CaO.Al_2O_3.CaCl_2.H_2O$).[8-10] Consequently, higher concentrations of C_3A, up to a maximum level,[11] will be helpful to reduce the amount of free chloride ions. However, the sulfate content of cement and the source of chlorides have to be considered in selection of the proper type of cement and its C_3A content. Type II and V are normally used in sea water exposure conditions and both have lower C_3A contents. One author[8] has concluded these type cements do not have sufficient C_3A to remove the chloride added in the mix or which diffuse into the hardened concrete. Therefore, corrosion problems can be assumed to be probable with these cements.

Finally, the size of cement particles may indirectly influence the corrosion phenomena.[7] Fine cements increase the water demand and thus increase w/c ratio which in turn effects the permeability.

The pH of concrete has also some influence in this corrosion process. As stated earlier the high alkaline evironment of concrete (pH ∿ 12.5) provides the protective layer of γ-Fe_2O_3 on the steel surface and prevents corrosion. However, if the pH drops below 11.5, the protection will be diminished. It has been reported[12] that chloride ions lower the pH which results in the destruction of the protective layer. The higher the pH the lower the capacity of chlorides to disrupt the passive state and the higher the amounts of chloride ions to be tolerated.[13] It has also been reported that CO_2 has the same effect in reacting with alkaline solutions of the concrete and lowering the pH.[12] Carbonation process however, is not significant for dense concrete due to low diffusion rate of CO_2.[2]

Other factors which should also be mentioned are aggregate size, shape and composition; addition of other chemicals such as air entraining agents, water reducers (retarders), accelarators, sulfides, curing time and method and finally mixing procedures and placing. These will not be discussed here.

Reinforcing Steel

The existence of heterogenities on the surface of steel results in the formation of local cells which in turn intensifies the corrosion. The surface of reinforcing steel is covered with a layer of several different iron oxides (usually called mill scale). Ferrous oxide (FeO) is adjacent to the steel, magnetite (Fe_3O_4) is in the middle and ferric oxide on top.[14] The electrochemical behavior of steel is effected by these oxides. In some cases, the protective layer of mill scale is flaked off during transportation which will later causes the formation of localized cells in which mill scale will serve as the cathode and the steel as anode. It has been observed[15] that the external steel structures attached to the concrete platforms corrode severly. This is also due to the formation of galvanic cells between embedded steel and external steel.

Environment

As stated earlier, the major cause of steel corrosion in concrete is chloride ions. Chlorides come from different sources. Deicing salts have been

used to remove snow and ice from highways. Sea water may sometimes be used as mix water and sand or aggregates may be contaminated with salt. In some cases, calcium chloride has been used as an accelerator to improve the strength and accelerate the setting time of concrete. The addition of $CaCl_2$ has been controversial in the past several years. Although most reports strongly prohibit the mixing of $CaCl_2$ with concrete, some have suggested that addition of up to 2% $CaCl_2$ by weight of cement is in the chloride tolerance range of concrete.[16] Several investigators have reported the existence of a chloride ion concentration threshold beyond which the corrosion manifestation increases drastically. This critical concentration is between 1-2 lb/yd^3 (0.6-1.2 kg/m^3)[6] of chloride ion. It has been shown that for saturated $Ca(OH)_2$ solution, this value is 700 PPM of chloride ions,[17] the larger the ratio of Cl^-/OH^- the larger the corrosion rates. Nonuniform distribution of salts on the concrete surface forms differential concentration cells in which one portion of the reinforcement will be more active than the other which will increase the corrosion hazards.

The effect of chloride ions on the electrochemistry of steel in concrete has been studied by the authors.[18] Reinforced concrete specimens with different salt contents were cast. Anodic, cathodic polarization tests (Figure 1) and polarization resistance tests (Figure 2 and 3) were carried out on these specimens. Anodic and cathodic polarization tests not only provide some information about the electrochemistry of steel in concrete, but they can also be used to calculate the Tafel slopes for corrosion rate calculations. The results of the polarization resistance tests together with the anodic and cathodic Tafel slopes (β_a and β_c) were used to calculate corrosion current (i_{corr}) by using the Stern-Geary equation:

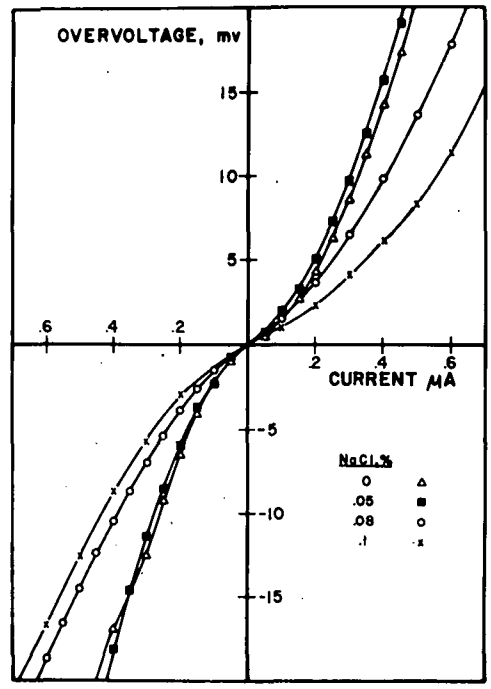

FIGURE 2

Polarization Resistance of Reinforcing Steel for 0, 0.05, 0.08 and 0.1 Percent Salt

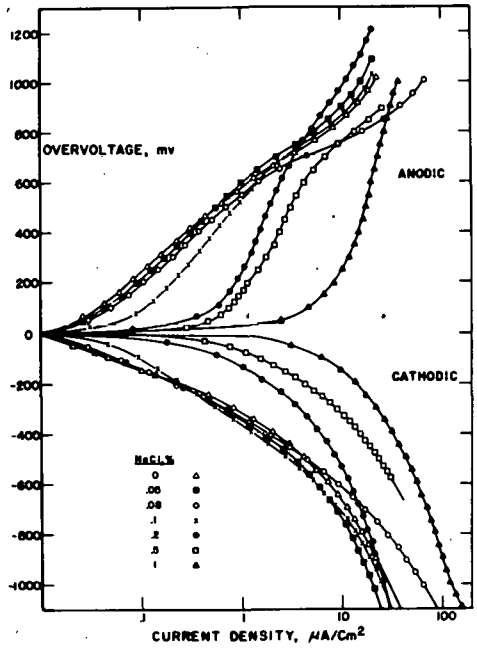

FIGURE 1

Anodic and Cathodic Polarization of Reinforcing Steel in Concrete

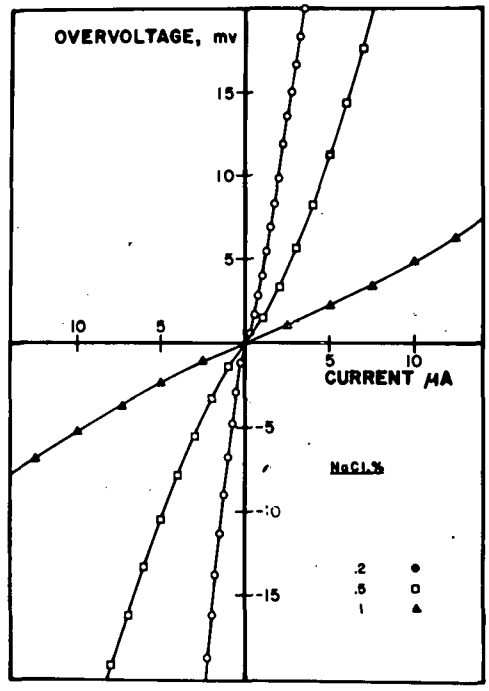

FIGURE 3

Polarization Resistance of Reinforcing Steel 0.2, 0.5 and 1 Percent Salt

$$i_{corr} = \left(\frac{di}{dE}\right) \frac{\beta_a \beta_c}{2.3(\beta_a+\beta_c)} \quad (3)$$

where $\frac{di}{dE}$ is the slope of polarization resistance at the free corrosion potential (i=0).

The corrosion currents were then converted to corrosion rates according to equation (1) and Faraday's law.

The results of this investigation which are tabulated in Table 2 are in reasonable agreement with some other reports using different methods of corrosion rate measurement such as weight loss[19] tests, electrical resistance[20] and electrical impedence[21] technique.

It was concluded that for the concrete specimens containing more than 0.1% NaCl the corrosion rate increases drastically which is in good agreement with some field studies too.

Table 2

CORROSION RATE OF REINFORCING STEEL

NaCl%	$\frac{di}{dE} \times 10^6$ A/mv	β_a mv	β_c mv	Corrosion Rate Mpy
0	.1	320	460	.08
.05	.08	360	450	.07
.08	.07	360	380	.06
.1	.1	470	400	.09
.2	.25	860	1050	.52
.5	.7	850	950	1.39
1	2	1570	1080	5.66

Other environmental factors include the presence of oxygen and carbon dioxide. According to equation (2), oxygen has to be present so that the overall reaction can proceed. The effects of oxygen depends on the concrete porosity and moisture content. It has been reported that the corrosion is lower if the experiment environment is replaced with nitrogen instead of air.[12] The corrosion rates have also been increased when the tests were conducted under the pressures more than atmospheric pressure.[22] Thus, the dissolved oxygen of the oceans may be a factor in submerged concrete structures. It has been shown that the oxygen oontent of the oceans is a function of location, salinity and depth.[23] It decreases to some depth and rises again and levels off. Table 3 indicates some of these variation with respect to location and depth. Although many investigators believe that 0_2 diffusion may not be a problem for submerged structures, differential aeration cells can be formed between the portions of the structure below and above the sea level. On the other hand, the penetration of sea salts under the hydrostatic pressure may also increase the corrosion hazards. For a high quality concrete it takes less than a year to penetrate 3 inches (75 mm) under around 470 feet (140 m) of sea water.[24]

Table 3

VARIATION OF DISSOLVED OXYGEN CONCENTRATION AT DIFFERENT DEPTHS AND LOCATIONS*

Depth M	dissolved oxygen ml/L		
	Gulf of Mexico	N. Atlantic	N. Pacific
0	5	5	6.2
100	4	4.8	5.5
300	2.8	4.6	4.6
500	2.9	--	1.8
1000	4.2	3.7	0.5
2000	--	5.9	2
3000	--	5.9	2.6
5000	--	6	3.4

*Reference 23

The cover thickness is another major corrosion factor. A uniform cover is of great importance. A homogeneous distribution will prevent formation of differential concentration cells (chloride penetration) and differential aeration cells (0_2 diffusion). Finally, a 2-3 inch (50-75 mm) of high quality, impermeable concrete which has been properly placed seems to provide good protection for embedded steel.

Methods of Protection and Prevention

A variety of methods have been proposed to protect steel from corrosion which mostly are restricted to bridge decks and some are still in the experimental stage. These include: Latex modified concrete, corrosion inhibitors, internally sealed concrete, epoxy coated reinforcement, galvanized reinforcement, chloride removal, polymer impregnated concrete, overlays and membranes and cathodic protection.

One of the most effective solutions in halting the corrosion of steel in concrete is cathodic protection which has drawn a lot of attention recently. The unique feature of this method is its application to any concrete structure such as offshore rigs, bridge decks and concrete pipeline in offshore. It is thought that the controlled potential of steel in concrete has to be in range of -700 to -1100 mv with respect to $Cu/CuSO_4$ in order to protect the steel and prevent hydrogen evolution. Since the potential has to be controlled some reference electrodes have to be developed for this service. There are many types of reference electrodes available, each of those is practical and suitable to a certain environment. The most common types are standard hydrogen electrode, calomel, silver/silver halides, copper/copper sulfate and metal/metal oxide electrodes.

Solid reference electrodes can be easily used in any orientation. These electrodes are not only used in solution, but also they may be used in concrete to monitor the protected steel potential. The authors have done some work on the area of solid reference eletrodes.[25]

Some interesting data has been found which will be discussed here.

Solid Molybdenum-Molydenum Oxide Reference Electrode

The potentials of these electrodes were measured in sodium hydroxide solution with concentration ranging up to 40% by weight. Figure 4 shows the variation of the electrode potentials with sodium hydro hydroxide concentration. This data agrees with the work of Every and Bank.[26] The potentials of these electrodes also were measured in saturated $Ca(OH)_2$ with respect to time. There was no variation in potential as function of time as shown in Figure 5. The agreement between electrodes is satisfactory. Similar data was obtained as a function of salt concentration in saturated $Ca(OH)_2$ (See Figure 6). Figure 7 presents the electrode potentials with respect to $Cu/CuSO_4$ as a function of time with the electrodes in concrete cylinders. The electrode potentials started to shift towards more positive potential at the end of the curing period. The potentials did not vary when cylinders were again placed and later removed from a 100% humidity atmosphere. This 200 mv shift is due to the portland cement matrix reaction with MoO_3 or possibly a change in the electrode environments due to a change in the portland cement matrix.

The molybdenum/molybdenum oxide electrode will be a stable reference if in manufacturing process the MoO_3 is produced on its surface. The following mechanism presents the behavior of the electrodes with varying OH^- concentration.[27]

$$Mo^{+6} + 6e^- \longrightarrow Mo \quad (3)$$

$$MoO_3 \longrightarrow M^{+6} + 3O^{=} \quad (4)$$

$$3\bar{O} + 3H_2O \rightarrow 6OH^- \quad (5)$$

$$6OH^- + 6H^+ \longrightarrow 6H_2O \quad (6)$$

A batch of the electrode which has been in concrete for a period of one year and a half indicated that the potentials after the initial change were stable and slight changes were observed. The potential shift in concrete should not halt the use of these electrodes in concrete. The potentials seem to be shifted permanently with proper aging techniques.

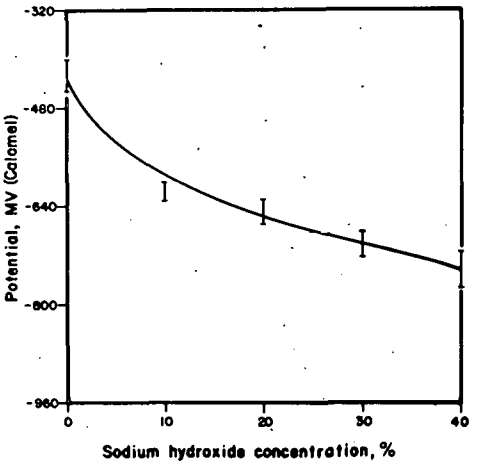

FIGURE 4

Potential of Mo/MoO_3 Electrodes Versus Sodium Hydroxide Concentration Wt%

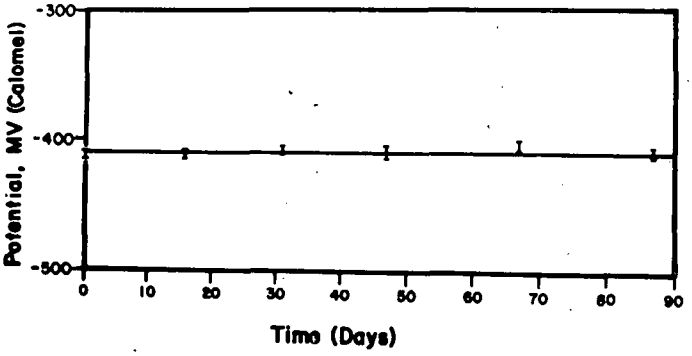

FIGURE 5

Variation of Mo/MoO_3 Electrode Potential With Time Measured in Saturated $Ca(OH)_2$

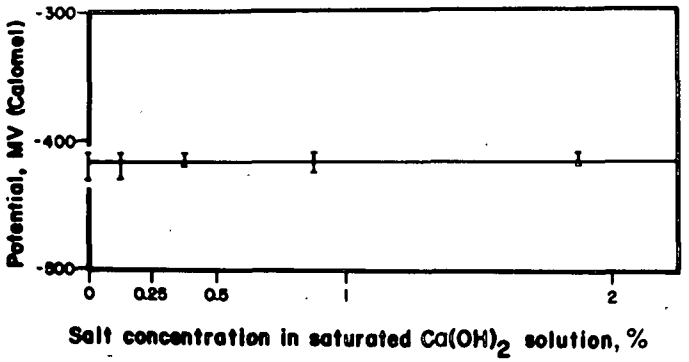

FIGURE 6

Potentials of Mo/MoO_3 Electrodes as a Function of NaCl Concentrations in Wt%

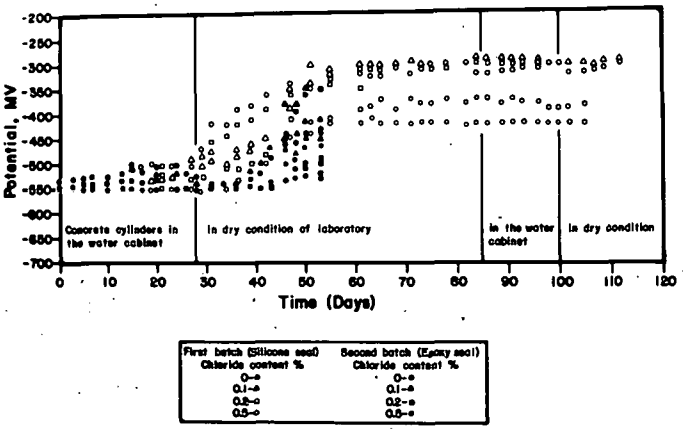

FIGURE 7

Plot of Electrode Potentials Compared to Copper/Copper Sulfate as a Function of Time

Conclusion

The present knowledge of electrochemistry of steel in concrete has verified the importance of such factors as chloride effects on passive layer and its reaction with cement, access of oxygen to the embedded steel and moisture content. More research is underway to better determine these effects and clear this corrosion phenomena. For OTEC plants, it would be both logical and economical to provide a corrosion preventive technique together with a monitoring system. Cathodic protection for example is a reliable method which has already been used in offshore platforms.

References

1) Cady, P.D. "Corrosion of Reinforcing steel in Concrete—A General Overview of the Problem," ASTM STP629, pp. 3-11, 1977.

2) OTEC Power Technical and Economic Feasibility, Vol. II, Report No. NSF/RANN/SE/GI-C937/FR/75/1. LMSC-D056566, April 12, 1975.

3) Mozer, J.D., et al. "Corrosion of Reinforcing Bars in Concrete," ACI Journal Proceedings, Vol. 62, No. 8, pp. 909-930, 1965.

4) Monfore, G.E. "The Electrical Resistivity of Concrete," Journal of the PCA-R&D Vol. 10, No. 5, pp. 35-48, 1968.

5) Gjorv, O.E., et al. "Electrical Resistivity of Concrete in the Oceans," Paper No. OTC 2803, Offshore Technology Conference, pp. 581-588, 1977.

6) Clear, K.C. and Hay, R.E. "Time-to-Corrosion of Reinforcing Steel in Concrete," Report No. FHWA-RD-73-32, Vol. 1, 1973.

7) Whiting, D. "Influence of Concrete Materials, Mix, and Construction Practices on the Corrosion of Reinforcing Steel," Materials Performance Vol. 17, No. 12, pp. 9-15, 1978.

8) Mehta, P.K. "Effect of Cement Composition on Corrosion of Reinforcing Steel in Concrete," ASTM STP 629, pp. 12-19, 1977.

9) Neville, A.M. Properties of Concrete. John Wiley & Sons, New York, 1975.

10) Ben Yair, M. "The Effect of Chlorides on Concrete in Hot and Arid Regions," Cement and Concrete Research, Vol. 4, No. 3, pp. 405-416, 1974.

11) Tremper, B. "Corrosion of Reinforcing Steel," Significance of Tests and Properties of Concrete and Concrete Making Materials, ASTM STP 169-A, pp. 220-229, 1966.

12) Berman, H.A. "Soldium Chloride, Corrosion of Reinforcing Steel, and the pH of Calcium Hydroxide Solution," ACI Journal Proceedings, Vol. 72, No. 4, pp. 150-157, 1975.

13) Reizin, B.L. "Depassivation of Reinforced Concrete Equipment by an Extra Anode Current," Protection of Metals, Vol. 6, pp. 510-512, 1970.

14) Shrier, L.L. Corrosion. Newnes-Brutterworths, London, 1976.

15) Heuze, B. "Cathodic Protection on Concrete Offshore Platforms," NACE, Corrosion/79, Paper No. 138.

16) Cook, H.K. and McCoy, W.J. "Influence of Chloride in Reinforced Concrete," ASTM STP629, pp. 20-29, 1977.

17) Hausmann, D.A. "Steel Corrosion in Concrete," Materials Protection, Vol. 6, No. 11, pp. 19-23, 1967.

18) Locke, C.E. and Siman, A. "Electrochemistry of Reinforcing Steel in Salt Contaminated Concrete," Presented at ASTM International Symposium on Corrosion in Concrete, Miami Beach, 1978.

19) Alekseev, S.N. and Rozental, N.K. "Characteristics of the Protective Capacity of Cement Concrete with Respect to Steel," Protection of Metals, Vol. 10, pp. 536-538, 1974.

20) Griffin, D.F. and Henry, R.L. "Effect of Salt in Concrete on Compressive Strength, Water Vapor Transmission, and Corrosion of Reinforcing Steel," ASTM Proceedings, Vol. 63, pp. 1046-1075, 1963.

21) Dawson, J.L., et al. "Electrochemical Impedence Measurements Applied to the Corrosion of Reinforcing Steel in Concrete," NACE, Corrosion/78, Paper No. 125.

22) Akimova, K.M. "Effect of Oxygen on the Corrosion of the Steel Reinforcement in the Presence of Chlorides," Protection of Metals, Vol. 13, pp. 157-159, 1977.

23) Dexter, S.C. and Culberson, C.H. "Global Variability of Natural Sea Water," NACE, Corrosion/79, Paper No. 227.

24) Bury, M.R.C. and Domone, P.L. "The Role of Research in the Design of Concrete Offshore Structures," Paper No. OTC 1949, Offshore Technology Conference, pp. 155-168, 1974.

25) Locke, C.E. and Dehghanian, C. "Embeddable Reference Electrodes for Chloride Contaminated Concrete," Materials Performance, Vol. 18, No. 2, pp. 70-73, 1979.

26) Every, R.L. and Banks, W.P. "Reference Electrodes in Acid and Base Systems," Corrosion, Vol. 23, p. 151, 1967.

27) Ives, D.J.G. and Janz, G.J. Reference Electrodes. Academic Press, New York, 1961.

DISCUSSION

A. Alexiou, Seagrant/NOAA: Can you say something about the effects of pressure and prestressing on the rates of corrosion of steel reinforced concrete in seawater.

C. Locke, University of Oklahoma: There has been little work done on the effect of hydrostatic pressure on the corrosion rate. The variables affected by hydrostatic pressure that might be important would be the mobility of the chloride ions diffusing to this steel and oxygen availability. In general, the problem of the corrosion rate below the surface of the sea is usually not as large as in the splash zone because of the limited availability of oxygen. The hydrostatic pressure of water would have little effect on the corrosion process. There has been little work done on a comparison of prestressed steel and nonprestress steel.

J. Rynewicz, Lockheed: If you were in a position to make a decision on mix material and a protection approach, and it was your responsibility to make that decision for the 10/40 platform to provide it with a 10-year life or 30-year life—whatever the criteris is—what would your recommendations be if you have to do that 12 months from now?

C. Locke: I would depend on specification of the concrete mix design, construction practice, and cathodic protection. The concrete mix should have a low water-to-cement ration (less than 0.5) and a high cement factor (at least 7 sacks per cubic yard of concrete). A sulfate resistive cement like Type V or Type II with pozolan aggragate should be used. The concrete cover over the reinforcing steel should be at least 50 mm. and in the splash zone 75 to 100 mm. The cathodic protection system's primary function is to protect the metallic components exposed directly to sea and not covered by concrete. Most of these would be in contact with the reinforcing steel and, because of the different environment, would be anodic and would corrode at a very rapid rate unless properly protected. The cathodic protection system could be the sacrificial anode or impressed current design.

J. George, JHU/APL: It seems to me that with the post-tension concrete structural design that there would be a tendency to keep the cracks from forming during all service loadings. This should minimize some of the problems; is that true?

C. Locke: That is the practice now used in the large concrete structures put in the North Sea. They do use post tensioned concrete to prevent cracks from forming but they do have problems with the post tensioned cables. Some of these problems are as a result of the grout used around the cables.

P. Walsh, Value Engineering: We all know that there are concrete structures in the sea that have been there 40 or 50 years. I am thinking particularly of some of the large structures that were built in the North Sea during World War II and they seem to be surviving happily. Would you comment on that please?

C. Locke: That is true to some extent, although some of these structures you speak of are not necessarily in very good shape. I recently attended a conference in which one of those structures built during World War II was discussed. It is presently being investigated as to the corrosion progress, chloride content in the concrete, etc. This structure has evidences of severe corrosion of the reinforcing steel. However, what you'r speaking of does point up some of the items that indicate our lack of knowledge concerning this complicated corrosion phenomena.

THE EFFECTS OF BIOFOULING AND CORROSION ON HEAT TRANSFER MEASUREMENTS

B. E. Liebert, L. R. Berger, H. J. White,
J. Moore, Wm. McCoy, J. A. Berger, and J. Larsen-Basse
University of Hawaii
Honolulu, Hawaii 96822

Abstract

Four different metal heat exchanger tubes were deployed on a submerged buoy 40 ft. below the surface 1000 ft. from Keahole Pt., Hawaii. Nominal sea water velocity of 6 ft./sec. was maintained on the internal surfaces of these tubes from Nov. 6, 1978 through March 9, 1979. Periodic samples from titanium, stainless steel, aluminum, and copper-nickel tubes were removed for biological and corrosion analyses. Weekly measurements of changes in heat transfer were made on each sample and attempts are made to correlate observed biofouling and corrosion data with changes in heat transfer. A discussion of predictive techniques for changes in heat transfer is also discussed.

Introduction

The success or failure of OTEC plants for large-scale power generation is critically dependent on the efficiency of heat transfer between the warm and cold ocean waters and the working fluid used to drive a turbine. This is a much more important consideration for the OTEC concept than for conventional power plants because of the relatively small temperature difference available, which results in a Carnot efficiency of only about 6%.

In order to determine the suitability of the OTEC concept for power generation, it is necessary to understand what happens to the metal surfaces of heat exchangers when exposed to flowing sea water over an extended period of time.

Basically, two processes, which may or may not be independent, can occur. First, living organisms in the ocean water can attach themselves to any available substrate resulting in the formation of films that increase the thermal resistance of the heat exchanger. Second, corrosion of metal surfaces may result in either premature failure of the heat exchanger module or the formation of thermally insulating inorganic films, or combination of both.

The important property that must be maximized is the rate of heat transfer from one fluid, through the walls of the heat exchanger tube, to the other fluid. The presence of microscopic films of either biofouling or corrosion products can significantly increase the fouling resistance, R_f.

In the experiments presently being conducted at Keahole Pt., Hawaii, as well as at other sites, the fouling resistance of a number of metal alloys is being measured under simulated OTEC conditions to determine the degradation of heat transfer as a function of time. The major goal of such research is to qualify metals for OTEC heat exchanger applications. This means suitable metals must be found that possess an acceptably low corrosion rate and either be resistant to biofouling or to the mechanical or chemical cleaning techniques used to remove the biofouling layer. In addition, the mechanisms of biofouling and corrosion should be understood so that cleaning or control techniques can be optimized and predictive models of biofouling activity and corrosion can be formulated.

Our immediate goal has been to find ways to measure quantitatively the nature and amount of early biofouling and corrosion under simulated OTEC flow conditions and to be able to relate these changes to measurements of R_f.

The four alloys considered in this investigation include 5052 aluminum (Al), grade 2 titanium (Ti), AL-6X stainless steel (SS), and CA706 copper-nickel (Cu-Ni). In addition to these four, serious consideration is being given to Alclad aluminum alloys because of their resistance to pitting and crevice corrosion, although evaluation of this class of materials under OTEC conditions has not yet begun.

Each of these alloys has advantages and disadvantages for OTEC applications. The greatest advantage of Al is that it is inexpensive and appears to corrode at an acceptably low rate.[1,2] However, biofouling films readily form and its hardness is fairly low, which has caused some concern as to its ability to resist mechanical cleaning for removal of the biofouling films. Neither Ti nor SS corrode at a significant rate under these conditons, although both form biofouling films, and their hardness is sufficiently high to resist all but the most vigorous mechanical cleaning techniques. Unfortunately, both are significantly more expensive than Al. Cu-Ni is unique among the other alloys in that the growth of biofouling films is significantly less than for the other three metals, although it does corrode at a fairly substantial rate.

Experimental Methods

Details of some of the methods employed in this work were discussed at the Jan. 1979 OTEC Workshop on Biofouling and Corrosion and will be found in the proceedings of that Conference.[2,3,4]

The Carnegie-Mellon University (CMU) heat transfer measuring device was used to measure the influence of both biofouling and corrosion on the rate of heat transfer through the four metals used in this investigation. The combined thermal resistance of the turbulent convective flow, biofouling layer and/or corrosion layer was determined by repeatedly measuring the temperature decay in a preheated hollow copper cylinder that surrounds, and is thermally bonded to, each of the simulated heat exchanger tubes.[5,6] This measurement was repeated from four to sixteen times for each data point, and no data point has been discarded.

Up until Nov. 15, 1978, Ramapo flowmeter data was available from the buoy; thereafter, all flowmeter signals were lost. Flowmeter data was not available again until Feb. 9, 1979; with these and all subsequent flow rates being obtained by divers with a

portable Ramapo flowmeter. Hence, unless a diver-obtained flow rate was available for the day on which a heat transfer experiment was conducted, the influence of a relatively large flow velocity uncertainty must be added to the standard deviation in R_f in order to obtain a proper estimate of the total error[7].

The portable flowmeter was calibrated in the laboratory by repeatedly recording the time required to fill a measured volume that was downstream of a fluid circuit that contained the flowmeter and a flow restrictor valve (for varying the flow velocity). These measurements were then repeated without the flowmeter in the fluid circuit in order to correct for the in-line effect of the flowmeter. Finally, a salt water/fresh water density correction is utilized to yield the final relationship between velocity and flowmeter voltage.

Sample coupons were placed downstream of the CMU heat transfer instrument but upstream of the pump. The coupons were cleaned at the same time, and in the same manner, as the heat transfer section using a M.A.N. brush modified to spin while being lowered into the tubing sections. This modification reduced the number of cleaning passes required to achieve an acceptable reduction in R_f from twenty to two. After removal for biological and corrosion analyses, the coupons were either drained and frozen or filled with a 2.5% glutaraldehyde-sea water mixture, depending on the type of analysis desired.

Except for SEM and x-ray fluorescence studies, the fouling film was removed from the tubing as follows. One-inch sections of tubing were sealed with silicone rubber caps after the addition of 0.5 ml ballitini-type micro-glass beads (Scotch-Lite, MMM Co.) and 3 ml filtered double distilled water. The sample was then placed in a type Vi2 vibrating ballistic disintegrator (RHO Scientific Co., Commack, NY) and processed at approximately 100 Hz for 5 minutes. After allowing the glass beads to settle, 2.5 ml of the turbid liquid was removed from the sample. Two ml filtered dH_2O was then added to the sample and the film removal procedure was repeated. The sequence was repeated a third time and the aqueous suspensions were pooled.

One ml aliquots of the film extract were hydrolyzed in 4N HCl at 121°C for 1 hour. The hydrolysate was then dried over P_2O_5 and NaOH in vacuo, then taken up in 0.15 ml water. The dry weight of the film (less carbonates) was computed from a portion of the hydrolysate and is reported in mg/cm^2 of inner surface of the tube.

Organic carbon and total nitrogen assays were done on aliquots of the same hydrolysate in an automatic carbon-nitrogen-hydrogen analyzer (Hewlett-Packard Co.) Values obtained were converted to $\mu g/cm^2$ of inner surface of the tubes.

Aliquots of the film extract were analyzed fluorometrically for protein by the method of Robrish, et al.[8]

Coupons from sections of tubes were coated with carbon for EDAX analysis. Background and overlapping non-Kα-band quanta were subtracted by computer.

A portion of the loose corrosion film on the Cu-Ni coupons was lifted off the interior surface, mounted perpendicular to the SEM holder, and coated with carbon for film thickness measurements.

Experimental Results

The water temperature at the buoy varied between 23 and 28°C during this portion of the deployment. This is shown in Fig. 1 along with the salinity, pH, alkalinity, dissolved oxygen, nitrate, and phosphate levels over the same time period.

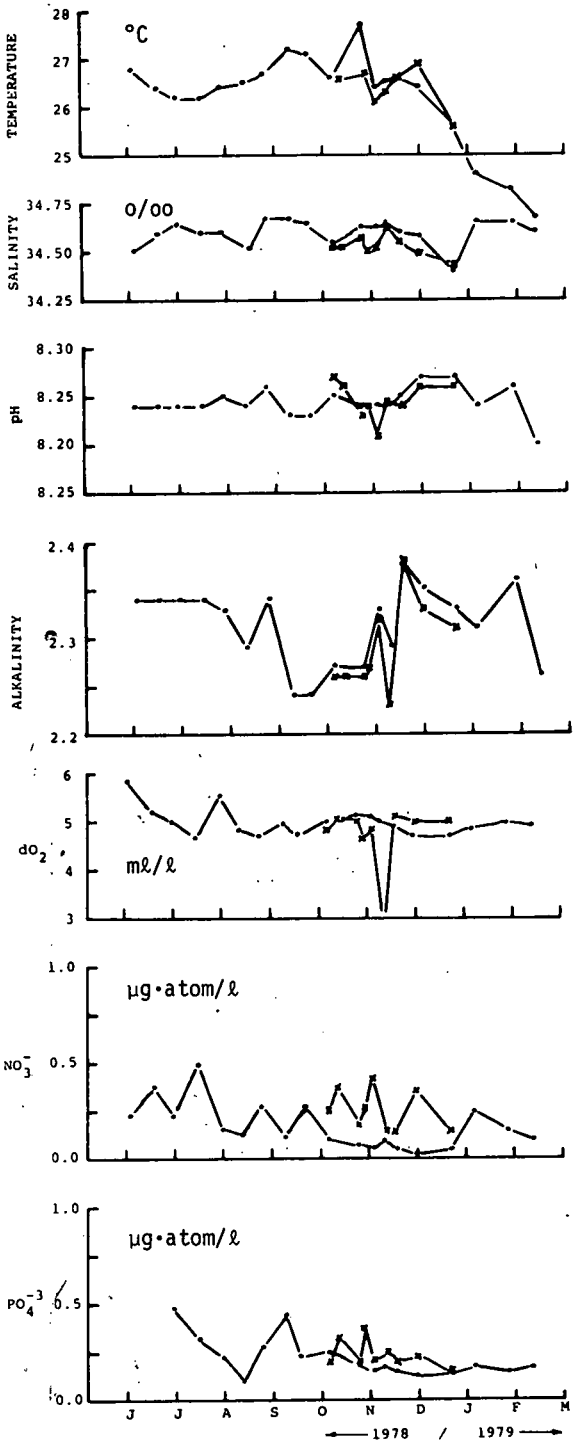

Fig. 1 Variation of the temperature, salinity, pH, alkalinity, dissolved oxygen, nitrate, and phosphate levels at Keahole Pt., Hawaii.
x = measurement taken at the underwater buoy
• = measurement taken at a site near shore

Flow velocity measurements are given in Table 1 for the four different instruments. The jump in velocity for the Cu-Ni and SS instruments was due to a change in a flow restrictor valve on the pump.

Table 1 Velocity Measurements, ft./sec.

Days in Flow	Al	Ti	CuNi	SS
2	5.89	--	--	--
3	R.P.*	7.58	7.15	--
7	--	--	--	7.25
8	5.65	--	--	--
9	--	7.64	--	--
93	--	--	R.P.	--
95	5.97	6.86	7.59	7.03
100	--	--	R.P.	R.P.
102	6.34	6.75	7.04	7.04
102	--	--	R.P.	R.P.
102	6.24	6.82	7.49	7.08
106	--	--	R.V.**	--
107	--	--	--	R.V.
109	6.15	6.98	8.97	8.97
115	R.P.	--	--	--
119	--	--	R.P.	R.P.
124	5.73	6.91	9.01	9.01

* indicates replacement of the pump
**indicates replacement of the pump and flow restrictor valve

The change in thermal resistance from its initial deployment value, the fouling factor R_f, is shown in Fig. 2 for the four metals studied, along with the total film weight during the first 101 days of the experiment. The R_f data have been normalized to 21°C and 6 ft/sec[9].

Typical values of the error in R_f are shown in Fig. 3 for the SS instrument. The error bars for the data gathered up to Nov. 15, 1978 (9 days in flow) represent one standard deviation in the value for R_f, assuming a normal error distribution. Most of this error is due to the thermopile reference cylinder being out-of-tune with the preheated copper cylinder when both are subjected to ocean temperature fluctuations.

As shown in Fig. 2, except for Al, the changes in the total mass of the film closely follow those in R_f. In the case of Al most of the hydrated aluminum oxide layer is probably not removed by the brushing procedure in the field. Therefore this layer does not contribute significantly to the changes in R_f.

Fig. 4 shows the results of the analyses of organic carbon and total nitrogen. The data, again, are plotted together with the R_f values vs time. When the tubes were cleaned at either 59 days, 94 days, or both, there were drops in carbon and

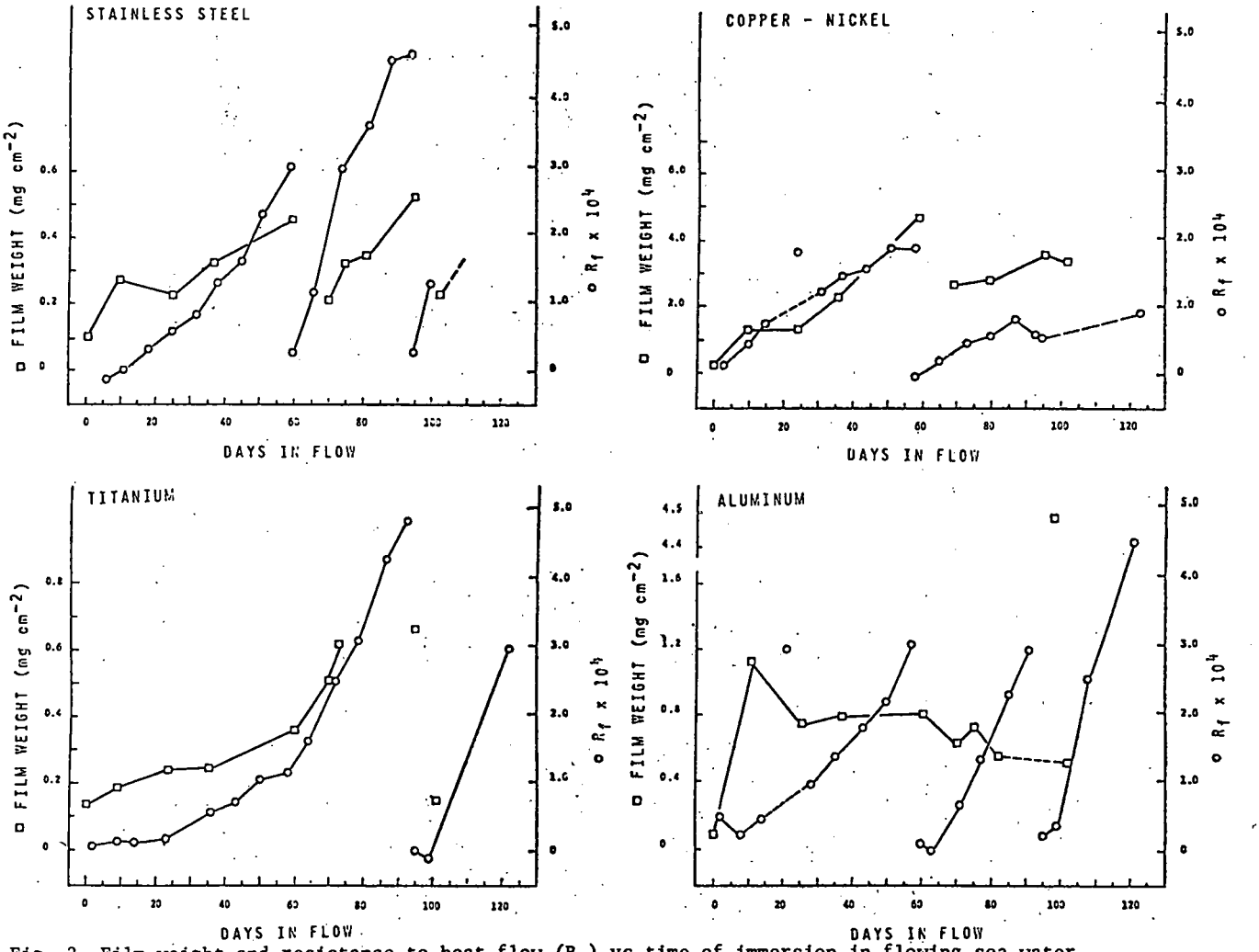

Fig. 2 Film weight and resistance to heat flow (R_f) vs time of immersion in flowing sea water.

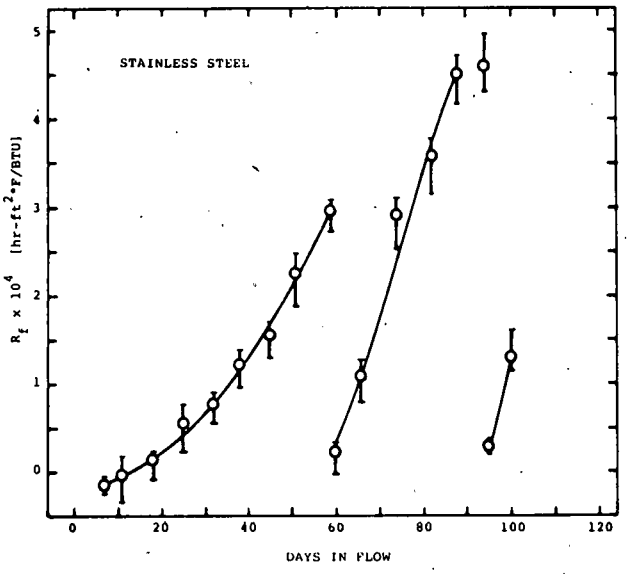

Fig. 3 Estimates of error of R_f for stainless steel. Typical of that found for Ti, Al, and Cu-Ni.

nitrogen which paralleled the drops in R_f. This correlation is least evident in the Cu-Ni tubes. Whether this implies that the biofouling is not removed along with much of the corrosion layer during the cleaning is not certain. There is a 10 day period between cleaning and the next sample during which considerable corrosion of the Cu-Ni could have taken place. The "after-brushing" samples are presently being analyzed.

The increase with time in the amount of protein correlates with R_f for all metals except Cu-Ni, as shown in Fig. 5. However, the amounts of protein detected in the Cu-Ni tubes are at the lower limits detectable by the analytical procedure. Nevertheless, SEM micrographs clearly show the presence of biological fouling on the Cu-Ni tubes after 94 days' immersion.

The change in the thickness of the Cu-Ni corrosion product with time in flow is shown in Fig. 6. The linear increase in thickness parallels the linear increase in R_f for times earlier than the first cleaning. After brushing, which restored R_f to its original value, the measured film thickness did not

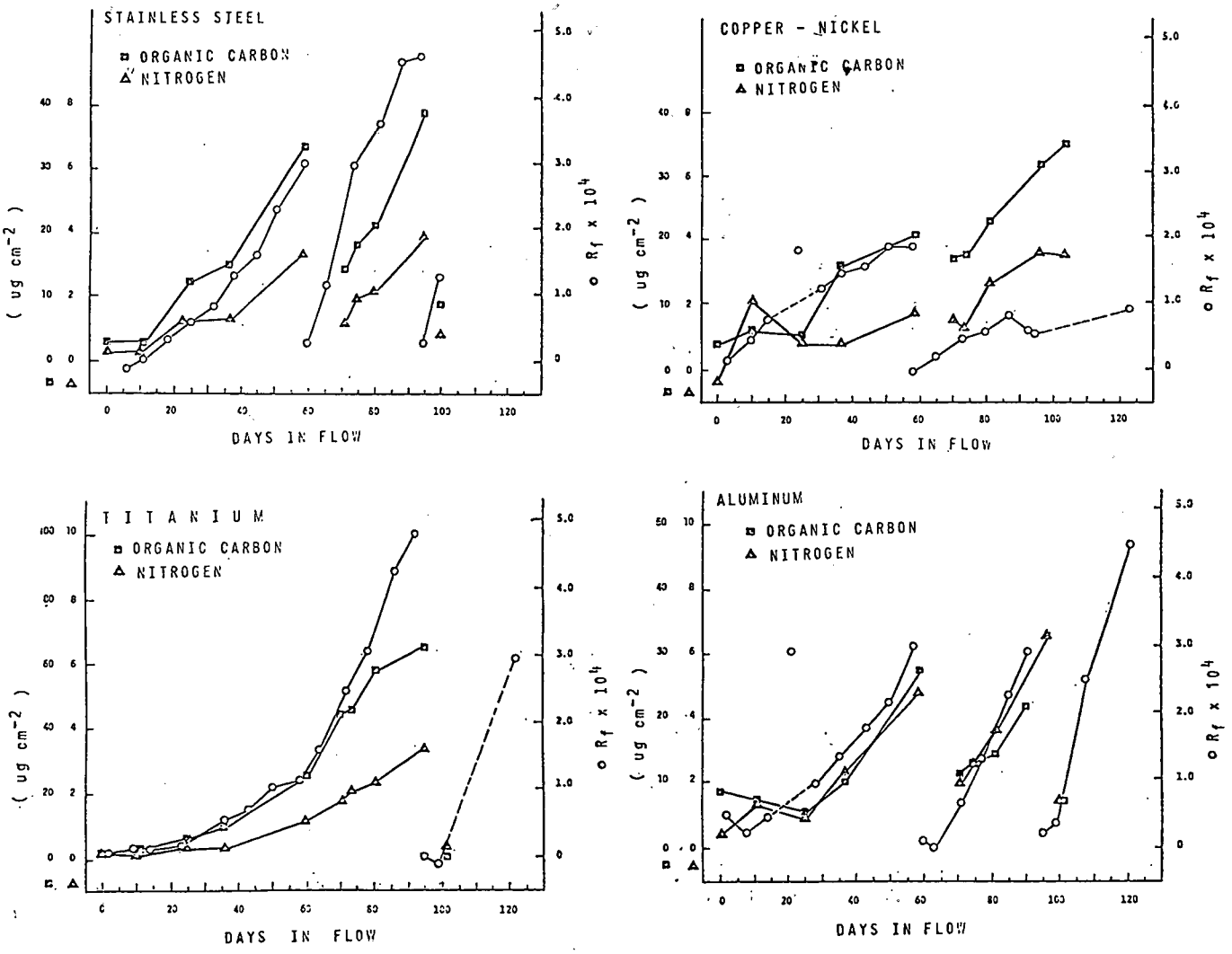

Fig. 4 Organic carbon, total nitrogen, and resistance to heat flow (R_f) vs time in flowing sea water.

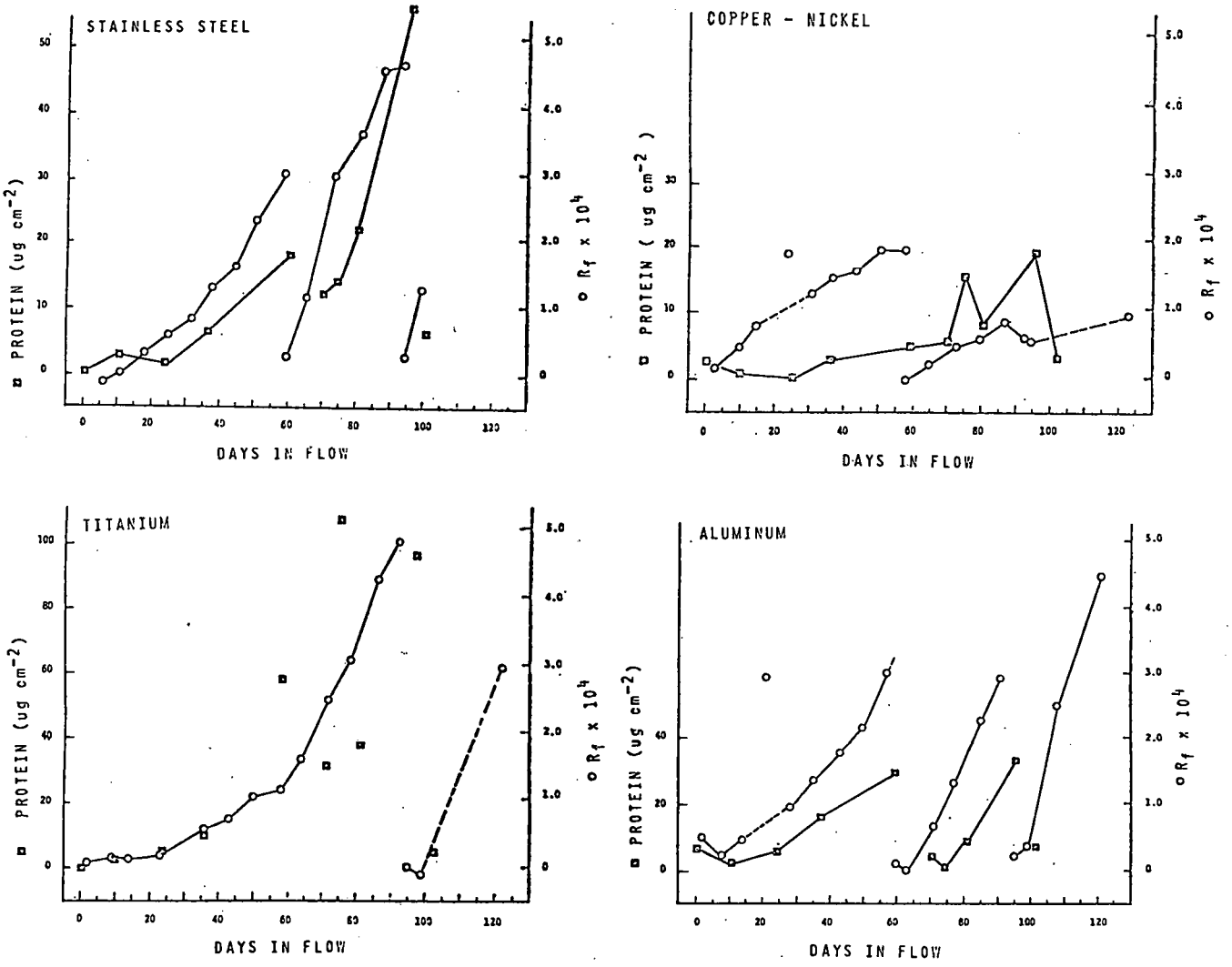

Fig. 5 Film protein and resistance to heat flow (R_f) vs time in flowing sea water.

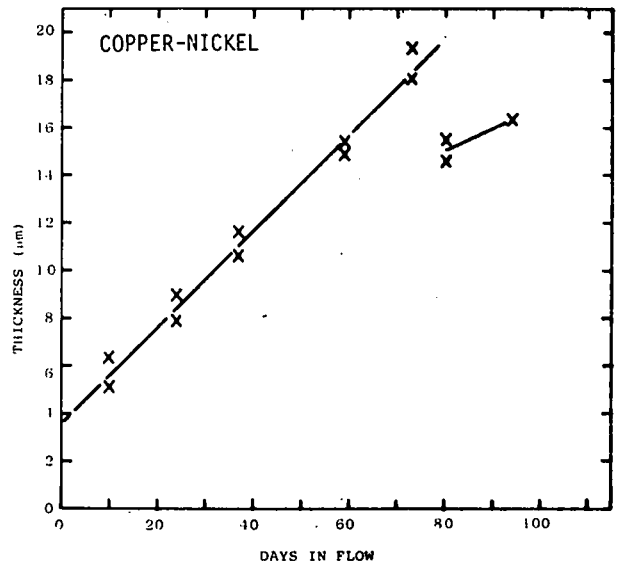

Fig. 6 Thickness of Cu-Ni corrosion film thickness measured in the SEM vs time in flowing sea water.

decrease back to its original value; rather, it decreased only slightly.

It is possible that the cleaning of the heat transfer instrument resulted in a more complete removal of the film compared to the samole coupon test section and that the film which was removed for thickness measurements was not representative of the entire inside surface. These results are in general agreement with the dry film weight measurements of Cu-Ni shown in Fig. 2.

The nature and color of the Cu-Ni film was found to change substantially with exposure time. Initially, a blue-green film, containing a high percentage of Cl over a "rust-colored" film, was present. As time increased, the blue-green regions were replaced by a loosely adherent "rust-colored" film that gradually became darker with time. Finally, after 94 days the film returned to the light "rust-colored" appearance of earlier times but was much more tightly adherent than before and could only be removed with difficulty.

The percentage of Fe present in the film increased with time, reaching values of 65% as indicated by the ratio of counts from the EDAX fluorescence analysis. This result is in agreement with recent work

on copper-based alloys using Auger electron spectrometric analysis.[10]

All the Al samples showed the familiar "mud-cracked" appearance seen before.[2] Although the dry film weight of Al, shown in Fig. 2, apparently reaches a limiting value within the first 10 days of exposure, the film appeared to be thicker at the end of the exposure, under the SEM, than after the first 10 days. This is also in agreement with the size of the platelets formed by dehydration of the gelatinous film, which was found to increase with time. No evidence of pitting was found in any of the Al specimens examined.

EDAX analysis revealed that the corrosion film of the Al also had become greatly enhanced in Fe during exposure. Whereas a freshly exposed bare metal substrate showed Fe only at the background level, the corrosion products had an Fe count actually higher than the Al count. The source of this large enhancement in Fe is not clear at this time.

Laboratory experiments of the same alloy, but in sheet form, carried out in stagnant, aerated sea water did not produce the expected continuous "mud-cracked" pattern seen in the coupons removed from the buoy. Rather, only a relatively small number of these isolated areas were found, although each had an associated central region containing a high concentration of Fe. Fe seems to be necessary for the growth of the thick hydrated oxide layer found when Al is exposed to sea water.

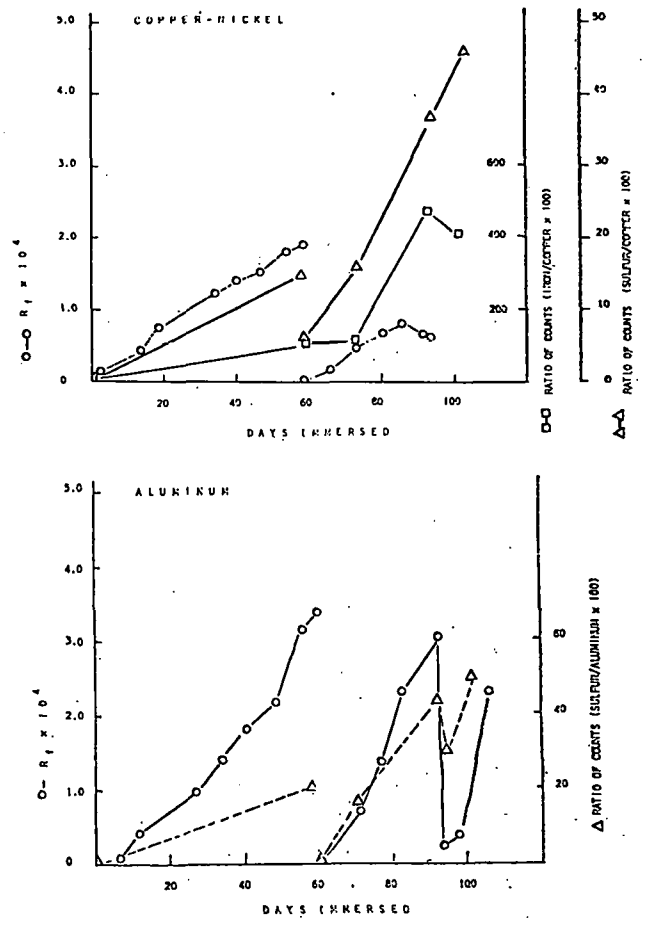

Fig. 7 Resistance to heat flow of Cu-Ni and Al tubing and elemental analysis of tubing surfaces by x-ray fluorescence analysis.

Fig. 7 shows the results obtained from EDAX analysis of the inner surfaces of the Cu-Ni and Al tubes. The ratios of both S and Fe to that of Cu in the Cu-Ni tubes and of S to Al in the Al tubes are plotted with the R_f values. The patterns observed with S were also similar to those of P, Ca, and Si though the amounts of the latter elements were significantly lower than those for S. None of the measured elements appeared to increase significantly for the Ti and SS tubes during the experimental period nor do the data correlate in any obvious way with R_f values.

Discussion

Since neither Ti nor SS corrode under these conditions, the increase in R_f must be solely due to the colonization and growth of a biofouling layer. In contrast, Cu-Ni shows very little biofouling; consequently the increase in R_f with time must be dominated by the formation of a corrosion product layer. Al, on the other hand, forms both corrosion and biofouling films simultaneously; however, based on the results of Fig. 2, the influence of the corrosion film on R_f appears to be negligible compared to that of the biofouling film. Therefore, the increase in R_f with time for Al should be similar to that found for Ti and SS.

How can these changes in R_f be justified in terms of what is physically known about the systems in question?

The rate of growth of biomass under conditions of a constant supply of nutrients, unimpeded growth, and continuous removal of waste products, is similar to that found for a first-order autocatalytic chemical reaction; i.e., the rate of increase in the biomass is proportional to the amount of biomass at any instant in time:

$$dM/dt = \mu M \qquad (1)$$

This may be integrated to yield (for a constant μ)

$$M = M_o \exp(\mu t) \qquad (2)$$

where M_o is the amount of biomass at time = 0 and μ is the specific growth rate constant.[11] This relationship predicts that, for unimpeded growth, the amount of biomass should increase exponentially with time with the biomass doubling time given by:

$$t_d = \ell n\ 2/\mu = 0.693/\mu \qquad (3)$$

For OTEC conditions, the growth constant μ will be influenced by the nutrient content in the water, how fast waste products are removed, temperature, etc. In fact, μ should be exponentially dependent on temperature over the limited OTEC temperature range, i.e.

$$\mu = \mu_o \exp\text{-}(Q/RT) \qquad (4)$$

where μ_o is a constant, Q is the activation energy for growth, R is the gas constant, and T is the absolute temperature. This equation predicts that the rate of fouling of the cold water condenser may be much less than that of the warm water evaporator, unless the higher nutrient concentration of the cold water increases the growth rate to compensate for the reduced temperature.

Since measurements of R_f were obtained with a temperature variation of only a few degrees, the

effect of temperature on the growth rate of biomass is not expected to be significant in this experiment.

Eqn. 2 may be rewritten:

$$\log M = \log M_o + (\mu/2.303)t \qquad (5)$$

Therefore, since R_f is known to be proportional to the film thickness[6], a plot of log R_f vs time should result in a straight line with a slope of $\mu/2.303$ for the Al, SS, and Ti alloys. The results are shown in Fig. 8.

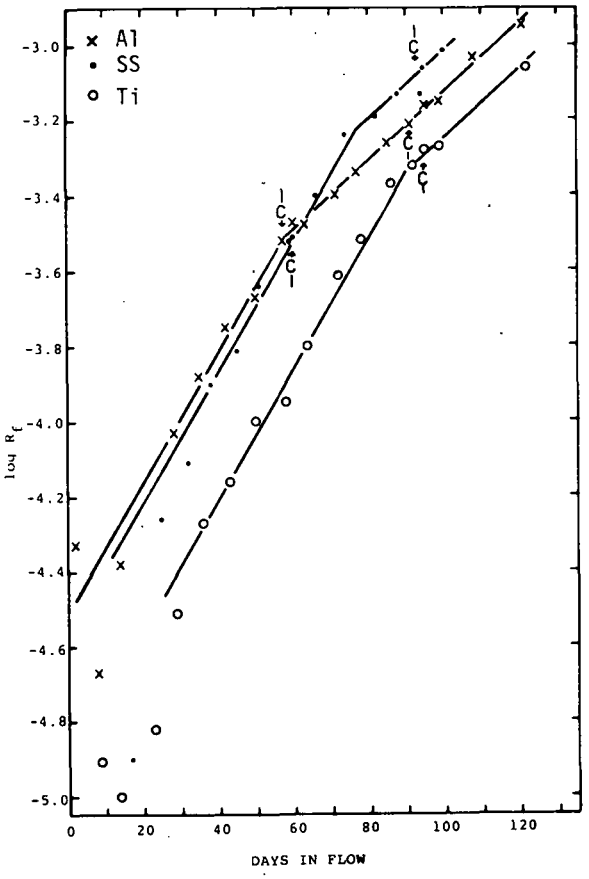

Fig. 8 Logarithm of resistance to heat flow (R_f) vs time in flowing sea water. The "C" indicates the point at which the tube was cleaned. After cleaning the measured value of R_f was adjusted upward to coincide with the value it would have had if the tube had not been cleaned.

All three alloys show an initial "lag-period" of 30-40 days in which the data are sufficiently scattered to prevent any growth rate from being assigned to the initial period. The initial period for the Ti tube is significantly longer than that for the Al or SS tubes, which are seen to behave similarly. This may be due to the difficulty of colonization on the relatively smooth, inert surface of Ti compared to the rough surface of SS and the gelatinous corrosion film present on Al.

After the initial period, however, all three alloys foul at nearly identical and constant rates indicating that the growth is indeed exponential. The change in R_f with time, obtained by a least squares fit to a log R_f vs time plot, is given by:

$$R_f(Al) = 3.30\times10^{-5}\exp(3.87\times10^{-2}t) \qquad (6)$$

$$R_f(SS) = 2.45\times10^{-5}\exp(4.26\times10^{-2}t) \qquad (7)$$

$$R_f(Ti) = 1.23\times10^{-5}\exp(4.08\times10^{-2}t) \qquad (8)$$

where R_f is in hr-ft^2°F/BTU and t is in days. The biomass is predicted to double in just over 17 days from the heat transfer results. If the results of the change in film weight, organic carbon, and nitrogen for the Ti tube (shown in Figs. 2 and 4) are plotted in this fashion, a doubling time of 19 days is obtained from the change in both organic carbon and nitrogen but 38 days from the change in film weight. This suggests that changes in film weight may be measuring a different effect than changes in R_f, organic carbon, and nitrogen.

After cleaning by two passes of the modified M.A.N. brush, indicated by a "C" on the figure, all three alloys show a drop in R_f to the original low value. However, if the new R_f values are moved upward to coincide with what R_f would have been if no cleaning had occurred, as is done in Fig. 8, the growth rate again is found to be exponential, but with a growth rate about one-half of the previous rate for Al and Ti. SS, on the other hand, continues to foul at the same rate for about 15 days, as if cleaning had not occurred. After 15 days, however, the growth rate on the SS tube becomes nearly identical to that found on the Al and Ti tubes.

After the Al and SS tubes were cleaned for the second time, the growth rate did not change, suggesting that the primary biofouling film remaining on the interior of the tubes after cleaning had stabilized. The change in the modified value of R_f after cleaning is given by:

$$R_f(Al) = 9.12\times10^{-5}\exp(2.09\times10^{-2}t) \qquad (9)$$

$$R_f(SS) = 1.20\times10^{-4}\exp(2.08\times10^{-2}t) \qquad (10)$$

$$R_f(Ti) = 9.12\times10^{-5}\exp(1.83\times10^{-2}t) \qquad (11)$$

with a biomass doubling time of about 34 days. In this case, the doubling time calculated from the change in film weight, organic carbon, and nitrogen for the SS tube (only four points are available) is found to be 21, 20, and 15 days, respectively.

On the basis of these results, it does not seem practical to attempt to achieve a smoother surface finish on the interior of the tubes by another processing operation since all three surfaces of the Al, SS, and Ti alloys foul at approximately the same rate after the primary biofouling film has been established. Even after cleaning, the rate of growth on the three alloys is essentially the same.

Since the biofouling on the Cu-Ni tube is significantly less than on the other metals, and its influence on R_f can be neglected compared to the effect of the corrosion products, it is expected that the increase in R_f with time would show a different behavior than for the Al, SS, and Ti alloys. The increase in R_f (Fig. 2) and film thickness (Fig. 6) is linear with time, rather than exponential.

A linear growth rate is expected if the film that forms on the surface is porous but remains attached to the metal substrate, permitting the growth rate to be interface, rather than diffusion, controlled.

The Cu-Ni corrosion film was found to have numerous cracks and be rather porous when viewed in the dehydrated condition in the SEM. This morphology would permit the easy access of O_2 to the Cu-Ni interface, resulting in a linear growth rate.

The Cu-Ni dried film density was estimated to be 2.6 g/cm^3 from the film weight and thickness measurements given in Figs. 2 and 6, respectively. Since the film has a "rust-colored" appearance, along with a high concentration of Fe, this estimate compares favorably with the density of the principal component of "rust", $Fe_2O_3 \cdot xH_2O$, which is reported to fall between 2.44 and 3.60 g/cm^3.[12]

An estimate of the thermal conductivity of the Cu-Ni corrosion product film can be made from the influence of film thickness on R_f. A value of 0.23 BTU hr^{-1} ft^{-1} °F^{-1} is obtained, which compares with 235, 10, and 0.35 BTU hr^{-1} ft^{-1} °F^{-1} for Cu, CuO, and H_2O, respectively.[12] This suggests that most of the thermal resistance may be due to a stagnant water film, which is essentially equivalent to a thicker sublaminar boundary layer.

There is a significant difference in the ratios of carbon to nitrogen in the fouling layer of the Cu-Ni tubes and those on the other metals, as shown in Fig. 9. This is consistent with the report of Gerchakov, et al.[13], who proposed that organisms able to colonize Cu-Ni surfaces produce more extracellular matter than those that colonize stainless steel and glass surfaces. These polymeric films are in large part carbohydrate and low in nitrogen.

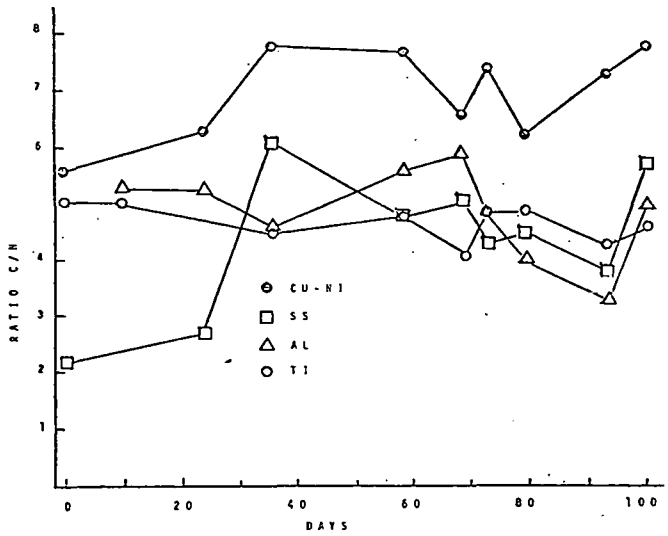

Fig. 9 Ratio of carbon to nitrogen in the fouling layer of the four metal tubes vs time of immersion in flowing sea water.

Fig. 10 shows the trend in the influence of the amount of organic carbon on R_f for the four metal alloys. Cu-Ni and Al are shown both before [1] and after [2] cleaning. These results suggest that the nature of the biofouling film that forms on SS and Al is different than that found on Ti since any amount of organic carbon present on Ti results in a value of R_f about one-third of that for SS and Al. It is not clear what is responsible for this difference in behavior at this time.

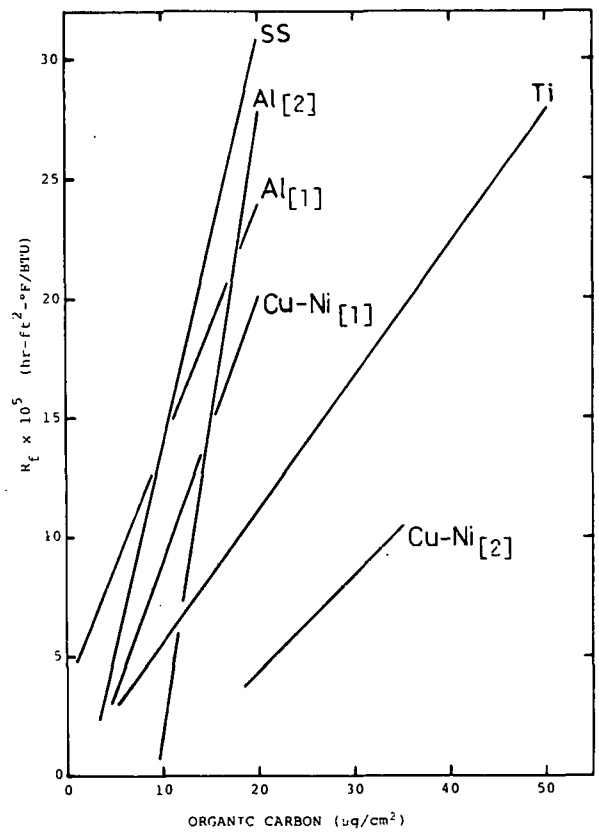

Fig. 10 The trends in the resistance to heat flow (R_f) vs organic carbon in the fouling layer. The results for Cu-Ni and Al are shown before [1] and after [2] cleaning.

Summary

- The weight of the film, organic carbon, total nitrogen, and protein in OTEC tube samples can be correlated to the fouling resistance, R_f.
- The dry weights of the film, which may include biofouling and/or corrosion products increase with R_f in all metals tested except Al.
- The parameters that measure biofouling, i.e. organic carbon, nitrogen, and protein, correlate to a greater or lesser degree with R_f for all metals.
- The ratio of C:N in Cu-Ni fouling is higher than that for the other metals.
- Biofouling increases exponentially with time after a delay period of 30-40 days.
- The growth rate of biomass is identical in Al, SS, and Ti tubes and is responsible for the increase in R_f with time.
- The corrosion film on Al does not influence R_f to any measurable degree.
- The corrosion film on Cu-Ni increases linearly with time, has an effective thermal conductivity about that of water, and is responsible for the increase in R_f with time.

- Certain elements accumulate in the corrosion layers of Cu-Ni and Al that may be used to indicate fouling and perhaps changes in R_f.

- Fe is present in high concentration in both the Cu-Ni and Al corrosion products.

- The fouling resistance of all four metal tubes is able to be reduced to its initial value with only two passes of a spinning M.A.N. brush.

Future Work

The present Keahole deployment No. 3 is continuing although, due to signal transmission problems, data has not been acquired since Mar. 9, 1979. Water flow through the test sections is being maintained despite periodic outages of up to 53 hours on one occasion. R_f data should again be available toward the end of May with the installation of a new signal cable. Further cleaning experiments will be attempted after successful data acquisition.

Additionally, the State of Hawaii has funded the installation of a 3-inch pipeline, 1500 ft long with a capacity of 50 gal/min, between the present submerged buoy location and a shoreside location. Upon installation (July-Aug., 1979) this will permit comparative experiments of the effects of biofouling and corrosion on heat transfer between the sea water at the buoy site and that same water after being subjected to an 11 min traverse through the pipeline and pump system.

References and Notes

1. Brenda Little and Dennis Lavoie, *Gulf of Mexico Ocean Thermal Energy Conversion (OTEC) Biofouling and Corrosion Experiment*, Proceedings of the OTEC Biofouling, Corrosion, and Materials Workshop, Rosslyn, VA, Jan. 8-10, 1979.

2. Bruce E. Liebert, *Corrosion of Aluminum and Titanium at Keahole Point Over an Eight Month Period*, Proceedings of the OTEC Biofouling, Corrosion, and Materials Workshop, Rosslyn, VA, Jan. 8-10, 1979.

3. Hank White and Cullen Tendick, *Preliminary Results from Ke-Ahole Buoy Deployment #3*, Proceedings of the OTEC Biofouling, Corrosion, and Materials Workshop, Rosslyn, VA, Jan. 8-10, 1979.

4. L. R. Berger, W. F. McCoy, and J. A. Berger, *Biofouling Assays for OTEC Pipes*, Proceedings of the OTEC Biofouling, Corrosion, and Materials Workshop, Rosslyn, VA, Jan. 8-10, 1979.

5. John G. Fetkovich, *A System for Measuring the Effect of Fouling and Corrosion on Heat Transfer Under Simulated OTEC Conditions*, U. S. Energy Research and Development Administration Report, Contract No. E(1101) 4041, Dec. 1976.

6. J. G. Fetkovich, G. N. Grannemann, L. M. Mahlingam, D. L. Meier and F. C. Munchmeyer, *Degradation of Heat Transfer Rates Due to Biofouling and Corrosion at Keahole Point, Hawaii*, Proceedings of the Ocean Thermal Energy Conversion (OTEC) Biofouling and Corrosion Symposium, Seattle, WA, Oct. 10-12, 1977.

7. The measured flow rate variations, other than that attributed to equipment changes, are primarily due to the substantial changes in ocean current velocity that have been observed at the buoy (a calibration of the portable flowmeter yields a standard deviation of only ±0.1 ft/sec).

8. S. A. Robrish, C. Kemp, and W. H. Bowen, *The Use of O-phthalaldehyde Reaction as a Sensitive Assay for Protein and to Determine Protein in Bacterial Cells and Dental Plaque*, Analyt. Biochem. 84, 196 (1978).

9. This, in turn, requires the adoption of a steady-state convective heat transfer law. In particular, a value of 0.8 is utilized for the exponent of the flow velocity in this adopted law, which is only accurate for hydraulically smooth pipes.

10. J. W. Wilson, *Composition of Seawater Corrosion Product Films on Copper Base Alloys: Auger Electron Spectrometric Analyses*, Corrosion/79, NACE, Atlanta, GA, Mar. 12-16, 1979.

11. S. John Pirt, *Principles of Microbe and Cell Cultivation*, John Wiley & Sons, NY (1975).

12. *Handbook of Chemistry and Physics*, 48th ed.

13. S. M. Gerchakov, F. J. Roth, B. Sallman, and L. R. Udey, *Observations on Microfouling Applicable to OTEC systems*, Proceedings of the Ocean Thermal Energy Conversion (OTEC) Biofouling and Corrosion Symposium, Seattle, WA, Oct. 10-12, 1977.

Appendix

Days in Flow	Protein $\mu g/cm^2$	Total Nitrogen $\mu g/cm^2$	Organic Carbon $\mu g/cm^2$	Dry Weight mg/cm^2
Cu-Ni				
0	2.7	0.6	3.5	0.15
10	0.5	3.1	5.6	1.19
24	0.0	0.8	5.2	1.13
36	2.8	1.8	15.9	2.14
59*	5.0	2.7	20.5	4.59
70	5.2	2.5	16.7	2.57
73	15.4	2.3	17.4	2.33†
80	8.1	3.7	22.9	2.66
94	18.7	4.6	33.5	3.5
101	2.9	4.5	35.0	3.35
Ti				
0	0.0	1.1	2.4	0.13
10	2.5	0.5	5.9	0.18
24	4.6	2.2	59.	0.24
36	10.5	1.6	9.6	0.24
59	58.5	5.1	24.9	0.35
70	32.0	8.6	44.1	0.50
73	107.0	10.4	45.2	0.62
80	38.0	12.5	56.8	0.72
94*	96.0	16.9	64.8	0.66
101	4.5	1.6	9.3	0.15
SS				
0	0.0	0.5	2.7	0.10
10	2.4	0.5	2.7	0.26
24	1.5	0.9	11.8	0.21
36	5.9	2.8	12.5	0.31
59*	18.5	7.0	33.5	0.45
70	12.4	2.8	11.4	0.20
73	14.0	3.7	18.1	0.31
80	21.8	4.3	21.1	0.33

Appendix (cont'd)

Days in Flow	Protein $\mu g/cm^2$	Total Nitrogen $\mu g/cm^2$	Organic Carbon $\mu g/cm^2$	Dry Weight mg/cm^2
SS				
94*	55.6	8.8	30.0	0.51
101	6.5	1.8	8.4	0.22
Al				
0	6.5	0.5	8.4	0.094
10	1.9	1.3	6.9	1.12
24	4.6	1.0	5.4	0.74
36	14.9	2.2	10.0	0.78
59*	20.9	4.9	27.5	0.79
70	3.5	2.0	11.7	0.63
73	0.8	2.6	12.8	0.72
80	7.8	3.6	14.4	0.56
94*	33.5	6.6	21.8	4.51
101	7.4	1.4	6.9	0.50

*indicates measurement before cleaning
†indicates sample partially spilled

DISCUSSION

S. Dexter, Univ. of Delaware: I would expect a change in slope upon cleaning at least the first time on the R_f curve you showed because you are starting off with a different surface. The question is, will that slope continue to change with repeated cleanings or do you reach a steady state where, after several cleanings, you always come back to the same condition?

B. Liebert: For the two metals that we have R_f data after several cleanings, aluminum and stainless steel, no steady state is found; the slope of R_f versus time continues to increase with time.

R. Mitchell, Harvard: The difference between the metals may become irrelevant after a couple of cleanings because the conditioning film of polymer that forms on the surface will coat all the metals, and the biofilm will no longer see the metal itself; all it will see is the conditioning film. The next question that has been raised is: can you use some parameter that is common to all of your systems to relate to the change in R_f? Initially, we thought we could use film thickness, and then we thought we could use ATP. It is obvious that neither of these work. We begin to see from your data that you can use total organic carbon. The next stage to that, and I think the reason you have confusion in some of your biomass data, is the total organic carbon is still far too crude to measure. What you need to know is the nature of the polymeric film, because what really goes on in that surface is that the microorganism has laid down a layer and after that polymeric film starts to fill in the matrix, the nature of that polymeric film may be consistently the same or may be different; we really don't know. You may get variations that we know nothing about. We need more sophisticated techniques now to measure the nature of that polymeric film, not simply to use total organic carbon; we also need to know about that conditioning film because your data seem to indicate that the conditioning film builds up with additional cleaning. You may, in fact, have the same sort of thing that I mentioned yesterday, that you have with dental placque in teeth. That is, the layer keeps building until eventually it becomes uneconomical from OTEC's point of view, and not very smart from the health point of view with teeth, to just keep cleaning. You have to go in there and clean that surface off. However, before you get to that point, you had better know the nature of that conditioning film. We know nothing about it, we also don't know if it keeps building or if it eventually reaches a plateau.

Question: Does copper-nickel have any substantial benefit from your point of view concerning the systems that build up on heat transfer surfaces?

B. Liebert: No. The only advantage copper-nickel might have is that the rate of increase in R_f with time is initially less than that of the other metals. Whether this behavior will remain the same at longer exposure times is not known at this time.

D. Sasscer, Univ. of Puerto Rico: It looks to me as though your after-cleaning curves were linear but with a different slope than before. Doesn't that indicate then that your slopes are getting higher or your periods between cleanings getting smaller?

B. Liebert: I'm not sure you can say the slopes of R_f are linear, but you are right about the slopes increasing after cleaning. This would, of course, result in the periods between cleanings becoming shorter in order to maintain a minimum R_f.

M. Kaminsky, Argonne National Laboratory: You indicated that the significant difference in the R_f-values for aluminum, stainless steel, and titanium (your Fig. 8) for different exposure times to seawater is due, in part, to differences in the initial surface roughness. Can you indicate quantitatively what the initial surface roughness of the aluminum, stainless steel, and titanium samples prior to seawater exposure has been?

B. Liebert: We do not have any quantitative information on the initial surface roughness of aluminum, stainless steel, and titanium. However, when examined under the SEM, it is very clear that the surface roughness of stainless steel is far greater than that of the titanium, which is greater than that of the aluminum. During the next deployment, we hope to use a titanium tube that has been machined to varying degrees of roughness in order to determine if surface roughness influences the nature and amount of biofouling.

EXPERIMENTS ON ULTRASONIC CLEANING OF A SHELL-LESS FOLDED-ALUMINUM-TUBE, OTEC HEAT EXCHANGER

Peter P. Pandolfini[+], William H. Avery,[++] and Freeman K. Hill[+++]

Applied Physics Laboratory
The Johns Hopkins University
Johns Hopkins Road
Laurel, Maryland 20810

Abstract

Experiments on ultrasonic removal of biofouling from geometrically similar models of a shell-less, folded-aluminum-tube, Ocean Thermal Energy Conversion (OTEC) heat exchanger were conducted in seawater at Ke-Ahole Point, Hawaii and in the Gulf of Mexico. In this type of heat exchanger, conceived by The Johns Hopkins University's Applied Physics Laboratory, the seawater is outside the tubes. For the Hawaiian experiments, an ultrasonic device was designed to be raised and lowered through the 1.25-in. clear space between the tube elements of the test model; this device developed an intensity of 0.43 W/cm^2 at 29 kHz on its surface. Results indicate that a resistance coefficient of 0.0002 to 0.0003 Btu^{-1}hr-ft^2-°F was maintained on the fouled surfaces with periodic ultrasonic radiation exposures (weekly, biweekly, and triweekly) over the twelve-week test period. In the Gulf experiments, aluminum tubes with 3.5 to 13 weeks of biofouling were cleaned in a 2.5-gal tank of water with acoustic transducers cemented to the bottom; an intensity of 0.72 W/cm^2 at 44 kHz was developed on the transducers' surfaces. Exposure times of 30 to 150 sec in the bath were needed to return the heat transfer characteristics of the fouled surfaces to a near clean condition. The results of these experiments offer encouraging evidence that a well-designed, low-cost cleaning system using ultrasonic radiation can be developed which will keep the fouling resistances developed during operation of OTEC-plantship heat exchangers at acceptable levels, probably averaging 0.0002 Btu^{-1}hr-ft^2-°F.

Introduction

An essential element in the implementation of Ocean Thermal Energy Conversion (OTEC) systems will be the development of heat exchangers which will yield minimum overall system cost. OTEC heat exchangers must operate at low temperature differences (5 to 12°F) between the working fluid and seawater, and must be designed to permit periodic removal of biofouling, which can degrade their performance.

In the heat exchanger concept being developed by APL, arrays of 3-in.-O.D. aluminum tubes are arranged in a horizontal multipass configuration (Refs. 1-4). Ammonia is used as the working fluid that flows inside the tubes. Seawater is pumped into head ponds above the tube banks and flows over the tubes by gravity. No heat exchanger shells are required; compartments in the concrete ship structure channel the water flow. In the evaporator, the ammonia is partially vaporized to 60 to 70% mass quality as it rises through successive horizontal passes connected by U-bends. Ammonia vapor, separated from the liquid by a demister, drives the OTEC power turbine. The ammonia is condensed in downward flow through an array of multiple horizontal passes similar to those of the evaporator. The liquid from the demister is mixed with that from the exit of the condenser and pumped back into the evaporator.

Biofouling of the heat transfer surfaces on the seawater side can seriously degrade the overall heat exchanger performance. Therefore, an OTEC power system should be designed to employ cost-effective measures to periodically remove the biofouling and maintain the fouling resistance at or below an acceptable level. A fouling resistance of 0.0002 Btu^{-1}-hr-ft^2-°F currently is used in projecting power system performance for the APL/OTEC concept. In the concept seven 3-in-O.D., multipass tubes are "nested" to follow parallel paths in one vertical plane to form an "element." This configuration provides a 1.25-in. clear passage between the elements to permit use of cleaning heads to remove exterior biofouling.

This paper describes experiments on ultrasonic removal of biofouling from geometrically similar models of a shell-less, folded-aluminum-tube, Ocean Thermal Energy Conversion (OTEC) heat exchanger conducted in seawater at Ke-Ahole Point, Hawaii and in the Gulf of Mexico. The object of these experiments was to test a practical, cost-effective method of biofouling control directly applicable to the APL OTEC power system.

Ke-Ahole Point Experiment

Test Equipment

The test equipment shown in Fig. 1 (and described further in Ref. 5) consists of an array of 5 rows of 10 horizontal tubes of Alclad 3004 H34 aluminum each 4-in. in diameter* and 18 in. in length. For these tests, three tubes with 6061T2 heat sinks were instrumented and located in the first (A), fourth (B), and seventh (C) positions of the center row. A staggered array with 1.25-in. clear space between tube rows and 0.75-in. vertical spacing between tubes (2.63 transverse and 0.59 longitudinal pitch ratios) was used.

[+] Senior Staff Engineer

[++] Director of Ocean Energy Programs

[+++] Aeronautics Division Staff

*At the time the present test model was built it was believed that 4-in.-O.D. tubes would be used, so this model has 4-in. tubes. In February 1977 the design of the plantship heat exchangers was changed to use 3-in.-O.D. tubes.

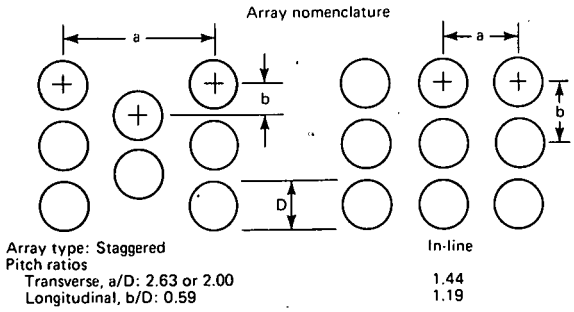

Fig. 1 Test setup showing the 2.63 by 0.59 staggered tube arrangement simulating full-scale plant-ship heat exchanger geometry.

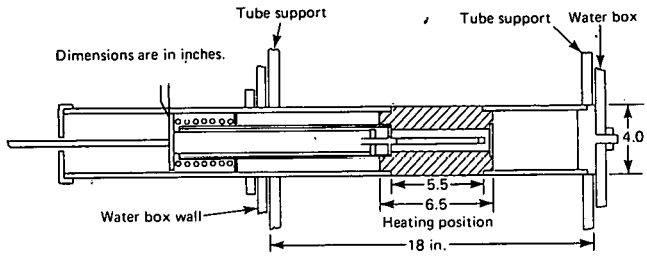

Fig. 2 Schematic diagram of instrumented tube.

The test section was located inside a water box as illustrated in Fig. 1. Seawater was pumped at a rate of 1700-2000 gpm to provide a flow velocity of 2.9 to 3.5 ft/sec through the minimum lateral spacing (1.762 in.) between adjacent tubes in the array. All data were normalized to 3.2 ft/sec by correcting the water-side heat-transfer coefficient, h_w, by (flow rate) 0.6^* . The flow passed into the test assembly through one or the other of two 8-in. risers to a head pond located above the tube array. The seawater flowed by gravity through the tube array into a lower chamber and out through a 12-in. pipe and control valve onto the lava bed at the test site.

As shown in Fig. 2, each instrumented tube consisted of a 1.25-in.-I.D., 4-in. O.D., 6061T2 aluminum heat sink with an exposed length of 5.5 in. mounted coaxially between 4-in.-O.D. Plexiglas tubes. The Plexiglas tube on one side of the test section was long enough to extend through one side of the test box. The heat source was a 5.5-in.-long, 400-watt (nominal) quartz lamp that was centered within the heat sink.

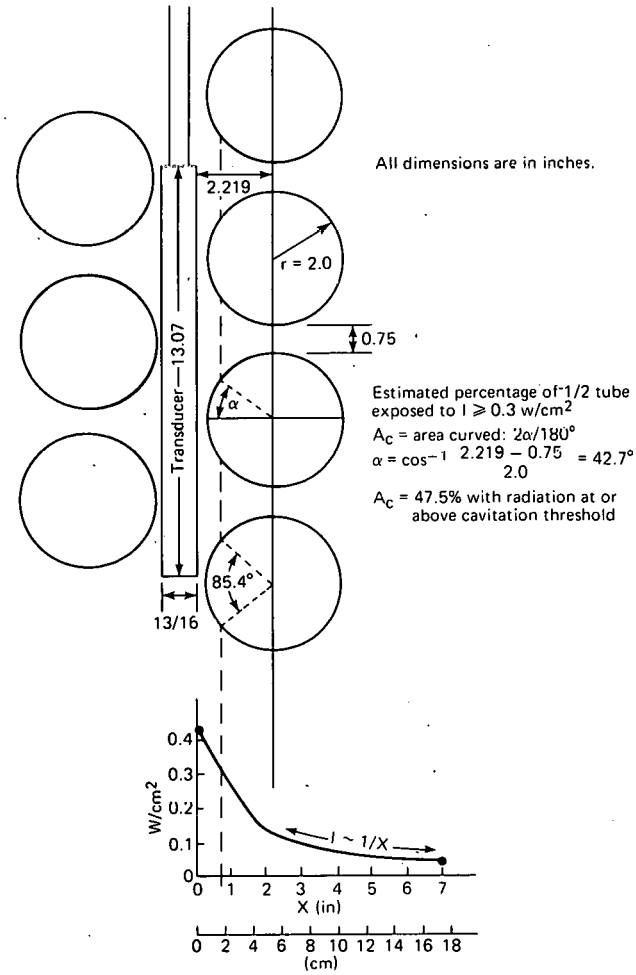

Fig. 3 Geometry of ultrasonic cleaning device inserted into tube bank.

The ultrasonic cleaning concept that was tested involved the use of a planar array of twelve ultrasonic transducers (piezo-electric ceramic) mounted on a steel plate. They were driven at 29 kHz and produced an acoustic intensity of 0.43 W/cm² at the face of the plate slightly above the cavitation threshold, which is ~ 0.3 W/cm². The transducer assembly was enclosed in a stainless steel case 13-in. long x 10-in. wide x 13/16-in. thick. This device was built for APL by Alpha Ultrasonics and Electronics Corporation. Figure 3 shows it located

---

* The equation used for h_w in the APL computer code is the Zukauskas equation for Reynolds numbers (Re's) < 200,000:

$$h_w = 0.4 \frac{k}{D} Re^{0.6} Pr^{0.36} \quad (1)$$

where D = tube O.D. (4 in. here); k = seawater conductivity, and Pr = Prandtl number.

Table 1 Values of 10^4 R_f (Btu^{-1}-hr-ft^2-°F) from Tests at Ke-Ahole Point, Hi. Seawater Velocity, 3.2 ft/sec; Tank Top Covered; Staggered Tube Array

Day/Quadrant	1	2	3	4	Avg[a]
Tube A					
0	0[b]	0[b]	0[b]	0[b]	0
6	< 1	< 1	2	4	1
6[c]	< 1	< 1	< 1	1	< 1
12	< 1	2	2	-	< 1
14[c]	1	< 1	2	3	1
20	2	2	3	1	2
21[c]	2	1	3	1	2
45	< 1	2	2	-	1
46[c]	< 1	< 1	2	4	2
46[d]	3	2	1	< 1	2
52	3	< 1	4	2	3
54[e]	4	1	3	< 1	3
62	6	1	4	< 1	3
67	7	1	4	5	4
82[f]	11	5	g	3	8
82[f]	7	< 1	g	< 1	3
Tube B					
0	0[h]	g	0[h]	0[h]	0
7	1	-	< 1	< 1	< 1
13	2	-	3	3	3
14[c]	4	-	3	2	3
20	3	-	2	3	3
21	3	-	3	2	3
52	4	-	2	5	4
54[e]	3	-	3	1	3
81[f]	3	-	g	2	4
82[f]	1	-	-	1	2
Tube C					
2	0[i]	0[i]	0[i]	0[i]	0
20	1	< 1	2	2	1
21[c]	2	< 1	2	3	< 1
45	g	g	3	3	-
52[c]	g	g	2	3	-
62	2	1	4	4	4
67[e]	3	< 1	4	< 1	2
81[f]	4	4	3	4	4
82[f]	2	1	3	2	2

[a] Tube average based on average for the sum of instrument signals at the average of the individual tube calculations. By this method the uncertainty in the measurement was slightly reduced since the sum of the instrument signals on a particular tube showed better consistency than the individual thermocouple readings.

[b] h_{w_o} values (Btu-hr-ft^2-°F) for Tube A Quadrants 1 through 4 were 1300 ± 70, 1270 ± 110, 1350 ± 210, and 1230 ± 80, respectively.

[c] 15-sec exposure each side

[d] 15-sec exposure on Quad 2; 1 min on Quad 4

[e] 15-sec exposure on Quad 2; 3 min on Quad 4

[f] 3-min exposure on Quads 2 and 4

[g] Outside thermocouple bad, open circuit. Tube average based on remaining working quadrants. See note a.

[h] h_{w_o} = 1540 ± 260, 1490 ± 150, and 1570 ± 320 Btu/hr-ft^2-°F for Quads 1, 3, and 4, respectively.

[i] h_{w_o} = 1490 ± 520, 1760 ± 100, 1380 ± 130, and 1620 ± 60 for Quads 1-4, respectively.

between vertical rows of 4-inch aluminum heat transfer tubes. Below the diagram is a plot of intensity versus distance from the transducer face which indicates that ultrasonic irradiation at the cavitation level of 0.3 W/cm^2 would cover just over half the exposed area on one side of each tube.

Results of the Experiment

In the tests, which were conducted October 6 - December 27, 1978, tube A was cleaned at approximately weekly intervals while tubes B and C were cleaned approximately biweekly and triweekly, respectively. The exposure time with the ultrasonic cleaning device was varied from 15 sec early in the series to 3 min at the end of the series. Instrument problems prevented data gathering between the 22nd and 44th days but the cleaning schedule was maintained throughout the test. From the 46th day until the end of the tests, the exposure time on the No. 4 quadrants (left sides) was increased to 3 min but was held to 15 sec on the No. 2 quadrants (right sides).

The data for tube A in Table 1 show that the ultrasonic cleaning at weekly intervals retarded the fouling, especially on quadrants 2 and 4 (sides) which received the radiation intensity expected to cause cavitation. Since the experimental apparatus required that the flow be stopped for cleaning operations, some dislodged fouling may have settled back on the surfaces; in some instances the cleaning showed no benefit when an immediate subsequent measurement of R_f was made. However, the periodic cleaning did show retardation of the growth of the fouling coefficient over several weeks when compared to results of previous tests in which there was no periodic cleaning.[6] For example, Ref. 6 shows that after 46 days of exposure without periodic cleaning, the values of 10^4 R_f were 5, 3, 5, and 3 for quadrants 1 through 4, respectively. During the present series, after 46 days with weekly cleaning, the values of 10^4 R_f were 3, 2, 1 and < 1 for the same quadrants. The overall tube value of 10^4 R_f was 2 for this test versus 4 for the previous test. On day 46 the exposure time on quadrant 4 was increased to 3 min, and this exposure time was employed in the cleaning procedure on this quadrant thereafter. In the final test both side quadrants (2 and 4) were exposed to the radiation for 3 min. The results for this final day show that cleaning of quadrants 2 and 4 returned the values of 10^4 R_f to < 1. The instruments on quadrant 3 were not functioning properly on the final day; however, the value 10^4 R_f on quadrant 1 (top) was 7, which indicates that this level of exposure did not work as well on the top. Since there is no tube above tube A and the water velocity is low at its top, a larger fouling layer may be expected to form there. Before the cleaning on the final day, 10^4 R_f on the top quadrant was 11, so when compared to the value after cleaning (7) there was some beneficial effect of the very low radiation intensity.

For tubes B and C, biweekly and triweekly cleaning, respectively, also retarded the growth of R_f. For tube B, the values of 10^4 R_f were 1 for quadrants 1 and 4 on the final day after cleaning. For tube C, the values of 10^4 R_f on the 82nd day were 2, 1, 3, and 2 on quadrants 1 through 4 after the cleaning. In contrast, the values of 10^4 R_f on the 41st day of a previous test series[6] without periodic cleaning were much higher (5, 5, 7, and 5) showing the overall effectiveness of the periodic ultrasonic cleaning.

Summary and Conclusions from Tests at Ke-Ahole Point

1) The tests with a crude initial version of an ultrasonic cleaner showed that 15-sec exposure with 0.43 W/cm^2 intensity at the cleaner surface was marginally effective in preventing fouling buildup on surfaces within the heat exchanger array; exposure reduced R_f to 0.0002.

2) Weekly exposure of 15 sec did not prevent fouling buildup after 46 days on the top quadrant of the top tube where the water velocity was low. However, a 3-min exposure after 82 days removed about 40% of the fouling from this quadrant.

3) Weekly cleaning with ultrasonic radiation will keep $R_f \simeq 0.0001$ provided that the surface receives a sufficient intensity of radiation.

4) Cleaning with ultrasonic radiation at 2- or 3-week intervals will return a fouled surface to a near clean condition ($R_f < 0.0001$) provided that the surface receives a sufficient intensity of radiation.

Gulf of Mexico Experiment

Test Equipment and Methods

The experimental apparatus consisted of a water box into which were placed 12 sets of 3-in.-diameter aluminum (3004 H8) tubes (each containing a full tube and two half tubes) so that a staggered configuration geometrically similar to the APL heat exchanger was formed. Seawater was continuously pumped through the water box at a rate to give a maximum velocity of 2.5 ft/sec in the minimum gap between the tube surfaces. Each specimen was removable so that it could be tested for heat transfer before and after immersion in an ultrasonic bath.

The change in heat transfer characteristics due to fouling and cleaning were determined by calorimeter measurements. The calorimeter consisted of a Dewar flask into which a specimen (either fouled or cleaned) was inserted; two stirrers were also placed in the container so that one was on the inside and the other on the outside of the specimen tube. Water at approximately room temperature was placed in the Dewar flask; cold water at the ice point was placed inside the specimen which was sealed to prevent direct mixing of the two fluids. Thermocouple measurements of the temperature in the hot and cold fluid were monitored as a function of time and an overall heat transfer coefficient U was deduced from these transient measurements.

The ultrasonic cleaning bath consisted of a 2.5-gallon tank of water with acoustic transducers cemented to the bottom producing an intensity of 0.72 W/cm^2 at 44 kHz for controlled periods of time. During immersion, the specimens were kept in motion to produce a flow over the cylindrical surface washing away the material loosened by the ultrasonic radiation. Visual inspection was used to determine when the surface was clean. Generally when all green, wispish biofouling material was removed and the surface had a noticeably brighter color (although some residual discoloration may have remained) the specimen was judged clean and the heat transfer characteristics remeasured.

Results of the Experiment

Specimens with 3.5 to 13 weeks of exposure to seawater flow were removed for heat transfer measurements. Some of the testing was done at sea immediately upon removal from the water box while others were shipped in plastic bags containing seawater back to APL. The delayed measurement with samples shipped could perhaps distort the results; typically it took at least 2 weeks between removal of the sample and arrival at APL. In some cases the shipped tubes were exposed to air and a scale and corrosion appeared on their surfaces while in other cases some of the grainy filamentary material was removed; in still other areas the specimens appeared to undergo no change from their condition when removed from the water box. The results of the measurements made to date on those specimens for which no disturbance on the biofouling growth occurred are presented in Table 2.

For the 2.5 ft/sec minimum gap velocity, 10^4 R_f was measured at 2-3 for 3.5 weeks' exposure, 4-5 for 7 weeks' exposure, and 8-9 for 13 weeks' exposure. Cleaning times needed to return these specimens to a bright appearance and remove all greenish wispy material averaged about 30 sec for the specimens with 3.5 to 7 weeks' exposures; the specimen with 13 weeks' exposure needed a much longer time in the ultrasonic bath to clean. These results are encouraging because they indicate that a cleaning device with this acoustic intensity (0.7 W/cm^2) could restore the tubes to a thermally clean condition on a time scale that is longer than what is presently planned for periodic cleaning of the plantship heat exchangers. Because of the relatively short duration of the program, no refouling (and subsequent recleaning) of the tubes was conducted, so the frequency of cleaning needed to maintain the desired average R_f level (≤ 0.0002) was not established. However, the results indicate that the period between cleanings would be 3 to 4 weeks, with 30 sec of ultrasonic exposure.

Closure

The results of the two experiments indicate that ultrasonic cleaning at modest intensities (≤ 1 W/cm^2) and at intervals from 1 to 3.5 weeks for exposure times of 30 to 180 sec is a viable concept for maintaining thermally clean heat transfer tubes. Development of a prototype cleaning device that would keep all of the surfaces (including tops and bottoms of tubes and bends) clean is still needed. Also, there must be investigation of the longer term use with tubes that are cyclically fouled and cleaned to establish more precisely the cleaning interval and ultrasonic exposure times.

Table 2 Results for Six Specimens from Gulf of Mexico Biofouling and Ultrasonic Cleaning Experiment; 3-in.-OD Aluminum (3004 H8) Tubes; Water Velocity, 2.5 ft/sec.

Specimen No.	Test Location	Biofouling Exposure Time (weeks)	U (Btu/hr-ft^2-°F) Measured by Calorimeter "Fouled"	"Cleaned"	$10^4 R_f$ hr-ft^2-°F/Btu	Time To Clean sec.
1	APL	3.5	220	235	3	30
5	APL	3.5	187	195	2	30
9	APL	7	195	211	4	45
12	Sea	7	195	217	4	25
5'	Sea	7	191	227	5	30
4	APL	13	178	210	9	150

Acknowledgment

The experiment at Ke-Ahole Point was supported by a grant from the Office of Sea Grant, U.S. Department of Commerce and the State of Hawaii. The authors wish to express their appreciation to these organizations for their continued support. Many people on the staffs of the Applied Physics Laboratory and the Natural Energy Laboratory of Hawaii have contributed to the design, fabrication, maintenance and execution of this experiment. We gratefully acknowledge the cooperation of our colleagues in this effort. At APL, Mr. A.S. Polk designed the test box and the tube matrix components, Mr. J. Malek developed the portable data acquisition system, Mr. J. Creeden fabricated and installed the instrumentation, Mr. M. Rose fabricated the wiring harnesses, and Mr. E. Wallace fabricated the instrumented tubes. At NELH, the test site was prepared and the piping installed under the direction of Dr. Jim Jones and Mr. Hank White and the tests were run and the equipment maintained under the direction of Mr. C. Tendrick. Messrs. Scott Bickel and Jan War conducted the field measurements.

The Gulf of Mexico experiment was supported by a grant from the Argonne National Laboratory funded by the Department of Energy and under the direction of Dr. G.F. Popper. Mr. F. Spiehler of the NOAA Data Buoy Office supervised the fabrication, installation, and calibration of the water box test assembly. Mr. E. Wallace of APL built the calorimeter equipment. We gratefully acknowledge their assistance in this effort.

References

1. Dugger, G.L. et al, "Experiments on and Design of Low-Cost Aluminum Heat Exchangers for OTEC Plant Ship, Applied Physics Laboratory AEO-77-073," March 1977.

2. Keirsey, J.L. et al, "Core-Unit Testing of the APL/JHU Shell-less, Folded-Tube Heat Exchanger," this Conference.

3. George, J.F., "System Design Considerations for a 10/40 MW_e OTEC Pilot Plantship," this Conference.

4. Richard, E., McEvaddy, P.J., and Perini, L.L., "Off-Design Performance and Control Considerations for the Power System of an OTEC Plantship," this Conference.

5. Pandolfini, P.P. and Makofski, R.A., "Circumferential Heat Transfer and Pressure Drop in Tube Arrays with a Low-Lateral-Pitch Ratio in Crossflow," Applied Physics Laboratory CP-066, June 1978.

6. Pandolfini, P.P. and Avery, W.H., "Measurement of the Effect of Biofouling and Cleaning on the Heat Transfer Characteristics of Large Diameter Tubes," March 1979, final report to the Office of Seagrant.

DISCUSSION

G. Kinelski, DOE: You said in the areas where you had cavitation you got cleaning by the ultrasonic device. What effect will the cavitation have on an aluminum surface, bearing in mind what Frank LaQue said this morning about the instantaneous corrosion layer formed on aluminum. Now that we are going to add to it the cavitating affect I just wonder what this is going to do to the aluminum surface that you are trying to protect.

F. Hill: The maximum value we are using in this case was 0.7 W/cm^2, whereas it takes 100 W/cm^2 or more to erode aluminum.

R. Webb, Penn State: Could you possibly comment on the possibility of applying this concept to cleaning inside circular tubes or noncircular passages and how small a device might be made?

P. P. Pandolfini: The particular device we used at Keahole Point had a thickness of 0.812 in., which is about as thin as practical for a plate type device. It consisted of 12 transducers between the plates. For use inside circular tubes, a 1-in.-square by 2-ft-long device could be made for use in tubes with diameters $\geq$ 1.6 in. or so. For other noncircular passages, such as the rectangular seawater passages in a heat exchanger that the Trane Co. tested at Argonne National Laboratory, this concept also may be applied. If the width of those passages can be increased to somewhat greater than 1.0 in., a suitable ultrasonic cleaner could be built.

S. Dexter: Let me comment on Gene Kinelski's question for a moment. He mentioned that your power levels were considerably lower than that necessary to cause appreciable short-term damage to aluminum

itself, but what we are more concerned with is the damage to the protective film oxide. Do you have any data to show that the power levels needed for biofouling removal will not damage the aluminum oxide film, which is more erodible than the base metal, the Al 7072 cladding in your case.

F. Hill: Data in the literature indicate than an intensity of the order of 10 W/cm^2 would be required to erode the oxide film. This greater resistance to damage of the oxide film compared to the bio-film was qualitatively confirmed by our tests: samples that were exposed to air for a few weeks due to shipping-bag failure had discolored areas that were not readily removed by the cleaner.

THE LMSC BIOFOULING MEASUREMENT DEVICE

W. L. Owens

Lockheed Missiles & Space Company, Inc.
Sunnyvale, California 94088

ABSTRACT

Three concepts for measuring biofouling thermal resistance are discussed. These methods employ electric heating either directly or indirectly to determine the overall thermal resistance for water flowing in a tube. An analysis of experimental uncertainty is presented for two of the concepts in terms of the measurement uncertainties associated with heater power, temperature, and fluid velocity. A description of the LMSC device is given along with fouling factor data for San Diego Bay water in aluminum and copper-nickel tubes. Also considered is the effect of seawater temperature variation on the measurement accuracy of the LMSC device. Finally, a comparison is presented for the three concepts in terms of accuracy, complexity, cost, ease of data reduction, and the influence of seawater temperature variation on measured fouling factor.

NOMENCLATURE

A	area
b	rate of temperature change
C_p	specific heat
D	diameter
e	Reynolds number exponent
h	heat transfer coefficient
L	total heated tube length
ℓ	partial heated tube length
M	tube mass
q	rate of fluid heat transfer
R_F	fouling factor
R_W	wall thermal resistance
T	temperature
t	time
U	overall heat transfer coefficient
V	fluid velocity

GREEK

Δ	increment
ΔT_{LM}	log-mean-temperature difference
ρ	fluid density
τ	thermal time constant

SUBSCRIPTS

1	inlet or reference block
2	heater block
c	seawater
c1	seawater inlet
c2	seawater outlet
h	secondary fluid
h1	secondary fluid inlet
h2	secondary fluid outlet
i	inside or initial
L	liquid
o	clean tube
W	wall

INTRODUCTION

A problem of some concern in the design of OTEC heat exchangers is the level of biofouling thermal resistance, and the effectiveness of various biofouling countermeasures. One part of the problem is the capability of measuring this thermal resistance in an accurate and repeatable manner. The biofouling film thickness associated with OTEC fouling factors (~ 0.001 in.) makes physical measurement of the film a difficult and inaccurate means of determining the in situ fouling factor. At present, the most effective means of determining biofouling thermal resistance is through measurement of the overall heat transfer coefficient. The portion of the total thermal resistance due to biofouling is obtained by subtracting the contribution due to the seawater and the wall from the measured overall thermal resistance. There are several ways in which this can be accomplished. Three of these methods will be discussed and compared in this paper.

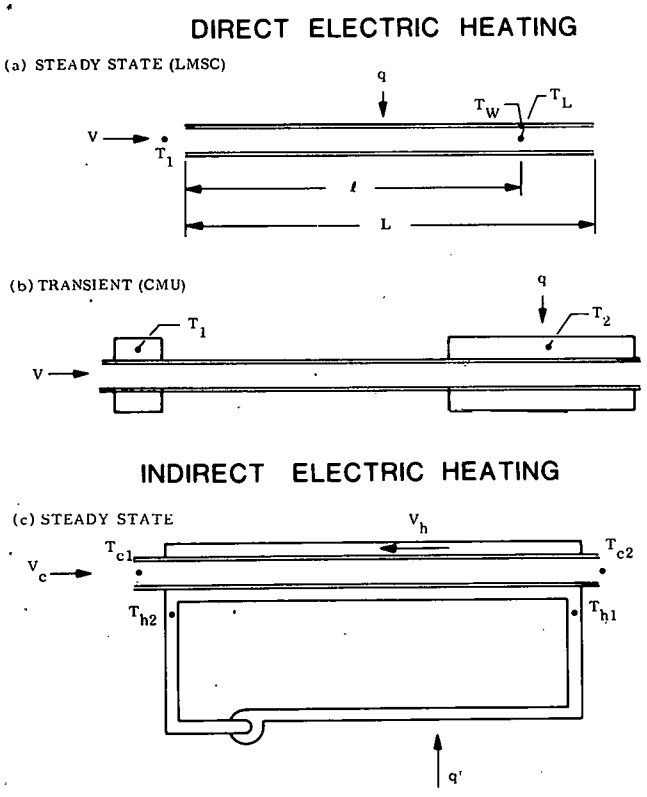

Fig. 1 Three Electrically Heated Biofouling Measurement Concepts

CONCEPTS

The three biofouling measurement techniques to be considered can be categorized by the method of heating. Figure 1 shows the basic arrangements and subdivision by direct or indirect electrical heating of the test section. Direct electrical heating has been employed by Carnegie Mellon University (CMU) and Lockheed Missiles & Space Co., (LMSC) for measurement of seawater biofouling in tubes of various materials. The LMSC device shown in Fig. 1(a) employs a steady-state method of electric heating where a uniform heat flux is applied to a tubular test section using an electric heater tape. The measured quantities consist of heater power, tube-wall temperature, seawater velocity, and inlet temperature as indicated.

The relationship between heat rate and temperature difference is given by

$$q = UA_i (T_W - T_L) \tag{1}$$

where

$$T_L = T_1 + \frac{\ell}{L} \frac{4q}{\pi \rho C_p V D_i^2} \tag{2}$$

The reciprocal of the overall heat transfer coefficient is given by

$$\frac{1}{U} = \frac{1}{h} + R_W + R_F \tag{3}$$

since, from Eq. (1)

$$\frac{1}{U} = \frac{A_i (T_W - T_L)}{q} \tag{4}$$

the fouling factor can be obtained by setting Eq. (3) equal to Eq. (4) and solving for R_F.

$$R_F = \frac{A_i (T_W - T_L)}{q} - \left(\frac{1}{h} + R_W\right) \tag{5}$$

Equation (5) indicates that the fouling factor can be determined from a measurement of the local temperature difference, heat flux, and seawater heat transfer coefficient. The wall resistance term, R_W, which includes the thermal resistance associated with wall temperature measurement, is obtained from a Wilson plot for the unfouled tube.

Figure 1(b) shows a schematic of the CMU device which has been described previously in a number of publications.[1-3] The device is basically composed of a tube with two copper cylinders clamped to the outside surface. Both cylinders are 3 in. in outside diameter and approximately 1.3 in. in inside diameter. The smaller cylinder is called the reference block and is 2 in. long. The larger cylinder is called the heater block and is in three sections, each 4 in. long. Operation is essentially composed of heating the heater block until steady state conditions are obtained, and then interrupting the power and observing the transient decay of the temperature difference between the heater and reference blocks.

Equation (6) represents a simplified solution for the transient temperature response of the block, ignoring its thermal resistance.[1]

$$T_2 - T_1 \approx (T_2 - T_1)_i \exp(-t/\tau) \tag{6}$$

Measurement of the temperature difference as a function of time allows determination of the time constant τ. The time constant can be related to the seawater, biofouling, and block contact thermal resistances. This allows a solution for the fouling factor in terms of the initial (clean tube), and subsequent values of the time constant and seawater heat transfer coefficient.

$$R_F = \frac{A}{C_p M}(\tau - \tau_o) + \frac{1}{h_o} - \frac{1}{h} \tag{7}$$

The actual calculation of fouling factor is somewhat more involved and requires consideration of block and tube thermal conductivity and heat loss to the environment and along the tube. These items are discussed in Ref. 1. The measured quantities are seawater velocity and heater and reference block temperature difference as a function of time.

The indirect heating concept, shown in Fig. 1(c), uses a secondary heat transfer fluid to provide test section heating for the determination of the overall heat transfer coefficient. Seawater passes through the tube while a second larger tube provides an annulus for the secondary heat transfer fluid. The secondary fluid loop contains a reservoir, pump, heater, flow measurement device, and inlet and outlet temperature probes. The primary seawater flow path requires flow measurement and inlet and outlet temperature probes.

The derivation of the expression for fouling factor is similar to that for the LMSC device.

$$R_F = \frac{T_{h1} - T_{c2} - (T_{h2} - T_{c1})}{q/A \ln \frac{T_{h1} - T_{c2}}{T_{h2} - T_{c1}}} - \left(\frac{1}{h_c} + \frac{1}{h_h} + R_W\right) \tag{8}$$

The principal difference is the use of the log-mean-temperature difference and the inclusion of the secondary fluid heat transfer coefficient.

The indirect heating concept is also suitable for biofouling measurements on plate heat exchanger surfaces whereas the other two approaches may be somewhat difficult to implement.

FOULING FACTOR MEASUREMENT UNCERTAINTY

Estimation of the expected experimental uncertainty in the determination of fouling factor is

possible using the expression for fouling factor and estimates of the various measurement uncertainties. Typical measurements used in the determination of fouling factor are heater power, velocity, and temperature difference. Assuming that the measurement uncertainties for these variables are normally distributed, the experimental uncertainty will be given by [4]

$$\Delta R_F = \pm \left\{ \left[\frac{\partial R_F}{\partial (T_W - T_L)} \Delta (T_W - T_L) \right]^2 + \left(\frac{\partial R_F}{\partial q} \Delta q \right)^2 + \left(\frac{\partial R_F}{\partial V} \Delta V \right)^2 \right\}^{1/2} \quad (9)$$

The expression for experimental uncertainty for the LMSC device is obtained by substituting the various partial derivatives of Eq. (5) into Eq. (9).

$$\Delta R_F = \pm \left\{ \left(R_F + \frac{4\ell}{C_p \rho D_i V} + \frac{1}{h} + R_W \right)^2 \times \left[\left(\frac{\Delta (T_W - T_1)}{T_W - T_1} \right)^2 + \left(\frac{\Delta q}{q} \right)^2 \right] + \left(\frac{4\ell}{C_p \rho D_i V} + \frac{e}{h} \right)^2 \left(\frac{\Delta V}{V} \right)^2 \right\}^{1/2} \quad (10)$$

The quantities $\Delta(T_W - T_1)/(T_W - T_1)$, $\Delta q/q$, and $\Delta V/V$ represent the ± uncertainty ratio for temperature difference, heater power, and seawater velocity. The quantity e represents the Reynolds number exponent for the seawater heat transfer coefficient.

Figure 2 shows the variation of fouling factor measurement uncertainty with temperature difference measurement uncertainty for the conditions noted. The test section was assumed to be an aluminum tube with an outside diameter of 1.66 in., 0.14-in. wall thickness, and a heated length of 27 in.

The selected values of $\Delta V/V$ and $\Delta q/q$ represent the assumed bounds of experimental accuracy which can be expected with careful measurement techniques. The present temperature difference measurement uncertainty for current versions of the LMSC device is believed to be on the order of ± 0.04°F. This indicates an experimental uncertainty in the determination of fouling factor between approximately ±2 x 10^{-5} and ±4 x 10^{-5} $(Btu/hr\text{-}ft^2\text{-}^oF)^{-1}$. Figure 2 also emphasizes the increasing importance of heater power measurement accuracy as fouling progresses.

Following the same procedure for the indirect device, the expression for biofouling measurement uncertainty is obtained by substituting the partials of R_F from Eq. (8) into Eq. (9).

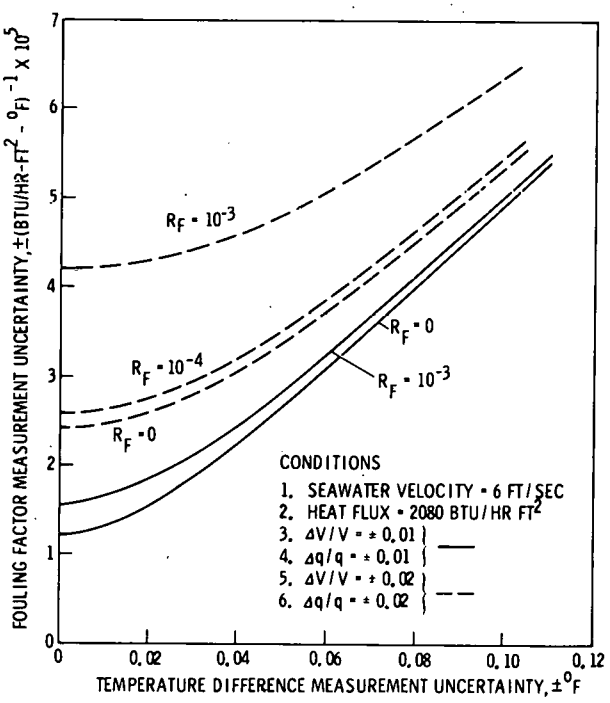

Fig. 2 LMSC Biofouling Measurement Device Uncertainty

$$\Delta R_F = \pm \left\{ \left[\frac{A}{q} \Delta (\Delta T_{LM}) \right]^2 + \left[\left(R_F + \frac{1}{h_c} + \frac{1}{h_h} + R_W \right) \frac{\Delta q}{q} \right]^2 + \left[\left(\frac{e}{h_c} \right)^2 + \left(\frac{e}{h_h} \right)^2 \right] \left(\frac{\Delta V}{V} \right)^2 \right\}^{1/2} \quad (11)$$

where

$$\Delta T_{LM} = \frac{T_{h1} - T_{c2} - (T_{h2} - T_{c1})}{\ln \frac{T_{h1} - T_{c2}}{T_{h2} - T_{c1}}} \quad (12)$$

and

$$\Delta (\Delta T_{LM}) = \pm \left\{ \left[\frac{\partial \Delta T_{LM}}{\partial (T_{h1} - T_{c2})} \Delta (T_{h1} - T_{c2}) \right]^2 + \left[\frac{\partial \Delta T_{LM}}{\partial (T_{h2} - T_{c1})} \Delta (T_{h2} - T_{c1}) \right]^2 \right\}^{1/2} \quad (13)$$

The variation of fouling factor uncertainty for the indirect tubular device is shown in Fig. 3 as a function of temperature difference measurement uncertainty. The two sets of velocity and heat rate measurement uncertainties were chosen to bracket the expected limits for these quantities.

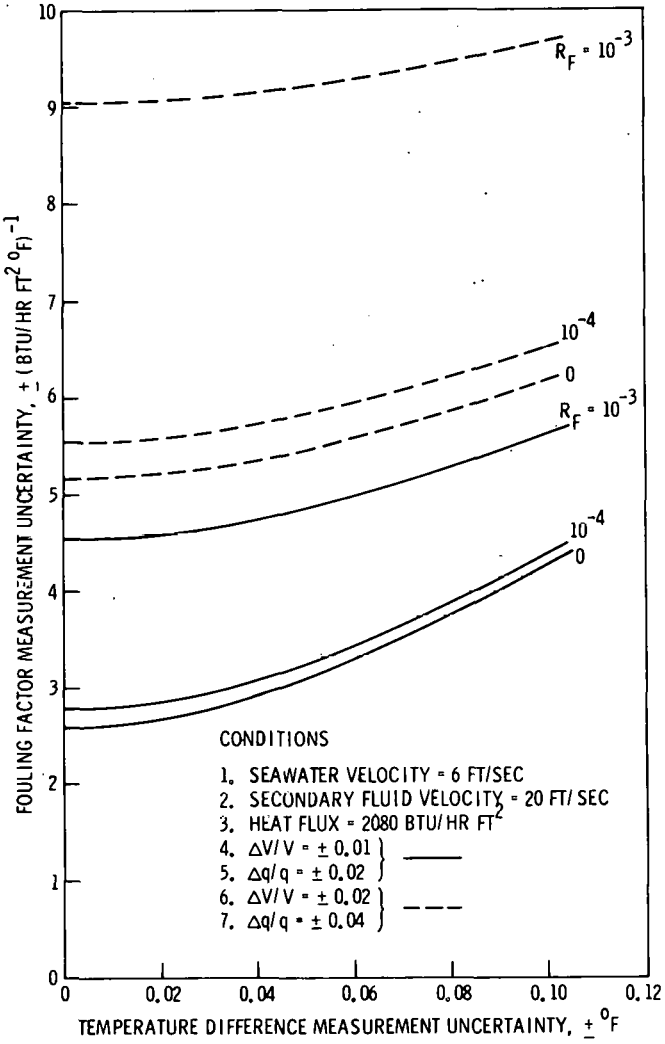

Fig. 3 Indirect-Tubular Biofouling Measurement Device Uncertainty

The seawater velocity, heat flux, tube-wall resistance, and tube dimensions were the same as the previous uncertainty determination for the LMSC device. The principal difference for measurement uncertainty between the two devices has been assumed to be in the area of test section heat rate. Use of the secondary fluid heater power will require correction for heat loss in the secondary flow loop which is not necessary for the LMSC device. Also, use of the liquid mass rate and temperature change to calculate the heat flux would be less accurate because of the relatively small temperature rise ($\sim 0.1^{\circ}F$) for the seawater and secondary fluid (water). The indirect device would also require care in obtaining the mixed mean temperatures, T_{c2} and T_{h2}, shown in Fig. 1(c). Incomplete mixing of the effluent would result in a temperature difference measurement uncertainty greater than that experienced for the LMSC device. For the conditions shown in Fig. 3, the estimated fouling factor measurement uncertainty would be expected to lie in the range of $\pm 3 \times 10^{-5}$ to $\pm 9 \times 10^{-5}$ $(Btu/hr\text{-}ft^2\text{-}{}^{\circ}F)^{-1}$, depending on the level of fouling and velocity and heat flux uncertainty.

The indirect device, while not as accurate as the direct steady-state concept for tubes, offers considerable potential as a plate heat exchanger bio-

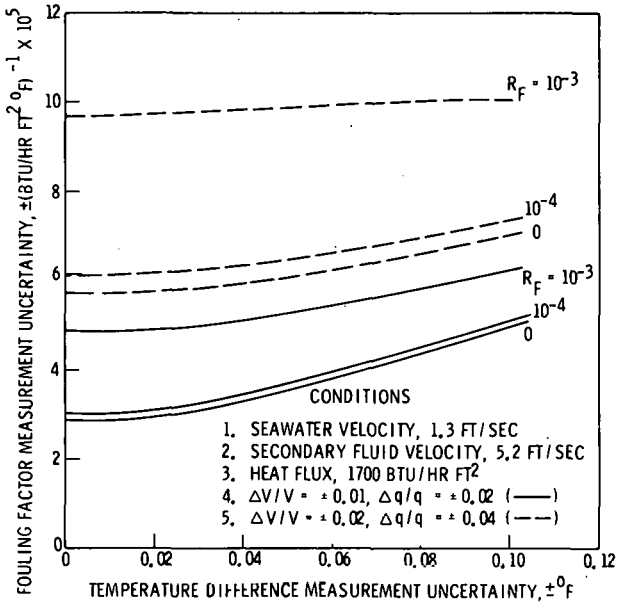

Fig. 4 Indirect-Plate Biofouling Measurement Device Uncertainty Versus Temperature Difference Uncertainty

fouling measurement device. Figure 4 indicates the expected fouling factor measurement uncertainty for the range of conditions shown. A typical OTEC plate heat exchanger seawater velocity of 1.3 ft/sec was used along with an arbitrarily chosen value for the secondary fluid (water) of 5.2 ft/sec. Some improvement in measurement uncertainty can be obtained by an increase in the secondary fluid velocity although this would not be significant for the present conditions. Of greater importance is the influence of heat rate measurement uncertainty on the measured fouling

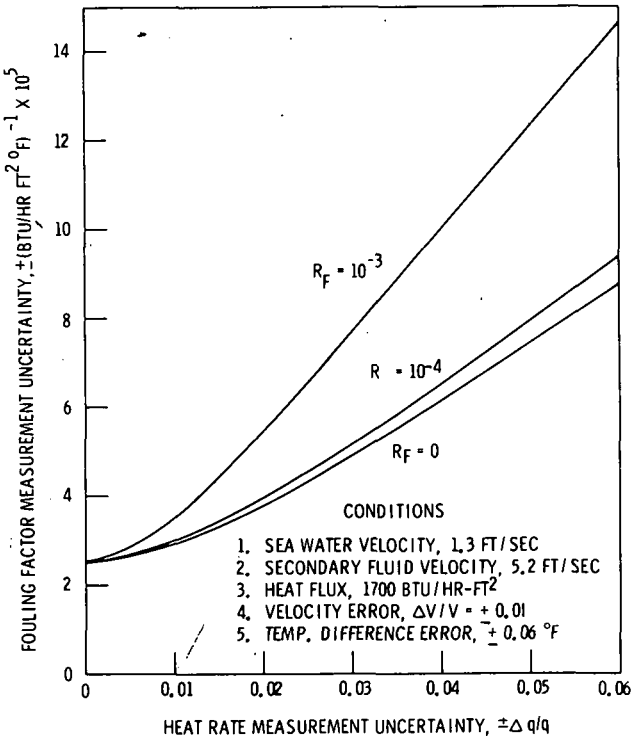

Fig. 5 Indirect-Plate Biofouling Measurement Device Uncertainty Versus Heat Rate Measurement Uncertainty

factor which is shown in Fig. 5. Based on the assumed conditions, it should be possible to obtain plate biofouling measurements within an uncertainty range of approximately $\pm 4 \times 10^{-5}$ to $\pm 8 \times 10^{-5}$ $(Btu/hr\text{-}ft^{2}\text{-}^{o}F)^{-1}$ with this type of device.

The effectiveness of the CMU device has been previously evaluated on the basis of fouling factor measurements taken at Keahole Point, Hawaii, St. Croix, Virgin Islands, and the Gulf of Mexico.[5] Specific sources of measurement uncertainty related to the CMU device include nonidentical thermal response of the reference and heater blocks to seawater temperature fluctuations, thermal boundary layer development under the heater block, thermal contact resistance between the tube and the heater block, heat losses to the environment, and the use of low thermal conductivity tubes. Suggestions for improving some of these problem areas include the use of thermal grease to reduce the contact resistance and "tuning" of the two copper blocks to reduce the influence of seawater temperature variation. Analysis of the test data for the various CMU devices produced a wide range of fouling factor uncertainty. The best results were from Keahole Point where the fouling factor uncertainty ranged between $\pm 2 \times 10^{-5}$ and $\pm 6 \times 10^{-5}$ $(Btu/hr\text{-}ft^{2}\text{-}^{o}F)^{-1}$. The worst were from data taken from a tugboat in the Gulf of Mexico and ranged between $\pm 12 \times 10^{-5}$ and $\pm 108 \times 10^{-5}$ $(Btu/hr\text{-}ft^{2}\text{-}^{o}F)^{-1}$. Based on the Keahole Point results, it may be said that the CMU device is capable of fairly accurate fouling factor determination under favorable conditions.

LOCKHEED BIOFOULING MEASUREMENT DEVICE

The LMSC device was conceived and developed in 1978 in connection with a Lockheed biofouling research program being carried out at the Lockheed Ocean Laboratory (LOL) in San Diego, Calif. The basic design objectives for the tubular device were as follows:

- o Simple design, fabrication, and operation
- o Fouling factor measurement uncertainty $< \pm 5 \times 10^{-5}$ $(Btu/hr\text{-}ft^{2}\text{-}^{o}F)^{-1}$
- o Capability of measuring local values of fouling factor
- o Simple data acquisition and reduction

Based on the above objectives, the direct electric heating, steady-state concept was chosen for development.

Description. The LMSC biofouling measurement device (BMD) is essentially a tube wrapped with heater tape and covered with insulation as indicated in Fig. 6. To date, BMDs have been fabricated from schedule 40 pipe in aluminum, copper-nickel, and titanium. The overall length is 31 in. with a heated length of 27 in. Wall temperatures are measured with imbedded thermistors at eight positions along the heated portion of the tube. Electrical heating is provided by a wrap-on heater tape which is covered with 2 in. of polyurethane foam insulation.

The heated length is primarily established on the basis of the thermal entry length. With fully developed turbulent flow at the entrance, approximately 15 diameters is sufficient to ensure a fully developed temperature profile. The total

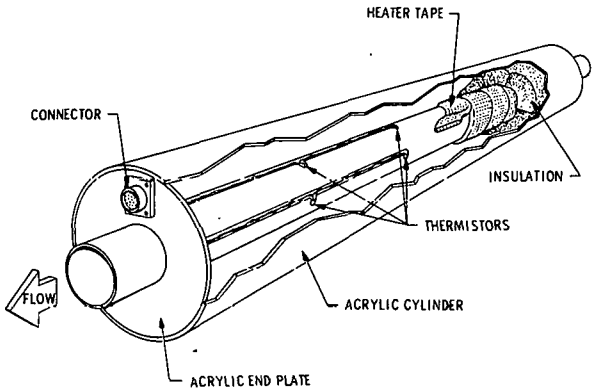

Fig. 6 Sectional View of LMSC Biofouling Measurement Device

heated length L, shown in Fig. 1(a), must be adequate to provide a suitable thermal entrance length in addition to an adequate downstream length to eliminate end effects on the measured wall temperature.

For a particular application, the choice of BMD tube material and inside diameter are generally fixed by the particular tubular heat exchanger design under investigation. The seawater velocity is a dependent variable which is fixed by the OTEC heat exchanger operating conditions or experimental objectives. The only BMD test condition with some degree of freedom is tube wall heater power. The choice of heater power is important in that it influences the accuracy of fouling factor determination as indicated in Eqs. (10) and (11), and the temperature gradient across the biofouling film. The expression for the temperature difference between the inside wall and the local liquid bulk temperature is given by

$$T_{Wi} - T_L = \frac{q}{A_i}\left(\frac{1}{H} + R_F\right) \qquad (14)$$

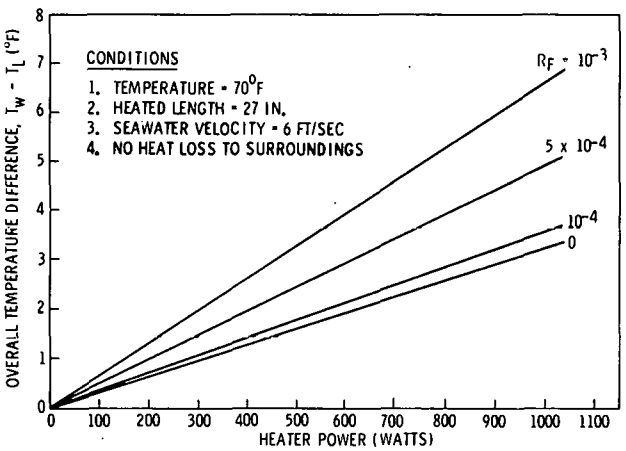

Fig. 7 LMSC Device Overall Temperature Difference Versus Heater Power

Figure 7 shows a plot of Eq. (14) for typical conditions with fouling factor as a parameter. For a clean tube with $R_F = 0$, the indicated temperature difference results entirely from the thermal resistance of the water. The resultant temperature drop across the biofouling film is given by the difference between the overall temperature difference for a particular R_F value and the clean tube value. As an example, the clean tube

temperature drop at 600W from Fig. 7 is 2°F. For a fouling factor of 10^{-4} (Btu/hr-ft^2-°F)$^{-1}$, the overall temperature drop is 2.2°F. This results in a 0.2°F drop across the biofouling layer with the assumption of an unchanged seawater heat transfer coefficient. A nominal heater power of 600W has been selected for the LMSC BMD although lower values will yield acceptable results.

Instrumentation consists of heater current and voltage, venturi pressure differential, and thermistor resistances. Thermistor calibration is obtained by operating the BMD at zero power and recording the seawater and wall thermistor readings for a seawater velocity on the order of 6 ft/sec. This allows calculation of the wall thermistor temperature corrections used in the data reduction program.

Calculation of fouling factor from Eq. (5) requires prediction of the seawater heat transfer coefficient, h. Since h is a function of velocity, inside diameter, bulk temperature, and surface roughness, accurate estimation under all conditions may not be possible. One means of reducing the uncertainty in h due to the change in surface conditions with fouling, is through the use of Wilson plots.[6] This entails making temperature measurements at three or four values of seawater velocity, and can serve as the principal means of determining fouling factor or as a check on the correlation used to calculate h.

Seawater Temperature Variation. A problem of some concern for the CMU device has been the influence of seawater temperature variation on fouling factor determination.[1,5] Application of the LMSC device, to date, has been limited to San Diego Bay which has relatively constant seawater temperatures. An assessment of the thermal response of the LMSC device to seawater temperature variations has been limited to a relatively simple analysis. Assuming a lumped wall and seawater temperature and the notation of Fig. 1(a), an energy balance yields

$$C_p M \frac{dT_W}{dt} = q - h A_i (T_W - T_L) \qquad (15)$$

Equation (15) was solved for the assumption of a ramp change in seawater temperature given by

$$T_L = T_{Li} + bt \qquad (16)$$

Substituting Eq. (16) into (15) and solving for $T_W - T_L$ gives the change in wall-seawater temperature difference ratio as a function of time.

$$(T_W - T_L)/(T_W - T_L)_i = 1 - \frac{C_p Mb}{q}\left[1 - \exp(-t/\tau)\right] \qquad (17)$$

where $\tau = C_p M/h A_i$ (18)

The temperature ratio given by Eq. (17) varies between one at $t = 0$ and some minimum value as $t \to \infty$

$$\lim_{t\to\infty} \frac{T_W - T_L}{(T_W - T_L)_i} = 1 - \frac{C_p Mb}{q} \qquad (19)$$

Typical values for Eqs. (18) and (19) have been tabulated in Table 1 for several candidate BMD materials. The assumed conditions are as follows: D_o = 1.66 in., D_i = 1.38 in., h = 1000 Btu/hr-ft^2-°F, q/A = 2500 Btu/hr-ft^2, and b = 10°F/hr. It will be noted that the LMSC device has a relatively short time constant for all five materials. In addition, the calculated temperature ratios, for a seawater temperature change rate of 10°F/hr, indicate errors in temperature difference which are substantially less

Table 1 THERMAL RESPONSE FOR VARIOUS TEST SECTION MATERIALS

MATERIAL	SPECIFIC HEAT (BTU/LBM-°F)	DENSITY (LBM/FT^3)	TIME CONST. (SEC)	$(T_w - T_{sw\infty})/(T_w - T_{sw})_i$
ALUMINUM	0.22	171	1.7	0.998
STAINLESS	0.12	501	2.8	0.997
TITANIUM	0.13	282	1.7	0.998
CUNI	0.09	558	2.3	0.997
COPPER	0.09	558	2.3	0.997

than the assumed temperature difference uncertainty of ±0.040°F. Although a more exacting analysis would include the response of the heater tape and insulation, it is felt that the LMSC BMD will be relatively insensitive to most seawater temperature variations.

Fouling Factor Measurement. The seawater test loop at LOL has been described elsewhere.[7] At the present, four BMDs of aluminum and one of Cu-Ni have been fabricated and tested using San Diego Bay water. Figure 8 shows a typical clean tube Wilson plot for the first BMD fabricated from 6061 aluminum. The intersection with the abscissa allows determination of the wall thermal resistance associated with each thermistor while the slope provides an indication of the seawater heat transfer coefficient. The use of a velocity exponent of 0.86 is a departure from convention and is based on the correlation of Sleicher and Rouse.[8] Our experience with turbulent flow heat transfer in tubes indicates that the Sleicher-Rouse correlation is to be preferred over the more conventional Dittus-Boelter, Colburn, or Sieder-Tate correlations.

An indication of the influence of heater power on measured overall thermal resistance and general data repeatability is given in Fig. 9. The data points at 600W are those from Fig. 8 along with similar measurements taken at 200W and 400W. The individual values are calculated from Eq. (4) using measured temperature difference and heater power. These data show the expected lack of dependence on heater power as well as a measurement variation on the order of ±2 x 10^{-5} (Btu/hr-ft2-°F)$^{-1}$ for the higher velocities. The variation for the data taken at 3.4 ft/sec is on the order of ±3 x 10^{-5} (Btu/hr-ft2-°F)$^{-1}$ and is believed to result,

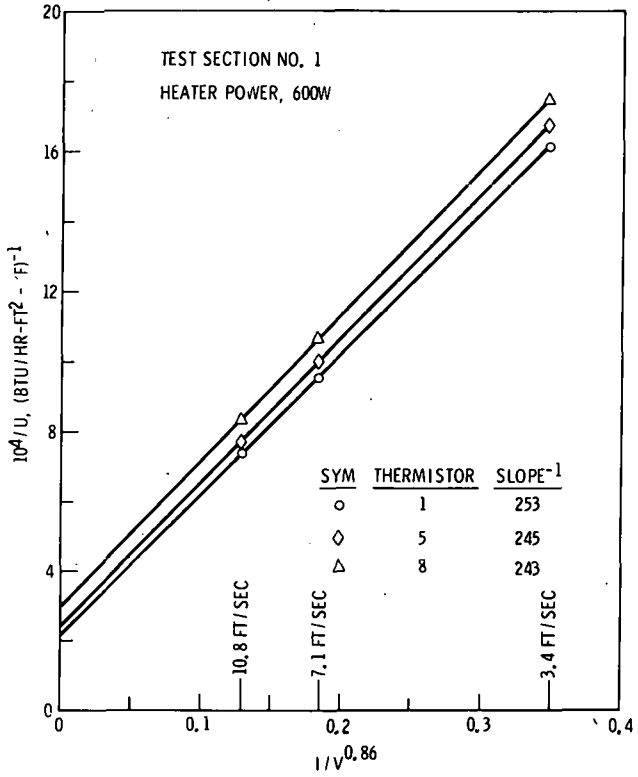

Fig. 8 Wilson Plot for LMSC Test Section No. 1

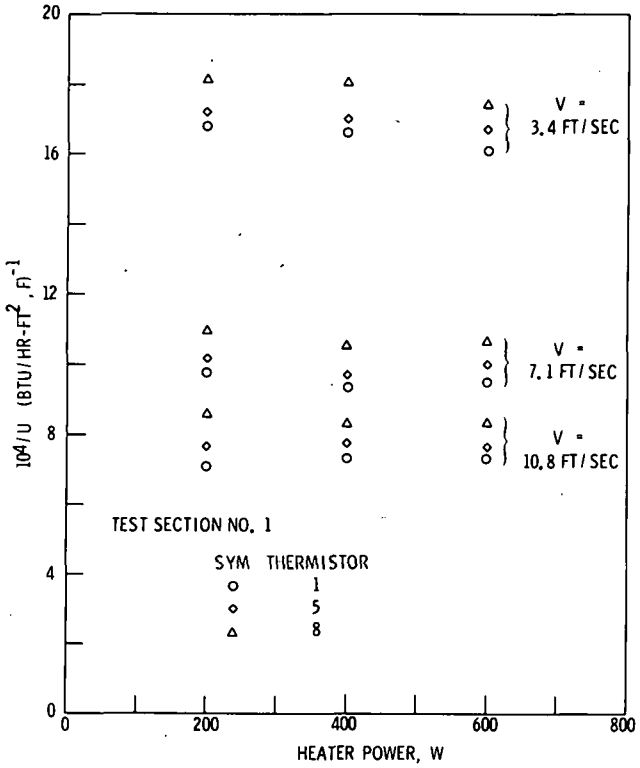

Fig. 9 Overall Thermal Resistance as a Function of Heater Power

primarily, from a reduction in the velocity measurement accuracy at the lower velocities. This problem has since been corrected through the use of more accurate differential pressure transducers for the measurement of venturi pressure drop.

An indication of the current fouling factor measurement accuracy is provided by the most recent LMSC biofouling data shown in Fig. 10. The test conditions noted were selected to provide a velocity comparison for aluminum, a material comparison for aluminum and Cu-Ni at 3.4 ft/sec, and a low dose chlorination/no chlorination comparison for aluminum at 7 ft/sec. The apparent accuracy for the Cu-Ni data is quite good and appears to have a variation of less than $\pm 1 \times 10^{-5}$ $(Btu/hr\text{-}ft^2\text{-}^oF)^{-1}$. The chlorination data, with one exception, exhibits an error band on the order of $\pm 2 \times 10^{-5}$ $(Btu/hr\text{-}ft^2\text{-}^oF)^{-1}$. Determination of the error band for the aluminum tube data at 3.4 and 7.0 ft/sec is somewhat more difficult as some of the indicated fluctuation in fouling factor could result from sloughing off of the biofouling layer. The largest changes are associated with the 7.0 ft/sec velocity which lends some credence to this explanation. With one exception, the data essentially lie within an error band of $\pm 2 \times 10^{-5}$ $(Btu/hr\text{-}ft^2\text{-}^oF)^{-1}$. Based on the preceding, generally it is felt that the LMSC device is capable of fouling factor measurement accuracies on the order of $\pm 2 \times 10^{-5}$ $(Btu/hr\text{-}ft^2\text{-}^oF)^{-1}$.

The influence of velocity on fouling factor as indicated by the 6061 aluminum data at 3.4 and 7.0 ft/sec appears to be negligible. The data points, with one exception, fall within the expected measurement accuracy of the device. The efficacy of continuous low dose chlorination is demonstrated by a comparison of the 7.0 ft/sec data for aluminum. The relatively low dosage rate

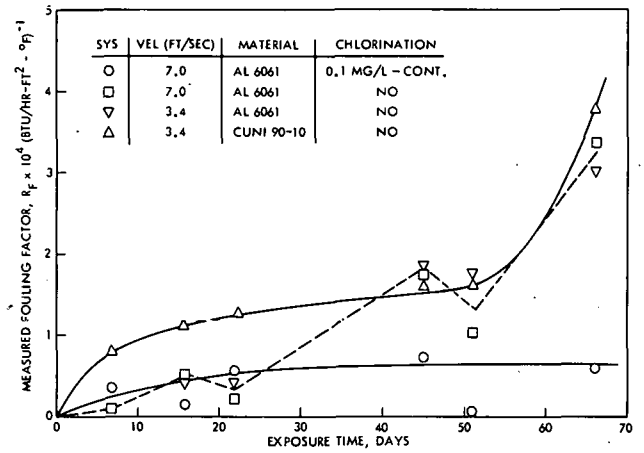

Fig. 10 Measured Fouling Factor Versus Exposure Time - San Diego Bay

of 0.1 mg/ℓ is sufficient to maintain the fouling factor at a value of approximately 6×10^{-5} $(Btu/hr\text{-}ft^2\text{-}^oF)^{-1}$. The actual thermal resistance resulting from biofouling alone could not be determined, but it is very likely that a substantial portion of the indicated fouling factor is due to the corrosion layer which forms on the initially clean tube. Runs at various chlorination rates will be necessary to determine the optimum rate for particular seawater conditions.

A comparison of the data for Cu-Ni with that for aluminum at 3.4 ft/sec in Fig. 10, shows the Cu-Ni to have the larger fouling factor for the first forty days. This is quite similar to the University of Hawaii data for 90-10 Cu-Ni and 5052 aluminum taken off Keahole Point, Hawaii.[9] Their data also showed Cu-Ni to have a larger fouling

factor than aluminum for approximately the first forty days for seawater velocities which were approximately twice the present values (6-7 ft/sec). The principal difference lies in the period beyond forty days where the present data from San Diego Bay indicate a similar fouling rate for both Cu-Ni and aluminum. The Hawaii data, on the other hand, showed the aluminum fouling factor to be approximately 50 percent greater than the Cu-Ni at the end of 59 days of fouling. The approximately linear increase in fouling factor with time for the Cu-Ni tube was shown to be almost directly attributable to a linear increase in the thickness of the Cu-Ni corrosion film. The present data for Cu-Ni suggest the formation of a corrosion layer during the first 50 days followed by biofouling at a rate similar to that for an aluminum tube.

COMPARISON OF CONCEPTS

A completely objective comparison of the three concepts is not possible at the present. This is primarily due to the different levels of development for the three devices. The CMU device has benefited from a rather extensive development program while the indirect device is still basically conceptual in nature. The LMSC device has a development status somewhere in between, but with considerably less data acquisition experience than the CMU device. The subjective comparison shown in Table 2 tends to indicate an advantage for the LMSC device for most of the items considered. Present results appear to support the claim of superior accuracy although biofouling data are not currently available for the indirect device. One of the attractions of the LMSC device is its simplicity and relatively low cost. A comparison of the instrumentation required is given by a consideration of the necessary measurements for the three devices; LMSC - one temperature differential, one velocity, and one heater power. CMU - one temperature differential, one velocity, and time. Indirect - two temperature differentials, two velocities, and one heater power. Data reduction should favor the steady state devices over the CMU transient concept. Calculation of the fouling factor for the LMSC and indirect devices involves the relatively simple algebraic computations given by Eqs. (5) and (8) while the CMU device involves a transient analysis for the experimental time constant.

The accuracy of the LMSC device with large seawater temperature variations remains to be demonstrated although present expectations are that it will be relatively insensitive to seawater temperature change. The larger thermal mass and recirculation secondary fluid of the indirect device should make it less suitable than the LMSC device for operation in an environment with significant seawater temperature variation. Should it become desirable to replace the tubular biofouling section of the BMD, the indirect device has a decided advantage over the other two. The LMSC device would present the greatest expense because of the embedded thermistors.

Table 2 SUBJECTIVE COMPARISON OF BIOFOULING MEASUREMENT TECHNIQUES

	LMSC	CMU	INDIRECT
Accuracy	1	2	2
Complexity	1	2	3
System Cost	1	2	2
Data Reduction	1	3	2
Development Status	2	1	?
SW Temp Variation	1	2	2
Tube Replacement	3	2	1
Fouling Factor	Local	Average	Average

There are definite advantages to being able to measure local values of fouling factor as opposed to the average values obtained by the CMU and indirect devices. An additional advantage of measuring local fouling factors is the ability to specify the state of development of the seawater velocity and temperature profiles. The LMSC device has been designed to provide fully developed velocity and temperature profiles at the locations for which fouling factor measurements are obtained.

In summary, it is felt that the LMSC biofouling measurement device enjoys several significant advantages over the other two methods considered; not the least of which are accuracy and cost.

ACKNOWLEDGEMENT

The experimental fouling factor data presented in this paper were obtained under a Lockheed Independent Research Program by P. C. Springer of Lockheed Ocean Laboratory, San Diego, Calif.

REFERENCES

1. Fetkovich, J.G., "A System for Measuring the Effect of Fouling and Corrosion on Heat Transfer under Simulated OTEC Conditions," COO-4041-10, Carnegie-Mellon Univ., Pittsburg, PA, Dec. 1976.
2. Fetkovich, J.G., et al., "Degradation of Heat Transfer Rates Due to Biofouling and Corrosion at Keahole Point, Hawaii," Proceedings of the OTEC Biofouling and Corrosion Symposium, Seattle, Wash., 1977.
3. Fetkovich, J.G., et al., "Studies of Biofouling in Ocean Thermal Energy Conversion Plants," Proceedings of the Fourth Annual Conference on Ocean Thermal Energy Conversion, Univ. of New Orleans, La., 22-24 Mar 1977.
4. Kline, S. J. and F. A. McClintock, "Describing Uncertainties in Single-Sample Experiments," Mechanical Engineering, Jan 1958.
5. Bird, S. P., "Uncertainties in Heat Transfer Measurements Obtained With the CMU Biofouling Device," Proceedings, Condenser Biofouling Control Symposium, Atlanta, GA 26-28 Mar 1979.
6. Wilson, E. E., Trans ASME, Vol. 37, p 47, 1915.
7. Springer, P.C. and W.L. Owens, "A Measurement Technique for Condenser Tube Biofouling," Proceedings, Condenser Biofouling Control Symposium, Atlanta, GA, 26-28 Mar 1979.
8. Sleicher, C. A. and M. W. Rouse, "A Convenient Correlation for Heat Transfer to Constant and Variable Fluid Property Fluids in Turbulent Pipe Flow," Int. J. Heat Mass Transfer, Vol. 18, 1975, pp 677-683
9. Liebert, B. E., et al., "The Effects of Biofouling and Corrosion on Heat Transfer Measurements," Proceedings, Sixth Ocean Thermal Energy Conference, Washington, D.C., 19-22 June 1979

DISCUSSION

E. Kinelski: Are other people also finding that biofouling on Cu-Ni is greater than they had anticipated?

W. Owens: That apparently is the general assumption. I am not aware of other data, but Joe Rynewicz tells me that other people have also found this general occurrence. Can you elaborate on that, Joe?

J. Rynewicz: This corresponds to the Gulf of Mexico results reports there and the Hawaiian results reported by them. I think the term "fouling" is really the wrong description. The heat transfer resistance may be due to slime or corrosion; we can't say.

Basically you have to remember that copper base alloys inhibit biofouling through the generation of corrosion products which are toxic to marine organisms. Copper-nickel is more corrosion-resistant than copper, just the fact that you'd have a lower corrosion rate implies less resistance to biofouling.

Now, you again have to differentiate between macro- and microfouling. Copper-nickel alloys are presumably very resistant to macrofouling but not necessarily to microfouling. It seems from some of the Hawaii data, some of our data, and I think from somewhere else, I believe from EPRI, that very, very thin films of microorganisms accumulate on copper-nickel alloys. But there is no real evidence for or against copper-nickel alloys preventing microfouling.

I think there is evidence in the case of antifouling paints in the marine environment that you do, in fact, get high sliming rates on copper-based antifouling paints.

Another point is that with high-copper compounds I get the impression that you get an oxide or some kind of corrosion product that comes off rather easily, and I wonder whether, as this product comes off, it probably will take any biofouling away with it.

F. LaQue: We used to think that the antifouling properties of the copper-nickel alloys were attributable to some toxic effect of soluble ions released, copper ions, particularly, from the metal. That mechanism has recently been challenged, and there is some evidence that perhaps it wasn't well-founded in the first place. Even though I have published critical rates of release that are supposed to prevent biofouling, the present feeling seems to be that the alloys resist fouling because the organisms do not settle well on corrosion products having a particular characteristic, but once that characteristic has changed, which it does with time, the alloy becomes foulable. And I think perhaps we ought to make a distinction between the rate at which the resistance to heat flow is increased and the ease with which the original heat flow can be restored. Perhaps if the copper alloys have an advantage with respect to microfouling, it may be with respect to the ease by which some cleaning method will restore the heat transfer performance.

W. Owens: I'd also mention that one of these devices is being installed on Mini-OTEC that will be used to measure the cold water fouling rate, which should be very interesting.

POSSIBLE Cu-Ni-CLAD STEEL MATERIAL AND ABRASIVE SLURRY CLEANING SYSTEM FOR PLATE-FIN-TYPE OTEC HEAT EXCHANGERS

Michael J. Mann

General Electric Company
Schenectady, New York 12345

Abstract

The use of a copper-nickel-clad low-carbon steel (Cu-Ni/LCS) material for Ocean Thermal Energy Conversion (OTEC) heat exchangers would have the advantage of placing corrosion- and fouling-resistant Cu-Ni on the seawater side and low-cost steel on the working-fluid (Freon or ammonia) side. This clad material can be produced by a cold, 100% metallurgical bonding process. Estimates of relative costs of materials for plate-fin heat exchangers indicate that this material, 0.01 in. of 90-10 Cu-Ni on 0.04 in. of LCS, would cost less than unclad Al 5052, titanium, or stainless steel. For cleaning these plate-fin heat exchangers with their small, non-circular passages, neither Amertap rubber balls nor M.A.N. brushes (mechanical systems used inside the tubes of shell-and-tube heat exchangers) is appropriate. Therefore, experimental development of a slurry (sand/water) cleaning system is recommended. With a flow velocity of 12 ft/s through the exchanger, it is believed that a closed-cycle slurry system would prove successful and low in capital cost.

Use of Cu-Ni-Clad Steel

Introduction

The OTEC heat exchanger concept being developed by GE and Sea Solar Power is a cross-flow, plate-fin type (Fig. 1). This work on material selection and slurry cleaning was done under Phase I of the U.S. Department of Energy's (DOE's) Power System Development II (PSD II) program. Further details on the heat exchanger design and the heat transfer experiments done to date are given by Anderson and Pribis.[1a] The design requirements for PSD-II established by DOE led to our selection of the following criteria for material selection:

- The heat exchanger must be designed for 30-year life in a marine environment.
- The wall thickness shall be determined by developing strength requirements in conformance with ASME Pressure Vessel Codes (Sections II, V, VIII Division 1 and IX) and adding appropriate corrosion loss values.
- The material must meet the thermal requirements of the system.
- The material must be readily available and compatible with the fabrication requirements of the heat exchanger, including surface enhancement.
- Use of a fouling-resistant material is desirable.

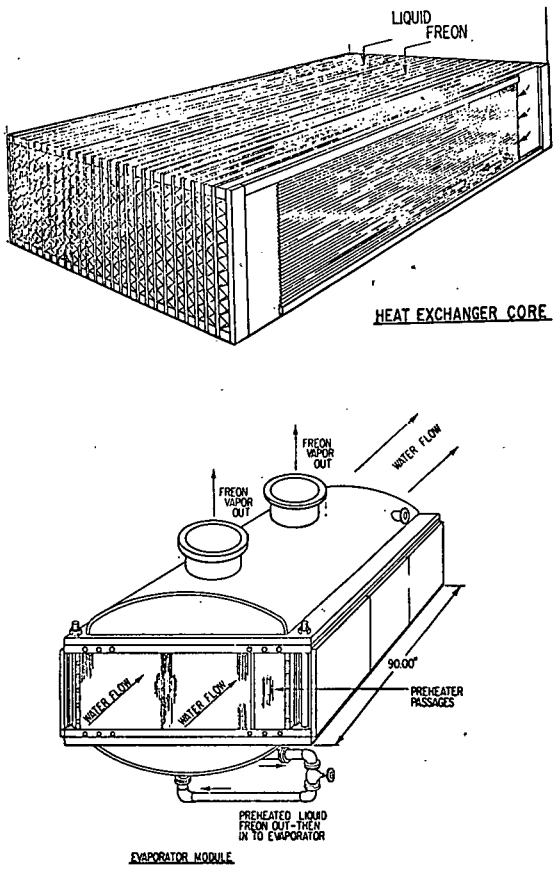

Fig. 1 Schematic diagrams of the plate-fin heat exchanger concept.

- The material must be cost effective and must support the final design requirement.

Freon is proposed as the working fluid with ammonia as an alternate. The surfaces on the working fluid side are enhanced. Water channel flow velocity will be approximately 2.0-4.0 fps and no passive corrosion control features will be incorporated in the exchanger. No enhancement will be required on the seawater side since the design will take advantage of the fin effect. Because of the configuration of the water channel, crevice corrosion becomes a major consideration.

Discussion of Major Materials

Titanium. Titanium is the best available candidate material because it is resistant to all types of corrosion, and no corrosion allowance is required even in thin plates, to meet the design life criterion

(Tables 1 and 2). It has good strength characteristics and low density. Its thermal conductivity is poor but in thin sheets it is adequate. For the GE application, however, the fabrication of titanium poses some limiting problems in that the material cannot be readily extruded and is very difficult to bend or roll. The availability of titanium has been an area of frequent concern to the OTEC program. Current U.S. production of titanium sheet, strip and plate stands at 3500 tons/year.[2] For the GE base case design, this amount would be consumed by the production of one 100-MW_e OTEC plant. Although industry production priorities could be expected to be reordered, material availability could be a problem. Titanium's main drawback is its high cost (Table 2).

Aluminum Alloys. Aluminum alloys have been leading contenders for OTEC applications. Current leading alloys in descending order seem to be roll-welded, Alclad 3003 or 3004 and bare 5052.[3] These alloys have low density and excellent thermal conductivity and are low in cost. The 5052 alloy is included in Table 2; the cost of Alclad 3003 or 3004 would be lower than the cost of 5052 for tubular heat exchangers. Although normally believed to be easily worked, the leading aluminum alloys present some interesting fabrication problems to the GE design. While bare 3003 is extrudable, cladding cannot be included in a complex extruded shape. Some attempted extruded shapes are shown in Fig. 2. Although some arguments dispute this, bare 5052 is too hard to be extruded into smooth, acceptable shapes. Options left on the GE design were extensive machining or mechanical assembly.

Beyond the fabrication difficulties, however, the key issue is whether corrosion will limit the design life. LaQue[1b] has concluded that 10-yr life can be expected for the aforementioned alloys in tubular heat exchangers (and Al suppliers say a greater life is probable), but its use in plate-type heat exchangers probably will be ruled out by crevice corrosion.

Stainless Steel. Allegheny 6X (high nickel - high chronium) has been generally accepted as the most appropriate stainless steel product available

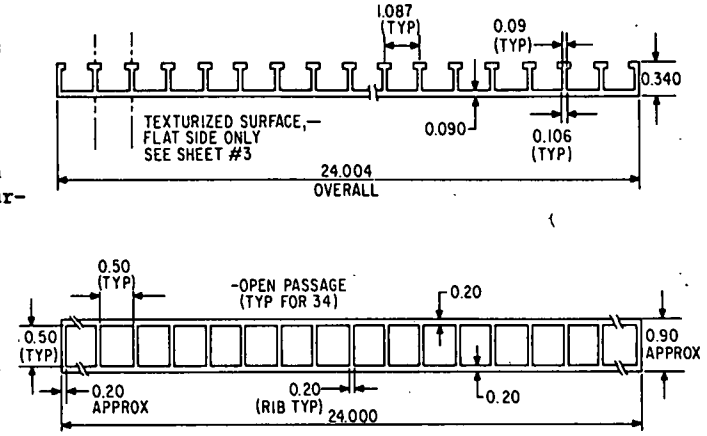

Fig. 2 Extruded shapes attempted with aluminum alloys.

for OTEC use.[1b] The alloy has demonstrated excellent corrosion resistance and has good strength characteristics, thus allowing thin walls. Currently, Allegheny-Ludlum is producing the material only in tubes, but no technical limitation prevents strip production. The thermal conductivity is poor. The material is not easily worked and fabrication may present problems (see Table 2). A newer alloy, Crucible's "Sea Cure," has also shown a good ability to resist corrosion in sea water. While long-term test results are not available, investigations to date have been promising.

Copper-Nickel Alloys. Copper-nickel alloys have provided stalwart duty in naval seawater systems for many years.[3] Recent Argonne analyses of candidate materials indicate substantial anti-fouling protection obtained from Cu-Ni alloys; 90-10 Cu-Ni has good fouling resistance due to minute release of copper ions at the freely corroding surface. Information recently developed by the University of Hawaii at Keahole Point substantiates this.[1c] The alloys are very resistant to seawater corrosion, which is normally experienced as a generalized attack and subsequent loss of material.[4] On the other hand, concerns have been raised over Cu-Ni's

Table 1

Material performance in seawater.[(2)]

Material	Corrosion rate, mil/yr			Crevice	Erosion at 4-8 FPS	Biofouling	Stress Corrosion Cracking
	General	Pitting	Galvanic				
Titanium Ti-50A	Nil	Nil	Excellent	Excellent	Nil	Poor	Excellent
Aluminum 5052	4.0 Initially 1.5 Continuous	10-30	Poor	Poor	1-5	Poor	Excellent
Copper-Nickel 706 Cu 90%Cu-10%Ni	C = 1.5 + 0.005T	Nil	Excellent	Excellent	0-1	Excellent	Good
Stainless Steel	1.0	0.5	Excellent	Good	Nil	Poor	Excellent

[a]Based on Ref. 8.

Table 2

Cost comparison of candidate core materials (solid and clad) for OTEC flat plate heat exchanger design.

Material	Density[a] (lb/ft^3)	Thermal[a] Conductivity (Btu/ft^2/hr) (1°F/in.)	Design[b] Stress (ksi)	30-Year-Life Design Thickness (in.) St.	30-Year-Life Design Thickness (in.) Corr.[c]	U Factor (Btu/hr/°F/ft^2)	Weight Per Sq Ft (lb/ft^2)	Estimated Cost Per Pound[d] ($/lb)	Relative[e] Material Cost Al = 1.0	Delta[h] Plant Costs ($/kWe)
SOLIDS										
Al 5052	168	960	6.3	0.09	0.10	541	2.66	1.05	1.0	0
9010 Cu-Ni	558	312	9.5	0.065	0.01	514	3.48	1.50	1.91	+66
Stainless Steel AL-6X[f]	506	95	18[6]	0.03	0.01	483	1.68	3.50	2.36	+163
Stainless Steel Sea-Cure SC-1[g]	483	114	18(+)	0.03	0.01	500	1.61	2.25	1.40	+28
Titanium SB265,GR.2	282	114	12.5	0.04	0.0	500	0.94	6.45	2.35	+115
CLADS										
9010 Cu-Ni/LCS	9010-558 LCS-490	349	13.7	(LCS) 0.04	(9010 Cu-Ni) 0.01	558	2.09	1.60	1.16	-11
9010 Cu-Ni/SS	9010-558 SS-501	134	18	(SS) 0.03	(9010 Cu-Ni) 0.01	513	1.71	2.85	1.71	+45
Al 5052/LCS /Al 5052	Al-168 LCS-490	920	12.5	(Al) (LCS) 0.06/0.01	(Al) 0.06	558	2.08	2.00	1.45	+46
Ti Al 3003	Al-168 TI-282	241	12.5	(Al) (Ti) 0.05/001	0.0	564	0.935	5.50	1.76	+55

[a] Ref. 5.
[b] Ref. 6.
[c] Based on total amount of metal expected to be lost due to corrosion and/or erosion - see text.
[d] Based on expected metal market costs on May 1, 1979.
[e] Cost ratioed by U factors relative to AL5052.
[f] Allegheny-Ludlum trademark — see Ref. 6.
[g] Crucible Metals trademark.
[h] Costs are relative to aluminum with core materials representing approximately 25% of total H.E. cost. For the purpose of this analysis, aluminum heat exchanger costs are assumed to be $700/kWe and no consideration is given to fabrication difficulties between materials.

vulnerability to stress corrosion cracking in an ammonia environment. Although Dow Chemical is currently investigating this problem,[1d] current best engineering practices avoid the Cu-Ni/ammonia interface. The alloys are readily available but pose certain fabricational problems for the GE design; they are not extrudable and would need to be machined or formed. The alloys are quite dense but have fairly good strength.

Potential New Clad Materials. Texas Instruments' Metallurgical Materials Division in Attleboro, Massachusetts has found that with a cold pressing process, metals can be 100% bonded to provide dissimilar physical characteristics in one final material. This process can bond materials as thin as 0.010 in. each and provide a product width of 24 in. Some combinations are ruled out because of temper dissimilarities causing warping or bond failure. However, several viable alternatives have emerged. It should be pointed out initially that galvanic dissimilarities have been considered in the application of these components. Extensive design concern has been taken in GE's approach to insure that the base material will not come in contact with seawater to form a galvanic couple with the cladding material.

The current leading clad candidate is 90-10 Cu-Ni on the seawater side bonded to a low carbon steel (LCS) on the working-fluid side. The Cu-Ni provides the desired resistance to fouling and corrosion while the LCS provides strength and compatibility with ammonia or freon. The material has relatively good thermal properties and can be cost effective (Table 2).

Other clad materials being considered include Cu-Ni/stainless steel, Alclad/LCS/Alclad and Al/SS. The item that becomes limiting in clad approaches is the fabrication, particularly when an enhanced surface on the working-fluid side is desired.

Cost Trade-Off Calculations

The relative heat transfer characteristics of the candidate materials have been assessed by the heat transfer equation,

$$Q = UA\ (LMTD) \quad (Btu/hr) \qquad (1)$$

where: U = heat transfer coefficient(Btu/hr/ft^2/°F), A = effective area for heat transfer (ft^2), and LMTD = log mean temperature difference (°F).

Relative surface areas and resulting relative costs are referenced to the estimated cost for unclad Al 5052. It is assumed that the LMTD does not change appreciably for the materials considered.

The U is computed from

$$U \simeq (1/h_w + R_f + t/k + 1/h_f)^{-1} \qquad (2)$$

where h_w is the film coefficient on the seawater side, R_f is the fouling resistance, t is the wall thickness and k is its thermal conductivity, and h_f is the film side. For this trade off, the following values are assumed: h_w = 1209, R_f = 0.00025, and h_f = 1750.

Substitution of these values into Eq. (2) yields

$$U = 1/(0.001648 + t/k)$$

Table 2 gives the results of this tradeoff analysis. The prices of the materials listed are representative of current market quotes and do not represent firm prices from any vendor.

A Sand Slurry Cleaning System

Introduction

It would be fruitless to select working materials and optimize heat exchanger design if no means for removing fouling from the heat transfer surfaces were provided. In compact, plate-fin heat exchangers the water flow channels are small and irregularly shaped, so that mechanical cleaning systems based on balls (e.g., Amertap) or brushes can not be used. An alternative is needed.

Abrasive/sand cleaning was probably used to clean the first dishes and scour the first pots. Gold miners were very familiar with the cleaning capabilities of abrasives and even used the technique in early gold processing systems. Train locomotive engineers found that when confronted with a steep upgrade crossing the Rockies that a shovel or two of sand into the locomotive fire box was enough to provide that extra bit of power needed. In current state-of-the-art machinery, General Electric uses sand and walnut-shell slurries in turbine cleaning. On Lake Ontario, the Niagara-Mohawk Company (a private utility) takes advantage of a high solids concentration in the cooling water to effect condenser tube cleaning; no other cleaning technique or abatement measure is used, and performance and service of these condensers is believed to be above average.

The mechanism of abrasive cleaning is quite simple: When the impact force of the solid medium on the biofouled surface is sufficient to overcome the fouling attachment strength, the attached material is removed to become part of the cleaning flow system. Media currently being considered for OTEC abrasive slurry cleaning include several types of sand, diatomaceous earth, shells, and detergents. The design requirements addressed are listed in Table 1.

An interesting observation from OTEC biofouling/cleaning experiments[1c,e] is that the fouling rate is lower on Cu-Ni surfaces than on Ti, Al, or stainless steel, and that the fouling rate on Cu-Ni does not increase after cleaning as it does for the other materials.

The Slurry Cleaning System Concept

In the General Electric concept for heat exchanger cleaning, sand is used as the cleaning medium in a single-pass, flow-reversible mode. The cleaning cycle is controlled by referenced heat transfer monitor units and the module is cleaned to a fouling resistance coefficient R_f of 0.0001 hr-ft^2-^{o}F/Btu. The slurry is then directed to a solids/water separator where floatable material is removed, seawater is discharged overboard, and the sand is returned to the sand hopper. A schematic representation of the system is shown in Fig. 3, and the components are described in Table 3.

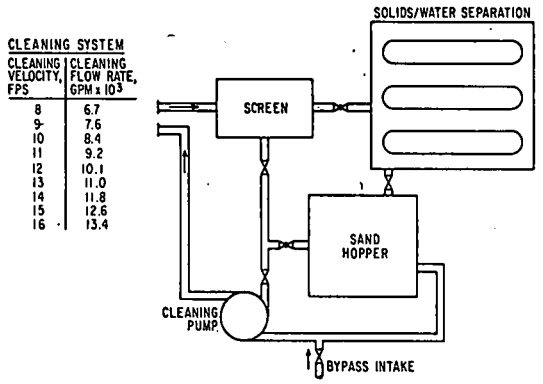

Fig. 3 Schematic diagram of the cleaning system.

Table 3

Characteristics of proposed cleaning system.

Components	Type	Capacity	Material/construction	Estimated cost
Pumps (2)	Solids handling, centrifugal	7500 gpm at 40-ft head	"Nihard", 24% Cr; 100 HP driver w/variable speed controller	$15 k each
Solids/water separator	Coalescing vertical plate	10,000 gpm	Fiberglass	$10 k
Sand hopper	Vertical cylinder	300 ft^3 (8-ft diam, 10-ft high)	Epoxy coated, self-dewatering	$ 2.5 k
Sand feeder	Volumetric, trap	-	-	$ 2 k
Piping & control				$25 k
			Total	$55 k

Some make-up sand may be required periodically. Although the separator is 99+% efficient for removal of particles near 70 μ some sand will undoubtedly be lost.

The system is easy to operate. Flow directional channels and valves allow the cleaning volume to be directed to an isolated heat exchanger section (Fig. 2). There is no requirement to shut down the rest of the plant. Mechanics and a schematic of the coalescing plate separator are shown in Fig. 5.

Operational control parameters include:

Cleaning flow velocity:	12 fps
Cleaning duration/module:	1 min.
Sand concentration:	3%
Mean particle size:	70 μ

This cleaning system should meet the stated design objectives at a price expected to be near $\$20/kW_e$ including installation and operating expenses. Current best estimates for other mechanical cleaning systems exceed $\$50/kW_e$.

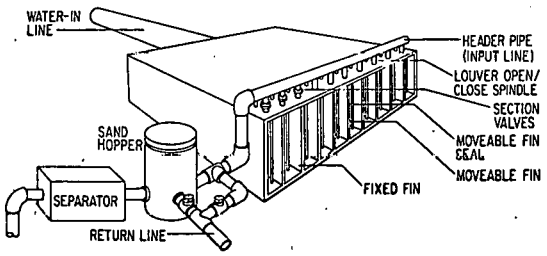

Fig. 4 Schematic diagram of cleaning system for 0.2-MW_e heat exchanger.

Concluding Remarks

For the slurry cleaning system, a great deal of work needs to be done to validate and then fine-tune the proposed system. Since there is no definitive literature on abrasive cleaning, developmental concerns include:

- A need for data on optimum abrasive media concentrations and velocities.
- An understanding of the material "break-away" velocity in an abrasive environment.
- A verification of the effectiveness of the coalescing plate solids/liquid separator.
- An understanding of potential momentum problems on the fluid turn.

If these concerns are successfully met, the abrasive cleaning system will offer a simple, cost-effective solution. Testing on OTEC-1[1f] would be invaluable in proving this capability.

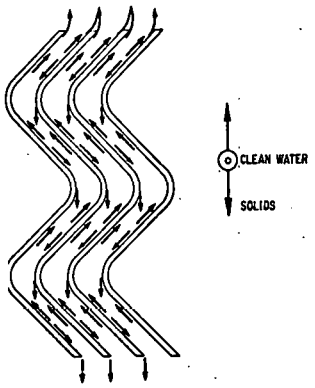

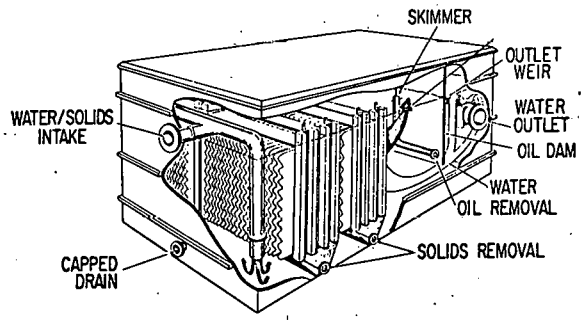

Fig. 5 Coalescing plate separator.

References

1. Dugger, G. L., editor, Proceedings of the 6th Ocean Thermal Energy Conversion (OTEC) Conference, Washington, D.C. June 19-22, 1979:

1a) Anderson, J. H., Jr. and Pribis, P. B., "Compact Heat Exchanger Design Progress," Vol. II.

1b) LaQue, F. L., "Qualification of Aluminum Stainless Steel for OTEC Heat Exchanger Tubing," Vol. II.

1c) Liebert, B. E., Berger, L. R., White, H. J., Moore, J., McCoy, W., Berger, J. A. and Larsen-Basse, J., "The Effects of Biofouling and Corrosion on Heat Transfer Measurements," Vol. II.

1d) Schrieber, C. F., Grimes, W. D. and McIlhenny, W. F., "Interleakage of Ammonia and Seawater in OTEC Heat Exchangers Effects on Corrosion and Scale Formation," Vol. II.

1e) Little, Brenda, Morse, J., Loeb, G. and Spiehler, F., "A Biofouling & Corrosion Study of Ocean Thermal Energy Conversion (OTEC) Heat Exchanger Candidate Metals," Vol. II.

1f) Svensen, N. A., "An Overview of the OTEC-1 Design," Vol. I.

2. Engineering and Mining Journal, McGraw-Hill, p. 172, March 1979.

3. Perry, D. A. and Kelso, J. M., "A Disucssion of Cupro-Nickel Heat Exchangers in Seawater Service," Harrison Radiator Div., General Motors Corp., Report #H361-A.

4. Personal Communication with Frank Ansuini, Kennecott-Copper, Lexington, Mass., January 5, 1979.

5. "Properties of Some Metals and Alloys," INCO Report No. A-297-A, April 1977.

6. ASME Boiler and Pressure Vessel Code, Section VIII, Division 1, 1979.

7. Wagner, R. H. and Bonewitz, R. A., "Catalog Information on the Performance of Aluminum in Seawater," Alcoa Rept. NXS-3 prepared for Battelle Pacific Northwest Laboratory, April 5, 1978.

8. Rosales, L. A., Dvorak, T. C., Kwan, M. M. and Bianchi, M. P., "Materials Selection for Ocean Thermal Energy Conversion Heat Exchangers," Proceedings of The Fifth Ocean Thermal Energy Conversion Conference, February 20-22, 1978, Miami Beach, Florida, Vol. 4, pp. VIII-231-264.

DISCUSSION

Question, Union Carbide: I do not think your aluminum costs and general corrosion rates do justice to materials like Alclad 3004, let alone the general corrosion rate estimate for Sea Cure and AL-6X. You can drop the general corrosion rate by 25% for both the Sea Cure and the AL-6X equivalent materials and certainly come up with economic considerations that would be among the best options that you have, competitive with the duplex alternative you are proposing.

M. Mann: First, we are not looking at the general corrosion weight. We are trying to look at an integrated general pitting, crevice effective corrosion rate, so we can design a wall thickness that will not give a penetration in the 30-yr design life we want. I agree with you on general corrosion, and the numbers possibly could be dropped.

POSSIBLE USE OF THE CATHELCO SYSTEM TO CONTROL FOULING IN OTEC SYSTEMS

Clifford W. Smith
CV Associates
McLean, Virginia 22101

Barry J. Kirk
Cathelco Ltd.
Chesterfield S40 1JS, England

William J. Blume
Blume Worldwide Services
Scarsdale, New York 10583

Abstract

The success of an OTEC plant is very dependent on the control of marine fouling without adverse effects on heat exchanger performance, corrosion, environment or cost. Cathelco is a unique fouling control system employing two anodes at very low current: a) marine growth anodes which release copper ions which prevent the settlement of the primary forms of biofouling on surfaces within the system being protected, and b) trap corrosion anodes which release aluminum, which serves as a surface conditioner to enhance deposition of the copper antifoulant throughout the system and forms a protective coating thereby reducing corrosion.

Introduction

The successful use of the Cathelco system for the prevention of biofouling and corrosion in seawater systems in over 100 ships, submarines and offshore structures has led to the examination of the suitability of the system for use in electric utility applications, shore-based test plants, OTEC, etc. in which the water flows are considerably greater than in any previous application of the system. We believe that the system can be scaled up, that it will offer protection against marine fouling acceptable cost, and that it will be easy to install, operate and maintain without significant adverse environmental consequences.

The discovery that it could be used to control biofouling occurred by accident during trials being carried out to descale a large sheet of steel that was encrusted with scale and rust, situated below the waterline at the end of a wooden pier. Some 150 ft away, anodes were suspended from a floating log. The steel sheet was acting as a cathode to generate hydrogen which lifted off the scale and rust and inhibited further scale formation.

At the same time, experiments were being conducted on the control of 'teredo' in the dock pilings and log booms using different combinations of anode materials. Between the anodes and the cathode were wooden piles which were heavily encrusted with numerous variations of marine growth (Fig. 1a). With one particular combination of anodes, the marine growth started to detach from the piles and within 6 months the piles were virtually clean (Fig. 1b). Since the wooden piles were non-cathodic, the explanation appeared to be that the marine life found the environment to be unhospitable and departed. This observation led to the development of the present Cathelco Marine Growth Control System.

It has been known for years that marine growth will not attach to surfaces where active copper corrosion is taking place. The corrosion products being formed can inhibit adhesion. More importantly, copper is a toxic substance above certain levels and proves intolerable to marine life. Finally, it was observed that the use of certain combinations of copper and aluminum was highly effective in the treatment and prevention of fouling on underwater surfaces which fell within the tidal flow path of the seawater.

Cathelco was approached by Vickers Shipbuilding Group (U.K.) concerning the possible use of this system to protect the hulls of ships from fouling. Under their sponsorship a research program was undertaken. The method was found to be effective for hull protection but critically dependent upon the efficiency with which the treated water was kept in contact with the surface being protected. The

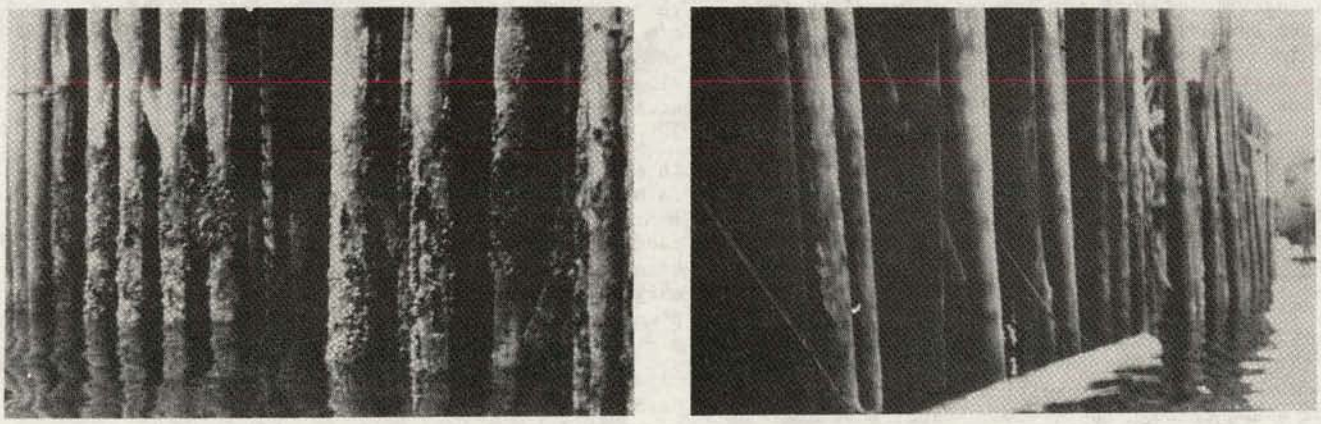

a b

Fig. 1 The marine fouling seen on the wooden piles at left disappeared, as shown at right, after 6 months' exposure in a tidal flow between anodes and a cathode.

amounts of anode materials generated were remarkably small, and the accumulative effect was wholly dependent on the direction of flow.

System Design and Operation

The systems presently in use comprise two anodes, either mounted individually, or, where space is limited, in a single assembly: a) the marine growth (MG) anode, which can be of pure copper but is most effective when manufactured from special alloys, and b) the trap corrosion (TC) anode which may be aluminum or iron. System hardware normally comprises a control panel which incorporates anode monitoring and controls which converts main voltage to low voltage DC, cabling, mounting arrangements for the anodes, watertight glands to ensure system integrity and safety caps.

The anodes are normally installed as near as possible to the point of entry of the water into the system to be protected and care is taken to ensure that no untreated water is introduced into the system at some downstream point. In some cases, where the water system is in intermittent use, it is possible to link the anode controls to the inlet valve controls so that when the inlet valve is shut, the anodes are switched off, thus reducing anode wastage. Occasionally, iron anodes may be used, particularly in systems using Al-Br or Cu-Ni alloys, since the iron compounds released by these anodes provide corrosion protection to condenser tubes.

The mechanism by which the system works is believed to be as follows:

a) Anodic dissolution of aluminum in sea water produces a flocculent gel of hydroxylated alumina, which coagulates due to the high ionic strength of seawater. The gel is likely to carry a small charge, either positive or negative.

b) Simultaneous dissolution of copper provides Cu^{++} ions which are presumed to adsorb on the alumina gel where they confer a net positive charge to the surface. Other stray metallic ions present in the seawater are also likely to be collected by the gel.

c) The presence of dissolved copper ions will contaminate any passive films forming on aluminum in the vicinity which will allow the aluminum anodes to continue to dissolve.

d) Where the water velocity is sufficiently low, the gel collects and adsorbs on metal surfaces exposed downstream from the treatment area. The Cu^{++} ions become sufficiently concentrated in just those areas most susceptible to marine fouling. Without this concentrating/collecting effect of the alumina gel, the copper concentration is insufficient to control fouling.

e) Adsorbtion is likely to be favored at surfaces carrying a charge of opposite sign to that of the gel. In the case of metallic pipework acting as the cathode, a thin film of alumina, which will provide a degree of corrosion protection, builds up. If the pipework is nonmetallic, a dummy cathode must be used to complete the electrical circuit, and the gel will tend to settle in stagnant areas, be adsorbed in metallic sections of opposite charge, or be swept through the system. Since most heat-exchanger tubes are likely to have a small net positive charge, there may be no deposition of alumina, particularly as water velocity is higher in the tubes.

Evidence from water samples taken upstream and downstream of the anodes indicates that the treatment tends to purify the water by the action of the alumina gel in mopping up stray metals. Any Al-Cu complex which may be carried through the system will contain very low concentrates of copper, since the actual production of copper in solution is less than 2 parts per billion (ppb) in the first place.

Application to OTEC

Cathelco systems have been supplied to a number of ships and installations whose water flow and configurations vary considerably. Systems have been successfully employed for flows of 3,000 to 17,000 gpm. Since the effectiveness of the system depends on its ability to keep the electrolytic products near the surface to be protected, the principle remains the same whether the flow is 5000 gpm or 50 million gpm. The use of Cathelco for OTEC poses the following problems, some of which may be answered by laboratory work or small-scale test installations and some of which may not be resolved.

a) Consider the problem of macrofouling. The water flow through each of the cold and warm water pipes is of the order of 60,000 gpm per net megawatt. There may be no macrofouling problem in the cold water pipe, but for the time being it will be assumed that there is. Clearly, if the pipe does not need treatment, the figures given below should be halved. Our experience to date shows that about 2 ppb of copper is sufficient to control macrofouling and to ensure adequate aluminum as a carrier, the Cu/Al ratio being of the order of 4. This means, therefore, that the copper usage would be 3.5 lb/day/MW_t, and the aluminum usage 0.9 lb/day/MW_t. To give a two-year anode life in a 400-MW_t plant, 456 tons of copper and 114 tons of aluminum would be needed. A rough estimate of installation cost is about $50 M, with an anode replacement cost at 2-yr intervals of about $20 M, and a power consumption of about 12 kW_e. Several things may affect this calculation. First, 2 ppb of Cu^{++} may be considerable over-protection; it may be possible to reduce the anode usage by a factor of 10 or more, which would also considerably reduce the power consumption and annualized replacement cost. Second, we have assumed a linear relationship between anode usage and water flow, and this may not be valid. What we are trying to ensure is that fouling is prevented on the pipe surfaces. Why not, therefore, aim to treat the boundary layers only by putting anodes radially around the pipe at certain intervals along the pipe, particularly just downstream of areas of turbulent flow?

b) In systems containing long pipe runs, is it sufficient to treat the water at the inlet? It is believed that the presence of copper deters marine organisms from settling, but at some distance downstream, where the effects of Cathelco have been diluted or have disappeared, it may be necessary to increase the current at the anodes, or to place booster anodes.

c) What happens to the floc? In a metallic pipe system the pipe itself is normally used as the cathode. This has a beneficial side effect, because ionic products, gradually deposited on the pipe walls, form a thin corrosion-resistant film, which is fine until we reach the heat exchangers where this film may cause a reduction in heat transfer. However, as has already been stated, if the

heat exchanger tubes carry a small positive charge then the floc should be carried straight through. Only trials will give the answers we seek here, but it could be that by deliberately making the heat exchangers carry a positive charge, any potential buildup of film could be obviated. (In a nonmetallic pipe system the floc may settle in stagnant or low velocity areas or be carried straight through the system; under these circumstances a false cathode is needed to complete the electrical circuit.)

d) Will the system also prevent microfouling? Our belief that it may is based only on visual and tactile inspection of heat exchanger tubes, with no evidence of slime. Furthermore, we have had no reports of any evident deterioration of condenser performance in ships at sea. We have also treated ships where algae growth has been the main problem. We are fully aware that this can not be classified as hard evidence, but it is remotely encouraging. Trials will be carried out in the near future on a number of test rigs which may tell us more about this aspect.

e) What about the ecological implications? We know that in systems where the pipework is used as the cathode there appears to be no problem. The water is purer than it was prior to treatment. In the case of nonmetallic pipes, where more of the floc is likely to be carried through the system; does this pose an environmental problem? Again, further trials should provide some answers, but bear in mind that we are still talking of 2 ppb or less of copper.

In summary, evaluation work, here and in England, would provide answers to some of the questions about the applicability of the Cathelco system to OTEC. If the answers are encouraging, the system might prove to be a simple, affordable solution to a number of problems associated with the OTEC program.

FOULING COUNTERMEASURES – STATUS OF TWO MECHANICAL CLEANING SYSTEMS AND CHLORINATION

Daniel F. Lott* and Susan M. Tuovila†

Naval Coastal Systems Center
Panama City, Florida 32407

Abstract

Initial tests of two commercial mechanical systems for removal of biofouling primary films indicate that: (1) for flow-driven brushes, acceptable fouling resistances (R_f) result from 4- or 8-hour cleaning cycles in titanium tubes. For a 4-hour cycle, R_f was held to approximately 0.001 ft^2-hr-^oF/Btu for 17 days. The 8-hour cycle held R_f to < 0.0005 ft^2-hr-^oF/Btu for 3 months. The R_f for aluminum tubes has been held to < 0.0002 ft^2-hr-^oF/Btu with a 4-hour cycle; but exceeded 0.0005 ft^2-hr-^oF/Btu with the 8-hour cycle; (2) for flow-driven, sponge-rubber balls and 15-minute cycling, an acceptable R_f level (< 0.0002 ft^2-hr-^oF/Btu), has not been achieved. Mechanical problems have plagued this system and the initial data cannot be considered valid. Modifications to correct operational deficiencies are required in both cleaning systems as well as the chlorination system. Plans for further evaluation of all 3 systems are discussed.

Introduction

Central to the success of Ocean Thermal Energy Conversion (OTEC) will be the ability to keep the fouling resistance (R_f) on the seawater side of the heat exchanger tubing well below 0.0005 ft^2-hr-^oF/Btu.[1,2] With this point in mind, a program to evaluate biofouling countermeasures was established on St. Andrew Bay near Panama City, Florida, a test site which provides heavy year-round fouling and avoids many of the problems at remote test sites.

Test systems were designed and built by David Taylor Naval Ship Research and Development Center (DTNSRDC), Annapolis, Maryland. The rationale for system design has been documented by Fritsch et al.[1] System design features have been continuously modified and upgraded in response to problems identified during system operation. Three systems are presently under evaluation: flow-driven brushes, recirculating sponge-rubber balls, and chlorination. The advantage of these systems is "off-the-shelf" components providing in situ cleaning and requiring limited maintenance.

St. Andrew Bay is characterized by narrow, meandering, deep water channels surrounded by extensive Thalassia beds. The bay is classified as a positive estuary although fresh water input barely exceeds evaporation;[3] salinities are in the 24-32‰ range. Maximum diurnal tidal range averages 1.5 feet. The characterization data in Table 1 indicate a relatively nonpolluted environment with an extensive microbial community.

*Daniel F. Lott, Microbiologist, Naval Coastal Systems Center (NCSC)

†Susan M. Tuovila, Mathematician, Naval Coastal Systems Center (NCSC)

Test Systems and Procedures

The test system (Fig. 1) comprises 6 major components: (1) water supply and distribution; (2) data acquisition and analysis; (3) controls; (4) flow-driven brushes; (5) recirculating balls; and (6) chlorination units. Water is supplied to test sections from a distribution header which is, in turn, supplied by suction pumps from an intake depth of 7 feet. A feed tank into the distribution header has been removed from the system to eliminate problems associated with marine growth inside the tank. Therefore, the present system is a single-stage pumping system operating at a pressure of 30 psig.

Data acquisition and data reduction are done by a DEC PDP 11/34 operating with software by Fetkovitch[4] and modified by Fritsch et al.[1] Current operational characteristics have required further modifications and will be reported at a later date. Dependent on system operations, a cooling curve is generated for each tube every 30 minutes.

Controls

Controls generally consist of 2 types: (1) controls cleaned daily and (2) freely fouling controls. For each type, both aluminum and titanium heat transfer monitors (HTM's) are used.

The controls that are cleaned daily serve as an internal check of the data gathering system since R_f seldom exceeds 0.0001 ft^2-hr-^oF/Btu. Cleaning consists of 20 passes of a nylon bristle brush on an extended handle. The bristle length and stiffness have been chosen to assure that considerable shear forces are exerted on the tube walls without much scoring of the pepe. This maintenance is generally not performed on weekends or holidays.

The purpose of the freely fouling controls is to provide a measure of the fouling rate until R_f reaches 0.0005 ft^2-hr-^oF/Btu. At that time, the tubes are cleaned and returned to service.

Flow-Driven Brushes and Recirculating Ball Subsystems

As shown schematically in Fig. 2, each heat transfer monitor (HTM) is supplied with a brush slightly larger than the HTM pipes (approximately 1"). Brush movement is controlled by electrically-operated ball valves and a timer. Flow reversal followed by regular flow provides a single cleaning cycle. Depending on cycle intervals, brush movement should generate sufficient shear forces to prevent a buildup of the primary film.

The system for recirculating sponge-rubber balls utilizes unidirectional flow by peristaltic pumps as shown in Fig. 3

Ball movement is controlled by a variable

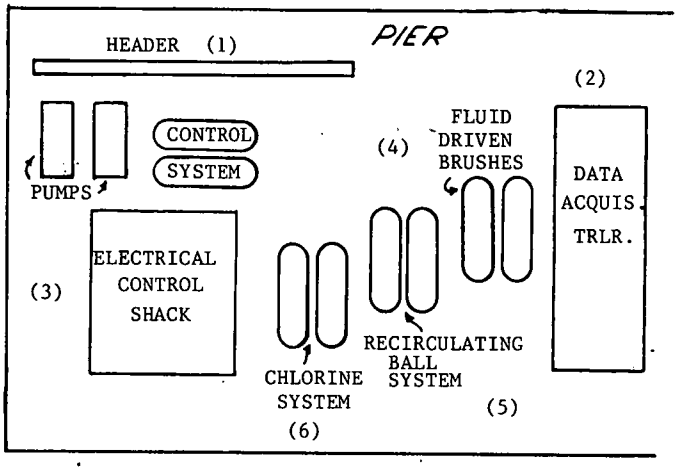

Fig. 1 - Test System Components

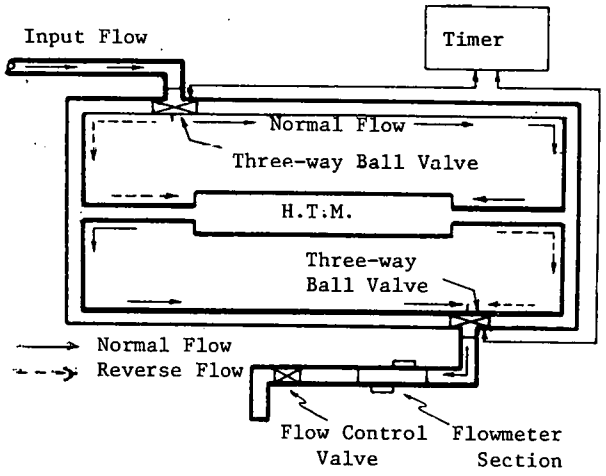

Fig. 2 - Flow-Driven Brush Cleaning System

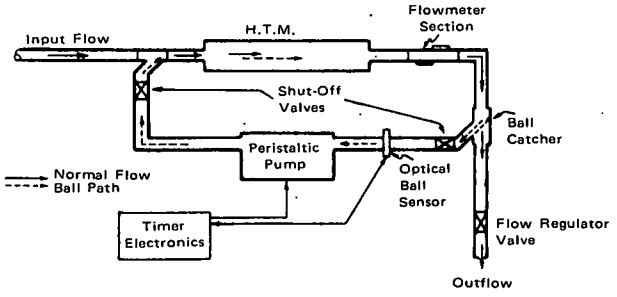

Fig. 3 - Recirculating Sponge Ball Cleaning System

timer. When the specified cycle interval has lapsed, the timer starts the peristaltic pump, which drives a single ball into the HTM loop, through the HTM, and into the ball catcher. The catcher diverts the ball past an optical sensor which simultaneously cuts off the peristaltic pump and resets the timer.

Chlorination

The chlorination system is diagrammed in Fig. 4.

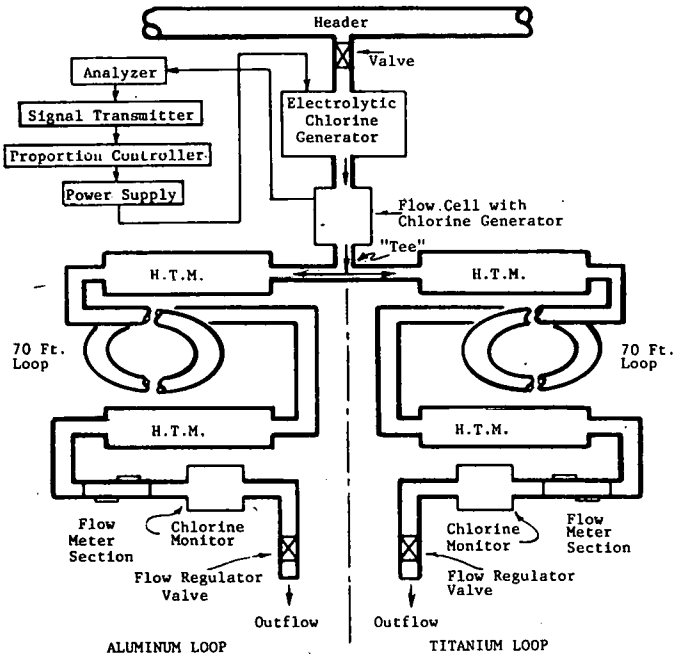

Fig. 4 - Chlorination System

In identical parallel loops for aluminum and titanium, each containing 2 HTM's, input chlorine concentration and residual chlorine concentration are monitored. Input chlorine concentration is maintained at a preset value (0.1 ppm total residual chlorine concentration) by electronic conditioning between the chlorine analyzer and the chlorine generator. This approach eliminates the wide variations in daily chlorine demand that are encountered in this estuary. Chlorine demand for St. Andrew Bay may vary between 0.5 and 4.0 ppm.

Results

Table 2 presents the code for the location and the purpose of each test unit throughout all tests.

Results obtained from the tests initiated 10 May 1979 are plotted as time versus fouling resistance. Each point on the curve generated represents the daily mean R_f. The number of cooling curves used varied from day to day because of change in data analysis specifications and/or operational requirements (i.e. flow within specified ranges, over-

TABLE 2

Code for HTM Tube Purposes and Materials

Tube #	Purpose	HTM Material
1	Control, cleaned daily	Aluminum 5052
2	Control, cleaned daily	Titanium
3	Control, freely fouling	Aluminum 5052
4	Control, freely fouling	Titanium
5	Flow-Driven Brush	Aluminum 5052
6	Flow-Driven Brush	Titanium
7	Recirculating Sponge Ball	Aluminum 5052
8	Recirculating Sponge Ball	Titanium

Odd tube numbers denote aluminum HTM's; even tube numbers, titanium HTM's.

voltages, etc.). R_f's generated from curves with high flow rate standard deviations or poor curve fits were not used in calculation of daily mean R_f.

Discussions and Conclusions

Fig. 5 indicates that daily cleaning of both the aluminum and the titanium HTM's kept R_f in the 0.0001-0.0002 range. Daily maintenance of both aluminum and titanium began on 14 May with the effects of cleaning readily apparent. Throughout the test, Tube 1 has experienced fluctuations in V_0, the thermopile amplifier offset, which have resulted in some lost data during the test period. Two steps have been taken to reduce these effects: (1) insulation of Tube 1 thermopile/thermistor and (2) software modification to reduce drift effects. Present plans call for Tube 1 to be replaced as new HTM's become available. Peaks on the curve for Tube 2, titanium cleaned daily, correspond to weekends when daily maintenance is not performed. This effect is not seen for Tube 1. Apparently, titanium fouls faster and to a greater magnitude for these controls.

The freely fouling aluminum control (Tube 3 in Fig. 6) showed a steady increase in R_f for 10 days. As R_f approached 0.0005, the tube experienced a flow in excess of 20 gpm. Thus, scouring of the primary film occurred. From this point on, R_f decreased gradually until the tube was cleaned on 29 May. Cleaning decreased fouling resistance to initial values.

The titanium freely fouling control (Tube 4 in Fig. 6) experienced two periods of accelerated R_f increase. The initial increase peaked after 5 days at 0.00025 ft^2-hr-^oF/Btu. Fouling resistance then gradually increased for 9 days and was followed by extremely intense fouling for another 5 days. During this period, R_f exceeded 0.0010 ft^2-hr-^oF/Btu. Total time required to reach the maximum R_f limit was 15 days. Cleaning effects were much more dramatic than seen in the aluminum tube.

Although the titanium tube required longer to reach 0.0005 ft^2-hr-^oF/Btu, the maximum R_f in the titanium HTM greatly exceeded that of the aluminum HTM. It is interesting that on 29 May (cleaning day) there was no visual difference between fouling layers on both tubing materials. A thick uniform layer of fouling covered the interior of each tube. Brush cleaning the aluminum tubes removed most of the fouling but sizable patches remained after 20 brush passes. The titanium was essentially as clean as Day 1 after 4 brush passes. Thus, it appears that fouling adherence to titanium was much less rigid than that to aluminum.

Results obtained with the flow-driven brushes (Fig. 7) are encouraging. In both aluminum and titanium HTM's, R_f for a 4-hour cleaning cycle remained well below 0.0005 ft^2-hr-^oF/Btu. The aluminum tube showed a general increasing trend in R_f to approximately 0.00025 in 3 weeks. For the titanium tube, R_f showed small oscillations but remained at or below 0.0001 with no discernible trend toward an increase with time.

Performances of recirculating sponge balls on a 15-minute cycle are shown in Fig. 8. For the aluminum tube, there was a gradual increase in R_f to 0.0002 in 2 weeks. Results for the titanium tube are not as clear. Oscillations in the curve reflect problems that occurred in this test system. The present system, using peristaltic pumps for ball recirculation, is inadequate. During the 14-day period, there are five major problems th t affected system performance. Tests were finally terminated when the pump motors burned out

At least two candidate systems were evaluated as a replacement for the peristaltic pumps to recirculate the sponge balls. The system selected was designed by Pete Gavin, Argonne National Laboratories, and is similar to those proposed for OTEC-1. In conclusion, flow-driven brushes have performed well in current testing. Results with recirculating sponge balls are inconclusive since the current system cannot be construed as a fair test of the sponge ball system.

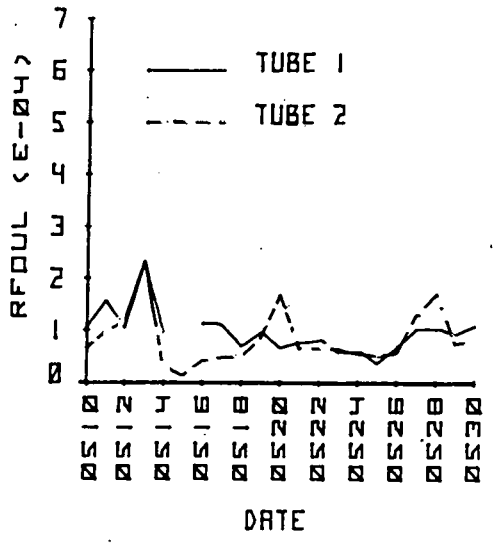

Fig. 5

TABLE 1

PANAMA CITY OTEC TEST SITE CHARACTERIZATION DATA

MEAN VALUES

Parameter	Sep	Oct	Nov	Dec	Jan	Feb	Mar	Apr	May
Conductivity (mmhos/cm)	42.8	44.5	44.8	39.3	31.4	28.2	33.8	34.9	36.6
Salinity °/oo	26.5	30.8	31.9	31.0	27.2	23.9	25.7	25.9	23.9
Temperature (°C)	28.2	22.9	21.3	16.1	9.4	12.2	17.8	21.9	25.1
Acidity (pH)	7.6	7.9	7.6	7.8	7.9	8.0	8.0	8.0	8.0
Turbidity (NTU)	1.7	1.7	1.3	0.9	2.3	1.8	1.6	1.8	1.7
Dissolved Oxygen (ppm)	4.7	6.9	6.6	7.3	9.0	8.6	7.3	6.5	6.0
Biochemical Oxygen Demand (ppm)	2.1	3.0	3.4	3.2	3.6	3.8	1.8	3.2	2.6
Total Organic Carbon (mg/L)	5.21	4.42	6.15	5.58	19.70	9.28	3.67	3.70	N/A
Adenosine Triphosphate (ng/L)	3.33	8.73	1.15	4.70	2.08	1.72	9.70	11.65*	N/A
Total Bacteria (cfu/ml)*	3076	5973	554	1382	339	302	254	989	D
Nitrogen, Ammonia (ug/L)	12	5	10	13	6	14	36	21	26
Nitrogen, Nitrate (ug/L)	.2	.4	.3	.3	.4	.4	.3	.4	.4
Phosphate, Phosphorous (ug/L)	34	40	8	59	71	59	34	37	41
Silicates (ug/L)					56	550	290	150	90

* Colony Forming Units/ml

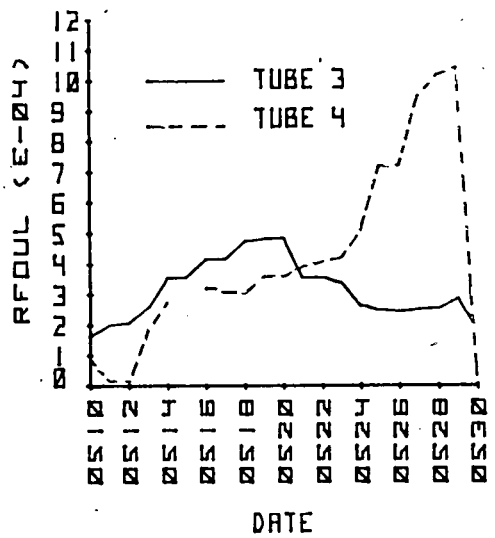

Fig. 6

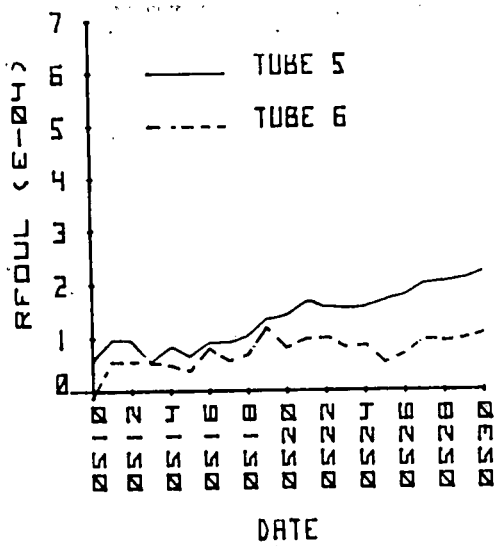

Fig. 7

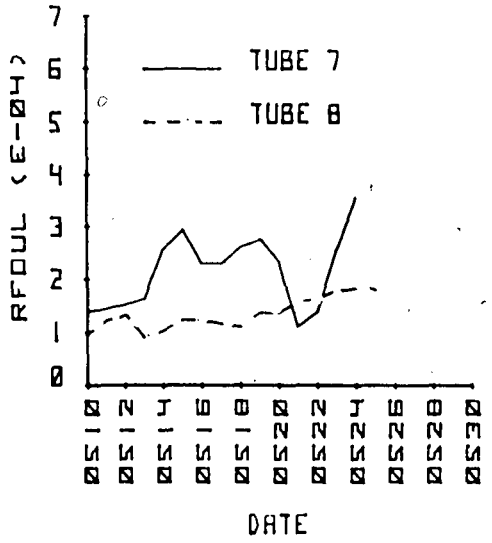

Fig. 8

References

1. Fritsch, A.; W. Adamson; and V. Castelli, "An Evaluation of Mechanical Cleaning Methods for Removal of Soft Fouling from Heat Exchanger Tubes in OTEC Power Plants," Proceedings of the Ocean Thermal Energy Conversion (OTEC) Biofouling and Corrosion Symposium, Washington, D.C., 1978.

2. Conn, A. F.; M. S. Rice; and D. Hagel, "Ultra Clean Heat Exchangers - A Critical OTEC Requirement," Proceedings of the Fourth Annual Conference on Ocean Thermal Energy Conversion, New Orleans, La., 1977.

3. McNulty, J. K.; W. N. Lindall; and J. E. Sykes, "Cooperative Gulf of Mexico Estuarine Inventory and Study, Florida: Phase I, Area Description," NOAA Technical Report NMFS CIRC-368, Seattle, Wa., 1972.

4. Fetkovich, J. G., "A System for Measuring the Effect of Fouling and Corrosion on Heat Transfer Under Simulated Conditions," Report COO-4041-10, Carnegie-Mellon University, December 1976.

DISCUSSION

Question: I believe you mentioned that in the aluminum tube you didn't get all of the fouling out. The Amertap balls did not remove all of the biological material. Is that correct?

D. Lott: Yes. I have further information on that. As of three cleaning cycles, the R_f after cleaning increased in each successive cycle. This is not true for the titanium; with each cleaning, the R_f for the titanium tube was restored to the initial value.

W. Grimes, Dow Chemical: What percentage of your Amertap balls had an abrasive on the ball?

D. Lott: For this testing - none. We were using the commercially available "normal" ball which was approximately 28 mm in diameter. For the M.A.N. system also we were using the commercially available brush that was suggested to us by the manufacturer, and again it has bristle length of approximately 28 mm.

A BIOFOULING & CORROSION STUDY OF OCEAN THERMAL ENERGY CONVERSION (OTEC) HEAT EXCHANGER CANDIDATE METALS

Brenda Little*, John Morse**, George Loeb***, and Frank Spiehler****

Abstract

A field test was undertaken in the Gulf of Mexico to correlate decreased heat transfer efficiency with the characteristics of the biofouling/corrosion film on heat exchanger surfaces of aluminum (5052), titanium (grade 2), copper-nickel (90-10), and stainless steel (AL 6X). Subsurface water from a 75-foot depth was pumped through the heat exchangers at a flow rate of 6 ft/sec for approximately fourteen weeks. Sections of sample loops were removed periodically and the biofouling/corrosion characterized using the following parameters: inorganic constituents, wet-film thickness, adenosine triphosphate (ATP), and total organic carbon. Scanning electron microscopy coupled with energy-dispersive x-ray spectrometry was used to describe the topographical features and elemental composition of the film. Heat transfer efficiency across the materials was measured using a device developed at Carnegie-Mellon University.

The various metals exhibited dissimilar heat transfer responses and biofouling rates from the onset of the experiment. Early degradation of the heat-transfer efficiency was measured in the copper-nickel and aluminum heat exchangers. Both surfaces were covered with a corrosion layer and the aluminum surfaces were also heavily biofouled. The stainless steel and titanium exhibited a much slower initial loss in heat transfer efficiency, minimal corrosion, and patchy colonization by microorganisms.

Introduction

The efficiency of OTEC heat exchangers is dependent on the maintenance of a surface with a high heat-transer coefficient. Materials exposed to natural seawater typically develop a layer of attached organisms that is referred to as biofouling. A biofouling film can contain dead cells and cellular debris, organic secretions, and inorganic precipitates, in addition to viable cells. Metal surfaces in contact with seawater may be further altered by the formation of a scale layer produced by corrosion. The resulting biofouling and/or corrosion derived deposits have poorer thermal conductivity than the original metal surface, introducing resistance to heat transfer between seawater and the working fluid[1]. The objective of the Gulf of Mexico OTEC biofouling and corrosion experiment was the same as similar experiments in Hawaii[2], St. Croix, U.S. Virgin Islands[3], and a previous Gulf of Mexico experiment[4]: to characterize the biofouling and corrosion in heat exchangers exposed to flowing oceanic water as a function of time and to correlate these phenomena with the measured decay in heat-transfer efficiency.

A model system incorporating the basic elements of an ocean thermal energy conversion (OTEC) plant was mounted on a National Oceanic and Atmospheric Administration (NOAA) 40-foot discus buoy and deployed in the Gulf of Mexico 160 nautical miles west of Tampa, Florida (27°33'N, 85°31'W) on 2 December 1978. The flow-through system consisted of four individual heat exchangers, one each of 5052 aluminum, grade 2 titanium, 90-10 copper-nickel, and AL 6X stainless steel, through which water from a 75-foot depth was pumped at a flow rate of 6 ft/sec. A fifth heat exchanger experiment developed at Applied Physics Laboratory (APL) John's Hopkins University was included to provide similar data for roll-welded Alclad aluminum 3004 heat exchangers over which seawater flowed at a rate of 2.6 ft/sec.

Methods and Materials

Each of the four flow-through heat-exchange experiments consisted of a 90-inch sample, vertically oriented and designed to contain standing water during sample collections and flow interruption due to pump failures. The in situ heat transfer surfaces were composed of lengths of tubing identical to those of the sample loops and connected in series to them. The pressure water system consisted of three pumps located below the deck, with their suction inlets below the level of the buoy waterline. Each pump took in water through a common all-plastic suction strainer. The synthetic rubber suction hose was 6 inches in diameter and 75 ft long. All pump components in contact with seawater were polyvinylchloride (PVC) or an equivalent inert nonmetallic material. The discharge line of each pump had a check valve to prevent backflow, a pressure indicator, and a vacuum gage for the detection of obstructions. Each pump was driven by a close-coupled, totally enclosed, fan-cooled motor. The electric motors were 115-V single-phase and developed approximately 3 horsepower each. The APL water box loop, designed by Southwest Research Institute, San Antonio, Texas, contained 12 tubes, of which one half were used for biofouling/corrosion analysis and the other half, for heat-transfer and cleaning tests.[5]

Figures 1 and 2 provide details of the flow schematic and the relationship of the flow-through and APL experiments.

*Naval Ocean Research and Development Activity, NSTL Station, MS 39529

** Rosensteil School of Marine and Atmospheric Science, University of Miami, Miami FL 33149

*** Naval Research Laboratory, Washington, D.C.

**** NOAA/Data Buoy Office, NSTL Station, MS 39529

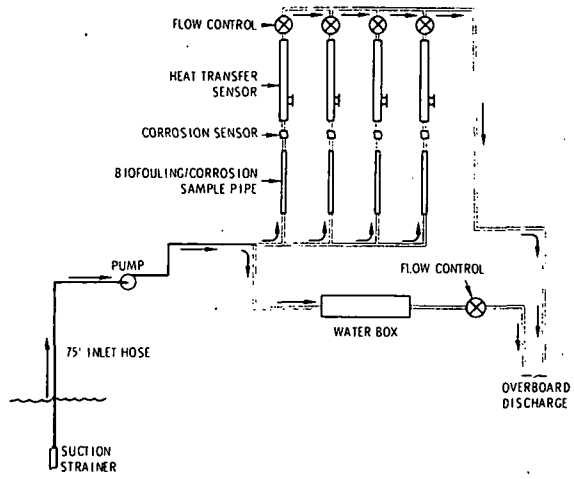

Figure 1. Biofouling/Corrosion Experiment Flow Schematic

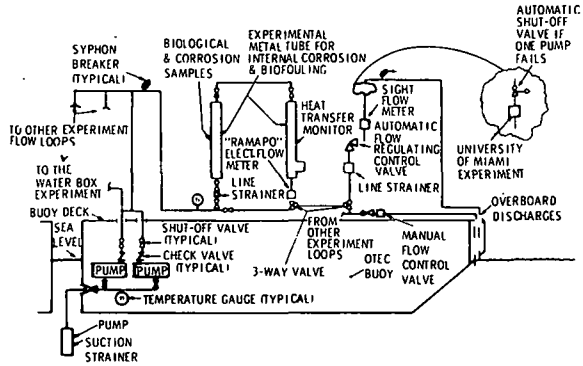

Figure 2. Biofouling/Corrosion - Heat Transfer Experiment Flow Loop

The pressure water system contained a Kates flow-control valve to maintain a constant flow rate regardless of upstream or downstream pressure changes. The primary flow measurement was obtained with a (RAMAPO) strain-gage-type electronic flow-meter located downstream of the heat transfer measurement system.

The power system consisted of two diesel-powered alternators with 115-V, 60-Hz, 30-amp capacity each.

The heat transfer monitor was designed by John Fetkovich of Carnegie-Mellon University[6]. On command, an electrically heated ring clamped on the outside of the metallic tube being tested heated the tube to 1.8° C above the water temperature or applied heat for 10 time constants, and then cut off. The time series of the temperature difference between the tube wall and water was used to accurately establish a time constant.

The heating collar was positioned 36 inches from the upstream end of the test pipe. The temperature was determined some distance from the center of the pipe and compared to the inlet water temperature 12 inches upstream. Ten seconds after the heat was turned off, data collection began. As the biofouling film formed, the cooling time increased. Decreased heat transfer efficiency or increased resistance due to fouling was reported as R_f in hr ft^2 °F/BTU units. R_f was defined as the difference between 1/h where h is the measured heat transfer coefficient at any given time and the initial value of 1/h. Reference 6 discusses the corrections, based on water temperature and flow rate, used to calculate the heat transfer coefficient and fouling factor.

The Shore Collection Station at NSTL Station, MS, was used to control the OTEC-GOME experiment. Data were received at the NSTL and printed out immediately to permit evaluation of data quality before the experiment continued. A data tape was produced for Argonne National Laboratories from which the resistance due to fouling (R_f) was calculated.

All pipe samples were degreased with trichloroethylene before installation in the experiment. The 90-inch sample loop was prescored at 9-inch intervals to facilitate sample removal. The sample section was prescored at 1/2-inch intervals for subsampling.

The biofouling on the heat-exchanger surfaces was characterized by the following parameters: adenosine triphosphate (ATP) and total organic carbon. Wet-film thicknesses were measured with the light section microscope. All methods for sample collection and handling, as well as procedures for microscopy and biochemical analyses were presented at OTEC Workshop on Biofouling and Corrosion, 1979.[4]

The procedure used for the determination of concentration of inorganic scale componenets on OTEC heat exchanger test pipes was that of Morse and Craig[7]. A 1-inch pipe sample was given a quick rinse in double-distilled water to remove excess sea salt. It was then immersed in a 3% acetic acid solution for 24 hours. The initial volume of the acid solution was 40 ml. The pipe sample was removed and a rinse of the pipe was added to the acid solution. The solution was then transferred to a 50-ml volumetric flask and the beaker rinsed into the volumetric flask until a volume of 50 ml was obtained. Selected metal concentrations in the solution were then determined by graphite furnace and flame atomic absorption and spectroscopy[8]. The geometric surface area of the pipe was calculated and the metal concentration in nanomoles per cm^2 of surface area was determined. The concentrations of the selected metals on a control pipe not exposed to seawater were subtracted from those on the test pipes.

Results

The Gulf of Mexico biofouling/corrosion experiment was plagued with equipment failures. Biofouling/corrosion samples were collected three times during the course of the 14-week experiment. Each of the samples was collected after a period of decreased flow

(<6 ft/sec) or flow stoppage (fig. 3). The system operated without interruption for the first 31 days. A hose failure at 32 days resulted in flow fluctuations as low as 2.6 ft/sec until the suction hose was replaced at day 54. The first biofouling/corrosion sample was collected at day 48. Flow was resumed at approximately 5.5 ft/sec for 14 days, when both of the diesel generators failed due to fuel contamination. The diesels were restarted at day 72, functioned for 4 days, failed on day 76, restarted on day 77, and functioned at a flow of 6 ft/sec until day 86, when the pump seals failed and the experiment was terminated. The second biofouling/corrosion sample was collected at day 78 and the final sample was collected on day 99 (13 days after the pump failure). Flow data were not recorded for the APL system.

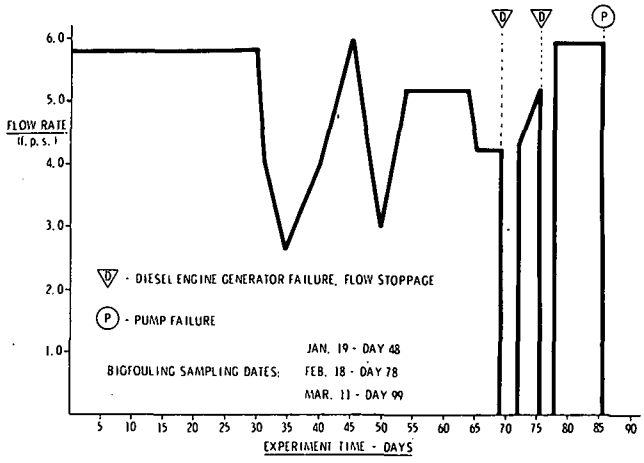

Figure 3. OTEC-GOME — Flow Rate Versus Time

Heat Transfer Resistance

Heat transfer data are presented in figure 4. The 90-10 copper-nickel (Cu-Ni) surfaces exhibited immediate loss of heat transfer efficiency but reached a platcau of about $R_f = 1.3 \times 10^{-4}$ at about 34 days. Though the R_f increased slightly after that, it remained less than 2.0×10^{-4}. After the first flow stoppage at 72 days, the R_f values for the Cu-Ni pipe fluctuated slightly in comparison to much larger decreases in R_f values in the other heat exchangers.

The aluminum surfaces also experienced early decay in heat transfer efficiency and at day 72 had reached $R_f = 3.6 \times 10^{-4}$. After the flow stoppage at 72 days, the next measured R_f showed a decrease to 1.3×10^{-4}. Resumed flow resulted in an increasing R_f when the experiment concluded.

The heat transfer properties of the titanium surface remained essentially unaffected by biofouling/corrosion until day 37. The maximum observed R_f was at day 72, as in aluminum, at a value of 2.7×10^{-4}. An abrupt decline in R_f coincided with the flow stoppage at day 72 with an increase immediately after the resumption of flow.

Stainless steel had a slow initial loss of efficiency, but experienced the greatest loss of efficiency in the shortest time ($R_f = 3.7 \times 10^{-4}$ at day 66), that also declined during the stagnant period.

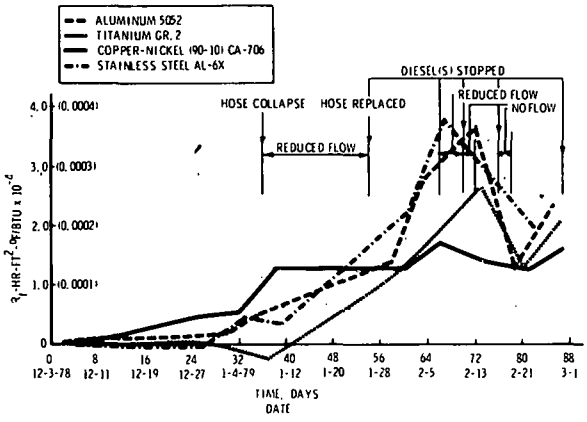

Figure 4. Gulf of Mexico Experiment (GOME)

Inorganic Constituents

The blank-corrected surface concentrations are presented in table 1. The aluminum 5052 alloy corroded vigorously during the first few minutes of exposure to flowing seawater. The amount of aluminum present in the scale after 15 minutes exposure was 70% of the amount present at the end of the 48-day exposure. Therefore, the initial build-up of corrosion product on the aluminum surface is very rapid. Scale formation on the copper-nickel was also rapid. The scale on the copper-nickel surface was enriched in iron with respect to the original alloy. The titanium and AL6X stainless steel pipe surfaces accumulated less than 10% as much inorganic material as the copper-nickel pipe surfaces. Inorganic deposits on the surfaces of all materials decreased after the 13-day stagnation period.

Wet Film Thickness

Because of the opaque nature of the corrosion film on the copper-nickel surface, the light-section microscope could not be used to measure wet film thicknesses. Film thickness measurements for the other surfaces are presented in figure 5. The corrosion film and associated biofouling developed a much thicker film (31μ) on the exterior of the aluminum surfaces in the APL water box experiment than did that of the aluminum pipe interiors (15μ) during the first 48-day exposure period. The film thickness in the aluminum flow-through system was predominately corrosion product, while that of stainless steel and titanium was due primarily to biofouling. It appears that some sloughing of the fouling film took place in the aluminum pipe after the period of stagnation of 13 days. The film thickness decreased approximately 5 microns during that period. during that period.

ATP

Adenosine triphosphate (ATP), a constituent of living cells only, was below detection limits for all samples taken during this experiment.

Table 1. Selected Metal Concentrations in Inorganic Scale.

Sample		Na	K	Ca	Mg	Fe	Cu	Ni	Cr	Al
Aluminum	15 min.	232	9.8	18.5	913	71.3	2.59	–	—	5820
	1 hr.	51.3	6.1	34.3	670	194	0.019	–	–	5020
	24 hrs.	83.5	8.7	39.1	560	138	1.56	–	–	5490
	48 days	103	2.10	211	816	199	0.70	–	–	8120
	78 days	71.6	1.36	202	1240	292	49.6	–	–	13500
	99 days	0.244	-0.008	0.322	1.25	-0.066	0.002	–	–	7.9
Stainless Steel	48 days	105	1.95	34.3	60.9	391	34.5	2.57	48.1	—
	78 days	225	4.62	46.2	54.8	177	16.5	12.5	13.7	–
	99 days	0.186	-0.010	0.129	0.077	-0.23	1.10	0.158	-0.0222	–
Copper-Nickel	48 days	322	7.12	191	365	3680	9180	2370	–	–
	78 days	96.3	2.13	141	237	3600	8810	2070	–	–
	99 days	0.566	-0.0083	0.462	0.548	5.56	8.5	2.53	–	–
Titanium	48 days	83.6	1.78	12.2	36.5	118	44	–	–	–
	78 days	70.7	1.55	18.5	38.2	83.3	7.6	–	–	–
	99 days	0.309	0.0001	0.041	0.049	-1.18	0.058	–	–	–

All concentrations in nmoles/cm^2 All Ti values < 0.003

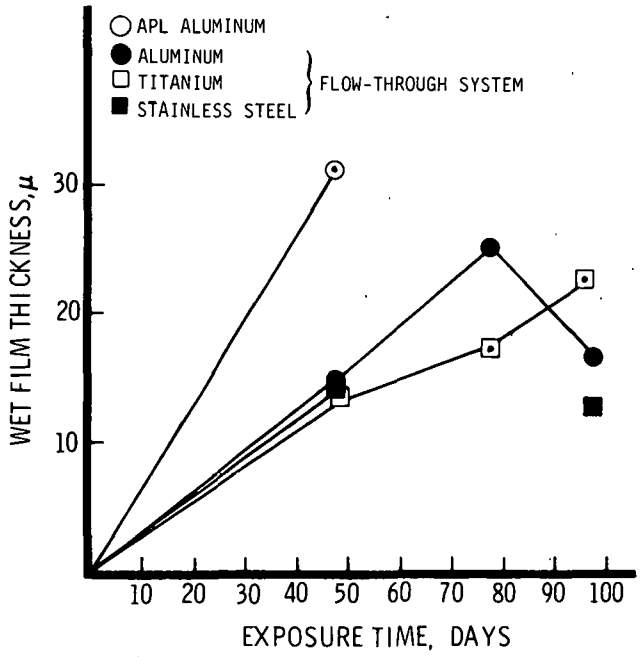

Figure 5. Wet-Film Thickness Measurements Versus Time

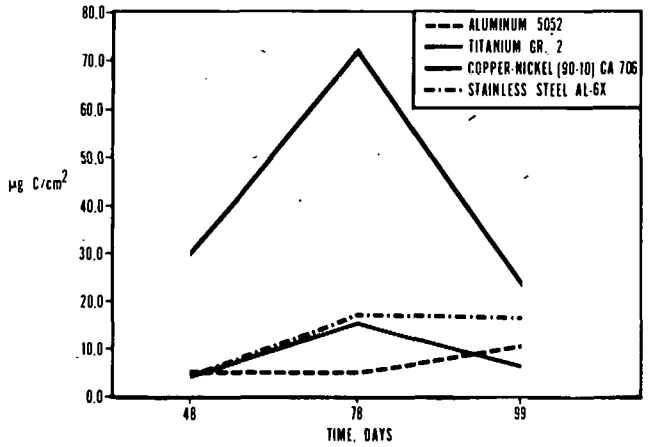

Figure 6. Total Organic Carbon Versus Time

Total Organic Carbon

Total organic carbon data are presented in Figure 6. Total values generally increased from the start of the experiment to day 78. After the 13-day stagnation period drops in the total organic carbon values were observed for the copper and titanium surfaces and slight increases for aluminum and stainless steel surfaces.

Scanning Electron Microscopy

After a 48-day exposure, the aluminum surface exhibited a uniformly corroded surface and patchy colonization by filamentous bacteria (fig. 7). Areas in which discrete cells were not present were covered with a slime film presumably exuded by microorganisms (fig. 8). Samples collected at 78 and 99 days, after prolonged stagnation, were covered with slime and cellular debris. Copper-nickel specimens from the three exposures were covered with a rust-colored corrosion film. There was no visible indication of biofouling for the period of investigation (fig. 9). The corrosion film was porous and brittle and easily removed from the surface after critical-point drying. The corrosion film was enhanced in iron

with respect to the original copper-nickel pipe, as indicated by the EDAX florescence spectrum and atomic absorption analysis of the scale (table 1). A similar observation was reported by Wilson using Auger electron spectrometric analysis[9].

The titanium surface was covered with a thin oxide layer and microorganisms after the 48-day exposure. Surface of the 78- and 99-day exposures were covered with crystalline structures - sometimes occurring singly and sometimes in clusters (fig. 10). Gerchakov et. al., observed the same structure on copper-based alloys[10]. The crystalline material is always attached to the surface by means of a filament.

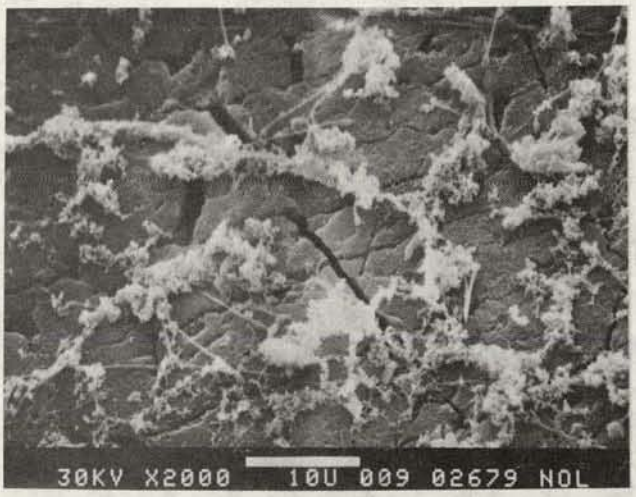

Figure 7. Aluminum 48-day Exposure
Filamentous Cells Attached to Corrosion Layer

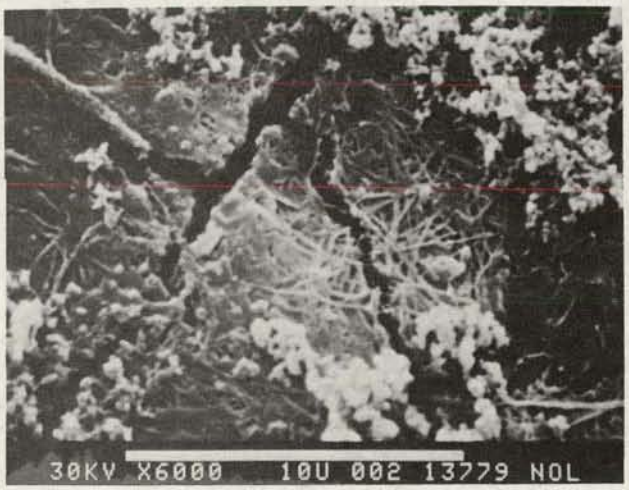

Figure 8. Aluminum 78-day Exposure
Cells Enmeshed in Slime

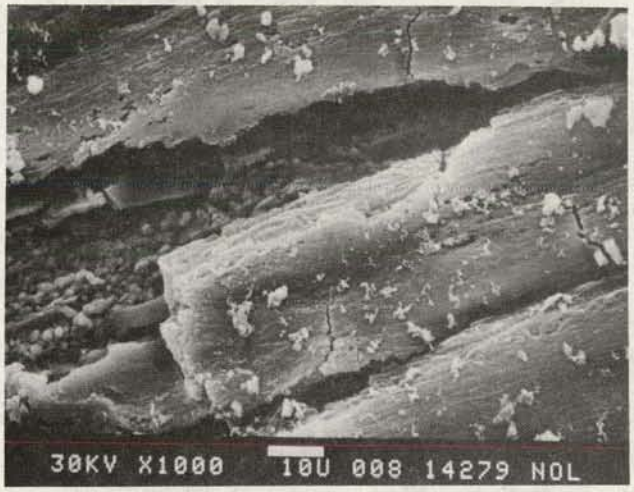

Figure 9. Copper-Nickel 99-day Exposure
Cracked Corrosion Film Detached from Underlying Surface

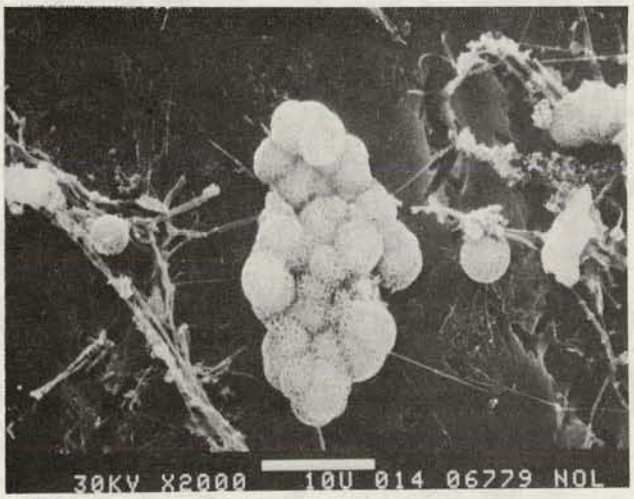

Figure 10. Titanium 78-day Exposure
Crystalline Structures Occurring Singly and in Clusters

The stainless steel surface was highly irregular with pits and grooves, typically, 1-5 μm wide, 20 μm deep and ranging from 10 to hundreds of micrometers long, present as a result of the extrusion process (fig. 11). After the 78-day exposure, the surface features were obscured by the presence of slime-enmeshed diatoms, coccoliths, and other debris (fig. 12).

The APL water-box samples fouled much faster and showed more diversity than the flow-through system (figs. 13, 14, & 15) under the experimental conditions described. Hydroids were attached to the surface at 48 days.

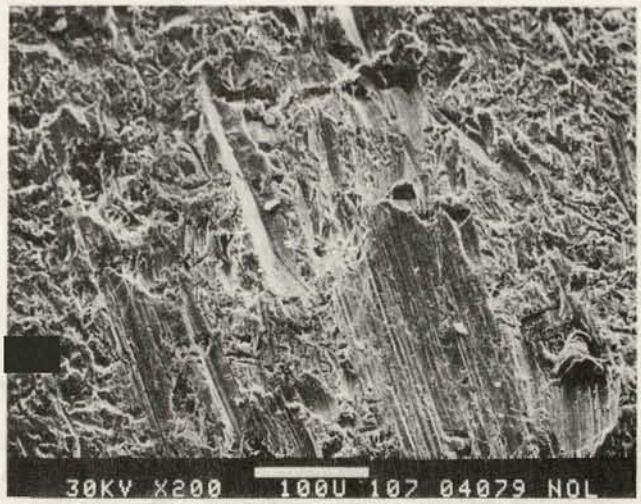

Figure 11. Stainless Steel 48-day Exposure

Figure 14. APL - Aluminum Surface 99-day Exposure Complex Fouling Layer Containing Coccoliths, Diatoms, and Other Plankters.

Figure 12. Stainless Steel 78-day Exposure Surface Roughness Obscured by Slime and Debris

Figure 15. APL - Aluminum Surface 99-day Exposure Hydroids Attached to Corrosion Film

Figure 13. APL - Aluminum Surface 48-day Exposure

DISCUSSION

There are major problems in interpreting the results of the Gulf of Mexico experiment.

Each of the biofouling/corrosion samples was collected during or after a catastrophic equipment failure. The composition of a biofilm is strongly dependent on environmental factors - flow conditions, oxygen and nutrient concentrations. The titanium, stainless steel, and aluminum surfaces had been colonized by filamentous bacteria before the first sample was collected at 48 days. Even small perturbations of short duration can alter the constituents of the film. The absence of measurable quantities of ATP, found only in living cells, in the samples for this experiment is an indication that the flow interruptions adversely affected the microorganisms present in the film. Microorganisms colonizing solid surfaces grow until these surfaces are completely covered. Subsequent growth is from the surface outward with aerobes in areas where

the oxygen supply is sufficient and anaerobes in the depths of the film into which oxygen cannot diffuse. When nutrients are no longer available for those basal microorganisms, they die or lyse and thus destroy the attachment of the film to the solid surface so that sloughing occurs[11]. The flow stoppages between days 65 and 78 resulted in substantial drops in R_f for those surfaces that were colonized (aluminum, stainless steel and titanium); a much slighter decrease was observed in the copper-nickel pipe where fouling was predominately due to corrosion.

Film thickness decreased on the aluminum and stainless steel surfaces after the 13-day stagnation period and the inorganic chemical analyses of the corrosion film indicated sloughing of the corrosion film from all surfaces.

The high content of total organic carbon (a measure of adsorbed, dissolved organic matter; living and dead biomass; and associated secretions) in the films from copper-nickel surfaces indicates that microorganisms had been present, although no intact individuals were found. Microorganisms attached to copper-base surfaces secrete copious quantities of polymer,[10] and a comparatively high carbon-to-nitrogen ratio is characteristic of these materials.[14] Decreases in total organic carbon on the Cu-Ni and Ti samples following the stagnation period indicate sloughing or removal of organics from those surfaces.

Stainless steel, which exhibited the greatest apparent loss of heat-transfer efficiency for the period of investigation, is inert in seawater. On the one hand, it forms no corrosion products; on the other, it does not resist fouling.[12] The large Rf increase can probably be attributed to the insulating properties of the biofilm layer, whose development may have been enhanced by the highly irregular surface of the particular pipe specimens that were used. The aluminum surface underwent an early degradation of heat-transfer efficiency and reached an R_f slightly less than that of stainless steel at about 79 days. The 5052 aluminum alloy corroded vigorously during the first few minutes of exposure - approximately 70% of the aluminum scale component found at 48 days was present after only 15 minutes. The corrosion film is hydrated and may be responsible for the initial minimal losses in efficiency. Greater losses appear to be due to the presence and constituents of the biofilm.

The copper-nickel pipes exhibited the greatest initial loss of efficiency. During the first 32 days, R_f reached a value of 1.5×10^{-4}. All losses were attributable to the rapidly forming corrosion film.

The titanium surface experienced slow initial losses and a maximum R_f value of 2.7×10^{-4}. Titanium, like stainless steel, is resistant to corrosion and is nontoxic to marine organisms[13]. The loss of efficiency was due to biofouling.

The fouling resistance data from the Gulf of Mexico Experiment (prior to the first shutdown) and those from the Keahole Point, Hawaii, experiment have been compared in figures 16, 17, 18, and 19. Except for the longer lag period for all surfaces in the Gulf of Mexico experiment, the data are remarkably similar. The slopes of the curves after the lag phase are identical. The second and third curves for the Hawaii data represent the R_f data after cleaning.

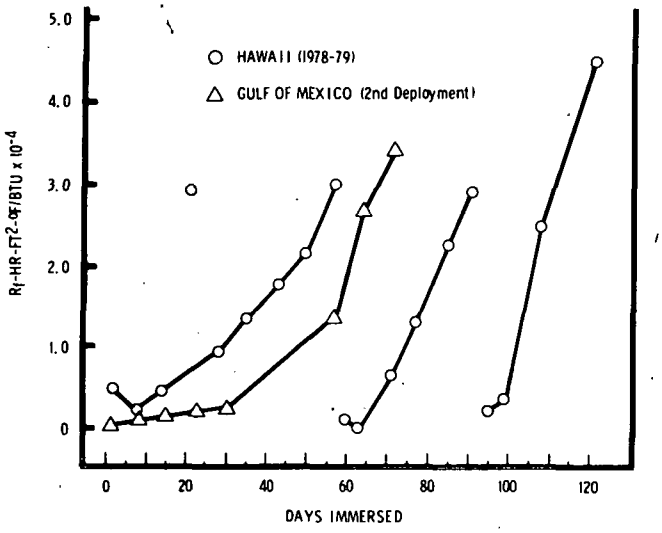

Figure 16. Fouling Resistance Versus Time - Aluminum

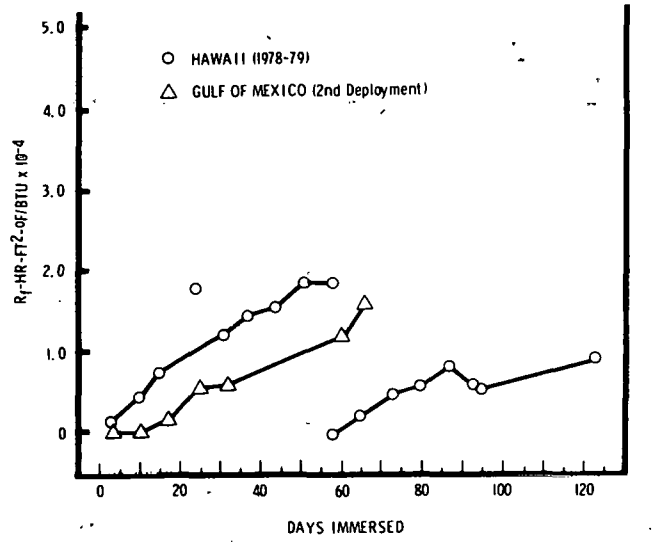

Figure 17. Fouling Resistance Versus Time - Copper-Nickel

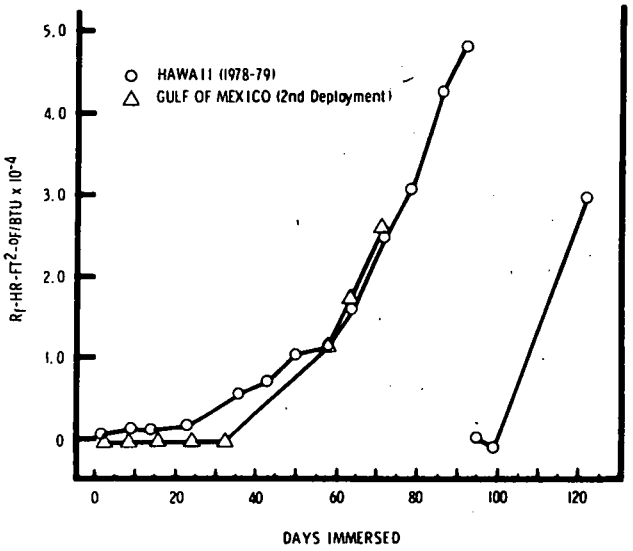

Figure 18. Fouling Resistance Versus Time - Titanium

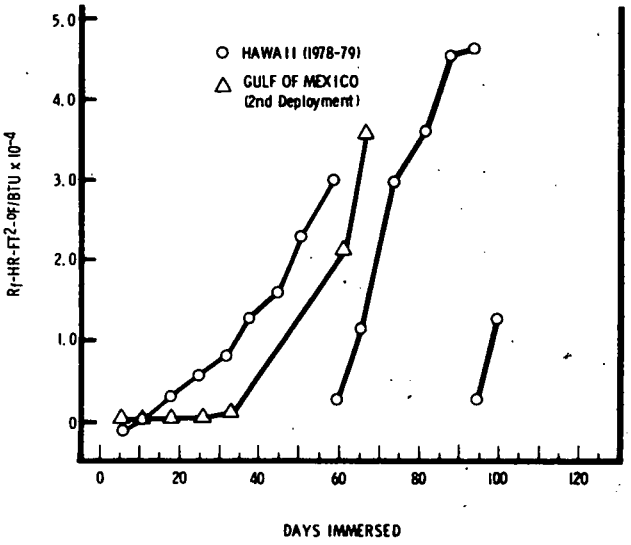

Figure 19. Fouling Resistance Versus Time - Stainless Steel

CONCLUSIONS

1. Biofouling on the exterior aluminum surfaces of the APL device was more diversified and formed faster than the biofouling observed on the pipe interiors for the system described.

2. Titanium and AL6X stainless steel pipe surfaces accumulated less than 10% as much inorganic material as the aluminum and copper-nickel pipe surfaces.

3. The formation of inorganic deposits on the aluminum pipe surfaces was initially very rapid, with approximately 70% of the material found after 48 days exposure being deposited during the first 15 minutes.

4. Reduced heat-transfer efficiency across the stainless steel and titanium surfaces was due to biofouling. The increase in R_f of the copper-nickel surface was due to corrosion. Corrosion products on the aluminum surface may impede heat transfer in the early stages of exposure, but biofouling and its related processes appear to control the observed increase in R_f.

5. After a 13-day stagnation period inorganic and organic deposits are lost from fouled surfaces. A short stagnation period of four days resulted in a decrease in R_f for surfaces colonized by microorganisms. All decreases may be due to the sloughing of the biofouling/corrosion film.

6. Surface irregularities may enhance biofouling.

7. The Gulf of Mexico and Hawaii heat transfer data are virtually superimposable after the lag periods.

REFERENCES

1. Bell, K. J. The effect of fouling on heat exchanger design, construction and operation, Proccedings of the Ocean Thermal Energy Conversion (OTEC) Biofouling and Corrosion Symposium, Seattle, WA, October 10-12, 1979.

2. Berger, L. R., W. F. McCoy and J. A. Berger, Biofouling Assays for OTEC Pipes, Proceedings of the OTEC Biofouling, Corrosion and Materials Workshop, Rosslyn, VA, January 8-10, 1979.

3. Aftring, R. P., D. G. Capone, L. Duguay, J. W. Fell, I. M. Master and B. F. Taylor, Biofouling and site characterization studies in Ocean Thermal Energy Conversion (OTEC) experiment at St. Croix, U.S. Virgin Islands. Report to Department of Energy. 1978.

4. Little, B. J. and D. M. Lavoie, Gulf of Mexico Ocean Thermal Energy Conversion (OTEC) Biofouling and Corrosion Experiment, Proceedings of the OTEC Biofouling, Corrosion, and Materials Workshop, Rosslyn, VA, January 8-10, 1979.

5. Pandolfini, P. P., W. H. Avery, and F. K. Hill, Experiments on Ultrasonic Cleaning of a Shell-less, Folded-Aluminum-Tube, OTEC Heat Exchanger, Paper 8A-1 at 6th OTEC Conference, Washington, D. C., June 19-22, 1979.

6. Fetkovich, J. G., G. N. Granneman, L. M. Mahalingham and D. L. Meier. Degradation of heat an enzyme fer rates due to biofouling and corrosion at Keahole Point, Hawaii. Proceeding of the OTEC Biofouling and Corrosion Symposium, Seattle, WA.

7. Morse, J. W. and H. L. Craig, Jr., 1978, Test procedures to define the ranges of balance between dissolved CO_2 and carbonates in seawater that could lead to deposition of calcareous deposits on heat transfer surfaces within the temperature range of OTEC heat exchangers, Final Report to Department of Energy, Contract No. EY-76-C-1830; Pacific Northwest Laboratories, Battelle Memorial Institute, Special Agreement No. B-07455-A-E, 35 pp.

8. Segar, D. A. and A. Y. Cantillo, 1975, Direct determination of trace metals in seawater by flameless atomic absorption spectrophotometry, In: Analytic Methods in Oceanography, T. R. P. Gibb, Jr. (ed), American Chemical Society, Washington, D. C., 56-81.

9. Wilson, J. W., Composition of seawater corrosion product films on copper base alloys: Auger Electron spectrometric analyses, Corrosion, March, 1979.

10. Gerchakov, S. M., F. J. Roth, B. Sallman and L. B. Udey and D. S. Marszalek. Observations on Microfouling Applicable to OTEC systems, Proceedings of the Ocean Thermal Energy Conversion (OTEC) Biofouling and Corrosion Symposium, Seattle, WA, October 10-12, 1977.

11. Hohen, C. H. and A. D. Ray. Effects of thickness on bacterial film. Journal WPCF 45:11, November, 1973.

12. LaQue, F. L. Qualification of stainless steel for OTEC heat exchanger tubing. ANL/OTEC Prepared for the U. S. Department of Energy Division of Central Solar Technology under contract W-31-109. Enc-38. January 1979.

13. Franson, I. A. and L. C. Covington. Titanium and the OTEC environment, Proceedings of the Ocean Thermal Energy Conversion (OTEC) Biofouling and Corrosion Symposium, Seattle, WA, October 10-12, 1977.

14. Liebert, B. E., L. R. Berger, H. J. White, J. M. Moore, W. M. McCoy, J. A. Berger and J. Larsen-Basse. The effects of biofouling and corrosion on H Heat Transfer Measurements. Proceedings of the Ocean Thermal Energy Conference, Washington, D. C. June 19-22, 1979.

DISCUSSION

J. Lorenz, ANL: What was the error band on R_f?

B. Little: Will you answer that, Glenn Popper, Argonne National Laboratories?

G. Popper, ANL: The uncertainty in h_a is ±15 in 1000 Btu/hr-ft^2-°F. The guy who runs the OTEC plant has rather little interest in R_f and rather little interest in the R_f versus time curve. He cares about heat transfer coefficients.

W. H. Avery, APL: Although knowledge of the initial surface changes within an hour or two of exposure is of fundamental importance in understanding the biofouling and corrosion processes taking place, the problem of interest is the rate of biofouling in a particular environment with a selected heat exchanger material. Therefore the value of R_f should be referred to the measured heat transfer at the start of the experiment with the as-manufactured and delivered condition of the surface rather than to the heat transfer coefficient of a theoretically clean surface.

J. Morse: The problem with the R_f is that if your're designing a plant, you take a heat exchanger tube of a given metal of a given conductivity and you make it so thick and you think you know what your heat transfer is going to be. If you then put down 20μ or so of highly insulating aluminum hydroxide that is 90% water on the surface, very quickly you have changed the thermal conductivity and the heat transfer rate between the working fluid and the seawater. We found when we plotted R_f measurements from the first Gulf of Mexico experiment versus time and compared the measured thickness and calculated thermal conductivity of the film, that the material was conducting like a pure metal because the influence of the aluminum hydroxide layer had been tuned out. As the film dehydrated with time to about 60% water, its conductivity actually should go up. However, the data indicated that it went down, and the thermal conductivity was 4 to 5 times that reported by earlier investigators. They had curves of calculated film thickness versus thermal resistance that were radically different. And so, in working with these results and interpreting them, it is important to know what is going on on the surfaces with these rapid film formations. It is not just a theoretical thing--it is a real thing that is happening to increase thermal resistance.

P. P. Pandolfini, APL: With respect to the conclusion that the APL device fouled more quickly and showed more diversity in the fouling species, emphasis should be made on the different maximum flow rates causing this result. Comparison of measured R_f (see our paper) is perhaps more useful.

FIELD DEMONSTRATION OF RAPID MICROFOULING IN MODEL HEAT EXCHANGERS: GULF OF MEXICO, NOVEMBER 1978

V. A. DePalma, D. W. Goupil, C. K. Akers

Calspan Corporation
P.O. Box 100
Buffalo, New York 14225

Abstract

Field demonstrations were performed at the Stage I experimental platform of the Naval Coastal Systems Center, 19 Kilometers off Panama City, Florida in the Gulf of Mexico. Subsurface water from the 15 meter level beneath the platform was delivered at constant fluid flow conditions through model heat exchangers for periods from 24 hours through 144 hours. The volumetric exposure of seawater to heat exchanger surface area was controlled to simulate conditions in proposed full-scale OTEC units. The proposed OTEC grades of titanium and aluminum alloy surfaces were evaluated. Corrosion-resistant optical flats of germanium, especially useful in qualitative/quantitative diagnosis of the acquired fouling films, were also evaluated. Combined analyses by internal reflection infrared spectroscopy, ellipsometry, surface potential, wettability (contact angle), and scanning electron microscopy illustrate that fouling films are acquired by spontaneous adsorption of glycoproteinaceous matter within the first day of seawater exposure. This is quickly followed (72 hours) by prolific attachment of pioneer microorganisms (rod, flagellated and stalked), circular entities with mineral skeletons, and build-up of gross fouling. The titanium and aluminum alloys both showed considerable corrosion films in addition to the biological slimes.

Introduction

Prior to the accumulation of the bacterial slime layer and ultimate film growth to visible levels of fouling, a clean solid/liquid interface is conditioned by the adsorption of naturally occurring macromolecules. It is hypothesized that this adsorption alters the molecular conformation that these macromolecules possess in bulk solution and hence, change their interaction with the remainder of the biological community. The extent of the macromolecular denaturation appears to be dependent upon the surface chemistry of the substrate. It is generally known[1] that surfaces exposed to seawater are colonized by bacteria that are important in terms of material corrosion and gross fouling. It has been shown[2,3] that surfaces placed in a solution containing proteins will acquire an adsorbed protein film.

The aim of the research described within this paper was to develop techniques to obtain and characterize surfaces exposed to ocean waters in order to examine the early events of marine biofouling. The exposure of the test surfaces was made by flowing ocean water from the Gulf of Mexico through a specially designed flow cell during the period from November 20, 1978 to December 8, 1978. The flow conditions within the flow cell matched the volume of water per unit surface area per unit time of a typical heat-exchanger surface. Although the results of this work are preliminary, they do support the general observations we have reported elsewhere: (a) surfaces exposed to flowing solutions of biological species and proteins acquire adsorbed protein films which alter both the electrical and chemical nature of the surface, and (b) subsequent reactions with the surface are dominated by the outermost properties of this adsorbed film[4].

Materials and Methods

In these experiments, water from 15 meters below the sea surface was pumped to a polyethylene reservoir, which was attached to flow cells[5] containing pairs of germanium, titanium or aluminum plates. The plates, measuring 2 cm x 5 cm x 0.10 - 0.13 cm and separated by a 0.089 cm spacer, were placed within the flow cell in such a manner as to define a rectangular flow region.

The experimental apparatus shown in Figure 1 is fed by a deep well submersible pump (TEEL Model #3P614) positioned at the 15 meter level (see Figure 2). A polyethylene tube (1.6 cm O.D.) transferred the seawater from the pump to the 19-liter polyethylene reservoir. The reservoir was fitted with an overflow tube, establishing a constant fluid pressure head for the flow cells. Fluid flow through the cells was maintained at 100 ml/min. The flow cells were connected via latex rubber tubes 10 cm long to plastic tubing connectors positioned near the bottom of the reservoir.

Prior to connecting the flow cells to the reservoir, the inside surfaces of the pump, supply tubing and reservoir were exposed to flowing feed water for 48 hours. After this "conditioning" period, three flow cells containing germanium internal reflection plates and three flow cells containing polished titanium (type 50-A) plates were connected to the reservoir. One flow cell of each type was removed from the reservoir after an exposure period of 24, 72 and 144 hours. Next, three flow cells having polished aluminum (type 5052-0) plates were connected to the reservoir, and tested in a similar fashion.

Preparation of the Test Plates

The germanium plates used in this study were purchased from Harrick Scientific Corporation, Ossining, New York in the form of polished internal reflection plates. The titanium test plates were cut from sheet material supplied by TIMET, Pittsburgh, Pennsylvania. A sheet of ALCOA aluminum (obtained from Brace, Mueller & Huntley, Tonawanda, New York) was used for the aluminum test plates.

Prior to insertion into the flow cell, the germanium plates were freed of adventitious organic contamination by a washing with a commercial detergent (Sparkleen, Fisher Scientific Co.). This step was followed by a distilled water rinse and air dry-

ing. The titanium and aluminum plates were polished on one side by rubbing first with 400 grit wet and dry abrasive paper and then with 600 grit abrasive paper. This was followed by polishing on a motorized polishing wheel using .3 μ - alumina polishing compound. Polishing was stopped when a reflecting surface suitable for ellipsometry was achieved. The plates were then cleaned using the detergent washing procedure outlined above.

Analytical Methodology

After a given exposure, the test plates were removed from the flow cells and allowed to air dry in a horizontal position. Subsequently, the plates were briefly rinsed with distilled water to remove the attached sea salts. The rinsed plates were then dried again in a horizontal position and returned to Calspan for examination.

The germanium internal reflection test plates were analyzed using the following techniques:

1. Internal reflection infrared spectroscopy
2. Ellipsometry
3. Surface potential
4. Scanning Electron Microscopy (SEM)
5. Wettability (contact angles)

The titanium and aluminum test plates were examined only by ellipsometry, surface potential, SEM and wettability measurements.

Internal Reflection Infrared Spectroscopy

Internal reflection infrared spectra[6] of the germanium internal reflection plates were recorded using a Perkin-Elmer model 710b infrared spectro meter equipped with a Wilks internal reflection attachment. Figure 3 is a typical internal reflection spectrum of a clean germanium plate before exposure to flowing sea water. This figure gives the baseline spectrum for the plate and is used to establish the initial surface condition of the plate. A similar control spectrum was run for each of the six germanium plates used in these experiments.

Ellipsometry

In these experiments, a Rudolph and Sons Model 43603-200E ellipsometer was used to obtain optical properties of the surface from which the thickness of the adsorbed film is determined. This is done by using the ellipsometric measurements made on the surface and the computational program written by McCrackin[7]. This technique can be used to determine a film thickness of 1 - 1000A.

Surface Potential

Surface potential measurements were made with the ionizing electrode-type device[8] utilizing a null technique to measure the potential of the adsorbed film. The reported values represent the change in surface potential before and after exposure. This surface potential difference gives information on the magnitude and direction of the electric dipoles within the adsorbed films.

Scanning Electron Microscopy

The test plates used in this experiment were examined in an ETEC scanning electron microscope. The surfaces of the plates were examined both as received (noncoated) and coated with metal. The noncoated plates of germanium and titanium examined in the SEM resulted in micrographs which were quite satisfactory and in some cases enhanced the presence of adsorbed cellular species. In the case of aluminum, the surface was coated with a thin gold-palladium film that prevented charging of the oxide layer which formed as a result of exposure. In the lower left-hand part of all SEM micrographs in this paper there is a bar whose length in micrometers is given by the number preceeding the bar.

Wettability (contact angle)

Equilibrium contact angle data, determined for a series of liquids placed on the flow region of each test plate, were used to make Zisman plots[9] from which the critical surface tension, γ_c, and the slope, s, of the best straight line fit through the data are obtained. In addition, the contact angle data have been examined further in order to determine the dispersive γ_d and polar, γ_p, parts of the surface energy[10,11] of the test plates before and after exposure to flowing water.

The above techniques, with the exception of SEM and wettability, are nondestructive and do not alter the chemical or physical aspects of the surface. The SEM procedure, on the other hand, exposes the plates to a vacuum and/or some modification, as with an evaporated metallic film. Wettability compromises the surface properties by the application of a liquid drop on the surface film. Consequently, only one of the two plates in each flow cell per exposure time was examined in the SEM, while the remaining plate was reserved for wettability measurements.

Results

It should be noted that the results reported in this section are from a single set of test plates for each exposure time. Therefore, until these experiments are repeated they must be considered preliminary.

The data from the five independent measurements made on the germanium and titanium plates are summarized in Table I. As a result of the accumulation of a thick oxide layer, which cracked upon dehydration, only data for the control plates are given for aluminum. Information on Figures 4 to 9 may be found in the column on "Observation from SEM Micrographs," given in Table I.

Figure 10 shows two SEM views of an Al plate exposed for 144 hr to warm subsurface ocean water. Note the surface is severely distorted due to dehydration of the oxide film. In spite of this only diatoms and plankton were observed on this plate. Due to the induced surface roughness of the Al plate, the wettability data were unusually low, giving a false high critical surface tension for the exposed surface.

Discussion

The main conclusion of the investigation is that the test surfaces rapidly acquire an adsorbed film when exposed to flowing warm subsurface ocean water. Table 1 lists the ellipsometrically determined film thicknesses which have been measured for the germanium and titanium test plates. The film thickness for the titanium plate probably includes the adsorbed film and some oxide film. The internal reflection spectra shown in Figures 7a, b, and c provide evidence that the film is probably a glycoprotein which very slowly increases in thickness and mass (deduced from increase in area under Amide I and II infrared bands) as the exposure time increases. It is speculated that a similar film adsorbs on the titanium plate.

• Another important finding is that the surface energy (γ_c, γ_d, γ_p) of the test plates change substantially within the first 24 hours of exposure and only slightly thereafter. Table I provides the initial surface energy data for the test plates prior to testing and after the various exposure times. For the germanium plate the critical surface tension, γ_c, is reduced from 38.6 to 29.2 dynes/cm after an exposure of 24 hours. Concurrent with this change is a decrease in the polar part of the surface energy, γ_p, as reflected by the change in the slope. It should be stressed that the surface energy data refer to the outer-most properties of the adsorbed film, to which subsequent reactions will take place. The large changes in the surface potential may indicate that there is a substantial alteration of the molecular configuration of the film with increased exposure.

With both the germanium and titanium test plates, it is clearly observed that the number and type of adhering bacteria as well as the quantity of observed diatoms present requires an induction period which is at least 24 hours. This statement is deduced from the fact that no bacteria were detected on either the germanium plate (see Figure 4) or the titanium plate during this time. The large number of submicron deposits seen on the germanium plate are currently unresolved. After 72 hr of exposure many rod-shaped bacteria are seen on both the germanium plate (see Figure 5) and on the titanium plate (see Figure 6). The test plates examined after 144 hr clearly show the presence of many rod, flagellated and stalked bacteria as seen in Figures 8a, b, c, for germanium and Figure 9 for titanium. These stalked bacteria have been tentatively identified[12,13] as members of the genus Caulobacter. Although the exposure of the aluminum plates was made without the benefit of germanium plates being exposed at the same time, it is believed that similar films would be acquired. Note, however, that no bacteria were detected on any of the Al plates even after 144 hr of exposure. As Figure 10 shows, these plates acquired instead many diatoms and related organisms during the 144 hr exposure.

It is important to note that numerous barnacles had attached to the inside of the reservoir as shown in Figure 11. (An examination of the supply tube indicated barnacles did not attach to it.) The barnacles in the reservoir were measured to have bases from 0.3 to .6 cm in diameter. This finding indicated that numerous barnacle nauplii were available within the system; however, none were detected on the test plates during the time period studied. This was most likely due to the fluid flow conditions within the flow cells. The fluid flow conditions resulted in a fluid shear rate of 980 sec^{-1} with an average fluid velocity of 14.4 cm/sec. In spite of this high shear rate, an adsorbed film was deposited at the solid/liquid interface of the test plates.

This adsorbed film is the primary film which modifies a surface prior to attachment of bacteria. Control of this primary film by selective modification of the surface properties is postulated as a means of controlling microfouling and macrofouling of the surface. At the present time, additional characterization of the adsorbed films and their roles in influencing the attachment of bacterial and other species is required before control of the surface can be achieved.

Acknowledgments

This investigation was supported by internal research funding from Calspan Corporation, Buffalo, NY. We would like to express our thanks to Dr. R. E. Baier for his discussions on the subject, to Ms. R. Zontek and Ms. A. Meyer for their assistance in the wettability studies, to Mrs. B. J. Spahr who typed the manuscript and to the staff at Calspan who worked on the figures.

References

1. Gerchakov, S.M., Marszalek, D.S., Roth, F.J., and Udey, L.R., "Succession of Periphytic Microorganisms on Metal and Glass Surfaces in Natural Seawater," 4th Int'l Congress on Marine Corrosion and Fouling, Antibes, France, p. 203-211, 1976.

2. Goupil, D.W., DePalma, V.A. and Baier, R.E., "Prospects for Nontoxic Fouling-Resistant Paints," Proceedings of 9th Annual Conference Marine Technology Society Marine Industries:Problems and Opportunities, p. 445-458, 1973.

3. Baier, R.E., Editor, Applied Chemistry at Protein Interfaces, Advances in Chemistry Series #145, American Chemical Society, Washington, DC, 1973.

4. DePalma, V.A., Baier, R.E., "Microfouling of Metallic and Coated Metallic Flow Surfaces in Model Heat Exchange Cells," Proceedings of the Ocean Thermal Energy Conversion (OTEC) Biofouling and Corrosion Symposium, Robert H. Gray, Editor, Seattle, Washington, p. 89-106, 1978.

5. DePalma, V.A., "Characteristics of Biofouling on Underwater Surfaces," Calspan Report #ND-6028-M-1, Calspan Corporation, Buffalo, NY, 1977.

6. Harrick, N.J., Internal Reflection Spectroscopy, Intersciences, 1967.

7. McCrackin, F.L., "A Fortran Program for Analysis of Ellipsometer Measurements," National Bureau of Standards, Technical Note 479, 1969.

8. Schulman, J.H. and Rideal, E.K., "On the Surface Potentials of Unimolecular Films of Long Chain Fatty Acids - Part I Experimental Method," Proc. Roy Soc (London) A 130, 259-284, 1931.

9. Zisman, W.A., "Relation of the Equilibrium Contact Angle to Liquid and Solid Constitution," Advances Chem. 43, 1, 1964.

10. Kaelbel, D.H., "Dispersion-Polar Surface Tension Properties of Organic Solids," J. Adhesion, 2, 66-81, 1970.

11. Akers, C.K., Dardik, H., Dardik, I., Wodka, W., "Surface Properties of the Inner Walls of Isolated Human Veins," Journal of Colloid and Interface Science, 59, 461, 1977.

12. Corpe, W., Private communication.

13. Brock, T.D., Biology of Microorganisms, Prentice-Hall Inc., NJ, p. 595-597, 1970.

Table I
SUMMARY OF RESULTS

	OBSERVED RESULT						
TEST PLATE AND EXPOSURE TIME	γ_c (dyne/cm) AND SLOPE (cm/dyne)	γ_d (dyne/cm)	γ_p (dyne/cm)	FILM THICKNESS Å	SURFACE POTENTIAL DIFFERENCE V (mv)	OBSERVATION FROM SEM MICROGRAPHS	INTERNAL REFLECTION INFRARED SPECTRUM
Ge (CONTROL	38.6; -0.011	24.4	23.4	--	+300*	VERY FLAT, SOME SCRATCHES SEEN AT 5000X	TYPICAL BASELINE, SEE FIGURE 3
Ti (CONTROL)	36.7; -0.005	30.4	28.4	--	+300*	A SMOOTH BUT WAVY SURFACE, SOME SCRATCHES SEEN AT 500X	--
Al (CONTROL)	35.4; -0.006	24.7	30.7	--	+1000	SMOOTH WITH SCRATCHES SEEN AT 500 AND 5000X	--
Ge (24 hr)	29.2; -0.020	29.9	5.8	62, 34**	0, -16**	MANY SUBMICRON DEPOSITS SEEN, SEE FIGURE 4	DEFINITE INDICATION OF A GLYCOPROTEINACEOUS FILM DETECTED, SEE FIGURE 7a
Ti (24 hr)	43.7; -0.026	33.3	11.9	72, 76**	-98, -153**	LIKE CONTROL BUT WITH AN EASILY SCRATCHED FILM, ALSO MANY SUBMICRON DEPOSITS	--
Ge (72 hr)	30.3; -0.017	29.5	6.5	53, 98**	50, -66**	MANY ROD-SHAPED BACTERIA 1-2 μ IN LENGTH, ALSO AREAS OF DIATOM DEPOSITS, SEE FIGURE 5	A DEFINITE INCREASE IN A GLYCOPROTEINACEOUS FILM DETECTED SEE FIGURE 7b
Ti (72 hr)	42.1; -0.007	35.6	12.6	706, 674**	-202, -313**	SURFACE OXIDIZED, MANY ROD BACTERIA EMBEDDED IN OXIDE, SEE FIGURE 6	--
Ge (144 hr)	32.4; -0.020	30.3	6.2	70, 67**	107, 220**	LARGE NUMBER OF STALKED BACTERIA ALONG WITH AREAS OF DIATOM DEPOSITS, SEE FIGURE 8a, b, c	SLIGHT INCREASE IN A GLYCOPROTEINACEOUS FILM ABOVE 72 hr CASE, SEE FIGURE 7c
Ti (144 hr)	45.6; -0.032	43.1	4.8	772, 773**	-275, -200**	LARGE NUMBER OF STALKED BACTERIA ALONG WITH AREAS OF DIATOM DEPOSITS, SEE FIGURE 9	--

* INITIAL SURFACE POTENTIAL

**MEASUREMENTS FROM BOTH PLATES IN FLOW CELL

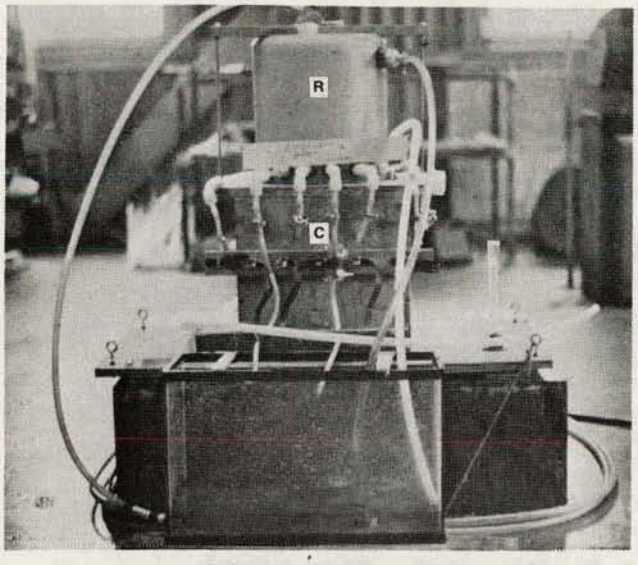

Figure 1 EXPERIMENTAL APPARATUS CONSISTING OF POLYETHYLENE RESERVOIR (R) AND FLOW CELLS (C) USED AT STAGE I PLATFORM

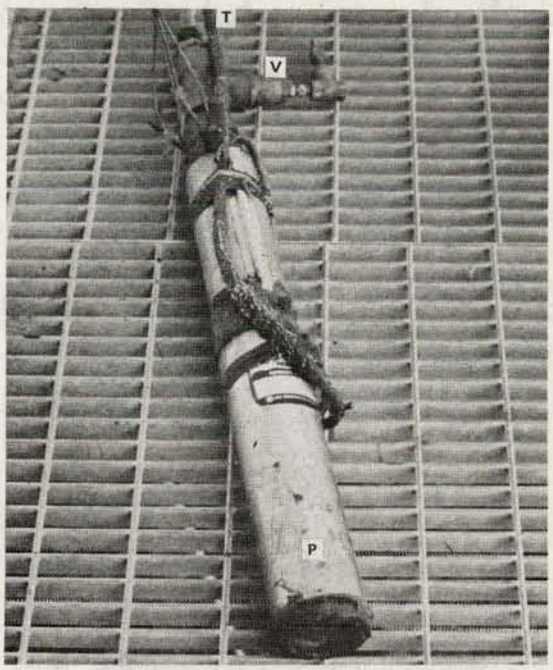

Figure 2 DEEP WELL SUBMERSIBLE PUMP, P, USED TO PUMP WATER TO RESERVOIR IN FIGURE 1. NOTE VALVE, V, USED TO DIVERT WATER FROM DELIVERY TUBE, T

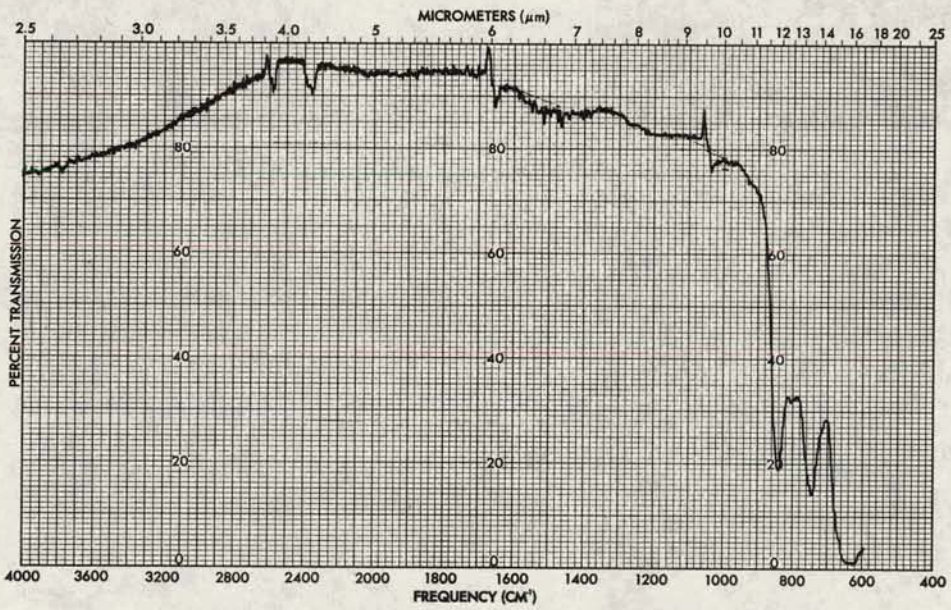

Figure 3 INTERNAL REFLECTION INFRARED SPECTRUM OF GERMANIUM INTERNAL REFLECTION PLATE #108 BEFORE EXPOSURE – BASELINE SPECTRUM

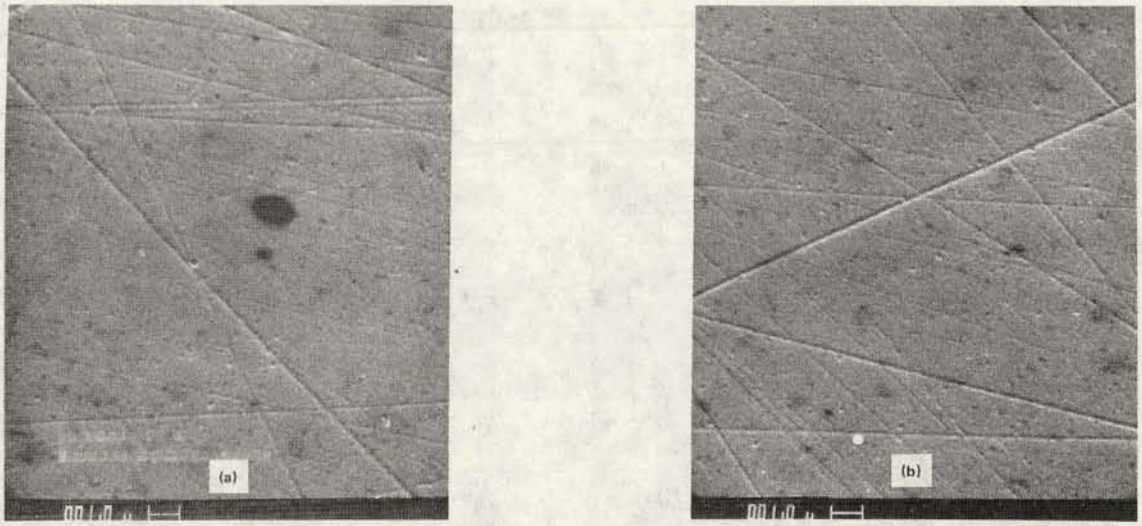

Figure 4 SEM VIEWS OF GERMANIUM INTERNAL REFLECTION PLATE #111 AFTER 24 HR. EXPOSURE TO SUB-SURFACE WARM OCEAN WATER (45° TILT, UNCOATED)

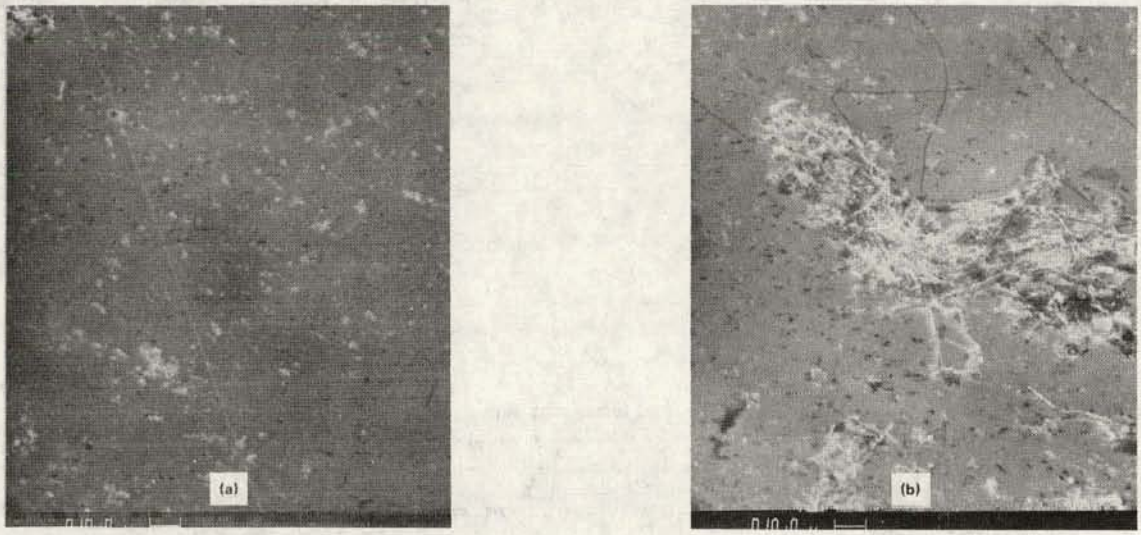

Figure 5 SEM VIEWS OF GERMANIUM INTERNAL REFLECTION PLATE #115 AFTER 72 HR. EXPOSURE TO SUB-SURFACE WARM OCEAN WATER (45° TILT, UNCOATED)

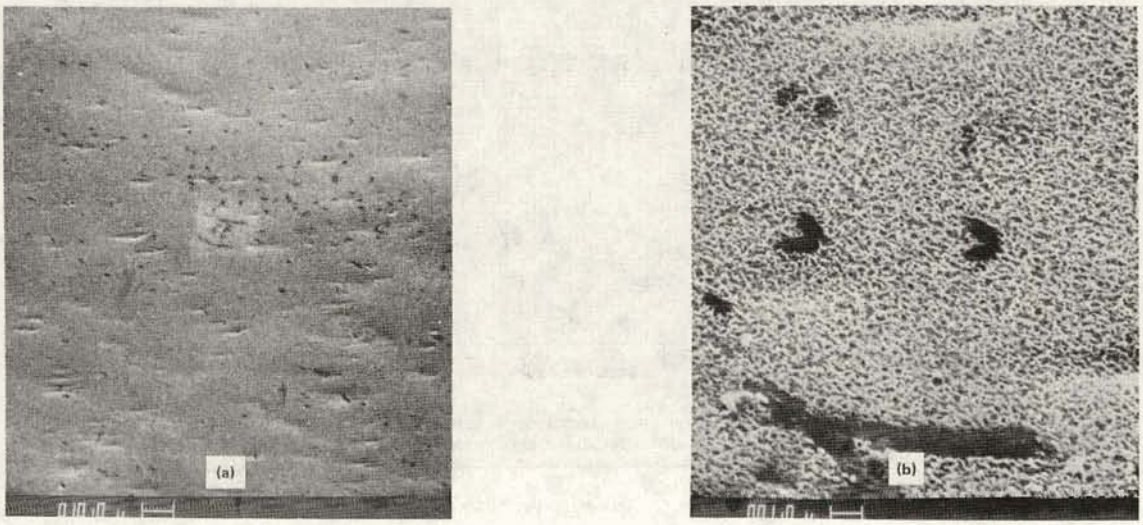

Figure 6 SEM VIEWS OF TITANIUM PLATE #4 AFTER 72 HR. EXPOSURE TO SUB-SURFACE WARM OCEAN WATER (VIEW a, b, 45° TILT, UNCOATED)

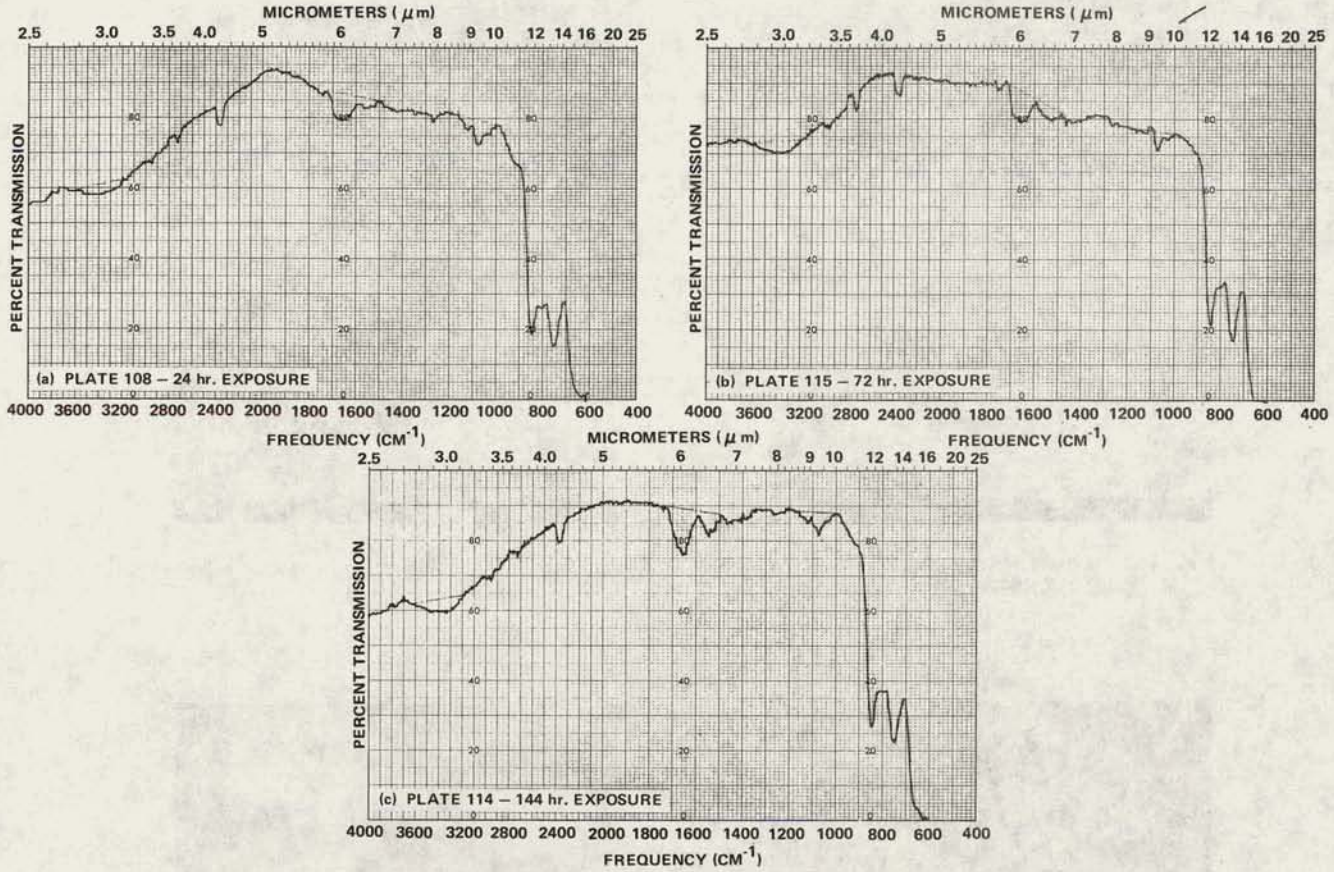

Figure 7 INTERNAL REFLECTION INFRARED SPECTRA OF ADSORBED FILM ON GERMANIUM INTERNAL REFLECTION PLATES EXPOSED TO FLOWING SUB-SURFACE WARM OCEAN WATER

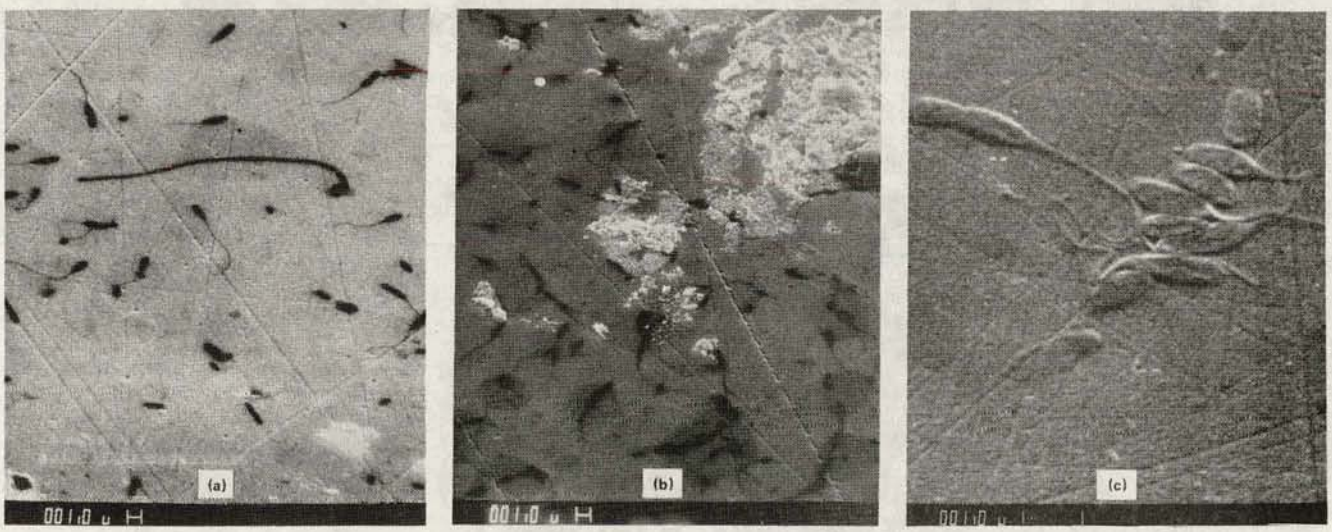

Figure 8 SEM VIEW OF GERMANIUM INTERNAL REFLECTION PLATE #103 AFTER 144 HR. EXPOSURE TO SUB-SURFACE WARM OCEAN WATER (45° TILT, a & b 20 KV BEAM, UNCOATED, c 10 KV BEAM COATED)

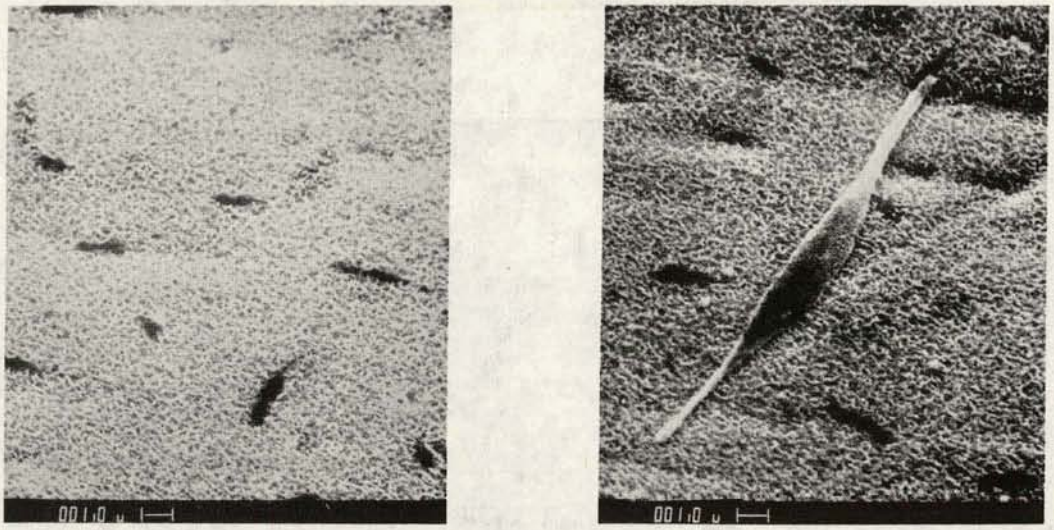

Figure 9 SEM VIEWS OF TITANIUM PLATE #6 AFTER 144 HR. EXPOSURE TO SUB-SURFACE WARM OCEAN WATER (45° TILT, UNCOATED)

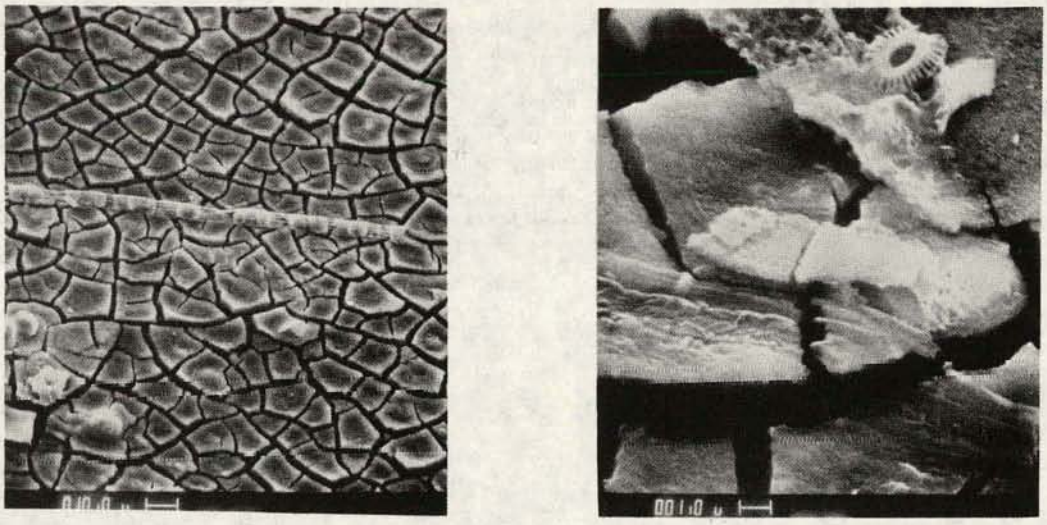

Figure 10 SEM VIEWS OF ALUMINUM TEST PLATES AFTER 144 HR. EXPOSURE TO SUB-SURFACE WARM OCEAN WATER (BOTH AT 45° TILT AND COATED)

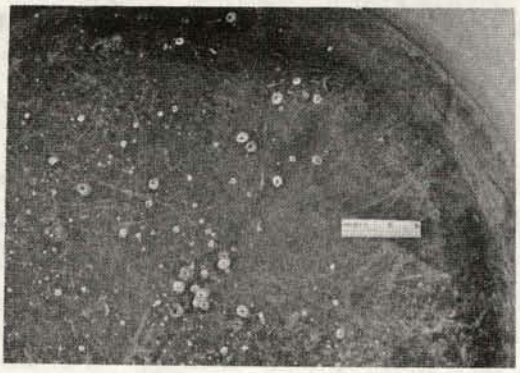

Figure 11 PHOTO OF THE INSIDE SURFACE OF THE RESERVOIR AFTER EXPOSURE TO SUB-SURFACE OCEAN WATER – NOTE THE PRESENCE OF BARNACLES ATTACHED TO THE SURFACE (SMALLEST SCALE DIVISIONS ARE .1 cm)

DISCUSSION

B. Freedman, General Dynamics: When you talk about corrosion, do you mean corrosion of the aluminum? I do not observe any pits either under the scanning electron microscope. Did you really look for pits?

V. DePalma: No.

R. Mitchell, Harvard: Glenn Zeeland with Argonne National Laboratory is supposed to be doing that. He's just a little slow in getting the results to us.

B. Liebert, Univ. of Hawaii: In an experiment similar to yours, using the same material, Aℓ 5052 and same flow rate, I did not observe any pitting either.

MICROBIAL FILM DEVELOPMENT AND ASSOCIATED ENERGY LOSSES

J. D. Bryers**, W. G. Characklis*, N. Zelver†, and M. G. Nimmons†

Environmental Science and Engineering Dept.
George R. Brown School of Engineering
Rice University
Houston, Texas 77001

Abstract

Microbial fouling in power plant condensers increases heat transfer and fluid frictional resistance resulting in energy losses. Biofouling control is generally by chlorine addition creating potential toxicity problems in receiving waters. A better understanding of biofouling film development and destruction (i.e., stoichiometry and kinetics) is necessary to maintain effluent water quality while minimizing biofouling effects.

This paper reviews research progress in the following areas:

1) development of various sensitive biofilm detection methods for monitoring the extent of biofouling;

2) determination of effects of certain variables on the kinetics and stoichiometry of biofilm accumulation;

3) correlation of biofilm development to increases in both heat transfer and fluid frictional resistance; and

4) determination of the effects of chlorine applications on established biofilms.

Introduction

The term fouling refers to the formation of inorganic and/or organic deposits on surfaces. In cooling systems, these deposits form on condenser tube walls increasing fluid frictional resistance, accelerating corrosion and impairing heat transfer. Four types of fouling, alone or in combinations, may occur:

1. crystalline fouling caused by precipitation of $CaCO_3$, $CaSO_4$ or silicates
2. corrosion fouling resulting from formation of insulating layers of metal oxides on the tubes
3. fouling due to adherence of particulate matter on tube surfaces
4. biological fouling resulting from attachment and growth of microbial organisms

This investigation was restricted to the study of biological fouling.

The Problem

The most common method for controlling the fouling biofilm development and maintaining condenser performance is periodic chlorination. However, concern over residual toxicity from hypochlorous acid or its reaction products has resulted in federal regulations which limit the allowable concentrations of free available chlorine in cooling water discharges. At the present time, there is no sound basis for assessing the impact of the regulations.

This investigation stems from the apparent need for a more basic understanding of fouling biofilm development and fouling biofilm destruction.

Project objectives included the following:

1. Develop a better understanding of fouling biofilm development, with particular emphasis on the effects of fluid flow rate, bulk water temperature, wall surface temperature and limiting nutrient concentration.
2. Determine the effectiveness of fouling biofilm destruction by chemical oxidants, primarily chlorine.
3. Develop a practical, reliable, sufficiently sensitive device for monitoring biofouling and for effectively operating and controlling biofouling destruction processes at operating power plants.

Laboratory experiments and a limited number of field tests were conducted with two reactor configurations:

1. a tubular reactor
2. an annular reactor consisting of a stationary outer cylinder and a rotating inner cylinder.

The tubular reactor geometry and its turbulent flow regime are identical to those existing in cooling water condensers. The annular reactor was tested as a biofouling monitor because it is very sensitive to fouling and is easy to operate and maintain. The annular reactor has the potential of being used in a sidestream from the cooling water supply to continuously monitor biofouling for control of the addition of oxidant. Biofouling in the experimental reactors was measured by observing changes in the following parameters:

1. biofilm thickness
2. attached biomass
3. fluid frictional resistance
4. heat transfer resistance

Processes in Fouling Biofilm Development

Microbial fouling is the combined result of phys-

*Professor, Environmental Science and Engineering Dept., Rice University.

**,†,†Graduate Assistant, Environmental Science and Engineering Dept., Rice University.

ical transport and biological growth rate processes as shown in Fig. 1. The following processes contribute to overall biofouling accumulation:

Biofouling Processes

1. Organic Adsorption
2. Transport of Microbial Particles to the Surface
3. Microorganism Attachment to the Surface
4. Growth of Attached Microorganisms
5. Reentrainment of Biofilm by Fluid Shear Stress

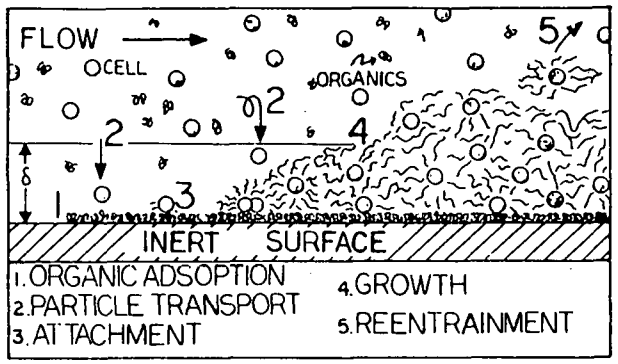

Fig. 1 Biofouling Development Processes

Organic adsorption. Figure 1 illustrates an initially "clean" surface exposed to a turbulent flow of fluid containing dispersed microorganisms, nutrients, and organic macromolecules. Adsorption of an organic monolayer occurs within minutes of exposure. Investigations have shown that, once exposed to natural waters with low organic concentrations, materials of originally diverse surface properties (i.e., wettability, surface tension, electrophoretic mobility) are rapidly conditioned by adsorbing organics.[2,3,4,5,11,12,18,19]

Transport of microbial particles to the surface. Figure 1 indicates the physical transport of bacterial particles from the bulk fluid to the organically-coated surface. Within a turbulent flow regime, particles suspended within the fluid are transported to the solid surface by only two mechanisms: molecular diffusion and turbulent eddy transport. Theory indicates that the flux of particles to the surface increases with increasing fluid velocity and particle concentration in the bulk fluid. However, particle flux is also strongly dependent on the physical properties of the particles (e.g., size, shape, density).[6]

Microorganism attachment to the surface. Bacteria do not attach to solids very tenaciously unless left in contact with the water source for several hours. Then, some cells are attached so strongly that they are not dislodged by washing or staining. This suggests that bacteria grow on, and/or attach themselves to solid surfaces rather than merely being passively stuck.

Research confirms the existence of a two-stage attachment process: reversible adhesion followed by an irreversible attachment. Reversible adhesion refers to an initially weak attachment of a bacterium to a surface. Organisms still exhibit Brownian motion and are readily removed by mild rinsing. Conversely, irreversible attachment is a permanent cohabitation with the surface, usually aided by production of cellular exopolymers. Photomicrographs show that biofilms do not consist of successive layers of microorganisms, but rather microorganisms entrapped in a gelatinous matrix.[10,15] Irreversibly attached bacteria can only be removed by severe methods.

Most attachment studies were concerned with the biological sequences of early fouling and were conducted at very low shear rates. Kinetics determined from these studies may be mass transfer limited and not necessarily applicable to condenser biofouling.

Growth of attached microorganisms. Attached and dispersed microorganisms assimilate nutrients, produce extracellular polymers, maintain biosynthesis, and replicate. Biofilm "growth" is considered the combined effect of cellular reproduction and exopolysaccharide production, as shown in Fig. 1.

Biofilm growth can be described by a wide variety of rate expressions whose rate constants are functions of pH, temperature, limiting nutrient concentration, nutrient type, terminal electron acceptor, and organism concentration.

Postulated rate expressions for nutrient depletion by a fixed biofilm are numerous, but all agree that nutrient depletion rates are first order in biofilm mass and, generally, diffusion-limited in the biofilm.[1,14,16,17,24]

Reentrainment of biofilm by fluid shear. At any point in the development of a biofilm, portions of biofilm peel away from the inert surface and are reentrained in the fluid flow (Fig. 1). Reentrainment is a continuous process of biofilm removal and is highly dependent on hydrodynamic conditions. Sloughing, on the other hand, appears to be a random, massive removal of biofilm attributed to oxygen/nutrient depletion deep within biofilms. Sloughing is more frequently witnessed with thicker, dense films. More work is needed to quantify either effect.

In summary, biofouling is the net result of all these rate processes occurring simultaneously. Naturally, at specific times in the overall development certain processes may contribute more significantly than others.

Experimental

Protocol

The experimental methods used in this laboratory study were chosen to simulate the fundamental processes of biofilm development and destruction occurring in a small portion of a power plant condenser.

Nutrients, glucose and, in some cases, a synthetic growth media were added to provide the necessary mineral, energy and carbon requirements for microbial growth. The feed water to the various experimental reactors was tap water which had been treated to remove residual suspended solids and chlorine.

Apparatus

Two reactor geometries were used in this research

to study biofilm development and destruction:

1. The circular tube was used because it is the prevalent geometry in power plant condensers.

2. The sensitivity of the rotating annular reactor was tested because it could provide a more practical, reliable means for monitoring biofouling in the field since it requires little maintenance or support equipment. This paper will not discuss results from the annular reactor.

Tubular fouling reactors. The tubular fouling reactors are chemostats (continuous stirred tank reactors) with internal recycle as indicated in Fig. 2. Advantages of this configuration for laboratory experimentation include the following:

1. At high recycle rates employed (F_r>>F), the reactor contents are completely mixed and no concentration gradients exist. This simplifies mathematical descriptions and sampling. It also provides a relatively uniform biofilm in the recycle section while allowing simple control of pH and temperature. From a practical standpoint, this system minimized the consumption of water and microbial nutrient medium.

2. A short mean residence time can be maintained which minimizes biomass activity in the bulk fluid and restricts microbial activity to the reactor surfaces.

3. Fluid shear stress at the wall in the recycle loop is independent of mean residence time in the reactor system.

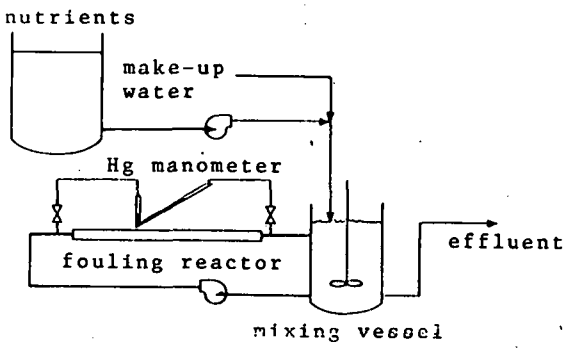

Fig. 2 Biofouling Reactor System

Results from three tubular reactor systems are discussed in this paper. Each system is similar to the design depicted in Figure 2 but differ from each other according to their specific intent as follows:

Tubular Fouling Reactor 1 (TFR1) was used for determining the effect of fluid shear rate at the wall, bulk water temperature, and limiting substrate concentration on biofilm development as determined by attached biomass, biofilm thickness and fluid frictional resistance. Tubular Fouling Reactor 3 (TFR3) was an improved version of TFR1.

Tubular Fouling Reactor 4 (TFR4). Biofilm thickness, fluid frictional resistance, and heat transfer resistance were measured by TFR4 experiments. Heat transfer resistance was measured in a Test Heat Exchanger (THE) which was an integral part of the recycle reactor.

Tubular Fouling Reactor 5 (TFR5) was used for studying biofouling development during the initial fouling phase. It consists of a continuous culture reactor (i.e., chemostat C.S.T.R.) with internal recycle loops. In this way one can maintain a constant bulk microbial culture at a desired activity while independently varying fluid flow rate.

Further details concerning methods and experimental protocol can be found elsewhere.[7,13,21,25]

Analytical Methods

Biofouling was measured by observing changes in the following parameters:

1. biofilm thickness
2. attached biomass
3. fluid frictional resistance
4. heat transfer resistance
5. biofilm constituent chemical analysis

Details of the analytical methods are presented elsewhere.[7,13,21,25]

Results and Discussion

Biofilm Development

The process of biofilm development on a surface exposed to turbulent flow is adequately described by a sigmoidal-shaped curve. The progression of biofilm development can be conveniently divided into three phases:

1. Induction Phase - the initial development period during which the biofilm accumulation increases but fluid frictional resistance remains constant.

2. Logarithmic Growth Phase - the period of time during which the accumulation increases logarithmically (may include a portion of the induction period).

3. Plateau Phase - the period during which deceleration of the accumulation rate is observed and pseudo-steady state in biofilm accumulation occurs.

The three phases of biofilm development are indicated in Fig. 3.

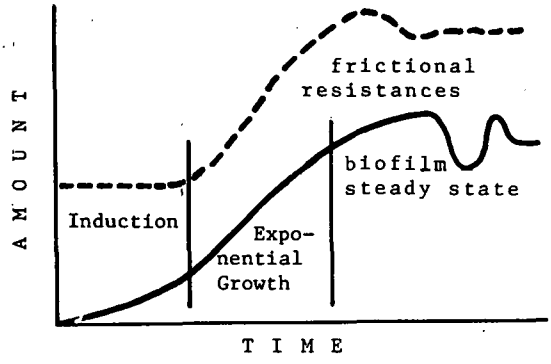

Fig. 3 Phases of Biofilm Development

Induction Phase. Primary biofilm formation occurs during that period of time from "clean" surface conditions to the onset of frictional resistance increase.

Experiments were conducted to ascertain the rate of primary biofilm formation as a function of dispersed biomass concentration (X), Reynolds number (Re), and dispersed organism growth rate (μ). The relationship can be described by Eq. 1:

$$R_i = dX_A/dt = k \cdot f(x,Re,\mu) \qquad (1)$$

where X_A = attached biofilm amount/area; R_i = rate of initial biofilm formation.

All primary biofilm experiments were conducted in TFR5. Details of the experimental protocol for this research are provided by Bryers.[7]

Results of the primary biofilm formation experiments can be summarized as follows:

1. Biofilm develops faster at higher Reynolds number (i.e., increased velocity) at constant dispersed biomass concentration and dispersed growth rate.

2. Increasing dispersed biomass concentration, at constant Re and dispersed growth rate, increases the rate of initial biofouling

3. An increased dispersed organism growth rate increases the rate of primary biofilm formation, at constant Re and dispersed biomass concentration

Growth and plateau phase. Biofilm development progression for a typical experiment is illustrated in Fig. 3. The logistic or sigmoidal curve for biofilm development can be described analytically by the following function:

$$Th = \frac{Th_o e^{kt}}{1-(Th_o/Th_{MAX})\ (1-e^{kt})} \qquad (2)$$

where Th = biofilm thickness (L); Th_o = Th at t = 0 (L); Th_{MAX} = maximum value to Th attained (L); k = rate constant (t^{-1}). The rate of change of Th can be described by the following:

$$\frac{d(Th)}{dt} = k(Th) - \frac{k(Th)^2}{Th_{MAX}} \qquad (3)$$

The rate constant, k, describes the logarithmic rate of development which occurs at $Th << Th_{MAX}$. The second term accounts for a process opposing development. Regardless of mechanism, k(Th) represents the logarithmic development rate or fouling rate characteristic of the growth phase while Th_{MAX} characterizes the plateau phase.

The logarithmic fouling rate (based on either biofilm thickness or biofilm mass) varies with nutrient loading rate as indicated in Fig. 4. The effect of wall shear stress is also indicated. As wall shear stress increases, the second term in Eq. 3 becomes more important in controlling biofilm development rate. This suggests that Th_{MAX} decreases with increasing wall shear stress. Figure 5 indicates that, in fact, Th_{MAX} decreased with increasing wall shear stress, especially at high nutrient loading rates.

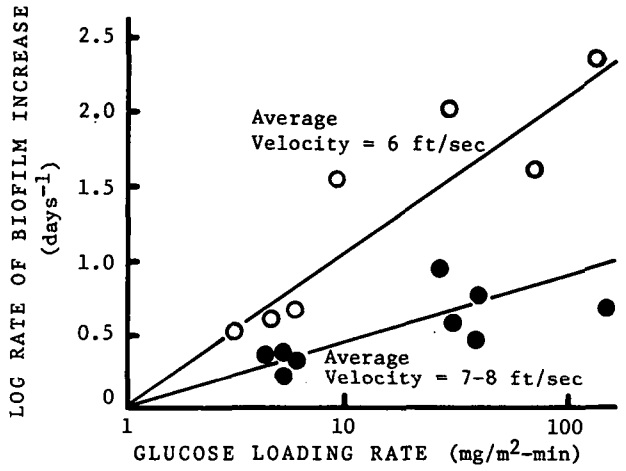

Fig. 4 Glucose loading and rate of biofilm Increase

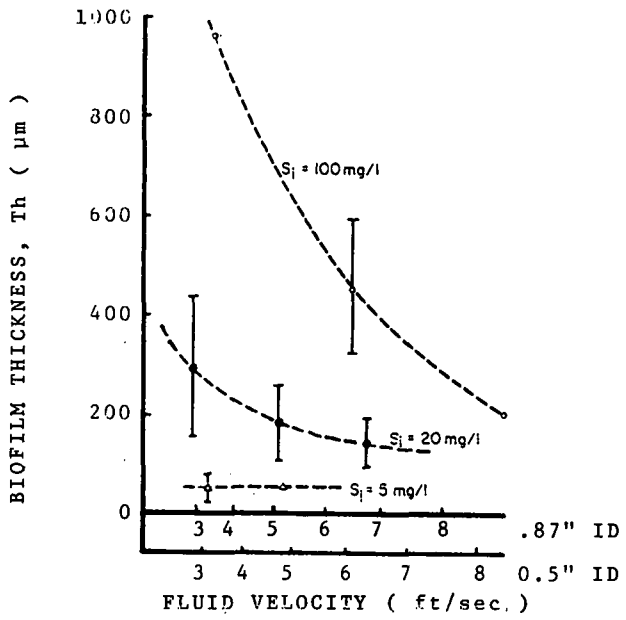

Fig. 5 Velocity effect on maximum biofilm Th

Biofilm Detriments

Effects on frictional resistance. Increase in fluid frictional resistance due to biofilm accumulation during experiments in which flow rate is maintained constant causes an increase in pressure drop and power requirements for pumping as shown in Fig. 6 for a typical experiment.

Conversely, if pressure drop is held constant, flow capacity is reduced. Fig. 7 shows a typical experimental curve where flow capacity was reduced to 42% of the original capacity in a 100-hour laboratory experiment.

Frictional resistance can be represented by a dimensionless friction factor defined as follows:

$$f = 2.0 \frac{d}{L} \frac{\Delta P}{\rho_w \bar{v}^2} \qquad (4)$$

where f = friction factor; d = tube diameter (L); ρ_w = fluid density (M/L^3); $\bar{v}$ = average fluid velocity; (L/t); ΔP = pressure drop along length L ($M/L\text{-}t^2$).

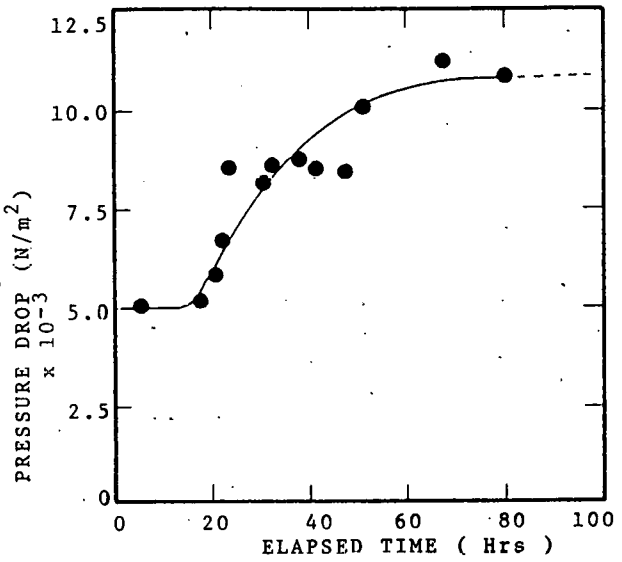

Fig. 6 Change in ΔP with time; constant flow

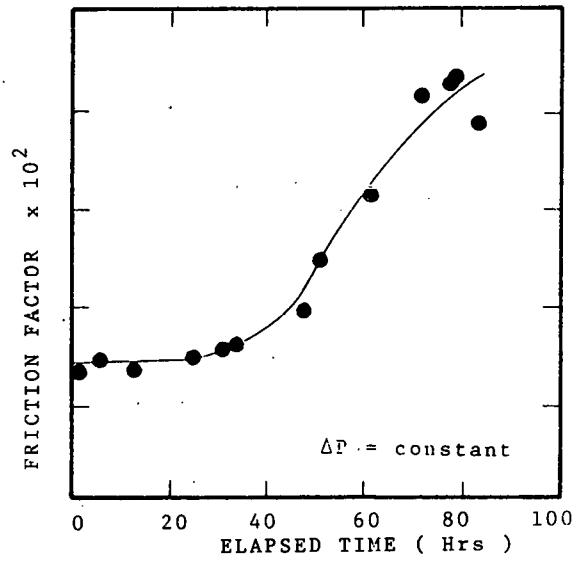

Fig. 8 Change in friction factor with time

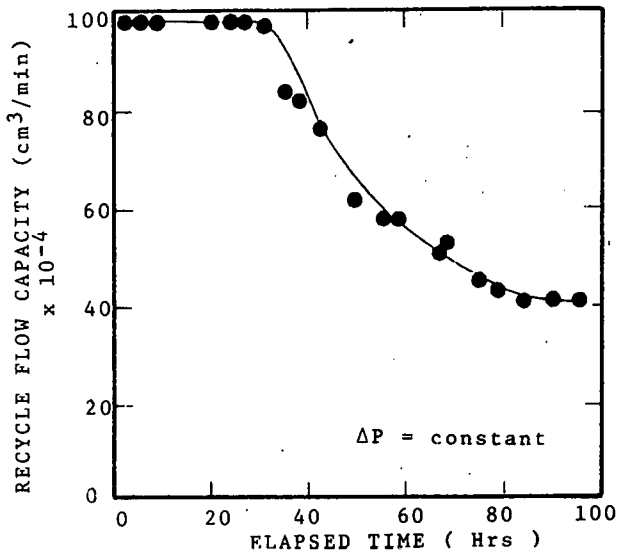

Fig. 7 Change in flow capacity with time

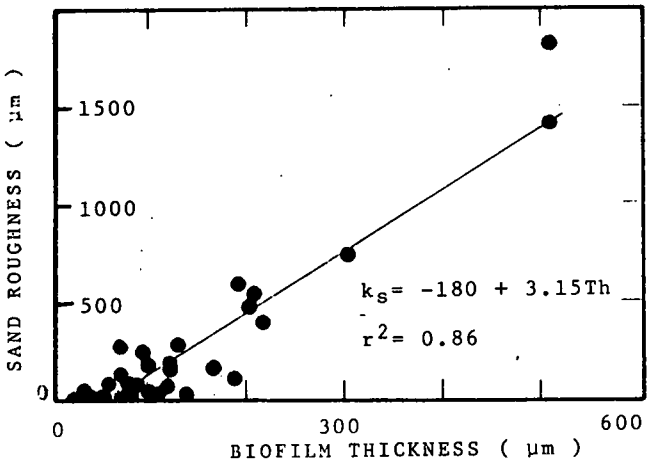

Fig. 9 Change in equivalent sand roughness with biofilm thickness for all constant ΔP experiments

The change in friction factor with time for a typical experiment is shown in Fig. 8. The measured biofilm thickness for the same experiment is also indicated.

The friction factor is related to the Reynolds number and the equivalent sand roughness k_s through the empirical Colebrook-White equation:

$$k_s = \frac{d}{2}\, 10^{(0.87-0.50f^{-\frac{1}{2}})} - \frac{18.70}{Re\, f^{\frac{1}{2}}} \qquad (5)$$

where d = tube diameter (L); Re = vd/ν = Reynolds number; $\bar{v}$ = mean fluid velocity (L/t); ν = kinematic viscosity (L^2/t). This expression can be used to compute an equivalent sand roughness for the biofilm from a measurement of the flow rate and pressure drop. In all TFR experiments except TFR5, k_s increases with time. Figure 9 indicates the dependence of k_s on biofilm thickness for the range of shear stress investigated (6.5 - 7.9 N/m^2).

The Blasius-Stanton or Moody diagram can be used to compare frictional resistance due to biofilm development with frictional resistance of rigid rough surfaces.[20] The Blasius-Stanton diagram is a plot of friction factor vs. Reynolds number for a series of pipes with different equivalent sand roughness; the friction factor in a pipe with a rigid rough surface depends on both the relative roughness and the Reynolds number.

The relationship between friction factor and Reynolds number for the fouled TFR3 system is presented in Fig. 10. This figure shows the dependency of friction factor on Reynolds number is similar to that for a tube with a rigid rough surface between the range of Reynolds numbers investigated (5,000 to 48,000).

The relationship between biofilm thickness and friction factor for all experiments at a wall shear stress from 6.5 - 7.9 N/m^2 is shown in Fig. 11. Friction factor is dependent on film thickness after a critical thickness (TH_{crit}) approximately equal to the thickness of the viscous sublayer is attained. Thickness of the viscous sublayer is defined by Eq. 6:

$$\delta = \frac{10d}{Re}\left(\frac{f}{2}\right)^{-0.5} \qquad (6)$$

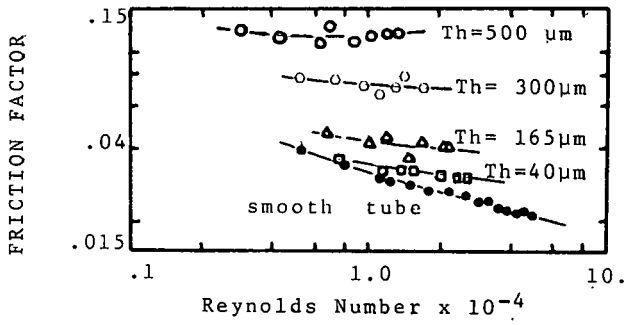

Fig. 10 Friction factor vs Reynolds Number for a fouled constant pressure system

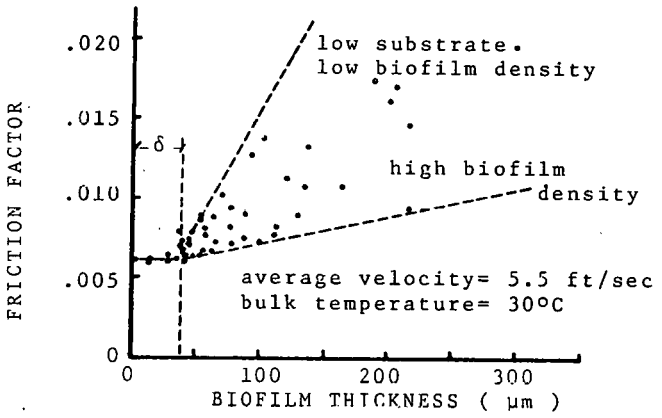

Fig. 11 Effect of biofilm thickness on friction factor in a circular tube

The critical film thickness corresponds to the stage of biofilm development at which surface irregularities protrude through the viscous sublayer. Until this stage, the roughness peaks are smaller than the viscous sublayer thickness ($k_s < \delta_1$) and friction factor does not increase (the tube is hydraulically smooth). For a wall shear stress of 6.5 - 7.9 N/m^2, the viscous sublayer is approximately equal to 40 micrometers; this corresponds well with the observed TH_{crit} 30-35 micrometers for the same wall shear stress range.

Although the frictional resistance effects of biofilm can be adequately described by formulae suitable for rigid rough surfaces, the conclusion should not be drawn that indeed the biofilm presents a rigid rough surface to the flow. Such a notion is an oversimplification and cannot account for all experimental observations. Picologlou et al., discuss mechanisms of hydraulic deterioration due to biofilm development in more detail.[23]

Effects on heat transfer resistance. Biofilm development and resulting fluid frictional resistance have been discussed and both influence heat transfer. Changes in heat transfer resistance arise from the combined effects of increased biofilm thickness (conductive heat transfer) and increased frictional resistance (convective heat transfer).

Conductive heat transfer can be related to biofilm thickness and its effective thermal conductivity. Experimental biofilm thermal conductivity determinations indicate no significant difference from that of water at the same temperature.[25] This is not surprising since biofilm is approximately 98-99% water.

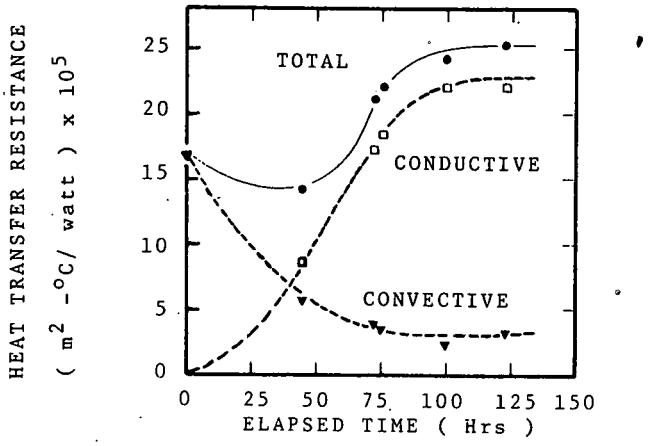

Fig. 12 Change in heat transfer due to biofilm development

Convective heat transfer resistance due to biofouling film development can then be calculated if the following are known:

1. biofilm thickness and thermal conductivity
2. frictional resistance
3. wall temperature and bulk temperature

Figure 12 describes a typical experiment in TFR4 and illustrates the relative effects of conductive and convective heat transfer resistance on overall heat transfer resistance.

Biofilm Destruction by Chemical Oxidants

The most common method for controlling fouling biofilm development and maintaining power plant condenser performance is periodic chlorination. Chlorine, added to cooling water, serves either to kill the microorganisms in the biofilm or to hydrolyze the extracellular polymers which hold the biofilm together.

One objective of this study was to further define the chlorine-biofilm reaction, its rate and stoichiometry. Batch experiments were conducted primarily in the tubular fouling reactor (TFR1) under turbulent flow conditions with "mature" biofilms.

Rate of chlorine consumption by biofilms. Batch experiments were initiated by injecting a pulse of chlorine into the recycle tubular reactor section of the TFR1 and observing the disappearance of chlorine (actually, total oxidant). The input pulse invariably resulted in an exponential decrease of chlorine, as illustrated in Fig. 13, for seven successive injections of equal magnitude. Chlorine disappearance rate for an individual injection can be described as follows in a batch reactor:

$$V \frac{d[OX]}{dt} = -k_1 A_s [OX] \qquad (7)$$

where [OX] = chlorine concentration (ML^{-3}); A_s = reactor surface area covered by biofilm (L^2); V = reactor volume (L^3); k_1 = process rate coefficient (Lt^{-1}); t = reaction time (t). k_1 has units of velocity (Lt^{-1}) or a surface rate coefficient since the reaction is occurring at the water-biofilm interface. Figure 13 indicates that each successive injection resulted in a decreasing k_1 for a given biofilm. The decrease in k_1 with successive injections is satisfactorily described by the following expression:

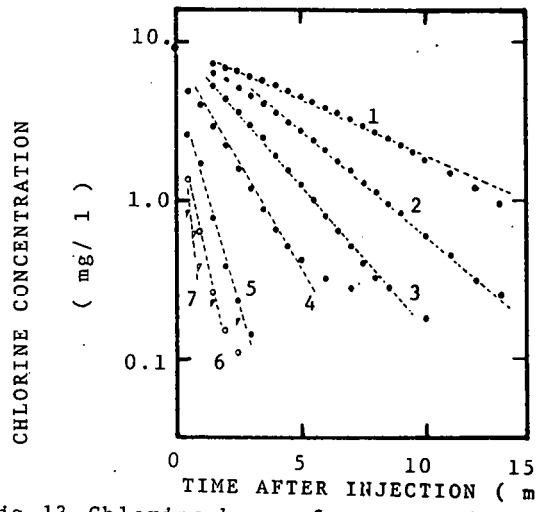

Fig. 13 Chlorine decay after several injections

$$k_1 = k_2 \exp[-k_3 OX_R] \quad (8)$$

where OX_R = cumulative chlorine reacted (ML^{-2}); k_2 = process rate coefficient (Lt^{-1}); k_3 = constant (L^2M^{-1}).

The first order rate expression Eq. 8 may be indicative of a first order reaction or a mass transfer limitation occurring in the bulk fluid or within the biofilm. The potential for diffusion limitation in the biofilm appears reasonable since chlorine is extremely reactive in the biofilm. In view of these results, biofouling control strategies can be more effective when chlorine is present at higher concentrations in the bulk fluid, even if only for short periods.

Biofilm destruction. Biofilm destruction rates could not be directly determined because biofilm sampling techniques used in this study were not amenable for use during chlorination tests which lasted for very short periods (30 minutes or less). Therefore, biofilm thickness data are restructed to before and after chlorination. However, biofilm destruction rates were indirectly monitored during chlorination by pressure drop measurement (TFR1). Figure 14 illustrates changes in pressure drop for typical experiments as a function of chlorine reacted. Assuming a direct relationship between pressure drop and biofilm thickness, the following expression describes the rate of biofilm destruction in a batch reactor:

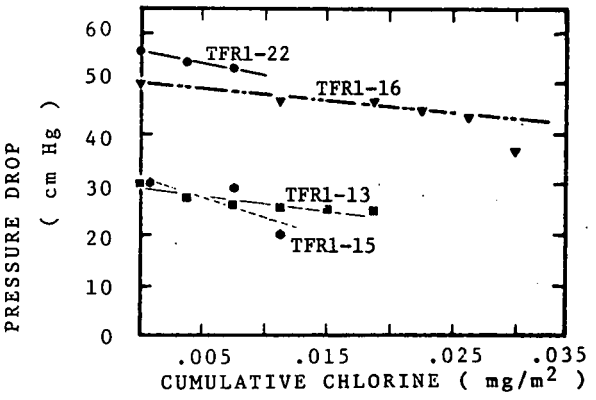

Fig. 14 Change in ΔP due to biofilm treatment with chlorine

$$\frac{dTh}{dt} = Th_i \exp(-k_4 [OX_R]) \quad (9)$$

where Th_i = biofilm thickness prior to chlorination (L); k_4 = constant (L^2M^{-1}). More experimental work is needed to yield a relationship incorporating instantaneous bulk chlorine concentration and biofilm thickness.

Studies indicate that chlorine attacks the extracellular polymers which maintain the integrity of the biofilm matrix.[8] Chlorine causes depolymerization and results in removal of the weakened biofilm matrix by fluid shear stress. Continued biofilm removal is frequently observed even when all chlorine is dissipated which implies the important role of fluid shear stress in the overall biofilm destruction process. Norrman et al., also recorded the enhancing effect of fluid shear stress on biofilm destruction by chlorination.[22]

Biofilm regrowth subsequent to chlorination. Established biofilms in this study were exposed to extremely severe treatments, including sequential strong acid, strong base and strong hypochlorite solutions. Microscopic inspection subsequent to such treatments frequently indicated a significant residual deposit composed of microbial cells and associated organic matter, especially when the biofilm was highly filamentous. When growth was reinitiated, the residual deposit apparently enhanced redevelopment of the biofilm. Regrowth rates subsequent to chlorination were measured by Norrman.[22]

Summary

Current research has provided some insight into the overall biofouling problem. Specifically:

1. Biofouling film development is the combination of several physical transport and biological growth rate processes.

2. Rate of biofouling in the induction phase increases with increasing dispersed solids concentration, fluid flow velocity, and dispersed organism growth rate.

3. Beyond a "critical" thickness, biofilm accumulation creates large increases in both frictional and heat transfer resistances. The "critical" biofilm thickness, observed experimentally, compares favorably with the viscous sublayer thickness calculated for the clean tube.

4. Increased frictional resistance resulting from biofilm development can be attributed to several biofilm characteristics including its viscoelasticity, filamentous morphology and/or rippled surface morphology. Regardless of mechanism, the increase in friction factor can be described by traditional "equivalent sand roughness" deposits.

5. Changes in overall heat transfer resistance arise from the effect of biofilm development on both conductive and convective heat transfer.

6. Chlorine oxidizes parts of the biofilm resulting in a weakened matrix which is more easily removed by fluid shear forces. Chlorine removal rate is approximately first order in chlorine concentration. The extent of biofilm removal is dependent on the amount of biofilm (measured as thickness) present prior to chlorine addition.

Acknowledgments

The authors gratefully acknowledge the following:

- The Electric Power Research Institute (RP902-1); The National Science Foundation (ENG74-11957 and ENG77-26934); and the Amoco Foundation Fellowship for partial financial support.
- Drs. B.F. Picologlou and L.V. McIntire for significant contributions to the experimental program.
- Ms. Maurine Lee and Ms. Linda Graetz for manuscript preparation.
- Duane Marks for the graphic illustration.

References

1. Atkinson, B. and M.E. Abdel Rahman Ali. 1976. Wetted area, slime thickness, and liquid phase mass transfer in packed bed biological film reactors. Trans. Instn. Chem. Engr., 54, pp. 239-250.

2. Baier, R.E., E.G. Shafin, and W.A. Zisman. 1968. Adhesion: mechanisms that assist or impede it. Science, 162.2, p. 1360

3. Baier, R.E. 1972. Influence of the initial surface condition of materials on bioadhesion. Proc. 3rd Int'l. Cong. on Mar. Corrosion and Biofouling, Gaithersburg, Md.

4. Baier, R.E. 1973. Applied chemistry at protein interfaces. Adv. Chem. Series, No. 145, p. 1.

5. Baier, R.E. and V.A. Depalma. 1977. Microfouling of metallic and coated metallic flow surfaces in model heat exchanger cells. Calspan Corp. Report, P.O. Box 235, Buffalo, N.Y.

6. Beal, S.K. 1970. Deposition of particles in turbulent flow on channel or pipe walls. Nucl. Sci. and Engr., 40. pp. 1-11.

7. Bryers, J.D. and W.G. Characklis. 1979. Measurement of primary biofilm formation. Proc. Biofouling of Power Condenser Symposium - EPRI, Atlanta, Ga.

8. Characklis, W.G. and T. Dydek. 1975. Influence of carbon to nitrogen ratio on the chlorination of microbial aggregates. Water Res., 10, pp. 515-522.

9. Colburn, A.P. 1933. Correlation of momentum and energy transfer. Trans. A.I.Ch.E., 29, pp. 174-210.

10. Costerton, J.W., G.G. Geesey and K.J. Cheng. 1979. How bacteria stick. Scientific American, Jan., p. 86.

11. Dexter, S.C., J.D. Sullivan, J. Williams, and S.W. Watson. 1975. Influence of substrate (surface) wettability on the attachment of marine bacteria. Appl. Microb., 30.2, pp. 298-308.

12. Dexter, S.C. 1976. Influence of surface wettability on the formation of bacterial slime films on solid surfaces immersed in natural sea water. Proc. 4th Int'l. Cong. on Mar. Corr. and Fouling. Antibes, France.

13. EPRI. 1979. Biofilm development and destruction. Final Report. EPRI No. RP902-1. Proj. Director: Roger M. Jordan. EPRI - Palo Alto, Ca. Res. Dir.: W.G. Characklis.

14. Harremoes, P. 1977. Half order reactions in biofilm kinetics. Vatten, 2, pp. 122-143.

15. Jones, H.C., I.L. Roth, and W.M. Sanders. 1969. Electron microscipic study of a slime layer. J. Bacter., 99.1, pp. 316-325.

16. Kornegay, B.H. 1967. Characteristics and kinetics of biological fixed film reactors. Ph.d. dissertation, Clemson University, Clemson, S.C.

17. LaMotta, E.J. 1974. Evaluation of diffusional resistances in substrate utilization by biological films. Ph.D. dissertation, Univ. of No. Carolina at Chapel Hill.

18. Loeb G. and R. Neihoff. 1972. Molecular fouling of surfaces in seawater. Proc. 3rd Int'l. Cong. on Mar. Corrosion and Biofouling, Gaithersburg, Md.

19. Loeb, G. and R. Neihoff. 1973. Marine conditioning films. Adv. Chem. Ser., 145, p. 319.

20. Moody, L.F. 1944. Friction factor dependency on Reynolds number and pipe roughness. Trans. ASME, 66, p. 671.

21. Nimmons, M.J. 1979. Biofilm effects on heat transfer resistances within a turbulent flow system. M.S. Thesis, Rice University, Houston, Tx.

22. Norrman, G. 1976. Control of biofilms in circular tubes with chlorine. M.S. Thesis, Rice University, Houston, Tx.

23. Picoglou, B.; N. Zelver, and W.G. Characklis. 1979. Influence of biofilms on hydraulic deterioration in circular tubes. Submitted for publication, J. Hydraulics Div., ASCE.

24. Trulear, M. 1979. Dynamics of biofilm processes. Proc. 34th Annual Industrial Wastewater Trtmnt. Conf., Purdue University, Purdue, In.

25. Zelver, N. 1979. Biofilm development and associated energy losses in water conduits. M.S. Thesis, Rice University, Houston, Tx.

DISCUSSION

Question: ...OTEC...what is the relative (inaudible) between warm water and cold-water concentration.

W. Characklis: I don't know what the concentrations are of warm water and cold water. This work wasn't done for OTEC.

J. Edwards, inaudible question:

W. Characklis: The organic content is relatively low, 5 to 10% by weight.

Question: It's not done in sea water though?

W. Characklis: No, it is not.

Question: I'm a little confused between the results of the two papers where, as I understood, Brenda Little's samples ended up without a slime. And I gather that you do end up with slime, mostly water. Is there a disparity, or am I confused by the whole situation?

W. Characklis: We ended up with a slime; Brenda will have to tell you what she had. Under normal circumstances, we have maintained flow and have found a film that is predominantly water. Several of the micrographs that Brenda showed had quite a bit of polymer material on them, but it does not look the same after it has been dried; it looks very different under those conditions.

Question: Your curves show no lag phase and the R_f data show a lag phase, particularly in relation to the filling-in of the film with polymers rather than the laying down of micro-organisms in a thick mat. There is a change in the chemistry.

W. Characklis: R_f is, of course, a measure of heat transfer resistance, and there are data in my paper regarding the heat transfer resistance that we also measured with film. There is a lag in heat transfer resistance even though the biofilm thickness is increasing. There are a couple of possible reasons for this: in many of our experiments there was a decrease in heat-transfer resistance for a short period. And we hypothesize that it's due to the nature of these films. The film comprises filaments that grow quickly through the thermal boundary layer so that there is some increase in convective heat-transfer resistance when, in fact, the conductive heat-transfer resistance has gone up, and they counterbalance. And our sensitivity was not enough to do anything but give us a lag period. Now, in addition, metallurgy and chemistry are involved in your systems, which we did not have, because we used glass tubes to eliminate the corrosion processes from the biofouling processes. We did use aluminum alloy for heat-transfer experiments, but only for those experiments. I would also expect a lag period for your OTEC experiments because of the food availability. Probably the number and concentration of particles are much less than what we had in our system. But we have data in a report that is being prepared now that are compared with some of the data from OTEC and from HTRI in seawater, and the data compare very well.

ULTRASONIC DETECTION OF MICROBIAL SLIME FILMS

George Loeb* and Jacek Jarzynski†

Naval Research Laboratory
Washington, D.C. 20375

Abstract

The acoustic attenuation and speed of sound were measured in a microbial slime. An ultrasonic interferometer was used, with sample length of 0.094 cm, and measurements were made at frequencies near 10 MHz. The bacteria used were obtained from a Chesapeake Bay slime sample. The acoustic impedance of the microbial matter is found to be ~3% higher relative to seawater, and the attenuation coefficient is 1.3 cm^{-1} at 10 MHz. On the basis of this acoustic data, detection of slime fouling on the inside of seawater-filled heat exchanger tubing from the outside seems to be feasible with current techniques. Estimates are given for the amplitude of the ultrasonic echo from the slime-seawater interface, and the shift in the resonance of the tubing due to the fouling layer.

Introduction

The growth of microbial slime layers on heat exchanger surfaces exposed to seawater is a basic problem in the development of an Ocean Thermal Energy Conversion (OTEC) plant. The presence of such layers decreases heat transfer, and may also have an adverse effect on the pumping efficiency. Consequently, a significant effort has been directed toward detecting, measuring, and characterizing fouling layers. The layer material is believed to be mainly of biological origin, but may also contain chemical precipitates from seawater (scale), and/or corrosion product films. At present, characterization of the fouling layers is mostly done by micoscopic examination of samples taken from heat exchanger tubes. This involves removing sections of tubing from a test rig, and fixing of the layer in some way for further examination at a shore laboratory if electron microscopy is to be used. Optical microscopy is also useful, but microscopy is not suited to measurement of the physical properties of the fouling layers important to the heat transfer and hydrodynamic drag enhancement properties of these layers. It is herefore desirable to supplement microscopic examination by techniques which allow convenient on-site, in situ measurement of the layer properties of importance. As a prospective tool for such measurements, we are considering the application of ultrasonic techniques. The work reported here is part of a feasibility study aimed in particular at developing an ultrasonic method for on-site nondestructive measurements of the layer thickness.

The heat exchangers currently considered for a pilot OTEC plant are thin metallic tubes. The requirements for the ultrasonic method are that it should be capable of making direct measurements of fouling layers in the thickness range from 2 to 50 microns, while still in contact with seawater.

The aim of the first phase of our program was to determine the acoustic properties of the fouling layer material, and the results are presented in the next section. In Section 3 several ultrasonic methods for monitoring the layer thickness are described, and the performance of each method is predicted using our data for the relevant physical properties of the layer material.

Experimental Methods

Measurements of the acoustical properties were made for laboratory-grown slime films grown from slime collected on a titanium sample in the Chesapeake Bay. It is reasonable to assume that our data can be used to estimate the acoustical behavior of the slime to be found in the OTEC heat exchanger pipes. The choice of the method of measurement and instrument design was dictated by the fact that only small quantities of the microbial matter were available at a time.

The ultrasonic interferometer used to measure longitudinal sound velocity is shown in Fig. 1. It was designed specifically for use with samples available only in small quantities. Its sample chamber is a circular cavity of 0.794 cm radius and is 0.094 cm deep, formed by placing an annular spacer between two aluminum delay rods. The spacer

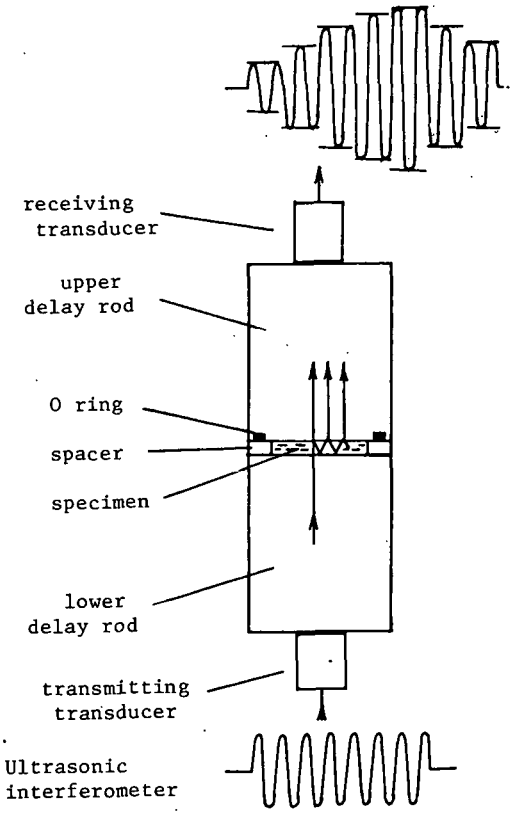

Fig. 1 Ultrasonic interferometer

*Marine Biology Branch, Ocean Sciences Division

†Physical Acoustic Branch, Acoustics Division

is cemented to the lower delay rod, and with an O-ring makes a seal with the upper delay rod (which is spring loaded to maintain firm contact with the spacer).

The electrical signal applied to the transmitting transducer is a gated sinusoidal oscillation (see Fig. 1). The duration of the signal is sufficiently long so that multiple reflections of the ultrasound occur within the specimen, but is short enough so that successive echoes in the delay rods do not overlap. If the signal frequency is adjusted so that the sample length L equals an integral number, n, of half-wavelengths of the ultrasound

$$L = n\,\frac{\lambda}{2} = \frac{n\,c}{2f} \qquad \text{----------(1)}$$

then the successive reflections within the sample are in phase and the received signal is as shown in Fig. 1. The frequency at which this in-phase (resonance) condition occurs can be determined very precisely if a lock-in amplifier is used in the receiving system. The application of a lock-in amplifier to determine resonance frequencies is described, for example, by Bolef and Miller[1]. Even when the resonance frequency is determined precisely, it follows from Eq. 1 that the accuracy with which the absolute value of the sound speed, c, can be determined is limited by the uncertainty in the value of L. Since L is small, the precision to which it can be determined is relatively low. However, as is explained in the next section, the quantity of interest for the present application is the ratio c/c_ℓ, where c_ℓ is the speed of sound in the medium (saline water) in which the fouling layer was grown. The value of c/c_ℓ can be determined quite accurately from the observed shift in resonance frequency when the microbial matter in the sample chamber is replaced by the medium. The length L remains constant (determined by the spacer between the delay rods) and therefore it follows from Eq. 1 that

$$\frac{c}{c_\ell} = \frac{f}{f_\ell} \qquad \text{----------} \qquad (2)$$

where f_ℓ is the corresponding (same value of n) resonance frequency when only the medium is in the sample chamber.

It is also possible to determine the attenuation of longitudinal sound in the sample by measuring the amplitude of the received signal. As shown in Fig. 1, at a resonance frequency the amplitude of the received signal increases by stepwise increments as successive echoes in the sample are superimposed in phase. It can be shown[1] that when k echoes in the sample combine in phase the amplitude of the resulting signal in the upper rod is,

$$p_k = \frac{(1 - y^k)}{1 - y}\, x p_o \qquad \text{----------} \qquad (3)$$

where: $y = (re^{-\alpha L})^2$

$x = t_{21} t_{12}\, e^{-\alpha L}$

r is the (pressure) reflection coefficient at the sample-delay rod interface, t_{21} and t_{12} are the delay rod-sample and sample-delay rod transmission coefficients respectively, p_o is the amplitude of the incident sound in the lower delay rod, and α is the sound attenuation coefficient in the sample. The reflection and transmission coefficients are determined from the densities (ρ, ρ_2) and sound velocities (c, c_2) in the sample and delay rods[2]

$$r = (\rho_2 c_2 - \rho c)/(\rho_2 c_2 + \rho c)$$

$$t_{12} = 2\rho_2 c_2/(\rho_2 c_2 + \rho c) \qquad \text{------} \qquad (4)$$

$$t_{21} = 2\rho c/(\rho_2 c_2 + \rho c)$$

Medium in equilibrium with slime samples used for these measurements was obtained by membrane filtration (Gelman, 0.2μm) of portions of the microbial culture.

Density of the slime material relative to the saline medium was determined by displacement in a specific gravity bottle. Thus, the mass of filtered medium required to fill a 25 ml specific gravity bottle (M_1) was compared with the mass of medium (M_2) required to fill the same bottle when it contains a mass M_s of slime. The ratio of slime density (ρ) to medium density (ρ_ℓ) is then given by

$$\frac{\rho}{\rho_\ell} = \frac{M_s}{M_1 - M_2} \qquad \text{----------} \qquad (5)$$

Measurements were made at frequencies in the vicinity of 10 MHz. This relatively high frequency range was chosen in order to observe a measurable change in amplitude due to attenuation in the sample. The signal pulse width was ~ 5 μsec, which is long enough to observe five reflections in the sample. Three successive resonance frequencies were determined, corresponding to n = 10, 11 and 12. Also the peak amplitude of the received signal was measured. This amplitude is the result of superposition of five echoes in the sample (k = 5 in eq. 3). The attenuation coefficient of the slime was determined relative to the filtered medium, for which the attenuation coefficient of water at 23°C and 10 MHz was assumed. This value is sufficiently close to those of saline waters that estimates of the effects of slimes are valid.

Results

The relative sound speed, relative density, and attenuation coefficient observed for the slime examined in this work are listed in Table 1.

Table 1 Measured values of sound speed and density relative to medium and of sound attenuation, for the microbial slime. The sound speed and attenuation measurements were made at frequencies near 10MHz.

Relative sound speed, c/c_ℓ	Relative density ρ/ρ_ℓ	Attenuation coefficient $\alpha(cm^{-1})$
1.011	1.02	1.3

Discussion

The data presented in the previous section was used to evaluate two possible ultrasonic techniques for monitoring the growth of slime layers, and the results are reported in this section.

The most direct method (illustrated in Fig. 2) for detecting and monitoring the thickness of the fouling layer would be to measure the amplitude

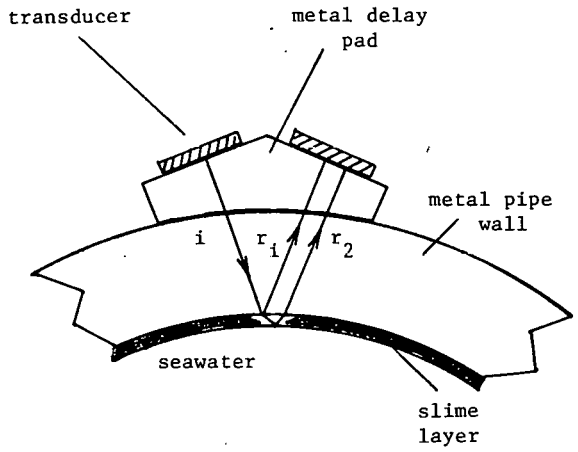

Fig. 2 Detection of layer by direct reflection from layer-seawater interface

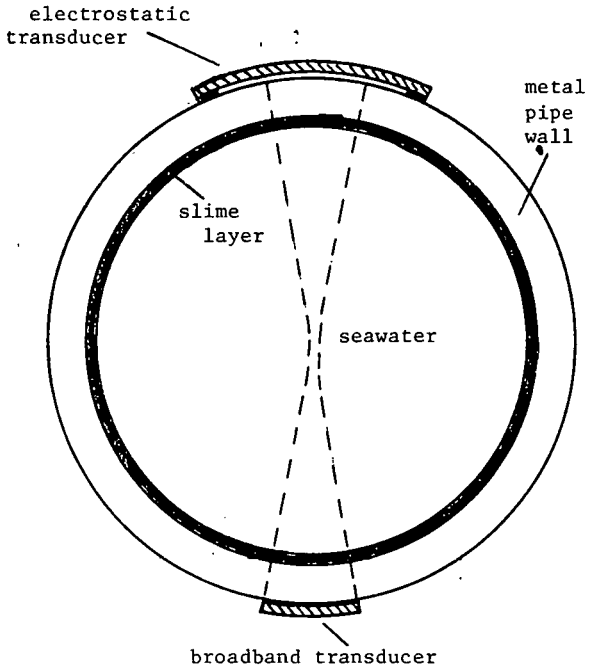

Fig. 3 Detection of layer by measuring the resonance frequency of the metal tube

and time-of-flight of ultrasonic echoes from the slime-medium interface. There are two potential problems in applying this method in practice, and these are due to the fact that the fouling layer is thin, and the ultrasonic echo from the layer-medium interface is weak. Using the data in Table 1 the calculated return time of flight for longitudinal waves through a fouling layer 10μm thick is ~ 0.013μsec. This time of flight corresponds to λ/10 at 10 MHz or λ/3 at 30 MHz, where λ is the ultrasonic wavelength. A shift of λ/10 in the return echo is about the smallest which can be measured using standard ultrasonic equipment.

To calculate the amplitudes of the echoes from the metal-slime and slime-liquid interfaces the expressions (Eq. 4) for the reflection and transmission coefficients are used together with the data in Table 1. Values for the acoustic impedance of aluminum, titanium, and steel, taken from Kaye and Laby[3] are 1.72×10^6, 2.76×10^6 and 4.71×10^6 cgs units respectively. The results are presented in Table 2. It can be seen that the echo from the layer-liquid interface will be between 47 and 55 dB down relative to the echo from the metal-layer interface. This difference in echo levels is due to the large impedance mismatch between the metal and the layer, and the relatively close impedance match between the layer and medium. In principle it should be possible to detect the weak signal from the layer-liquid interface, since broadband receivers are available with gains up to 120 dB. In practice, however, this will require special signal processing because the weak signal from the slime-liquid interface is superposed on the much stronger signal from the metal slime interface. One possible approach would be to use, as reference, a short piece of identical metal tubing filled with seawater and cleaned periodically to prevent slime growth. The ultrasonic echo from the metal-seawater interface in this reference pipe could be used to cancel the strong echo from the metal-slime interface in the heat exchanger pipe.

The echo amplitudes in Table 2 were calculated for normal incidence of the ultrasound. In practice it may be better to let the ultrasound be incident at an angle, as shown in Fig. 2. The advantage of this arrangement is that separate transducers are used to generate and receive the ultrasonic signals, which avoids initial overload of the receiving electronics by the strong signal from the transmitter.

Table 2 Calculated values of the relative amplitudes (see Fig. 2) of ultrasonic echoes from the metal-slime and slime-seawater interfaces respectively.

Metal	r_1/i	r_2/i
Aluminum	0.837	4.6×10^{-3}
Titanium	0.895	3.1×10^{-3}
Stainless steel	0.937	1.9×10^{-3}

A second possible technique for detecting the slime layer is to monitor the resonance frequency of the metal pipe. The experimental arrangement is shown in Fig. 3. A broadband transducer is used to insonify a diametrically opposite region of the pipe, and a second transducer is used to monitor the amplitude of vibrations at the outside surface of the insonified metal. It may be advantageous to use a transducer which does not load the

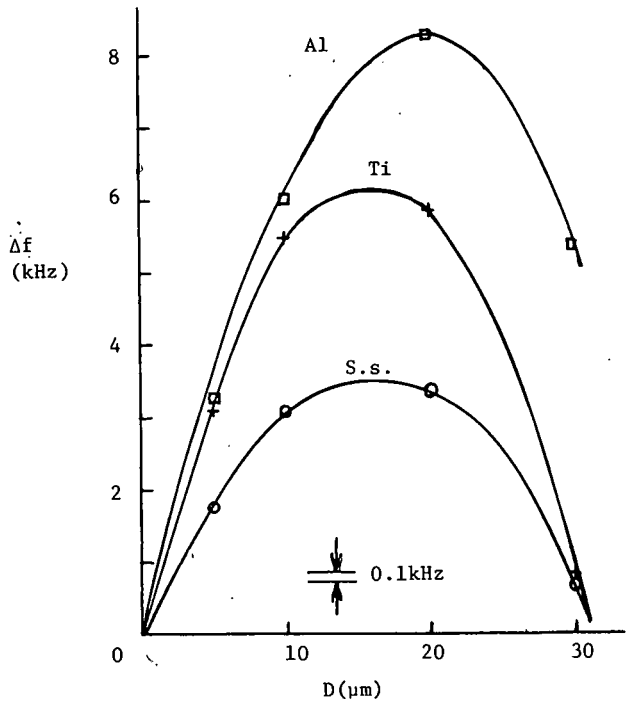

Fig. 4 The shift in resonance frequency as a function of layer thickness

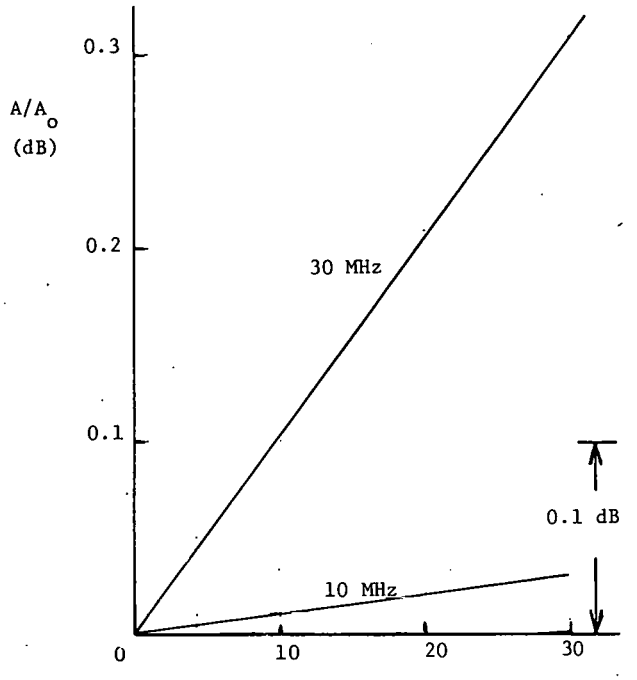

Fig. 5 The relative signal amplitude, at resonance, as a function of layer thickness

vibrating metal, and a contactless electrostatic transducer is one possible choice. The experimental procedure is to vary the frequency of the incident ultrasound until a (resonance) peak is observed in the amplitude of vibration of the insonified metal. The amplitude of vibration and resonance frequency are measured.

When a slime film develops on the metal surface its effect will be to shift the resonance frequency and decrease the amplitude of vibration. Both these changes were calculated, using the data in Table 1, as follows. The slime and metal were treated as a two layer system, in contact with seawater on one side and air on the other side. An expression was derived, using the theory of sound propagation through multiple layers (Brekhovskikh[4]), for the amplitude of vibration at the outside surface of the metal as a function of the amplitude and frequency of the ultrasound incident on the seawater-slime interface. The changes in resonance frequency and amplitude of vibration as a function of the thickness D of the slime layer were found to be

$$A/A_o = 1 - \alpha D \qquad (6)$$

$$\Delta f/f_o = \frac{2\rho_\ell c_\ell}{\pi \rho_2 c_2} \sin\left(\frac{2\pi f D}{c}\right) \cos\left(\frac{2\pi f D}{c}\right) \left(\frac{\rho c}{\rho_\ell c_\ell} - 1\right) \qquad (7)$$

where f_o and A_o are the resonance frequency and signal amplitude for the metal without a slime layer, while f ($= f_o + \Delta f$) and A are the corresponding values with the slime. The ultrasound attenuation coefficient in the slime is α, and c_ℓ, c and c_2 are the sound velocities in seawater, slime and the metal respectively, whilst ρ_ℓ, ρ and ρ_2 are the corresponding densities.

Calculations were made for the following metal tubes at their resonance frequencies near 10 MHz - aluminum (0.065 inches thick, f_o=9.652 MHz), titanium (0.03 inch, f_o=12.099 MHz), and stainless steel (0.03 inch, f_o=11.803 MHz). The calculated Δf and A/A_o vs. slime thickness are shown in Fig. 4 and the lower line of Fig. 5. A similar treatment may be made near 30 MHz. Assuming α increases as f^2, α=11.7 cm^{-1} at 30 MHz, and the upper curve of Fig. 5 shows the effect of this increased attenuation.

Conclusions

When evaluating the significance of the above results it should be noted that resonance frequencies can be measured to within 100 Hz or better using the lock-in amplifier technique described in Ref. 1, whilst relative changes in amplitude can be measured to within 0.1 dB. Therefore, it follows from Fig. 4 that the shift in resonance frequency can be used to determine the presence of a slime layer. However, Δf is not proportional to the thickness D of the layer. Rather, it follows from Eq. 7 that Δf = maximum when D = $\lambda/8$, $3\lambda/8$,..and Δf=0 when D = $\lambda/4$, $\lambda/2$,.... Also, a shift in resonance frequency can be produced by changes in ambient temperature. The effect of temperature change was estimated using the values for temperature coefficients of the elastic constants of metals given in Ref. 3. For a temperature change of 0.1°C, and for resonance frequencies near 10 MHz, the estimated frequency shift is largest for aluminum, $\Delta f \approx 90$ Hz, and smallest for steel, $\Delta f \approx 60$ Hz. In practice it may be necessary to monitor the temperature of the heat exchanger pipe and subtract the effect of temperature changes from the measured Δf.

The relative decrease in amplitude A/A_0 is proportional to D, and at a higher frequency, such as 30 MHz, this effect could also be used to monitor the slime layer, at thicknesses greater than 10 microns.

In conclusion it can be said that the shift in resonance frequency would seem to be a feasible method for monitoring slime growth at the beginning of the fouling process. The amplitude of the signal would be valuable at later stages, and as an indication of the pertinent cycle of the frequency curve at a given time. Finally, it should be noted that both methods described in the previous section are non-invasive. Therefore, the heat exchanger need not be opened for measurement, as both the transmitting and receiving transducers are attached to the pipe from the outside.

References

1. D.I. Bolef and J.G. Miller in Physical Acoustics, Vol. 8, edited by W.P. Mason and R.N. Thurston (Academic Press, New York, 1971).

2. L.E. Kinsler and P. Frey, Fundamentals of Acoustics, (Wiley, New York, 1962).

3. G.W.C. Kaye and T.H. Laby, Tables of Physical and Chemical Constants, 14th edition, (Longman, London, 1973).

4. L.M. Brekhovskikh, Waves in Layered Media, (Academic, New York, 1960).

DISCUSSION

W. Avery, APL: If you have an outside layer as well as slime, will you be able to distinguish the two?

G. Loeb: We would have a composite signal, but we have not analyzed it. It certainly is a point of interest, but we have not done that calculation. We know that we can detect an oxide layer by itself, and we know we can detect the slime layer by itself. However, we have not thoroughly analyzed the interaction between the two. Obviously it's something that should be done.

W. Avery: You probably could use a couple of frequencies...

G. Loeb: That's a point for further investigation.

R. Mitchell, Harvard: It would be extremely useful if we could use ultrasonic detection for nondestructive measurement of microbial films, particularly in relation to cleaning. If I understood your past slide correctly — what you're saying is that a frequency of less than 30 MHz is not really useful for measuring very thin film.

G. Loeb: Well, not in terms of the amplitude. But you can still see it in terms of the frequency.

Question: Can you tell anything about the chemistry, the density? How much more can you tell than film thickness?

G. Loeb: We hope to be able to measure the elastic moduli. I think the elastic moduli are going to be very important in determining such things as pressure drops and pumping power requirements. As far as density is concerned, we have not analyzed it sufficiently to be able to determine clearly whether we can disentangle density from thickness. One would have to use a few frequencies, perhaps.

Question (inaudible):

G. Loeb: The question was, would we expect to get different responses, say, from polysaccharide than from protein? One can hope, but we can't say.

J. Lorenz, ANL: You have plans relating to the thickness.....

G. Loeb: Well, that was really the motivation. One has satisfactory thickness measurement. The question is how to relate this to another parameter, which one understands, that would allow one to understand better the decay in the heat-transfer coefficient. More experimentation is required to answer that question. We can not yet make a quantitative correlation, but we hope that we will be able to.

DESIGN FOR AN OTEC SEACOAST TEST FACILITY AT KE-AHOLE POINT, KONA, HAWAII

W. Grantz and J. Belvedere

Parsons Brinckerhoff Quade & Douglas, Inc.
Honolulu, Hawaii 96813

L. Hallanger*, E. Noda+ and H. White≠

Research Corporation of the University of Hawaii
Honolulu, Hawaii 96826

Abstract

This paper provides a comprehensive look at the proposed OTEC Seacoast Test Facility which is to be located at Ke-ahole Pt. on the Island of Hawaii and planned for construction late this year. The paper explains the advantages of a land-based facility and includes a description of all the major features of the project. Also covered are the more unusual construction problems that are presented by this project, in particular the design, fabrication and deployment of the cold water intake pipeline which is to reach a depth of 2100 ft.

Introduction

Ever since the Ocean Thermal Energy utilization began to receive serious consideration, the development of a shore-based test facility has been a very attractive concept. Such a facility was first tried in 1930 by Claude/Bouchardt at a location near Havana, Cuba. While this first attempt failed due to the lack of technology at the time, and has not been repeated since, the principle was sound: To identify a location where large depths are available near shore (due to steep bottom slopes) and where the water at depth has an acceptable temperature differential from the surface water. Ke-ahole Pt. near Kona on the Island of Hawaii has been determined to be such a location. In fact, conditions in this area are so attractive that the area has become the focus for the first three OTEC test programs being undertaken by the Department of Energy and various industrial firms. OTEC-1, a test facility constructed on a converted tanker with a deep water intake pipeline, is to be located 18 miles northwest of Ke-ahole Pt. Mini-OTEC, a moored barge test facility also with a deep water intake, is to be located offshore from Ke-ahole Pt., and the OTEC Seacoast Test Facility (STF) which is the subject of this paper.[1,2] The important differences which should be noted regarding the STF are that, unlike the other two programs, it is land-based and designed to be a long term research facility.

A land based facility has many important practical advantages. Access and comfort of personnel, ease in delivery of units to be tested, flexibility and room for expansion of test areas and supporting laboratories, are but a few. The STF being designed at Ke-ahole Pt. will permit continuous testing and operation under heavy storm conditions. All in all it is felt that the Seacoast Test Facility proposed at Ke-ahole Pt. on the Island of Hawaii will provide an ideal environment for the studies needed to evaluate OTEC equipment components and power cycle configurations.

The challenge of this project focuses mainly on the underwater pipeline systems for warm and cold water supply and discharge. In particular the cold water intake pipeline poses the most difficult engineering problems. Engineering studies and estimated construction costs for traditional concrete coated steel pipes of the type presently used in the offshore oil fields and the state-of-the-art for their deployment, particularly along the 30 to 40 degree ocean bottom slope that exists at Ke-ahole Pt., indicated that the costs of installation to depths of 2000 ft. or more would be prohibitive.

Background

Investigations of ocean thermal resources were initiated in Hawaii as early as 1971. In 1974 the Hawaii State Legislature enacted a bill which created the Natural Energy Laboratory of Hawaii (NELH) and dedicated a 320 acre site at Ke-ahole Pt. for further development of the NELH facility. A major element of the NELH ocean thermal resources development program is the design and construction of the OTEC Seacoast Test Facility.

On June 15, 1978 the Research Corporation of the University of Hawaii (RCUH) submitted to the Argonne National Laboratory (ANL) a comprehensive two-volume design and construction proposal for the

---

* Project Manager, OTEC Seacoast Test Facility

+ University of Hawaii, Project Manager

≠ Natural Energy Laboratory of Hawaii, Operations Manager

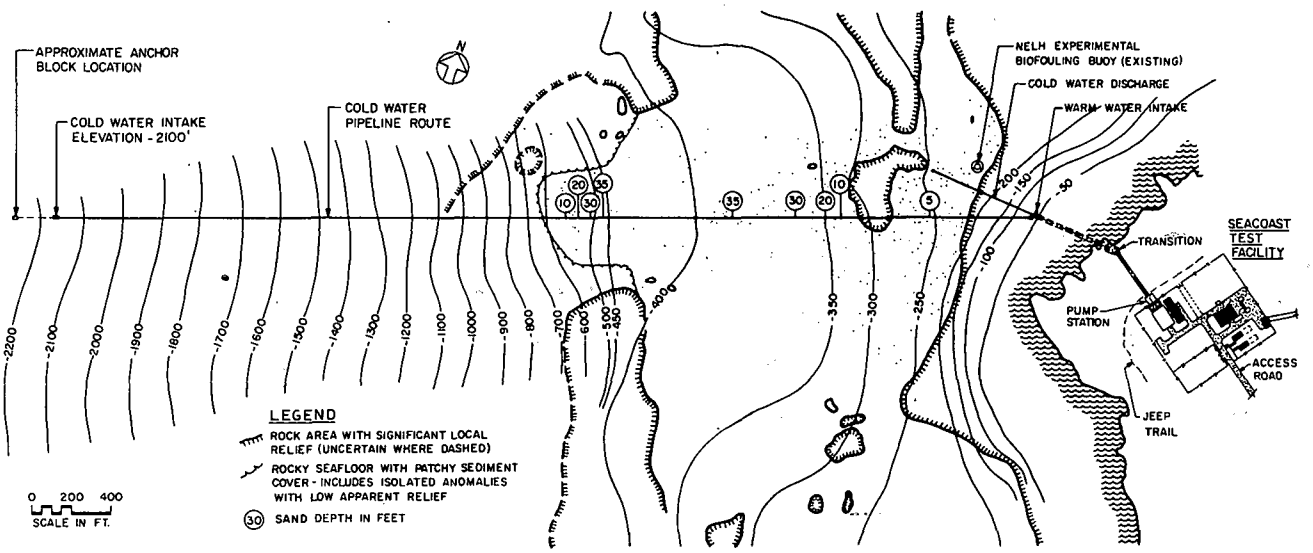

Fig. 1 General Plan of Seacoast Test Facility at Ke-ahole Pt.

OTEC-STF. Included in the proposal was the RCUH's conceptual design for the onshore and offshore facilities of the Project. The offshore facilities include: cold water intake and discharge pipelines; warm water intake and discharge pipelines; a pumping station; and constant head tanks and a test pad which are located onshore but, due to their relationship to the pipelines and pump station, are included as components of the offshore facilities. The onshore facilities consist of conventional elements of any test facility and include laboratories, a warehouse, offices, utilities and other support facilities.

The RCUH and Makai Ocean Engineering developed the original conceptual design and construction report submitted to ANL. Based upon this report, ANL contracted with the RCUH to design and construct the proposed facility. The RCUH in turn selected the consulting engineering firm of Parsons Brinckerhoff Quade & Douglas, Inc. to provide A/E services for the design and construction supervision of this facility. Since that time Parsons Brinckerhoff has, with the assistance Makai Ocean Engineering, Dames and Moore and several other Honolulu-based subconsultants developed a revised conceptual design and is presently preparing construction bid documents for the construction of the Onshore and Offshore Seacoast Test Facilities.

Site Description

Ke-ahole Pt. is situated on the western coastline of the Island of Hawaii (also known as the "Big Island"). Located in the district of North Kona, Ke-ahole Pt. is approximately nine miles north of the town of Kailua-Kona and 23 miles south of the deepwater port of Kawaihae. The Kailua area is the major population center on the west side of the island.

The general topography of the Ke-ahole Pt. area is relatively level with an average elevation of approximately twenty feet. The shoreline is characterized by a five to ten foot cliff which drops into the ocean to a depth of ten to twenty feet. The land surface at the site is an uneroded lava flow with numerous crevices and lava tubes. The geological formation of the project site was developed by the progressive layering of cinders and pahoehoe lava flows from the volcano Hualalai.

The ocean environmental conditions at Ke-ahole Pt. are excellent for the proposed facility. The area is sheltered from the prevailing trade winds and, although severe storms can occur and must be considered in the design, normal day-to-day wave activity is quite mild. The ocean bottom contours are very steep and therefore only about a mile of cold water intake pipeline is required to reach the required water depth of 2100 ft.

Bathymetric and seismic surveys were conducted to determine the bottom topography. In the deep water, instrument resolution was not sufficient to depict surficial features less than fifty feet in height. For this reason three dives have been made in a submersible down to depths of approximately 1400 ft. to make visual reconnaissance along the proposed pipeline path.[3] These observations and surveys have revealed the following general topography (see Fig. 1).

A 250-foot wide nearshore shelf extends seaward from the shoreline to a distinct shelf break occurring in 45 to 50 feet of water. Below the shelf break is a near shore slope with an average dip of between 25 to 30 degrees which consists of basalt bedrock. The upper slope is covered by a section of live corals overlying thin coralline debris; the lower parts of the slope are largely exposed basalt bedrock

with shallow pockets of coralline sands and debris.[4]

The bottom of the nearshore slope ends abruptly at about 200 feet below sea level at a distance of about 600 to 700 feet from the coastline along the proposed route. Seaward of the nearshore slope is a relatively flat sandy shelf about 1,700 to 1,800 feet wide which descends to approximately 450 feet below sea level. Emerging from the unconsolidated sediments of this mid-depth shelf are a number of rock outcrops. A tongue of sediment extends seaward at the offshore edge of the mid-depth shelf in the area surveyed and provides a relatively smooth transition zone to the deeper slope.[4]

The deep slope is concave with steeper overall slopes of about 35 degrees in the upper zone, above the approximate 1,200-foot depth, and gentler average slopes of about 28 degrees below the 1,200-foot depth. Nearly vertical relief features have been observed on the upper zone of this slope that may drop precipitously as much as 40 feet. The lower part of that slope has not been observed from the submersible and features of this scale are not resolved in these water depths and steep slopes from high-resolution profiling from the sea surface. Since the same geological process that formed the shallower areas are assumed to have been at work in the deeper area, it is prudent to assume that local relief features of similar magnitude occur at all depths.[4]

Design Criteria

The following briefly summarizes the basic parameters which are being used for the design of the facility:

- System Design Life to be ten years minimum.

- Intake Depths: Warm Water 50 feet
  Cold Water 2100 feet

- Minimum Intake and Discharge Flows:
  Warm Water 9600 gpm
  Cold Water 6400 gpm

- Uninterrupted flow for both warm and cold water (up to 50 percent reduction from full rated flow is permissible).

- Cold water temperature rise (from 2100 ft. depth to shore) not to exceed 1°C.

- Provision shall be made for degassing the cold water intake ahead of the pumps.

- Screening to permit uninterrupted flow at both intakes.

- Pipeline materials to be biologically inert and not introduced corrosion product contamination.

- Cold water must be discharged at a depth of not less than 180 ft.

- Design shall include provisions for pipeline cleaning.

- Pipeline protection in active surf zone and onshore for 100 year deisgn storm waves.

- Ocean Waves: A significant wave height of 30 ft. with a period of 11.64 seconds was determined for a 100 year storm frequency at Ke-ahole Pt. by Bretschneider and Rocheleau.[5]

- Currents: Based on data collected and prepared by RCUH and current profile developed for OTEC-1 by Bretschneider.[6]

Offshore Facilities

Nearshore Overview

The purpose of the facility is to test OTEC components on a laboratory scale, under realistic operating conditions and using the actual ocean thermal resources of warm surface waters and the deep cold waters. The offshore pipelines will deliver these waters to constant head tanks located adjacent to a laboratory building and an open concrete slab test area. Experiments which are weather or temperature sensitive will be conducted within the airconditioned laboratory space while other weather insensitive or large experiments will utilize equipment mounted outdoors on the test pad.

As shown in Fig. 4 the pumping station, to be constructed adjacent to the constant head tanks, will continuously deliver the full rated flows to the tanks. In this way the desired temperature differential between warm and cold water can be maintained as constant as possible. Excess warm and cold water will be discharged back to the ocean.

High molecular weight polyethylene pipe has been selected for the cold and warm water intake pipelines. This material has three properties that are all basic to this project. The material, unlike metal pipes, does not contaminate the water with metal ions. This is important for biofouling experiments which will be conducted under controlled conditions. The polyethylene is a sufficiently good insulator to keep the cold water from exceeding the allowable temperature rise in the distance from the intake to the header tanks. Finally, the polyethylene is less dense than the seawater and therefore floats.

Between the shoreline and the pumping station the cold and warm water intake and discharge pipelines will be placed in a trench to protect them from storm waves in the surf zone. At the shoreline transition the two intake pipelines and the cold water discharge pipeline will turn downward to an elevation below the ocean bottom. Degassing equipment will be provided in the

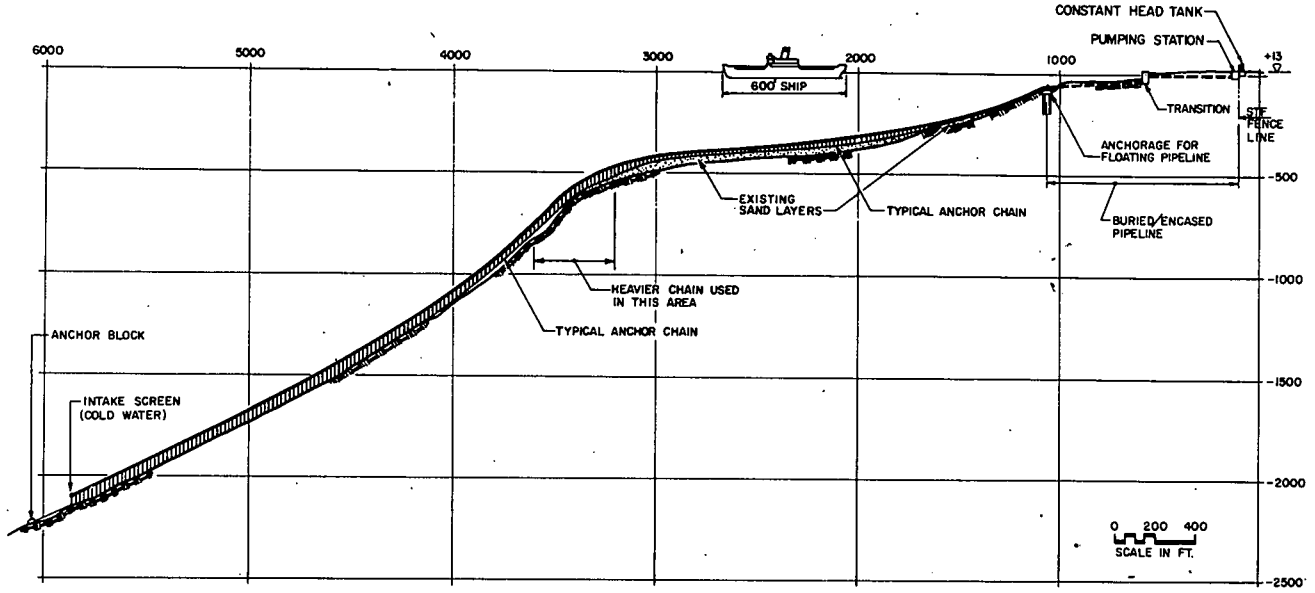

Fig. 2 Profile of Offshore Facilities

transition. Dissolved gas, primarily nitrogen, will be released from the cold water due to the reduced hydrostatic pressure and increased temperature which occur as the water travels up from the depth of the intake.

The warm water discharges directly into the surface waters at the shoreline. The cold water discharge line is carried 1000 ft. offshore to a depth where the higher density of the cold water permits it to run downhill away from the warm water intake. The warm water intake is set at a depth of 50 ft., somewhat above the ocean bottom to avoid sediments from being sucked into it. The cold water intake and discharge lines and the warm water intake line are placed in a trench and encased in tremie (concrete placed under water). The reason for the concrete encasement of these pipes is protection against the design storm waves which can have a peak value of over 50 ft. Such waves start to break at a depth of 70 ft. and consequently the shelf between the depths of 20 and 60 ft. will be subjected to severe surf conditions. It was decided that attempts to anchor these pipes to the bottom by yokes or straps would not be reliable or practical.

Cold Water Intake Pipeline

Pipeline Design

The most difficult and challenging aspect of this Seacoast Test Facility has been the development of the cold water intake pipeline design. Because of limitations on funding, the mobilization and use of state-of-the-art petroleum industry pipelaying equipment (often costing in the $100 million range) was judged prohibitive in cost. Since a polyethylene pipeline can not lay exposed on the rugged ocean floor, consideration was given to using a concrete-encased steel pipe pulled out from shore. Once the steel pipe was deployed, a polyethylene pipeline would be inserted inside the steel pipe. Although the pulling of such pipes is common practice in the oil industry, this method of deploying the cold water intake pipeline did not appear to be feasible due to the abrupt change in the ocean bottom slope beyond the 500 ft. depth.

Considering the irregular ocean bottom and the abrupt changes in ocean bottom slopes, various configurations of a floating polyethylene pipeline were studied. Based upon these studies the final design configuration selected involves the use of a polyethylene pipeline tethered to a heavy pretensioned anchor chain (see Fig. 2).

Under this pretensioning the anchor chain will lay on the ocean bottom along the upper flat slopes while in the steep area the chain will tend to span irregular surface features. In this way the length of anchor chain and the spacing of the tethers can be established with sufficient accuracy. The lower portion of the tethers will be protected from abrasion by a length of chain (see Fig. 3). The weight of this tether chain will be neutralized by a syntactic float. The length of the tethers will be selected to avoid possible contact of the floating pipeline with rock outcrops and protuberances. The main anchor chain will be attached to a special anchorage located at a depth of about 70 feet.

Fabrication and Deployment

The selection of the fabrication site will be dictated by such factors as sea conditions and protection, topography, and access to the ocean. Kawaihae harbor could be used, or land near the Seacoast Test Facility itself. The size of the fabrication yard should be sufficient to

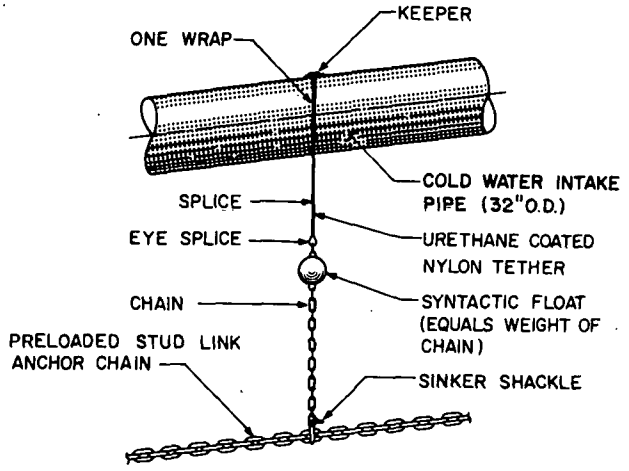

Fig. 3 Tether Detail

permit the assembly and launching of about 1,000 foot long section of pipeline. Each 1,000 foot section involves welding 25 joints of polyethylene pipe, 12 chain connections and the assembly of 50 tethers.

Once all the 1,000 foot sections are fabricated, and the project site and equipment are ready for the deep pipeline deployment, each section would be launched closed-ended with the anchor chain and tethers secured to the side of the polyethylene pipe. Each section would be towed to its assigned mooring area and, once secured, the tethers and chain would be deployed below the pipe. The anchor chain could be used for securing the pipeline at its mooring area by attaching it to mooring buoys previously anchored.

When all the sections are prepared, assembly of the entire pipeline would proceed by lining up sections and successively bolting the pipe flanges together and connecting the chains while holding the mating ends at a barge. During this operation, one end of the pipeline is moored while the other is under tow. When the entire length of the pipeline is connected together it is towed to the site.

Several possible deployment systems were studied to accomplish the desired alignment and preloaded pipeline configuration. Of these, two basic schemes emerged:

1. Deployment Seaward. In this scheme the anchor chain is first connected at the underwater anchorage. The pipeline anchor chain assembly is pulled into alignment and attached to an anchor block supported on a derrick barge on the seaward end. A long tow line is also attached to the anchor block and pulled by a tug. The anchor block is lowered as the pipeline is progressively flooded first with fresh water and then with salt water to increase its negative bouyancy. In this way the pipeline lays down on the bottom slope in a gentle, controlled manner and the anchor chain retains the preload force introduced by the tug pulling outward on the whole system (see Fig. 4).

2. Deployment Shoreward. In this method the pipeline is connected to a shore winch by a cable attached to the anchor chain. The deep anchor block is lowered to the bottom in its plan location taking the intake end of the pipeline with it. The pipeline and anchor chain/tethers assembly is controlled during the sinking operation by feeding it over a chute installed on a barge. As the pipeline is placed, the barge moves toward shore while maintaining tension in the system. Once the major part of the pipeline is deployed in this way, friction along the bottom will prevent loss of the preload when the force in the shore end is relaxed to permit final adjustment and attachment to the anchorage at the 70 ft. depth. An important consideration is the fact that in this system the total length would have to be adjusted at the end of the operation by either adding or removing fabricated sections of pipeline and chain. The amount of adjustment could be substantial depending on the accuracy used in placing and locating the deep anchor block (see Fig. 6).

It is likely, in the end analysis, that the construction contractor will propose a modification to one of the two basic deployment systems described above which will best suit his equipment and capabilities. Both these systems can be accomplished with conventional marine construction equipment and do not require the expensive pipelaying rigs used in the petroleum industry.

Pumping Station

An important aspect of the Seacoast Test Facility was the selection of the most suitable pumping station design. A number of different arrangements were studied including a submerged pumping station in 50 ft. of water; various combinations of submersible pumps placed in sumps at the site's shorebreak inlet area; centrifugal pumps placed in a pumping station located at the shorebreak inlet area; and centrifugal pumps on shore placed in a pumping station located near the constant head tanks. It was decided that the best compromize of cost and functionality would be the last arrangement with the pumping station on shore using centrifugal pumps. The low cost of the centrifugal pumps, their conventional, off-the-shelf design and the accessibility of the station during nearly all weather conditions were all deciding factors for selection of this alternative.

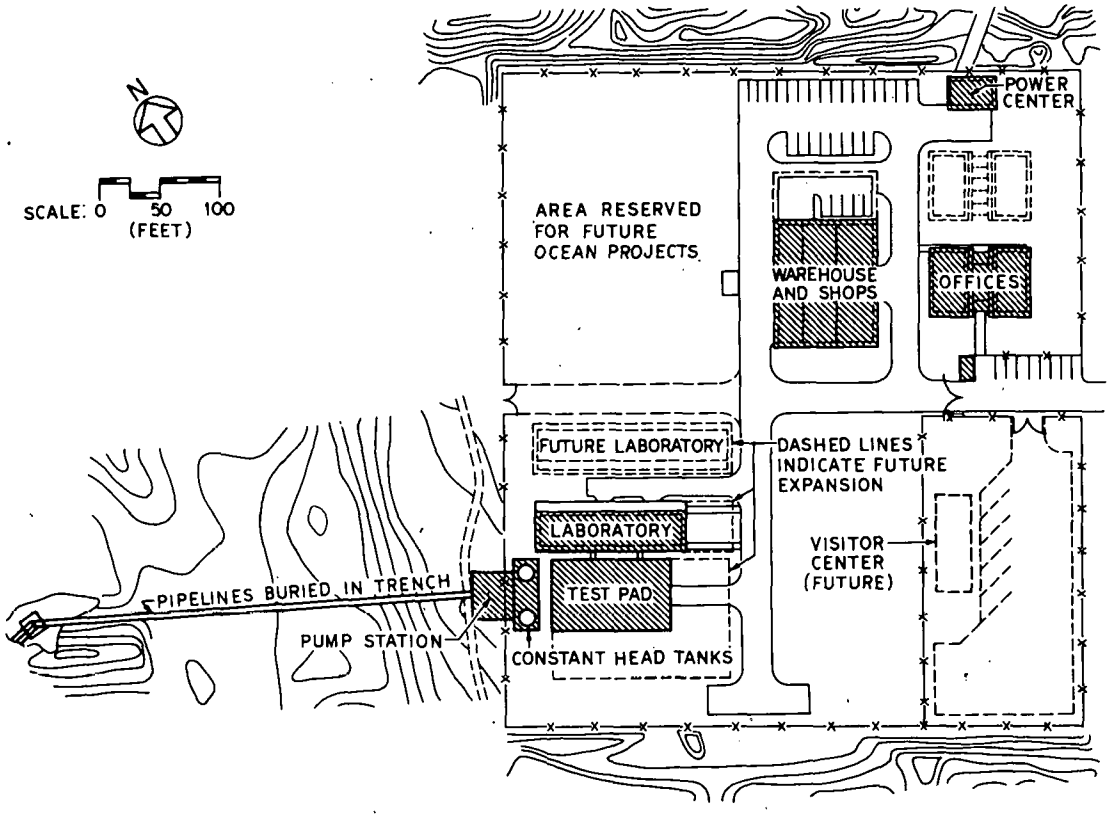

Fig. 4 Plan of Onshore Facilities

The selected pumping station alternative will provide the design flow rates using seven 50 HP centrifugal pumps. Four warm water pumps will deliver a total flow of 10000 gpm and three cold water pumps will deliver 7500 gpm. The pumps are interchangeable and were selected to provide for anticipated capacity loss due to subsequent wear. Should two warm water pumps or one cold water pump become inoperative, there is sufficient redundancy in the system to maintain reduced flow to the experiments within acceptable limits.

Degassing of the cold water will occur at the transition and at the pumping station. By maintaining a net positive suction head on the cold water intake pipeline cavitation of the pumps is avoided and automatic priming is assisted.

Constant Head Tanks

The system design includes two constant head tanks - one for the warm water supply and one for the cold water. The tanks will be sized so that, at full flow conditions, a changeover rate of 1.5 minutes and 2.2 minutes for the warm and cold water supplies respectively will be maintained.

In addition to supplying water to the test facility at a constant head of 22 feet, each tank will also be equipped with approximately 120 square feet of screening media. The screens will be designed so that they can be manually removed and cleaned without disrupting flow to the test facility. Additionally, each tank will be designed with a bypass so that full flow can be maintained to the test facility while the tank is being cleaned.

Onshore Facilities

The siting of the Onshore laboratories and support buildings evolved from two basic criteria. The arrangement had to be operationally efficient from the point of view of the OTEC program, not only the Seacoast Test Facility presently planned but also potential future OTEC programs as well. In addition the buildings had to be arranged to provide a nucleus for the Natural Energy Laboratory of Hawaii and its programs. These programs include a future aquaculture laboratory and solar experiments. The NELH also may prove to be an important visitor attraction for the area in consideration of the promise OTEC brings to the now critical energy field. Consequently, although construction funding is limited, the appearance of the structures and the area landscaping are also important considerations. The style of the individual building arrangement will be in keeping with the ideal climate of the area. Open passengerways and lanais will provide the pleasant ambience one comes to expect in Hawaii (see Fig. 4).

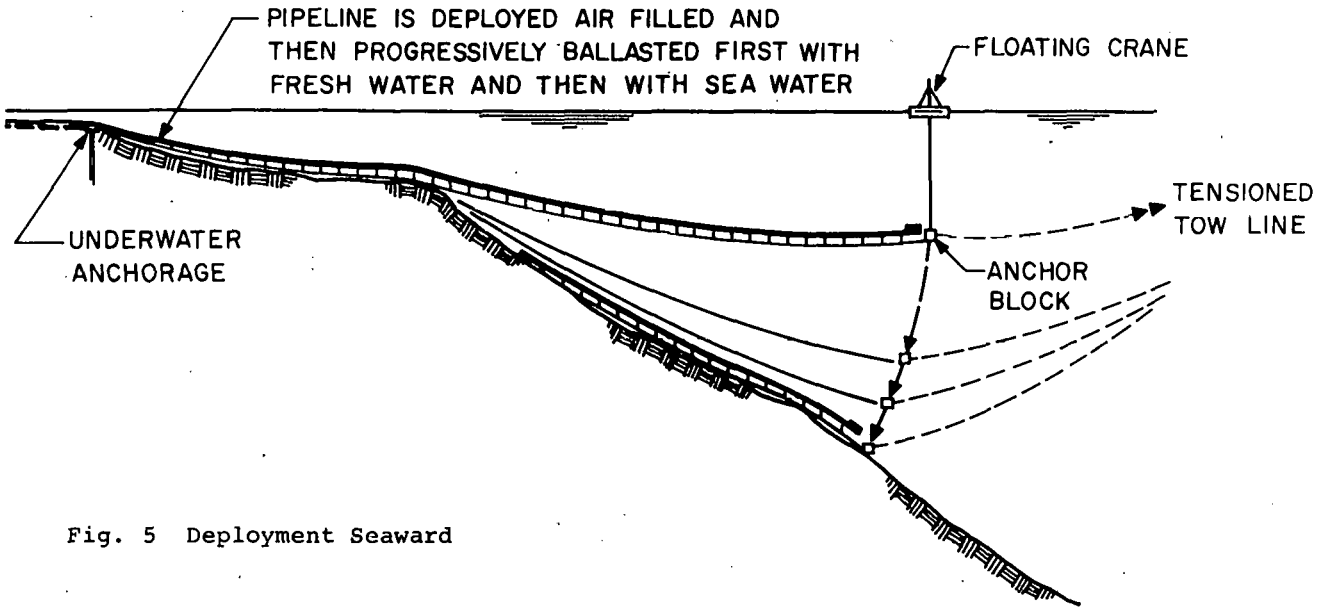

Fig. 5 Deployment Seaward

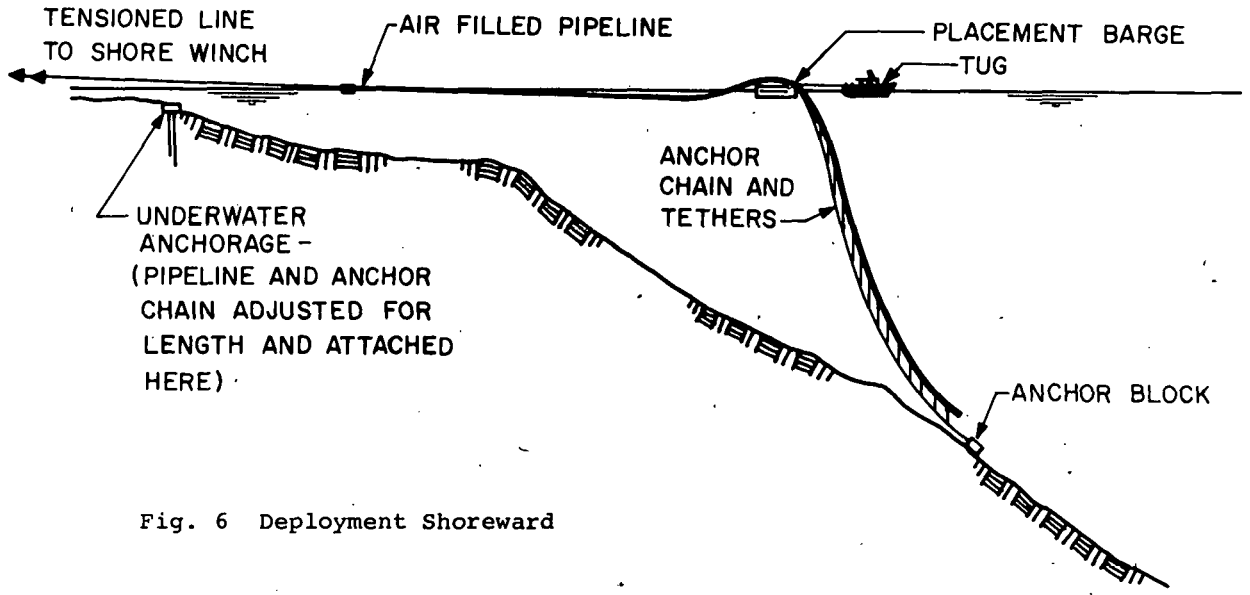

Fig. 6 Deployment Shoreward

Final Comments on the OTEC Testing Program

When completed the Seacoast Test Facility will become a center for investigation of biofouling and corrosion problems that may affect OTEC Systems. Early investigations will emphasize research into the effectiveness and applicability of various heat exchanger tube cleaning systems along with both short and long term biofouling and corrosion tests using a variety of potential OTEC heat exchanger materials and configurations. During its 10 year design life many, if not most, of the biofouling and corrosion questions on the component level pertaining to the technical and economic viability of OTEC Systems will be answered by the work done at the STF.

References

1. OTEC-1, Global Marine Development Inc.'s conversion of U.S. Navy Tanker Chepachet to OTEC test platform for one-megawatt pilot generator.

2. Mini-OTEC, Lockheed Missiles and Space Co. and Dillingham Corporation's outfitting of a U.S. Navy barge for an OTEC test platform for a 50-kW generator.

3. Star II Submersible, owned by the University of Hawaii and leased to Maui Divers of Hawaii Ltd.

4. Dames and Moore, "Bathymetric and Marine Geological Surveys-Proposed OTEC Pipeline Route Offshore Ke-ahole Point, Island of Hawaii for Parsons Brinckerhoff Quade and Douglas", January 1979 pg. 2-3.

5. Charles L. Bretscheider and Richard E. Rocheleau, "An Evaluation of Extreme Wave Climate at Ke-ahole Point, Hawaii", undated, no pagination.

6. Charles L. Bretscheider "Design Wave and Current Criteria for Potential OTEC Sites" (1977) and OTEC 1 RFP, Enclosure A," OTEC-1 Site Environmental Profile.

DISCUSSION

Question: Will this particular seawater intake correspond to a cold-water input or a warm-water input in terms of the OTEC facility?

L. Hallanger: We will have both. The warm-water input is from 400-600 ft offshore; the water is near oceanic quality at that location. The cold-water intake at the 2100 ft-depth is over 5000 ft offshore. We will be able to use either one or both if desired.

Question: What is your completion date?

L. Hallanger: That depends on when DOE funds the construction; approximately one year after the full construction is initiated. It could be September '80.

Question: What is the cost for the offshore pipeline?

L. Hallanger: The offshore pipeline from the 70-ft depth is approximately $1.5 million including installation. For reference, the original estimate made a number of years ago for a conventionally laid oil-field technology pipeline using lay barges was in the order of $10 to 12 million for the cold-water pipeline only.

Question: Why were your gallons per minute listed as minimums?

L. Hallanger: That is a guaranteed minimum flow rate because of standard off-the-shelf pump capacities. We will actually be pumping about 7500 gpm of cold water and 10,000 gpm of warm water. The contract specifies minimum performance requirements of 6400 and 9600 gpm, respectively.

Question: Your cold-water pipe cable ...(inaudible)

L. Hallanger: The chain is on the bottom, the pipeline is floating above the bottom.

Question: With regard to corrosion, are you using anodes on the chain also?

L. Hallanger: Those will be put on in addition. The life is based on no cathodic protection of any kind.

Question: Is it on the bottom everywhere or are there catenaries?

L. Hallanger: We can encounter vertical drops of up to 40 ft that have been observed from submersible tracks. We've done it down to 1200-ft depth. The tension in the chain allows it to span a short irregularity, so that if there is a vertical 40-ft drop, you don't try to make your pipeline make too abrupt changes. So we will span small irregularities, the tension is such that we will not create long catenaries.

Question: Can you tell me, on financing of the facility, what is the current status or whatever; what parts are in operation or when will they be?

L. Hallanger: Current status is: final design is due on my desk the 30th of this month and will be delivered to Argonne by the 6th of July. Financing: this is a joint effort between the State of Hawaii and the Department of Energy. The water supply facility (pipelines, pumps, etc.) is a federal investment. The onshore facilities, buildings, laboratory, utilities, that sort of thing are a State of Hawaii investment.

Inaudible Question:

L. Hallanger: We will bring in a crane from local construction sources. We do not plan to have a large crane on board at the present time.

Question: How are you going to truck things back to the test pad?

L. Hallanger: There is adequate paved access all the way to the test pad.

DESIGN AND CONSTRUCTION PHASE OF A BIOFOULING, CORROSION, AND MATERIALS STUDY FROM A MOORED PLATFORM AT PUNTA TUNA, PUERTO RICO

Donald S. Sasscer*, **Thomas R. Tosteson****, **Kund B. Pedersen**†, **Ferdinan Rosa**‡ **and Fernando L. Benitez**††

Center for Energy and Environment Research
University of Puerto Rico
Mayaguez, Puerto Rico 00708

Abstract

In November 1978, a contract was awarded to the Center for Energy and Environment Research to initiate a three phase research project for the design, construction and operation of an OTEC biofouling corrosion and materials study to be conducted from a moored platform at Punta Tuna, Puerto Rico. The design, which has now been completed, specifies a Landing Craft, Utility (LCU) type vessel, modified to enable it to be used as a versatile research platform, by the addition of auxiliary electrical power units and by the construction of a well through the bottom of the vessel through which the water supply intake and exhaust hoses will be placed. Research data will be acquired by a sea water system installed onboard the LCU. The system will consist of four independent flow loops with each flow loop having four parallel flow paths. Heat transfer will be monitored in one of the flow paths, and biofouling and corrosion, in the other three parallel paths. Construction is estimated to be completed in approximately four months.

Introduction

Considerable knowledge has been gained during the past several years about biofouling and corrosion and their effects on the transfer of heat through various materials which have potential for use in OTEC heat exchangers. Continued studies, however, are needed in order to confirm or deny the tentative conclusions which have been reached concerning the nature and extent of biofouling and corrosion. These studies should be sufficiently intensive to enable statistically valid conclusions and should be of sufficient length to determine temporal variability.

*Head, OTEC Division, CEER
**Professor, Department of Marine Science, Mayaguez Campus, UPR
†Professor, Department of Mechanical and Nuclear Engineering, Mayaguez Campus, UPR, and Scientist, OTEC Division, CEER
‡Professor, Department of Mechanical and Nuclear Engineering, Mayaguez Campus, UPR.
††Professor, Department of Mechanical and Nuclear Engineering, Mayaguez Campus, UPR.

In November 1978 the OTEC Biofouling, Corrosion and Materials Project of Argonne National Laboratory funded the Center for Energy and Environment Research (CEER) for the first phase of a three phase (design, construction and operation) project to conduct an OTEC biofouling, corrosion and materials study at Punta Tuna, Puerto Rico. This paper will be devoted primarily to a discussion of the design phase of the project.

Objectives

The major objective of this investigation is to obtain a better understanding of the nature of the biofouling and corrosion which can be expected to occur in OTEC heat exchangers. This will be accomplished through replicated multi-seasonal determination of the relationships which exist among biofouling, corrosion, materials, cleaning methods, location and the heat transfer coefficient. An additional objective is to determine the compatibility between Caribbean open ocean surface water and OTEC heat exchangers, at a site where the electrical utility and the local government have expressed an interest in cooperating with DOE in building and operating the world's first commercial OTEC power plant.

A third objective is to conduct these investigations from a versatile, moored vessel/research platform which can be used for continued and/or expanded testing with surface water, and which can serve as the prototype for an OTEC test facility using both surface and deep water.

Overview

The research will be performed from a 115-ft long, modified landing craft type vessel. During the study, the vessel/research platform will be attached by a 400-ft nylon rope to a buoy which has been moored in 1100 m deep water approximately two miles southwest of Punta Tuna, Puerto Rico. The electrical-Hydraulic system for the research facility has been designed, and is presently being assembled and constructed by the Southwest Research Institute (SwRI), of San Antonio, Texas. Heat transfer data will be acquired using the heat transfer monitoring system designed and built by Carnegie-Mellon University (CMU) and which was used for the biofouling experiment conducted by Tracor Marine Inc. at

St. Croix. Biofouling and corrosion sample coupons will be obtained by periodically cutting sections from sacrificial tubes which will be in flow paths parallel to the CMU heat transfer monitoring devices.

Overhaul and modification of the vessel for research use will be performed at New Bern, North Carolina, where the LCU is presently docked. After the experimental system has been built and tested at SwRI, it will be shipped to New Bern, and installed on board the vessel. The vessel/research platform will then sail to Puerto Rico under its own power, and be moored to the buoy at Punta Tuna.

The research platform will have housekeeping facilities to accomodate approximately 10 visiting scientist for short periods of time. In order to assure safe operation, the platform will be continuously manned by a crew of three seamen and will be equipped with VHF, UHF and SSB radios. A 34-ft diesel power boat will be available to transport crew, scientist, fuel, and light equipment between the research platform and the harbour of Yabucoa, Puerto Rico, approximately 5 miles away.

Research Site

The bathymetric chart of Figure 1 shows the site at which the study will be conducted, and the proximity of Punta Tuna to the harbour of Yabucoa. As is indicated on the chart, water 1000 m deep occurs within 2 miles of Punta Tuna. This fact, along with the nearby convenience of Yabucoa, makes Punta Tuna a prime site for an OTEC plant and for conducting research. Yabucoa (population 1500) has living accomodations such as hotels and guest houses for visiting scientist, and is less than 2 hours driving time from San Juan. The buoy to which the platform will be moored is installed in 1100 m of water at the site. The buoy is tension-moored with a 3000-lb anchor, 12 shots of 1-inch anchor chain, and a 2-inch diameter nylon rope.

Physical oceanographic studies funded by the DOE/OTEC program are presently being conducted at the site by Dr. Gary Goldman and others of the CEER staff. The preliminary results of this study are being presented by Dr. Goldman and Mr. Daniel Pesante in another paper at this conference. Next year it is planned that biological as well as physical oceanographic research will be conducted at the site, and it is expected that a significant portion of this research will be conducted from the moored biofouling research platform.

Vessel/Research Platform

A sketch of the modified vessel which will be used as a research platform is shown in Figure 2. The vessel is the Landing Craft, Utility (LCU) 1470, and was an active vessel of the U.S. Army Heavy Boat Company of Morehead City, North

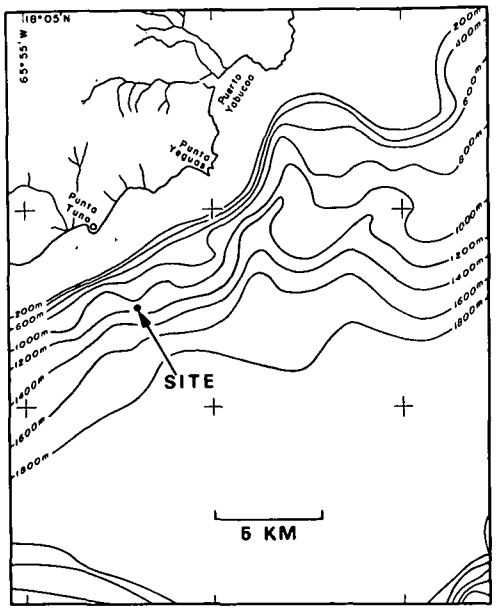

Fig. 1 Site of Experiment near Punta Tuna, Puerto Rico.

Carolina, until the summer of 1978, at which time it was transferred to DOE for OTEC experimental use. The vessel is presently awaiting overhaul and modification at the Barbour Boat Works at New Bern, North Carolina. The 350-ton vessel is 115-ft long and has a beam of 34-ft. It has accomodations for 14 persons, is powered by three 165 hp diesel engines and has two 20-kw DC diesel-electric generators to provide electrical power, for housekeeping purposes.

Two 50-kw AC generators and additional fuel storage facilities will be added to the vessel to provide electrical power for research use. An 18-inch diameter well from the deck through the bottom of the vessel will be constructed to provide a passage for the intake and exhaust water hoses. The experimental flow loops will be installed on deck near the well, and the heat transfer data acquisition system will be housed in an 8-ft x 10-ft x 8-ft air-conditioned fiberglass house on deck.

Experimental Set-Up

Water Intake and Exhaust System

Figure 3 shows the schematic of the "A" frame which will be used for the deployment of the intake and exhaust hoses through the well. The intake hoses will draw water from approximately 45-ft below the center of the platform, through the well to the experiment, and the exhaust hoses will discharge water approximately 30-ft below the center of the vessel. Both the intake and exhaust hoses will be attached to a weighted cable suspended from the "A" frame. A torid-type bumper system will be attached to the cable so that the hoses will not

chafe against the sides of the well. In order to prevent the hoses from bending through a small radius, due to motion of the platform, they will be reinforced as they exit from the bottom of the vessel. Considerable difficulty has been experienced with intake hoses during other biofouling experiments conducted at sea. For this reason, substantial effort has been expended in designing a simple, trouble free intake system.

Flow Loop Modules

As can be seen in Figure 4, the experiment will consist of four parallel-flow, experimental modules. Each module will have its own pump, and intake and exhaust system; however, to guarantee continuous operation, each two modules will be served by three pumps. Two modules will be vertically mounted back to back on a frame as shown in Figure 5. The modules themselves have four parallel flow paths which insure that the heat transfer monitoring devices will have the same potential for biofouling as each of the "coupon" tubes. The Carnegie-Mellon Heat Transfer measurement device shown in Figure 6 will be installed in one flow path and the three remaining parallel flow paths of each module will consist of coupon tubes. Each heat transfer monitor and coupon tube will have an independent flow meter and flow calibration system. Two of the modules will be constructed of 1-inch diameter 5052 aluminum tubes and the other two will consist of 1-inch

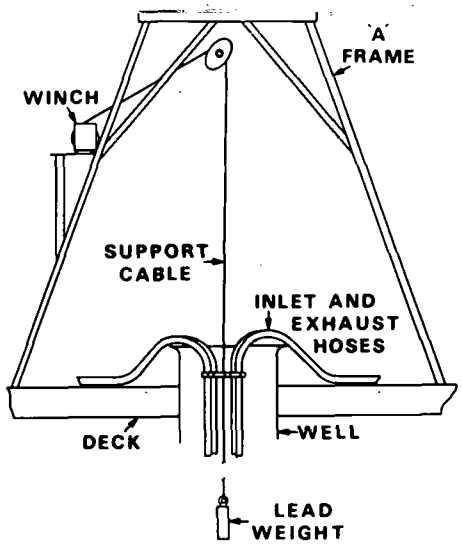

Fig. 3 Through deck well and "A" frame for deployment of intake and exhaust hoses.

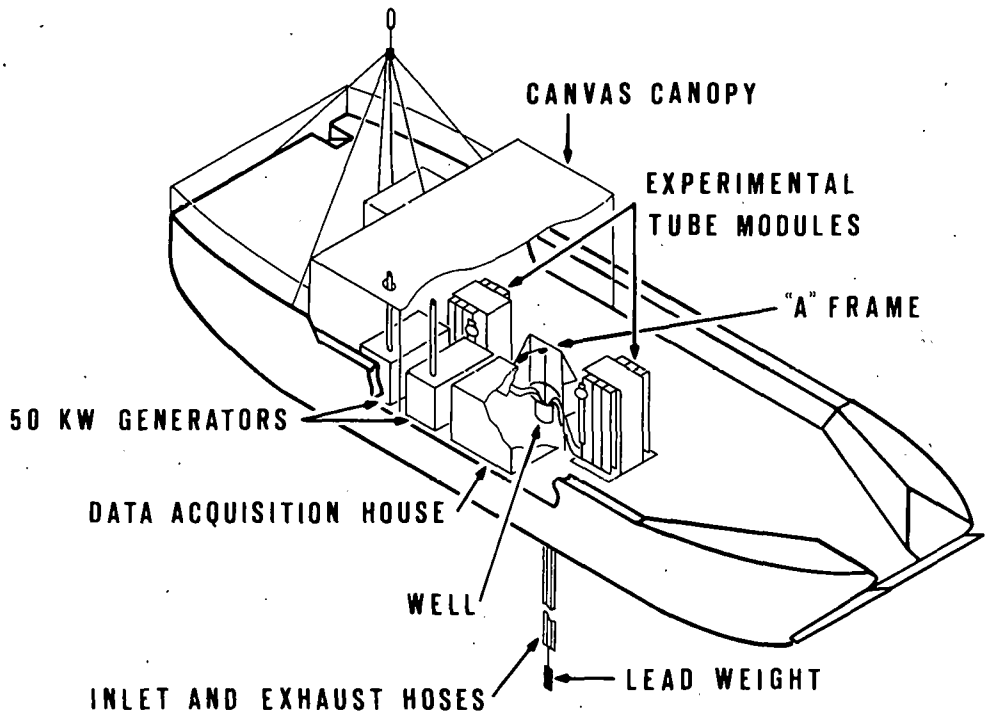

Fig. 2 Cutaway view depicting the modification of LCU-1470 for use as a moored OTEC research platform.

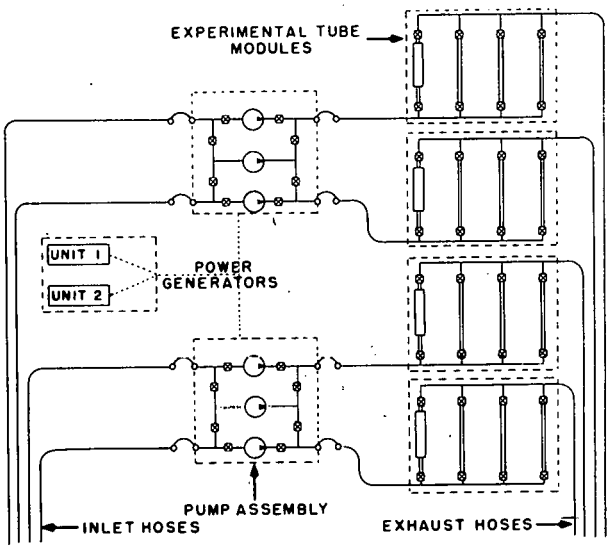

Fig. 4 Skematic diagram of the four modular flow loops of the hydrolic system.

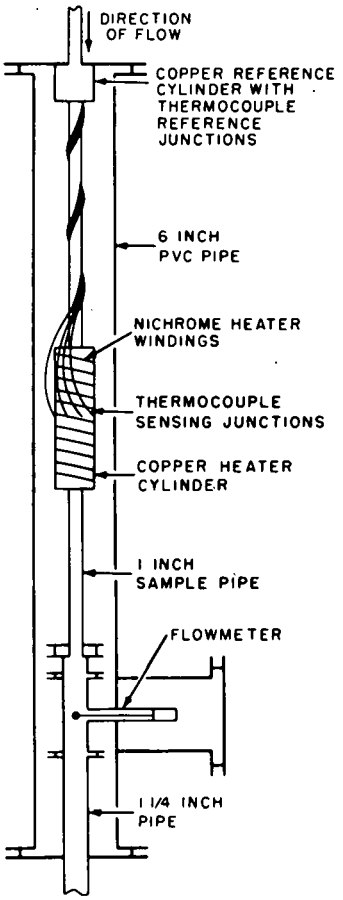

Fig. 6. Carnegie Mellon University heat transfer monitoring device.

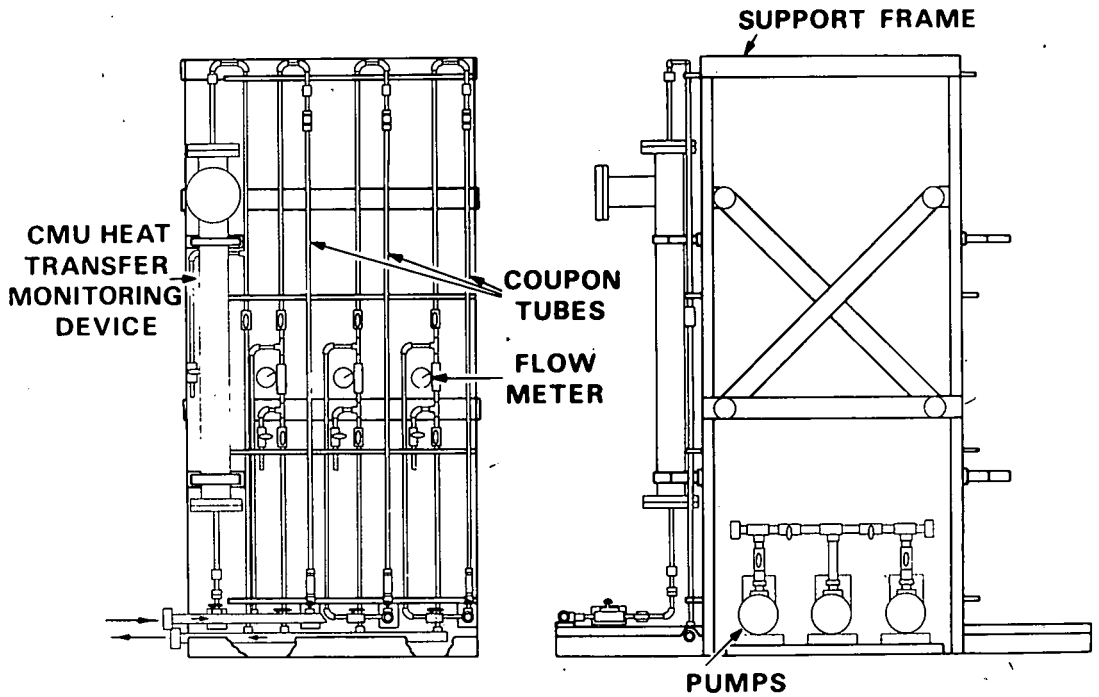

Fig. 5. Drawing of one modular flow loop showing the arrangement of the CMU heat transfer device and the coupon tubes (left) and the mounting of the module on deck (right).

diameter ASTM 8-338 grade 2 titanium tubes. As near as possible, the water intake and exhaust system has been kept symmetrical in order to minimize the acceleration of the water in the test units due to the motion of the vessel.

One of the primary advantages of using a large vessel such as an LCU for a research platform is that it will have sufficient space to accommodate four independent parallel flow modules, which can provide independent replicated data on materials, heat transfer, biogrowth, and corrosion.

Heat Transfer Data Acquisition System

Heat transfer data will be acquired by using the monitoring device developed by CMU (Figure 6), and the CMU PS-105 data acquisition system. The CMU PS-105 will transmit and amplify the low-level signals of heat transfer decay constant, flow rate, and water temperature, from the monitor to a teletype readout in the data acquisition house, on deck adjacent to the flow loops. The data will be stored on tape and heat transfer calculations will be performed at convenient intervals.

Biofouling and Corrosion Sample Collection System

The coupon tubes of the flow loops are 90 inches long. Pediodically 9-inch sections of tube will be removed to serve as biofouling and corrosion samples. After removal of the first down stream 9-inch section, a replacement 9-inch section of PVC tube will be installed in its place. After removal of the second 9-inch sample section, the 9-inch PVC replacement section will also be removed and the two will be replaced by a single replacement section 18 inches long. This process will be repeated throughout the duration of the experiment so that the length of the sample loop remains constant.

Experimental Procedures

The experiment will correlate biogrowth, corrosion, materials and cleaning effectiveness with the change in heat transfer through aluminum and titanium tubes which simulate the tubes of OTEC heat exchangers.

During the first three months of the experiment, emphasis will be given to understanding the onset of biogrowth. For this reason no cleaning will be performed during this phase of the study. A weekly R_f determination will be made on the two aluminum and two titanium tubes instrumented with the CMU heat transfer monitoring devices. Simultaneously 9-inch long sections will be cut from three of the aluminum and three of the titanium coupon sample tubes for biogrowth study and for correlation between biogrowth and the change in heat transfer coefficients. This procedure will provide one replica of each R_f determination and two replicas of each biogrowth sample on a weekly basis over a three month period for both aluminum and titanium heat exchanger tubes and should provide sufficient data to enable statistically valid conclusions to be reached concerning the nature of the onset of biogrowth and its effect on the heat transfer of two potential OTEC heat exchanger materials.

After completion of the initial intensive three month study, new coupon sample tubes will be installed in the experiment and a multiseasonal experiment will be conducted. During this phase of the study, R_f will normally be determined weekly, as in the initial phase of the study. Cleaning with hand operated M.A.N. brushes will be performed each time R_f reaches a predetermined value, (perhaps 0.0002), coupon samples for both biogrowth and corrosion studies will be collected at this time and R_f will be determined just before and after each cleaning. This procedure is expected to result in a schedule of ten to twelve sampling periods during the year and should enable multi-seasonal correlations to be made among biogrowth, corrosion, materials, cleaning and heat transfer coefficient changes. As in the initial phase of the study, replicas of all R_f data biofouling and corrosion coupon samples will be obtained.

Biogrowth

Selected samples of heat exchanger tubing will be examined in order to determine the rate at which these surfaces are fouled by materials present in ambient seawater and acquire adherent marine microorganisms. Four major aspects will be examined concerning the accumulation of materials on the test surfaces:

1. Film Thickness. The wet film thickness found on the test surface will be determined microscopically and the volume per unit area calculated. Segments of the exposed surfaces will be preserved in a hydrated condition, transported to the laboratory and examined by reflectance microscopy.

2. Film Density. The film density will be calculated on the basis of film volume described above, and a determination made of the total amount of solute accumulated on the test surfaces. Samples of exposed surfaces will be foiled (aluminum foil) and frozen (liquid nitrogen) at the sampling site. These surfaces will be transported to the laboratory in a frozen condition and subsequently freeze dried. The total amount of material accumulated will be removed from the test surface and weighted.

3. Chemical Composition of the Film. The solute materials accumulating on the test surfaces, isolated as described in #2 above, will be analyzed for organic carbon content and for the presence of selected inorganics (Ca^{++}, Mg^{++}, $SO_4^{=}$ and $PO_4^{=}$).

These analyses will be contracted to an analytical laboratory. The ATP and Chlorophyll "a" contents of the isolated materials will also be determined by the contracted analytical facility.

4. Scanning Electron Microscopy of Exposed Surfaces. The condition of the exposed surfaces will be visualized using SEM. Such facilities are available at the University of Puerto Rico, Mayaguez. Samples of exposed surfaces will be frozen at the OTEC site (as described in #2 above), and transported to the laboratory. The subsequent drying and coating of the sample in preparation for the SEM will have to be assessed with the specific material or sample at hand. This procedure will be analyzed prior to the field experiment, employing typically fouled surfaces of the heat exchanger tubes.

Additional studies will be conducted on selected samples of solute materials that accumulate on the surfaces employed in this study. The high molecular weight components accumulated will be examined with high pressure liquid chromatography (HPLC). These materials will be fractionated on HPLC cationic exchange columns and the resulting materials (fractions) examined for their ability to enhance the adhesion of micro-organisms to the test surfaces.

The second phase, multiseasonal determination of biogrowth, will utilize the same techniques as the initial phase; however, the sample period will be extended to approximately one month to six weeks rather than one week, as in the initial phase.

Heat Transfer

To measure changes in heat transfer properties of the tubes as a result of biofouling and/or corrosion, a device developed at Carenegie-Mellon University will be mounted on one tube in each four-tube experimental module (Figure 4). The CMU device (Figure 6) consists of a copper heater cylinder and a copper reference cylinder, both of which are clamped to the tube. A temperature sensing devices, a thermistor and a flow meter are attached directly to the tube. A small amount of heat is applied to the outer surface of the heater cylinder, and when the temperature of the cylinder reaches a steady state, the heat is turned off. Measurements of water temperature, flow velocity, and the temperatures of the heater and reference cylinders are taken at 6-sec intervals until the temperature of the heater and reference cylinders again reaches a steady state. Using these data, the CMU group has developed a program to calculate a mean conductance coefficient and the standard deviation of the mean. This program will be used for data reduction along with the uncertainty analysis developed by Battele PNL as a sub-routine to the CMU program.

Major sources of variation in characteristics and sources of error, with plans of how these will be avoided or at least minimized are as follows:

Pump Stoppage. It is essential to maintain a steady flow of water through the experimental tubes. Once the flow has been interrupted, all subsequent data are of questionable value. The LCU will have a full-time crew of three who will be responsible for checking the pumps at hourly intervals to assure that they are functioning properly. Each pair of modules will be provided with a spare pump which can be activated if one of the primary pumps fails.

Flowmeter Fouling. Since the heat transfer coefficient is a function of water velocity, among other factors, it is important to measure the flow rate accurately. The CMU device uses an intrusion-type flowmeter, and biofouling of the sensor may alter its calibration. Therefore, flowmeters will be calibrated before and after each run.

Flow Rate Fluctuations. When the experimental equipment is mounted on the platform, rolling and pitching of the platform due to wave action results in fluctuations in the flow rate. To minimize this effect, both intake and outlet hoses for each system will be passed through a well which passes through the bottom of the research platform near its center of mass.

Rapid Variation of Sea Water Temperature. Measurements of the heat transfer coefficient will be influenced by the water temperature. This measurement is sensitive to fluctuations as small as 0.1°C. Error resulting from variations of sea water temperature can be minimized by making several measurements (16 on the same day). Erratic values caused by temperature changes can then be eliminated by statistical procedures.

Contact Resistance between Cylinder and Tube. With the CMU device, it is assumed that the contact resistance between the heater, reference cylinder and the heat transfer tube remains constant throughout the experiment. Thermal conductivity will be tested between the tube and the device prior to the experiment and again at the termination of the experiment.

Corrosion

During the initial three-month experiment it is not expected that significant corrosion will occur; however, for completeness, several samples each of aluminum and titanium will be collected and analyzed. Corrosion coupons will be collected on the same schedule as biological samples during the year-long, multiseasonal phase of the study.

Starting with the evaluation of a cleaned set of control samples, the samples progressively removed from the coupon tubes will be examined for type, rate, and severity of corrosion, and composition of the corrosion products and scale which are found on the tubes. The corrosion potential and corrosion rates will be measured at the tubes. These results will be correlated with the data from the biofouling and heat transfer experiments. Corrosion data will include: corrosion potentials, polarization currents, and physical samples representing corrosion phenomena. Examination of samples will include visual observation of type of attack, including any pitting, description of the corrosion product film, microscopic examination, recording of the film thickness and texture, and elemental analysis using SEM microprobe analysis.

Conclusion

The design phase of a three-phase contract for design, construction and operation of an OTEC study of biofouling, corrosion and materials at Punta Tuna, Puerto Rico has been completed and the construction phase has commensed. The design has resulted in a four loop, modular, parallel path, experiment flow system which will be mounted upon, and operated from, a 115-ft long moored vessel/research platform. The system was designed to be versatile and capable of expansion, and yet simple and of low cost. The construction phase of the project should be completed in approximately four months, and data acquisition should start before the beginning of 1980.

References

1. T.R. Tosteson, and W.A. Corpe. 1975. Enhancement of adhesion of the marine Chlorella vulgaris to glass. Canad. J. Microbiol. 21:1025-1031.

2. K. Verner, and T.R. Tosteson. 1973. The aggregation of planktonic algae. Proc. 10th Meeting Assoc. of Island Marine Labs. of the Caribbean.

3. T.R. Tosteson, D.K. Atwood and R. S-C. Tsai. 1976. Surface active, high molecular weight organics in the Caribbean Sea. MITS-IEEE Oceans 76 Symp., 13C1-13C7.

4. B. Jiménez-Vélez, T.R. Tosteson, B.R. Zaidi, D.K. Atwood and R. S-C. Tsai. 1977. Adhesion enhancing organics in the Eastern Caribbean Sea. Proc. CIGAR II Symp. (in press).

5. D.R. Hale. 1975. The physiological effects of the extracellular products of marine micro-organisms. M.S. Thesis, Dept. of Mar. Sci., Univ. Puerto Rico CAAM, Mayaguez, Puerto Rico.

6. T.R. Tosteson, and B.R. Zaidi. 1976. Surface active macro-molecules in the marine environment: a sugar specific lectin-like activity. Proc. 4th Symp. on Food and Drugs from the Sea, pp. 457-466.

7. D.R. Hale, and T.R. Tosteson. 1975. Interaction of marine microbial populations. Proc. 11th Meeting Assoc. of Island Marine Labs. of the Caribbean.

8. B.R. Zaidi, and T.R. Tosteson. The differential adhesion of Chlorella cells during the life cycle. Proc. VII Seaweed Symp., pp. 323-328.

9. T.R. Tosteson, and L.R. Almodóvar. The Adhesive properties of Chlorella vulgaris and the enhancement of the adhesion by substance found in ambient sea water. ONR Tech. Rep. No. 2, NR 306-849.

10. B. Little, D. Lavoie. 1978. Summary Report, OTEC-2 Gulf of Mexico Biofouling and Corrosion Experiment. U.S. Department of Energy.

11. J.G. Fetkovich. 1976. A System for Measuring the Effect of Fouling and Corrosion of Heat Transfer under Simulated OTEC Conditions. N.T.I.S., Springfield, VA 22161.

12. S.P. Bird. 1976. Uncertainty Analysis Routine for the Ocean Thermal Energy Conversion (OTEC) Biofouling Measurement Device and Data Reduction Procedure. BATTELLE Pacific Northwest Laboratories, Richland, Washington 99352.

13. H.L. Graig, Jr., R.S.C. Munier and J. Morse. Corrosion Results from a 72-day Field Test of Simulated OTEC Aluminum Heat Exchanger. Surface of St. Croix, U.S.V.I. Proc. The Fifth Ocean Thermal Energy Conversion Conference, VIII-147, Miami Beach, Fla., February.

14. Tracor Marine Inc. 1978. Final Report, Ocean Thermal Energy Conversion (OTEC) Biofouling and Corrosion Experiment. (1977) St. Croix, U.S. Virgin Island. PNL-2739, Part I. Pacific Northwest Laboratories Richland, Wash. U.S. Dept. of Energy.

15. R.W. Finley and D.L. Meier. 1977. Design Report for PS-105 Data Acquisition system for Biofouling Studies of Heat Exchangers in Sea Water. U.S. Department of Energy COO-4041-6.

DISCUSSION

Question: Why was the flow system symmetric with respect to the inlet and outlet sides?

D. Sasscer: As the tubes move through the heaving of the vessel there will be an acceleration of the water and, therefore, it will diminish the consistency of the velocity. In order to keep a constant velocity, we would like to limit the differential so we have the same head on the input as on the output as the vessel heaves.

Question: What will you do if the flow meters do not read correctly?

D. Sasscer: We will not depend just on our flow meters; we will calibrate every flow meter with the bucket method exactly. In addition, we can, if we wish to, pull in exhaust hoses or intake hoses separately. It's like pulling it back up the well. But we will calibrate them on a periodic schedule by the bucket method by module and by individual flow tubes.

H. White, U. of Hawaii: How do you moor this vessel? Are your pumps either self-priming or are they below the water line?

D. Sasscer: We are depending upon our mooring that was designed, and given to us, and put in by Dan Probert at the Naval Air Development Command. He has had quite extensive experience. In fact, his job is laying deepwater moorings; a 3000-ft mooring was nothing to him because he lays 12,000-ft moorings. Now, I know we haven't solved the problem yet as to what happens when that ship pulls on the tension moor buoy. It has a 3000-lb anchor, it's got 25 shots of chain on the bottom of the buoy, and our hope is that the LCU moored to the buoy will not cause any motion of the bottom of the buoy.

H. White: I was just suggesting — we looked carefully at the problem with Mini-OTEC, and the risks involved if it ever starts to cascade down the cliff can be pretty catastrophic. And you're probably aware of the Mini-OTEC solution, which might lend itself to your problem.

D. Sasscer: Well, we don't; our slope is not deep enough to cascade down. It certainly could move, it's about a 30% slope or one to three. And in answer to the other question, our pumps will not be below water, they'll be on deck.

G. Goldman, EER: We have used that mooring already for many weeks of mooring vessels off and on and so far we have't gone down the slope, thank goodness. We also should ask whether anybody is interested in negotiating for time on this vessel. It is going to sit out there three months to a year in 1050 m of water. Please contact Don Sasscer and we'll be able to make some arrangements as to how you can use it. Not only is space available, water that we are pumping through it is available.

D. Sasscer: Yes, we have had 125-ft, 250-ft vessels moored to it for a matter of days in fairly heavy weather and nothing has moved.

Question: I've got some experience with the heat transfer measurement devices and I'm concerned about electromagnetic interference.

D. Sasscer: The electronic aspect of the layout was designed by Southwest Research Institute, which has considerable experience in this area. Now I haven't necessarily requested that they address that particular problem. The heat transfer data acquisition shack will be 10 or 12 ft from the motor generator. That might be too close. I hope their electronics man considered that when he did the layout of the wiring, and the data acquisition. But I can not answer it specifically.

Question: What did you say was the utility bill for Puerto Rico in a year?

D. Sasscer: Last year more than $23 million was spent by the power company to buy fuel oil to produce electricity. The electrical capacity of the system is, I'd say, 44 MW_e, 99% oil-powered.

Response: That's $7.00 per person per year. Pretty cheap. We envy you.

D. Sasscer: Our electricity cost is about 5.5¢/kWh, so it's not cheap.

13. THE OTEC RESOURCE: ENVIRONMENT AND SITING

OTEC ENVIRONMENTAL AND RESOURCE ASSESSMENT PROGRAM

Lloyd F. Lewis*

U.S. Department of Energy
600 E Street N.W.
Room 400
Washington, D.C. 20585

Abstract

The Ocean Thermal Energy Conversion (OTEC) Environmental and Resource Assessment Program is that part of the Department of Energy's activity which assesses the Environmental and Resource requirements for continued OTEC development and ensures not only that the appropriate research is done, but also that it matches the scheduled time frame for development.

The initial requirement is to locate possible OTEC sites not only by their available thermal resource and environmental response but also by other considerations such as their operational and survival design requirements. The program ensures that the information on conditions at the sites is acquired and that the best possible estimates of OTEC induced changes are made.

The present program plan calls for a significant near term effort in site characterization at locations of probable OTEC deployment. This characterization is undertaken using historically acquired oceanographic data, models, hindcasts, and other techniques to the extent possible. Field measurements are made as necessary, to augment the archival data and, if required, for design and/or environmental assessment. Design requirements and site characterization data provide much of the necessary basis for environmental impact and resource assessments.

Introduction

The principal objective of the OTEC Environmental and Resource Assessment (ERA) program is to collect and analyze sufficient oceanic data to make defensible judgements on:

- o The impact of OTEC plants on the environment.
- o The impact of the environment on OTEC plants.

Initial studies to support this objective were begun in 1974 funded through the National Science Foundation. Comprehensive environmental/socio-economic assessments were made for possible OTEC development in Hawaii[1] and Puerto Rico.[2] The ERA program has grown steadily under the Energy Research and Development Administration, and now DOE, to a present effort including some 18 contracts totaling approximately $2.2 million (FY 79).

This paper will briefly present an overview of the ERA program[3-5] and characterize its recent and projected accomplishments. Companion papers by Wilde, Ditmars, and Molinari in this session will examine the program components in detail.

*Program Manager
Environmental Planning and Analysis Branch

OTEC Environmental Issues

The recently published DOE Environmental Development Plan for OTEC[6] describes in detail the following environmental concerns:

I Redistribution of Oceanic Properties
- Ocean Water Mixing
- Impingment and Entrainment of Biota
- Climatic and Ocean Thermal Impacts

II Chemical Pollution
- Biocide Discharges
- Working Fluid Leaks
- Corrosion Products Discharges

III Structural Effects
- Artificial Reef
- Nesting and Migration Impacts

IV Socio-Legal Economic
- Worker Safety
- Environmental - Maritime Law
- Secondary Economic Impacts

(I) above concerns the set of problems associated with very large volumes (4.5 m^3/sec/MWe) of flow through each the evaporator and condenser cycle and the effects of these intakes and combined volume discharges. Nutrient rich water from 1000 m depth will be displaced to the upper thermocline. Twenty degree centigrade difference water masses will be mixed and discharged at the same intermediate temperature. Biota will be both impinged on intake screens and entrained into the OTEC plant. If, as in open cycle OTEC, condenser water is deaerated, relatively large volumes of carbon dioxide and other gases may evolve into the atmosphere.

(II) describes the set of discharges due to OTEC operations. Some biocide (i.e., chlorine) is likely to be required in addition to mechanical cleaning to keep OTEC heat transfer surfaces free of biofouling. Ammonia, the baseline design working fluid, will leak to some extent from the very large (10^4 m^2/MWe) surface area of thin walled heat exchangers. It is anticipated that some near- plant toxicity will be attributable to corrosion product releases.

(III) represents the set of issues associated with OTEC platforms and cold water pipes acting as artificial islands for fish and seabirds. These could prove to be beneficial impacts, but their effects warrant examination.

(IV) above attempts to combine the legal, institutional, health, and safety issues attributable to OTEC. Most of those concerns are governed by maritime, Federal, or state law and will be handled by OTEC design options in compliance with permits. An undecided issue set involves the international

aspects of OTEC deployment and possible controls implicit in the pending United Nations Law of the Sea treaties.[7]

OTEC-ERA Program

Figure 1 describes the management structure of the present OTEC-ERA program. Utilizing the lead laboratory concept, Dr. Wilde's OTEC group at Lawrence Berkeley Laboratory serves as a focus of program planning and technical direction. In turn, they rely heavily on Dr. Molinari and his staff at NOAA/AOML for measurement and analytical support and Dr. Ditmar's group at ANL for hydrodynamical and numerical modeling. All three of these groups monitor the 18 contracts mentioned earlier.

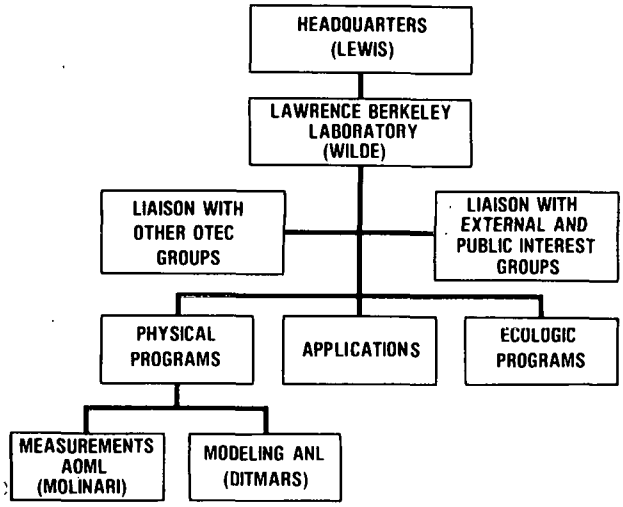

Fig. 1 OTEC-ERA Research Management.

OTEC sites

The sites of principal interest to OTEC are indicated on Figure 2. Ocean Data Systems, Inc. has prepared brief site data summaries[8] and worldwide ocean thermal difference charts[9]. It is anticipated that OTEC interest will expand into plant ship site locations in the Carribean and Pacific as well as moored electricity producing sites internationally.

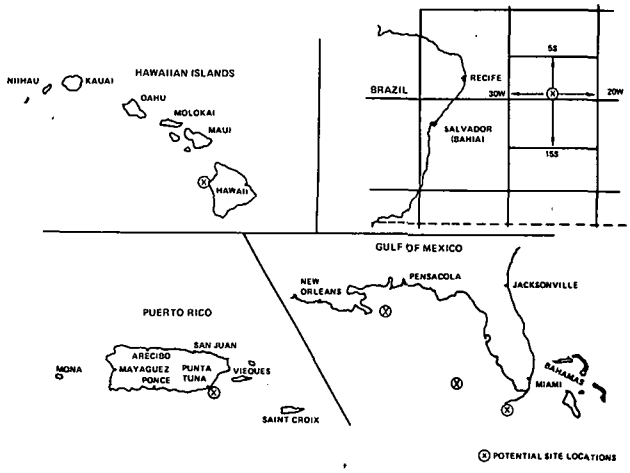

Fig. 2 OTEC General Site Locations.

The OTEC-ERA program has been supporting an oceanic measurement program at the locations noted on Table 1 since July 1977. Survey objectives and results have been published[10-14] and will be described more fully in companion papers in this and other environment and siting sessions.

SITE/REGION	PHYSICAL MEASUREMENTS	CHEMICAL MEASUREMENTS	BIOLOGICAL MEASUREMENTS
MOBILE	8	6	6
TAMPA	7	5	5
SOUTH ATLANTIC	2	2	2
PUERTO RICO	5	5	5
HAWAII	2	2	2

Table 1 OTEC-ERA Measurements Program Status: July 1977-May 1979 Site Occupations.

Environmental research

In addition to the oceanic measurements, a program of environmental research has been implemented to address the environmental concerns previously noted. Figure 3 briefly lists these research projects and their near term schedules.

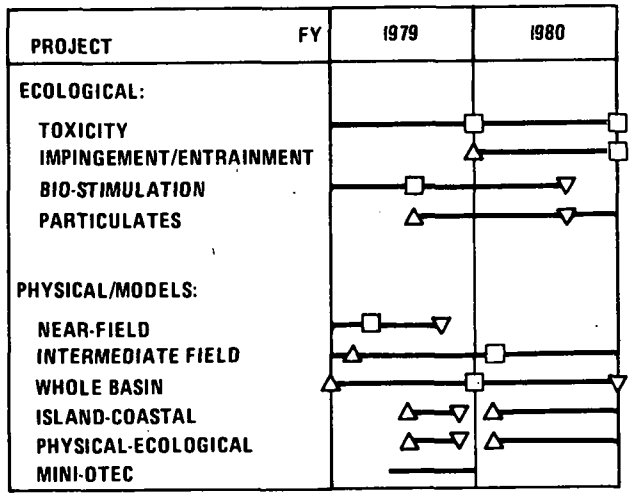

Fig. 3 OTEC-ERA Environmental Research Program Milestones: 1979-1980.

NEPA compliance

In compliance with the National Environmental Policy Act, the OTEC-ERA program has produced a series of documents. An environmental impact assessment was published for OTEC-1.[15-16] Based on that effort, DOE declared[17] that no environmental impact statement for OTEC-1 would be required. By October 1979, Interstate Electronics Corp. will have completed a draft programmatic environmental assessment of OTEC. It is expected that this document will further refine our knowledge of OTEC environmental issues and assist us in environmental research and monitoring planning. An environmental assessment for the 10/40 MWe OTEC facility is planned to begin in FY 80. In addition to these NEPA documents, DOE has prepared an Environmental Development Plan.[6]

OTEC-ERA 1978 accomplishments

During the past year, the OTEC-ERA program has accomplished the following tasks:

- Oceanic measurements under way at Gulf of Mexico, Hawaii, Puerto Rico, South Atlantic sites.
- Preliminary Environment Data Guideline issued.[18]
- World Thermal Resource Data published.[8-9]
- OTEC oceanic Data Base established at National Oceanographic Data Center.[19]
- OTEC-1 Environmental Impact Assessment published.[15-17]

Results of the measurements and research program have suggested the following as OTEC design considerations:

- A mixed discharge below mixed layer depth is a preferred design option (with possible environmental constraints).
- OTEC plant size might be limited to 400 MWe due to recirculation into evaporator.
- Sea state, thermal difference and currents in the South Atlantic plantship region are more limiting than predicted.
- Thermal differences at the Gulf of Mexico sites were smaller than predicted last year.

OTEC-ERA planned activities

Within the next two years, the following will have been accomplished:

- OTEC Programmatic Environmental Assessment completed (October 1979).
- OTEC discharge pollution guidelines established in cooperation with Environmental Protection Agency and U.S. Coast Guard (1980).
- Toxic effects of probable OTEC discharges will be established(1980).
- Guidelines will be set for OTEC plant size and spacing consideraing both recirculation and environmental impacts (1979).

References

1 Bathen, K.M. (1975) "An Evaluation of Oceanographic and socio-economic aspects of near shore ocean thermal energy conversion power plant in subtropical Hawaiian waters." University of Hawaii, Honolulu, HI, April 30, 1975, (PB - 242167, NTIS).

2 Attwood, D.K. et. al. (1976) "OTEC: Resource assessment and environmental impact using a proposed Puerto Rico site." University of Puerto Rico, Maguquez, P.R., August 1976, NSF Grant Report AER 75 - 00145.

3 Lewis, L.F. and W.R. McCluney (1977) "Proceedings, OTEC Resource and Environmental Assesment Workshop," Florida Solar Energy Center, Cape Canaveral, FL, October 1977, FSEC Report RD-77-2.

4 Lewis, L.F. (1977) "Status of OTEC environment and resource assessment studies," Proc. OTEC Biofouling and Control Symposium, USDOE, Seattle, WA, October 10-12 1977, PNL-SA-7115.

5 Lewis, L.F. and C.P. Duncan (1978) "OTEC environmental and resource assessment program," Proc. 5th OTEC Conference, USDOE and University of Miami, Miami, FL, February 20-22 1978, Conf-780236 (vol. 1).

6 U.S. Department of Energy (1979) Environmental Development Plan (EDP): OTEC, USDOE, Washington, D.C., March 1978, DOE/EDP-0034.

7 American Society of International Law (1978) "International, legal, political and institutional aspects of OTEC demonstration and development", ASIL, Washington, D.C., December, 1978, USDOE Contract Report EG-77-C-01-4118.

8 Wolff, P.M. (1979) "OTEC thermal resource reports for 10 sites," Ocean Data Systems, Inc. Monterey, CA , March, 1979, USDOE Contract Report ET-78-C-01-2898.

9 Wolff, P.M. (1978) "Large scale distribution of OTEC thermal resource (2 charts)", Ocean Data Systems, Inc., Monterey, CA , USDOE Contract ET-78-C-01-2898.

10 Lee, T.N. et.al. (1978) "Water mass structure and variability north of St. Croix, U.S. Virgin Islands as observed during the summer of 1977 for OTEC assessment", University of Miami, Miami, FL , June, 1978, UM-RSMAS #78004.

11 Molinari, R.L. and J.F. Festa (1978) "Ocean thermal and velocity characteristics of the Gulf of Mexico relative to the placement of a moored OTEC plant," National Oceanic and Atmospheric Admin., Miami, FL , October, 1978, NOAA Tech. Memo. ERL-AOML-33.

12 Thomas, G.G. et.al. (1979) "Data from the Atlantic Oceanographic and Meterological Laboratories OTEC plant site study in the Gulf of Mexico: July 1977," National Oceanic and Atmospheric Admin., Miami, FL, January 1979, NOAA Tech. Memo. ERL-AOML-34.

13 Molinari, R.L. and F. Chew (1979) "Ocean thermal and current structures in the tropical South Atlantic relative to the placement of a grazing OTEC plant," National Oceanic and Atmospheric Admin., Miami, FL , January, 1979, NOAA Tech. Memo. ERL-AOML-35.

14 Cummings, S.R., Jr. et.al. (1979) "Inorganic nutrients and dissolved oxygen variation determined from historical data at three proposed OTEC sites: Puerto Rico, St. Croix and Northern Gulf of Mexico", National Oceanic and Atmospheric Admin., Miami, FL , February, 1979, NOAA Tech. Memo. ERL-AOML-36.

15 U.S. Department of Energy (1979) Environmental Assessment: OTEC Preoperational Ocean Test Platform, USDOE, Washington, D.C., March, 1979, DOE/EA-0062.

16 TRW, Inc. (1979) "Supplement to draft environmental impact assessment: OTEC: preoperational ocean test platform", TRW, Inc. Redondo Beach, CA , March, 1979, Preliminary Draft.

17 U.S. Department of Energy (1979) "Environmental assessment: OTEC-1", letter Ruth Clusen, ASEV to John Deutch, ASET of March 16, 1979, USDOE, Washington, D.C.

18 Molinari, R.L. and J.F. Festa (1978) "Ocean thermal and current velocity data requirements for design of an OTEC demonstration plant", National Oceanic and Atmospheric Admin., Miami, FL, January, 1978, NOAA Tech. Memo ERL-AOML-30.

19 U.S. Department of Commerce (1978) "Oceanographic data base for OTEC", National Oceanic and Atmospheric Admin., National Oceanographic Data Center, Washington, D.C., NODC-DOE IAA EX-76-A-29-1041.

OCEAN THERMAL AND CURRENT VELOCITY DATA REQUIREMENTS FOR DESIGN OF AN OTEC PLANT - AN UPDATE

Robert L. Molinari*

Atlantic Oceanographic and Meteorological Laboratories
National Oceanic and Atmospheric Administration
15 Rickenbacker Causeway
Miami, Florida 33149

Abstract

Oceanographic data are required in the OTEC plant design effort to evaluate the effect of plant operations on the environment and the effect of the environment on operations. The program designed to obtain current and thermal data at several proposed OTEC sites has been updated. The update is based on the results of workshops, reports, meetings with design engineers, journal articles and at sea experience. Data requirements for moored plant sites are somewhat different than those for grazing plants in that data are required over a larger area in the case of the grazing plant. Data requirements include upper layer temperature data to evaluate the resource available at the site. Sea surface data are not sufficient because the plant ingests water from a layer of finite thickness rather than just the plane of the sea surface. Current meter data are needed to evaluate the tendency for vortex shedding and the current loading on the cold water pipe. Surface drift is monitored at the grazing sites to determine propulsion requirements. Accuracy and required spatial and temporal resolution for these and other required measurements are given. In addition, the types of reports and formats used to present these data are also described.

Introduction

Molinari and Festa[1] presented a list of oceanographic data required for the design of an OTEC plant. These requirements are updated herein based on reviews of journal articles and technical reports, workshop discussions, and at-sea experience. In addition, measurement programs for obtaining the data, and suggested format for presenting the data are given.

Two modes of operation for OTEC plants have been proposed. In one mode, the plant is moored and the electricity generated at the plant is hardwired ashore to a land-based power grid. In the other mode, the plant is self propelled, and the electricity generated at the plant is used to manufacture an energy intensive product such as ammonia or hydrogen.[2] Designers of either plant require oceanographic data to evaluate the effect of the plant on the environment and the effect of the environment on the plant. Certain types of data are required for both moored and grazing design efforts, and others are more specific to a particular mode of operation (see, e.g., Ref. 3). The general data needs and design-specific needs are discussed next.

*Physical Oceanography Laboratory

Thermal and Current Data for Design of Moored and Grazing OTEC Plants

General Data Needs

Table 1 lists various properties of temperature distribution and the design factor which they effect. In the case of the moored plant, the property must be defined essentially at a point. In the case of the grazing plant, the data are required over a larger area which encompasses the grazing pattern. Table 2 lists properties of the current distribution which must be defined to insure a successful design.

The current and temperature requirements can be satisfied by a combination of new observations and re-analysis of historical data. The observational effort now described is minimal, in the sense that if additional funds are available the effort could be expanded. Moorings which provide continuous measurements in time, but normally discrete measurements in the vertical, and site visits by a research vessel, which provide discrete measurements in time, but continuous measurements in the vertical, are required.

Two types of moorings are suggested, a subsurface taut wire current meter mooring and a surface slack wire thermister chain mooring. Separate moorings are recommended in order to obtain temperature data at and near the sea-surface. Surface mooring motions could reduce the usefulness of current meter data placed on such a mooring. Two thermister chains, each 100 m in length, are recommended for the thermister mooring. One chain should be placed immediately below the surface float, and the other in the thermocline.

Two current meter moorings are a minimum requirement to obtain some data on the spatial variability at the site. A 10 km to 25 km separation is probably adequate for the initial deployment to ascertain the representativeness of single point measurements at the site.

Over-the-side operations from a research vessel are required to establish the shape of the vertical profile of horizontal currents. These profiles can be used to place the current meters. For instance, subsurface current maxima and current reversals should be sampled by the current meters. Bimonthly site visits are adequate at this time for the profiling program.

Density data can also be collected during the site visits. An expendable bathythermograph (XBT) grid should be occupied during each visit. A 25 km grid and surveillance of satellite imagery for the region is adequate to insure no significant thermal fronts exist near the site.

Table 1: Properties of the temperature field, their effect on design, and required accuracy and spatial and temporal resolution of an observational program.

Property	Design Requirement	Accuracy	Spatial Resolution	Temporal Resolution	Remarks
1)Temperature distribution a)0-100 m b)900 m -1100 m	Thermal resource Length of cold pipe Size of heat exchanger	±.1°C	a) 0-100 m 10 m's b) 900 m-1100 m 50 m's	daily	Resource determined by a layer of finite thickness; therefore data required over larger interval than merely sea-surface or 1000 m.
2)Mixed layer depth	Depth of intake and discharge Recirculation studies	±10 m		daily	
3)Thermocline depth	Depth of intake and discharge Type of discharge Recirculation studies	±10 m		daily	Seasonal thermocline can cause significant temperature gradients near sea-surface
4)Density distribution	Pumping requirements Effect of discharge on environment	±.0002 gm/cm³	Continuous to 1000 m	seasonal	Salinity observations required to determine density.
5)Horizontal distribution of temperature	Thermal resource Effect of discharge on plant	±.1°C	a) Moored-25 km around site b) Grazing-entire site	bi-monthly	The existence of temperature fronts and their spatial and temporal evolution is required.
6)Extreme events (hurricanes, cold fronts)	Thermal resource	+.5°C	Event spatial scale	Event time scale	Duration of recovery period to pre-event conditions must be determined.

Table 2: Properties of ocean current distribution, their effect on design, and required accuracy and spatial and temporal resolution of an observational program.

Property	Design Requirement	Accuracy	Spatial Resolution	Temporal Resolution	Remarks
1)Vertical distribution of horizontal currents	Mooring Cold water pipe Loading Fatigue Propulsion	± 10° ±5 cm/sec	Minimum -4 depths, 100, 200 m 500 m, 800 m	hourly	Time series required to compute statistics of flow variability. Meter depths can vary depending on local conditions.
	Same as above	±10° ±10 cm/sec	Continuous in vertical	seasonal	Necessary to insure proper placement of current meters.
2) Near-field circulation	Recirculation Environmental impact	±10° ±5 cm/sec	5 km-25 km	hourly	Requires placement of several current meter moorings at site.
3) Large-scale circulation	Environmental impact	±20° ±20 cm/sec	50 km-100 km	seasonal	Circulation patterns can be inferred from geostrophic calculations, drift bottle studies, water mass distributions, etc. Important to define vertical as well as horizontal motions.
4) Extreme events (hurricanes, cold fronts)	Plant survival	±20° ±20 cm/sec	Event spatial scale	Event time scale	Duration of recovery period to pre-event conditions must be determined.

Re-analysis of historical data and some modeling effort are required to provide data on events, and time and space scales which are difficult and/or expensive to measure. For instance, geostrophic current distributions can be generated to study the large-scale circulation and its possible effect on OTEC discharges. Distributions of water mass properties can be used to determine regions of significant vertical motion near the site. Such information is required for impact studies if these motions bring plant discharges into the photic zone. An estimate of the ocean response to severe events can be obtained from analytical and/or numerical models. These events (hurricanes, cold fronts, etc.) are likely to represent the survival conditions for the plant. It is important to use models which have been calibrated with the few available data, and which, in particular, represent the decay stage of the ocean's response to these events. The length of the decay stage will determine, in part, when operations can resume, if they must be discontinued.

Data Requirements Specific to Moored OTEC Plants

The specific data needs of the moored plant design effort are related primarily to the requirements for a mooring and a transmission cable to the shore. Additional current data at the ocean bottom are required to design an efficient anchor. In addition, temperature and current data are required along the transmission cable route from the site to the shore. Data during extreme events are particularly important because of the potential for current scouring around the anchor and other bottom mounted equipment.

Figure 1 represents a suggested mooring array and ship track. This is a minimum array, any additional mooring equipment could be used to obtain more refined estimates of the near-field circulation, for use in recirculation and impact studies. Additional ship time could be used to define vertical

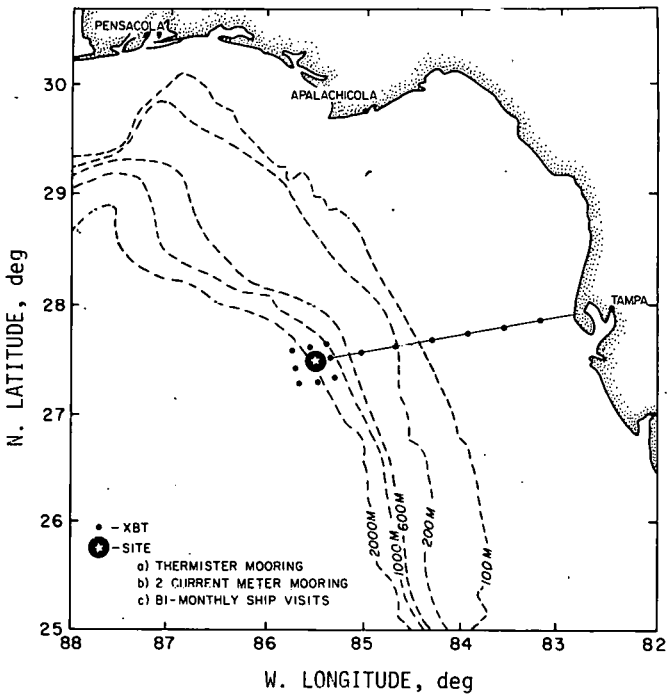

Figure 1. Suggested observational strategy for an offshore OTEC plant site.

profiles of current and density structure. Table 3 gives the data available from each operation shown on Figure 1.

Data Requirements Specific to Grazing OTEC Plants

For grazing plants, environmental data are required over larger areas than in the case of the moored plant.[4] This requirement is important since the plant moves continually to obtain the maximum resource. The spatial character of the thermal

Table 3: Observational strategy for a moored plant site

Data Requirement	Instrument	Deployment Strategy Vertical	Horizontal	Sampling Rates	Remarks
1) Warm water thermal resource, mixed layer depth, thermocline depth	Thermister chain	Two chains a) 0 to 100 m b) Vicinity of thermocline depth	One mooring	hourly	Thermister chains should be deployed from a slack-wire surface mooring. Surface buoy should be instrumented with a meteorological sensor package.
2) Current Profiles	Current meter	Five meters	2 moorings 25 km separation	½ hourly	Meters should be deployed on a taut-wire subsurface mooring in vicinity of important current features, and at ocean floor.
3) Current Profiles	Profiling current meter	Continuous 0 to 500 m	On-site	Continuous 10 hr. station	Continuous station should be longer than semi-diurnal tidal period.
4) Cold water thermal resource, density profiles	STD	Continuous 0-to 1000 m	On-site	Continuous 10 hr. station	
5) Horizontal temperature structure	XBT	Continuous 0 to 750 km	25 km grid around site	Bi-monthly	Needed to study frontal activity near site.
6) Horizontal temperature structure	XBT	Continuous 0 to 750 km	20 km, site to shore	Bi-monthly	Needed to define bottom temperature structure along transmission cable route.

resource (as in the case of the moored plant, defined in terms of the upper water column, rather than merely the sea surface) must be defined. In particular the major length scales of the variability must be determined to develop grazing strategies.

Furthermore, the temporal evolution of the thermal distribution is required. Grazing strategies also are dependent on the time scales of thermal variability, i.e., seasonal, weekly, daily. These strategies in turn determine the requirements for propulsion, a parasitic power drain.

In contrast to moored plant requirements, detailed data on current variability in the horizontal direction as well as the vertical direction are necessary. These data correlated with temperature define the motion of surface waters. In particular, the relation of local heating to advective effects determines local thermal conditions. Propulsion requirements differ for the case of dominant local heating as compared to the case of dominant advective effects.

The observational program for the grazing option, complicated by the large areas to be studied, requires unattended and remote sensing devices. Although satellite observations provide an inexpensive and easy method of obtaining relative surface temperatures (horizontal contours) to indicate the direction for the plant to move,[2] satellite-derived data are insufficient at the present time to satisfy all design needs. For instance, the accuracy of present satellite systems is inadequate to provide accurate measurements of absolute sea surface temperature to satisfy OTEC needs.[5]

Furthermore, neither data on the subsurface thermal field nor data on current structures can be obtained reliably from satellites. These data are best obtained from moored thermister chain and current meter arrays and satellite tracked drifting buoys. The most efficient distribution of thermister moorings can be developed from satellite studies of the distribution of the sea-surface temperature. A minimum of three moorings is recommended. Satellite tracked drifting buoys instrumented with thermister beads can provide data on the distribution of surface currents and the relation of these currents to the sea-surface temperature structure. Finally, some current meter moorings are necessary to sample the sub-surface current structure. These data are particularly important in the tropics where subsurface current reversals and maxima are frequently observed.

Site visits by a research team are required, minimally on a seasonal basis. Continuous vertical profiles of horizontal current are needed to insure adequate coverage from the current meter arrays. In addition, density data can be collected during these cruises. Table 4 presents a suggested measurement program for the proposed grazing plant sites.

Data Reporting and Formats

Three types of reports are planned for the dissemination of thermal and current velocity data collected and analyzed for OTEC. Data reports will contain plots and listings of reduced data. These reports will include descriptions of instruments and analysis techniques applied to the data. Summary reports will summarize one-year long data

Table 4: Observational strategy for a grazing plant site

Data Requirements	Instrument	Deployment Strategy Vertical	Horizontal	Sampling Rates	Remarks
1) Warm water thermal resource, mixed layer depth, thermocline depth	Thermister chain	Two chains a) 0 to 100 m b) Vicinity of thermocline depth	Three moorings, are a minimum deployment. Spacing a function of results of historical data analysis	One to two hours	Thermister chains should be deployed from a slack-wire mooring. Surface buoy should be instrumented with a meteorological sensor package.
2) Current profiles	Current meters	Four meters	Minimum no. of moorings a function of current distribution	One to two hours	Meters should be placed so as sample important current features.
3) Current profiles	Profiling current meter	Continuous 0-500 m	60 to 120 km sampling grid to cover grazing area	seasonal	
4) Surface currents	Drifting buoys	Drogued at 30 m	Minimum deployment 3 buoys; if no data available determine deployment strategy as STD data being collected.	one position/ day	Buoy trajectories can provide current patterns in data sparse areas.
5) Cold water thermal resource and density profiles	STD	Continuous 0 to 1000 m	Same as for 3	seasonal	

sets. The relation of the temperature and current variability to atmospheric and oceanic phenomena will be addressed in an attempt to determine the cause of the variability. These relations are necessary to determine how representative the one-year data set is of longer term conditions. Re-analysis of historical data reports are prepared to present long-time series of data, if they exist, and to address environmental impact questions.

Three types of reports offer temporal resolution of environmental events on different time scales. Data reports present data pertinent to the time-scales ranging from hourly to monthly, with little analysis of the data included. Summary reports will include analysis and discussion of features with time-scales ranging from hourly to seasonal. Re-analysis reports can provide data on long-term and interannual trends and variability.

The format selected to present these data have been determined after discussions with data users both individually and at workshops. As in the case of the observational program, the formats are subject to change depending on the needs of the OTEC program. However, the formats discussed appear best suited for present needs.

The vertical profiles of temperature, salinity, and density obtained during the site visits will be listed in the data reports. In addition, composite plots and time series by cruise of temperature, salinity, and density are given. Figure 2 from Thomas et al.[6], shows examples of composite and time history plots. Listings of profiling current meter data and plots of speed components by station are also included, along with time-series plots of speed components and total speed (Figure 3).

Time-series plots of raw and filtered current meter data are generated for inclusion into the data reports (Figures 4 and 5). Histograms of current speed and direction (Figure 6) are given to demonstrate the observed variability. Time-series plots of raw thermister chain data similar to Figure 2, but with more detail, are constructed and put into the data reports.

Summary reports are to include data on the thermal variability on time-scales ranging from diurnal to seasonal. Plots and/or listings of diurnal variability of sea-surface temperature, upper layer temperatures, mixed layer depth, etc. are constructed by cruise, if no thermister data exist, or by month if thermister data exist.

The seasonal evolution of both the temperature and density mixed layer and seasonal thermocline will be shown as composite and time-series plots such as shown on Figure 2. If subsurface inversions exist, particularly during the winter, their characteristics will be quantified.

Temperature spectra will be computed from the temperature sensors on the current meter and thermister chains (Figure 7). In addition, histograms defining percent occurrences of thermal resource, mixed layer depth, etc. are given (Figure 8). Horizontal charts of the temperature distribution at various depths are necessary to identify any frontal activity in the region.

Stick plots presenting average velocities for various time intervals are constructed (Figure 9). Tables of major tidal constituents at the current meter depths are computed. In addition, spectra are computed to quantify the current variability (Figure 10).

The meteorological and oceanographic phenomena likely to impact on the site are to be identified. For instance, Figure 11 shows the wind speed and air temperature observed at a site, in addition to frontal passages. These data, when compared to

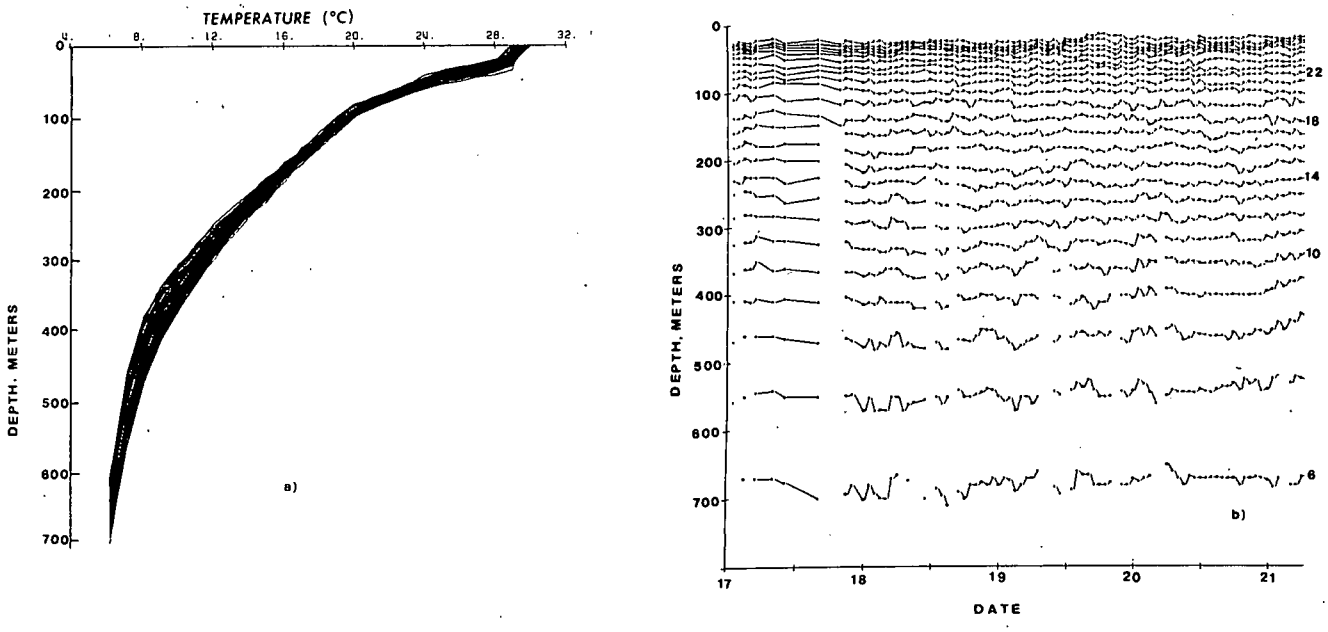

Figure 2. Composite (a) and time-history plots (b) of temperature observations taken by XBT's in July 1977 at the Mobile site in the Gulf of Mexico (from Ref. 6).

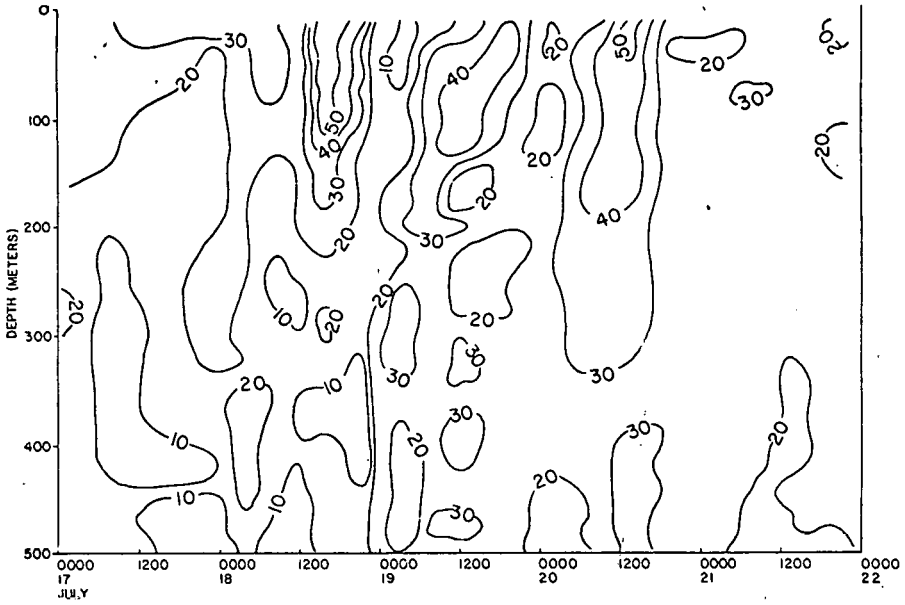

Figure 3. Time series plot of total speed (cm/sec) obtained by a profiling current meter at the Mobile site in the Gulf of Mexico.[6]

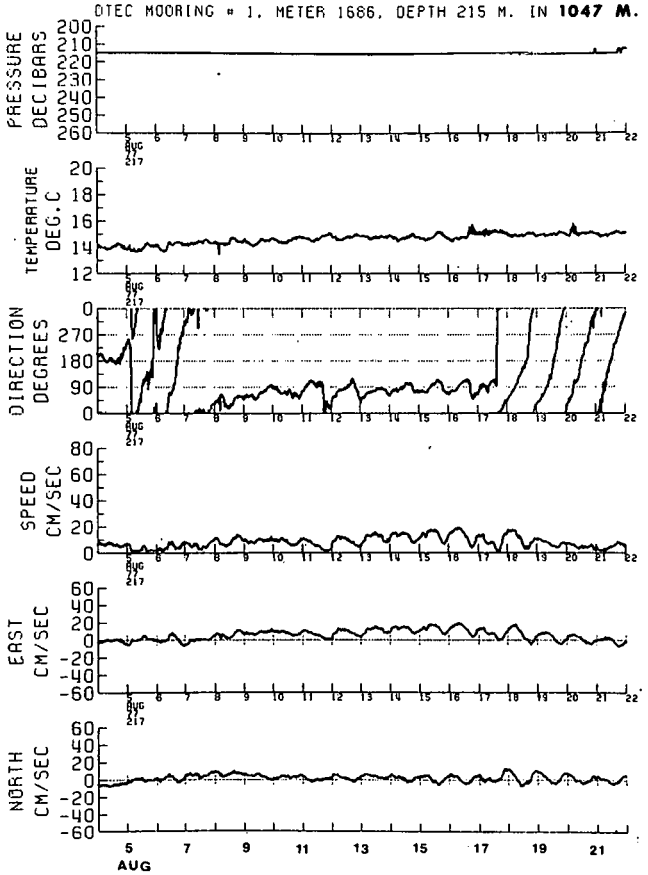

Figure 4. Time series plot of raw current meter data obtained at the Mobile site in the Gulf of Mexico.[6]

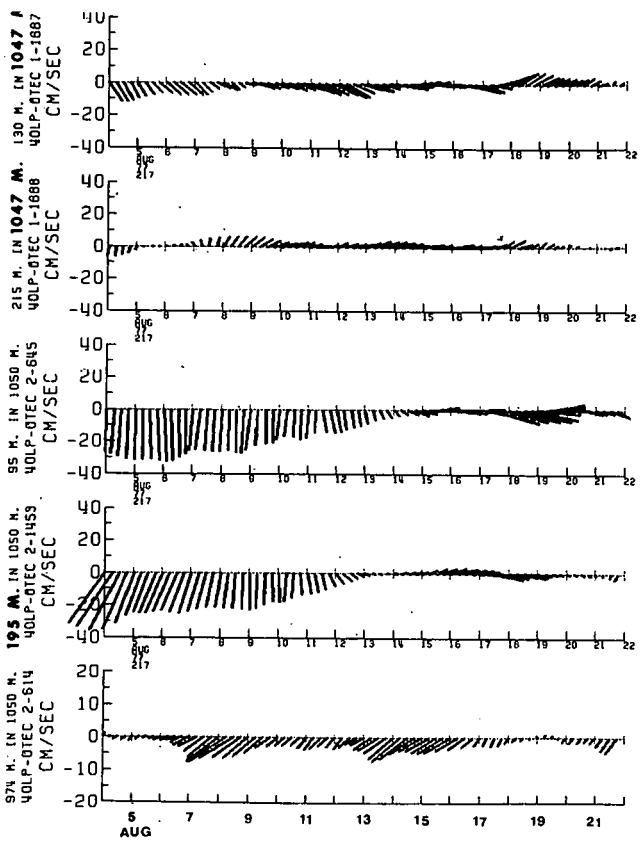

Figure 5. Time series plot of smoothed current meter data obtained at the Mobile site in the Gulf of Mexico.[6]

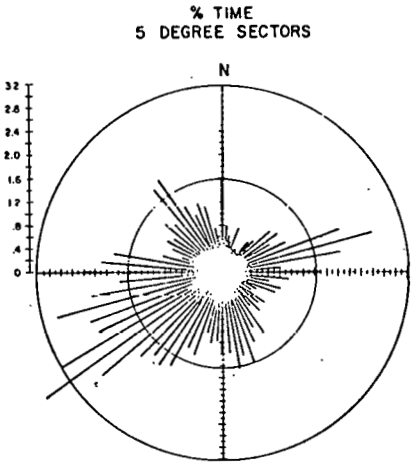

OTEC MOORING 1
METER 1686
DEPTH 215 METERS

Figure 6. Current histogram representing per mil occurrences in each 10° direction and 5 cm/sec interval.[6]

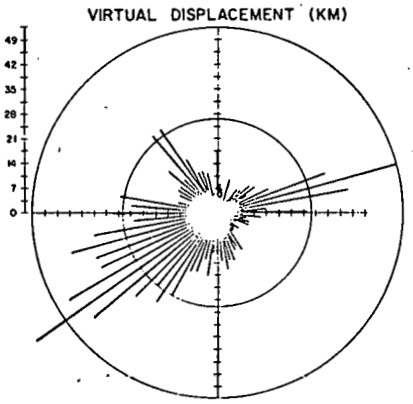

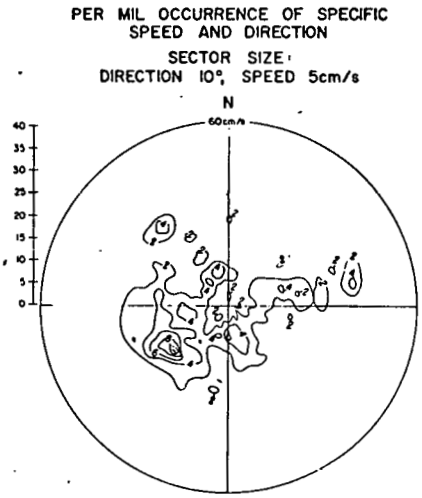

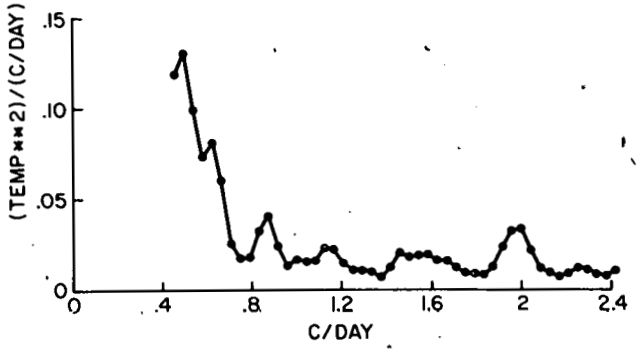

Figure 7. Typical temperature spectra showing high energy at low frequency.

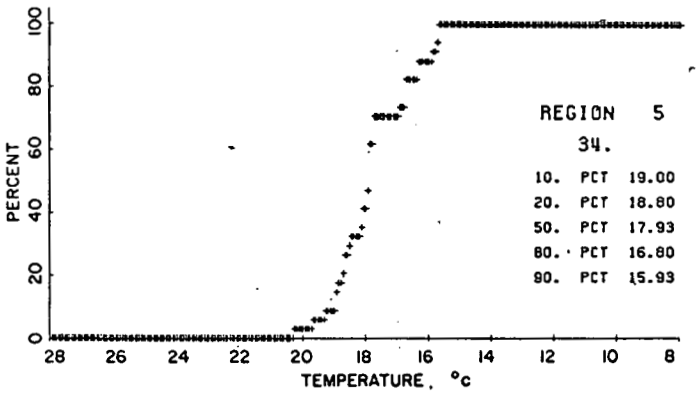

Figure 8. Histograms showing percent occurrences of thermal resource (ΔT, °C, 0-1000 m) greater than a given ΔT for an area encompassing the Mobile site, January to March 1978.[1]

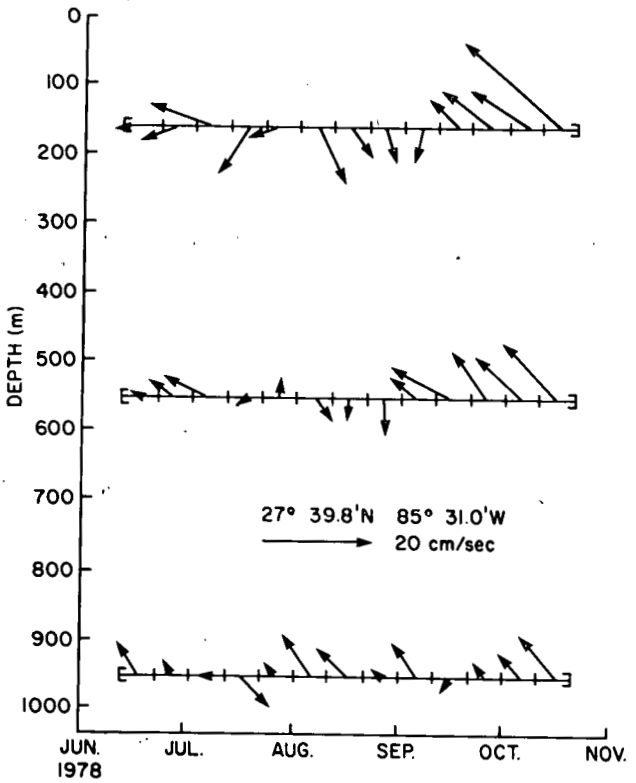

Figure 9. Stick plots representing ten-day average currents at various depths from data collected at the Tampa site.

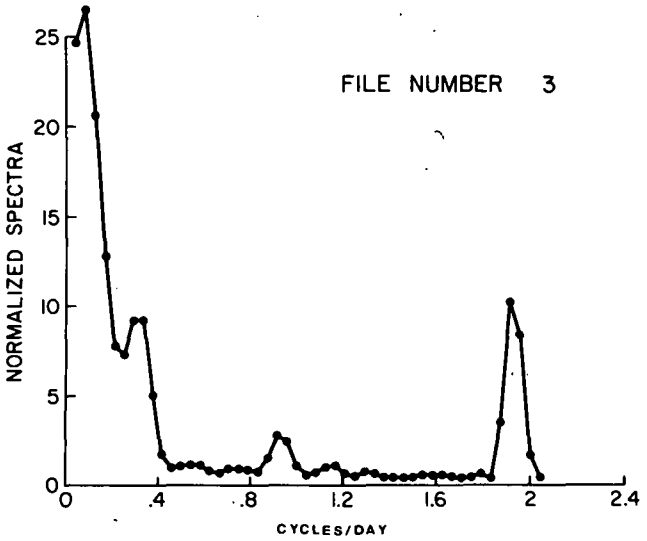

Figure 10. Typical current spectra where semi-daily tidal energy exceeds daily tidal energy.

climatological data, will provide a measure of the representativeness of the one-year data-set.

Data available from historical studies at the site are also included in the summary report. For instance, time-series plots of sea-surface temperature in the vicinity of the site, and subsurface vertical sections can be constructed for a site in the Gulf of Mexico (Figure 12, for instance). These plots provide additional information on inter-annual variability and the representativeness of the one-year data set. Drift bottle data can provide qualitative information on surface currents near the site (Figure 13), and should be included in the summary report if they exist.

An adequate historical data set can be re-analyzed to provide baseline design information, to plan observational programs, to provide environmental impact data, and to define areas which require further study. For instance, basin wide maps of thermal resource can be produced for siting studies (Figure 14). Major current patterns can be deduced from average dynamic height maps (Figure 15). The impact of these currents on OTEC operations and vice versa can then be ascertained (Table 5).

Discussion

Ideally, the data collection and formatting effort will evolve with the design effort. More detailed oceanographic data will be required as the plant design becomes more refined. Thus, this manuscript should be considered more a working document than the final data collection plan. This evolution can occur only if there is a constant interchange between data generators and data users. Thus, any comments on the data collection effort and formats should be forwarded to the Department of Energy, to insure a steady stream of required data to the OTEC program.

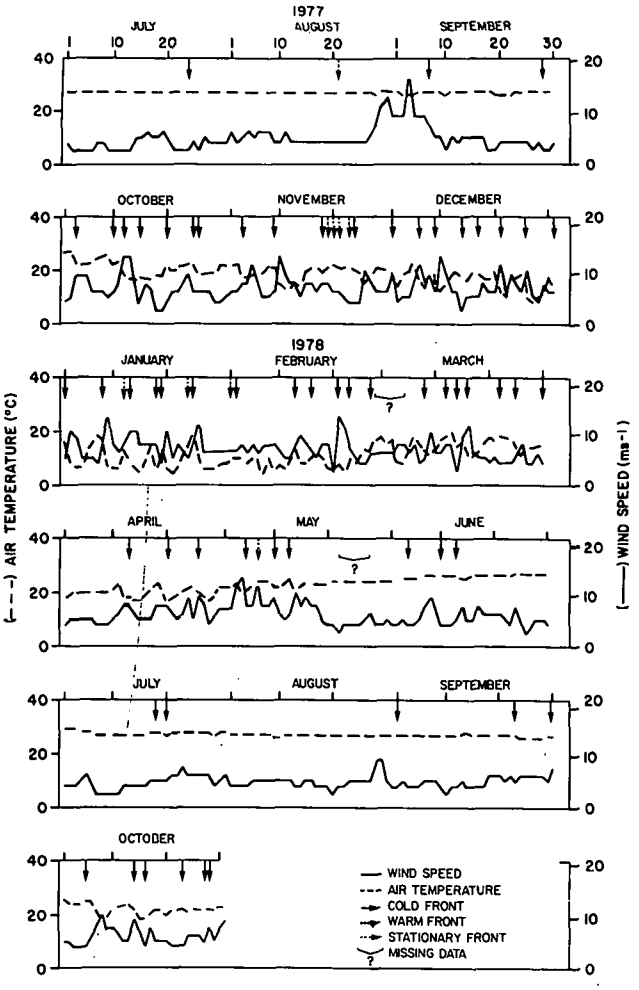

Figure 11. Wind and air temperature observations at the Mobile site. Also shown are frontal passages.

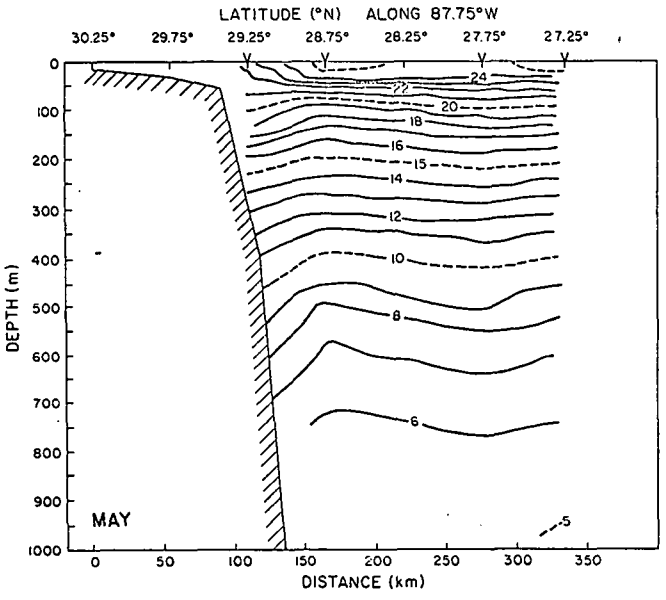

Figure 12. Vertical section of temperature for the region near the Mobile.

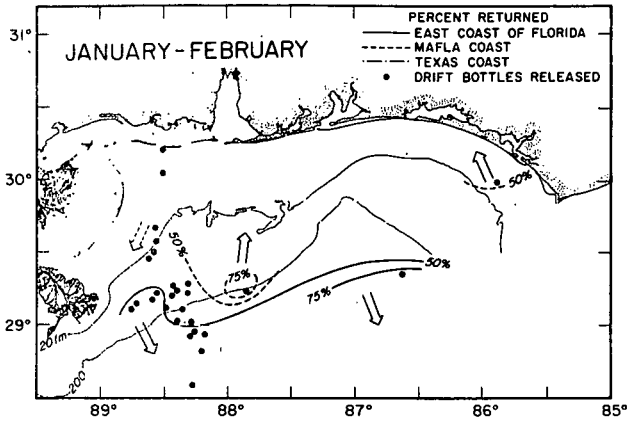

Figure 13. Summary of results of drifting bottle experiment conducted near the Mobile site. Numbers represent percentage of drifters recovered, not deployed. MAFLA refers to recoveries on the Mississippi, Alabama and Louisiana coasts.

Acknowledgment

This work was funded by the Department of Energy through Interagency Agreement EX-76-A-29-1041, Task Order T027 with the National Oceanic and Atmospheric Administration.

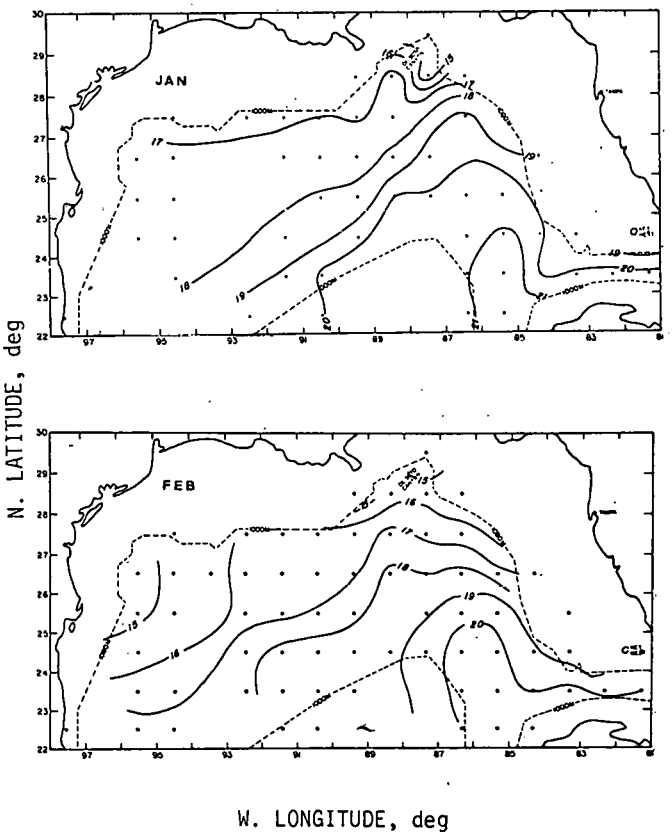

Figure 14. Gulf-wide thermal resource distributions computed on a 1° x 1° grid (ΔT's in °C).[1]

Table 5. Summary of thermal and velocity characteristics of the major currents in the Gulf of Mexico relative to the placement of an OTEC PLANT, and the possible impacts of these currents.

Currents	Characteristics				Impact				
	Scale		Thermal	Current	Resource	Design	Operation	Biofouling Corrosion	Environmental
	Vert.	Hori.							
Yucatan Current	1500m	100km	a) Looking downstream warmest water to the right b) Large slopes in isothermal surfaces, which rise from east to west in Yucatan Strait	a) Speeds approaching 2.5 m/sec in axis	a) Source of warm water to Gulf in winter b) Source of deep cold water			a) Transports tropical biological and chemical species into the Gulf	a) Same advection of water out of Gulf in Yucatan Strait: impacts on residence time of OTEC discharges
Loop Current	1500m	100km	a) Same as (a) for Yucatan Current b) Large slopes in surfaces which rise from right to left looking downstream. c) Encompasses a core of warm water	a) Speeds approaching 2m/sec in axis	a) Can increase resource in winter b) Currents can serve to reduce potential for recirculation	a) Large speeds a factor in design	a) When Loop present-increase in thermal resource b) If grazing plant-increase in parasitic power loss due to station keeping	a) Replace Gulf species with tropical species	a) Current can advect away plant discharges reducing concentrations in plant vicinity
West Florida Current	Same As For Loop Current →								

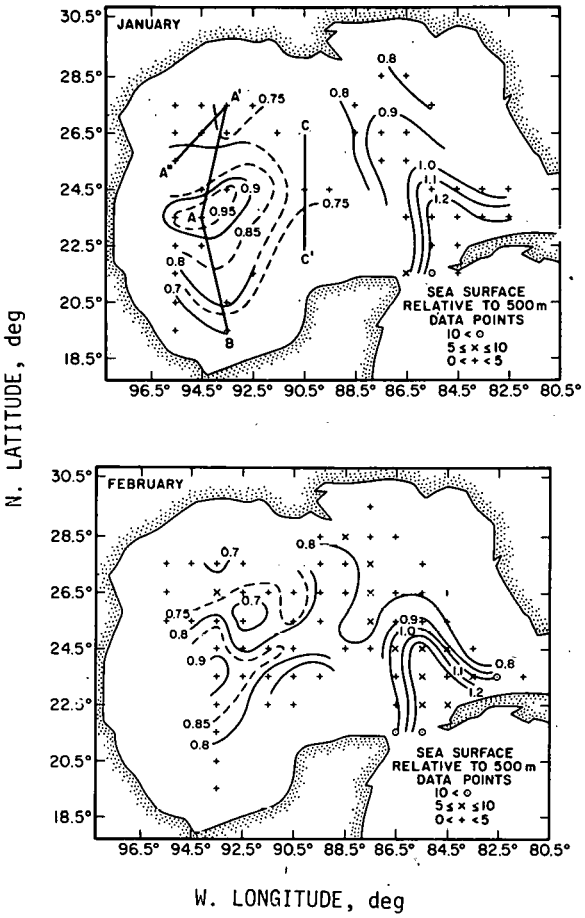

Figure 15. Gulf-wide dynamic topography distributions computed on a 1° x 1° grid from mean monthly dynamic height data.[3]

References

[1]Molinari, R. L. and J. F. Festa, "Ocean Thermal and Current Velocity Requirements for Design of an OTEC Demonstration Plant," NOAA Tech. Memo. ERL AOML-30, 1978.

[2]Hill and Dugger, this conference.

[3]Molinari, R. L. and F. Chew, "Ocean Thermal and Current Structures in the Tropical South Atlantic Relative to the Placement of a Grazing OTEC Plant," NOAA Tech. Memo. ERL AOML-35, 1979.

[4]Avery, W. H., "Ocean Thermal Energy Status and Prospects," Mar. Tech. Soc. Jour., 12, 916, 1978.

[5]Maul, G. A., this conference.

[6]Thomas, G. G., S. M. Minton and R. L. Molinari, Data from the Atlantic Oceanographic and Meteorological Laboratories OTEC Plant Study in the Gulf of Mexico," NOAA Tech. Memo. ERL AOML-34, 1979.

THERMAL AND CURRENT DATA FROM THE GULF OF MEXICO AND SOUTH ATLANTIC RELATIVE TO PLACEMENT OF OTEC PLANTS

Robert L. Molinari*

Atlantic Oceanographic and Meteorological Laboratories
National Oceanic and Atmospheric Administration
15 Rickenbacker Causeway
Miami, Florida 33149

Abstract

Temperature and current data required for design of Ocean Thermal Energy Conversion (OTEC) plants have been collected at two proposed sites in the Gulf of Mexico, south of Mobile and west of Tampa, and in the tropical South Atlantic east of Brazil. The The Gulf sites are proposed as possible locations for moored plants and the South Atlantic site for grazing plants. The seawater temperature difference (ΔT) between 0 and 1000 m at the Mobile site for the July 1977 through October 1978 period ranged from an August maximum of 24.7°C to a February-March minimum of 10.5°C. The ΔT's at Tampa from March through October 1978 ranged from a low of 15°C to a high of 24°C. The July-August ΔT's of the South Atlantic site ranged from a low of about 21.4°C to a high of 22.5°C. Current speeds at Mobile at 90 m ranged from about 5 to over 30 cm/sec during all months; at 1000 m, from 2 to 15 cm/sec. The maximum speed observed at 90 m at Mobile was 60 cm/sec. Similar speeds were observed at Tampa. The highest surface speeds in the South Atlantic were about 50 cm/sec. From 3°S to 5°S, the surface flow was to the west, but the subsurface flow was to the east, as speeds as high as 30 cm/sec.

Introduction

Physical oceanographic data have been collected at two potential OTEC sites in the Gulf of Mexico and one in the tropical South Atlantic. Current meter moorings have been deployed at 29°N, 88°W, approximately 150 km due south of Mobile, for 15 months and at 27.5°N, 85.5°W, approximately 275 km due west of Tampa (Fig. 1), for eight months. Bimonthly site visits were made to the Tampa and Mobile sites from June through October 1978. Ship-of-opportunity

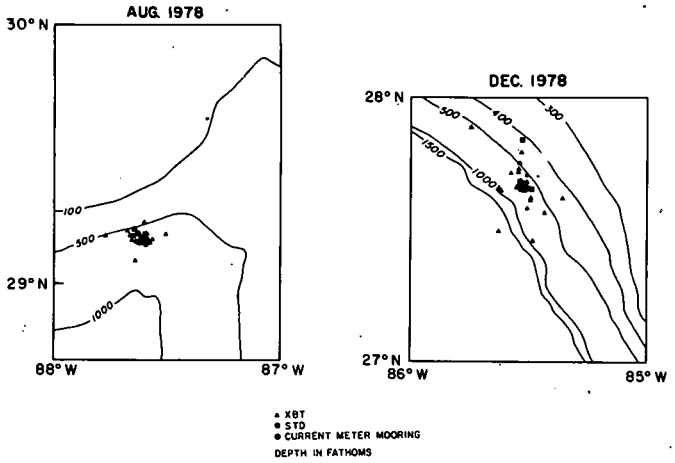

Fig. 1. Sample site occupations at the Mobile (left) and Tampa (right) sites.

Table 1: Timetable of measurement program

	J	A	S	O	N	D	J	F	M	A	M	J	J	A	S	O	N
Mobile																	
a) Site visits	X				X			X		X		X			X		X
b) Current meters	D X				D X R			D X R				D X R					X R
Tampa									X	X		X		X			X
b) Current meters												D X					D X R
South Atlantic													X				
b) Current meters													X D				

D = deployed
R = recovered

*Physical Oceanography Laboratory

visits were made to the Mobile site from July 1977 through June 1978; to the Tampa site from March 1978 through June 1978; and to the South Atlantic during July-August 1978.

The data are part of a package required to characterize the environmental conditions at these sites. The specific needs for these data relative to evaluating the potential of a site for OTEC operations have been given in Molinari and Festa[3] and Molinari and Chew.[2] The data needs are to characterize a) the effect of plant operations on the environment and b) the effect of the environment on plant operations. Table 1 shows the timetable of site visits and current meter records through 1978. During the site visits, expendable bathythermograph (XBT), STD and profiling current meter data were collected to obtain profiles, which are continuous in the vertical, of temperature, density and current. These data supplement the continuous records in time of currents and temperature collected at discrete positions in the vertical by the current meters.

The original data used to plot Figs. 1 and 2 are listed in Thomas et al.[7] and Molinari et al.[6] Preliminary site characterizations based on re-analysis of historical data are given in Molinari and Festa[3] and Molinari and Chew.[2] The final report describing the results of the one-year measurement program conducted at Mobile is given in Molinari et al.[6]

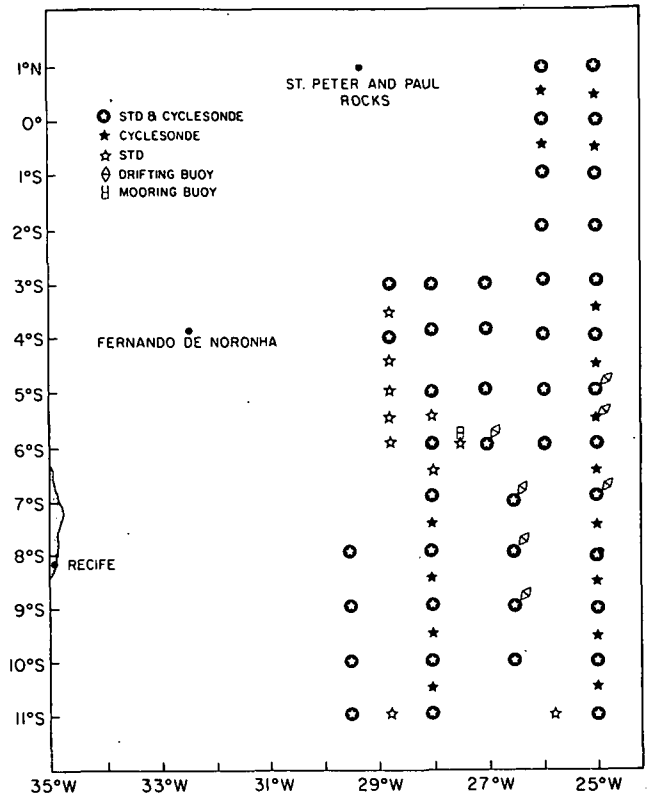

Fig. 2. Trackline occupied in the tropical South Atlantic during July-August 1978.

Large-Scale Meteorological and Oceanographic Conditions

The temperature and current fields at the Gulf of Mexico site are affected by both meteorological and oceanographic phenomena. Comparison of mean monthly meteorological conditions observed at the Mobile site for the period 1977-1978 with mean conditions observed during the period 1960-1973, indicate that the air temperatures of the winter of 1977-1978 were considerably lower than normal (Fig. 3). The summer air temperatures of 1977 and 1978 were closer to normal. The mean monthly wind speeds and directions for 1977-1978 were close to the monthly means obtained from the longer record. A similar analysis has not yet been performed for the Tampa site, but the results should be similar.

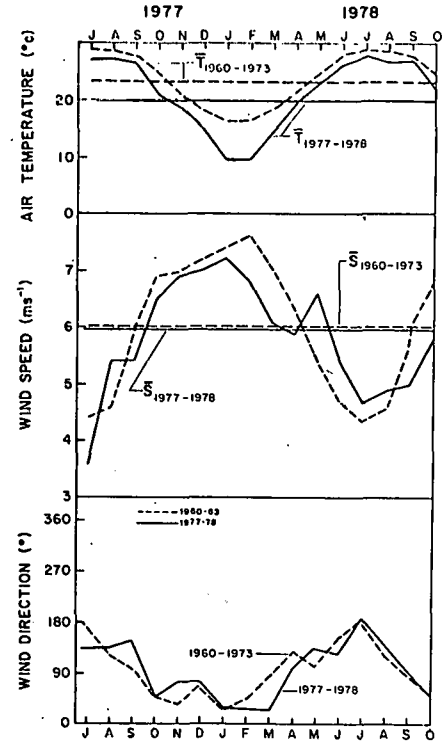

Fig. 3. Mean monthly air temperature, wind speed, and wind direction determined from data collected from July 1977 through October 1978, $\bar{T}$ 1977-1978, and from a data set obtained from 1960 through 1973, $\bar{T}$ 1960-1973 (from Molinari, et al., 1979).

The Loop Current is a major circulation feature in the eastern Gulf of Mexico (Molinari & Festa[4]). Loop Current positions were generated from ship and satellite data and are shown in Fig. 4. The Loop was far to the south during the summer of 1977, gradually penetrating to the north during the late fall and winter. Maximum penetration of the Loop was in the late spring, with an eddy separating sometime in May or June. The Loop did not intrude north again until the fall of 1978. Thus, the Loop was closest to both sites during May and June, 1978. The intrusion cycle of the Loop Current observed during 1977-1978 is similar to the average intrusion cycle described by Behringer et al.[1]

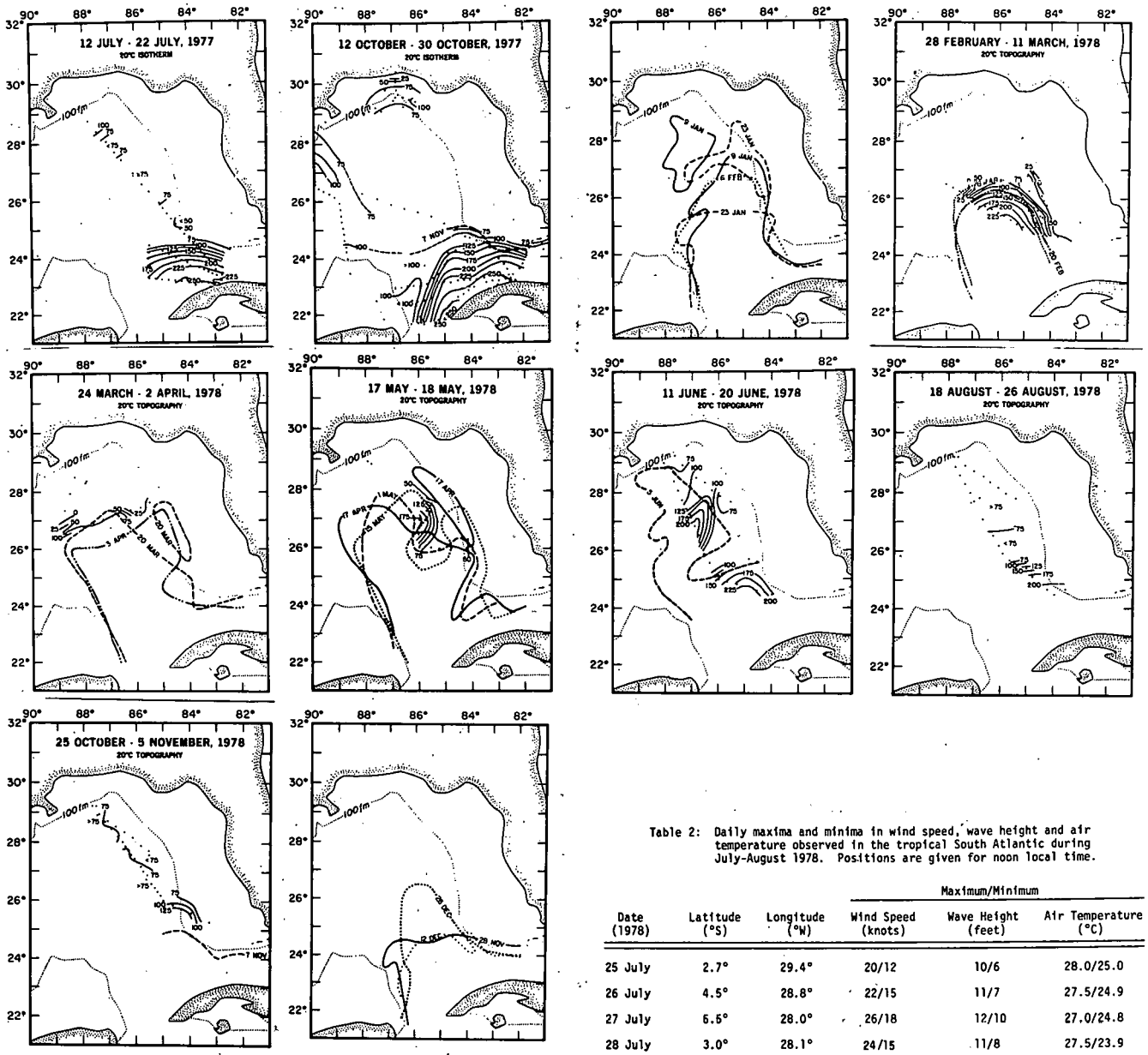

Fig. 4. Distributions of the depth of the 20°C and positions of the axis of the Loop Current determined from satellite imagery. The 150 m contour of the 20°C surface is located near the axis of the Loop Current.

A detailed analysis determining the large-scale meteorological and oceanographic conditions in the tropical South Atlantic has not yet been performed. In qualitative terms, the July-August 1978 cruise was conducted during the Southern Hemisphere winter when the southeast trades should be the strongest. Table 2 lists daily maxima and minima in the wind speed, sea height and air temperature observed during the July-August 1978 cruise.

Table 2: Daily maxima and minima in wind speed, wave height and air temperature observed in the tropical South Atlantic during July-August 1978. Positions are given for noon local time.

Date (1978)	Latitude (°S)	Longitude (°W)	Maximum/Minimum Wind Speed (knots)	Maximum/Minimum Wave Height (feet)	Maximum/Minimum Air Temperature (°C)
25 July	2.7°	29.4°	20/12	10/6	28.0/25.0
26 July	4.5°	28.8°	22/15	11/7	27.5/24.9
27 July	6.5°	28.0°	26/18	12/10	27.0/24.8
28 July	3.0°	28.1°	24/15	11/8	27.5/23.9
29 July	4.5°	27.0°	21/14	10/8	27.0/24.5
30 July	6.0°	26.0°	22/13	10/6	27.0/24.0
31 July	3.0°	26.0°	17/10	7/5	28.0/24.0
1 August	0.5°	26.0°	20/10	5/3	27.0/24.0
3 August	1.0°	25.0°	23/14	10/6	26.0/23.0
4 August	3.8°	25.0°	24/16	10/8	26.5/23.5
5 August	6.5°	25.0°	22/12	13/8	27.0/24.0
6 August	9.0°	25.0°	22/15	13/6	26.0/23.0
7 August	11.0°	25.1°	28/16	13/6	25.5/22.0
8 August	8.0°	26.5°	28/14	8/6	26.0/22.0
9 August	6.0°	27.5°	19/12	7/5	27.0/23.8
10 August	8.0°	28.0°	20/14	7/7	27.0/23.0
11 August	10.5°	28.0°	22/12	8/5	25.0/22.0
12 August	10.0°	29.5°	24/8	8/4	26.0/23.9
13 August	8.0°	30.1°	24/17	10/8	27.0/24.5

Site Specific Thermal Resource Data

Gulf of Mexico

Composite temperature plots for the Mobile and Tampa sites are given in Figs. 5 and 6. The winter traces at the Mobile site show the presence of inversions just below the sea-surface. The summer traces indicate that strong seasonal thermoclines develop immediately below the sea-surface.

The warm water resource will be a layer of finite thickness rather than merely the plane of the sea-surface. Thus, it is not sufficient to consider only the sea-surface temperature (SST) when defining the thermal resource, because of the presence of inversions and seasonal thermoclines at the Gulf sites. Therefore, average temperatures for several layers of varying thickness are given as potential warm water resource layers. The cold water resource is taken as 5°C at Mobile (Molinari et al.[6]) and Tampa. Average thermal resources computed for the sea-surface, upper 20 m and upper 40 m relative to 1000 m are given in Table 3 for data collected during the site visits. The upper layers seem to warm quicker at Tampa, with April temperatures at Tampa some 2°C higher than those at Mobile. Both sites exhibit similar resources from June through October 1978.

Some information on the higher frequency variability of the thermal resource can be inferred from data obtained during the site visits. Table 4 gives the minimum and maximum temperatures and the standard deviations about the mean (Table 3) for the site visit data. The range between minimum and maximum temperatures for the three layers is generally less than 1°C, with the majority of the temperatures falling within ±.5°C of the respective means.

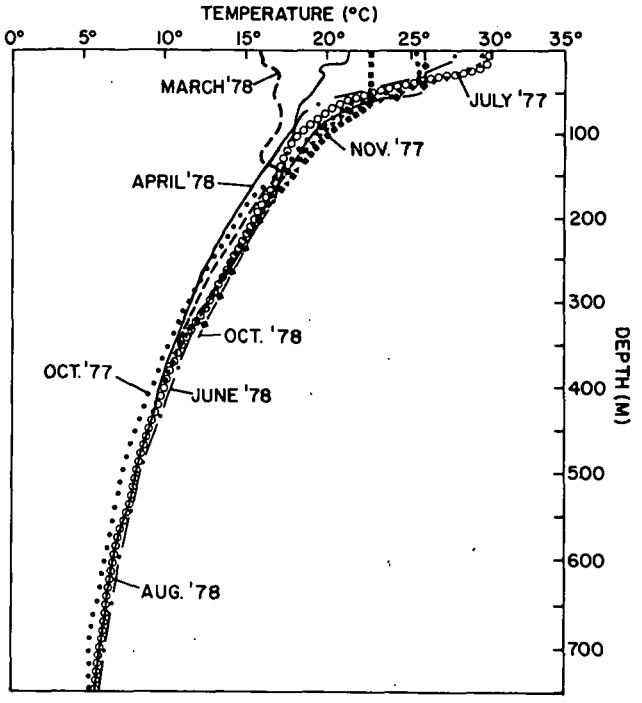

Fig. 5. Representative XBT traces from Mobile site visits.

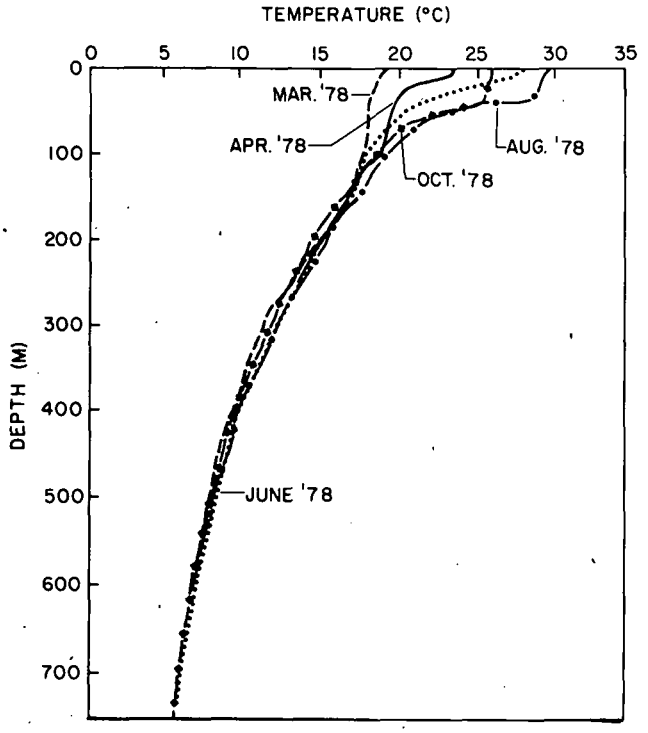

Fig. 6. Representative XBT traces from Tampa site visits.

The mixed layer and thermocline depths are required for the successful design of an OTEC plant.[2,3] For purposes of this report, two mixed layer depths are defined; the first depth at which the temperature is 0.2°C colder than the SST, and the first depth at which the temperature is 0.4°C colder than the SST. In winter, the temperature of the mixed layer is frequently higher than the SST because of inversions. Table 5 lists average mixed layer depths observed during the site visits. The range of mixed layer depths is quite large, from less than 10 m in the summer to greater than 200 m in winter.

The thermocline depth is taken as the depth of the 12°C isotherm. This isotherm is at the bottom of the main thermocline. Temperature gradients above 12°C are about 1°C/25 m and decrease to about 1°C/50 m below 12 C. The average thermocline depths observed during the site visits are given on Table 6. Throughout the year, the bottom of the thermocline is about 300 m.

South Atlantic, July-August 1978

Figure 7 is the plot of the distribution of the mixed layer depth, defined as the first depth at which the temperature is 0.2°C less than the SST. The 0.4°C less than SST depths are not shown because these depths are almost identical to the 0.2°C depths. The mixed layer is shallowest in the far northeastern corner of the survey area, where depths less than 50 m are observed. Throughout most of the OTEC area, 5°S to 10°S and 25°W to 30°W, the mixed layer is greater than 90 m.

Because of the deep mixed layer, the SST is sufficient to define the warm water resource for this period of time. Figure 8 shows the SST and $T_{1000\ m}$

Table 3: Available thermal resource (°C) between the sea-surface and 1000 m (A), the upper 20 m and 1000 m (B), and the upper 40 m and 1000 m (C). The temperature at 1000 m is taken as 5°C.

Year	Date	Number of Data Points	A		B		C	
			Mobile	Tampa	Mobile	Tampa	Mobile	Tampa
1977	17-21 July	25	24.2		24.1		23.0	
	18 October	1	20.4		20.7		20.9	
	18-20 November	16	17.5		17.5		17.4	
	1 December	2	18.4		18.4		18.4	
1978	26 Feb-2 March	28	10.5		10.6		11.0	
	24 March	7		15.0		14.2		13.7
	26 March	1	13.7		14.0		14.1	
	2 April	6		18.3		18.0		17.4
	12 April	4		18.4		17.4		16.3
	13 April	3	16.1		15.6		15.0	
	12-14 June	15		23.0		22.0		20.2
	14-16 June	19	23.1		22.1		20.6	
	18-21 August	14		24.7		24.5		23.3
	21-23 August	13	24.7		24.4		23.5	
	25-28 October	17		20.7		20.7		20.1
	30 Oct-3 Nov	20	20.4		20.5		20.6	

Table 4: Minimum (1) and maximum (2) temperatures (°C) at sea surface (A), and minimum (1) and maximum (2) values of the average temperature of the upper 20 m (B) and the upper 40 m (C). Also given are standard deviations (3) about the mean.

Year	Date	Number of Data Points	A						B						C					
			Mobile			Tampa			Mobile			Tampa			Mobile			Tampa		
			1	2	3	1	2	3	1	2	3	1	2	3	1	2	3	1	2	3
1977	17-21 July	25	29.0	29.8	.2				28.8	29.6	.2				27.5	28.5	.2			
	18-20 November	16	22.2	22.7	.1				22.2	22.6	.1				22.2	22.6	.1			
1978	28 Feb-3 March	28	14.4	16.7	.6				15.1	15.2	.2				15.6	16.6	.3			
	12 April	4				23.2	23.7	--				21.9	22.8	--				21.7	21.7	--
	13 April	3	20.7	21.3	--				20.0	21.0	--				19.6	20.0	--	24.7	25.8	.3
	12-14 June	19				27.7	28.4	.1				26.8	27.4	.2	24.7	26.8	.5			
	14-16 June	15	27.7	28.8	.2				26.5	27.9	.3							27.2	28.8	.3
	18-21 August	15				29.4	30.3	.2				29.3	29.7	.1	25.2	25.8	.3			
	21-23 August	13	29.7	30.5	.2				29.6	30.1	.1							25.4	25.7	.1
	25-28 October	17				25.5	26.0	.1				25.5	25.9	.1	25.4	25.8	.1			
	30 Oct- 3 Nov	20	25.2	25.8	.2				25.2	25.8	.1									

Table 5: Average mixed layer depths (m) defined as the first depths at which the temperature is 0.2°C (A) and 0.4°C (B) lower than SST. Also shown in parenthesis is the standard deviation (in m) about the mean.

Year	Date	Number of Data Points	A		B	
			Mobile	Tampa	Mobile	Tampa
1977	17-21 July	25	20 (± 3)		23 (± 2)	
	18-20 November	16	60 (± 17)		72 (± 6)	
	1 December	2	60		60	
1978	28 Feb-2 March	8*	6 (± 4)			
		20*	202 (± 17)			
		27			201 (± 19)	
	12 April	3		5		7
	13 April	3	14		16	
	12-14 June			7 (± 3)		8 (± 3)
	14-16 June	18	7 (± 4)		8 (± 3)	
	21-23 August	13	7 (± 2)		11 (± 4)	
	25-28 October			26 (± 12)		37 (± 7)
	30 Oct-3 Nov	20	49 (± 4)		50 (± 4)	

*The distribution is strongly bimodal because of the occurrence of inversions. Therefore, averages for each mode are given.

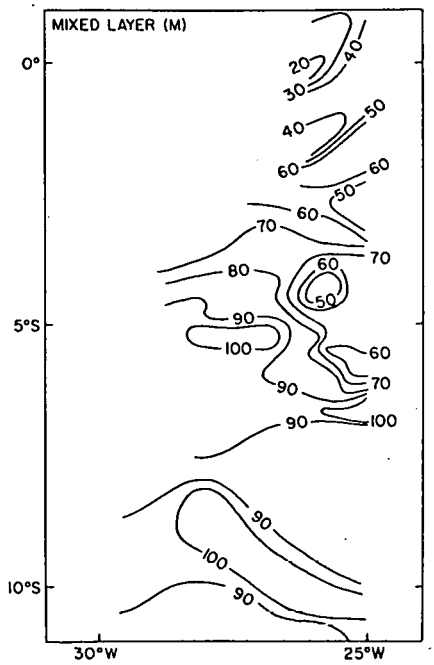

Fig. 7. Depth of the bottom of the mixed layer (m), taken as the first depth at which the temperature is 0.2 C colder than SST, obtained from data collected in July-August 1978 for the South Atlantic site.

Table 6: Average depth of the bottom of the thermocline (taken as the depth of the 12°C isotherm, see text) observed during the site visits.

Year	Date	Number of Data Points	Depth of the bottom of the thermocline: Mobile	Tampa
1977	17-21 July	25	291 (± 7)	
	18-20 November	15	316 (± 25)	
	1 December	2	298	
1978	28 Feb-2 March	28	304 (± 6)	
	24 March	7		299 (± 15)
	12 April	3		319
	13 April	3	292	
	12-14 June	15		326 (± 4)
	14-17 June	18	330 (± 7)	
	18-21 August	14		347 (± 7)
	21-23 August	13	283 (± 9)	
	25-28 October	17		295 (± 9)
	30 Oct-3 Nov	20	343 (± 11)	

distributions. The SST's south of 5°S range from 25.4°C to 26.4°C. The highest SST's appear as a tongue centered just south of 5°S. A temperature front appears at about 26°W between 5°S and 7°S. A cell of colder water appears at 27°W and 7°S. This feature may be a manifestation of the front observed along 26°W, after it has advected to the west.

The temperatures at 1000 m south of 5°S are about 4°C. Thus, the thermal resource ranges from about 21.4°C to 22.4°C during the observational period. The quarterly average ΔT's for July-September computed from a very small historical data set range from about 20.5°C to 22°C.[2] Thus, the thermal resource observed during July-August, 1978 appears within the range of "normal" conditions.

Figure 9 shows some vertical temperature sections. The large temperature gradients representing the thermocline begin to weaken at about the 10°C isotherm. If this isotherm is taken as the bottom of the thermocline, thermocline depths south of 5°S range from about 250 m to 300 m.

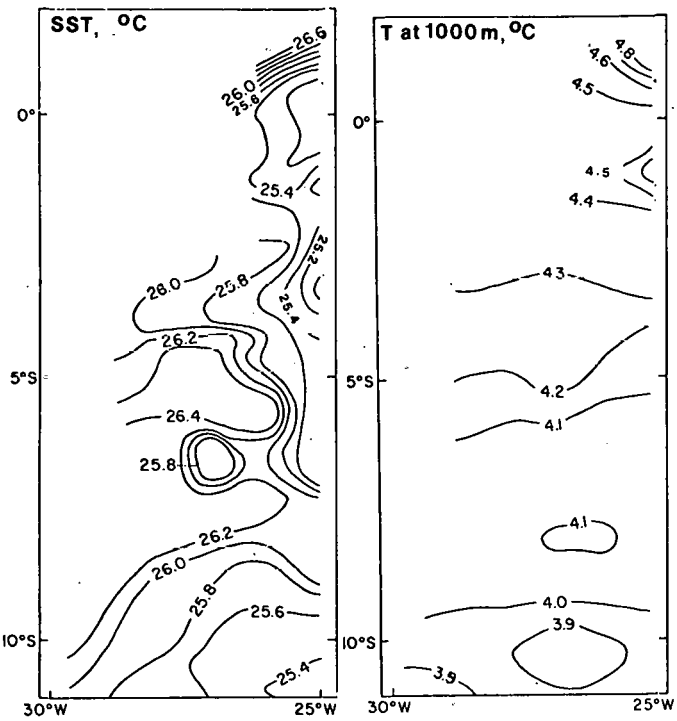

Fig. 8. SST (left) and 1000 m (right) distributions (°C) observed during the period July-August 1978 in the South Atlantic site.

Site Specific Ocean Current Conditions

Gulf of Mexico

Current meter data are available at the Mobile site from 18 July 1977 through 16 August 1978. The array was moored at 29°6.5'N, 87°55.1'W from July through October 1977 and at 29°11.4'N, 87°38.2'W from October 1977 through August 1978 (Fig. 1). Data collected at the Tampa site, 27°39.8'N, 85°31.0'W, from June through October 1978 have been analyzed.

Figure 10 is a stick plot showing ten-day average current vectors. Considerable variability is obvious in these ten-day average data. A measure of this variability can be obtained from histograms of speed constructed from the data. Table 7 summarizes the results of the histograms for the various deployment intervals. Figure 11 shows the maximum speeds observed during each month of observation.

There appears little difference in the seasonal ranges of current speeds at the three depths sampled at Mobile (Table 7). For instance, the speeds at 70 m to 95 m range from about 5 cm/sec to 30 cm/sec. Those at 980 m range from about 2 cm/sec to 15 cm/sec.

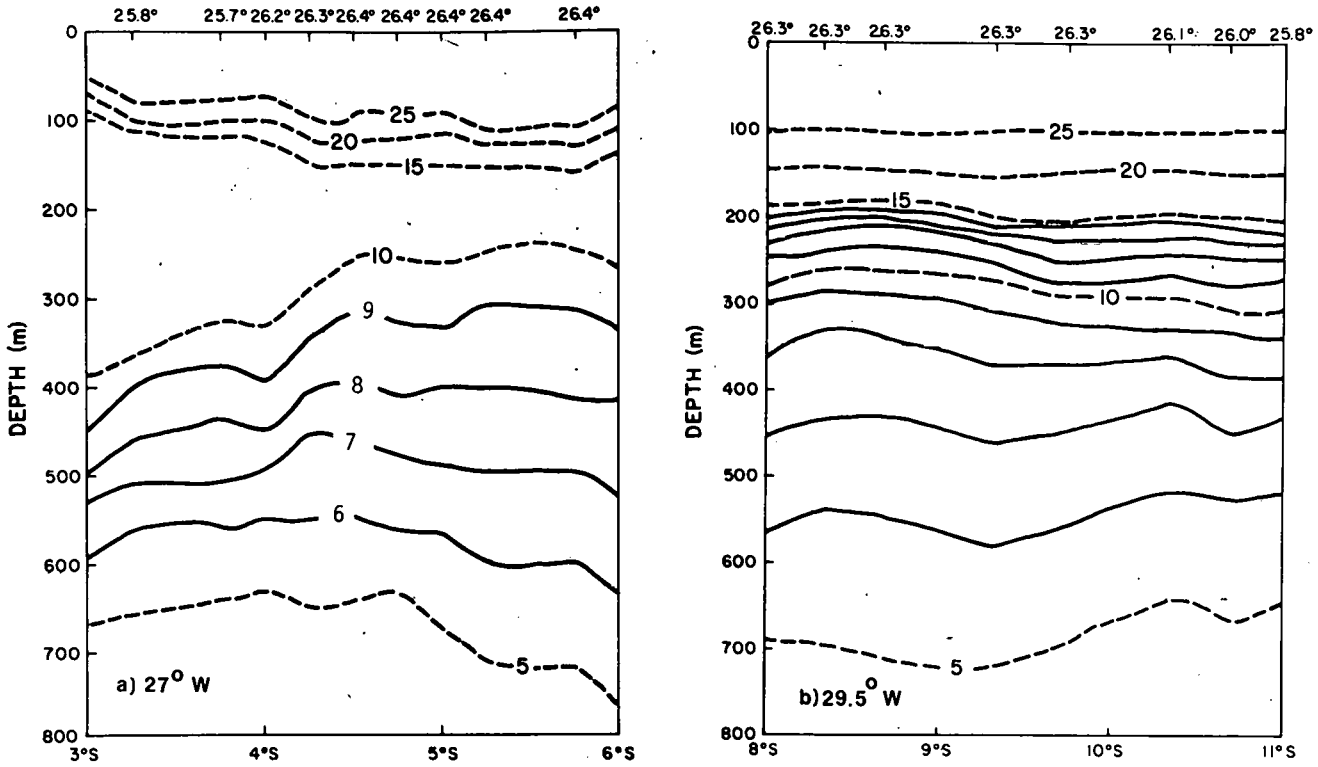

Fig. 9. Vertical section of temperature observed at 27° and 29.5°W, South Atlantic site, July-August 1978.

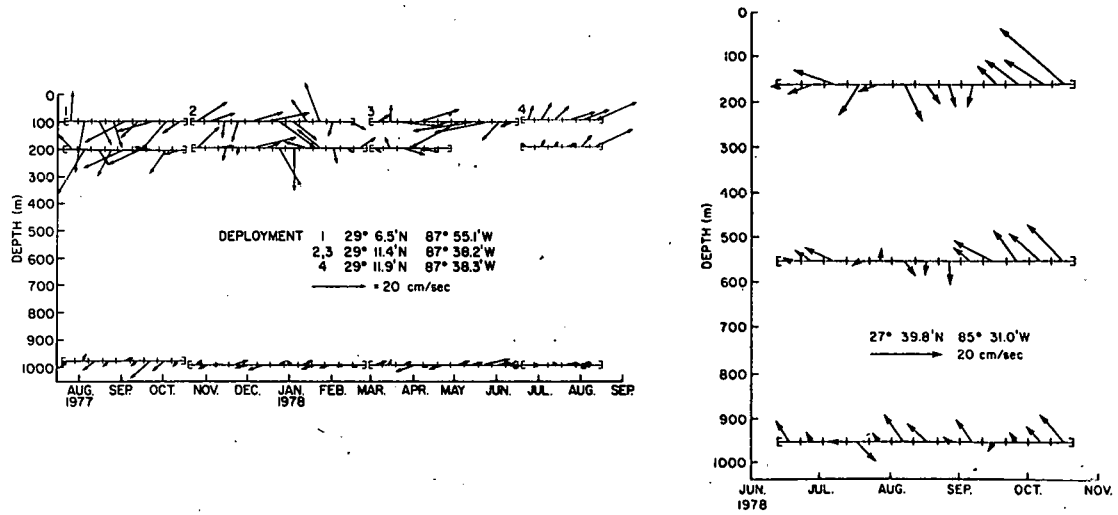

Fig. 10. Stick plots of ten-day averaged current meter data collected at the the Mobile and Tampa sites.

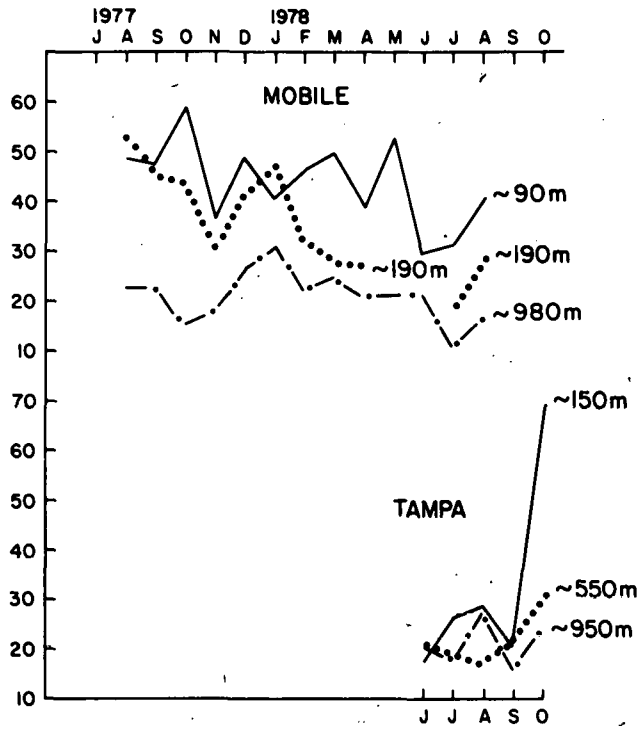

Fig. 11. Maximum speeds observed during each month of available records.

Table 7: The values of speed (cm/sec) exceeded by 10%, 50% and 90% of the observations during the deployment intervals indicated.

Deployment Interval	Meter Depth (m)	Mobile 10%	Mobile 50%	Mobile 90%	Tampa 10%	Tampa 50%	Tampa 90%
19/Jul-18/Oct, 1977	95	34	18	4			
	195	33	15	5			
	974	13	6	2			
19/Oct, 1977-25/Feb, 1978	90	31	17	6			
	190	28	14	4			
	985	15	7	3			
27/Feb-16/Jun, 1978	95	33	14	3			
	190	20	8	2			
	985	15	7	2			
18/Jun-23/Aug, 1978	70	26	14	4			
	168	21	7	1			
	970	11	5	2			
13/Jun-25/Oct, 1978	153				20	11	4
	549				16	9	4
	950				15	7	2

The maximum speed observed at Mobile was approximately 60 cm/sec during October 1977 (Fig. 11). During most of the year, except for during August and October 1977 and May 1978, the maximum speeds at Mobile were less than 50 cm/sec. A maximum speed of 69 cm/sec was observed in the four-month Tampa record during October 1978.

South Atlantic

Figure 12 shows the distribution of the dynamic height anomaly of the sea-surface computed relative to 900 m. The distribution of surface currents inferred from this pattern is quite complicated, suggesting several regions of strong flow. In addition, an easterly flow appears at 6°S in contrast to the primarily northwesterly flow throughout the remainder of the OTEC area.

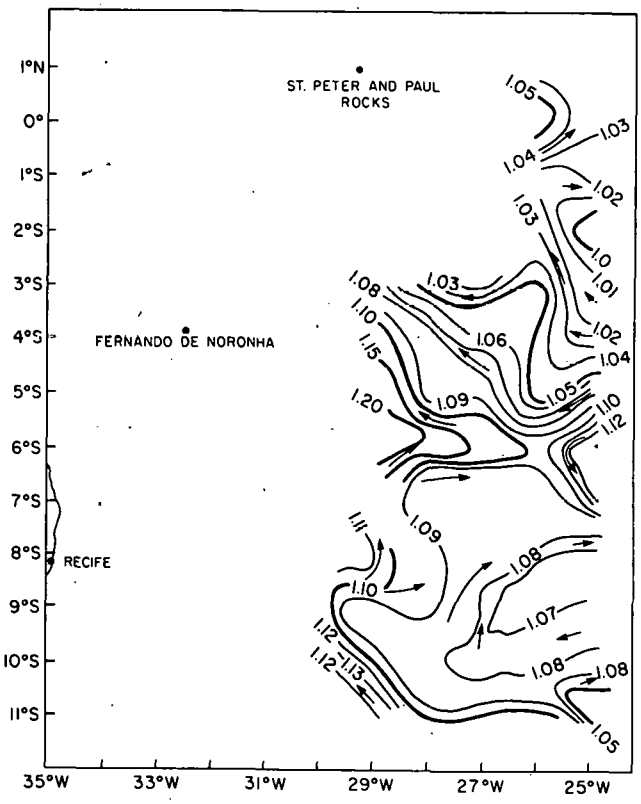

Fig. 12. Dynamic topography (dyn-m) of the sea-surface computed relative to a reference level at 900 m from data obtained in July-August 1978, South Atlantic site.

Vertical sections of geostrophic speed computed relative to 900 m are given in Figure 13. The east-west component of speed is given by the north-south sections. The subsurface circulation is also quite complicated. For instance, subsurface maxima in current speed are observed; see e.g., 8.5°S, 29.5°W and 7.5°S, 25°W. It should be noted that these geostrophic speed may underestimate the actual speeds, because of large station spacing and inherent limitations of geostrophic computations.

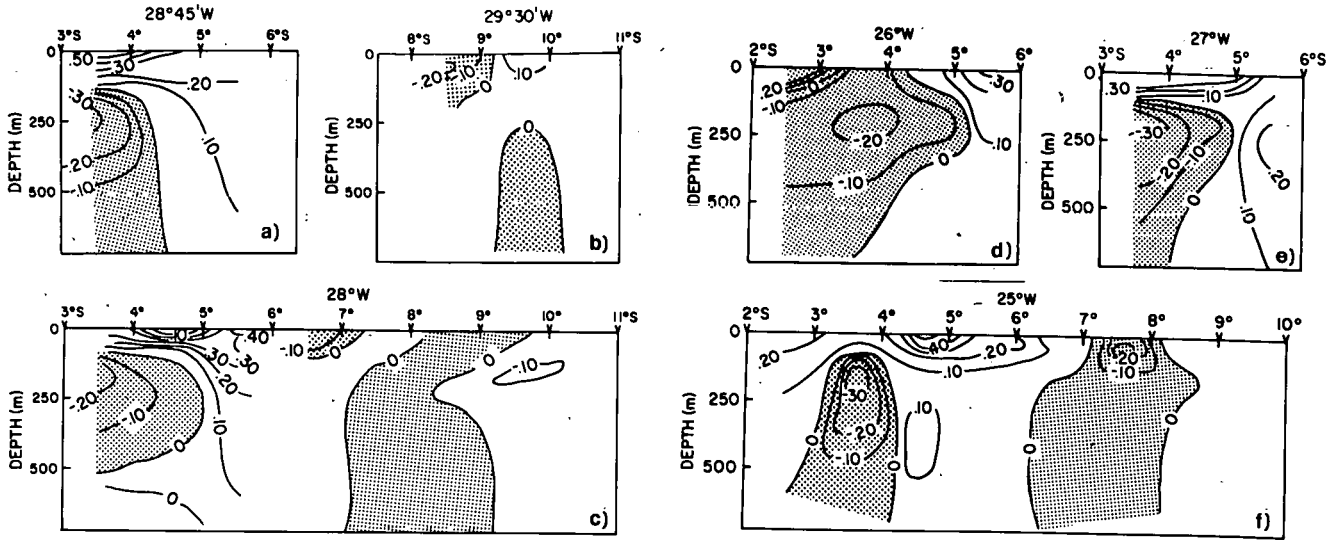

Fig. 13. Vertical sections of geostrophic speed (m/sec) computed relative to 900 m from data collected in July-August 1978, South Atlantic site. Shaded areas represent flow to the east.

References

1. Behringer, D. W., R. L. Molinari and J. F. Festa. "The Variability of Anticyclonie Current Patterns in the Gulf of Mexico," J. Geophys. Res., 82, 1977, pp. 5469-5476.

2. Molinari, R. L. and F. Chew. "Ocean Thermal and Current Structures in the Tropical South Atlantic Relative to the Placement of a Grazing OTEC Plant," NOAA Tech. Memo, ERL AOML-35, 1979.

3. Molinari, R. L. and J. F. Festa. "Ocean Thermal and Current Velocity Data Requirements for Design of an OTEC Demonstration Plant," NOAA Tech. Memo., ERL AOML-30, 1978.

4. Molinari, R. L. and J. F. Festa. "Ocean Thermal and Velocity Characteristics of the Gulf of Mexico Relative to the Placement of a Moored OTEC Plant," NOAA Tech. Memo., ERL AOML-33, 1978a.

5. Molinari, R. L., J. Hazelworth and D. Ortman. "Data from OTEC Site Characterization Studies in the Gulf of Mexico and Tropical South Atlantic." To appear as a NOAA Tech. Memo, 1979.

6. Molinari, R. L., D. Mayer and F. Chew. "Physical Oceanographic Conditions at a Potential OTEC Site in the Gulf of Mexico, 88°W, 29°N." To appear as a NOAA Tech. Memo, 1979a.

7. Thomas, G. G., S. M. Minton and R. L. Molinari. "Data from the Atlantic Oceanographic and Meteorological Laboratories OTEC Plant Site Study in the Gulf of Mexico, July 1977," NOAA Tech. Memo, ERL AOML-34, 1979.

OTEC DATA BASE AND DATA PRODUCTS

James Churgin* and Harry Iredale**

U.S. Department of Commerce
National Oceanic and Atmospheric Administration
Environmental Data and Information Service
National Oceanographic Data Center
Washington, D.C. 20235

Abstract

The National Oceanographic Data Center's (NODC) historical data files used to establish the Ocean Thermal Energy Conversion (OTEC) project's environmental data base are discussed. Additional data and literature services provided by NODC are introduced. The status of the data base and data products developed and maintained at NODC is discussed. A potential data format conversion problem is addressed. The need for improved specification of OTEC products is commented upon. A brief description is given of the Generalized Applications System (GAS) used by NODC to access all its data files in order to generate products. Samples of products available are illustrated; computer graphics currently under development and those being considered for future generation are listed.

Introduction

Two years ago managers of the Federal OTEC program asked the National Oceanographic Data Center (NODC) to initiate the establishment of an Ocean Thermal Energy Conversion (OTEC) Data Base, identify historical data required by OTEC contractors, generate data products and provide services specifically designed to meet the needs of OTEC developers. The establishment of the Data Base and other related functions is envisioned to provide: (1) environmental data and data products to contractors and others engaged in engineering design of OTEC plants; (2) environmental data and data products required for the investigation of potential OTEC sites; (3) information required in order to assess the environmental impact of OTEC development; (4) a uniform system for acquisition, storage and retrieval of site-specific data collected in connection with OTEC investigations; and (5) a focal point for environmental data related to OTEC needs, including meteorological data, satellite-derived data and marine geological data.

This paper describes the activities at NODC related to the objectives mentioned above and, hopefully, will provoke some thought among those actively engaged in OTEC development regarding the nature and types of data services they require. NODC strives to provide data products specifically tailored to the needs of the user. It has been our experience that these products can be developed most effectively through a continuing dialogue with the potential user.

A step toward this goal was begun at the OTEC Workshop last year, but since that time NODC has not had any direct involvement with OTEC developers concerning desired products. In order to provide a basis for these discussions this paper will describe the present NODC processing system, the OTEC product definition impact on NODC, the kinds of products now available to OTEC contractors, products being generated which will meet perceived OTEC needs and the types of requests which NODC has serviced for OTEC researchers.

Data from Historical Files

Although most people in the marine sciences community should be aware of the NODC and the services it provides, we are continually surprised by colleagues who state that they have just learned of our existence. For persons not familiar with the historical marine data files currently available from NODC, we will describe some of the major files that have contributed to the OTEC data base. Table 1 summarizes by file type the volume of data available in our major historical files.

Station Data File

The Oceanographic Station Data or Hydrographic Cast file consists of depth versus some or all of the following parameters: seawater temperature, salinity, dissolved oxygen, nutrient chemistry, pH, sigma-t,* dynamic height anomaly and sound speed. All but the latter three are direct measurements, and the latter are computed from available measured temperature, salinity and depth. Auxiliary information for each station can include identifying data, bottom depth, meteorological observations and seawater visibility (Secchi disk) measurements. Temperature and salinity values are generally considered accurate to $\pm.03^{\circ}$C and $\pm.05$ PPT, respectively. Quality control is routinely performed on incoming data by comparing them against historical models and performing normal range and valid character checks. Doubtful data are flagged.

The present worldwide Ocean Station Data file has about 635,000 stations, and the annual growth rate is approximately 25,000 stations. Nearly 80 percent of the Oceanographic Station Data file originated from sources outside the United States. Although the total number of stations may appear impressive, there are very few good time-series observations, particularly in regions of potential OTEC interest.

---

*Director, Data Services Division, NODC

**Oceanographer, Data Services Division, NODC

*Sigma-t (σt) = (density - 1.0) x 1000

Expendable Bathythermograph (XBT) Data File

The XBT file contains digitized temperature/depth profiles obtained from expendable bathythermographs. Under recently adopted procedures these data are quality controlled by checking them against historical data by ocean area and by performing normal range and valid character checks.

The XBT is a relatively new instrument, with the bulk of the data having been collected within the last 10 years by U.S. organizations. More than 300,000 observations are in the file, and the majority of these are between 0 to 450 meters, with some to depths of 750 meters. Only a few of the newest observations go as deep as 1,400 meters.

Temperature accuracy is normally $\pm$ .1°C, although recent studies have indicated that systematic errors, especially with deeper probes, may yield data of slightly less accuracy.

XBT data provide generally reliable continuous temperature records with depth and can furnish excellent data on relative vertical temperature variations.

Mechanical Bathythermograph (MBT) File

The mechanical bathythermograph is an instrument which scratches a temperature trace on a glass slide and requires a grid, specifically calibrated for each instrument, for translation to digital temperature/depth data. The MBT was widely used from the mid-1940's until the advent of the XBT in the late 1960's, and in the past resulting temperature traces were hand-digitized at 5-meter intervals. NODC no longer processes these data, and the file is considered virtually closed at its present total of 760,000 records. Figure 1 shows the distribution of MBT's off the U.S. East Coast.

For a number of reasons, the value of these data as absolute temperature measurements can be seriously questioned. However, when large numbers of observations are available, they are good tools for examining vertical temperature structure (layer and thermocline depths), and they can be used as a source of statistical data when compared with more accurate observations. Most MBT measurement depths do not exceed 300 meters; the majority are 150 meters or less.

Data from all three of these files, MBT, XBT and Station Data, have been used extensively in initially outlining areas of potential thermal resources for OTEC.

Other Data of Potential Interest to OTEC

There are numerous additonal data files at NODC and other Centers of the Environmental Data and Information Service (EDIS) which may have some applicability to OTEC development. A few that have been queried in response to OTEC requests and other files and services of possible interest to OTEC investigators are described in the following sections.

Surface Current Data System (SCUDS)

The SCUDS file contains ship set and drift observations, obtained from 1850 through 1974, from which estimated surface current speeds and directions have been derived. These data can be quite useful to statistically model long-term trends and major current systems and are usually provided in summary form when requested. There are about 4 million observations in the present historical file.

Subsurface Current Data

For several technical reasons no single historical Subsurface Current file exists at NODC. Instead, NODC has archived discrete files of current data in specific individual formats. It is doubtful, however, that many subsurface current records in these files will meet OTEC needs. In order to correct this deficiency, we are specifically soliciting current data from other institutions for use in the OTEC Data Base. To date we have received 64 current measurements off Florida, Puerto Rico and the Hawaiian Islands. These data have been reformatted with considerable effort and are now available in the OTEC Data Base. Figure 2 shows the location of some of these data obtained from the University of Hawaii last year.

The OTEC Subsurface Current file contains records of east and north current components, speed, direction and simultaneous measurements, such as temperature, conductivity and associated identifying information for the observations. The observations themselves may be either time-series data collected at one depth or current depth profiles collected over several depths in the same location. Current data collected with the newer instruments are usually accurate to $\pm$ 8 degrees true and $\pm$ 2 cm/sec.

Biological Data Files

The NODC Biological Data files are void of any observations in OTEC areas. Most of the biological data currently at NODC have been collected for specific projects, such as the Outer Continental Shelf Environmental Program and the Marine Ecosystem Analysis Program. A suite of formats and an accompanying taxonomic code are available, and have been proposed for use by OTEC investigators.

Environmental Data Index (ENDEX) and Oceans and Atmospheric Scientific Information System (OASIS)

ENDEX and OASIS are two referral systems available to OTEC users through the NODC. The ENDEX computer file is used to locate environmental data not archived by EDIS which has been collected by Federal, State and local governments, private industry, universities and research institutions. This system can be queried for potentially useful data located in various research facilities throughout the continental United States.

OASIS is a retrieval service that provides references to published literature and ongoing research efforts concerning coastal resources

and environmental studies in marine sciences. This is done through computerized searches of multidisciplinary bibliographic data bases.

EDIS Data Sources for which NODC is the OTEC Focal Point

NODC is the contact for OTEC people desiring any of the environmental data held by the National Climatic Center (NCC) or the National Geophysical and Solar-Terrestrial Data Center (NGSDC). A few of their files are briefly described in the following paragraphs.

Summary of Synoptic Meteorological Observations (SSMO)

The SSMO is a publication prepared by the Naval Weather Service Detachment at NCC in Asheville, North Carolina. Various tables summarizing precipitation, wind, clouds, visibility, humidity, temperature and wave measurements are presented for various coastal regions.

Satellite Infrared Imagery

These are weather satellite images maintained by NCC which show cloud, frontal and storm structures over portions of the earth's surface.

Marine Geological Data

The NGSDC marine geological data consist of lists and descriptions of cores, samples and bottom sediments. Other data maintained by NGSDC that have potential OTEC use are earthquake, tsunami mareograms and bathymetry.

NODC OTEC Support Activites

The OTEC Data Base

At present the OTEC Data Base consists of six files: (1) Oceanographic Station Data, (2) XBT, (3) MBT, (4) SCUDS, (5) Subsurface Current and (6) STD. Data in these files are from the Gulf of Mexico and ocean areas contiguous to the Hawaiian Islands, Puerto Rico and the Atlantic coast of Florida. The first four files contain historical data only, with the exception of OTEC Project generated XBT data provided by the Atlantic Oceanographic Meteorological Laboratory (AOML). The Subsurface Current file consists entirely of data accessioned by AOML and data received as a result of NODC solicitations. All the data in the STD file were accessioned by AOML. Table 2 provides the total number of observations in each of these files. AOML has been exceptionally cooperative in OTEC work, and all their data submitted for accessioning has been in NODC file formats.

Potential Data Format Conversion Problems

Historically, the NODC has accepted data in any format, but it is becoming increasingly unrealistic to do so. Even with data on magnetic tape, the conversion from a new format to an NODC file format is painstakingly slow (Figure 3). Nonetheless, we are forced to deal with numerous and varied input formats because of lack of standardization among investigators which results in a large overhead on essentially redundant work. For example, when we located subsurface current data of interest to OTEC at four institutions and began to access the data, we had to go through the eight steps shown in Figure 3 five times for five different data sets.

Obviously, if we were to receive several data sets from OTEC data collectors all in their own formats, very little data could be accessioned to the OTEC Data Base in any reasonable amount of time. In order to assist in our efforts, we strongly recommend that anyone submitting data for inclusion in the OTEC Data Base check with us first for accession format specifications. This would greatly expedite data accessioning as can be seen by comparing Figures 3 and 4.

Data Products

OTEC Products. To date we have not received formal specifications for working products from OTEC investigators, but we have received examples in the form of two documents; a paper called "Description of Data Formats" from the February 1978 Data Users Workshop for Developing Ocean Data Monitoring Needs and Data Reformatting Specifications for the OTEC Program, and the next iteration of the same subject entitled "OTEC Oceanographic Data Reports" (August 1978).

Rather than wait for further iterations, it was decided to begin software development in a systematic fashion by working our way through the February 1978 Workshop's product papers. This proved to be a mistake, however, because many of the products in the first iteration of data formats were not included or were substantially modified in the second iteration.

A significant programming effort was thus rendered of little value, and products were developed whose further usefulness is unclear. In order to avoid this in the future, it was decided to concentrate on those data products illustrated in the second iteration that were similar to already existing NODC products and to develop those products which would be useful regardless of OTEC requirements. When OTEC requirements become firm, we will then address our attention to the entire spectrum of OTEC products.

Generalized Application System (GAS). At the NODC there were many data files and many more software applications programs to generate various products for our users. This meant that to process R data files with S application routines we had to have at least R x S programs to generate products. The GAS software flow shown in Figure 5 was developed to eliminate much of the redundant software. Now one module with subroutines reads the many files and converts them to GAS format for processing by the application routines, all of which read GAS outputs.

Sample Products. Categories of products are: inventories and geographic searches; parameter computations (listings and tapes); graphic illustrations, including histograms, profiles, vertical sections, horizontal contours, progressive vectors, composite plots and exceedence diagrams; data summaries and limited data analysis. Some of the graphic products are shown in Figures 6 through 15.

The vertical section in Figure 6 shows the spatial variability of water temperature over depth. Figure 7 is a horizontal temperature contour which illustrates the spatial distribution of the surface isotherms for the winter season in the ocean area shown. The isotherms in Figure 8 present temporal variability over a 13-day period. The points are the individual temperature profile observations or interpolations, the isopleths are not smoothed, and no interprofile interpolation was performed. Some examples of current graphics are shown in Figures 9 through 11. The current roses in Figure 9 are averaged currents from moored meters at a specific depth, with resultant direction and magnitude averaged over a season for each 1-degree square in Figure 10. The progressive vector diagram in Figure 11 represents the resultant sample interval vectors placed end-to-end for a 25-day period for a stationary meter. Figure 12 is a composite plot of sigma-t for several profiles in the same area; and temperature, salinity and sigma-t are plotted versus depth in Figure 13. An exceedence diagram showing the cumulative percentage of temperature differential (0 to 1,000 meters) values is presented in Figure 14. For example, in Figure 14, 50% of the observed temperature differentials were greater than or equal to 22.58°C for a year in this 1-degree square in the Gulf of Mexico. Walrus sightings per 1/2-degree square presented in Figure 15 is a sample biological plot. These are just a few examples of the many graphic products that are available from NODC. Publications describing NODC products and formats are given in the references at the end of this paper. The products publication is currently being updated and will describe all NODC products in more detail.

Future OTEC Products. Products under development are: current histograms representing time percentage of total currents flowing in a specified direction, virtual displacement and per-unit occurrence of component speeds from moored current meter observations; the addition of sigma-t lines on temperature-salinity plots; and parameters contoured over a depth-time grid.

In the future, we expect to develop computed Brunt-Väisälä frequency for high-resolution data, the various spectra plots and the biological histograms illustrated in the working document "OTEC Oceanographic Data Reports" of August 1978.

NODC Support to OTEC Contractors

NODC has responded to over 40 requests from OTEC contractors for data and information including salinity, temperature, dynamic height anomalies, surface currents, inventory searches, SSMO's, satellite infrared imagery, charts, plots and miscellaneous publications.

Numerous publications from OTEC contractors and the Department of Energy have been received by NODC. We are in the process of developing an automated inventory listing for them and now have these reference materials available for use on the premises.

Summary

This paper has discussed the historical data files, their status and their usefulness in establishing the OTEC Data Base. Other data and information sources available through NODC were introduced for the purpose of expanding our useful services to OTEC contractors and investigators.

The support activities of NODC were included in the discussions concerning the status of the OTEC Data Base, the data products available now and in the future and the responses of NODC to OTEC requests.

Two problem areas, the lack of firm definition of product requirements from OTEC data users and the potential need for multiple formats, were addressed with the intention of making all involved aware of their impact and to initiate action toward their resolution. To provide the best service possible in our efforts to support the OTEC project, we need to establish and continue close communications between the NODC and the OTEC community.

References

Division of Solar Technology, "Environmental and Resource Assessment Program," DOE/ET-0020/1, Washington, D.C., January 1978.

Environmental Data and Information Service, "User's Guide to ENDEX/OASIS," Washington, D.C., January 1976.

Kramer, William P., "A Storage Format for Current Meter Data," Tech. Rep. Ref. No. 75-2, University of R.I., May 1975.

Morawski, Walter J., "The Generalized Applications System of NODC," The Proceedings of the Fifth Biennial International Data Conference, Pergamon Press, New York, 1977.

National Oceanographic and Atmospheric Administration and Lawrence Berkley Laboratory, "OTEC Oceanographic Data Report," Unpublished, August 1978.

National Oceanographic Data Center, "GAS System Reference Manual," Unpublished, Washington, D.C.

National Oceanographic Data Center, "NODC Application Products," Unpublished, Washington, D.C.

National Oceanographic Data Center, "NODC OTEC Support Activity Quarterly Status Report," Washington, D.C., April 1978.

National Oceanographic Data Center, "Oceanographic Data Base for OTEC," Washington, D.C., November 1977.

National Oceanographic Data Center, "Oceanographic Data Base for OTEC," Washington, D.C, July 1978.

National Oceanographic Data Center, "User's Guide to NODC's Data Services," Washington, D.C., February 1974.

Thomas, Gregg G, Minton, S. Michael and Molinari, Robert L., "Data From the Atlantic Oceanographic Meteorological Laboratories OTEC Plant Site Study in the Gulf of Mexico July 1977," NOAA Tech. Memo. AOML, Miami, Fla., January 1979.

	NUMBER OF OBSERVATIONS
OCEANOGRAPHIC STATIONS	635,000
EXPENDABLE BATHYTHERMOGRAPHS	300,000
MECHANICAL BATHYTHERMOGRAPHS	760,000
SURFACE CURRENTS	4,000,000

Table 1. Inventory of NODC Worldwide Historical Data Files

	NUMBER OF OBSERVATIONS
OCEANOGRAPHIC STATIONS	3,637
EXPENDABLE BATHYTHERMOGRAPHS	8,633
MECHANICAL BATHYTHERMOGRAPHS	13,125
SURFACE CURRENTS	896,827
SUBSURFACE CURRENTS	66
SALINITY, TEMPERATURE DEPTH PROFILES	20

Table 2. Inventory of OTEC Data Base

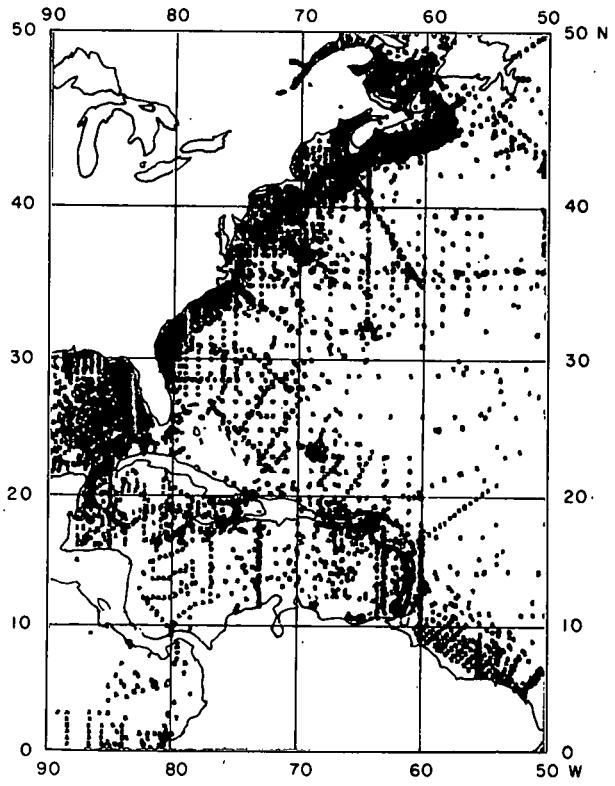

Figure 1. Geographic distribution of bathythermographs.

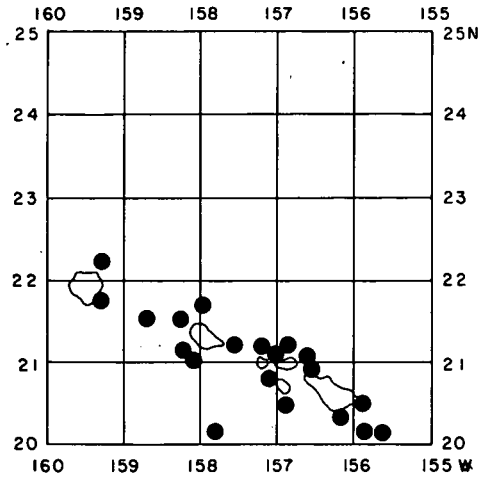

Figure 2. Subsurface current observations near Hawaiian Islands.

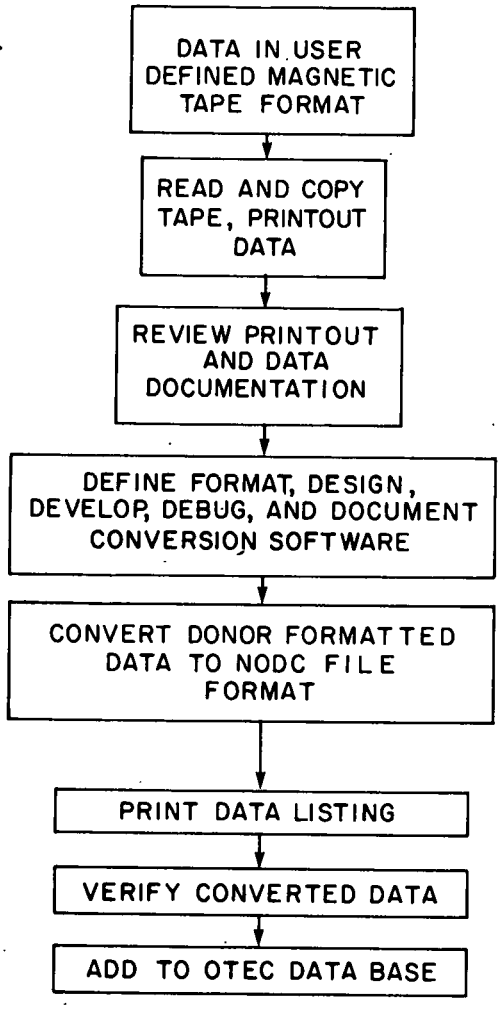

Figure 3. Usual data accession procedure at NODC.

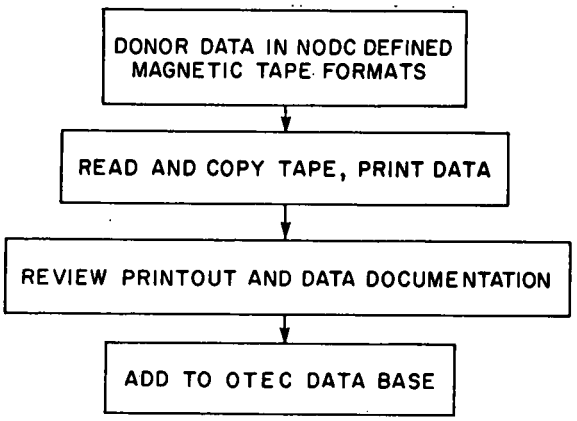

Figure 4. NODC preferred data accession steps.

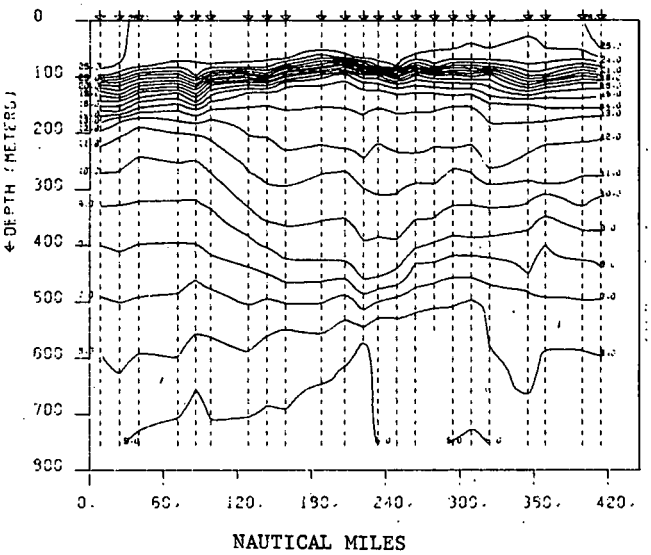

Figure 6. Temperature contour on a depth-distance grid.

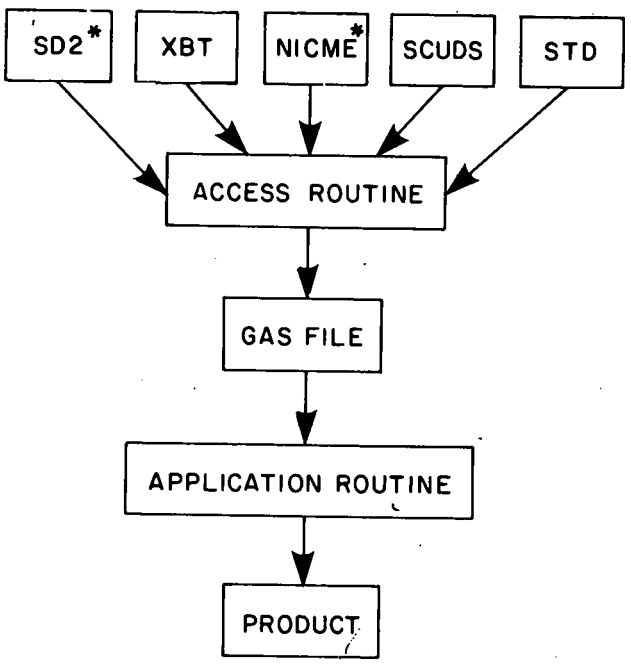

Figure 5. GAS processing system flow.

*SD2 - Station Data (Nansen Cast)
NICME - Subsurface Current Data

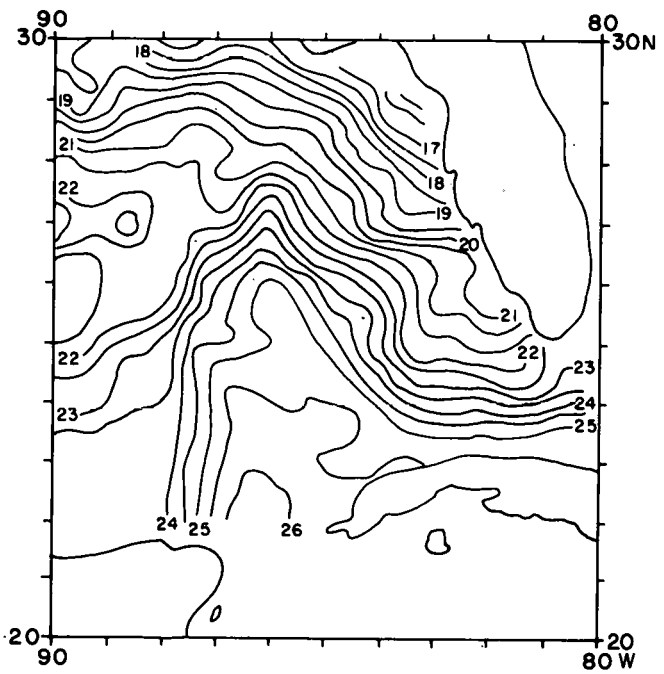

Figure 7. Horizontal temperature contours at the surface.

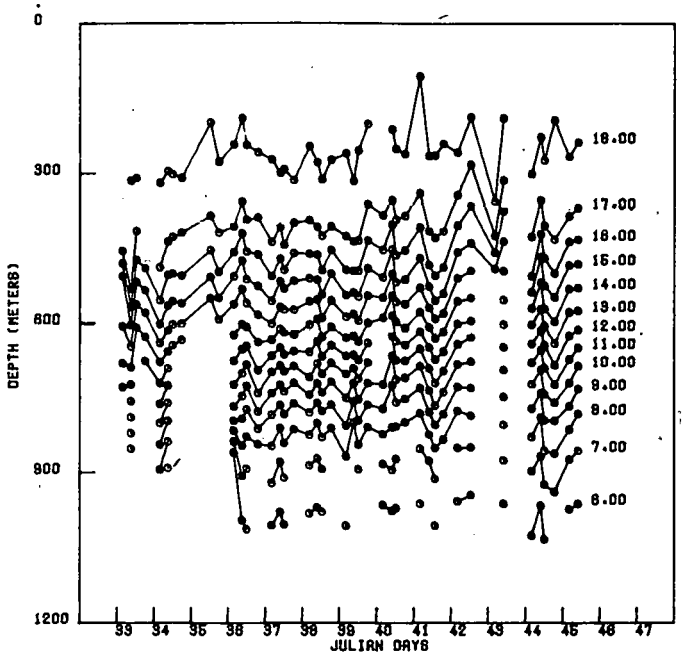

Figure 8. Raw isotherms on depth-time grid. February 1963 35°N 48°W

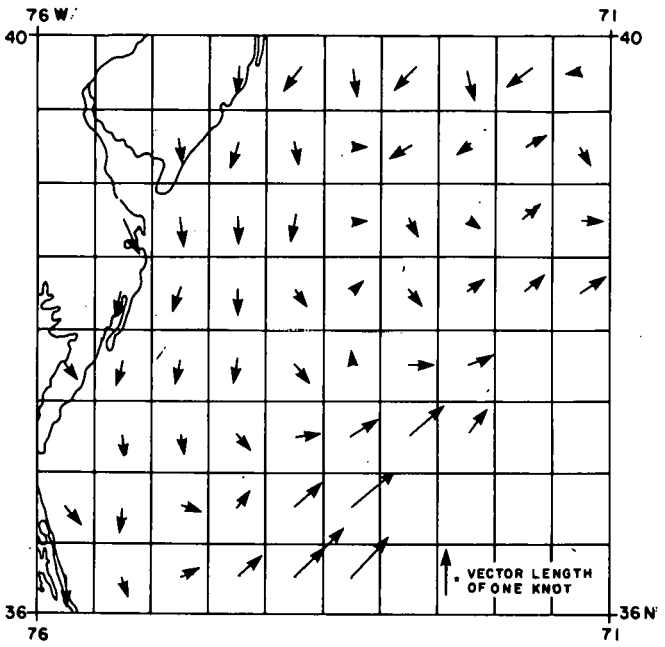

Figure 10. Average surface current vectors for one-half degree square.

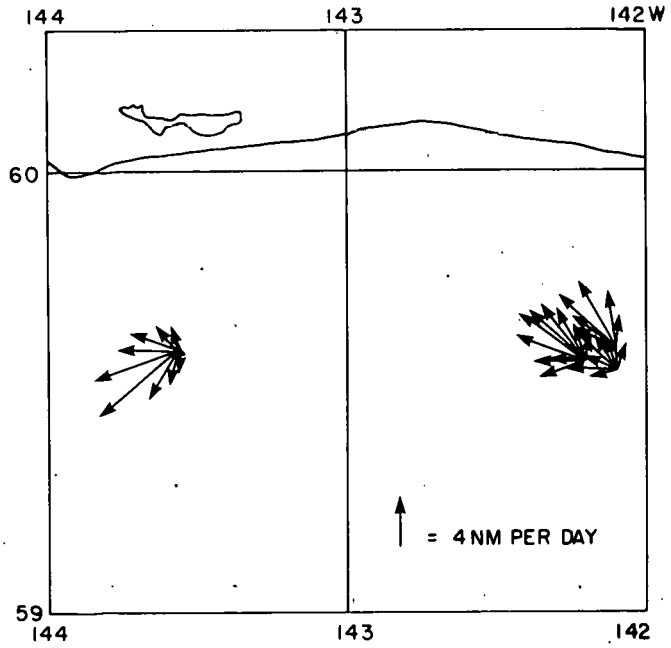

Figure 9. Average current vectors at 20 meters depth.

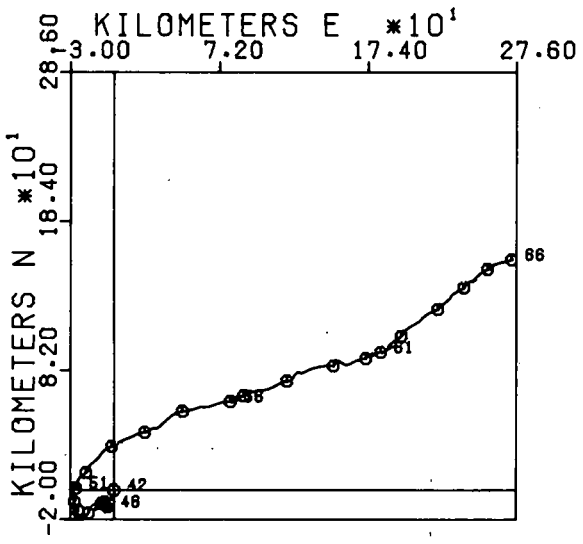

Figure 11. Progressive current vectors for a 25-day period in Hawaiian OTEC area. February - March 1965 21°16'N 157°36'W

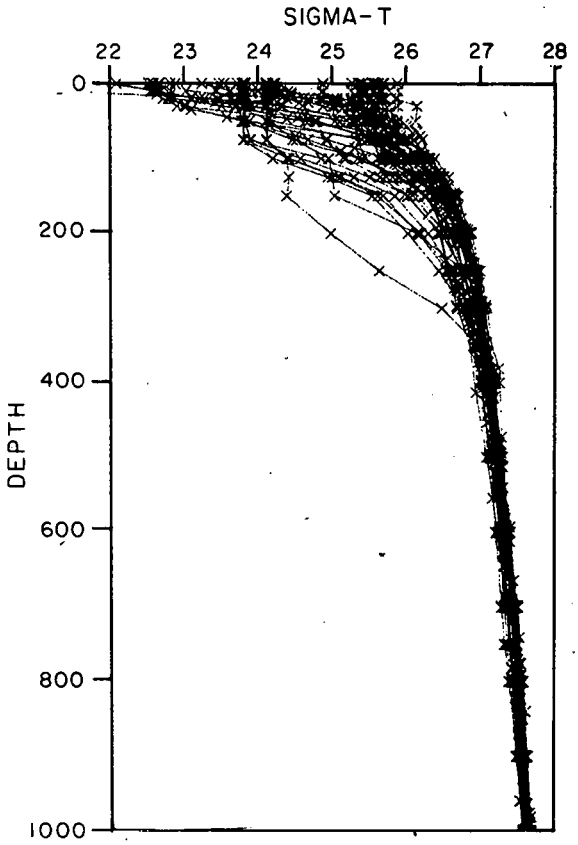

Figure 12. Composite sigma-t profiles.

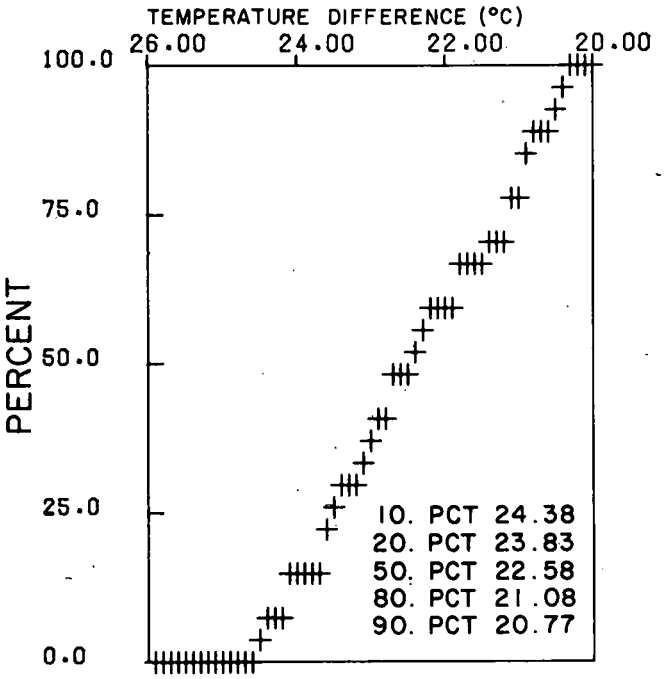

Figure 14. Exceedence diagram of vertical temperature differential (0 to 1000 meters), yearly in the Gulf of Mexico. One Degree Square 58

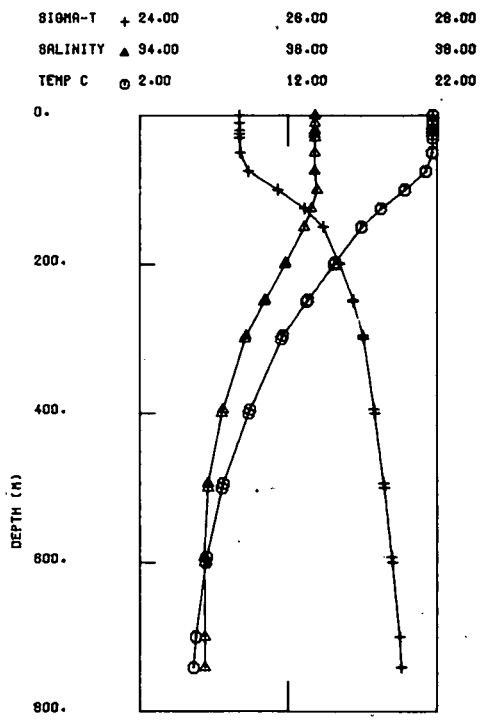

Figure 13. Temperature, salinity and sigma-t profiles in the Gulf of Mexico. February 14, 1962 28°32'N 88°58'W

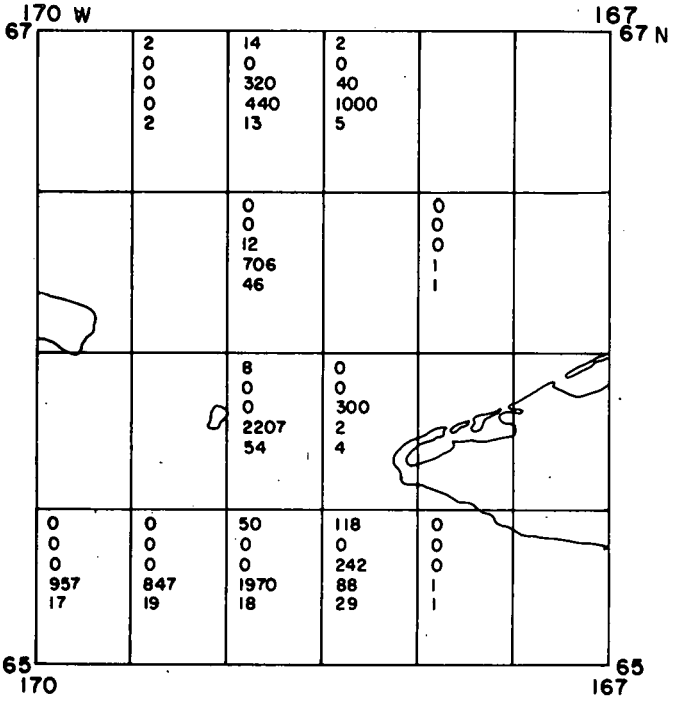

Figure 15. Sample biological plot. Geographical distribution and ecological niche that a particular species was occupying at the time of sighting, e.g. land, water, ice, etc.

OTEC WORLD THERMAL RESOURCE

William A. Wolff, William E. Hubert, and Paul M. Wolff

Ocean Data Systems, Inc.
2400 Garden Road
Monterey, California 93940

Abstract

The Ocean Thermal Energy Conversion (OTEC) thermal resource in terms of ΔT (°C) between the surface waters and waters at depths to 1500 meters has been determined. Charts of the large-scale distribution of this resource potential have been printed for worldwide distribution by the U.S. Department of Energy (Division of Solar Technology). This definition of global resource was based upon monthly analyses of sea surface temperature and subsurface temperatures at space scales determined by data availability. Subsurface soundings of all types were subjected to computer processing for latitude/longitude rectangles varying from 1° to 5° in extent; monthly ΔT values were then averaged to obtain the gross potential fields shown. For ten selected sites (Guam, Ivory Coast, Sri Lanka, Dampier Land, Manila, Jakarta, Mombasa, off Mexico, and a Plant Ship location in each ocean) more detailed OTEC thermal resource studies are described. Tables are presented which summarize the most probable ΔT values from surface to 1200 meters, the greatest depth expected to be of practical interest for OTEC. All ten sites examined have the necessary thermal resource for potential OTEC exploitation and several of the most promising are comparable with any resource previously examined. In addition, bathymetric, upper mixed layer weather, sea/swell, and current features peculiar to each site are discussed in less detail.

Introduction

Since the OTEC plants will be most efficient where there is a large, consistent temperature difference resource, an early evaluation of this resource at potential OTEC sites is necessary. For NSF/RANN, Ocean Data Systems, Inc., assembled a data base to examine the availability of this thermal resource on a seasonal basis for the ocean areas surrounding the North American continent (Wolff and Hubert [1]). A definition of thermal structure on finer space and time scales with an updated and expanded data base was done under the Energy Research and Development Administration program. Regions examined in terms of 1° latitude and longitude squares and months of the year included Hawaii, Puerto Rico, Key West, Florida Atlantic Coast, and the western and eastern regions of the Gulf of Mexico. The worldwide OTEC thermal resource is being examined in further detail under Department of Energy Contract (ODSI[2]). The large-scale distribution of OTEC thermal resource from 40° south to 40° north latitude in terms of ΔT (°C) between the uniformly warm waters of the upper mixed layer and waters to depths of 1500 meters has been determined. Charts of this resource potential have been printed for worldwide distribution by the Department of Energy. Also under the contract, the thermal resource at each of ten new sites selected by the Department of Energy were analyzed.

Worldwide ΔT Maps

This ocean thermal resource study was based upon all available soundings - mechanical bathythermographs (MBT), expendable bathythermographs (XBT), salinity temperature depth systems (STD), and Nansen casts. Existing hydroclimatological atlases were consulted in each of the world's oceans. Data files were obtained from the National Oceanographic Data Center and the U.S. Naval Fleet Numerical Weather Central. The temperature difference resource was examined for all of the world's oceans. The sites with sufficient temperature differences are generally limited to the area between 25° south and 30° north. Japan may be an exception; we have not studied potential Japanese sites in detail. Though the OTEC data file contains a high percentage of all soundings ever taken, there are areas where the data is sparse and non-uniform in time and space. In areas where all soundings are similar and uniform in shape and show small total variability, this is not a serious problem. Where there was great variability, some investigation of the physical oceanography of the region with respect to the factors causing temperature changes was necessary. The total data sample covering over seventy years is not uniform with time.

Sea surface temperatures (SSTs) and upper mixed layer depths were analyzed monthly on space scales consistent with data availability. Mean temperatures at depths of 1000 meters or greater, where observations were generally quite sparse, were also analyzed monthly. Data were examined on scales of 2.5° latitude by 2.5° longitude and on 5° latitude scales in areas with fewer observations. In numerous areas ΔT values were determined for one degree by one degree rectangles. For areas void of observed data subjective interpolation was used. When using discrete sets of observational data containing errors, smoothing is both necessary and justified. Four smoothing passes were made. The magnitudes of changes tend to be smaller than a few hundredths of a degree after four passes. The actual smoothing procedure consisted of the replacement of the ith temperature value with the three point average value using :

$$T_i^{\nu+1} = \frac{1}{3}\left(T_{i-1} + T_i + T_{i+1}\right)^{\nu} \qquad (1)$$

where ν indicates the iterate. Periodic boundary conditions are used. The smoothing techniques applied are described by Wolff[3]. Monthly average ΔT figures from the warm waters near the surface to depths of 1000 meters or more were computed, from which gross annual ΔT values were derived.

Since latitudinal variation in ocean temperature diminishes with depth, sea surface temperature is an important factor in determining temperature difference resources. Despite this consideration, the data shows that the shape and location of the 1000 meter ΔT contour cannot be inferred from the surface conditions. Temperatures at 1000 meters show considerable variation in different ocean basins due to a variety of physical and oceanographic causes. Table I provides a comparison of

the gross resource availability for selected sites off Hawaii, Puerto Rico and in the Gulf of Mexico. Table 2 provides some representative Δ T figures for various worldwide locations. The Red Sea and Mediterranean locations are obviously of no OTEC interest, unless possibly connected with an iceberg melting scheme as described in these proceedings. The values for the site off Brazil in Table 2 are for stationary operations near 7° S, 29° W. With this siting area, as with others on the open seas in Tables 2 through 5, the values tabulated do not take into account the higher annual averages achievable by cruising within a certain area to attain the highest Δ T each month and hence a 1°-2°C higher annual average due to cruising.

The primary need for OTEC in terms of temperature difference resource is the availability of an adequate Δ T from uniformly warm waters near the surface to some depth probably not exceeding 1200 meters. For continuous efficient operation of an OTEC plant an annual average Δ T greater than 20.0°C (36°F) is required. The mean Δ T of the coldest month should exceed 16.7°C (30°F). The temperature difference resource at most locations is generally quite stable from day to day but many sites show large seasonal variations. A considerable portion of the world's oceans have the necessary thermal resources advantageous for OTEC exploitation. Several locations have excellent Δ Ts very close to shore, where OTEC plants could be land based. Others are accessible to land with submarine cables, and extensive open ocean areas have necessary the thermal resource for exploitation by OTEC plant ships producing energy-intensive products at sea. Figure 1 maps the global annual average Δ T contours for 1000 meters.

Zener and G. Lavi[5] showed that the gross power output of an OTEC plant is a function of the Δ T raised to a power near 2. Net power varies with Δ T raised to a higher power. Therefore, small increases in Δ T are important for the resulting net power. Costs of stronger pumps, greater pipe lengths, electric cable cost, and mooring costs must be weighed also.

TABLE 1: Resource Availability
(Δ Ts to 1000 Meter Depth, °C)

	Mean Annual Δ T	Δ T in Coldest Month
Hawaii (Keahole Port)	21.4	20.0
Puerto Rico (Punta Tuna)	22.3	20.9
Western Gulf of Mexico	20.6	16.3
Eastern Gulf of Mexico (Tampa)	22.6	20.8
Northern Gulf of Mexico (New Orleans)	21.0	16.0
Key West	20.1	17.4
Florida East Coast	20.6	18.7

TABLE 2: Resource Availability
at Other Sites, °C

	Mean Annual Δ T	Δ T in Coldest Month
Red Sea	4.3	0.3
Mediterranean	8.3	2.6
Brazil (S. Atlantic)	22.1	21.2
Equator E. Pacific	20.5	19.5
Central Pacific	23.0	22.5
West Pacific	25.0	24.6
Equator Indian Ocean	22.5	22.0
Equator W. Africa	21.2	18.6
Saudi Arabia	17.1	15.2
Persian Gulf	19.0	13.5
Iran-Gulf of Oman	18.5	14.2
India	21.5	20.0

TABLE 3: Locations and Resource Availability
(Δ Ts to 1000 meter depth, °C) of the
Ten Most Recently Investigated Sites

Site	LAT	LONG	Range Distance Kilometers from shore to 1000 meters	Annual Mean Δ T	Coldest Monthly Δ T
Dampier Land	13-18° S	118-121°E	265-417	22.6	20.7
Manila	14-16° N	118-120°E	6-82	24.0	22.6
Guam	12-15° N	142-146°E	7-18	24.1	23.4
Ivory Coast	3-6°N	3-8° W	33-52	22.1	19.7
Jakarta	6-9°S	104-109°E	18-60	22.8	21.9
Off Mexico	20-23°N	105-110°W	5-104	20.9	18.0
Sri Lanka	5-10°N	78-83° E	22-55	21.3	20.8
Mombasa S.	5S-0°N	40-45° E	33-130	20.2	18.5
Mombasa N.	0-3°N	40-45° E	33-56	19.5	18.2
Plant Ship	13-15°N	75-80° W	370	22.4	21.3
Plant Ship	5-10°N	90-95° W	370	22.8	21.7

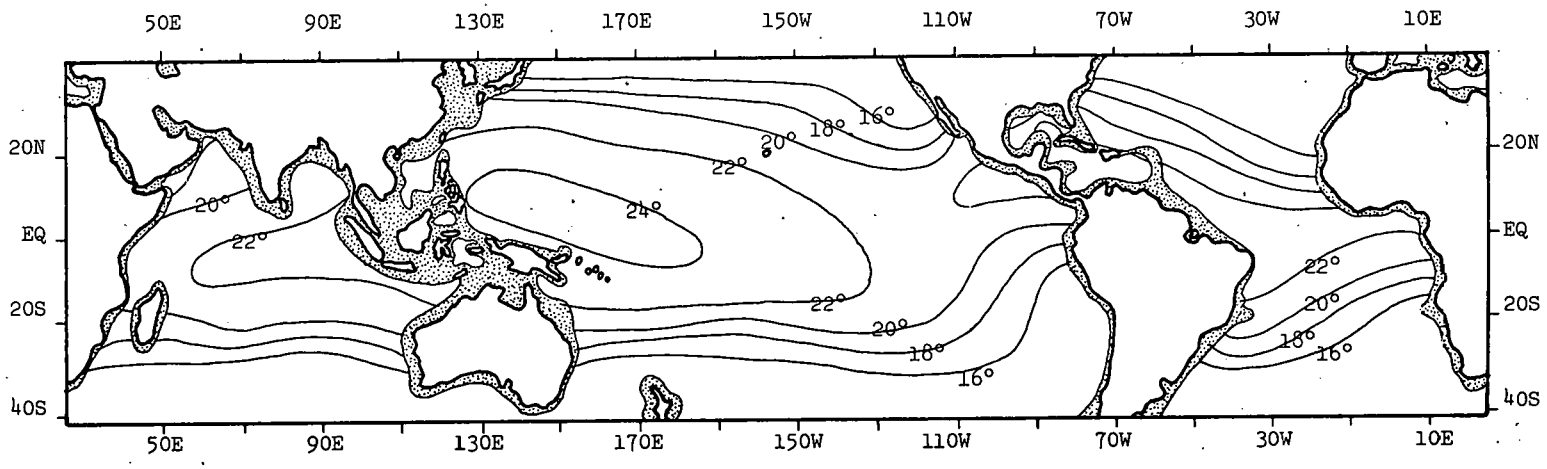

FIGURE 1: Large-scale Distribution of OTEC Thermal Resource Based on ΔT (° C) Between Surface and 1000-m Depth.

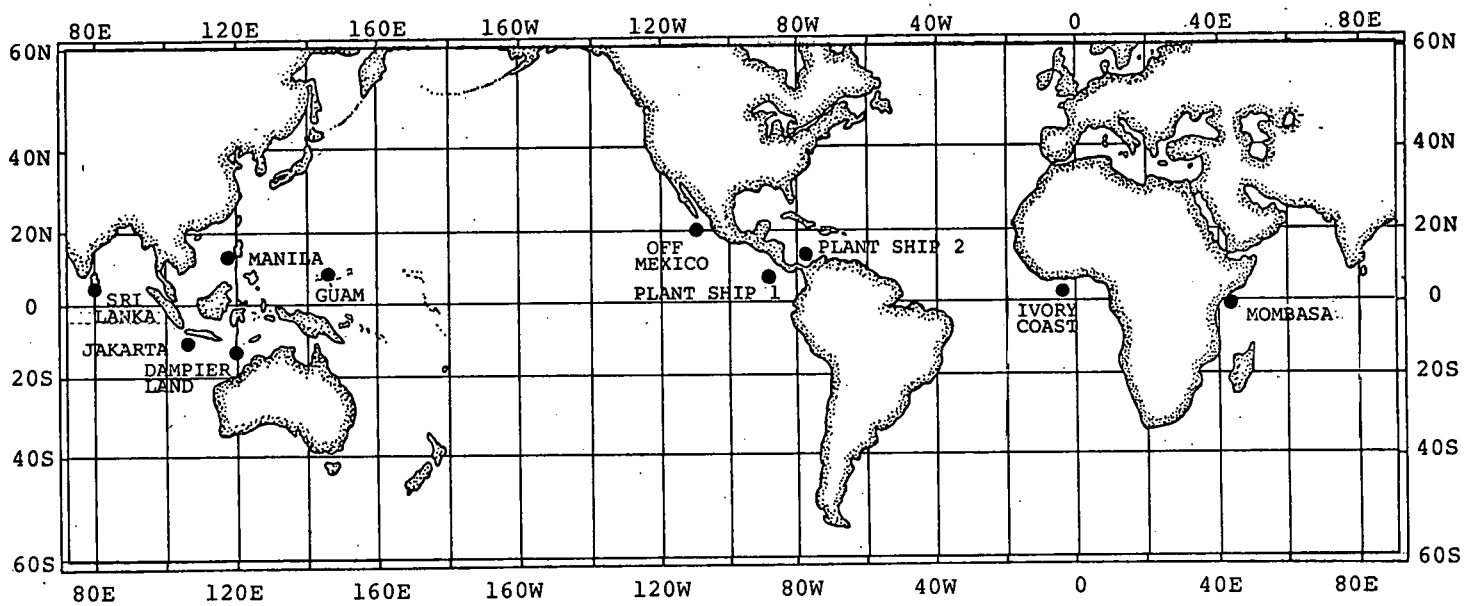

FIGURE 2: Locations of the Ten Most Recently Investigated Sites.

Ten Selected Sites

Ten new potential OTEC sites were selected by the U.S. Department of Energy for detailed thermal resource analysis. The latitiude and longitude of the specific rectangles for each site are included in Table 3. Figure 2 illustrates the location of these ten sites. A separate report was prepared for each site.

For each area, the most probable temperature structures were determined to a depth of fifteen hundred meters. In order to define the temperature structure, the OTEC data file was updated. The primary sources for the data were NOAA's National Oceanographic Data Center and the U.S. Naval Fleet Numerical Weather Central. When the most probable temperature soundings were plotted, some month-to-month variability was present which was caused by the non-uniform data sample rather than by real changes in the ocean. These short-period time variations were removed by a filtering process described by Wolff[3].

Tables 4, 5, and 6 provide summaries of key temperature parameters for the ten newly investigated sites. Figures 3 and 4 show temperature-bands for which the boundaries are the curves for the best and poorest months at a given site. Figure 3 is from Dugger [6].

Other Environmental Considerations

Some potential plant sites may have the required thermal potential throughout the year but may not be ideal for OTEC operations because other environmental parameters are not within specified limits. Bathymetry is an important consideration. Where mooring is required, the ocean bottom can not be deeper than about 2000 meters. OTEC systems transmitting power to shore within submarine AC cables can be located out to about thirty kilometers (20 miles). DC transmissions costs will limit transmission via cable to about 300 kilometers (200 miles) from shore (Cohen [4]). Of the ten locations studied, eight have sites with an annual average ΔT of 20°C within 30 kilometers of shore, and, thus, will be appropriate sites for AC transmission. The Guam, Manila, and off-Mexico locations all have excellent thermal resources within ten kilometers of their shores. Sites along the coast of Kenya 1000 meters deep, the depth needed to achieve a ΔT of 20°C for this area, range between 33 and 130 kilometers from shore, hence DC transmission will probably be required. Similarly, DC transmission will be required if plants using submarine cables are placed off Dampier Land, Australia where the minimum distance to water 1000 meters deep is approximately 265 kilometers. A cruising Plant Ship producing energy-intensive products would be better suited to this site.

TABLE 4: Monthly and Annual Mean ΔTs for Four Sites (°C)

Depth	Month												
	1	2	3	4	5	6	7	8	9	10	11	12	Annual Mean
A. Sri Lanka, 5-10° N/78-83° E													
50	0.3	0.2	0.8	1.1	1.6	1.5	2.2	2.1	2.2	0.8	0.6	0.3	1.1
100	4.7	3.6	5.4	6.3	7.0	7.2	7.3	7.9	7.4	6.2	6.3	5.0	6.2
700	19.0	19.0	19.8	20.0	20.0	19.3	18.9	19.0	19.2	19.3	19.4	19.3	19.4
900	20.3	20.3	21.2	21.5	21.4	20.7	20.2	20.4	20.5	20.6	20.7	20.6	20.7
1000	20.9	21.0	21.8	22.1	22.0	21.3	20.8	20.9	21.1	21.2	21.3	21.2	21.3
1200	22.0	22.0	22.8	23.1	23.1	22.4	21.9	22.0	22.1	22.1	23.3	22.2	22.3
B. Plant Ship, 13-15° N/75-80° W													
50	0.0	0.3	0.3	0.4	0.4	0.7	0.6	0.8	1.0	0.8	0.5	0.0	0.5
100	1.0	1.3	1.3	2.0	2.7	3.6	3.4	3.6	4.0	3.7	2.3	1.2	2.5
700	20.1	19.7	19.6	20.2	20.6	21.2	21.0	21.3	21.5	21.0	20.7	20.0	20.6
900	21.4	20.9	20.9	21.6	22.1	22.6	22.4	22.6	22.7	22.3	22.1	21.6	21.9
1000	21.6	21.3	21.3	22.0	22.5	23.0	22.8	23.0	23.2	22.8	22.7	22.0	22.4
1200	22.4	21.9	21.8	22.5	22.9	23.5	23.3	23.6	23.7	23.4	23.2	22.6	22.9
C. Dampier Land, 13-18° S/118-121° E													
50	1.6	0.6	1.0	0.8	0.4	0.2	0.4	0.4	0.8	1.5	2.0	1.5	0.9
100	4.7	4.6	4.5	4.3	3.0	1.8	1.4	1.5	2.0	3.3	4.3	4.7	3.3
700	21.7	21.1	20.9	21.3	21.0	20.4	19.3	19.3	19.8	21.2	21.9	21.9	20.8
900	22.0	21.5	21.3	21.7	21.4	20.7	19.6	19.6	20.1	2.4	22.2	22.2	21.1
1000	23.1	22.5	22.4	22.9	22.6	21.9	20.7	20.7	21.2	22.5	23.3	23.2	22.6
1200	23.8	23.2	23.0	23.5	23.2	22.6	21.4	21.4	21.9	23.2	23.9	23.9	22.9
D. Plant Ship, 5-10° N/90-95° W													
50	9.6	9.0	9.2	10.1	11.3	12.3	12.4	12.0	11.1	10.6	10.5	10.2	10.7
100	12.8	13.4	13.9	14.9	15.0	14.7	14.2	13.8	13.9	13.7	13.5	13.3	12.8
700	20.1	21.0	21.7	22.6	22.6	21.9	21.2	20.8	21.1	21.2	20.8	20.6	21.3
900	21.3	22.0	22.8	23.6	23.6	23.0	22.3	22.0	22.3	22.3	22.0	21.8	22.4
1000	21.7	22.4	22.9	23.9	23.9	23.4	22.7	22.4	22.7	22.7	22.4	22.2	22.8
1200	22.5	23.2	23.6	24.6	24.6	24.1	23.5	23.2	23.5	23.5	23.3	23.1	23.6

The upper mixed layer depth at each potential site was also considered. Mixed layer depths are affected by several types of processes including stirring by the wind, mixing caused by radiative cooling and heating, by advection, and by divergence and convergence of currents causing organized vertical motions. An upper mixed layer ideally is deep enough to assure an intake of uniformly warm water. Ideally, it is not so deep that the effluent can be discharged below the upper mixed layer in order to minimize the possibility of recirculation. An adequate upper mixed layer depth is available at nearly every one of the ten potential OTEC locations studied. Each of the ten sites has an adequate mixed layer during some seasons of the year and most throughout the year. The Pacific Plant Ship site and the Ivory Coast site may be subject to occasional periods in which the upper mixed layer is not deep enough to assure a $\Delta T > 16.7\,^{\circ}C$.

The most desirable OTEC sites are not subject to frequent tropical storms, have minimum sea and swell, and do not have extreme current conditions. Predictable periods of good weather and calm sea and swell occur at each of these ten newly investigated potential OTEC plant areas with sufficient frequency and duration, to permit installation of floating, bottom mounted or on-shore systems. Many of the areas which have the best thermal potential have relatively high-tropical and/or extra tropical storm damage potential from high winds and heavy seas. Guam and Manila, for example, have excellent thermal resources, but are also frequently subjected to damage by storms. Storm damage potential due to heavy seas can be reduced by putting the power plant on shore, where the bathymetry and thermal resources make this feasible. It is also possible that a cruising plant ship could avoid the brunt of some storms. Current structure is another important site selection consideration. Currents contribute to the replenishment of the warm water supply and help accomplish dispersion of the mollifed water discharged by the plant. Current stresses and horizontal and vertical shears are also important design considerations.

TABLE 5: Monthly and Annual Mean ΔTs for Four Sites (°C)

A. Guam, 12-15° N/142-146° E

Depth	Month												
	1	2	3	4	5	6	7	8	9	10	11	12	Annual Mean
50	0.1	0.0	0.1	0.3	0.3	0.3	0.2	0.5	0.3	0.4	0.3	0.2	0.3
100	1.0	0.7	0.6	0.9	1.2	1.5	1.8	2.2	2.4	2.7	2.3	1.9	1.6
700	22.5	22.2	22.4	22.5	22.8	23.1	23.3	23.4	23.4	23.4	23.3	22.7	22.9
900	23.3	22.9	23.2	23.2	23.5	23.9	24.2	24.4	24.4	24.3	24.1	23.5	23.7
1000	23.7	23.4	23.6	23.6	23.9	24.2	24.5	24.8	24.8	24.7	24.5	23.9	24.1
1200	24.5	24.1	24.3	24.4	24.6	24.9	25.1	25.3	25.3	25.3	25.2	24.7	24.8

B. Off Mexico, 20-33° N/105-110° W

50	1.3	3.8	3.2	4.6	6.4	7.2	7.7	7.8	7.7	6.4	5.1	5.2	5.5
100	9.2	8.0	7.8	8.8	9.8	11.3	11.9	13.5	13.0	12.5	11.7	9.9	10.6
700	18.3	17.1	16.6	17.4	17.8	19.4	20.5	22.0	22.1	21.6	21.2	19.3	19.4
900	19.5	18.2	17.7	18.4	18.8	20.5	21.6	23.2	23.1	22.7	22.2	20.4	20.5
1000	19.9	18.7	18.0	18.7	19.1	21.0	22.1	23.6	23.5	23.1	22.6	20.8	20.9
1200	20.6	19.4	18.7	19.4	19.8	21.7	22.8	24.3	24.2	23.8	23.3	21.5	21.6

C. Ivory Coast, 3-6° N/3-8° W

50	8.4	8.4	7.7	7.0	5.9	6.2	6.1	6.8	6.4	5.1	6.4	8.5	6.9
100	11.7	11.6	11.5	11.4	11.2	10.3	9.4	8.6	8.3	8.3	10.4	11.6	10.4
700	21.9	21.9	22.3	22.6	22.5	21.4	19.9	18.7	18.6	18.9	21.1	22.1	21.0
900	22.8	22.8	23.1	23.4	23.4	22.3	20.7	19.1	19.4	19.7	22.0	22.9	21.8
1000	23.1	23.1	23.3	23.6	23.5	22.4	20.9	19.8	19.7	20.0	22.2	23.2	22.1
1200	23.3	23.3	23.5	23.8	23.7	22.6	21.1	20.0	19.9	20.2	22.4	23.4	22.3

D. Manila, 14-16° N/118-120° E

50	0.4	0.9	1.6	2.4	2.6	2.0	1.4	0.9	0.9	0.8	0.7	0.4	1.3
100	5.4	5.6	6.2	7.2	7.6	7.1	6.4	5.6	5.5	5.5	5.8	5.1	6.1
700	20.9	20.6	21.0	21.8	22.4	22.4	22.2	22.2	22.3	22.2	21.9	21.3	21.8
900	22.3	22.1	22.5	23.5	24.3	24.5	24.1	23.9	23.9	23.7	23.3	22.8	23.4
1000	22.8	22.6	23.1	24.1	25.0	25.1	24.7	24.4	24.4	24.2	23.9	23.2	24.0
1200	23.5	23.4	23.9	24.9	25.7	25.9	25.5	25.3	25.2	25.1	24.7	24.0	24.8

TABLE 6: Monthly and Annual Mean ΔTs for Three Sites (°C)

A. Jakarta, 6-9° S/104-109° E

Depth	Month												Annual
	1	2	3	4	5	6	7	8	9	10	11	12	Mean
50	0.6	0.5	0.6	0.7	0.5	0.1	0.3	0.3	0.4	0.6	0.7	0.3	0.5
100	4.4	5.3	6.0	6.0	5.9	5.9	5.9	5.7	4.8	4.6	4.1	4.1	5.2
700	21.2	21.0	21.1	21.3	21.4	21.5	21.2	20.5	19.8	19.5	20.2	20.7	20.8
900	22.6	22.5	22.5	22.8	22.9	22.9	22.7	21.4	21.3	21.0	21.8	22.3	22.3
1000	23.1	23.0	23.1	23.4	23.5	23.4	23.2	22.4	21.9	21.7	22.5	22.9	22.8
1200	23.9	23.8	23.9	24.3	24.4	24.3	24.0	23.2	22.8	22.7	23.4	23.7	23.7

B. Mombasa (North Section), 0-3° N/40-45° E

50	0.5	0.6	0.4	1.0	0.9	0.9	0.2	0.2	0.8	0.8	0.7	0.9	0.6
100	2.0	2.5	3.2	5.7	7.5	7.5	5.4	4.0	4.6	5.5	5.8	6.9	5.1
700	17.6	18.0	18.7	19.6	19.5	18.7	17.3	16.6	16.9	17.2	17.7	17.2	17.9
900	18.8	19.1	19.7	20.4	20.3	19.7	18.4	17.7	18.0	18.3	18.8	18.3	19.0
1000	19.2	19.7	20.5	21.1	21.0	20.2	19.0	18.2	18.4	18.7	19.3	18.8	19.5
1200	20.3	20.8	21.9	22.5	22.2	21.3	20.2	19.4	19.7	19.9	20.4	19.8	20.7

C. Mombasa (South Section), 0-5° S/40-45° E

50	0.8	1.0	1.1	1.5	1.1	0.7	0.4	0.4	0.6	0.8	1.1	1.1	0.9
100	5.3	4.7	4.7	6.4	6.8	6.4	4.7	4.0	3.5	3.9	4.9	5.6	5.1
700	18.6	18.9	19.4	20.2	19.8	18.9	17.9	17.1	17.2	18.0	18.9	19.1	18.7
900	19.8	20.0	20.4	21.4	21.2	20.0	18.8	18.0	18.2	18.8	19.7	20.1	19.7
1000	20.1	20.4	21.2	22.0	21.7	20.5	19.3	18.5	18.7	19.3	20.2	20.3	20.2
1200	21.1	21.4	22.1	23.0	22.6	21.5	20.3	19.4	19.7	20.4	21.3	21.4	21.2

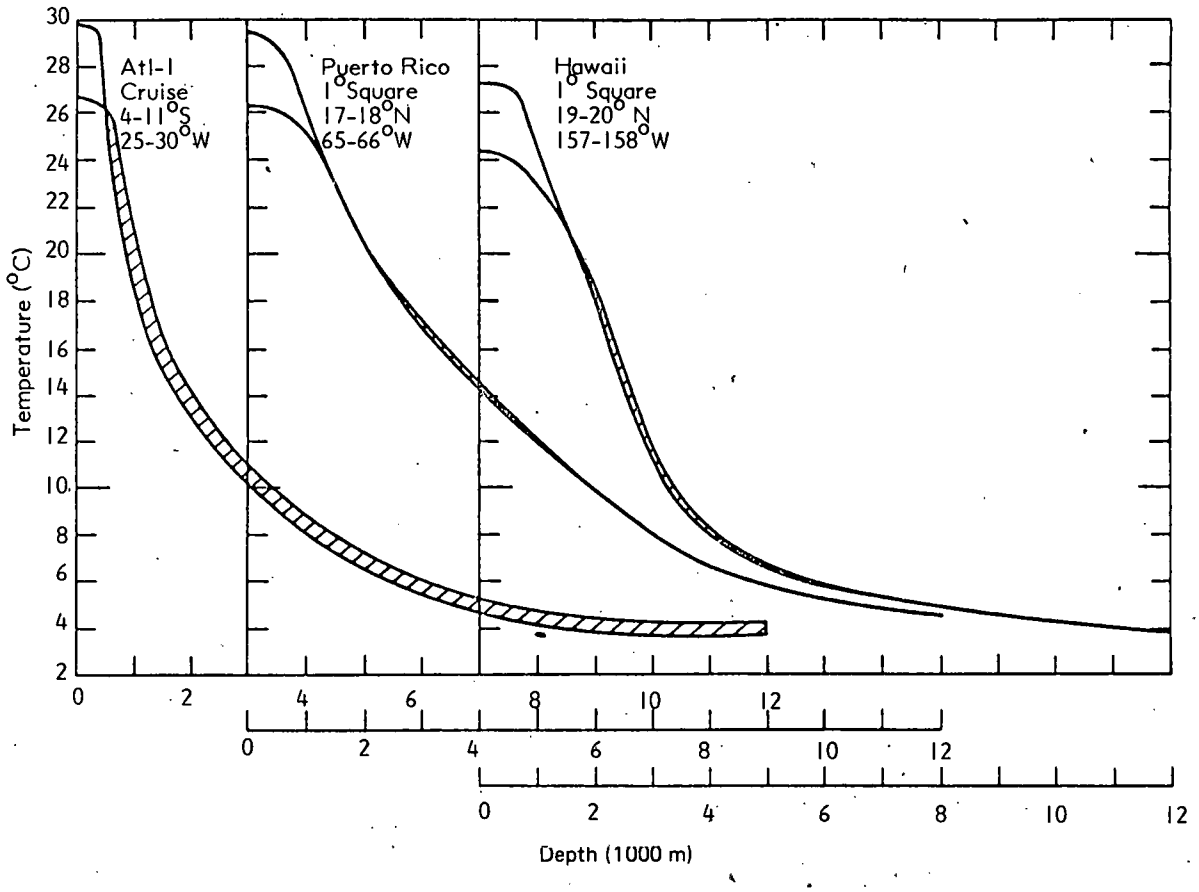

FIGURE 3: Temperature-Depth Variations for Three Sites.

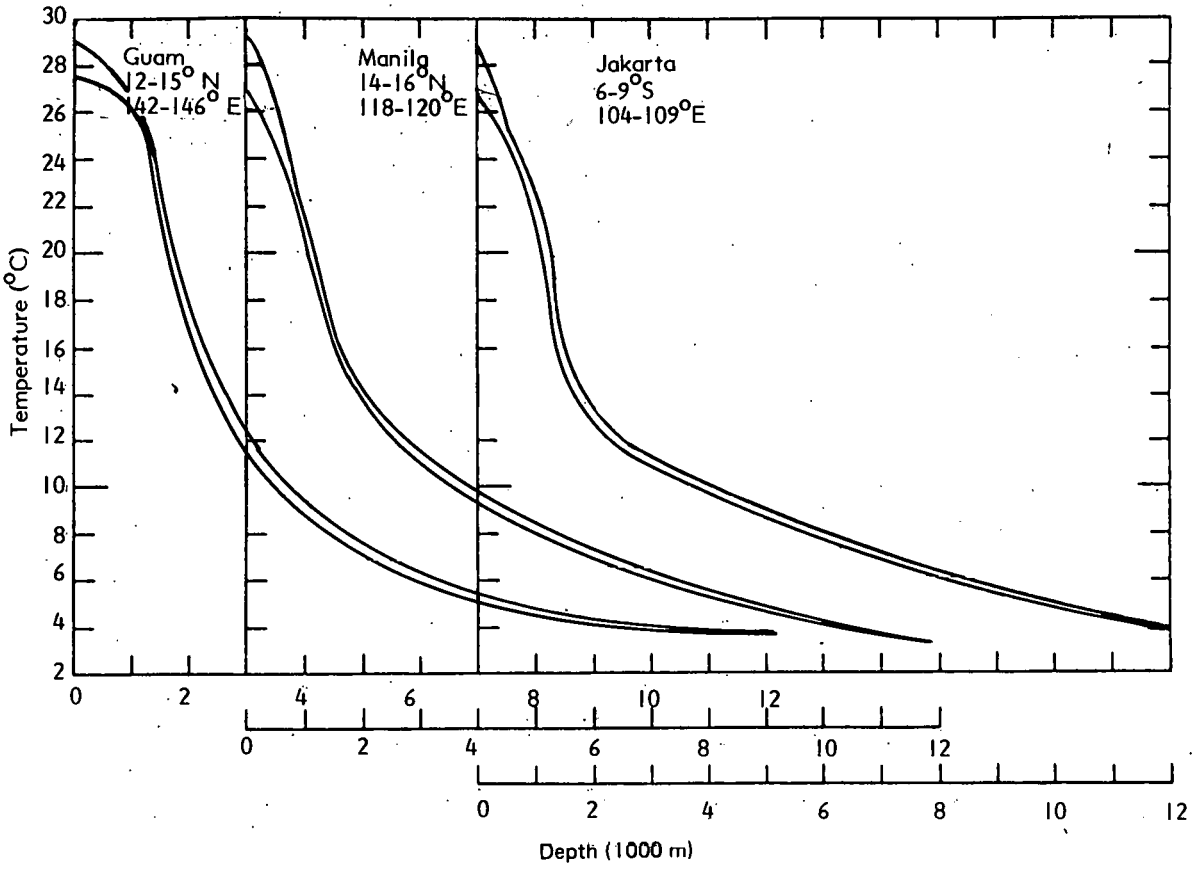

FIGURE 4: Temperature-Depth Variations for Three Sites.

References

1. Wolff, Paul M., and William E. Hubert, "Ocean Thermal Energy Conversion Resource, Ecological and Environmental Studies", Contract No. NSF-C1020, Ocean Data Systems, Inc., Monterey, California, March 1976.

2. Ocean Data Systems, Inc., U.S. Department of Energy Contract No. ET-78-C-01-2898, 1979.

3. Wolff, Paul M., et al, "OTEC Thermal Resource Report for Hawaii", Contract No. EG-77-L-01-4028, Ocean Data Systems, Inc., Monterey, California, October 1977.

4. Cohen, Robert, "An Overview of the U.S. OTEC Development Program", U.S. Department of Energy, Washington, D.C. 20545, November 1978.

5. See Appendix A of G.H. Lavi and C. Zener, "A Comparison of Two Generic OTEC Systems and Missions", G.E. loup, editor, Proceedings, Fourth Annual Conference on Ocean Thermal Energy Conversion, OTEC, University of New Orleans, Louisiana, March 22-24, 1977, pp. II-11-25.

6. Dugger, G.L., Naef, F.E. and Snyder, J. Edward, III, "Ocean Thermal Energy Conversion", Chapter 19, Solar Energy Handbook, (McGraw Hill), to be published.

REGIONAL-SCALE SEA SURFACE TEMPERATURE DETERMINATION FROM THE GEOSTATIONARY ENVIRONMENTAL OPERATIONAL SATELLITE

George A. Maul

National Oceanic and Atmospheric Administration
Atlantic Oceanographic and Meteorological Laboratories
Miami, Florida 33149

Abstract

Sea surface temperatures determined from the digital GOES data base require five steps for quantification: First, the data have to be remapped into a rectangular matrix. Second, using optional decision strategy, cloud-free pixels are identified from joint visible-infrared probability distributions. Third, atmospheric corrections for infrared radiative transfer are calculated from upper air soundings in the region of interest. Fourth, the corrected satellite data are least-squares adjusted to surface observations because the GOES data have no absolute blackbody reference calibration. Fifth, the data are composited and prepared for analysis of variability with application to OTEC thermal resource. Error analysis of this scheme suggests that the rms error for 10 km resolution surface temperature will be ± 1° K or less.

Introduction

Determining the sea surface temperature distribution for a regional-scale area such as the Gulf of Mexico at high spatial resolution is a problem to which earth observation satellites are well suited. Since August 1976, the National Climatic Center (NCC) has archived visible and infrared observations from the Geostationary Operational Environmental Satellite (GOES) in digital form. These data are the only multi-year digital archive at NCC at full sensor resolution prior to the autumn of 1978, when storage began on data from the newly launched TIROS-N polar orbiting spacecraft. The archived GOES data are the basis for this analysis of sea surface temperature variability in a regional-scale area because 10 km spatial resolution is required for the last few years.

Visible and infrared data are collected on GOES by the Visible-Infrared Spin Scan Radiometer (VISSR). Although the VISSR observes the full earth disk on a nominal 30 minute repeat schedule, only data that were observed at 0930, 1000, 1600, 2130, and 2200 GMT are archived on computer compatible tapes (from the geostationary satellite which orbits above 0°N, 75°W). The geographic coverage is 88° latitude by 99° longitude from August 1976 to the present, but only the 1600 GMT observation is a visible-infrared pair. Resolution of both the visible and the infrared data is about 8 km at mid-latitudes, and the earth-location of each picture element is about ± 10 km.

The infrared data are not calibrated in the accepted sense of the word. Output from the detector on the spacecraft is corrected on a weekly basis to compensate for an annual fluctuation in the sensor response. There is no routine comparison between the detector output and a blackbody calibration source in the VISSR as designed for GOES. Accuracy of VISSR temperatures is 2°K - 4°K except near

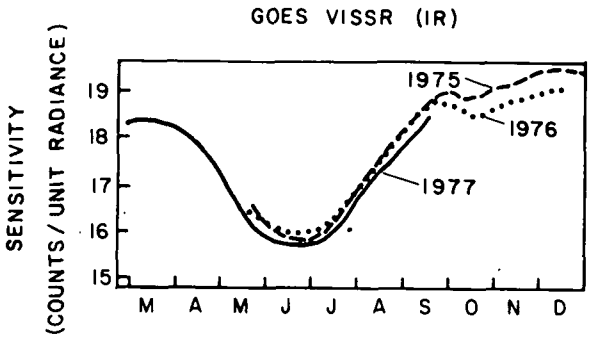

Fig. 1 Long period fluctuation in GOES infrared sensitivity per unit radiance (J. Lienesch, NOAA/NESS, personal communication).

eclipse times (three weeks on either side of the equinoxes) when an additional 4°K error can occur due to thermal fluctuations on board the spacecraft as it moves through the earth's shadow (Hunolt, 1978). Precision of the equivalent blackbody temperatures measured on GOES is very good with a NEΔT of 0.22°K at 300°K, so that while the absolute values are in error, the relative values are stable. VISSR visible data, on the other hand, are completely uncalibrated even in the sense shown in Figure 1 for the infrared.

The above discussion on VISSR accuracy applies only to the radiances measured at the spacecraft. In order to convert the VISSR values to accurate surface values, the atmospheric effects must be quantified and then the relative (atmospherically corrected) surface values must be calibrated by using surface ship or aircraft observations. Correction for the atmosphere involves solving the infrared radiative transfer equation for the distribution of temperature and relative humidity as a function of pressure at a number of stations in the region of interest. An example of the range of atmospheric corrections to GOES observations (Maul, et al., 1978) is shown in Figure 2 for the western North Atlantic Ocean. The values plotted for a winter and summer month are the differences between sea surface temperature (T_S) and the temperature calculated (T_C) from the radiative transfer model of Maul and Sidran (1973). Even for an area the size of the Gulf of Mexico, differences in atmospheric correction of more than 1° - 2°K exist which precludes using surface values only to correct the VISSR data.

The background information given in this introduction provides the framework around which VISSR data will be used to quantify sea surface temperature in a regional-scale area. The procedure is to first remap the satellite data at full resolution

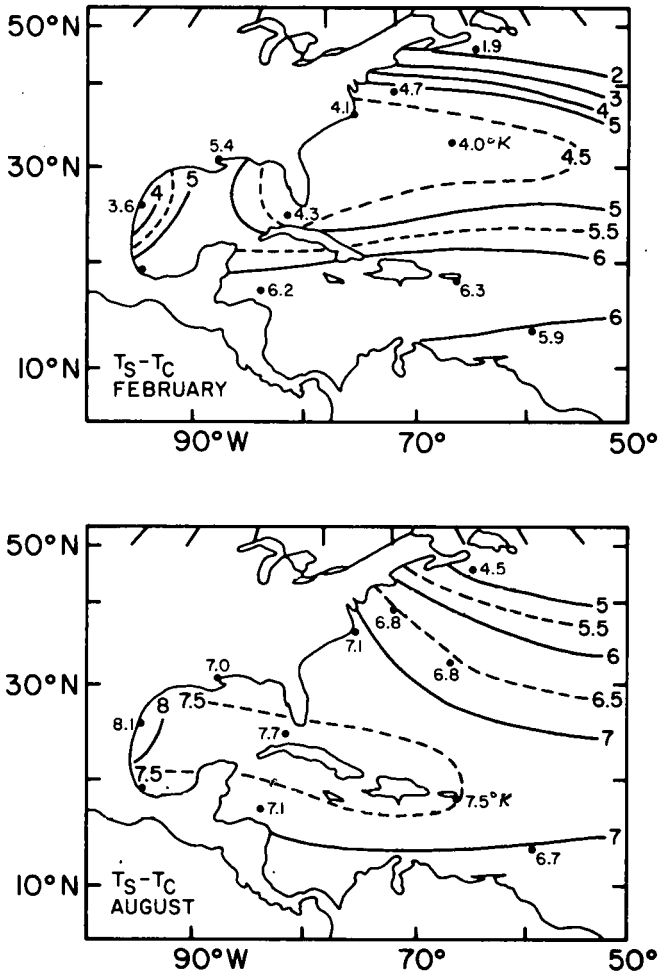

Fig. 2 Correction to mean sea surface temperature for February and August using cloud free radiosondes (Maul, et al., 1978).

into a regularly spaced rectangular matrix using Herman's (1978) algorithm. Second, from a chosen training set, an optimal (Bayesian) pattern classifier is computed to objectively determine the cloud-free matrix elements using the technique outlined by Swain (1978). Third, the cloud free data are corrected for the atmosphere using the procedure derived by Maul and Sidran (1973) except that the LOWTRAN-4 (Selby et al., 1978) radiance model is used for the radiative transfer. Fourth, the cloud-free, atmospherically corrected data are least squares adjusted to observed values of surface temperature from reporting stations, ships, and aircraft. Finally, since cloudiness will leave gaps in a single data matrix, composites will be compiled for various time periods depending on the application. Details of each of these steps and an error analysis is given in the following sections.

Forming the Data Matrix

Data from the VISSR, if viewed on an earth coordinates projection, would appear as a series of curved lines on a non-linear geographic system. This is a cumbersome format to efficiently handle the data and a study was performed (Herman, 1978) to fit NCC photogrammetrically located pixels to a least squares determined surface which covers a regional-scale area such as the Gulf of Mexico. Herman (1978) found the order of the least squares surface necessary to best fit the VISSR data was linear by comparing a multiple linear polynomial regression with a multiple quadratic polynomial regression. This allows a geographic matrix with 0.1 degree (~ 10 km) intervals of infrared and visible data to be formed for the regional scale area of interest. Location error of any individual pixel is ± 3 km which is a factor of three less than the surface resolution of the VISSR.

The matrix of located satellite data are next masked in order to eliminate any land features. This translates the satellite data into an n x m matrix with zeros at any unwanted pixel location. The matrices of visible and infrared data are now ready for an objective analysis to determine which infrared pixels are cloud free based on their thermal and visible properties. This procedure is discussed in the next section.

Pattern Classification

Fundamentals of objective pattern classification have been studied by mathematicians and is known as Bayes decision theory (Duda and Hart, 1973). The approach is based on the assumption that the decision problem can be stated in probabilistic terms and that the relevant probabilities are known. The objective analysis needed in sea surface temperature determination from GOES data is to decide which pixels are cloud-free measurements of ocean surface radiance.

As a test case, data from October 1977 over the Gulf of Mexico are chosen because the research ships GYRE and RESEARCHER were at sea providing surface calibration information. An example of a visible and an infrared image recorded simultaneously at 1600 GMT on 22 October is shown in Figure 3. Data shown in Figure 3 are typical of the region, and form the basis for the pattern classification discussion to follow.

Many schemes have been suggested to identify or eliminate clouds using an infrared channel only (e.g., La Violette and Chabot, 1969; Smith et al., 1970; Tarpley and Raymond, 1975). Each of these methods has the advantage of requiring only one channel of information to process a temperature value, but each ignores the possibility that some clouds are thermally indistinguishable from the ocean. This is clearly illustrated in Figure 4 which is a portion of the joint histogram between visible and infrared data shown in Figure 3 of the Gulf of Mexico; values over land are excluded by using a binary mask in the mapping routine and excluding zeros from the statistics.

The maximum in the correlation of Figure 4 occurs at 295°K and visible radiance count 12. There are correlations with 295°K at visible counts as high as 30. Visible count 30 has temperatures associated with it as low as 237°K, which is well below freezing and clearly represents a cloud. Results such as these eliminates any serious consideration of using infrared data only in order to adequately determine sea surface temperature. Unfortunately in the GOES data, only one visible-infrared pair is recorded per day, which according to the Nyquist sampling theorem, limits time-series analysis to periods of two days and longer.

The second important feature of Figure 4 is that there is only one maxima of any significance. A cursory glance at Figure 3 would have suggested at least two: one high temperature/low visible radiance peak representing open ocean, and one low temperature/high visible radiance peak representing clouds. Careful reexamination of Figure 3 supports the histogram and shows a wide range of visible radiances which probably represents the range of cloud heights and sizes expected over the Gulf. This result eliminates the possibility of objective clustering techniques (cf. Swain, 1978) to partition the data into cloud-free and other categories. Further, the one-dimensional visible radiance histogram (Figure 4) shows that an arbitrary visible count cut-off for cloud-free data is unrealistic because the visible histogram is strongly skewed to the right. Conversely, the infrared one-dimensional histogram (Figure 4) is skewed to the left but with a more clearly defined central tendency. It may be possible to perform unsupervised

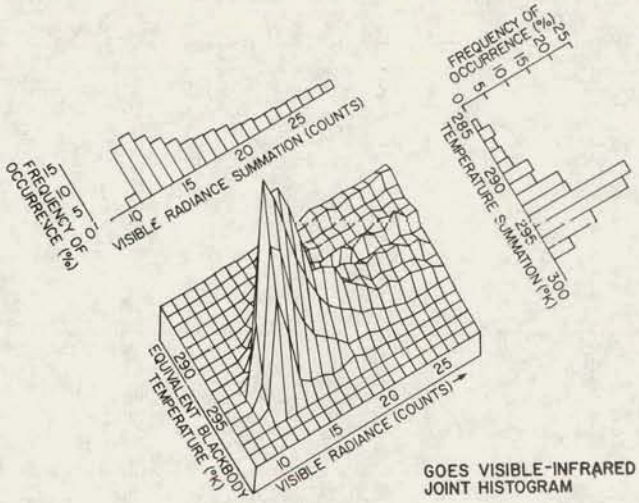

Fig. 4 Joint visible and infrared histogram from the GOES data over the Gulf of Mexico shown in Figure 3, data points over land are excluded.

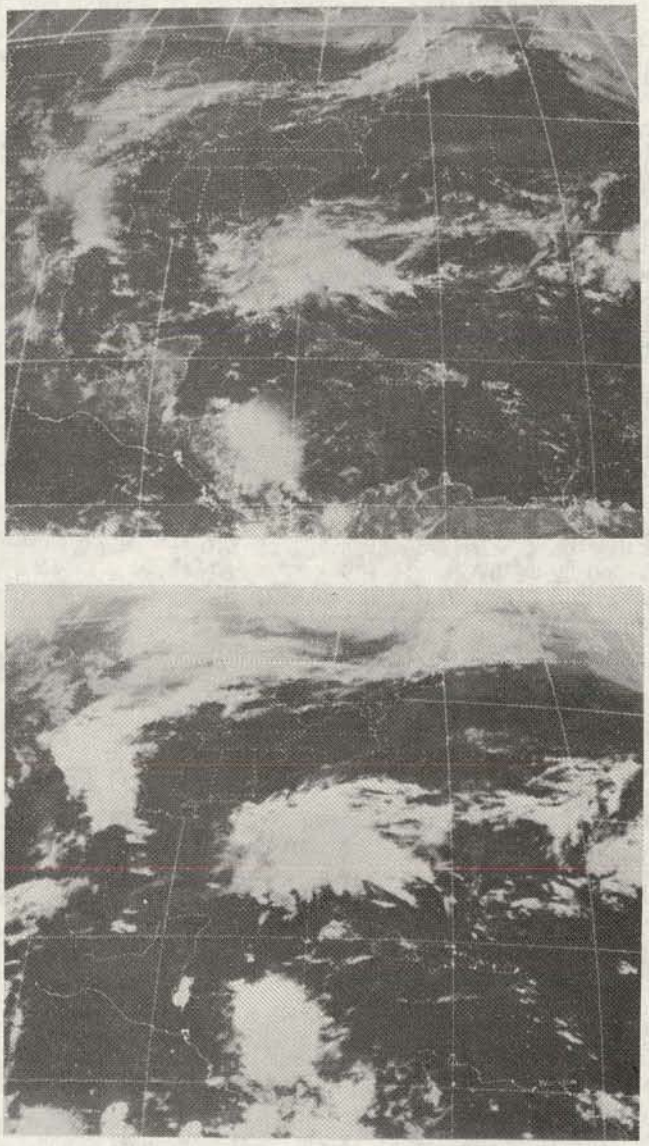

Fig. 3 GOES visible (upper panel) and infrared (lower panel) images simultaneously observed at 1600 GMT, 22 October 1977.

analysis of the data using several cloud levels as well as clear day clusters, but statistical separability would be poor using any measure of Euclidean cluster center divergence.

The usual approach to objectively classifying a cluster is to choose a discriminant function $[g_i(X)]$ based on a maximum likelihood decision rule. Swain (1978) has shown that

$$g_i(X) = p(X|\omega_i)p(\omega_i) \qquad (1)$$

where $p(X|\omega_i)$ is the probability density function associated with the measurement vector X, given that X is from a pattern in class i, and $p(\omega_i)$ is the probability of observing a pattern from class i independent of any other information. For application to the GOES data, $p(X|\omega_i)$ will be calculated from a training pattern and a threshold will be assigned to the probability density function so as to conservatively select a cloud free area.

Due to the sensor characteristics of the VISSR, training patterns will have to be selected for each visible/infrared image pair. For the infrared image shown in Figure 3, a typical partly cloudy training pattern is shown in the upper panel of Figure 5, and a typically mostly clear training pattern is shown in the lower panel. The upper panel of Figure 5 shows a bimodal frequency distribution which is the type of pattern anticipated for the entire image, and the type of pattern to which clustering would be applicable. Temperature distribution for a relatively cloudless area (lower panel in Figure 5) appears to have a Gaussian distribution which is known (Swain, 1978) to be a useful approximation even if the distribution was markedly asymmetrical. The assumption that the distribution is Gaussian allows the multivariate probability density function to be written:

$$p(X|\omega_i) = \frac{1}{(2\pi)^{n/2}\,|\Sigma_i|^{\frac{1}{2}}} \exp\left[-\tfrac{1}{2}(X-U_i)^T\,\Sigma_i^{-1}(X-U_i)\right] \qquad (2)$$

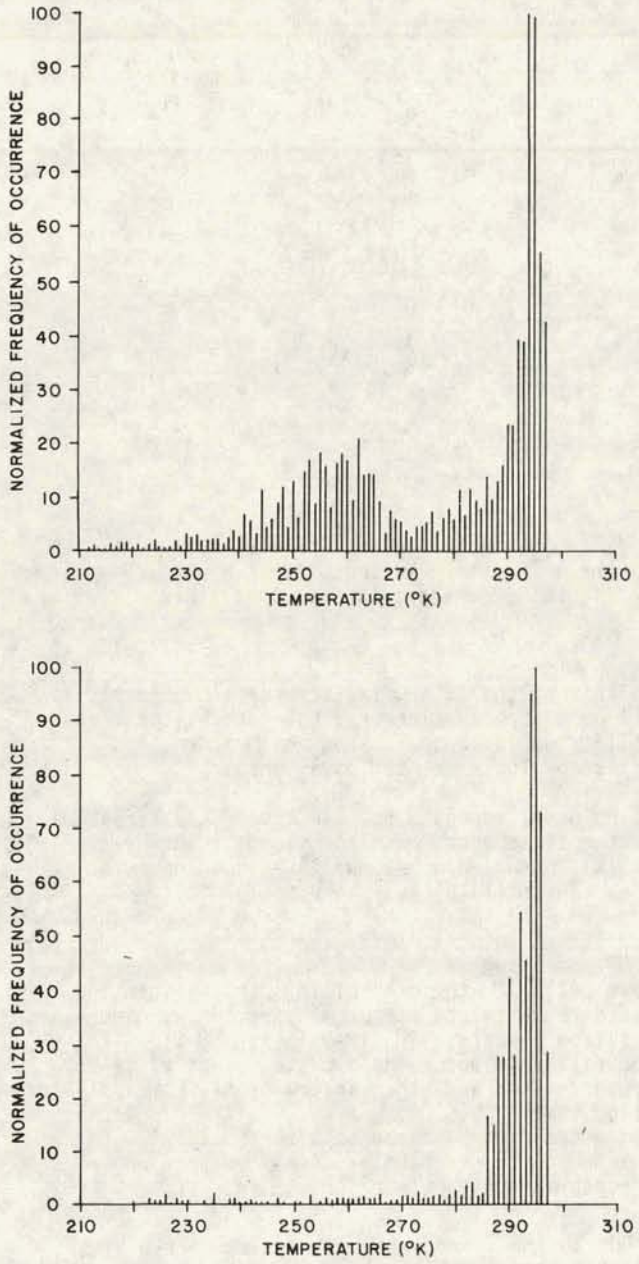

Fig. 5 Infrared histograms from portions of the GOES image shown in Figure 3. Upper panel is from the upper quarter of Figure 3; lower panel is from the lower quarter of Figure 3.

where $|\Sigma_i|$ is the determinant of the covariance matrix Σ_i, $(X-U_i)^T$ is the transpose of the vector $(X-U_i)$, and U is the mean vector for class i. With this formulation, the discriminant function based on the maximum likelihood decision rule that X is contained in ω_i if and only if $g_i(X) \geq$ a threshold value.

Atmospheric Correction

Magnitude of the atmospheric correction is summarized in Figure 2. Physically, radiation received at the spacecraft is the sum of the radiation reflected and emitted by the surface after atmospheric attenuation, plus the radiation emitted by the atmosphere itself. The radiation temperature of the sea is often cooler than the equivalent blackbody temperature due to the complex heat flux across the interface. For most practical problems, the sea can be assumed to be a blackbody and the radiative transfer equation expressed by:

$$L(0) = \int_0^\infty \phi(\nu)\, L(s,\nu)\, \tau(s,\nu) d\nu + \int_0^\infty \int_0^S \phi(\nu)\, L(a,\nu)\, \frac{\partial \tau}{\partial p}\, dp\, d\nu \qquad (3)$$

where L(0) is the radiance received by the VISSR which has a filter function $\phi(\nu)$; ν is the wave number of the radiation in cm^{-1}. The term $L(s,\nu)$ is the radiance of the sea surface given by Plank's Law, $\tau(s,\nu)$ is the transmissivity of the atmosphere from the spacecraft to the surface s, and $L(a,\nu)$ is the radiance of the atmosphere which is a function of atmospheric temperature, pressure, and relative humidity. The first term on the right hand side is the probability ($0 < \tau < 1$) that a surface photon will not interact with the atmosphere, times the energy density of that photon. The second term on the right-hand side of equation 3 represents the contribution from the photons emitted by the atmosphere.

Equation 3 is numerically solved by computer using the transmissivities and the algorithm discussed by Selby et al. (1978). Typical values for the ratio $L(o,\nu)/L(s,\nu)$ are 0.97 to 0.99. Values for τ, however, range from 0.4 to 0.9 (Maul, et al., 1978) which emphasizes the importance of quantitatively assessing the contribution of the second term on the right hand side of equation 3.

Quantitative correction for the atmosphere involves using all the radiosonde data from the perifery of the region, at the hour nearest to image acquisition time. Only cloud-free radiosondes are used, or radiosondes in which the cloud layers can be identified and excluded. Maul and Sidran (1973) showed that a linear relation exists between the equivalent blackbody temperature (calculated from radiosonde data) at the satellite and the surface temperature. Following the arguments set out by Maul et al. (1978), the reason for the linearity in the correction is that the radiative transfer equation can be written:

$$T_0 = T_s\, \tau + (1-\tau)\overline{T}_a \qquad (4)$$

for the 10.5-12.5 μm VISSR channel. In equation 4, T is the equivalent blackbody temperature, the subscripts are the same as in equation 3, and the overbar on the mean air temperature is a result of using the mean value theorem to rewrite the last term on the right hand side of equation 3. Manipulation of

equation 4 shows that a correction, $T_S - T_O$, is a function of T_S, τ, and $\overline{T_a}$; that is, the conversion of T_O to T_S is a function of T_S itself. Therefore, a simple map such as is shown in Figure 2 cannot be constructed to correct the satellite data for the atmosphere.

Correction for the atmosphere is accomplished by objectively mapping the slope and intercept given in equation 4 over the region of interest, and computing corrections based on the matrices of τ and $(1 - \tau)\overline{T_a}$. Resolution of the matrices is such that no error in T_S larger than $0.1^{o}K$ results from the calculations. The cloud-free corrected pixels are now prepared for adjustment to the known surface reports and for compositing.

Adjustment and Compositing

The scheme of deriving sea surface temperatures at full GOES VISSR resolution requires final comparison with reports from the ocean itself in order to convert gradients into absolute values. Ship reports of T_S are generated several times each day as part of their routine weather observations. These reports will form the basis of the satellite data calibration. During special periods where intensive research vessel observations are available, such as with POLYMODE in the Atlantic Ocean, the routine reports are strongly augmented and higher quality values of T_S will be calculated. Since the satellite data are being corrected for a calibration offset only at this point, linear least squares adjustment procedures are employed.

Once the cloud-free, atmospherically corrected, and calibrated data matrices are generated, an objective compositing routine is used to produce time averaged maps. For the Gulf of Mexico, Vukovich, et al. (1978) have shown that variations in the thermal fronts associated with the Loop Current have periods less than a fortnight. It is therefore necessary to composite no more than five to seven days in order to stochastically analyze for these variations.

The nature of cloudiness, however, is that it is associated with atmospheric frontal passages. Usually there are several days following frontal passage which are relatively dry and cloud free. Compositing, which takes advantage of the timing of frontal passages, need involve only two or three days, but then a gap of several days will result between maps. This approach has the advantage of emphasizing the higher frequencies, but with the disadvantage of having randomly spaced data (although randomly spaced data can be analyzed for their spectral content; Vanicek, 1971). Whatever the method finally used, there still is the question: Are the changes in T_S coupled with wind events associated with cloudiness?

Error Analysis

Each stage in the above procedure is a source of error and should be considered separately. Herman's (1978) positioning algorithm reformats the data with location error less than one pixel, i.e., less than 8 km. Many oceanic fronts, however, have temperature changes of several degrees over distances much less than 8 km (cf. Figure 3 near $40^{o}N$, $70^{o}W$). Comparison of satellite derived values of T_S with conventional methods will show large rms deviations if data near strong fronts are included in the comparisons. The question of comparing point data with scan spot data is open to debate; however, errors due to positioning the VISSR data, especially over an enclosed sea whose very boundaries act as additional horizontal control points, are negligible.

Classification errors from the discriminant function (equation 1) depend on how well the training set is chosen, and the threshold level used. For example, the mean and standard deviation (σ) of the peak on the right hand side of the bottom panel in Figure 5 is $293^{o} \pm 3^{o}$. If the threshold in this one-dimensional sample were set at $\pm 1\sigma$, 68% of the data under the normal curve would be included. This choice would exclude temperatures outside the range $290^{o} \leq T \leq 296^{o}$. If the probability of a value belonging to a chosen training set is to be ≥ 0.05, then $\sigma = \pm 1.6$ and the range of acceptable temperatures is $288^{o} \leq T \leq 298^{o}$. This example suggests that σ should be less than ± 2, and that error will be minimal if the threshold is conservatively chosen.

Selby et al. (1978) show remarkable agreement between their calculated spectra and observed spectra. Since the radiative transfer calculations will be to $0.1^{o}K$, the results of the calculations themselves will contribute negligible error. A significant error source will be lack of knowledge about the atmospheric conditions between radiosonde stations. Based on the calculations of Maul et al. (1978) over the western North Atlantic, this error is about $\pm 0.4^{o}K$ for a basin the size of the Gulf of Mexico.

Error due to compositing several days data can be quite large, greater than $1^{o}K$ near oceanic fronts. However, if these areas are excluded in the comparisons, and ship reports are correlated with satellite data, the scatter diagram should be without form. The diameter of this cluster is the final statement of error for the procedure outlined above. With care in choosing the training set and upper air data, and conservative threshold limits, it appears that full resolution satellite derived sea surface temperatures should not be in error by more than $1^{o}K$.

References

Duda, R. O. and P. E. Hart (1973). Pattern classification and scene analysis. Wiley, New York, 482 pgs.

Herman, A. (1978). An algorithm for positioning satellite radiometer data. NOAA-AOML, Miami, FL 33149. Unpublished manuscript.

Hunolt, G. W. (1978). VISSR archive users' guide. NOAA-NCC, Satellite Data Services Branch, Washington, D.C. 20233. Unpublished manuscript.

La Violette, P. ahd P. Chabot (1969). A method of eliminating cloud interference in satellite studies of sea surface temperature. Deep Sea Res., 16 (5), pp. 539-548.

Maul, G. A. and M. Sidran (1973). Atmospheric effects on ocean surface temperature sensing from the NOAA Satellite Scanning Radiometer. J. Geophys. Res., 78 (12), pp. 1909-1916.

Maul, G. A., P. W. deWitt, A. Yanaway and S. R. Baig (1978). Geostationary satellite observations of Gulf Stream meanders: Infrared measurements and time series analysis. J. Geophys. Res., 83 (C12), pp. 6123-6135.

Selby, J. E. A., F. X. Kneizys, J. H. Chetwynd, Jr. and R. A. McClatchey (1978). Atmospheric transmittance/radiance: Computer code LOWTRAN 4. U. S. Air Force, AFGL-TR-78-0053, Hanscom AFB, Mass. 01731, 100 pgs.

Smith, W., P. Rao, R. Koffler and W. Curtis (1970). The determination of sea surface temperature from satellite high resolution infrared window radiation measurements. Mon. Wea. Rev., 98 (8), pp. 604-611.

Swain, P. H. (1978). Fundamentals of pattern recognition. In: Swain, P. H., and S. M. Davis (1978). Remote Sensing, The Quantitative Approach. McGraw-Hill, New York, pp. 136-187.

Tarpley, J. D. and B. A. Raymond (1975). Automated measurement of sea surface temperature from a geostationary environmental satellite. Proceedings of tenth international symposium on remote sensing of environment, Vol. 1, Environmental Research Institute of Michigan, Ann Arbor, pp. 139-148.

Vanicek, P. (1971). Further development and properties of spectral analysis by least-squares. Astrophys. and Space Sci., 12, pp. 10-33.

Vukovich, F. M., B. W. Crissman, M. Bushnell and W. J. King (1978). Sea surface temperature variability analysis of potential OTEC sites utilizing satellite data. Research Triangle Institute, Research Triangle Park, NC 27709, 153 pgs.

DISCUSSION

Question: Is there spectrographic data from GOES that you could use?

G. Maul: No, the GOES satellite has two narrow spectral windows; one visible around 0.5 to 0.9 μm, and one IR channel which is 10.5 to 12.5 μm. We only have two bits of information to work with. We don't have spectrographic information.

Question: Are there other satellites with spectrographs looking at the earth?

G. Maul: Not spectrographs; there are other satellites which have more channels that look at the earth. The Tiros-AVHRR, for example, has four channels, and it turns out that one channel is not useful (first of all, the channel is not operating properly) but also it's not useful because in the daytime, when cloud information is available from visible channels, it is contaminated with reflected infrared radiation, so you can't use it for this type of analysis. So again you are stuck with basically two channels on either spacecraft. The only reason we're using GOES is that it's the only data set that goes back several years...

Question: For areas like the Hawaiian Islands and some of the more classical OTEC locations, you are talking about a probable total error in measurement of 1+ °C, and you are only getting a 3° or 4°C variation throughout the semitropical and tropical areas of the oceans. Maybe it's not such a good tool.

G. Maul: That is a possibility, particularly in an area including Hawaii where the temperature gradient at the surface is going to be reduced in the summertime because of water vapor in the atmosphere.

Question: In terms of the mechanics of all this, you say this is pretty detailed, is it labor intensive, computer intensive?

G. Maul: Labor intensive. Once we get the system set up and running, I think it will be computer intensive. It can be mechanized.

LARGE COLD TONGUES IN THE EASTERN GULF OF MEXICO AND THEIR POTENTIAL EFFECT ON OTEC

Fred M. Vukovich

Research Triangle Institute
P. O. Box 12194
Research Triangle Park, N. C. 27709

Abstract

A large, narrow, cold tongue was detected in May 1978, extending southward from the northern boundary of the Loop Current. Similar tongues were detected in the spring of 1977 and 1975. The 1977 intrusion was described by Vukovich et al. (1978). These tongues penetrated as far as 400 km southward and persisted for as long as 73 days. They originated as meanders on the northern boundary of the Loop Current. Limited *in situ* data (one case study) has indicated that there is greater cooling in the subsurface layers than in the surface layers in the cold tongues. This, in fact, produced an increase in the vertical temperature difference or enhancement of the OTEC resource. Further study is needed to provide more substantial statistics.

Introduction

The primary purpose of this research was to continue the analysis of the variability of the sea surface temperature in the eastern Gulf of Mexico. Satellite infrared data for the periods 1973-1978 were used to identify and locate major thermal fronts at the sea surface. The primary emphasis, however, was placed on the analysis of 1978 NOAA-5 infrared data. *In situ* data were used, whenever available, to determine the magnitude of various aspects (e.g., temperature difference and depth of layers) of the ocean features.

In the course of this study, it was noted that the most prominent perturbation that developed in the eastern Gulf of Mexico during 1978 was a large cold tongue that surged into the Loop Current. The cold tongue began to develop in late April and was fully developed by the end of May. In reviewing data in the period 1973-1977, similar features were noted in the spring of 1975 and 1977. The feature in 1977 was discussed to some extent in the previous study (Vukovich et al., 1978). More detailed results of the analysis of these features are now presented.

Analysis Results

Cold tongue was noted in the winter of 1975. Though the thermal contrast was sufficient to represent the life history of this event using infrared images, the boundaries of the Loop Current were used to demonstrate the life history in order not to confuse the principal feature of interest with other phenomena that occurred during that period. The boundaries of the Loop Current were transposed to gridded maps.

Cold tongue initiated from a meander on the northern boundary of the Loop Current. The meander was detected on 26 December 1974 (Figure 1) and

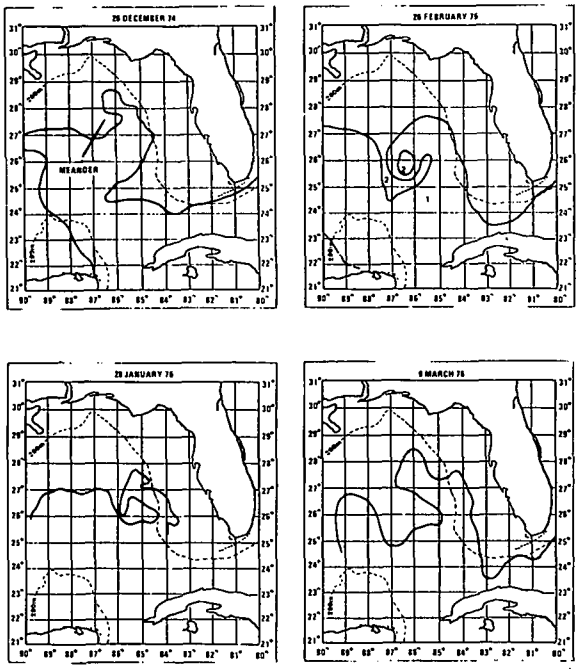

Fig. 1 Graphical presentation of the history of the development of a cold tongue in the eastern Gulf of Mexico based on NOAA VHRR data for the period 26 December 1974 through 9 March 1975

was centered around 27.5°N and 86.5°W. The wavelength of the meander was approximately 250 km and the amplitude was 140 km. The position of the meander remained relatively constant for the rest of the month.

Cloudiness obscured the sea surface for most of the early part of January 1975. It was not until late January that an unobstructed view of the sea surface in the region of interest was acquired. On 28 January, a cold tongue was noted on the northern boundary of the Loop Current extending some 140 km to the south. The cold tongue was narrow at its origin, the northern boundary of the Loop Current, but then broadened as it turned in a cyclonic manner to the east and north forming a large cold zone. The position of the cold tongue was somewhat east and south of that for the meander noted on 26 December 1974.

Over the next 30 days, the feature drifted westward and the cold tongue surged southward at an average speed of 4 cm s^{-1}. On 26 February 1975, the cold tongue extended some 280 km to the south rela-

tive to the northern boundary of the Loop Current. The southern part of the cold tongue turned in a cyclonic manner to the east and then northward. The narrowing of the cold tongue was evidently due to the surging of the Loop Current water in a cyclonic manner to the west, then to the south, and finally to the east, apparently isolating a lens of cold water. The circulation, to some extent, appeared to be centered around the cold lens, which was located at about 26°N and 86°W.

By 9 March 1975, mixing had apparently taken place within the cold tongue, leaving a broad zone of cold water extending some 240 km from the northern boundary of the Loop Current. The cold zone separated two zones of warm Loop Current water and appeared similar to the meander detected on 26 December 1974.

This case yielded indications of a cyclonic circulation system associated with development of the cold tongue. The thermal structure at the surface on 26 February associated with the circulation has a cold central core encircled by warm Loop Current water and by cold ambient Gulf of Mexico water (the cold tongue) at the outer fringes. This structure is very similar to that associated with cyclonic rings in the Sargasso Sea (Vukovich, 1976) and suggests that the circulation system entrained both Loop Current and ambient Gulf of Mexico water, producing the apparent cold and warm tongues. This would imply that the cold tongue, the warm tongue of Loop Current water, and the thermal structure associated with cyclonic circulation systems are separate thermal features but are all related to the same circulation system. Therefore, the potential exists for a variety of effects on the OTEC resource. Effects are conditional on the location of the feature relative to an OTEC system. However, this explanation is conjectural because there were no supporting in situ data.

A similar event was noted in the spring of 1977. On 2 March 1977 (Figure 2), a large amplitude meander was noted on the northern boundary of the Loop Current centered at approximately 28°N and 88°W. The wavelength of the meander was approximately 250 km and the amplitude was 220 km. By 9 March, significant changes had taken place in the surface thermal structure in the region where the meander was located. Warm loop current water had surged southwestward in a cyclonic manner with an average speed of 28 cm s^{-1}. A tongue of cold water had moved northward in a cyclonic manner, but the southeastern boundary had surged eastward and turned in an anticyclonic manner to the south. The average speed of the water in the southwestward direction was 30 cm s^{-1}. Because of these processes, the meander was transformed into a cold tongue which extended some 390 km southeastward from the northern boundary of the Loop Current.

Over the next 30 days the cold tongue underwent minor changes. A significant change occurred in early April. The 7 April image showed that the cold tongue had become very narrow and elongated. It was oriented in a north-northwest to south-southeast manner, extending some 450 km to the south-southeast from the northern boundary of the Loop Current. Between 7 and 11 April cold water surged westward and northward from the west Florida shelf. This water merged with the cold tongue and produced an isolated zone of warm Loop Current water in the northeastern portion of the Gulf of Mexico.

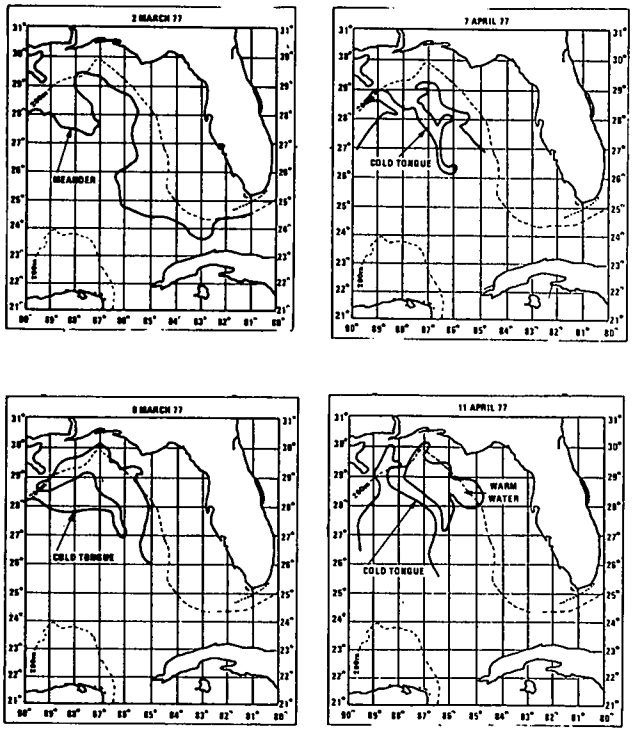

Fig. 2 Graphical presentation of the history of the development of a cold tongue in the eastern Gulf of Mexico based on NOAA VHRR data for the period 2 March through 11 April 1977

This case also showed indications of a cyclonic circulation associated with the development of cold tongue. This, of course, raises the same issue concerning the subsurface thermal structure and the potential effects on the OTEC resources. However, no in situ data could be found to support or refute the contention.

The large cold tongue that developed in the spring of 1978 originated from a meander on the boundary of the Loop Current (Figure 3). The meander was positioned at around 86°W and 26°N and had a wavelength of approximately 250 km and an amplitude of about 90 km. The figure is a NOAA-5 infrared image for 28 April 1978 and the persistence of the feature (it was observed in four separate images over a ten-day period) supports the notion that it was a phenomena occurring at the sea surface and not due to atmospheric interference. The NOAA-5 infrared image on 8 May 1978 (Figure 4) shows that a transition had occurred in the meander. The feature now most closely resembles a cold tongue extending some 250 km from the northern boundary of the Loop Current. The transition was due to two factors. There was a southward surge of cold water from 26°N to 25.5°N latitude; but more importantly, there was a northward surge of Loop Current water east of the cold tongue from about 26°N (which was the farthest north any warm water was detected in the 28 April infrared image) to about 27°N on 8 May. The cold water moved southward to an average speed of 6 cm s^{-1} and the warm water moved northward at an average speed of 12 cm s^{-1}.

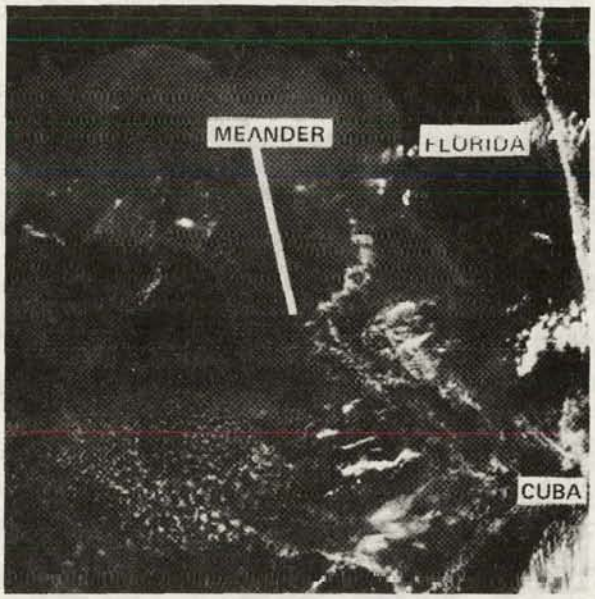

Fig. 3 NOAA-5 VHRR image for 28 April 1978

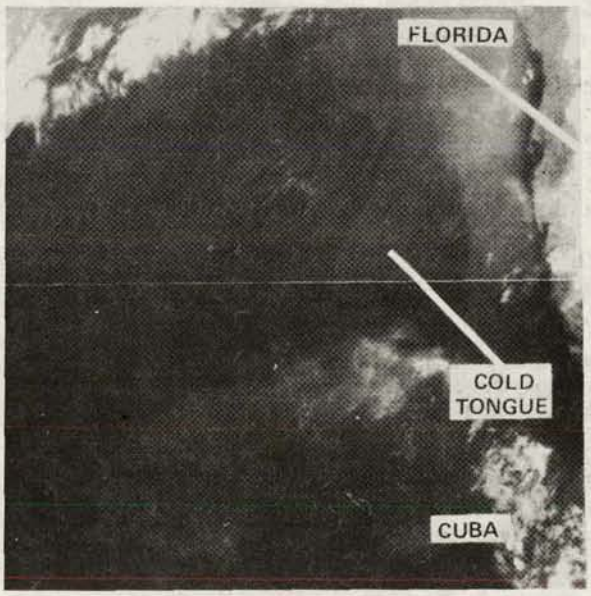

Fig. 4 NOAA-5 VHRR image for 8 May 1978

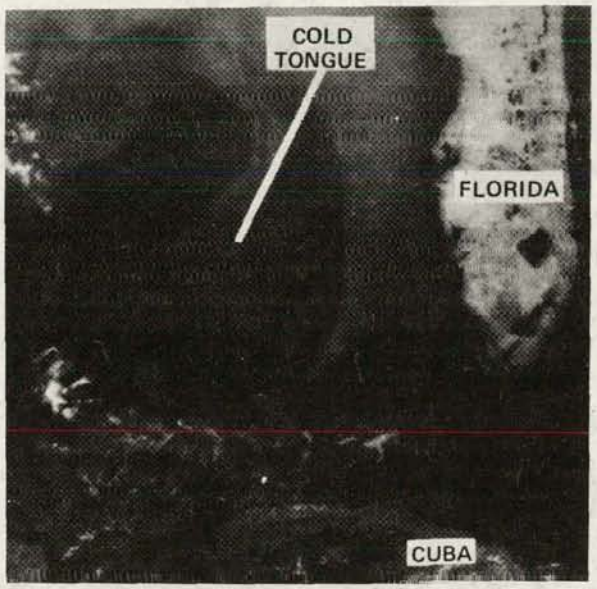

Fig. 5 NOAA-5 VHRR image for 15 May 1978

On 15 May 1978 (Figure 5) an elongated cold tongue was formed in the eastern Gulf of Mexico separating the eastern and western zone of Loop Current water and extending some 360 km southward from the northern boundary of the Loop Current. The cold tongue had surged as far south as 25°N and the warm water to the east had surged as far north as 28°N. The speed of motion of the cold water was, on the average, 9 cm s^{-1} southward, and the warm water averaged 18 cm s^{-1} northward.

The near proximity of the northward and southward moving water measses indicates the presence of cyclonic shear, which suggests a cyclonic circulation. In order to support the cyclonic circulation on the scale indicated in the satellite imagery, a significant subsurface density perturbation is required. This generally would mean a temperature and/or salinity perturbation whose general structure would be similar to the temperature and salinity structure found in cold rings (a dome of cold, low salinity water) on the eastern side of the Gulf Stream (Vukovich and Crissman, 1978, and Vukovich, 1976). Such thermal perturbations generally extend to a significant depth (greater than 1000m) in the ocean. Furthermore, the perturbation was detected for 22 days without any obvious decrease in the thermal contrast in the perturbation. It was not detected after 20 May because cloudiness obscured the sea surface until June and at that time the thermal contrast across the entire Gulf of Mexico was not sufficient to detect any features at the surface.

Figure 4 gives an analysis of in situ temperature data obtained from NOAA's Atlantic Oceanographic and Meteorological Laboratory. XBT data were collected in the cold tongue down to about the 700-m depth during the period 27 to 29 May 1978. The position of the 7 stations used in this analysis relative to the 20 May 1978 position of the cold tongue, as determined from the NOAA-5 data, is given in Figure 6a.

The cross-sectional analysis (Figure 6b) shows a very intense cold dome extending to depths greater than the 700-m depth in the region where the section passed through the cold tongue. The warm Loop Current is found north and south of the center of the cold dome. The cold water to the north is ambient Gulf of Mexico water. It is interesting to note that the horizontal temperature changes, relative to the center of the cold dome and the Loop Current water to the north or south, is greater at depth. The maximum change at the surface is about 0.5°C, and that at the 700-m depth, about 3.0°C. Greater cooling in the subsurface in the cold tongue compared to the surface increases the OTEC resource. This is shown in Figure 6c. In Figure 6c, the vertical temperature difference was computed using the surface and 700-m temperature. It is expected that a similar effect would be found if 1000-m temperature were available instead of the 700-m temperature.

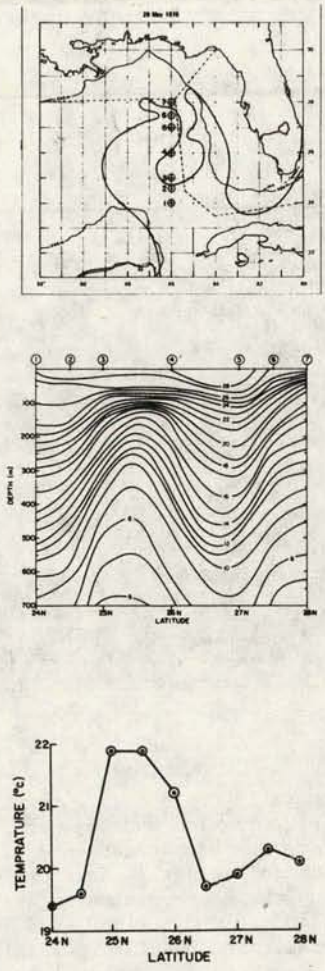

Fig. 6 (a) Graphical presentation of the NOAA-5 VHRR image for 20 May 1978 with XBT stations dicated. (b) Temperature cross-section through cold tongue. (c) Vertical temperature difference through cold tongue.

The satellite data on 20 May would suggest a greater contrast (greater than or equal to 1.5°C) at the surface than indicated in the in situ data 7 to 9 days later. The discrepancy may be due to mixing in the intervening period. In any case, if the subsurface temperature remains constant between 20 and 29 May, there will still be an increase in the vertical temperature difference through the cold tongue on 20 May but not as great as that around 28 May (about 1°C increase of a 2.5°C increase).

Table 1 yields the lifetimes of the three cold tongues. It can be seen that the 1975 tongue may have had as large a lifetime, but this could not be determined because the thermal contrast disappeared in mid June.

Discussion of Results

In summary, large cold tongues and associated warm tongues were detected in the eastern Gulf of Mexico. The cold tongues apparently originated from meanders found on the northern boundary of the Loop Current. These tongues extended as far as 400 km southward from the northern boundary of the Loop Current. The transformation of a meander into a cold tongue appears to be due to two processes: a surging of warm Loop Current water northward and a surging of cold water southward in a cyclonic manner. As indicated in the three cases, the effect of the transformation processes can have results that can vary from extending deep into the Loop Current to the isolation of Loop Current water.

In any event, it is obvious that marked changes in the sea surface temperature are associated with this feature. A cyclonic circulation appears to be associated with the feature. In one case, the feature moved eastward and westward along the northern boundary of the Loop Current. These factors suggest that the feature may have a pronounced influence on the OTEC resource in the Gulf of Mexico. The potential of a cyclonic circulation being associated in this feature also indicates that the feature may have a pronounced effect on the transport of water and thus affect the operations associated with OTEC.

Table 1. Statistics on Large Cold Intrusions

Date	Lifetime (days)	Comment
Winter-Spring 1975	73	Large narrow cold intrusion originated as a meander and evolved back into a meander.
Spring 1977	40	The intrusion was involved in the development of a warm lens.
Spring 1978	>40	The intrusion was still evident in early June but soon could not be detected because of the lack of thermal contrast at the sea surface. Therefore, the lifetime could not be determined.

References

Vukovich, F. M., B. C. Crissman, M. Bushnell, and W. J. King, 1978: "Sea-Surface Temperature Variability Analysis of Potential OTEC Sites Utilizing Satellite Data." Final Report DOE Contract No. EG-77-C-05-0544. Research Triangle Park, N.C., 27709, 153 pp.

Vukovich, F. M., 1976: "An Investigation of a Cold Eddy on the Eastern Side of the Gulf Stream using NOAA 2 and NOAA 3 Satellite Data and Ship Data." J. Phys. Oceanogr., 6, pp. 605-612.

Vukovich, F. M., and B. C. Crissman, 1978: "Further Studies of a Cold Eddy on the Eastern Side of the Gulf Stream Using Satellite and Ship Data." J. Phys. Oceanogr., 8:5, pp. 838-845.

USE OF SATELLITE-DERIVED SEA SURFACE TEMPERATURES BY CRUISING OTEC PLANTS

F. K. Hill and G. L. Dugger

Applied Physics Laboratory
The Johns Hopkins University
Johns Hopkins Road
Laurel, Maryland 20810

Abstract

The greatest resource for Ocean Thermal Energy Conversion (OTEC) plants is in the millions of square miles of the tropical areas of the Atlantic and Pacific Oceans within 10°-15° of the Equator. Of particular interest for early OTEC plantship deployment is a 360,000 square nautical mile area in the Atlantic, 5-15°S latitude by 20°-30°W longitude (a siting area called ATL-1), where annual average temperature differences between surface water and 900-m deep water of 22°-23.9°C can be found. To attain the highest value, 23.9°C (43°F), an OTEC plantship would cruise continually at an average speed near 0.4 knot to seek out the warmest spot each month. To do this, the navigator must know what course to follow in terms of increasing relative sea surface temperature T_S. This T_S gradient can be obtained from satellite observations of T_S much less expensively than from data from surface vessels, floating buoys, or low-flying aircraft. Data supplied to the authors by the National Oceanic and Atmospheric Administration (NOAA) from the historical files of the National Oceanographic Data Center (NODC) are compared to T_S isoline charts generated from the data provided by ITOS/NOAA polar orbiting satellites. Agreement in terms of T_S gradients is good even though absolute values of T_S in ATL-1 may differ, with a bias of 1.0°C colder from the satellite data. The satellite data for an alternative siting area in the Pacific Ocean 200 n.mi. WSW of Acapulco, Mexico, are in somewhat better agreement with ship measurements of T_S, however. It is concluded that use of T_S data from satellites for OTEC plantship navigation looks very promising.

Introduction

A survey of the thermal resource available in the oceans indicated that high annual average values of the ΔT between surface- and deep-water temperature could be obtained in tropical ocean regions in the south Atlantic and the eastern north Pacific. The historical records showed that over an area 360,000 square nautical miles (a 10° x 10° square), the surface temperature T_S could vary by 2 to 4°C. Since the temperature at 900-m depth is nearly constant, changing a few tenths of a degree with latitude but very little with longitude or season, the change in T_S essentially determines the ΔT (i.e., $T_S - T_{900m}$) available. Thus a ΔT from 1 to 2°C above the monthly local mean temperature can be obtained by cruising through the area to seek out the highest T_S at all times. National Oceanographic Data Center (NODC) files make available 3170 valid points of temperature in the area 10°N to 20°S, 20°W to 30°W, which includes the area 5°-15°S, 20°-30°W, that we call ATL-1. These data, collected from 1922 to 1974, form the historical record taken by oceanographic surface vessels. Since this data base is small, the T_S distribution is less well substantiated than in other more heavily traveled areas.* However, two other sources of data--the Summary of Synoptic Meteorological Observations (SSMO) records and the weekly satellite surveys published by NOAA's National Environmental Satellite Service (NESS)--provide a good statistical distribution of T_S by month.

The objective of the APL effort is to determine what ΔT can be obtained by a cruising OTEC plantship and whether the warm areas can be reached by navigation based on NESS or other satellite-derived T_S data.

A cruise pattern for an OTEC plantship for one year is deduced from historical T_S data, and two years of satellite data are analyzed to assess the utility.

Data Base

In the region we call OTEC site ATL-1, the temperature at 900-m depth, T_{900}, is 3.9°C at 15°S, 4.0°C at 10°S, and 4.1°C at 4°S.

The aforementioned 3170 points for T_S used by NOAA to generate monthly T_S isolines for us were made up of MBT, XBT, and SD listings.** A second set of contours was generated by NOAA from only the XBT and SD listings (~1500 points). Figure 1 represents these data sets for the month of May. Since the MBT data are less accurate than the XBT data, the sets of data with and without MBT were compared, and it was observed that there was more scatter when the MBT data were included but no significant bias to either colder or warmer temperatures.

The aforementioned SSMO data can also be useful. In the ATL-1 area, 55,384 observations of T_S were recorded from 1854 to 1976. These data, randomly

---

* For determining monthly contours ideally, the computer programmer wishes to have two valid data points for each 0.2° x 0.2° square in the area for each month, or some 60,000 data points in a 10° x 10° OTEC site. In the case discussed here an area 3 times that of the 10° square OTEC site was chosen for contouring. Consequently whereas 180,000 points were needed for ideal contouring, only 3170 or 1.7% of the ideal number were available.

** All data tabulations and T_S isotherm plots based on MBT, XBT, and SD listings were obtained directly from the Oceanographic Service Branch of NODC, NOAA, U.S. Dept. of Commerce. Here MBT = Mechanical Bathythermograph, XBT = Expendable Bathythermograph and SD listings are Station Data listings, e.g., Nansen casts.

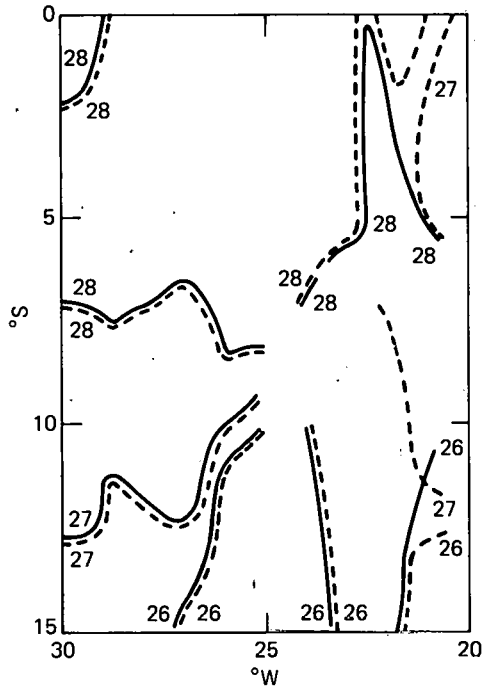

Fig. 1 Comparison of T_s Contours (Surface Isotherms °C) in the South Atlantic. Based on XBT + Station Data (Solid Lines) and on MBT + XBT + Station Data (Dashed Lines).

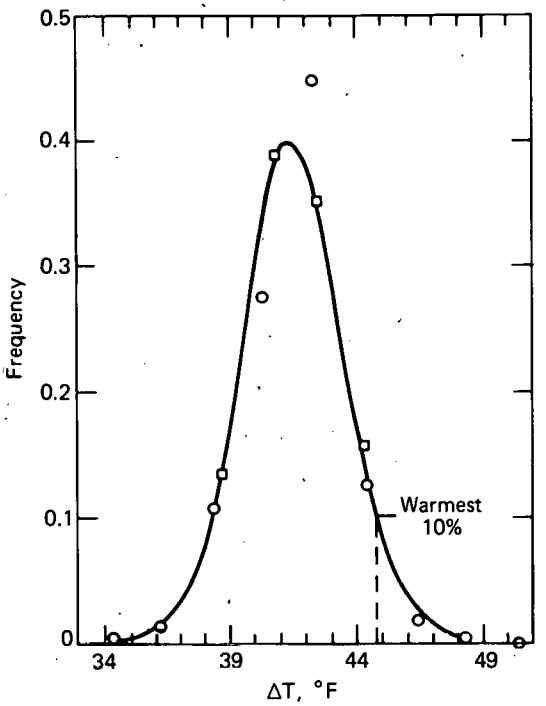

Fig. 2 Distribution of ΔT in May at ATL-1. Mean ΔT = 41.5°F, Warmest 10%, ΔT = 44.8°F. o = SSMO Data; □ = MBT + XBT + Station Data from NODC.

distributed over the area, were compiled by the National Climatic Center, U.S. Dept. of Commerce, NOAA Environmental Data Source (NCC) and were tabulated monthly showing essentially a normal distribution in temperature. The data for May are shown as an example in Fig. 2 with the normal frequency distribution fitted to these points (circles). In addition, the area percentages for each 1°C ΔT increment obtained from the May NODC contour plots are shown (squares). As is to be expected, the greater data base provided by the SSMO data permits the distribution curve to be drawn indicating ΔT's (at reduced probabilities) which are above the cut-off values indicated by the more restricted NODC data base. From the historical, statistical records it is apparent that when cruising if navigation is good enough to keep the OTEC plantship in the best 10% of the surface area, there will be an average ΔT of 43°F.

For the future, satellite observations of T_s may be most useful of all for cruising OTEC plantships. From April 1976 through February 1979 the Global Operational Sea Surface Temperature Computational (GOSSTCOMP) procedures supplied T_s isoline charts from polar orbiting ITOS/NOAA satellites. The GOSSTCOMP isotherms for May 2, 1978, are compared with those for May from the historical data in Fig. 3. The new TIROS-N satellite data now being received should have better accuracy.

Figure 4 compares the average highest monthly ΔT's from the satellites for 1977 and 1978 with the historical average. They all follow the same annual variation, but the satellite-derived ΔT's are averaging up to 1°C lower. The significant item for OTEC cruising, however, is that the T_s isoline charts provided by the satellites (Fig. 3) accu-

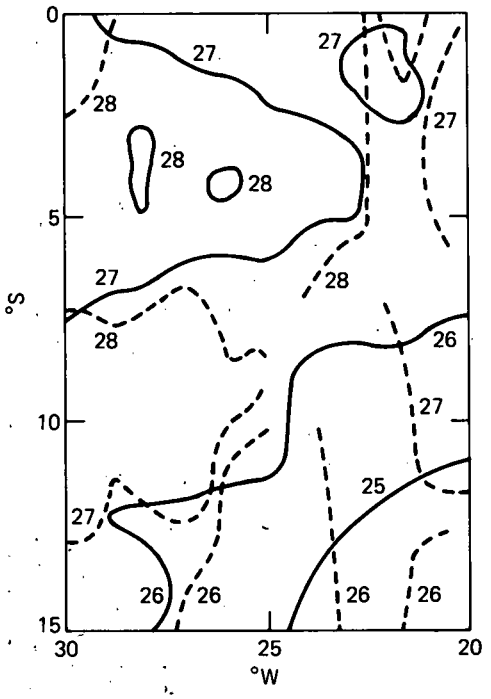

Fig. 3 Comparison of T_s Isotherms (°C) Obtained from the Historical Data (Dashed Lines) for May in ATL-1 and from Satellite Data for May 2, 1978 (Solid Lines).

rately depict the gradients needed to navigate to the warmest areas. Other comparisons of satellite-derived surface temperatures with ship measurements have been made, for example, in the Indian Ocean east of Africa. In Ref. 1, Leetmaa and Cestari report satellite values in some areas below and in other areas above surface measurements.

OTEC Plantship Cruise Patterns in ATL-1

All monthly contours similar to Fig. 1 were analyzed, and in Fig. 4 the values of best thermal resource as a function of time through the year are plotted. Figure 5 illustrates the cruising pattern which corresponds to Fig. 4. The greatest distance that would have to be covered in 31 days (744 hr) is between positions 7 and 8 (July and August), 275 n.miles; this would require an average speed of 0.37 knot. The selection of a cruise pattern may be improved by continuous synoptic observations, and the temperatures along the course integrated to optimize the average obtained. The cruise pattern shown is only an example based on the 52-year average temperature history. It will most likely change each year, so that the plantship needs a constantly updated synoptic display of T_s. The polar-orbiting satellites can provide this twice daily, provided that there is no atmospheric interference. For cases where the IR-scanning system is invalidated, the ship will remain on course until a valid update picture is transmitted.

Figure 6 compares the area coverages by the satellite, the NODC isotherm plots, and the cruise patterns selected from them.

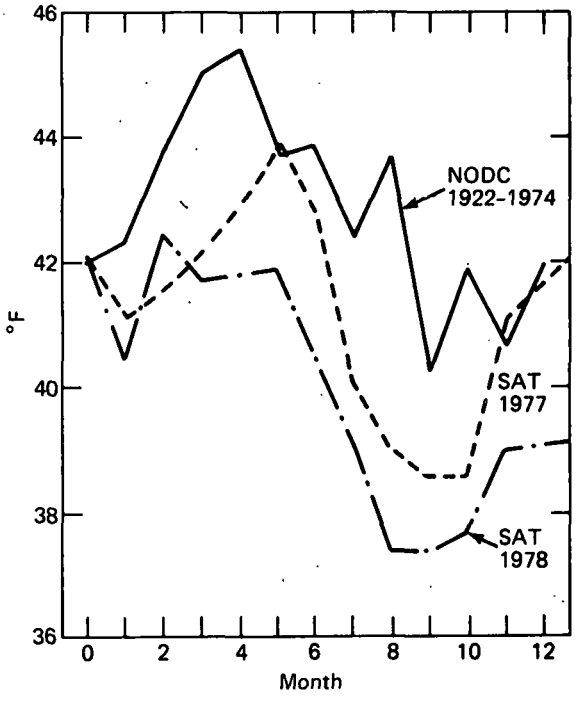

Fig. 4 Optimum Monthly ΔT's for the Cruise Pattern in ATL-1 based on Historical Averages (NODC) and for Satellite Surveys in 1977 and 1978.

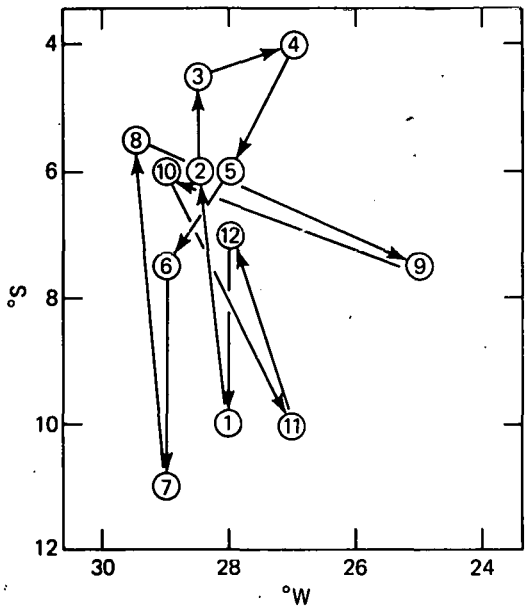

Fig. 5 Cruise Pattern in ATL-1 for OTEC Plantship Based on T_s Contour Plots of NODC Data. This Pattern Provides an Annual Average ΔT of 23.9°C (43.0°F).

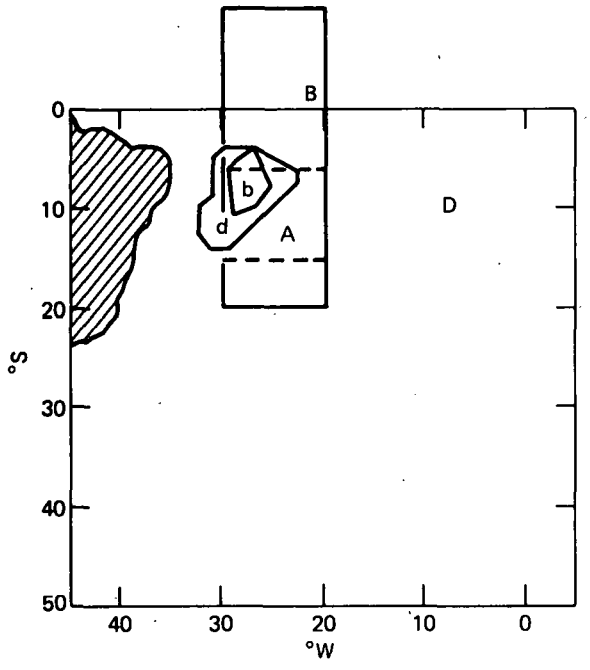

Fig. 6 Comparison of Surface Vessel and Satellite Surveys. A = ATL-1, B = Area of NODC Contours, b = Area Selected for Cruise from NODC T_s Contours, D = Area Surveyed by Satellites, d = Area Selected from Satellite T_s Contours.

Other means of obtaining data for cruise pattern selection may be considered such as drifting buoys, surface vessels moving at moderate speeds and using XBT casts, and low-flying aircraft. Table 1 summarizes the numbers of units and times required to survey a 10°x 10° OTEC site.

Table 1 Comparison of Numbers of Buoys, Ships, Low-Flying Aircraft, and Satellites Required for an OTEC Site Survey

Device	Number Required to Cover 10° x 10°	Time Required	Accuracy
Drifting Buoys	2500	1 hr	0.2°C
Surface Vessels	10	40 days	0.2°C
Aircraft	3	12½ days	0.01°C
Satellite	1	0.5 days	1.7°C

It is clear that synoptic coverage from a satellite is the only practical means, even though accuracy is poor.

Questions to be Answered (1) How accurate will the satellite determinations of T_s gradients become? Aside from the general agreement in picking out cruise patterns that we have observed, a study by Huh[2] on detecting thermal fronts off Korea with satellites indicated that although the absolute T_s indicated was 2 to 10°C below the surface-measured values, the T_s gradients were accurate within 0.1°C. On the other hand, work by Maul et al[3] measuring Gulf Stream meanders, indicated that the recorded T_s gradients were significantly affected by atmospheric moisture. Such effects on the T_s gradients appear to be understood, and in some areas corrections are made.

(2) Can the satellite-scanning data be processed and transmitted to an OTEC plantship in a few hours? Based on a small improvement over today's capability, this should be feasible. Drifting buoys monitor sea surface conditions and emit a signal which is received by an overpassing satellite measuring the doppler shift, from which the buoy location is computed and transmitted via a ground station and subsequently to the National Data Buoy Office of NOAA. A similar communications method could be arranged for a ship at sea.

(3) Are the warm areas contiguous? That is, as the ship cruises from one optimum ΔT area to another, can it remain in relatively warm water? Some loss in thermal resource may be experienced with long transit paths and adverse weather and sea conditions intervening. The synoptic view of T_s and cloud cover (for corrections) may enable the ship to select the best of several alternative cruising paths.

(4) What propulsion capability is required to attain the optimal OTEC performance? For example, there may be times when the plantship should go north from ATL-1, perhaps even north of the equator. The equatorial currents can be negotiated with the 1-knot propulsion capability to be provided. However, since the propulsion power varies with the cube of velocity, tradeoff studies of propulsion power vs power gain through ΔT gain are needed. The gross power delivered by the OTEC power plant varies with $(\Delta T)^2$, the net power with $(\Delta T)^{2.5}$.

Cruise Patterns in PAC-2

In the northeast tropical Pacific an area was selected in the same manner as described above for ATL-1. It is south of lower Mexico and is closer to the United States via water or air routes than ATL-1 is. It has an equally favorable thermal resource but is close to the spawning area of eastern Pacific tropical cyclones. Figure 7 shows the area selected first by NODC contours as the best, excluding regions closer than 200 n.mi. from the Central American coast. The best cruising area as illustrated in Fig. 7 is from 10°N to the 200 n. mi. limit and between 97° and 107°W. The figure includes historical average NODC contours for August as a comparison with the August 29, 1978 satellite isoline plot for T_s. While the two sets of contours are different, they have important similarities: the 27°C to 29°C contours predominate in the region above 10°N, and very similar groups of contours are seen between 0° and 7°N. The satellite contours indicate that the plantship should cruise back and forth just beyond the 200-n. mi. limit from shore. Better results would be obtained if an agreement with Mexico would permit going nearer shore. Figure 8 compares the cruise pattern derived from the NODC historical data (monthly averages) with weekly-averaged satellite data points mentioned above. For the pattern from the historical data, the longest path, again between July and August, requires three weeks at 0.5-knot speed.

Table 2 Comparison of Satellite and Surface Measurements in PAC-2

Month	ΔT NODC (1922-1974) $T_s - T_{900\text{-m}}$	ΔT, XBT	ΔT 1977 Satellite $T_s - T_{900\text{-m}}$	ΔT 1978 Satellite $T_s - T_{900\text{-m}}$
Jan.	40.7°F	41.6°F	41.5°F	41.7°F
Feb.	41.2	40.1	43.1	43.1
Mar.	42.5	42.3	42.4	41.7
Apr.	45.2	44.1	44.1	41.9
May	45.2	45.2	44.5	42.3
June	44.1	no data	42.1	43.0
July	43.4	42.7	45.0	41.7
Aug.	43.0	45.0	42.8	42.0
Sept.	42.8	43.2	42.8	41.8
Oct.	42.5	no data	41.6	40.2
Nov.	43.4	no data	43.9	41.8
Dec.	41.8	41.8	42.6	41.3
Average	43.0°F	42.9°F	43.0°F	41.9°F

Table 2 lists the locations of the sites shown in Figure 8 as well as the computed ΔT values. For the 900-m temperature a constant value of 4.9°C was taken, since there is only a difference of about 2° in latitude for most of the sites. A check on this assumption is given by including ΔT data derived directly from XBT casts. Unfortunately there were not sufficient data to permit NODC contouring in the cruise area during June, October and November.

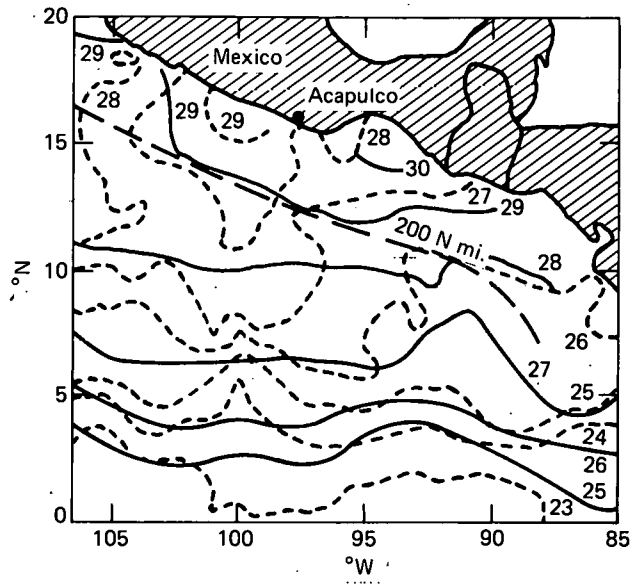

Fig. 7 Comparison of T_s Contours (Surface Isotherms, °C) in the PAC-2 Site for NODC Historical Date for August (Solid Lines) and Satellite Date for August 29, 1978 (Dashed Lines).

Figure 9 compares the ΔT variations by month deduced from the historical data and from satellite data for 1977 and 1978.

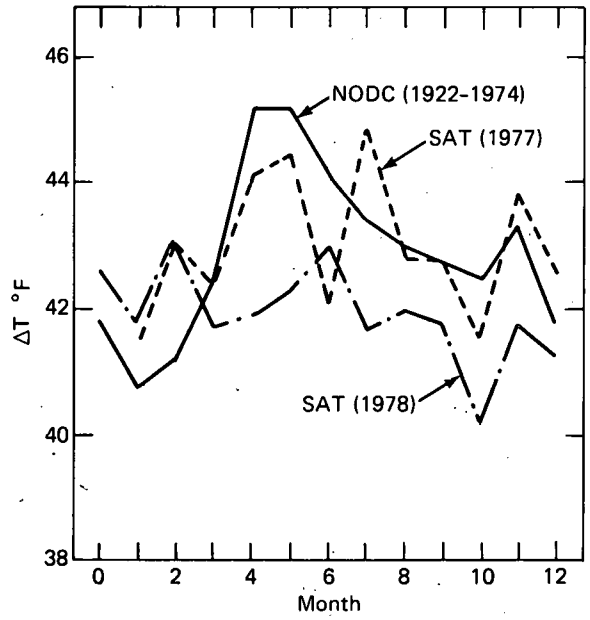

Fig. 9 Optimum Monthly ΔT's from Historical Average (NODC Data), and 1977 and 1978 Satellite Surveys. The Annual Average ΔT's are 23.9°C (43.0°F) for the NODC and 1977 Satellite Cases and 23.3°C (41.9°F) for the 1978 Satellite Case.

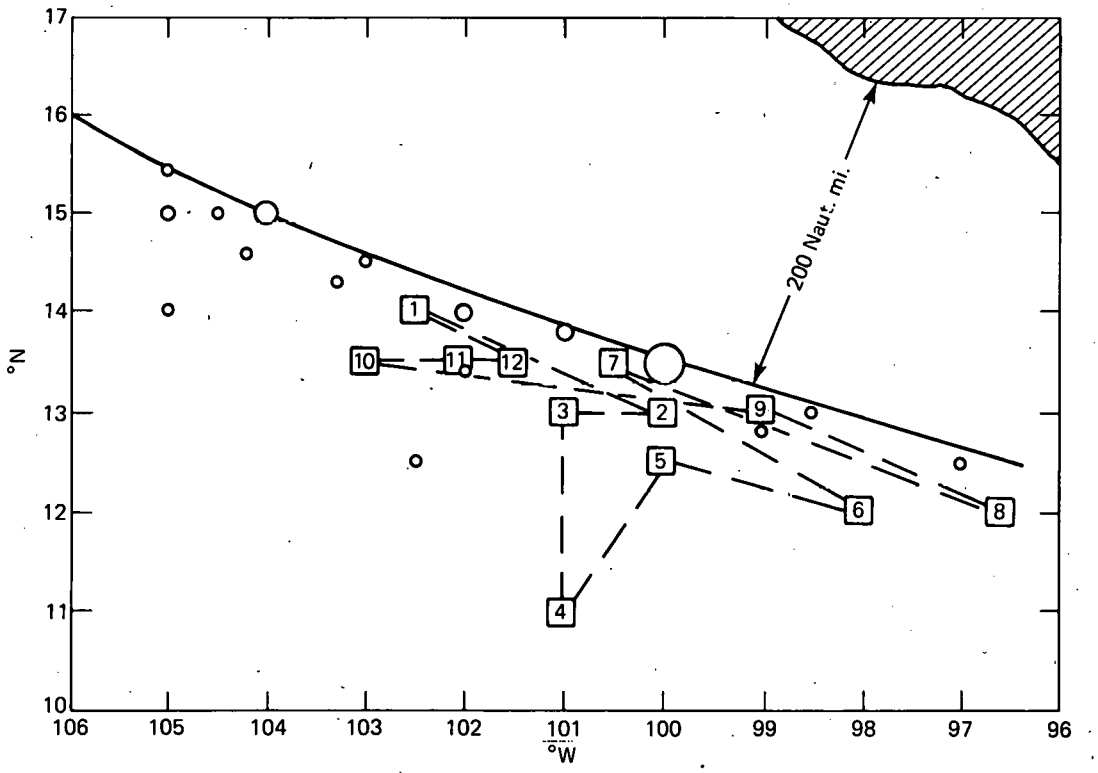

Fig. 8 Cruise Patterns for Optimum Annual Average ΔT in the PAC-2 Site. □ = Monthly NODC Historical (1922-1974) Average; ○ = Optimum Weekly Satellite Positions for 1978 Operation (Size of O Proportional to Number of Weeks).

Conclusions

There is a substantial variation of T_S over the ATL-1 site (5°S to 15°S, 20°W to 30°W) which averages about 26°C annually. A variation of 2 to 5°C monthly enables a cruising plantship to improve the available thermal resource by 2°C so that on a statistical basis a ΔT of 23.9°C (43°F) should be available to an OTEC plantship cruising in the best (highest temperature) 10% of the area. In the PAC-2 area, both the historical data and the data from satellites indicate that the best area lies along the 200-n.mile offshore limit between 97° and 106°W, where an annual average ΔT of 23.9°C is available. To navigate to these optimum areas of high ΔT requires a synoptic view of the site and surrounding area on a continuing basis. Comparison of satellite measurements with surface measurements indicates that the view from space provides not only the areal coverage needed but the necessary resolution with respect to gradients in T_S to navigate OTEC plantships to stay in the warmest water. The absolute accuracy of satellite measurements of T_S should be better several years from now when the first pilot plantship starts its cruise.

Acknowledgment

The modest APL effort in this area has been supported by IR&D funding plus a few man-weeks under the technical assistance project funded by Dr. Robert Cohen of the DOE Ocean Systems Branch, to whom we are grateful. Advice and aid from Dr. W. H. Avery and R. W. Henderson of APL were also appreciated. Ellsworth C. Smith of the Ocean Service Branch of NOAA was very helpful in providing the T_S contour maps and associated sources of information at minimum cost. We appreciate the extensive tabulation of SSMO data in the Atlantic and Pacific areas furnished by Dr. Robert G. Quayle of NCC and the weekly GOSSTCOMP Contour Charts provided through the various service groups of NESS.

References

1. Leetmaa, Hans; and Cestari, Mathew, "A Comparison of Satellite-Observed Sea-Surface Temperatures With Ground Truths in the Indian Ocean," NOAA Technical Report ERL375-AOML 22, Aug. 1976.

2. Huh, Oscar Knob, "Detection of Oceanic Thermal Fronts off Korea with Defense Meteorological Satellites," Remote Sensing of Environment Vol. 5, 1976, pp 191-213.

3. Maul, George A; De Witt, O. Webb; Yanaway, Alan; and Baig, Stephen R., "Geostationary Satellite observations of Gulf Stream Meanders: Infrared Measurements and Time Service Analysis," Jour. Geophysical Res. Vol. 83, No. C12, Dec. 20, 1978.

OBSERVATIONS OF WATER MASS STRUCTURE AND VARIABILITY NORTH OF ST. CROIX, U.S. VIRGIN ISLANDS FOR OTEC ASSESSMENT

Robert S. C. Munier*

Ocean Technology Division
Tracor Marine, Inc.
P.O. Box 13114
Port Everglades, Florida 33316

Thomas N. Lee† and Sherman Chiu‡

Division of Meteorology and Physical Oceanography
Rosenstiel School of Marine and Atmospheric Science
4600 Rickenbacker Causeway
Miami, Florida 33149

Abstract

A 72-day time series of measurements of temperature, salinity, and current velocity were made to determine the water mass structure and hydrographic variability to 1500m depth at a tropical oceanic site 15km north of St. Croix, U.S.V.I., for OTEC assessment. The study was performed in conjunction with a comprehensive heat transfer, biofouling, and corrosion experiment of simulated OTEC heat exchanger tubes conducted for DOE by Tracor Marine and the University of Miami. The largest temporal fluctuation in water properties occurred in the Tropical Surface Waters of the upper 100m due primarily to advection of this spatially inhomogeneous water mass past the moor. Variations in water properties below the Tropical Surface Water were small. The OTEC thermal resource (ΔT) between the surface mixed waters and subsurface water averaged 23°C at a depth of 1000m with a standard deviation of ±0.2°C. The depth to reach a ΔT of 20°C varied from a minimum of 660m to a maximum of 740m. Historical data indicate that the maximum depth to reach a ΔT of 20°C occurs in the winter and does not exceed 956m. From thermal resource considerations, the waters north of St. Croix may be considered an excellent location for an OTEC site.

Introduction

The variability of oceanographic properties may determine the viability of potential OTEC sites. An adequate mean ΔT does not guarantee a sufficient thermal resource every day of the year. Water mass variations will alter local fouling regimes and impact the corrosion behavior of certain OTEC components. Current velocity changes will affect plant station-keeping. For these reasons, OTEC site characterization studies should include determination of the variability as well as the mean of the pertinent oceanographic properties and avoid the presumption of a "snap shot" survey.

Hydrographic variability can be expected from a number of sources including the development of a shallow seasonal thermocline, wind and island wake induced upwelling, internal gravity and tidal waves, disturbances produced by upstream flow over sills and around islands, storm-induced vertical mixing, surface tides, and diurnal changes in the local heat budget. The general hydrographic features of the waters in the vicinity of St. Croix are well documented in the literature; however, the temporal variability of conservative and non-conservative water properties and current fluctuations are not well understood.

In the summer of 1977, the University of Miami and Tracor Marine, Inc., conducted a comprehensive at sea heat transfer, biofouling and corrosion experiment on simulated OTEC heat exchanger tubes in seawater service. The work was performed aboard a 130' instrumented test barge operated by Tracor Marine for the Navy, which was anchored in the Virgin Island Basin at a permanent "deep moor" in 3600m depth. To support the heat exchanger experiments and to evaluate the location for OTEC assessment, daily measurements of temperature, salinity and current velocity were made from the barge. The duration of the investigations was approximately 2.5 months, from mid-July to the end of September 1977.

We were fortunate to have a platform on station for an extended period from which a time series of measurements could be conducted and an analysis of variability made. Even so, this study was limited to the summer season; as a minimum, a similar time series of measurements should be conducted during the winter. Other potential OTEC sites may warrant similar programs during all seasons.

In this paper, the hydrographic variability at St. Croix is discussed in detail. The site description and discussion of the mean property characteristics are abbreviated; they are presented in detail elsewhere.[9,8] The corrosion, biofouling, and chemical (nutrient) results are reported by Craig, et al., (1978)[4] and Aftring, et al., (1978).[1]

Study Area

The bathymetry of the study area and location of the deep moor are shown in Figure 1. The most significant features are the Virgin Islands Basin, which has a flat floor 4400m deep, and the Anegada

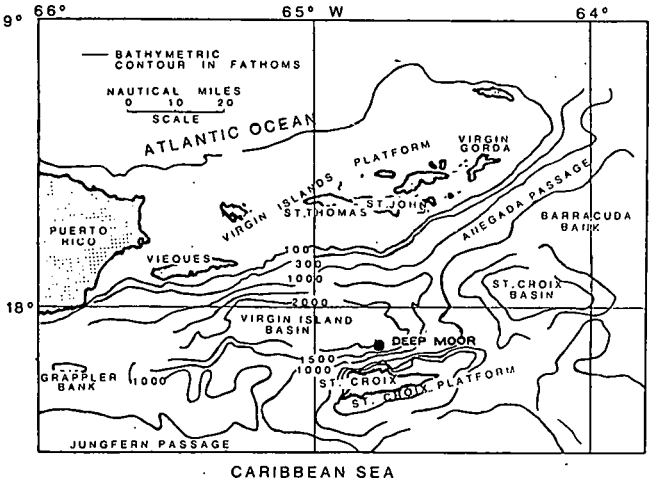

Figure 1. General bathymetry of the U.S. Virgin Islands area[6] and the location of the Tracor Marine deep moor.

*Director of Project Coordination.

†Associate Professor.

‡Research Associate.

and Jungfern Passages which comprise one of the deepest pathways for deep water renewal between the Atlantic Ocean and the Caribbean Sea.

St. Croix has a marine tropical climate dominated by the easterly trades which blow steadily at least 10 months of the year. The average mean air temperature is 26°C and has an annual range of only ±2°C. This consistent weather is interrupted occasionally by easterly tropical waves, and rarely by hurricanes. Much a function of the easterly trades, seas at the deep moor are from the eastern quadrant the entire year and are generally steep and of short period.

The tidal range near St. Croix is small. The spring tide range is typically 30-35cm and markedly diurnal; neap tides have a range of about 15cm and exhibit a mixture of diurnal and semi-diurnal periods.

The deep moor is within the influence of the Caribbean Current which is made up of waters from the north and south equatorial regions that enter the Caribbean through passages in the Lesser Antilles. Historical data indicate that surface currents in the vicinity of St. Croix vary in speed from 20 to 100cm/sec with 40cm/sec average, and in direction from WSW to NW.[10, 9] Deep currents are poorly understood; speeds of 5 to 10cm/sec between 750 and 1050m have been measured, but with extremely variable direction.[7, 3]

The water mass structure north of St. Croix is typical of the northeastern Caribbean Sea, and is described fully in a later section.

Methods

The hydrographic measurement program is outlined in Table 1. STD casts were made daily, initially to 600m, and later to 1500m when additional wire became available. During spring and neap tide periods, casts were made bi-hourly for 24 hours to observe the tidal influence on the T-S structure. Water samples for chemical analyses were taken daily from the experimental intake depth of 20m, and from weekly 10-bottle hydrocasts to 1500m. Hourly current measurements were made at 10m with Bendix Q-15 and Hydroproducts current meters. A single current profile was obtained using an Aanderaa current meter. Weather data were logged by barge personnel and supplemented with information for shore stations and weather maps.

The STD strip chart records were digitized by hand in 20m intervals. The data was post calibrated using linear regression by comparison with salinity, temperature, and depth values determined from Niskin bottle samples collected during each STD cast. The corrected temperature and salinity data were input into the computer and analyzed for mean, minimum, maximum, standard deviation and variance at 40 depths. Further analysis included determination of density (σ_t), the behavior of T, S, σ_t, and ΔT in time series and T-S profiles.

Data Analysis

Mean Data Profiles

The mean and scatter of the total set of temperature (T) and salinity (S) derived in this study are given versus depth in Figures 2 and 3, respectively. The mean ΔT versus depth is also shown in Figure 2. A mean density (σ_t) profile was computed from the mean S and T data, and is shown in Figure 4.

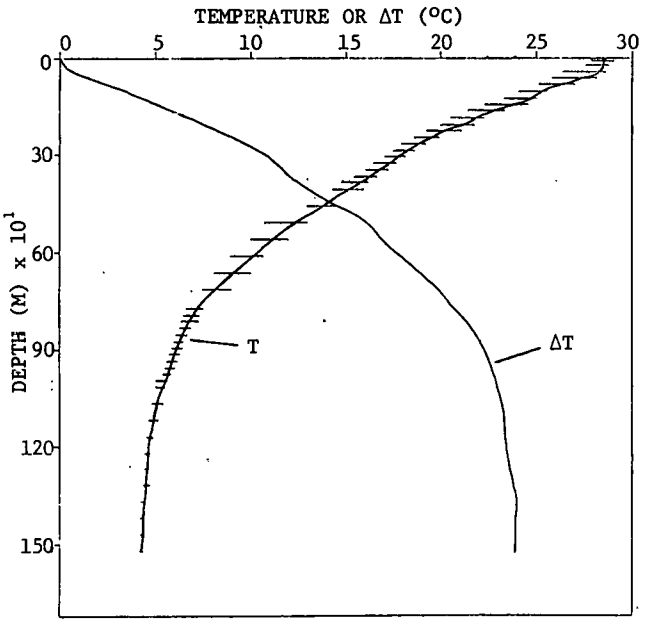

Figure 2. Mean and scatter of temperature profiles and mean ΔT vs. depth, 22 July to 29 September, 1977.

Table 1. Summary of physical oceanographic data collected during St. Croix OTEC experiment.

Data Type	Sample Frequency	Depth (m)	Total Number Samples	Parameters Processed
STD	Daily (Mon-Fri)	600	14	T, S, σ_t
		1000	9	T, S, σ_t
		1500	19	T, S, σ_t
	2-hourly (during tidal study)	1500	21	T, S, σ_t
Intake Bottle	Daily	20	54	T, S, O_2, pH, nutrients
Hydrocasts	Weekly	600	3 casts x 10 bottles	T, S, O_2, pH, nutrients
		1500	7 casts x 10 bottles	T, S, O_2, pH, nutrients
Surface Currents	Hourly	10	≈600 (incomplete)	Current velocity
Current Profile	One	990	1 profile	Current velocity vs. depth
Wind	6-hourly		540	Wind velocity

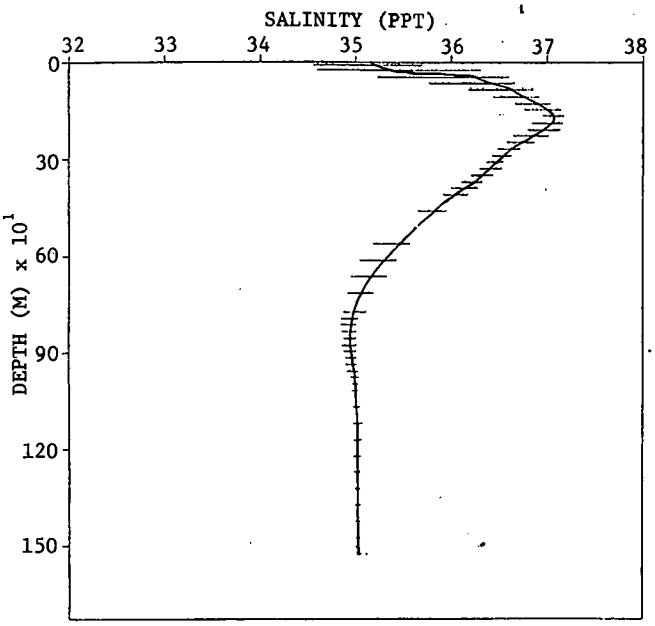

Figure 3. Mean and scatter of salinity profiles, 22 July to 29 September 1977.

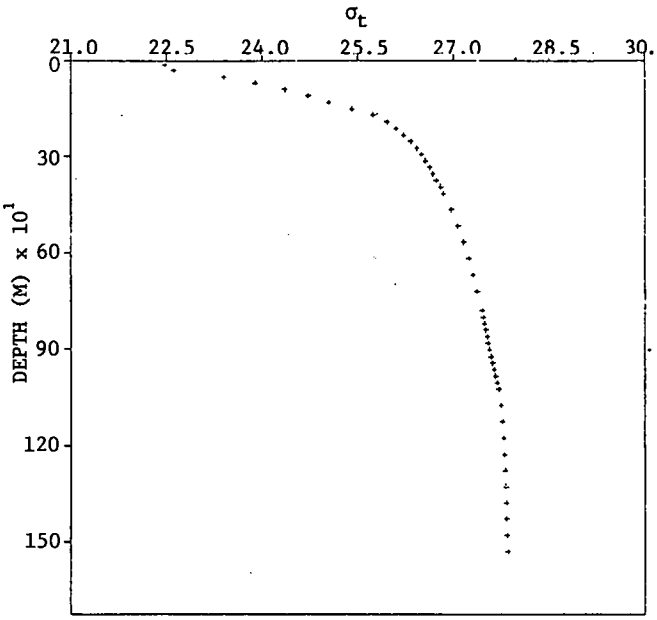

Figure 4. Mean density (σ_t) profiles, 22 July to 29 September 1977.

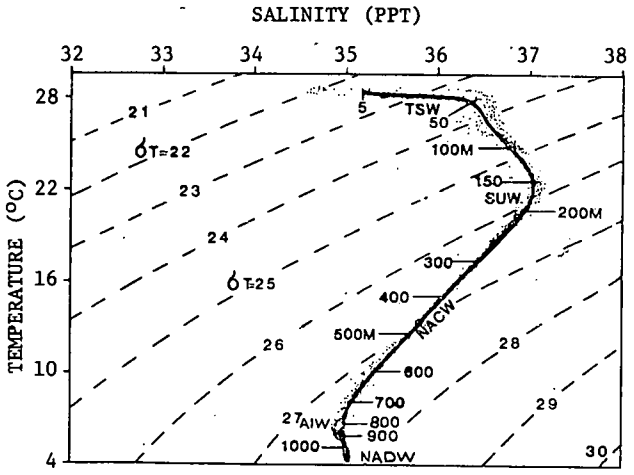

Figure 5. Mean and scatter of T-S relationships, 22 July to 29 September 1977.

The T-S diagram given in Figure 5, which was constructed from the mean and scatter of the T and S profile data, is diagnostic of the water mass structure at the site. Table 2 gives the general characteristics of water masses which can be identified from the T-S plot.

The temperature, salinity and water mass data presented above are in good agreement with that collected by Atwood, et al., (1976)[2], in their OTEC site assessment study off of Pt. Tuna, Puerto Rico, 100km west of our site, and with the recent OTEC archival data assemblies of Munier, et al., (1978)[9] and Cummings, et al., (1978)[5] covering the Virgin Islands Passage. This suggests that both sites have nearly identical water mass structures characterized by consistent prevailing tropical oceanic conditions.

Water Structure Variability

The temporal variability of the water column structure north of St. Croix can be seen in graphs of T, S, and σ_t vs. time for selected depths (Figures 6 and 7). The time of each profile is identified with a tick mark above the day time axis. The depth of each time series is labeled on the right hand side. A vector time series of the 6-hourly winds is also included in Figure 6. Winds during the experiment appear to be typical of the region, around 5 to 8m/sec, primarily from the southeast; however, east and northeast winds are also common. There were two periods where the wind intensified to 10-12m/sec from the southeast, on 6 and 22 September. Associated with these wind events were substantial increases in local rainfall.

Table 2. Water mass characteristics

	DEPTH	TEMP	SALINITY
Tropical Surface Water (TSW)	0-80m	25-29°C	34.6-36.8‰
Subtropical Underwater (SUW)	160-180m	20-25°C	36.8-37.2‰
North Atlantic Central Water (NACW)	200-700m	8-18°C	36.6-35.2‰
Antarctic Intermediate Water (AIW)	720-920m	6-7°C	34.9‰
North Atlantic Deep Water (NADW)	>1000m	5.8-42°C	34.9-35.1‰

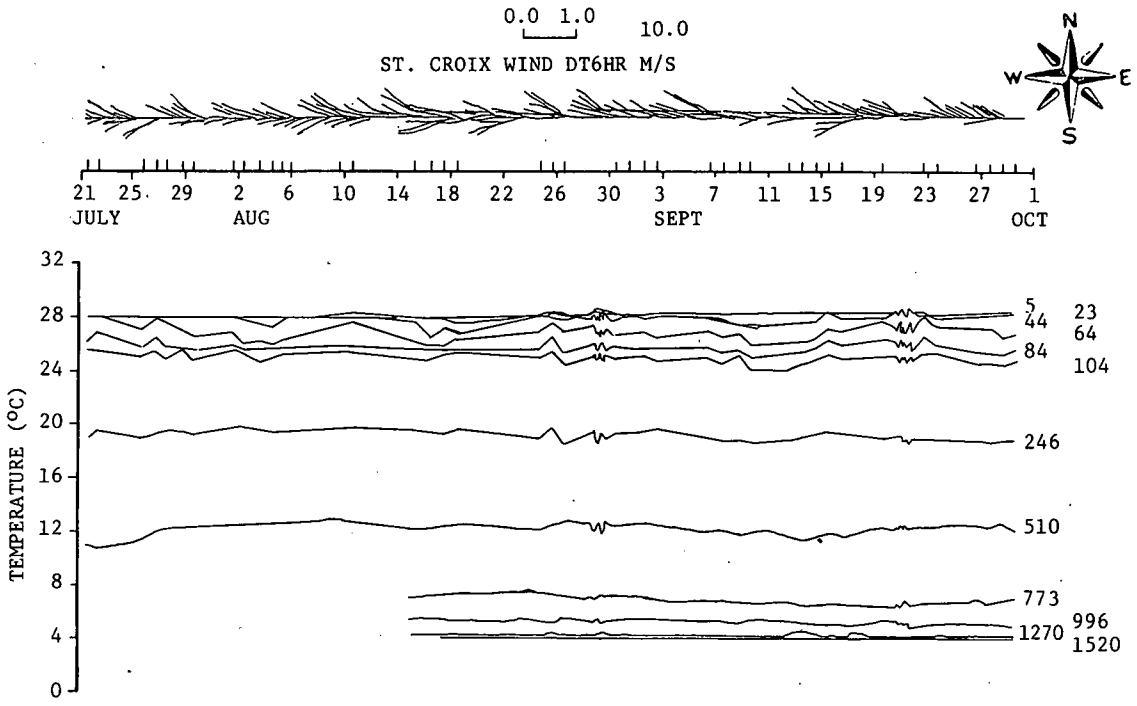

Figure 6. Six-hourly wind vectors (m/sec) (top), and temperature (°C) at selected depths, 22 July - 29 September 1977.

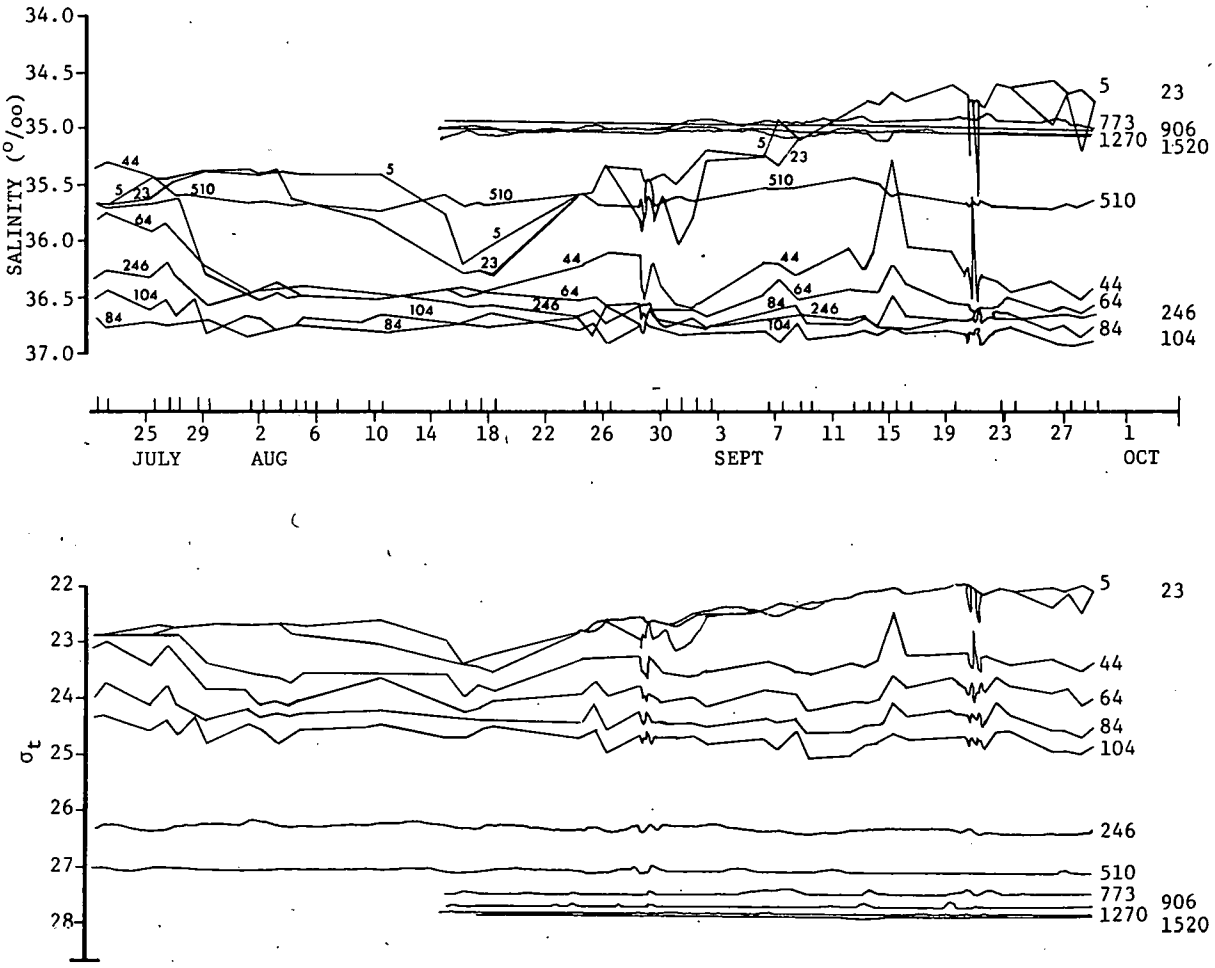

Figure 7. Time series of salinity (°/oo) and density (σ_t) at selected depths.

Temperature. The temperature (T) structure remained relatively consistent throughout the study period. Temperature of the surface mixed layer at 20m was quite steady with a mean of 28.3°C, range of 27.8 to 28.7°C, and a standard deviation of only ±0.23°C. The depth of the surface mixed layer defined by temperature underwent changes of about 40m, from 60m early in the experiment, to 20m by mid-August, with a period of approximately 20 days that does not appear to be connected to local winds. Visually coherent T fluctuations occurred from 44 to 1000m depths on time scales of tidal (semi-diurnal) and longer. The amplitude of these oscillations was approximately 1°C in the upper 500m of the thermocline and decreased to about 0.5°C at 1000m. The most likely source of the tidal fluctuations is the semi-diurnal internal tide. The temperature at 1270 and 1520m was almost invariant in time with standard deviations of only ±0.04°C, respectively.

The mean and deviation of the depths of selected isotherms are given in Table 3.

Table 3. Relevant statistics for depth deviations of selected isotherms from profile data.

Isotherm °C	# Data Points	Mean Depth (m)	±S.D. (m)	Min (m)	Max (m)
28	54	44	12	4	66
25	63	108	8	88	128
20	63	336	9	206	243
15	63	405	10	383	438
10	58	611	21	561	655
5	40	1073	27	1027	1140

The vertical deviation in isotherm depth was largest where the vertical temperature gradients were smallest: The 5 and 10°C isotherms, which lie below and above the core of AIW, had the largest standard deviations, whereas the smallest vertical displacements were in the main thermocline above and below the core of SUW (25 and 20°) and in NADW (15°C).

Variations in ΔT. Temporal deviations in the temperature differences (ΔT) between near surface (5m) and subsurface depths of 773, 996, 1270 and 1520m are shown in Figure 8; the variability in ΔT was small for the depths concerned.

A ΔT ≥20°C was present throughout the experiment at depths ≥773m. The mean ΔT at this depth was 21.4°C with a standard deviation of ±0.4°C. At depths ≥1000m, the standard deviations were only ±0.2°C. Internal tides appear to influence the ΔT to a depth of at least 1000m, producing variations of about ±0.2°C in ΔT with a 12-hour period.

Depth deviations of the 20°C ΔT are also shown in Figure 8. The largest depth variations were about 50m and occurred on time scales of less than one day. The greatest depth to obtain a 20°C ΔT was 740m; the shallowest, 660m.

Salinity. The salinity structure displayed the largest deviations over the measurement period. This information is shown in time series in Figure 7, which is rather confused due to the presence of subsurface salinity maximum and minimum layers. To help clarify this, depth has been labeled at various places on each time series. The near surface waters (5m) showed an S increase in the 3rd and 4th week of

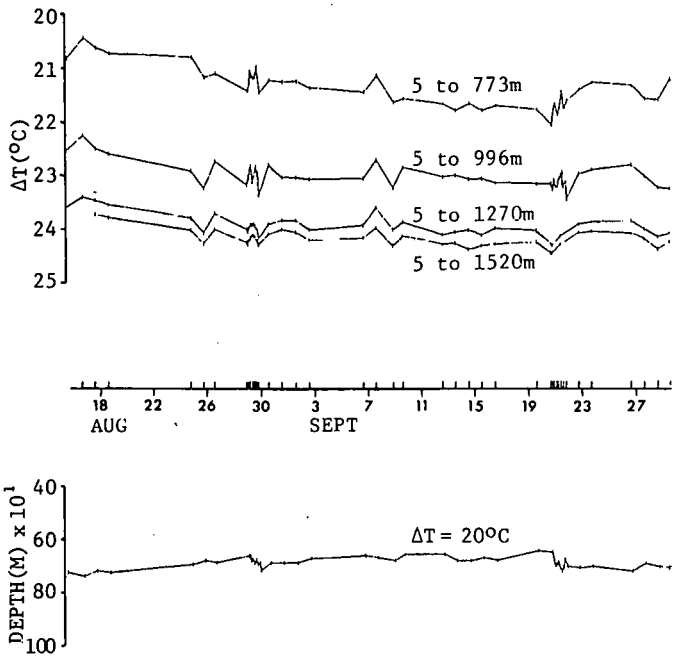

Figure 8. Temporal behavior of vertical temperature differences (ΔT) between the near surface (5m) and depths of 773, 996, 1270 and 1520m; and vertical displacement of the 20°C ΔT.

the experiment of about 0.9 ‰, followed by a gradual decrease of around 1.7 ‰ over the last 1.5 months. The surface mixed layer as defined by salinity was 20m thick; however, occasional salinity differences of 0.5 ‰ developed even in the upper 20m. The largest S variations occurred near the base of the surface mixed layer at a depth of 44m, where salinity variations up to 1 ‰ occurred over time scales of several days. Below the surface mixed layer and above the subsurface salinity maximum was a region of high visual coherence at periods of tidal (semi-diurnal) and longer. The salinity of the SUW subsurface maximum, between 104 and 246m, remained relatively constant. The standard deviation in the core of this layer was only ±0.05 ‰. At depths of 773 to 1520m in the AIW and NADW, the salinity remained nearly constant at about 35.0 ‰ for the duration of the experiment.

Vertical displacements of isohalines were generally small and tended to follow the same trend as previously described for isotherms: deviations were smallest in the main thermocline where vertical stability is greatest, and largest in the deeper well-mixed waters.

The large variations in salinity in the upper layer (above the SUW) probably results from the advection of poorly mixed TSW past the moor rather than local convective or wind mixing. TSW, which is comprised of waters from the equatorial region with a freshwater input from the Amazon and Orinoco Rivers, can be significantly altered during transport by mixing and air-sea interaction resulting in salinity patchiness.

Density. The σ_t variations shown in Figure 7 reflect the combined fluctuations of T and S. The temporal deviations are mainly produced by the previously discussed changes in salinity over the experiment duration. The stable (density increasing) configuration of the density structure is primarily a result of the temperature stratification. Visually coherent tidal variations extend from near sur-

face to approximately 1000m and are thought to be produced by the semi-diurnal internal tide in the main pycnocline. In general, isopycnol depths were quite stable over the duration of the experiment.

Tidal Variability. The vertical variability of the water mass structure that occurs with tidal periodicities was investigated during spring and neap tide periods with bi-hourly STD casts. The range of the T fluctuation was about 0.7 to 1.0°C in the main thermocline and decreased to about 0.3 to 0.5°C at 1000m. The range of S variation was approximately 0.3 to 0.8 °/oo in the main thermocline and decreased to nearly zero below 775m. The tidal range of σ_t was about 0.2 to 0.5 in the main thermocline, and also decreased to almost zero below 775m. Since these fluctuations appear to be restricted to the main thermocline, their source is probably the semi-diurnal barotropic surface tide which excites an internal tide within the pycnocline. Depth deviations of T, S and σ_t associated with the semi-diurnal internal tide were generally small, ranging from about 10 to 40m.

Vertically coherent T fluctuations with semi-diurnal periods occurred in the upper part of the thermocline (between 64 to 104m depths) during both tidal experiments, with variation bounds of about 0.5 to 1.0°C. During the spring tide, oscillations extended to a depth of 1000m, with the amplitude decreasing to about 0.2 to 0.5°C, and phase increasing with depth. The largest S variations occurred at the base of the surface mixed layer (23 to 44m). The bounds of the tidal deviations here were about 0.5 to 0.8 °/oo. Below 44m, tidal variations of S were difficult to detect.

Currents. Most reports in the literature indicate that currents north of St. Croix are westward with speeds of 10-50cm/sec. Our data, however, demonstrated considerable variability in current velocity. Near surface currents were toward the east at speeds of approximately 25cm/sec during the first 2.5 weeks of the study, which is a 180° reversal from normal. On August 10, the current direction shifted to the west and continued on this course with little deviation until August 22. Current speed also increased during this period to be between 25 and 50cm/sec. This period of westward currents coincides with the occurrence of a salinity maximum in the surface mixed layer (Figure 7), which may reflect the westward advection of a patch of north equatorial water past the site. From August 22 to 28, a strong diurnal tidal current developed with speed amplitudes of about 25cm/sec and 180° direction reversals. This coincided with the spring tide, when the tidal sea level fluctuations were also diurnal. After August 28, the currents became weak and variable.

A vertical profile of the horizontal currents and temperature to a depth of approximately 1000m was obtained on September 29 by lowering an Aanderaa current meter to desired measuring depths. These data are shown in Figure 9. Currents at 40m were toward the southeast at about 14cm/sec. A current reversal occurred at 100m with currents toward the west at speeds of 10 to 16cm/sec down to 800m. Below 800m, the current shifted toward the north.

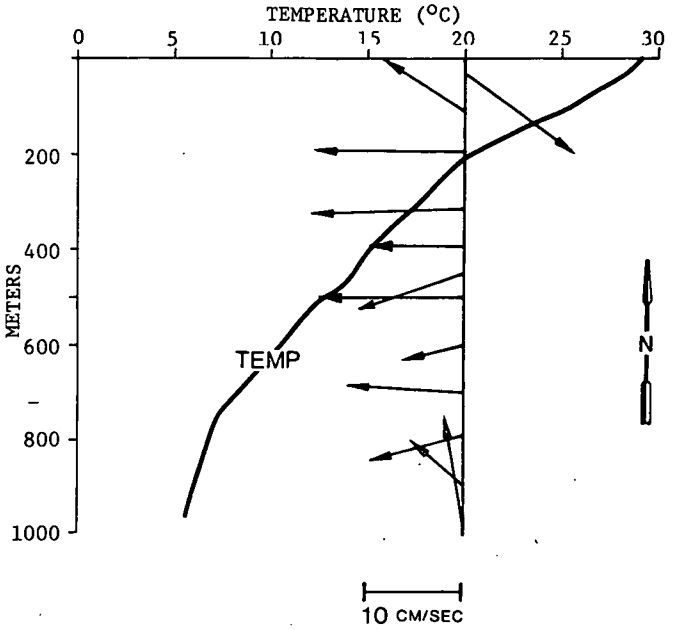

Figure 9. Current and temperature profiles, September 29, 1977

Consequences for OTEC

Thermal Resource

The thermal resource defined in terms of a vertical temperature difference (ΔT) of 20°C between the surface mixed waters and subsurface waters, was available at the deep moor for the duration of this experiment. The deep waters showed very little deviation in temperature: At 1000m, temperature varied 0.5°C from about 5.1 to 5.6°C. Temperature of the surface mixed waters exhibited a total range of only 0.9°C, from 27.8 to 28.7°C. The mean ΔT at 1000m was 23°C with standard deviation ±0.2°C. The mean ΔT at 773m was 21.4°C with a standard deviation of ±0.4°C. The depth to reach a 20°C ΔT varied from 660m minimum to 740m maximum during the experiment.

Historical data from NODC indicates that a 20°C ΔT thermal resource is available year round at St. Croix from depths less than 1000m and distances a few kilometers from shore. The temperature variations measured during the 2.5 month experiment at 1000m are typical of those found in the historical data set at this depth. The seasonal variation of near surface temperature is about 3°C in the NODC data base, from a minimum of 26°C in winter to a maximum of 29°C in summer. Using the 26° winter surface temperature, a mean ΔT of 20°C would occur at a depth of 895m. The maximum possible depth to reach a ΔT of 20°C would be 956m. Thus, from thermal resource considerations the waters north of St. Croix are considered an excellent location for an OTEC site.

Variability

The temperature variations observed in this study, when viewed in conjunction with the historical data set, do not seriously degrade the potential thermal resource for OTEC exploitation of the St. Croix site. The implications of the substantial salinity and current velocity changes measured in the surface waters at the deep moor, however, should be considered.

Significant salinity variations occurred to a depth of 100m. Based on our summer data, locating an OTEC evaporator seawater intake at the 20m depth would place it near the bottom of the mixed surface layer defined by T and below the mixed surface layer defined by S. Tropical Surface Waters consist of a mixture of equatorial waters and freshwater input

from the Amazon and Orinoco Rivers. Salinity patchiness develops in this layer due to incomplete mixing of water types and air-sea exchanges during transport and will produce S variations in the intake waters as it is advected past the site. Variations may also be caused by vertical displacement of isohalines. Although salinity variations alone probably would not have a detrimental impact on OTEC performance, the consequences of significant variations in non-conservative properties such as oxygen, nutrients, and plankton implied by the surface water patchiness should be considered, especially from the viewpoint that the subtropical waters of St. Croix and Puerto Rico are remarkably invariant when compared to more temperate sites such as the Gulf of Mexico and the Gulf Stream.

Variability in current velocity will impact the station-keeping ability of an OTEC plant. 180° direction reversals of surface currents occurred several times during our 2.5 month study; easterly surface currents were recorded nearly 50% of the time, whereas historical data indicates westward flow throughout the year. Although our current profile is merely a snapshot, it demonstrates a complicated structure and requires further investigation.

Acknowledgments

Funding for this project was provided by NOAA (AOML), Contract No. 3-7-022-35217 through a Grant from ERDA/DOE. We thank Jules Hirshman, Robert Molinari, and Lloyd Lewis for their assistance in project development. We are extremely grateful to the Tracor Marine personnel in St. Croix for their generous and helpful aid during the field program, and to Marilyn Baker, who typed the manuscript.

References

1. Aftring, R.P., D.C. Capone, L. Duguay, J. Fell, I.M. Master, and B.F. Taylor. 1978. Biofouling and site characterization studies in an ocean thermal energy conversion (OTEC) experiment at St. Croix, U.S. Virgin Islands. In: Proceedings of the Fifth Ocean Thermal Energy Conversion Conference. (A. Lavi and T.N. Veziroglu, eds.). Miami Beach, Florida. pp. VIII-45 - VIII-72.

2. Atwood, D.K., P. Duncan, M.C. Stalcup, and M.J. Barcelona. 1976. Ocean Thermal Energy Conversion: Resource Assessment and Environmental Impact for Proposed Puerto Rico Site. Final Report, NSF Grant No. AER 75-00145. 104pp.

3. Burns, D.A. 1977. The Oceanographic and Meteorological Environment West of St. Croix. Physical Oceanography Div. Naval Oceanographic Laboratory. NORDA Report #13. 81pp.

4. Craig, H.L., R.S.C. Munier, and J.W. Morse. 1978. Corrosion results from a 72-day field test of simulated OTEC aluminum heat exchanger surfaces at St. Croix, U.S. Virgin Islands. In: Proceedings of the Fifth Ocean Thermal Energy Conversion Conference. (A. Lavi and T.N. Veziroglu, eds.). Miami Beach, Florida. pp. VIII-148 - VIII-192.

5. Cummings, S.R., D.K. Atwood, and J.M. Parker. 1978. Synthesis and description of the existing historical inorganic nutrient data sets from three potential OTEC sites: Northern Gulf of Mexico, Puerto Rico, and St. Croix. In: Proceedings of the Ocean Thermal Energy Conversion (OTEC) Biofouling and Corrosion Symposium. (R.H. Gray, ed.). Seattle, Washington. pp. 423-446.

6. Frassetto, R. and J. Northrup. 1957. Virgin Islands bathymetric survey. Deep Sea Research, 4, 138-146.

7. Gordon, A.L. 1967. Circulation of the Caribbean Sea. J. Geophysical Research. 72(24), p. 6207.

8. Lee, T.N., R.S.C. Munier, and S. Chiu. 1978. Water Mass Structure and Variability North of St. Croix, U.S. Virgin Islands, as Observed during the Summer of 1977 for OTEC Assessment. U. Miami-RSMAS-78004. 81pp.

9. Munier, R.S.C., S.C. Hess, T.N. Lee, and H.B. Michel. 1978. St. Croix: Supplement to a Source Book of Oceanographic Properties Affecting Biofouling and Corrosion of OTEC Plants at Selected Sites. U. Miami-RSMAS, TR78-2. 56pp.

10. Wust, G. 1964. Stratification and Circulation in the Antillean-Caribbean Basins. Columbia University Press, New York. 201pp.

OTEC PHYSICAL AND CLIMATIC ENVIRONMENTAL IMPACTS

John D. Ditmars and Robert A. Paddock

Energy and Environmental Systems Division
Argonne National Laboratory
Argonne, Illinois 60439

Abstract

Assessment of Ocean Thermal Energy Conversion (OTEC) environmental impacts and resource utilization requires an understanding of the physical processes underlying the interactions between an OTEC plant or plants and the ocean. This paper presents an overview of the U.S. Department of Energy program for the development and application of analyses and models for the prediction of the physical aspects of OTEC impacts. Predictive tools are necessary to address problems at different site areas, scales of OTEC deployment, and time horizons.

The effects of intake/discharge designs and of ambient ocean conditions on recirculation and near-field effluent plume behavior have been investigated by means of physical models. Further study of the intake flow fields may be necessary to make estimates of intake impingement and entrainment effects. Mathematical analysis of intermediate-field mixing of plant effluents has shown that effluent plumes may have vertical dimensions on the order of meters and lateral dimensions on the order of kilometers. Models of oceanic regional and island coastal circulation are required to investigate far-field effects on the scale of tens of kilometers. Basin-wide resource renewal and physical environmental effects are being studied by means of a numerical model of the Gulf of Mexico with detailed vertical resolution. Concerns regarding climatic impacts presently are focused on atmospheric CO_2 loading and modification of air-sea heat exchange processes due to OTEC operation.

Introduction

The assessment of the physical aspects of OTEC environmental impacts and resource utilization is an integral part of the overall OTEC Environmental and Resource Assessment program. That broader program includes the biological and chemical aspects of OTEC impingement on the ocean environment and is managed for DOE by the Lawrence Berkeley Laboratory.[1] The purpose of the Argonne program is to provide the development and application of analyses and models necessary for the assessment of potential OTEC environmental and resource utilization problems. Physical transport and mixing processes are at the base of ecological impact assessment, and predictive means for simulating these processes are required. Predictive tools are necessary to address environmental and resource questions for a variety of potential site areas, scales of OTEC deployment, and time horizons. That is, not only must questions regarding initial demonstration plants be addressed, but also questions regarding future large-scale deployments must be addressed in terms of environmental impacts and thermal resource utilization and availability.

The purpose of this paper is to present an overview of the physical impacts program. The overview describes the status of the program outlined at the previous OTEC conference[2] and emphasizes progress achieved and projects initiated within the past year. The approach is to identify the specific problems being addressed, to summarize what we know about their solutions or what tools are available to address them, and to indicate those problem areas where we know little and need tools developed. The details of model development, applications, and results will not be discussed in this overview paper, and the reader is directed to the papers by individual investigators, cited below, where such information can be found.

The discussion here is focused on three general problem areas: thermal resource utilization, physical environmental impacts, and climatic impacts. The problems of thermal resource utilization and physical environmental impacts are treated in terms of single- and multiple-plant deployments and various spatial scales. Several physical processes affect both resource utilization and environmental impacts. Distinct separation of the tools to deal with such processes, in terms of different problems, is not possible, and, in some cases, the same tool will be applicable to more than one problem.

Thermal Resource Utilization (Single Plant)

The OTEC power cycle is driven by a relatively small temperature difference (thermal resource) compared to most other power generating schemes, using a thermodynamic cycle with typical temperature differences expected to be in the 18-24 C° range. Due to the fact that about 25% of the normal gross electric power generated must be used to operate the plant and the fact that only about half of the total temperature difference exists across the power cycle, any fractional loss in thermal resource is magnified by a factor of about 2.7 in terms of fractional loss in generating capacity. For example, a 1 C° loss in thermal resource will reduce the net output of an OTEC plant by about 12%.

The temperature difference available to an OTEC plant depends both on the ambient ocean conditions at the site and on the design of the plant itself. The problem is to predict the effects of plant-ocean interactions on available thermal resource as a function of plant design and ocean conditions. Because the temperature of the deep, cold water resource is expected to remain relatively constant, the available temperature difference depends primarily on the warm sea water intake temperature. Warm water (evaporator) intakes will be located in the upper mixed layer, near the surface, where ambient water temperatures are usually greatest. Ambient water temperatures in this region may exhibit variability with hourly, daily, and seasonal time scales in response to perturbations to the heat balance by the passage of weather fronts and ocean circulation features. The water temperature available at the evaporator is a function not only of ambient ocean temperature variability, but of the interactions between the flow fields generated by the intake and the plant discharges with the surface water. The extent of these interactions and the

resulting warm water intake temperature will depend on the ambient temperature, density, and current structures in the vicinity of the plant and on the location and configuration of the intake and discharge ports. The thickness of the mixed layer, the ambient currents in the mixed layer, the depth of the intake, the orientation of the intake, the separation of the intake and the discharges, and the orientation of the discharges are all important in determining the resulting flow field and thus the intake temperature.

The effects of intake design and discharge design on warm water intake temperature may not be independent. However, it is convenient to assume initially that discharge effects can be minimized by prudent design and to consider separately what is known about intakes. A discussion of direct recirculation from discharges to intakes will follow.

Evaporator Intake Temperatures

The variability of evaporator intake water temperatures depends both on temporal changes in the ambient water temperature and the mechanics of the intake flows. In physical model experiments the effects of the unsteadiness of the water temperature field in the vicinity of a plant were neglected, and the temperature of water drawn into the evaporator depended on the intake flow fields. An intake in a homogeneous (with respect to density) mixed layer will draw water from over the entire vertical extent of the mixed layer. Withdrawal of colder water from the thermocline region below the mixed layer is possible under certain conditions, but physical model studies[3] have indicated that such withdrawals would not be likely for typical 200-MW OTEC plant designs until the intake structure was within about 10 m of the bottom of the mixed layer. In cases where the mixed layer is so shallow that the evaporator intake is in the thermocline or where some vertical density stratification exists in the "mixed layer," intake water may be selectively withdrawn from over limited vertical extents. While the thickness of such a withdrawal layer grows with distance away from the plant and is not easily predicted, it is likely to be on the order of tens of meters within a kilometer of the plant.[4] The intake temperature is determined by the distribution of flow in the withdrawal layer and vertical ambient temperature distributions. Given relatively symmetric distributions of both flow and temperature, mean intake temperatures will be about equal to ambient temperatures at the elevation of the intake centerline. Limited observations of intake temperatures in physical model experiments with ambient stratification do not contradict that suggestion.[5] The evaporator intake flows, then, act to integrate spatial variations in water temperature.

Temporal changes in intake temperature depend on the degree to which temporal variations in ambient water temperatures are damped out by the integrating effect of the intakes. Clearly, the unsteadiness of near-surface water temperatures will not be felt in intake temperatures, if water temperatures over the bulk of the mixed layer remain constant. On the other hand, if temporal variability exists throughout the mixed layer, intake water temperatures may reflect it. Present observational programs for OTEC[6] at potential site areas include the use of thermistor chains that record water temperatures on an hourly basis at ten-meter intervals in the upper 100 m of the water column. Data from the thermistor chains will provide adequate statistics on relatively short-period ambient water temperature variability. Those data and a more detailed understanding of the mechanics of the intake flow fields for various plant designs are needed to assess the potential for short-period variability of intake water temperatures.

Direct Recirculation of Plant Effluent to the Evaporator

The temperature of the warm water drawn in by an OTEC plant can also be affected by the presence of the discharges from the plant, and some fraction of the discharge effluent may recirculate directly into the warm water intake. The mode of discharge (separate evaporator and condenser discharges or a mixed discharge), the vertical separation of the evaporator intake and discharge ports, the depth of the discharge with respect to the mixed-layer depth, the angle of the discharge with respect to the horizontal and to the ambient current, and the discharge and ambient current velocities will all affect the near-field behavior of the discharge jet and its interaction with the evaporator intake flow field. Prediction of the magnitude of the effects of the discharge on the warm water intake temperature is necessary so that the potential for resource degradation through recirculation can be given proper consideration in the process of selecting a discharge mode and designing the discharge ports. The complexity of the near-plant flow fields has resulted in the use of laboratory physical models to examine these effects.

Initial physical model studies focused on highly schematic versions of OTEC plant intakes and discharges and/or of the ambient ocean. The direct recirculation from a single round, non-buoyant jet directed horizontally into a uniform ambient current to a horizontal, radial intake located above the jet was studied by Hydronautics.[7] Discharges into counterflowing (head-on), crossflowing, and coflowing currents were examined, and separation distances between intakes and discharges were varied from 1-2 discharge port diameters. These studies showed that direct recirculation varied with the magnitude of the ambient current such that it increased with increases in ambient current to some maximum (at ambient currents ≈50-70% discharge velocity) and then decreased for further increases in ambient current. The amount of direct recirculation was a function of the orientation between the discharge velocity and ambient current, and the maximum recirculation values observed, for the range of intake/discharge separations considered, were 30%, 10%, and 3% for counterflowing, crossflowing, and coflowing conditions, respectively. Tests with different intake designs yielded recirculation values of the same magnitude or less. Increases in the vertical separation distance between intake and discharge and making the discharge negatively buoyant acted to decrease recirculation below the values given above.

Additional studies[7] on the inhibition of recirculation due to the negative buoyancy of the effluent relative to mixed-layer water involved an intake port positioned 0.5-2.0 port diameters above the interface with a stagnant, denser layer. The inhibiting effect of the density difference was found to be substantial, and the largest withdrawal from the lower layer was found to have occurred for the case of a round intake port drawing water vertically upward. Even in this case, a separation equivalent to 10-15 m was sufficient to keep recirculation to less than 10% for an intake equivalent to a typical 200-MW OTEC plant. The use of a horizontal radial intake was found to reduce recirculation to less

than 5% even with vertical separations of only 10 m, and intakes drawing flow from the surface vertically downward were found to reduce recirculation even further.

To put these recirculation values into perspective, if the discharge is 3 C° cooler than the intake temperature (typical of the evaporator discharge) and the total thermal resource is 22°C, a 25-30% recirculation corresponds to a 12-16% loss in net power. This corresponds to experimental results for essentially a worst case situation with a neutrally buoyant discharge located only 1-2 port diameters below the intake and directed into a strong oncoming current. A more typical situation is the one in which only part of the discharge will be directed into the current while part of the effluent will be directed perpendicular to the current and part of the effluent in the same direction as the current. The maximum total recirculation would then be 10-15% even for an intake/discharge separation of 1-2 port diameters and a neutrally buoyant effluent. The corresponding net power loss is only 4-8%.

Additional schematic physical model experiments were carried out at MIT by Jirka et al.[8,9] to study a mixed discharge from an OTEC plant discharged at the mixed-layer depth. Actually only the upper layer of a two-layer ocean was simulated in the model, and it was modeled in an inverted configuration with a 1:200 geometric scale reduction. The model showed no measurable recirculation for a range of discharge conditions for radial slot and symmetric 4-port discharge configurations with an intake drawing flow from the surface vertically downward. Intake/discharge separations ranged from 8 to 48 discharge port/slot heights, and ambient currents were zero or small. Jirka et al. also adapted existing analytical model techniques to the configurations studied in the physical model experiments (mixed discharge at the mixed-layer depth with no ambient current). Based on the predictions of the analytical model and insights gained from the physical model results, an approximate criterion was developed to predict possible onset of recirculation. The criterion is expressed in terms of flow rate, discharge velocity, plant radius, density difference of the mixed discharge with respect to the mixed-layer density, and the mixed-layer depth. They concluded that for a reasonable plant design and mixed-layer depth on the order of 50 m, OTEC plants with capacities up to 200 MW (net) could operate using mixed discharges with little or no recirculation.

The results of these recirculation studies suggested that, under the conditions studied, recirculation could be minimized by appropriate vertical separation of the intake and discharge. More detailed examinations of recirculation for large OTEC plants in flowing ocean environments with realistic vertical temperature stratification were undertaken this past year at MIT.[10] Completed experiments involved both evaporator-only and mixed discharges into stagnant, temperature-stratified receiving waters. Discharge flow rates corresponding to a net capacity of 400 MW were used in most cases, and radial slot and symmetric 4-port discharges were studied. Realistic stratifications were used with mixed-layer depths in the range of 30-70 m, and intake/discharge separations varied from 30-91 m. Recirculation was found to be small in most cases corresponding to changes in intake temperatures of 0.0-0.2 C°. Only in two experiments was significant recirculation observed. These two experiments corresponded to an evaporator-only discharge directed 21° upward above the horizontal and to an evaporator-only discharge from a 600-MW plant. Experiments with a realistic ocean current present, as well as temperature stratification, have been initiated only recently and are expected to provide the first data on a symmetric 4-port discharge in currents of as large as 1 m/s. Additional laboratory studies at MIT concern the near-plant interaction of separate, but closely-spaced, evaporator and condenser discharges. Interactions may result in the formation of effective mixed discharges without the necessity of mixing the heat exchanger effluents inside the plant and with the apparent advantage of reduced probability of recirculation for mixed discharges.

There are areas related to direct recirculation at individual plants that need further investigation. The effect of large ambient currents upon recirculation is not well understood. There is some evidence from the Hydronautics studies[7] that discharge into an oncoming current of speeds comparable to the discharge velocity may result in substantial recirculation (on the order of 25-30%) for certain intake and discharge configurations. The experiments underway at MIT that involve towing an OTEC model in a stratified tank to simulate large ambient currents will help quantify the extent of the recirculation under realistic stratification conditions. The possibility of using directional discharges or vertically downward discharges to avoid the potential for recirculation, if it exists, should also be investigated. Plants in the 50- to 100-MW size range require additional study. While many of the trends indicated in the investigations of larger plants are likely to hold for this range in plant size, hydraulic scaling does not allow consistent scale-down of existing results for parameters describing both the plant and the ambient environment. Also, little is known specifically about the potential for recirculation for the conditions under which a plant ship would operate. Recirculation may not be a problem for a plant ship underway because its discharge plume would be left behind by the motion of the ship and the intake could be placed forward of the direct influence of the discharge. However, for the small headways expected to be maintained by OTEC plant ships, recirculation might still occur under certain conditions. The potential for recirculation under plant ship conditions should be investigated.

It is not adequate to design intake and discharge systems on the basis of recirculation avoidance alone. The impact on the ocean environment must be considered as well.

Thermal Resource Utilization (Many Plants)

It has been proposed that eventually many OTEC plants may be deployed relatively near one another to form a power park. This type of deployment might minimize undersea power transmission and shore-based power conditioning costs by allowing a single cable and shore facility to service many plants. However, the concentrated deployment of OTEC plants in a power park raises additional questions concerning thermal resource utilization. The spacing between the plants must be selected such that the effluent from one plant does not degrade the thermal resource for other nearby plants. Also, with large quantities of warm and cold water being removed from near the surface and from a depth of 500-1000 m and injected at some intermediate depth, the question of resource renewal arises.

Spacing of Plants to Avoid Resource Degradation

The effluent from one OTEC plant may reduce the thermal resource available to other plants within a power park either by directly entering the warm water intake of a plant downcurrent or by effectively "thinning" the mixed layer downcurrent and therefore increasing the likelihood that cooler water near the bottom of the mixed layer will be drawn up into the intake of neighboring plants.

Jirka[11] has presented a preliminary analysis that can be used for estimating the minimum plant spacing that will preclude the effluent from one plant from degrading the effective thermal resources available to neighboring plants. In his analysis, Jirka assumes that a mixed-discharge mode is used and that the ambient ocean can be approximated by a two-layer system. After initial dilution due to jet entrainment, the mixed-discharge effluent is assumed to form a layer of intermediate density between the upper and lower layers of the ambient ocean. The effluent then drifts with the ambient current and spreads laterally due to buoyancy. The intermediate layer reduces the effective thickness of the mixed layer at neighboring plant sites and increases the potential for recirculation. Using the aforementioned recirculation criterion developed at MIT, the maximum allowable decrease in mixed-layer thickness before the onset of recirculation can be estimated and used to estimate minimum plant spacing that will result in this maximum amount of mixed-layer thinning. This analysis has been applied by Jirka to two power park configurations. For a row of plants oriented orthogonal to the dominant current direction and an ambient mixed-layer depth of 70 m, a minimum lateral spacing of 480 m is predicted for 100-MW plants and 36,000 m for 400-MW plants. In the case of a rectangular grid of plants, the minimum spacing depends on the ambient mixed-layer depth, the magnitude of the ambient current, and the number of rows in the grid. For the case of a mixed-layer depth of 70 m, an ambient current of 0.1 m/s, and five rows, a minimum spacing of 5,570 m is predicted for 100-MW plants, and 160,000 m for 400-MW plants.

The above analysis of plant spacing requirements is a rather tentative one because the model for plant interactions is extremely simple and the model for buoyancy spreading in the intermediate field region downcurrent from the plant is quite approximate. Jirka[12] has been developing a two-dimensional analysis of the buoyancy spreading regime of intermediate-scale plume motions. That analysis deals more directly with the problem of a source of buoyancy in a current than earlier analyses, and initial approximate results suggest that lateral spacing requirements may exceed those indicated above. That is, minimum lateral spacing for 100-MW plants may be on the order of 2 km rather than 0.5 km. It is necessary to caution here that plant spacing requirements may not be driven solely by thermal resource considerations, and assessments of downcurrent environmental impacts may provide other constraints on plant spacing.

Resource Renewal for Large Deployments

The preservation of the thermal resource for utilization by large numbers of OTEC plants, while not an issue for early OTEC plant deployments, requires consideration now in terms of assessment of the power potential of various site areas. The term resource renewal is meant to denote the general availability, on an ocean-regional or basin scale, of the warm surface and cold deep water. In large measure the question of resource renewal is related to the oceanic circulation or water mass transports responsible for replacement of water in various regions, although surface water temperatures may be governed in part by local air-sea exchange processes that might be modified by OTEC plant operations. Our understanding of transport patterns is founded almost entirely on observational data, and in many potential OTEC site areas observational data on transport are sparse -- a prime motivation for the collection of such data under OTEC aegis. Of course, long time-series and synoptic data sets are required to provide data for the evaluation of net transport quantities. Moreover, the effects of OTEC plants on natural resource renewal processes are likely to be subtle and may be evident only after long times. Consequently, numerical modeling of circulation including simulated OTEC effects may provide some insight into the resource renewal question. To date the question of resource renewal at island sites has not been addressed but will receive some attention in relation to modeling efforts of large-scale environmental perturbations at such sites. The past activities related to resource renewal have focused on the Gulf of Mexico.

The Gulf of Mexico basin, with open boundaries at the Yucatan Strait and the Straits of Florida, is large with respect to even large-scale OTEC deployment. However, the warm water requirement for production of 100 GW (1000 100-MW plants) in the Gulf is on the order of 3-6% of the geostrophic transport (relative to 500 m) estimated[13] to enter the Gulf through the Yucatan Strait. Cold water neither enters nor leaves the Gulf through the Straits of Florida, and net transports of cold water from the Gulf through the Yucatan Strait have been estimated on occasion from observations. Estimates[13] of outward cold water flows have been as large as three times the cold water requirements for 100 GW of OTEC production. The long-term transports of cold water to and from the Gulf are not known, and cold water renewal for OTEC operations is also a consideration for the Gulf.

A simple one-dimensional model of the Gulf of Mexico (assuming lateral homogeneity) by Martin and Roberts[14] indicated that 1000 100-MW OTEC plants distributed uniformly throughout the Gulf might result in perturbations to natural ocean temperatures in the water column of as much as 1 C°. The model results are very approximate because of the spatial averaging of the effects of the Loop Current and are sensitive to assumptions regarding exchanges through the straits. While the behavior of the Loop Current and exchanges through the straits are not well-understood, it is apparent that they may influence significantly the thermal resource renewal in the Gulf.

Prediction of the circulation in the Gulf, particularly with regard to intrusions of the Loop Current into the regions of interest for OTEC deployment, is a formidable numerical modeling task. However, questions related to basin-wide environmental impacts also require simulation of the transport field, and these numerical modeling activities may provide insight into the resource renewal question as well. Previous modeling efforts by Thompson and Hurlburt[15,16] were directed toward two-layer baroclinic models of the Gulf driven both by wind and flows through the Yucatan Straits. Circulation patterns similar to Loop Current structures were noted in preliminary integrations. During the past year, a numerical model with the capability for greater spatial resolution in the vertical has been

readied for application to the Gulf of Mexico by Dynalysis of Princeton, Inc., as reported by Mellor and Blumberg.[17] This model uses layers of variable thickness in the vertical (a sigma coordinate system) and will be run with 10 (and eventually 20) layers. While the primary motivation for application of this model to the Gulf is assessment of environmental impacts (as discussed below), sensitivity studies regarding exchanges through the Yucatan Strait and simulated OTEC power park perturbations are relevant to resource renewal concerns.

Environmental Impact (Single Plant)

The environmental concerns attributable to the operation of an individual OTEC plant have been grouped in four general categories[18]: redistribution of oceanic properties, chemical pollution, structural effects, and socio-legal/economic matters. Specific problem areas include impingement and entrainment associated with seawater intakes, particularly the evaporator intake, perturbations to the ambient temperature, salinity and nutrient distributions by the discharge plume that entrain ambient water as it sinks or rises to some equilibrium elevation, and discharge plumes as conveyers of biocides, corrosion products, and working fluid (due to leaks) into the water column downcurrent of the plant. Many of the physical processes related to these problem areas are the same as the processes governing resource utilization.

Intake Flows and Entrainment/Impingement

The physical problem associated with intakes and entrainment and impingement effects is the estimation of the mass flux of biota into the sea-water intakes. If the distributions of biota of concern were uniform throughout the water column, the mass flux would be simply the product of the concentration and the intake flow rate. However, because vertical distributions of biota exist, particularly relative to the evaporator intakes, the distribution in the water column of flow to the intake may be important for estimates of impingement/entrainment impacts. Determination of the zone of influence of the intake flows involves the same processes described above in the discussion of evaporator intake water temperature. Additional work on intake flow hydrodynamics is required along with the results of biological sampling to improve estimates of mass fluxes to intakes.

Near-Plant Impacts of Discharges

In order to design a discharge system for an OTEC plant that will be environmentally acceptable, one must first be able to predict the fate of the effluent and then assess its impact on the environment. The immediate fate of the effluent depends on both the plant discharge configuration and the ambient ocean conditions. Initially the effluent will behave as a buoyant jet, entraining ambient seawater as it sinks (or rises) and eventually becoming neutrally buoyant, on the average, with respect to the surrounding ocean water. In this near-field region of the plume the physical impact of the effluent plume can be characterized by the equilibrium depth, the dilution, the plume width and thickness, and the disturbances to the ambient temperature and salinity profiles. Determination of these plume characteristics has been an objective of near-field physical model studies. Most of the experiments carried out to investigate direct recirculation provide the additional opportunity for measurements of gross plume characteristics. Analytical and numerical model approaches are difficult in cases where intake flows and ambient currents make external flow fields complex, but they may provide some guidance for the simpler conditions.

Physical model studies at MIT reported by Adams et al.[5,10] included both evaporator-only and mixed discharges into stagnant, stratified receiving waters. Radial discharge ports and flow rates corresponding to a net generating capacity of 400 MW were used in most cases. Realistic stratifications were used with mixed-layer depths in the 30-70 m range. In the case of the evaporator-only discharges, the near-field plume equilibrium depth was 10-15 m below the mixed layer for discharge depths varying from 10 m above the bottom of the mixed layer to 40 m below. The thickness of the plume at equilibrium ranged from 15-50 m, with plume thickness increasing with increasing distance between the discharge port and plume equilibrium elevations. The centerline dilution 900 m from the point of discharge (well after equilibrium depth had been reached) was measured using dye to be 5-10. In the mixed-discharge tests, the equilibrium depth was found to be 25-75 m deeper than for the corresponding evaporator-only discharge tests, and the plume thickness 60% larger. Dilutions were typically in the same range as observed in the evaporator-only discharge tests, that is, 5-10. A few tests were conducted with 4-port discharge configurations. The limited results suggest that the resulting plume behaves similarly to the plumes from the axisymmetric radial discharge.

Integral-type jet analyses were also applied to estimate discharge plume behavior for various discharge modes, discharge depths, and discharge orientations. Calculations were made using an analysis[19] of a submerged round buoyant jet into a stagnant stratified receiving water body for an ambient density profile based on the average temperature profile for the month of September at Keahole Point, Hawaii. Discharge flow rates corresponding to a 50-MW OTEC unit and discharge velocities of 2 m/s were used. The plume equilibrium depths predicted for the horizontal discharge cases are in general agreement with the recent MIT physical model results for both the evaporator-only and mixed discharge modes. The equilibrium depths in the mixed-discharge cases are about 40 m deeper than for the evaporator-only discharge cases. Vertically downward discharges resulted in equilibrium depths that are 60 m deeper for the evaporator-only cases and 80 m deeper for the mixed discharge cases than found for horizontal discharges. The dilution at the jet centerline when the jet has leveled out at the equilibrium depth are predicted to be in the range of 3-5 (average dilution of 6-10), with horizontal discharges producing slightly larger dilutions than vertical discharges. The diameter of the jet at this point (defined here arbitrarily as the diameter of the contour corresponding to a dilution of 20) is about 90 m for the horizontal evaporator-only discharge cases and 130 m for the horizontal mixed discharge cases. The jet diameter is predicted to be 1.7-1.9 times larger in the case of vertically downward discharges.

The following general conclusions can be drawn from the above physical model and analytical model studies. Mixed discharges and vertically downward discharges produce significantly deeper (50-75 m) equilibrium depths and only slightly smaller

dilutions than separate discharges (assuming no interfering interaction) and horizontal discharges. Whether such differences are important in terms of potential biostimulation or biocide distributions is not known presently. The results of biological sampling at OTEC sites and laboratory studies on biostimulation and toxicity will be used with the plume predictions to assess potential ecological impacts.

The near-field behavior of the discharge plume will also be affected by ambient ocean currents. Currents may increase dilutions by increasing the supply of ambient ocean water, but they may also cause the plumes from individual ports to interact with one another and effectively block the inflow of dilution water. Also, ambient currents may act to inhibit the degree of vertical penetration of the plume to depths less than those found for stagnant environments. Physical model experiments presently underway at MIT will study the effect of currents on the external flow field in a stratified environment. If near stagnant conditions exist for long periods of time, however, there may be a buildup of the effluent in the vicinity of the plant. This may also occur in the presence of small currents which reverse periodically and return the effluent to the immediate plant site. Data on ambient ocean conditions and the time scale of changes in ambient ocean conditions at proposed OTEC deployment sites are needed to predict the physical near-plant behavior of the effluent and thus assess the possible environmental impacts.

Downcurrent Effects of Discharges

When the discharge effluent from the plant has reached its equilibrium depth, it has lost its jet-like characteristics and has a velocity only slightly different than the ambient current. Its intrusion into the stratified ocean results in a collapse of the plume in the vertical direction and spreading laterally due to gravity forces. The interaction of the spreading layer and the ambient current in the intermediate field produces a plume that extends upcurrent of the plant and grows in width downcurrent of the plant due to gravity spreading until gravity forces become small and turbulent diffusion takes over as the dominant mixing process.

Jirka[12] has been studying the spreading of plumes from OTEC plants in the intermediate-field region. As indicated above in the discussion of plant spacing for resource utilization purposes, one-dimensional analysis provide estimates of plume spreading downcurrent of the plant. For example, for a 100-MW plant in an ambient current of 0.125 m/s, the plume between the layers of a two-layer ocean is predicted to be about 15 km wide and 4 m thick near the plant and about 30 km wide and 2 m thick 10 km downcurrent. Even in the case of an ambient current as large as 0.5 m/s, the plume is predicted to be 6 km wide 10 km downstream. Recent analysis by Jirka[12] of the two-dimensional (lateral and longitudinal) aspects of intermediate-field spreading allows approximate solutions for the cases of two-layer and linearly-stratified environments. Initial results indicate that the lateral spreading is particularly sensitive to the magnitude of the ambient current and that downcurrent plume widths may exceed predictions from the one-dimensional analysis. Laboratory experiments by Jirka, at Cornell, are being performed to evaluate the approximate solutions in the vicinity of the plant.

Transient plume motions in the intermediate field are being investigated by Jirka in addition to the steady cases discussed above. Little additional dilution of the plant effluent can be expected in the intermediate field, although the plume will be collapsed to a thin, wide layer. Passive turbulent diffusion of that layer at distances downstream of the intermediate field will result in additional reduction in constituent concentrations. Such mixing processes are rather slow and may not result in large dilutions, however, vertical thinning due to gravity spreading may result in breakup of the discrete layer into patches that in turn might experience enhanced mixing with ambient waters.

Environmental Impacts (Many Plants)

Prediction of the large-scale effects of many interacting plants requires an understanding of the interactions among individual plants and of the transport characteristics of the region in which the plants are located. The interactions among plant effluent plumes depend largely on the intermediate-field spreading and plant spacing. Criteria for spacing from an environmental impact viewpoint require some assessments of downcurrent biostimulation potentials and/or biocide levels and are yet to be established. However, the predictive tools for the physical transport are being developed presently and the biological sampling activities are underway. The problem of regional transport pathways and regional accumulation of certain effluent constituents is more difficult to address. Field observations of currents, both historical and those undertaken for the OTEC program, will provide some insight into the transport processes. However, consideration of long-term net transports, of particular interest for the assessment of regional effects at OTEC sites, may require a combination of observational data and numerical modeling. Island site areas, while unbounded in some sense, may be of concern because of the proximity to island coastal waters. Thus, circulation around and in the coastal waters of islands will receive attention in the near future.

The Gulf of Mexico, because of its basin-like features, raises obvious questions about residence times and transport pathways for effluents in the instance of large-scale OTEC operation. Preliminary transport calculations for marked tracers in the two-layer Gulf of Mexico model by Thompson and Hurlburt[15] indicated the differences in transport features for sites in the northern Gulf off New Orleans, in the rather quiet central Gulf, and in the active transport area in the eastern Gulf off Tampa. The focus of the application of the more detailed circulation model of the Gulf of Mexico under development by Dynalysis of Princeton, Inc.,[17] is the examination of the transport and mixing of effluents from OTEC power parks at several locations in the Gulf. The enhanced vertical resolution in the 20-layer Dynalysis model will permit investigation of the large-scale implications of plant designs that result in different near-plant effluent behavior (e.g. evaporator-only vs. mixed discharges). The effects of park location and size on effluent transport pathways and residence times will be investigated as well.

Climatic Effects

Impacts on the climate due to the operation of a small number of OTEC plants are not likely to be

measurable. However, the possibility of large-scale deployments of OTEC plants in the future requires that the climatic consequences of such deployments be considered. The possible impacts of immediate concern are atmospheric loading of CO_2 and weather/climate modification due to modification of air-sea heat exchange processes.

CO_2 Loading to the Atmosphere

Deep ocean water is enriched with inorganic carbon with respect to the surface waters, and, because of the buffering capacity of the surface water, CO_2 may evolve from deep water brought to the surface for OTEC condensers. The potential excess CO_2 in cold water brought to the surface over surface water values is on the order of 1.7×10^{-5} kg CO_2/kg H_2O. In terms of a 200-MW OTEC plant, the excess flux of CO_2 available to the atmosphere would be about 1.2×10^6 kg/day.[20] For comparison, the amount of CO_2 released to the atmosphere by a fossil-fuel-fired power plant of the same electrical capacity is two to three times as much.[21] This analysis should yield an upper bound on potential CO_2 additions to the atmosphere, although the results of site-specific measurements may indicate slightly different values of that upper bound. However, condenser effluents from closed-cycle OTEC plants could well be discharged below the mixed layer (as indicated in earlier sections), and the total evolution of excess carbon to CO_2 may not be realized. The fate of the deep-water carbon depends on both the complex carbonate chemistry of seawater and the physical mixing of the effluent in the ocean. Estimates of physical mixing are available from physical model studies and mathematical analysis, but present limited understanding of oceanic carbonate systems precludes defensible estimates of the fate of carbon in the water column.

Air-Sea Heat Exchange Processes

OTEC plants remove heat from the surface layers of the ocean and, consequently, may produce sea surface temperature depressions. The zeroth-order estimate of sea surface temperature depressions for 1000 100-MW OTEC plants operating in the Gulf of Mexico is less than 1 C°.[14] This is a small number, certainly in the noise of ambient ocean temperature fluctuations, but there are suggestions that even small temperature changes may be responsible for climatic changes. Moreover, models for the prediction of climatic changes are not adequately developed to be sensitive to such small temperature changes.

The zeroth-order estimates of sea-surface temperature depressions were found in a laterally-averaged model of the Gulf of Mexico. Actual three-dimensional distributions of water temperature perturbations may be different. That is, local depressions in the vicinity of OTEC power parks may have larger magnitudes and smaller surface areas associated with them than indicated by laterally-averaged models. Application of the multilayer circulation model of the Gulf of Mexico by Dynalysis to the case of large-scale OTEC deployment will provide some estimates of sea-surface temperature depressions. These estimates will, of course, be limited in that the Gulf of Mexico model will not be a coupled ocean-atmosphere model and will not predict atmospheric impacts due to change in the ocean. The results of this study will certainly not overcome the difficulties of modeling climatic changes, but they will provide bounds on the ocean areas affected. The means of assessing the climatic impact from such ocean temperature perturbations remains to be found.

Summary

Physical model studies are being employed to provide answers to questions regarding resource utilization and environmental impacts in the near-plant region. Studies of intake flow fields are required for better definition of the magnitude of evaporator intake water temperature variability and of impingement/entrainment impacts. Mathematical modeling of density spreading in the intermediate field of effluent plumes is producing guidelines for downcurrent impact assessment and plant-spacing requirements. Oceanic regional and island coastal circulation models are necessary for the assessment of far-field effluent plume impacts and resource renewal. A basin-wide numerical model is being applied to the Gulf of Mexico to investigate the transport pathways and residence times for effluents and resource renewal characteristics associated with large-scale deployments of OTEC plants. Determinations of climatic impacts are presently limited to estimates of upper bounds for CO_2 loading to the atmosphere and of sea-surface temperature depressions that drive air-sea heat exchange processes.

Acknowledgments

The Argonne project of OTEC program management support in the area of assessment of OTEC physical and climatic environmental impacts is supported by the U.S. Department of Energy under contract W-31-109-ENG-38.

References

1. Wilde, P., *OTEC Site Investigations: Hawaii, Puerto Rico, Guam,* these proceedings (1979).
2. Allender, J.H., J.D. Ditmars, R.A. Paddock, and K.D. Saunders, *OTEC Physical and Climatic Environmental Impacts: An Overview of Modeling Efforts and Needs,* Proc. Fifth Ocean Thermal Energy Conversion (OTEC) Conf., Miami, pp. III-165 to III-189 (Feb. 20-22, 1978).
3. Sundaram, T.R., S.K. Kapur, and A.M. Sinnarwalla, *Some Further Experimental Results on the External Flow Field of an OTEC Plant,* Hydronautics, Inc., Tech. Rept. 7621-2, Laurel, Md. (April 1978).
4. Fry, D.J., *Effects of Oceanic Flow Patterns on the Thermal Efficiency of Ocean Thermal Energy Conversion (OTEC),* M.S. Thesis, Dept. Civil Eng., Carnegie-Mellon Univ., Pittsburgh (April 1976).
5. Adams, E.E., D.J. Fry, D.H. Coxe, and D.R.F. Harleman, *Research on the External Fluid Mechanics of Ocean Thermal Power Plants, Interim Report Covering Experiments in Stagnant Water,* MIT Energy Laboratory Rept. COO-4683-1, Cambridge (Oct. 1978).
6. Molinari, R.L., and J. Festa, *Ocean Thermal and Current Velocity Data Requirements for Design of an OTEC Demonstration Plant,* NOAA Tech. Memo. ERL AOML-30, Miami (Jan. 1978).
7. Sundaram, T.R., E. Sambuco, A.M. Sinnarwalla, and S.K. Kapur, *The External Flow Field Associated with the Operation of an Ocean Thermal Power Plant,* Hydronautics, Inc., Tech. Rept. 7621-1, Laurel, Md. (Feb. 1977).

8. Jirka, G.H., R.P. Johnson, D.J. Fry, and D.R.F. Harleman, *OTEC Plants: Experimental and Analytical Study of Mixing and Recirculation,* R.M. Parsons Lab. for Water Resources and Hydrodynamics, MIT, Tech. Rept. No. 231, Cambridge (Sept. 1977).
9. Fry, D.J., E.E. Adams, and G.H. Jirka, *Evaluation of Mixing and Recirculation in General OTEC Discharge Designs,* Proc. Fifth Ocean Thermal Energy Conversion (OTEC) Conf., Miami, pp. III-104 to III-116 (Feb. 20-22, 1978).
10. Adams, E.E., D.J. Fry, and D.H. Coxe, *Results of a Near Field Physical Model Study,* these proceedings (1979).
11. Jirka, G.H., *Preliminary Guideline for the Siting of Multiple Ocean Thermal Energy Conversion (OTEC) Plants (Draft),* Dept. Envir. Eng., Cornell Univ., Ithaca (June 1978).
12. Jirka, G.H., *Modeling of the Intermediate Field of OTEC Discharges,* these proceedings (1979).
13. Molinari, R.L., and J.F. Festa, *Ocean Thermal and Velocity Characteristics of the Gulf of Mexico Relative to the Placement of a Moored OTEC Plant,* NOAA Tech. Memo. ERL AOML-33, Miami (Oct. 1978).
14. Martin, P.J., and G.O. Roberts, *An Estimate of the Impact of OTEC Operation on the Vertical Distribution of Heat in the Gulf of Mexico,* Proc. Fourth Ocean Thermal Energy Conversion (OTEC) Conf., New Orleans, pp. IV-26 to IV-34 (Mar. 22-24, 1977).
15. Thompson, J.D., and H.E. Hurlburt, *Gulf of Mexico -- OTEC Far-Field Numerical Studies: Description and Results of a Two-Layer Model,* Code 322, NORDA, NSTL Station, Miss. (July 1978).
16. Thompson, J.D., and H.E. Hurlburt, *Gulf of Mexico -- OTEC Far-Field Numerical Studies: Code and Documentation and User's Guide,* Code 322, NORDA, NSTL Station, Miss. (July 1978).
17. Mellor, G.L., and A.F. Blumberg, *A Whole Basin Model of the Gulf of Mexico,* these proceedings (1979).
18. U.S. Department of Energy, *Environment Development Plan (EDP): OTEC,* USDOE, Washington, D.C. DOE/EDP-0034 (March 1979).
19. Ditmars, J.D., *Computer Program for Round Buoyant Jets into Stratified Ambient Environment,* W.M. Keck Lab. Tech. Memo. 69-1, Calif. Inst. Tech., Pasadena (March 1969).
20. Saunders, K.D., Argonne Nat. Lab., personal communication (1978).
21. Williams, R.H., *The Greenhouse Effect and Ocean-Based Solar Energy Systems,* Center for Envir. Studies, Princeton Univ., Working Paper No. 21, Princeton (Oct. 1975).

RESULTS OF A NEAR FIELD PHYSICAL MODEL STUDY

E. Eric Adams, David J. Fry and David H. Coxe

R.M. Parsons Laboratory for Water Resources and Hydrodynamics
Department of Civil Engineering
Massachusetts Institute of Technology
Cambridge, Massachusetts 02139

Abstract

A physical model study is ongoing to investigate the sensitivity of recirculation and near field plume dynamics to variation in OTEC plant design and ambient ocean conditions. A thermally-stratified 18 x 12 x 0.6 m basin at a nominal scale of 1/300 allows the upper 180 m of the ocean to be studied for plant sizes up to 600 MWe. Tests have been conducted for stagnant conditions and for conditions with a current, using both the mixed discharge (combined evaporator and condenser) and non-mixed discharge concepts. Separate tests were made to investigate interactions between evaporator and condenser discharges in a non-mixed concept. Measurements include temperature, dye concentration, mean velocity and visual observations obtained from still and motion pictures. Results for the stagnant water tests showed no significant recirculation except for those tests where the discharge ports were oriented (slightly) upward or where the largest plant size (600 MWe) was tested. No significant difference in recirculation could be discerned between the mixed and the non-mixed discharge designs although differences in the equilibrium positions of the discharge plumes were noted. Tests in a current are still in progress but some preliminary results are presented.

Introduction

OTEC plants interact with the ocean environment by withdrawing water through their intake ports and exhausting it through their discharge ports. The resulting flow field external to the plant is of significance in regards to plant performance (as affected by any potential recirculation) and environmental impacts (such as the transport of nutrients, ocean temperature modification, etc.). The goal of the experimental research program at MIT is to understand the external fluid mechanics associated with generic OTEC designs, under a range of ocean environments, so that these considerations can become a part of OTEC plant optimization.

With the present program it will be possible to extend the range of conclusions which could be drawn from previous physical model studies reported in Jirka, et al.(1977), and Fry et al.(1978). By way of background, these previous tests were performed for a somewhat narrower range of plant and ambient conditions. In particular

a) the ocean was assumed to be discretely stratified, consisting of a warm, well-mixed upper layer, and a cold, well-mixed lower layer.
b) the evaporator and condenser flows were assumed to be mixed within the plant and discharged horizontally at the interface between upper and lower layers.
c) plant sizes were limited to a range of 100-200 MWe, and
d) ambient currents were limited to a range of 0 - .1 m/s.

The original motivation for these tests was to provide detailed documentation of typical OTEC flow fields for the purposes of calibrating mathematical models and studying the underlying physical processes. In addition, it was possible to draw some direct conclusions regarding plant performance, and recirculation in particular, within the range of conditions which were tested. For instance, a formula was developed to estimate the onset of recirculation, and an exercise of this formula suggested that for typical ocean profiles (and the relatively low range of current speeds tested) recirculation could be avoided for plants employing mixed discharges with capacities up to about 200 MWe.

The objective of the present set of tests is to extend the range of plant and ambient conditions which can be modeled by relaxing each of the limitations a-d) described above. The resulting tests will thus provide a direct measure of OTEC performance under a more realistic range of operating conditions. Of course the tests can also be used for the calibration/verification of mathematical models.

Model Description

Experimental Characterization

The OTEC plant type. Several different designs have been proposed for a prototype OTEC power plant. The designs considered in this study are limited to those which can be modeled as symmetrical vertical columns.

Figure 1 shows the parameters which characterize the OTEC plant model and the range within which these parameters vary in the model. The evaporator intake, drawing a flow Q_i, is located at a depth of h_i below the surface. The condenser intake is not modeled. The previous study (Jirka, et al.1977) utilized a model which assumed that the evaporator and condenser flows would be mixed within the plant and that the combined discharge flow ($Q_o = 2Q_i$) would be discharged horizontally as shown in Figure 1. This study examines both mixed discharges and non-mixed discharges (flow rate $Q_o = Q_i$). In either case the discharge depth is h_d and the vertical angle is α. (α is positive downward.) For the non-mixed discharges, only the evaporator discharge is modeled, thus assuming that no interaction between evaporator and condenser discharge takes place.

Two types of generic discharge configurations

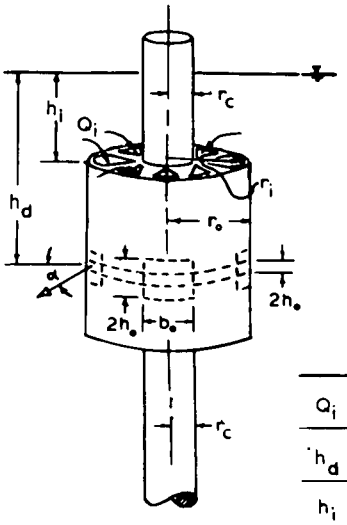

RADIAL OR SEPARATE JET DISCHARGE

	EXPERIMENTAL MODEL (1:300)
Q_i	500-2500 m^3/sec
h_d	23-170 m
h_i	0-60 m.
α	0° ≤ 45°
r_i	20 m.
r_o	23 m.
r_c	11 m.
h_o	Depends on Q_i
b_o	

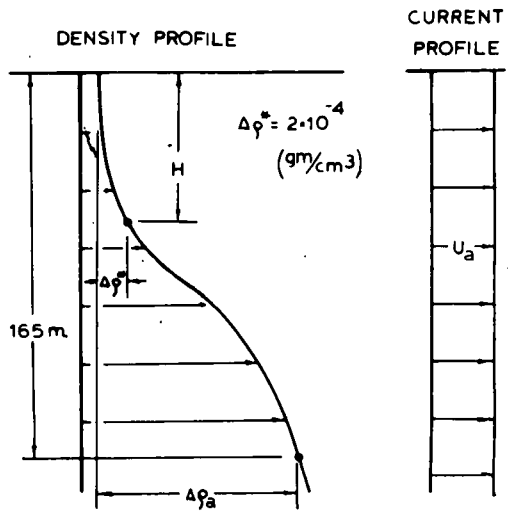

	EXPERIMENT PROFILES (1:300)
U_a (m/sec)	0 - 1.
$\Delta\rho_a (10^{-4}\ gm/cm^3)$	4. - 34.
H (m.)	25. - 150.

Figure 1 New Experimental OTEC Schematizations (with experimental parameter ranges)

were evaluated in this study (see left side of Figure 1).

a) Radial discharge: The discharge geometry is assumed as a radial slot of height $2h_o$ which completely encircles the plant circumference. Although none of the presently proposed OTEC designs exhibit this geometry, it is a useful basis for evaluation. It has an obvious advantage for analytical (cylindrically two-dimensional) and experimental modeling and it preserves many of the characteristics of more complicated three dimensional separate discharge designs as long as equality of mass, momentum and heat fluxes is maintained.

b) Separate discharge: Four separate jets with rectangular cross-sections (height $2h_o$ and width b_o) are arranged around the plant circumference at angles of 90° to one another. This closely approaches probable (round port) design conditions with the mixed or non-mixed discharge concept.

For either discharge geometry, A_o is defined as a characteristic cross-sectional area equal to 1/8 of the total port area. Thus for the radial discharge, $A = \pi/2\ r_o h_o$, while for four separate jets, $A_o = h_o b_o$. Using the square root of A_o as a length scale, a discharge densimetric Froude number is defined, for either radial or separate jet discharge, as

$$F_o^* = \frac{u_o}{\sqrt{g\left|\frac{\Delta\rho_o}{\rho}\right| A_o^{1/2}}}$$

where u_o is the discharge velocity ($Q_o/8A_o$) and $\Delta\rho_o/\rho = [\rho_{amb}(z = h_d) - \rho_o]\ /\rho_{amb}(z = h_d)$ where $\rho_{amb}(z)$ describes the ambient density profile and ρ_o is the discharge density. A positive value of $\Delta\rho_o$ implies positive buoyancy and corresponding values of F_o^* are denoted with an upward arrow. Negative values of $\Delta\rho_o$ imply negative buoyancy, and values of F_o^* have a downward arrow. A final parameter used to characterize the discharge is the jet Reynolds number, defined for either radial or separate discharge configurations as

$$R_e = \frac{4u_o r_h}{\nu}$$

where r_h is the hydraulic radius of the discharge structure. ($r_h = h_o$ for the radial jet and $h_o b_o / (2h_o + b_o)$ for the separate jet experiments.)

The ambient ocean. Figure 2 (Miller, 1977) shows ocean density profiles for several tropical locations. Near the surface water is typically well-mixed, while below densities increase with the steepest density gradient (pycnocline) usually located near the bottom of the mixed layer. The previous study (Jirka, et al.,1977) approximated the ocean profile with two well-mixed layers of

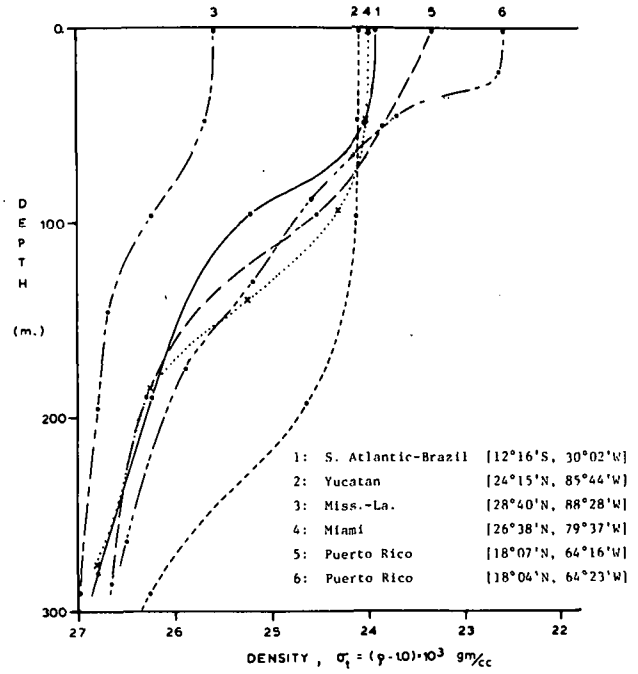

Figure 2 Ocean Density Profiles [Miller, 1977]

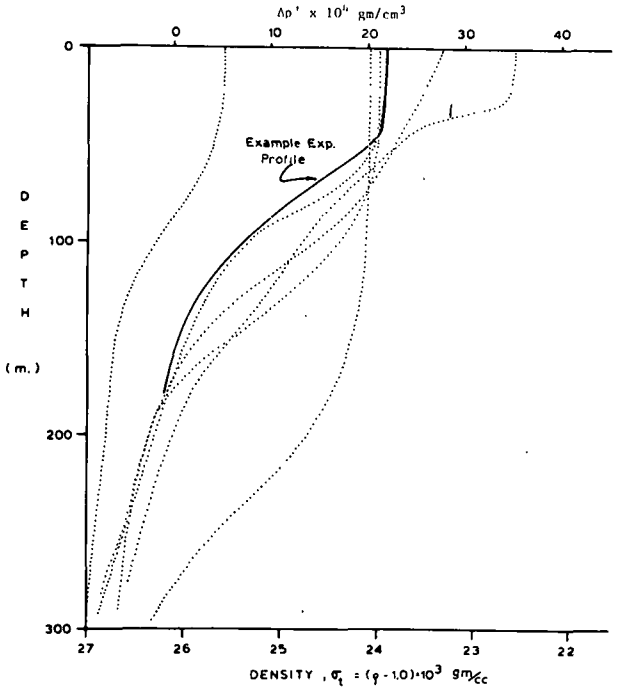

Figure 3 Superimposed Experimental Profile (Scale 1:300) for Comparison of Density Variation

water of distinctly different densities. Thus the profile was characterized by a density difference and a surface layer depth. As shown in Figure 1, the present study considers more realistic, continuous, density profiles. Since the profiles are experimentally produced, each is somewhat different. However, for purposes of summary they are characterized by the parameters H and $\Delta\rho_a$. H is the mixed layer depth, defined as the depth at which the ambient density differs by an arbitrarily small amount - taken here as $2 * 10^{-4}$ gm/cm^3 - from the surface density. $\Delta\rho_a$ is the density difference between the surface and 165 meters. Figure 3 shows a typical profile generated in the lab and indicates that it is representative of actual ocean conditions.

Experiment Layout

The OTEC model. The experiments were conducted in a 12.2 m x 18.3 m x 0.60 m (40' x 60' x 24") basin located on the first floor of the Ralph M. Parsons Laboratory for Water Resources and Hydrodynamics at M.I.T. The basin has a 4.57 m (15 ft) long plexiglass window in one wall of the basin which allows for visual observation and photography of the velocity field close to the wall. Figure 4 presents a general layout of the basin and the water flow circuits for both the set up for the stagnant water tests and the tests in a current.

An undistorted Froude scale model with length ratio of 1:300 was chosen to provide a compromise between the competing objectives of obtaining large jet Reynolds number and measurement resolution (dictating large scale ratios) and ability to model large ocean depths (dictating a small ratio). The 1:300 scale and 0.60 m basin depth allows the upper 180 m of the ocean to be tested. This was sufficient depth to prevent interaction of the discharge with the bottom for any of the horizontal discharge configurations. The basin was not deep enough to model either the condenser discharge in a non-mixed design involving large separation between evaporator and condenser discharge, or the condenser intake at the bottom of the cold water intake. These limitations were not considered to be significant. With the 1:300 scale ratio, the minimum jet Reynolds number was 3100 obtained for the case of a 200 MWe plant with a non-mixed (evaporator), radial discharge.

For stagnant water tests only half of the OTEC model is used; the half model is attached to the plexiglass window so that the wall is taken as a plane of symmetry. For tests in a current, the model is towed along the center of the basin with the discharge and intake flows conveyed to and from the model by flexible 2" hoses. In either case, the intake flow (hot water) enters the model through a radial configuration of circular port holes. It then travels through a large plexiglass tube where it is pumped out of the model. The discharge flow enters the top of the model through brass tubes, which pass inside the intake flow tube to the discharge ports. To simulate a radial discharge, twelve discharge ports (6 for the half model) are used while for separate jet tests four ports (2 for the half model) are used. To insure uniformity, flow to each of the ports is individually metered.

Stratification system. In order to simulate an actual ocean density profile, the basin is filled with water of different temperatures starting with cold city water on the bottom followed by warm water near the surface. During filling, diffusion takes place resulting in a smooth thermocline. Also, once filling has ceased, surface cooling

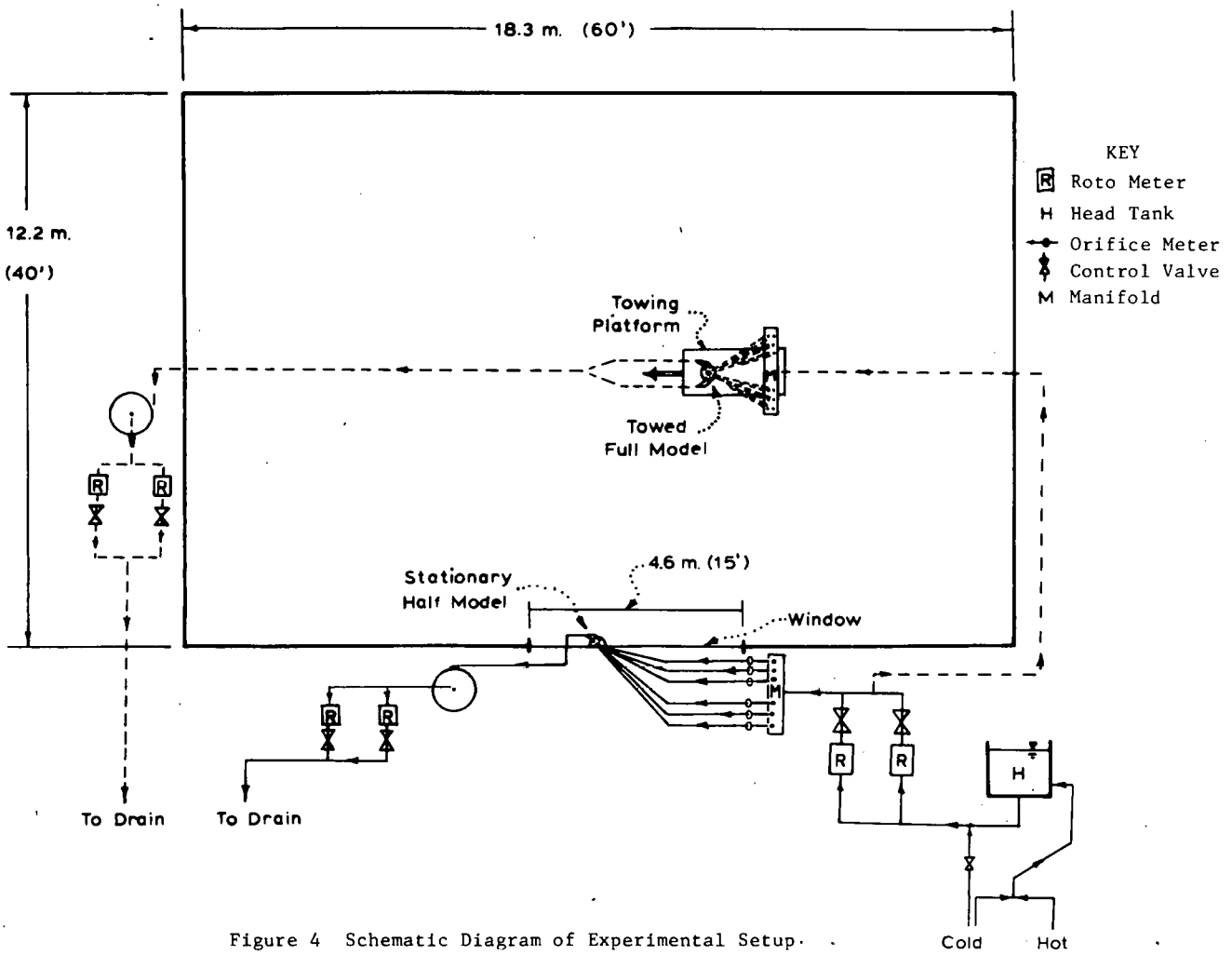

Figure 4 Schematic Diagram of Experimental Setup.

mixes the upper layers thereby decreasing the surface temperature. Because the difference in density between the entering hot and cold water is designed to be greater than the desired density difference $\Delta\rho_a$, a run is begun once the surface has cooled and the desired density difference between the upper and lower layers has been achieved. This takes from 1-4 hours from the time the hot water inflow is turned off.

The spatial and temporal variability of typical temperature profiles obtained with this procedure was examined. The maximum standard deviation in horizontal temperature variation was about .25°C while the maximum rate of change of the mean temperature was about 1°C per hour occuring on the surface. Since a typical experiment lasts for 30 minutes this was considered small, but was nonetheless accounted for in the data reduction.

Measurement systems. Temperatures are measured by approximately 100 Yellow Springs Incorporated thermistors (time constant = 1 sec.) located throughout the basin, and in the discharge and intake lines. A digital electronic volt meter with the capability to scan the 100 thermistor probes records temperature on a paper printout and on punched paper tape. During a typical experiment between 5000 and 6000 temperature readings are recorded.

Fluorescent dye measurements are used to complement temperature measurements in determining recirculation and discharge dilution. Concentrations are measured with a Turner Model IV fluorometer with a threshold detection of 1 part per billion (ppb). Experiments can be run with discharge concentrations of as much as 50,000 ppb and basin background concentrations of less than 30 ppb. A dye concentration of 10 ppb above the background concentration is distinguishable and thus it is estimated that measurement of direct recirculation down to 10 ppb/50,000 ppb = 0.0002 or 0.02% is possible.

Injection of the fluorescent dye into the flow stream serves to tag the discharge jet for photographic purposes. A pair of slide projectors supported above the water are used to emit a narrow slit of light which illuminates a cross section of the flow stream. In order to quantitatively measure the position and thickness of the spreading layer, six marker poles containing fiber optic strands are mounted beneath the light slit. When illuminated, these strands produce dots of light down the marker pole providing a reference grid. Figure 5 shows tracings, made from photographs, of the dyed discharge plume for two typical runs involving an ambient current.

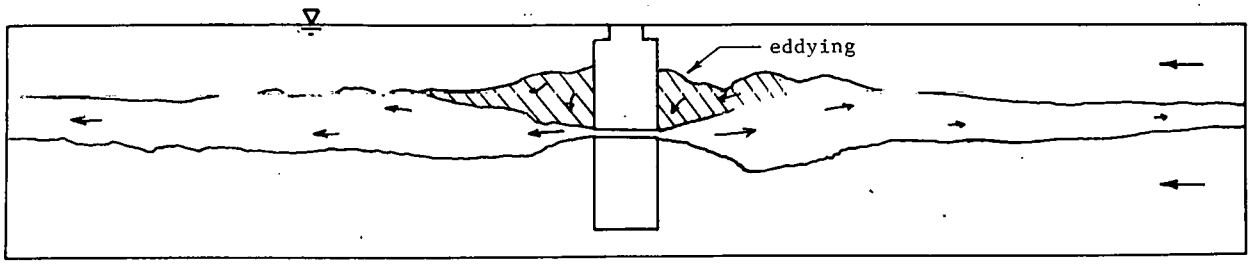

a) ambient current speed = .15 m/s

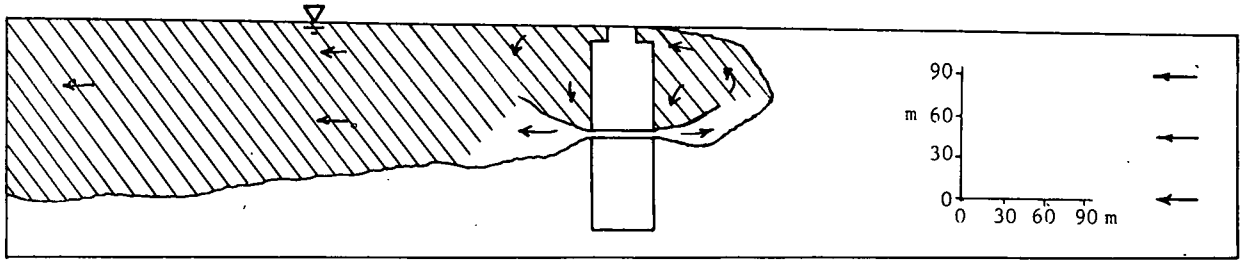

b) ambient current speed = .51 m/s

Figure 5 Photographic Tracings of Longitudinal Plume Crossections for a 400 MWe Plant with Horizontal Radial Evaporator Discharge

Results

Experiments are being performed in three parts. The first two, involving observations of OTEC external fluid mechanics in stagnant water, have been completed. The first set was designed to study OTEC performance under a range of realistic plant designs and profiles of ambient stratification. The second set looked in detail at the interaction which might take place between adjacent discharge jets in a non-mixed discharge concept or between a single discharge and the free surface in either a mixed discharge concept or a non-mixed discharge concept involving substantial separation between evaporator and condenser discharges. The third set of experiments is presently ongoing and involves observations of OTEC external fluid mechanics in ambient currents up to 1 m/s for similar ranges of plant designs and profiles of ambient stratification tested under stagnant conditions. A summary of the results of parts one and two, and preliminary results from part three are described below.

Stagnant Water Tests

An experimental program involving 21 tests was established to examine the influence of discharge type (mixed or non-mixed and radial or individual jet), nominal net power (200 MWe - 600 MWe), relative discharge and mixed layer depths h_d and H, discharge angle α and discharge area A_o. The results of each run are presented in Adams et al. (1978) and include, for each run, photographic tracings of the plume outline, undisturbed and disturbed temperature profiles, intake temperature depression (if any), percentage of direct intake recirculation, and the equilibrium jet dilution, thickness and position (vertical elevation). While it is not practical to present the results here, several observations can be summarized.

Perhaps the most important is that direct recirculation was observed in only two tests. In the first, the discharge trajectory had a vertical component ($\alpha = -21°$) due to improper distribution of flow emanating from the discharge ports. The fact that changing the discharge angle by 21° (to a horizontal discharge) completely eliminated recirculation suggests that recirculation is very sensitive to discharge angle. The second observance of recirculation involved a larger plant (nominally 600 MWe) which was selected so as to produce recirculation. The percentage recirculation (40%) was high suggesting that a nominal plant size of 400 MW (with horizontal discharge in stagnant water) may be near the limit of no recirculation. This is confirmed by the photographic tracings which show the plumes from many "400 MW experiments" approaching, but not quite reaching the water surface and thus not recirculating. These two runs were, not surprisingly, the only runs in which significant intake temperature drops were observed. Because the discharge mixes with a (stratified) ambient, any direct recirculation involves a lowering of intake temperature due both to the direct recirculation itself and the fact that the discharge has been mixed with ambient water of lower temperature (than that which the intake would normally draw). In each of the two cases where recirculation occurred, the latter (indirect) type accounted for more than 50% of the intake temperature drop.

Although dilution was measured for each test it was hard to discern any trends in the variation of dilution with discharge or ambient conditions. The mean value of dilution was about 7 indicating that peak concentrations in the intermediate field of

any chemicals contained in the discharge will be about 14% of the discharge concentrations. It should be noted that the discharge velocities in these tests are relatively high (u_o = 3.5 to 7.8 m/sec).

In contrast to dilution, the shape and the equilibrium depth of the plume are strongly correlated with the discharge and ambient conditions. For instance, for cases of horizontal discharge, all positively buoyant plumes rose while all negatively buoyant plumes fell. For this reason it was often difficult to notice the effect of the discharge on the ambient profiles; the plumes tended to hide in ambient water of their own density (temperature). However a general tendency for the density gradient to decrease at the equilibrium depth was observed. Also, profiles at the smaller radii often show positive temperature anomalies above the plume (indicating that warm entrainment water is being drawn down from above) and negative anomalies below the plume (indicating that cooler water is being drawn up from below).

Interaction Tests

These tests studied in detail the balance of forces involved in two possible near field flow phenomena. Both can significantly affect the vertical trajectory of the discharge jets.

The first involves interaction between the discharge and the free surface which was the cause of the only significant recirculation observed in the previously described tests. This attachment is associated with an attraction or Coanda effect between the discharge jet and the water surface which occurs despite any negative buoyancy of the jet. The evaporator intake flow helps magnify this interaction. The second interaction phenomena studied was the possible mixing of evaporator and condenser jets exterior to the OTEC plant. The jets originate at different vertical levels with different buoyancies. Analogous to the previous phenomena, a low pressure zone exists between the jets tending to attract them together. The vertical trajectory of the discharge jets in both cases, then, is a function of buoyancy and low pressure zones (created by jet-surface or jet-jet interactions). The low pressure is caused by water flowing toward the OTEC plant outside the jet boundaries and originates due to both the evaporator intake and the discharge entrainment demand.

Two sets of tests were carried out to investigate this phenomena. In both cases the OTEC discharge was radial to insure that all flows directed toward the OTEC plant were either above or below the jets. Furthermore the receiving water was stagnant and unstratified. Because any interaction is expected to take place near the plant, this is not a significant limitation. In the first set of tests a single submerged, negatively buoyant jet was discharged horizontally with the water surface much closer than the basin floor. In some tests an intake of equal flow rate existed near the surface. In other tests the intake was absent. Temperature measurements and photographs were used to observe under what conditions jet-surface interaction forced the jet to the surface overcoming the jet's negative buoyancy. For the tests with an intake recirculation was also measured. Either the jet reached the surface resulting in 30-40% recirculation or the jet did not reach the surface and there was 0% recirculation. There were no observations of a steady flow regime with recirculation between these values. A movie of the experiments, shown at the conference, clearly indicates the two regimes.

Dimensional analysis shows that if the discharge radius is kept constant and the intake geometry is ignored, two dimensionless members should characterize the flow. Two such numbers are the discharge Froude number and the relative port width,

$$\mathbb{F}_r = \frac{u_o}{\sqrt{g \frac{|\Delta\rho_o|}{\rho_a} h_o}} \qquad W = \frac{h_o}{H}$$

(Note that this definition of $\mathbb{F}_r$ differs slightly from the definition of $\mathbb{F}_o^*$ used previously.) As $\mathbb{F}_r$ decreases, buoyancy effects can be expected to increasingly dominate. As W goes down the surface interaction should decrease as low pressure affects the jet path less. Experiments established critical sets of $\mathbb{F}_r$ and W values where the flow pattern switched between jet-surface attachment (30-40% recirculation) and no jet attachment (0% recirculation). A hysteresis effect was also observed analogous to those found in other Coanda effect experiments. For a given value of W, it took a higher value of $\mathbb{F}_r$ to obtain attachment than the value needed to get an attached jet to fall away (detach) from the surface. The presence of an intake flow increased surface interaction and hence lowered the critical $\mathbb{F}_r$ values (for a given W). Figure 5 presents the experimentally determined critical value of $\mathbb{F}_r$ and W. Figure 6 shows jet centerlines (obtained from photographs) for a series of tests with an intake flow and the same value of W.

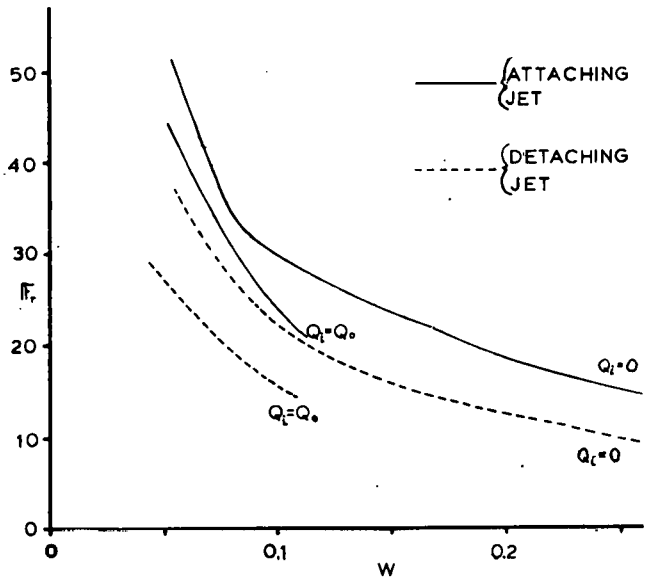

Figure 6 Critical Values of $\mathbb{F}$ and W as Determined by Experiments

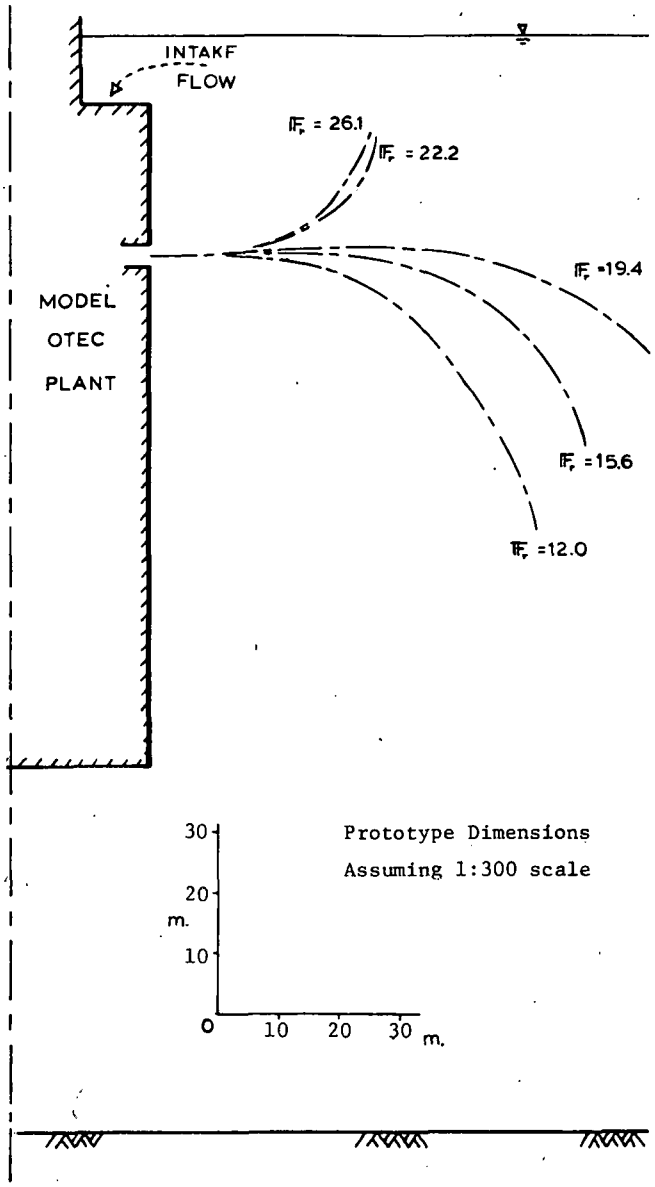

Figure 7 Experimental Discharge Jet Centerline Trajectories W = .105

In the second series of tests, two jets were discharged horizontally at different vertical levels. They were closer to each other than either was to the water surface or basin floor. The upper jet was positively buoyant and the lower jet was negatively buoyant. Both had the same port characteristics and value of

$$IF_r = \frac{u_o}{\sqrt{g \frac{|\Delta\rho_o|}{\rho_a} h_o}}$$

Also, there was no intake. For the case of no jet-jet attachment the flow field was symmetrical about a horizontal plane placed midway between the jets. The observed behavior was exactly similar to the jet-surface interaction experiments (with no intake flow) with the plane of symmetry replacing the surface boundary. Therefore the analogous dimensionless port width is

$$W' = \frac{2h_o}{h_{sep}}$$

where h_{sep} is the separation distance between evaporator and condenser water discharge. For a given value of W', the jets merged when IF_r for both jets reached a critical number. Just as with recirculation in the surface interaction experiments, either the merger was complete or did not occur at all. The experimental data for these experiments is still being reduced.

Tests in a Current

To date approximately twenty tests have been performed. Recirculation results are presented herein for one set of tests involving a 400 MWe plant with a horizontal, non-mixed (evaporator), radial discharge at a depth of h_d = 77 m into a stratified ambient with a mixed layer depth of H = 54 m. Current speeds of .15, .28, .40, .51 .87 and 1.00 m/s were tested to complement a corresponding test in stagnant water. Photographic tracings in Figure 5 show vertical plume crossections for runs with current speeds of .15 m/s (indicating little or no recirculation) and .51 m/s (indicating partial recirculation). Percentage dye recirculation (direct recirculation) for all the current speeds is plotted in Figure 8, which indicates that maximum recirculation occurs at intermediate current speeds. This confirms observations made by Sundaram et al. (1977, 1978) under more idealistic conditions. The maximum percentage recirculation for these tests is approximately 6-7% suggesting that, even under recirculating conditions, much of the intake flow is still being drawn from fresh ambient water. This situation is contrasted to that of the stagnant water tests in which the direct recirculation percentage was either zero (all intake flow being drawn from fresh ambient water) or in the neighborhood of 30-40% (about one third of the intake flow being drawn directly from the discharge flow with

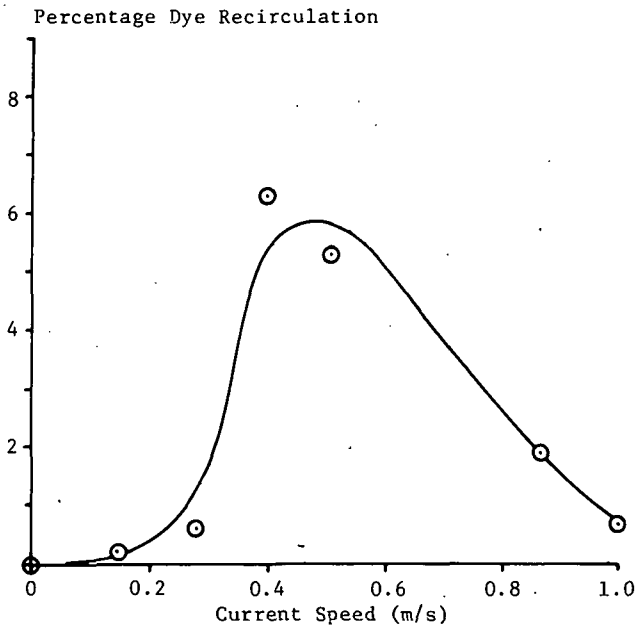

Figure 8 Recirculation Percentage as a Function of Ambient Current Speed for a 400 MWe Plant with Horizontal Radial Evaporator Discharge

most of the remainder being drawn from the near field plume).

Summary

This paper has described an ongoing experimental program to investigate the detailed external fluid mechanics associated with OTEC Plants. Results have been discussed for tests performed in stratified, stagnant, ambient receiving water and for special tests which investigate jet-boundary interaction. Further detail concerning these tests is available in Adams, et al. (1978). Together with tests presently being performed in stratified, flowing, ambient receiving water, these tests should provide valuable data concerning potential recirculation and near field plume transport for a range of both OTEC plant designs and ambient conditions.

Acknowledgement

This work is being performed under the sponsorship of the U.S. DOE, Division of Solar Technology, under contract No. ET-78-S-02-4683.

References

Adams, E., D. Fry, D. Coxe, and D. Harleman, "Research on the External Fluid Mechanics of Ocean Thermal Power Plants," Interim Report Covering Experiments in Stagnant Water, R.M. Parsons Laboratory for Water Resources and Hydrodynamics, Report COO-4683-1, October 1978.

Fry, D., G. Jirka, and E. Adams, "Evaluation of Mixing and Recirculation in Generic OTEC Discharge Designs," paper presented at Vth OTEC Conference, Feb. 1978.

Jirka, G.H., R.P. Johnson, D.J. Fry, and D.R.F. Harleman, "Ocean Thermal Energy Conversion Plants: Experimental and Analytical Study of Mixing and Recirculation," R.M. Parsons Laboratory for Water Resources and Hydrodynamics Technical Report No. 231, prepared for Div. of Solar Energy, U.S. ERDA under Contract No. EY-76-S-02-2909.M001.

Miller, Arthur R., "Ranges and Extremes of the Natural Environment Related to Design Criteria for Ocean Thermal Energy Conversion Plants," Woods Hole Oceanographic Institution, Oct. 1977.

Sundaram, T.R., S.K. Kapur, A.M. Sinnarwalla, and E. Sambuco, "The External Flow Field Associated with the Operation of an Ocean Thermal Power Plant," Hydronautics, Inc., Report No. COO-2348-1, December 1977.

Sundaram, T.R., S.K. Kapur, and A.M. Sinnarwalla, "Some Further Experimental Results on the External Flow Field of an OTEC Power Plant," April 1978.

ENVIRONMENTAL IMPACT ASSESSMENT FOR OTEC-1

Linda Sinay-Friedman

TRW Defense and Space Systems
One Space Park Drive
Redondo Beach, California 90278

John Reitzel

1694 Main Street
Concord, Massachusetts 01742

Abstract

Operation of a one megawatt electric (MW_e) set of OTEC heat exchangers aboard the OTEC-1 Early Ocean Test Platform, approximately 39 kilometers (km) northwest of Kawaihae, Hawaii, will begin in April 1980 and continue for three and one-half years. In accordance with the National Environmental Policy Act (NEPA) of 1969, governmental activities must consider environmental impacts resulting from the project by preparing an Environmental Impact Assessment (EIA). This paper presents the latest results of the OTEC-1 Environmental Impact Assessment Study.[1] This Study serves as a supplement to an earlier DOE-sponsored generic EIA for OTEC-1.[2]

The key environmental issues considered applicable to OTEC-1 which were assessed during the study relate to: (1) organism entrainment; (2) organism impingement; (3) ocean water mixing; (4) platform attraction; (5) chlorine releases; (6) ammonia leakage to the sea; (7) oil spills; (8) atmospheric pollution; (9) endangered species; and (10) socioeconomics.

Major concerns have focused on the biological impacts. The OTEC-1 tests involve no electrical power generation, and negligible extraction of heat from the ocean. Nearfield effects of OTEC-1 will be localized and negligible in view of the broad distribution of pelagic organisms. Farfield effects could reach nearshore populations whose habitats may be more restricted, although this is not expected.

Introduction

The OTEC-1 project will be conducted by a team of contractors, under the auspices of DOE. Their functions are listed below.

Firm Name	Function
Global Marine Development Inc. (GMDI) and TRW Defense and Space Systems	Systems Integration Contractor
Energy Technology Engineering Center	Test Director Contractor
TRW Defense and Space Systems	Test Article Contractor

The Systems Integration Contractor will design, convert and operate the OTEC-1 platform; the Test Director Contractor will provide guidance for conducting the field test; and the Test Article Contractor will provide a set of 1 MW_e heat exchangers to be tested on the platform.

Conversion of the OTEC-1 vessel, a T2 Tanker (the USNS CHEPACHET) is currently being performed at Northwest Marine Shipyard, Portland, Oregon.

The primary purpose of OTEC-1 is to operate and test an OTEC module at sea, without generating electricity, to:

- assess developing heat exchanger technology
- evaluate biofouling, corrosion, and biofouling control techniques
- determine potential environmental impacts

OTEC-1 will be the world's first field test of a closed-cycle OTEC system of this size, and the technical results of the experiment will substantially further OTEC research and development.

Project Description

The OTEC-1 vessel is shown in Figure 1 below.

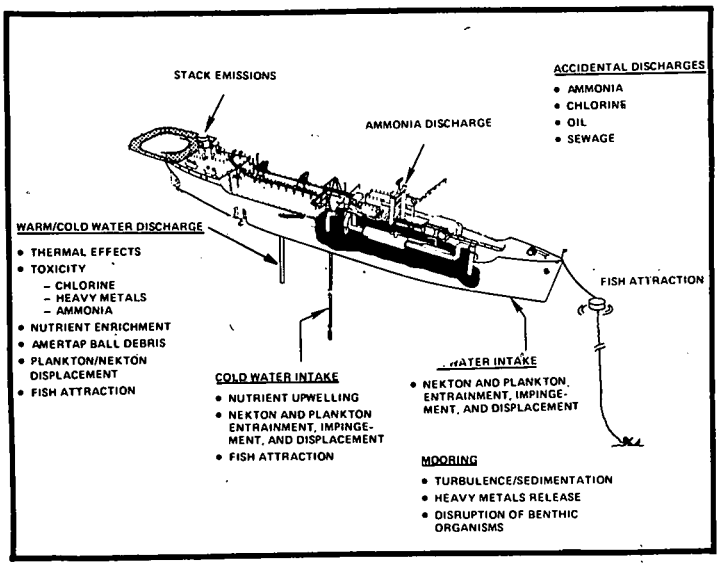

Fig. 1 OTEC-1 Vessel.

The OTEC-1 vessel will be a single-point moored platform that supports a 640 meter (m) cold water intake pipe capable of intaking 4°C water at a rate of 4.3 cubic meters per second (m^3/sec). The cold water pipe will be a symmetrical arrangement of three 1.2 m-diameter extruded polyethylene pipes, strung together and weighted at the bottom. Warm water at 26°C will be pumped through an intake located at the bow of the vessel at a rate of 5.4 m^3/sec. Both intakes and other key points in the system will have self-cleaning gridded screens designed to prevent large marine organisms from being ingested into the OTEC-1 system. A solid velocity cap will cover the bottom of the warm water screen to eliminate vertical current flows and the potential for organism ingestion into the warm water intake. Intake water is to be supplied mainly by ambient horizontal currents. OTEC-1 is not expected to change conditions appreciably at the intake depths, since the overall effect is the physical removal of water at that depth.

The warm and cold water will be mixed prior to being discharged to the ocean at a rate of 9.7 m^3/sec and a temperature of about 16°C. The depth of discharge can be varied from 10 to 70 m. Part of the OTEC-1 test involves evaluating environmental effects of discharging to different depths.

Ammonia is the working fluid selected for use in the OTEC-1 field test. Large quantities of ammonia (up to 16 metric tons) will be stored onboard the OTEC-1 vessel. Although the OTEC-1 system is a closed-loop, some ammonia will be lost to the atmosphere. Waste ammonia will be separated into volatile products and discharged during normal operations via a discharge stack at an average concentration of over 500 parts per million (ppm). Periodic start-up and subsequent maintenance of the ammonia system will require purging with nitrogen and the subsequent release of both ammonia and nitrogen to the atmosphere. During a total ammonia purge, expected to be of one to two hours duration, up to 1200 kilograms of ammonia may be released.

To control micro- and macrofouling on the seawater side of the heat exchanger, both chemical and mechanical methods will be employed. Between 40 and 840 kilograms of free chlorine per day will be generated onboard the vessel for injection into the seawater streams at a continuous baseline concentration of 0.05 ppm and a maximum concentration of 1.0 ppm (three times per day at 15 minutes per injection).

The mechanical cleaning system is designed to remove biofouling by circulating balls through the titanium and steel heat exchanger tubes. The balls are natural biodegradeable sponge rubber, 2.6 centimeters in diameter. Abrasive silicon-carbide-coated balls can be used if severe fouling or mineral encrustation is encountered.

Two research facilities will be integrated aboard the vessel. These are a Control Van and a Biofouling and Corrosion Van, both used in conducting the OTEC-1 scientific and engineering tests. An on-site monitoring plan is being designed to comply with governmental regulations and permits, as well as to evaluate the environmental impacts.

The monitoring plan consists of three profiling and sampling systems, primarily designed to track the discharge plume. The first is an oceanographic buoy containing a string of instruments, moored at a distance from the OTEC-1 vessel to obtain unperturbed environmental data. The second consists of an onboard meteorological station and a moveable profiling and sampling system designed to detect the nearfield plume. Last is an instrumented work boat, located downstream of the vessel to study farfield effects.

Site Description

The OTEC-1 mooring site, as shown in Figure 2, is located off the western coast of the Island of Hawaii, approximately 27 km northwest of Keahole Point and 39 km west of Kawaihae, on the mid to outer continental shelf at 19° 56'N and 156° 10'W. For the purposes of the environmental assessment study, the OTEC-1 site was considered a tropical pelagic site bordering on the large open water masses of the Central Pacific. This site classification is based on its distance from the shoreline and the depth of the water column (approximately 1150 m).

Land-based facilities are planned for the deep water port town of Kawaihae. To evaluate potential impacts resulting from the OTEC-1 project, an onshore study area, extending along a 36-mile-long narrow coastal band from Kawaihae in the north to Kailua-Kona in the south (see Figure 2) was established. The eastern boundary of the zone was set far enough inland to include nearby facilities and connecting transportation routes.

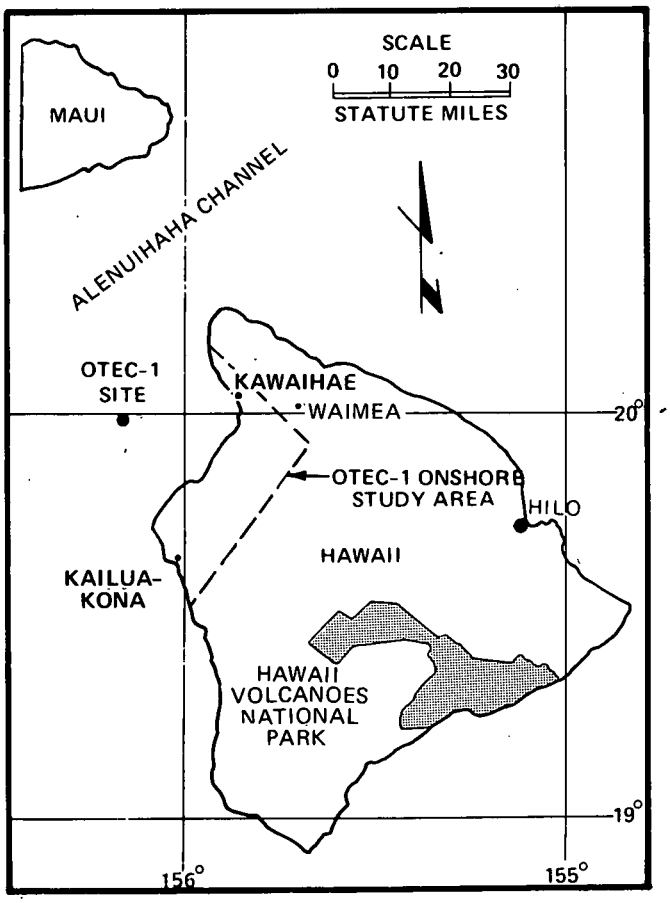

Fig. 2 Location of OTEC-1.

Environmental Impacts

An assessment of the potential environmental impacts resulting from the OTEC-1 field test was performed for the issues identified below and shown in Figure 1.

- organism entrainment
- organism impingement
- ocean water mixing
- platform attraction
- chlorine releases
- ammonia leakage to the sea
- oil spills
- atmospheric pollution
- endangered species
- socioeconomics

(Only critical issues are discussed in this paper due to space constraints.)

Approach

The potential impact of OTEC-1 on any pelagic population can be put in perspective by comparing the size of the region in which farfield effects from OTEC-1 may be perceptible to that population (referred to as the reference parcel) with the size of the habitat of that population. The impacts on nearshore populations will depend on the extent to which farfield effects overlap nearshore habitats. For the OTEC-1 study, the reference parcel was chosen to represent the largest region affected in the long-term by each intake or discharge, so as to focus more sharply on the effects on populations at specific depths and to assess the possible farfield effects of OTEC-1 on coastal (nearshore) populations.

To estimate the range of farfield effects from OTEC-1, dilution ratios for the discharge and ingestion probabilities for the intakes, were calculated as limiting steady-state solutions of the diffusion equation with time-dependent diffusivity, $K=\frac{1}{2}vt$ (see Reference 1, Appendix L). Figure 3 shows a pear-shaped plume defined by the surface on which the dilution ratio/ingestion probabilities have a chosen value. The stem of the plume is centered at the bottom of the intake or discharge pipe. The dilution ratio plume extends downstream from the discharge, while the ingestion probability plumes extend upstream from the intakes and represent the regions from which intake water is drawn. The plume for each intake and discharge has a length (L), width (W) and depth (D) as shown on Figure 3. Table 1 presents numerical values for the length, half-width and half-depth of plume defined by the surfaces on which dilution ratio or ingestion probabil-

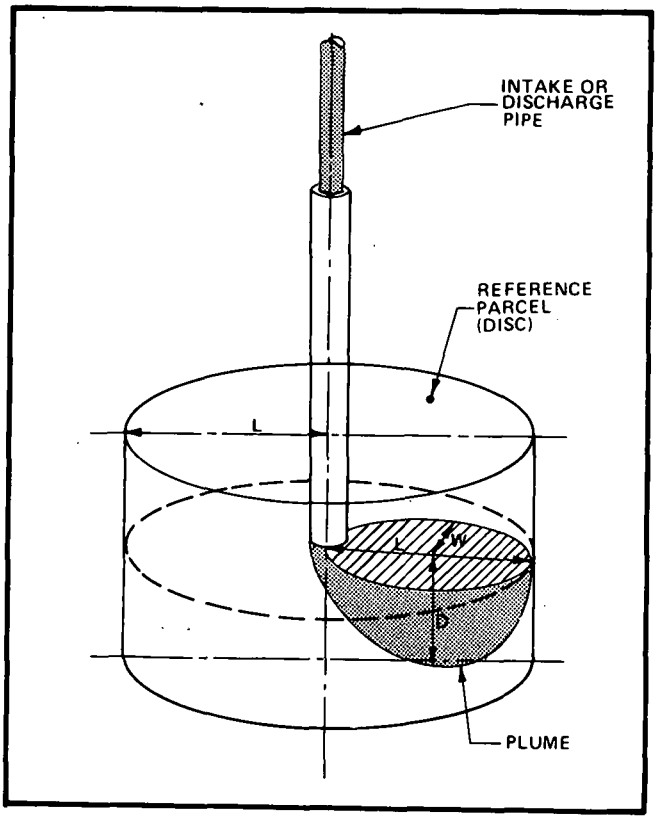

Figure 3 Bottom Half of the Pear-Shaped Plume and the Disc-Shaped Reference Parcel.

Table 1 Plume Dimensions for Intakes and Discharge.

AMBIENT CURRENT VELOCITY (cm/sec)	ρ/ρ_0 = INGESTION PROBABILITY OR DILUTION RATIO								
	0.01			0.001			0.0001		
	Half Length (Radius) (km)	Half Width (m)	Half Depth (m)	Half Length (Radius) (km)	Half Width (m)	Half Depth (m)	Half Length (Radius) (km)	Half Width (m)	Half Depth (m)
COLD WATER INTAKE (Q = 5 m^3/sec, v_h = 1 cm/sec, v_z = 0.1 cm/sec)*									
10	1.3	75	8	4.0	240	25	13	750	80
20	1.8	55	6	5.6	170	20	18	550	60
30	2.2	45	5	6.9	140	15	22	450	50
WARM WATER INTAKE (Q = 5 m^3/sec, v_h = 1 cm/sec, v_z = 0.1 cm/sec)									
10	1.8	110	11	5.6	340	35	18	1100	110
20	2.5	75	8	8.0	240	25	25	750	75
30	3.1	65	6	9.8	200	20	31	650	65
MIXED DISCHARGE (PLUME) (Q = 10 m^3/sec, v_h = 1 cm/sec, v_z = 0.01 cm/sec)									
10	5.6	340	3.5	18	1100	11	56	3500	35
20	8.0	240	2.5	25	750	8	80	2500	25
30	9.8	200	2	31	650	6	98	2000	20

*Q = Volume flow of intake/discharge.
v_h = Horizontal dispersion velocity.
v_z = Vertical dispersion velocity.

ities have values of 0.01, 0.001 and 0.0001. These are calculated for representative current velocities of 10, 20 and 30 cm/sec.

The disc-shaped region swept by any plume as the current swings through all possible current directions is defined as the reference parcel for that plume as shown on Figure 3. This is a conservative estimate of the largest region in which given values of dilution ratio or ingestion probability ever occurs. The reference parcels for the warm water and cold water intakes and for the discharge are shown in Figure 4. The entrainment intake in this figure represents the ambient water that is entrained in the nearfield of the discharge.

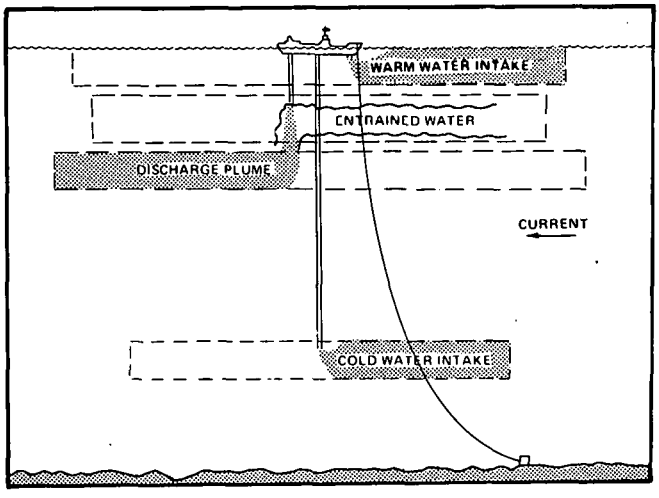

Fig. 4 Regions Affected by Intakes and Discharges

Ingestion

Organisms ingestion (entrained) through the OTEC-1 cold and warm water intakes will be subjected to physical, chemical and thermal stresses, including pressure changes, shear forces and exposure to potentially toxic chemicals and heating and cooling water. Organisms in the water entrained near the discharge will also be subject to displacement in addition to comparable thermal and chemical stresses. For the study, a maximum 100 percent mortality rate was assumed for organisms ingested into the OTEC-1 system and entrained into the discharge. To put into perspective the significance of ingestion to planktonic populations, the daily losses by ingestion from an OTEC-1 intake were compared to the daily losses due to natural causes within the reference parcel surrounding the intake.

Warm Water Intake and Entrainment Intake. The warm water intake and the entrainment intake both affect planktonic populations of the uppermost 100 m and are considered together here. The following table shows estimates of the fractional increase over the natural mortality rates [3,4] within a 2 km^3 reference parcel, extending from the surface to 100 m. The fractional increase is produced by ingestion from the combined OTEC-1 warm water and entrainment intakes, at an entrainment intake rate of about 40 m^3/sec.

CATEGORY	FRACTIONAL INCREASE IN MORTALITY RATE WITHIN REGION OF IMPACT (%)
Phytoplankton	4
Microzooplankton	2
Macrozooplankton	10
Micronekton	10

As can be seen, the anticipated maximum increase in mortality from ingestion of OTEC-1 is 40 percent for phytoplankton populations at the 100 m level in the reference parcel. Under typical conditions (current velocity of 20 cm/sec), the largest region or disc affected by the two intakes is estimated to be 2 km^3, with its entirety located more than 10 km from shore in water depths exceeding 1000 m (see Table 1).

The habitat of most pelagic organisms is on the order of 10^6 km^3. Therefore, by comparison, these intakes will affect a negligible portion of the habitat of any pelagic plankton species. Additionally, effects of the intakes will not extend to nearshore species, which prefer the proximity of an ocean bottom, since the habitat of nearshore species is within 10 km from shore.

Cold Water Intake. Since phytoplankton and microzooplankton are limited in vertical distribution to the upper 200 m of the water column, only macrozooplankton and micronekton will be ingested by the cold water intake. The reference parcel defined by the cold water intake under conditions of 1 percent ingestion probability and a typical current velocity of 10 cm/sec (see table 1) is only a small (approximately 0.1 km^3) fraction of the total habitat (i.e. over 10^6 km^3) of the species. Thus, ingestion mortality is expected to have only negligible effects on overall populations, since the reference disc is small, deep, and far from shore.

Impingement

Impingement in OTEC-1 will take place in two stages for both the warm and cold water intakes: (1) against the coarse screens protecting the intakes and (2) against the fine screens in the wells upstream from the pumps. Impingement should be reduced by a screened velocity cap over the warm water intake designed to induce a horizontal rather than a vertical current into the intake, since most nekton are better adapted to sensing and avoiding horizontal currents. The velocity cap would also decrease the current flow at the intake, thus reducing the probability of impingement of weakly swimming organisms such as jellyfish. It is possible that organisms small enough to pass through the first stage (larger mesh) screens may be impinged on the finer second stage screens in the pump wells. Periodical removal of the biomass will be necessary to keep these screens clean.

Ocean Water Mixing

Intake water will be supplied primarily by ambient horizontal currents. The 16°C discharged water will be a mixture of warm water pumped from the surface and cold water pumped from 640 m. Since the intake water will be returned to the ocean at a different depth, the net effect of each intake will be to remove water without changing

conditions appreciably at the intake depth. The discharge will entrain and mix with an unknown amount of ambient water, and the combined plume will sink to a depth between 80 and 150 m, depending on the ambient density profile and the amount of water entrained. The amount of initial entrainment will have a strong effect on the sinking rate and the subsequent entrainment of ambient waters in the plume. Entrainment and sinking of ambient water will act like another intake, moving water from one depth range to another.

At the depth where the average density of the discharged and entrained water is the same as the ambient density, the plume will stop sinking and will be transported downstream by the ambient current. If there is a significant density gradient at this depth, the plume will be squeezed by residual buoyancy forces and spread horizontally into an increasingly thin layer. Thus, the farfield plume will disperse in a region characterized by a small vertical dispersion and will be effectively isolated from the mixed layer.

Upon initial release, the physical, chemical and biological characteristics of the mixed discharge will vary from the ambient. However, at the stabilization depth, the temperature and salinity in the plume will be close to ambient values, although the concentrations of chemical constituents and the amount of detritus and nutrients may differ noticeably.

The strength and spatial extent of these differences is ultimately determined by dispersion parameters of the ocean that describe the speed with which the plume is mixed with ambient waters.

Nutrient Redistribution. The artificial upwelling of plant nutrients (nitrate, phosphate and silicate) in the discharged water may locally enhance the growth of phytoplankton. The upper limit of eutrophication can be estimated by nitrate concentrations, which appear to be a limiting factor in primary phytoplankton growth in open ocean waters. During the OTEC-1 study, it was estimated that the discharge will have a concentration of about 15 μgm-atoms/ℓ^5, which will be diluted by a factor of 100 by dispersion at the plume limits. At the OTEC-1 site, only trace amounts of nitrate in the waters above 150 m have been measured. Thus, the overall effect from nutrient redistribution will be a small local increase in the growth of phytoplankton.

Detrital Food. Dead plankton and nekton in the discharged water will be food for plankton, nekton and heterotrophic bacteria. This detritus, which represents a small biological oxygen demand, is negligible in comparison to the oxygen concentration of the discharged water and is not expected to appreciably deoxygenate the ambient water.

Carbonate Equilibrium. Changes in CO_2 saturation might lead to its release at the surface from artificially upwelling deep water from OTEC-1. CO_2 could evolve in the mixed discharge and rise to the surface if receiving waters are saturated with CO_2. The impact from the change in CO_2 saturation from OTEC-1 is anticipated to be insignificant.

Thermal Effects. Out to a few hundred meters horizontally from the OTEC-1 discharge, the mix of discharged and entrained water could vary as much as 0.3°C to 0.4°C from the ambient. Information about thermal effects on marine organisms in the vicinity of the discharge is limited mainly to thermal shock data from power plant discharges. Observations of thermal shock effects reveal that an abrupt cold thermal change does less harm to an organism's metabolism than an abrupt warm change. Also, the survival rate and time for recovery from cold shock is more favorable than for a warm shock. More detailed data will be available upon completion of the OTEC-1 test.

Chlorine Release

Chlorine toxicity to marine organisms is based on a temperature-time-dosage relationship. In general, the lower the temperature, the shorter the time of exposure and/or the lower the dosage, the less likely a toxic reaction will occur.

During the study, the region possibly affected by chlorine release from the OTEC-1 discharge was estimated to be small in comparison to the habitats of pelagic organisms, and removed from any nearshore habitat. The extent of any possible toxic effect is a plume with a volume of 0.04 km^3, defined by a length of 8 km, width of 500 m, and depth of 10 m, estimated from Table 1 for a discharge plume with ambient current velocity of 20 cm/sec. It is at the boundary of this plume that the concentration of residual chlorine will be diluted by a factor of 100, to levels that are marginally toxic, depending on the species. Any organism entrained in this plume near the discharge will remain in the affected region for about 10 hours, exposed to a chlorine concentration dropping from 0.05 ppm (baseline injection) to 0.0005 ppm. Use of the 1.0 ppm dosage may increase potential toxicity.

A more significant long-term impact is the possible formation of long-lived chlorinated organics which have a tendency to bioaccumulate. Chlorine could react with ammonia to form toxic, persistent chloramines. Surface waters at the OTEC-1 site contain small concentrations of ammonia, which should reduce the potential amount of chloramines. Ammonia leakage from OTEC-1 to the seawater system will tend to increase chloramine formation.

Conculsion

In general, major concerns about the OTEC-1 project have focused on biological impacts. The overall findings of the environmental assessment study are that the nearfield biological effects of OTEC-1 will be localized within a few hundred meters of the vessel. Compared to the overall distribution of pelagic organisms, whose habitats and populations are large and widespread, impacts will be negligible. Farfield effects on nearshore populations, whose habitats may be more restricted, will be insignificant. The significance of these impacts will be further determined by on-site environmental monitoring of the OTEC-1 project.

References

1. Sinay-Friedman, L. 1979. SUPPLEMENT TO THE DRAFT ENVIRONMENTAL IMPACT ASSESSMENT, OCEAN THERMAL ENERGY CONVERSION (OTEC) PREOPERATIONAL OCEAN TEST PLATFORM. Prepared by TRW, Redondo Beach for the United States Department of Energy.

2. Sands, M. D., et. al, 1978. DRAFT ENVIRONMENTAL IMPACT ASSESSMENT OCEAN THERMAL ENERGY CONVERSION (OTEC) PREOPERATIONAL TEST PLATFORM. Prepared by Interstate Electronics Corp. for the United States Department of Energy.

3. Beers, J. R., Reid, F. M. H., and Steward, G. L. 1977. MICROPLANKTON IN THE CENTRAL GYRE OF THE NORTH PACIFIC OCEAN: PART II, POPULATION STRUCTURE AND ABUNDANCE. Institute of Marine Resources, Reference 77-1.

4. Eppley, R. W., Ranger, E. H., Venrich, E. L., Mullin, M. M. 1973. A STUDY OF PLANKTON DYNAMICS AND NUTRIENT CYCLING IN THE CENTRAL GYRE-OF THE NORTH PACIFIC OCEAN. *Liminology Oceanography*, 18: 534-551.

5. Lawrence Berkeley Laboratory and University of Hawaii. UNPUBLISHED OCEANOGRAPHIC DATA FROM HOTEC-1 CRUISE, October-November 1978.

DISCUSSION

A. Thorhaug, FIU: Why did you exclude artificial reef effects in your OTEC-1 EIA?

L. Sinay-Friedman: Let me rephrase your question please: You are referring to whether we considered the artificial attraction of the ship itself. We did not disregard it. Our report was a supplement to a previous study that included a lengthy section on the artificial reef effects of the OTEC platform. In the two reports there is quite a bit of information on the attraction of fish to an OTEC ship. Many papers have been written on the artificial reef effects of a platform, and there are references to it in our report. I simply did not mention them today, other than to say that we will attract fish. Our study was geared to cover areas that were not discussed in the first report.

MODELING THE INTERMEDIATE FIELD OF OCEAN THERMAL ENERGY CONVERSION PLANT DISCHARGES

Gerhard H. Jirka*, Janet M. Jones+ and Frank E. Sargent+

School of Civil and Environmental Engineering
Cornell University
Ithaca, New York 14853

Abstract

The intermediate field of an Ocean Thermal Energy Conversion (OTEC) plant is defined as that region in the surrounding stratified ocean where the plant effluents are distributed through the interaction of buoyancy-driven currents and the ambient ocean current. The intermediate field determines the area over which physical, chemical and biological disturbances from the plant can be felt and measured. The governing equations of the intermediate field motion are derived, and first-order solutions are given. The results, including some experimental verification, document the significant horizontal (order 10km) and vertical extents (order 10m) of the intermediate field layer. The results provide guidelines for the siting of multiple OTEC plants, as plants should be spaced sufficiently apart to prevent intermediate field interaction. Also, the intermediate field causes additional hydrodynamic drag effects which should be considered in the mooring design.

Introduction

Ocean Thermal Energy Conversion (OTEC) plants will produce physical, chemical and biological perturbations in the ambient ocean. The analysis and prediction of these changes is best performed by considering different areas (scales) of impact, from near-field (order 1km) over intermediate field (10km) to far field (100km) and, beyond that, ocean basin wide (1000km) scales. This breakdown by scales is convenient in terms of the physical processes, and their mathematical treatment, which need to be considered and is a practical necessity given the current state-of-the-art of modeling of oceanic processes. A more extensive framework for OTEC environmental impact analysis, including a discussion of important physical processes within each scale, has been given by Allender et al (1a).

This paper deals with the modeling of the intermediate field perturbations produced by OTEC plants. In the intermediate field the OTEC effluent forms an internal layer (or layers) within the ambient stratified ocean. The motion within the layer is predominantly horizontal as determined by the interaction of buoyant forces and of drag effects due to the ambient ocean current.

The analysis of the size, shape and motions of the intermediate field is important for several reasons. First, and from an environmental viewpoint, it determines the horizontal (lateral, up-current and down-current) range of influence of an OTEC plant. This will be the zone over which the primary physical, chemical and biological disturbances of the plant will be felt, and will, in fact, be large enough to be measurable. The typical size (horizontal extent) of the zone is of the order of 10km with a residence time of the order of a few days. For example, depending on phytoplankton kinetics and photic conditions, it seems that this zone could be an area in which significant biostimulation due to the artificial upwelling of nutrient laden deep ocean water would occur. By the same token, the effects of OTEC discharged chemicals (as biocides or for corrosion control) would have an impact over the same region. Thus, for environmental impact determinations (excepting climatic impacts) the intermediate field may indeed be the most crucial and most interesting zone. In contrast, the residence time in the near-field is usually so short that no significant biochemical reactions can take place, while the additional long term advection and mixing processes in the far-field (and beyond) will limit the practical detectability of environmental perturbations. Obviously, these considerations become even more important if multiple OTEC plants (arranged in a grid like pattern) are considered.

The second reason concerns the thermal resource effects of one OTEC plant on another (and possibly as a feedback on itself). While initial near field studies (1a,2) have demonstrated that moderately sized single OTEC plants (say less than 200 MWe) in typical subtropical ocean conditions can be operated without significant recirculation, this may not be the case if several OTEC plants interact with each other. Hence, one plant can alter the thermal and density profile at another site sufficiently strongly to cause a decrease in thermal resource recovery. Thus, the analysis of the intermediate field motions must be an integral part of siting studies for multiple OTEC arrangements.

Another effect has to do with the additional drag effect due to the pressure disturbances caused by the interactions of the ambient ocean flow with the OTEC effluent flow in the near-field. These pressure disturbances lead to a loss of momentum in the ambient flow which ultimately must be balanced as an increased force, on top of the direct drag of the flow around the plant, on the mooring of OTEC plants.

Analysis

A definition diagram for the intermediate field motion (Fig. 1) shows a fluid layer of thickness $h(x,y)$ and width $b(x)$, where $b >> h$, sandwiched within the structure of the ambient stratified ocean which has a current velocity u_a. Two simple types of ambient stratification are considered in the analysis (Fig. 1): Case A: A step-wise stratification simulating a two-layer ocean with effluent discharge at the discontinuity. Case B: A linearly varying stratification with the effluent discharge

*Assistant Professor
+Research Assistant

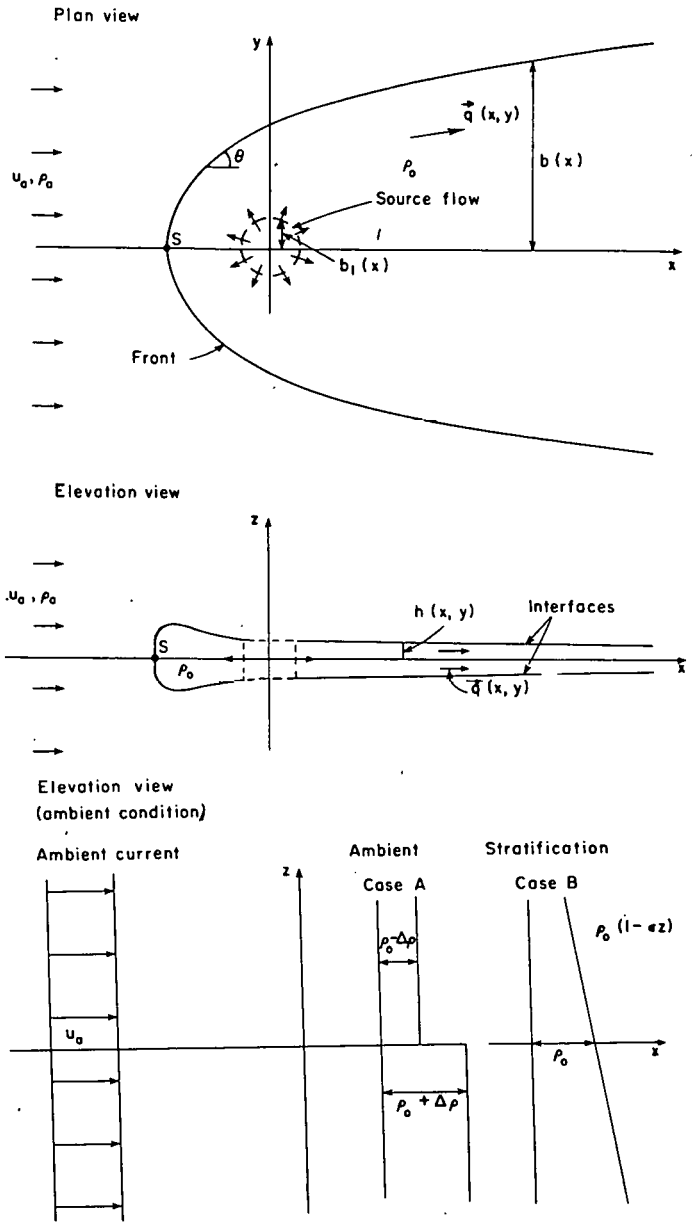

Fig. 1 Definition diagram for analysis of OTEC intermediate field motion.

occurring at the equilibrium level (equal density level). Case B is much more representative for conditions in the thermocline (or pycnocline) of the real ocean. Case A, however, is conveniently simulated in the laboratory, thereby providing a validation of the analytical predictions.

Coupling to the near-field

As indicated in Fig. 1, the near-field flow provides a source boundary condition for the intermediate field. Several possibilities exist here as the behavior in the near-field is closely linked to the design of the OTEC plant, (1b,2), notably its discharge ports. For mixed (evaporator and condenser) discharges, with release level at the thermocline, the near-field zone will remain horizontal and will have a smooth transition to the intermediate field. This was the case considered by Jirka et al, (1b,2) who determined the amount of near-field mixing (dilution factor S) and its geometric extent (radius). For example, for typical 100 MWe designs, S would be of the order of 5 to 10 and the near-field radius from 0.5km to 1km. An entirely different situation would hold for separate discharge designs. In this case, the near-field plumes coming from the evaporator and condenser discharges, respectively, could follow separate (rising or sinking) paths until their equilibrium level is found. Turbulent entrainment along the trajectory of the plumes causes dilution (2,3). At the equilibrium level the density inside the plume is equal to the ambient density and the horizontal intermediate field spreading motion commences. Thus, in principle, there can be one, two or more intermediate field spreading zones within the ambient ocean. The analysis would apply to any of them and the source boundary conditions are given by the amount of flow (initial discharge flow times dilution) which is arriving at the equilibrium level.

Governing equations

Several assumptions are made in the analysis of the intermediate field density current motion. Most of these assumptions can be justified by a formal scaling analysis. 1) Hydrostatic Conditions. The density current is shallow ($h/b \ll 1$) and is well submerged below the surface of the ocean. Thus, the pressure in both ambient flow and density current flow can be taken as hydrostatic everywhere, except for a narrow zone along the front of the density current in which significant local vertical accelerations take place in the ambient flow. This pressure deviation results in a form drag F_D normal to the front

$$F_D = C_D \rho_a \frac{(u_a \sin\theta)^2}{2} h_B \qquad (1)$$

where u_a = ambient velocity, θ = local front angle, h_B = thickness along front, ρ_a = ambient density and C_D = drag coefficient (of order 0.5 (5)). This drag force arrests the density current. 2) Stable interface. All turbulent entrainment processes across the interface between effluent flow and ambient flow are assumed to be limited to the near-field. The interface is stable in the intermediate field. This assumption appears reasonable at this time, but may need further study (experiments) for certain regions with strong shear effects (e.g. upstream intrusions in Fig. 1). 3) Negligible vertical diffusion. Diffusion by molecular or turbulent (shear instabilities) processes across the interface is a slow process and therefore negligible in the intermediate field. 4) Inviscid approximation. Both horizontal and vertical shear effects have a negligible effect on the dynamics of the density current. This assumption would become invalid over large distances when vertical interfacial shear would dominate.

Thus, the governing equations are the vertically averaged two-dimensional long-wave equations

$$\nabla \cdot (\vec{q}h) = 0 \qquad (2)$$

$$\vec{q} \cdot \nabla\vec{q} = -\sigma \nabla h^{s+1} \qquad (3)$$

where $\vec{q} = (u,v)$ = internal velocity and σ, s are ambient stratification parameters for the two types of stratification:

Case A: Step-wise stratification

$$\sigma = \frac{\Delta\rho}{\rho} g \ , \ s = 0 \qquad (4)$$

where $\Delta\rho/\rho$ = relative density difference between density current and ambient flow, g = gravitational acceleration.

Case B: Linear stratification

$$\sigma = \frac{1}{2}\,\varepsilon g = \frac{1}{2}\,N^2 \quad , \quad s = 1 \qquad (5)$$

where ε = density gradient, N = Brunt-Vaisala frequency.

Boundary conditions are specified at the horizontal front line, at the source and far downstream.

Front conditions: The front is a streamline

$$v_B = u_B \frac{db}{dx} \quad \text{at } y = b(x) \qquad (6)$$

where (u_B, v_B) is the front velocity. Furthermore, pressure continuity across the front requires that the local drag force F_D, Eq. (1), be balanced by a buoyant force, $\frac{1}{s+1}\rho_o\,\sigma\,h_B^{s+2}$, so that

$$h_B = \left(\frac{s+2}{2\sigma}\,C_D\,u_a^2\,\sin^2\theta\right)^{\frac{1}{s+1}} \quad \text{at } y = b(x) \qquad (7)$$

gives a relation between the boundary angle θ and boundary thickness h_B.

Source conditions: The flow is specified at the source boundary

$$\vec{q} = \vec{q}_i \quad , \quad h = h_i \quad \text{at } y = b_i(x) \qquad (8)$$

such that the total inflow is equal to the flow determined form a near-field analysis.

Downstream condition: At large distances the current will collapse such that

$$\vec{q} \to \vec{u}_a \quad , \; h \to 0 \quad \text{at } x \to \infty \qquad (9)$$

while the total outflow remains finite (equal to the inflow).

Since Eq. (3) describes irrotational flow, it can be replaced by a Bernoulli equation

$$\frac{1}{2}\,q^2 + \sigma\,h^{s+1} = C \qquad (10)$$

where q = speed and the Bernoulli constant C is calculated from the conditions at the stagnation point S (Fig. 1)

$$C = \sigma\,h_S^{s+1} = \frac{s+2}{2}\,C_D\,u_a^2 \qquad (10a)$$

The buoyancy term in Eq. (10) is related to a local critical velocity c (the speed of a small amplitude long wave) by

$$\sigma\,h^{s+1} = \frac{c^2}{s+1} \qquad (11)$$

Use of Eqs. (10) and (11) in the continuity Eq. (2) gives the potential equation

$$(c^2 - \phi_x^2)\phi_{xx} - 2\phi_x\phi_y\phi_{xy} + (c^2 - \phi_y^2)\phi_{yy} = 0 \qquad (12)$$

where $\vec{q} = \nabla\phi$.

Solutions

The above equation system with its boundary condition is, in principle, a well posed one, even though the front matching conditions, Eqs. (6) and (7), will require some iterative approach. However, a formal solution (analytical or numerical) is confounded by the fact that the equation system has mixed type characteristics. This is best seen from Eq. (12) which shows an elliptic type in regions of $q < c$ and a hyperbolic type in regions $q > c$, where $q^2 = \phi_x^2 + \phi_y^2$. Defining a Froude number, $F = q/c$, the first type is commonly referred to as subcritical flow ($F < 1$) and the second as supercritical flow ($F > 1$). The density current clearly includes both such regions and can therefore be called transcritical flow: this is easily seen from Fig. 1 by considering the stagnation point S ($F = 0$) and the downstream condition ($F \to \infty$). The flow may exhibit considerable complexities as regards transitions between these regions which may be in the form of critical lines or shock (hydraulic jump) lines. The mechanics of this flow situation is related to the one for transonic gas dynamics (a review for transonic airfoil flow analysis is given by Nieuwland and Spee (6)).

In the following, the results of two approximative methods are given, also a more detailed numerical solution is outlined. The results are conveniently non-dimensionalized using h_s as the vertical length scale and $Q_o/(2\pi u_a h_s)$ as the horizontal length scale. This non-dimensionalization should give a unique presentation of the density current properties as it includes all relevant parameters: the source flow Q_o, the ambient velocity u_a, and (implicitly through h_s) the ambient stratification s, σ and the drag coefficient C_D.

1. One-dimensional approximation: At sufficiently large distances x downstream from the source (Fig. 1) the initial velocity non-uniformity due to the source condition is damped so that a simple one-dimentional analysis is possible. The density current consists of transverse slabs (of unit length in x) which are advected with the ambient velocity u_a while spreading laterally. Assuming a uniform thickness $h(x,y) = h_B(x)$, Eq. (7) can be used together with a continuity relation $Q_o = 2\,b\,h\,u_a$ and the boundary geometry $db/dx = \tan\theta$. The solution is the normalized boundary width

$$b^* = \pi + \left[\frac{s+3}{2}\,\pi^{\frac{s+1}{2}}\,x^*\right]^{\frac{2}{s+3}} \qquad (13)$$

where b^* and x^* are the normalized horizontal distances. Eq. (13) has been derived originally by Larsen and Sorensen (7) for the special case of step-wise stratification ($s = 0$).

2. Constant thickness approximations: Clearly, Eq. (13) will be invalid in the source vicinity where the lateral dimensions (y) are of equal order as the longitudinal ones (x), so that the one-dimensional approximation breaks down. Recognizing that the flow around the stagnation point S will be largely subcritical, it seems possible to use a

technique which has some features of the Raleigh-Janzen method of compressible gas dynamics. The method starts by first finding a constant thickness (equal to h_s) solution for the density current which meets all boundary conditions and then adjusting the solution to account for the variable collapsing thickness. Details of the method are described elsewhere (8). The results for current width are plotted in Fig. 2 for the two cases of stratification and include Eq. (13) as the asymptotic behavior for large x*.

3. Numerical solutions: The above methods do not provide detailed predictions of the internal velocity field and thickness distribution over the major portion of the intermediate field, notably the upstream intrusion region. Different transition phenomena are likely to occur in this region. Additional calculations are being planned using a modification of the mixed type numerical solution scheme by Jameson and Caughey (9). This model has found efficient application in transonic aerodynamic problems.

Experiments

A series of special experiments is in progress in order to verify the initial approximative theories for the intermediate field and to provide detailed data for the development of the numerical model. The experiments are carried out in a 6.7m x 8.5m x 0.6m Stratified Flow Basin at Cornell University which has a pumping system for ambient current generation. The current experimental set-up simulates the step-wise stratification (Case A) in which the OTEC discharge is a less dense flow which occurs at the free surface of the unstratified current. Thus the free surface can be considered as a symmetry line according to Fig. 1. A similar approach has been used in earlier near-field studies (1b,2). The lighter discharge fluid is a methanol-water mixture. Current speeds of up to 3 m/min with a water depth of about 20 cm can be produced. The discharge density difference $\Delta\rho/\rho$ can be up to 0.02 (10% methanol) at a flow-rate of up to 2 ℓ/s which is obtained from a constant head tank. The discharge device is a radial plexiglass structure and discharge velocities are kept small so that any near-field mixing is minimized.

Photographs of the intermediate field for a typical experiment are shown as Fig. 3. The density current has been marked by a continuous dye discharge. Comparing Fig. 3 with the predictions of Fig. 2 (Case A) shows good qualitative agreement regarding the relative horizontal proportions of the density current. A series of experiments in which all governing parameters are systematically varied will be conducted. Both horizontal and vertical dimensions will be measured. Close-up inspection of the preliminary experiments revealed flow features, such as internal hydraulic jumps, which are not predicted by the approximate theories, but can be simulated in the numerical model.

Intermediate Field for a Typical OTEC Plant

Typical plant design and oceanographic conditions are now assumed in order to demonstrate the magnitude of the intermediate field. A linear stratification, Case B, is assumed here as being well representative of the real ocean. A well established thermocline (0.1°C/m or $\varepsilon = -4 \times 10^{-5}$ m^{-1}) has a Brunt-Vaisala frequency of about $N = 0.02$ s^{-1}. A typical ocean current speed at the thermocline is u_a = 0.1 m/s. A 100 MWe OTEC plant is assumed with a mixed discharge flow of about 1000 m^3/s. Taking an average near-field mixing ratio of 10, this gives Q_o = 5000 m^3/s (half of the flow goes above and half below the symmetry line, see Fig. 1).

With these values the vertical length scale for the intermediate field is (Eq. 10a)

$$h_s = \sqrt{3\, C_D}\, \frac{u_a}{N} \approx 6.2 \text{ m} \qquad (14)$$

with $C_D = 0.5$(5) and the horizontal length scale is

$$\frac{Q_o}{2\pi\, h_s\, u_a} \approx 1300 \text{ m} \qquad (15)$$

Fig. 4 is a plot of the intermediate field density current for these conditions, obtained by multiplying the data of Fig. 2 by the scaling length. Also shown in Fig. 4 are the boundary heights ($2\, h_B$) along the current front. Fig. 4 demonstrates the considerable extent of the intermediate field. The effect of parameter changes is readily seen from Eqs. (14) and (15): smaller velocities u_a or larger

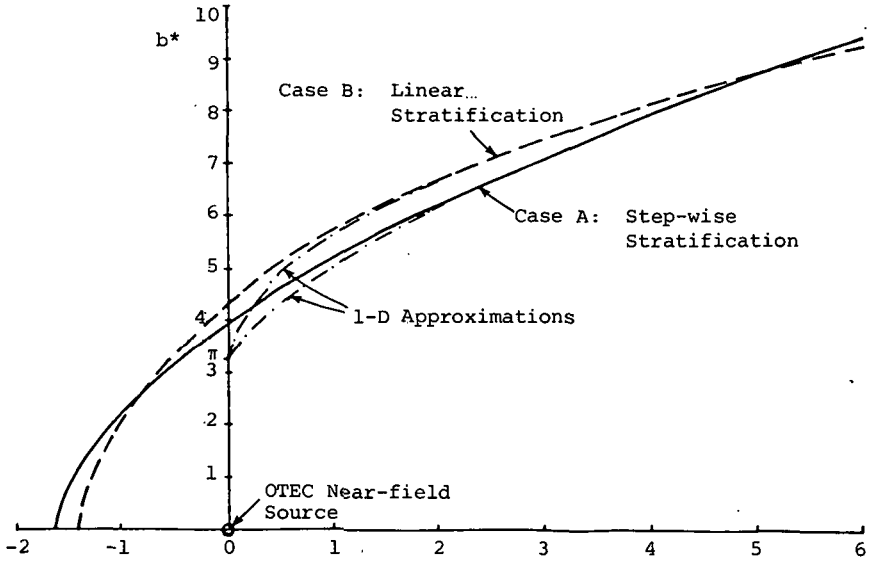

Fig. 2 Non-dimensional plots of plan view of intermediate field shapes. For x* > 2 the one-dimensional approximation is used and for x* < 2 the constant thickness approximation. Ambient current from the left.

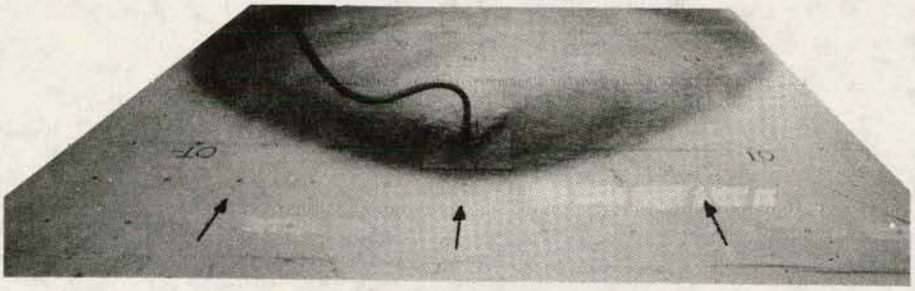

a) Oblique frontal view of density current.

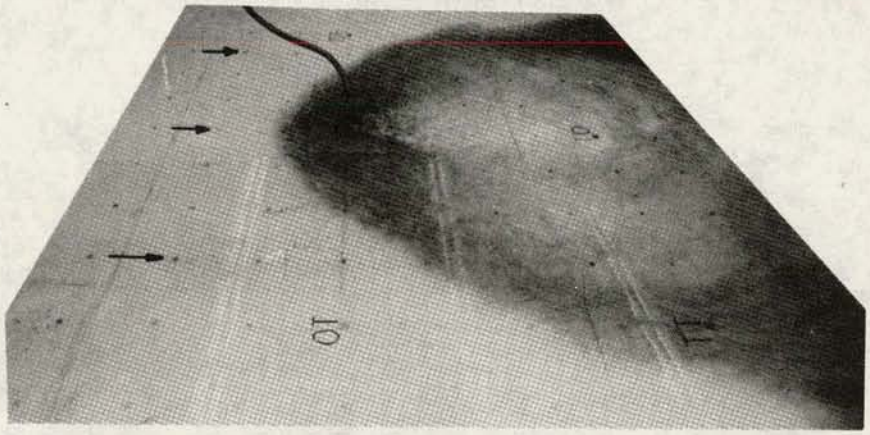

b) Oblique side view of density current.

Fig. 3 Photographs of OTEC intermediate field simulations in the laboratory. Ambient current direction is indicated by arrows. Discharge flow to OTEC model is supplied through flexible hose shown. Grid spacing is 0.5m.

stratification N decreases its thickness, but expands its horizontal extent. Larger discharges (or near-field mixing) Q_o does not affect the thickness but expands the horizontal dimensions.

Siting Consequences

The effect of the intermediate field on the siting of multiple OTEC plants, i.e. the choice of a geometrical arrangement and separation distances, has been discussed in the introductory remarks. Fig. 4 implies two factors: First, within the density current zone the ambient temperature profile will be perturbed; in particular the original linear temperature (density) gradient is replaced by a locally uniform temperature zone. If another plant were located within the density current zone of the first plant, it could experience changes in its thermal resource utlization. Utilization criteria, such as those proposed by Jirka et al. (2) could be used to address this possibility. Second, the density current zone defines the region of bio-chemical activity, as related to nutrient upwelling and/or chemical releases from the plant. Other plants will both be subject to this influence, but also add their incremental effect. The consideration of these effects must be in the form of predictive models which include both the transport terms (on the basis of the intermediate field velocity distribution) and the reaction kinetics.

Effect on Hydrodynamic Plant Drag

The pressure disturbances which are caused in the ambient ocean are reflected as form drag on the plant. The usual direct drag effect due to high Reynolds number flow separation is the subject of several OTEC related studies. However, the drag effect due to ambient flow disturbances in the intermediate field should be considered as an additional force component. Using the approximate one-dimensional theory, Eq. (13), the magnitude of this drag force F_B in the x-direction can be estimated as

$$F_B = F_o + \int_o^\infty F_D \tan\theta \, dx \qquad (16)$$

where F_D is the drag force per unit boundary length normal to the boundary, Eq. (1), θ is the boundary angle and F_o is the total drag force acting on the initial width ($b^* = \pi$ in Eq. (13) or Fig. 2) of the density current. Substituting Eqs. (1) and (7) and integrating,

$$F_B = \left(1 + \frac{1}{s+1}\right) C_D \rho_a u_a Q_o \qquad (17)$$

where b is the stratification parameter and Q_o the source flow. This density current drag force may be compared to the direct plant drag (assuming a uniform ambient velocity)

$$F_p = \frac{1}{2} C_p \rho_a u_a^2 A_p \qquad (18)$$

where C_p = plant drag coefficient and A_p = plant cross-sectional area perpendicular to the flow. Taking linear stratification (s = 1), typical drag coefficients ($C_D = 1/2$, $C_p = 1$), a plant area A_p = 20,000 m^2 and using the data from the example in the preceeding paragraph one finds a ratio

$$\frac{F_B}{F_p} \approx 4$$

This means that for moderate current velocities (u_a = 0.1 m/s) the density current drag may in fact dominate over the direct plant drag. On the other hand, for larger current (including the more realistic case of large current velocities in the surface layer) the direct plant drag becomes dominant. In any case, the results point out that the current drag may be a significant factor in the mooring design of OTEC structures. Additional drag producing effects may be in the form of internal hydraulic jump (shock) zones. This need to be considered in the context of the detailed numerical analysis of the

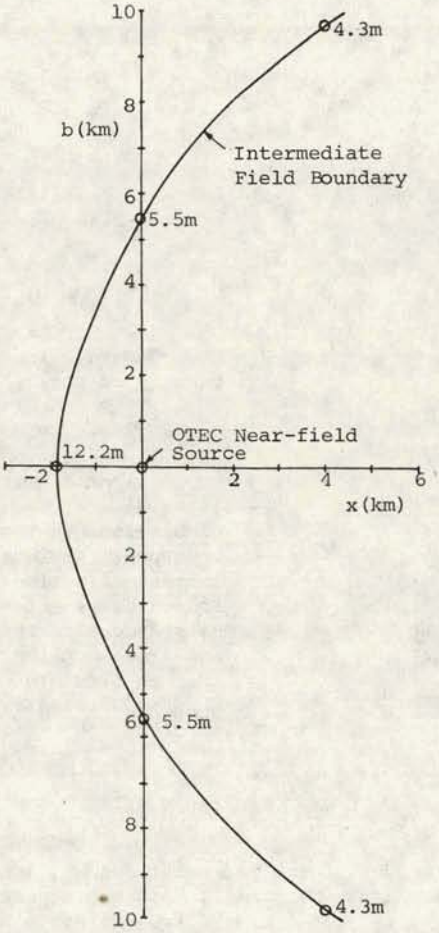

Fig. 4 Plan view of predicted boundary shape and thickness (at selected points) for intermediate field of a 100 MWe OTEC plant with mixed discharge design. Ambient current from the left with velocity 0.1 m/s.

density current velocity field. The ambient flow energy will be dissipated locally in a head wave effect at the density current front (for a discussion of the dissipating mechanism see Benjamin (5)) or, in the case of continuous stratification, will be particularlly radiated away from the front in form of internal waves.

Concluding Remarks

This study has documented and analysed the intermediate field of OTEC discharges as an important fluid zone as regards environmental impact determination and thermal resource utilization. The behavior of steady density currents has been stressed in the preceeding. However, the actual ocean environment is much more dynamic with frequent changes in ambient current magnitude and direction. Additional work is underway to analyze transient motions and thus to estimate the typical adjustment time from one current mode to another.

Acknowledgments

This work has been supported by the U.S. Department of Energy, Ocean Systems Branch, under contract No. ET-78-S-02-4683 (subcontract from M.I.T.). The cooperation of Drs. R. Cohen and L. Lewis of DOE and of Dr. J. Ditmars of Argonne National Laboratory is gratefully acknowledged.

References

1. Proceedings of the 5th Ocean Thermal Energy Conversion Conference, Miami Beach, Feb. 1978, N. Veziroglu, University of Miami, Coral Gables, FL.

   a) Allender, J.H., Ditmars, J.D., Paddock, R.A., and Saunders, K.D., "OTEC Physical and Climatic Environmental Impacts: An Overview of Modeling Efforts and Needs," pp. III-165 to 185.

   b) Fry, D.J., Jirka, G.H. and Adams, E.E., "Evaluation of Mixing and Recirculation in Generic OTEC Discharge Designs," pp. III-104 to 116.

2. Jirka, G.H., Johnson, R.P., Fry, D.J. and Harleman, D.R.F., "Ocean Thermal Energy Conversion Plant: Experimental and Analytical Study of Mixing and Recirculation," R.M. Parsons Laboratory, Report No. 231, M.I.T., 1977.

3. Bathen, K.H., "A Further Evaluation of the Oceanographic Conditions Found Off Keahole Point Hawaii, and the Environmental Impact of Nearshore OTEC Plants on Subtropical Hawaiian Waters," G. Ioup, editor, Proc. 4th OTEC Conference, New Orleans, March 1976, University of New Orleans.

4. Fry, D.J., "Effects of Oceanic Flow Patterns on the Thermal Efficiency of OTEC," M.S. Thesis, Dept. of Civil Eng.g, Carnegie-Mellon University, 1976.

5. Benjamin, T.B., Gravity currents and related phenomena, J. Fluid Mech., 31, 1978, pp. 209-248.

6. Nieuwland, C.Y. and Spee, B.M., "Transonic airfoils: Recent Developments in Theory, Experiment and Design," Ann. Rev. Fluid Mech., 5, 1973, pp. 119-150.

7. Larsen, J. and Sorensen, T., "Buoyancy Spread of Wastewater in Coastal Regions," Proc. 11th Conference on Coastal Eng.g, 2, London, 1968.

8. Jirka, G.H. and Jones, J., "Analysis of the Intermediate Field of OTEC Induced Density Currents," Interim Report to DOE, School of Civil and Environmental Eng.g, Cornell University, 1979.

9. Jameson, A. and Caughey, "A Finite Volume Method for Transonic Potential Flow Calculations," Proc. AIAA, 3rd Computational Fluid Dynamics, Conf., Albuquerque, New Mex., 1977.

A WHOLE BASIN MODEL OF THE GULF OF MEXICO

Alan F. Blumberg* **and George L. Mellor†**

Dynalysis of Princeton
20 Nassau Street
Princeton, New Jersey 08540

Abstract

An ocean model has been developed which includes the following characteristics: (1) A second moment turbulence closure model capable of accurate prediction of small scale turbulent mixing and derivative ocean features such as mixed layer temperature and depth. (2) An algorithm which calculates the external (tidal) mode separately from the internal mode. The external mode, an essentially two-dimensional calculation, requires a short integrating time step whereas the costly, three-dimensional, internal mode can be executed with a long step. The result is a fully three-dimensional code which includes a free surface at no sacrifice in computer cost compared to rigid lid models. (3) A "σ" coordinate system with 20 levels in the vertical independent depth so that the continental shelf, shelf break and slope will be resolved; furthermore, the model features increased resolution in the surface and bottom layers. (4) Coding designed for modern array processing computers, which is essential to three-dimensional ocean simulations requiring long integrations at tolerable cost. Some preliminary tests of the model as applied to the Gulf of Mexico are presented herein. The results to date indicate that the model should be useful in evaluating the environmental impact of many OTEC power plants deployed in the Gulf of Mexico or subsequently in other regions of the World Ocean. Conversely, the model should be useful in establishing oceanographic parameters (e.g. current shear) required by power plant designers.

1. Introduction

In the last several years, second moment models of small scale turbulence have been developed at Princeton University (Mellor, 1973; Mellor and Durbin, 1975; Mellor and Yamada, 1974) such that mixing or the inhibition of mixing of momentum, temperature and salinity (or any other ocean property) can be predicted with considerable confidence. A number of other investigations have tested the simplest version of the model (Martin, 1976; Martin and Roberts, 1977; Weatherly and Martin, 1978) and it is now a part of the large weather and climate General Circulation Models at NOAA's Geophysical Fluid Dynamics Laboratory (Miyakado and Sirutis, 1977).

A three-dimensional, time dependent, numerical ocean model, incorporating an advanced version of this turbulence model (Mellor and Yamada, 1977) has been constructed. Mean velocity, temperature, salinity, turbulent kinetic energy and turbulent macroscale are prognostic variables. Free surface elevation is also calculated prognostically with no sacrifice in computational time. The model incorporates a "σ" coordinate system such that the number of grid points in the vertical is independent of depth. Furthermore, the spacing in this transformed coordinate system is also variable so that, for example, one may stipulate finer resolution near the surface and bottom layers resulting in an algorithm which will be very economical on modern array processing computers.

The model responds to tidal forcing, surface wind stress, heat flux, salt "flux" (i.e., evaporation minus precipitation), estuarine outflow and to the specification of temperature, salinity and sea surface elevation at open inflow boundaries.

The model is now operational and some preliminary simulations of the Gulf of Mexico are presented in this paper. Subsequent reports will describe details of the meteorological forcing, oceanographic climatology and, finally, a multi-year simulation of the Gulf of Mexico.

The goal of the first phase of this investigation is a five year integration of the Gulf of Mexico model which will then be compared with the oceanographic climatology. In the second phase, simulated OTEC power plants will be inserted in the model and a second, five year integration will be executed; the results will be compared with the control case. The model should subsequently be useful in answering a great many engineering and environmental questions.

2. The Governing Equations

The set of equations governing ocean circulation must describe the velocity and surface elevation fields, the salinity and temperature fields. Two simplifying approximations are used; first, it is assumed that the weight of the fluid identically balances the pressure (hydrostatic assumption), and second, density differences are neglected unless the differences are multiplied by gravity (Boussinesq approximation).

Consider a system of orthogonal Cartesian coordinates with x increasing eastward, y increasing northward and z increasing vertically upwards. The instantaneous velocities are then U+u, V+v and W+w whereas the corresponding ensemble mean and fluctuating velocities are U,V,W and u,v,w respectively.

The continuity equation is

$$\frac{\partial U}{\partial x} + \frac{\partial V}{\partial y} + \frac{\partial W}{\partial z} = 0 \qquad (1)$$

The "Reynolds" momentum equations in conservative

*Research Scientist
†Consultant to Dynalysis, Professor Princeton University

form are

$$\frac{\partial U}{\partial t} + \frac{\partial U^2}{\partial x} + \frac{\partial UV}{\partial y} + \frac{\partial UW}{\partial z} - fV = -\frac{1}{\rho_o}\frac{\partial P}{\partial x} - \frac{\partial}{\partial z}\overline{wu} + F_x \quad (2)$$

$$\frac{\partial V}{\partial t} + \frac{\partial UV}{\partial x} + \frac{\partial V^2}{\partial y} + \frac{\partial VW}{\partial z} + fU = -\frac{1}{\rho_o}\frac{\partial P}{\partial y} - \frac{\partial}{\partial z}\overline{wv} + F_y \quad (3)$$

$$\rho g = -\frac{\partial P}{\partial z} . \quad (4)$$

(The mean density, ρ, is the only symbol where a mean variable is denoted by a lower case letter.) We define ρ_o, the reference density; ρ, in the in situ density; g, the acceleration due to gravity, P, the pressure; and $-\overline{wu}$, $-\overline{wv}$, the vertical Reynolds (kinematic) stresses. A latitudinal variation of the Coriolis parameter, f, is introduced by use of the β plane approximation as

$$f = f_o + \beta y \quad (5)$$

For the Gulf of Mexico, we set $f_o = 6.147 \times 10^{-5}$ sec^{-1} and $\beta = 2.070 \times 10^{-11}$ m^{-1} $^o sec^{-1}$ for a latitude of 25°N.

The pressure at a depth z can be obtained by integrating the vertical component of the equations of motion, Equation (4), from z to the free surface, η, is

$$P(x,y,z,t) = P_{atm} + g\rho_o\eta + g\int_z^o \rho(x,y,z',t)dz' \quad (6)$$

Henceforth, the atmospheric pressure, p_{atm} is assumed constant.

The equations for the mean of any scalar, Θ_i, may be written

$$\frac{\partial \Theta_i}{\partial t} + \frac{\partial U\Theta_i}{\partial x} + \frac{\partial V\Theta_i}{\partial y} + \frac{\partial W\Theta_i}{\partial z} = -\frac{\partial}{\partial z}\overline{w\theta_i} . \quad (7)$$

Thus, Θ_i may represent mean potential temperature, Θ, salinity, S, or a contaminant, C, whereas $\overline{w\theta_i}$ may represent the corresponding turbulent fluxes of temperature, salinity or contaminant.

Once the temperature and salinity have been computed, the density is represented as

$$\rho = \rho_\theta(\Theta,S) \quad (8)$$

where ρ_θ is the potential density.

The turbulence is characterized by

$$\frac{\partial q^2/2}{\partial t} + \frac{\partial Uq^2/2}{\partial x} + \frac{\partial Vq^2/2}{\partial y} + \frac{\partial Wq^2/2}{\partial z} = \frac{\partial}{\partial z}\left(K_q\frac{\partial q^2/2}{\partial z}\right) - \overline{wu}\frac{\partial U}{\partial z} - \overline{wv}\frac{\partial V}{\partial z} - \frac{g}{\rho_o}\overline{w\rho'} - \frac{q^3}{\Lambda_1} + F_g \quad (9)$$

$$\frac{\partial q^2\ell}{\partial t} + \frac{\partial Uq^2\ell}{\partial x} + \frac{\partial Vq^2\ell}{\partial y} + \frac{\partial Wq^2\ell}{\partial z} = \frac{\partial}{\partial z}\left(K_q\frac{\partial q^2\ell}{\partial z}\right) - \ell E_1\left(\overline{wu}\frac{\partial U}{\partial z} + \overline{wv}\frac{\partial V}{\partial z} + \frac{E_3}{\rho_o}\overline{w\rho'} - \frac{q^3}{B_1}\tilde{W}\right) + F_\ell \quad (10)$$

where $q^2/2$ is the turbulent kinetic energy and is a turbulent macroscale. The fluxes are given by

$$(\overline{-uw}, \overline{-vw}) = K_M\left(\frac{\partial U}{\partial z}, \frac{\partial V}{\partial z}\right) \quad (11a,b)$$

$$\overline{-w\theta_i} = K_H\frac{\partial \theta_i}{\partial z} \quad (11c)$$

$$\overline{-w\rho'} = K_H\frac{\partial \rho}{\partial z} \quad (11d)$$

where

$$K_M \equiv \ell q\, S_M, \quad K_H \equiv \ell q\, S_H \quad (12a,b)$$

and furthermore

$$K_q \equiv \ell q\, S_g \quad (12c)$$

S_M and S_H are analytically derived algebraic relations emanating from closure hypotheses described and implemented by Mellor (1973), Mellor and Yamada (1974), Yamada and Mellor (1975) and most recently by Mellor and Yamada (1977). Empirical constants in these algebraic relations are derived from neutral data but the result has been shown to predict the stabilizing or destabilizing effects of density stratification. The reader is referred to these references for the remaining details.

The terms, F_x, F_y, F_T, F_S, F_q and F_ℓ represent horizontal diffusion terms which are usually required by models to damp small scale numerical computational modes. For the calculations on a 1/2° x 1/2° grid, the horizontal viscosity and diffusion coefficient is 10^3 m^2 s^{-1}. We hope to reduce this value with this grid resolution and, of course, can do so with finer resolution.

Boundary Conditions

The boundary conditions at the free surface, $z = \eta(x,y)$, are

$$K_M\left(\frac{\partial U}{\partial z}, \frac{\partial V}{\partial z}\right) \sim (\tau_{ox}, \tau_{oy}) \text{ as } z \to \eta \quad (13a,b)$$

$$K_M\left(\frac{\partial}{\partial z}, \frac{\partial S}{\partial z}\right) \sim (\dot{H}, \dot{S}) \quad \text{as } z \to \eta \quad (14a,b)$$

$$q^2 = B_1 u_\tau^2, \quad z = \eta \quad (15)$$

$$q^2\ell = 0, \quad z = \eta \quad (16)$$

$$W = U\frac{\partial \eta}{\partial x} + V\frac{\partial \eta}{\partial y} + \frac{\partial \eta}{\partial t}, \quad z = \eta \quad (17)$$

where (τ_{ox}, τ_{oy}) is the surface wind stress vector, $\dot{H}$ is the net ocean heat flux and $\dot{S} = S(0)[\dot{E}-\dot{P}]/\rho_o$ where (E-P) is the net evaporation-precipitation fresh water surface flux rate. In equation (15), $u_\tau = |\tau_o|^{1/2}$ is the friction velocity and B_1 is one of the empirical constants in the turbulent con closure relations.

At the bottom, $z = -H(x,y)$, boundary conditions for Θ, S, q^2 and $q^2\ell$ are similar to (14a,b), (15) and (16) where, however, $\dot{H} = \dot{S} = 0$. In place of (17) we have

$$W = -U \frac{\partial H}{\partial x} - V \frac{\partial H}{\partial y} \qquad (18)$$

where H(x,y) is the bottom topography. The horizontal velocities are not set to zero at the bottom; instead, they are matched to the "law of the wall" which extends the solutions of U and V into the viscous or roughness sublayer. Thus,

$$(U,V) \sim \frac{(\overline{-wu}, \overline{-wv})}{\kappa u_\tau} \ell n \frac{(H+z)}{z_o} \quad \text{as} \quad z \to -H \qquad (19a,b)$$

Here, u_τ is the bottom friction velocity and von Karmen's constant, $\kappa = 0.40$; and z_o is roughness height. For a smooth bottom it can be shown that

$$z_o = \frac{\nu}{u_\tau} e^{-4.9\kappa} = 0.141 \frac{\nu}{u_\tau} \qquad (20)$$

Basically, two types of open boundaries exist, inflow and outflow. The outflow condition is one which allows phenomena generated in the region of interest to pass through the boundary, and the inflow condition is one which requires the prescription of temperature and salinity as a function of depth all along the inflowing open boundary. On the outflow, it is assumed that advective processes dominate. Velocity, turbulent kinetic energy and turbulent macroscale will be determined by neglecting the advection in comparison with the other terms in their respective equations. The boundary surface elevation or total transport must also be prescribed.

3. Coordinate Transformation

The ordinary x,y,z coordinate system has certain computational disadvantages in the vicinity of large bathymetric irregularities. It is advantageous to introduce a new set of independent variables that transforms both the surface and the bottom into coordinate surfaces. The governing external and internal modal equations are transformed from (x,y,z,t) to (x*,y*,σ,t*) coordinates, where

$$x^* = x, \; y^* = y, \; \sigma = \frac{z-\eta}{H+\eta}, \; t^* = t. \qquad (21)$$

If now we let $D \equiv H+\eta$ and applying the chain rule, the following relationships linking derivatives in the old system to those in the new system are obtained:

$$\frac{\partial G}{\partial x} = \frac{\partial G}{\partial x^*} - \frac{\partial G}{\partial \sigma}\left(\frac{\sigma}{D}\frac{\partial D}{\partial x} + \frac{1}{D}\frac{\partial \eta}{\partial x}\right) \qquad (22a)$$

$$\frac{\partial G}{\partial y} = \frac{\partial G}{\partial y^*} - \frac{\partial G}{\partial \sigma}\left(\frac{\sigma}{D}\frac{\partial D}{\partial y} + \frac{1}{D}\frac{\partial \eta}{\partial y}\right) \qquad (22b)$$

$$\frac{\partial G}{\partial z} = \frac{1}{D}\frac{\partial G}{\partial \sigma} \qquad (22c)$$

$$\frac{\partial G}{\partial t} = \frac{\partial G}{\partial t^*} - \frac{\partial G}{\partial \sigma}\left(\frac{\sigma}{D}\frac{\partial D}{\partial t} + \frac{1}{D}\frac{\partial \eta}{\partial t}\right) \qquad (22d)$$

where G is an arbitrary field variable, and σ ranges from σ = 0 at z = η to σ = -1 at z = -H. A new vertical velocity can now be defined,

$$\omega \equiv w - u\left(\sigma\frac{\partial D}{\partial x} + \frac{\partial \eta}{\partial x}\right) - v\left(\sigma\frac{\partial D}{\partial y} + \frac{\partial \eta}{\partial y}\right) - \left(\sigma\frac{\partial D}{\partial t} + \frac{\partial \eta}{\partial t}\right) \qquad (23)$$

which transforms the boundary conditions, equations (17) and (18), into

$$\omega(x,y,0,t) = 0 \quad \text{and} \quad \omega(w,y,-1,t) = 0 \qquad (24)$$

Equations (1), (2), (3), (7), (9) and (10) are all transformed according to the above relations before they are written in finite difference form.

4. Mode Splitting Technique

The equations governing the dynamics of coastal circulation contain the influences of fast moving barotrophic effects (surface gravity waves and slow moving baroclinic effects (internal gravity waves). It is desirable in terms of computer economy to separate out vertically integrated equations (external mode) from the vertical structure equations (internal mode). This separation allows the resulting three dimensional (x,y,z) internal mode equations to be solved using a much longer time step than required for the two dimensional (x,y) external mode equations.

The external mode equations are obtained by integrating the internal mode equations over the depth, thereby eliminating all vertical structure. The continuity equation becomes

$$\frac{\partial \eta}{\partial t} + \frac{\partial \bar{U}D}{\partial x} + \frac{\partial \bar{V}D}{\partial y} = 0 \qquad (25)$$

and the momentum equations become

$$\frac{\partial \bar{U}D}{\partial t} + \frac{\partial \bar{U}^2 D}{\partial x} + \frac{\partial \bar{U}\bar{V}D}{\partial y} - \overline{fVD} + gD\frac{\partial \eta}{\partial x} = -\overline{wU}(0) + \overline{wU}(-1) - \frac{\partial D\overline{U'U'}}{\partial x} - \frac{\partial D\overline{U'V'}}{\partial y} - \frac{gD^2}{\rho_o}\int_{-1}^{0}\left[\frac{\partial}{\partial x}\int_{\sigma}^{0}\rho d\sigma\right]d\sigma + \frac{g}{2\rho_o}\frac{\partial D^2}{\partial x}\int_{-1}^{0}\left[\int_{\sigma}^{0}\sigma\frac{\partial \rho}{\partial \sigma}d\sigma\right]d\sigma + D\overline{F_x} \qquad (26)$$

and

$$\frac{\partial \bar{V}D}{\partial t} + \frac{\partial \bar{U}\bar{V}D}{\partial x} + \frac{\partial \bar{V}^2 D}{\partial y} + f\bar{U}D + gD\frac{\partial \eta}{\partial y} = -\overline{wV}(0) + \overline{wV}(-1) - \frac{\partial D\overline{U'V'}}{\partial x} - \frac{\partial D\overline{V'^2}}{\partial y} - \frac{gD^2}{\rho_o}\int_{-1}^{0}\left[\frac{\partial}{\partial y}\int_{\sigma}^{0}\rho d\sigma\right]d\sigma + \frac{g}{2\rho_o}\frac{\partial D^2}{\partial y}\int_{-1}^{0}\left[\int_{\sigma}^{0}\sigma\frac{\partial \rho}{\partial \sigma}d\sigma\right]d\sigma + D\overline{F_y} \qquad (27)$$

where the pressure has been obtained from (6) and the vertically integrated velocities are defined as

$$(\bar{U},\bar{V}) \equiv \int_{-1}^{0}(U,V)\,d\sigma \qquad (28a,b)$$

the wind stress components are $-\overline{wu}(0)$, $-\overline{wv}(0)$ and the bottom stress components are $-wu(-1)$ and $-\overline{wv}(-1)$. The terms in equations (26) and (27) involving $\overline{U'^2}$, $\overline{U'V'}$ and $\overline{V'^2}$ represent vertical averages of the cross-products of the velocity departures from the vertically integrated (average) velocity. Thus

$$(\overline{U'^2},\ \overline{V'^2},\ \overline{U'V'}) = \int_{-1}^{0} (\overline{U'^2},\ \overline{V'^2},\ \overline{U'V'})d\sigma \quad (29a,b,c)$$

where $(U', V') = U-\bar{U}, V-\bar{V})$. The quantities $\bar{F}_x$ and $\bar{F}_y$ are vertical integrals of the horizontal diffusion of momentum.

5. Aspects of the Numerical Scheme

As previously mentioned, computational economy is achieved if the program is divided into external and internal mode subprograms. The first, call it the XYt subprogram, computes the vertically averaged velocity and the surface elevation fields with a short time increment (≈30 sec.) imposed by the shallow water wave speed, CFL criterion

$$\Delta t \leq \frac{1}{2}\left[\sqrt{gD_{max}}\ \left(\frac{1}{\Delta x} + \frac{1}{\Delta y}\right)\right]^{-1} \quad (30)$$

The second, call it the XYZT subprogram, computes the full three-dimensional velocity, temperature and salinity fields with a much longer time increment (100 times the short increment) governed by

$$\Delta t \leq f^{-1} \quad (31)$$

and

$$\Delta t \leq \left[C_b\left(\frac{1}{\Delta x} + \frac{1}{\Delta y}\right)\right]^{-1} \quad (32)$$

where C_b is the gravest mode internal gravity wave speed. The XYZT subprogram incorporates the second moment turbulent closure model. It supplies computed bottom friction and vertical integrals of density and vertical variances of horizontal velocity to the XYt subprogram where they behave as lateral friction-like terms in the vertically averaged horizontal eddy viscosities in models which do not adequately resolve vertical structure. In turn, the XYt subprogram supplies sea surface elevation to the XYZT subprogram. This may sound complicated, but in the final analysis, the full three-dimensional field equations are solved with a free surface boundary condition at no additional cost in computer time as compared to rigid lid models (Bryan and Cox, 1978).

The time differencing is the conventional leap-frog technique. However, the scheme is quasi-implicit in that vertical diffusion is evaluated at the forward time level. Thus, small vertical spacing is permissible near the surface without need to reduce the time increment or restrict the magnitude of the mixing coefficients. It should be remarked that the finite difference equations conserve volume, θ_i, mass and momentum. Also, they are second order accurate in space and time.

Leap-frog time differencing introduces a tendency for the solutions at even and odd time steps to split. This time splitting is removed by a weak filter (Asselin, 1972) where the solution is smoothed at each time step according to

$$F_s^n = F^n + \frac{\alpha}{2}\left(F^{n+1} - 2F^n + F_s^{n-1}\right) \quad (33)$$

where $\alpha = 1/10$ and F_s is a smoothed solution. This technique introduces less damping than either the Euler-backward or forward stepping techniques.

A flow chart of the model logic is displayed in Figure 1.

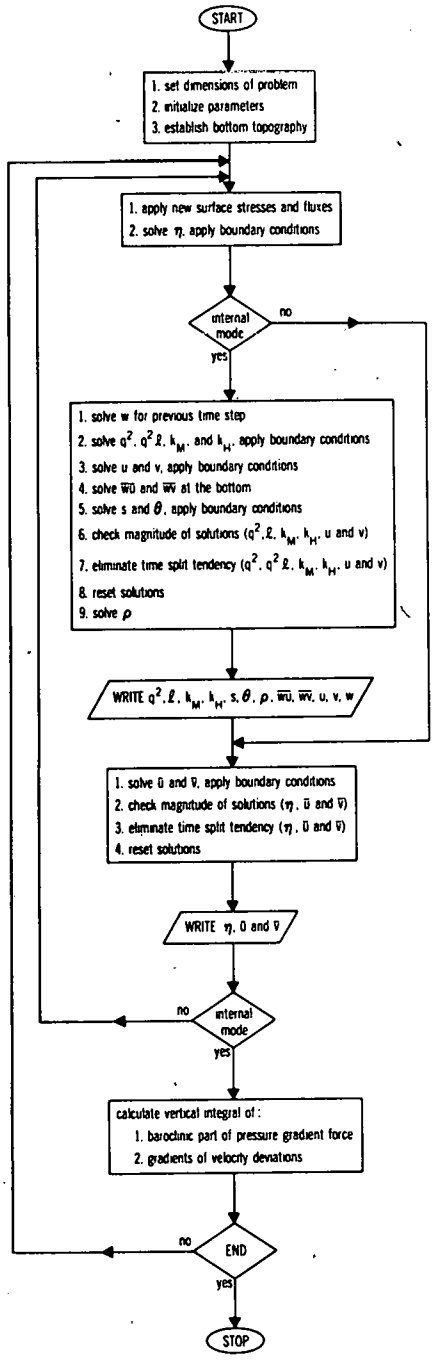

Fig. 1. Flow Chart of the Numerical Model

The model can be run exclusively in an external mode by removing the internal mode option; however, in equations (26) and (27) the vertical structure terms involving density must be prescribed from data and the structure terms involving velocities must be empirically estimated or set to zero. A bottom friction term must also be empirically estimated.

6. Vertical Resolution Requirements

After some time, it was decided that the fully operational model should run with 20 levels (note, however, that the preliminary runs, discussed in Section 9, were only 10 levels). Table I shows the distribution of σ and z for depths of 100, 1000 and 4000 m. Near the surface and the bottom the distribution of points is logarithmic; in the center portion, the distribution is linear.

Table I. Vertical σ coordinate system and corresponding z for D = 100m, 1000m, and 4000m. The arrows on the left column mark a change from a logarithmic to a linear distribution.

	K	D	100m	1000m	4000m
		σ	z	z	z
	1	0	0	0	0
	2	.0012	0.12	1.2	4.81
	3	.0024	0.24	2.4	9.62
	4	.0048	0.48	4.81	19.23
	5	.0096	0.96	9.62	38.46
	6	.0192	1.92	19.2	76.92
	7	.0385	3.85	38.5	153.85
	8	.0769	7.69	76.9	307.69
→	9	.1538	15.38	153.38	615.38
	10	.2303	23.08	230.8	923.08
	11	.3077	30.77	307.7	1230.77
	12	.3846	38.46	384.6	1538.46
	13	.4615	46.15	461.5	1846.15
	14	.5385	53.85	538.5	2153.85
	15	.6154	61.54	615.4	2461.5
	16	.6923	69.23	692.3	2769.2
	17	.7692	76.92	769.2	3076.9
	18	.8462	84.62	846.2	3384.6
→	19	.9231	92.31	923.1	3692.3
	20	.9615	96.15	961.5	3846.2
	21	1.00	100.00	1000.0	4000.0

The bottom boundary layer will not be resolved very well. Nevertheless, the resolution of the bottom layer on the shelf when H ≃ 100m is about the same as the surface layer when H ≃ 4000m and we will see that the surface layer is computed surprisingly well when H ≃ 4000m.

Figures 2 and 3 display the results of a sample, one dimensional calculation after 10 days when an eastward wind stress of 2 dynes cm^{-2} is applied at day zero. As mentioned above, it will be seen that the surface layer is resolved fairly well even when the vertical increments correspond to H = 4000m.

We have also run the above case but with an imposed oscillatory wind stress prescribed by $\tau_{oy} = 0$ and

$$\tau_{ox} = \frac{2\text{dynes}}{\text{cm}^2}\left[1 - \cos\left(\frac{2\pi t}{4\text{days}}\right)\right] \qquad (34)$$

The calculated velocity profiles differ in detail from those of Figure 3, of course, but the temperature profile and mixed layer depth were virtually identical to those in Figure 2 for the constant stress case. Therefore, it appears that temperature profiles are not sensitive to the temporal variation of wind stress at least on scales of a few days. However, as discussed in Section 8, it is nevertheless quite possible that the temporal distribution of winds may be important during the spring heating season.

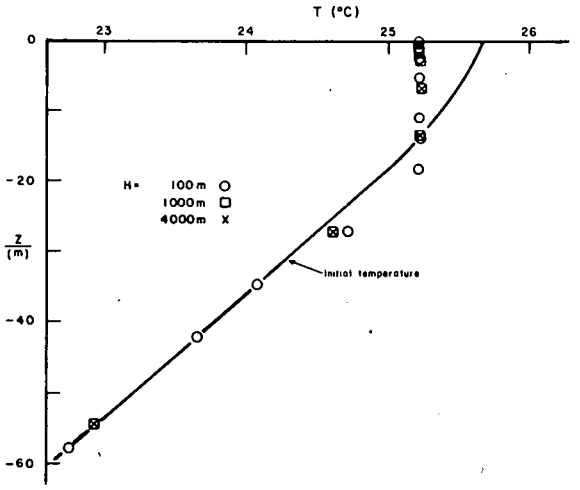

Fig. 2. Temperature distribution for a one-dimensional simulation to assess vertical resolution requirements. Time = 10 days after imposition of a 2 dyne cm^{-2} wind stress.

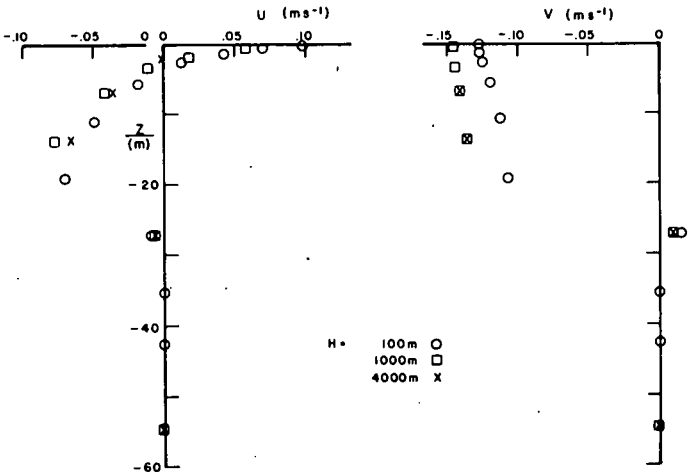

Fig. 3. Same as Fig. 2 except that the eastward and northward velocity components are plotted.

7. Surface Stress Data Requirements

It is our plan to drive the model with climatological surface stresses derived from surface winds. The data will be averaged monthly; that is, for each month of the year, statistics of the wind stress will be determined for each 1° square. The choice of statistics is governed and complicated somewhat by the fact that surface layer mixing depends synoptically on $\tau_o \equiv |\underset{\sim}{\tau}_o|$ where $\underset{\sim}{\tau}_o$ is the surface wind stress vector and, as evidenced by the discussion of Section 6, the required climatological average should be $\overline{\tau}_o = \overline{|\underset{\sim}{\tau}_o|}$. On the

other hand, Ekman transport and the resulting general circulation depend on τ_x and τ_y and the required climatological average is $\bar{\tau}_x$ and $\bar{\tau}_y$. To satisfy both requirements we propose to drive the model with

$$\tau_x = \bar{\tau}_x(x,y,t) + \sqrt{2}\sigma_\tau(x,y,t) \cos \omega t \qquad (35a)$$

$$\tau_y = \bar{\tau}_y(x,y,t) + \sqrt{2}\sigma_\tau(x,y,t) \sin \omega t \qquad (35b)$$

where $\omega = 2\pi T^{-1}$ and T is a period of the order of a week. The averages $\bar{\tau}_x(x,y,t)$, $\bar{\tau}_y(x,y,t)$, and variances $\sigma_{\tau x} = [\overline{(\tau_x - \bar{\tau}_x)^2}]^{1/2}$, $\sigma_{\tau y} = [\overline{(\tau_y - \bar{\tau}_y)^2}]^{1/2}$ are slowly varying functions of time interpolated from climatological monthly averages.

The one dimensional, sensitivity simulation discused in Section 6 prescribed $\bar{\tau}_y = \sigma_{\tau y} = 0$, $\sqrt{2}\sigma_{\tau x} = -\bar{\tau}_x$ and T = 4 days.

8. Area Averaged Seasonal Simulations

To gain some a priori understanding of the model's ability to simulate seasonal variability, we have made calculations with the one-dimensional model driven by wind stress and surface heat flux. The one-dimensional equations may be regarded as the three-dimensional equations after averaging horizontally over the basin. The correct equation for Θ, for example, is

$$\frac{\partial A\Theta}{\partial t} + \oint \Theta \, \underset{\sim}{V} \cdot \underset{\sim}{n} ds + \frac{\partial}{\partial z}(AW\Theta) = -\frac{\partial}{\partial z}(A\overline{w\theta}) \qquad (36)$$

where A(z) is the basin area and Θ is here taken to be the area averaged temperature. The term $\oint \Theta \, V \cdot n ds$ represents the horizontal advection of Θ into the basin ($\underset{\sim}{V} \cdot \underset{\sim}{n}$ is the volume flux rate and s is distance along the perimeter of the basin) dominated in this case by flow through the Straits of Yucatan and Florida.

In this study we will neglect both horizontal and vertical advection, $\partial(AW\Theta)/\partial z$, which we will see does not seriously distort the results in the present, one-dimensional study and over time scales of a year (horizontal and vertical advection are, of course, included in the full three dimensional model). NODC data tapes provide a large number of temperature and salinity observations collected over the last 80 years. The data have been averaged on 1° squares which are depicted in Figure 4. The Caribbean Sea region in the southeast has been excluded. There are a total of 36,000 observations at the surface decreasing to 21,000 at the 250m depth. The area averaged temperature climatology was then observed and is plotted in Figure 5. Below 100m there seems to be a semi-annual oscillation which might merit further study in the future. The oscillation is also manifest in salinity contours at the lower depths. When $z \gtrsim -100$ the salinity is nearly constant.

The heat storage, $\int_{-100}^{0} \Theta \, dz$, was obtained for each month. (Extending the integration to lower depths incorporated the semi-annual oscillation which, if real, must be related to horizontal advection which we are neglecting here). The result was Fourier transformed into a series consisting of a constant and six cosine and six sine functions. To obtain the surface heat rate, the series was differentiated and the result is shown in Figure 6. The data points represent the full Fourier series whereas the solid line is the data smoothed by dropping the two highest harmonics in the series. The smoothed curve is the surface heat flux used to drive the model.

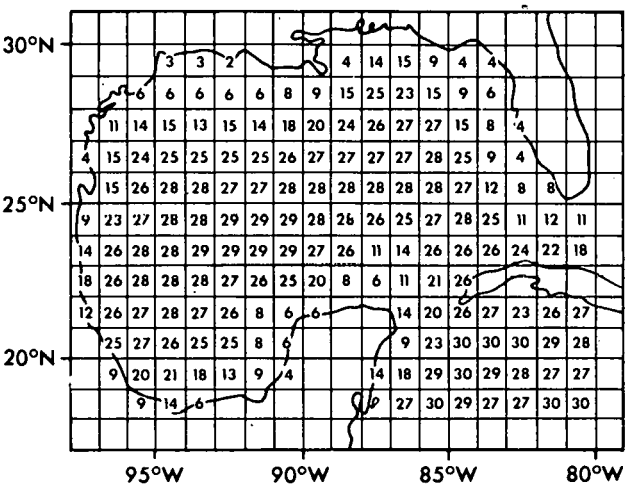

Fig. 4. The number of standard levels in each 1° square containing data from the NODC (National Oceanographic Data Center) files. Area averages of this data are shown in Fig. 5.

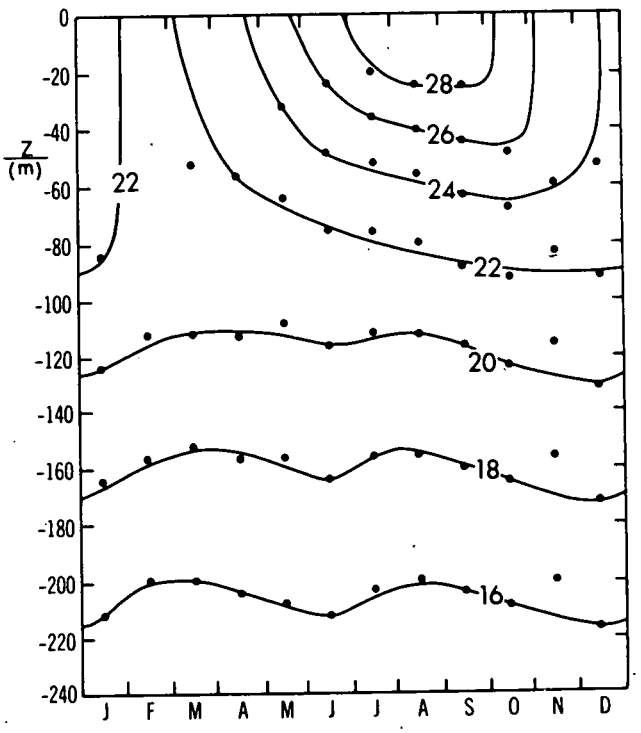

Fig. 5. Area averaged temperature climatology. The contours are in °C.

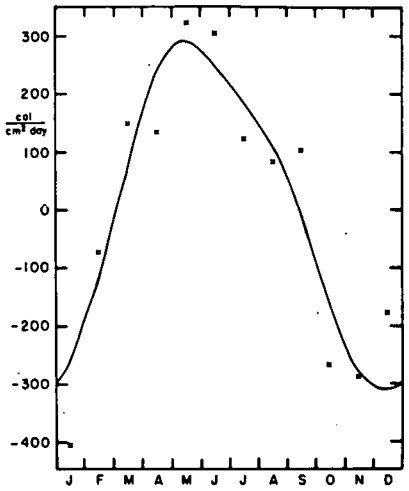

Fig. 6. The area average surface heat flux into the Gulf of Mexico. The solid line is the Fourier smoothed result.

It should be noted that we have in progress a determination of heat flux from meterological surface data. When this work is complete, it will be interesting to compare the area integrated result with Figure 6. Martin and Roberts (1977) have already estimated the monthly surface heat flux from meterological data (using, however, averaged wind data rather than individual observations to obtain stress and fluxes) and obtained a result that differs a bit but is not inconsistant with Figure 6.

Various estimates of the annual heat budget from meterological data have also been summarized by Martin and Roberts. They conclude that the Gulf loses heat to the atmosphere at a rate of about 30 cal cm^{-2} day^{-1}, about 10% of the maximum or minimum shown in Figure 6. If we were to subtract 30 cal cm^{-2} day^{-1} from the heat flux of Figure 6 and drive the model with the corrected heat flux, it would be necessary to balance the model calculation with horizontal advection into the system. However, it is not expected that the final results would be significantly altered.

Our preliminary estimates of the average wind stress over the Gulf from the meterological data is that $|\overline{\tau_0}| \approx$ 1-2 dynes cm^{-2}.

Figures 7a and 7b are model calculations for (τ_x, τ_y) = (1 dynes cm^{-2}, 0) and (2 dyne cm^{-2}, 0) respectively. (Note that absolute direction of the stress vector has no significance in the present study.) For the higher stress we note that the model prediction compares quite favorably with the data. However, after the initial deepening of the model isotherms, they remain nearly constant until cooling begins in the Fall; the data, on the other hand, exhibits further slow deepening. At this point we note that a "background" or minimum value of $K_M = K_H = 0.1$ cm^2 s^{-1} has been included in the model. (In the mixed layer, the turbulence closure generates values in the order of 100-200 cm^2 s^{-1}). If we raise this to 1.0 cm^2 s^{-1}, we obtain the result obtained in Figures 7c and 7d. Thus, in a one-dimensional calculation it seems that the model requires this completely empirical adjustment. The actual physical mechanism responsible for this level of background mixing may reside in nonlinear breaking of internal waves or bottom boundary layer mixing on the lateral boundaries of the basin (Armi, 1978) with subsequent advection into the interior. (The full, three dimensional model should account for lateral bottom mixing.) An area average of the temperature data over an interior 4°x4° region (whose southwest corner is at 23°N and 94°W in Figure 4) yields a result similar to Figure 5 but, due to paucity of data, is much noisier; w have therefore not reproduced this result here. However, it does appear that the secondary deepening of the isotherms is about half that shown in Figure 5 thus suggesting that the origins of the additional mixing are the lateral boundaries.

From the deepening of, say, the 16° isotherm in Figure 7d, one might deduce a required upwelling to conteract the deepening as did Martin and Roberts who used one of our simpler ("Level 2") models. However there is no reason to suppose that the background K is constant down to the 16° isotherm as we have assumed in Figure 7d.

We have also performed two calculations corresponding to $\tau_y = 0$ and τ_x = (2 dynes cm^{-2})[1-cos (2 t/T)] where T = 4 days and 8 days for a background K = 1 cm^2 s^{-1}. Below (20m) the results were nearly the same as in Figure 7d, but, in both cases the maximum surface temperature was nearly 2°C higher; this contrasts with the fact that there was no difference in the results of Figure 3 where an

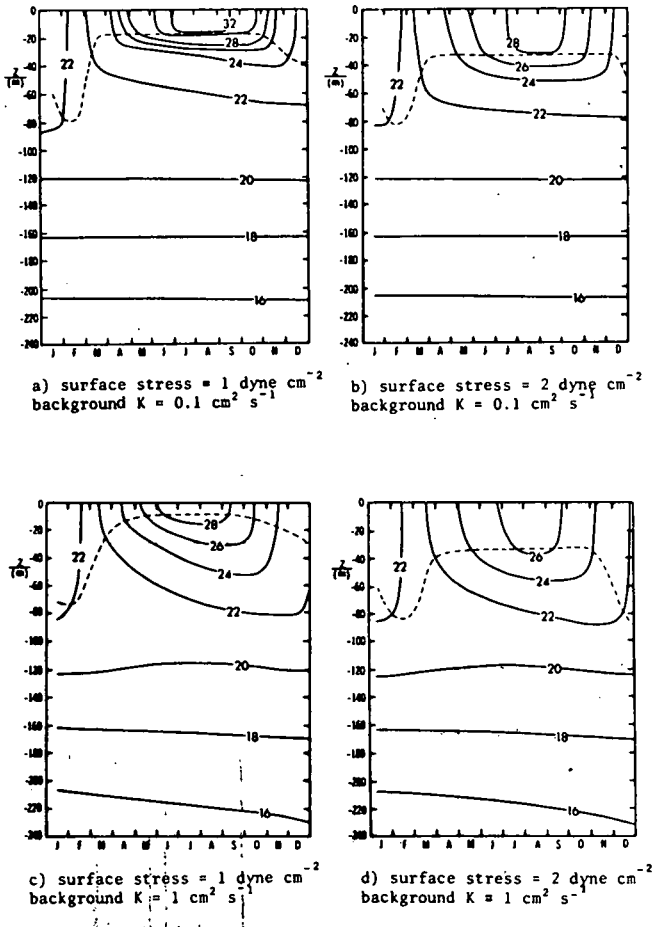

Fig. 7. One dimensional simulation using the surface heat flux of Fig. 4. The base of the mixed layer is denoted by the dashed line.

oscillatory stress was applied. Thus the application of wind stress during Spring heating is a rela-relatively delicate matter and may, if one were to consider individual years, govern the mixed layer depth and surface temperature of the entire Summer. This appears to be a ripe subject for further, in-depth study.

9. 20 Day Gulf of Mexico Simulations

It will be the purpose of a separate report to present results of multi-year model simulations of the Gulf of Mexico and then subsequently, simulations which include upwards of a 1000 model OTEC power plants.

During the development of the model which has necessitated a long programming, reprogramming and debugging period, we have, to save computer time and storage, used ten layers (in "σ" space) whereas the final simulations will use twenty layers as discussed in Section 6. Note that we would wish also to halve the horizontal grid spacing (thereby quadrupling the number of grid nodes and doubling the required time steps) but at the present time this would seem to excessively increase computer costs.

—Although the computer code is configured to accept arbitrary distributions of wind stress, heat flux and effective salt flux, these surface forcing quantities have been set equal to zero for the present since problems inherent in code development do not involve these effects. The 20 day simulation discussed here is initialized with climatological data for the Spring season. Inflow and outflow boundary conditions are prescribed at the Straits of Yucatan and the Straits of Florida as set forth in Section 2.

The bottom topography, smoothed somewhat compared to the real topography, is shown in Figure 8. The initial temperature and salinity fields are plotted in Figure 9. Clearly seen - expecially at 250m - is the hydrographic manisfestation of the Loop Current. The initial velocity field is null, so that the model must survive an initial startup shock.

After 20 days, the computed total transport and sea surface elevation are plotted in Figure 10. The velocity fields at 10m and 250m are shown in Figure 11; at 500m and below the velocity vectors are barely visible using the present scale. The temperature and salinity fields are plotted in Figure 12.

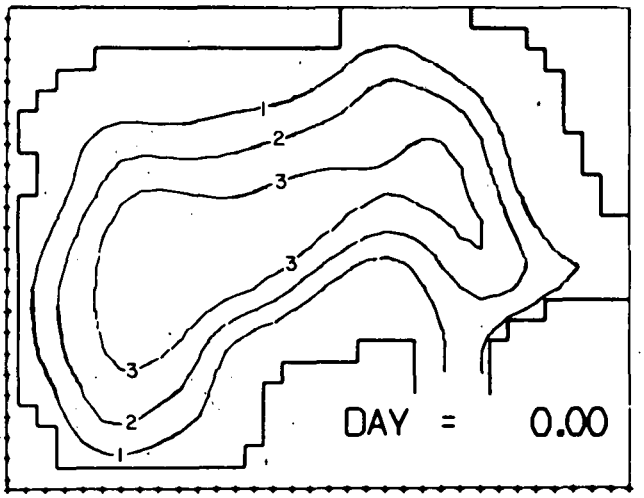

Fig. 8. Bottom topography of the Gulf of Mexico as used in the model. Contours are in 1 km increments

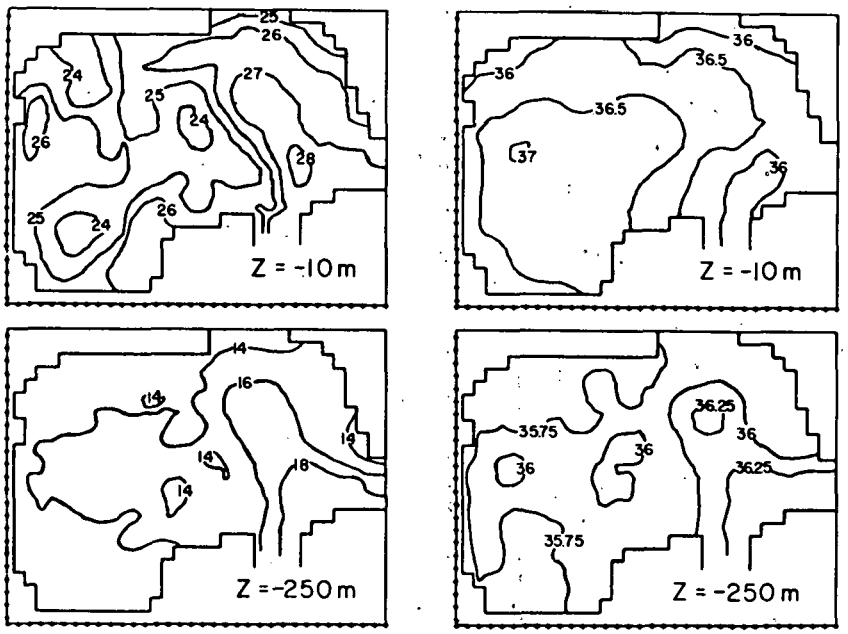

Temperature (°C) Fields

Salinity (0/00) fields

Fig. 9. The initial (day zero) temperature (°C) and salinity (0/00) fields. April - June climatology.

Twenty days is a fairly short period and changes in mass field and velocity field - from 10 to 20 days - are apparently small. However, it does appear that the initial two gyre Loop Current system evolves such that the northern gyre weakens while the southern gyre strengthens a bit.

10. Summary

A fully three-dimensional, time dependent numerical model is available for assessment of the environmental impact of many OTEC power plants in the Gulf of Mexico and other regions of the World Ocean.

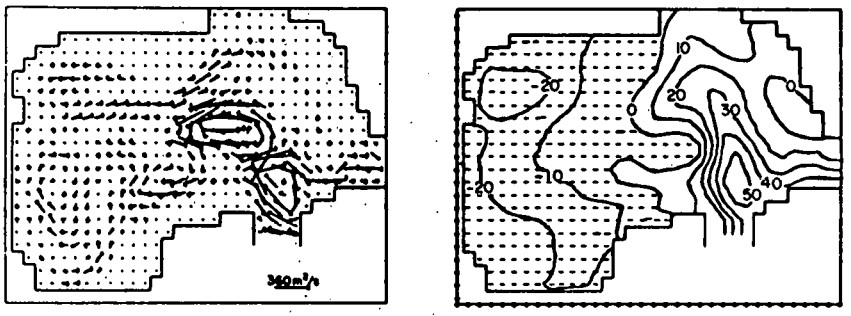

Fig. 10. Computed total transport (left side) and surface elevation (right side) after 20 days.

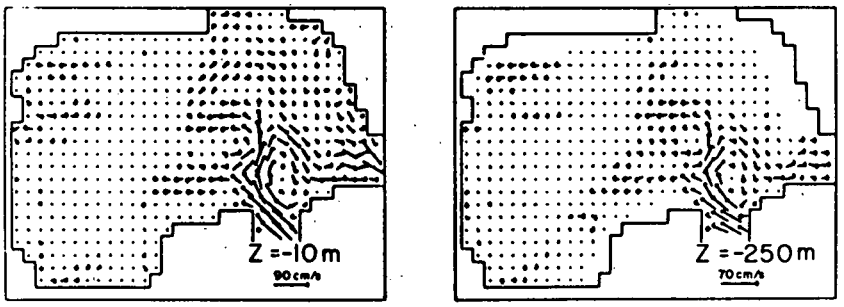

Fig. 11. The computed velocity fields after 20 days.

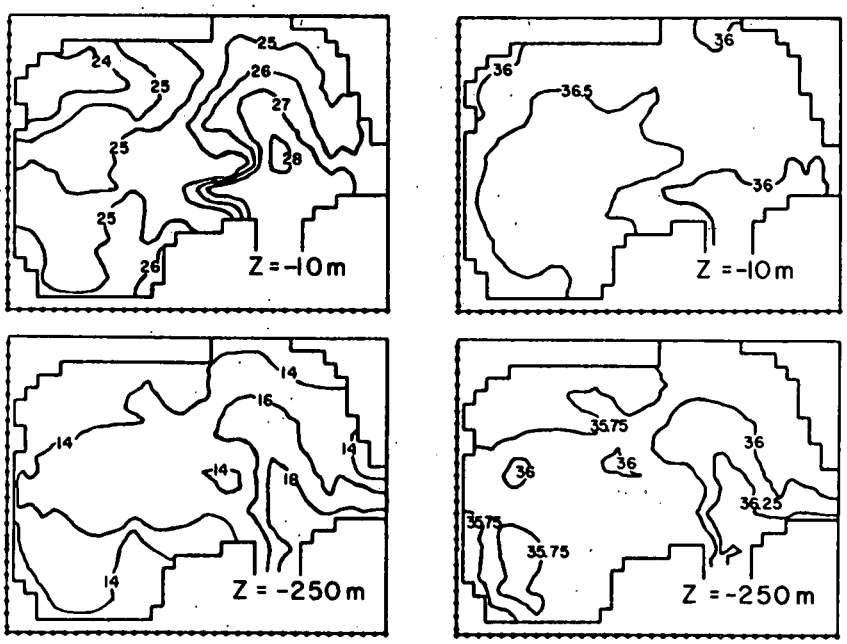

Temperatures, °C

Salinities, 0/00

Fig. 12. The computed temperature and salinity fields after 20 days.

Acknowledgements

This work is supported by the Department of Energy under Grant Number ET-78-C-02-5028.

References

Armi, L., 1978: Some evidence for boundary mixing in the deep ocean. J. Geoph. Res., 83, 1971-1979.

Asselin, R. , 1972: Mon. Wea. Rev. 100, No. 6, 487-490.

Blumberg, A., 1977: Numerical Tidal Model of Cheasapeake Bay. J. of the Hydraulid Division, ASCE, 103, (HY1), 1-10.

Blumberg, A. F., G. L. Mellor and S. Levitus, 1977: The Middle Atlantic Bight: A climatological atlas of oceanographic properties. Princeton University Sea Grant Report No. NJ/P-SG-01-8-77.

Bryan, K. and M. D. Cox, 1968: A nonlinear model of an ocean driven by wind and differential heating, Parts I and II, J. Atmos Sci., 25, 945-978.

Fofonoff, N. P., 1962: The Sea.

Mamayev, O. I., 1975: Temperature-Salinity Analysis of World Ocean Waters, Elsevier Publishing Co., Amsterdam-Oxford-New York.

Martin, P. J., 1976: A comparison of three diffusion models of the upper mixed layer of the ocean. NRL-GFD/OTEC 4-76, 1-56.

Martin, P. J. and G. O. Roberts, 1977: An estimate of the impact of OTEC operation on the vertical distributions of heat in the Gulf of Mexico. Proceeding, Forth Annual Conference on Ocean Thermal Energy Conversion, New Orleans.

Mellor, G. L., 1973 Analytic prediction of the properties of stratified planetary surface layers. J. Atmos. Sci., 30, 1061-1069.

Mellor, G. L. and T. Yamada, 1974: A hierarchy of turbulence closure models for planetary boundary layers. J. Atmos. Sci., 31, 1791-1806.

Mellor, G. L. and P. A. Durbin, 1975: The structure and dynamics of the ocean surface mixed layer. J. Phys. Oceanogr. 5, 718-728.

Mellor, G. L. and T. Yamada, 1977: A turbulence model applied to geophysical fluid problems. Proceedings: Symposium on Turbulent Shear Flows, Pennsylvania State University, University Park, Pennsylvania, April 1977, 1-14.

Miyakado, K. and J. Sirutis, 1977: Comparative integrations of global models with various parameterized processes of subgrid-scale vertical transports: Description of the parameterizations. Beitrage zur Physik der Atmosphare., 50, 445-487.

Richtmyer and Morton, 1967: Differential Methods for initial value problems.

Rodi, W., 1972: The prediction of free turbulent boundary layers by use of a 2-equation model of turbulence. Ph.D. Thesis, University of London.

Weatherly, G. and P. J. Martin, 1978: On the structure and dynamics of the oceanic bottom boundary layer. J. Phys. Oceanogr., 8, 557-570.

Yamada, T. and G. L. Mellor, 1975: A simulation of the Wangara atmospheric boundary layer data. J. Atmos. Sci., 32, 2309-2329.

Yamada, T., 1977: A numerical experiment on pollutant dispersion in a horizontally-homogeneous atmospheric boundary layer., Atmosphere Environment., 11, 1015-1024.

PROGRAMMATIC ENVIRONMENTAL ASSESSMENT FOR OPERATIONAL OTEC PLATFORMS - A PROGRESS REPORT

M. Dale Sands

Oceanic Engineering Division
Interstate Electronics Corporation
Anaheim, California 92803

Abstract

As the Ocean Thermal Energy Conversion (OTEC) Program advances toward commercialization, the potential environmental impacts must be assessed. Several OTEC plant types, configurations, sizes, and uses are being considered: closed- and open-Rankine cycles; land-based, moored-offshore, and cruising plant types; barge and spar platform types; pilot/demonstration and commercial sizes; cabled electricity to shore and production of energy-intensive products such as ammonia and aluminum. Uses of various heat exchanger types, biofouling countermeasures, and seawater intake and discharge geometries add to this matrix. In some cases multiple plants may be coordinated in, or used to serve, industrial parks or utility grids, or to have the closest practical spacing when cruising to attain the highest monthly ocean temperature differences within given open-ocean areas. Design modifications that will mitigate or reduce potentially adverse effects must be identified and incorporated into the design configurations. The key issues to be considered for siting these platforms include minimum operational site characteristics, market potential, social considerations, and potential for environmental impacts. The approach being taken to develop a programmatic Environmental Assessment (EA) is to describe the environmentally significant design options of the platforms and generically characterize a subtropical oceanic environment where the platforms will be sited. The potential environmental impacts are then examined as these two interact: the platform on the environment and the environment on the platform.

Introduction

With the construction of the preoperational Ocean Thermal Energy Conversion (OTEC-1) Platform underway,[1a, 1b, 2-4] it is time to evaluate the social, economic, and environmental issues associated with the operation of several demonstration- and commercial-size OTEC platforms. The Environmental Development Plan prepared by the Department of Energy listed several key issues associated with OTEC.[3] The environmental impact assessment (EIA) published in March 1979 specifically considered the potential environmental effects associated with OTEC-1.[4] The Ocean Engineering Division of Interstate Electronics Corporation was awarded Subcontract 450101 by the Lawrence Berkeley Laboratories to prepare this Programmatic Environmental Assessment (EA), which has been underway since January 1979 and has a completion date of December 31, 1979.

The approach taken for this EA calls for the definition of the candidate designs for commercial-size OTEC platforms and an oceanographic characterization of the potential siting locations. Once these components are defined, the key social and environmental issues associated with the OTEC platform are to be evaluated. This Programmatic EA is performed in compliance with the 1969 National Environmental Policy Act requirements for the preparation of a detailed report addressing the environmental effects of the OTEC Program. If, through the preparation of this EA, significant potential impacts are deemed likely to occur, a Programmatic Environmental Impact Statement (EIS) will be prepared.[5,6]

Platform Configurations

Three principal OTEC platform types are under consideration in this assessment: moored, land-based, and grazing plant-ship. Many studies have been funded by various government agencies to examine the different components for an OTEC platform.[7-9] From the available information, the environmentally significant design components were selected. The design options for the operating mode, the intake/discharge systems, and the stationkeeping and uses are shown in matrix form in Figs. 1, 2, and 3, respectively. Various combinations of these components and options will be examined for their environmental acceptability specific to each of the three platform types.

Site Selection

The candidate regions for OTEC development in this study are listed in Table 1. The suitable environmental characteristics for siting may be ranked as follows:

1) Minimal siting criteria
2) Economic feasibility and potential markets
3) Social issues
4) Potential environmental consequences

For each of the preferred sites identified for each type of OTEC platform, the associated critical impacts can be examined as briefly described below.

Minimum Siting Criteria

The three principal criteria in siting OTEC plants are:

1) An annual average ΔT (temperature difference) between surface and deep seawater $\geq 20°C$ (the greater, the better). The candidate areas have been determined;[1c, 1d, 10]
2) Oceanographic currents not consistently exceeding 60 cm/sec (moored and plantship only), because of the strains imparted on the cold water pipe (CWP), and the cost and/or power requirements for holding position or maneuvering in higher currents; and
3) Low frequency of occurrence of extreme meteorological conditions ($<3\%$ of the year).

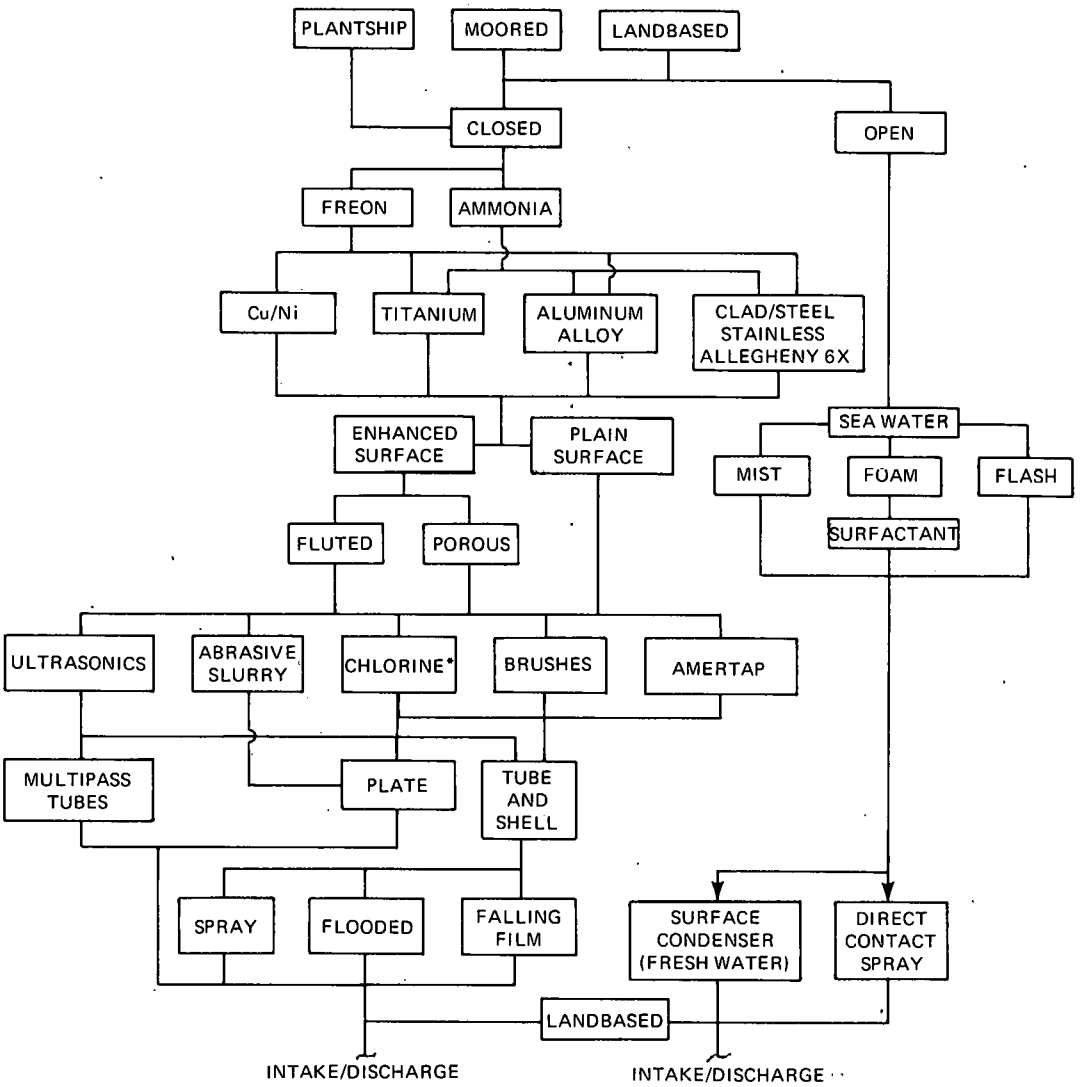

*Chlorine may be used in conjunction with any other cleaning system.

Fig. 1 Design options for OTEC operating mode.

Mooring technology is not judged to be adequate to permit siting in water deeper than 2200 m (7200 ft).

Economic Feasibility and Potential Markets

Paramount after identifying the locations meeting the minimum siting criteria are the economics surrounding plant installation, operation, and maintenance:

a) Present and projected power requirements. For instance, the tourism industry will inevitably be developing for the Marianas Islands, and OTEC power may facilitate development;

b) Potential for industrial growth requiring electric power;

c) Market potential for the energy-intensive products, availability of necessary raw materials, cost to produce the product, and distance to the market(s); and

d) Cost-competitiveness with alternative local energy sources.

As a further example of (c) above, the richest deposits of manganese nodules are located 1000 to 1800 km southeast of Hawaii, in water depths near 2200 m.[11] The processing of manganese nodules by the hydrochloric-acid-leach process to extract nickel, cobalt, copper and manganese requires chlorine gas, ammonia, and electric power. A chlorine plant is presently in the planning phase in Hawaii, but the current high costs of electricity still pose an obstacle to processing. An OTEC plant-ship could work in conjunction with a deep-ocean mining platform.[1e]

As part of this programmatic EA, a deployment scenario was prepared to describe the projected commercialization plan. OTEC commercialization investigations[11-15] conducted from 1977 to 1979 were reviewed to project the numbers and types of plants to be deployed by the years 1990 to 2020 in various oceanic regions. The development of this deployment scenario was complicated by the wide number of program options depicted in Figs. 1-3, the varying depths of detail of the investigations,[11-15] and the fact that their deployment scenarios are based on several assumptions ranging from the uncertainty

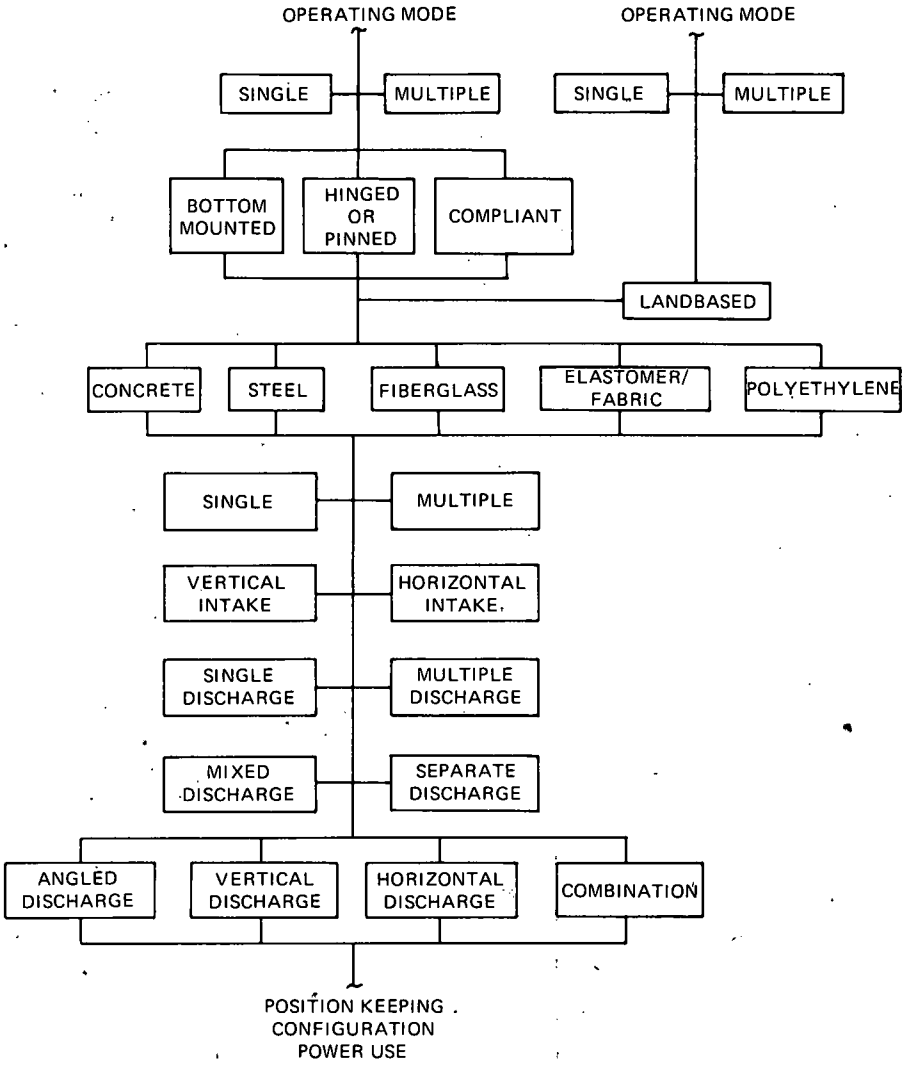

Fig. 2 Design options for OTEC intake/discharge systems.

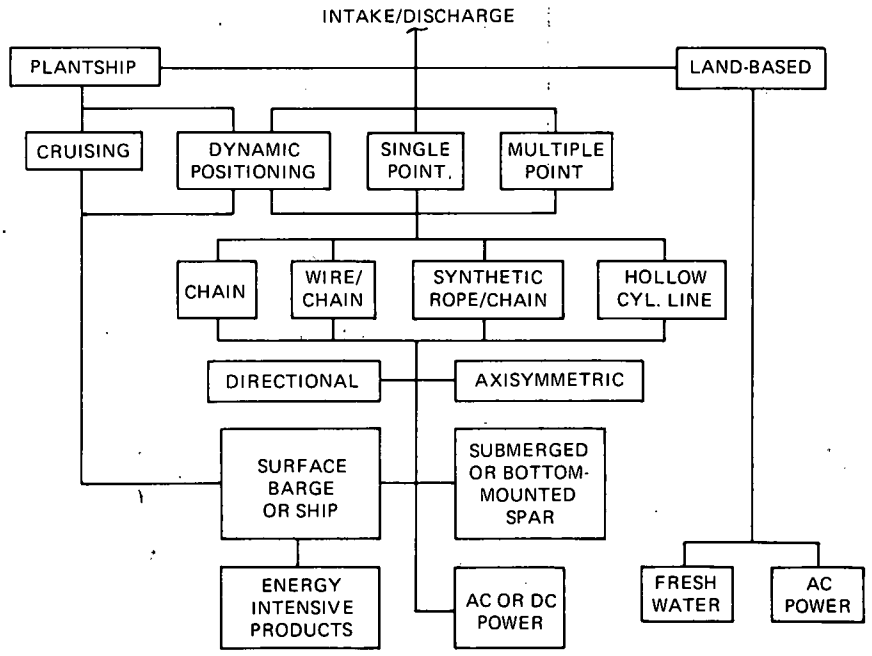

Fig. 3 Design options for station keeping, configuration, and power use for OTEC plants.

of optimal platform size, type, and cost, to the problem of estimating a realistic level of Federal involvement in the development, demonstration, and deployment.

In the programmatic EA scenario, mixes of the various platform types and power cycles are projected for deployments. For baseload electricity, the deployment scenario prepared by Jacobsen and Manley[14, 15] is used. It bases OTEC power entry to the southeast continental U.S. grids on the amount of previously installed island capacity, which would occur in three phases:

Phase 1 - Two 10-MW_e pilot plants;

Phase 2 - One 50- to 100-MW_e precommercial pilot plant: and

Phase 3 - Combined installed capacity in the 1995 to year 2000 period of 500 to 4,000 MW_e

After the completion of these phases, the total projected power from moored platforms located in the Gulf of Mexico for the southeastern sector in the year 2020 is projected to range from 22 to 72 GW_e as a result of various levels of federal incentives. The moderate incentive calls for 58 GW_e in the Gulf of Mexico by 2020 with a demonstrated island capacity of 500 MW_e in 1995. This amount of power represents an 8% to 25% displacement of the projected baseload market in 2020 in the OTEC target area. Approximately 146 platforms of 400-MW_e size would be required to produce this amount of power. Because of the limitations for deep ocean mooring and the requirement for an annual average $\Delta T \geq 20^{\circ}C$, the available space in the Gulf of Mexico will be limited by both the local bathymetry and the possible environmental interactions among the plants.

Table 1. Candidate Regions for Siting of the Three Types of OTEC Platforms

Platform type			
Plant-ships	Land-based	Moored	Region
x	x	x	Hawaiian Islands
x	x	x	U.S. Trust Territories including Guam, American Samoa, and the Marianas Islands
x	x	x	Puerto Rico and the Virgin Islands
x		x	Gulf of Mexico, incl. FL, AL, LA, AR, and TX
x			South Atlantic $\geq$200 miles east of Brazil or west of Africa
x			Pacific $\geq$ 200 miles west of Central America

While the studies reviewed[11-15] were based on closed-cycle systems, open-cycle systems may prove to be more cost-effective for some uses, particularly when fresh water is desired as a byproduct.[16] Thus, open-cycle platforms are included in the present assessment.

For ammonia plant-ships, General Electric[13] estimated the demand for ammonia to increase by an annual rate of 3%. If new demand after 1990 is provided by OTEC plants, 10 platforms of 400-MW_e size would be needed by 1995, 12 more by 2000, and a continual addition of 2 or 3 per year thereafter (regarded as a conservative estimate by General Electric), which means that 72 plants could be operational by 2020. These plants will "graze" in the Atlantic and Pacific Oceans within approximately 20 degrees of the equator, or will be on or moored near tropical islands.

For aluminum, General Electric projected an annual growth of 4.9%. If all new aluminum demand in the 2000-2025 period were provided by OTEC plants, some 154 plants of 400-MW_e size would be required. The reserves for bauxite, which is the ore converted to aluminum, exist primarily in Australia, Jamaica, and South America, with lesser quantities reported in Asia and West Africa.[12] Correspondingly, the primary locations of plants are in the South Atlantic and the South Pacific, with a few to be located in the Gulf of Mexico and North Pacific by 2020.

Social and Cultural Issues

The social and cultural concerns related to OTEC siting must be assessed next. The areas within the 200-mile economic resource zone (ERZ) surrounding the U.S. and its territories and possessions are under evaluation. Surrounding the Pacific Trust Territories, and encompassed within the ERZ, is the highest ΔT water in the world. For land-based or moored plants located in high population or tourism environments, land use and visual effects will be important. An OTEC plant 70 m high would be visible 28 km offshore to an individual at sea level. This observation provides a rough rule of thumb for the distance from shore to which offshore OTEC platforms would have to be architecturally pleasing. Also, the presence of sacred or culturally significant areas may preclude OTEC siting. Relative to other countries, plant-ships are considered to graze the world's oceans beyond the 200-mile ERZ's.[3,14]

Environmental Issues

The key environmental issues may be divided into the following generic categories:

1) Institutional/management issues
2) Oceanographic site/region characterization
3) Impact evaluation
4) Monitoring to evaluate impact
5) Health and safety

The forward planning of OTEC design considerations related to the environmental features of a specific region will preempt or mitigate severe environmental conflicts. Among the institutional or management issues are the coastal zone management (CZM) plans or policies and the discharge or siting Federal Permits. Most of the U.S. territories have completed their CZM Environmental Impact Statements but these studies require close scrutiny to evaluate potential conflicts.[2] On an international basis, the Law of the Sea negotiations have not resolved the OTEC-related issues.

Oceanographic data for the Gulf of Mexico, Puerto Rico, Hawaii, the South Atlantic east of

Brazil, Guam, and the Pacific subtropical ocean are being pooled by their predominant features. Environmental impacts will be considered with these data for a single moored plant, single land-based plant, a cluster of 8 moored plants, and a total of 18 clusters of plants in the Gulf of Mexico case.

Environmental issues are divided into air quality, water quality, and land effects. Air quality effects include the release of carbon dioxide from redistribution of ocean waters and the release of ammonia, chlorine, and other gases from the plant. Water quality impacts include: platform attraction; ocean redistribution from ocean mixing of nutrients and temperature; release of trace elements from erosion and corrosion; organism impingement and entrainment; trace releases of oil, grease, and wastewater; cable and mooring implantation; working fluid leaks; and biocide release. Land effects may result from construction and changes in land use. Each of these issues is presently under thorough evaluation. Progress to date for each will be presented for the generic platforms.

REFERENCES

1. Dugger, G. L., editor, Proceedings of the 6th OTEC Conference, Washington, D.C., June 19-22, 1979, Applied Physics Laboratory, The Johns Hopkins University, Laurel, MD 20810, for the U.S. DOE Dept. of Central Solar Technology, Nov. 1979:

   a) Svenson, N. A., "An Overview of the OTEC-1 Design," Vol. I.

   b) Friedman-Sinay, L. and Reitzel, J., "Environmental Impact Assessment for OTEC-1," Vol. II.

   c) Wolff, W. A., Hubert, W. E. and Wolff, P. M., "OTEC World Thermal Resource," Vol II.

   d) Hill, F. K. and Dugger, G. L., "Use of Satellite-Derived Sea Surface Temperatures by Cruising OTEC Plants," Vol. II.

   e) Harlow, E. H., "OTEC Power for Ocean Minerals," Vol. I.

   f) Jacobsen, W. E. and Manley, R. N., "Analysis of Prospects for OTEC Commercialization for Baseload Power," Vol. I.

   g) Rabas, T. J., Wittig, J. M. and Finsterwalder. K., "OTEC 100-MW_e Alternate Power Systems Study," Vol. I.

2. Sands, M. D., "Progress Report for the Environmental Assessment Program for the 1-MW_e Early Ocean Test Platform," N. Veziroglu, editor, Proceedings of the Fifth OTEC Conference, Feb. 20-22, 1978, Miami Beach, FL, University of Miami, Coral Gables, FL, pp. III-186-202.

3. U.S. Department of Energy, "Environmental Development Plan (EDP) Ocean Thermal Energy Conversion 1977." Available as NTIS DOE/EDP-0006, Springfield, VA, 1978, 48 pp.

4. Sands, M. D., Andrews, M., Howard, M. K., Smookler, M. and Sullivan, S. M., "Draft Environmental Impact Assessment--OTEC Preoperational Ocean Test Platform," U.S. Department of Energy Contract No. EG-77-C-06-1033, 1978, 2 volumes, 381 pp.

5. Council on Environmental Quality, "National Environmental Policy Act," Federal Register, November 29, 1978, 43(230):55978-56007.

6. U.S. Energy Research and Development Administration, "Part 711--Guidelines for Environmental Review," Federal Register, January 26, 1977, 42(17).

7. U.S. Department of Energy, "Ocean Thermal Energy Conversion Program, FY 1977 Program Summary," Division of Central Solar Technology, Washington, D.C., DOE/ET-002/1, Feb. 1978, 201 pp.

8. U.S. Department of Energy, "Ocean Systems Program Summary," Office of Solar, Geothermal, Electric and Storage Systems, Washington, D.C., DOE/ET-0083, 1979, 269 pp.

9. U.S. Department of Energy, "OTEC Objectives and Status Conference: (1) Early Applications and Environment, (2) Later Applications and Program Support, (3) Longer Range Research and Summary," The Johns Hopkins University/Applied Physics Laboratory, Laurel, MD, 1979, 3 volumes, 689 pp.

10. U.S. Department of Energy, "OTEC Thermal Resource," Division of Central Solar Technology, Washington, D.C., Contract No. ET-78-C-01-2898, 1978

11. State of Hawaii, Department of Planning and Economic Development, "Hawaii and the Sea," 1974, 111 pp.

12. Washom, B. J., Niles, J. M., Lutz, R. E., Nachtigal, D. and Schmidhauseer, J. R., "Incentives for the Commercialization of Ocean Thermal Energy Conversion Technology," U.S. DOE, Washington, D.C., PB-268097, 1977, 353 pp.

13. General Electric Company, "Ocean Thermal Energy Conversion Mission Analysis Study: Phase I," Volumes I and II, Tempo Center for Advanced Studies, Washington, D.C., ERHQ/2421-77-1, 1977.

14. Francis, E. J., "Investment in Commercial Development of Ocean Thermal Energy Conversion (OTEC) Plant-Ships," The Johns Hopkins University/Applied Physics Laboratory, Laurel, MD, for U.S. Department of Commerce, 1977.

15. Jacobsen, W. E. and Manley, R. N., "OTEC Commercialization Analysis," The MITRE Corporation, Metrek Division, McLean, VA, Draft, 1979, 132 pp.

PRELIMINARY RESULTS OF A PROGRAM TO STUDY OTEC OCEANIC ENVIRONMENTAL PARAMETERS AT PUNTA TUNA, PUERTO RICO

Gary C. Goldman* and Daniel Pesante**

Center for Energy and Environment Research
University of Puerto Rico
College Station
Mayaguez, Puerto Rico 00708

Abstract

Measurements of pertinent OTEC oceanic parameters are being taken on a bimonthly basis at Punta Tuna, Puerto Rico. To date, four cruises have been conducted, and this paper will attempt to discuss the up-to-date analyses. The emphasis in the paper shall be those data which are probably most meaningful to the plant designers, such as surface temperature, thermal resource, Mixed Layer Depth, salinity, current profiles, and zooplankton. The surface temperatures seen so far are compared to the historical data, with no significant differences. The thermal resource values seen appear to indicate that the literature values may have tended to be somewhat conservative. The Mixed Layer Depth frequently was seen to range deeper than expected by the literature values. The observed salinity values were consistent with the historical values. As there is virtually no existing historical-current profile data, the results of this program is revealing many interesting situations. Apparently the water column has considerable variation in both direction and speed. Also, some tidal influence is seen. With regards to zooplankton, at this early stage, most common copepoda are beginning to be recognized, varying both with time and depth. Finally, suggestions are made as to statistical improvements in the zooplankton program and future work at this and other OTEC sites for the collection of data for both designers and environmental purposes.

Introduction

Currently, the University of Puerto Rico's Center for Energy and Environment Research is conducting a measurement program under contract with the U.S. Department of Energy to study the variability of oceanic parameters relatable to an OTEC plant at the potential OTEC site at Punta Tuna, Puerto Rico (Figure 1). This paper, describes some of the preliminary results of this program. But first, the reader should understand the scope of the existing OTEC oceanographic program at the CEER.

Besides this field program, CEER has a small project that is funded by the Puerto Rico Power Company to duplicate these measurements at a station south of Vieques, about 35 km from Punta Tuna (Figure 1). This Vieques program is designed to help the designers understand the spatial variation that may be experienced from site to nearby site. The field work for the Vieques program coincides with the cruises of the other oceanographic program. A second, related program, funded by the U.S. Department of Energy, involves implanting current-meter moorings at two sites near Punta Tuna. This current-meter work is being done by the Naval Underwater Systems Center, New London, Conn. The two field programs began in the summer of 1978, and the current-meter program began in January, 1979.

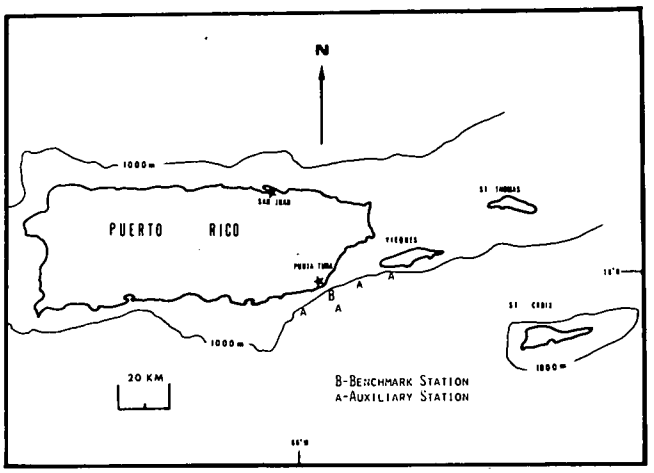

Fig. 1 - Puerto Rico and Vicinity with 1000 m Deep Contour and Stations Visited.

The Fourth program is somewhat different in nature. The OTEC/Biofouling and Corrosion group has contracted the Center to place a vessel/research platform (40 m long LCU) in 1150 m deep water at the Punta Tuna site. The purpose of this project is to duplicate the biofouling and corrosion studies that have been made elsewhere, as well as develop long-term measuring capabilities at sea. The LCU is scheduled to begin operations early this fall. As this effort is being conducted aboard a seaworthy vessel, tied continuously to a fixed deepwater mooring, the vessel can also be used for any other oceanographic measurements. The actual mooring buoy for the LCU has been in place since September of 1978, and the other oceanographic measurement programs have been using this buoy to secure our vessel on every cruise since that time.

The CEER OTEC oceanic measurement program is not quite a year old, having started about the first of August, 1978. Bimonthly cruises are conducted to the Punta Tuna area, where we stay on station for 2-4 days. During that time, we take hydrocasts, temperature, XBT (expendable bathythermographs), STD, plankton casts, and perform transmission and water current profiles. All the above samples and data are collected while secured to the mooring. While apart from the moor, we take horizontal plankton tows, XBT, STD, and current profiles at two or three

*Project Director
**Senior Associate

nearby stations. We also duplicate at least once, the entire data set at the Vieques station. Since the program began, there have been five cruises: August, October, and December 1978, and February and April 1979. This paper shall discuss some of the preliminary results of the first four cruises.

Procedure

The CEER data-taking procedure is similar to, but not exactly the same, as that done at the other OTEC sites. As we understand, one of the similarities is that we spend at least two days at our Benchmark Site (Figure 1, point B). During that time, we collect, or plan to collect, at least six zooplankton tows, four hydrocasts, four water current profiles, two transmission profiles, and an XBT and STD at the time of each of the above. The other sites have no deep water buoy at this time. Also, we plan to visit at least one or two auxiliary stations (Figure 1) and cast an XBT and STD at each, as well as take a current profile at each. Standard methods are used wherever possible.

Over time, our cruise procedure has been modified somewhat, to accommodate the circumstances. To begin with, as CEER/UPR has no STD, and unless we are fortunate enough to cruise on a vessel with an STD, that portion of the cruise plan is usually lost. Also, after our measurement program began, the large surface mooring buoy was placed at our Benchmark station (17° 57.6'N, 65° 51.9'W) to accommodate the future LCU/Biofouling studies. Since this mooring is available, and is at a fixed location (namely our Benchmark station) our procedure now includes securing the vessel to the mooring, after having taken the preliminary horizontal zooplankton tow. We remain at the buoy until all the work is completed for that station. Then, we release from the moor, and collect the second horizontal zooplankton tow. This is followed by our visitation to the auxiliary stations. At these stations, we again were forced to modify the initial procedure. Now we refrain from taking the drifting current profiles, as they were yielding such poor results, as to be virtually meaningless.

During the cruises, we try to collect samples at two different light periods, about noon, and about midnight. We take a hydrocast to 1000 m at each of these periods, a hydrocast to 400 m at each of these time periods, horizontal light transmission profile at each of the periods, and we try to take a horizontal near-surface zooplankton tow during each of these periods. The current profiles are taken at six-hour intervals over a 24 hour period.

During the deep hydrocasts, we sample for temperature (using reversing thermometers), salinity, oxygen, and nutrients (nitrate, nitrite, phosphate, and silicate) using 5-liter Niskin sampling bottles. During the shallow hydrocasts, we sample for temperature, salinity, and chlorophyll.

Preliminary Results of Physical Parameters

Probably the most important parameters to discuss at this stage of the OTEC development are those which will affect the design of the OTEC plant. CEER is also studying the parameters that will indicate how the plant will affect the environment, but much more, the long-term environmental analysis will be necessary before anyone can begin to make any predictions of this nature. Although the data are few and scattered throughout space and time, some ranges of values and trends are starting to develop. These are based on both historical data and CEER results. Probably the most meaningful physical parameters to discuss at this time are the ones constraining the design engineers. These are surface water temperature, thermal resource, mixed layer depth, water current profile, and salinity/density.

Surface Temperature

Numerous investigators (Atwood et al., 1976; Wolff, 1978; Sands et al., 1978) have discussed the surface temperature at the Punta Tuna site. As this is an important aspect of the design, and environmental and climatological criteria, it should be mentioned at this time. While taking at least four, and usually many more surface temperature measurements in the 48 hour period while we are on station, we have not seen any new phenomena that would either change or detract from those already existing data available to-date. Figure 2 contains the ODSI (1977) statistical monthly mean values of surface temperature, with CEER values superimposed. Never did the two values vary by more than 0.35 C°. The shape of the temperature distribution does show the seasonal trend to range from a low of slightly more than about 26°C in the late winter to a high of slightly more than 29°C in the early autumn.

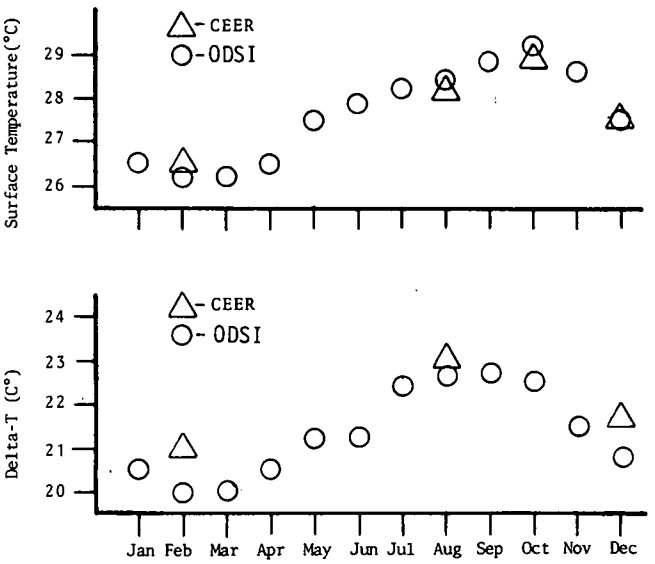

Fig. 2 - Surface Temperature and Temperature Difference from the Surface to 1000 m Depth (Delta-T) at Punta Tuna, P.R.

Thermal Resource

The thermal resource is defined as being the heat energy available between the surface mixed layer and the water at about 1000 m depth. This heat energy is directly relatable to the temperature difference, in Centigrade degrees, between the surface waters and

the 1000 m deep water. It is this temperature difference with which the engineers are designing the thermal engines to run the OTEC power plants. Knowledge of this parameter is somewhat available in the literature (Atwood et al., 1976; Wolff, 1978; Sands et al., 1978; ODSI, 1977). The monthly averages from the literature are shown in Figure 2, as well as our values from three of our cruises. Our values seem to indicate that the historical averages may be a bit conservative, but again, not to any significant amount.

Mixed Layer Depth

This parameter is important to both the design engineers and to the environmentalists. The designers must use great volumes of water to run the power plant. The plant intake openings will have some non-zero vertical dimension. The designers must know to what depth they can reach to maintain the same surface water characteristics, with little or no chance of intrusion of "subsurface" water, to reduce the thermal efficiency or to change the water chemistry in other ways. The environmentalists are aware that the upper mixed layer is usually identified with the Tropical Surface Water, the upper water mass in the Caribbean Sea. This water has certain ranges of temperature, salinity, and light transmission. Also, many organisms spend much of their life in or reacting to this water mass. If this water mass is altered, unnaturally, by the presence of one or many OTEC plants, this may affect the natural balance between predator and prey, or between flora and fauna, in ways man can not even begin to understand.

The actual definition of the Mixed Layer Depth (MLD) varies from person-to-person, group-to-group. Molinari (1979) defines the MLD as "the depth to the center of the first depth interval in which the temperature changes by 0.3 C°." This definition is very tight in terms of temperature, but also leaves room for much ambiguity in the definition of the other words used. Sands et al., (1978) on the other hand, uses a definiton that is easier to understand and use, but not as thermally restrictive. Sands says the MLD is the depth where the temperature drops 1 C° from the surface water value. Unfortunately, the latter definition could result in a great loss of thermal efficiency in an OTEC power plant. The MLD may also be defined in terms of salinity, instead of temperature (Lee et al., 1978).

Using the thermal criteria of Sands, a drop of 1 C° from surface value, we can show how the depth of the MLD has varied, both from cruise-to-cruise, and over the four cruises, by looking at the cast-to-cast range. The criteria of a change of 1 C° is not difficult to justify, as usually the temperature is virtually invariant with depth to the lower limit of the MLD. Then the temperature undergoes a great change within a small vertical distance, overcoming both the 0.3 C° and the 1 C° criteria at about the same depth.

Figure 3 shows the results of the data compiled by ODSI (1977). Shown are the most probable values and the maximum and minimum values seen in the literature. CEER values are superimposed in this Figure for comparison. The noteworthy points to see are those two cases in which the maximum depth of the MLD, as we measured it, exceeds that seen before. The more frequent data supplied by cruises like ours, and the data taken often at the same location over a 48 hour period, are seeming to help expand the statistical sampling base.

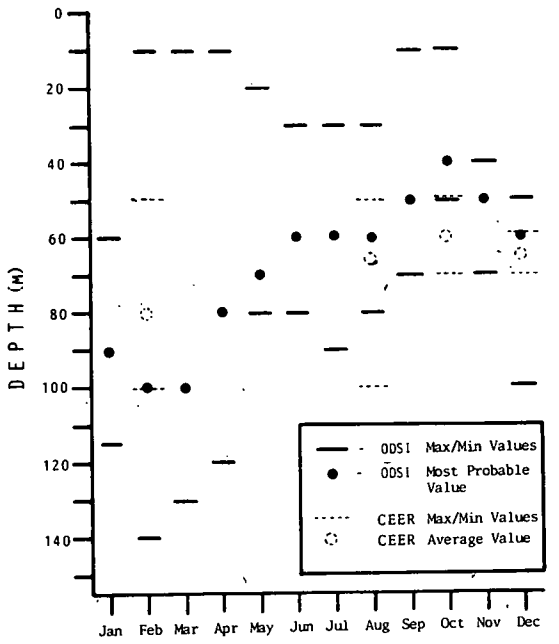

Fig. 3 - Values of Mixed Layer Depth for Literature (ODSI, 1977) and CEER Measured Vieques at Punta Tuna, P.R.

Salinity/Density

Salinity throughout the water column is important, as it concerns the source of the particular water mass, and its density. The density is important, as it is the parameter that will ultimately determine the depth at which the OTEC exhaust water will settle.

In general, the literature (Sands et al., 1978; Haminski, 1975; Shanley & Duncan, 1972) shows considerable variations in the salinity of the upper waters, both as a function of time and depth. As examples let us discuss the surface and 50 m depth and their variations of salinity. Figure 4 shows many of these results together. For the sake of simplicity, and because of the specific grouping of some of the historical data, this Figure shows the year divided into four seasons, of three months each. The surface and 50 m depth values are shown, as they are the values most likely to be used to design the intake of an OTEC power plant.

Initial observations of the Figure indicate that the range of surface values of salinity usually exceeds the range of values for the 50 m depth. The values of surface salinity depend on the spatial and temperal distribution of precipitation, evaporation, and solar insolation, which in turn, are somewhat seasonally dependant. Also, the surface salinity is somewhat affected by the large freshwater inputs from the Amazon and Orinoco Rivers, in South America. The salinity values of the 50 m depth are less affected by the above conditions, but are probably more affected by the thickness of the MLD and the climatic

conditions. In oceanic, tropical areas, normal variations in atmospheric pressure are very small, compared to temperate areas--a 0.2 inch of mercury change over a couple of months is normal. During large tropical weather systems, such as tropical depressions, waves, storms, or hurricanes, the pressure is reduced considerably, causing a rise in the water surface. This consequentially pulls the lower water masses upward (specifically, the Subtropical Underwater, lying directly beneath the Tropical Surface Water). The underlying water may actually penetrate the water surface. Considering all these factors, it is not surprising to see such large variations in the surface-water salinity.

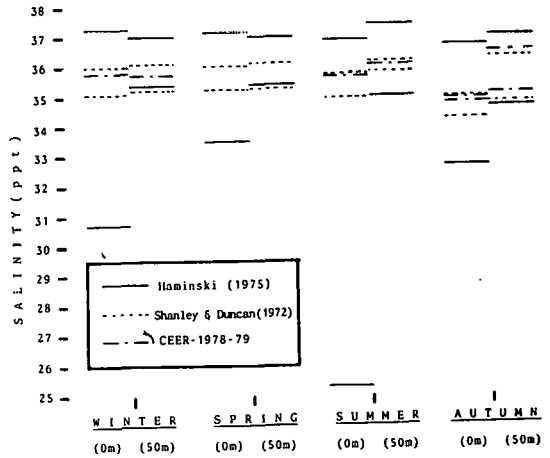

Fig. 4 - Variations in Salinity Throughout the Year at the Surface and 50 m Depth at Punta Tuna, P.R.

In general, the salinity at 50 m is usually higher than that at the surface. The reason for this is not only as seen in the above discussion, but also, as the temperature changes very little over this depth, the more dense, higher salinity water will be found beneath the less dense surface water. The water mass directly beneath the Tropical Surface Water, the Subtropical Underwater, has the highest salinity of any water in the entire water column in the Caribbean Sea.

The Figure also shows the trend to low surface salinities in the wetter, late summer, through early winter. As spring approaches, the salinity increases somewhat. The salinity at the 50 m depth does not seem to show as much seasonal variation as does the surface water. In the wetter, more frequent storm period of late summer and autumn, there appears to be greater excursions of values seen for the 50 m depth salinity.

As an OTEC power plant intake system may be drawing in the water over a 10-20 m vertical extent, these salinity variations with depth are important. They not only affect the chemistry of the water, they also affect the density of the water, and at what depth the exhaust water will settle.

Water Current Profiles

As of this reporting, CEER's water current profile measurements have not been well analyzed. We have made profile measurements while drifting and while tied to the mooring. Only those made while moored shall be reported here.

Figure 5 shows the results of some of the CEER water current profile data for October and December, 1978, and February, 1979. Also, data taken from two moored arrays, described in Burns & Car (1975) are shown with our February data for comparison.

For the October cruise, the data presented shows two measurements taken on 11 October. At 1300 hr, the wind was coming from the southeast at about 5 m/sec. At that time, the upper 50 m was moving westerly, and the water from 75 m to between 150 m-250 m was moving easterly. Below that, the water again was moving westerly. During the set taken at 1900 hr, the wind was out of the northeast at about 10 m/sec. The upper water was moving easterly and the water from 100 m downward was moving westerly. The two measurements were taken at times that coincide with the maximum flood and ebb tide currents (1300 and 1900 hr, respectively NOS, 1977; NOS, 1978). According to the tidal current tables above, the flood tide will probably move westerly, and the ebb tidal current will probably move easterly in that area. These are the directions seen in the upper waters for the October data set in the Figure.

The December data set were taken at about 8 hours apart on 2-3 December 1978. Both of these two measurements were taken during slack tidal current period. During these periods, the upper water seems to be moving northwest, in spite of the wind coming from the northeast at 7-8 m/sec. The water between 100 m and 250 m depth is moving easterly on 2 December, then reverses itself 8 hours later. The lower portion of the water column is moving westerly, with the anomalous northerly value at 700 m depth on 3 December.

The final set of measurements were taken on 11 February at 1900 hr and 2400 hr. These periods again coincide with slack tidal current. The wind was out of the northeast at about 5-6 m/sec. The entire water column seems to show considerable variation, both from each other and from the other data. Any attempt to fully interpret this data set has thus far proven unsatisfactory. Included with the February data set are the results of two current meter moorings, one from March 1967, and the other from March 1972. These two moorings were both in the water for about 20 days. Generally, the moored instruments show a westerly direction most of the time, and except for the 100 m depth meter, the frequency of recorded events not showing westerly direction was quite small. The upper meter shows about 20% of the time being spent toward the east. This may be due to the tidal current in the area, but others (Lee et al., 1978) have also reported easterly movements in the upper waters.

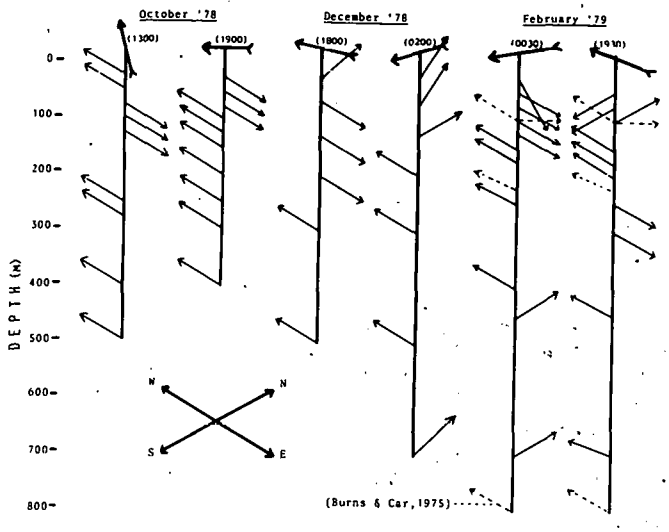

Fig. 5 - Current Profile Results from Three Cruises and One Mooring (Burns & Car, 1975) at Punta Tuna, P.R.

Zooplankton

As part of the environmental studies conducted at Punta Tuna, plankton is being collected to observe which members of the zooplankton community are present and to try to assess the zooplankton dynamics. Samples are collected on a bimonthly basis, during the above mentioned cruises. The depths being sampled are: 1000-800 m, 800-200 m, 200- surface, 1000- surface, and two horizontal tows at 25 m, one during the day, and one at night. The vertical hauls are made while the vessel is moored. The 25 m deep horizontal tows are taken while underway at approximately 3 knots.

The net that is used has a .75 m diameter opening, with a 5:1 length to diameter ratio. The mesh size is 202 microns. The nets are coupled to a General Oceanics "Double-Trip Mechanism", to enable the net to be opened and/or closed remotely. The collected samples are preserved in 4% buffered formaldehyde solution. The specimens are later identified and measured. The copepods are identified to species, while all other organisms are identified to family. All the plankters are measured to determine their length.

Subsamples are handled in the following way. From a particular sample, an aliquot is made and taken to a convenient volume, depending on the number of plankton present. This may range from 200 to 1000 ml. Subsamples are then drawn from this new concentration and the size of the final subsample for analysis varies from 1 to 12 ml, in order to contain from 300 to 400 copepods. As the present program stands, only one such subsample is being analyzed per sample.

Table 1

Most Common Species of Copepods as a Function of Depth, Seen at Punta Tuna, P.R.

1000-800 m	Clausocalanus arcuicornis
	Haloptilus longicornis
	Oithona plumifera
	Pleuromama abdominalis
	P. piseki
800-200 m	Oithona plumifera
	Oithona spp.
	Pleuromama abdominalis
	P. piseki
	P. xiphias
200-sfc	Calocalanus pavo
	Clausocalanus furcatus
	Mecynocera clausi
	Oithona plumifera
	Paracalanus parvus
25 m	Acartia tonsa
	Calocalanus pavo
	Clausocalanus furcatus
	Coricaeus spp.
	Farranula gracilis
	Mecinocera clausi
	Macrosetella gracilis
	Oithona plumifera
	Oncaea mediterranea
	Oncaea venusta
	Paracalanus parvus
	P. aculeatus
	Temora turbinata
	T. stylifera
	Undinula vulgaris

Results of Zooplankton

Due to insufficient statistics, and the few number of samples and cruises carried out to date, we have only a relative idea of the species present, and some very approximate numbers of the quantities present. Some species have been observed to be most common or dominant. Table 1 summarizes these most commonly seen copepod species at the various depths. Larvaceans, caridean larvae, ostracoda, and chaetognatha are among the most common members of the zooplankton present at the site, particularly in the upper 200 m. As of now, 60 species of Copepoda have been identified from the Punta site. This fact shows that the sampling regime is not adequate, as that area should have yielded up to 200 species, if not more, according to Owre and Foyo (1967). A typical tow includes plankters seen in Table 2. These are both holoplankton and meroplankton.

Table 2

Plankters seen in a typical tow at Punta Tuna

ALIMA
AMPHIPODA
CARIDEAN LARVAE
CHAETOGNATHA
CLADOCERA
COPEPODA
  calanoid
  cyclopoid
  harpacticoid
CTENOPHORA
CYPHONAUTES
DOLIOLARIA
ECHINOPLUTEUS
EPHYRA LARVAE
EUPHAUSIDS
LARVACEA
MEDUSAE
MYSIDACEA
NAUPLIUS LARVAE
OSTRACODA
PAGURID LARVAE
POLYCHAETA
PTEROPODA
SIPHONOPHORA

Conclusions and Recommendations

From the results in Puerto Rico so far, we can conclude that we are only beginning to learn about the physical and biological environment at Punta Tuna. And OTEC has not even begun to look at the geology and chemistry of the area.

The Mixed Layer seems to vary considerably in time. There are apparent seasonal changes in temperature and salinity. There are also variations in depth. The thermal resource, part of which is contained in the Mixed Layer, also has seasonal variations. Furthermore, it seems there are even variations in the 1000 meter deep water temperature. Water currents in this area are still virtually unknown. Lastly, CEER's zooplankton program has done little to increase the understanding of the area, due to the lack of statistical validity of our present methods.

We therefore would like to make some recommendations to enhance the collection of information and understanding of the oceanic processes in the area.

The Mixed Layer must be studied much more intensively for short term variations in both temperature and depth. This might be accomplished easily from the moored platform on a 3-6 hour interval basis.

The cold water temperature has shown enough apparent variation to justify monthly observations with 3-6 replications for reliability.

As remote sensing is a reliable, inexpensive method of collecting sea surface temperature, this tool should be exploited to a greater extent. Careful ground truth measurements can enhance even marginally acceptable infra-red data to the level of acceptability. Furthermore, as we improve understanding of the thermal structure of the upper waters, the remotely sensed data will become even more valuable. Planned measurements, coordinated with overpass events, should be carried out as frequently as possible.

Climatic variations, such as wind, atmospheric pressure, and temperature should be correlated closely with changes in the Mixed Layer temperature and depth. This would involve low frequency, but faithful monitoring of these variables on site.

Water currents must be measured for a variety of reasons, and in a variety of ways. Moored array (eulerian) measurements are necessary at Punta Tuna to help determine the stress on the cold water pipe. High frequency data is probably not necessary. But, several depths must be monitored at the same time. These depths can be either combinations or compromises between the probably water mass movements, and the major stress criteria of the pipe. Also, langrangian measurements are needed to understand the trajectory of water at given depths as it leaves the plant site. Of specific importance are the upper waters, and the water immediately below the thermocline.

Waves, both surface waves and internal waves, have been almost completely ignored. Except for some historical analysis and hindsight predictions, the waves have not been studied. This phenomena must be measured, to protect the mechanical structures, personnel, and the thermal efficiency of the plant. Wave riders might be deployed from the mooring buoy or the LCU to look at the surface waves. Thermistor strings should be suspended from the LCU to observe the frequency and amplitude of any internal waves that might affect the plant. As the area is near a very steep slope, reflection of these internal waves may also prove to be problematic to plant operation.

The zooplankton program also needs expansion. Monthly, or more frequent intervals, rather than the present bimonthly collection should be implemented. This would help clarify the plankton dynamics. The sampling time at each depth should be extended by a factor of 2 or more. Although zooplankton are mainly drifters, sampling should be extended away from the site to develop a "basin wide" understanding of the biota. Also, high frequency sampling should be attempted for a short time to examine the validity of any low frequency sampling program. Finally, laboratory subsamples should be analyzed in triplicate, to determine the variance between the subsamples, and subsequently, determine if the subsamples and the original sample is representative.

If the results of the measurement program at each of the OTEC sites are to be comparable, they must be done in the same, or comparable ways. Although the locations and conditions are different, a common methodology must be developed or decided upon, that gives the scientist and engineers an interchangeability from site to site.

Finally, as we begin to develop more understanding of each of the locations, we must not loose sight of the relationship of that location, and the OTEC plant or plants and their larger impacts. Large scale measurement programs should be started to develop norms over large possible impacted areas. As the area increases, the variation will probably also increase. To assure ourselves that the operation of an OTEC plant is actually producing or not producing, some far, downstream effect, we must have looked

downstream before the plant existed.

References

Atwood, D. K., P. Duncan, M. Stalcup & M. Barcelona. 1976. Ocean Thermal Energy Conversion: Resource Assessment and Environmental Impact for Proposed Puerto Rico Site. University of Puerto Rico, Mayaguez, P.R. NSF Grant #75-000145, 105 pp.

Burns, C. A. & M. Car. 1975. Current Meter Data Report for the Eastern Part of the Caribbean Sea. Naval Oceanographic Office, Physical Oceanography Division, Washington, D.C. Tech Note 6110-6-75, 185 pp.

Haminski, S. J. 1975. Temperature, Salinity, Oxygen, and Phosphate in Waters off Eastern Central America and Northern South America. NODC, Washington, D.C. 189 pp.

Lee, T. N., R. S. C. Munier, & S. Chiu. 1978. Water Mass Structure and Variability North of St. Croix, U.S. Virgin Islands, as Observed During the Summer of 1977 for OTEC Assessment. University of Miami, Resentiel School of Marine and Atmospheric Science. Tech Report #78004, 81 pp.

Molinari, R. & F. Chew. 1979. Ocean Thermal and Current Structure in the Tropical South Atlantic Relative to the Placement of a Grazing OTEC Plant. NOAA Tech Memo ERL-AOML-35, 57 pp.

National Ocean Survey (NOS). 1977. Tidal Current Tables 1978; Atlantic Coast of North America. Rockville Md. 214 pp.

National Ocean Survey (NOS). 1978. Tidal Current Tables 1979; Atlantic Coast of North America. Rockville Md. 218 pp.

Ocean Data System, Inc. (ODSI). 1977. Ocean Thermal Resource Report for Puerto Rico. ODSI. Monterez, California, 39 pp.

Owre, H. E. & M. Foyo. 1967. Copepods of the Florida Current. Fauna Caribaea Number 1. Crustacea, Part 1: Copepoda Institute of Marine Science, University of Miami. 137 pp.

Sands, M. D., M. Andrews, M. K. Howard, M. Smookler, & S. M. Sullivan. 1978. Draft Environmental Impact Assessment-Ocean Thermal Energy Conversion (OTEC) Preoperational Ocean Test Platform. Interstate Electronics Corp. Anaheim, Ca., under contract to U.S. Dept. of Energy #EG-77-C-06-1033, Volume I, II.

Shanley, G. E. & C. Duncan. 1972. Hydrographic Data for Caribbean Sea and for Pesca Serial Station at 17° 38'N, 67° 00'W for 1971. University of Puerto Rico, Dept. of Marine Science, Mayaguez, P.R. 34 pp.

Wolff, P. M. 1978. Temperature Difference Resource. In Fifth Ocean Thermal Energy Conversion Conference, 20-22 February, 1978. Miami Beach, Fla. pp III-11 to III-37.

DISCUSSION

Comment: I might interject a comment for those of you who are not familiar with the problem. Gary recognized that one can calculate the neutral point for these two mixed water masses, i.e., where they would end up if you could enclose them in plastic bags and dump them into the ocean. The fact is, as I indicated earlier, that where there is mixing, there is entrainment of the surface waters, which are of lesser density, so the water will not end up at the depth you would calculate by that simple equilibrium calculation. Gary was acknowledging that calculation to the modeling types. And the other point that he made was quite valid, that that kind of information or the variability of mixed-layer depth and density structure of the earth is quite important to mixing calculations.

G. Goldman: This was just a simple-minded third step to just show some other conditions that might have to be considered somehow. There had been a number of calculations made of where the plume might end up given a number of potential plant designs, and a number of potential density gradients. As the data come in, we can sharpen those estimates, but we have a fairly good idea that the discharged plume, either from a mixed or evaporated type discharge, is probably going to end up toward the bottom of the mixed layer or below it. That's a very general statement to which there are lots of exceptions.

ENVIRONMENTAL MONITORING AND ASSESSMENT PROGRAM AT POTENTIAL OTEC SITES

P. Wilde

Earth Sciences Division
Lawrence Berkeley Laboratory
University of California
Berkeley, California 94720

Abstract

Ecologically sound operations of projected Ocean Thermal Energy Conversion (OTEC) plants can be insured by careful attention to the marine environment during the design phase. This requires quality information from regions of potential OTEC interest, coordinated with required assessment studies to insure legal compliance. Currently, preliminary or actual surveys and laboratory studies are being conducted in the waters of Puerto Rico, the Gulf of Mexico, Hawaii, and Guam for potential moored or seacoast OTEC plants and in the equatorial South Atlantic for proposed plant-ship operations to provide such benchmark and baseline data. These data plus existing archival information can be used to model effects of OTEC operations based on projected design schemes. Four major areas of concerns (1) redistribution of oceanic properties, (2) chemical pollution, (3) structural effects, and (4) socio-legal-economic; and 11 key issues associated with OTEC deployment and operation have been identified. In general mitigating strategies can be used to alleviate many deleterious environmental effects of operational problems as biostimulation, outgassing, etc. Various assessment research studies on toxicity, biocide releases, etc., are under way or are planned to investigate areas where no clear mitigating strategy is available. Data from the monitoring and assessment programs are being integrated into a series of environmental compliance documents including a comprehensive programmatic environmental assessment.

Purpose

The goals of this paper are to present a logical strategy for the evaluation and eventual monitoring at Ocean Thermal Energy Conversion (OTEC) sites or regions so that

- the effects of an OTEC plant on the environment, and
- the influence of the environment on OTEC operations can be assessed.

This should result in information which can be used by engineers, designers, and planners to insure practical, safe, and efficient operations of any OTEC plant and provide sufficient justification for operational permits for OTEC plants from the involved regulatory agencies.

Environmental Concerns

The four major classes of environmental concerns and the key issues in these classes associated with OTEC deployment and operation are:

- redistribution of oceanic properties (ocean water mixing, impingement/entrainment, climatic/thermal)
- chemical pollution (biocides, working fluid leaks, corrosion)
- structural effects (artificial reef, nesting/migration)
- socio-legal-economic (worker safety, enviro-maritime law, secondary economic impacts).

The potential changes in the oceanographic properties of sea water due to OTEC pumping operations are a major environmental concern. Because large amounts of cold deep water and warm shallow water will be pumped to the heat exchangers, likely at some third depth; parameters such as temperature, salinity, density, dissolved oxygen, nutrients, carbonates, particulates, etc. will be modified by mixing with ambient ocean water in the vicinity of the eventual discharge. Discharges in the photic zone may cause biostimulation due to the increased nutrient contribution from the deep waters, with potential changes in either the size, relative abundance or species composition with respect to the resident marine population resulting in secondary effects on the food web. Displacement of sea water also could have toxic effects on ambient species by the introduction of trace chemical substances such as trace metals, organic decay products, etc., from other depths. Certain species, particularly those with low mobility, will be harmed by impingement/entrainment in the pumping system either by contact with the screens and walls of the pipe/heat exchanger system or by the pressure and temperature changes encountered in transit of the system from intake to discharge. Surface discharges may produce climatic effects by alteration of the air-surface-water-temperature ratio. Such an alteration, at sufficient scale such as in an OTEC park, could affect the microclimate by modification of locally generated winds and currents. Long-term operation of a large number of OTEC plants could result in reduced available heat due to the thermal extraction. Surface discharges also could enhance the release of CO_2 and other gases dissolved in cold deep waters with potential climatic effects for large scale operations. This is particularly true for open cycle systems where gases even normally dissolved in the surface ocean, must be separated from vaporized sea water so that gas bubbles do not impede plant efficiency. Such gases will be vented into the atmosphere potentially modifying the local microclimate as discussed above. However, subsurface discharges below the surface mixed layer in the pycnocline could mitigate all or most of the potential problems associated with surface discharges.

Chemical pollution could result as functions of various OTEC plant operations and maintenance procedures. Of major concern are biocides proposed to keep the system components clean of biological growth. There are alternative ways (various mechanical systems) to clean heat exchanger systems, but these may not clean surfaces to the extent necessary for efficient operation. The major problem with biocides is the levels of concentration needed to impede biological growth in the system which unquestionably will affect organisms in the vicinity of the discharge. Furthermore, if chlorine is used as a biocide and ammonia as a working fluid, accidental combinations of these chemicals can produce compounds even more toxic to ambient organisms than the separate chemicals. Leaks of the working fluid of a closed cycle system also will pollute ambient ocean water. The effects and chemical fate of proposed working fluid leaks into sea water are not well understood. Ammonia, for example, is a nutrient in proper amounts and could stimulate marine growth complicating the biofouling problem. However, the excessive doses associated with a major leak are toxic to both marine and human life. Chemical pollution also will be produced by the corrosive effect of sea water passing through the heat exchanger system. Corrosion would produce metallic ions, and scale particles which could have direct toxic effects or long-term effects through incorporation of corrosion products into the particulate food supply of marine organisms through the process of bioaccumulation.

The physical presence in the ocean of a structure the size of an OTEC system itself has an impact on the ocean. The structure of whatever configuration will become an attractive habitat for a wide range of organisms based on experience from artificial reefs. The long-term effects of the structure on the environment will depend on the types, size, and abundance of the organisms attracted to or attached to the structure and this will modify the local population. Regional effects on populations might occur by either interference with, or modification of, nesting habits or migration pathways.

The first three major classes of concerns chiefly dealt with impacts on marine life. However, there are human consequences of OTEC operations which are grouped here as socio-legal-economic issues. Worker safety is of prime concern regulated by the Occupational Health and Safety Administration (OSHA) and the Coast Guard for strictly marine occupational concerns. Potential work hazards are the chemicals used or produced by the OTEC system such as ammonia or chlorine, foul weather during marine operations, collision and systems accidents. Because of the novelty of OTEC operations standard safety procedures will be augmented by procedures unique to OTEC. The siting of OTEC facilities either in international waters or where the downstream effects of OTEC operations might intrude into international waters, will raise the issues of international rights, economic zones and responsibilities beyond those treated by conventional maritime law and treaties. At present the law of the sea is in a state of flux so that the resolution of potential international issues may be complicated and time-consuming. Probably multilateral agreements or treaties among concerned parties, as is done for fishing rights, may be the interim solution of potential legal problems which may impede OTEC operations. Finally, the construction and operations of an OTEC facility may affect existing social and institutional structures. New jobs will be created and shore-based "boomtown" growth may occur with its associated impacts on housing, education, sanitation, etc. The electrical energy produced by OTEC plants may be transmitted to consumers either by AC or DC transmission lines. The cable needed to transmit this power could have impacts on marine ecosystems at the sea bed and at the shoreline. DC transmission will require two converter facilities, one at sea and one on shore, causing land use problems. If OTEC systems are used to produce energy-intensive products, they will produce air/water emissions typical of those produced in similar land-based industries.

The present and projected status of the resolution of these issues is listed in Table 1. Detailed discussion of these issues is found in the Environmental Development Plan (EDP, 1978) for OTEC.

Present Program

Monitoring

The monitoring strategies are designed for shipboard operations, manned platforms as well as instrumented buoys (Table 2). This program is to be integrated with those proposed by OTEC groups for bio-fouling and corrosion, and by NOAA for synoptic oceanographic parameters. An additional goal is to develop a packaged monitoring program which can be mobilized rapidly to aid in site selection for larger OTEC platforms (Fig. 1). Data collection and monitoring strategies will be done in view of compliance with NEPA and EPA, Corps of Engineers, Coast Guard, etc. regulations.

Specifically the program initiated pre-operational studies in four areas (Fig. 2).

- o Hawaii - one site off the Kona coast (OTEC-1 site);
- o Puerto Rico - one site near Punta Tuna;
- o Gulf of Mexico - regional survey using two station locations: (1) west of Tampa, (2) south of Biloxi;
- o South Atlantic - regional survey, 5-10°S, 20-30°W and affected zone.

In the areas considered for the sea coast or moored OTEC option - Hawaii, Gulf of Mexico, and Puerto Rico - a program has been initiated to take background data before placement of any operating OTEC system in these areas. This is required to insure that baseline information is available to evaluate the effects of OTEC on the ambient environment and to provide environmental data useful in the design of the operating system. At this time, only attractive thermal regions are known with any certainty. It is premature, therefore, to pick exact sites for potential OTEC plants until knowledge of other important environmental siting factors is obtained. Accordingly, for the initial studies each thermal region is divided into subregions in which it is expected that the basic environmental conditions relating to OTEC are spatially homogeneous, although likely to vary seasonally.

Table 1 Issues, required research, and projects

Issues	Required Research	Status of Projects Completed	Current	Planned
Ocean Water Mixing	-Develop computer model to predict the impact of OTEC operations on oceanographic characteristics	2	3	3
	-Establish baseline oceanographic data at potential OTEC test sites	3	2	7
	-Characterize changes in oceanographic characteristics resulting from OTEC test operations	2	2	1
	-Determine impacts of oceanographic changes on site-specific marine ecosystems		4	2
Impingement/Entrainment	-Search existing literature to determine extent of impact at similar ocean water pumping operations		2	1
	-Monitor impacts at OTEC testing sites and define factors responsible for attraction of organisms		2	1
Climatic/Thermal	-Develop computer models to predict impacts of OTEC operation on micro- and macroclimate	2	2	1
	-Characterize site-specific climatic impacts resulting from OTEC test module operations	1	2	1
	-Determine potential increase in levels of atmospheric CO_2 resulting from OTEC operations			1
	-Determine potential microclimate effects of degassing during open cycle OTEC operations			
Biocides	-Survey existing literature to determine impacts of biocides on marine species		2	1
	-Monitor, sample, and characterize biocide discharges during OTEC testing operations		2	1
	-Conduct laboratory tests to determine the effects of varying levels of biocide use on marine ecosystems		2	1
Working Fluid Leaks	-Survey existing literature to characterize impacts of various levels of potential working fluid leaks on marine ecosystems		2	1
	-Monitor, sample, and characterize the extent of working fluid leaks during OTEC operations		2	1
Corrosion	-Survey existing literature to determine effects on marine species of metallic element compounds discharged from heat exchangers constructed of various metals		2	1
	-During OTEC testing operations, monitor, sample, and characterize metallic elements discharged and dispersed into ambient ocean water, and determine the impacts of these discharges on indigenous marine species		1	2
Artificial Reef Nesting/Migration	-Define factors responsible for attraction of organisms		3	1
Worker Safety	-Develop worker safety programs for OTEC facilities using input from land-based facilities using/producing the same chemicals		1	1
	-Develop a warning system for OTEC facilities to prevent collisions with other ocean vessels		1	1
Enviro-maritime Law	-Conduct survey of international law of the sea applicable to OTEC operations; update biennially	1		1
	-Conduct in-depth study of potential legal/institutional issues involving the particular site(s) chosen for OTEC operations			
Secondary Economic Impacts	-Assess the secondary impacts (e.g., land use, air/water emissions, solid wastes) associated with construction of OTEC plants		1	1
	-Assess the socioeconomic impacts of OTEC development	1	1	1
	-Assess the ecological and secondary impacts of electricity transmission			
	-Survey existing literature to characterize air/water emissions expected to be encountered in the production of chemicals at OTEC plants; develop applicable control technologies			1

Table 2 Proposed ecological monitoring strategies

		Time Schedule
STEP I	Pre-OTEC site occupation studies; background sampling of significant ecological and chemical parameters in conjunction with a literature review to define preoperational environmental conditions.	Initiated FY 78 in Hawaii, Puerto Rico, Gulf of Mexico, South Atlantic
	Sampling from survey ships or from fixed moorings.	
	Sampling frequency bi-monthly initially for one year, further sampling frequency to be determined by experience.	
STEP II	Non-interference with Platform Operations	Initiated FY 79 Platform
	No permanent work space on platform	
	Sampling equipment self-contained and transported to and from site	
	Sampling frequency a function of operations schedule	
	All analyses done on beach	
STEP III	Limited interference with platform operations	Plan FY 79
	Limited permanent work space on platform	RFP late FY 79 or Early FY 80
	Sampling equipment and some analytical equipment on site	Operational FY 80
	Most analyses done on beach	
STEP IV	Limited interference with platform operations (crane operations, etc.)	Plan FY 79-80 (experience from Phase I and II)
	Permanent work space in container/vans	
	Power/water from platform but with backup systems	RFP late FY 80
	Operations Van (sensor packages on buoy) A. Wet Lab - sample preparation - gross equipment repairs B. Dry Lab - instruments/analyses/electronic repairs C. Dry Lab II - data reduction/storage/remote monitors	Operational FY 81 (first unit) Additional units as required
	Storage Van (not applicable to buoy) A. Wet Storage - nets, over the side gear B. Dry Storage - equipment, paper C. Sample Storage - refrigerator	

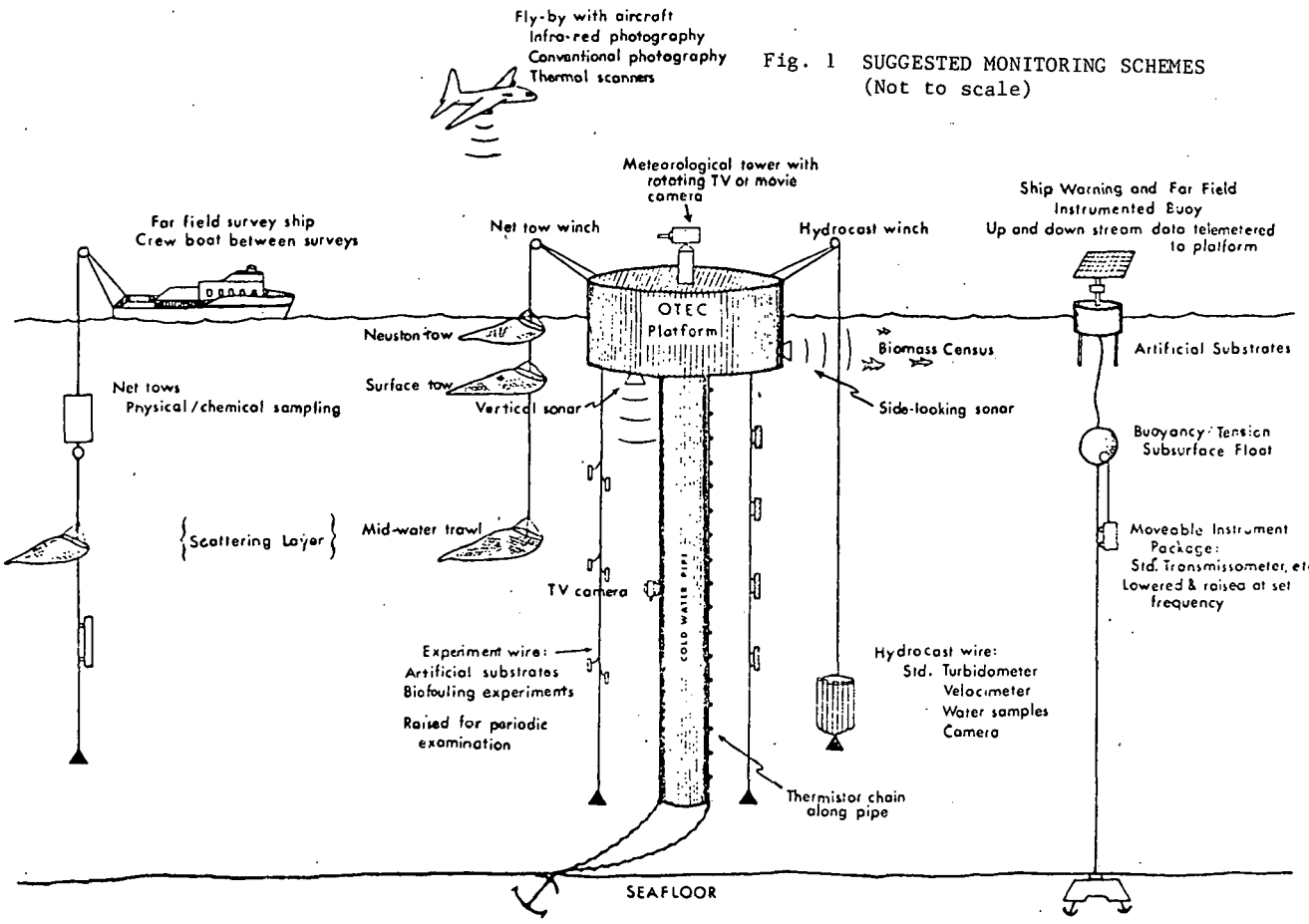

Fig. 1 SUGGESTED MONITORING SCHEMES (Not to scale)

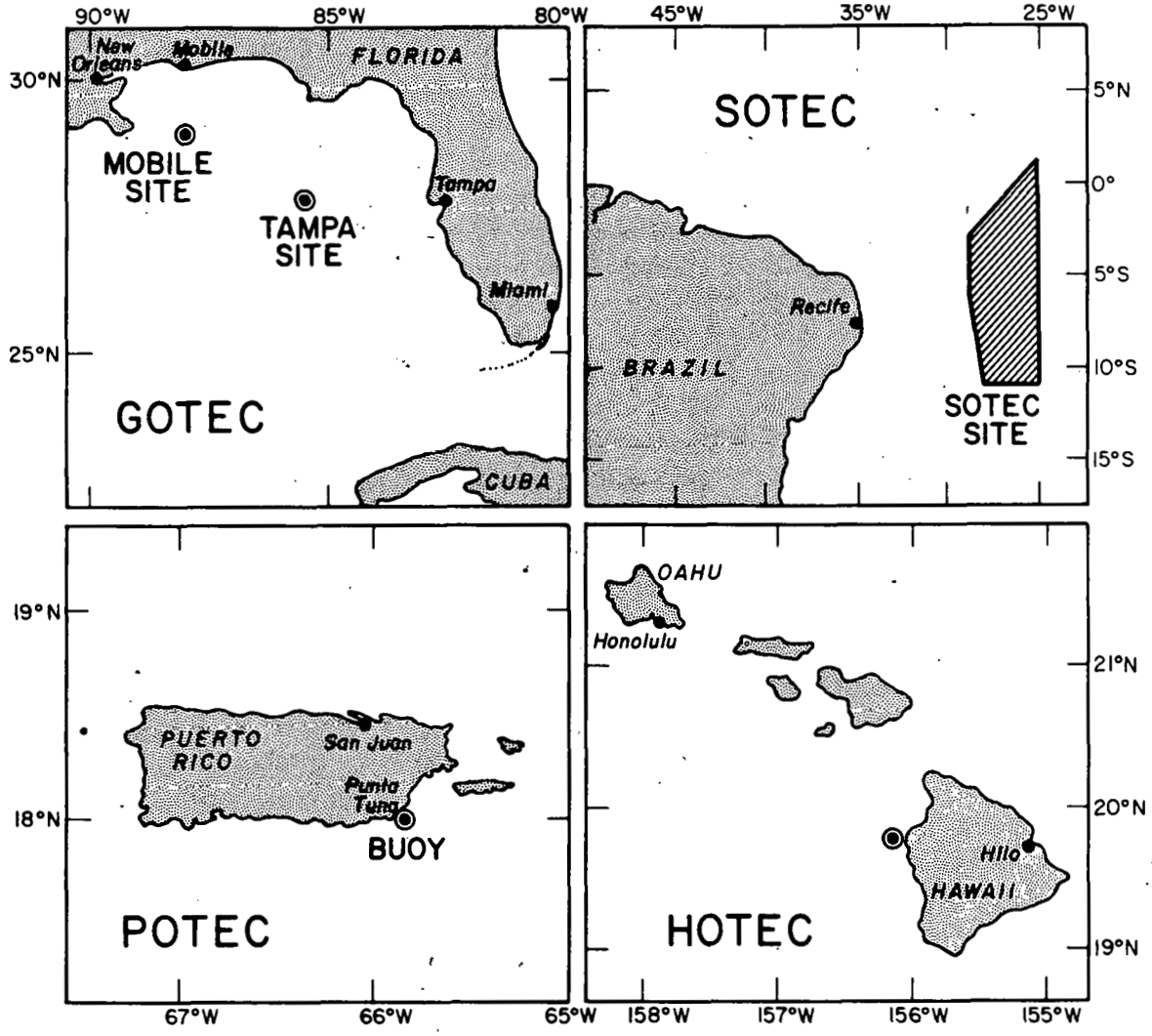

Figure 2. OTEC SITES WHERE ENVIRONMENTAL DATA HAVE BEEN TAKEN

To characterize each subregion a reconnaissance benchmark is located. A benchmark is defined as a specific location, typical of a subregion, where serial data are taken and to which historical data may be referred. Because of the lack of serial, long-term records of any kind in attractive thermal regions, we believe that the benchmark approach is more valuable in the long term than initiating broad regional surveys where variations in measurements may be attributed to site as well as time variability. Where substantial subregional variability is found, the benchmarks will be used as starting points for potential regional surveys. The intent of taking measurements at benchmarks is to provide data, at a specific location, which will form the basis, in conjunction with previously obtained data from the area, for defining longer term and more comprehensive environmental surveys required for the siting and permitting OTEC plants in the designated thermal regions. Station operations at the reconnaissance benchmark sites are given in Tables 3 and 4. In addition to this station operation at each benchmark, a current meter array will be deployed to complement current profiler runs during station operations, except in Hawaii due to the loss of the Holoholo. A current meter array is planned at the Hawaii benchmark prior to the deployment of OTEC-1. Satellite data, when available, will be used to assist the interpretation of data from the arrays. Because of costs and reliability factors, measurements for the initial surveys will be mainly from survey ships rather than from instrumented buoys. The survey ship will occupy each benchmark site bi-monthly for a minimum of three days with augmented sampling every four months. Sampling at each station occupation is designed to give, at a minimum, day-night variations as well as bi-monthly variations for the biologically significant parameters. Parameters sampled bi-monthly are thought to have variations which may be detected at that frequency. Parameters sampled every four months are thought: (1) to have less variation annually; or (2) to have potential but unresolved significance to OTEC. The augmented sampling every four months also is done to develop optimal measurement and sampling techniques for parameters which may become routine during future site occupations. Upon completion of the initial study (actually, during the surveys) the sampling frequencies and choice of parameters will be re-examined. Results from augmented samplings, from serial samplings, and historical data reviews will be used to design subsequent site data collections. In progress comparison of data from the various OTEC sites is given in other papers at this conference. Status of these sites is shown in Table 5.

Table 3

Station operation		Class of Stations	
Profiler	Vertical profiles of horizontal currents	PRIMARY	3-DAY DURATION
Hydrocast	Discrete samples at depth of: a. temperature b. salinity c. dissolved oxygen d. nutrients e. phytoplankton	Occupied in locations of prime OTEC interest - sampling frequency to ascertain diurnal changes	2 Deep Hydrocasts 2 Shallow Hydrocasts 2 Oblique Net Tows 4 Current Profilers 12 XBT 4 STD
STD	Vertical profiles of salinity, temperature	CURRENT PROFILER	2-1/2 HOUR DURATION
Net tows	Biological samples	Occupied to determine spatial variability of current regime	1 Current Profile
XBT	Vertical profiles of temperature to 750 m		
Current meter arrays	Discrete measurements of horizontal water currents at depth		
Transmissometer	Vertical profiles of light transmittance		

Table 4 Ecological/chemical parameters

Parameter	Station operation	Station Frequency	Sampling Frequency
Temperature	hydrocast	bi-monthly	all hydrocasts
Temperature	STD, XBT	bi-monthly	4 STD, 12 XBT
Salinity	hydrocast	bi-monthly	all hydrocasts
Salinity	STD	bi-monthly	4 STD
Water Currents	current meter	continuous	one/30 min
	profiler	bi-monthly	4 per station
Light transmittance	transmissometer	bi-monthly	2 traces/cruise
Dissolved oxygen	hydrocast	bi-monthly	2 casts
Orthophosphate	hydrocast	bi-monthly	2 casts
Total phosphate	hydrocast	every 4 months	2 casts
Silicate	hydrocast	bi-monthly	2 casts
Nitrate	hydrocast	bi-monthly	2 casts
Ammonia	hydrocast	every 4 months	2 casts
Urea	hydrocast	every 4 months	2 casts
Total nitrogen	hydrocast	every 4 months	2 casts
Alkalinity	hydrocast	yearly	2 casts
Trace metals	hydrocast	yearly	1 cast
Chlorophyll/phaeophytin	hydrocast	bi-monthly	2 shallow casts
ATP	hydrocast	every 4 months	2 shallow casts
Phytoplankton census	hydrocast	bi-monthly	1 shallow cast
^{14}C uptake	hydrocast	every 4 months	1 cast
POC	hydrocast	yearly	1 cast
DOC	hydrocast	yearly	1 cast
Zooplankton census	net tow	bi-monthly	6 tows

Assessment

Complementary to the monitoring program are a series of studies to ascertain those effects of potential OTEC operations that are not site-dependent but are generic to OTEC. Also included in such studies are the legal compliance activities (Sands et al., 1979) and model studies (Ditmars this volume) which are discussed in detail in this symposium. Initial studies on toxicity to organisms of various OTEC operations are under way at the Gulf Coast Research Laboratory. The toxicities of aluminum (heat exchanger material), ammonia (working fluid), and chlorine (biocide) are being investigated by bioassays of mullet (fish), copepods (zooplankton). Biostimulation studies using ^{14}C uptake techniques investigating the potential for artificial upwelling effects due to redistribution of nutrients have been started in conjunction with nitrogen fixation studies. Entrainment/impingement, artificial reef, and chlorine studies are being planned through DOE's Office of Health and Environmental Research (OHER).

Table 5 OTEC-ERA number of visits/site (July 1977 - May 1979)

Site/Region	Measurements Physical	Chemical	Biological
Mobile	8	6	6
Tampa	-	5	5
South Atlantic	2	2	2
Puerto Rico	5	5	5
Hawaii	2	2	2

Afterword

As the initial OTEC test module contract has just been let (September, 1978) it is too early to determine if the environmental strategies advocated here need to be augmented or modified greatly. Unquestionably strong interactions among environmental groups, regulatory agencies, designers, engineers, and DOE will be required to insure the success of the OTEC environmental program in attaining the goal of ecological compatibility and economical viability for OTEC systems.

To insure continuity among states DOE program positions and interim reports of this nature, portions of existing documents such as the OTEC Program Summary (1977 and 1978), the OTEC Environmental Development Plan (1977 and 1978), and DOE Assessment Seminar (November meeting) have been quoted here exactly or with minor modifications.

References

Commins, M., 1979. Preliminary Analysis of Zooplankton from potential OTEC sites. 6th OTEC conference, Washington, D.C.

Ditmars, J.D. and R.A. Paddock, 1979. OTEC physical and climatic environmental impacts: 6th OTEC Conference Washington, D..C

Environmental Development Plan (EDP) 1978. Ocean Thermal Energy Conversion. U.S. Dept. of Energy, (in prep. May 1979).

Johnson, P.W. and A. Horne. 1979. Phytoplankton and biomass distribution at potential OTEC sites. 6th OTEC conference, Washington, D.C.

Payne, S.F. 1979. The marine mammal fauna of potential OTEC sites in the Gulf of Mexico and Hawaii. 6th OTEC conference, Washington, D.C.

Program Summary: FY78 Ocean Systems Branch, Department of Energy, Office of Solar Systems. DOE/ET 0083, December 1978.

Quinby-Hunt, M.S. 1979. Comparison of nutrient and dissolved oxygen data from four possible OTEC sites. 6th OTEC conference, Washington, D.C.

Sands, M.D. and others, (1979). Environmental assessment Ocean Thermal Energy Conversion (OTEC) program preoperational test platform, Department of Energy, Division of Solar Technology. DOE/EA 0062.

A REVIEW OF THE BIOLOGICAL INFORMATION RELATING TO OTEC OPERATION

S. Mack Sullivan

Oceanic Engineering Operations
Interstate Electronics Corporation
707 E. Vermont Ave.
Anaheim, California 92803

Abstract

Ocean Thermal Energy Conversion (OTEC) power plants will operate in tropical and subtropical waters that exceed 500 m in depth. The organisms inhabiting these ocean areas have adapted to a stable, pristine environment. The installation and operation of an OTEC power plant may disturb this environment, which could result in potentially serious environmental impacts on the biota. Some of these impacts include the entrainment of plankton, impingement of organisms on the intake screens, and release of biocides used for fouling control. Conversely, schooling fish and large planktonic organisms, such as siphonophores and medusae, may seriously impair the operation of the plant by clogging the intake screens.

The assessment of these issues requires a thorough characterization of both the site and the plant engineering and is an integral part of the OTEC program. Interstate Electronics, as part of the OTEC-1 Environmental Assessment Program, examined the historical data in three potential OTEC resource areas: Keahole Point (HA), Punta Tuna (PR), and the Eastern Gulf of Mexico. The available information on zooplankton and micronekton for these sites is presented. A comparison of the biological information at the sites is made and the site similarities are shown. The life history, behavior, density, and spatial distribution of these organisms is discussed in terms of how the plant and the biota may interact. Additionally, suggestions to complete the site characterization are given when the available information is insufficient to assess the effects of an OTEC plant.

Introduction

The installation and operation of an Ocean Thermal Energy Conversion (OTEC) power plant could result in potentially serious environmental impacts on pelagic organisms. OTEC power plants will operate in tropical and subtropical waters, utilizing warm water drawn from the epipelagic zone (0-200m) and cold water drawn from the mesopelagic zone (200-1000 m). Before passing through the heat exchangers, large organisms will be removed from the water by screens having openings approximately 0.8 by 7.6 cm. The warm and cold water intakes will entrain minute planktonic organisms and impinge any organism larger than approximately 2.5 cm[12] on the intake screen that is not able to avoid or withstand the intake current. In addition, the mixed discharge from an OTEC plant will be released near the surface and form a descending plume downstream of the plant. Pelagic organisms encountering this plume may be exposed to biocides used for fouling control.

The entrainment of organisms through an OTEC plant and the effect of the discharge plume on pelagic organisms are environmental issues. The impingement of organisms on the intake screens is a plant operational concern as well as an environmental issue. The assessment of these issues requires a thorough characterization of the site and the plant engineering and is an integral part of the OTEC program. Interstate Electronics, as part of the OTEC-1 Environmental Assessment Program[12], examined the historical data in three potential OTEC resource areas: Keahole Point (HA), Punta Tuna (PR), and the Eastern Gulf of Mexico. Although the operation of an OTEC plant necessitates the impingement and entrainment of organisms, it was shown that OTEC-1 will have a negligible effect on pelagic populations[12]. However, a large OTEC plant could potentially affect the pelagic biota. The available biological information for the three potential OTEC resource areas is presented for the zooplankton and micronekton, two key members of the marine food chain, and their abundances at the OTEC-1 intake depths are put into perspective by estimating the impingement and entrainment rates assuming the organisms display no avoidance or attraction behavior.

Zooplankton

The zooplankton represent the passively swimming animals of the water column and are generally considered to form the second tropic level of the food chain. In addition to the dominant zooplankton groups, such as copepods and chaetognaths, the zooplankton also includes the eggs and larvae of the micronekton and nekton. The zooplankton will be entrained along with the incoming water at the warm and cold intakes located at 8 and 640 m, respectively, pass through the plant, and be expelled along with the mixed discharge. The entrained organisms at the warm water intake will be subjected to chlorine and the physical abuse (acceleration, impaction, shear forces, and abrasion) associated with passage through the plant. At the cold water intake entrained organisms will be exposed to these conditions plus a temperature change of 16 to 20° C and pressure change of over 60 atmospheres, all within a few minutes. Since any organism surviving to the discharge will be exposed to an altered environment, and increased predation, it is suspected that entrainment will result in 100 percent mortality. The amount of zooplankton that is entrained by an OTEC plant is related to the vertical location of the warm and cold water intakes as well as the vertical distribution of the zooplankton populations.

The numerical vertical distribution of the dominant types of zooplankton near the Punta Tuna and the Eastern Gulf of Mexico sites is shown in Figures 1 and 2[10]. These investigators found the greatest zooplankton abundance occurred in the epipelagic zone. At the depth of the warm water intake (8m), the concentration of zooplankton was found to be approximately 18 individuals/m^3, while at the depth of the cold water intake (640m), there were less than 2 individuals/m^3. As an illustration of these abundances, OTEC-1 will entrain approximately $9x10^7$ zooplankton individuals at the warm water intake and $9x10^5$ individuals at the cold water intake each day. These estimates were made assuming OTEC-1 will pump 520,000 m^3 through the warm water intake and 430,000 m^3 through the cold water intake each day. Entrainment of zooplankton will be much greater at the warm water intake than at the cold water intake.

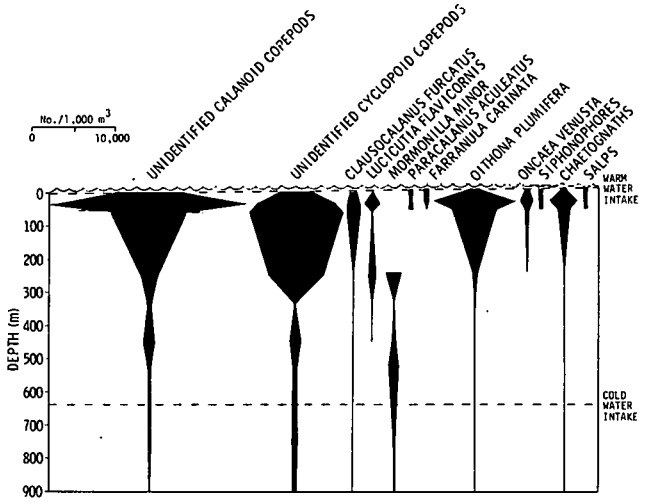

Fig. 1 Diel Vertical Distribution of Zooplankton Near Puerto Rico (Michel and Foyo, 1976).

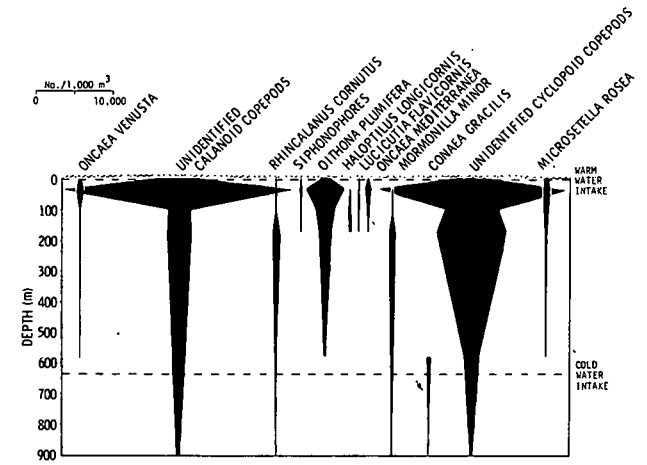

Fig. 2 Diel Vertical Distribution of Zooplankton in the Eastern Gulf of Mexico (Michel and Foyo, 1976).

The most abundant zooplankton group is the copepods. The abundance of copepods is greatest at 50 m, and decreases with depth. Near the surface there are approximately 15 copepods/m^3, while approximately 4 copepods/m^3 are present at 640 m. After the copepods, the chaetognaths are the next most abundant group. Chaetognaths display the same distributional pattern as the copepods; a large concentration at the surface, increasing to 50 m, and then decreasing with depth. At 8 m, the chaetognath abundance was approximately 0.5/m^3 while at 640 m the abundance was estimated at 0.02/m^3. The abundance of salps and siphonophores is low and these organisms appear to be usually confined to waters above 100 m. Siphonophores had an average abundance of 0.3/m^3 in the surface layers, while salps were reported in concentrations of approximately 0.1/m^3.

No information was found on the vertical distribution of zooplankton numerical abundance in Hawaii. However, the vertical distribution of Hawaiian zooplankton biomass has been reported[6]. In confirmation to the other regions, the zooplankton biomass increases to 50 m and then decreases with depth. Above 300 m, the night biomass exceeded the day biomass, indicating vertical migration of the zooplankton at night into the upper layers of the water column and perhaps greater net avoidance during the day than at night[6]. These studies illustrate that the zooplankton entrainment rate will be the greatest at the warm water intake. In addition, entrainment rates will be greater at night than during the day.

Micronekton

Micronekton are a group of organisms composed of mesopelagic fishes, cephalopods (octopus and squid), and large crustaceans (shrimp). These organisms can move rapidly for a short period of time, but normally move in conjunction with the currents. Since these organisms are larger than the OTEC-1 intake screens and are abundant in the open ocean, they will be the organisms most heavily influenced by impingement.

Micronekton play important roles in the oceanic ecosystem. These organisms act as an important intermediate step in the food chain between the zooplankton and many commercially important fish, such as tuna, marlin, and swordfish[7]. In addition, the micronekton inhabit the mesopelagic during the day and vertically migrate to the epipelagic at night to feed. By so doing, micronekton serve as an important step in a ladder that brings the energy produced in the photic zone to the organisms living in the deeper regions of the ocean.

The micronekton are exposed to the full range of environmental effects associated with OTEC operation. A vertically migrating member of the micronekton will be susceptible to impingement by the cold water intake of OTEC during the day, the warm water intake at night, and it will be exposed to the mixed discharge while in transition at dawn and dusk.

The relative composition of the micronekton near Hawaii was reported to consist of approximately 57% fish, 32% crustaceans, 1% cephalopods, and 10% other invertebrates (salps, siphonophores, ctenophores, pteropods, etc.)[9]. The vertical distribution and abundance of the latter organisms is not known. However, since salps, siphonophores, and medusae are large gelatinous organisms exhibiting no avoidance capabilities, it is expected that these organisms will cause the greatest operating problems of cleaning the screens. The diel vertical distribution of the mesopelagic fish, shrimps, cephalopods, and fish larvae near Hawaii are summarized in Figure 3.

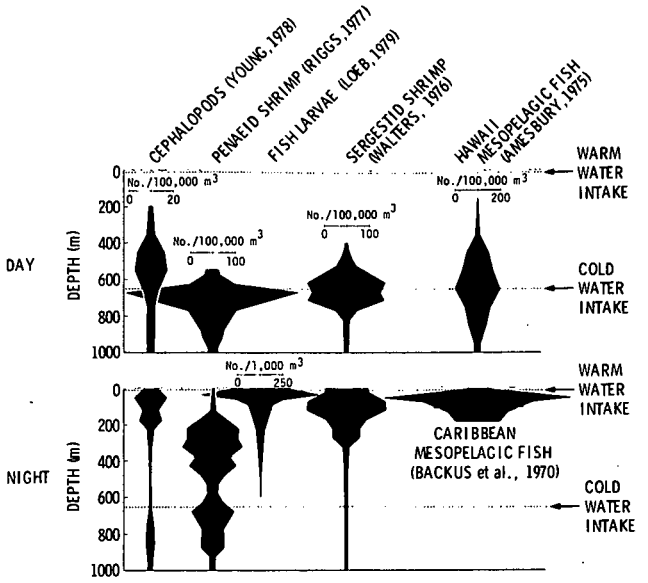

Fig. 3 Diel Vertical Distribution of Cephalopods, Penaeid Shrimp, and Sergestid Shrimp near Hawaii. The Day Distribution of Mesopelagic Fish and Night Distribution of Fish Larvae near Hawaii is shown, as well as the Night Distribution of Mesopelagic Fish in the Upper 200 m of the Caribbean Sea.

Mesopelagic Fish

The mesopelagic fish fauna is dominated by gonostomatids and myctophids (lanternfish). The genus Cyclothone (a gonostomated fish) represents the most populous fish[4] Mesopelagic fish are not expected to be impinged at the warm water intake during the day. Amesbury[1] sampled the micronekton near Hawaii and reported that during the day, the mesopelagic fish community is confined primarily to depths between 400 and 900 m, with a peak abundance of approximately 400/100,000 m^3 between 600 and 700 m. The upper boundary at 400 m is quite abrupt, and Amesbury reports the few fishes collected shallower than this were largely larval forms of inshore and benthic species. Light seems to be the single most important physical parameter affecting the upper boundary. Presumably visual predators restrict midwater fishes to depths at which illumination is below a critical range.

There is no information available pertaining to the vertical distribution of mesopelagic fish at night near Hawaii. However, the vertical distribution of mesopelagic fish larvae at night north of Hawaii is reported by Loeb[8]. Loeb found the ichthyoplankton to be distributed between the surface and 600 m at night, with the greatest abundance, 652 larvae/1000 m^3, occurring in the surface layer. The night distribution of mesopelagic fish is available from the other OTEC resource areas. Collections at night in the Gulf of Mexico and the Caribbean Sea,[2] indicate that the mesopelagic fish extend to the surface with the greatest abundance at 50-75 m. Near the surface, the mesopelagic fish abundance is between 100 and 900/100,000 m^3. Although the results from the different studies are not directly comparable, due to different oceans, season, and methods, the results from the Eastern Gulf of Mexico and Caribbean Sea illustrate the upward movement of the mesopelagic fish fauna at night.

The abundance of mesopelagic fish near the surface is minimal during the day. If these organisms display no attraction or avoidance behavior, the expected daily impingement rate at the warm water intake would be between 200 and 1800 fish. Since the abundance of mesopelagic fish at the cold water intake at night is not known, the daily impingement rate cannot be calculated. However, during the daylight hours, approximately 900 fish would be impinged at the cold water intake.

Cephalopods

Data on the vertical distribution of cephalopods is difficult to obtain: many species are uncommon and some are fast swimming and cannot be sampled since they avoid the trawls. Young[15] examined the vertical distribution of pelagic cephalopods taken off Hawaii and found that during the day, the greatest abundance of individuals occurred between 400 and 700 m. This peak in abundance reflects the dominance of the enoploteuthids, especially Pyroteuthis and Pterygioteuthis spp. At 640 m during the day, the cephalopod abundance is estimated at 7 individuals/100,000 m . Young reported no cephalopods near the surface during the day.

At night the largest catches were made in the upper 200 m[15]. In this region two peaks are apparent. The peak in the 50 to 100 m zone was largely due to Pterygioteuthis microlampas, the most abundant species collected. The peak in the 150 to 200 m zone was composed of Pyroteuthis addolux, Heteroteuthis hawaiiensis, and young Histioteuthis dofleini. In the upper 50 m at night, the cephalopod abundance was estimated at 6 individuals/100,000 m^3. The zone between 200 and 700 m was sparsely inhabited at night. The peak between 700 and 1000 m represented the deep nonmigrating population. The capture rate in this region was almost identical to the day capture rate at the same depths: deep-living migrators were few. At 640, the night cephalopod abundance was estimated to be approximately 1 individual/100,000 m^3. Calculating as before, approximately 16 cephalopods would be impinged on the warm water intake screens and 17 cephalopods on the cold water intake screens each day, assuming no attraction or avoidance.

Young concluded that over 80% of the individuals occur in the upper 250 m at night and nearly 60% of the species exhibit diel shifts in habitat. Species not exhibiting diel migrations belonged primarily to the Cranchiidae and Octopoda families.

Pelagic Shrimps

The pelagic shrimps are composed of five families: Penaeidae, Sergestidae, Oplophoridae, Pandalidae, and Pasaphaeidae. No information is available on the latter three families of shrimp.

The impingement of penaeid shrimp is expected to be greater at the cold water intake than at the warm water intake. Riggs[11] found the penaeid shrimp to be the most abundant between 600 and 800 m during the day and between 200 and 450 m at night. During the day, the penaeid shrimp population begins quite abruptly around 500 m, with the greatest abundance occuring between 650 and 700 m. Between 600 and 650 m, the population is approximately 100 penaeid shrimp/100,000 m^3. At night, Riggs found 5 penaeid shrimp/100,000 m^3 near the surface and 42 penaeid shrimp/100,000 m^3 between 600 and 650 m. Using

these abundances, approximately 13 penaeid shrimp will be impinged on the warm water intake screens and 300 on the cold water intake screens each day.

Sergestid shrimp have day distributions beginning at 400 m in Hawaii, with the greatest abundance between 550 and 750 m[13]. The concentration of sergestid shrimp between 600 and 650 m during the day is approximately 165 individuals/100,000 m^3. At night the population extends to the surface, with the greatest abundance between 50 and 150 m. The night sergestid shrimp population was estimated to be 98 individuals/100,000 m^3 in the surface 50 m and 8 individuals/100,000 m^3 between 600 - 650 m. The daily impingement rate of sergestid shrimp is estimated at 254 individuals at the warm water intake and 375 individuals at the cold water intake.

Behavior

Although preliminary information is available on the vertical distribution of the micronekton near Hawaii, additional information is necessary at the sites to assess the impact of biota impingement and entrainment. A better description of the seasonal differences between vertical migration in the zooplankton and micronekton is necessary along with an evaluation of the relative behavior of the organismsto the OTEC structure itself. Studies in the Eastern Gulf of Mexico[14] and off Keahole Point, Hawaii[5] have shown that epipelagic fish congregate around an offshore structure seeking protection and food. The number and species of fish attracted to offshore structures depend on a number of parameters, including the distance offshore, water depth, type of structure, water clarity, and the availability of attractable fish moving through the area where the structure is deployed. It is suspected that artificial structures do not increase the number of fish within a region, but only concentrate the fish already available in an area. The rate of attraction of the micronekton to artificial structures has not been documented.

It is not known if the zooplankton or micronekton will display avoidance capabilities toward the OTEC intakes. The avoidance capabilities of the organisms may differ not only between species, but perhaps also by time of day. It has been suggested that vertically migrating species of mesopelagic fish may be nearer their exhaustion point at night, and less capable of escape, than are the inactive, resting daytime fishes at depth[3].

Suggested Future Studies

Baseline information that is essential for the environmental assessment of an OTEC plant includes: 1) a better description of the diel vertical distribution and abundance of micronekton during different seasons, 2) information on the degree to which the OTEC plant increases the concentration or alters the vertical distribution of the biota, and 3) a study correlating the number of organisms impinged and entrained with physical, biological, and plant operation parameters. To obtain this information, acoustic monitoring may be performed at the selected site before an OTEC plant is deployed and around the OTEC plant at regular time and distance intervals after deployment. Monitoring of this type will determine the amount and rate of accumulation of attracted organisms around an OTEC plant. The acoustical monitoring could occasionally be supplemented with field collections to identify the organisms being acoustically monitored. Monitoring of this type, coupled with the collection of impinged organisms, will provide invaluable information on the pelagic biota not only to the OTEC plant designer and operator, but also to the marine biologist who has found it extremely difficult to study these interesting organisms.

Acknowledgements

This report was performed as a part of the Environmental Assessment of the OTEC Preoperational Ocean Test Platform, sponsored by the United States Department of Energy (Contract number EG-77-C-06-1033) under the supervision of Drs. Lloyd Lewis and Pat Wilde.

The author gratefully acknowledges the assistance and contributions made by M. Dale Sands, Dr. Arthur Barnett, and Dr. Jed Hirota.

References

1. Amesbury, S.S. 1975. The Vertical Structure of the Midwater Fish Community Off Leeward Oahu, Hawaii. Ph.D. Thesis. University of Hawaii. 106 pp.

2. Backus, R.H., J.E. Craddock, R.L. Haedrich, and D.L. Shores. 1970. The Distribution of Mesopelagic Fishes in the Equatorial and Western North Atlantic Ocean. Journal of Marine Research. 28(2): 179-201.

3. Barham, E.G. 1970. Deep-Sea Fishes Lethargy and Vertical Orientation. p. 100-118. In: G.B. Farquhar (Ed.), Proceedings of an International Symposium on Biological Sound Scattering in the Ocean. Maury Center for Ocean Science. Dept. of the Navy. Washington, D.C. MC Rept. 005. 629 pp.

4. Clarke, T.A. 1973. Some Aspects of the Ecology of Lanternfishes (Myctophidae) in the Pacific Ocean Near Hawaii. Fishery Bulletin. 71(2): 401-433.

5. Gooding, R.M. and J.J. Magnuson. 1967. Ecological Significance of a Drifting Object to Pelagic Fishes. Pacific Science. 21: 486-497.

6. King, J.E. and T.S. Hida. 1954. Variations in Zooplankton Abundance in Hawaiian Waters, 1950-1952. U.S. Dept. of Interior, Fish and Wildlife Service. Special Scientific Report: Fisheries No. 118. 65 pp.

7. Kort, V.G. (Ed.). 1967. Biology of the Pacific Ocean. Book III. Fishes of the Open Waters. Available from the Defense Documentation Center or National Technical Information Service. AD 370633. 273 pp.

8. Loeb, V.J. 1979. The Ichthyoplankton Assemblage of the North Pacific Central Gyre: Spatial and Temporal Patterns. Ph.D. Thesis. University of California, San Diego. Available from University Microfilms International. 300 N. Zeeb Rd., Ann Arbor, Michigan. 220 pp.

9. Maynard, S.D., F.V. Riggs, and J.F. Walters. 1975. Mesopelagic Micronekton in Hawaiian Waters: Faunal Composition, Standing Stock, and Diel Vertical Migration. Fishery Bulletin. 73(4): 726-736.

10. Michel, H.B. and M. Foyo. 1976. Caribbean Zooplankton. Part 1- Siphonophora, Heteropoda, Copepoda, Euphausiacea, Chaetognatha, and Salpidae. Office of Naval Research. Dept. of the Navy. 712 pp.

11. Riggs, F.V. 1977. Vertical Distribution and Migration Patterns of the Hawaiian Mid-Water Penaeidae. Ph.D. Thesis. University of Hawaii. 47 pp.

12. United States Department of Energy. 1978. Environmental Assessment. Ocean Thermal Energy Conversion (OTEC) Program Preoperational Ocean Test Platform. Washington, D.C. DOE/EA-0062. 2 Vols. 381 pp.

13. Walters, J.F. 1976. Ecology of Hawaiian Sergestid Shrimps (Penaeidea Sergestidae). Fishery Bulletin. 74(4): 799-836.

14. Wickham, D.A., J.W. Watson, Jr., and L.H. Ogren. 1973. The Efficacy of Midwater Artifical Structures for Attracting Pelagic Sport Fish. American Fisheries Society, Transactions. 102(3): 563-572.

15. Young, R.E. 1978. Vertical Distribution and Photosensitive Vesicles of Pelagic Cephalopods from Hawaiian Waters. Fishery Bulletin. 76(3): 583-616.

COMPARISON OF NUTRIENT DATA FROM FOUR POTENTIAL OTEC SITES

Mary S. Quinby-Hunt
Earth Sciences Division
Lawrence Berkeley Laboratory
University of California
Berkeley, California 94720

Abstract

An in-progress assessment of nutrient chemical data (phosphate, nitrate, nitrite, and silicate) from four potential OTEC sites (Puerto Rico, the Gulf of Mexico, Hawaii, and the South Atlantic) show reasonable comparison with archival data. At this time sufficient data is available only at the Tampa site (Gulf of Mexico) to discern seasonal variations which show an influx of nutrient-rich water in February, which decreases with time to a minimum in December. Results show a greater potential for stimulation of primary productivity at the Hawaii site than in the northern Gulf of Mexico due to the discharge of the cold water pipe into the photic zone.

Introduction

The operation of an Otec plant will transport nutrient-rich waters from the deep ocean and discharge them into nutrient-poor waters nearer the surface. This 'artificial upwelling' could potentially alter the local species composition near each OTEC site by increasing primary productivity.

In order to adequately assess the impact of artificial upwelling and other possible ecological impacts of OTEC operations on the chemistry of the water column at OTEC sites, a study was initiated at LBL to establish baseline levels of nutrients at four potential OTEC sites: the Gulf of Mexico

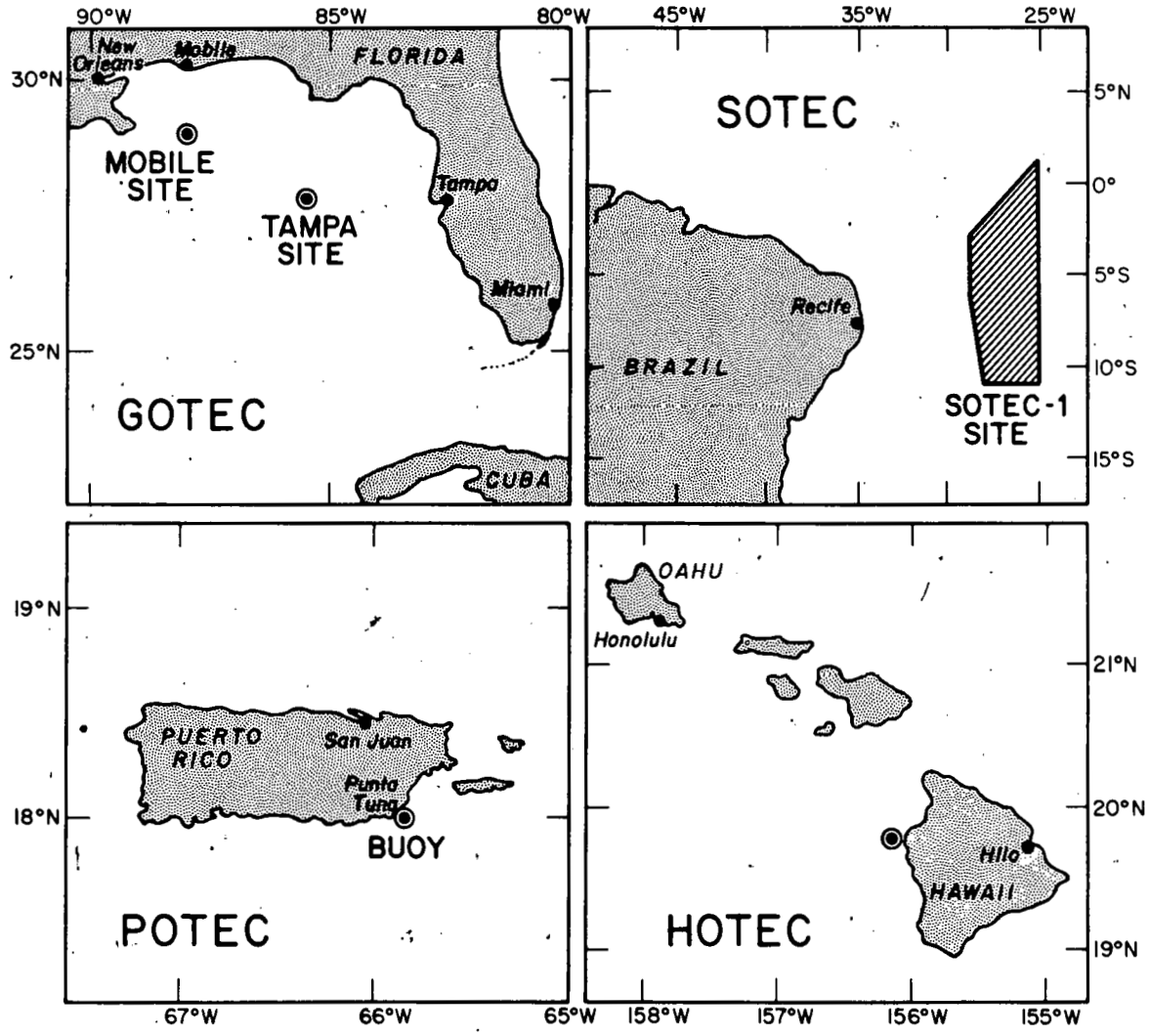

Fig. 1. Maps of four general OTEC areas, the northern Gulf of Mexico (GOTEC), Puerto Rico (POTEC), the South Atlantic (SOTEC), and Hawaii (HOTEC) showing the location of the areas where samples were taken.

Table 1. Results of nutrient measurements at the Tampa GOTEC site, GOTEC 04-08, June 1978-February 1979

Std. Depth (m)	Phosphates (µg-at/ℓ) 04 Jun	05 Aug	06 Oct	07 Dec	08 Feb	Nitrates and Nitrites (µg-at/ℓ) 04 Jun	05 Aug	06 Oct	07 Dec	08 Feb	Silicates (µg-at/ℓ) 04 Jun	05 Aug	06 Oct	07 Dec	08 Feb
0	0.05	0.05	0.1	0.2	0	1	0	0	0	0	0	0	1	1	0
50	0.2	0.0	0.05	0.2	0	0	0	0	1	1	0	0	0	0	0
100	0.2	0.1	0.2	0.2	0.7	5	3	8	3	11	1	0	2	0	2
150	0.4	0.2	0.3	0.2	0.9	8	6	13	4	15	2	2	4	0	5
200	0.6	0.4	0.4	0.2	0.5(?)	14	9	16	4	8(?)	4	3	6	0	0(?)
300	0.9	0.4	0.5	0.2	1.6	20	13	21	7	26	6	6	8	0	12
400	1.2	0.6	0.4	0.3	1.9	26	16	16	4	31	10	10	7	1	16
600	1.5	0.8	0.6	0.3	2.1	31	20	24	10	33	15	17	13	2	21
800	N.D.	0.8	0.8	0.4	1.9	N.D.	19	29	12	31	N.D.	20	18	9	23
1000	1.5	0.6	0.8	0.6	1.8	35	17	23	15	28	16	20	16	5	24

(GOTEC sites), Puerto Rico (POTEC site), the South Atlantic (SOTEC site), and Hawaii (HOTEC site). All are shown in Figure 1. Serial data were taken on a bimonthly interval and thus cover both temporal fluctuations, as well as variation with depth.

This paper will present and compare preliminary data on nitrates and nitrites, phosphates and silicates from each of the potential OTEC sites shown in figure 1. The data will also be compared to archival data from all four locations. Details of the analytical schemes and discussion of specific sets of data will not be presented here. In general, analyses have been performed by researchers whose laboratories are located near each potential site. They are: Dr. John Morse of the University of Miami (Gulf of Mexico and South Atlantic sites), Dr. Gary Goldman of the University of Puerto Rico (Puerto Rico site), and Dr. S. Allen Cattell of Aecos, Inc. for Dr. Gary Niemeyer of the University of Hawaii (Hawaii site).

Results

Gulf of Mexico—GOTEC. Eight cruises were made to the GOTEC sites from July 1977 to February 1979. The Mobile site (29°N 88°W, see Figure 1) was visited in GOTEC cruises 01-06 (01 - July 1977; 02 - November 1977; 03 - February 1978; 04 - June 1978; 05 - August 1978; and 06 - October 1978). Samples were taken at the Tampa site (27°30'N 85°30'W) in in GOTEC's 04-08 (07 - December 1978, and 08 - February 1979). Samples were collected at several depths and a series of nutrients were determined: dissolved oxygen, nitrates and nitrites, nitrites, ammonia, phosphates, and total phosphate.

The data is most complete for the Tampa site and is presented for phosphates, nitrates and nitrites, and silicates in table 1 and figure 2. As can be seen from both the table and figure, preliminary data show seasonal fluctuations which are pronounced and the envelope of concentrations over an entire year's time is extremely broad as can be seen from the shaded areas in figure 2.

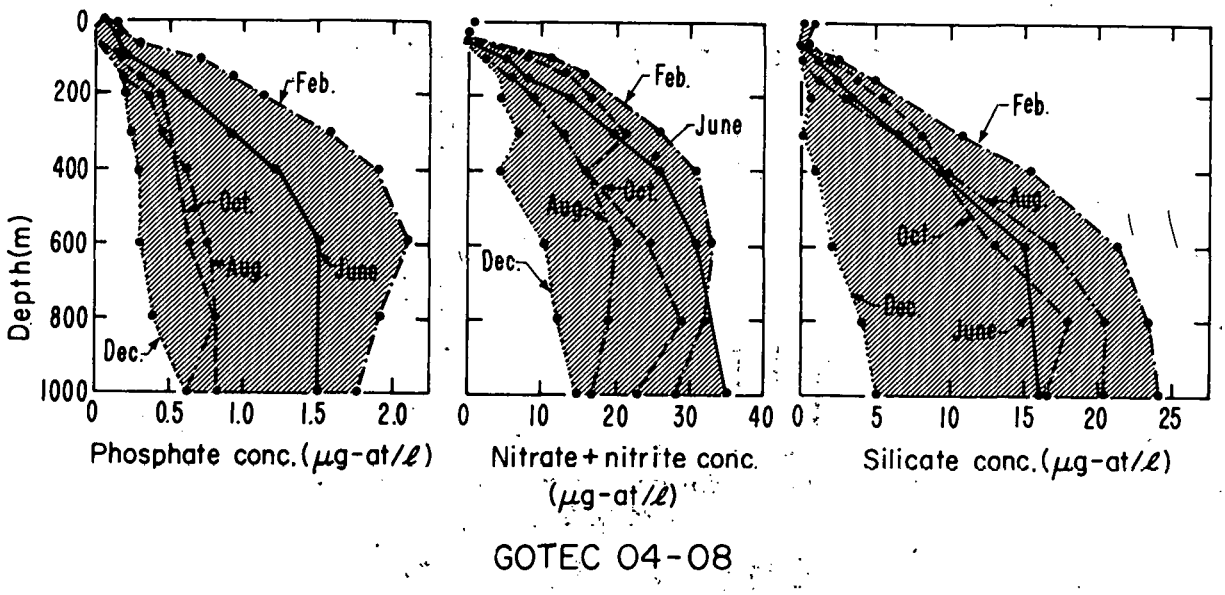

Fig. 2. Phosphate, nitrate and nitrite, and silicate concentrations determined during GOTEC's 04-08.

Table 2. Results of nutrient measurements made during SOTEC-01 (July-August 1978). Comparison of analyses made on shipboard and later at Rosenstiel School of Marine and Atmosphere Science.*

Std. depth (m)		Phosphates (µg-at/ℓ)		Nitrates and Nitrites (µg-at/ℓ)		Silicates (µg-at/ℓ)	
		STA. 20	STA. 42	STA. 20	STA.42	STA. 20	STA. 42
30	Ship	0.2	0.2	N.D.	1	3	2
	RSMAS	0.0	0.7	0	11	0	
1							
250	Ship	1.8	2.1	N.D.	26	22	27
	RSMAS	0.8	1.2	21	28	10	18
500	Ship	--	--	--	--	--	--
	RSMAS	1.0	--	26	--	16	--
1000	Ship	2.2	2.2	N.D.	31	35	32
	RSMAS	0.9	1.7	24	29	25	29

*Measurements made at Oceanographic station 20 (3°S x 26°30'W., 8 August, 1978, 1500 hrs. local) and station 42 (6°S x 26°30'W, 8 August, 1978, ~1700 hrs local).

The envelopes seen for these three nutrients generally correspond to those reported by Cummings, Atwood, and Parker[1], although in all cases the December results (GOTEC 07) appear to be lower than have previously been reported.

The February data represent the maximum values for all three nutrients; the phosphates, nitrates, and nitrites reach a maximum value (2.1 and 33.2 µg at/ℓ, respectively) at 600 m. This corresponds to the values reported for northern Gulf of Mexico by Cummings, Atwood, and Parker[1]; also to those reported by Sverdup, Johnson, and Fleming[2] for the Atlantic Ocean. The February data for silicates show a similar correspondence to the earlier data; no maximum is seen at depths less than 1000 m in either the GOTEC or archival data. The concentrations reported increase steadily until 600 m at which point the rate of increase decreases.

Several questions remain about this data. The nitrogen/phosphorus ratio is extremely high for October data (29:1 to 46:1) and the December values for all three nutrients are noticeably lower than those found in the archives. Before any real conclusions can be drawn, the values should be substantiated and then must be considered in conjunction with other oceanographic data which was taken simultaneously.

South Atlantic—SOTEC. Results are available from one cruise to the south Atlantic to an area roughly between 1°N-11°S and 26°W-29°W (shown in figure 1). Fifty-six oceanographic stations were visited, samples were taken and preserved to be analyzed in Miami upon the ship's (OSS *Researcher*) return. Determinations were made for dissolved oxygen, phosphates, nitrates and nitrites, nitrites, silicates, ammonia, and total phosphate.

At two stations samples were taken in duplicate. One sample at each depth was preserved, stored and analyzed at a later date in Miami. The other sample was analyzed at sea for phosphates, nitrates and nitrites and silicates. The results of both sets of analyses are given in table 2 and the results of the shipboard analyses are plotted in figure 3.

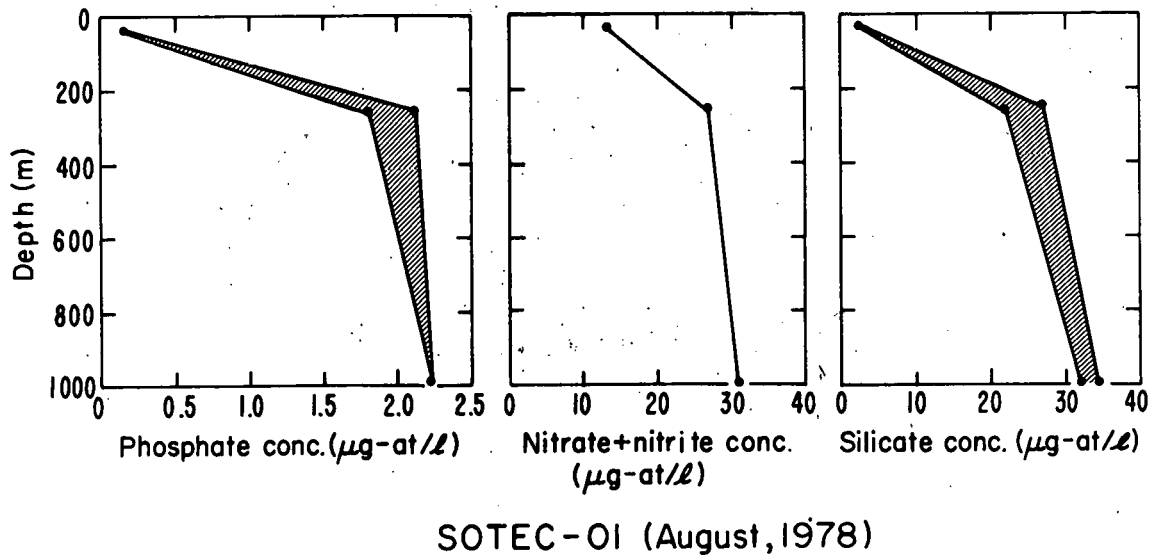

Fig. 3. Concentrations of phosphates, nitrates and nitrites, and silicates observed at the south Atlantic site and analyzed at sea.

Table 3. Results of nutrient measurements made during POTEC-02 (October, 1978) and POTEC-03 (December, 1978)

STD Depth (m)	Nitrates and Nitrites (μg-at/ℓ) POTEC-02	POTEC-03
0	2	0
50	3	N.D.
100	3	0
150	3	1
200	4	3
250	5	4
300	8	4
400	13	15
600	35	25
800	27	35
1000	38	39

The concentrations found for phosphates and silicates in samples analyzed in Miami are with one exception significantly lower than those found in the samples analyzed at sea. The nitrate and nitrite results were comparable. The results for phosphates and silicate, however, have raised questions about the preservation or storage of the samples analyzed in Miami. As a result a comprehensive nutrient preservation study will be undertaken this summer.

The values for the nutrients obtained in the shipboard analyses correspond well to preliminary results of the GEOSECS expedition[3] to the same area. The phosphate values are significantly higher than those reported by the "Meteor" expedition of 1925-1927[4]. Silicate values are somewhat less than those reported by Armstrong[5].

Puerto Rico—POTEC. Four cruises have taken place to the Punta Tuna (18°N 66°W, Puerto Rico) and Punta Vaca (18°N 65°W, Vieques) sites, however, nutrient data reports have been limited to the nitrate and nitrite results for POTEC 02 and 03 (October and December 1978). These are presented in table 3 and figure 4. While the values determined fall within the envelope reported by Atwood et al.[6] for nitrates at this site, the maximum which they report at 600 m does not appear. The data from this site is so incomplete that it is impossible to draw any conclusions.

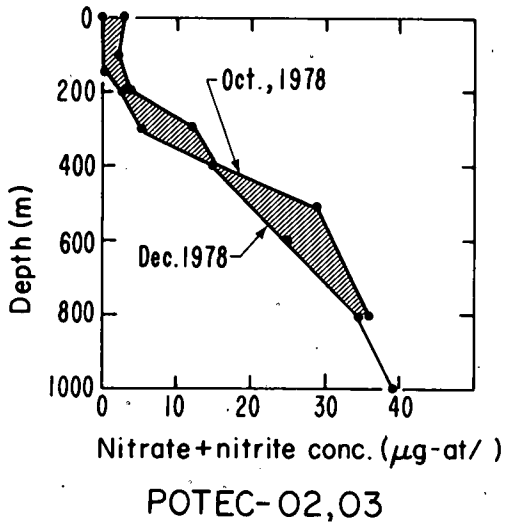

Fig. 4. Nitrate and Nitrite concentrations observed at the Puerto Rico OTEC site.

Hawaii—HOTEC. Data is available from only one cruise (HOTEC 01) to this site off the Kona Coast, 20°N 156°W, which took place in October 1978. The data are presented in figure 5 and table 4.

The nitrate results show the same general curve shape and approximate maximum values (slightly lower) as that reported by Gunderson et al.[7] Sverdup, Johnson, and Fleming[2] report slightly lower values

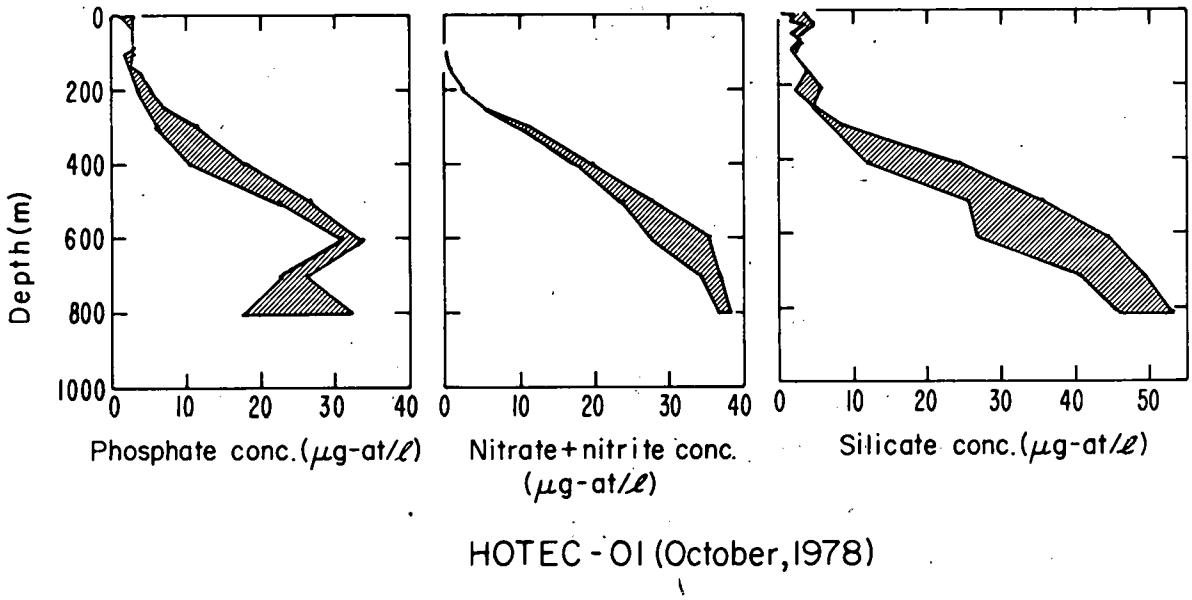

Fig. 5. Phosphate, nitrate and nitrite, and silicate concentrations observed at the Hawaii OTEC site.

Table 4. Results of nutrient measurements taken on HOTEC-01 (October, 1978).

STD Depth (m)	Phosphates (µg-at/ℓ)	Nitrates & Nitrites (µg-at/ℓ)	Silicates (µg-at/ℓ)
0	0.2 - 0.3	0	2 - 3
50	0.2	0	1 - 3
100	0.1 - 0.3	0	1 - 2
150	0.3 - 0.4	1	3
200	0.3 - 0.5	2	2 - 5
250	0.4	5	4
300	0.6 - 1.1	11 - 12	7 - 8
400	1.5 - 1.8	18 - 25	12 - 24
500	2.2 - 2.7	24 - 33	25 - 35
600	3.0 - 3.3	28 - 36	26 - 44
700	2.2 - 2.6	35 - 37	40 - 49
800	1.8 - 3.2	37 - 38	45 - 53

at 800 m. None of the archival data shows a maximum in the concentration depth curve at depths less than 800 m which agrees with these preliminary results. The concentrations found for phosphates are somewhat higher than those reported by Sverdup, Johnson, and Fleming[2] for the Pacific Ocean, and by Gundersen and Palmer[8] for Hawaiian waters. Sands reports no archival data for silicates at this site[9] however the values reported agree with those reported for the Pacific Ocean.[2]

Discussion

When reliable data covering a minimum of a year is available from all four OTEC sites, it will be valuable to compare them and to project corresponding responses to the perturbation produced by an operating OTEC plant. At this stage, the value of such a comparison is questionable for at least two important reasons. First, the quantity of the data which has been collected so far is uneven in terms of quality and extent, and must be rechecked. Secondly, the possibility of temporal variation at each site which has been raised by the GOTEC (Tampa) results and suggests that until an entire year's data has been collected, it will be impossible to assure that corresponding seasons, minima, maxima (etc.) are being compared.

Nonetheless, an initial comparison has been made of the data reported by the cruises to the three sites in the northern hemisphere; GOTEC 06, HOTEC 01, and POTEC 02, which took place in October 1978. The data from these three cruises are shown and related in figure 6.

The results for phosphates and silicates are generally what might be expected from the archives, roughly similar values from the upper 200 m of the water column and then, by 800 m in depth the values reported from Hawaii are nearly three times those reported at the Mobile site. Although the differences are less, the values for nitrates at the HOTEC site are generally higher than those at the GOTEC site in waters beneath the photic zone.

From these preliminary results, it is possible to conclude that a greater increase in primary productivity might be expected at the Hawaiian site than at the Gulf of Mexico site if the water from the cold water intake pipe is released in the photic zone. When the results of these experiments are more complete it should be possible to make more quantitative predictions regarding these potential effects.

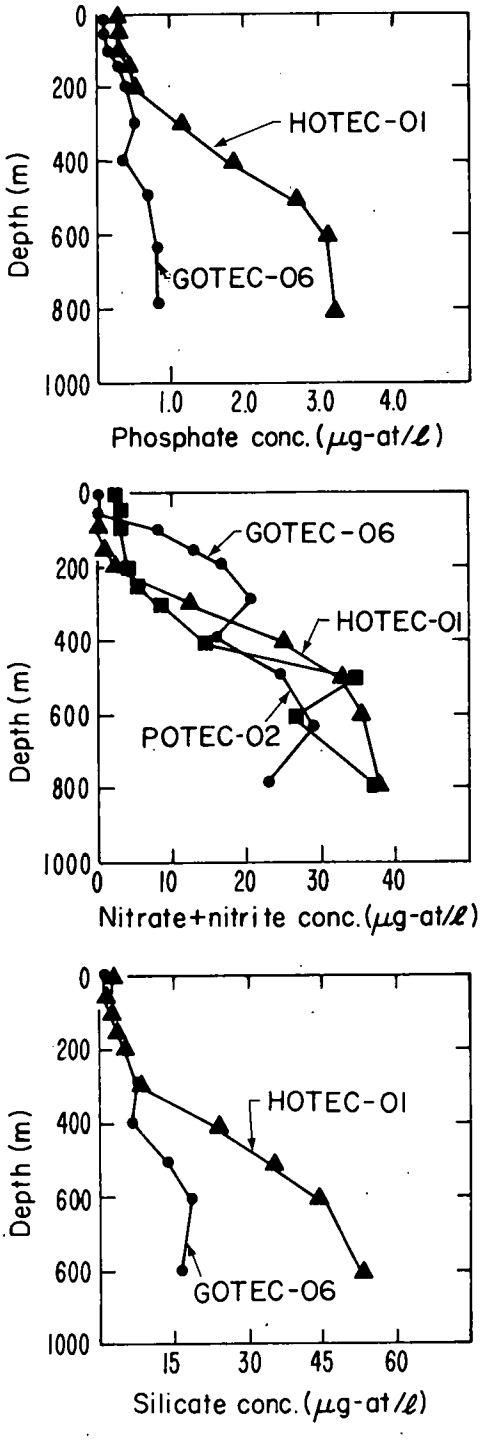

Fig. 6 Comparison of phosphate, nitrate and nitrite, and silicate concentrations observed during October cruises to the Gulf of Mexico (Tampa) site, Puerto Rico (Punta Tuna) site, and Hawaii sites.

References

[1] Cummings, S. R., Jr., D. K. Atwood, and J. M. Parker (1979). Inorganic nutrients and dissolved oxygen variation determined from historical data at three proposed Ocean Thermal Energy Conversion (OTEC) sites; Puerto Rico, St. Croiz and northern Gulf of Mexico. NOAA Technical Memo. ERL AOML-36, Miami, Florida 67 pp.

[2] Sverdup, H. V., M. W. Johnson, and R. H. Fleming (1942). The Oceans: Their Physics, Chemistry and General Biology. Prentice-Hall, Inc., Englewood Cliffs, N. J., 1087 pp. (pp.241-245).

[3] Morse, J. W. (1979). Private communication.

[4] Wattenberg, H. (1933). Das Chemische Beobachtungs —Material und Seine Gewinnung, Kalzium Karbonat und Kohlensauregehalt des Meerwassers. In: Deutsche Atlantische Expedition auf dem Forschungs und Vermessungschiff "Meteor." 1925-1927, A. Defand, editor, VIII, Verlag von Walter de Fruytes Co. 333 pp. (pp. 78 et seq.).

[5] Spencer, C. P. (1975). The Micronutrient Elements In: Chemical Oceanography, J. P. Riley and G. Skirrow, eds., Second edition, Academic Press, 2, 245-300.

[6] Atwood, D. K., P. Duncan, M. C. Stalcup, and M. J. Barcelona (1976). Ocean thermal energy conversion: Resource assessment and environmental impact for proposed Puerto Rico site. Final report for NSF Grant No. AER 75-00145, August 1976, 104 pp.

[7] Gundersen, K., C. W. Mountain, D. Taylor, R. Ohye, and J. Shen (1972). Some chemical and microbiological observations in the Pacific Ocean off the Hawaiian Islands. Limnol Oceanogr.,17(4), 524-531.

[8] Gundersen, K. and R. O. Palmer (1972). Report on Aquaculture and Ocean Energy Systems for the County of Hawaii, Center for Engineering Research, University of Hawaii, Honolulu, Hawaii.

[9] Sands, D. et al., (1978), Draft Environmental Impact Assessment: Ocean THermal Energy Conversion (OTEC) Program, Preoperational test platform, Interstate Electronics Corporation, Anaheim, CA. U.S. Department of Energy, Washington D.C. 20545, DOE/EA-0062, 2 vols. Available as: U.S. Department of Energy (1979) Environmental Assessment.

ZOOPLANKTON FROM OTEC SITES IN THE GULF OF MEXICO AND THE CARIBBEAN

M. L. Commins and A. J. Horne

Earth Sciences Division
Lawrence Berkeley Laboratory
University of California
Berkeley, California 94720

Abstract

The spatial and temporal variations in the abundance of major classes of zooplankton were measured using standard methods, between June and October 1978, at two OTEC sites in the Gulf of Mexico and in the Caribbean near Puerto Rico. The usual oceanic patterns were found with highest numbers near the surface, especially at night, and lowest numbers at 800 - 1000 m. Absolute numbers varied considerably from site to site. As expected, copepods (usually divided between calanoids and cyclopoids) dominated the zooplankton at all sites.

Introduction

Zooplankton are small, relatively slow-moving aquatic animals. They are widely distributed even in oligotrophic oceans and link marine plants (phytoplankton) with small fish in the overall trophic structure of the marine community. Zooplankton samples have been collected at three OTEC sites off Tampa and Mobile in the Gulf of Mexico and in the Caribbean off Puerto Rico. Studies on distribution and taxonomy at specific OTEC sites are lacking although various general surveys have been made.[1,2,3,4]

Samples for OTEC zooplankton were collected using standard methods employing 202 μ mesh net with a 0.75 m diameter and a 5:1 cone. This type of net adequately samples the majority of zooplankton but some small organisms pass through the net. Very large zooplankton may avoid the net or be so uncommon that they are rarely captured by this diameter net. At present logistic problems have prevented uniform methodology. This will presumably be overcome in the future but may have contributed to between-site differences in the data presented here.

This report presents part of the information obtained so that comparisons can be made between OTEC sites. We present data from at least two sites collected in June, August, and October 1978. This accommodates seasonal variation in zooplankton which occurs in the Gulf of Mexico.

Temporal and Spatial Variation in Zooplankton Abundance

Maximum zooplankton number in the Gulf of Mexico at the Tampa site for the 5-month period was 1110.0 individual organisms per m^3. This peak occurred in October during the day at a depth of 25 m. The minimum number for the Tampa site was 2.2 individuals per m^3 in June at 1000 - 800 m. Populations at 800 - 1000 m are unlikely to be significantly influenced by the day-night light regime although we have not made measurements at these sites (Table 1). Zooplankton abundance for the Gulf of Mexico Mobile site ranged from 3995.6 per m^3 collected during the nighttime 25 m tow in June to a low of 7.6 per m^3 at 1000 - 800 m in August (Table 2).

Table 1. Zooplankton abundance (# per m^3) and percent copepods, Tampa site.

	Jun	Aug	Oct
25 m Horizontal Night			
Total	512.7	896.2	1106.9
% copepods	75	46	86
25 m Horizontal Day			
Total	953.7	582.1	1110.0
% copepods	84	49	81
200 m - 0 m			
Total	408.0	332.7	213.6
% copepods	68	70	70
800 m - 200 m			
Total	26.7	16.8	9.0
% copepods	86	84	76
1000 m - 800 m			
Total	2.2	2.5	--
% copepods	93	92	--

Table 2. Zooplankton abundance (# per m^3) and percent copepods, Mobile site

	Jun	Aug	Oct
25 m Horizontal Night			
Total	3995.6	1962.1	1340.1
% copepods	62	29	59
25 m Horizontal Day			
Total	1049.6	1137.3	1370.5
% copepods	79	29	48
200 m - 0 m			
Total	--	685.3	414.0
% copepods	--	57	56
800 m - 200 m			
Total	102.7	62.8	58.9
% copepods	84	84	78
1000 m - 800 m			
Total	11.8	7.6	--
% copepods	78	72	--

Over the same time period in the Caribbean off Puerto Rico samples are only available from August. Here the zooplankton abundance peak was 858 per m^3 at 25 m during the day (Table 3). Equipment failure prevented collection of deep samples, including 1000 - 800 m so no useful comparisons about minimum numbers can be made with the Gulf of Mexico.

Table 3. Zooplankton abundance (# per m^3) and percent copepods, Puerto Rico site

	August
25 m Horizontal Night	
Total	407
% copepods	86
25 m Horizontal Day	
Total	858
% copepods	87
1200 m - 0 m	
Total	141
% copepods	72

The vertical distribution of zooplankton is shown in Fig. 1. At both the Mobile and the Tampa sites approximately 98% of the zooplankton occurred in the upper 200 m of water with over half occurring near the surface. The 200 to 1000 m region was sparsely populated. Increased zooplankton numbers in near-surface waters is due to their need to feed on algae which only grow in the photic zone. Normally some daily vertical migration by zooplankton out of the photic zone in the daylight hours occurs to avoid predation by fish and squid. Detailed studies on diel migration are in progress for the Gulf of Mexico.

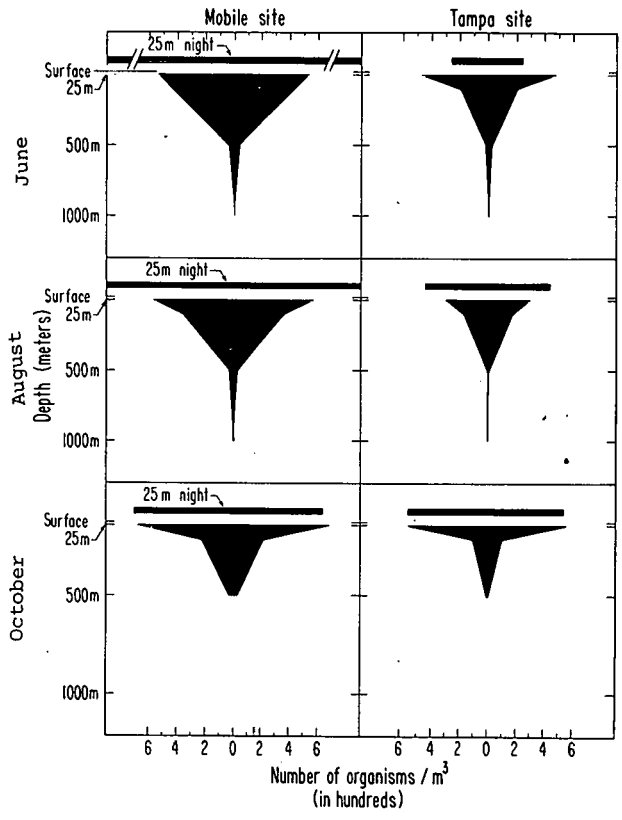

Fig. 1 Daytime vertical distribution of zooplankton during June, August, and October, 1978.

Major Taxonomic Groups

In general environmental surveys of the type carried out for OTEC by LBL, it is desirable to subdivide the zooplankton into their major functional groups in the food chain. This is not possible in detail but some idea of the importance of each type of organism can be gained from a breakdown of total numbers into the main taxonomic groups and also by division into size classes.

As usual in ocean waters, copepods comprised a major portion of the total plankton, ranging from 46% to 93% at the Tampa site, 29% to 84% at the Mobile site, and 72% to 87% at Puerto Rico (Tables 1-3). The copepods were quite evenly divided between the two major free-living oceanic taxonomic groups, the calanoids and the cyclopoids. Usually only a small number of the third group, the harpacticoids, occurred at both the Tampa and Mobile sites. In contrast, although the data are somewhat limited, at the Puerto Rico site the calanoids were approximately three times more numerous than the cyclopoids.

At the Tampa site the most frequently occurring copepods genera in the upper 200 m were the cyclopoids, *Oithona* and *Oncaea* and the calanoid, *Clausocalanus*. The most common genera at deeper levels were the calanoids *Eucalanus*, *Rhincalanus*, and *Mormonilla* and the cyclopoid *Conaea*. In the upper 200 m at Mobile the most common genera of copepods were the same as those at Tampa, *Clausocalanus Oithona*, and *Oncaea*. A fourth copepod, the calanoid genus *Temora*, not abundant at Tampa, was quite common at the Mobile site. The deeper samples were also similar to the Tampa site in having *Conaea*, *Mormonilla*, and *Eucalanus* occurring most frequently, in addition to *Oithona* and *Oncaea*. The most numerous copepod genera in the 25 m samples from Puerto Rico were the calanoids *Clausocalanus*, *Acartia*, and *Calocalanus* and the cyclopoid *Oithona*.

Size Frequency Distribution

Unlike their algal or bacterial food most zooplankton pass through a variety of distinct stages before becoming reproductive adults. In general, adult reproduction and survival of very early stages are most prone to environmental disturbances such as may be caused by full-scale OTEC plants. Thus size-frequency distribution of correctly identified organisms may enable prediction of future effects on the most sensitive section of each functional unit of the ecosystem. At present a size class distribution is all that can be obtained for each data set.

The size class distribution of the zooplankton collected at the Tampa site is shown in Fig. 2. Most of the organisms in the upper waters fell in the 0.5 - 1.9 mm size range. There was an increased frequency of the larger sizes in deeper samples. Zooplankton in the 2.0 - 2.9 mm range were almost as numerous at 800 - 200 m and more numerous at 1000 - 800 m than the 0.5 - 1.9 mm organisms. Organisms in the 0.5 - 1.9 mm size range were also the most frequently occurring in the upper waters at Mobile (Fig. 3). There was a slight increase in larger size ranges in deeper waters but this was not so pronouced an increase as that found at the Tampa site.

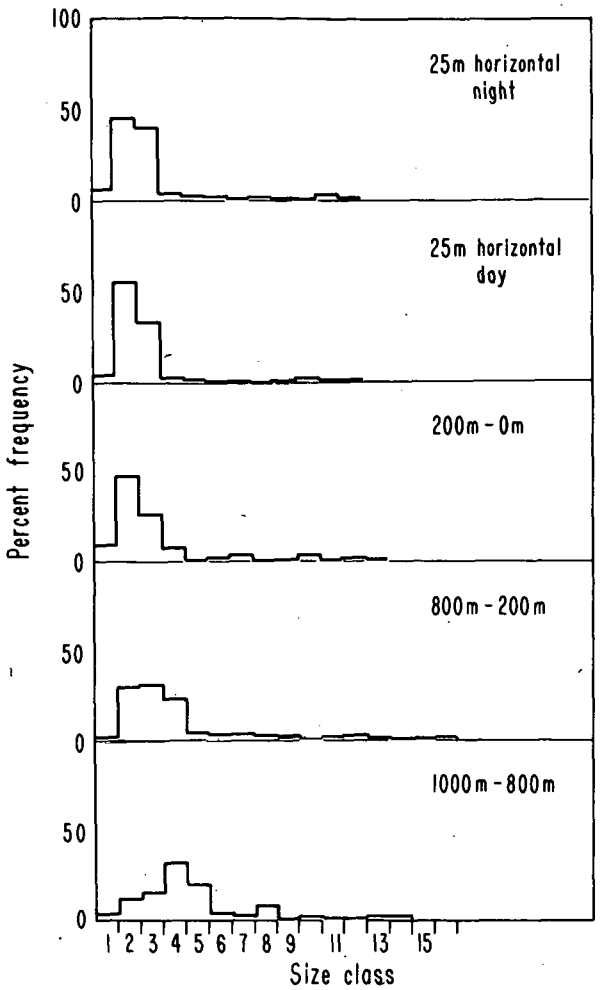

Fig. 2 Zooplankton size distribution for the Tampa site during June, August, and October, 1978. Actual size range of size classes are (in mm): 1 = <0.5; 2 = 0.5-0.9; 3 = 1.0-1.9; 4 = 2.0-2.9; 5 = 3.0-3.9; 6 = 4.0-4.9; 7 = 5.0-5.9; 8 = 6.0-6.9; 9 = 7.0-7.9; 10 = 8.0-8.9; 11 = 9.0-9.9; 12 = 10.0-19.9; 13 = 20.0-29.9; 14 = 30.0-39.9; 15 = 40.0-49.9; 16 = >50.0.

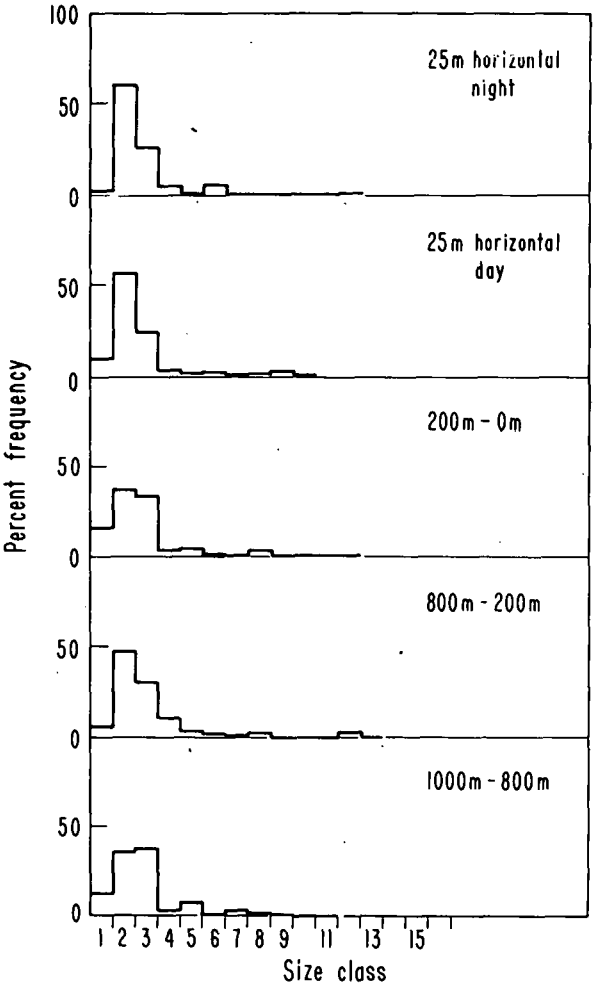

Fig. 3 Zooplankton size distribution for the Mobile site during June, August, and October, 1978. Actual size range of size classes are (in mm): 1 = < 0.5; 2 = 0.5-0.9; 3 = 1.0-1.9; 4 = 2.0-2.9; 5 = 3.0-3.9; 6 = 4.0-4.9; 7 = 5.0-5.9; 8 = 6.0-6.9; 9 = 7.0-7.9; 10 = 8.0-8.9; 11 = 9.0-9.9; 12 = 10.0-19.9; 13 = 20.0-29.9; 14 = 30.0-39.9; 15 = 40.0-49.9; 16 = >50.0.

References

1. Khromov, N.S. 1965. Distribution of plankton in the Gulf of Mexico and some aspects of its seasonal dynamics. In: Soviety-Cuban Fishery Research. A.S. Bogdanov, ed.

2. _____. 1965. Distribution of plankton in the Caribbean Sea. In: Soviet-Cuban Fishery Research. A.S. Bogdanov, ed.

3. Hopkins, T.L. 1973. Zooplankton. In: A summary of knowledge of the Eastern Gulf of Mexico. J.I. Jones, ed. State University of Florida Institute of Oceanography.

4. Michel, H. and M. Foyo. 1976. Caribbean zooplankton. Part I. Siphonophora, Heteropoda, Copepoda, Euphausiacea, Chaetognatha, and Salpidae. Office of Naval Research. Dept. of Navy. 549 pp.

Acknowledgement

Zooplankton samples were collected and counted by John Steen of he Gulf Coast Research Laboratory. Jim Bennett, Tom Hopkins and Paul Shuert of the Univ. of South Florida and Daviel Pesante of the Center for Energy and Environment Research, Puerto Rico.

PHYTOPLANKTON AND BIOMASS DISTRIBUTION AT POTENTIAL OTEC SITES

P. W. Johnson and A. J. Horne

Earth Sciences Division
Lawrence Berkeley Laboratory
University of California
Berkeley, California 94720

Abstract

Net or large phytoplankton species composition and most phytoplankton abundance was measured at three OTEC sites. In the Gulf of Mexico and at Hawaii, diatoms dominated, while the blue-green algae Trichodesmium was most common at Puerto Rico. The species ratio of diatoms to dinoflagellates was approximately 1:1 at all sites. The species diversity varied from site to site, Hawaii > Puerto Rico > Gulf Mexico. Chlorophyll a, which is a measure of the pigment of all alga size ranges, showed a subsurface peak of 0.14-0.4 µg per liter at 75 to 125 m. Occasional surface peaks up to 0.4 µg per liter occurred. Further refinement of collection techniques is needed to delineate possible changes in species composition and biomass due to OTEC plant discharges.

Introduction

Phytoplankton are microscopic floating plants which constitute the photosynthetic base of the food chain in tropical oceans. Phytoplankton in the surface waters of tropical oceans are normally scarce due to lack of nutrients. Upwelling of deep, nutrient-rich water from OTEC plants could increase phytoplankton growths, and various antifouling toxicants could decrease phytoplankton. The effects on the food web could be severe and quite extensive. However, deleterious consequences can be restricted to local areas if ecological knowledge is used in the design and maintenance of OTEC plants. Also, changes in environmental conditions may be reflected in the characteristic biota living in, or passing through, the areas involved.

To establish base-line data on phytoplankton abundance and taxonomic composition, samples were taken at potential OTEC sites. Proposed OTEC sites studied are at the following locations: Gulf of Mexico (GOTEC), near Mobile, Alabama, 29°N 88°W; Hawaii (HOTEC), located off Kawaihae, Hawaii, at 20°N 154°5'W; Puerto Rico (POTEC), located off Punta Tuna, Puerto Rico, at 17°45'N 65°51'W. Sample counts were made for only one cruise from each site: POTEC during July 1978; HOTEC during October 1978; and GOTEC during June 1978. Samples were collected and counted by the authors with assistance from other LBL scientists.

Larger phytoplankton were collected using standard net tows. Total algal abundance was estimated by chlorophyll a concentrations from filtered water samples. Vertical net tows (25 µg mesh) and bottle casts for chlorophyll a were taken at each station within the photic zone (approximately 0-200 m). The algae in the net tows (net phytoplankton) were identified and counted. Net tows provide a quantitative sampling of algae (larger than the mesh size) due to the large volume of water filtered. However, smaller algae are missed. In some, but not all, oceans smaller algae (the nannoplankton, 2-20 microns in diameter) are responsible for a large part of the primary productivity and/or biomass.[1,4,5]

An estimate of total phytoplankton biomass is provided by chlorophyll a pigment analyses. Unfortunately only small volumes of one or two liters could be filtered. This greatly increased the variability of replicate samples since large, uncommon algae may have been missed. Base-line data obtained from both net tows and chlorophyll a measurements must be considered together to compare algal standing crop and species composition through time.

Phytoplankton

Species Composition and Abundance

The net phytoplankton population at the Hawaii (HOTEC) site was diverse (Tables 1, 2). Seventy-six species were identified, with numerical abundance being dominated by four species of pennate diatoms: Dactyliosolen mediterraneus, Nitzschia closterium, Navicula sp., an unidentified pennate; and unidentified athecate dinoflagellates. D. mediterraneus is generally a neritic or nearshore species but is occasionally oceanic, while N. closterium is an ubiquitous species, found in many different oceanic areas.[2] Athecate dinoflagellates are difficult to preserve and identify but are common in many ocean areas.

The ratio of the number of diatom species to the number of dinoflagellate species (Table 1) gives some idea of community structure. HOTEC had a ratio of 1:1. This indicated that although diatoms dominated numerically, there were approximately the same number of dinoflagellate species as diatom species. The total number of species at the HOTEC site is probably larger than the 76 found on this one cruise. But most of the organisms of the area were probably represented in the sample taken since seasonal variations are much reduced in tropical oceans compared to temperate waters. The diversity index measures the evenness with which a group of individual organisms is distributed among the species present.[7] At the HOTEC site diversity was quite high (H' = 4.1).

All species and groups identified at the HOTEC, GOTEC, and POTEC sites, and their rank of abundance at each are listed in Table 2. In Hawaii, only a few species were present as more than a few individuals and most species were rare. Thirty-four species of diatoms and thirty-three of dinoflagellates were found. One species of blue-green algae, the colonial, filamentous Trichodesmium sp. occurred. This species is a facultative nitrogen-fixing organism that may be the most important replenisher of fixed nitrogen in oceanic waters.[3] Although their abundance was low in the sample examined, dense growths are known to occur. Trichodesmium sp. is not sampled very well using current single net tows.

Table 1. Biological parameters at potential OTEC sites from the results of net tows.

	Site		
	Hawaii	Gulf	Puerto Rico
Dominant organism	Dactyliosolen mediterraneus Navicula sp. Nitzschia closterium Uniden. pennate Athecate dinoflagellate	Chaetoceros lorenzianus Nitzschia sp.	Trichodesmium sp. Nitzschia closterium
No. of species diatom vs. no. species dinoflagellates	33 : 32	10 : 8	23 : 13
Total number of species	73	18	38
Diversity (H^s)	4.1	--	2.8

Two species of silicoflagellates and five species of coccolithophorids were found. This contrasts with a study by Muller[6] in which small and large coccolithophorids were more important components of the plankton near Hawaii. These small cells may not have been sampled quantitatively with our net.

The chlorophyll a profile shown in Fig. 1 indicates a pigment maximum at approximately 125 m. Below this depth the concentration dropped off significantly approaching zero near 300 m. A deep chlorophyll a maximum (50-100 m) is a common feature of all oligotrophic waters including the Pacific Ocean.[8] The deep maxima have been attributed to differential zooplankton grazing, an increase in the chlorophyll a/carbon ratio of cells with depth, increased nutrient availability in deeper waters, and pycnocline location.[8] The maximum chlorophyll a concentration was 0.27 µg per liter which is a fairly typical value for the subsurface maximum near Hawaii.[1,4] Continued data collection will provide an accurate description of seasonal variations.

At the Gulf of Mexico (GOTEC) site two diatoms dominated the net phytoplankton, Chaetoceros lorenzianus and Nitzschia sp. (Table 2). Also common were the dinoflagellates Exuviella sp., Peridinium pendunculatum, and Prorocentrum micans. The ratio of diatom species to dinoflagellate species was basically 1:1, which was similar to that found at the HOTEC site. A lesser total number of species were identified than at either the HOTEC or POTEC sites (Table 1). This may be a sampling artifact as the expected number of species from past records is greater than this. Diversity was not calculated because the initial phytoplankton counts were done using a qualitative rank abundance. The GOTEC site is probably less diverse than either the HOTEC or POTEC sites.

Trichodesmium sp. was not found in these GOTEC samples, but we have recently observed dense growths at the GOTEC site. No silicoflagellates or coccolithophorids were identified at the GOTEC site.

A subsurface chlorophyll a maximum occurred between 25 and 75 m (Fig. 2). A surface peak occurred in September 1978, with a pigment concentration of 0.4 µg per liter. The November 1977 and September 1978 subsurface maxima were of similar magnitude, as were the June 1978 and December 1978 values. These pairs differed in magnitude by a factor of 2.5. It appears that the depth of the chlorophyll a maximum decreased from early summer to winter. As in the HOTEC samples, pigment concentrations were greatly reduced below 150 m, with zero values being approached near 300 m.

At the Puerto Rico (POTEC) site, the dominant phytoplankters were Trichodesmium sp., Nitzschia closterium, and several species of Thalassiothrix (Table 1). Tichodesmium sp. was by far the most abundant both in terms of biomass and numbers of cells, and may have been responsible for the surface chlorophyll a peaks seen at the Puerto Rico site (Fig. 3). The large proportion of N. closterium was similar to the HOTEC site. The ratio of diatom to dinoflagellate species was weighted towards diatoms (60:40). Although numerically different from the HOTEC and GOTEC sites, the general equality of numbers of diatom species and dinoflagellate species was preserved.

The total number of species identified from the POTEC site was less than the number from HOTEC, and greater than the number from GOTEC. The diversity index was lower than that shown for HOTEC. This is probably due to the great abundance of Trichodesmium sp. found at the POTEC site. Silicoflagellates were not found at the POTEC site and coccolithophorids were rare.

The chlorophyll a profiles for the POTEC site (Fig. 3) show quite large surface concentrations for October 1978, and February 1979, of approximately 1.9 to 2.5 µg per liter. Subsurface maxima from 0.14 to 0.35 µg per liter occurred between 75 and 150 m. A double-maximum was found in October 1978. Multiple peaks can be a common feature of chlorophyll a profiles.[9] As in Hawaii and in the Gulf of Mexico the chlorophyll a concentrations were very low below 200 m.

Table 2. Phytoplankton species and abundance at potential OTEC sites.

Phytoplankton	Hawaii	Gulf	Puerto Rico
Diatoms	Rank	Rank	Rank
Amphiprora sp.	--	--	Rare
Asterionella sp.	--	--	Rare
Bacteriastrum delicatulum	Rare	--	--
B. elongatum	Rare	--	--
Bacteriastrum sp.	Rare	--	Rare
Chaetoceros coarctatus	Rare	--	--
C. convolutum	Rare	--	--
C. didymus var. anglica	--	Rare	--
C. lorenzianus	Rare	Dominant	--
C. messancase	Common	--	--
Chaetoceros sp.	Common	--	Rare
Climacodium frauenfeldianum	Rare	--	--
Coscinodiscus excentricus	Common	--	--
C. lineatus	Rare	Common	--
C. marginatus	Rare	--	--
Dactyliosolen mediterraneus	Dominant	--	--
Eucampia zoodiacus	Rare	--	--
Grammatophora sp.	--	--	Rare
Guinardia flaccida	--	Rare	--
Hemialus hauckii	Common	--	Rare
Hemiaulus sp.	Rare	--	Rare
Leptocylindrus danicus	Rare	Common	--
Licomorpha abbreviata	--	--	Rare
Licomorpha sp.	--	--	Rare
Mastogloia rostrata	Rare	--	--
Navicula carnifera	--	--	Rare
Navicula sp.	Dominant	--	Common
Nitzschia closterium	Dominant	--	Dominant
N. delicatissima	Rare	--	--
N. longissima	Rare	Rare	Rare
Nitzchia sp.	--	Dominant	Common
Planktoniella sol	Rare	--	--
Pleurosigma sp.	--	--	Rare
Pseudoeunatia deliolus	Rare	--	--
Rhizosolenia alata	Rare	--	--
R. bergonii	--	Rare	--
R. cylindrus	Rare	--	--
R. hebetata f. hiemalis	Rare	--	--
f. semispina	Rare	--	--
R. imbricata var. shrubsolei	Rare	--	Rare
R. styliformis	--	--	Rare
Surirella sp.	--	--	Rare
Synedra vaucheriae	Rare	--	--
S. undulata	Rare	--	--
Thalassionema nitzschioides	--	Rare	Common
Thalassiothrix frauenfeldii	--	Rare	Common
T. longissima	--	--	Common
Thalassiothrix sp.	--	--	Common
Unidentified pennate	Dominant	--	Common
Unidentified centric	Rare	--	--
Total number Diatom species	33	10	23

Table 2 (continued)

Phytoplankton	Hawaii	Gulf	Puerto Rico
Dinoflagellates	Rank	Rank	Rank
Amphidinium sp.	--	--	Rare
Ceratium fusus	Rare	--	--
C. incisum	Rare	--	--
C. karsteni	Rare	--	--
C. pentagonum	Rare	Rare	--
C. setaceum	Rare	--	--
Ceratium sp.	--	--	Rare
Cochlodinium sp.	Common	--	--
Dinophyris exigua	Rare	--	--
Dinophysis sp.	--	--	Rare
Exuviella apora	Rare	--	--
E. baltica	Rare	--	Common
E. compressa	Rare	Common	--
E. vaginula	--	Rare	--
Exuviella sp.	--	Common	Rare
Goniaulax sp.	Rare	--	Rare
Gymnodinium sp.	Rare	--	Rare
Gyrodinium sp.	Rare	--	--
Ornithocercus quadratus	--	Rare	--
Oxytoxum gigas	Rare	--	--
O. variabile	Rare	--	--
Parahistioneis sp.	--	--	Rare
Peridinium globulus	Rare	--	--
P. hirobus	Rare	--	--
P. pendunculatum	--	Common	Rare
P. tube	Rare	--	--
Peridinium sp.	Rare	--	Rare
Phalacroma ovum	Rare	--	--
Podolampas bipes	Rare	--	--
P. elegans	Rare	--	--
P. palmipes	Rare	Rare	--
Podolampas sp.	Rare	--	--
Pronoctiluca pelagica	--	--	Rare
Prorocentrum lebourae	Rare	--	--
P. micans	--	Common	--
Prorocentrum sp.	--	--	Rare
Protoerythropsis crassicaudata	Rare	--	--
Pyrocystis fusiformis	Rare	--	--
P. hamulus var. semicircularis	Rare	--	--
P. lunula	Rare	--	--
P. pseudonoctiluca	Rare	--	--
P. robusta	Rare	--	--
Unidentified athecate dino-flagellates	Dominant	--	Common
Total number Dinoflagellate species	32	8	13

Table 2 (continued)

Phytoplankton	Hawaii	Gulf	Puerto Rico
Blue-green Algae	Rank	Rank	Rank
Trichodesmium sp.	Rare	--	Dominant
Silicoflagellates	Rank	Rank	Rank
Dictyocha fibula	Rare	--	--
Ebria sp.	Rare	--	--
Coccolithophroids	Rank	Rank	Rank
Discosphaera tubifer	Rare	--	--
Gephryocapso pcsamosa	Rare	--	--
Rhabdosphaera sp.	Rare	--	--
Umbellosphaera sp.	Common	--	--
Unidentified coccolithophorids	Common	--	Rare
Total number coccolithophorid species	5	0	1

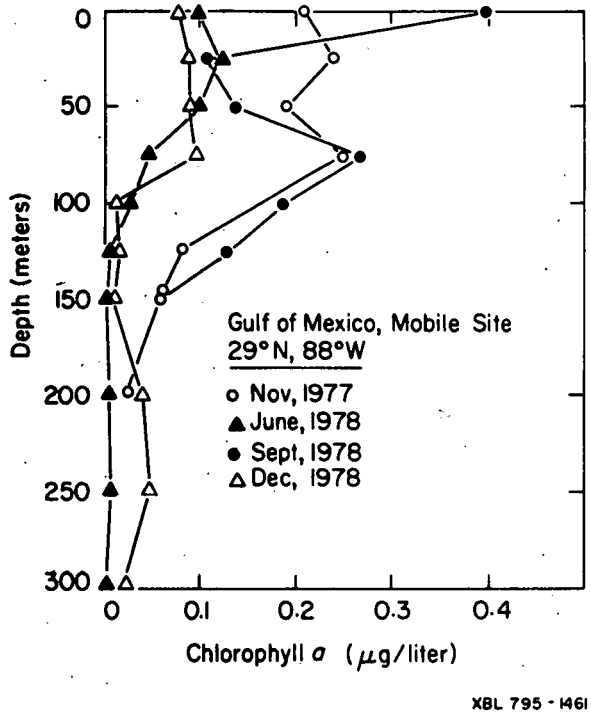

Fig. 2 Chlorophyll a concentrations with depth at the Mobile Site, Gulf of Mexico.

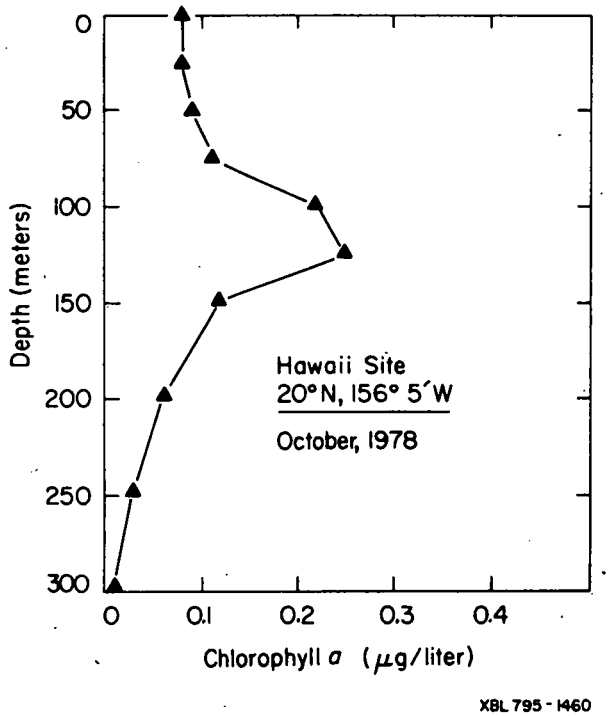

Fig. 1 Chlorophyll a concentrations with depth at the Hawaii site.

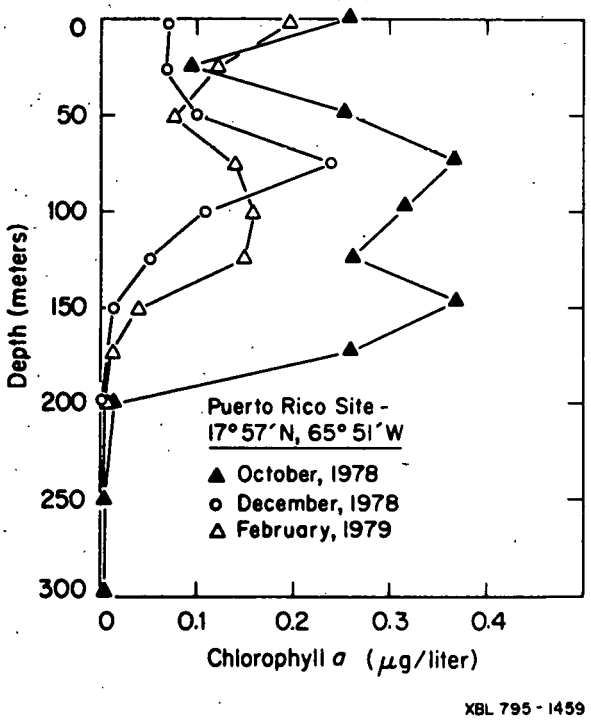

Fig. 3 Chlorophyll a concentrations with depth at the Puerto Rico site.

References

1. Beers, J.R., F.M.H. Ried, and G.L. Stewart. 1975. Microplankton of the North Pacific Central Gyre. Population Structure and abundance, June 1973. Int. Rev. Hydrobiol. 60:607-638.

2. Cupp, E.E. 1943. Marine Plankton Diatoms of the West Coast of North America. Bull. Scripps Inst. Oceanogr., Univ. of Calif. 5(1):1-238.

3. Fogg, G.E. 1978. Nitrogen fixation in the oceans. Ecol. Bull. (Stockholm) 26:11-19.

4. Gundersen, K.R., J.S. Corbin, C.L. Hanson, M.L. Hanson, R.B. Hanson, D.J. Russel, A. Stollar, and O. Yamada. 1976. Structure and biological dynamics of the oligotrophic ocean photic zone off the Hawaiian Islands. Pacific Science 30 (1): 45-68.

5. Hobson, L.A. and C.J. Lorenzen. 1972. Relationships of chlorophyll maxima to density structure in the Atlantic Ocean and Gulf of Mexico. Deep-Sea Research 19:297-306.

6. Muller, R.G. 1971. Phytoplankton observations through fourteen months at a tropical oceanic station. Masters thesis, University of Hawaii.

7. Shannon, C.E. and W. Weaver. 1963. The mathematical theory of communication. University of Illinois Press, Urbana. 117 pp.

8. Venrick, E.L. J.A. McGowan, and A.W. Mantyla. 1973. Deep maxima of photosynthetic chlorophyll in the Pacific Ocean. Fishery Bulletin, 71(1): 41-52.

9. Wood, E.J.F. 1965. The vertical distribution of phytoplankton in tropical waters. Ocean Science and Ocean Engineering, pp. 111-115.

THE MARINE MAMMAL FAUNA OF POTENTIAL OTEC SITES IN THE GULF OF MEXICO AND HAWAII

Susan F. Payne

Earth Sciences Division
Lawrence Berkeley Laboratory
University of California
Berkeley, California 94720

Abstract

Twenty-seven marine mammal species have been recorded for the Gulf of Mexico, including 7 Mysticetes or baleen whales, 17 Odontocetes or toothed whales, 1 Sirenian (manatee), and 1 or 2 Pinnipeds or seals. The most common species in the Gulf is *Tursiops truncatus*, the bottlenosed dolphin, an inshore species. Offshore, *Stenella plagiodon*, the spotted dolphin, is fairly common. Most other species are recorded from very few sightings or strandings. None of the endangered species is common in potential OTEC sites in the Gulf of Mexico. Twenty-two marine mammals may occur in Hawaii; 2 Mysticetes, 19 Odonotocetes, and the endemic Hawaiian monk seal. The monk seal *(Monachus schauinslandi)*, an endangered species, lives in the extreme northwestern island chain away from potential OTEC sites. Among the most common cetaceans in Hawaii is the endangered humpback whale *(Megaptera novaeangliae)*. *Stenella longirostris*, the spinner dolphin; and *Tursiops* sp., the bottlenosed dolphin are also fairly common. The baleen whales feed on zooplankton during the summer in polar waters; and are migratory, while the toothed whales feed mainly on fish and squid, and are found in temperate or tropical regions year-round. The manatee is vegetarian and the pinnipeds are fish- or squid-eaters. Environmental effects of OTEC which may affect mammals are: toxic effects of biocide release or ammonia spill, biostimulating effects of seawater redistribution, oil spills, or effects of the physical presence of OTEC plants.

Introduction

A knowledge of marine mammal distribution, migrations, and feeding habits in relation to OTEC siting and operation is necessary because of the importance of mammals in the marine environment. Marine mammals are often top predators in marine food chains, show complex social systems, communication, and high intelligence, and are an integral part of the ocean environment. In addition, many marine mammals have an endangered or threatened status and are protected under the Endangered Species Act of 1973, and all marine mammals in United States waters are given protection under the Marine Mammal Protection Act of 1972.

This report surveys current literature on tropical marine mammal ecology in the Gulf of Mexico and Hawaii. Much information was found in reviews (Caldwell and Caldwell, 1973; Gunter, 1954; Hershkovitz, 1966; Layne, 1965; Lowery, 1974; Marcuzzi and Pilleri, 1971; and Moore, 1953) as well as newly published records and accounts scattered throughout the literature. Where possible, distribution maps are presented and food habits are discussed.

General Information

The marine mammals potentially found at OTEC sites in the tropical ocean are divided into three main groups; the Sirenia or manatees and dugongs, the Pinnipedia or seals and sea lions, and the Cetacea or whales, dolphins, and porpoises.

Order Sirenia

The order Sirenia contains only two species, the manatees *(Trichechus* sp.) and dugongs *(Dugong* sp.), but only the manatee is found near potential OTEC sites. Manatees are wholly aquatic inhabitants of salt water bays or slow-moving brackish or fresh water streams. The front limbs are modified into flippers, there are no external hind limbs, and there is a broad, flat tail. They may measure up to 15 feet long and weigh over 1/2 ton. Manatees are entirely vegetarian. Based on anatomical considerations, they are considered to be close to the evolutionary line which gave rise to the elephants.

Order Carnivora, Suborder Pinnipedia

The suborder Pinnipedia includes the seals, sea lions, fur seals, and walruses. In tropical OTEC sites, the only pinniped representatives are true seals in the family Phocidae, and possibly one feral sea lion in the family Otariidae. Seals and sea lions have limbs modified as flippers for swimming. True seals have no external ears, and the hind flippers cannot be brought under the body, making movement on land difficult. They are mostly aquatic but do come on to land for breeding and basking. Pinnipeds are carnivorous mammals which feed mainly on fish and squid.

Order Cetacea

Most marine mammals are in the order Cetacea, which contains the whales, dolphins, and porpoises. A wholly aquatic group, they are represented in all oceans and seas of the world. Like other marine mammals, they have the front limbs modified as flippers and there are no external hind limbs. The body is streamlined for efficient locomotion and skeletal and physiological modifications for deep diving are present. The cetaceans are divided into two suborders; the Mysticeti or baleen whales and the Odontoceti or toothed whales. The mysticetes have the embryonic teeth replaced by beleen or whalebone, and feed by straining small crustaceans and molluscs through the baleen plates. Most feed in Arctic or Antarctic seas during the polar summer, and undertake long migrations to tropical seas to breed. Included in the baleen whale group is the blue whale *(Balaenoptera musculus)*, the largest animal that has ever lived.

Most living cetaceans are toothed whales or odontocetes. They have no baleen, but may contain anywhere from a few to a great many calcified teeth. The skull has undergone great modification, including pronounced telescoping. Some species possess a "melon" or spermaceti organ in the skull, thought to function in echolocation. Whales and dolphins often show complex social systems, and are considered highly intelligent. They feed mainly on fish and squid, although the killer whale *(Orcinus orca)* also feeds on other whales and seals.

Marine Mammals of the Gulf of Mexico

Twenty-seven marine mammal species, mostly cetaceans, have been seen or stranded within the Gulf of Mexico (see Table 1). The most common are the bottlenosed dolphin *(Tursiops truncatus)* inshore, and the spotted dolphin *(Stenella platiodon)* offshore. Both of these small odontocetes are primarily fish-eaters, and travel in groups. The common dolphin *(Delphinus delphis)* is also fairly numerous, and the false killer whale *(Pseudorca crassidens)* and pygmy killer whale *(Kogia breviceps)* may be sighted less frequently. Although six endangered marine mammals have occasionally been seen or stranded in the Gulf of Mexico, none of the endangered species is common there. The West Indian manatee *(Trichechus manatus)*, an endangered species, is fairly numerous in Florida, but it is found so close inshore that it will be little affected by offshore OTEC operation. Some effects could occur with large surface chemical spills or shore buildings unless knowledge of the manatee is considered.

Table 1 Marine Mammals of the Gulf of Mexico and Hawaii

Species	Gulf of Mexico	Hawaii
Order Sirenia		
Family Trichechidae		
**Trichechus manatus*, West Indian manatee	common inshore	—
Order Carnivora, Suborder Pinnipedia		
Family Phocidae		
**Monachus shauinslandi*, Hawaiian monk seal	—	Common away from OTEC sites
**M. tropicalus*, Caribbean monk seal	extinct?	—
Family Otariidae		
Zalophus californianus, California sea lion	Rare, introduced	—
Order Cetacea, Suborder Mysticeti		
Family Balaenidae		
**Balaena glacialis*, Black Right whale	Rare	—
Family Balaenopteridae		
Balaenoptera acutorostrata, Minke whale	Rare	—
B. borealis, Sei whale	Rare	—
B. edeni, Bryde's whale	Rare	Occasional
**B. musculus*, Blue whale	Rare	?
**B. physalus*, Fin whale	Rare	?
**Megaptera novaeongliae*, Humpback whale	—	—
Suborder Odontoceti		
Family Delphinidae		
Delphinus delphis, Common dolphin	Fairly common	Fairly common†
Feresa attenuata, Pygmy killer whale	Rare	Fairly common
Globicephala macrorhyncus, Short-finned pilot whale	Rare	Rare
Grampus griseus, Risso's dolphin	Rare	Rare
Lagenodelphis hosei, Shortsnouted whitebelly dolphin	—	Rare
Orcinus orca, Killer whale	Rare	—
Peponocephala electra, Little blackfish	—	Rare
Pseudorca crassidens, False killer whale	Fairly common	Fairly common
Stenella attenuata, Spotted dolphin	—	Fairly common
S. coeruleoalba (= S. styx), Striped dolphin	Fairly common	Fairly common
S. frontalis (= S. clymene, Bridled dolphin	Fairly common	—
S. longirostris, Spinner dolphin	Rare	Common
S. plagiodon, Spotted dolphin	Common	Rare
Steno bredanensis, Roughtoothed Dolphin	Rare	Rare
Tursiops gilli, Pacific bottlenosed dolphin	—	Fairly common
Tursiops truncatus, Bottlenosed dolphin	Common	Fairly common
Family Physeteridae		
Kogia breviceps, Pygmy sperm whale	Common inshore in western Gulf	Rare
K. simus, Dwarf sperm whale	Rare	Rare
**Physeter catodon*, Sperm whale	Fairly common in past, now rare	Occasional
Family Ziphiidae		
Mesoplodon densirostris, Dense-beak whale	—	Rare
M. europaeus, Gulfstream beaked whale	Rare	—
Ziphius cavirostris, Goose-beak whale	Rare	Rare

*denotes endangered or threatened species

Trichechus manatus, West Indian manatee

The West Indian manatee is widespread in the eastern Gulf of Mexico, especially peninsular Florida (Caldwell and Caldwell, 1973). They are concentrated in Florida during the winter, but may be found as far north as North Carolina during summer (Irvine and Campbell, 1978). Manatees are adversely affected by cold temperature and generally remain within 5 km of a warm water source. Preferred manatee habitat is shallow salt-water bays and fresh- or brackish-water sluggish, coastal rivers (Moore, 1951), and they feed on aquatic vegetation such as eelgrass. The manatee is protected under Florida law, and the population, which numbers somewhere near 1000, has shown an increase in recent years. Manatees are located in coastal areas, and this endangered species should not be affected by offshore OTEC operation unless unforeseen large surface chemical spills occur.

Suborder Mysticeti, Baleen whales

Of the seven baleen whales which have been reported for the Gulf of Mexico, five are classified as endangered or threatened species. These are the black right whale *(Balaena glacialis)*, sei whale *(Balaenoptera borealis)*, blue whale *(B. musculus)*, fin whale *(B. physalus)*, and the humpback whale *(Megaptera novaengliae)*. The other two mysticetes which may occur in the Gulf are the minke whale *(B. acutorostrata)* and Bryde's whale *(B. edeni)*. All are apparently rare within the Gulf. The humpback whale apparently was common in the Gulf of Mexico in the past, as commercial whaling for this species in the central Gulf and off of Florida occurred during the 19th century (Townsend, 1935).

Delphinus delphis, Common dolphin

The common dolphin may be one of the most numerous cetaceans near potential OTEC sites. The common dolphin is widely distributed in warm temperate and tropical waters of all oceans (Ricc, 1977). It is a pelagic migrant which follows the migrations of its food source, especially sprat *(Clupea spratus)* and anchovy *(Engraulis encrasicholus)* (Marcuzzi and Pilleri, 1971). Sightings of common dolphins in the eastern Gulf of Mexico from both coastal and offshore areas are shown in Figure 1. They have been observed in the Gulf in waters 1200-1500 meters, (m) deep and 120-148 miles from land (Caldwell, 1955).

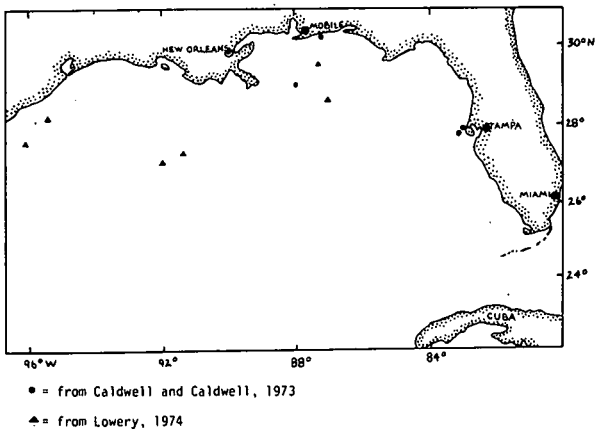

Fig. 1 Sightings of the common dolphin, *Delphinus delphis*, in the Gulf of Mexico.

Stenella spp., Spotted and spinner dolphins

The spotted dolphin *(S. plagiodon)* is probably the most common cetacean species offshore in the Gulf of Mexico. Spotted dolphins occur 12 or more miles offshore, in waters greater than 10 m deep (Caldwell and Caldwell, 1966). During the spring they move close inshore off of Florida, which suggests either an annual northward migration or a seasonal inshore-offshore movement at the same latitudes. Groups of from 1 to 30 spotted dolphins have been seen offshore in the Gulf of Mexico (Caldwell, 1955; Caldwell, 1960) (see Figure 2), and are apparently fairly numerous in potential OTEC areas. They feed on cephalopods and fish, including herring (Clupeidae), anchovies (Engraulidae), and the carangid fishes *Decapterus* sp. and *Selar* sp. (Caldwell and Caldwell, 1966). Occasional records of other *Stenella* species have been recorded for the Gulf. *S. coeruleoalba*, the striped dolphin, and *S. longirostris*, the spinner dolphin were reported by Caldwell and Caldwell (1973), and *S. frontalis*, the bridled dolphin, by Schmidly et al. (1972).

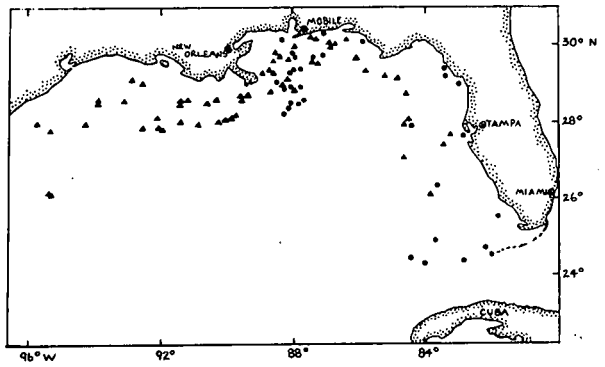

Fig. 2 Sightings of the spotted dolphin, *Stenella plagiodon*, in the Gulf of Mexico.

Tursiops truncatus, bottlenosed dolphin

The bottlenosed dolphin is the most common inshore cetacean species in the Gulf of Mexico, with a continuous distribution around the Gulf from Texas to Florida (Caldwell and Caldwell, 1973) (see Figure 3). *Tursiops* probably rarely exceeds the limit of the continental shelf offshore, beyond which it is replaced by the spotted dolphin, *Stenella plagiodon*. It occurs most frequently in bays and brackish water, and near large passes in Texas (Gunter, 1942). A food habits study of the bottlenosed dolphin in Texas (Gunter, 1942) showed that they eat a variety of species, with mullet *(Mugil cephalus)* constituting 83% of the fish eaten (see Table 2). Nine different fish species were reported in this study, and Odell (1975) reports six more fish species eaten by *Tursiops*, as well as eel and squid (Table 2).

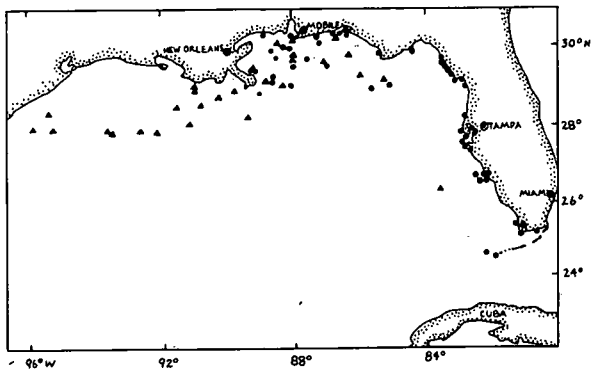

Fig. 3 Sightings of the bottlenosed dolphin, *Tursiops truncatus* in the Gulf of Mexico.

Table 2 Prey items of the bottlenosed dolphin *(Tursiops truncatus)* in the Gulf of Mexico

Species	Number taken	Source
Mugil cephalus, Striped mullet	423 (83%)	
Dorosoma cepedianum, Gizzard shad	40	
Sphoeroides marmoratus Puffer	3	
Archosargus probatocephalus Sheephead	2	
Strongylura marina, Needle-gar	1	
Pogonias cromis Black drum	1	Gunter, 1942
Cynoscion nebulosis Spotted trout	1	
C. arenarius Sand trout	1	
Paralichthys lethostigmus Flounder	1	
Leiostomus xanthurus Spot	12?	
Micropogon undulatus Croaker	12?	
C. arenarius Sand trout	12?	
Penaeus setiferus Shrimp	1	

Species		Source
Astroscopus y-graecum	Stargazer	
Galeicthys felis	Sea catfish	Caldwell and Caldwell, 1972
Scaenidae	Croaker and Drum	
Clupeidae	Herring	Reported in Odell, 1975
Belonidae	Needlefish	
Eels		
Squid		

Other Delphinids

The remaining dolphins within the family Delphinidae listed in Table 1 as occurring in the Gulf are in general little known and not expected to occur in large numbers near potential OTEC sites. The pygmy killer whale *(Feresa attenuata)* is one of the least known cetaceans. Its distribution is thought to be circumglobal (Caldwell and Caldwell, 1971). A single specimen has been recorded from the Gulf of Mexico in Texas (James et al. 1970).

The short-finned pilot whale *(Globicephala macrorhynca)* is represented in the Gulf of Mexico by numerous strandings along the southern Florida coast, Louisiana, and Texas (Caldwell and Caldwell, 1973). Strandings of this species far outnumber those of other cetaceans, and the seasonality of stranding data suggest either that actual seasonal movements occur, or that seasonal biological or abiological factors may affect the tendency to strand (Layne, 1965). The pilot whale has not been frequently sighted at sea, however.

Risso's dolphin *(Grampus griseus)* is a cosmopolitan, pelagic species found in all seas. It is uncommon in the Gulf; one stranding has been reported in Florida (Paul, 1968). Risso's dolphin may winter in southern waters and move north during summer (ibid.).

The killer whale *(Orcinus orca)* is a pelagic and oceanic species which occurs circumglobally, although more frequently in cold seas (Marcuzzi and Pilleri, 1971). The killer whale is carnivorous and feeds on a wide variety of prey, including other whales and seals as well as fish and squid. The killer whale is uncommon in the Gulf of Mexico. (Caldwell and Caldwell, 1973; Moore, 1953).

The false killer whale *(Pseudorca crassidens)* has been sighted in the central Gulf at 26°30'N, 89°15'W (Bullis and Moore, 1956), and Texas (Schmidly and Melcher, 1974). Brown et al. (1966) report that fishermen working in the northeast Gulf from shore to 50 miles offshore have seen "blackfish" *(Pseudorca)* singly or in herds up to 100, in waters 60 m deep or greater, and 20+ miles offshore. It is considered a very social form, as evidenced by the large herds at sea and mass strandings. False killer whales have been observed feeding on amberjack *(Seriola lalandi)* and bonito *(Sarda lineolata)*, and are frequent predators on large pelagic fishes.

The rough-toothed dolphin *(Steno bredanensis)* is recorded in the Gulf of Mexico from an unpublished record offshore and one in Texas (Schmidly and Melcher, 1974), and from a mass stranding of 16 dolphins in Florida (Layne, 1965). Stomach content analysis of the stranded dolphins revealed that they had fed on the blanket octopus *(Tremoctopus violaceus)*, a fairly common pelagic cephalopod.

Family Physeteridae, sperm whales

There are three members of the family Physeteridae; the sperm whale *(Physeter catodon)*, pygmy sperm whale *(Kogia breviceps)*, and dwarf sperm whale *(K. simus)*. The sperm whale, classified as a threatened species, is the largest Odontocete cetacean. It is found in all oceans except polar ice-fields (Rice, 1977), and most often in tropical, subtropical, and very warm currents (Marcuzzi and Pilleri, 1971). Deep water is preferred, and sperm whale distribution coincides with areas of major upwelling. At one time sperm whales were common enough in the Gulf to support whaling efforts, especially in the area

from 28-29°N and 88-90°W, and in the central Gulf (Caldwell and Caldwell, 1973). Since 1910, four strandings in Florida have occurred, and two in Texas. Sperm whales are now rarely seen or stranded in the Gulf. They feed primarily on squid, and also on octopuses, sharks, skates, and bony fishes (Lowery, 1974).

The pygmy sperm whale and dwarf sperm whale are closely related pelagic species which occur in warm waters worldwide (Marcuzzi and Pilleri, 1971). It is not known whether they migrate. Both have been stranded in the Gulf several times in Florida and Texas, and the pygmy sperm whale is considered one of the most common cetaceans in coastal Texas waters (Shane and Schmidly, 1978). A seasonal distribution of strandings suggests that *Kogia* spp. may move northward toward the pole in summer to feed and return to warmer waters to breed during winter (Schmidly and Melcher, 1974). The stomach contents of a specimen of the dwarf sperm whale from the Gulf of Mexico were examined by Raun, et al. (1970). Squid beaks predominated, and of these only *Ommastrephes* sp. could be identified. Also found were the mysid shrimp *Gnathophausia ingens,* and the peneid shrimp *Aristaemorpha foliacea,* a pelagic shrimp from depths of below 300 m.

Family Ziphiidae, Beaked whales

Two beaked whales have been reported in the Gulf of Mexico; the Antillean or Gulf Stream beaked whale *(Mesoplodon europaeus = M. gervaisi)* and the goose-beaked whale *(Ziphius cavirostris)*. The Gulf Stream beaked whale occurs in the North Atlantic and a few strandings have occurred in the Gulf of Mexico (Moore, 1966). A specimen from Texas first identified as *M. densirostris* (Gunter, 1955) was later found to be *M. europaeus* (G. Gunter, pers. comm., and Moore, 1960).

The goose-beaked whale has stranded in the Gulf on six occasions, in Florida, Louisiana, and Texas (Schmidly and Melcher, 1974).

The Marine Mammals of Hawaii

Twenty-two marine mammal species may occur in Hawaii, including two mysticetes, 19 odontocetes, and one pinniped (see Table 1). In contrast to the Gulf of Mexico site, where no endangered species are common offshore, one of the most abundant cetaceans in Hawaii is an endangered species, the humpback whale *(Megaptera novaengliae)*. This large mysticete occurs in Hawaii during the winter months, where it migrates to breed. Another endangered species, the Hawaiian monk seal *(Monachus schauinslandi)* is present in fairly large numbers in Hawaii and nowhere else in the world, but its habitat is the far northwestern island chain, away from potential OTEC sites in Hawaii. As in the Gulf of Mexico, dolphins in the genus *Stenella* are the most numerous small odontocetes in Hawaii. They have been sighted in coastal areas throughout the island chain, and a 250-member population of *Stenella longirostris,* the spinner dolphin, occurs off of Keahole Point, a potential OTEC area. The bottlenosed dolphin, *Tursiops* spp., is also fairly common in Hawaii, while the false killer whale *(Pseudorca crassidens)* and pygmy killer whale *(Feresa attenuata)* may be sighted less frequently.

Monachus schauinslandi, Hawaiian monk seal

The Hawaiian monk seal is a member of the rare pinniped genus *Monachus*, which includes the now extinct Caribbean monk seal *(M. tropicalus)* which once flourished in the Gulf of Mexico, and the rare Mediterranean monk seal *(M. monachus)*. Hawaiian monk seals, an endangered species endemic to Hawaii, breed on Kure, Pearl, Lisianski, Laysan, and French Frigate Shaoals atolls in the leeward island chain. Breeding occurs from late December through mid-August, with a peak between March and May (Kenyon, 1973). The population is considered non-migratory, although occasional individuals may "straggle" as far as the big island of Hawaii. They are bottom feeders whose diet consists of coral-reef and shallow-water cephalopods and fish. Because the population is localized far from potential OTEC sites, they should not be impacted by OTEC operation.

Megaptera novaengliae, Humpback whale

Of the larger cetaceans which may occur in Hawaii, the humpback whale is encountered most frequently. The estimated worldwide population of humpbacks, protected as an endangered species since 1970, is 5200-7000, 1200 of which are found in the north Pacific, and no more than a few hundred of these east of 140°W. (Jurasz and Wolman, 1977). In 1977, a census of the Hawaiian population indicated a population estimate of 500 (Rice and Wolman, 1978). Humpback whales feed in colder temperate and sub-polar waters during summer, and migrate to tropical waters to breed during winter. Hawaii is one of five breeding areas in the world. The whales are at the Hawaiian breeding ground from December to May, and are usually found on the leeward sides of islands, in waters less than 180 m deep (see Figure 4). Calving occurs in five shallow sand-bottomed areas in Hawaii, four of which are shown in Figure 4 of this report. They are found most frequently in areas with little human disturbance, and there is evidence that the whales may be leaving certain areas of human activity. The humpback whale is probably the most important marine mammal to consider when examining potential OTEC sites and operation in Hawaiian waters.

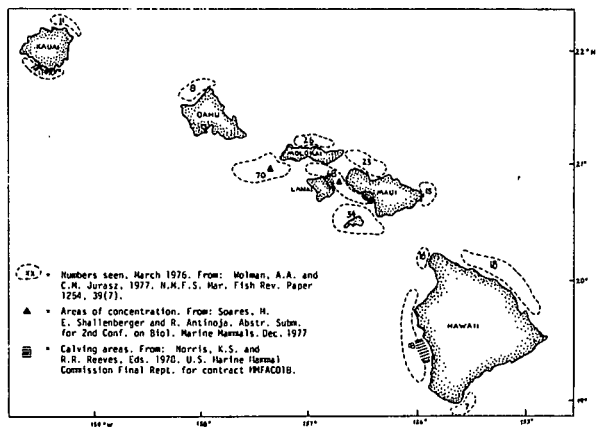

Fig. 4 Humpback whale *(Megaptera novaeangliae)* distribution in Hawaii.

Other Mysteceti

The Bryde's whale, *Balaenoptera edeni*, has been sighted in Hawaii (DeLong and Brownell, 1977). Although most likely of the rorquals (genus *Balaenoptera)* to be found near Hawaii, the scanty data suggests that its presence is not common. The Bryde's whale feeds primarily on herring and also on *Euphausiacea* (Marcuzzi and Pilleri, 1971). Other balaenopterids may occur near Hawaii only as occasional migrants.

Delphinus delphis, Common dolphin

The common dolphin is widely distributed in warm temperate and tropical waters, and in the eastern tropical Pacific is often found in association with other dolphins *(Stenella* spp.*)* and yellowfin tuna *(Thunnus albacares)*. It may be expected to occur near Hawaii. A wide variety of fish is eaten by these dolphins, which may be deep-water or bottom-feeders (200 m depth) (Fitch and Brownell, 1968).

Feresa attenuata, Pygmy killer whale

The pygmy killer whale is considered a regular resident of the Hawaiian Islands (Pryor, et al., 1965). It may be one of the more common odontocetes at potential OTEC sites, although its habits are not well known.

Pseudorca crassidens, False killer whale

The false killer whale may be fairly common in Hawaii. It has been observed feeding on dolphinfish *(Coryphaena* sp.*)* off the Kona coast of Hawaii (Brown, et al. 1966). It is a frequent predator on large pelagic fishes.

Stenella spp., Spinner, spotted and striped dolphins

Three main groups of dolphins in the genus *Stenella* may be differentiated based upon differences in snout length and color pattern (Rice, 1977). Most abundant of the small odontocetes in Hawaii is the spinner dolphin, *S. longirostris* (see Figure 5). Also present are the spotted dolphin, *S. attenuata*, and the striped dolphin, *S. coeruleoalba*. Spinner dolphin distribution in Hawaii is heterogeneous, with concentrated areas of congregation and stretches where the dolphins are not seen (Norris and Dohl, 1978). A 250-member population at Keahole Point moves offshore from shallow rest areas to waters of 2000 m depth. They are nocturnal feeders which feed upon fish and crustaceans which approach the surface only at night.

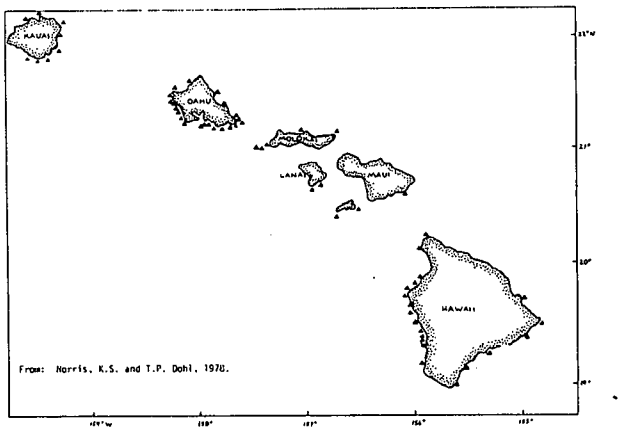

Fig. 5 Sightings of spinner dolphins *(Stenella longirostris)* off Hawaii.

Both spotted and spinner dolphins are often found in close association with yellowfin tuna *(Thunnus albacares)* in the eastern tropical Pacific ocean. The dolphins are sometimes taken in tuna nets incidental to tuna fishing. Stomach-content analysis of 140 spotted and 46 spinner dolphins was performed by Perrin, et al. (1973). Of the 46 spinner dolphin stomachs examined, 19 were empty. Squid and fish, especially myctophids, each made up approximately one-half of the stomach contents of the remaining dolphins. An ommastrephid squid, probably *Doscidius gigas*, was the predominant squid species. *Benthosema panamense, Diogenichthys* sp., *Vinciguierra* sp., and *Bregmaceros* sp. were important fish species in the spinner dolphin stomachs (see Table 3).

Table 3. Summary of important fish and squid species from stomachs of Stenella sp. taken in the Eastern Tropical Pacific *

	Spotted *S. attenuata*	Spinner *S. longirostris*
Fishes:		
Oxyporhampus micropterus	+ + + +	
Auxis Sp.	· · ·	
Diogenicthys sp.	+ +	·
Benthosema panamense		+ ·
Vinciguierra sp.	+	+ ·
Bregmaceros sp.	+ +	·
Squids:		
Onykis sp.	+ ·	+ ·
Ommastrephid A (*Doscidius gigas*?)	· · · · ·	· ·
Ommastrephid B (*Symplectoteuthis*?)	+ + + · · ·	
Abraliopsis affinis	+ + · ·	
	6 hauls examined	2 hauls examined

+ = present in one haul
· = common in one haul

*Modified from Perrin, et. al. (1973)

The stomachs of 140 spotted dolphin, taken from six net hauls were examined in this same study. In four of six hauls, squid predominated, especially *Symplectoteuthis* sp. (see Table 3). In two of the net hauls, ommastrephid squid made up over 85% of the food content by number. Onyctoteuthid squid, especially *Onykis* sp., were also found. Small mesopelagic fishes are apparently a much less significant food source for the spotted dolphin as compared to the spinner dolphin. Of the fish present, *Oxyporhampus micropterus, Diogenichthys* sp., and *Bregmaceros* sp. were found most often.

Spinner dolphin and spotted dolphin apparently have mostly different prey items and feed at different times of day. Spotted dolphins feed at the surface and largely on epipelagic prey; while the spinner dolphin feeds in deeper water and mainly on mesopelagic ommastrephid squid.

Steno bredanensis, Rough-toothed dolphin

The rough-toothed dolphin, a pelagic species which inhabits deep water, is fairly common in Hawaiian waters. It has been reported from the eastern tropical Pacific by Perrin and Walker (1975). Little is known of the habits or actual numbers of this species at potential OTEC sites.

Tursiops spp., Bottlenosed dolphin

Both *Tursiops truncatus* and the closely related form *T. gilli* may be found near Hawaii. *T. truncatus* was sighted most frequently during cetacean observations in the leeward Hawaiian chain (DeLong and Brownell, 1977). The size of the Hawaiian *Tursiops* population, not including the leeward chain, is estimated at 500-1000 individuals (Orr, 1978). No migration patterns are known; the animals apparently stay near the islands, and travel in groups of 5-20 individuals.

Other Delphinidae

Little literature exists on the other members of the family Delphinidae listed in Table 1. All are tropical species which are expected to occur in Hawaiian waters.

Family Physeteridae, Sperm whales

The sperm whale *(Physeter catodon)* is the largest of the toothed whales. Sperm whales are at the apex of the food chain, feeding on giant squid, a second or third level predator. Cephalopods such as squid occur in large numbers where warm and cold currents meet, coinciding with higher sperm whale density (Gulland, 1974). North Pacific catch records show that sperm whales were found near Hawaii in the summer and more frequently in winter (Rice, 1974). Sperm whale populations have decreased as a result of whaling, and they may occasionally be seen near Hawaii. They are classified as a threatened species.

The pygmy sperm whale *(Kogia breviceps)* and dwarf sperm whale *(K. simus)* are little-known, relatively uncommon relatives of the sperm whale. They feed on squid, crabs, and shrimp (Handley, 1966).

Family Ziphiidae, Beaked whales

The densebeak whale, *Mesoplodon densirostris*, is a widely but sparsely distributed species which has been reported for Hawaii by Moore and Gilmore (1967). The goosebeak whale, *Ziphius cavirostris*, is a cosmopolitan, pelagic species which undertakes long migrations. Little is known of the habits of these two species, and they are probably uncommon in Hawaii.

Possible Environmental Effects of OTEC Plants

Operation of OTEC plants in the Gulf of Mexico and Hawaii may have several environmental effects which could affect marine mammals. These include (modified from U. S. Dept. of Energy, 1979):
(1) toxic effects of discharge of chlorinated compounds (biocides) used in cleaning heat exchangers;
(2) toxic effects of accidental spillage of working fluid (NH_3) from storage tanks, or heat exchanger leaks;
(3) biostimulating effects of redistribution and release of deep nutrient-rich seawater to the photic zone;
(4) a possible petroleum spill due to increased boat traffic at the site;
(5) toxic effects of release of some waste effluents;
(6) effects due to the physical presence of an OTEC plant.

Continuous discharge of chlorinated compounds might cause a change in phytoplankton, zooplankton, and fish depending on resistances to total residual organics. A change in biomass at all trophic levels may adversely affect the ichtyophagous cetaceans which normally feed in an OTEC area.

Accidental ammonia spillage would probably be detected by taste or smell by marine mammals in the vicinity, and the animals would rapidly move away. Since the ammonia spills are likely to be a thin plate of toxicant moving mostly downstream, they should be relatively easy to avoid.

The redistribution of cold, nutrient-rich seawater to a higher level in the water column may increase primary productivity. Increases in zooplankton are expected to be small and effects on planktophagous marine mammals will be negligible since they apparently do not feed in tropical waters. If the biostimulating effects of OTEC could affect fish or squid, it is highly unlikely that any such indirect effects on cetaceans will be detectable.

Mammals in the vicinity of a temporary oil spill from boat traffic will be less affected than most other organisms because they will most likely be able to avoid the area.

Release of waste effluents such as sewage should have a minimal effect on air-breathing mammals if the effluent is rapidly diluted.

The physical presence of an OTEC plant may induce avoidance behavior in mammals or desertion of the area, especially if construction is prolonged. Eventual habituation to its presence may occur, or they may even be attracted to it. As the OTEC plant will cause some fish or squid to be attracted, this may affect the feeding ecology of ichthyophagous cetaceans in the area.

Special attention must be given to siting of an OTEC plant away from the critical habitat of any endangered species. The humpback whale in Hawaii is the most numerous endangered species at potential OTEC sites; construction of an OTEC plant there should be restricted to periods when the humpbacks are not present (i.e., summer) and the site should be away from humpback calving and breeding areas.

References

Brown, D. H., M. C. Caldwell, and D. K. Caldwell, 1966. Observations on the behavior of wild and captive false killer whales, with notes on associated behavior of other genera of captive delphinids. L. A. Co. Mus. Contrib. Sci. 95: 1-32.

Bullis, H. R. and J. C. Moore, 1956. Two occurrences of false killer whales and a summary of American records. Amer. Mus. Novitiates. 1756: 1-5.

Caldwell, D. K. 1955. Notes on the spotted dolphin *Stenella plagiodon* and the first record of the common dolphin *Delphinus delphis* in the Gulf of Mexico. J. Mammal. 36(3): 467-470.

_____. 1960. Notes on the spotted dolphin in the Gulf of Mexico. J. Mammal. 41(1): 134-136.

_____ and M. C. Caldwell. 1966. Observations on the distribution, coloration, behavior, and audible sound production of the spotted dolphin, *Stenella plagiodon* (Cope). L. A. Co. Mus. Contrib. Sc. 104.

_____ and M. C. Caldwell. 1969. Gray's dolphin, *Stenella styx*, in the Gulf of Mexico. J. Mammal. 50: 612-614.

_____ and M. C. Caldwell. 1971. The pygmy killer whale, *Feresa attenuata*, in the western Atlantic with a summary of world records. J. Mammal. 52: 206-209.

_____ and M. C. Caldwell. 1972. The world of the bottlenosed dolphin. Lippincott, Philadelphia, Pa. 157 pp.

_____ and M. C. Caldwell. 1973. Marine mammals of the eastern Gulf of Mexico. pp.III-1-1 to III-1-23 in: Jones, J., ed. A Summary of Knowledge of the Eastern Gulf of Mexico. State Univ. System of Fla., Inst. of Oceanography, St. Petersburg, 602 pp.

DeLong, R. L. and R. L. Brownell. 1977. Hawaiian monk seal *(Monachus schauinslandi)* habitat and population survey in the northwestern (leeward) Hawaiian Islands, April 1977. N.M.F.S., N.W. and Alaska Fish. Cent., Seattle, Washington. Unpubl. 1-30.

Fitch, J. E. and R. L. Brownell, Jr. 1968. Fish otoliths in cetacean stomachs and their importance in interpreting feeding habits. J. Fish Res. Bd. Can. 25(12): 2561-2574.

Gunter, G. 1942. Contributions to the natural history of the bottlenosed dolphin, *Tursiops truncatus*, (Monatague) on the Texas coast with particular reference to food habits. J. Mammal. 23: 267-276.

_____. 1954. Mammals of the Gulf of Mexico. pp. 543-551 in: Gulf of Mexico, its origin, waters and marine life. P. S. Galtsoff, ed. U. S. Fish and Wildl. Serv. Fish Bull. vol. 55.

_____. 1955. Blainville's beaked whale, *Mesoplodon densirostris*, on the Texas Coast. J. Mammal. 36: 573-574.

Hershkovitz, P. 1966. Catalog of living whales. Bull. U. S. Nat. Mus. 246: 1-259.

Irvine, A. B. and H. W. Campbell, 1978. Aerial census of the West Indian manatee, *Trichechus manatus*, in the Southeastern United States. J. Mammal. 59(3): 613-617.

James, P., F. W. Judd, and J. C. Moore. 1970. First western Atlantic occurrence of the pygmy killer whale. Fieldiana: Zool. 58: 1-3.

Jurasz, C. M. and A. A. Wolman. 1977. Humpback whales in Hawaii: vessel census 1976. Mar. Fish. Rev. paper 1254, vol. 39 no. 7.

Kenyon, K. W. 1973. The Hawaiian monk seal. In: Seals; Proc. workshop of seal specialists on threatened and depleted seals of the world, 18-19 Aug. 1972, Guelph, Canada. IUCN (World Wildlife Fund, publ.) Switzerland. pp. 88-97.

Layne, J. N. 1965. Observations on marine mammals in Florida waters. Bull. Fla. State Mus. Biol. Sci. 9(4): 132-181.

Lowery, G. H. 1974. The mammals of Louisiana and its adjacent waters, Louisiana State Univ. Press, Louisiana Wildlife and Fisheries Commission.

Marcuzzi, G. and G. Pilleri. 1971. On the zoogeography of Cetacea. Investigations on Cetacea, G. Pilleri, Ed.

Moore, J. C. 1951. The status of the manatee in the Everglades National Park, with notes on its natural history. J. Mammal. 32(1): 22-36.

_____. 1953. Distribution of marine mammals to Florida waters. Amer. Midl. Nat., 49(1): 117-158.

_____. 1966. Diagnoses and distributions of beaked whales of the genus *Mesoplodon* known from North American waters. In: Norris, K. S., ed. Whales, dolphins, and porpoises. U. C. Press, 1966.

_____ and R. M. Gilmore. 1967. A beaked whale new to the western hemisphere. Nature 205: 1239-1240.

Norris, K. S. and T. P. Dohl. 1978. ms. The behavior of the Hawaiian spinner porpoise, *Stenella longirostris* (Schlegl, 1841). Center for Coastal Marine Studies, U. C. Santa Cruz.

Odell, D. K. 1975. Status and aspects of the life history of the bottlenosed dolphin, *Tursiops truncatus*, in Florida. J. Fish. Res. Bd. Canada 32(7): 995-1004.

Orr, J. M. 1978. A survey of *Tursiops* populations in the coastal United States, Hawaii, and territorial waters. U. S. Marine Mammal Comm., Requisition no. PL 92-522.

Paul, J. R. 1968. Risso's dolphin, *Grampus griseus*, in the Gulf of Mexico. J. Mammal. 49(4): 746-748.

Perrin, W. F. and W. A. Walker, C. H. Fiscus, and D. B. Holts. 1973. Stomach contents of porpoise, *Stenella* spp., and yellowfin tuna, *Thunnus albacares*, in mixed-species aggregations. U.S.F.W.S. Fish. Bull 71: 1077-1092.

Pryor, T., K. Pryor, and K. S. Norris. 1965. Observations on a pygmy killer whale *(Feresa attenuata* Gray) from Hawaii. J. Mammal. 46: 450-461.

Raun, G. G., H. D. Hoese, and F. Mosely. 1970. Pygmy sperm whales, genus *Kogia*, on the Texas coast. Texas J. Sci. 21: 269-274.

Rice, D. W. 1974. Whales and whale research in the Eastern North Pacific. Chap. 6 in: W. E. Schevill, ed., The Whale Problem.

_____. 1977. A list of the marine mammals of the world. NOAA Tech. Rep. NMFS SSRF-771.

_____ and A. A. Wolman. 1978. Humpback whale census in Hawaiian waters—February 1977. Preliminary report of an ongoing study. Appendix V in: Norris, K. S. and R. R. Reeves, eds. Report on a workshop on problems related to humpback whales in Hawaii, M.M.C. Contract MM7AC018.

Schmidly, D. J., M. H. Beleau, and H. Hildebran. 1972. First record of Cuvier's dolphin from the Gulf of Mexico with comments on the taxonomic status of *Stenella frontalis*. J. Mammal. 53(3): 625-628.

_____ and B. A. Melcher. 1974. Annotated checklist and key to the cetaceans of Texas waters. Southwestern Nat., 18: 453-464.

Shane, S. H. and D. J. Schmidly. 1978. A biological assessment of the cetacean fauna of the Texas coast. Final report to U. S. Marine Mammal Commission, Contract MM4AC008. June 1978.

Townsend, C. H. 1935. The distribution of certain whales as shown by loggbook records of American whaleships. Zoologica 19: 1-50.

United States Department of Energy. 1979. Environmental Assessment: Ocean Thermal Energy Conversion (OTEC) Program; Preoperational Ocean Test Platform, DOE, Washington, D. C. 2 vols. DOE-EA-0062.

14. LEGAL AND INSTITUTIONAL

LEGAL ASPECTS OF SITING OTEC PLANTS OFFSHORE THE UNITED STATES, ON THE HIGH SEAS, AND OFFSHORE OTHER COUNTRIES

J. D. Nyhart*

Sloan School of Management
Department of Ocean Engineering
Massachusetts Institute of Technology
Cambridge, Massachusetts 02139

Abstract

Likely sites for OTEC plants identified by the Department of Energy for purposes of legal analysis are within 200 miles of the United States or other nations, or elsewhere on the high seas. In the first two cases, OTEC operations will be within the Exclusive Economic Zone of the coastal state, assuming such zones are created by a future Law of the Sea Treaty. Possible policy goals and problem areas for U.S. policy planners concern coastal state dominance and conflicting interests among coastal states; the arrangement of mutually beneficial international legal arrangements; the protection of major U.S. interests in maximum access for OTEC plants in high seas deployment; creation of protected rights, interests or influence in other countries' economic zones; establishment of standards and liability for transzonal environmental effects; the acquisition of MARAD incentives to reduce investor uncertainty; and, potential inconsistencies among U.S. policies. Additional problem areas concern inertia in global institution building, the desirability of optimizing goals with minimum institutional innovation, the nature of legal status accorded sea-borne OTEC plants, the nature of national legislation concerning OTEC operations, and the location of U.S. sites. (112 references)

Introduction

This paper highlights the analyses and conclusions from eight papers comprising a report undertaken for the U.S. Department of Energy's Oceans System Branch, Division of Solar Energy (DOE) by the American Society of International Law (DOE Contract #EG-77-C-01-4118). Authors of the papers were: Robert S. Faron, Eugene R. Fidell, Ann L. Hollick, H. Gary Knight, J. D. Nyhart, Robert E. Stein and Byron J. Washom. Fuller identification is found in note 1. As the author of this paper and the longer summary submitted to DOE, I have acted as much as a consolidating editor as a writer. Passages from the panel papers are frequently found in this summary, and are referenced to the full, individual reports, to which readers are referred.

Six Sites in Three Legal Zones

Research summarized in this report was conducted largely in the context of specific projected locations for OTEC emplacements, identified by Department of Energy research staff.[1] They present a broad range of legal contexts and problems. The six major sites are:

U.S., West Coast Florida: A system of moored, floating plants of 400 megawatts each, located 150 miles offshore in a U.S. exclusive economic zone (EEZ), supplying power to U.S. grid by D.C. cable; the system comprises two or three parks or clusters of plants, each park growing in number from one to two to up to eight plants or approximately 3000 megawatts per park by the year 2000.

U.S., Puerto Rico: A system of one to eight individual plants located about 10 miles offshore, each of 400 megawatts or less, probably connected by A.C. cable to Puerto Rico's power system, although production of energy intensive commodities is an option.

Mexico: One, perhaps more, 400 megawatt plant located 200 or fewer miles offshore.

Cuba: One, perhaps more, 400 megawatt plant located 200 or fewer miles offshore in Cuba's EEZ, and cable linked to shore, or possible commodity producing.

Bahamas: One, perhaps more, 400 megawatt plant located 200 or fewer miles offshore, in Bahamas' EEZ, and cable linked to shore, or possible commodity producing.

High Seas, Brazil: A system of up to 10 floating, non-moored plants operating in clusters as a migrating flotilla spaced nominally one to nine kilometers apart, and moving in an area located approximately 300 miles offshore, but sometimes moving into area claimed as territorial by Brazil.

These six sites fall into three generic zones for the purpose of legal analysis: offshore U.S. (Florida and Puerto Rico sites), offshore a foreign country (Mexico, Cuba and Bahamas) and on the high seas nominally beyond the claimed zonal jurisdiction of any state. These three categories form the basis for the analyses in section III.

Six Issue Areas

The legal issues for each specific site, grouped in the three zones just identified, were analyzed in terms of six issue areas: 1) international legal and political framework, 2) international arrangements, 3) international regulatory law, including that pertaining to environmental protection, 4) criminal law, 5) private and residual law, and, 6) financing.

U.S. Legal Policy Goals for OTEC Planners

Several possible policy goals pertaining to legal developments can be identified for consideration by OTEC policy planners. Many are not mutually exclusive. They include several pertaining to jurisdictional issues:

*Associate Professor of Management and Coordinator of Law-Related Studies

1) To facilitate the deployment of research and commercial OTEC devices generally.

2) To maximize the area of world ocean space available for deployment of OTEC devices without consent.

3) To ensure exclusivity of control over OTEC devices deployed within 200 miles of the U.S. coast.

4) To ensure that the conditions of access for an OTEC device to another nation's economic zone are as unrestrictive as possible.

5) To ensure that any jurisdictional arrangement for OTEC devices does not prejudice other U.S. ocean interests, particularly interests in maximizing freedom of navigation.[2]

Another set relates to the creation of an adequate legal regime or regimes for OTECs:

1) To provide recognition in international law of OTECs as a legitimate ocean use.

2) To provide for means of registration or other mechanisms by which OTECs are recognized as belonging to and subject to the laws of one or more nations (that is, it may be that OTECs might "belong" to one state, and be subject as well to the laws of another).

3) To provide, if necessary, exclusive access to the spot or area of the ocean in which OTECs operate.

4) To make applicable to OTECs,[3] as appropriate, existing and proposed international regulations and standards.

5) To identify the regulations which may be applicable to OTECs operating within the economic zone or other extended jurisdiction zones of coastal states, and to establish and make applicable, any additional regulations which may be appropriate.

6) To identify the body or bodies of criminal law applicable to OTEC.

7) To identify existing, and where appropriate, to create new mechanisms for establishing liability for harm from collisions, personal injury, environmental damage, etc., caused by conduct or non-conduct of the OTEC or its operators, which fall below statutory or non-statutory standards of care, and to identify means for recovering damages arising from contractual infractions.

8) To identify the body or bodies of law which will serve as the residual law, filling any interstices left by laws falling under 5-7, above.

9) To establish the judicial fora which will have jurisdiction over criminal, statutory and common law cases pertaining to OTEC.[4]

Site Analyses

As indicated, the six hypothetical OTEC locations involve three generic legal contexts -- an (assumed) U.S. Exclusive Economic Zone, the economic zones of other states, and the high seas. Legal and policy issues in the six areas just identified are reviewed for each context.

The U.S. Exclusive Economic Zone: The Florida West Coast[5]

The assumption here is that OTECs would be built at an average of fewer than one a year, with perhaps 14 to 20 400-megawatt plants on line by the end of the century, clustered in two or three "parks" (with five to eight plants per park). They will be moored approximately 150 miles offshore and feed power to a park collector station, which will transmit it to shore by D.C. cable. The cable requires a right-of-way zone six miles wide.[6]

International Jurisdictional and Political Issues. In terms of present international law, the site will be on the high seas. To the extent that OTEC does not interfere with the exercise of rights recognized by other principles of international law, any nation is free to engage in such energy production exercises on the high seas.[7] Under prospective future developments, the site is likely to be in a future U.S. Exclusive Economic Zone[8] and this assumption as to the future is made throughout this section.

The major political issues raised are those stemming from adverse effects of the U.S. OTECs on neighboring nation states that are further "downstream". The waters which move through the site pass by the northern coast of Cuba, the Bahamas and become the Gulf Stream. The Gulf Stream moderates the climate of Europe.

Also, other U.S. domestic users in the West Florida coast area -- fishers, shippers, sportsmen, and coastal residents -- may raise domestic political problems over the dislocation caused by dredging, changes in water quality, assembling plant on site and their emplacement.[9]

Thus the same environmental concerns impinging on U.S. politics will be of concern internationally.[10] Political assertion that these concerns are exclusively domestic would be double-edged, as the United States itself may also be interested in OTEC activities in the economic zone of other nations.[11]

International Arrangements. Attention will have to be given to the possible interaction with interests of other states, such as Cuba, which have declared (or might declare) their own 200-mile maritime zone.

For example, the United States and Cuba have negotiated a boundary agreement in the context of the U.S. Fishery Conservation and Management Act[12] and have negotiated a Governing International Fishery Agreement (GIFA).[13] Under it, Cuba enjoys rights to obtain permits to fish within the U.S. Fishery Conservation Zone. The impact of one or many OTECs in this site on Cuba's fishery rights, both in terms of physical and environmental hazards, would have to be weighed.[14]

If the number of OTECs grew to the point where navigation could be impeded, the need for a concurrent use agreement to ameliorate another state's objection at the diminishing of its free use of the high seas might be considered.[15] If rights other than navigation were in issue, still additional specific arrangements might be necessary.[16]

OTECs built in a foreign yard may be subject to legislation barring the transfer of vessels to other flag states.[17] If such foreign legislation was held to apply, then arrangements concerning title, operation, manning and financing might be affected.[18] Also, should the OTEC structure be of foreign flag or nationality, then the United States might insist upon the conclusion of an appropriate agreement with the other country before permitting the operation in the U.S. EEZ.[19]

Regulatory and Environmental Law. Generally, only those international regulatory standards which the United States has voluntarily agreed to imple-

ment for its vessels and/or non-vessel marine entities, would affect operation of moored OTECs within a zone subject to U.S. jurisdiction[20] although U.S. domestic regulations would be applicable in many circumstances.[21]

Safety considerations may suggest the creation of safety zones around OTEC structures which would constrain the freedom of navigation of vessels within the U.S. EEZ. Such zones are provided for presently around continental shelf fixed structures. Whether a safety zone concept around an OTEC would be acceptable in an international law in abssence of a specific international agreement is questionable.[22]

Environment. In this arena, the fallout of events such as the Amoco Cadiz may force an accelerated evolution of regulation tending toward limiting the freedom of action of vessels and other structures outside territorial limits.[23]

NEPA and section 311 of the FWPCA will apply to the OTEC work involved in burying the cable connecting the structure to the land power grid.[24]

A site specific environmental assessment should be begun.[25]

The United States, independently of its right to exploit the resource under its extended jurisdiction, may wish to agree to international monitoring of the environment through UNESCO, IMCO, or UNEP in order to allay other nations' fears about OTECs' environmental impacts[26] and to provide information on any environmental impacts of OTEC deployment.[27] Adjudication of environmental disputes could be preagreed, using the 1958 LOS Conference Optional Protocol on Dispute Settlement as a model.[28] If the new LOS treaty comes into effect, its dispute settlement procedures would presumably provide alternatives.

Criminal Law. Three significant issues concerning criminal law will need resolution. First, how much federal criminal law will or should be extended to the EEZ in which the OTECs will be operating? Provided legislation creating the EEZ follows the language of the Outer Continental Shelf Lands Act and the Deepwater Port Act, apparently the full range of federal criminal law will apply. If the legislation creating the EEZ is not explicit on this point, it is recommended that OTEC implementing legislation seek the full extension.[29]

The criminal law of the adjacent state should be made applicable, either in any EEZ legislation, or in OTEC implementing legislation.[30]

Private Law. Here, OTEC policy planners face a significant choice among two bodies of law -- maritime and the law of the U.S. states -- or some combination thereof. It is recommended that the admiralty and maritime jurisdiction be applied to OTEC operations on this site, and that the substantive law of admiralty be the primary source of private law on and about OTEC operations. Adjacent state law should supplement admiralty on a non-conflicting basis where appropriate.[31] This arrangement would provide a work for uniformity in OTEC-related private law matters wherever located, while still providing for application of state based law where maritime law does not supply the answer or where local interests are particularly important.[32] OTEC operations would thus share a common ocean environment with vessels which have formed the core of traditional maritime nexus concepts.[33]

Financing. The financing of the Florida West Coast OTECs, assuming they are public utilities, would probably follow traditional forms of public utility financing. However, the U.S. government would be required to stimulate investment in the initial OTEC units by providing tax and institutional incentives.[34] Leveraged lease financing would probably be used, thus enabling the public utility to provide only a minor portion of the initial costs, and providing a tax shelter situation for the investor institutions.[35] However, both federal and state governments may be required to provide tax and other incentives over and above existing tax credits.[36]

Mexico

This OTEC facility, a 400-megawatt plant cable linked to Mexico's eastern coast, would be sited within that country's EEZ[37]. Energy would be produced either for local energy-intensive commodities, or for transmission by power lines to central grid systems, including that of the United States.[38] The OTEC is assumed to have vessel status, to be a U.S. flag vessel, be built in the United States, have American crew and be eligible for MARAD subsidies. (An alternative was also considered: the OTEC is foreign built and manned and flies a flag of convenience.) The facility would probably be a Mexican government owned public utility.[39]

International Jurisdictional and Political Issues. It is assumed that the OTEC operation falls within the competence of Mexico's Exclusive Economic Zone and so makes that government's consent a necessary prerequisite to access to its zone and its regulation of OTEC a fact of life.[40] This consent regime would hold even if the electrical supply were not owned by the Mexican government.

Politically, the United States should not expect to be in a position to leverage OTEC deployment primarily benefitting the United States in exchange for some favors to Mexico. If development of this site is to occur, it will result from negotiations in which both nations share in the benefits from OTEC activity.[41]

International Arrangements. The international arrangements would most likely divide into two kinds: those establishing or promoting OTEC operations on a mutual interest basis and those of a defensive nature.

The mutual interest category might include agreements on the fees to be paid Mexico for overland transmission of energy to the United States, in technology transfer, on location of OTECs along the coasts of some of the remote areas to provide electricity as inducements to reduce migration to the cities, or for remote area industries processing ammonia or manganese nodules.[42]

Many arrangements useful for the Florida West Coast site would be applicable off Mexico. These include agreements protecting any U.S. fishing or navigation rights the United States may have negotiated with Mexico, and those concerning multinational agreements such as the Rules of the Road.[43] An additional area of negotiation with Mexico might concern sharing of thermal energy resource in the Gulf of Mexico should there be competition for it from U.S. sites.[44]

A more defensive array of international agreements might be sought to protect U.S. interests in the area, rather than on allowing maximum benefits to the OTEC owner-operator.[45] One concern is whether the United States can rely on the coastal state (Mexico) to uphold U.S. interests vis-à-vis

flag of convenience OTECs which might operate in Mexico's zone. Perhaps the flag of convenience state itself might; if not, some means ought to be found to reach the real party of interest.[46]

In summary, Mexico will assert its legal regimes in its economic zones, just as the United States will be expected to impose its laws in the U.S. EEZ. U.S. Policy planners will have to decide whether this nation's interests are best protected through bilateral negotiations, multilateral arrangements, or some combination of both.

Regulatory and Environmental Law. Certain non-technology-specific international regulation -- in the fields of safety, communications, labor, for example -- will influence OTEC operations in the Mexican site. The U.S. interest is in establishing minimum, non-prejudicial international standards which would support stable OTEC development and operation, rather than leaving such regulation subject solely to the other states' interest.[47] Regulations which are specific to OTEC technology, on the other hand, are unlikely to be left to international authority.

Environment. A major concern is that the Mexican (or other Caribbean) site is not used as a "pollution haven" to avoid U.S. or other countries' more stringent environmental regulations. Such might be the temptation should OTECs be used primarily to power energy intensive industry.[48] The United States could be a co-victim in the case of environmental accident or degradation.[49] The United States could seek agreements on pollution prevention via mandatory information exchange, consultation, conceivably compensation for damage, creation of a compensation fund, clean-up responsibilities, and prevention of imminent environmental damage to U.S. interests.[50]

Under a broad interpretation of NEPA requirements, the U.S. would have to carry out a site-specific environmental impact analysis, assuming that there is the requisite federal connection.[51] The development and evolution of laws governing shared natural resources and for environmental protection are rapidly changing. And so the basis for internationally recognized responsibilities of owner-operators is likely to grow by the time OTECs are commercially established.

Criminal Law. In criminal law, Mexico's interest is in a non-discriminatory, effective criminal regime. Any specific desired additional arrangements should be negotiated directly with Mexico or as part of a multilateral regional pact.[52] Successful classification of the OTEC structure as a vessel might provide the United States with an argument for some application of its own criminal law if it is the flag state. However, Mexico's interest is likely to prevail, just as that of the United States will in its EEZ.

Private Law. Again, Mexico can be expected to assert its system of private law for its EEZ. In the interest of building toward roughly comparable principles of private law, the United States could urge that, where applicable, maritime law be relied upon as the primary source of private law for the OTEC off Mexico's shore. That course of action, coupled with a similar reliance within the United States's own EEZ, is recommended.[53]

Financing. The financing of an OTEC off Mexico would, so long as it were classified as a U.S. flag vessel and met other requirements, proceed along the leveraged lease/MARAD support lines already discussed, unless existing law blocked MARAD support because of Mexican government ownership of the electricity supply.[54]

High Seas, Brazil

This site is located on the high seas, mainly outside Brazil's 200-mile territorial seas claim. Structures are not moored; they move in order to follow the maximum thermal gradient. Up to ten such structures are postulated by the year 2000, operating as a flotilla, nominally at one to nine kilometers distance apart. They may mix their warm and cold discharge waters.

Attention is mostly paid to the high seas aspects of this site, those pertaining to operations within 200 miles being analogous to the situations off Mexico and the United States.

International Jurisdictional and Political Issues. The OTECs on this site would, in terms of international law, be able to operate in the future much as they would today.[55] In legal theory, if migrating OTECs are treated as vessels; if the zone state, Brazil, is not the flag state (which it isn't); and if the site is also beyond the limits of the Brazilian continental shelf, then the site would be wholly free of coastal state competence.[56] However, Brazil has evidenced a readiness to extend its claims to the continental margin where this reaches beyond 200 miles. The continental margin (primarily the rise) extends to roughly 400 miles along the northern coast of Brazil.[57] Thus, prospectively, the jurisdictional question may not be as free of challenge as appears at first blush.

International Arrangements. Agreements further clarifying the status of OTECs on this site would be desirable. Political considerations dictate that the owner/operator of the OTECs will want to seek an understanding with the Brazilian government as to OTEC operations even though they are located on the high seas.[58] A powerful nation such as Brazil may react negatively to uninvited industrial activities on the fringes of its claimed waters.[59] (Note, however, that Brazil's position in terms of international law would probably not be strong.)[60] But, Brazil may react favorably to overtures for cooperative development.[61] Also, there are important issues that prudent investors will insist upon clarifying as a precondition to financing such OTEC programs.[62]

Regulatory and Environmental Law. It is unlikely that any existing international regulatory authority or scheme will regulate the initial development and operation of OTEC on the high seas in the way that navigational vessels are regulated. Some international schemes may be wholly or partially applicable to OTEC devices.[63] The regulatory schemes most likely to apply under current perception of international regulation would be those of the flag state(s), tempered by the international standards, referred to above, voluntarily accepted by the flag state.[64]

If international standards become desirable, there are existing institutions, notably IMCO, which could expand their competence to deal with regulatory aspects of OTEC operations.[65] Alternatively, a regional multilateral pact could include these matters along with private law issues.[66]

Environment. The desirability of seeking Brazil's approval even for operations 300 miles off its coast has already been noted.[67]

The international reach of United States's NEPA

requirements would apply to this site under both the CEQ approach and that requiring impact statements on the commons.[68]

Criminal Law. Criminal law is traditionally a part of admiralty law and hence in international law generally within the competence of the flag state.[69] However, in the United States, at least, there is ambiguity as to whether a non-traditional object not clearly identifiable as a vessel would be held by the courts to fall within the statutory special maritime jurisdiction.[70] In order to avoid this uncertainty, it is recommended that OTEC planners urge explicit Congressional clarification of 18 USC 7, which would apply the jurisdiction to OTEC structures and, given the opportunity, to other non-traditional vessel structures.[71]

There is case law to support the position that the courts can infer Congressional intent to make specific statutory offenses apply to the high seas, and also that common law offenses can be applied under traditional principles of admiralty law's criminal competence. Development of these sources is seen as preferable to a statutory extension of federal law.[72]

Private Law. U.S. courts would, under present law, probably find connections between the functions of OTECs and the concepts of navigation (and between an OTEC structure and a vessel) sufficient to apply maritime law. This outcome should be codified in any future OTEC legislation.[73]

However, because policy considerations argue against creeping nationalization of the high seas, it is recommended that there be no general extension of federal or U.S. state law to OTECs on the high seas, reliance being placed upon principles and rules of admiralty law.[74]

Financing. Financing of the high seas OTECs could be similar to those operating off the West Coast of Florida which might be owned by a private corporation not operating as a public utility. However, there may be a problem of the rental income being considered as a foreign source for tax purposes. Assuming vessel status, the lessor in a leveraged lease could elect to treat the income as a U.S. source.[75]

Conclusions

In comparing the prospects for OTEC sites in the U.S. Exclusive Economic Zone, on the high seas, and in the Exclusive Economic Zone of other states in terms of the six substantive areas identified in the first section, several problem areas appeared as pervasively affecting the international institutions and arrangements for research on development and commercialization of OTECs.

Twelve points should be made.

Coastal State Dominance

The most likely evolution of the Law of the Sea will bring coastal state dominance of ocean thermal energy sites located within 200 miles offshore, whether cable linked to shore or not.[76] This dominant competence will most likely apply to research as well as commercial phases.[77] Even beyond these economic zones, adjacent coastal nation political and legal interests are likely to be of growing importance.[78] An illustration is the view that even in high seas deployment of OTEC 300 miles off Brazil, the United States would be advised to seek prior approval of that nation.[79]

Also, those states whose land territories or ocean economic zones are affected environmentally by OTEC operations can be expected to assert legal claims or to seek legal arrangements for regulating or redressing any environmental impacts.[80]

Three General Objectives

The international Law of the Sea and political prospects identified above suggest that international arrangements or domestic legal policy decisions for OTEC development will have one or more of three general objectives. They will seek to effect benefits for both the United States and foreign countries interested in OTEC development,[81] they will be defensive in nature in seeking to protect U.S. interests or rights,[82] they will seek to facilitate or make more attractive investment in OTEC development by private sources of finance.[83]

Achievement of Mutual Benefits

Although the United States will retain its dominant position in the Western Hemisphere, politically, the power and assertiveness of the foreign countries having interests in OTEC development will increase in relative terms by the time OTECs are deployed commercially.[84] A major consequence is that negotiations with other countries will focus on attainment of benefits for both the United States and other countries and for accommodation of multiple uses.[85]

Defensive Aspects

The major interests or rights to be protected in defensive aspects of arrangements and policies include: maximum access for OTECs in high seas deployment; maintenance of other characteristics of freedom of the high seas; creation of protected rights, interests or influence in other countries' economic zones; and, establishment of operational standards and/or liability for transzonal environmental effects which have an impact on the United States or U.S. interests.[86]

Investment Incentives

In order to facilitate private financial investment, OTEC policy planners can seek to make a range of MARAD incentives applicable to OTEC structures.[87] They can also seek to ensure that a balance is kept in the fashioning of international arrangements in order to reduce uncertainty sufficiently that confidence will be instilled in investors, while simultaneously avoiding stifling private interest by hedging OTEC development in with conditions.[88] OTEC operations in foreign economic zones can benefit from U.S. government acts to secure agreements which provide for orderly, equitable development of standards and allocation of development costs [89] and in achieving agreement as to principles of private law.[90]

Potential for Inconsistency Among U.S. Objectives

A major problem with which OTEC legal policy planners will have to contend arises from the potential inconsistencies inherent in pursuit of the above objectives.

First, it is likely that in its own future economic zone, the United States will seek full control over economic activities, constrained only by those principles of international law protecting the rights of other nations to navigation and a limited number of other uses. In contrast, in other nations' economic zones, the United States would ideally like to preserve as much influence, flexibility and freedom of action as possible.[91]

This problem of doubled edged policies is nearly ubiquitous. It arises in the issue of whether or not an OTEC use within 200 miles of land will be subject to a "consent" or a free access regime;[92] in the conditions under which OTEC related research may be undertaken;[93] in regard to environmental standards;[94] in claiming competence over criminal activities;[95] and, in asserting a nation's own law as the operative body of private law at sea.[96]

A second potential inconsistency is related -- that between achieving agreements of maximum mutual benefits and of maximizing the defensive positions described above.

Inconsistency is not new in policy making. Nevertheless, OTEC policy planners should be alert to the attendant problems.

Alternatives of Land Law and Ocean Law Orientations of OTEC Legal Regimes

OTEC policy planners are likely to be among the first building new legal regimes for new technologies operating offshore. They are likely to have to decide the extent to which land based legal concepts are extended to sea, the extent to which sea based concepts are adapted to the new technology, or the degree to which land based and maritime based laws are melded to derive new concepts. Illustrative areas are the nature of the right the owner or operator will have in the thermal gradient resource,[97] the extension of adjacent state private law as opposed to maritime law[98] and the choice between applying all federal criminal law or the more limited sanctions specified within the special maritime and territorial jurisdiction.[99]

Vessel Status

Many of the U.S. and international laws and regulations presently in force on the ocean are couched in terms of being applicable to vessels. The question arises repeatedly as to whether OTEC structures will or should be considered vessels for a particular purpose. Among the pertinent areas are the applicability of various international conventions,[100] the applicability of the special maritime and territorial jurisdiction in U.S. criminal law,[101] the applicability of maritime law to OTECs generally,[102] the applicability of U.S. Federal Maritime Administration financial incentives[103] and the applicability of different environmental laws.[104]

The significance of the "vessel status" issue arises from the fact that existing incentives and standards have largely been created to deal with problems relating to traditional vessels. Lawmaking for the most part has not caught up with the introduction of new technology. Whether OTECs would be found by the courts or regulatory bodies to be within the class for which a particular incentive, standard or legal rule was intended is uncertain and will probably remain so until tested on an instance-by-instance basis. Notwithstanding, a trend in IMCO to include and to anticipate non-traditional structures in the ambit of its conventions does appear. The desirability of OTECs being classified as vessels will also vary from instance to instance. OTEC policy planners should take the initiative in seeking legislation which will bring those desirable benefits, standards or legal regimes to bear on OTEC rather than awaiting judicial or regulatory construction.

Advantage of U.S. Coastal Site

In comparing the proposed sites from the perspective of international arrangements, the U.S. Florida West Coast site promises the simplest web of new institutional agreements, being limited to those concerned with transzonal effects.[105] In this and other siting situations, participation of another government in the ownership or benefits of OTEC operation could lessen the difficulty of securing the international agreements. Those sites in foreign economic zones will present the most difficult and intricate set of relationships.[106]

Prospects for Agreements

International arrangements for OTEC may usefully be distinguished along two lines. The first is level: global, multilateral/regional, and bilateral. The second is scope: non-technology specific, technology specific, site specific and venture specific. Even if an LOS treaty comes into force which answers many jurisdictional questions, the operation of OTECs in the commercial phase will require a technology specific global convention.[107] The speed with which such a convention is likely to come into existence will depend upon the impacts or perceived threats of impacts on other interests and uses future OTECs have -- the greater they are, the more likely the institutional inertia at the global level is likely to be overcome.[108]

However, even before a technology-specific agreement, modification of existing global, non-technology specific regulatory agreements will be required to take OTEC operations into account.[109]

Multilateral or bilateral agreements will be required on a site- or venture-specific basis to settle boundary, transzonal and investment facilitating agreements.

Optimizing Goals with Minimal Institutionalization

In discussing the multitude of international arrangements and legal regimes which might be designed to facilitate the development of OTEC,[110] the panel agreed that an operating criterion should be the achievement of policy planners' goals with the minimum mass and most simply conceived arrangements or regimes which could get the job done. The wisdom of using or adapting what exists rather than creating a new institution will be a part of the policy planners' design problem.

Anticipating Inertia in Global Institution Building

As a corollary to the above, the difficulty in moving a large institution building body such as the U.N. Conference on the Law of the Sea, IMCO or other global groups to give attention to technology specific legislation in anticipation of, rather than reaction to, events will be a problem should the creation of institution building at such levels be felt desirable.[111] Similarly, bending the collective will of such bodies to the interests of one country, the United States, will be difficult if not frequently impossible.[112]

Recommendations

Regarding OTEC and the Law of the Sea Conference

Those within the U.S. government wishing to maximize opportunities for deployment and operation of OTEC should:

1) attempt to recast the language of the Informal Composite Negotiating Text dealing with scientific research so as not to require consent of the coastal state for exploratory OTEC deployment within 200 miles of the coast of any nation;

2) consider carefully whether the coastal state competence over commercial OTEC plants is not a de-

sirable option, taking into consideration that acceptance of the principle of coastal state competence would apply to the United States as well as to other nations; and,

3) take appropriate measures in the Law of the Sea Conference to ensure that for the area beyond the Exclusive Economic Zone no competences are accorded to the international seabed agency that would give it any jurisdiction with respect to OTEC in the scientific research mode or commercial production mode.

Regarding Ocean Jurisdiction

Given the trend with respect to the Exclusive Economic Zone in the Third United Nations Conference on the Law of the Sea, the United States probably has jurisdiction to adopt legislation regulating the deployment and operation of OTEC devices within 200 miles of its coast. Such enabling legislation thus has a basis in international law should it be decided on other bases that such enabling legislation is desirable.

Regarding the Status of OTECs under Various IMCO Regulatory Conventions

1) The question of whether OTECs would be covered under the various IMCO treaties should be put on the IMCO agenda. The format might be that outlined in Hallberg, Chapter 6 of Knight, Nyhart and Stein (page 114), i.e., referral to an IMCO standing committee for study, formulation by the Assembly of a recommended practice, trial by member states, and finally, if accepted, formulation as part of the pertinent conventions.

2) Similarly, the work under Task III may suggest that IMCO be urged to consider placing drafting and consideration of an international convention for OTECs on its agenda. If so, the same path might be appropriate.

3) However, Hallberg's caution as to the prospect for IMCO's giving serious attention to a new use before it comes into being should be borne in mind. It gives impetus for U.S. unilateral legislation covering roughly the same ground.

Regarding Criminal Law Applicable To, On and About OTEC Operations

1) The Department of Energy should support the extension of U.S. criminal law (in the form of Title 18 and other criminal statutes, rules or regulations) to any future U.S. Exclusive Economic Zone, or failing that, its extension to OTECs in any legislation applying to OTEC development and commercialization at sites within an area encompassed by the U.S. Fisheries Conservation and Management Zone. This extension explicitly should include the application to OTECs of the Special Maritime and Territorial Jurisdiction of 18 USC 7. Further, the Department of Energy should support the application on a non-conflicting basis of adjacent U.S. state criminal law.

2) In addition, the Department of Energy should urge an explicit Congressional clarification of 18 USC 7 which would apply that jurisdiction to OTEC structures owned by U.S. nationals on the high seas.

3) Further, the Department of Energy should support exploration by appropriate parties of the application as a part of admiralty jurisdiction, of common law and the law pertaining to offenses under the law of nations.

Regarding Private Law Applicable To, On and About OTEC Operations

1) It is recommended that maritime law be adopted as the primary substantive body of private law for OTEC operations on the West Coast Florida site, with adjecant state law, e.g., that of Florida, applying concurrently on a non-conflicting basis. If an Exclusive Economic Zone is created prior to OTEC specific legislation, it is recommended that the Department of Energy urge that this same course be adopted in the EEZ legislation.

2) It is recommended that for any high seas, migrating sites, OTEC legislation or any other applicable acts, Congress statutorily establish that maritime law be applicable. It is further recommended that no statutory extension of adjacent state law be made for operations on the high seas site, although Congress might state a legislative intent that U.S. state law be the applicable residual law unless established international conflicts of law practice is thereby violated.

3) Further, a regional convention, participated in by OTEC operating and affected nations, should be pursued drawing up a set of principles harmonizing the application of different private law concepts which might be significant to OTEC operations in the area.

Notes

1. The papers comprising the report included: Summary, J. D. Nyhart (hereinafter, Summary); OTEC and the Law of the Sea: The Jurisdictional Problems, H. Gary Knight (hereinafter, Knight); International Political Aspects of OTEC Siting, Ann L. Hollick (hereinafter, Hollick); Six Scenarios of OTEC Commercialization, Byron J. Washom (hereinafter, Washom); International Regulatory Aspects of OTEC Development and Demonstration, Robert S. Faron (hereinafter, Faron); Environmental Aspects of OTEC Development and Demonstration, Robert E. Stein (hereinafter, Stein); Criminal, Private and Residual Law Aspects of OTEC Siting, J. D. Nyhart (hereinafter, Nyhart, Vessels); Alternative Intergovernmental Arrangements for OTEC Deployment, Eugene R. Fidell (hereinafter, Fidell)

2. Knight 87.

3. The term "OTECs" is used in this paper to refer to OTEC plants, those structures on and in which the process of ocean thermal energy takes place.

4. Nyhart 259-75.

5. The study also considered a Puerto Rico site, located close to shore, most likely within the anticipated twelve-mile territorial sea. Up to eight OTEC facilities of 400 megawatts would be dispersed along the coast, each directly linked to shore by A.C. cable. The resulting energy source would cut the island's imported petroleum costs significantly. Hollick 117.

The problems distinguishing this site are largely political. Hollick 114-118. They include the relationship between the U.S. and Puerto Rico, the environmental consequences for neighboring states and the use of OTEC siting as an ideological opportunity to attack U.S. colonialism. Hollick 114.

The environmental problems are mainly those which might involve other states and are therefore similar to those discussed in the Florida West Coast and Mexican sites. Hollick 117. There is in addition the question of U.S. regulatory control. Under U.S. law, NEPA and FWPCA would apply. Stein 207. However, ambiguity arising from interpretation of the constitutional compact between Puerto Rico and the United States could cause complications for OTEC planners. Hollick 114.

6. Hollick 110. As additional assumptions (Washom 135), it is taken that the owner-operator is a U.S. public utility, limited on its allowed rate of return, that the structures are not considered vessels for purposes of the Federal Mortgage Act of 1920, and that they are constructed either in a U.S. or foreign yard.

7. Knight 66.

8. Knight 71.

9. Hollick 111.

10. Hollick 113, Stein 205-7.

11. Hollick 113, Fidell 288.

12. Fidell 288, Knight 85.

13. Fidell 291.

14. Fidell 291-2.

15. Fidell 288-9.

16. Fidell 291.

17. Washom 137.

18. Fidell 292.

19. Fidell 292.

20. Faron 92-114.

21. Faron 92-114. See also Teftt, Kelley & Motley report, and Knight, Nyhart & Stein, Ocean Thermal Energy Conversion, Lexington Books, Lexington, Mass. (1976), Chapters 6-10.

22. Fidell 290-1.

23. Stein 206.

24. Stein 206.

25. Stein 207.

26. Stein 207.

27. Fidell 293.

28. Fidell 294.

29. Nyhart 220. There is the question as to whether the special maritime and territorial jurisdiction applies to OTEC structures, an issue discussed in detail under the High Seas, Brazil site. Nyhart 226.

30. Nyhart 221.

31. Nyhart 238, 244.

32. Nyhart 242, 244.

33. Nyhart 241-3.

34. Washom 140.

35. Washom 141.

36. Washom 141-2. If the OTEC were uncoupled from permanent attachment to the seabed, making it capable of being either moored or migrating, it might be assumed to qualify as a vessel for purposes of the Federal Ship Mortgage Act and qualifications for U.S. Maritime Administration (MARAD) loan guarantees, capital construction funds and construction differential subsidies. The vessel would fly the U.S. flag and would be built in an existing U.S. shipyard.

Further, if the OTEC is owned and operated by a private U.S. corporation not considered a public utility (Washom 137), MARAD economic incentives, coupled with traditional vessel leveraged lease financing, might be available to facilitate raising the large amounts of necessary capital at a greatly reduced risk. Washom 142-3, Fidell 295. The loan guarantee, coupled with the normal 10% Investment Tax Credit (ITC) and perhaps under new legislation a supplemental fully reimbursable ITC of 15%, would make the OTEC plant a most attractive investment venture. Washom 143.

In another variation, a government owned, private corporation operated (GOCO) scheme is specified, with Mexico possible joining the United States as a co-owner government. The funds for a GOCO OTEC could come from a variety of government sources, e.g., general funds, special federal trust fund authorities, special government bonds, etc. Washom 146-7.

The intergovernmental arrangements required here would be the most extensive of all those examined. The selection of a GOCO mode would provide sufficient U.S. governmental involvement to invest virtually all arrangements with a governmental character, as was done with the development of the nuclear ship Savannah. Operations within the U.S. Exclusive Economic Zone would subject the venture primarily to U.S. regulation regarding its operations. However, spillover effects on the adjacent coastal states' zones would require similar pollution and conflicting use agreements discussed for other sites. Mexican involvement, either through a joint management plan or through part ownership, would also bring Mexican regulatory schemes into play. A detailed agreement setting forth joint rights and responsibilities would be essential. Furthermore, the contemplated transfer of products under one alternative in the Scenario would require an agreement on distribution, control, payment, and schedule for the joint disbursement of products. Fidell 303-4.

Provisions for arbitration of disputes, customs regulation, liability assessment and criminal and private law jurisdiction might also have to be negotiated if two governments were jointly involved. Fidell 304.

37. Puerto Rico was also analyzed as a site, emphasizing the beneficial impact an OTEC energy supply would have on cutting the costs of imported petroleum. Hollick 117. The problems distinguishing this site are largely political. Hollick 114-8.

38. Washom 130, Hollick 118.

39. Washom 138, Hollick 120. Alternatively, Mexico might lease a U.S. owned facility. Hollick 120.

40. Knight 84, Hollick 118, Stein 208, Nyhart 246.

41. Hollick 120.

42. Hollick 120-22.

43. Fidell 300.

44. Fidell 301.

45. Fidell 300.

46. Fidell 301.

47. Faron 185.

48. Stein 208.

49. Stein 208.

50. Fidell 300.

51. Stein 208.

52. Nyhart 231.

53. Nyhart 246-7.

54. Washom 138. Discussion of the Cuban and Bahamian sites is summarized in Summary, 50-1.

55. Knight 78-83.

56. Fidell 295.

57. Hollick 127.

58. Hollick 127, Stein 209.

59. Hollick 127.

60. Fidell 249.

61. Hollick 127-30, Stein 209.

62. Fidell 296.

63. Faron 155-77.

64. Faron 186.

65. Faron 186.

66. Nyhart 249.

67. Stein 165.

68. Stein 165.

69. Nyhart 214.

70. Nyhart 223-5.

71. Nyhart 225-7.

72. Nyhart 227-30.

73. Nyhart 245.

74. Nyhart 245-6.

75. Washom 143.

76. Knight 71-2, Hollick 88-93, Faron 104-16, Stein 193-200, Nyhart 219.

77. Knight 88-93.

78. Knight 78, Hollick 105.

79. Hollick 127, Stein 209.

80. Hollick 112-3, Stein 205-6.

81 Hollick 120.

82. Fidell 299.

83. Washom 141, Fidell 305-6.

84. Hollick 104-6, 109.

85. Hollick 109, 120.

86. Knight 87, Hollick 102, 111-13, Stein 205-6, Fidell 299-301.

87. Washom 139-47.

88. Fidell 305-6.

89. Faron 181-2.

90. Nyhart 249.

91. Knight 87, 90-2.

92. Knight 90-3.

93. Knight 88-90.

94. Stein 208, Hollick 113.

95. Nyhart 221, 230-1.

96. Nyhart 243-4, 246.

97. Knight 73-6.

98. Nyhart 239-44.

99. Nyhart 220-3.

100. Faron 154-77, Nyhart Vessels 263-71.

101. Nyhart 223-7.

102. Nyhart 239-44.

103 Washom 142-3.

104. Stein 201-2.

105. Fidell 306.

106. Fidell 306.

107. Fidell 305.

108. Faron 177-80.

109. Faron 177-80.

110. Fidell, generally.

111. Faron 178-79.

112. Knight 91, 93.

LEGAL AND INSTITUTIONAL ASPECTS*

Ved P. Nanda

University of Denver College of Law
200 West 14th Avenue
Denver, Colorado 80204

Abstract

The paper has as its primary focus those legal and institutional aspects of the jurisdictional, regulatory, and environmental issues that will ostensibly have a significant bearing upon the commercialization of OTEC. They are discussed in the context of both the current and the evolving law, with particular emphasis on the relationship between the coastal States and the Federal government, and the ongoing negotiations of the Third United Nations Conference on the Law of the Sea (LOS III). The current state of the law is examined, and the exisiting ambiguities, gaps and uncertainties are identified. The need is demonstrated for the development of an imaginative and effective legal and institutional framework. Specific recommendations are made. For example, on the domestic front it is urged that through legislation a comprehensive ocean management system for U.S. coastal areas be established; in the international area, it is suggested that consideration be given to the drafting of a convention which mandates environmental impact assessments of a state's major projects which could harm the environment of another state or the shared global environment, and provides for consultative mechanisms. This should be followed by the drafting of another convention specifically of OTEC activities including a code on conduct. (126 references)

Introduction

The discussion in this paper is premised on three assumptions. First, the United States will need new technologies to meet its increasing energy demands by the end of the century. While the world energy demand is expected to double in a period of twenty to thirty years,[1] a recent study by the U.S. Department of Commerce indicates that the country's need for energy will grow 1.2% per person through the end of the century, and that the economy will grow by about 2.2% per year.[2] Second, this increasing demand for energy (deemed essential in order to maintain an acceptable level of economic activity), coupled with the oil crises of 1973-74 which gave rise to the demand for energy security in the United States, will necessitate the exploration of all reasonably promising energy alternatives.[3] According to the National Energy Plan,[4] these principal alternative energy sources available to the United States -- coal, nuclear power, and solar power (direct and indirect) -- will be used in the years ahead. Finally, the steadily rising cost of fossil fuel, especially coal, the likely scarcity and increasing costs by the year 2000 of petroleum, natural gas, and U-235, and a growing concern over their detrimental environmental effects, will make these sources uneconomical for large scale electrical generation. Substitute sources will include OTEC, non-U-235 nuclear, and geothermal energy.

OTEC, an unconventional energy source and a unique energy technology, is an attractive alternative for several reasons. "[I]t can provide utilities with 'baseload capability' on line 24 hours a day. It can economically generate power at a level of 250 megawatts and up, enough for a moderate-sized city. Using a renewable resource, the sun, its 'fuel' is delivered directly to the site in usable form without charge. It is environmentally benign, emits no poisonous byproducts (barring the remote contingency of a massive leak of the working fluid -- probably ammonia), and it is necessarily situated unobtrusively offshore, away from the population centers. All evidence to date indicates that it has no harmful effect on ocean life; indeed, cold water upwellings are known to be beneficial to fish populations."[5]

Despite these attractive features however, established utilities have thus far shown little interest in pursuing technological studies and hardware demonstrations related to OTEC. This apparent lack of serious interest stems mainly from the perception that OTEC is an expensive, unproven and risky undertaking. A combination of factors, including unproven economics (based on presently noncompetitive estimated costs of OTEC-generated energy), unverified social and environmental effects, and uncertainty as to the potential of energy from OTEC as well as how OTEC fits into the national energy policy is responsible for the prevailing skepticism. The absence of an adequate legal and institutional framework further clouds the picture.

It seems that the uncertainty OTEC faces on technological and economic grounds will be dispelled by further studies and demonstration projects which are likely to be undertaken by the Department of Energy (DOE).[6] While the "engineering challenges to be bridged demand solutions of scale rather than technical innovation,"[7] it is estimated that "the OTEC power plant should have an economic advantage over fossil fuel plants and nuclear plants well before the year 2000."[8]

However, these economic and technological issues will not be discussed here, nor will the financial aspects be investigated.[9] This study has as its primary focus those legal and institutional aspects

*This paper is an adapted version of a study, "Selected Legal and Institutional Issues Related to Ocean Thermal Energy Conversion (OTEC)," prepared by the author as a consultant to the Solar Energy Research Institute (SERI), Golden, Colorado.

†Professor of Law and Director, International Legal Studies Program.

which will ostensibly have a significant bearing upon the commercialization of OTEC. These issues are broadly classified as (1) jurisdictional, (2) regulatory, and (3) environmental. They will be discussed here in the context not only of existing international law -- both customary and treaty law -- but also of the current developments in the law and the probable changes in it, particularly those resulting from ongoing negotiations of the Third United Nations Conference on the Law of the Sea (LOS III).[10] Several alternatives will be discussed and recommendations offered in each area in light of the United States' interests.

This discussion will be prefaced by a short assessment of the possible arrangements for the siting of OTEC plants, their functions, and their potential for the United States.[11] The most likely configurations for OTEC plants will be: (1) an OTEC facility operating individually as a semi-permanent fixture, or a number of plants moored in clusters of eight to ten plants around a central collection device, and connected to shore by a transmission cable, supplying electrical power for general consumption to a land-based electricity grid; or (2) an open sea OTEC facility, a plant-ship, migrating and "grazing" on the surface, seeking the maximum thermal differential gradient and supplying power for an energy-intensive industry at sea. The energy produced could be converted into other forms of energy, such as hydrogen, and the products produced onsite transported to shore by vessel. Such products could also be manufactured and processed in such places as Hawaii and Puerto Rico, which are close to some of the prospective sites of OTEC facilities.

Because of the thermal gradient needed to make OTEC operative, tropical regions within 10° of the equator, comprising about twenty million square miles, where the surface water is around 80° F., while the cold water 3,000 feet below is around 40° F., offer the most promising sites for OTEC facilities which fit into configuration one discussed above. For the United States, however, these sites are limited to the Gulf Coast, Hawaii, Puerto Rico, and the Pacific territories. According to the studies of the Energy Research and Development Administration (ERDA), a thermal resource of at least 300,000 megawatts lies just off the west coast of Florida.[12] It is anticipated that the technological developments expected from DOE's current OTEC Research, Development and Demonstration (RD&D) Program would allow the exploitation of this resource. Other studies indicate that the off-grid applications mentioned in configuration two type facilities will have a market potential of an average of 30,000 to 40,000 megawatts during the years 2000 to 2025.[13]

Jurisdictional, Regulatory, and Environmental Issues

Regardless of the site of an OTEC facility or its system and configuration, ownership, operation, energy potential and use, the move toward OTEC commercialization will be facilitated if the prevalent uncertainties regarding the issues to be discussed in this section are removed and an adequate legal and institutional framework is established, offering guidelines to interested parties. The following discussion, which is designed to present a broad outline of such a framework, surveys the current state of the law, suggests likely changes, identifies existing ambiguities, gaps and uncertainties, and makes recommendations to remove them.

Jurisdictional Issues

In the United States offshore areas, questions of jurisdiction, that is, questions pertaining to the competence to prescribe and apply the governing law to peoples, events, and activites in these areas, arise in two contexts: national-international and Federal-State. In the former, activities are governed by norms established by multilateral treaties, regional and bilateral arrangements, and customary law, supplemented by unilateral action; in the latter, by statutory law and judicial pronouncements.

National-international issues. The unsettled state of the Law of the Sea is responsible for the presence of unresolved jurisdictional issues pertaining to the installations of OTEC devices in offshore areas. The law is still in an evolutionary state and LOS III, which convened its resumed eighth session in Geneva on March 19, 1979,[14] is attempting to formalize a comprehensive and generally acceptable convention on all aspects of ocean space. The negotiations have shown a remarkable consensus on most issues likely to affect OTEC deployment and operation. Also, regional and bilateral arrangements and unilateral state practices and claims are instrumental in changing the traditional Law of the Sea.

The basic issue pertinent to the present discussion is a coastal state's rights in adjacent waters and on the high seas. Under traditional international law, the inquiry has centered on the limit of territorial waters, and additionally, since the 1958 Geneva Conventions on the Law of the Sea,[15] on the extent of contiguous zones and the outer limit of the continental shelf. Beyond these areas, the universally applicable concept has been freedom of the high seas.

OTEC devices under traditional international law regarding the territorial sea. Historically, coastal nation states have enjoyed certain exclusive rights and privileges with respect to adjacent waters over a narrow belt of three marine miles along their coasts, measured from the low water mark, which constituted their territorial waters.[16] During the last fifty years, however, the breadth of territorial waters has been marked by a lack of uniformity. While the international conferences in 1930,[17] 1958,[18] and 1960,[19] failed to reach agreement on the limits of the territorial sea, under traditional international law, an OTEC device deployed for research[20] or commercial purposes within the territorial limits would be within the exclusive competence of the coastal state, since the term "sovereignty" has been continuously used to describe a coastal state's rights in territorial waters.[21]

OTEC devices under the emerging law on the territorial sea. Although the 1958 convention failed to set a definite limit on the breadth of the territorial waters, state practices were fast eroding the traditional three-mile limit. A United Nations Secretariat study in 1968 revealed that

fewer than one-third of the states reporting (30 of 92) had opted for less than six miles while nearly half (43 of 92) opted for twelve miles or more, and only a small number (9) were claiming more than twelve miles.[22]

The current product of the LOS III negotiations is the Informal Composite Negotiating Text (ICNT), a massive document containing 303 articles and 7 annexes,[23] which sets the breadth of the territorial sea at twelve miles,[24] and that of contiguous zones for similarly specified purposes as were contained in the 1958 convention at 24 miles.[25] Within this adjacent maritime belt, a coastal state's sovereignty is recognized as extending to the air space over the territorial sea as well as to the seabed and subsoil,[26] and is limited only by the right of innocent passage.[27] There is an almost universal consensus on the twelve mile limit for the territorial seas. Within this zone, the coastal state will have almost total control over the installation and operation of an OTEC facility, both for research and commercial use.

OTEC devices on the exclusive economic zone and the continental shelf.

Exclusive economic zone. Beyond the twelve mile territorial sea and the twenty-four mile contiguous zone, ICNT recognizes a special area known as the Exclusive Economic Zone (EEZ) which extends seaward to a distance of 200 nautical miles from the baseline from which the breadth of the territorial sea is measured. The establishment of EEZ is perhaps the most significant development in the Law of the Sea since President Truman's Proclamation on the Continental Shelf in 1945, which claimed for the United States the natural resources of the seabed and the subsoil of its continental shelf lying beyond the traditional three mile limit.

Although ICNT does not specifically mention coastal states' jurisdiction over OTEC activities within EEZ, it would be a valid conclusion that coastal states will have exclusive competence over the deployment and regulation of OTEC installations within their EEZ for research purposes or commercial operations. Any reasonable interpretation of ICNT provisions will support this conclusion. To illustrate, article 56(a) grants a coastal state "sovereign rights" within EEZ for "other activities for the economic exploitation and exploration of the zone, such as the production of energy from water, currents and winds." This would obviously include the energy produced by an OTEC operation. Article 60 explicitly provides for a coastal state's "exclusive right to construct and to authorize and regulate the construction, operation and use of: (a) Artificial islands; (b) Installations and structures for the purposes provided for in article 56 and other economic purposes; (c) Installations and structures which may interfere with the exercise of the rights of the coastal State in the zone." Article 247(2) provides that "[m]arine scientific research activities in the exclusive economic zone and on the continental shelf shall be conducted with the consent of the coastal State." Moreover, there is such an overwhelming consensus among the participants at LOS III on EEZ that even if the efforts to formalize a comprehensive treaty on the Law of the Sea were to fail, EEZ will in the near future be accorded legitimacy by state practices, transforming it into a rule of customary international law.

It appears that the coastal state's permission would be required to install an OTEC device in its EEZ either for research purposes or commercial operations. Until now, no nation state has adopted specific legislation addressing this issue. However, once OTEC technology and economics are proven, such legislative measures prescribing conditions for access to EEZ and outlining the legal and institutional arrangements under which a foreign entity is permitted to operate an OTEC facility within that zone will in all probablity be adopted by countries wishing to attract a foreign owned/operated OTEC facility within its EEZ. Bilateral and regional arrangements regarding the deployment and operation of an OTEC device within a coastal state's EEZ would be another way of establishing conditions for the installation of OTEC devices within an EEZ.

Continental shelf. Under the 1958 Geneva Convention on the Continental Shelf,[31] "sovereign rights" of the coastal states in the continental shelf (defined as beginning at the seaward limit of the territorial sea and continuing to the 200-meter isobath),[32] are restricted to "exploring it and exploiting its natural resources,"[33] leaving unaffected the "legal status of the superjacent waters as high seas, or that of the airspace above those waters."[34] A coastal state's consent is imperative for any scientific research concerning the continental shelf and conducted there.[35]

Thus, although theoretically an OTEC device of another nation could be moored on a coastal state's continental shelf, while the device itself is located on the high seas, provided it did not interfere with the coastal state's exclusive right to exploit natural resources in that area,[36] the prospects that this would happen are unlikely without the consent of the coastal state. A coastal state's special rights in adjacent waters with regard to scientific research and pollution control are widely accepted, and with the emergence of EEZ, such a possibility without the coastal state's consent could be ruled out.

ICNT modifies the definition of the continental shelf by providing that it extends to the outer edge of the continental margin or to a distance of 200 miles when the outer edge of the continental margin does not extend that far.[37] While other ICNT provisions[38] do not substantially change the prior law, a reading of articles 60, 80, and 247 provides the inescapable conclusion that a coastal state will have exclusive competence over the installation of any OTEC device located over its continental shelf for research or commercial purposes.

OTEC devices on the high seas.

Traditional law. Under the freedom of the seas concept, every nation has unrestricted access to the high seas, but none is permitted any long term appropriation of any part of the high seas for its exclusive use. In 1958, the Geneva Convention on the High Seas codified the essence of the freedom of the seas by providing freedoms such

as commercial navigation, fishing, laying of submarine cables and pipelines.[39] Obviously, many of these freedoms may give rise to conflicting uses of the high seas. For the management of these conflicting uses, the standard is that of "reasonableness" with regard to the interests of other users, that is, not unreasonably interfering with their uses. The deployment of an OTEC device for research or commercial purposes could be justified under this "reasonable use" concept. The recent U.S. legislation authorizing the construction of deep water ports beyond the limits of its territorial sea,[40] which it justified on this reasonable use theory,[41] offers an appropriate precedent. Since states traditionally have the primary responsibility for regulating the activities of vessels flying their flags on the high seas, applying that analogy to OTEC devices, any OTEC installation owned or authorized by a state on the high seas would be under its authority and control. Similarly, under the laws of nationality, nationals are always and everywhere subject to the laws of their nation state[42] and their activities on an OTEC device on the high seas would be governed by the laws of the state of their nationality.

LOS III and the deep seabed. Current negotiations in LOS III are still stymied on the nature and scope of the proposed regime for deep seabed mining.[43] However, ICNT attempts to give concrete shape to the "common heritage" concept enunciated by the U.N. General Assembly in its Resolution 2749 of December 17, 1970.[44] It declares the area constituting "the sea-bed and ocean floor and subsoil thereof beyond the limits of national jurisdiction"[45] (Area), and its resources to be "the common heritage of mankind,"[46] and envisages the establishment of an International Sea-Bed Authority (ISA) to organize and control activities in the Area. No state is to claim or exercise sovereignty there and no exclusive appropriation is permissible.[47] The legal status of the waters superjacent to the Area or that of the airspace above those waters are left unaffected.[48] There is considerable ambiguity regarding ISA's control in the Area.[49]

Resources are defined as "mineral resources in situ,"[50] which are subject to ISA's licensing and regulation.[51] Minerals include "water, steam, hot water."[52] While it can be argued that ISA's jurisdiction extends to "fresh water aquifers and similar sub-surface water sources, not the cold water lying near the seabed that might be used by an OTEC device,"[53] a broad interpretation by ISA of these provisions is possible, under which OTEC deployment for scientific research or commercial purposes would be covered.[54] Also, despite the current provision, under which ISA has no jurisdiction over the superjacent waters of the high seas,[55] it is possible that its jurisdiction in the near future will extend to activities in the water column and on the surface,[56] thereby affecting OTEC operations. Such an outcome would be consistent with the growing demands of the developing states for a strong ISA which could give meaning to "the common heritage" concept. Similarly, the mooring of an OTEC device on the high seas, which would require corings and other physical investigations of the ocean floor and the seabed, could be perceived as an economic use of the Area, and, therefore, subject to ISA's jurisdiction. Additionally, ISA could assume jurisdiction, should such mooring pose any actual or potential interference to seabed mining activities which are to be regulated by ISA. Of course, ISA could assert jurisdiction over marine scientific research in the Area which is to be carried out "exclusively for peaceful purposes and for the benefit of mankind as a whole."[57]

Consequently, it appears that under the envisaged seabed regime, OTEC activities on the high seas could be subjected to the jurisdiction of the proposed ISA. Perhaps two exceptions to ISA jurisdiction are possible: (1) A coastal state extends its competence to an OTEC facility which lies beyond its EEZ, but which poses an actual or potential threat to its living and nonliving resources by adversely affecting the marine environment, or (2) if there is no accord at LOS III on a deep seabed regime and the existing law applies under which the deployment of an OTEC facility on the high seas could be justified under the "reasonable use" concept.

Federal - State Issues Related to OTEC Devices[58]

In the United States' coastal waters, there still remain unresolved questions regarding the demarcation of authority between the Federal government and the adjacent coastal states. Further uncertainty is likely when the United States decides to expand its territorial seas to a twelve mile limit and subsequently to claim its 200 mile EEZ, the two probable prospects with or without a comprehensive Law of the Sea treaty. The primary question is, what would be the States' rights in the newly acquired territory?

Current law. The 1945 Truman Proclamation which extended United States' jurisdiction to its continental shelf left unresolved the question of Federal versus State authority over the shelf.[59] In May, 1963, U.S. Congress responded to the ensuing uncertainties by enacting the Submerged Lands Act.[60] This Act gave the States title and ownership of land and resources lying beneath the water extending seaward to its three mile limit,[61] subject, however, to the continued U.S. authority and rights over such lands and waters "for the purposes of navigation or flood control or the production of power."[62]

Six years after the enactment of the statute, a Federal district court specifically recognized the paramount power of the United States to control such waters for the purposes of navigation in interstate and foreign commerce.[63]

In August 1953, just three months after the enactment of the Submerged Lands Act, the Outer Continental Shelf Lands Act[64] implemented the 1945 Truman Proclamation by declaring the policy of the United States: "that the subsoil and seabed of the outer Continental Shelf[ocs] appertain to the United States and are subject to its jurisdiction, control, and power of disposition."[65]

The Act provides for the application of the civil and criminal law of coastal States existing on the effective date of the Act to the activities on the subsoil and seabed of OCS including artificial islands and fixed structures erected there.[66] In 1975 Congress amended the Act to apply current State laws.[67]

These statutes did not resolve the Federal-State controversy regarding the proper authority and control for the exploration and exploitation of OCS. The States continued to claim a stronger voice in the decision making process because of the direct impact on the States of OCS development. In response to a U.S. complaint against thirteen Atlantic coastal States that they were interfering with the exclusive U.S. rights to explore and exploit the natural resources of OCS, in 1975 the Supreme Court decided United States v. Maine,[68] in which it reaffirmed its earlier decisions that the Federal government had "paramount rights in the marginal seas"[69] as attributes of its external sovereign powers.

More recently, however, the recognition of the coastal State's interest in activities over OCS has been evident in several new developments, including: (1) the formation of regional OCS advisory boards with State representatives on them;[70] (2) the devising of a new system under which the Department of the Interior will share with the States information regarding lease tracts;[71] and (3) the 1978 Amendments to the Outer Continental Shelf Lands Act[72] under which States will be given a significant role in decision making pertaining to leasing.[73]

Several other Federal statutes permit Federal-State participation in planning offshore activities,[74] including the Deepwater Port Act (DPA)[75] and the Coastal Zone Management Act (CZMA).[76]

CZMA Amendments of 1976 created a coastal energy impact program[77] which authorizes $800 million for the creation of a coastal energy impact fund for loan guarantees and grants to States which must have an approved coastal zone management program or be making satisfactory progress in developing such a program.[78]

Federal-State issues in light of LOS III. When the United States extends its boundaries to a twelve mile territorial sea and a 200 mile EEZ, two questions become pertinent: (1) would the State zone be extended from three to twelve miles? and (2) if such a State expansion were to take place, would the Federal government pre-empt the States in energy matters, including OTEC? Who would be the licensing authority and what would be the licensing requirements? Since the coastal State is given police power over such islands and structures, the question arises as to which laws would be made applicable to them. In regard to the last question, the model provided by the Outer Continental Shelf Lands Act,[79] and DPA,[80] applies the law of the adjacent coastal State. This would seem to be the desirable approach to adopt. Thus, the law of the State where the transmission cables go ashore will apply to the extent that it is not inconsistent with Federal law. Other possibilities include the general maritime law or the law of the State in which the OTEC firm is incorporated.

Regulatory Issues

Regulatory issues will be considered in this section in two contexts -- international and Federal-State. This examination will be prefaced by a brief investigation of the legal status of OTEC devices.

Legal status of OTEC devices. It is important to determine the legal status of OTEC devices because many rights and obligations of such entities and those owning, operating, and manning them will often flow from such a determination. Additionally, the conferring of legal status on OTEC devices, whether fixed to the ocean floor or moveable either for stationkeeping or for grazing on the high seas, will legitimize their presence as well as their operation.

Whether an OTEC device is considered a vessel will not be dispositive of the complex legal issues raised by OTEC presence as a new user of the sea. However, because of the status of commercial navigation as an ocean use of long-standing, there are existing international guidelines, standards, and regulations applicable to vessels. It is useful to inquire whether the existing standards and regulations -- those of safety, design and construction, collision and navigation, communication, and labor -- will apply to OTEC devices and whether these regulations need to be modified in order to meet OTEC needs. Otherwise, new arrangements will have to be devised. In the national context, the status of OTEC devices as vessels could confer upon them substantial economic benefits, in view of the fact that the U.S. shipping industry is subsidized by the United States government by means of providing mortgage guarantees, construction and operation subsidies, and tax advantages.[81]

It appears that only during the last decade have international agreements regulating activities on the sea broadened their reach to cover OTEC-type structures by using terms such as "floating crafts" and "floating platforms" to define ships. These agreements include the 1969 Convention on Intervention on the High Seas, dealing with oil pollution casualties;[82] the 1972 Convention on the Prevention of Marine Pollution by Dumping of Wastes and Other Matter;[83] the 1973 Convention for the Prevention of Pollution from Ships;[84] and the 1976 Convention on the International Maritime Satellite Organization.[85] However, there are many conventions adopted under the auspices of the International Maritime Consultative Organization (IMCO), which do not cover OTEC-type facilities.[86] Which of these conventions should be made applicable to OTEC will depend upon the purpose of the convention and the probable benefit of its application to OTEC activities - both to the research and demonstration and development phases - so that its commercialization is facilitated and expedited.

ICNT provisions on pollution, on the other hand, would cover OTEC devices. Dumping is defined to include wastes or other matter from "vessels, aircraft, platforms or other man-made structures at sea."[87] The terms used are "installations and devices,"[88] and "vessels, installations, structures and other devices," flying the flag of the mining states or of their registry.[89] Therefore, regardless of the status of OTEC devices, they would be regulated under ICNT.

International Regulatory Mechanisms and OTEC [90]

Current law. It should come as no surprise that no regulatory mechanism exists for specific application to OTEC, for as a new technology it has yet to make its debut as a user of ocean space.

It seems likely that in the initial stages of OTEC development for research and demonstration purposes and subsequently for commercial operation, broader guidelines and standards with built-in flexibility, rather than narrow, precise norms will be established. Developments in another relatively new area, transnational pollution,[91] show that the important tasks of setting and harmonizing standards and establishing appropriate machinery for implementation, usually occur first in regional settings[92] and appear later in a global setting where such need and feasibility have been clearly demonstrated. Because of unique regional situations, it is unrealistic to expect or even pursue universality and uniformity. The Regional Seas Program of the United Nations Environmental Program (UNEP),[93] which has developed in the last four years and is still developing action plans for seven regions -- Mediterranean, Gulf of Arabia, Red Sea, Gulf of Guinea, Caribbean and adjacent regions, East Asian Seas, and South Pacific -- illustrates regional efforts on environmental management.

Several existing arrangements regulating other activities in ocean space such as the ones established under the 1958 Geneva Convention, could be construed to cover OTEC-type structures and activities on them, or with modifications could be made applicable to OTEC. However, the question of who would authorize operation of OTEC devices on the high seas is at present unsettled. Would the current state practice on vessels, the flag state approach (which raises a further issue of the flags of convenience),[94] be made applicable. Or, would the OTEC issue become as controversial as is the deep seabed mining issue at present?[95] It is premature to suggest the precise nature of the conditions and arrangements for OTEC activities on the high seas, for the current debate on the seabed mining issue and the conclusions which are finally reached at LOS III will substantially affect the OTEC licensing and operations.

Regulations applicable to marine pollution which might have a bearing on OTEC activities will be discussed in the next section dealing with environmental problems.

Federal-State Regulatory Mechanisms and OTEC

Current law. In a recent study, Tefft, Kelly, Dick, and Stevenson postulate the following scenario for OTEC exploitation to the year 2025:[96]

U.S. OTEC
Megawatts on Line

1980	85	90	95	00	05	10	15	20	25
	.5	2.5	5	10	50	100	150	200	250

The authors conclude that "decisive Federal action will be needed to carry out this scenario,"[97] and offer a model of Federal legislation.[98] The proposed "Ocean Thermal Energy Conversion, Development, Expolitation, and Regulation Act of 1980," would establish, among other policy objectives, the following: OTEC shall be subject to exclusive Federal regulation; while in the short term, Federal participation in OTEC development, ownership, and/or operation will be necessary to stimulate deployment to meet the established energy generation goals, a long term objective shall be non-Federal development, ownership, and operation. The authors provide a detailed institutional framework to carry out these policies.[99]

Regarding the application of Federal versus State laws to OTEC activities in adjacent offshore areas, pending the enactment of a comprehensive Federal legislation regardint OTEC, pertinent guidelines are provided by the Supreme Court test of uniformity versus locality or diversity:

> if a case falls within an area in commerce thought to demand a uniform national rule, state action is struck down. If the activity is one of predominantly local interest, state action is sustained. More accurately, the question is whether the state interest is outweighed by a national interest in the unhampered operation of interstate commerce.[100]

More recently, the court applied the test in Ray v. Atlantic Richfield Co.[101]

Environmental Considerations

A recent study[102] has outlined several environmental problems associated with the deployment of OTEC devices in the ocean. Obviously, such an inquiry is at present speculative, however it is desirable that environmental issues be addressed at this preliminary stage of OTEC development.

Domestic (Federal-State) issues. Potential environmental impacts from OTEC facilities in coastal waters include those from construction and operation of such facilities, cables and transmission lines, and onshore services and support facilities. The existing U.S. legislation relevant to OTEC activities includes the OCS Lands Act, CZMA, DPA, and the National Environmental Policy Act of 1969 (NEPA).[103]

NEPA requires Federal agencies to prepare records on environmental effects of and alternatives to "every recommendation or report on proposals for legislation and other major Federal actions significantly affecting the quality of the human environment."[104] Since Federal involvement in OTEC development is expected to be substantial, at least during the initial stages, preparation of Environmental Impact Statements (EISs)[105] -- programmatic, site-specific, and regional -- are likely to be required during the research phase of OTEC development.

Among other significant developments, the Coast Guard, on December 4, 1978, proposed rules for administering an offshore oil pollution compensation fund,[106] which is expected to cover "all marine oil pollution, including that discharged from onshore facilities and deepwater ports."[107] Also, the Council on Environmental Quality (CEQ) is proposing new pollution clean up plans in which coastal States' interests are recognized.[108]

Unilateral U.S. actions related to the marine environment. During the recent past, the U.S. Congress has adopted legislation with potential extraterritorial reach in the marine environment. For example, the Clean Water Act[109] extended the

application of Section 311 (Oil and Hazardous Substance Liability) of the Federal Water Pollution Control Act[110] to cover activities which affect the resources of the 200 mile U.S. fisheries zone or its OCS. Earlier, the Fishery Conservation and Management Act of 1976 [111]extended the U.S. fishery zone to 200 miles. Other U.S. acts with potential effect on maritime activities include the U.S. Ports and Waterway Safety Program,[112] the Marine Protection, Research and Sanctuaries Act of 1972,[113] the New Coast Guard Regulations concerning navigational aids,[114] and the DPA.[115]

The debate continues as to whether NEPA applies to major Federal actions abroad.[116] Under a proposed Executive Order, certain Federal actions having a significant adverse effect upon the environment of nonparticipating third countries or natural resources of global importance will be required to have abbreviated environmental reviews.[117]

Multilateral actions. The 1972 U.N. Conference on the Human Environment in Stockholm[118] acknowledged the emerging norms of state responsibility and liability for transnational environmental damage. Principles 7, 21 and 22 of the U.N. Declaration on the Human Environment contain pertinent provisions.

Following the Stockholm conference, several conventions were concluded. Also, there have been substantial bilateral and multilateral efforts to conclude new conventions for the prevention of marine pollution and the conservation and management of the marine environment[119] which might have some bearing on OTEC operations.

ICNT provisions. Part XII of ICNT contains 46 articles on the protection and preservation of the marine environment. States are obligated to protect and preserve the marine environment,[120] to refrain from polluting the environment of other states or areas beyond their national jurisdiction,[121] and to take measures to prevent, reduce, and control marine pollution.[122] In another article ICNT calls upon states "[i]n taking measures to prevent, reduce and control pollution of the marine environment...not to transfer, directly or indirectly, damage or hazards from one area to another or transform one type of pollution into another."[123] States would also assume positive legal responsibility to cooperate in internationa monitoring programs,[124] and to assess the environmental impacts of their activities on the marine environment.[125] Articles 210 and 236 provide for the establishment of rules and standards and responsibility and liability respectively. OTEC activities and operations would certainly be covered under many of the principles and specific provisions contained in the chapter on the ocean's environment.

Appraisal and Recommendations

OTEC holds sufficient promise to warrant vigorous research efforts on its systems and technology. However, an efficient and effective legal and institutional framework would further facilitate and expedite OTEC development and commercialization. Accordingly, only selected issues, the most pertinent ones seeking resolution on a priority basis, have been addressed in this paper.

Specific recommendations made here relate to both Federal-State and international aspects. On national-international jurisdictional issues, it is suggested that the U.S. opt for the 200 mile coastal state competence related to OTEC siting and deployment, and that Congress enact as an interim measure legislation creating a 200 mile Coastal Energy Conservation and Management Zone. Under such a zone the United States will claim limited jurisdiction for the specific purpose of energy conservation and management. To engage in OTEC activities on the high seas, the United States could invoke a "reasonable use" theory. On Federal-State issues, it is essential that a cohesive and equitable U.S. policy be formed and strong institutional structures built to implement it so as to ensure an efficient management of the 200 mile marine zone.

On national-international regulatory issues, two issues deserve urgent consideration: (1) the prescription of unilateral U.S. regulations on licensing and registration, safety, conflicting sea uses, communications, import and export, foreign labor, insurance, liability and compensation schemes, etc; and (2) the devising of imaginative bilateral and regional arrangements to address questions related to: the management of conflicting claims of ocean users caused by OTEC presence; the apparently competing interests of a coastal state and the licensing-registry state, where a foreign registered/licensed OTEC device is operating adjacent to a coastal state EEZ; and bilateral or regional schemes under which a combination of a state or states and private enterprises pool their resources, technology, and know-how to construct, operate and own OTEC devices. Also, dispute settlement mechanisms will have to be devised. Regarding OTEC siting on the high seas, mechanisms on a global scale might have to be devised to set pertinent standards and regulations to ensure the optimal use of the oceans for OTEC development. On Federal-State issues, under a proposed mechanism, the licensing and regulatory authority will be the Federal government, while the DOE/Federal Energy Regulatory Commission (FERC) will be the lead Federal Agency. OTEC facilities in offshore areas will be considered a utility in interstate and foreign commerce under FERC jurisdiction. Effective Federal/State consultative mechanisms, administrative advisory boards, and Federal-State revenue sharing schemes will ensure an accommodation of Federal-State interests.

On environmental issues, in the domestic arena, NEPA requirements of EIS and CZMA will apply. In the international arena, several existing multilateral agreements and ICNT provisions, and possibly EIS requirements, will apply.

In sum, it seems imperative that through legislation a comprehensive management system for U.S. coastal areas be devised. In the international arena, consideration should be given to the drafting of a convention mandating environmental impact assessments of a state's major projects which could harm the environment of another state or the shared global environment, and providing for consultative mechanisms,[126] and of another convention specifically on OTEC activities, including a code of conduct.

Acknowledgments

I am especially grateful to John Lawrence Hargrove, Director of Studies, American Society of International Law (ASIL), for sharing with me a recent study prepared by ASIL under an Energy Research and Development Administration (ERDA) contract and entitled, "International, Legal, Political and Institutional Aspects of OTEC Demonstration and Development," and to R. C. Teffts, President, Tefft, Kelly & Motley, Inc., for a study prepared by his firm entitled, "Toward a Legal, Institutional and Financial Framework for OTEC Demonstration and Commercialization." I have greatly benefited from these studies as well as from my discussions with Jan Laitos, George Morgan, and John Veigel of the Solar Energy Research Institute. However, I alone am responsible for the contents of the paper.

References

1. Cited in Council on Environmental Quality, Solar Energy--Progress and Promise 1 (1978).

2. Reported in Denver Post, Nov. 23, 1978, at 38, col. 1.

3. See, e.g., Nye, Jr., "Nuclear Policy: Balancing Nonproliferation and Energy Security," 78 Dep't State Bull., Oct. 1978, at 39. See also 78 Dep't State Bull., Sept. 1978, at 3.

4. Energy Policy and Planning, Executive Office of the President, The National Energy Plan (U.S. Govt. Printing Off., April 1977).

5. Whitmore, "OTEC: Electricity from the Ocean," 81 Technology Rev., Oct. 1978, at 58-60.

6. Id. at 58.

7. Id. at 61.

8. Id. at 63.

9. On technical, economic, and financial aspects, see generally H. Knight, J. Nyhart & R. Stein, Ocean Thermal Energy Conversion (1977) [hereinafter cited as Knight, Nyhart & Stein]; Science Policy Research Division, Congressional Research Service, Subcomm. on Advanced Energy Technologies and Energy Conservation Research, Development and Demonstration of the House Comm. on Science and Technology, 95th Cong. 2d Sess., Energy from the Ocean 25-79 (Comm. Print 1978); E. Francis, Investment in Commercial Development of Ocean Thermal Energy Conversion (OTEC) Plant-Ships (1977) (Prepared by Johns Hopkins University Applied Physics Laboratory for U.S. Dept. of Commerce); Solar Energy Research Institute, Economic Feasibility and Market Readiness of Eight Solar Technologies: Interim Draft Report 130-45 (1978) (Prepared for U.S. Dep't of Energy) [hereinafter cited as SERI Interim Draft Rep.]; R. Tefft, R. Kelly, C. Dick, Jr., & K. Stevenson, Toward a Legal, Institutional and Financial Framework for OTEC Demonstration and Commercialization (1978) (Prepared for ERDA by Tefft, Kelly and Motley, Inc.) [hereinafter cited as Tefft, Kelly & Motley, Inc. Study]; B. Washom & J. Nilles, Incentives for the Commercialization of Ocean Thermal Energy Conversion Technology (OTEC) (1977) (Prepared for RANN, Nat'l Sci. Found.); J. Witwer, J. Alich, S. Kohan, M. Levine, P. Meagher, E. Pickering, F. Schooley, A. Slemmons, & T. Thompson, 1 A Comparative Evaluation of Solar Alternatives: Implications for Federal RD&D 95-101 (1978) (Submitted to Solar Working Group, U.S. Dep't of Energy); and 5 Sharing the Sun: Solar Technology in the Seventies 392-548 (K. Boer ed. 1976).

10. The Conference which began in Caracas in 1974 concluded its resumed seventh session on Sept. 15, 1978 convened its eighth session in Geneva on March 19, 1979. For a short report on the last session, see 15 UN Monthly Chronicle, Sept. 1978, at 41-42. Voluminous legal literature has grown around the Conference issues. See, e.g., various publications of the Law of the Sea Institute including the papers and proceedings of its annual conferences, and its occasional and special papers; 1-6 New Directions in the Law of the Sea (R. Churchill, M. Nordquist, S. Lay, K. Simmonds & J. Welch eds. 1973-77); R. Dupuy, The Law of the Sea: Issues in Ocean Resource Management (D. Walsh ed. 1977); Symposia in volumes 6-15 of San Diego L. Rev. (1969-78).

11. The assessment is based on a study of sources cited in note 9 supra.

12. Cited in Tefft, Kelly & Motley, Inc. Study, supra note 9, at 3.

13. Cited in id.

14. UN Chronicle, Aug.-Sept. 1978, at 41-42.

15. The four conventions are found at 499 U.N.T.S. 312; 559 U.N.T.S. 285; 450 U.N.T.S. 82; and 516 U.N.T.S. 205.

16. See generally arts. 1-13 of the Territorial Sea Convention; M. McDougal & W. Burke, The Public Order of the Oceans 174-304, 446-564 (1962) [hereinafter cited as McDougal & Burke].

17. League of Nations Publication C. 74. M. 39. 1929. V.

18. See U.N. Doc. A/CONF. 13 (1958).

19. See U.N. Doc. A/CONF. 19/8 (1960).

20. Historically, there has been no freedom of scientific research within the territorial sea.

21. Arts. 1 and 2 of the Territorial Sea Convention.

22. See U.N. Doc. A/AC.135/11 and A/AC./135/11/Add.V (1968).

23. U.N. Doc. A/CONF.62/WP. 10 & Corr. 1-3(1977) [hereinafter cited as ICNT].

24. Id. art. 3.

25. Id. art. 33.

26. Id. art. 2.

27. Id. arts. 17-32.

28. See generally D. Johnston & E. Gold, The Economic Zone in the Law of the Sea: Survey, Analysis and Appraisal of Current Trends (Occasional Paper No. 17, Law of the Sea Institute, University of Rhode Island, June 1973).

29. ICNT, Art. 57.

30. Pres. Proc. No. 2267, 3 C.F.R. 67 (1943-48 Compilation).

31. See note 15 supra.

32. Art. 1 of the Continental Shelf Convention.

33. Id. art. 2.

34. Id. art. 3.

35. Id. art. 5(8).

36. Based on arts. 4-5 of the Continental Shelf Convention, Knight makes this argument in Knight, "International Jurisdictional Issues Involving OTEC Installations," in Knight, Nyhart & Stein, supra note 9, at 45-73.

37. ICNT, art. 76.

38. Id. arts. 77-85.

39. Art. 2 of the High Seas Convention. See note 15 supra.

40. The Deepwater Port Act of 1974, 33 U.S.C. §§ 1501-24 (1976) [hereinafter cited as DPA].

41. See Hearings on S.1751 and S.2232 93d Cong., 1st Sess., pt. 1, 606-19 (1973)(Statement of John Norton Moore).

42. See generally H.Van Panhuys, The Role of Nationality in International Law (1959).

43. For a recent commentary, see LaQue, "Different Approaches to International Regulation of Exploitation of Deep-Ocean Ferromanganese Nodules," 15 San Diego L. Rev. 477 (1978).

44. G.A.Res. 2749,25 U.N. GAOR, Supp. (No. 28) 24, U.N. Doc. A/8028 (1970).

45. ICNT, art. 1(1).

46. Id. art. 136.

47. Id. art. 137(1).

48. Id. art. 135.

49. Id. arts. 1(3), 133(a), 143-49.

50. Id. art. 133(b).

51. Id. Annex II.

52. Id. art. 133(c)(1).

53. Knight, "OTEC and the Law of the Sea: The Jurisdictional Problems," in American Society of International Law, International, Legal, Political and Institutional Aspects of OTEC Demonstration and Development 15 (Study prepared for ERDA, Sept. 1978)[hereinafter cited as ASIL Study].

54. Knight acknowledges this possibility. Id. at 15.

55. ICNT, art. 135.

56. The Delegation of Malta made this claim in the United Nations seabed committee in 1971. See 26 U.N. GAOR, Supp. (No. 21) 105, U.N. Doc. A/8421 (1971).

57. ICNT, art. 143 (1).

58. For a thorough and incisive study of Federal-State issues in the U.S. coastal waters, see M. Ball, Law of the Sea: Federal State Relations and the Extension of the Territorial Sea (The Dean Rusk Center for International and Comparative Law, University of Georgia, Monograph No. 1, 1978) [hereinafter cited as M. Ball].

59. See 13 Dep't State Bull. 484 (1945).

60. 43 U.S.C. §§ 1301-1315 (1970).

61. 43 U.S.C. § 1311(a),(b)(1970).

62. Id. § 1311(d).

63. See Organized Village of Kake v. Egan, 174 F. Supp. 500 (D. Alaska, 1959).

64. 43 U.S.C. §§ 1331-43 (1970).

65. 43 U.S.C. § 1332 (1970).

66. Id. § 1333(a)(2).

67. 43 U.S.C.A. § 1333(2) (Supp. 1978).

68. 420 U.S. 515 (1975).

69. Id. at 522-23.

70. Cited in M. Ball, at 42 n. 159.

71. 43 Fed. Reg. 3883, 3887, 3889, 3895 (1978).

72. Pub. L. No. 95-372, 92 Stat. 629.

73. Id. Title II, § 208 (adding a new § 19), 92 Stat. 652-53.

74. See, e.g., 33 U.S.C. §§ 1251-1376 (1976), as amended by Pub. L. No. 95-217, 91 Stat. 1566; Pub. L. No. 94-265, 90 Stat. 331; 16 U.S.C. §§ 1401-34 (1976); and 16 U.S.C. §§ 1361-1407 (1976).

75. 33 U.S.C. §§ 1501-24 (1976).

76. 16 U.S.C. §§ 1451-64 (1976).

77. 16 U.S.C.§ 1456(a) (1976).

78. 16 U.S.C. §§ 1456 (a),(c),(d), 1464(b)(1976).

79. 43 U.S.C. §§ 1331-43 (1970).

80. 33 U.S.C. §§ 1501-24 (1976).

81. See,e.g. on ship mortgages, 46 U.S.C.§§911-84, 1271-80(1970 & Supp. IV 1974), as amended by Pub. L. No. 92-507. See generally Cook, Jr., "Government Assistance in Financing Title XI Federal Guarantees," 47 Tul. L. Rev. 653 (1973); Kominers, "Federal Government Aids to Merchant Shipping," id. at 691.

82. Article II (2), 26 U.S.T. 765, T.I.A.S. No. 8068.

83. 26 U.S.T. 2403, T.I.A.S. No. 8165.

84. Reprinted in 12 Int'l Legal Materials 1319 (1973).

85. Reprinted in 15 id. 1051 (1976).

86. For these conventions see 536 U.N.T.S. 27; 536 U.N.T.S. 27; 14Int'l Legal Materials 959 (1975); 327 U.N.T.S. 3, as amended by 600 U.N.T.S. 332; 640 U.N.T.S. 133;and 9 Int'l Legal Materials 45 (1970).

87. ICNT art. 1(1)(5)(a)(i & ii).

88. Id. art. 195(3)(c & d).

89. Id. art. 210(2).

90. See generally Faron, "International Regulatory Aspects of OTEC Development and Operation," in ASIL Study, at 86-148.

91. See generally J. Barros & D. Johnston, The International Law of Pollution (1974); Nanda, "The Establishment of International Standards for Transnational Environmental Injury," 60 Iowa L. Rev. 1089 (1975).

92. See generally Nanda, supra note 91, at 1101-08, 1126-27; Okidi, "Toward Regional Arrangements for Regulation of Marine Pollution," 4 Ocean Dev. & Int'l L. 1(1977).

93. See InternationalCenter, Industry and Environment, Executive ReportNo. 30, Octo. 30, 1978.

94. See generally B. Boczek, Flags of Convenience (1962).

95. See note 43 supra.

96. Tefft, Kelly& Motley Study at 8.

97. Id.

98. Id. at 11-24.

99. Id. See also Tefft, Kelly & Motley, Inc., Working Draft, OTEC Development, Exploitation, and Regulation Act of 1980 (1978).

100. California v. Zook, 336 U.S. 725, 728 (1949).

101. 98 S. Ct. 988 (1978).

102. SERI Interim Draft Rep. at 137-39.

103. 42 U.S.C. § 4321-47 (1976).

104. 42 U.S.C. § 4332(c). See generally R. Linoff, A National Policy for the Environment: NEPA and its Aftermath (1976).

105. See generally Note, "The Scope of the Program EIS Requirement: The Need for a Coherent Judicial Approach," 30 Stan. L. Rev. 767 (1978); Friedman, "The NationalEnvironmental Policy Act of 1969 - The Brave New World of Environmental Legislation," 6 Natural Res. Law, 44 (1973); Kleppe v. Sierra Club, 427 U.S.390 (1976) rev'g Sierra Club v. Morton, 514 F. 2d856 (D.C. Cir. 1975).

106. 43 Fed. Reg. 56840 (1978). See 9 Environ. Rep. (BNA) 1413 (1978).

107. 43 Fed. Reg. 56840 (1978).

108. See 9 Environ. Rep. (BNA) 1416-17 (1978).

109. Pub. L. No. 95-217,91 Stat. 1566, 1593-96 (1977).

110. 33 U.S.C. § 1321 (1976).

111. Pub. L. No. 94-265, 90 Stat. 331(1976).

112. 33 U.S.C. §§ 1221-27 (1976).

113. 16 U.S.C. §§ 1401-34 (1976).

114. See, e.g., 42 Fed. Reg. 5964, 5966 (1977).

115. 33 U.S.C. §§ 1501-24 (1976).

116. See generally Comment, "Renewed Controversy Over the International Reach of NEPA," 7 Envt'l L. Rep. 10205 (1977).

117. See 9 Environ. Rep. (BNA) 304-305 (1978).

118. U.N. Doc. A/CONF.48/14/Rev. 1 (1972).

119. See generally 4 New Directions in the Law of the Sea, supra note 10, at331-518; 6 id. at 456-562.

120. ICNT art. 193.

121. See id. arts. 195(2), 238.

122. Id. art. 195(1).

123. Id. art. 196.

124. Id. art. 205.

125. Id. art. 207 For a critical appraisal of ICNT provisions on the marine environment, see Schneider, "Something Old, Something New: Some Thoughts on Grotius and the Marine Environment," 18 Va. J. Int'l L. 147 (1977).

126. A Senate Resolution, S.49, was introduced in 1978 urging the United States "to negotiate an international treaty requiring environmental impact assessments on major projects that could harm the environment of another nation or the global commons. International impact statements could be filed with the ... (UNEP)." The Resolution would require states parties to the treaty to "consult with affected nations, or with the UNEP in cases involving global commons, to minimize harmful impacts across international boundaries." 9 Environ. Rep. (BNA) 539 (1978).

RESEARCH IN OTEC INSTITUTIONAL AND LEGAL MATTERS

R. Clark Tefft, Ratus L. Kelly,
C. Mathews Dick, Jr., and Kathleen M. Stevenson

Tefft, Kelly and Motley, Inc.
1225 Connecticut Avenue, N.W.
Washington, D.C. 20036

Abstract

In this investigation two principal issues were examined: (1) the legal status of OTEC power plants as "vessels," and (2) possible institutional and financial arrangements which could facilitate OTEC commercialization. With regard to the former, the probable existing status and suggested Federal legislation to change or confirm the existing situation are discussed. Present vessel status is examined in four contexts: financing, civil law, criminal law, and regulatory law. Important conclusions are that: (a) the applicability of the Merchant Marine Act construction and operating incentives to OTEC is questionable; if beneficial features of this Act are to apply to OTEC, it should be amended. However, other Federal approaches to OTEC incentivization are probably preferable; (b) for civil liability and regulatory purposes, grazing OTEC plants are vessels under existing law. Thus they would be registered as such and fly a flag; Admiralty law would apply. (c) the current legal status re civil liability and regulation of floating/moored OTEC plants as vessels or otherwise is doubtful.

With regard to possible institutional and financial arrangements beneficial to OTEC commercialization, potential entrepreneurial arrangements that range from direct Federal ownership/operation to private ownership operation with special Federal incentives are discussed.

Finally, recommended Federal legislation would set goals for OTEC deployment and establish a legal regime for OTEC plant operation.

Introduction

Under ERDA/DOE Contract EG-77-C-01-4119, we studied various legal, institutional, and financial aspects of OTEC commercialization. At the Fifth OTEC Conference in February 1978,[1] we suggested many of the tentative findings and probable recommendations that would likely be made in our final report, which we have completed and submitted, and of which this paper is a summary.

Our work has been conducted in close coordination with the American Society of International Law (ASIL) that was doing related research. In effect, our focus was domestic, theirs was international. As both groups of researchers were aware, this division of labor was not precise, there being a substantial number of interlocking and/or overlapping issues. We are pleased to report that our mutual efforts to consider and coordinate our overlapping areas went well and that both our research efforts and reports are harmonious.

Two primary issues were examined in our undertaking: (1) the legal status of OTEC power plants as "vessels," and (2) possible legal, institutional, and financial arrangements that would facilitate OTEC commercialization. A summary of our approach, findings, and recommendations follows.

Possible Legal, Institutional, and Financial Arrangements That Could Facilitate OTEC Commercialization

We assumed that OTEC commercialization is a situation in which OTEC is an accepted and economic way to generate power and that its products have entered the mainstream of commerce on a sizable scale. The initial step in developing possible legal, institutional, and financial arrangements capable of facilitating OTEC commercialization was to determine potential impediments to its accomplishment. To develop these we reviewed the OTEC technical and non-technical literature as well as other appropriate literature and conducted interviews with potential debt and equity investors, insurance brokers, and government officials. Based on an analysis of this work we distilled the following as prime investment impediments:

a) High cost of early plants.
b) High investment risks - hostile environment/new technology, large dollar amounts, uncertain legal status, insurability, and extent of government regulations.
c) No natural parent industry.
d) High front end expense and risk.

We then developed seven scenarios representing different combinations of legal, institutional, and financial arrangements under which OTEC commercialization might occur. The first basic

scenario represented the current situation, i.e., non-Federal entities acting under existing domestic law proceed without additional Federal assistance or incentive to assemble and finance OTEC facilities ventures, and to design, build, and operate plants or plant ships, delivering electricity and energy-intensive products to the United States, its territories and/or possessions including Puerto Rico. We concluded that under this scenario, OTEC would not commercialize. The impediments are too many and too great.

Since Federal policy generally favors OTEC commercialization, we assumed that the Federal Government would wish to take actions that would eliminate or mitigate impediments by modifying the legal, institutional, and financial status quo. Based upon literature and interview research and our own analysis, a menu of potential eliminating or mitigating actions were cast in six alternative scenarios, including various combinations of change in status quo strategies. (See Table 1)

Common to all of the alternative scenarios is a "legal regime package" the adoption of which we feel is a baseline essential to OTEC commercialization. Included in this package would be Federal legislation that, at a minimum, would establish (1) a United States Energy Management Zone, (2) an OTEC licensing requirement authority and fee policy, (3) applicable law (i.e., Federal/State, Maritime/terrestrial) and jurisdiction, and (4) OTEC regulatory requirements and authorities.

We went on to assess the other changes in status quo strategies, pointing out their various probable utilities and disutilities. In our final report to DOE, we also proposed a draft of Federal legislation, the "Ocean Thermal Energy Conversion Act," that would, as a policy of Congress, (a) have OTEC research, development, and demonstration proceed on an urgent basis, (b) establish goals for OTEC deployment (c) recognize the necessity of Federal actions to assist OTEC commercialization, (d) establish Federal regulation of OTEC, and (e) have the U.S. encourage international OTEC activities. This suggested legislation also includes the necessary provisions to enact the legal regime package elements as outlined above plus certain other legal regime elements of lesser significance.

Table 1 - Summary of Alternative Scenarios

Scenario	Features
1	a) Legal regime package b) Enactment of pending Senate investment tax credit bill c) DOE contracts with two entities to develop venture package for a plant ship and an umbilical plant
2	a) Legal regime package b) Enactment of pending Senate investment tax credit bill c) Investment loans guarantee program up to 75% of facility (ies) cost d) DOE contracts with a substantial number of entities to develop venture packages for plant ships and umbilical plants
3	a) Legal regime package b) Enactment of pending Senate investment tax credit bill c) Investment loans guarantee program up to 75% of facility (ies) cost d) DOE contracts with a substantial number of entities to develop venture packages for plant ships and umbilical plants e) Direct investment loans program f) DOE participation as partner in facilities ownership and operation through cooperative agreements
4	a) Legal regime package b) Enactment of pending Senate investment tax credit bill c) Establishment of COMSAT like corporation to package, own, and operate OTEC facilities
5	a) Legal regime package b) Enactment of pending Senate investment tax credit bill c) Federal lease-in of commercially owned and constructed facilities d) Federal program of last resort property and liability insurance
6	a) Legal regime package b) Government agency or corporation ownership, construction, and operation of facilities via contracts with industry (GOCO arrangement)

References

1. Tefft, R. Clark, Kelly, Ratus L., Dick, C. Mathews, Stevenson, Kathleen M., "Toward A Legal, Institutional and Financial Framework for OTEC Demonstration and Commercialization," Proceedings of The Fifth Ocean Thermal Energy Conversion Conference, February 20-22, 1978, Miami Beach, Florida.

DISCUSSION

Question: Can you foresee the federal government auctioning offshore ocean thermal energy rights?

C. Tefft: Our legislation scenario deals with that and says no. In effect, the cost of the license for operating within the suggested 200-mile U.S. Energy Management Zone (EMZ) is constrained to administrative costs only. The idea would be that the resource is free once the applicant gets a license, and the license fee would not depend on some kind of built-in price for the resource. There would be another problem if the U.S. Government were to charge a royalty for OTEC rights, because that would clearly define ocean thermal energy as a resource. Then, in terms of international law on the high seas there would be a stronger case for treating the OTEC resource as a part of the common heritage of mankind. And that would be the beginning of an expansion of the international Seabed Authority to an extent that a lot of nations don't want to see happen. We believe that the U.S. EMZ should be set up in parallel with the way the fishing zones are set up, that is, the government's role would be management and conservation, not ownership in legal terms.

Question: With regard to resource allocation, suppose utilities in two adjacent states wanted to develop the same OTEC sites. How do you think that would be handled?

C. Tefft: First come first served on acceptable license application.

Question: Would public utilities have a priority here as they do with state agencies?

C. Tefft: That probably is going to be an extremely difficult issue. We were not asked to cover that in our work statement under our contract, and we dealt with it simply by putting a footnote in the report saying that it is likely to be a problem. It is the public versus private power issue that we've fought in this country for years and years, and it goes back and forth quite obviously.

Question: How many agencies could be involved in regulating OTEC installations and operations?

C. Tefft: The proposed lead agency, the DOE/Federal Energy Regulatory Commission (FERC), would provide one-stop service. I would guess that the lead agency will have to coordinate about 10 Federal agencies and possibly the counterpart State agencies. One of the legal regime issues that we dealt with was State and Federal relationships. And one specific issue was whether a state excise tax or sales tax or something like that could be levied on the power as it comes ashore. Our answer was no, except that the states would be allowed to tax the energy coming ashore to the extent that they had economic impact from that cable coming ashore, etc. But not, again, on a royalty type of basis. This is parallel to the final resolution in the Deep Water Ports Act, incidentally. We did use precedents, as lawyers are prone to do, including the Deep Water Ports Act, the Fisheries Act, and the Outer Continental Shelf Act.

Question: As I understand the preseent situation, the DOE is just trying to set up a tracking system to determine where problems may arise with regard to various licensing procedures at the State and Federal levels. Is it realistic to assume that it will be possible to establish a lead agency concept by the time that OTEC has been tested and is ready for the commercial market as far as the technical status is concerned?

C. Tefft: I don't know. That will depend upon how soon a demonstration plant will be operating and whether the schedule of construction of the first commercial plant will overlap the demonstration plant schedule. I think that, if action begins today, it will take 3 or 4 years to get the legislation in place. After that another two years probably will pass before the administrative agencies get themselves organized to accept and process license applications.

C. Cochran, Naval Academy: Along these lines, yesterday afternoon F. Perez Bracetti of the Puerto Rico Water Resources Authority in San Juan indicated that they were going to walk through an application to simulate the licensing procedure for an OTEC plant. It seems to me that this will be a very valuable experience. Everybody will be watching to see how they make out. This experience may enable them to make recommendations for change, or relate what the picture is as they see it and how the action should be streamlined.

D. Nyhart, MIT: Here again, the Deep Water Port Office within the Department of Transporation provides a model, because that new office was created and given the so-called lead agency responsibility with definite statutory specified time limits for handling an application. Admittedly they only had two applications, one of which fell through, but my understanding is that it has been marginally useful to have one lead office. Still, all of the licenses and permits at the federal level still have to be obtained, but the feedback that I have received so far is that both the government people and the private people think that having a designated agency has been an improvement in the process.

LEAD AGENCY DESIGNATION AND PROPOSED LICENSING PROCEDURES FOR OCEAN THERMAL ENERGY CONVERSION FACILITIES**

Edward J. Linky, Esq.*

State of New Jersey
Department of Energy
Trenton

Abstract

Ocean Thermal Energy Conversion (OTEC) in its basic form is channeling the solar heated surface waters of the ocean and deeper bottom waters through a heat exchanger containing fluid capable of vaporization which then propels a turbine for primary generation of electricity or as a catalyst to an energy producing process. OTEC appears to be an environmentally desirable alternate energy form. However, by influencing the circulation of ocean waters, OTEC creates the potential to modify the marine environment.

The physical components of OTEC, platform, power modules, mooring systems and transmission cables to shore, do not distinguish OTEC in a regulatory sense from other types of offshore facilities such as a deepwater port. However, the use of the oceans water column does distinguish OTEC from these other facilities and therefore warrants a separate regulatory regime. Thus, an opportunity exists to design a licensing regulatory mechanism which, while relevant and safeguarding the public interest, will avoid some of the obstacles of past regulatory programs.

For OTEC to be implemented at the federal level, it has been assumed that a lead agency designation will prove beneficial. Such may not be the case at the state level. The federal lead agency, however, must meet several criteria: 1. engineering competence, 2. satisfactory interfaces with state and local agencies and the public, and 3. satisfactory interfaces with federal agencies. The federal lead agency must be more than an OTEC advocate. It must be sensitive to state and local interests.

Because New Jersey has a highly developed regulatory network for energy facility siting, it ~~will be~~ are instructive to examine its programs as an example of the types of problems that a lead federal agency may encounter in siting an OTEC facility. Also, by examining the state process, several pitfalls in the lead agency concept ~~will be~~ are uncovered.

*Administrator, Office of Planning and Policy Analysis, New Jersey Department of Energy - Former staff attorney, New Jersey Department of Enrironmental Protection, Office of Coastal Zone Management.

** The views expressed herein do not necessarily reflect those of the New Jersey Department of Energy or Environmental Protection.

Introduction

Concern about long-term supply and negative environmental impacts of fossil fuels and nuclear has spurred consideration of new technologies. Ocean Thermal Energy Conversion (OTEC) is not a new technology but one for which no economic incentive existed until the current state of energy affairs. Bringing new technology on stream is much more than an engineering exercise. Regulation and licensing procedures potentially consume at least as much time as the basic engineering for energy facilities. The attempt of Public Service Electric and Gas Company to build the Atlantic Generating Station (AGS) 2.8 miles off the New Jersey coast is but one example of offshore energy facility siting caught in a regulatory web.[1] Deepwater Port siting is another example, although these facilities have generally fared better in the regulatory process than the floating nuclear power plants. In recent years, state planning and regulatory programs have gained jurisdiction over offshore energy facilities principally through the federal Coastal Zone Management Act P.L. 92-583, 16 USC 1451 et seq. and the Outer Continental Shelf Lands Act Amendments of 1978 P.L. 95-372. This paper examines the concept of a lead agency both at the federal and state levels in an attempt to determine whether such a concept will aid the permitting of an OTEC facility. Key features of a licensing procedure at the federal and State levels will be set forth. Offshore siting of energy facilities is particularly susceptible to competing and often conflicting regulatory and planning programs of federal agencies.

State Regulatory Programs

In New Jersey the siting and operation of an OTEC facility would be subject to concurrent jurisdiction by the Departments of Energy (DOE) and Environmental Protection (DEP). Both of these agencies have planning programs which directly affect the licensing and siting of energy facilities. For purposes of this paper it is not suggested that New Jersey is particularly suited for an OTEC facility by oceangraphic conditions.

The DEP-Division of Coastal Resources (DEP-DCR) administers the New Jersey Coastal Management Program: Bay and Ocean Shore Segment (BOSS) while the DOE possesses coextensive jurisdiction on energy matters pursuant to N.J.S.A. 52:27F-15. The New Jersey Energy Master Plan (EMP) provides guidance to the DOE in administering its coextensive jurisdiction on state permits.

Co-extensive regulation of energy facilities extends not only to state permits, but also to federal consistency determinations as authorized for approved state management programs.[2] The federal consistency provisions, 307 (c)(1)(2), require federal activities and development projects to be consistent to the maximum extent practicable with state management programs. Section 307 (c)(3)(A), and 307 (c)(b) and 307 (d) require federally licensed and permitted activities to be consistent with state management programs.[3] A Memorandum of Understanding between the DOE and DEP is the implementing mechanism on co-extensive federal consistency determination.[4]

Co-extensive versus Lead Agency Approaches for OTEC in New Jersey

State agencies which would have direct regulatory authority over various components of an OTEC system are the Departments of Energy and Environmental Protection and the Board of Public Utilities (BPU). A Determination of Need for the OTEC Facility would be performed by the DOE. DEP and DOE have co-extensive siting authority and the BPU would decide if the construction costs of OTEC are to be included in the operating utility's rate base. This proliferation of state authority on energy facilities has given rise to proposed legislation which would supposedly expedite the siting process by concentrating all authority in the DOE. The legislation, New Jersey Senate Bill No. 1179, became known as a one-stop shopping bill; that is, all the regulatory functions would take place in the DOE. Section 13 of the bill states that the provisions of other law notwithstanding that the DOE shall have the coordinative and lead role, jurisdiction, and authority with respect to the siting of any energy facility in any part of New Jersey.[5] Would passage of the bill with Section 13 intact aid the siting of an OTEC facility in the State?

Lead agency designation at the state level may be useful only for coordinating information gathering for permit reviews at least with respect to OTEC facilities. The extensive oceanographic analyses associated with OTEC make it virtually impossible for one agency to perform the functions outlined by Section 13. Moreover, such a concentration of authority would bring into question the continued approval by the National Oceanic and Atmospheric Administration (NOAA) of the state's Coastal Management Program.

The federal CZMA pursuant to Section 306 requires all state management programs to contain a process by which facilities of greater than local benefit and in the national interest can be accommodated.[6] Even with this provision it was not the congressional intent in the CZMA that energy facilities (national interest facilities) should always prevail in siting conflicts. All that is required is a process to ensure that these types of facilities will not be unreasonably excluded from state management programs. Lead agency designation under proposed Senate No. 1179 would swing the pendulum too far in trying to rapidly effectuate siting of energy facilities and, in this instance, OTEC.

Senate bill No. 1179 was drafted to respond to what was perceived to be a problem with the concurrent jurisdiction of DOE and DEP. In actuality the concurrent jurisdiction acts as a check and balance system. When the two agencies ultimately come to loggerheads, an Energy Facility Review Board is convened and makes the final decision which is binding on both agencies. Thus, in New Jersey, lead agency status, defined as true one-stop permitting capability is unnecessary and potentially harmful because of its negative effects on the State's Coastal Management Program. Lead agency status does, however, make more sense at the federal level.

Federal Lead Agency Designation

Lead agency designation with regard to energy facilities has not worked well in the past. A general criticism of lead agencies is that few have congressional mandates and staffs to evaluate technology and facilities from a balanced perspective. A case in point is the Nuclear Regulatory Commission (NRC) which is the lead agency for nuclear powered electric generating facilities. The processing of the application for the Atlantic Generating Station the so-called floating nuclear power plants has repeatedly turned up environmental issues which the NRC has been unsuccessful in resolving. For example, the so-called Liquid Pathways Study, a portion of the Environmental Impact Statement, was commissioned only after vigorous insistence by the New Jersey Departments of the Public Advocate and Environmental Protection. This study dealt with Core-Melt scenarios involving releases of radioactivity into the marine environment and was considered unnecessary by the NRC.[7]

Deepwater Ports, another offshore energy facility, are the responsibility of a lead agency, the federal Department of Transportation (DOT). The experience of the Louisiana Offshore Oil Port (LOOP) now under construction has pointed out deficiencies in the processing of this facility. Indeed the project nearly terminated several times principally because of antitrust questions. The lead agency DOT initially was not able to adequately deal with certain of the issues raised by the Department of Justice and valuable time was lost. The Energy Mobilization Board proposed by President Carter could have resolved the difficulties associated with LOOP or an OTEC facility but it is unclear whether such a board is an expedient substitute for the challenging task of creating an effective permitting process. The Deepwater Ports Act[8], however, provides an illustrative example of a lead agency process which can make a contribution to an OTEC licensing regime.

The Deepwater Ports Act

The Act authorizes the Secretary of Transportation to license facilities with potential large scale environmental impacts on an adjacent coast. To address these concerns, 33 USC 1504(b) states that the Secretary of Transportation in consultation with the Secretary of the Interior and Administrator of the National Oceanic and Atmospheric Administration is to prescribe regulations involved with site evaluations, and preconstruction testing at potential deepwater port locations, that may, (1) adversely affect the environment, (2) interfere with authorized uses of the Outer Continental Shelf, and (3) pose a threat to human health and welfare. Further, pursuant to 33 USC 1505 the Secretary must obtain recommendations from the Environmental Protection Agency (EPA), NOAA and other Federal departments and agencies to establish environmental review criteria consistent with the National Environmental Policy Act (NEPA).[9]

Additional features of the Act which are desirable for a federal OTEC regime is the adjacent state provision. The Governor of an Adjacent Coastal State possesses a defacto veto over the approval of a license application. Section 33 USC 1508(b)(1) states that, if the Governor of such adjacent state notifies the Secretary that an application which would otherwise be approved is inconsistent with State programs relating to environmental protection, land and water use, and coastal zone management, then the Secretary must condition the license so as to make it consistent with State programs. Finally, a Deepwater Port liability Fund is established which allows persons affected by oil discharges to receive damages involving the loss of real or personal property, the resources of the marine environment, or the coastal environment of any nation, including damages claimed without regard to ownership of any affected lands, structures, fish, wildlife or biotic or natural resources. Perhaps the only criticism that can be leveled against the act is that the Secretary of Transportation need only consult with other agencies in adopting regulations on deepwater ports. This criticism leads one back to the initial issue raised by this discussion as to whether lead agency status or co-extensive jurisdiction, such as found in New Jersey Senate Bill No. 1179, would be desirable at the federal level.

Co-extensive Jurisdiction or Lead Agency Jurisdiction

Lead agency jurisdiction has decided advantages both from the standpoint of advancing the siting process and safeguarding the environment. The federal arena is too large and complex to entertain co-extensive authority such as exists at the state level in New Jersey. The Deepwater Port Act procedure is a decided improvement on the procedures used by the Nuclear Regulatory Commission and an OTEC licensing procedure could improve on that procedure still further. The desirable elements of an OTEC licensing procedure would include:

1. OTEC Liability Fund for damage to fisheries.

2. Adjacent state veto and consistency with State programs.

3. Mandatory acceptance by lead agency of other federal agency comments on proposed regulations.

4. Resolution of conflicts over agency regulations to be resolved by the Council on Environmental Quality.

5. Determination by the relevant State agency and U.S. Department of Energy that OTEC fulfills a regional energy need.

Candidate Federal Lead Agencies

Numerous federal departments and agencies have substantial interests in OTEC. The Departments of State, Interior, Transportation, and Energy, with the Environmental Protection Agency, National Oceanic and Atmospheric Administration, (NOAA) and the Council on Environmental Quality have key interests in OTEC. Although arguments can be made with respect to designation of these agencies, NOAA is the best overall candidate agency for OTEC facilities:

1. NOAA is already a comprehensive Oceans Agency with marine engineering and oceanographic expertise.

2. Through the National Marine Fishery Service and Coastal Zone Management Programs (CZM), it has an comprehensive environmental awareness.

3. Through its Coastal Zone Management Program, it has the experience and mandate to interact with state and local agencies.

4. Through the CZM programs, energy interests and environmental concerns must be constantly addressed and balanced.

References

1. See Final Environmental Impact Statement Floating Nuclear Power Plants U.S. Nuclear Registery Commission (NUREG) - 0502 December 1978.

2. Energy facility siting processes and issues under the CZMA is described in 11 Natural Resources Lawyer 495 (1979).

3. Coastal Zone Management Act of 1972 (CZMA) P.L. 92-583, 16 USC 1451 et seq.

4. See New Jersey Energy Master Plan Appendix A.

5. New Jersey Senate Bill No. 1179, P. 19

6. Ibid, Bay and Ocean Shore Segment (BOSS), P. 180.

7. Ibid, NUREG p. 3-9, Section 3.4.1.2.

8. P.L. 93-627, 313 USC 1501 et seq.

9. 42 USC 4321 et seq.

DISCUSSION

D. Nyhart, MIT: Let's take the case that I am most concerned about, which is one where an OTEC plant is 150 miles off a state shore. What is the state's interest other than where that cable comes on shore? If we assume that the link to the shore is a DC cable, obviously the state's immediate interests are in protecting where the power comes ashore and in the siting and the onshore impact of whatever activity is taking place offshore. There might be environmental impacts of whatever activity is taking place off shore. These might be economic impacts if crews are involved and on shore. As you see it from a state view, what are the other state concerns?

E. Linky: For one thing, I think the state would be very concerned about a preemptive cable route. Presumably through the regional management plan for fisheries and those types of things, an OTEC Routing Corridor for the cables could come into play. Right now, my office is having Rutgers University do an OCS Gas Pipeline Study. A lot of those questions will be answered when we try to find out how this whole process is going to work. There is, in fact, now an intergovernmental pipeline planning process under way which is basically supposed to say to the states, outline your corridor(s), say, from the mean high-tide line out to the edge of the three-mile limit, and then we'll pick it up. There are, in fact, existing mechanisms by which a state could couple up, but I will have to reserve judgment as to whether that will work or not. But there are some basic building blocks.

Question: Don't your dredge-and-fill permits give you enough involvement that you could put the cable where you wanted it and make sure there weren't any adverse environmental or onshore impacts?

E. Linky: The dredge-and-fill permits and many other permits are basically negative mechanisms. As a lawyer, I am not interested in waiting until a federal agency or a utility files an application that neglects some state concern and then go and stamp my feet around several federal agencies. We at the state level have seen how such uncoordinated regulatory processes eat into a project and may even kill it: to wit, the Floating Nuclear Power Plant. What I want to see is a coordinated planning process that includes participation by the states very early, at the preapplication stage. And this is one of the benefits of the so-called lead agency. I am not interested in running around and hitting people over the heads with threatened litigation. That doesn't do anybody any good.

Question: Do you consider the power that is coming as in interstate commerce or in federal commerce? If so, when do you consider that power non-state power?

E. Linky: Well, for purposes of regulation, we have to assume that the OTEC power is going to go into a regional power grid. If it is sited off New Jersey, it will go into the Pennsylvania-Jersey power pool. I think it will be power in interstate commerce and that the individual state public utilities boards will get involved.

Question: When will a state consider power derived from OTEC as state power as opposed to interstate or federal power? For example, if a coal-fired power plant were built in New Jersey, you wouldn't consider that power to be interstate commerce, would you? Would FERC (the Federal Energy Regulatory Commission) set the rates or would the state service commission set the rates?

E. Linky: As I understand things, e.g., for the offshore natural gas pipelines, FERC would set the rates if the plant were outside the three-mile limit. If a coal plant were built within the three-mile limit, then, given the fact that a state has exclusive use of the seabed, it would be a state board of public utilities question.

Comment: I think it's more complicated than that. For natural gas going from Texas into California by pipeline, FERC sets the rate at the California border and then the State Commission rules on how much can be added to that to establish the rate to the consumer. Although I have never looked into the equivalent situation in electricity, my superficial understanding is that it works much the same way. What comes out of the coal-fired plants at Four Corners goes to several states including California, and there are prices established by FERC at the borders, and the rates within the states depend upon what the various utilities that are participating in the system have invested and what they have to do, so there's always a two-headed situation on setting these rates.

D. Nyhart: Certainly FERC is going to have an impact on the pricing of OTEC energy when it comes ashore. But when this energy comes into a state jurisdiction, there still will be the problem of distributing it to the customers. The utility has an investment in a distribution system, and has operating costs. Hence the state utility commission probably will have to make decisions on a case-by-case basis within the state.

E. Linky: To defuse the issue I'll basically state that OTEC is potentially cost-competitive with offshore coal.

Comment: Licenses have been languishing for years because the people who had first made application decided that they were not going to pursue the license because it wasn't economically feasible because of some of the policies that existed. Now then, more recently FERC has been encouraged by legislation and its general policy is to try to encourage the generation of electricity from those sources that are nonpolluting. For example, small hydroelectric plants that previously weren't seen as being economically feasible have become so because of some change in policies.

15. LIST OF ATTENDEES

Attendance List

6th OTEC Conference, June 19-22, 1979

Washington, D.C.

ABATE, Richard
General Dynamics, Electric Boat
Eastern Point Rd.
Groton, CT 06340
(203) 446-3313

ABELSON, Harvey
Argonne National Laboratory
400 North Capitol Street, N.W.
Suite 185
Washington, DC 20001
(202) 376-5778

ADAMS, E. Eric, Dr.
Mass. Instit. of Technology
48-325
Cambridge, MA 02139
(617) 253-6595

ADCOX, Walt
Manager, Market Research
Morrison-Knudsen Co., Inc.
P. O. Box 7808
Boise, ID 83729
(203) 386-5832

ALEXIOU, A. G.
Assistant Director
Sea Grant/NOAA
Rockville, MD 20852
(301) 443-8894

ANDERSON, Henry S.
U. S. Department of State
Office of Marine Science &
Technology Affairs
Washington, DC 20520
(202) 632-9039

ANDERSON, James H., Jr.
Vice-President
Sea Solar Power, Inc.
2422 South Queen St.
York, PA 17402
(717) 741-0884

ANDERSON, J. Hilbert
President
Sea Solar Power, Inc.
2422 South Queen St.
York, PA 17402
(717) 741-0884

ANDERSON, Jennine
Economist
General Electric-TEMPO
777 14th St., N. W.
Suite 500
Washington, DC 20005
(202) 637-4533

ANDERSON, Kent
Manager, Govt. Liaison
The Trane Co.
2020 14th St.
Arlington, VA 22101
(703) 525-4015

ANDREWS, Molly
Economist
Interstate Electronics
707 E. Vermont, P. O. Box 3117
Anaheim, CA 92803
(714) 772-2811

ANSUINI, Frank
Senior Engineer
Kennecott Copper Co.
128 Spring St.
Lexington, MA 02173
(617) 862-8268

ANZAI, Takaaki
Assistant Professor
Florida Inst. of Technology
Melbourne, FL 32901
(305) 723-3701

ARCHBOLD, Phil
Project Engineer
ETEC (Rockwell International)
Canoga Park, CA 91307
(213) 341-1000

AREY, George
Stone & Webster Engineering Corp.
245 Summer Street
Boston, MA 02143
(617) 973-2257

ARMSTRONG, Robert
Manager, Contract Admin.
Rotoflow Corp.
2235 Carmelina Ave.
Los Angeles, CA 90064
(213) 477-3083

ARONSON, David
Consulting Engineer
David Aronson Associates
9 Riverview Drive West
Upper Montclair, NJ 07043
(201) 744-6112

ASHWORTH, David J.
Development Engineer
The Trane Co.
Building 12-2
3600 Pammell Creek Rd.
LaCrosse, WI 54601
(608) 787-4168

AUMENTO, F., Dr.
ELC-Electroconsult
Chiabrera 8
Milano - Italy

AVERY, William H., Dr.
Director, Ocean Energy Programs
Applied Physics Laboratory
The Johns Hopkins University
Johns Hopkins Road
Laurel, MD 20810
(301) 953-7100, EXT. 535

BAILEY, Frank
Project Manager
General Electric Co.
1 River Rd.
Building 23, Room 334
Schenectady, NY 12345
(518) 385-9009

BAKSTAD, Paal J.
TRW Ocean & Energy
One Space Park
Redondo Beach, CA 90278
(213) 535-1554

BARKMAN, Erik
Director, Applied Chem. & Math.
Reynolds Metals
47th & Canal St.
Richmond, VA 23261

BARNETT, Arthur M.
Vice-President
Marine Ecological Consultants
533 Stevens Ave., Suite B-57
Solana Beach, CA 92075
(714) 755-7729

BARR, Roderick
Head, Applied Hydrodynamics
Hydronautics, Inc.
7210 Pindell School Rd.
Laurel, MD 20810
(301) 776-7454

BARSNESS, E. J.
Advanced Programs Manager
Westinghouse Electric Corp.
P. O. Box 9175, M.S. N-206
Philadelphia, PA 19113
(215) 595-3124

BARTHOLOMEW, B. S.
Senior Vice President
VSE Corp.
2550 Huntington Ave.
Alexandria, VA 22303
(704) 960-4600, EXT. 372

BASAR, Nedret S.
Project Manager
M. Rosenblatt & Son, Inc.
350 Broadway
New York, NY 10013
(212) 431-6900

BASSIL, Leonard E.
Project Manager
Maritime Transportation
Research Board
2101 Constitution Ave., N. W.
Washington, DC 20418
(202) 389-6738

BAYLIS, J. R.
Sr. Consultant
M. Rosenblatt & Son, Inc.
2341 Jefferson Davis Hwy.
Arlington, VA 22202
(703) 892-5680

BEATTIE, Donald A.
Director, Energy Systems Div.
NASA Headquarters
Washington, DC 20546

BEAVER, Richard J.
Metallurgist
Union Carbide, Nuclear Div. (ORNL)
P. O. Box X
Oak Ridge, TN 37830
(615) 574-4341

BECKWITH, Walter C.
W. C. Beckwith Assoc.
1026 National Press Bldg.
Washington, DC 20045
(202) 628-3531

BELL, David L.
Technical Coordinator
Ocean Surveys, Inc.
91 Sheffield St.
Old Saybrook, CT 06475
(203) 388-4631

BELL, Kenneth J., Prof.
Dept. of Chemical Engineering
Oklahoma State University
EN 423
Stillwater, OK 74074
(405) 624-5280

BENSON, David K.
Principal Scientist
Solar Energy Research Institute
1536 Cole Blvd.
Golden, CO 80401
(303) 231-1162

BENSON, Peter H., Dr.
Argonne National Laboratory
EIS-11
Argonne, IL 60439
(312) 972-7802

BEORSE, Bryn
Research Associate
Sea Water Lab.
University of California
47th & Hoffman Blvd.
Richmond, CA 94804
(415) 235-6709

BERNDT, Torbjörn
Alfa Laval
Box 500
S-14700 Tumba
Sweden

BERNHISEL, James
311 California St., #700
San Francisco, CA 94104
(415) 435-5427

BIEWER, F. N.
President
Offshore Technology Corp.
578 Enterprise St.
Escondido, CA 92025
(714) 746-5511

BJUSTROM, Rebecca
The Mitre Corp.
1820 Dolley Madison Blvd.
McLean, VA 22043
(703) 827-6630

BLEVINS, Ralph W.
Applied Physics Laboratory
The Johns Hopkins University
Johns Hopkins Road
Laurel, MD 20810
(301) 953-7100 EXT. 7403

BLUESTEIN, Bruce A.
Staff Scientist
Science Applications, Inc.
101 Continental Bldg., Suite 310
El Segundo, CA 90245
(213) 640-0480

BLUMBERG, Alan, Dr.
Dynalysis of Princeton
20 Nassau St.
Princeton, NJ 08540
(609) 924-3911

BONNEMAIRE, Bruce
Engineer
Sea Tank Co. (CGE Group)-F
12 rue le Corbusies - Silic 303
94588 - Rurgis Cedex - France
687-23-32

BONNETT, Jr., Juan A.
Director
Center for Energy &
Environment Research
Caparra Heights Station
San Juan, PR 00935
(809) 765-7210

BOWDEN, Carl
Engineer
Westinghouse Electric Corp.
P. O. Box 9175 MS-N-206
Philadelphia, PA 19113
(215) 595-3323

BOWLES, Robert
Florida Power Corp.
3201 34th St., South
St. Petersburg, FL 33733
(813) 866-5151

BOYD, Hugh
Engr. Representative
Goodyear Aerospace Corp.
1210 Massillon Road
Akron, OH 44315
(216) 794-3627

BRADY, Robert
Tracor, Inc.
1601 Research Blvd.
Rockville, MD 20852
(301) 279-4256

BRETSCHNEIDER, Charles L.
Prof. & Chairman
Dept. of Ocean Engineering
University of Hawaii
2565 The Mall - Keller 219
Honolulu, HI 96822
(808) 948-7572

BREWER, John H.
Manager, Marine Division
Deep Oil Technology (FLUOR)
3333 Michelson Dr.
Irvine, CA 92730
(714) 975-7184

BRIGGS, Edward M.
Director
Southwest Research Institute
P. O. Drawer 28510
San Antonio, TX 78284
(512) 684-5111

BRIN, A. Y.
Charge de mission
Mission Interministerielle de
la Mer
64 rue de Varenre
75007 Paris, France
556-73-17

BROWN, Clinton
Chief Scientist
Hydronautics, Inc.
7210 Pindell School Rd.
Laurel, MD 20810
(301) 776-7454

BROWN, Luke
U. S. Coast Guard Academy (SNAME)
Box 1785
New London, CT 06320
(203) 443-8463

BRYAN, Jack A.
Vice President/General Manager
Irrig. Prod. Div.
Gifford-Hill & Co., Inc.
W. 601 Main, Suite 700
Spokane, WA 99201
(509) 456-8100

BUCK J.
Program Director
ORI, Inc.
1400 Spring St.
Silver Spring, MD 20910
(301) 588-6180

BULANG, W., Dr.
American M.A.N. Corp. - Munich
1114 Ave. of the Americas
New York, NY 10036
(212) 221-3340

BULLOCK, Harold O.
Technical Director
J. J. Henry Co., Inc.
2341 Jefferson Davis Hwy. #838
Arlington, VA 22202
(703) 920-3435

BURLEW, Donald R.
Vice President
ORI, Inc.
1400 Spring St.
Silver Spring, MD 20910
(301) 588-6180

BURROUGHS, Charles A.
Captain, NOAA Corps.
National Oceanic &
Atmospheric Administration
3300 Whitehaven St., N.W.
Washington, DC 20235
(202) 634-7379

BUTLER, A. F.
TRW, Inc.
One Space Park - Bldg. 81
Redondo Beach, CA 91740
(213) 535-0023

BUTLER, W. J.
Vice President/General Manager
Northwest Marine Iron Works
P. O. Box 3109
Portland, OR 97208
(503) 228-8222

CALISAL, S. M.
Assistant Professor
U. S. Naval Academy
Annapolis, MD 21402
(301) 267-3882

CALLANAN, John
Research Staff
Northwind Museum
18 E. 48th St.
New York, NY 10017
(212) 924-1767

CAMPAGMONE, Alfred F.
General Engineer
Department of Energy
9321 Warfield Rd.
Gaithersburg, MD 20760
(301) 353-4056

CAREW, Bob
Marine Engineer
MAR, Inc.
1335 Rockville Pike
Rockville, MD 20852
(301) 424-1310

CARLSTRÖM, Rolf
Alfa-Laval AB
14700 Tumba
Sweden
0753/31100

CARRENO, Manuel
Mechanical Dept. Manager
CH2M Hill
P. O. Box 1647
Gainesville, FL 32602
(904) 377-2442

CARSTAFF, Jr., Arthur E.
Technology Planning Associates
257 Newtonville Ave.
Newton, MA 02158
(617) 969-6969

CASSEE, Henry J.
Mechanical Engineer
U. S. Maritime Administration
Office of Ship Construction
Room 4409, Main Commerce Bldg.
Washington, DC 20230
(202) 377-4620

CASTELLANO, Carmine
Division of Solar Technology
Department of Energy
600 E St., N.W.
Washington, DC 20585
(202) 376-4995

CAYWOOD, William C.
Applied Physics Laboratory
The Johns Hopkins University
Johns Hopkins Road
Laurel, MD 20810
(301) 953-7100 EXT. 7406

CHALFANT, Arthur I.
Senior Project Engineer
United Technologies Research Ctr.
Silver Lane
East Hartford, CT 06108
(203) 727-7553

CHANG, George C.
Chief, Adv. Phy. Methods Br.
Department of Energy
600 E St., N.W.
Washington, DC 20545
(202) 376-9461

CHARACKLIS, William G., Prof.
Rice University
Environmental Science & Eng.
P. O. Box 1892
Houston, TX 77001
(713) 667-5587

CHARBONEAU, Ken
General Manager
Marine-Industrial Cable Corp.
14201 Gentilly Rd.
New Orleans, LA 70122
(504) 254-0754

CHARWAT, Andrew, Professor
UCLA
5731 Boelter Hall
Los Angeles, CA 90024
(213) 845-4197

CHEN, F. C.
Research Staff
Oak Ridge National Laboratory
P. O. Box y
Oak Ridge, TN 37830
(615) 574-0712

CHEN, Y. N., Dr.
American Bureau of Shipping
65 Broadway
New York, NY 10006
(212) 440-0467

CHRISTMAS, Susan V.
Staff Economist
Solar Energy Research Institute
1536 Cole Blvd.
Golden, CO 80401
(303) 231-1073

CHURGIN, James
Director, Data Services Div.
NOAA/EDIS/NODC
Washington, DC 20235
(202) 634-7500

CICCONE, Vincent J.
President
V. J. Ciccone & Assoc., Inc.
14045 Jefferson Davis Hwy.
Woodbrige, VA 22191
(703) 694-6503

CLARKE, Ralph L.
Marketing Director
Continental Shelf Assoc., Inc.
Box 3609
Tequesta, FL 33450
(305) 746-7946

COBBS, Jim
Systems Analyst
Tracor, Inc.
1701 Research Blvd.
Rockville, MD 20850
(301) 279-4242

COCHRAN, Charles, Professor
Department of Political Science
U. S. Naval Academy
Annapolis, MD 21402
(301) 267-3461

COFFAY, Brian
Project Manager
Westinghouse Electric Corp.
P. O. Box 9175 MS-N-206
Philadelphia, PA 19113
(215) 595-4912

COHEN, Robert, Dr.
Program Manager
Ocean Systems Branch
Division of Central Solar Tech.
Department of Energy
600 E St., N.W.
Washington, DC 20545
(202) 376-4773

COLEMAN, Howard S.
Division Director
Division of Central Solar Tech.
Department of Energy
600 E St., N.W.
Washington, DC 20585
(202) 376-4226

COLEMAN, William
Engineer
Westinghouse Electric Corp.
P. O. Box 9175 MS-N-205
Philadelphia, PA 19113
(215) 595-4118

COLEN, Melvin
Vice President, Advanced Programs
Avondale Shipyards, Inc.
P. O. Box 50280
New Orleans, LA 70150
(504) 436-5100

COMMINS, Marcie
Staff Scientist
Lawrence Berkeley Laboratory
University of California
Berkeley, CA 94720
(415) 486-6461

CONTI, R. J.
Sr. Staff Scientist
Lockheed Palo Alto Research Lab.
3251 Hanover St.
Palo Alto, CA 94034
(415) 493-4411 EXT. 45770

CORRADI, Charles J.
Gibbs & Cox, Inc.
2341 Jefferson Davis Hwy.
Arlington, VA 22202
(703) 979-7240

COSTELLO, J. P.
Corrosion Analyst
So. New England Tel. Co.
441 Washington Ave.
North Haven, CT 06473

COTTER, Dennis
Research Engineer
Chicago Bridge & Iron Co.
Route 59
Plainfield, IL 60544
(815) 436-2912

COWAN, Garald
Engineer
Westinghouse Electric Corp.
P. O. 9175 MS-N-206
Philadelphia, PA 19113
(215) 595-2806

COXE, Dave
Massachusetts Instit. of Tech.
83 Inman St.
Cambridge, MA 02139
(615) 253-1691

COYLE, John
Special Assistant
OP 60 B(SA) Navy Department
Pentagon
Washington, DC 20350
(202) OX. 5-5423 or 5431

COYNE, Pat
PRC Energy Analysis Co.
7600 Old Springhouse Rd.
McLean, VA 22102
(703) 893-1822

CREASMAN, Walter C.
Market Dev. Engineer
Ameron Utility Products Group
4700 Ramona Blvd.
Monterey Park, CA 91754

CREWS, James E., Jr.
Manager, Substation Engrg.
Florida Power Corp.
P. O. Box 14042
St. Petersburg, FL 33733
(813) 866-4170

CRUIT, Charles
Economic Analyst
General Electric-TEMPO
777 14th St., N.W., Suite 500
Washington, DC 20005
(202) 637-4533

CUNNINGHIS, S.
Manager of Projects
Gibbs & Hill, Inc.
393 7th Ave.
New York, NY 10001
(212) 760-4804

DAIDOLA, John C.
Head, Naval Architecture
M. Rosenblatt & Son, Inc.
350 Broadway
New York, NY 10013
(212) 431-6900

DANEK, George
Consultant
Argonne National Laboratory
1021 Harbor Dr., Route #7
Annapolis, MD 21403
(301) 263-3134

DANIELSON, R. V.
Bethlehem Steel Corp.
Ship Development & Sales
Sparrows Point Yard
Sparrows Point, MD 21219
(301) 477-7786

DARBY, Joseph B.
Argonne National Laboratory
9700 S. Cass Ave.
Argonne, IL 60439
(312) 972-7763

DAVIDSON, Alan
Costal Marine Research
P. O. Box 937
Toms River, NJ 08753
(201) 240-2222

DAVIES, Kent B., Dr.
Principal Res. Scientist
Battelle-Houston Operations
2223 W. Loop South
Houston, TX 77027
(713) 877-8034

DAVIS, Clayton W.
Mechanical Engineer
U. S. Maritime Administration
14th St. & Constitution Ave., N.W.
Washington, DC 20230
(202) 377-4620

DAVIS, F. H.
Project Manager
Globe Engineering Co.
222 No. Dearborn St.
Chicago, IL 60601
(312) 431-6882

DAVIS, W. L.
Executive Vice President
Southwest Alloy Supply
1256 Brittmoure Rd.
Houston, TX 77056
(713) 461-1907

DeLEON, M.
Director, N. A. Dept.
J. J. McMullen Associates, Inc.
One World Trade Center - Suite 3047
New York, NY 10048
(212) 466-2222

DePALMA, John R.
Oceanographer
U. S. Naval Oceanographic Office
NSTL, Bay St. Louis MS 39522
(601) 688-4717

DePALMA, Vito A.
Calspan Corp.
P. O. Box 400
Buffalo, NY 14225
(716) 632-7500

DeQUELEN, M. Louis
Tour Anjou
SGTE
33, Quai National
92806 Puteaux, France
(1) 776.43.34

DeSOMMA, A. Edward
Marine Engineer
G. G. Sharp, Inc.
2361 S. Jefferson Davis Hwy.
Arlington, VA 22202
(703) 892-4000

DENTON, J. W.
TRW, Inc.
One Space Park, Bldg. 81, Rm 1538
Redondo Beach, CA 91740
(213) 535-1554

DERRINGTON, John
Director
Sir Robert McAlpine & Sons Ltd.
40 Bernard St. - P. O. Box 74
London WC IN-1LG, England U.K.
01-837-3377

DEUCHLER, William P.
Gibbs & Cox, Inc.
2341 Jefferson Davis Hwy.
Arlington, VA 22202
(703) 979-1240

Deutch, John, Dr.
Acting Under Secretary
Department of Energy
1000 Independence Ave., S. W.
Washington, DC 20585
(202) 252-5704

DEXTER, Stephen C.
Assistant Professor
College of Marine Studies
University of Delaware
Lewes, DE 19958
(302) 645-4261

DICK, Richard J.
Group Leader
Battelle Columbus Laboratories
505 King Ave.
Columbus, OH 43201
(614) 424-5510

DITMARS, J. D.
Argonne National Laboratory
9700 South Cass Ave. EES-12
Argonne, IL 60439
(312) 972-3784

DONNELLY, H. L.
Applied Physics Laboratory
The Johns Hopkins University
Johns Hopkins Road
Laurel, MD 20810
(301) 953-7100 EXT. 7413

DORING, Jr., Walter F.
Executive Accounts Manager
Engelhard Industries
2655 U. S. Route 22
Union, NJ 07083
(201) 589-5000

DORN, S. J.
Pa. Dept. of Agriculture
610 Lee Dr.
Coraupolis, PA 15108
(412) 262-5407

DORSCH, F. E.
Sea Operations Engineering Mgr.
Western Electric Co.
Guilford Center - P.O. Box 20046
Greensboro, NC 27420
(919) 697-6947

DOUGLASS, Robert H., Jr.
TRW, Inc., 81-1538
One Space Park
Redondo Beach, CA 90278
(213) 535-2446

DRAGO, Christie
Developmental Engineer
Simplex Wire & Cable
P. O. Box 479
Portsmouth, NH 03801
(603) 436-6100

DRALEY, Joseph, Dr.
Argonne National Laboratory
Bldg. 212
9700 Cross Ave.
Argonne, IL 60439
(312) 972-7760

DRALLE, Carl W.
Manager, Market Development
AMPCO Metal Div.
AMPCO Pittsburgh Corp.
P. O. Box 2004
Milwaukee, WI 53201
(414) 645-3750

DREWRY, Jim
Technology Assessment
J. Ray McDermott & Co.
P. O. Box 60035
New Orleans, LA 70160
(504) 587-4691

DUGGER, Gordon L., Dr.
Supervisor, Aeronautics Div.
Applied Physics Laboratory
The Johns Hopkins University
Johns Hopkins Rd.
Laurel, MD 20810
(301) 953-7100 EXT. 7400

DUNCAN, Peter, Dr.
109 15th St., S.E.
Washington, DC 20003
(202) 567-5185

DUNNAVANT, Allan
Engineer
Westinghouse Electric Corp.
P. O. Box 9175 MS-N-206
Philadelphia, PA 19113
(215) 595-3544

DUNNING, Fred S. Jr.
Director, Ocean Systems Div.
Santa Fe Corp.
4660 Kenmore Ave., Suite 600
Alexandria, VA 22304
(703) 823-2233

EATON, Edward F.
Manager
Marine App. Engineering
General Electric Co.
650 Franklin St., Room 410
Schenectady, NY 12345
(518) 385-3381

EBNER, Dean
Logistics Analyst
Tracor, Inc.
1701 Research Blvd.
Rockville, MD 20850
(301) 279-4294

EDELMAN, Seymour
Physicist
National Bureau of Standards
Washington, DC 20234
(202) 921-3851

EISNER, Neil A.
Lehman Bros. Koehn Loeb
One William St.
New York, NY 10014
(212) 558-2496

ELION, Glenn R., Dr.
President
International Comm. & Energy, Inc.
66 Main St.
P. O. Box 249
Southborough, MA 01772
(617) 485-7641

ESTERLY, Henry
Solargistics, Inc.
P. O. Box 2667
Reston, VA 22090
(703) 437-8235

EVANS, Douglas J.
Evans-Hamilton, Inc.
4863 Cordell Ave.
Bethesda, MD 20014
(301) 652-6960

FAMADAS, Nelson
Partner
Consultores Tecnicos Asociades
P. O. Box 1875
Hato Rey, PR 00919
(809) 753-8976

FENDERSON, Maurice L.
Vice President Eng.
Simplex Wire & Cable Co.
Old Dover Rd.
Newington, NH 03801
(603) 436-6100

FICK, T. R.
Project Manager
Bechtel Corp.
P. O. Box 3965
San Francisco, CA 94119
(415) 768-5758

FIJAS, David F.
American Standard HTD
175 Standard Parkway
P. O. Box 1102
Buffalo, NY 14240
(716) 897-2800

FINK, William L.
5800 Quantrell Ave., #504
Alexandria, VA 22312
(703) 256-8065

FINSTERWALDER, K., Dr.
Dyckerhoff and Widmann
529 Fifth Ave.
New York, NY 10017

FIORATO, A. E.
Manager - Construction Methods
Portland Cement Association
5420 Old Orchard Rd.
Skokie, IL 60077
(312) 966-6200

FISH, Robert W.
Sr. Product Engineer
Supply Div.
U. S. Steel Corp.
P. O. Box 8252
Birmingham, AL 35218
(205) 783-2764

FISK, Sally
Program Coordinator
Department of Energy
1333 Broadway
Oakland, CA 94707
(415) 273-4265

FOLSOM, David L.
Commander
Third Coast Guard District
Governors Island
New York, NY 10004
(212) 668-7063

FOUST, Harry D.
Manager, Applied Projects
The Trane Co.
3600 Pammel Creek Rd.
La Crosse, WI 54601
(608) 787-2291

FRANCIS, E. J.
Executive Assistant
Applied Physics Laboratory
The Johns Hopkins University
Johns Hopkins Road
Laurel, MD 20810
(301) 953-7100 EXT. 537

FREEDMAN, Bernard J.
Principal Engineer
Electric Boat Div.
General Dynamics Corp.
Groton, CT 06340
(203) 446-3414

FRENCH, George C.
Project Engineer
Energy Tech. Engineering Center
P. O. Box 1449
Canoga Park, CA 91307
(213) 341-1000 EXT. 6689

FRENCH, Robert L.
Worthington Pump Corp.
1030 15th St., N.W.
Washington, DC 20005

FRIEDMAN, Linda Sinay
Assistant Project Manager
TRW, Inc.
One Space Park
Redondo Beach, CA 90278
(213) 536-4066

FRITSCH, Allen
Mechanical Engineer
Naval Ship R & D Center
Code 2722
Annapolis, MD 21402
(301) 267-3552

FRY, David J.
Research Assistant
MIT
15 Vassar St.
Cambridge, MA 02139
(617) 253-1639

FRY, Ruth
Envir. Project Spec.
Department of Energy
12th & Pennsylvania Ave., N.W.
Room 2317
Washington, DC 20461
(202) 633-8210

FRYBERGER, D. D.
Manager/Syst. Planning
Interstate Electronics Corp.
1745 Jefferson David Hwy.
Suite 601
Arlington, VA 22202
(703) 920-8990

FULLER, Roger D.
Program Manager
Lockheed Missiles & Space Co., Inc.
1111 Lockheed Way
Sunnyvale, CA 94086
(408) 988-3922

FULTON, R. P.
Vice President
Gibbs & Cox, Inc.
2341 Jefferson Davis Hwy.
Arlington, VA 22202
(703) 979-1240

FUNK, John A.
Applied Physics Laboratory
The Johns Hopkins University
Johns Hopkins Rd.
Laurel, MD 20810
(301) 953-7100 EXT. 2416

GAFFOGLIO, Carl
Manager - Engineering
Copper Development Assoc.
405 Lexington Ave.
New York, NY 10017
(212) 953-7316

GALEF, Arnold E.
TRW, Inc.
One Space Park
Redondo Beach, CA 91740
(213) 538-2920

GARCIA, Victor M.
Director
Interprofessional Service Group
GPO Box 2374
San Juan, PR 00936

GARRITY, Thomas
Department of Energy
Division of Solar Tech.
20 Massachusetts Ave., N.W.
Room 2221-C
Washington, DC 20545
(202) 376-4729

GEIGER, P. A.
Sante Fe Corp.
Kenmore Ave.
Alexandria, VA 22304
(703) 960-1821

GENGLER, Mark S.
Eastern Regional Manager
Water Services of America
2831 Heritage Lane
Shelby, NC 28150
(704) 487-0304

GEORGE, James F.
Applied Physics Laboratory
The Johns Hopkins University
Johns Hopkins Rd.
Laurel, MD 20810
(301) 953-7100 EXT. 7408

GERTZ, John
Manager
Westinghouse Electric Corp.
P. O. Box 9175 MS-N-207
Philadelphia, PA 19113
(215) 595-2931

GIANNINO, Steve
Senior Associate
PDC Energy Analysis Co.
7600 Old Springhouse Rd.
McLean, VA 22102
(703) 893-1822

GIANNOTTI, Julio
President
Giannotti & Associates
703 Giddings Ave., Suite U-3
Annapolis, MD 21401
(301) 261-1031

GIARDINA, Robert
Westinghouse Electric Corp
P. O. Box 9175 MS-N-206
Philadelphia, PA 19113
(215) 595-2807

GITTERMAN, Henry
Dir. Engineer
Burns & Roe
283 Route 17 S
Paramus, NJ 07666
(201) 265-8710

GLADFETTER, Harry A.
Director of Govt. Marketing
J. J. Henry Co., Inc.
2341 Jefferson Davis Hwy.
Suite 838
Arlington, VA 22202
(703) 920-3435

GLEITER, John
Manager Business Development
VETCO Offshore Group
250 E. Stanley
Ventura, CA 93001

GLUMACE, Roger J.
Project Manager
Rockwell International - ETEC
8900 DeSoto St.
Canoga Park, CA 91304
(213) 341-1000

GOLDMAN, Gary
CEER/UPR
College Station
Mayaguez, PR 00708
(909) 832-7912

GOMEZ, John D.
Director, Program Management
International Technology Corp.
1670 Highway AlA
Satellite Beach, FL 32937
(305) 777-1400

GONZALEZ, Juan G.
Center for Energy &
Environmental Research
College Station
Mayaguez, PR 00708
(809) 832-7212

GRANNEMANN, Glenn N.
Research Physicist
Physics Dept.
Carnegie-Mellon University
Pittsburgh, PA 15213
(412) 578-2748

GREEN, W. L.
Tech. Assessment
J. Ray McDermott Co., Inc.
P. O. Box 60035
New Orleans, LA 70160
(504) 587-4689

GRIEKSPOOR, Wilfred
Hollandsche Beton Group (HBG)
P. O. Box 1029
The Hague
The Netherlands
070-81-48-81

GRIFFIN, Arthur B.
TRW, Inc., 81-1538
One Space Park
Redondo Beach, CA 90278
(213) 536-3410

GRIFFIN, D. L.
Technical Director
CADCOM
Division of ManTech of New Jersey
107 Ridgely Ave.
Annapolis, MD 21401
(301) 261-1070

GRIFFIN, Owen M.
Naval Research Laboratory
Code 8441
Washington, DC 20375
(202) 767-2904

GRIFFITH, Steven K.
Senior Associate
PRC Energy Analysis
7600 Old Springhouse Rd.
McLean, VA 22102
(703) 893-1822

GRIMES, William D.
Dow Chemical Co.
Texas Division/A-2301
Freeport, TX 77541
(512) 238-4117

GRINSTEAD, C. E.
TRW, Inc.
One Space Park
Redondo Beach, CA 91740
(213) 536-3410

GRONICH, Sigmund
Program Manager
Ocean Systems Branch
Department of Energy
600 E St., N.W.
Washington, DC 20585
(202) 376-4771

GROSS, C. H., Jr.
Assistant Vice President
J. J. Henry Co., Inc.
Two World Trade Center
Suite 9528
New York, NY 10048
(212) 938-2144

GUILD, Donald
Project Manager
Stone & Webster Engineering Corp.
P. O. Box 2325
Boston, MA 02107
(617) 973-2501

GUNTER, Gordon
Director Emeritus
Gulf Coast Research Laboratory
Ocean Springs, MS 39564
(601) 875-2244

GUTSHALL, Nancy
Environmental Analyst
Energy & Environmental
Analysis, Inc.
1111 N. 19th St.
Arlington, VA 22209
(703) 528-1900 EXT. 265

HALACY, Dan
Communications Spec.
Solar Energy Research Institute
1536 Cole Blvd.
Golden, CO 80401
(303) 231-1151

HALCHAK, John A.
Rockwell International
Rocketdyne Division
6633 Canoga Ave.
Canoga Park, CA 91301
(213) 884-3527

HALE, William C.
University of Pennsylvania
The Energy Center
3221 Walnut St./K2
Philadelphia, PA 19104
(215) 566-5519

HALLANGER, Lawrence
Project Manager
Hawaii Natural Energy Institute
206 Holmes Hall
2540 Dole St.
Honolulu, HI 96822
(808) 948-6947

HAMADA, Hiroyoshi
Manager
The Tokyo Electric Power Co., Inc.
1901 L St., N.W., Suite 720
Washington, DC 20036
(202) 457-0790

HAMILTON, D. Heyward
Technical Representative
OHER/ASEV/US
Department of Energy
E-201
Washington, DC 20545

HAMMETT, Bobby E.
Sr. Project Engineer
American Society of Naval Eng.
12 Dogwood Cove
Gulfport, MS 39503

HARGROVE, J. L.
Director of Studies
American Society of Internatl. Law
2223 Massachusetts Ave., N.W.
Washington, DC 20008
(202) 265-4313

HARLOW, E. H.
Executive Vice President
Frederic R. Harris, Inc.
7500 Bellaire Blvd., Suite 411
Houston, TX 77036
(713) 981-7911

HART, G. K.
Project Engineer
DSS Engineers, Inc.
7483 NW 4th St.
Ft. Lauderdale, FL 33312
(305) 792-6660

HARTMAN, James K.
Project Manager
Department of Energy
P. O. Box 1446
Canoga Park, CA 91360
(213) 340-1722

HAZELWOOD, R. N.
Staff Scientist
Global Marine Development, Inc.
P. O. Box 3010
Newport Beach, CA 92663
(714) 752-5050

HEIMLICH, I. R.
Admin. Director
Reynolds Metals Co.
P. O. Box 1200
Sheffield, AL 35660
(205) 383-7141 EXT. 210

HEISE, Robert E.
Manager
Union Carbide Corp.
P. O. Box 44
Tonawanda, NY 14150
(716) 877-1600

HENDERSON, Richard W.
Applied Physics Laboratory
The Johns Hopkins University
Johns Hopkins Road
Laurel, MD 20810
(301) 953-7100 EXT. 7019

HENRY, Robert W.
Staff Engineer
U. S. Coast Guard
400 7th St., S.W.
Washington, DC 20590
(202) 426-2197

HERMAN, John B.
Systems Engineer
Automation Industries, Inc./Vitro
14000 Georgia Ave.
Silver Spring, MD 20910
(301) 871-3934

HERNANDEZ FRAGOSO, Julio
PRWRA
GPO 4267
San Juan, PR 00936
(809) 722-3236

HERRING, H. J.
Dynalysis
20 Nassau St.
Princeton, NJ 08540
(609) 924-3911

HERSHMAN, Haim
Manager, R & D Department
Ormat Systems, Inc.
98 South St.
Hopkinton, MA 01748
(617) 653-6300

HERVEY, Donald G.
Project Manager
Brown & Root
100 Waugh Dr.
Houston, TX 77007

HETTINGER, Fred
Manager, R & D
VETCO Offshore
250 W. Stanley Ave.
Ventura, CA 93001
(805) 653-2500

HIGGINS, E. Chipman
Director, Energy Supply
Hawaiian Electric Co.
P. O. Box 2750
Honolulu, HI 96840
(808) 548-7721

HIGGINS, George
Research Specialist
Dow Chemical
Bldg. 566
Midland, MI 48640

HIGGINS, Thomas P.
Manager, Ocean Energy Systems
Lockheed Missiles & Space Co., Inc.
P. O. Box 504
Sunnyvale, CA 94086
(408) 988-3922

HIGLEY, Paul D.
Senior Enginer
Raytheon Ocean Systems Co.
P. O. Box 360
Portsmouth, RI 02871
(617) 847-8000 EXT. 2533

HILL, Alan C.
Sanitory Engineer
U.S. Environmental Prot. Agency
Ocean Programs Branch (WH-548)
401 M St., S.W.
Washington, DC 20460
(202) 245-3054

HILL, Freeman K., Dr.
Physicist
Applied Physics Laboratory
The Johns Hopkins University
Johns Hopkins Road
Laurel, MD 20810
(301) 953-7100 EXT. 7455

HILLIS, David
Chief of Operations
Argonne National Laboratory
9700 South Cass Ave.
Argonne, IL 60439
(312) 972-8071

HINDLE, Robert A.
Manager, Adv. Eng. Systems
General Electric Co.
One River Rd. - B23/R352
Schnectady, NY 12345
(518) 235-0815

HIRAOKA, Hisao
Analyst
The Nikko Research Center, Ltd.
140 Broadway
New York, NY 10005
(212) 747-9840

HIRSHMAN, Jules
Sr. Scientist
NYIT Research Center
8000 N. Ocean Dr.
Dania, FL 33004
(305) 923-0551

HOFFMAN, Don
System Analyst
Tracor, Inc.
1701 Research Blvd.
Rockville, MD 20850
(301) 279-4273

HOGGE, Edward F.
Programmer
Wyle Laboratories
Route 1, Box 116
Hayes, VA 23072
(804) 642-4294

HOOD, Edwin M.
President
Shipbuilders Council of America
600 New Hampshire Ave., N.W.
Washington, DC 20037
(202) 338-7722

HOOVER, Thomas
Vice President
Parsons Brinckerhoff
One Penn Plaza
New York, NY 10001
(212) 239-6471

HORST, Ralph
Alcoa
Alcoa Laboratories
Alcoa Center, PA 15069
(412) 339-6651

HOVE, Duane
Manager, Applied Mechanics
Science Applications, Inc.
101 Continental Blvd. #310
El Segundo, CA 90245

HOWARD, M. J.
Emerson & Cuming
405 N. Bowser
Richardson, TX 75081
(214) 235-7394

HOWERTON, William M.
Marine Systems Proj. Engineer
Department of Energy
2311 Carrol Lane
Escondido, CA 92025
(714) 743-2995

HULTQVIST, Brigitta
Technical Assistant
Swedish Embassy
600 New Hampshire Ave.
Washington, DC 20037
(202) 298-3560

HUNT, Mary, Dr.
Chemist/Staff Scientist
Lawrence Berkeley Laboratory
University of California
Berkeley, CA 94720
(415) 486-6461

IREDALE, Harry
Oceanographer
NOAA/EDIS/NODC
3300 Whitehaven St., N.W.
Washington, DC 20235
(202) 634-7479

ISO, Shunya
Tokyo Kyuei Co., Ltd.
3-1-15 Nippon Bash 1
Chuo-Ky-
Tokyo, Japan
045-751-040

JAHNIG, Charles E.
Consultant
5 Auldwood Lane
Rumson, NJ 07760
(201) 842-0931

JAMES, Kenneth
Construction Manager
Tokola Offshore, Inc.
One Market Place
Spear Street Tower
San Francisco, CA 94105
(415) 777-4333

JANSON, J. Erik, Dr.
VBB
P. O. Box 5038
S-10241
Stockholm, Sweden
46-8228580

JAWISH, William
Giannott & Associates, Inc.
703 Giddings Ave.
Annapolis, MD 21401
(301) 261-1031

JAYADEV, T. S.
Senior Scientist
Solar Energy Research Institute
1536 Cole Blvd.
Golden, CO 80401
(303) 231-1014

JENNINGS, Stephen J.
Senior Engineer
Westinghouse Electric Corp.
P. O. Box 9175, Bldg. MS-206
Philadelphia, PA 19113

JIRKA, G., Professor
Cornell University
Ithaca, NY 14853
(607) 256-5140

JOHNSON, Arne E.
U. S. Navy
6001 Ridge Ford Dr.
Burke, VA 22015
(703) 569-5065

JOHNSON, Brent
Reg. Sales Manager
Southwest Alloy Supply Co.
1256 Britt Moore
Houston, TX 77043
(713) 461-1907

JOHNSON, David H.
Solar Energy Research Institute
1536 Cole Blvd.
Golden, CO 80401
(303) 234-7171

JOHNSON, E. Franklin
Oceanographer
NOAA/EDIS/NODC
2001 Wisconsin Ave., N.W.
Washington, DC 20235
(202) 634-7479

JOHNSON, Mansur
Alternative Direction in
Energy & Economics
34 Manomet Ave.
Hull, MA 02045
(617) 925-3058

JOHNSON, Peter
Research Assistant
Lawrence Berkeley Laboratory
University of California
Berkeley, CA 94720
(415) 486-6461

JOHNSON, Virgil E.
Senior Vice President
Hydronautics, Inc.
7210 Pindell School Rd.
Laurel, MD 20810
(301) 776-7454

JONES, Jr., M. S.
General Director
Reynolds Metals Co. - ECD
Box 1200
Sheffield, AL 35660
(205) 381-6121

JONES, Wilbert L.
General Engineer
U. S. Dept. of Commerce
14th & Constitution Ave., N.W.
Room 5898-C
Washington, DC 20230
(202) 377-2405

JONES, W. L.
Manager, Energy
Dillingham Corporation
Box 3468
Honolulu, HI 96801
(808) 735-3275

JOZAN, C.
Engineer
ETPM
33-35 rue d'Alsace
92300 Levallois - Perret, France
759-62-16

JUSTUS, John R.
Earth Science Analyst
Congressional Research Service/SPRD
10 First St., S.E.
Washington, DC 20540
(202) 287-6030

KAJIKAWA, Takenobu
Energy Div., Electrotechnical Lab.
Ministry Int'l Trade and Industry
5-4-1 Mukodai-Mach 1
Tanashi, Tokyo 188, Japan

KAMINSKY, M.
Senior Scientist
Physics Division D-203
Argonne National Laboratory
9700 S. Cass Ave.
Argonne, IL 60523
(312) 972-4074

KAMOGAWA, Hiroshi, Dr.
Toshiba R & D Center
Toshiba Corp.
1, Toshibacho, Saiwaiku, Kawasaki
Japan

KAPLAN, Paul, Dr.
President
Hydromechanics, Inc.
182 Fairchild Ave.
Plainview, NY 11803
(516) 349-9640

KAPUR, Suneel K.
TRW, Inc.
7600 Colshire Dr.
McLean, VA 22102
(703) 893-2000 EXT. 2321

KARPUK, Michael E.
Staff Engineer
Solar Energy Research Institute
1536 Cole Blvd.
Golden, CO 80401
(303) 234-7171

KATSURAMAKI, Tsuweo
Mihama Corp.
3-3-3, Akasaka
Minato-ku, Tokyo
Japan
03-586-3131

KATZER, Martin
General Electric Corp.
One River Rd.
Schenectady, NY 12345
(518) 385-0860

KATZIN, J.
Lehman Brothers Kuhnloeb, Inc.
One William St.
New York, NY 10004
(212) 558-2496

KAVLUM, K. W.
Oceanographer
ONR, COD480
NSTL Station
MS 39529
¢601) 688-4827

KAY, Mortimer I.
Senior Scientist
CEER
College Station
Mayaguez, PR 00708
(809) 832-1414

KAY, Robert
Chief Operations & Planning
NOAA
6001 Executive Blvd.
Rockville, MD 20038
(301) 443-8597

KAYTON, Myron
TRW Systems & Energy
Room 55-2182
Redondo Beach, CA 90278
(213) 535-4321

KEE, George
Engineer, Staff Assistant
General Dynamics Corp.
Electric Boat Division
Eastern Point Rd.
Groton, CT 06340
(203) 446-5035

KELLEHER, Matthew
Assoc. Prof.
Naval Post Graduate School
M. E. Department
Monterey, CA 93940
(408) 646-2530

KELLY, Andrew J.
Program Development
General Atomic Co.
P. O. Box 81608
San Diego, CA 92138
(714) 755-3746

KELLY, W. H. J.
Lt. Commander
20 Highclere Gardens
Plymouth Devon P1 7 EA6
United Kingdom
(301) 267-3881

KERAMATI, Bahram
Engineer
General Electric Corp.
One River Rd.
Schenectady, NY 12345
(518) 385-5122

KIDD, George R.
Mechanical Engineer
Energy Systems Div.
P. O. Box 106
So. Deerfield, MA 01373
(413) 665-7051

KIM, C. H., Dr.
Davidson Laboratory
Stevens Tech.
Castle Point Station
Hoboken, NJ 07030
(201) 420-5344

KINCAIDE, William C.
Manager
Teledyne Energy Systems
110 West Timonium Rd.
Timonium, MD 21093
(301) 252-8220

KINELSKI, Eugene H.
Program Manager
Department of Energy
600 E St., N.W.
Washington, DC 20585
(202) 376-4801

KING, Daniel S.
Senior Hydraulic-Envir. Eng.
Stone & Webster Engineering Corp.
245 Summer Street
Boston, MA 02107
(617) 973-5488

KISS, Ronald K.
Director, Offshore Ship Const.
Maritime Administration
14233 Briarwood Terrace
Rockville, MD 20853
(301) 377-4373

KLEIN, Alex
Project Manager
Energy Technology Engineering Ctr.
P. O. Box 1449
Canoga Park, CA 91304
(213) 341-1000 EXT. 6294

KOBAYASHI, H.
Chief, Ocean Engineering Dept.
Research Lab.
Shimizu Construction Co. Ltd.
4-17, Etchujima 3-chome
Kotoku, Tokyo, Japan
03-643-4311

KOGAN, Abraham, Professor
Solar Energy Research Institute
Thermal Conversion Branch
1536 Cole Blvd.
Golden, CO 80401
(303) 231-1758

KOSKE, P.
GKSS
2054 GEEITHACHT
Germany
331-3333

KOSTORS, Charles
Sr. Dev. Engineer
Elliott Co.
Jeanette, PA 15644

KOVACH, Curtis W.
Crucible, Inc.
P. O. Box 88
Pittsburgh, PA 15230
(412) 923-2955

KRATZ, Jay
Engineer
Westinghouse Electric Corp.
P. O. Box 9175 MS-N-206
Philadelphia, PA 19113
(215) 595-4921

KRISSINGER, Stu
Industrial Mkt. Manager
Harco Corp.
244 E. County Line Rd.
Hatboro, PA 19040
(215) 674-1400

KUMM, William H.
Prsident
Arctic Enterprises, Inc.
1220 L Gemini Dr.
Annapolis, MD 21403
(301) 261-2141

KURT, Jeff
Dev. Engineer
Simplex
P. O. Box 479
Portsmouth, NH 03801

KUSADA, Hisso, Dr.
Professor
Faculty of Science & Engineering
SAGA University
1, Honjomachi
Saga-shi, Saga-ken
Japan
0952-24-5191

LaBERGE, Jon J.
Advanced Technology, Inc.
7923 Jones Branch Dr.
McLean, VA 22102
(703) 790-1580

LACHMANN, Bengt
Director General
EUROCEAN
Villa Richard
Monaco-Ville, Monaco
33-93-304015

LANDRUM, T. C.
Director
Department of Natural Resources
P. O. Box 44156
Baton Rouge, LA 70804
(504) 342-4594

LaQUE, Frank L.
Consultant/Argonne
Claride House I
Claride Dr.
Verona, NJ 07044
(201) 239-6728

LAVI, Abrahim, Dr.
ERDI, Inc.
5530 Sunmoyle St.
Pittsburgh, PA 15217
(412) 683-6834

LAWNICZAK, George E., Jr.
Director
Nova University
Ocean Sciences Center
8000 North Ocean Dr.
Dania, FL 33004
(305) 587-6660

LEE, Theodore, T.
Department of Commerce
NOAA
6010 Executive Blvd.
Rockville, MD 20852
(301) 443-8655

LEE, T. S.
Section Manager
LaQue Center for Corrosion Tech.
P. O. Box 656
Wrightsville Beach, NC 28480
(919) 256-2271

LEITNER, Murray
Lockheed Missiles & Space Co.
Dept. 57-81, Bldg. 568
P. O. Box 504
Sunnyvale, CA 94086
(408) 988-6761/3922

LEVIN, R.
President
MAR, Inc.
3335 Rockville Pike
Rockville, MD 20852
(301) 424-1310

LEWANDOWSKI, Richard
Consultant
Fiberglass Structural Engineer
5000 Coastal Hwy.
Ocean City MD 21842
(301) 524-7030

LEWIS, Lloyd F., Dr.
Program Manager
Department of Energy
Room 400, 600 E St., N.W.
Washington, DC 20585
(202) 376-4835

LIBBY, David O.
Development Engineer
Simplex Wire & Cable
Box 479
Portsmouth, NH 03801
(603) 436-6100

LIEBERT, Bruce E.
Asst. Professor
University of Hawaii at Manoa
2540 Dole St., Holmes 202
Honolulu, HI 96822
(808) 948-7585

LINDMAN, Ross
Mechanical Engineer
Giannotti & Associates
703 Giddings Ave.
Suite U-3
Annapolis, MD 21401
(301) 268-0030

LINKY, Edward J.
Office of Planning & Policy
Analysis
New Jersey Dept. of Energy
101 Commerce St.
Newark, NJ 07102

LITTLE, Brenda
Biologist
NORDA
Bay St. Louis, MS 39466
(601) 688-4685

LIU, Han
Supv. Engineer
Burns & Roe, Inc.
185 Crossways Park Dr.
Woodbury, NY 11797
(516) 677-2240

LOCKE, Carl E.
Assoc. Professor
University of Oklahoma
202 W. Boyd, Room 23
Norman, OK 73019
(405) 325-5811

LOEB, George
Scientist
Naval Research Laboratory
Washington, DC 20375
(202) 767-3105

LORENZ, James J.
Argonne National Laboratory
9700 S. Cass Ave.
Argonne, IL 60439
(312) 972-5900

LOTT, Daniel F.
Microbiologist
Naval Coastal Systems Center
Panama City, FL 32407
(904) 234-4183

LUCAS, Dale K. S.
506 Mercantile-Towson Bldg.
Towson, MD 21204
(301) 821-5125

LUMBANG, A. L.
Design Engineer
Southwestern Engineering Co.
6111 E. Bandini Blvd.
Commerce, CA 90040
(213) 726-0641

LYON, R. N.
Consultant
Oak Ridge National Laboratory
P. O. Box Y
Oak Ridge, TN 37830
(615) 576-2537

McALEER, Stephen A.
Marketing Representative
J. J. Henry Co., Inc.
West Park Dr.
Mt. Laurel Industrial Park
Moorestown, NJ 08057
(609) 234-3880

McCAULEY, M. J.
Assoc. Prof. Physics
Winona State University
404 E. Howard
Winona, MN 55987
(507) 452-2484

McCLOSKEY, William
Applied Physics Laboratory
The Johns Hopkins University
Johns Hopkins Road
Laurel, MD 20810
(301) 953-7100 EXT. 2275

McCORMICK, Michael E., Dr.
Professor and Director
Ocean Engineering
Department of the Navy
United States Naval Academy
Annapolis, MD 21402
(301) 267-3873

McEVADDY, Patrick J., Dr.
Engineer
Applied Physics Laboratory
The Johns Hopkins University
Johns Hopkins Road
Laurel, MD 20810
(301) 953-7100 EXT. 7432

McGUINNESS, Terence, Dr.
NOAA
6010 Executive Blvd.
Rockville, MD 20852
(301) 443-8655

McHALE, F. A.
Project Manager
Dillingham
P. O. Box 3468
Honolulu, HI 96801
(808) 735-3211

McILROY, Kenneth
Program Manager
Union Carbide
Linde Division
P. O. Box 44
Tonawanda, NY 14150
(716) 877-1600

McMAHAN, Donald E.
Asst. Chief
Division of Production
U. S. Maritime Administration
M-723, Room 4867
Main Commerce Bldg.
Washington, DC 20230
(202) 377-3283

MacCUTCHEON, E. M.
Consultant6405 Earlham Dr.
Bethesda, MD 20034
(301) 530-7220

MACOMBER, H. L., Dr.
Vice President
Team, Inc.
6501 Loisdale Ct.
Springfield, VA 22150
(703) 971-3050

MAGER, David
President
Pacific Power and Protein
One Lincoln Plaza
New York, NY 10023
(212) 595-1325

MANLEY, Richard N.
Technical Staff
Mitre Corp.
1820 Dolly Madison Blvd.
McLean, VA 22180
(703) 827-6633

MANN, John W.
Engineer, Turbine Div.
General Electric Co.
1100 Western Ave.
Lynn, MA 01910
(617) 594-3581

MANN, Mike
Senior Environmental Engineer
General Electric Co.
One River Rd., 23-384
Schenectady, NY 12345
(518) 385-0860

MANNING, A. P., Jr., RADM
Chief, Office of Research & Development
U. S. Coast Guard Headquarters
Washington, DC 20590
(202) 426-1040

MANNING Paul E.
Corrosion Engineer
Satellite Division
Cabot Corp.
1020 W. Park Ave.
Kokomo, IN 46901
(219) 426-1040

MARCHAND, Philippe
66 Avenue d'Iena
75116 Paris, France
723-55-28

MARKEL, A. L.
Research Staff
Reynolds Metals Co.
P. O. Box 27003
Richmond, VA 23261
(804) 788-7325

MARKELS, Michael, Jr., Dr.
President
Versar, Inc.
6621 Electronic Dr.
Springfield, VA 22151
(703) 750-3000

MARKOFF, Del
Pacific Power & Protein
One Lincoln Plaza
New York, NY 10023
(212) 595-1325

MARTIN, James E.
Department of Energy
600 E St., N.W.
Washington, DC 20545
(202) 376-9034

MATHER, Elizabeth
Associate Economist
PRC Energy Analysis Co.
7600 Old Springhouse Rd.
McLean, VA 22102
(703) 893-1822

MATSUDA, Noriaki
Kyushu Elec. Power Co.
2-1-82, Watanabedori, Chuo-ku
Fukuoka-shi, Fukuoaka-ken,
Japan
092-671-5912

MATTHEWS, Charles D.
President
National Ocean Indus. Assoc.
Suite 410, 1100 17th St., N.W.
Washington, DC 20036
(202) 785-5116

MAUL, George A.
Oceanographer
NOAA-AOML
15 Rickenbacker Causeway
Miami, FL 33149
(305) 361-3363

MAURER, Jack R.
Manager, Marketing & Product Development
Allegheny Ludlum Steel Corp.
Research Center
Brackenridge, PA 15014
(412) 226-2000

MEHTA, G. D.
Inter Technology/Solar Corp.
100 Main St.
Warrenton, VA 22186
(703) 347-7900

MEIR-ALTHAUS, Dirk
Manager
American Tube Cleaning Systems
1114 Ave. of the Americas
New York, NY 10036
(212) 221-3340

MELLOR, George, Dr.
Dynalysis
Princeton, NJ 08540
(609) 924-3911

MEYER, Richard
Solar Ocean Energy Liaison
1303 South Michigan Ave.
Chicago, IL 60605
(312) 427-3000

MICHEL, John W.
Section Head
Oak Ridge National Laboratory
P. O. Box Y
Oak Ridge, TN 37830
(615) 574-5271

MIDBOE, Eric L.
Gibbs & Cox, Inc.
2341 Jefferson Davis Hwy.
Arlington, VA 22202
(703) 979-1240

MILIA, Louis
Vice President, Engineering
Amertap Corp.
1501 Franklin Ave.
Mineola, NY 11501
(516) 248-6402

MILLER, Bennett
Program Director for Solar, Geothermal, Electric, and Storage Systems
Department of Energy
600 E St., N.W.
Washington, DC 20545
(202) 376-4102

MILLER, Richards T., Capt. (Ret.)
Consulting Engineer
Naval Architect & Engineering
957 Melvin Rd.
Annapolis, MD 21403
(301) 268-8209

MITCHELL, Ralph
Professor
Harvard University
Pierce Hall
Cambridge, MA 02138
(617) 495-2846

MIXAN, James L., Jr.
Senior Design Engineer
AMP, Inc. 39-03
3711 Paxton St.
Harrisburg, PA 17105
(717) 564-0100

MOAK, Kevin E.
Gibbs & Cox, Inc.
2341 Jefferson Davis Hwy.
Arlington, VA 22202
(703) 979-1240

MOGHE, S. R.
B. F. Goodrich Research and Development Center
9921 Brecksville Rd.
Brecksville, OH 44141
(216) 527-4311

MOLINARI, Robert L., Dr.
Oceanographer
NOAA
698 Glenridge Rd.
Key Biscayne, FL 33149

MOLINI, A. E., Professor
Dept. of Chemical Engineering
Carnegie-Mellon University
Schenley Park
Pittsburgh, PA 15213
(412) 578-2234

MONTGOMERY, J. B.
Research Project Engineer
Newport News Shipbuilding
4101 Washington Ave.
Newport News, VA 23607
(804) 380-2319

MONTALSO, Edna E.
Puerto Rico Office of Energy
P. O. Box 41089
Santurce, PR 00940
(809) 726-4740

MOORE, Jeffrey A.
Research Associate
University of Hawaii (NELH)
74-5563Q Kaiwi St.
Kailua-Kona, HI 96740
(808) 329-9357

MORGAN, G. H.
Solar Energy Rearch Institute
1536 Cole Blvd.
Golden, CO 80401
(303) 231-1269

MORIMOTO, F.
Assistant Representative
Wako Securities Co., Ltd.
One World Trace Center
New York, NY 10048
(212) 432-0971

MORSE, John W.
Professor
University of Miami
4600 Rickenbacker Cswy.
Miami, FL 33149
(305) 340-7485

MORTALONI, L. R.
Staff Engineer
TRW, Inc.
Defense & Space Systems Croup
One Space Park 81/1212
Redondo Beach, CA 90278
(213) 536-3123

MORTON, Bob
Manager/Business Development
Naico
Division of Noimandeau Assoc., Inc.
Nashua Rd.
Bedford, NH 03102
(603) 472-5191

MUELLER, A. C., Dr.
Westinghouse Electric Corp.
P. O. Box 9173 MS-N-205
Philadelphia, PA 19113
(215) 595-4270

MUNIER, Robert S. C.
Director of Project Coordination
Tracor Marine
Box 13114
Port Everglades, FL 33316
(305) 463-1211

NAEF, Frederick E.
Lockheed Missiles & Space Co.
900 17th St., N.W.
Washington, DC 20006
(202) 872-5947

NAGASHIMA, Yoshinori
Engineer
Mitsui Engineering & Shipbuilding Co.
706 Tamahara, Tamano City,
Okayama, Japan

NAKAJI, Albert
Research Statistician
County of Hawaii
25 Aupuni St.
Hilo, HI 96720
(808) 961-8366

NAKAZAWA, M.
Manager, Mach & Elec. Dev.
Sumitomo Corp. of America
345 Park Ave.
New York, NY 10220

NANDA, Ved P.
Professor of Law
University of Denver
College of Law
200 West 14th Ave.
Denver, CO 80204
(303) 753-3427

NEELY, Dennis E.
Program Coordinator
Department of Energy
1333 Broadway
Oakland, CA 94612
(415) 273-4265

NEWMAN, Lawrence
Scientific Affairs Officer
United Nations
One UN Plaza
New York, NY 10014
(202) 754-8825

NEZAMES, Theodore H.
Methods Engineer
The Offshore Co.
Houston, TX 77001
(713) 871-7785

NIENDORF, Lynn
Manager UCC/Linde
Tonawonda, NY 14226
(716) 877-1600

NORDMAN, Dean T.
Solar Energy Research Institute
1536 Cole Blvd.
Golden, CO 80401
(303) 231-1013

NORLING, Rich
Professional Staff
Oceanographic Merchant Marine
& Fishery Subcommittee
3577 House of Representatives
Annex 2
Washington, DC 20515
(202) 225-3444

NUTTALL, L. J.
Applications Engineer
General Electric Co.
50 Fordham Rd.
Wilmington, MA 01887
(617) 657-4766

NYHART, J. Daniel
Associate Professor of Management
MIT
Room E52-544
Cambridge, MA 02139
(617) 734-2698

OBRADOVICH, J. N.
Project Engineer
VSE Corp.
2550 Huntington Ave.
Alexandria, VA 22303
(703) 960-4600 EXT. 475

O'CONNOR, J. S.
Engineer
Applied Physics Laboratory
The Johns Hopkins University
Johns Hopkins Road
Laurel, MD 20810
(301) 953-7100 EXT. 7414

O'CONNOR, Kevney J.
President
K. J. O'Connor Assoc.
1522 K St., N.W.
Washington, DC 20005
(202) 638-2652

OGIWARA, Hiroyasu, Dr.
Manager
Energy Science & Technology Lab.
Toshiba Research & Dev. Center
TOSHIBA Corp.
4-1, Ukishimacho, Kawasaki-ku
Kawasaki-shi, Kanagawan-ken
Japan
03-454-7111

OHLROGGE, K.
GKSS
2054 Geesthacht
Germany
331-3333

OHTSUKA, Yoshinori
Researcher
Mechanical Engineering Res. Lab.
Hitachi Ltd.
502, Kandatsu-Machi
Tsuchiura-Shi, Ibaraki, 3000
Japan
0298-31-5111

OKASZAKI, Yoshinobu
Chief of Development Section
Designing Department
Torishima Pump Mfg., Co., Ltd.
1-1-8, Miyatacho, Takatsuki-shi
Osaki-fu, Japan
0726-95-0551

OLDSON, John
Staff Scientist
Lawrence Berkeley Laboratory
University of California
Berkeley, CA 94720
(415) 486-6461

OLEJACK, John E.
President
Coastal Marine Research, Inc.
5 Robbins Parkway
P. O. Box 937
Toms River, NJ 08753
(201) 240-2222

OLIVA, Joseph A.
Supervising Engineer
New Jersey State Dept. of Energy
101 Commerce St.
Newark, NJ 07201
(201) 648-3595

OLIVER, James C.
Naval Architect
Giannotti & Associates, Inc.
703 Giddings Ave.
Suite U-3
Annapolis, MD 21401
(301) 268-0030

OLMSTED, Merle
Program Manager
General Electric Co.
One River Rd.
Schenectady, NY 12345
(518) 385-0825

O'ROURKE, Joseph J.
Principal Project Manager
The Ralph M. Parsons Co.
100 W. Walnut St.
Pasadena, CA 91344
(213) 331-0777

OWENS, William, Dr.
Staff Engineer
Lockheed Missiles & Space Co.
Dept. 57-22, Bldg. 150
Sunnyvale, CA 94086
(408) 988-1223

PADDOCK, Robert A.
Argonne National Laboratory
9700 South Cass Ave.
Argonne, IL 60439
(312) 972-7640

PAGE, Albert N.
Engineering Spec.
Electric Boat Div.
General Dynamics Corp.
Eastern Point Rd.
Groton, CT 06340
(203) 446-2480

PANDOLFINI, P. P., Dr.
Applied Physics Laboratory
The Johns Hopkins University
Johns Hopkins Rd.
Laurel, MD 20810
(301) 953-7100 EXT. 2424

PARKER, Charles D., Jr.
Engineer
Life Cycle Engineering, Inc.
145 King St., Suite 309
Charleston, SC 29401
(803) 723-4887

PARKER, C. W.
Proj. Cont. Officer
Department of Energy
P. O. Box 1446
Canoga Park, CA 91360

PAUL, Martin
Senior Engineer
Westinghouse Electric Corp.
M/S 9920, P. O. Box 1488
Annapolis, MD 21404
(301) 765-5312

PAYNE, Susan F.
Lawrence Berkeley Laboratory
University of California
Berkeley, CA 94720
(415) 843-2740

PENNINGTON, A. J.
Manager, Systems Engineering
Franklin Research Center
20th and the Parkway
Philadelphia, PA 19103
(215) 448-1567

PEPE, Diana
Westinghouse Electric Corp.
P. O. Box 9175 MS-N-206
Philadelphia, PA 19113
(215) 595-4185

PEREZ BRACETTI, Fernando
PRWRA
GPO 4267
San Juan, PR 00936
(809) 725-8156
725-7801

PÉREZ y PÉREZ, Leonardo
Naval Architect
Deep Oil Technology, Inc.
Fluor Corp.
3333 Michelson Dr.
Irvine, CA 92730
(714) 975-7182

PIERONI, Charles A.
Manager, Development Eng.
Simplex Wire & Cable Co.
P. O. Box 479
Portsmouth, NH 03801
(603) 436-6100

PITONIAK, Joseph E.
Engineer - Fluid Dynamics
General Electric Corp.
One River Rd.
Schenectady, NY 12345
(518) 385-0860

POMPA, J. A.
Senior Staff
ORI, Inc.
1400 Spring St.
Silver Spring, MD 20910
(301) 588-6180

PONT, Rosendo
Systems Engineer
Lockheed Missiles & Space Co.
P. O. Box 504
Bldg. 150, Org. 57-82
Sunnyvale, CA 94086
(408) 988-1223

POPPER, Glenn F.
Assistant Manager
Argonne National Laboratory
9700 S. Cass Ave., D-308
Argonne, Il 60439
(312) 972-5933

POTASH, Roger L.
Lockheed Ocean Systems
P. O. Box 504
Sunnyvale, CA 94086
(408) 988-6761

POTEAT, L. E.
Assoc. Professor
University of Miami
Miami, FL 33149
(305) 284-2571

POUCHER, Fred W.
Program Manager
ETEC (Rockwell International)
8900 DeSota St.
Canoga Park, CA 91304
(213) 341-1000 EXT. 6127

POWERS, Walter
Tracor, Inc.
1601 Research Blvd.
Rockville, MD 20850
(301) 279-4271

PRIBIS, Paul
Engineer
General Electric Corp.
One River Rd.
Schenectady, NY 12345
(518) 385-1590

PRICE, David
NOAA/OOE
6010 Executive Blvd.
Rockville, MD 20852
(301) 443-8655

PRICE, John
Engineer
NASA
Marshall Space Fight Center
Huntsville, AL 35812
(205) 453-1288

PRICHETT, Wilson
Alternate Energy Specialist
NRECA
1800 Massachusetts Ave., N.W.
Washington, DC 20036

PRINCE, Frank R.
Virgin Islands Energy Office
P. O. Box 2996
St. Thomas, U.S. VI
(809) 774-6726

PROACH, Don
General Electric Corp.
One River Rd.
Schenectady, NY 12345
(518) 385-9009

PUCCI, Paul F.
Professor
Naval Post Graduate School
Monterey, CA 93940

RABAS, Thomas
Engineer
Westinghouse Electric Corp.
P. O. Box 9175 MS-N-206
Philadelphia, PA 19113
(215) 595-3544

RAHM, Allen
Consultant
PTT/ETS
Department of Energy
600 E St., N.W.
Washington, DC 20545
(202) 376-9475

RAMIAH, A. Venkata
Physiologist
Gulf Coast Research Lab.
Ocean Springs, MS 39564
(601) 875-2244

RAMSDEN, Hal
Manager, Business Development
Global Marine Development
P. O. Box 3010
Newport Beach, CA 92663
(714) 752-5050

RANDALL, John M.
Research Chem. Engineer
Western Regional Research Ctr.
Sea-USDA
800 Buchanan St.
Albany, CA 94710
(415) 486-3726

READ, Kenneth, Prof.
Dept. of Mechanical Engineering
U. S. Naval Academy
Annapolis, MD 21402
(301) 267-3582

REITZEL, John
1694 Main St.
Concord, MA 01742
(617) 369-9095

RICHARDS, Dennis
Senior Staff Engineer
Applied Physics Laboratory
The Johns Hopkins University
Johns Hopkins Rd.
Laurel, MD 20810
(301) 953-7100 EXT. 539

RICHARDS, William E.
Chief, Ocean Systems Branch
Division of Central Solar Tech.
Department of Energy
600 E St., N.W.
Washington, DC 20585
(202) 376-4771

RIDGWAY, J. R., Jr.
Senior Consulting Engineer
Houston Lighting & Power Co.
P. O. Box 1700
Houston, TX 77001
(713) 481-7597

RIDGWAY, Stuart L., Dr.
R&D Associates
P. O. Box 9695
Marina Del Rey, CA 90291
(213) 822-1715

RILEY, Patrick
Senior Mar. Engineer
J. J. Henry Co., Inc.
2341 Jefferson Davis Hwy. #838
Arlington, VA 22202
(703) 920-3435

RITLAND, Paul
Manager
Westinghouse Electric Corp.
P. O. Box 9175 MS-N-206
Philadelphia, PA 19113
(215) 595-2861

ROBERTS, Kenneth P.
Sales Manager
Simplex Wire & Cable Co.
P. O. Box 479
Portsmouth, NH 03801
(603) 436-6100

ROGALSKI, W. W., Jr.
Asst. Hull Dept. Manager
Gibbs & Cox, Inc.
2341 Jefferson Davis Hwy.
Arlington, VA 22202
(703) 979-1240

RONEY, James
James R. Roney Ocean Engineering
152 Grover Ave.
Princeton, NJ 08540

ROONEY, David M.
Assistant Professor
Aerospace & Ocean Engineering Dept.
215 Randolph Hall
VPI&SU
Blacksburg, VA 24060
(703) 961-6740

ROSENDAHL, Gene
Project Manager
General Electric - TEMPO
777 14th St., N.W.
Washington, DC 20005
(202) 637-4501

ROSENSTEIN, Joel
Surveyor
American Bureau of Shipping
65 Broadway
New York, NY 10006
(212) 440-0364

ROTHFUS, Robert R.
Professor
Carnegie-Mellon University
5000 Forbes Ave.
Pittsburgh, PA 15213
(412) 578-2227

ROWAN, William
Technical Co-Director
Energy Systems Div.
P. O. Box 106
S. Deerfield, MA 01373
(413) 665-7051

RUMBAUGH, Jeff
Department of Energy
Div. of Central Solar Tech.
20 Massachusetts Ave., N.W.
Room 2208 MS-2203
Washington, DC 20545
(202) 376-4735

RUSSELL, Hubert E.
Chief Engineer
Morris Guralnick Associates, Inc.
620 Folsom St.
San Francisco, CA 94107
(415) 543-8650

RUSSELL, Ronald W.
Mechanical Engineer
General Electric Co.
One River Rd.
Schenectady, NY 12345
(518) 385-5394

RYNEWICZ, J. F.
Lockheed Ocean Energy Systems
Lockheed Missiles & Space Co.
Org. 57-02, Bldg. 150
P. O. Box 504
Sunnyvale, CA 94080
(408) 988-3925

SABIN, Cullen M.
Vice President
Geoscience Ltd.
410 Cedros Ave.
Solana Beach, CA 92075
(714) 755-9396

SAND, Duane
Senior Engineer
Westinghouse Electric Corp.
P. O. Box 1488
Annapolis, MD 21404
(301) 765-5312

SANDS, M. Dale
EIA Program Manager
Interstate Electronics Corp.
P. O. Box 3117
Anaheim, CA 92803
(714) 772-2811 EXT. 1819

SANTIAGO, Miguel, Professor
Dept. of Civil Engineering
University of Puerto Rico
Mayaguez, PR 00708
(809) 832-4040

SASSCER, Donald S.
Center for Energy &
Environment Research
Mayaguez, PR 00708
(809) 832-1414

SASSONE, R.
900 N. Broadway #715
Santa Ana, CA 92701
(714) 542-1111

SATHER, Norman F.
Associate Director
Argonne National Laboratory
9700 So. Cass Ave.
Argonne, IL 60439
(312) 972-3724

SATO, Shiro, Dr.
Technical Research Laboratories
Samito Light Metal Industries
3-1-12 Chitose Minato-ku
Nagoya 455, Japan
052-654-1111

SAVERER, D. R., Capt.
Searle Consultants
711 Hanford St.
Pismo Beach, CA 93445
(805) 773-4522

SCHAEFFER, James
Manager Management Systems
Tracor, Inc.
1701 Research Blvd.
Rockville, MD 20850
(301) 279-4263

SCHELLENBERG, V. R.
Engineering Section Manager
Newport News Shipbuilding
4101 Washington Ave.
Newport News, VA 23607
(804) 380-3583

SCHRIEBER, C.
Senior Res. Spec.
Dow Chemical Co.
Freeport, TX 77541
(713) 238-0244

SCOTT, Robert J.
Asst. Division Head
Gibbs & Cox, Inc.
2341 Jefferson Davis Hwy.
Arlington, VA 22202
(703) 979-1240

SCOTT, Sylvester
Market Manager
Aluminum Co. of America
Alcoa Building
Pittsburgh, PA 15219
(412) 553-3187

SCOTTI, Richard S.
Department of Commerce
NOAA
Office of Ocean Engineering
WSC-5 Room 1022
6010 Executive Blvd.
Rockville, MD 20852
(301) 443-8655

SEARLE, W. F.
MIT
808 Timber Branch Parkway
Alexandria, VA 22302
(703) 549-7775

SERIM, Feridun K.
Vice President & Manager
M. Rosenblatt & Son, Inc.
2341 Jefferson Davis Hwy.
Arlington, VA 22202
(703) 892-5680

SHAPIRO, David
Dir. Adv. Development
TRACOR
1601 Research Blvd.
Rockville, MD 20850
(301) 279-4318

SHEFFIELD, Richard C.
Naval Architect
M. Rosenblatt & Son, Inc.
350 Broadway
New York, NY 10013
(212) 431-6900

SHEETS, Herman E.
Chmn. & Professor
University of Rhode Island
Ocean Engineering Department
Bliss Hall
Kingston, RI 02881
(401) 792-2273

SHELPUK, Benjamin
Research Engineer
Solar Energy Research Inst.
1536 Cole Blvd.
Golden, CO 80401
(303) 231-1759

SHERWOOD, Wilbur G.
National Science Foundation
Ocean Drilling Project Team Ofc.
1800 G Street, N.W. - Room 602
Washington, D. C. 20550
(202) 632-4134

SINDT, Charles
Mech. Engineer
National Bureau of Standards
Boulder, CO 80302
(303) 499-1000

SKERRETT, Peter E.
Manager
Market Research & Planning
Avco Everett Research Lab.
2385 Revere Beach Parkway
Everett, MA 02149
(617) 389-3000 EXT. 677

SLEBODNICK, Robert
Engineer
Westinghouse Electric Corp.
P. O. Box 9175 MS-N-206
Philadelphia, PA 19113
(215) 595-4720

SMITH, Clifford W.
President
CV Associates
6613 Beverly Ave.
McLean, VA 22101
(703) 734-9626

SMITH, Fred A.
Argonne National Laboratory
9700 S. Cass Ave.
Chicago, IL 60439
(312) 972-3724

SNYDER, J. Edward, III
TRW, Inc.
One Space Park
Bldg. 81, Room 1538
Redondo Beach, CA 90278
(213) 536-3410

SOELAIMAN, T. M.
Professor
Embassy of Indonesia
2020 Massachusetts Ave., N.W.
Washington, DC 20036
(202) 293-1745

SOLON, Gene
President
Solargistics, Inc.
510 N St., S.W.
Washington, DC 20024
(202) 484-1184

SONENSHEIN, Nathan, RAdm. USN (Ret.)
Asst. to President
Global Marine Dev., Inc.
Box 3010
Newport Beach, CA 92663
(714) 752-5050

SOOY, Walt
Science Applications, Inc.
2361 S. Jefferson Davis Hwy.
Arlington, VA 22202
(703) 979-5900

SPIEHLER, F. A.
NOAA Data Buoy Office
NSTL Station, MS 39529
(601) 688-2806

SPROUSE, Alice M.
Project Engineer
TRW DSSG
One Space Park 81/1578
Redondo Beach, CA 90278
(213) 535-2130

STABINSKY, Leon
Director
Rockwell International
Rocketdyne Division
6633 Canoga Ave. MS AA53
Canoga Park, CA 91304
(213) 884-3374

STADTER, James T.
Senior Engineer
Applied Physics Laboratory
The Johns Hopkins University
Johns Hopkins Rd.
Laurel, MD 20810
(301) 953-7100 EXT. 7418

STEEN, John P., Jr.
Assistant Planktologist
Gulf Coast Research Lab.
East Beach Dr.
Ocean Springs, MS 39564
(601) 875-8724

STEVENS, Robert E.
Asst. Manager
Stone & Webster Engineering Corp.
245 Summer St.
Boston, MA 02107
(617) 973-8501

SUMITOMA, Hiroyuki
Chief Engineer
Hisaka Works, Ltd.
2-1-48, Higashi Konoikecho,
Higashi
Osaka-fu, Japan
0729-62-1451

SUMNER, William
Supvr., System Analyst
TRACOR, Inc.
1701 Research Blvd.
Rockville, MD 20850
(301) 279-4274

SUNDARAM, T. R.
President
TRS Associates
P. O. Box 1131
Columbia, MD 21044
(301) 596-4425

SURKEIN, Michael B.
Staff Scientist
Ocean City Research Corp.
Tenn. Ave. & Beach. Thoro.
Ocean City, NJ 08226
(609) 399-2417

SUTHERLAND, Paul
Sr. Project Coordinator
Florida Power & Light
P. O. Box 529100
Miami, FL 33152
(305) 552-3605

SVENSEN, Alf
Senior Project Engineer
Global Marine
P. O. Box 3010
Newport Beach, CA 92663
(714) 752-5050

SWENSON, James N.
Sales Engineer
Revere Copper & Brass, Inc.
605 Third Ave.
New York, NY 10016
(212) 578-1576

SZETO, F.
Ocean Engineer
NOAA
Office Ocean Engineering
6010 Executive Blvd., Room 1022
Rockville, MD 20852
(301) 443-8655

TAKAYANAGI, Mikio
Tokyo Shibaura Electric Co., Ltd.
Dept. of Thermal & Turbine Eng.
3-13-12, Mita, Minato-ku, Tokyo
Japan
103-454-7111

TAKESUE, Hiromitsu
Manager
Chemical Eng. & Equipment Dept.
Mikko Consulting & Eng. Co., Ltd.
2-10-1, Nikko Bldg.
Toranomon, Minato-ku, Tokyo
Japan
03-437-2505

TAM, Clement
Engineer
Southwestern Engineering Co.
6111 E. Bandini Blvd.
Los Angeles, CA 90054
(213) 726-0641

TAMADA, Toyoshige
International Dept.
Overseas Industry Research Center
4-4, Kojimachi, Chiyoda-ku, Tokyo
Japan

TATRO, Peter R.
Manager Ocean Science Division
Science Applications, Inc.
8400 Westpark Dr.
McLean, VA 22101
(703) 821-4470

TEFFT, R. Clark
President
Tefft, Kelly, and Motley, Inc.
1225 Connectivut Ave.
Washington, DC 20036
(202) 659-2650

THACKRAY, John
Product Manager
Trent Tube
East Troy, WI 53120
(414) 642-7321

THOMAS, Anthony
Manager, OTEC Power Systems
Argonne National Laboratory
9700 South Cass Ave.
Argonne, IL 60439
(312) 972-8071

THOMAS, E. Dail
Chemist
David Taylor Naval Ship R&D Ctr.
Code 2865
Annapolis, MD 21402

THORHAUG, Anitra
Professor
Florida International University
c/o 600 Grapetree Dr. #4EN
Key Biscayne, FL 33149
(305) 361-3340

TILLY, Lawrence
Ecologist
CEER/UPR
College Station
Mayaguez, PR
(809) 832-7912

TITCOMB, R. D.
Mktg. Manager
Oceanic Division
Westinghouse Electric Corp.
P. O. Box 1488
Annapolis, MD 21404

TOMINE, Koei
Manager, Technical Div.
Tobishima Corp.
3-28, Kudanminami 2-Chome
Chiyoda-ku, Tokyo
Japan
03-263-3151

TOMOMITSU, Kolke
Ishikawajima-Harima Heavy
Industries Co., Ltd.
3-2-16, Toyosu
Koto-ku, Tokyo
Japan
03-534-2446

TOSTESON, Thomas R.
Professor
University of Puerto Rico
Dept. Marine Sciences
Mayaguez, PR
(809) 832-4040

TOTH, Louis
Alexander Systems, Inc.
9161 Chesapeake Dr.
San Diego, CA 92123
(714) 292-7418

TRAUT, Richard T.
Dev. Engineer
Simplex Wire & Cable Co.
P. O. Box 479
Portsmouth, NH 03801
(603) 483-6100

TSU-You, Chu
Professor
Inst. of Oceanography N.T.U.
757 Cayuga Dr.
Horseheads, NY 14845
(607) 562-7416

TUCKEY, George
Northwest Marine Iron Works
P. O. Box 3109
Portland, OR 97408
(503) 228-8222

TURNER, Neil
General Electric Co.
Schenectady, NY 12345
(518) 385-0860

TURNIPSEED, Rhett
DOE Solar Technology
600 E St., N.W.
Washington, DC 20545
(202) 376-4745

UEHARA, Haruo
Associate Professor
Faculty of Science & Engrg.
SAGA University
1, Honjomachi, Saga-shi
Saga-ken Japan
0952-31-3731

UMBERGER, Robert
Supervisory Project Engr.
M. Rosenblatt & Son, Inc.
2341 Jefferson Davis Hwy.
Arlington, VA 22202
(703) 892-5680

VADUS, Joseph
Department of Commerce
NOAA
Office of Ocean Engineering
WSC-5, Room 1015
6010 Executive Blvd.
Rockville, MD 20852
(301) 443-8655

VAN DER POT, Bart, J.G.
Hollandsche Beton Groep (HBG)
P. O. Box 82
Ryswyk
The Netherlands
070-94.93.40

VAN HEMELRYCK, L.
Research Eng.
University of Texas at Austin
Marine Science Laboratory
Port Aransas, TX 78373
(512) 749-6779

VAN TETERING, J.
Vice President
Stork Werkspoor Can Ltd.
Pumps Div.
2000 Argentia Rd.
Plaza Two, Suite 402
Mississauga, Ontario
Canada L5N IV8
416-826-8700

VENEZIAN, Giulio
Assoc. Professor
Dept. of Ocean Engineering
University of Hawaii
2565 the Mall
Honolulu, HI 96822
(808) 948-8110

VEZIROGLU, T. Nejat
Professor
University of Miami
School of Engrg. & Arch.
Coral Gables, FL 33124
(305) 284-4666

VINCENT, Semon
Asst. Project Manager
TRW Systems & Energy
One Space Park 81/1538
Redondo Beach, CA 90278
(213) 535-1596

VOM SAAL, R. J.
Structural Engineer
Bethlehem Steel Corp.
Sparrows Point MD 21219
(301) 477-6187

VOS, Charles
Hollandsche Beton Groep (HBG)
P. O. Box 82
Ryswyk, The Netherlands
070-94.93.40

VUKOVICH, Fred
Research Triangle Institute
P. O. #12194
Research Triangle Park, NC 27709
(919) 541-6000

WACHTELL, G. P.
Principal Scientist
Franklin Research Center
20th St. & Parkway
Philadelphia, PA 19103
(215) 448-1555

WAID, Robert L.
Lockheed Missiles & Space Co.
P. O. Box 504
Sunnyvale, CA 94086
(408) 988-6594

WAITE, Keith
Environmental Analyst
EEA, Inc.
1111 N. 19th St.
Arlington, VA 22209
(703) 528-1900

WALLACE, John
Mgr. Business Development
Texas Instruments
Attleboro, MA 02703
MS 4-9
(617) 222-2800

WALLS, Donald
Senior Systems Engineer
Advanced Marine Enterprises, Inc.
2341 Jefferson Davis Hwy.
Suite 500
Arlington, VA 22202
(703) 979-9200

WALSH, J. P., Dr.
Value Engineering Co.
2550 Huntington Ave.
Alexandria, VA 22303
(703) 960-1820

WANDERER, E. T.
Senior Engineer
Aluminum Co. of America
Alcoa Center, PA 15069
(412) 339-6651

WANG, P. Y.
Research Engineer
Argonne National Laboratory
9700 S. Cass Ave., D-362
Argonne, IL 60439
(312) 972-6379

WASEL, Robert A.
NASA Headquarters
Washington, D. C.
(202) 755-2306

WASHOM, Byron
Mgr. Technology & Policy
Fairchild - Stratos Div.
1800 Rosecrans Ave.
Manhattan Beach, CA 90266
(213) 675-9111

WATSON, M. J.
OTEC-1 APM
TRW Systems
One Space Park
Redondo Beach, CA 90278
Attn: 88-2048
(213) 536-3466

WEBB, J. D.
Business Mgr.
TRW, Inc.
One Space Park
Redondo Beach, CA 90278
(213) 846-2203

WEBB, Ralph L.
Professor
Dept. of Mechanical Engrg.
Pennsylvania State Univ.
University Park, PA 16801
(814) 865-0283

WEBSTER, Lee R.
President
International Technology Corp.
1670 Highway A1A
Satellite Beach, FL 32937
(305) 777-1400

WECHSLER, Laskar Dr.
Chief Engineer
Hydronautics, Inc.
Pindell School Rd.
Laurel, MD 20810
(301) 776-7454

WEISS, Roger O., Dr.
Applied Physics Laboratory
The Johns Hopkins University
Johns Hopkins Road
Laurel, MD 20810
(301) 953-7100, EXT. 7467

WERTHEIMER, Jules
President
Vieques Development Corp.
299 Broadway
New York, NY 10001
(212) 267-6270

WESTERBERG, Arthur
Professor
Carnegie-Mellon Univ.
Dept. Chemical Engineering
Schenley Park
Pittsburgh, PA 15213
(412) 578-2228

WETMORE, Sherman B.
Vice President Engrg.
Global Marine Development, Inc.
4100 MacArthur Blvd.
Newport Beach, CA 92660
(714) 752-5050

WHITE, Harry J.
Operations Mgr.
University of Hawaii (NELH)
74-5563Q Kaiwi St.
Kailua-Kona, HI 96740
(808) 329-9357

WICKERSHAM, Jack
Project Engineer
Delmarva Power & Light Co.
800 King St., P. O. Box 231
Wilmington, DE 19899
(302) 429-3552

WILDE, Pat
Research Oceanographer
Lawrence Berkeley Laboratory
University of California
Berkeley, CA 94720
(415) 486-6461

WILKE, R. O.
Van Dresser Corp.
Suite 1610
7555 W. Big Beaver Rd.
Troy, MI 48084
(313) 362-4600

WILKINS, Mark A.
1st Secretary (Technology)
British Embassy
3100 Massachusetts Ave., N.W.
Washington, DC 20008
(202) 462-1340

WILLIAMS, Ralph
Senior Associate
PRC Energy Analysis Co.
7600 Old Springhouse Rd.
McLean, VA 22102
(703) 893-1822

WILLSON, J. J.
Deputy Director Planning
Burns & Roe, Inc.
5500 Kinderkamack Rd.
Oradell, NJ 07649
(201) 265-2000

WILSON, Arthur
Staff Analyst
National Advisory Committee on
Oceans & Atmosphere
3300 Whitehaven St., N.W.
Room 434 Page I Bldg.
Washington, DC 20235
(202) 254-8656

WILSON, Lewis A.
Manager, Advanced Energy Programs
Middle South Services, Inc.
P. O. Box 61000
New Orleans, LA 70161
(504) 529-5262

WILSON, Ted R.
Engineering Consultant
Harbridge House/Dev. Sciences
Services
2111 Jefferson Davis Hwy.
Suite 001-N
Arlington, VA 22202
(703) 892-6100

WILT, H. E.
Engr. Manager
B. F. Goodrich
Akron, OH 44309
(216) 379-2306

WITTE, Arvel
Manager, Energy Technology Dept.
TRW, Inc.
One Space Park
Redondo Beach, CA 90278
(213) 536-1967

WOLDIN, Richard
Congressional Fellow
Senate Energy Committee
U.S. Capitol Bldg.
Room S402
Washington, DC 20510
(202) 224-4431

WOLFF, Paul
Senior Vice President
Ocean Data Systems, Inc.
2400 Garden Rd.
Monterey, CA 93940
(408) 649-1133

WOODHULL, A. S.
United Engineers & Constructors
30 So. 17th St.
Philadelphia, PA 19101
(215) 422-3861

WRIGHT, David E.
Program Manager
Rocketdyne Div.
Rockwell International
6633 Canoga Ave., MS AB48
Canoga Park, CA 91304
(213) 884-3037

YAFFO, Jay E.
Administrative Director
Alfa-Laval Thermal, Inc.
So. Deerfield, MA 01373
(413) 665-7051

YAMPOLSKY, J. S.
Senior Technical Advisor
General Atomic Co.
P. O. Box 81608
San Diego, CA 92138
(714) 455-3645

YANG, Chic
Engineer
General Electric Co.
Bldg. 23, Room 384
Schenectady, NY 12345
(518) 385-7912

YARDEN, Abe
OTEC Project Manager
SEC
6111 E. Bandini Blvd.
Los Angeles, CA 90049
(213) 726-0641

YAREMA, Geoffrey
Nossaman, Krueger & Marsh
445 So. Figueroa St.
30th Floor
Los Angeles, CA 90266
(213) 628-5221

YOSHIHARA, Takeshi
Legislative Asst. to
Senator Matsunaga
362 Russell Senate Office Bldg.
Washington, DC 20510
(202) 224-6361

YUEN, Paul C.
Director
Hawaii Natural Energy Institute
University of Hawaii
2540 Dole St.
Honolulu, HI 96822
(808) 948-7886

YUNG, David
Argonne National Laboratory
CT-308
Argonne, IL 60439
(312) 972-5903

ZAWIERUCHA, Robert
Engineering Associate
Union Carbide Corp. - Linde Div.
P. O. Box 44
Tonawanda, NY 14150
(716) 877-1600

ZENER, Clarence
Professor
Carnegie-Mellon University
Pittsburgh, PA 15213
(412) 578-2538

ZIMMERMAN, Bob
Design Consultant
University of California - Irvine
1122 Verano Pl.
Irvine, CA 92715
(714) 752-2163

YOUNG, David S.
12727 Braewood Glen
Houston, TX 77072
(713) 498-6180

ATTENDEES FROM MEDIA

M. N. Abramovich	IEEE Newsletter
Eric Bender	Sea Technology
R. R. Benedict	Sears R. G. Weekly
John Bisney	NBC
Larry L. Booda	Editor, Sea Technology
C. Amos Bussmann	
Charles H. Bussmann	Sea Technology
Bill Buzenberg	National Public Radio
Paul Capros	WKAQ Radio - TV
Allan L. Frank	Solar Energy Intelligence Report
Alfred L. Gilmore	Triton Report
Anne Hinterlong	Government Executive Magazine
Dee Kominus	Nautilus Press Inc.
Bill Kovarik	Business Publishers Latin American Energy Report
Tom Kryan	UPI
Berta Lawn	An Nahar - Arab Report
Emile G. Louzada	Netherlands Embassy
Richard Meyer	Solar Ocean Energy Liaison
Stan Miller	ACS, Environmental Science and Technology

ATTENDEES FROM MEDIA (continued)

Michael Mulcahy	Sea Technology Magazine Arlington, Virginia
J. A. Quick	Arkin Magazine Synd.
Alain Raymond	Agence France Presse
Deborah Staats	Fortune
Mark Swann	Free-lance
Gordon Taylor	European Energy Report (Financial Times)
Harry Turner	San Juan Star
Seve Ungermark	Swedish Television
Edwin L. Wilber	Free-lance
Jane Winebrenner	Jack Anderson
K. Yamozaki	The Nihon Kiia

•U.S. GOVERNMENT PRINTING OFFICE : 1980 0-620-309/2679

United States
Department of Energy
Washington, DC 20585

Postage and Fees Paid
U.S. Department of Energy
DOE-350

Official Business
Penalty for Private Use, $300

FIRST CLASS MAIL